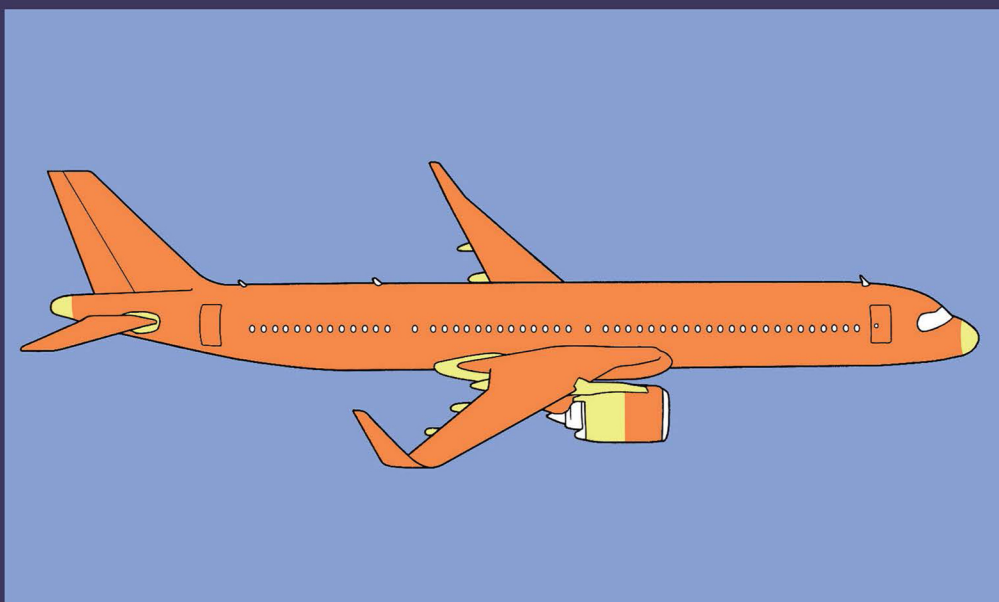


FOURTH EDITION

COMPOSITE MATERIALS

Design and Applications



Daniel Gay



CRC Press
Taylor & Francis Group

Composite Materials

For decades, *Composite Materials: Design and Applications* has guided readers on the efficient design of structural composite parts and has illustrated challenges encountered in modern engineering practice. The fourth edition of this perennial best-seller retains its pedagogical structure, featuring a technical level that rises in difficulty as the text progresses, while allowing each part to be explored independently, but has been updated to mirror recent advances and developments in manufacturing processes and applications.

- Gives numerous examples of the pre-sizing of composite parts, processed from industrial cases and reworked to highlight key information
- Provides a design method to define composite multilayered plates under loading, along with all numerical information needed for implementation
- Includes test cases for the validation of computer software using finite elements
- Proposes original study of composite beams of any section shapes and of transverse shear behavior of laminates, leading to technical formulations that are not found in the literature
- Reflects the latest manufacturing processes and applications in the aerospace, automotive, naval, wind turbine, and sporting goods industries, and now features new details on the recycling of composites and additive manufacturing
- Offers new coverage of ceramic-matrix composites and new concepts for design of laminates, including Double-Double and tapered laminates by means of Tsai homogenization

This book serves as a textbook for advanced students studying composite materials design, as well as a handy reference for industry professionals working with composite materials.



Taylor & Francis

Taylor & Francis Group

<http://taylorandfrancis.com>

Composite Materials

Design and Applications

Fourth Edition

Daniel Gay (<https://orcid.org/0000-0002-1775-2108>)



CRC Press

Taylor & Francis Group

Boca Raton London New York

CRC Press is an imprint of the
Taylor & Francis Group, an **informa** business

Fourth edition published 2023
by CRC Press
6000 Broken Sound Parkway NW, Suite 300, Boca Raton, FL 33487-2742

and by CRC Press
4 Park Square, Milton Park, Abingdon, Oxon, OX14 4RN

CRC Press is an imprint of Taylor & Francis Group, LLC

© 2023 Taylor & Francis Group, LLC

First edition published by CRC Press 2002
Third edition published by CRC Press 2014

Reasonable efforts have been made to publish reliable data and information, but the author and publisher cannot assume responsibility for the validity of all materials or the consequences of their use. The authors and publishers have attempted to trace the copyright holders of all material reproduced in this publication and apologize to copyright holders if permission to publish in this form has not been obtained. If any copyright material has not been acknowledged please write and let us know so we may rectify in any future reprint.

Except as permitted under U.S. Copyright Law, no part of this book may be reprinted, reproduced, transmitted, or utilized in any form by any electronic, mechanical, or other means, now known or hereafter invented, including photocopying, microfilming, and recording, or in any information storage or retrieval system, without written permission from the publishers.

For permission to photocopy or use material electronically from this work, access www.copyright.com or contact the Copyright Clearance Center, Inc. (CCC), 222 Rosewood Drive, Danvers, MA 01923, 978-750-8400. For works that are not available on CCC please contact mpkbookspermissions@tandf.co.uk

Trademark notice: Product or corporate names may be trademarks or registered trademarks and are used only for identification and explanation without intent to infringe.

ISBN: 978-1-032-04308-1 (hbk)
ISBN: 978-1-032-05048-5 (pbk)
ISBN: 978-1-003-19578-8 (ebk)

DOI: 10.1201/9781003195788

Typeset in Times
by codeMantra

Access the Support Material: <https://www.routledge.com/Composite-Materials-Design-and-Applications-Fourth-Edition/Gay/p/book/9781032043081>

Contents

Foreword	xxi
Preface.....	xxiii
Acknowledgments.....	xxv
Author	xxvii

PART I Principles of Construction

Chapter 1	Composite Materials: Interest and Physical Properties.....	3
1.1	What Is a Composite Material?	3
1.1.1	Broad Definition	3
1.1.2	Main Features.....	3
1.2	Fibers and Matrices	4
1.2.1	Fibers	4
1.2.1.1	Definition	4
1.2.1.2	Principal Fiber Materials.....	4
1.2.1.3	Processes for Obtaining Fibers.....	5
1.2.2	Materials for Matrices	6
1.3	What Can Be Made Using Composite Materials?.....	6
1.4	A Typical Example of Interest.....	8
1.5	Some Examples of Classical Design Replaced by Composite Solutions	8
1.6	Main Physical Properties.....	9
	Notes.....	15
Chapter 2	Manufacturing Processes	17
2.1	Molding Processes.....	17
2.1.1	Contact Molding.....	17
2.1.2	Compression Molding	18
2.1.2.1	Process	18
2.1.2.2	Bladder Molding Process.....	18
2.1.2.3	Forming by Stamping	18
2.1.3	Vacuum Molding Processes	18
2.1.3.1	Vacuum Molding	18
2.1.3.2	Autoclave Curing.....	19
2.1.4	Injection Processes	19
2.1.4.1	Resin Transfer Molding (RTM).....	19
2.1.4.2	Vacuum-Assisted RTM (VARTM).....	20
2.1.4.3	Injection Molding with Prepreg.....	20
2.1.4.4	Reaction Injection Molding (RIM/S-RIM)	21
2.1.5	Molding of Hollow Axisymmetric Components.....	21
2.2	Others Forming Processes.....	22
2.2.1	Sheet Forming	22
2.2.2	Pultrusion	23
2.2.3	Additive Manufacturing	23
2.2.3.1	Principle.....	23

2.2.3.2	Types of Additive Machines	23
2.3	Automated Preform Manufacturing	24
2.3.1	Necessity of Automation	24
2.3.2	Types of Machines	25
2.3.2.1	Fiber Placement Processes.....	25
2.3.2.2	Automated Tape Laying (ATL).....	25
2.3.2.3	Automated Fiber Placement (AFP).....	26
2.3.2.4	Example: Robots and Software for AFP – Automatic Fiber Placement Coriolis Composites (FR)	28
2.4	Practical Considerations on Manufacturing Processes; Acronyms.....	28
2.5	Recycling of Composites	29
2.5.1	Recycling Issues	29
2.5.1.1	The Problem of Waste	29
2.5.1.2	Examples.....	30
2.5.1.3	Specific Problems to Composites	31
2.5.2	Recycling of Polymer Matrix Composites	31
2.5.2.1	Main Processes	31
2.5.2.2	Case of Carbon/Resin Composites	31
	Notes.....	32

Chapter 3	Mechanical Properties of Reinforcement–Matrix Associations	33
3.1	Isotropy and Anisotropy	33
3.1.1	Isotropic Materials	34
3.1.2	Anisotropic Material	34
3.2	Characteristics of the Reinforcement–Matrix Mixture.....	36
3.2.1	Fiber Mass Fraction.....	36
3.2.2	Fiber Volume Fraction.....	37
3.2.3	Mass Density of a Ply.....	37
3.2.4	Ply Thickness	38
3.3	Unidirectional Ply.....	38
3.3.1	Elastic Modulus	38
3.3.2	Ultimate Strength of a Ply.....	41
3.3.3	Examples	42
3.4	Woven Ply	42
3.4.1	Forms of Woven Fabrics.....	42
3.4.2	Elastic Modulus of Fabric Layer	44
3.4.3	Examples of Balanced Fabric/Epoxy	45
3.5	Mats and Reinforced Matrices	46
3.5.1	Mats.....	46
3.5.2	Example: A Summary of Glass/Epoxy Layers	47
3.5.3	Microspherical Fillers	47
3.5.4	Other Classical Reinforcements	49
3.6	Metal Matrix Composites (MMC)	50
3.6.1	Materials.....	50
3.6.2	Some Examples	50
3.6.2.1	Aluminum-Reinforced Aramid (<i>ARALL</i> ®) and Aluminum-Reinforced Glass (<i>GLARE</i> ®).....	50
3.6.2.2	Short Silicon Carbide Fibers (Whiskers)/Aluminum	52
3.6.2.3	Boron/Aluminum.....	52
3.6.2.4	Unidirectional Fibers/Aluminum Matrix	53

3.7	Ceramic Matrix Composites (CMCs).....	53
3.7.1	CMCs: An Area of Growing Interest	53
3.7.1.1	Significant Industrial Importance	53
3.7.2	Fibers	54
3.7.2.1	Materials	54
3.7.2.2	Reinforcements	54
3.7.3	Matrices.....	54
3.7.3.1	Materials	54
3.7.3.2	Fatigue Resistance	55
3.7.4	Production Processes.....	55
3.7.5	Thermomechanical Properties	56
3.7.5.1	Laminates	56
3.7.5.2	Multidimensional Fabrics	56
3.7.5.3	Ranges for Mechanical Properties.....	57
3.7.6	Application Domains of CMCs.....	57
3.7.6.1	Recall	57
3.7.6.2	Aerospace and Defense.....	58
3.7.6.3	Space Applications	58
3.7.6.4	Automobile	58
3.7.6.5	Other Uses	59
3.8	Biocomposite Materials.....	59
3.8.1	Natural Plant Fibers.....	59
3.8.1.1	Natural Fibers	59
3.8.1.2	Pros	59
3.8.1.3	Cons	60
3.8.1.4	Examples.....	60
3.8.2	Natural Vegetable Fiber–Reinforced Composites.....	60
3.8.2.1	Mechanical Properties	60
3.8.2.2	Biodegradable Matrices.....	62
3.8.3	Manufacturing Processes	62
3.8.3.1	With Thermosetting Resins	62
3.8.3.2	With Thermoplastic Resins	63
3.9	Nanocomposite Materials.....	63
3.9.1	Nanoreinforcement.....	63
3.9.1.1	Nanoreinforcement Shapes.....	63
3.9.1.2	Properties of Nanoreinforcements.....	64
3.9.2	Nanocomposite Material	66
3.9.3	Mechanical Applications.....	68
3.9.3.1	Improvement in Mechanical Properties	68
3.9.3.2	Further Examples of Nonmechanical Applications.....	68
3.9.4	Manufacturing of Nanocomposite Materials	69
3.10	Tests	70
	Notes.....	71

Chapter 4	Sandwich Structures.....	73
4.1	What Is a Sandwich Structure?	73
4.1.1	Their Properties Are Surprising.....	73
4.1.2	Constituent Materials	74
4.2	Simplified Flexure	74
4.2.1	Stress	74
4.2.2	Displacements	75

4.2.2.1	Contributions of Bending Moment M and Shear Force T ...	75
4.2.2.2	Example: A Cantilever Sandwich Structure	76
4.3	Some Special Features of Sandwich Structures	77
4.3.1	Comparison of Mass for the Same Flexural Rigidity $\langle EI \rangle$	77
4.3.2	Deterioration by Buckling of Sandwich Structures	77
4.3.2.1	Global Buckling.....	78
4.3.2.2	Local Buckling of the Skins	78
4.3.3	Other Types of Damage.....	79
4.4	Manufacturing and Design Problems.....	79
4.4.1	Example of Core Material: Honeycomb.....	79
4.4.2	Shaping Processes	80
4.4.2.1	Machining.....	80
4.4.2.2	Deformation.....	80
4.4.2.3	Some Other Considerations	80
4.4.3	Inserts and Attachment Fittings	80
4.4.4	Repair of Laminated Facings	82
4.5	Nondestructive Inspection	83
4.5.1	Main Nondestructive Inspection Methods	83
4.5.2	Acoustic Emission Testing	83
Notes	86
Chapter 5	Conception: Design and Drawing	87
5.1	Drawing a Composite Part	87
5.1.1	Specific Properties.....	87
5.1.2	Guide Values of Pre-sizing.....	88
5.1.2.1	Material Characteristics.....	88
5.1.2.2	Design Factors	89
5.2	Laminate.....	89
5.2.1	Unidirectional Layers and Fabrics	90
5.2.1.1	Unidirectional Layer.....	90
5.2.1.2	Fabrics.....	90
5.2.2	Correct Ply Orientation	90
5.2.3	The Quadrangle Symmetric (Quad) Laminate	91
5.2.3.1	Standard Orientations	91
5.2.3.2	Laminate Middle Plane	93
5.2.3.3	Description of the Stacking Order: Drawing Code	93
5.2.3.4	Mid-plane Symmetry.....	94
5.2.3.5	Specific Case of Balanced Fabrics.....	95
5.2.3.6	Technical Minimum	96
5.2.4	Arrangement of Plies.....	96
5.2.4.1	Proportion and Number of Plies	96
5.2.4.2	Example of Pictorial Representation	97
5.2.4.3	Case of Sandwich Structure.....	97
5.3	Failure of Laminates	98
5.3.1	Damages.....	98
5.3.1.1	Types of Failure	98
5.3.1.2	Note: Classical Maximum Stress Criterion Shows Its Limits.....	99
5.3.2	Frequently Used Criterion: Tsai-Hill Failure Criterion.....	100
5.3.2.1	Tsai-Hill Number.....	100

	5.3.2.2	Notes	100
	5.3.2.3	How to Determine the Stress Components σ_{t_i} , σ_t , and τ_{t_i} in Each Ply	101
5.4		Pre-sizing of the Quadrangle Symmetric Laminate	101
	5.4.1	Modulus of Elasticity; Deformation of the Laminate	101
		5.4.1.1 Varying Proportions of Plies	101
		5.4.1.2 Example of Using Tables	102
	5.4.2	Case of Simple Loading	102
	5.4.3	Complex Loading Case: Approximative Proportions According to Orientations	110
		5.4.3.1 When the Normal and Shear Loads Are Applied Simultaneously	110
		5.4.3.2 Example	115
		5.4.3.3 Note.....	117
	5.4.4	Complex Loading Case: Optimum Composition of a Laminate.....	117
		5.4.4.1 Optimum Laminate	117
		5.4.4.2 Example	120
		5.4.4.3 Example	124
		5.4.4.4 Notes	125
	5.4.5	Notes for Practical Use Concerning Laminates	126
		5.4.5.1 Specific Aspects for the Design of Laminates.....	126
		5.4.5.2 Delaminations.....	127
		5.4.5.3 Why Is Fatigue Resistance So Good?.....	130
		5.4.5.4 Laminated Tubes	130
		Notes	131
Chapter 6		Conception: Fastening and Joining	133
6.1		Riveting and Bolting.....	133
	6.1.1	Local Loss of Strength	133
		6.1.1.1 Knockdown Factor.....	133
		6.1.1.2 Causes of Hole Degradation	133
	6.1.2	Main Failure Modes in Bolted Joints of Composite Materials	135
	6.1.3	Sizing of the Joint.....	135
		6.1.3.1 Recommended Values	135
		6.1.3.2 Evaluation of Magnified Stress Values	136
	6.1.4	Riveting	137
	6.1.5	Bolting	138
		6.1.5.1 Example of Bolted Joint.....	138
		6.1.5.2 Tightening of the Bolt.....	139
6.2		Bonding	139
	6.2.1	Adhesives Used	139
	6.2.2	Geometry of the Bonded Joints.....	140
	6.2.3	Sizing of the Bonding Surface Area	142
		6.2.3.1 Strength of Adhesive.....	142
		6.2.3.2 Design	142
		6.2.3.3 Stress in Bonded Areas.....	142
		6.2.3.4 Example of Single-Lap Adhesive Joint.....	145
	6.2.4	Case of Bonded Joint with Cylindrical Geometry	145
		6.2.4.1 Bonded Circular Flange.....	145
		6.2.4.2 Tubes Fitted and Bonded into One Another	145

6.2.5	Examples of Bonding	145
6.2.5.1	Laminates	145
6.3	Inserts	146
6.3.1	Case of Sandwich Parts	147
6.3.2	Case of Parts under Uniaxial Loads	147
	Notes	148
Chapter 7	Composite Materials and Aerospace Construction	149
7.1	Aircraft	149
7.1.1	Composite Components in Aircraft	149
7.1.2	Allocation of Composites Depending on Their Nature	150
7.1.2.1	Glass/Epoxy, Kevlar/Epoxy	150
7.1.2.2	Carbon/Epoxy	150
7.1.2.3	Boron/Epoxy	150
7.1.2.4	Honeycombs	151
7.1.3	Few Comments	151
7.1.4	Specific Aspects of Structural Strength	152
7.1.5	Large Transport Aircraft	152
7.1.5.1	Example	152
7.1.5.2	How to Determine the Benefits	153
7.1.5.3	Example: Civil Transport Aircraft A380–800, Airbus (EU) (Figure 7.4)	154
7.1.5.4	Example: Civil Transport Aircraft B 787–800, Boeing (US) (Figure 7.5)	155
7.1.5.5	Example: Civil Transport Aircraft A350–900, Airbus (EU) (Figure 7.6)	155
7.1.6	Regional Aircraft and Business Jets	157
7.1.6.1	Example: Regional Aircraft ATR 72–600, ATR (EU-IT)	157
7.1.6.2	Example: Business Aircraft Falcon 10X, Dassault Aviation (FR)	157
7.1.6.3	Example: Cargo Aircraft WK2 and Suborbital Space Plane SST2, Scaled Composites (US)-Virgin Group (GB)	158
7.1.7	Light Aircraft	159
7.1.7.1	Trends	159
7.1.7.2	Aircraft with Tractor Propeller	159
7.1.7.3	Aircraft with Pusher Propeller (Backward Propeller)	162
7.1.8	Fighter Aircraft	162
7.1.9	Architecture and Manufacture of Composite Aircraft Parts	164
7.1.9.1	Sandwich Design	164
7.1.9.2	Rib-Stiffened Panels	165
7.1.9.3	MMC Panels	169
7.1.10	Braking Systems	169
7.2	Helicopters	171
7.2.1	Composite Areas	171
7.2.2	Some Examples	171
7.2.2.1	Helicopter H160 Airbus-Helicopter (EU) 2020	171
7.2.2.2	Racer Airbus-Helicopter (EU)	172
7.2.2.3	SB-1 Defiant Sikorsky-Boeing (US)	173

	7.2.2.4	V 280 Valor Bell-Lockheed Martin (US).....	173
7.2.3		Blades	174
	7.2.3.1	Design of a Main Rotor Blade	174
	7.2.3.2	Advantages.....	174
	7.2.3.3	Consequences	174
7.2.4		Rotor Hub	175
	7.2.4.1	Example: Rotor Hub Starflex, Eurocopter (FR–DE)	176
	7.2.4.2	Example: Rotor Hub Spheriflex, Eurocopter (FR–DE), Airbus (EU)	177
7.2.5		Other Working Composite Parts	177
7.3		Airplane Propellers	178
7.3.1		Propellers for Conventional Aerodynamics	178
	7.3.1.1	Example: Propeller Blade, Hamilton Sundstrand (US)-Ratier Figeac (FR)	178
7.3.2		High-Speed Propellers	180
7.4		Aircraft Reaction Engine	181
7.4.1		Technological Developments and Progress.....	181
	7.4.1.1	Example: Jet Engine Leap®, CFM International, General Electric (US) – Safran Aircraft Engines (FR)....	181
7.4.2		Use of Ceramic Matrix Composites (CMCs)	183
	7.4.2.1	Interest of CMCs for Aerospace Engines	183
	7.4.2.2	Applications	183
	7.4.2.3	Example: Nozzle: COI Ceramics (US)/Rolls-Royce (GB)...	183
7.5		Space Applications	184
7.5.1		Satellites	184
7.5.2		Propellant Tanks and Pressure Vessels	185
7.5.3		Nozzles	186
7.5.4		Other Composite Components for Space Application	188
	7.5.4.1	For Engines.....	188
	7.5.4.2	For Thermal Protection	188
	7.5.4.3	For Energy Storage	189
		Notes.....	190

Chapter 8		Composite Materials for Various Applications	193
8.1		Comparative Importance of Composites in Applications	193
	8.1.1	Relative Importance in Terms of Market Value	193
	8.1.2	Mass of Composites Implemented According to the Geographical Area	193
8.2		Composite Materials and Automotive Industry	194
	8.2.1	Introduction	194
	8.2.1.1	Examples.....	194
	8.2.1.2	Relative Weight Importance of Materials.....	194
	8.2.1.3	Need for Making Cars Lighters.....	195
	8.2.2	Composite Parts	196
	8.2.2.1	Brief Reminder	196
	8.2.2.2	Current Functional Design	196
	8.2.2.3	Notable Composite Components	199
	8.2.2.4	Notes	199
	8.2.2.5	Use of Natural Fibers.....	200
	8.2.3	Research and Development	201

	8.2.3.1	Structure	202
	8.2.3.2	Mechanical Parts	202
	8.2.4	Motor Racing.....	202
8.3		Wind Turbines	203
	8.3.1	Components.....	203
	8.3.2	Manufacturing Processes	205
8.4		Composites and Shipbuilding.....	206
	8.4.1	Competition	206
	8.4.1.1	Example: Ocean-Going Maxi-Trimaran.....	206
	8.4.1.2	Example: Monohull IMOCA 60	207
	8.4.1.3	Example: Single Scull.....	209
	8.4.1.4	Example: Surfboard.....	209
	8.4.2	Vessels	210
8.5		Sports and Leisure	210
	8.5.1	Skis	210
	8.5.1.1	Equipment of a Skier	210
	8.5.1.2	Main Components of a Ski	211
	8.5.2	Bicycles.....	212
	8.5.2.1	Machine	212
	8.5.2.2	Other Specific Equipment.....	212
	8.5.3	Tennis Rackets.....	213
8.6		Diverse Applications	213
	8.6.1	Pressure Gas Bottle	213
	8.6.2	Bogie Frame	213
	8.6.3	Tubes for Offshore Installations	214
	8.6.4	Biomechanical Applications.....	214
	8.6.5	Cable Car	215
		Notes.....	216

PART II Mechanical Behavior of Laminated Materials

Chapter 9	Anisotropic Elastic Medium	219
9.1	Some Reminders.....	219
	9.1.1 Continuum Mechanics	219
	9.1.2 Number of Distinct ϕ_{ijkl} Terms.....	219
9.2	Orthotropic Material	221
9.3	Transversely Isotropic Material.....	221
	Notes.....	223
Chapter 10	Elastic Constants of Unidirectional Composites.....	225
10.1	Longitudinal Modulus E_ℓ	225
10.2	Poisson Coefficient	227
10.3	Transverse Modulus E_t	227
10.4	Shear Modulus $G_{\ell t}$	229
10.5	Thermoelastic Properties.....	230
	10.5.1 Isotropic Material: Recall.....	230
	10.5.2 Case of Unidirectional Composite	230
	10.5.2.1 Coefficient of Thermal Expansion along the Direction ℓ	

10.5.2.2	Coefficient of Thermal Expansion along the Transverse Direction t	232
10.5.3	Thermomechanical Behavior of a Unidirectional Layer.....	232
10.6	Hygroscopic Effects.....	233
10.6.1	Moisture Influence	233
10.6.1.1	Relative Humidity	233
10.6.1.2	Moisture Concentration	233
10.6.2	Coefficient of Moisture Expansion.....	234
10.6.3	Hygrothermal Behavior of a Unidirectional Layer	234
10.6.3.1	Coefficients of Moisture Expansion along ℓ and t Directions.....	234
10.6.3.2	Constitutive Equation	235
	Notes.....	235
Chapter 11	Elastic Constants of a Ply in Any Direction.....	237
11.1	Flexibility Coefficients	237
11.2	Stiffness Coefficients.....	241
11.3	Case of Thermomechanical Loading	243
11.3.1	Compliance Coefficients	243
11.3.2	Stiffness Coefficients.....	244
11.4	Case of Hygrothermal Loading.....	245
11.4.1	Preliminary Remark.....	245
11.4.2	Compliance Coefficients	245
11.4.3	Stiffness Coefficients.....	246
	Notes.....	246
Chapter 12	Mechanical Behavior of Thin Laminated Plates	247
12.1	Laminate with Mid-plane Symmetry	247
12.1.1	In-plane Behavior	247
12.1.1.1	Loadings	247
12.1.1.2	Displacement Field	248
12.1.2	Apparent Elastic Moduli of the Laminate.....	250
12.1.3	Consequence: Practical Determination of a Laminate Subject to In-plane Loading.....	250
12.1.3.1	Givens of the Problem	250
12.1.3.2	Principle of Calculation	251
12.1.3.3	Calculation Procedure	252
12.1.4	Flexure Behavior	254
12.1.4.1	Displacement Field	254
12.1.4.2	Loadings	255
12.1.4.3	Notes	257
12.1.5	Consequence: Practical Determination of a Quad-Laminate Subject to Flexure.....	259
12.1.6	Simplified Calculation for Bending.....	259
12.1.6.1	Apparent Failure Strength in Bending.....	259
12.1.6.2	Apparent Flexure Modulus	260
12.1.7	Thermomechanical Loading Case	261
12.1.7.1	In-plane Behavior	261
12.1.7.2	Behavior under Bending	263
12.1.8	Hygrothermal Loading Case	264

12.2	Laminate without Mid-plane Symmetry	265
12.2.1	Coupled In-plane–Flexure Behavior	265
12.2.2	Case of Thermomechanical Loading	266
12.2.3	Hygrothermal Loading Case	267
Notes	268

PART III Justifications, D-D Laminates, Composite beams, and Transverse Shear Behavior of Multilayered Plates

Chapter 13	Elastic Coefficients	273
13.1	Elastic Coefficients for an Orthotropic Material	273
13.1.1	Reminders	273
13.1.2	Elastic Behavior Equation in Orthotropic Axes	273
13.2	Elastic Coefficients for a Transverse Isotropic Material	275
13.2.1	Elastic Behavior Equation	275
13.2.2	Rotation about an Orthotropic Transverse Axis	278
13.2.2.1	Problem	278
13.2.2.2	Technical Form	282
13.3	Case of a Ply	283
Notes	284
Chapter 14	Damage in Composite Parts; Failure Criteria	285
14.1	Damage in Composite Parts	285
14.1.1	Industrial Emphasis of the Problem	285
14.1.1.1	Causes of Damage	285
14.1.1.2	Diversity of Composite Parts	285
14.1.2	Influence of Manufacturing Process	286
14.1.2.1	Example: Injected Part with Short Fibers	286
14.1.2.2	Example: Parts with Pronounced Curvatures	287
14.1.3	Smooth Area and Singularities in a Same Part	287
14.1.4	Degradation Process within the Smooth Area	287
14.1.4.1	Example: Composite Short Fiber Plate	288
14.1.4.2	Example: Laminate Consisting of Unidirectional Plies ...	288
14.2	Form of a Failure Criterion	291
14.2.1	Features of a Failure Criterion	291
14.2.1.1	Failure Criterion Is a Design Tool	291
14.2.1.2	Many Criteria	291
14.2.2	General Form of a Failure Criterion	291
14.2.2.1	Development of a Criterion	291
14.2.2.2	Case of an Orthotropic Material	292
14.2.3	Linear Failure Criterion	292
14.2.3.1	Example: Plane State of Stress in an Orthotropic Material	292
14.2.3.2	Example: Maximum Stress Failure Criterion	293
14.2.3.3	Note: Maximum Eligible Strain Criterion	294
14.2.4	Quadratic Failure Criterion	294

14.2.4.1	General Form.....	294
14.2.4.2	Orthotropic Material.....	294
14.2.4.3	Specific Case of Plane Stress: the Tsai-Wu Criterion.....	294
14.2.4.4	Note: Simplified Form for the Quadratic Criterion.....	296
14.3	Tsai–Hill Failure Criterion.....	297
14.3.1	Isotropic Material: The von Mises Criterion.....	297
14.3.1.1	Distortion Strain Energy	297
14.3.1.2	Notes	299
14.3.2	Orthotropic Material: the Tsai–Hill Criterion.....	300
14.3.2.1	Notes	300
14.3.2.2	Case of a Transversely Isotropic Material	301
14.3.2.3	Case of Unidirectional Ply under In-plane Loading.....	302
14.3.3	Evolution of Strength Properties of a Unidirectional Ply Depending on the Direction of Solicitation	303
14.3.3.1	Tensile and Compressive Strength.....	303
14.3.3.2	Shear Strength	304
14.4	Stress Criterion Translated into Strain Space.....	305
14.4.1	Advantage of the Approach.....	305
14.4.2	Form of the Criterion in the Ply Axes (ℓ, t).....	305
14.4.3	Example: Unidirectional Carbon/Epoxy.....	306
14.5	Taking into Account the Ply Failure	306
14.5.1	Mechanical Properties of Damaged Ply.....	306
14.5.2	Example.....	307
14.5.3	Consequences for Strength-Laminate Analysis	307
	Notes.....	308

Chapter 15 Quasi-Orthotropic Homogenized Laminates or D-D Laminates 309

15.1	Tsai Modulus and Stiffness Characterization of a Laminate.....	309
15.1.1	Tsai Modulus	309
15.1.1.1	Constitutive Equation of a Ply	309
15.1.1.2	Unidirectional Ply in a Plane Laminate	310
15.1.1.3	Trace-Normalized Moduli.....	310
15.1.2	Master Ply.....	311
15.1.3	Tsai Modulus of a Laminate.....	312
15.1.3.1	Reminder: Behavior Relationship.....	312
15.1.3.2	In-plane Stiffness Matrix $[A]$	313
15.1.3.3	Flexural Stiffness Matrix $[C]$	314
15.1.3.4	Coupling Stiffness Matrix $[B]$	315
15.1.3.5	Guide Values for the Stiffness of a Carbon/Resin Laminate.....	315
15.2	The Double-Double Sub-Laminated Set.....	316
15.2.1	Notes on Classical Quadrangle Symmetric Laminates or “Quad Laminates”.....	316
15.2.2	Definition of the “Double-Double” Sub-Laminated Set	316
15.2.3	Properties of the “Double-Double” Set.....	317
15.2.4	Arrangement of Plies.....	318
15.3	Contributions from a D-D Sub-Laminated Set	319
15.3.1	Arrangement \mathcal{A}	319
15.3.1.1	Notations.....	319
15.3.1.2	In-plane Stiffness Matrix $[A]$	319

15.3.1.3	Flexural Stiffness Matrix $[C]$	320
15.3.1.4	Coupling Stiffness Matrix $[B]$	322
15.3.1.5	Thermomechanical Loading.....	323
15.3.1.6	Hygromechanical Loading	325
15.3.1.7	Resulting Constitutive Relationship.....	325
15.3.2	Arrangement \mathcal{B}	326
15.4	Homogenization of a Double-Double Laminate	326
15.4.1	Behavior of a Homogeneous Orthotropic Plate.....	326
15.4.1.1	Recall	326
15.4.1.2	Constitutive Relationship with In-plane Forces and Flexure Moments	327
15.4.1.3	Stress-Strain Constitutive Relationship	328
15.4.1.4	Comparison with D-D Laminate.....	331
15.4.2	Evolution of the Laminate Behavior with the Number of Repeats r	332
15.4.2.1	Evolution of the Constitutive Equation.....	332
15.4.2.2	Consequence: Homogenized Laminate	333
15.4.3	Particular Case of Very Thin Laminates	336
15.4.4	Transverse Shear Behavior.....	337
15.4.5	Tape Laying of D-D Laminates	337
15.4.5.1	A Look Back on Sub-Laminate D-D Sets Arrangements	337
15.4.5.2	Classical Tape Laying.....	338
15.4.5.3	Bidirectional Tape Laying	338
15.5	Strength of Homogenized D-D Laminates.....	338
15.5.1	Ply Failure Criterion in Any Orientation	338
15.5.1.1	Criterion Expressed in Laminate Axes	338
15.5.1.2	Notes	339
15.5.2	Extension to Laminate Level.....	339
15.5.2.1	Variation with Angle θ	339
15.5.2.2	Example	340
15.5.3	Practical Form of the Failure Criterion	341
15.5.3.1	Preliminary Remarks.....	341
15.5.3.2	Principal Strain Components ϵ_I , ϵ_{II}	342
15.5.3.3	Unit Circle.....	343
15.5.3.4	The Nettles Circle	344
15.6	Incidence for the Design.....	344
15.6.1	Preliminary Remarks	344
15.6.2	Defining the Laminate Anisotropy	345
15.6.3	Strength of the Laminate.....	346
15.6.3.1	Preliminary Remark	346
15.6.3.2	Load Factor.....	346
15.6.3.3	In-plane Loading	347
15.6.3.4	Flexure Loading.....	348
15.7	Practical Benefits of Homogenized D-D Laminates	350
15.7.1	Impact on Design	350
15.8	Calculation Tool	352
15.8.1	Presentation	352
15.8.2	Characteristics	352
15.8.3	Computerized Integration	352
15.8.4	References	352
	Notes.....	353

Chapter 16	Bending of Composite Beams of Any Section Shape	355
16.1	Bending of Beams with Isotropic Phases and Plane of Symmetry	355
16.1.1	Degrees of Freedom	356
16.1.1.1	Equivalent Stiffnesses	356
16.1.1.2	Longitudinal Displacement	356
16.1.1.3	Rotation of the Section	357
16.1.1.4	Elastic Center	357
16.1.1.5	Transverse Displacement along y-Direction	357
16.1.1.6	Transverse Displacement along z-Direction	357
16.1.2	Perfect Bonding between the Phases	358
16.1.2.1	Displacements	358
16.1.2.2	Strains	359
16.1.2.3	Stresses	359
16.1.3	Equilibrium Relationships	359
16.1.3.1	Longitudinal Equilibrium	360
16.1.3.2	Transverse Equilibrium	360
16.1.3.3	Moment Equilibrium	361
16.1.4	Constitutive Equations	361
16.1.5	Technical Formulation	362
16.1.5.1	Assumptions	362
16.1.5.2	Expression of Normal Stress	363
16.1.5.3	Expression of Shear Stress	363
16.1.5.4	Shear Coefficient for the Section	366
16.1.5.5	Summary	366
16.1.6	Energy Interpretation	367
16.1.6.1	Energy Due to Normal Stress σ_{xx}	367
16.1.6.2	Energy Due to Shear Stress $\bar{\tau}$	368
16.1.7	Extension to the Dynamic Case	369
16.1.7.1	Inertia Forces	369
16.1.7.2	Summary	370
16.2	Case of Beams of Any Cross Section (Asymmetric)	370
16.2.1	Technical Formulation	370
16.2.2	Summary	372
16.2.2	Notes	374
16.2.3	Examples	375
	Notes	375
Chapter 17	Torsion of Composite Beams of Any Section Shape	377
17.1	Uniform Torsion	377
17.1.1	Torsional Degree of Freedom	377
17.1.2	Constitutive Equation	378
17.1.3	Determination of $\Phi(y, z)$	379
17.1.3.1	Local Equilibrium	379
17.1.3.2	External Boundary Condition	379
17.1.3.3	Internal Boundary Conditions	379
17.1.3.4	Uniqueness of Function Φ	380
17.1.4	Energy Interpretation	381
17.2	Location of the Torsion Center	381
17.2.1	Coordinates in Principal Axes	381

17.2.2	Summary of Results	383
17.2.3	Flexion–Torsion Coupling	384
Notes	385

Chapter 18 Transverse Shear Behavior of Multilayered Plates 387

18.1	Preliminary Remarks	387
18.1.1	Transverse Normal Stress σ_z	387
18.1.2	Transverse Shear Stress τ_{xz} and τ_{yz}	387
18.1.3	Assumptions	388
18.2	Displacement Field	390
18.3	Strains	392
18.4	Constitutive Equations	393
18.4.1	In-plane Behavior	393
18.4.2	Bending Behavior	394
18.4.3	Transverse Shear Behavior	395
18.4.3.1	Transverse Shear Resultant $Q_x = \int_{-h/2}^{h/2} \tau_{xz} dz$	395
18.4.3.2	Transverse Shear Resultant $Q_y = \int_{-h/2}^{h/2} \tau_{yz} dz$	396
18.5	Equilibrium Relationships	396
18.5.1	Transverse Equilibrium	396
18.5.2	Equilibrium in Bending	397
18.6	Technical Formulation for Bending	397
18.6.1	Stress Due to Bending	397
18.6.1.1	Plane Stress Values	397
18.6.1.2	Transverse Shear Stress Values	398
18.6.2	Characterization of Warping Increments in Bending η_x and η_y	399
18.6.3	Particular Cases	400
18.6.3.1	Orthotropic Homogeneous Plate	400
18.6.3.2	Cylindrical Bending of a Multilayered Plate with Proportionality Properties	400
18.6.3.3	Bending of a Multilayered Plate with Proportionality Properties	402
18.6.3.4	Consequences	402
18.6.4	Warping Functions	403
18.6.4.1	Boundary Conditions	403
18.6.4.2	Interfacial Continuity	404
18.6.4.3	Formulation of Warping Functions	404
18.6.5	Consequences	404
18.6.5.1	Expression of Transverse Shear Stress	404
18.6.5.2	Transverse Shear Coefficients	405
18.6.6	Energy Interpretation	407
18.7	Examples	408
18.7.1	Orthotropic Homogeneous Plate	408
18.7.2	Sandwich Plate	409
18.7.2.1	Case of Two Orthotropic Materials	409
18.7.2.2	Warping Functions	410
18.7.2.3	Transverse Shear Stress	411

18.7.2.4	Transverse Shear Coefficients	412
18.8	Quasi-orthotropic Homogenized Laminates (D-D Laminates)	412
18.8.1	Extension to Transverse Shear	412
18.8.1.1	Reminder	412
18.8.1.2	Equivalent Orthotropic Homogeneous Plate	413
18.8.1.3	Transverse Shear Stiffness.....	413
18.8.1.4	Transverse Shear Stresses.....	414
18.8.2	Example of D-D Laminate.....	415
18.8.2.1	Definition	415
18.8.2.2	Mechanical Characteristics	416
18.8.2.3	Bending in (x,z) Plane.....	416
18.8.2.4	Transverse Shear Stresses.....	417
18.8.2.5	Transverse Shear Coefficient	419
18.8.2.6	Warping of the Cross Section	419
18.8.2.7	Bending in (y,z) Plane	420
18.8.2.8	Increase in the Repetitions Number “ r ”	420
18.8.2.9	Conclusion	421
Notes.....		422

PART IV Applications

Chapter 19	Applications Level 1.....	425
19.1	Simply Supported Sandwich Beam	425
19.2	Poisson Coefficient of a Unidirectional Layer.....	427
19.3	Helicopter Blade	429
19.4	Drive Shaft for Trucks.....	434
19.5	Flywheel in Carbon/Epoxy	439
19.6	Wing Tip Made of Carbon/Epoxy.....	441
19.7	Carbon Fiber Coated with Nickel.....	451
19.8	Tube Made of Glass/Epoxy under Pressure	453
19.9	Filament-Wound Pressure Vessel: Winding Angle	456
19.10	Filament-Wound Pressure Vessel: Consideration of Openings in the Bottom Heads	458
19.11	Determination of Fiber Volume Fraction by Pyrolysis	461
19.12	Reversing Lever Made of Carbon/PEEK (Unidirectional and Short Fibers)	462
19.13	Glass/Resin Telegraph Pole	466
19.14	Unidirectional Layer of HR Carbon.....	469
19.15	Manipulator Arm for Space Shuttle	469
Notes.....		473
Chapter 20	Applications Level 2.....	475
20.1	Sandwich Beam: Simplified Calculation of the Shear Coefficient.....	475
20.2	Procedure for a Quad-Laminate Calculation Program	477
20.3	Kevlar/Epoxy Laminates: Stiffness in Terms of the Direction of Load	480
20.4	Residual Thermal Stress Due to the Laminate Curing Process.....	483
20.5	Thermoelastic Behavior of a Glass/Polyester Tube	485
20.6	Creep of a Polymeric Tube Reinforced by Filament Wound under Thermal Stress.....	488

20.7	First-Ply Failure of a Laminate; Ultimate Strength.....	493
20.8	Optimum Laminate for Isotropic Plane Stress.....	496
20.9	Laminate Made of Identical Layers of Balanced Fabric.....	500
20.10	Carbon/Epoxy Wing Spar.....	503
20.11	Elastic Constants of a Carbon/Epoxy Unidirectional Layer, Based on Tensile Test.....	509
20.12	Sailboat Hull in Glass/Polyester.....	510
20.13	Balanced Fabric Ply: Determination of the In-plane Shear Modulus.....	514
20.14	Quasi-Isotropic Laminate.....	516
20.15	Pure Torsion of Orthotropic Plate.....	518
20.16	Plate Made by Resin Transfer Molding.....	521
20.17	Thermoelastic Behavior of a Balanced Fabric Ply.....	527
	Notes.....	534
Chapter 21	Applications Level 3.....	537
21.1	Cylindrical Bonding.....	537
21.2	Double-Lap Bonded Joint.....	541
21.3	Composite Beam with Two Layers.....	545
21.4	Buckling of a Sandwich Beam.....	549
21.5	Shear Due to Bending in a Sandwich Beam.....	551
21.6	Shear Due to Bending in a Composite Box Beam.....	555
21.7	Torsion Center of a Composite U-Beam.....	558
21.8	Shear Due to Bending in a Composite I-Beam.....	559
21.9	Polymeric Column Reinforced by Filament-Wound Fiberglass.....	563
21.10	Cylindrical Bending of a Thick Orthotropic Plate under Uniform Loading.....	570
21.11	Bending of a Sandwich Plate.....	572
21.12	Bending Vibration of a Sandwich Beam.....	574
21.13	Transverse Shear in a Two Phases Circular Section Beam.....	576
	Notes.....	579
Appendix A:	Stresses in the Plies of a Carbon/Epoxy Quadrangle Symmetric Laminate Loaded in Its Plane.....	581
Appendix B:	Buckling of Orthotropic Structures.....	595
Bibliography	603
Index	607

Foreword

Textbooks are the most basic learning tools for everyone. They give comprehensive coverage on given topics from the first principles to steps for the subsequent levels of applications.

In the case of composite materials that suddenly burst into prominence for aeronautics in the 1960s, there were no textbooks to guide the engineers. New approaches and rules governing their operations had to be established. Among them were netting analysis, quadrangle symmetric laminates of 0° , $\pm 45^\circ$, and 90° plies, and carpet plots. Surprisingly they are still in use. Netting analysis is used to correlate burst pressure of pressure vessels to fiber strength; Quad laminates remain the current standard and subjected to a set of rules on symmetry, balanced, 10% rule, ply contiguity of no more than four plies, and limit on inter-ply difference no more than 45° ; and carpet plots can still be seen. These restrictions were more philosophical than science-based and have made composite laminates unnecessarily complex and not possible to be optimized. Carpet plots are deceptive because Quad laminates are discrete and cannot interpolate along continuous lines. Percent of $[\pm 45^\circ]$ plies can only be 20%, 40%, 60%, and 80% among 10% laminate increments. Other self-inflicted complexities by the Quad laminates include stacking sequence, symmetric ply drops, and blending.

In the past few years, we have taken an approach different from the traditional. New concepts include the recognition of tensor invariants of stiffness matrices that led to a highly accurate master ply for carbon/epoxy composites. One elastic invariant is there to distinguish one material from another. Laminate stiffness components are merely geometric factors from ply stacking multiplied by this stiffness invariant. Failure criterion can be similarly simplified with use of Omni envelope, which has the overlapping core of all ply orientations. This envelope is isotropic because it is ply orientation independent. Only laminate failure is needed, no need for ply-by-ply analysis.

Instead of the traditional Quad one, a new family of laminates based on Double-Double (DD) in $[\pm\Phi / \pm\Psi]$ will be so much simpler to work with. It is a field-based family replacing a collection of discrete Quad laminates. A DD laminate is stacked with repeated four-ply Sub-Laminates. It can be homogenized in its thickness as few as four repeats. It will be naturally symmetric, orthotropic, and need no rules on 10%, ply contiguity, and inter-ply angle difference. Being homogenized with repeated Sub-Laminates, DD laminate can be with fewer repeats for lightly loaded zones. Substantial weight savings would be possible. Ply drops can be in singles rather than in pairs when in Mid-plane symmetry. Such ply drops can be located on the exterior surfaces of laminate, thus clearing discontinuities and wrinkles from laminate interior. Such laminates will be stronger and not likely to trigger out-of-plane failures. Being homogenized across the thickness and across the entire component, there will be no thermal warpage. High-quality laminates can be expected in every design and actual production.

As we embark on a new approach to lamination, we expect more acceptance and greater confidence in these composite structures in the years to come.

In this new edition of a truly innovative textbook, the basic concepts of our new horizon for composite materials have been covered. They are done from the first principle onward and should be learned and practiced.

In a modest way, Double-Double is like the Maxwell's wave equations that can explain many electromagnetic phenomena not possible without them. Composite laminates can be simpler and more producible with DD principles, but not possible with the traditional Quad approach.

Students are urged to pay attention to the hard work by the author and gain confidence in composites to produce better airplanes and transportation systems.

Stephen W. Tsai

Professor Research Emeritus

Department of Aeronautics & Astronautics

Stanford University

January 2022

Preface

In a few decades, the field of composite materials has spread to all sectors of industry where new materials, processes, and applications are constantly being developed. Such development has made this field popular due to the breadth and universality of applications. The composite materials market is growing by around 5% per year, with more than 10% for the carbon fiber, a growth due notably to the transportation and wind power. The cost of composites is increasingly competitive compared to sophisticated metal alloys. The quality and variety of semi-finished products are remarkable and the manufacturing processes increasingly industrialized, with obvious consequences for the evolution of the quality of parts. In a market dominated by thermosetting matrices, composites with a thermoplastic matrix are gradually finding their place. Recycling issues are expected to further promote this development. Legislation on the recyclability obligation now has a significant influence on composite activities. It leads to research and development activities on subjects relating to the recovery of carbon fibers, use of natural fibers, biodegradable polymers....

The growth in the use of composites has been aided by the development of modern design and manufacturing methods for industrial components, which allow functional optimization based on multiple technical and economic criteria. A good knowledge of what already exists helps develop and use reliable numerical simulations for in-service behavior as well as for implementation during the manufacturing.

The development of simulation tools is an important component of industrial development in general and in composite domains in particular. Without trying to replace testing, these tools allow full exploitation of the experimental results in a much more complete manner, creating a powerful synergy that saves time and cost.

This updated volume has been amended and enlarged to take into account this rapid evolution as well as the emergence and development of additional areas such as recycling, ceramic-matrix composites, and advances in manufacturing processes.

However, more fundamental aspects are currently emerging for the design of laminates. The challenge is in particular to define laminates that are even more competitive both in terms of the optimized design of parts with variable thicknesses and their automated manufacture.

Accordingly, this fourth edition reports a break characterized by new concepts that go in the direction of history. We have to remember that when carbon laminates first appeared, slide rules and charts were still in use. Later, in the early 1980s, computer utilities arrived. We know what it is today where current resources allow the digital implementation of the laminate optimization process by means of powerful calculation tools. This is how a new chapter devoted to quasi-orthotropic laminates also called “Double-Double” here completes the heart of the work devoted to the methodical design of structural parts. It presents the work initiated by Pr. S.W. Tsai assisted by an international team of scientists to define and calculate more efficient and lighter laminates, much better suited to current and future resources, both in terms of calculation and manufacturing with automated tape laying. In addition, the notion of Tsai modulus introduced saves a large part of the experimental characterization.

Useful information is given on the corresponding free utility. The reader will be able to download this tool in open access as indicated in the book.

The chapters on composite beams of any cross-sectional shape and the chapter on transverse shear behavior of multilayered plates still retain their original character, both with regard to the proposed method and to the results. In particular, one will note a complementary study of transverse shear in quasi-orthotropic laminated plates in connection with the new theory of Double-Double laminates.

Also remember that the book is structured according to three levels of difficulty (even for the applications). The technical level becomes more and more complicated from one section to another.

The first section corresponds to the undergraduate level, while the second and third sections correspond to the graduate and postgraduate levels. One can, however, work on each part independently.

Section IV, “Applications”, consists of 45 examples, including numerous cases of pre-sizing of composite parts, processed from industrial cases reworked, so that the user can go directly to the essentials. As Pr. S.W. Tsai underlines, these practical problems “are treated in a closed form. Thus these solutions are useful for studying the parameters which may constitute the basis of optimization. Such observations are not always easy to do with numerical solutions like those resulting from finite element analysis. Another advantage of the closed solution is its speed in obtaining the answers, and it has no problem of numerical convergence”. In any case, it is useful to note that most of these applications provide usable results for numerical modeling, including tests for the validation of finite element computer software.

This book has had a run of three recent editions in English (since 2002) and six successive editions in French (since 1987), all of which out of print. It is addressed to engineers and technicians in the field who deal with problems of mechanical behavior that require designs, compositions, thicknesses, and fasteners to be defined. It is addressed to teachers who want to structure a course on the subject, or even simply talk about composites. It is also addressed to students pursuing undergraduate and postgraduate degrees and can help PhD students do an apprenticeship before moving on to specialized research.

This book does not focus on too detailed theoretical developments, which would not meet the requirements of the targeted audience. In industry, there is little time for the consultation of books, and the academic nature of initial training is often far from the daily concerns of the design office. I have therefore adapted this presentation by taking into account readers who are always in a hurry and who use the tools available to them or ones that they remember. The content of this book is nevertheless anchored on solid scientific basis and will allow potential users to derive maximum benefit from it.

Daniel Gay

May 2022

Acknowledgments

I would like to thank Prof. Stephen W. Tsai here for his foreword and for his encouragement and advice in writing this fourth edition. But above all, I would like to respectfully pay him tribute for his fundamental contributions to the knowledge of the field of high-performance composite structures, for his important contributions always renewed since the beginnings of the modern era of composites, and for his intensive activity highly unifying.

I warmly thank Dr. Thierry Massard for his comments and wise advice concerning quasi-orthotropic laminates as well as for his remarkable and sustained contribution for so many years to the development and dissemination of the optimized calculation of laminates and associated calculation tools.

I express my sincere thanks and gratitude to Dr. Stephane Gay, who reviewed and verified the appropriate use of technical terminology contained in this fourth edition, especially in the field of aeronautics.



Taylor & Francis

Taylor & Francis Group

<http://taylorandfrancis.com>

Author

Daniel Gay is a former student of the Ecole Normale Supérieure of Cachan-Paris-Saclay and served as a professor at the University Paul Sabatier Toulouse III. He led the Laboratory of Mechanical Engineering of Toulouse, now the Clément Ader Institute, from its inception for over 15 years.

Pr. Gay has taught composite materials and structures at the undergraduate, graduate, and post-graduate levels in many French schools and institutions (ENSAM, University of Toulouse III, IUT, INSA, ENSICA, Supaero (ISAE), ENSTA, etc.). He is the author of numerous books, articles, scientific publications, and industrial reports on the subject.



Taylor & Francis

Taylor & Francis Group

<http://taylorandfrancis.com>

Part I

Principles of Construction

This part of the book is important in terms of volume and content. First, it aims to succinctly present the following points, while remaining as clear as possible:

- Interest in the use of composite elements
- Products currently manufactured
- Manufacturing methods
- Presentation and definition of semi-finished products (fibers and reinforcements) with their characteristic properties

Second, it extends to the problems and solutions brought on when designing a composite component, and particularly the concerns related to the resistance and deformation under loading, as well as the connections of the part with its surrounding.



Taylor & Francis

Taylor & Francis Group

<http://taylorandfrancis.com>

1 Composite Materials

Interest and Physical Properties

1.1 WHAT IS A COMPOSITE MATERIAL?

1.1.1 BROAD DEFINITION

As the term indicates, a **composite material** is different from the conventional macroscopically homogeneous material.

Currently, composite materials refer to materials containing strong **fibers** — continuous or noncontinuous — embedded in a weaker material or **matrix**. The matrix keeps the geometric arrangement of fibers and transmits to these fibers the load acting on the composite component.

The resulting composite material is capable of **intermediate** mechanical performance, that is, superior to those of the matrix, but different and often lower than those of the fibrous reinforcement. Generally, this material also presents some other properties that are specific.

Notes: Composite materials are not new. They have been used since antiquity. Wood, clay, and mud reinforced with straw have been everyday composites. Composites have also been used to optimize the performance of some conventional weapons. For example,

- In the Mongolian bows, the compressed parts are made of horn, and the stretched parts are made of wood and cow tendons glued together.
- Damask sword or Japanese sabers have their blades made of steel and soft iron: the steel part is stratified like a flaky pastry, with orientation of defects and impurities in the long direction¹ (see Figure 1.1), and then formed into a U shape into which the soft iron is placed. The sword then has good resistance for flexure and impact.

This period marks the beginning of the distinction between the common composites used universally and the high-performance composites.

1.1.2 MAIN FEATURES

Composite material, as defined, has the following features:

- Very **heterogeneous**.
- Very **anisotropic**. This notion of **anisotropy** will be illustrated in Section 3.1 and also in Chapter 9. Simply put, this means that the mechanical properties of the material depend on the direction of the loading.

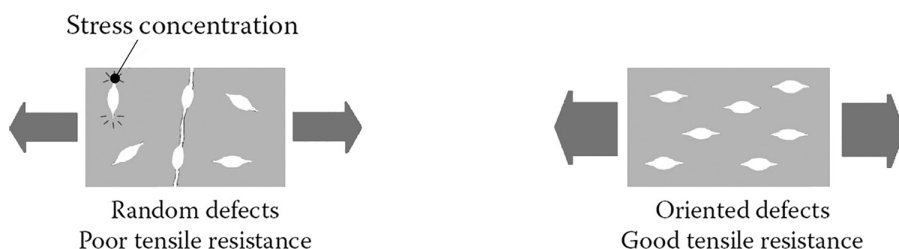


FIGURE 1.1 Effect of orientation of impurities.

1.2 FIBERS AND MATRICES

The bonding between fibers and matrices is created during the manufacturing phase of the composite material. This has fundamental influence on the mechanical properties of the composite material.

1.2.1 FIBERS

1.2.1.1 Definition

Fibers consist of several hundreds or thousands of filaments, each of them having a diameter of 5–15 μm , allowing them to be processable on textile machines²; for example, in the case of glass fiber, two semi-finished fiber products are obtained as shown in Figure 1.2.

These fibers are marketed in the following forms:

- Short fibers, with lengths of the order of a fraction of a millimeter to a few centimeters. These are **felts**, **mats**, and short fibers used in injection molding.
- Long fibers, which are cut during the time of fabrication of the composite material, are used as is or woven.

1.2.1.2 Principal Fiber Materials

Principal fiber materials include

- Glass
- Aramid or **Kevlar**® (very light)
- Carbon (high modulus or high strength)
- Boron (high modulus or high strength)
- Silicon carbide (high temperature resistant)
- High-density polyethylene
- Natural fibers (flax, hemp, sisal, etc.), the use of which is increasing

In forming fiber reinforcement, the assembly of fibers to make fiber forms for the fabrication of composite material can take the following forms:

- **Unidimensional:** Unidirectional tows, yarns, or tapes
- **Bidimensional:** Woven or nonwoven fabrics (Non-crimp fabrics, felts, or mats)
- **Tridimensional:** Fabrics (sometimes called **multidimensional fabrics**) with fibers oriented along several directions (>2)

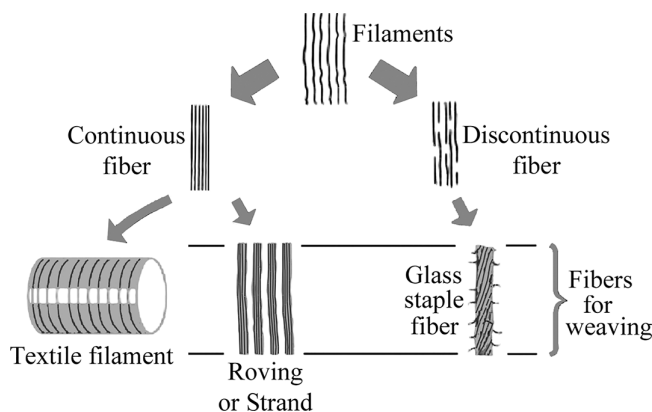


FIGURE 1.2 Different fiber forms.

Before the formation of the reinforcement, the fibers are subjected to a surface treatment or **sizing** to

- Decreasing the abrasion action of fibers when passing through the weaving machines
- Improving the fiber-matrix adhesion

Other types of reinforcements are also used as **fillers**: full or empty microspheres, powders³, and nanoreinforcements⁴.

1.2.1.3 Processes for Obtaining Fibers

A few notes about the fabrication of fibers are as follows:

- **Glass fiber**: Continuous glass filaments are drawn by pulling the glass (silicon+sodium carbonate and calcium carbonate; $T > 1,000^{\circ}\text{C}$) through the small orifices of a heated plate made of platinum alloy.
- **Kevlar fiber**: This is a **DuPont** trademark (US). Aramid fibers, which are yellowish in color, are made of aromatic polyamides (PAs) obtained by synthesis at -10°C . They are spun and stretched to obtain a high modulus of elasticity along the fiber direction.
- **Carbon fiber**: Filaments of polyacrylonitrile or pitch (obtained from residues of the petroleum products) are oxidized at high temperatures (300°C) and then heated further to $1,500^{\circ}\text{C}$ in a nitrogen atmosphere. Only the black and bright filaments of hexagonal carbon chains remain, as shown in Figure 1.3. The high modulus of elasticity is obtained by stretching at high temperature. Figure 1.4 helps to become aware of the rapid development of the carbon fiber industry⁵.
- **Boron fiber**: Tungsten filament (diameter $12\text{ }\mu\text{m}$) is used to catalyze the reaction between boron chloride and hydrogen at $1,200^{\circ}\text{C}$. The boron fibers obtained have a diameter of about $100\text{ }\mu\text{m}$ (the growth speed is about $1\text{ }\mu\text{m/s}$).
- **Silicon carbide**: The principle of fabrication is analogous to that of boron fiber: chemical vapor deposition ($1,200^{\circ}\text{C}$) of methyl trichlorosilane mixed with hydrogen.

The principal physical and mechanical properties of the fibers are indicated in Table 1.3 later in the chapter.

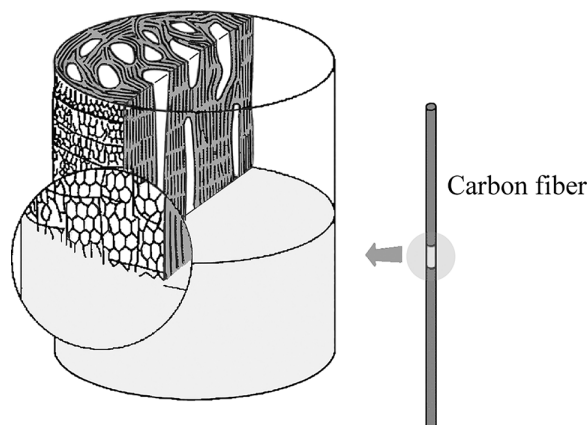


FIGURE 1.3 Structure of carbon fiber.

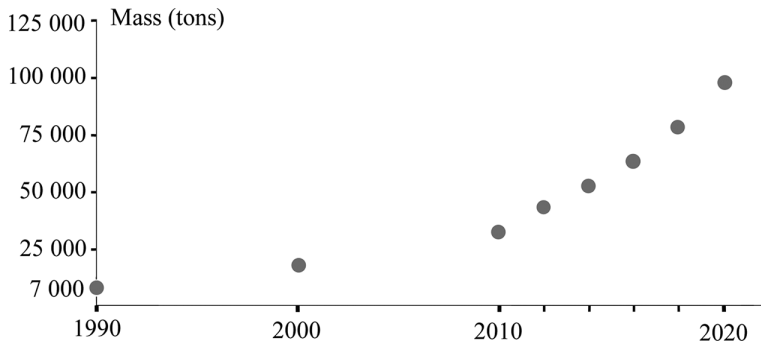


FIGURE 1.4 Annual demands for carbon fibers.

1.2.2 MATERIALS FOR MATRICES

Many materials are used as matrix materials:

1. Polymeric matrix:

- a. *Thermoplastic resins*: Polypropylene [PP], polyphenylene sulfone [PPS], polyamide [PA], polyether ether ketone [PEEK], polyether ketone ketone [PEKK], etc.
- b. *Thermoset resins*: Polyesters, phenolics, melamines, silicones, polyurethanes, and epoxies. Their principal physical properties are indicated in Table 1.4.

2. **Mineral matrix**: Silicon carbide and carbon. They can be used at high temperatures (see Sections 3.7, 7.1.10, 7.4, and 7.5).

3. **Metallic matrix**: Aluminum alloys and titanium alloys (see Sections 3.6 and 7.4).

1.3 WHAT CAN BE MADE USING COMPOSITE MATERIALS?

The range of applications is very large. A few examples are listed here:

1. Electrical, electronics:

- a. Insulation for electrical construction
- b. Supports for circuit breakers
- c. Supports for printed circuits
- d. Armors, boxes, and covers
- e. Antennas, radomes
- f. Tops of television towers
- g. Cable tracks
- h. Wind turbines

2. Buildings and public works:

- a. Housing cells
- b. Chimneys
- c. Concrete molds
- d. Various covers (domes, windows, etc.)
- e. Swimming pools
- f. Facade panels
- g. Profiles
- h. Partitions, doors, furniture, and bathrooms

3. Road transport:

- a. Body components
- b. Complete body
- c. Wheels, shields, and radiator grills
- d. Transmission shafts
- e. Suspension springs
- f. Bottles for compressed gas
- g. Chassis
- h. Suspension arms
- i. Casings
- j. Cabins and seats
- k. Highway tankers and isothermal trucks
- l. Trailers

4. Rail transport:

- a. Fronts of locomotives
- b. Wagons
- c. Doors, seats, and interior panels
- d. Ventilation housings
- e. Structural parts
- f. Bogies

5. Maritime transport:

- a. Hovercrafts
- b. Rescue crafts
- c. Patrol boats
- d. Trawlers
- e. Antimine ships
- f. Racing sailboats
- g. Pleasure boats
- h. Canoes

6. Cable transport:

- a. Cable cars
- b. Gondola lifts

7. Air transport:

- a. All-composite gliders
- b. All-composite light aircraft and drones
- c. Many aircraft components: vertical and horizontal tail plane, wing boxes, leading edges, winglets, flaps, center wing boxes, keel beams, fuselages, radomes, doors, aircraft brake disks, etc.
- d. Many helicopter components: blades, main rotors, tail rotors, transmission shafts, cabins, tails, etc.
- e. Aircraft engines: propellers, blades, fairings, fan housings, thrust reversers, etc.

8. Space transport:

- a. Bodies
- b. Tanks
- c. Nozzles
- d. Heat shields for atmospheric reentry

9. General engineering sector:

- a. Gears
- b. Bearings

- c. Housings and casings
 - d. Bodies of actuators
 - e. Robotic arms
 - f. Flywheels
 - g. Projectiles (shuttles) for looms
 - h. Pipes
 - i. Components of drawing tables
 - j. Compressed gas bottles
 - k. Tubes for offshore platforms
 - l. Radial-ply tires
10. **Sports and leisure:**
- a. Tennis and squash rackets
 - b. Fishing poles
 - c. Skis
 - d. Poles for pole vault
 - e. Windsurfing boards, sailboards, skateboards
 - f. Bows and arrows
 - g. Javelins
 - h. Protection helmets
 - i. Bicycles
 - j. Golf clubs
 - k. Oars and vessels for racing

1.4 A TYPICAL EXAMPLE OF INTEREST

In the field of commercial air transport industry, the following may be placed in parallel: the major concerns of manufacturers and the main characteristic properties of the composite material parts. The concerns of the manufacturers are performance and saving. The characteristics of composite components include the following:

- The subsequent weight reduction leads to fuel saving, increase in payload, or increase in range that improves performances.
- The good fatigue resistance leads to enhanced life, which involves saving in the long-term cost of the product.
- The good corrosion resistance means fewer requirements for inspection, which results in saving on maintenance cost.

Moreover, taking into account the cost of the composite solution as compared with the conventional solution, one can state that composites fit the demand of aircraft manufacturers.

1.5 SOME EXAMPLES OF CLASSICAL DESIGN REPLACED BY COMPOSITE SOLUTIONS

Table 1.1 shows a few significant cases illustrating the improvement on price and performance that can be obtained after the replacement of a conventional solution with a composite solution.

TABLE 1.1
Some Significant Cases

Application	Previous Construction	Composite Construction
65 m ³ reservoir for chemicals	Stainless steel+installation; Price=1	Price=0.53
Smoke stack for chemical plant	Steel; Price=1	Price=0.51
Nitric acid vapor washer	Stainless steel; Price=1	Price=0.33
Helicopter stabilizer	Light alloys+steel; Mass=16 kg; Price=1	Carbon/epoxy; Mass=9 kg; Price=0.45
Support for helicopter hoist	Welded steel; Mass=16 kg; Price=1	Carbon/epoxy; Mass=11 kg; Price=1.2
Helicopter motor hub	Mass=1; Price=1	Carbon/Kevlar/epoxy; Mass=0.8; Price=0.4
X-Y table for fabrication of integrated circuits	Cast aluminum; Rate of fabrication=30 plates/h	Carbon/epoxy honeycomb sandwich; Rate of fabrication=55 plates/h
Drum for drawing plotter	Drawing speed=15–30 cm/s	Kevlar/epoxy, 40–80 cm/s
Head of welding robot	Aluminum; Mass=6 kg	Carbon/epoxy; Mass=3 kg
Projectile for loom	Aluminum; Rate=250 shots/min	Carbon/epoxy; Rate=350 shots/min
Aircraft floor	Mass=1; Price=1	Carbon/Kevlar/epoxy; Mass=0.8; Price=1.7

1.6 MAIN PHYSICAL PROPERTIES

Tables 1.2–1.5 take into account the properties of only individual components, reinforcements, or matrices.

The characteristics of composite materials resulting from the combination of reinforcement and matrix depend on

- The proportions of reinforcements and matrix (see Section 3.2)
- The form of the reinforcement (see Section 3.2)
- The fabrication process

These characteristics can be observed in Figure 1.5, which shows the tensile strength for different fiber fractions and different forms of reinforcement for the case of glass/resin composite, and Figure 1.6, which gives an interesting view on the **specific resistance** of the major types of structural composites as a function of temperature. Here, the specific strength is defined as the tensile strength divided by the density: $(\sigma_{\text{rupture}}/\rho)$.

Other remarkable properties of these materials include the following:

- Composite materials **do not yield**: their elastic limits correspond to the rupture limit (see Section 5.4.5).
- Composite materials have high strength under **fatigue loads** (see Section 5.1).
- Composite materials **age** under the action of moisture⁶ and heat.
- Composite materials **do not corrode**, except in the case of contact **aluminum with carbon fibers** in which galvanic phenomenon creates rapid corrosion.
- Composite materials are not sensitive to the common chemicals used in engines: grease, oils, hydraulic liquids, paints and solvents, and petroleum. However, cleaners for paint attack the epoxy resins.
- Composite materials have medium- to low-level impact resistance (inferior to that of metallic materials).
- Composite materials have excellent fire resistance as compared with the light alloys with identical thicknesses. However, the smokes emitted from the combustion of certain matrices can be toxic.

TABLE 1.2
Properties of Commonly Used Metals and Alloys and Silicon

Metals and Alloys	Density, ρ (kg/m ³)	Elastic Modulus, E (MPa)	Shear Modulus, G (MPa)	Poisson Ratio, ν	Tensile Strength, σ_{rupture} (MPa)	Elongation, A (%)	Coefficient of Thermal Expansion at 20°C, α (°C ⁻¹)	Thermal Conductivity at 20°C, λ (W/m °C)	Heat Capacity, c (J/kg °C)	Temperature Limit for Use, T_{max} (°C)
Steels	7,800	205,000	79,000	0.3	400–1,600	1.8–10	1.3×10^{-5}	20–100	400–800	800
Aluminum alloy A92024 (2024)	2,800	75,000	29,000	0.3	450	10	2.2×10^{-5}	140	1,000	350
Titanium alloy R56400 (TA6V)	4,400	105,000	40,300	0.3	1,200	12	0.8×10^{-5}	17	540	700
Copper	8,800	125,000	48,000	0.3	200–500	4–45	1.7×10^{-5}	380	390	650
Nickel	8,900	210,000	80,000	0.3	300		1.3×10^{-5}	90	440	900
Beryllium	1,840	294,000	137,000	0.02	300		1.2×10^{-5}	200 (20°C); 90 (800°C)	1,750 (20°C); 3,000 (800°C)	900
Silicon	2,300	160,000	65,000	0.25		5	0.8×10^{-5}	1.4 (20°C); 3 (1,200°C)	750 (20°C); 1,200 (500°C)	1,300

TABLE 1.3
Properties of Commonly Used Reinforcements

Reinforcements (fibers)	Fiber Diameter, <i>d</i> (μm)	Density, ρ (kg/ m ³)	Modulus of Elasticity, <i>E</i> (MPa)	Shear Modulus, <i>G</i> (MPa)	Poisson Ratio, ν	Tensile Strength $\sigma_{rupture}$ (MPa)	Elongation, <i>A</i> (%)	Coefficient of Thermal Expansion, α (°C ⁻¹)	Coefficient of Thermal Conductivity, λ (W/m °C)	Heat Capacity, <i>c</i> (J/kg °C)	Temperature Limit for Use, <i>T</i> _{max} (°C)
“R” glass, high performance	10	2,500	86,000		0.2	3,200	4	0.3×10^{-5}	1	800	700
“E” glass, common applications	16	2,600	74,000	30,000	0.25	2,500	3.5	0.5×10^{-5}	1	800	700
Kevlar 49	12	1,450	130,000	12,000	0.4	2,900	2.3	-0.2×10^{-5}	0.03	1,400	
HR graphite, high strength	7	1,750	230,000	50,000	0.3	3,200	1.3	0.02×10^{-5}	200 (20°C); 60 (800°C)	800	>1,500
HM graphite, high modulus	6.5	1,800	390,000	20,000	0.35	2,500	0.6	0.08×10^{-5}	200 (20°C); 60 (800°C)	800	>1,500
Boron	100	2,600	400,000			3,400	0.8	0.4×10^{-5}			500
Alumina	20	3,700	380,000			1,400	0.4	0.8×10^{-5}	50 (20°C); 7 (800°C)	900	>1,000
Alumina silicate	10	2,600	200,000			3,000	1.5				
Silicon carbide	14	3,000	400,000		0.14	2,800	1.3	0.4×10^{-5}	120	750	1,300
Polyethylene	12	960	100,000			2,400	3.5	1.3×10^{-5}	20		70

TABLE 1.4
Properties of Commonly Used Resins

Resins	Density, ρ (kg/m ³)	Elastic Modulus, E (MPa)	Shear Modulus, G (MPa)	Poisson Ratio, ν	Tensile Strength, $\sigma_{rupture}$ (MPa)	Elongation, A (%)	Coefficient of Thermal Expansion, α (°C ⁻¹)	Coefficient of Thermal Conductivity, λ (W/m °C)	Heat Capacity, c (J/kg °C)	Temperature Limit for Use, T_{max} (°C)
Thermosets										
Epoxy	1,200	4,500	1,600	0.4	130	2 (100°C); 6 (200°C)	11×10^{-5}	0.2	1,000	90–200
Phenolic	1,300	3,000	1,100	0.4	70	2.5	1×10^{-5}	0.3	1,000	120–200
Polyester	1,200	4,000	1,400	0.4	80	2.5	8×10^{-5}	0.2	1,400	60–200
Polycarbonate	1,200	2,400		0.35	60		6×10^{-5}		1,200	120
Vinylester	1,150	3,300			75	5	5×10^{-5}			>100
Silicone	1,100	2,200		0.5	35					100–350
Urethane	1,100	700–7,000			30	100				100
Polyimide	1,400	4,000–19,000	1,100	0.35	70	1	8×10^{-5}	0.2	1,000	250–300
Thermoplastics										
PP	900	1,200		0.4	30	20–400	9×10^{-5}		330	70–140
PPS	1,300	4,000			65	100	5×10^{-5}			130–250
PA	1,100	2,000		0.35	70	200	8×10^{-5}		1,200	170
Polyether sulfone (PES)	1,350	3,000			85	60	6×10^{-5}			180
Polyetherimide (PEI)	1,250	3,500			105	60	6×10^{-5}	0.2		200
PEEK	1,300	4,000	1,450	0.38	90	50	5×10^{-5}	0.3	1,450	140–250

TABLE 1.5
Properties of Commonly Used Core Materials

Cores	Density, ρ (kg/m ³)	Modulus of Elasticity, E (MPa)	Shear Modulus, G (MPa)	Poisson Ratio, ν	Compressive Strength, $\sigma_{rupture}$ (MPa)	Elongation, A (%)	Coefficient of Thermal Expansion, α (°C ⁻¹)	Coefficient of Thermal Conductivity, λ (W/m °C)	Heat Capacity, c (J/kg °C)	Temperature Limit for Use, T_{max} (°C)
Balsa	100–190	2,000–6,000	100–250		8–18					
Polyurethane foam	30–70	25–60		0.4				0.05		75
Polystyrene foam	30–45	20–30		0.4	0.25–1.25					75
Impregnated carton			50–350							
Impregnated glass fabric			100–600							
Aluminum	15–130		130–910		0.2–8					
Steel			550–1250							
Nomex®	25–50		10–40		0.2–2.5					

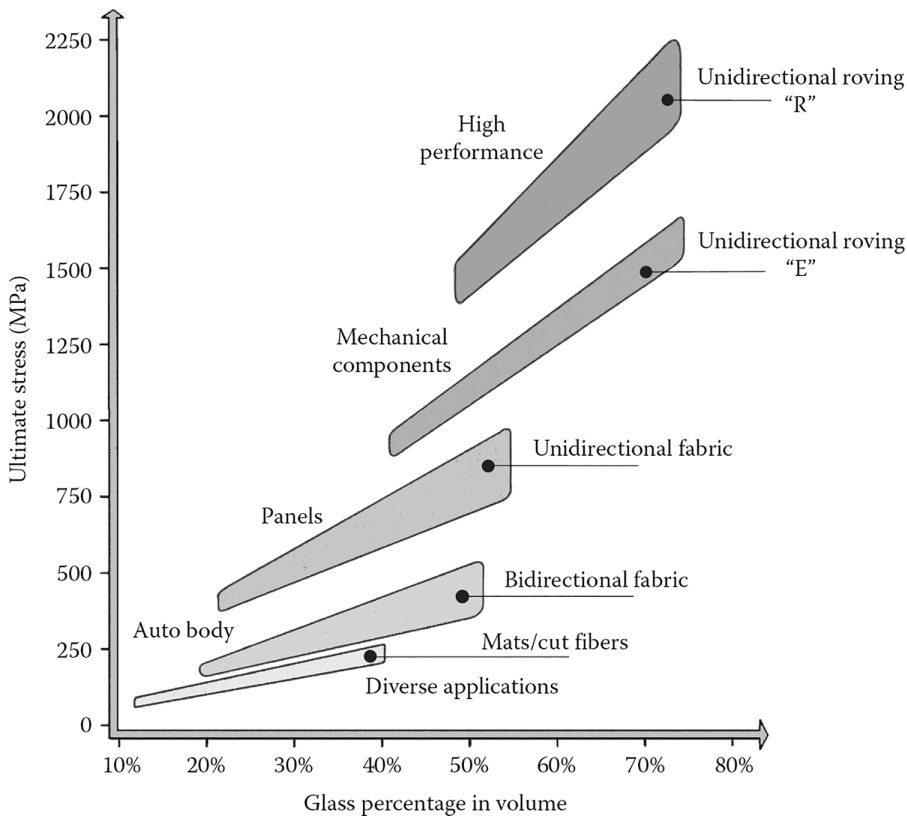


FIGURE 1.5 Tensile strength of glass/resin composites.

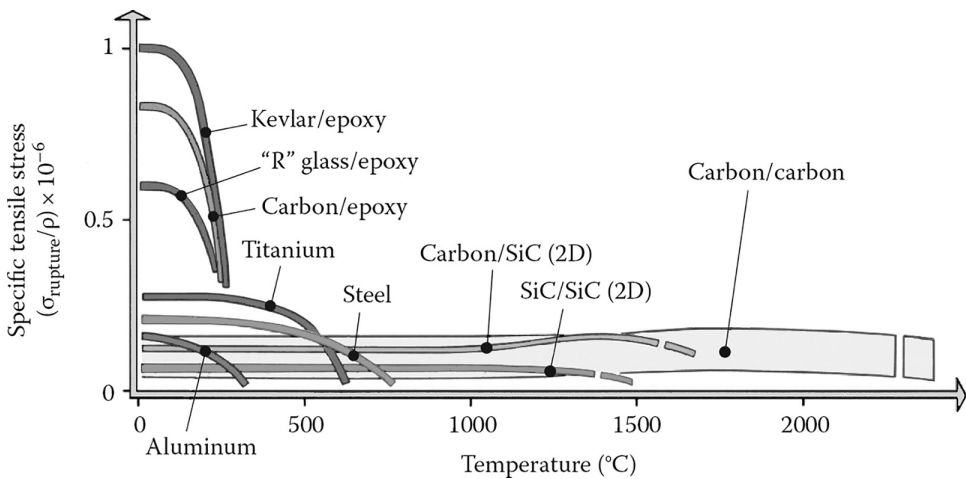


FIGURE 1.6 Specific strength of different composites.

NOTES

- 1 In folding a sheet of steel over itself 15 times, the final sheet is made of $2^{15} = 32,768$ layers.
- 2 The fibers have to be as thin as possible because
 - Their rupture strength decreases as their diameter increases.
 - Very small fiber diameters make it possible to bend fibers until they reach radii of curvature on the order of half a millimeter. However, an exception is made for boron fibers (diameter in the order of $100\text{ }\mu\text{m}$), which are formed around a tungsten filament (diameter = $12\text{ }\mu\text{m}$). Their minimum radius of curvature is 4 mm. Then, except for particular cases, weaving is not possible.
- 3 See Section 3.5.3.
- 4 See Section 3.9.
- 5 Non-pandemic forecasts: The drop in demand from the main industrial sectors (aerospace and defense, automotive, pipelines and tanks, and civil engineering) has temporarily led to a drop in demand for carbon fibers.
- 6 The cured epoxy resin can absorb water by diffusion up to 6% of its mass; the fiber-reinforced epoxy composite can absorb up to 2%. See Section 10.6.



Taylor & Francis

Taylor & Francis Group

<http://taylorandfrancis.com>

2 Manufacturing Processes

The mixture of reinforcement/resin leads to a composite part at the end of the last stage of manufacturing that is the hardening of the matrix. After this phase, it is not possible anymore to modify the material. The designer should not have in mind to change it later, as in the way he would like to modify the structure of a metal alloy using heat treatment, for example.

In the case of polymer matrix composites, for example polyester resin, the latter has to be polymerized. During the solidification process, it changes from the liquid state to the solid state by copolymerization with a monomer mixed with the resin. The phenomenon leads to hardening. This can be done using either heat or a chemical accelerator. The following pages will describe the principal processes for the manufacturing of composite parts. Next, the recycling of composites is discussed as well as the waste treatment methods.

2.1 MOLDING PROCESSES

Several processes use a tool that can be described as a mold and involve reinforcements of various types and geometries. The forming by molding processes varies depending on the nature of the part, the number of parts, and the cost. The impregnation of a reinforcement can be done before it is placed in the mold or afterwards, during the compaction phase. The nature of the resin also influences the course of the process. The material of the mold can be made of metal (steel, aluminum, invar), polymer, wood, or even plaster.

2.1.1 CONTACT MOLDING

Contact molding (see Figure 2.1¹) is an open molding process (there is only one mold, either male or female). The layers of fibers impregnated with resin and accelerator are placed on the mold. Compaction is done using a roller to squeeze out the air pockets. The duration for resin hardening varies, depending on the amount of accelerator and temperature, from a few minutes to a few hours. This way, parts of large dimensions can be produced at the rate of about 2–4 per day and per mold, depending on their complexity at lay-up stage.

- **Note:** Spray-up technique

This denotes the preceding process associated with short fibers. After application of the mold release agent and gel coat and curing of the latter, the short-fiber/resin mixture is projected onto the mold with a spray gun and compacted with a roller before polymerization. Depending on the part to be manufactured, one can combine plies such as mats and fabrics arranged manually and short fibers.

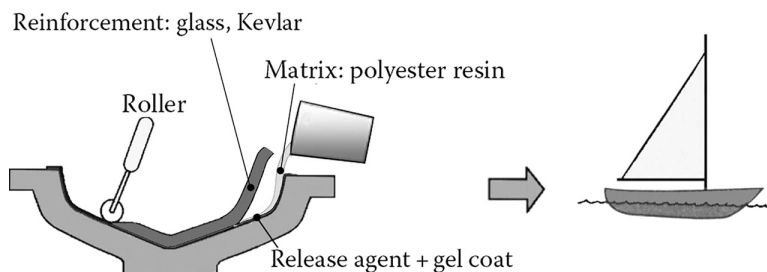


FIGURE 2.1 Contact molding.

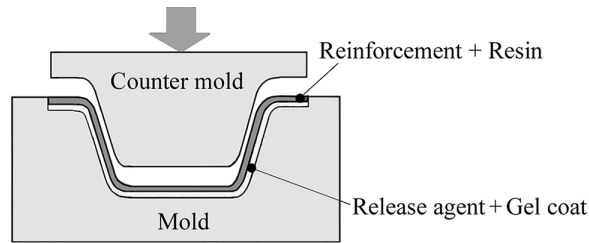


FIGURE 2.2 Compression molding.

2.1.2 COMPRESSION MOLDING

2.1.2.1 Process

With compression molding (see Figure 2.2), a countermold will close the mold after the impregnated reinforcements have been placed in it. The whole assembly is placed in a press that can apply a pressure of 1–2 bar. The polymerization takes place either at ambient temperature or higher.

The process is good for medium-sized series: several dozen parts a day can be manufactured (up to 200 with heating, depending on their complexity at lay-up stage). This is used for automotive and aerospace secondary parts.

2.1.2.2 Bladder Molding Process

The prepreg reinforcements are placed around an inflatable bladder and then put between mold and countermold. The bladder is then pressurized, and its expansion compacts the prepreg against the walls of the mold. Bladder evacuation after curing is not systematic.

2.1.2.3 Forming by Stamping

Also called thermoforming, such a process (see Figure 2.3) is only applicable to thermoplastic composites. One uses preformed plates that are heated, stamped, and then cooled down.

2.1.3 VACUUM MOLDING PROCESSES

2.1.3.1 Vacuum Molding

This process of molding with vacuum is still called **bag molding** or **depression molding**. As in the case of contact molding described previously, an open mold on which the impregnated reinforcements are placed is used for this process. Some cores for sandwich materials (see Chapter 4) can be placed in the mold. A sheet of soft plastic is used for sealing. It is bonded around the perimeter of the mold by means of seal putty. Vacuum is applied under the sheet of plastic (see Figure 2.4).

The part is then compacted due to the action of atmospheric pressure, and the air bubbles are eliminated. Porous felt absorbs excess resin. The whole material is polymerized in an oven.

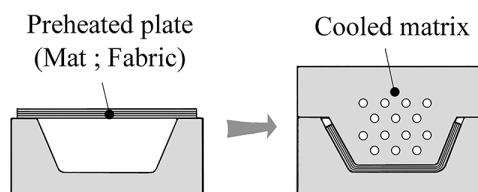


FIGURE 2.3 Stamp forming.

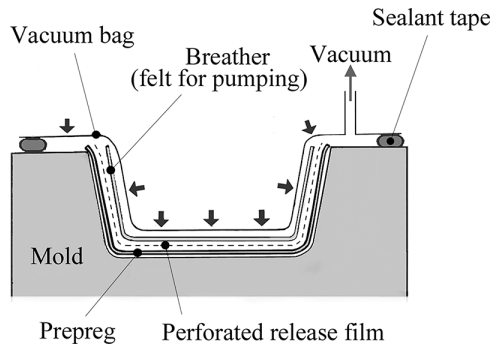


FIGURE 2.4 Vacuum molding.

2.1.3.2 Autoclave Curing

Autoclave is used for high-performance composites. The curing is done under pressure (see Figure 2.5), until 7 bar in the case of carbon/epoxy to obtain better mechanical properties with temperature cycling (see Figure 3.30). This process has applications for aircraft structures, with the rate of a few parts per day (depending on their complexity at lay-up stage). Autoclave's dimensions vary depending on the size of parts to be cured. They can be very important, for example, length up to 32 m with a diameter up to 6 m.

2.1.4 INJECTION PROCESSES

2.1.4.1 Resin Transfer Molding (RTM)

In this resin injection based process (see Figure 2.6), the reinforcements (mats, fabrics, plies) are put in place as a dry preform between mold and countermold. The resin is injected. The clamping pressure creating the locking force limits the resin injection pressure.

- **Medium series:** The molding pressure is low. The process can be fast with reactive resin
- **Small series:** For structural parts (high fiber content, high injection pressure)

Good surface condition on all sides

Shapes limited by undercut geometries

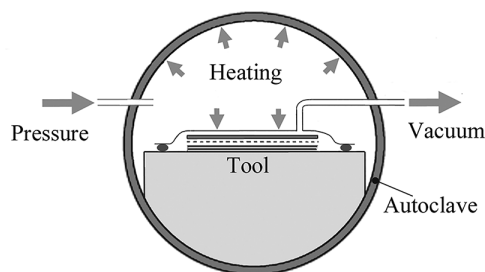


FIGURE 2.5 Autoclave curing.

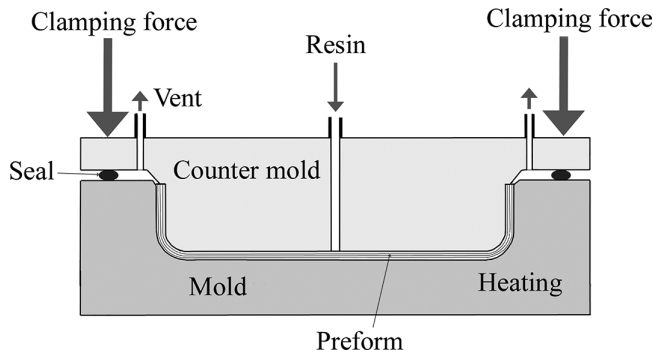


FIGURE 2.6 Resin Transfer Molding (RTM).

2.1.4.2 Vacuum-Assisted RTM (VARTM)

This process has variants, also called Light RTM, or SCRIMP^{®2}. It involves a lower mold and an upper flexible bag (See Figure 2.7). There is therefore only one finished face on the mold side.

It is suitable for very large parts with high-volume contents of fibers (up to 70%) and cored parts with all cores except honeycomb (shipbuilding, aircraft, and wind turbine parts).

The process requires a careful development adapted to each part geometry for impregnation defects have very costly consequences (carefully placed ports for resin entering and vacuum extract).

- **Note:** Resin Film Infusion

A variant of this process consists in placing a dry preform on the lower mold between films of high viscosity resin. Under the effect of heat and vacuum, the resin infuses into the preform. The resin content is then uniform.

2.1.4.3 Injection Molding with Prepreg

The process of molding by injection of prepreg allows automation of the fabrication cycle (rate of production up to 300 pieces per day).

- **Thermoset resins:** Can be used to make components of auto body. The schematic of the process is shown in Figure 2.8.
- **Thermoplastic resins:** Can be used to make mechanical components with high temperature resistance, as shown in Figure 2.9.

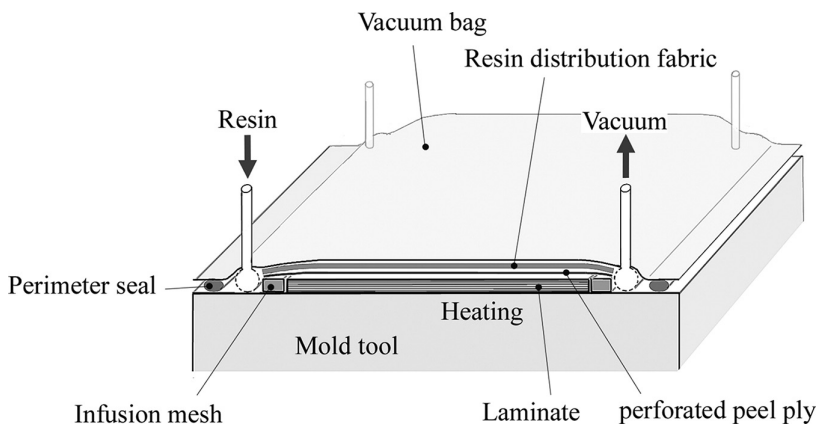


FIGURE 2.7 Vacuum-Assisted Resin Transfer Molding (VARTM).

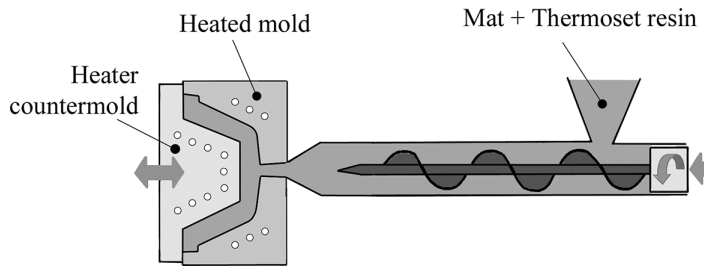


FIGURE 2.8 Injection of premixed.

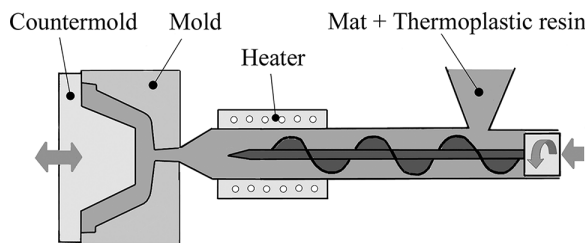


FIGURE 2.9 Injection of thermoplastic premixed.

2.1.4.4 Reaction Injection Molding (RIM/S-RIM)

Molding by foam injection (see Figure 2.10) allows the processing of pieces of fairly large dimensions made of polyurethane foam reinforced with glass fibers. These pieces remain stable over time, with good surface conditions, and have satisfactory mechanical and thermal properties.

With a dry preform previously placed in the mold, more resistant parts are obtained (Structural RIM or S-RIM). The production rate is about 1 min. However, polyurethane-type resins have lower mechanical properties than structural composites.

2.1.5 MOLDING OF HOLLOW AXISYMMETRIC COMPONENTS

- The process of **centrifugal molding** (see Figure 2.11) is used for the fabrication of tubes and pipes. It allows homogeneous distribution of resin with good surface finish, including the internal surface of the tube. The length of the tube depends on the length of the mold. The rate of production varies with the diameter and length of the tubes (up to 500 kg of composite per day).

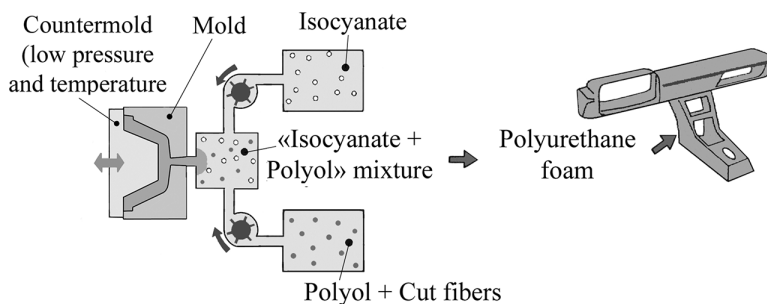


FIGURE 2.10 Reaction Injection Molding (RIM).

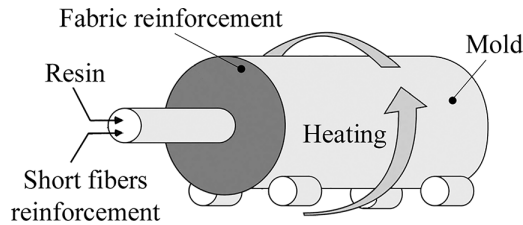


FIGURE 2.11 Centrifugal molding.

- The **filament winding** process as described in Figure 2.12 can be integrated into a continuous chain of production and can fabricate tubes of long length. The rate of production can be up to 500 kg of composite per day. Such a process can be used to make various types of tubes, for example, tubes for transporting petroleum and cylindrical shells for missile, rocket, torpedo, and container.

For revolution pieces with any meridian curves, filament winding can be done on revolution mandrels with adapted geometries. The composite is cured and the mandrel is removed (see Figure 2.13). The fiber volume fraction is high (up to 85%). This process is used to fabricate components with high internal pressure, such as reservoirs and propulsion nozzles.

2.2 OTHERS FORMING PROCESSES

2.2.1 SHEET FORMING

The technique of composite sheet forming (see Figure 2.14) allows the production of plane sheets or corrugated sheets showing increased stiffness. This process needs significant investments.

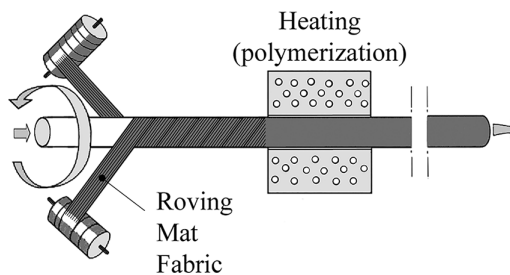


FIGURE 2.12 Filament winding.

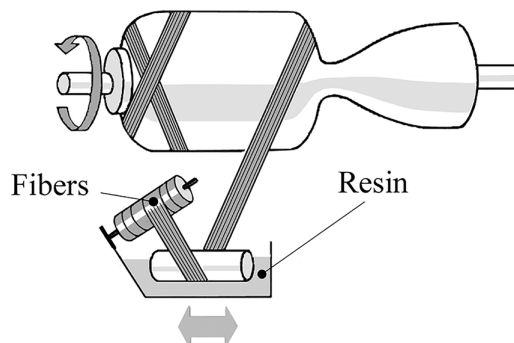


FIGURE 2.13 Filament winding on complex mandrel.

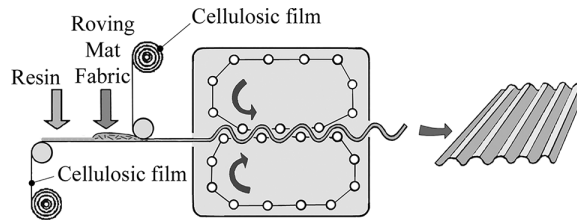


FIGURE 2.14 Sheet forming.

2.2.2 PULTRUSION

The composite pultruded profile shown in Figure 2.15 is made by pultrusion through a shaped die. This process makes possible the fabrication of continuous open or closed profiles. The fiber content can be important for high mechanical properties (more than 60% by volume). The rate of production varies between 0.5 and 3 m/min, depending on the nature of the profile³.

2.2.3 ADDITIVE MANUFACTURING

2.2.3.1 Principle

Additive manufacturing (also known as 3D printing technique) is a recent and rapidly evolving process. It starts with the digital model of the part and produces this part by depositing successive thin layers of material using a heated extrusion nozzle. It is thus possible to generate very complex geometries, which cannot be obtained by means of other methods mentioned.

The resins are thermoplastic (PEEK, PA...see Table 1.4) associated with short or continuous reinforcing fibers (carbon, glass, Kevlar).

2.2.3.2 Types of Additive Machines

Additive manufacturing machines can deposit short fibers or long fibers:

- **Short fibers (of the order of mm):** They are then integrated into the resin before extrusion.
- **Long fibers:** They can form a tape impregnated during extrusion with up to

$$V_f = 60\% \text{ (Carbon).}$$

Example: Machines with two extrusion nozzles: one for the current geometry of the part, with short fibers previously mixed with the resin, and the other with long fibers to adjust, in the most stressed areas the rigidity and the resistance of the part (see Figure 2.16). **Markforged (US)**⁴ and **Desktop Metal (US)** for small parts (print volume of 310×240×270 mm).

Example: Robotic 3D printing:

When the printing is done in successive layers on a plane table (x, y), strength of the finished part is lower in the z direction, which is a general property of conventional laminate materials.

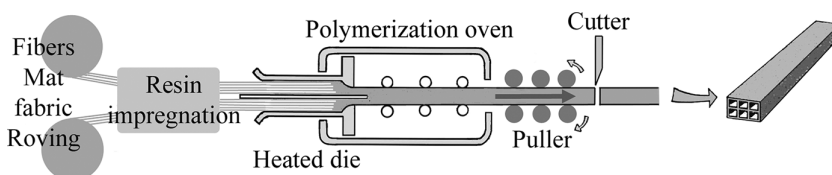


FIGURE 2.15 Pultrusion.

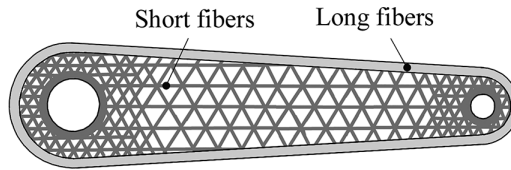


FIGURE 2.16 Rod cross section.

Nevertheless, possibilities of 3D laying can be considerably increased when the laying nozzle is robotized, i.e., mounted on a robotic arm. One can then reinforce any directions in space for parts of complex geometries: **Arevo** (US): 6-axis robot, and swivel table. High-performance parts are up to 1m^3 . The laying nozzle heats up with a laser and compacts the filament with a roller during deposit. Carbon/PEEK: $V_f = 50\%$.

Example: Composite fibers coextrusion (see Figure 2.17). Carbon fiber is pre-impregnated with a thermosetting resin, and then extruded with a thermoplastic resin. **Anisoprint** (RU; LU) printing volume: $297 \times 210 \times 145\text{ mm}$, fiber diameter 0.34 mm .

2.3 AUTOMATED PREFORM MANUFACTURING

2.3.1 NECESSITY OF AUTOMATION

Some composite parts require **numerous unidirectional layers** or fabric layers (tens to hundreds). For small- or medium-sized series, it becomes too risky and too costly to operate preforming manually:

- For following the form of a cutout template
- To respect the orientation specified by the design (see Chapters 5 and 15)
- To minimize waste of material

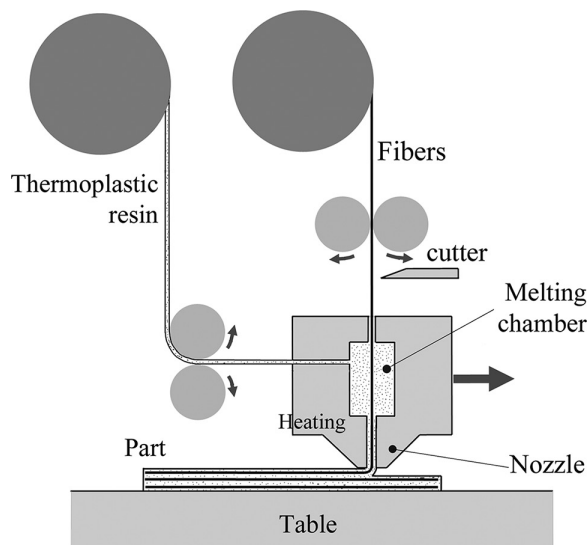


FIGURE 2.17 Composite fiber coextrusion.

This explains the use of automated machines for cutting and draping prepreg layers, with the following characteristics:

- A programmable trajectory of ply layer following several axis of movement
- A rapid cutting tool, such as an orientable vibrating cutting knife or a laser beam with the diameter of about 0.2 mm and a cutting speed varying from 15 to 40 m/min, depending on the power of the laser and the thickness of the part
- A productivity increased by a factor of 10 (carbon/epoxy laminates).

2.3.2 TYPES OF MACHINES

2.3.2.1 Fiber Placement Processes

There are two categories of fiber placement process depending on the characteristics of the laminates and the surfaces of the parts considered:

- Automated Tape Laying (ATL)
- Automated Fiber Placement (AFP)

In both cases of ATL and AFP, the fibers are placed using an elastomer compaction roller. They are successively put under controlled tension, cut, heated, compacted (see Figures 2.18–2.20).

For prepreg carbon fibers, Table 2.1 shows the performance ranges available from manufacturers of laying machines⁵.

With ATL process, it is also possible to lay up fabrics and Non-crimp fabrics. For glass/resin, the tape widths can be much larger.

2.3.2.2 Automated Tape Laying (ATL)

Examples:

- **MAD Forest-Liné** (FR), the draping is done in two steps by means of two distinct installations:
 - A cutting machine that produces a roller to which the cut pieces are attached (cassettes)
 - A depositing machine that uses the cassette of cut pieces to perform the draping

These two operations are shown schematically in Figure 2.18.

- Machines operating according to the principle illustrated in Figure 2.19.

TABLE 2.1
Performance Ranges of ATL and AFP Processes

Carbon Fibers	Tape Width mm	Slit-Tape (Tow) mm	Number of Tapes	Steering (Laying Radius) m	Laying Speed m/min	Weight per Hour kg/h
Automated Tape Laying (ATL)	60–75–150– 300–406 150		1–2–4	150	60–150	10–20
Automated Fiber Placement (AFP)		2.5–3.2–6.35– 12.7 6.35	6–16–32	1.5	6–30–60	2–6

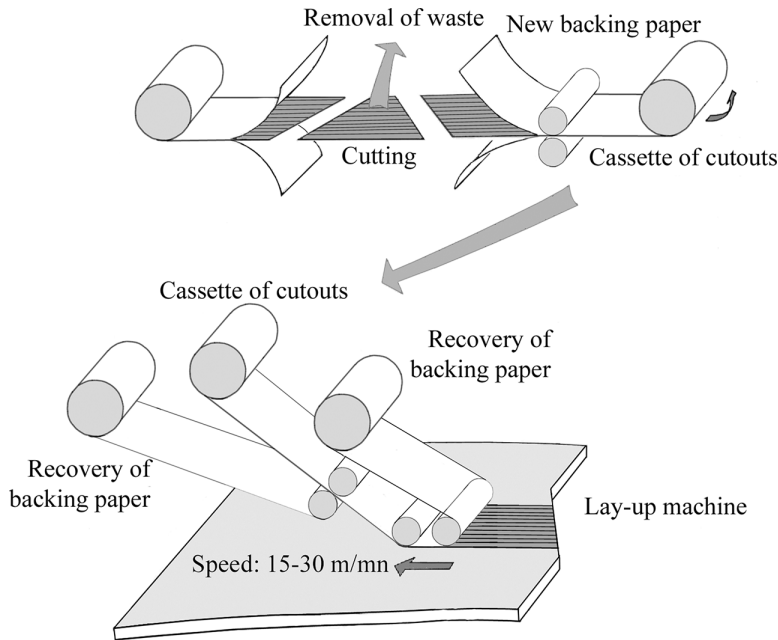


FIGURE 2.18 Two steps draping.

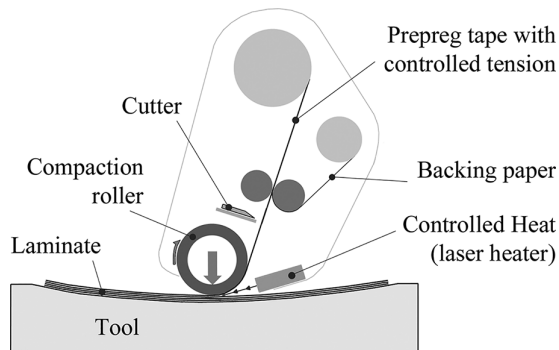


FIGURE 2.19 Automated Tape Placement head.

For example, the 11-axis high-speed ATL machine with ultrasonic cutters **MTORRESLAYUP®** M.Torres (ES):

- Layer feed rate 15 to more than 60 m/min
- Tape width 75 mm up to 600 mm in multitape configuration
- Draping of large parts with low curvatures

2.3.2.3 Automated Fiber Placement (AFP)

The tape of carbon fibers is replaced by tows obtained from bundles of pre-impregnated carbon fibers. Each tow is driven and cut independently. The independent control of the tows allows steered lay-up to be made on non-developable surfaces with different paths lengths for each tape (see Figure 2.20). A hybrid process is obtained between draping and filament winding: the possibilities

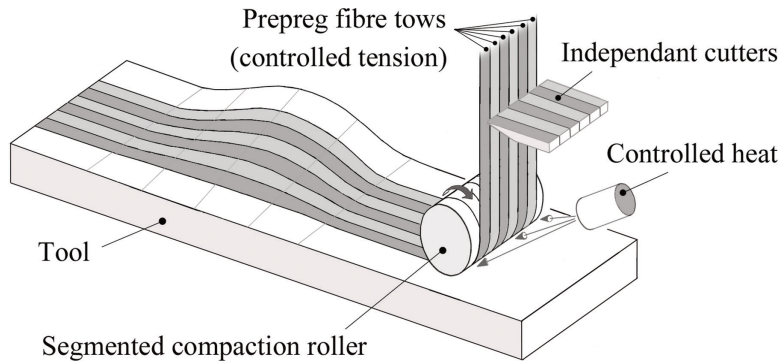


FIGURE 2.20 Automated Fiber Placement (AFP).

are thus extended to the production of laminated preforms with complex geometries: double curvatures, locally reinforced zones.

- **Remarks:**

- Quality of the laying

The quality of the path of the cut tows (start and end positions) depends on the laying speed. Productivity is reduced by at least half compared to that of the ATL process.

- Characteristics of AFP

The overlap of two ribbons is to be avoided. One admits a weak clearance (see Figure 2.21). It should be noted that the clearance between the tows increases when the laying radius decreases.

The tows can twist, come off, and get out of alignment.

If the laying radius is too small, one can observe the tow's wrinkling. In practice and to avoid this phenomenon, one should respect a minimum ratio as shown in Figure 2.22⁶.

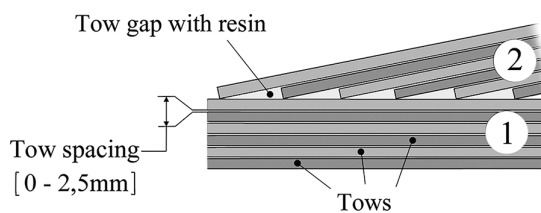


FIGURE 2.21 AFP: Junction between two layers.

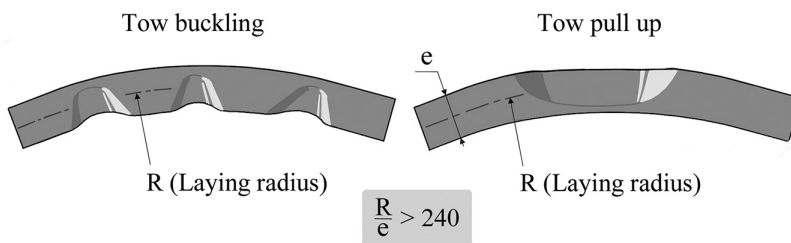


FIGURE 2.22 AFP: Influence of laying radius on steered tows.

2.3.2.4 Example: Robots and Software for AFP – Automatic Fiber Placement Coriolis Composites (FR)

The fiber placement process is implemented on standard polyarticulated robots commonly used in the automotive industry, combined with innovative fiber placement systems. The choice of robots rather than fixed machines allows benefiting of proven technology, readily available and relatively cheap.

The supply and fiber placement is obtained by means of a placement head of less than 50 kg associated with a simple and effective guidance solution for the fibers on nearly 3 m in length from the **creel**, which is located at the foot of the robot up to the head. The head that places fibers is compact and lightweight and can operate with all types of molds with complex geometries (male, female of concavity up to 1 m radius, etc.). The programming of the eight-axis robot and of the actuators of the head is optimized in order to obtain response time and accuracy of placement suitable for production rates of aircraft.

2.4 PRACTICAL CONSIDERATIONS ON MANUFACTURING PROCESSES; ACRONYMS

Professionals use many abbreviations to describe the fabrication processes of composite products. They are detailed here with the reference to the paragraph to which the corresponding processes refers:

- **Bladder molding:** Section 2.1.2.2.
- **BMC:** Bulk molding compound. Prepreg with thermoset resin, short fibers (6–12 mm and 10%–30% per volume), mineral fillers. Implementation process: pressure: 5–10 MPa. Temperature: 120°C–150°C. See Sections 2.1.2.1 and 2.1.4.3.
- **Centrifugation:** Matrix: resins. Reinforcement: cut fibers, mat, fabrics; see Section 2.1.5.
- **Compression molding:** Matrix: resins. Reinforcement: fabrics or unidirectional layers; see Section 2.1.2.1.
- **Contact molding:** Matrix: resins. Reinforcement: mat, fabrics; see Section 2.1.1.
- **Continuous fabrication processes:** See Sections 2.1.5, 2.2.1, and 2.2.2.
- **Filament winding:** Matrix: resins. Reinforcement: continuous fibers. See Section 2.1.5.
- **Pultrusion:** Matrix: resins. Reinforcement: mat, fabrics, continuous fibers. See Section 2.2.2.
- **R-RIM:** Reinforced-reaction injection molding (there is expansion in the mold). Pressure: 0.5 MPa. Temperature: 50°C–60°C. See Section 2.1.4.4.
- **RTM:** Resin transfer molding. The resin is injected in a closed mold. Matrix: thermosetting resins. Reinforcements: dry preforms with cut fibers or fabrics. Pressure: in vacuum or with low pressure 0.1–0.3 MPa. See Section 2.1.4.1.
- **RST:** Reinforced stamped thermoplastics. Reinforcement content about 30% per volume. Pressure: 15–20 MPa. Initial temperature \approx 200°C. See Section 2.1.2.3.
- **RTP:** Reinforced thermoplastics. Matrices: thermoplastic resins. Reinforcements: cut fibers (content about 30% per volume). Pressure: 50–150 MPa. Temperature: 120°C–150°C. See Section 2.1.2.3.
- **SMC:** Sheet molding compound. Prepreg made of fiberglass with resin and mineral filler. Matrix: polyester resin. Reinforcement: mat (25–50 mm fiber length), unidirectional glass, with content about 30% per volume. Pressure: 5–10 MPa. Temperature: 120°C–150°C. See Section 2.1.2.1.
- **Spray-up:** Matrix: resins. Reinforcement: short fibers. See Section 2.1.1.
- **S-RIM:** Structural reaction injection molding (structural parts, particularly for automobiles). Liquid thermoset resins with two components of very high reactivity are injected, as in the R-RIM process. See Section 2.1.4.4.

- **TMC:** Similar to SMC but with higher amount of glass fibers (a few millimeters in thickness).
- **Vacuum molding, Autoclave molding:** Matrix: resins. Reinforcement: fabrics or unidirectional layers; additional pressure if using autoclave. See Section 2.1.3.
- **VARTM:** Vacuum-assisted RTM. Vacuum infusion of dry preforms that are compressed by atmospheric pressure, with thermosetting resins. See Section 2.1.4.2.
- **ZMC:** Matrices: resins. Reinforcement: staple fibers longer than in the BMC process. Pressure: 30–50 MPa. Temperature: 120°C–150°C.
- **XMC:** Similar to SMC but with specific orientation of the fibers.

The diagram in Figure 2.23 summarizes these different processes

2.5 RECYCLING OF COMPOSITES

2.5.1 RECYCLING ISSUES

2.5.1.1 The Problem of Waste

Industrial composites activity regularly shows significant growth, with an estimated market value⁷ shown in Figure 2.24. Increasing in proportion is the total tonnage, about 18×10^6 t in 2017 (see Section 8.1.1).

Considering the importance of this tonnage today, composites industry is faced with environmental aspect and with the problem of waste. Regulations for the fate of waste are becoming more and more restrictive, with the risk of impacting the growth rate of composites, which, in some cases, can be abandoned in favor of materials more easily recyclable.

The volume of waste thus comprises two parts that are growing rapidly each year:

- Production waste
- End-of-life products

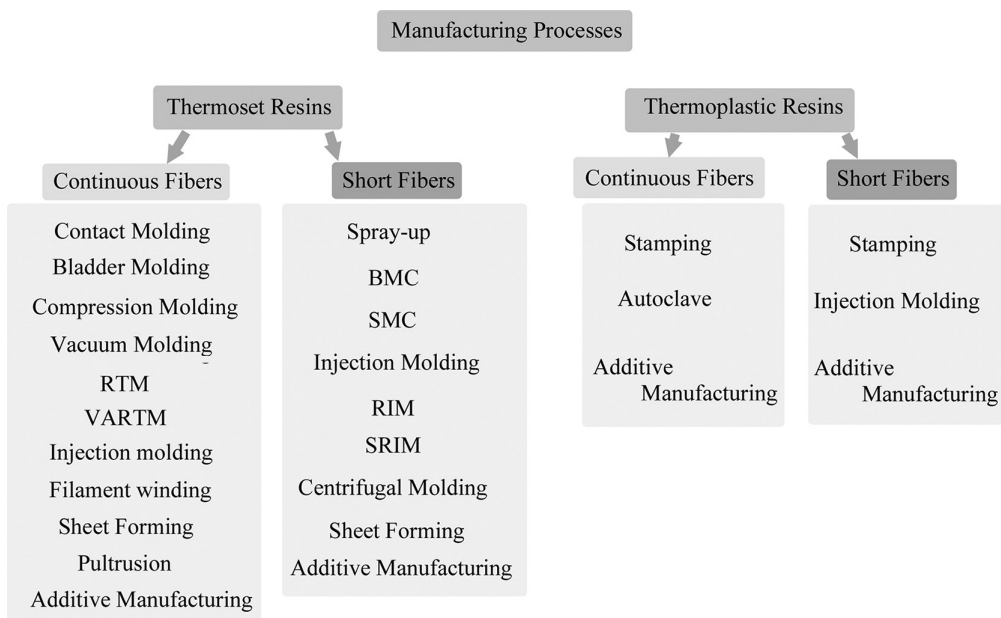


FIGURE 2.23 Classification of manufacturing processes.

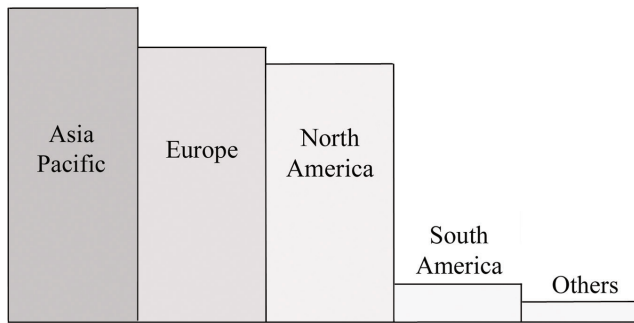


FIGURE 2.24 Global market estimated in 2024: $\$120 \times 10^9$.

Example:

Europe in 2015: Production waste: 50,000 tonnes

End-of-life products: 250,000 tonnes

Production waste is easier to treat because it is better identified and generally not associated with other materials.

For most of them, end-of-life products are difficult to identify and often associated with other materials including metals.

2.5.1.2 Examples

- **Aircrafts:** A total of 80%–85% of the constituent elements are potentially recoverable (aluminum alloys, titanium, steel, composite materials). The recent aircrafts contain a lot of composites and the quantity of planes to be processed is increasing rapidly (12,000 civil transport aircrafts in the next 20 years). In fact, the current life span of a commercial aircraft is of the order of 26 years versus 31 years previously. This is because of the consumption gains of new aircraft generations.
- **Wind turbines:** Wind farms have an estimated lifespan of 20 years.
- **Pleasure boats and yachts:** The legislation is not precise for end-of-life boats.
- For sport and leisure equipment, wrecks are abandoned or placed in landfill.

The aim today is to place composites in a renewable economy, as part of the energy transition.

Currently, 20% of plastic and composite waste is still placed in landfills. However, since 2002, the traditional method of burying in “technical landfill centers” is only considered as a solution for so-called “ultimate” waste, i.e., that cannot be treated otherwise by technical way.

Ideally, composite recycling should be considered when designing products and subsequently when it comes to production. Progress is real and visible: in 2016, recycling exceeded landfill.

We recall the main types of products mentioned in this book:

- Polymer matrix composites
- Metal matrix composites
- Ceramic matrix composites

Composites with polymer matrices are in the majority with nearly 70% of the total tonnage. And they also correspond to the oldest products. In what follows, we will focus on the latter category.

Note: In polymer matrix composites, the share of high-performance composites is largely in the minority. To fix ideas, the tonnage of carbon fiber composites in 2016 was estimated at 100,000 t. On the other hand, the corresponding waste is of great value.

2.5.1.3 Specific Problems to Composites

As can be seen in this book, composite materials involve complex and diverse products and treatments, for example:

- **Nature of the polymer matrix:** Thermosetting or thermoplastic with a variety of products (see Table 1.4), addition or not of fillers
- **Nature of fibers:** Short, long, of diverse materials (see Table 1.3), with various preforms, surface treated (sizing) to create a fiber-matrix bond that recycling aims to break
- **Incorporation into used and end-of-life products of other materials:** Core materials (see Table 1.5), metals, and inserts (see Section 4.4.3)

Notes: There is the problem of collecting used composite materials:

- We know how to collect production waste. On the other hand, it is difficult to recover obsolete material. Unless we put in place incentive measures yet to be defined.
- Recycled composites with glass and carbon fibers (thermoplastic and thermosetting compounds) can be found in the following industries:
Automobile
Civil engineering
Home furnishings and design
Aeronautics
Sports and leisures

2.5.2 RECYCLING OF POLYMER MATRIX COMPOSITES

2.5.2.1 Main Processes

To recover composite waste, several methods are used:

- **The thermal process:**
 - Incineration: Average calorific value of a thermosetting resin: 30,000 kJ/kg. Recovery of energy, clinker (*in principle* usable for road construction).
 - Pyrolysis: Allows fiber recovery.
- **The mechanical way:**
 - Conventional grinding to obtain a powder used as future reinforcement: damage to the fibers.
 - Impact crushing to recover fairly long fibers after sieving.
- **The chemical route:** Recovering reinforcements, fillers, possibly elements of the matrix: these are complex and expensive processes.
- **The biological method:** For certain biodegradable composites (see Section 3.8).

These main processes are illustrated in Figure 2.25.

2.5.2.2 Case of Carbon/Resin Composites

Carbon fibers are expensive. From a recycling point of view, they are therefore economically attractive. This is where the most significant R&D investments are found. In order to recover the fibers, the following routes are explored and illustrated in Figure 2.26:

- Pyrolysis of the part (400°C–750°C): The fibers are recovered, and the polymer matrix is recovered in the form of pyrolysis “coke”

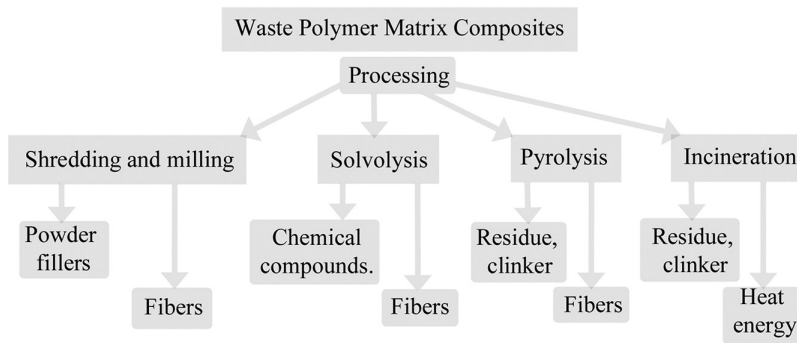


FIGURE 2.25 Main processing methods for polymer matrix composites waste.

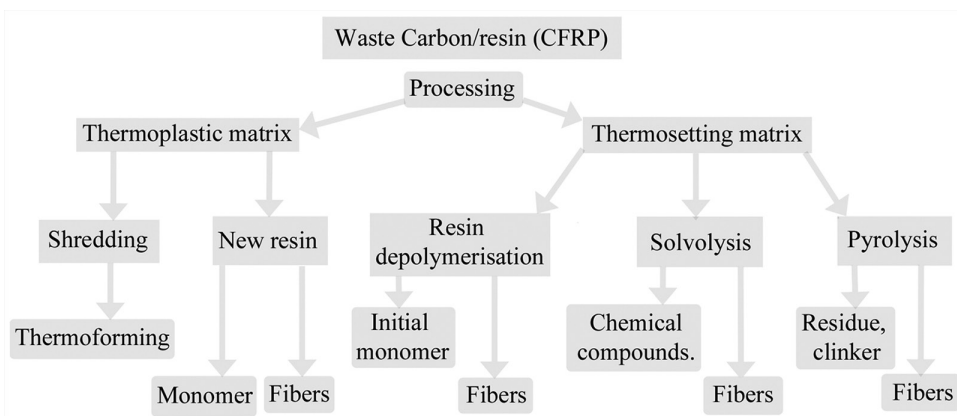


FIGURE 2.26 Recycling of carbon/resin composites (CFRP).

- Solvolysis (under temperature and pressure conditions) or acid catalysts to dilute a thermosetting matrix and recover fibers retaining their qualities
- Depolymerization of the resin to recover the initial resin monomer (under R&D)
- Vapothermolysis: Hot treatment with steam to recover almost intact carbon fibers (**Alpha Recyclage Composites** (FR))
- Thermoforming of plates with thermoplastic resins after preliminary grinding
- Development of thermoplastic resins from which the monomer can be recovered

NOTES

- 1 On Figure 2.2, **gel coat** means a colored polyester resin to get a smooth surface of the required color.
- 2 This acronym stands for “Seemann Composites Resin Infusion Molding Process”, **Seemann Composites** (US).
- 3 For example, carbon/epoxy pultruded profiles, **Epsilon Composites** (FR).
- 4 Code ISO 3166-1/alpha-2 for the representation of **names of countries**.
- 5 Including the following manufacturers: **Automated Dynamics** (US), **Cincinnati** (US), **Ingersol** (US), **M.Torres** (ES), **Forest-Liné** (FR), and **Coriolis** (FR).
- 6 According to **Coriolis** (FR).
- 7 Pandemic not taken into consideration.

3 Mechanical Properties of Reinforcement–Matrix Associations

It is essential for the designer to know precisely and understand the geometric and mechanical characteristics of a mixture of reinforcement and matrix after curing, which is the basic structure of composite parts. The description of these features is the focus of this chapter.

3.1 ISOTROPY AND ANISOTROPY

When studying the behavior of elastic bodies under mechanical loading (theory of elasticity), the following basic properties are highlighted, by means of considerations and tools that are not necessarily complicated:

- An **elastic** body subject to stress deforms in a **reversible** manner
- At each point within the body, the **principal planes** are the planes onto which only **normal stress** acts
- The **normal directions** to these planes are called the **principal stress directions**
- Inside of the body, a small **sphere** of material surrounding a point becomes a small **ellipsoid** after loading

The spatial position of the ellipsoid relative to the directions of principal stress enables to determine whether the material under study is isotropic or anisotropic. Figure 3.1 illustrates this phenomenon.

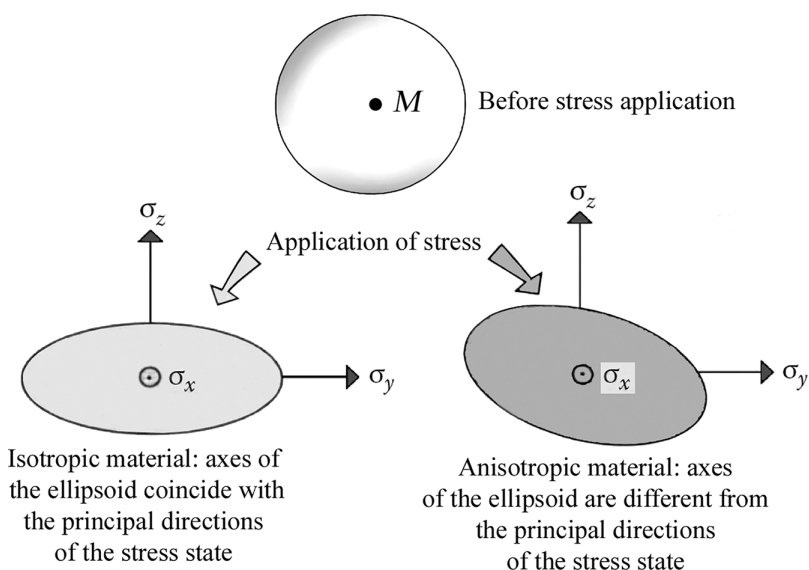


FIGURE 3.1 Schematic of deformation.

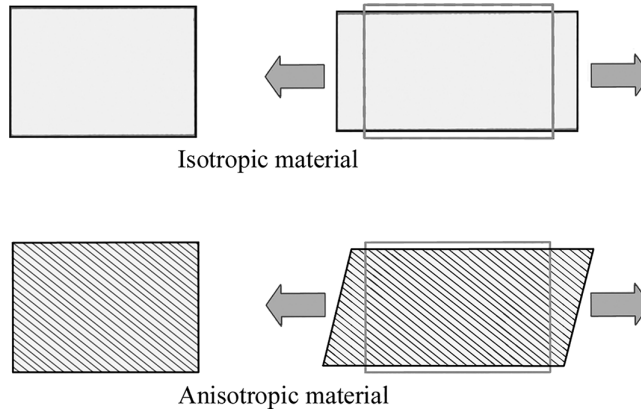


FIGURE 3.2 Isotropic and anisotropic plate: comparison of deformation.

An easy way to see the effects of anisotropy on the deformation of a sample consists in loading a plate-sample of anisotropic material in its own plane. Figure 3.2 illustrates the deformations under load, respectively, of an isotropic and anisotropic plate. In the latter case, the oblique lines on Figure 3.2 represent the reinforcement fibers. It should be recalled that a longitudinal loading applied to the isotropic plate creates an extension in the longitudinal direction and a contraction in the transverse direction. As seen in Figure 3.2, the same loading applied to an anisotropic plate creates an angular distortion **in addition** to the classical longitudinal extension and transversal contraction.

In the simple case of plane stress, as on the previous example, some elastic coefficients allow to link the stress components to the deformations that they induce. The corresponding relations are the so-called behavior relations, as written hereafter.

3.1.1 ISOTROPIC MATERIALS

The following relations are valid for a material that is elastic and isotropic.

The stress–strain relation can be written (see Figure 3.3) in matrix form as¹

$$\begin{Bmatrix} \epsilon_x \\ \epsilon_y \\ \gamma_{xy} \end{Bmatrix} = \begin{bmatrix} \frac{1}{E} & -\frac{\nu}{E} & 0 \\ -\frac{\nu}{E} & \frac{1}{E} & 0 \\ 0 & 0 & \frac{1}{G} \end{bmatrix} \begin{Bmatrix} \sigma_x \\ \sigma_y \\ \tau_{xy} \end{Bmatrix}$$

We can note three elastic constants: E , ν , G . There is a relation between them as

$$G = \frac{E}{2(1 + \nu)}$$

The earlier relation shows that a material isotropic and elastic can be characterized by only two independent elastic constants: E and ν .

3.1.2 ANISOTROPIC MATERIAL

The matrix equation for the anisotropic material in Figure 3.4 is

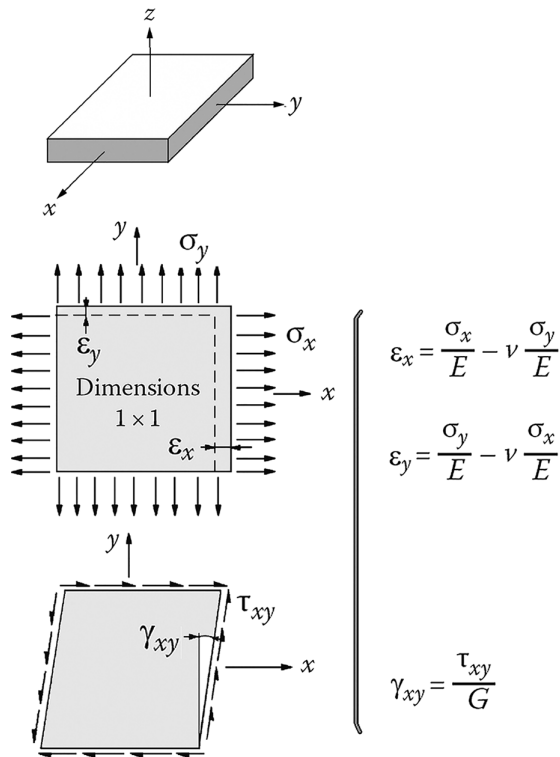


FIGURE 3.3 Stress–strain behavior of isotropic material.

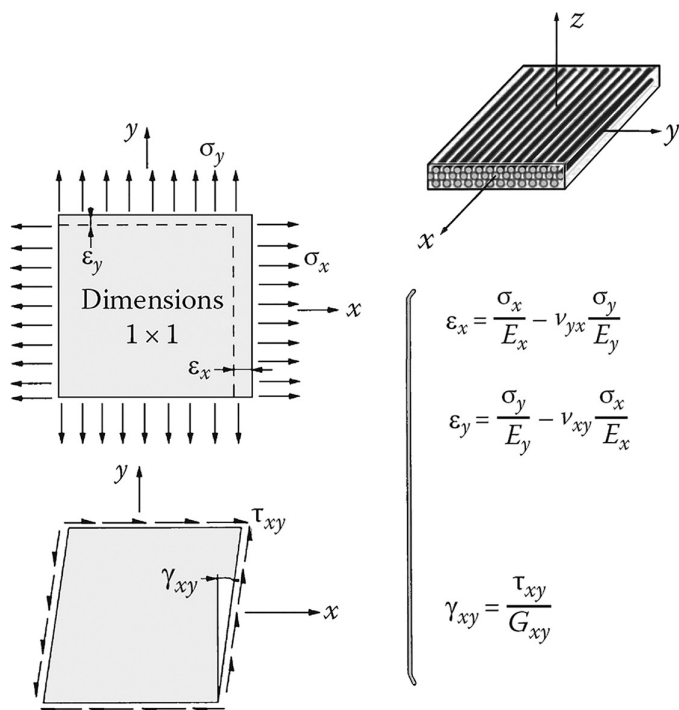


FIGURE 3.4 Stress–strain behavior of anisotropic material.

$$\begin{Bmatrix} \epsilon_x \\ \epsilon_y \\ \gamma_{xy} \end{Bmatrix} = \begin{bmatrix} \frac{1}{E_x} & -\frac{\nu_{yx}}{E_y} & 0 \\ -\frac{\nu_{xy}}{E_x} & \frac{1}{E_y} & 0 \\ 0 & 0 & \frac{1}{G_{xy}} \end{bmatrix} \begin{Bmatrix} \sigma_x \\ \sigma_y \\ \tau_{xy} \end{Bmatrix}$$

We can note an apparent asymmetry of the matrix of elastic coefficients earlier and five elastic constants:

- Two moduli of elasticity: E_x and E_y
- Two Poisson coefficients: ν_{yx} and ν_{xy}
- One shear modulus: G_{xy}

In fact this matrix is symmetric², and there are only four independent elastic constants³: E_x , E_y , G_{xy} , and ν_{yx} (or ν_{xy}). The fifth elastic constant can be obtained from the others using the symmetry relation.

$$\nu_{xy} = \nu_{yx} \frac{E_x}{E_y}$$

3.2 CHARACTERISTICS OF THE REINFORCEMENT–MATRIX MIXTURE

The term **ply** is commonly used to describe the semi-finished product **reinforcement + resin**, which presents as a quasi-2D thin layer⁴. This can be

- A layer of unidirectional fibers in a matrix
- A layer of woven fabric in a matrix
- A layer of mat in a matrix

These are examined in more detail in Sections 3.3–3.5.

3.2.1 FIBER MASS FRACTION

Fiber mass fraction is defined as

$$M_f = \frac{\text{Mass of fibers}}{\text{Total mass}}$$

And the matrix mass fraction is such as

$$M_m = \frac{\text{Mass of matrix}}{\text{Total mass}}$$

From which

$$M_m = 1 - M_f$$

3.2.2 FIBER VOLUME FRACTION

Fiber volume fraction is defined as

$$V_f = \frac{\text{Volume of fiber}}{\text{Total volume}}$$

As a result, the volume fraction of matrix is given as

$$V_m = \frac{\text{Volume of matrix}}{\text{Total volume}}$$

From which⁵

$$V_m = 1 - V_f$$

Note that mass fraction can be obtained from volume fraction and *vice versa*. If ρ_f and ρ_m are the specific mass of the fiber and matrix, respectively, we have

$$V_f = \frac{\frac{M_f}{\rho_f}}{\frac{M_f}{\rho_f} + \frac{M_m}{\rho_m}} \quad M_f = \frac{V_f \rho_f}{V_f \rho_f + V_m \rho_m}$$

Depending on the method of fabrication, the common fiber volume fractions are as shown in Table 3.1.

3.2.3 MASS DENSITY OF A PLY

The mass density of a ply can be calculated as

$$\rho = \frac{\text{Total mass}}{\text{Total volume}}$$

which can also be expanded as

$$\rho = \frac{\text{Mass of fiber}}{\text{Total volume}} + \frac{\text{Mass of matrix}}{\text{Total volume}}$$

$$\rho = \frac{\text{Volume of fiber}}{\text{Total volume}} \times \rho_f + \frac{\text{Volume of matrix}}{\text{Total volume}} \times \rho_m$$

TABLE 3.1
Common Fiber Volume Fractions in Different Processes

Molding Process	Fiber Volume Fraction (%)
Contact molding	30
Compression molding	40
Filament winding	60–85
Vacuum molding	50–80

TABLE 3.2
Ply Thicknesses of Some Common Composites

	M_f (%)	h (mm)
E glass	34	0.125
R glass	68	0.175
Kevlar®	65	0.13
HR carbon	68	0.13

or

$$\rho = \rho_f V_f + \rho_m V_m$$

3.2.4 PLY THICKNESS

The ply thickness is defined starting from the weight per unit area of fiber or **grammage** written as m_{0f} . The ply thickness, denoted as h , is then such that

$$h \times 1(\text{m}^2) = \text{Total volume} = \text{Total volume} \times \frac{m_{0f}}{\text{Fiber volume} \times \rho_f}$$

or

$$h = \frac{m_{0f}}{V_f \times \rho_f}$$

One can also express the thickness in terms of mass fraction of fibers rather than in terms of volume fraction:

$$h = m_{0f} \left[\frac{1}{\rho_f} + \frac{1}{\rho_m} \left(\frac{1 - M_f}{M_f} \right) \right]$$

Table 3.2 shows a few examples of ply thicknesses.

3.3 UNIDIRECTIONAL PLY

3.3.1 ELASTIC MODULUS

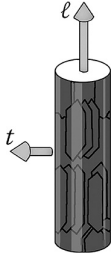
The mechanical characteristics of the fiber/matrix mixture can be estimated from the characteristics of each of the constituents. The literature provides a number of theoretical or semiempirical relations, the results of which do not always agree with the values derived from tests. One of the reasons is that the fibers themselves show a more or less pronounced anisotropy. Thus, for example, low values of the longitudinal modulus of elasticity in the transverse direction of both Kevlar and carbon fibers⁶ can be seen in Table 3.3. The glass fiber appears isotropic.

With definitions and writing conventions in the previous paragraph, we can retain the following expressions to characterize the unidirectional ply (reinforcement + matrix):

- **Elastic modulus along the fiber direction, E_ℓ**

A fairly accurate value is given by⁷

TABLE 3.3
Fiber Elastic Modulus

		Glass E	Kevlar	Carbon HR	Carbon HM
	Fiber longitudinal modulus in ℓ direction, E_{f_ℓ} (MPa)	74,000	130,000	230,000	390,000
	Fiber transverse modulus in t direction, E_{f_t} (MPa)	74,000	5,400	15,000	6,000
	Fiber shear modulus, $G_{f_{\ell t}}$ (MPa)	30,000	12,000	50,000	20,000
	Fiber Poisson ratio, $\nu_{f_{\ell t}}$	0.25	0.4	0.3	0.35
		Isotropic fiber		Anisotropic fiber	

$$E_\ell = E_f V_f + E_m V_m$$

or

$$E_\ell = E_f V_f + E_m (1 - V_f)$$

In practice, this modulus depends essentially on the longitudinal modulus of the fiber E_f because $E_m \ll E_f$ (for example, $(E_{m_{\text{resin}}}/E_{f_{\text{glass}}}) \approx 6\%$).

- **Elastic modulus in the transverse direction to the fiber axis, E_t**

In the following equation, E_{f_t} represents the elastic modulus of the fiber in the direction that is perpendicular to the fiber as indicated in Table 3.3:

$$E_t = E_m \left[\frac{1}{(1 - V_f) + \frac{E_m}{E_{f_t}} V_f} \right]$$

- **Shear modulus, $G_{\ell t}$** : An order of magnitude of this modulus (difficult to estimate by calculation) is given by the following expression in which $G_{f_{\ell t}}$ represents the shear modulus of the fiber as shown in Table 3.3:

$$G_{\ell t} = G_m \left[\frac{1}{(1 - V_f) + \frac{G_m}{G_{f_{\ell t}}} V_f} \right]$$

- **Poisson coefficient, $\nu_{\ell t}$** : The Poisson coefficient represents the contraction in the transverse direction t when a ply is subjected to tensile loading in the longitudinal direction ℓ (see Figure 3.5):

$$\nu_{\ell t} = \nu_f V_f + \nu_m V_m$$

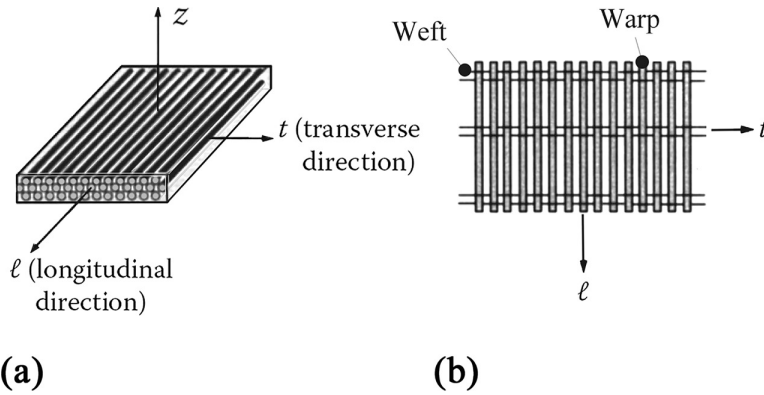


FIGURE 3.5 Orientations in composite layers: (a) unidirectional ply and (b) unidirectional fabric.

- **Modulus along any direction:** It is possible to evaluate elastic and shear modulus along any direction within the plane (ℓ , t)⁸. The longitudinal modulus along direction x , called E_x , is presented in the following equation where $c = \cos \theta$ and $s = \sin \theta$ (see Figure 3.6). It should be noted that this module decreases rapidly when x departs from the fiber direction

(i.e. as θ increases):
$$E_x = \frac{1}{\frac{c^4}{E_\ell} + \frac{s^4}{E_t} + 2c^2s^2 \left(\frac{1}{2G_{\ell t}} - \frac{\nu_{\ell t}}{E_\ell} \right)}$$

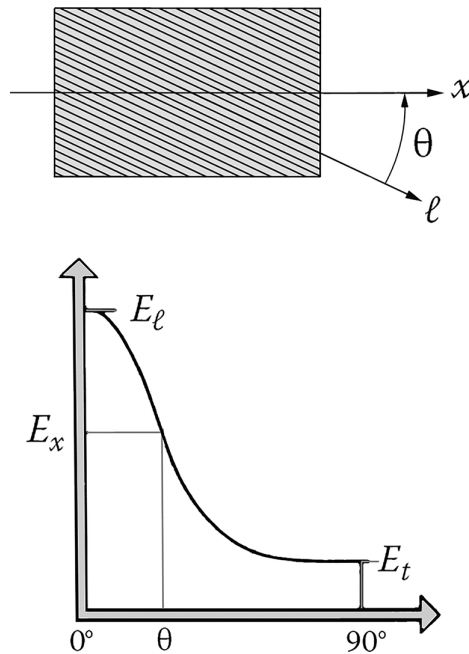


FIGURE 3.6 Off-axis modulus.

3.3.2 ULTIMATE STRENGTH OF A PLY

The curves in Figure 3.7 show the significant difference in failure behavior between classical metallic material and the unidirectional plies. Such difference can be summarized in the few points listed here:

- A lack of plastic deformation in the unidirectional ply: this is a disadvantage
- A high ultimate tensile stress for the unidirectional: this is an advantage
- An important elastic deformation of the unidirectional, which can constitute an advantage or a disadvantage depending on the applications: for example, this is an advantage for springs, bows, or poles

When the fibers break before the matrix during loading along the fiber direction, we obtain the following for the composite:

$$\sigma_{\ell_{\text{rupt.}}} = \sigma_{f_{\text{rupt.}}} \left[V_f + (1 - V_f) \frac{E_m}{E_f} \right]$$

Or approximately,

$$\sigma_{\ell_{\text{rupt.}}} \approx \sigma_{f_{\text{rupt.}}} \times V_f$$

The **ultimate strength along any direction**⁹ is given by the following relation where (see Figure 3.8)

$\sigma_{\ell_{\text{rupt.}}}$ is the fracture strength in the direction of the fibers

$\sigma_{t_{\text{rupt.}}}$ is the fracture strength transverse to the direction of the fibers

$\tau_{\ell t_{\text{rupt.}}}$ is the shear strength in the plane (ℓ , t) of the ply

$$\sigma_{x_{\text{rupt.}}} = \frac{1}{\sqrt{\frac{c^4}{\sigma_{\ell_{\text{rupt.}}}^2} + \frac{s^4}{\sigma_{t_{\text{rupt.}}}^2} + \left(\frac{1}{\tau_{\ell t_{\text{rupt.}}}^2} - \frac{1}{\sigma_{\ell_{\text{rupt.}}}^2} \right) c^2 s^2}}$$

With (see Figure 3.8) $c = \cos \theta$; $s = \sin \theta$.

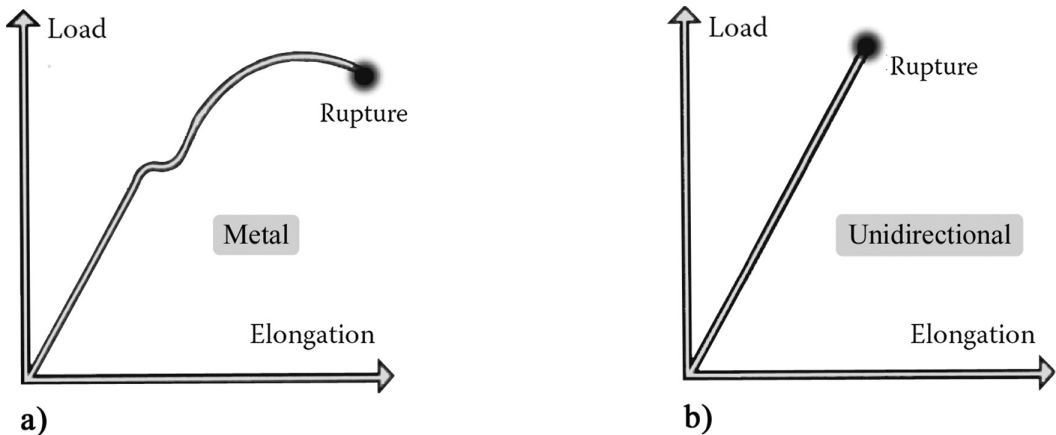


FIGURE 3.7 Loading curves of (a) metal and (b) unidirectional composite.

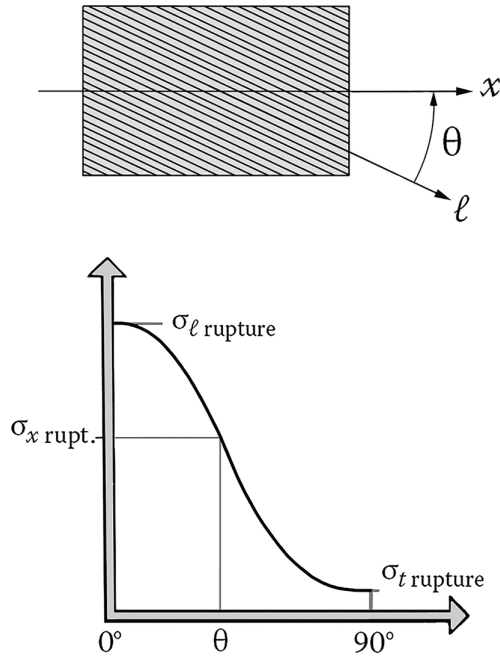


FIGURE 3.8 Off-axis rupture strength.

3.3.3 EXAMPLES

Table 3.4 gives the properties of the fiber/epoxy unidirectional ply at 60% fiber volume fraction¹⁰.

The compression strength along the fiber direction is smaller than the tensile strength along the same direction due to the **microbuckling** phenomenon of the fibers in the matrix (see Section 14.1.4 and Figure 14.6).

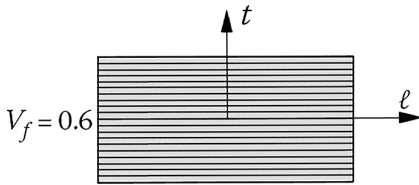
3.4 WOVEN PLY

3.4.1 FORMS OF WOVEN FABRICS

The woven fabrics are formed by fibers arranged along two mutually perpendicular directions: one is called the **warp** direction (the length direction of the roll of woven fabric) and the other is called the **weft** direction. The fibers are woven together, which means that the weft yarns pass over and under certain warp yarns, following a predetermined pattern. The way in which the warp yarns and the weft yarns cross each other defines the type of weave of the fabric. The weaves in Figure 3.9 are in ascending order for their ability to drape complex surfaces (see Figures 3.10 and 14.3), for their strength, for their rigidity, and for their cost.

Figure 3.9a shows a **plain weave** fabric where each weft yarn passes alternatively over and under the successive warp yarns. Figure 3.9b shows a **twill weave** fabric. Here, a weft yarn floats over a warp yarn (1) and under the two that follow (2, 3); in the next pass, the shuttle of the loom passes under warp yarns 1 and 2 and over the third one. Referring to Figure 3.9b, we see how the shuttle shifts during subsequent passages. A twill or diagonal effect is then formed on the fabric face. This is the simplest twill that can be made, so-called **3-harness twill**. Figure 3.9c shows a **satin weave** fabric: each weft yarn floats over four warp yarns before going under the fifth one. For this reason, it is called a **5-harness satin**.

TABLE 3.4
Properties of Fiber/Epoxy Unidirectional Plies



	Glass	Kevlar	Carbon
Specific mass, ρ (kg/m ³)	2,080	1,350	1,530
Longitudinal tensile strength, $\sigma_{\ell\text{rupture}}^{\text{tensile}}$ (MPa)	1,250	1,410	1,270
Longitudinal compressive strength, $\sigma_{\ell\text{rupture}}^{\text{compr}}$ (MPa)	600	280	1,130
Transverse tensile strength, $\sigma_{t\text{rupture}}^{\text{tensile}}$ (MPa)	35	28	42
Transverse compressive strength, $\sigma_{t\text{rupture}}^{\text{compr}}$ (MPa)	141	141	141
In-plane shear strength, $\tau_{\ell t\text{rupture}}$ (MPa)	63	45	63
Interlaminar shear strength, $\tau_{\ell z\text{rupture}}$ (MPa) = $\tau_{tz\text{rupture}}$ (MPa)	80	60	90
Longitudinal elastic modulus, E_{ℓ} (MPa)	45,000	85,000	134,000
Transverse elastic modulus, E_t (MPa)	12,000	5,600	7,000
Shear modulus, $G_{\ell t}$ (MPa)	4,500	2,100	4,200
Poisson ratio, $\nu_{\ell t}$	0.3	0.34	0.25
Longitudinal coefficient of thermal expansion at 20°C, α_{ℓ} (°C ⁻¹)	$0.4\text{--}0.7 \times 10^{-5}$	-0.4×10^{-5}	-0.12×10^{-5}
Transverse coefficient of thermal expansion at 20°C, α_t (°C ⁻¹)	$1.6\text{--}2.0 \times 10^{-5}$	5.8×10^{-5}	3.4×10^{-5}

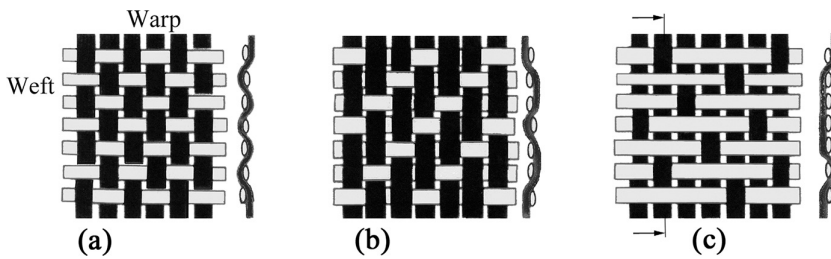


FIGURE 3.9 Forms of woven fabrics: (a) plain weave, (b) twill weave, and (c) satin weave.

For approximate values of the fabric elastic properties (about 15%), one can consider them to consist of two unidirectional plies crossing at 90° angle. The following notations can be used:

- e is the total layer thickness
- n_1 is the number of warp yarns per meter
- n_2 is the number of weft yarns per meter

$$k = \frac{n_1}{(n_1 + n_2)}$$

- V_f is the volume fraction of fibers

We can deduce the thickness of the equivalent unidirectional plies (see Figure 3.11) as

$$e_{\text{warp}} = e \times \frac{n_1}{(n_1 + n_2)} = k \times$$

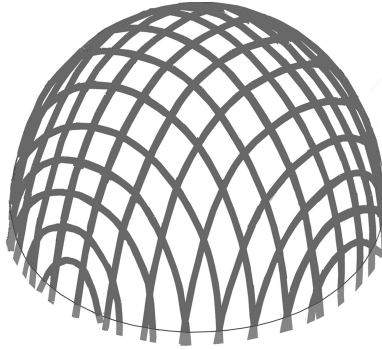


FIGURE 3.10 Ability of a fabric ply to drape complex surfaces.

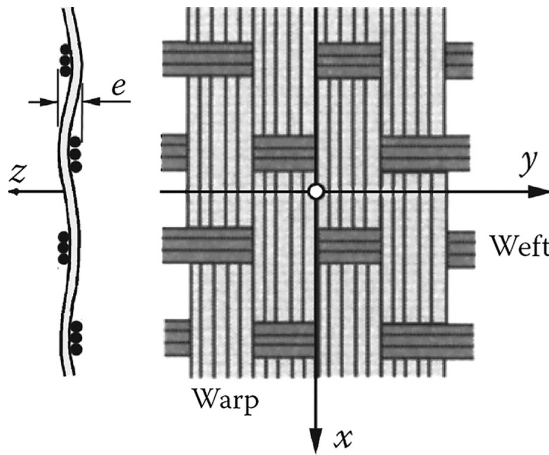


FIGURE 3.11 Notations for a fabric layer.

$$e_{\text{weft}} = e \times \frac{n_2}{(n_1 + n_2)} = (1 - k) \times e$$

3.4.2 ELASTIC MODULUS OF FABRIC LAYER

In order to obtain estimated values, the two layers of reinforcement can be taken into account either separately or together.

- **Separately:** The fabric layer is replaced by two unidirectional plies crossed at 90°, with the following thicknesses:

$$e_{\text{warp}} = k \times e; \quad e_{\text{weft}} = (1 - k) \times e$$

The average fiber volume fraction V_f being known, then the mechanical properties E_ℓ , E_t , $G_{\ell t}$, and $\nu_{\ell t}$ of these plies can be determined (see Section 3.3.1).

- **Together:** The fabric layer is replaced by a single anisotropic ply with thickness e . x -direction being the warp direction and y the weft direction (see Figure 3.9), we have then approximately¹¹

$$E_x \approx k \times E_\ell + (1 - k) \times E_t$$

$$E_y \approx (1 - k) \times E_\ell + k \times E_t$$

$$G_{xy} = G_{tt}$$

$$\nu_{xy} \approx \frac{\nu_{\ell t}}{\left(k + (1 - k) \frac{E_\ell}{E_t} \right)}$$

Notes

- The stiffness obtained with a woven fabric is less than what would be observed by superimposing two cross plies of unidirectionals. This is due to the curvature of the fibers during the weaving operation (see Figure 3.12). This curvature makes the woven fabric more deformable than the two cross plies when subject to the same loading. (There exist fabrics that are of **high modulus** where the unidirectional layers are not connected with each other by weaving. Stitched fine threads of glass or polymer hold the unidirectional plies together.)
- The fabric ply shows an upper tensile strength and a lower compressive strength, as compared with the corresponding strengths obtained when superposing two cross plies¹².

3.4.3 EXAMPLES OF BALANCED FABRIC/EPOXY

The fabric is said to be **balanced** when there are as many warp as weft yarns, made in the same material. Therefore, the warp and weft directions play equivalent roles with regard to thermomechanical characteristics. The corresponding plies are described in Table 3.5 with an epoxy resin matrix.

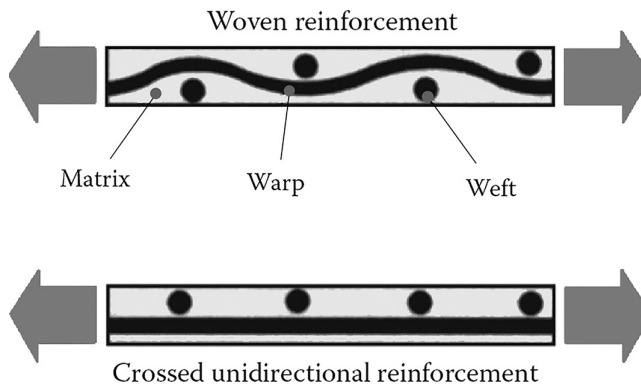
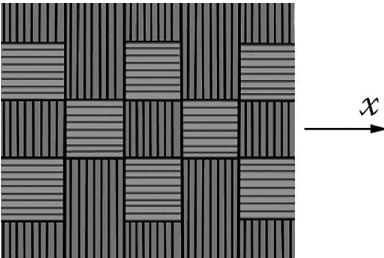


FIGURE 3.12 Cross section of a layer with fibers crossed at 90°.

TABLE 3.5
Properties of Balanced Fabric/Epoxy Composites



	"E" Glass	Kevlar	Carbon
Fiber volume fraction, V_f (%)	50	50	45
Specific mass, ρ (kg/m ³)	1,900	1,330	1,450
Tensile strength along x or y : $\sigma_{xrupture}^{tensile} = \sigma_{yrupture}^{tensile}$ (MPa)	400	500	420
Compressive strength along x or y : $\sigma_{xrupture}^{comp} = \sigma_{yrupture}^{comp}$ (MPa)	390	170	360
In-plane shear strength, $\tau_{xyrupture}$ (MPa)		150	55
Elastic modulus, $E_x = E_y$ (MPa)	20,000	22,000	54,000
Shear modulus, G_{xy} (MPa)	2,850		4,000
Poisson coefficient, ν_{xy}	0.13		0.045
Coefficient of thermal expansion, $\alpha_x = \alpha_y$ (°C ⁻¹)		-0.2×10^{-5}	0.05×10^{-5}
Elongation at break, A (%)		2.1	1.0

3.5 MATS AND REINFORCED MATRICES

3.5.1 MATS

Mats are made of cut fibers (fiber lengths between 5 and 10 cm) or of continuous fibers making a bidimensional layer. Mats are isotropic within their plane (x, y). They can therefore be characterized by two elastic constants only, as specified in Section 3.1.

If E_ℓ and E_t are the elastic moduli (longitudinal and transverse directions, respectively) of the unidirectional ply, which would have the same volume fraction V_f of reinforcement as that of the mat ply, we have then

$$E_{mat} \approx \frac{3}{8} E_\ell + \frac{5}{8} E_t; \quad G_{mat} \approx \frac{E_{mat}}{2(1 + \nu_{mat})}; \quad \nu_{mat} \approx 0.3$$

For example, mats with cut fibers made of **glass/epoxy** have the following characteristics:

Fiber volume fraction, V_f (%)	28
Specific mass, ρ (kg/m ³)	1,800
Elastic modulus, E (MPa)	14,000
Tensile fracture strength, $\sigma_{rupture}^{tensile}$ (MPa)	140
Heat capacity, c (J/g °C)	1.15
Coefficient of thermal conductivity, λ (W/m °C)	0.25
Linear coefficient of thermal expansion, α (°C ⁻¹)	2.2×10^{-5}

3.5.2 EXAMPLE: A SUMMARY OF GLASS/EPOXY LAYERS

Figures 3.13 and 3.14 summarize the main features of the different types of plies (unidirectional, fabric, mat) when the fiber volume fraction V_f varies.

3.5.3 MICROSPHERICAL FILLERS

Microspherical fillers are reinforcements associated with polymer matrices (see Figure 3.15). These fillers are made of solid or hollow microballs of glass, carbon, or polystyrene with diameters between 10 and 150 μm .

- The filler volume fraction V_f can reach up to 50%.
- The filler properties are such that $E_f \gg E_m$.

Defining

$$K = \frac{E_m}{3(1-2\nu_m)} \left[1 + 3 \left(\frac{1-\nu_m}{1+\nu_m} \right) \frac{V_f}{(1-V_f)} \right]$$

The composite (matrix+filler) is isotropic, with the elastic constants E , G , and ν given by the following relations:

$$E \approx \frac{9KG}{3K+G}; \quad G \approx \frac{E_m}{2(1+\nu_m)} \left[1 + \frac{15}{2} \left(\frac{1-\nu_m}{4-5\nu_m} \right) \frac{V_f}{(1-V_f)} \right]; \quad \nu \approx \frac{1}{2} \left(\frac{3K-2G}{3K+G} \right)$$

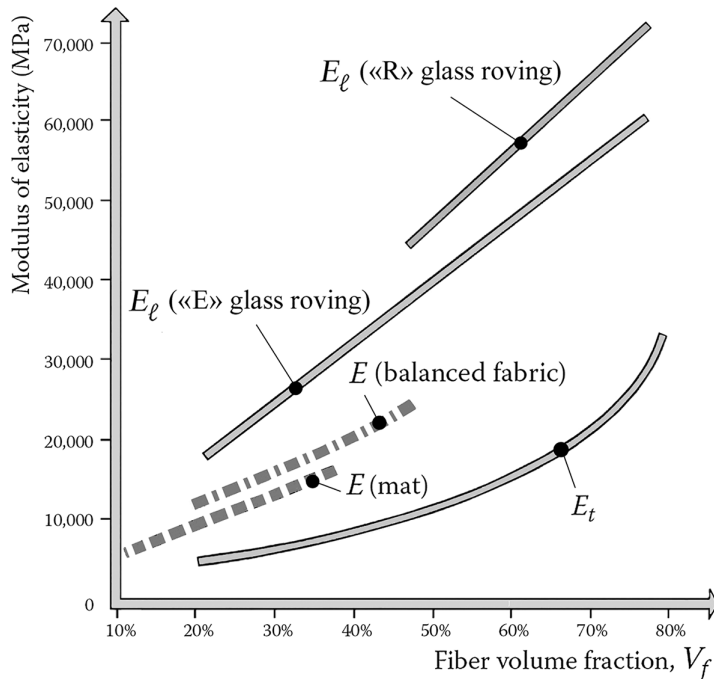


FIGURE 3.13 Elastic modulus of glass/epoxy layers.

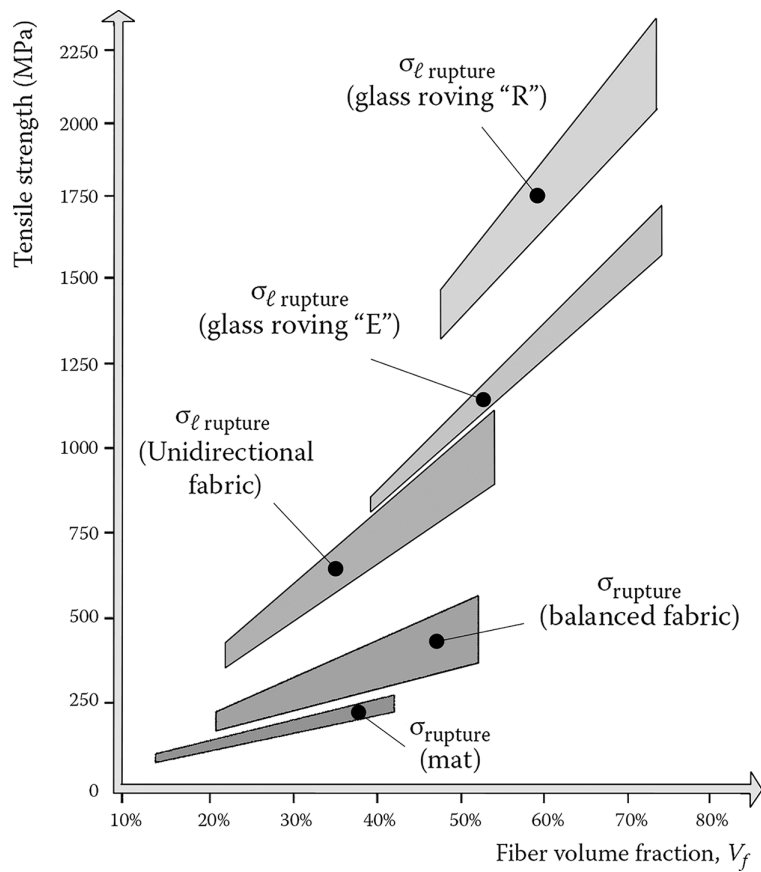


FIGURE 3.14 Tensile strength of glass/epoxy layers.

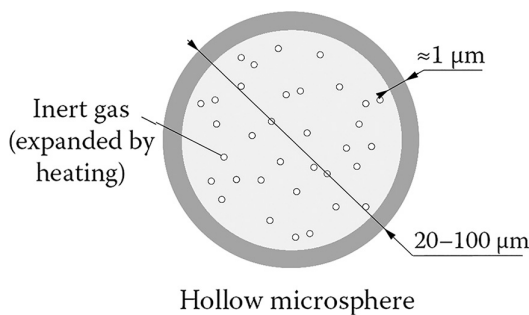


FIGURE 3.15 Spherical fillers.

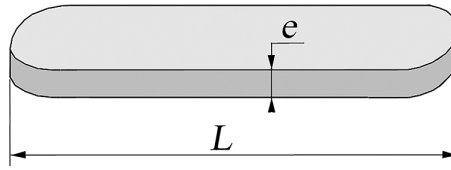


FIGURE 3.16 Form of flakes.

3.5.4 OTHER CLASSICAL REINFORCEMENTS

One may also use reinforcements in the form of milled fibers, flakes (see Figure 3.16), or powders made of any of the following materials:

- Glass
- Mica ($L \approx 100 \mu\text{m}$)
- Talc ($L \approx 10 \mu\text{m}$)
- Graphite
- Some metals
- Alumina

Example: The mica flakes when embedded in a resin with fiber reinforcement adopt a geometric-layered configuration as shown in Figure 3.17. It can then be observed the following impacts:

- First, an increase in the value of the resin's modulus as¹³

$$E = \left[1 - \frac{Ln(1+u)}{u} \right] \times E_{\text{mica}} V_{\text{mica}} + E_m V_m \quad \text{where} \quad u = \frac{L}{e} \sqrt{\frac{G_m}{E_{\text{mica}}} \times \frac{V_{\text{mica}}}{V_m}}$$

In this, the average properties of mica are

$$E_{\text{mica}} = 170,000 \text{ MPa} \quad \text{and} \quad \rho_{\text{mica}} = 2,800 \text{ kg/m}^3$$

- Second, a delay in the microcracking of resin (see Figure 3.18). It is also noteworthy that this remarkable property occurs when, in the absence of classical macroscopic reinforcements, the dimensions of the previously mentioned fillers decrease. We then get what is called **nanocomposites**. Their case will be examined in more detail in Section 3.9.



FIGURE 3.17 Mica flake arrangement.

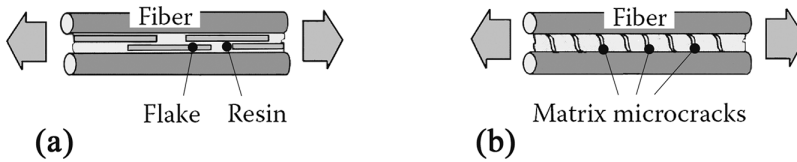


FIGURE 3.18 Cross section (a) with and (b) without mica flakes.

3.6 METAL MATRIX COMPOSITES (MMC)

3.6.1 MATERIALS

The area of MMC generally concerns highly loaded parts involving high added value.

It includes, in development or in service, a number of products consisting of:

- For reinforcements: aramid, carbon, boron, and silicon carbide (SiC)
- For matrices: aluminum, magnesium, titanium, casting, copper alloys (see also Chapter 7)

Depending on the application, the reinforcements take the forms shown in Figure 3.19.

3.6.2 SOME EXAMPLES

3.6.2.1 Aluminum-Reinforced Aramid (ARALL®) and Aluminum-Reinforced Glass (GLARE®)¹⁴

These composites consist of alternating layers of aluminum and glass/epoxy for GLARE (Glass Laminate Aluminum-Reinforced Epoxy) or Kevlar/epoxy for ARALL (ARamid ALuminum Laminate) (see Figure 3.20).

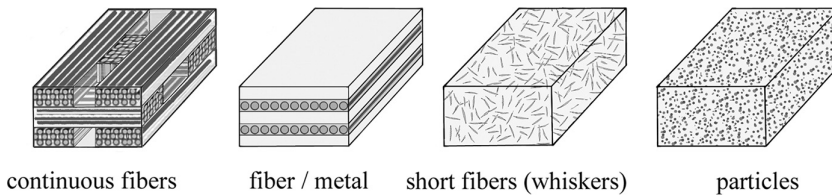


FIGURE 3.19 Reinforcement shapes

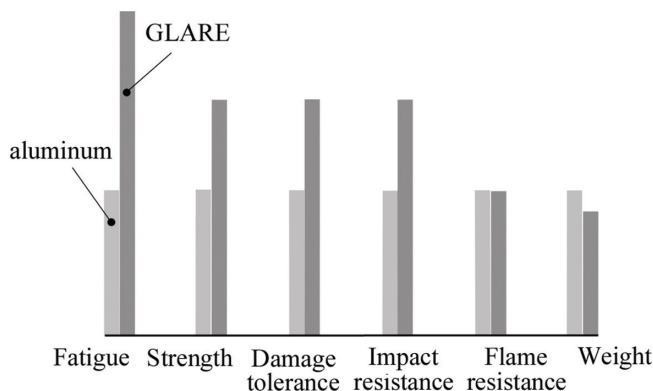


FIGURE 3.20 Advantages of GLARE.

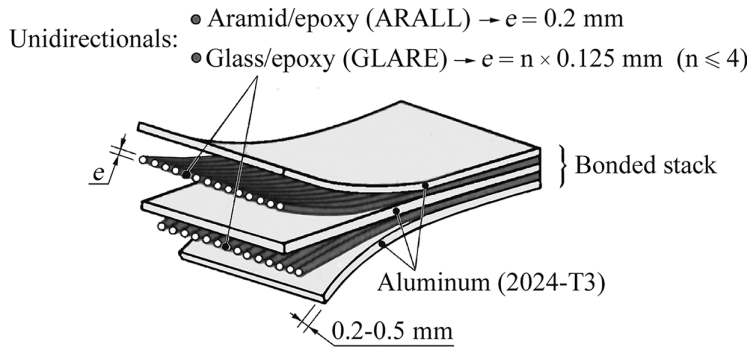


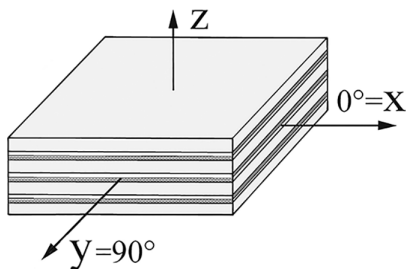
FIGURE 3.21 Layers of ARALL and GLARE.

The key advantages are as in Figure 3.20, and particularly better impact damage tolerance because of:

- Better resistance to failure due to thin metallic layers
- Better resistance against the crack propagation from one layer to the other

Example: Table 3.6 gives some mechanical properties for “GLARE3-4/3-0.4”, i.e., with four aluminum layers (each 0.4 mm thick) and three glass/epoxy layers (each $0^\circ \times 0.125 \text{ mm} + 90^\circ \times 0.125 \text{ mm} = 0.25 \text{ mm}$ thick).

TABLE 3.6
Mechanical Properties of GLARE3-4/3-0.4



Specific mass, ρ	kg/m ³	2,480
Longitudinal tensile strength, $\sigma_{xrupt.}^{tens.} = \sigma_{yrupt.}^{tens.}$	MPa	690 (yielding 365)
Longitudinal compressive strength, $\sigma_{xrupt.}^{compr.} = \sigma_{yrupt.}^{compr.}$	MPa	270
Longitudinal elastic modulus, $E_x = E_y$	MPa	58,000
Transverse elastic modulus, E_z	MPa	13,000
Shear modulus, G_{xy}	MPa	12,200
Poisson ratio $\nu_{xy} = \nu_{yx}$		0,22

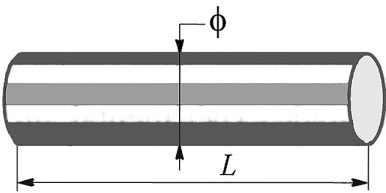


FIGURE 3.22 SiC whisker.

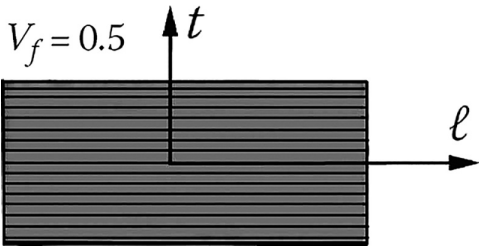
3.6.2.2 Short Silicon Carbide Fibers (Whiskers)/Aluminum

This is called an **incompatible** composite because of the large differences between the thermomechanical properties of the constituents. This leads to high stress concentrations as well as debonding between the fibers and the matrix. These types of composites are interesting for high-temperature applications. In Figure 3.22, the diameter of the whisker is about 20μm and the slenderness ratio ($L/\phi \approx 5$). The fiber volume fraction is about $V_f \approx 30\%$.

3.6.2.3 Boron/Aluminum

Unidirectionals in Table 3.7 have $V_f \approx 50\%$ boron fibers. These types of composites are used in aerospace applications (see Chapter 7). The manufacturing technology to obtain these materials

TABLE 3.7
Properties of Unidirectional Plies Made of Boron Fibers



	Boron/Epoxy	Boron/Aluminum
Specific mass, ρ (kg/m ³)	1,950	2,650
Longitudinal tensile strength, $\sigma_{t \text{ rupture}}^{\text{tens.}}$ (MPa)	1,400	1,400
Longitudinal compressive strength, $\sigma_{t \text{ rupture}}^{\text{compr.}}$ (MPa)	2,600	3,000
Transverse tensile strength, $\sigma_{t \text{ rupture}}^{\text{tens.}}$ (MPa)	80	120
Longitudinal elastic modulus, E_ℓ (MPa)	210,000	220,000
Transverse elastic modulus, E_t (MPa)	12,000	140,000
Shear modulus, $G_{\ell t}$ (MPa)		7,500
Longitudinal coefficient of thermal expansion at 20°C, α_ℓ (°C ⁻¹)	0.5×10^{-5}	0.65×10^{-5}

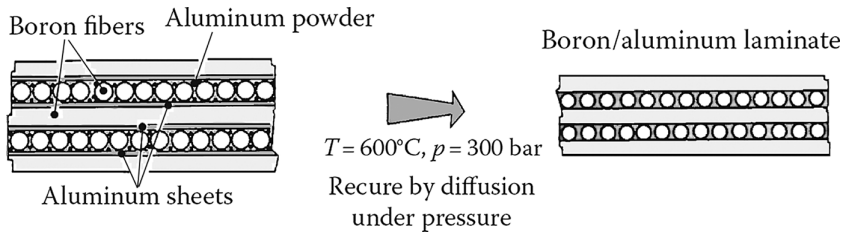


FIGURE 3.23 Boron/aluminum composite.

TABLE 3.8

Properties of Unidirectional Plies with Aluminum Matrix

	HR Carbon	Alumina	Silicon Carbide
Fiber volume fraction, V_f (%)	50	50	50
Specific mass, ρ (kg/m ³)	2,300	3,100	2,700
Longitudinal tensile strength, $\sigma_{\text{rupture}}^{\text{tens.}}$ (MPa)	800	550	1,400
Longitudinal compressive strength, $\sigma_{\text{rupture}}^{\text{compr.}}$ (MPa)	600	3,100	3,000
Longitudinal elastic modulus, E_L (MPa)	200,000	190,000	140,000

is summarized in Figure 3.23. Such composites allow high operating temperatures, in the order of 300°C for service temperature, while preserving significant mechanical properties (see Table 1.3 for the properties of boron).

3.6.2.4 Unidirectional Fibers/Aluminum Matrix

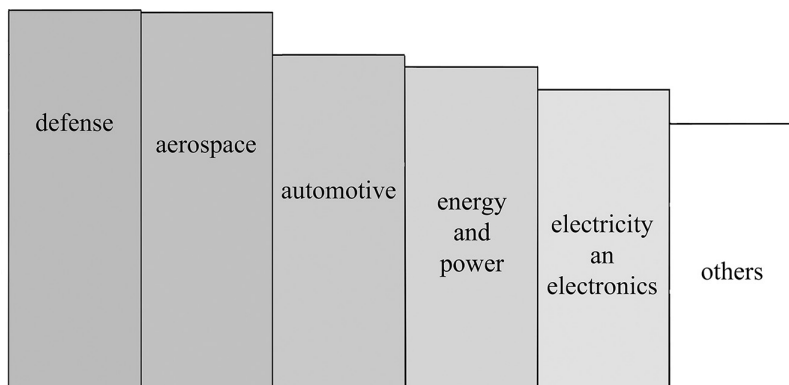
Table 3.8 shows the characteristics of some unidirectional reinforcements associated with an aluminum matrix A96061 (6061).

3.7 CERAMIC MATRIX COMPOSITES (CMCs)

3.7.1 CMCs: AN AREA OF GROWING INTEREST

3.7.1.1 Significant Industrial Importance

For these composite materials, the following diagram shows the areas of activity concerned as well as their relative economic importance (total 2018: \$ 8E9):



Ceramic Matrix Composites, or CMCs, are intended to be used at high temperature (1,000°C–1,200°C; the research development is carried out in the 1,400°C). The reinforcement and the matrix are ceramic type.

3.7.2 FIBERS

3.7.2.1 Materials

Developments of CMCs as well as the widening of the application area have been strongly favored by the emerging of long fibers on the market.

This has made it possible to greatly improve:

- Toughness and breaking strength
- Elongation at break
- Geometric stability
- Thermal shock resistance

The following materials lead to ceramic fibers:

- (C): Carbon
- (SiC): Silicon carbide
- (Ox): Aluminum oxide or alumina (Al_2O_3); mixed crystals of alumina and silicon oxide or silica (SiO_2) called “mullite” ($3\text{Al}_2\text{O}_3, 2\text{SiO}_2$)

3.7.2.2 Reinforcements

Ceramic fibers consist of 500 and up to 300,000 monofilaments.

Some can be weaved with standard textile machines to produce conventional reinforcements: weaving in two or three dimensions or more (see Section 3.6.5.2), braiding, winding.

- **Fibers that can be weaved** include carbon fiber, silicon carbide (SiC), and polyborosilazane (SiBN_3C), in rovings from 500 to 12,000 monofilaments of diameter 6 – 15 μm . The following table shows an example:

Reinforcement	Diameter ϕ (μm)	Temperature $^{\circ}\text{C}$	Elastic Modulus E MPa	Longitudinal Tensile Strength $\sigma_{\text{rupture}}^{\text{tens.}}$ MPa
Polyborosilazane fiber (SiBN_3C)	8–15	1,800	200,000	2,000

These fibers allow obtention of 2D layers, satin for example, or of 3D reinforcements, but also of layers obtained by winding and then stacked to obtain unidirectional layers or bidirectional, or even multidirectional.

- **Fibers that cannot be weaved** include alumina monocrystalline fiber and silicon carbide fiber (SiC) deposited on a tungsten core, the diameter of which is greater than 100 μm . These fibers are exclusively implemented by winding to get layers that are then stacked as described earlier for weavable fibers.

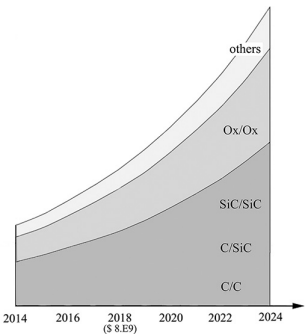
3.7.3 MATRICES

3.7.3.1 Materials

Matrices include carbon (C), silicon carbide (SiC), silicon nitride, alumina, mullite (Ox), and glass-ceramic. Thus, the classification of CMCs is as follows:

C/C, C/SiC, SiC/SiC, Ox/Ox.

One can see their fast industrial development on diagram below¹⁵.



3.7.3.2 Fatigue Resistance

This association of two fragile materials leads paradoxically to a composite material having an apparent ductility thanks to long fibers insertion, by a phenomenon similar to that described in Section 5.4.5 (see Figure 5.30) where the disembedding of the fiber from the matrix prevents the crack propagation. Simply substitute the resin with a fragile ceramic matrix. The fibers resist in a cracked matrix. The disembedding is achieved here by the presence of a third component, or inter-phase between fiber and matrix, that plays the role of **mechanical fuse**. It consists in fiber sizing or in porosities at the interface.

As a result, there is thus a fatigue resistance as can be seen on the following example:

	Elongation	Number of Loading Cycles
SiC/SiC	$A_{max} \times 80\%$	$> 8 \times 10^6$

Note: When the cracks develop in the part, only the fibers resist. As a result, the stiffness of the part decreases.

3.7.4 PRODUCTION PROCESSES

The process to manufacture ceramic composite parts generally follows three stages:

- a. **Production of a preform:** The fibers are processed on textile machines (see Section 3.6.2).
- b. **Infiltration of the future matrix:**
 - Polymer infiltration (Liquid Polymer Infiltration and Pyrolysis or LPIP): Five to eight cycles of infiltration and pyrolysis are required to fill the porosities because the pyrolysis takes place with a decrease in the volume of the polymer. Example: C/SiC obtained by infiltration of liquid polymer (LPI).
 - Gas mixture for Chemical Vapor Deposition (CVD): Pore closure is more successful than in the polymer infiltration case due to better gas circulation in the porous matrix.
 - Chemical reaction between a matrix already in place (powder, liquid) and another material (gas, liquid) ensuring a low final porosity. Example: SiC-silicon nitride.
 - Moderate-temperature sintering (1,000°C–1,200°C): Liquid charged with oxide ceramic powder impregnates the oxide fiber preform (CMC Ox/Ox). The heat welds the grains together without damaging the fibers. Example: mullite.
 - Electrophoresis: The preform constitutes an electrode in a liquid medium. The electrically charged ceramic particles fill the voids in the preform: a process still in the R&D phase.
- c. **Finishing of the part.**

3.7.5 THERMOMECHANICAL PROPERTIES

3.7.5.1 Laminates

Table 3.9 gives some characteristics of composites developed with the previous reinforcements and matrices. The fiber volume fraction is close to $V_f=40\%$, with a density of approximately $2,500\text{ kg/m}^3$. It should be pointed out that this density is $8,000\text{ kg/m}^3$ for superalloys.

3.7.5.2 Multidimensional Fabrics

When using CMCs in thermal environments with strong temperature gradients, one has to replace conventional multilayer laminates within which the plies would separate, with n -dimensional reinforcements with $n > 2$: multilayer weaving, 4D weaving (see Figures 3.24 and 3.25), needling, and braiding.

- **Example:** A Four-Dimensional Architecture of Carbon Reinforcement¹⁶

TABLE 3.9
CMC Laminates

<i>Laminate</i> [(0°/90°) _n] _s	Temperature	Elastic Modulus <i>E</i>	Longitudinal Tensile Strength $\sigma_{\text{rupture}}^{\text{tens.}}$	Elongation at Break
	°C	MPa	MPa	A (%)
2D C/SiC	20	90,000	350	0.9
	1,000	100,000	350	0.9
	1,400	100,000	350	
2D SiC/SiC	20	230,000	200	0.3
	1,000	200,000	200	0.4
	1,400	170,000	150	0.5
2D SiC/glass-ceramic (lithium aluminosilicate)	20		270	
	600		270	
	800		270	

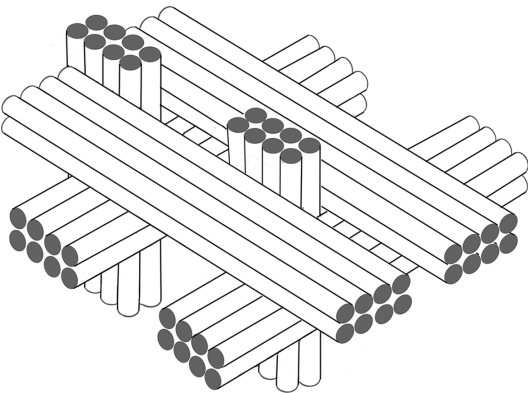


FIGURE 3.24 Orthogonal 3D reinforcement for C/C.

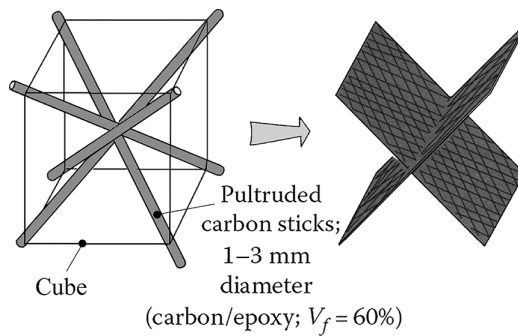


FIGURE 3.25 Four-dimensional architecture.

The reinforcement is assembled according to preset directions in space as seen in Figure 3.25. The fiber volume fraction is on the order of 30%. The matrix comes to fill the voids between the fibers¹⁷. The key advantages of these types of composites are as follows:

- The additional connection (compared to bidimensional plies) increases the damage tolerance versus impact (resistance to delamination)
- Mechanical resistance is maintained – and even improved – at high temperatures (up to 3,000°C for carbon–carbon)
- The coefficient of thermal expansion remains low
- These types of composites are thermal shock resistant
- The thermal conductivity of carbon–carbon is high
- The density is low
- The radio electrical waves travel easily through the silica/silica composites
- **Example:** Three-Dimensional Carbon/Carbon Components

Table 3.10 gives the characteristics of two composites made of tridimensional carbon/carbon. The mechanical properties are the same following any direction denoted as ℓ on the figure in Table 3.10. Therefore, the composite is referred as transversely isotropic¹⁸.

3.7.5.3 Ranges for Mechanical Properties

In Table 3.11, the wide range of variation for characteristics is due to the variety of reinforcements, their spatial arrangement, the matrix preparation, and the type of bonding between reinforcement and matrix (see above).

3.7.6 APPLICATION DOMAINS OF CMCs

3.7.6.1 Recall

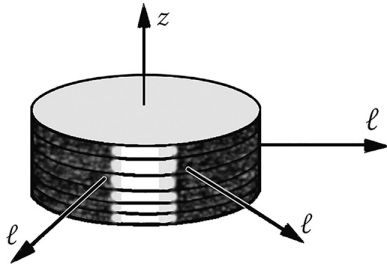
CMCs have many areas of application as shown in the diagram in Section 3.7.1.1.

Their growing importance and industrial development appear to be driven by the following benefits compared to previously used materials:

- A reduction in mass due to the lightening of parts
- More structural efficiency
- Increased service life

The uses of CMCs are summarized below. Some, which are pointed out, are detailed in later chapters.

TABLE 3.10
Properties of 3D Carbon/Carbon



		Aerolor® 41^a	Sepcarb® 4^b
Specific mass, ρ	kg/m ³	1,700–2,000	1,500–2,000
Longitudinal tensile strength, $\sigma_{\ell \text{ rupture}}^{\text{tens.}}$	MPa	40–100	95 and increasing, up to 2,000°C
Longitudinal compressive strength, $\sigma_{\ell \text{ rupture}}^{\text{compr.}}$	MPa	80–200	65
Tensile strength in the z direction, $\sigma_{z \text{ rupture}}^{\text{tens.}}$	MPa	>10	3
Compressive strength in the z direction, $\sigma_{z \text{ rupture}}^{\text{compr.}}$	MPa	80–200	120
Shear strength in (ℓ, z) plane, $\tau_{\ell z \text{ rupture}}$	MPa	20–40	10
Longitudinal elastic modulus, E_{ℓ}	MPa	30,000	16,000
Elastic modulus, E_z	MPa		5,000
Shear modulus, $G_{\ell z}$	MPa		2,200
Shear modulus, $G_{\ell \ell}$	MPa		5,700
Poisson ratio, $\nu_{z\ell}$			0.17
Poisson ratio, $\nu_{\ell \ell}$			0.035
Thermal expansion coefficient, α_{ℓ}	°C ⁻¹		
At 1,000°C		0.7×10^{-6}	3×10^{-6}
At 2,500°C		3×10^{-6}	4×10^{-6}
Thermal expansion coefficient, α_z	°C ⁻¹		
At 1,000°C		6×10^{-6}	7×10^{-6}
At 2,500°C		6×10^{-6}	9×10^{-6}
Coefficient of thermal conductivity, λ	W/m °C	300	

^a Aerolor® is a product of **Mersen Group**, the former **Carbone Lorraine Company** (FR).

^b Product of former **European Propulsion Company**, today **Safran Group** (FR).

3.7.6.2 Aerospace and Defense

Parts having to withstand high temperatures with abrasive environment and vibratory stresses are as follows: braking systems (see Section 7.1.10), engine and gas turbine parts, and stator and rotor blades (see Section 7.4).

3.7.6.3 Space Applications

Launcher and missile nozzles, ailerons, heat shield system parts (see Section 7.5).

3.7.6.4 Automobile

Pistons, bearings, coatings for exhaust pipes, clutch disks for Formula 1, and brake disks for Formula 1 and for sports cars (see Section 8.2).

TABLE 3.11
Range of Mechanical and Thermal Properties

		C/C	C/SiC	SiC/SiC	Ox/Ox
Fiber volume fraction	V_f (%)	40–60	10–70	40–60	30–50
Porosity volume fraction	V_p (%)	8–23	1–20	10–15	10–40
Density	ρ (kg/m ³)	1,400–1,700	1,800–2,800	2,300–2,900	2,100–2,800
Modulus of elasticity	E (GPa)	10–480	30–150	70–270	50–210
Tensile strength	$\sigma^{\text{tens. rupture}}$ (MPa)	14–1,100	80–540	150–360	70–280
Elongation	A (%)	0.1–0.8	0.5–1.1	0.1–0.7	0.12–0.4
Coefficient of thermal expansion	α (°C ⁻¹)	0.6–8.4	0–7	2.8–5.2	2–7.5
Coefficient of thermal conductivity	λ (W/m °C)	10–70	10–130	6–20	1–4
Limit temperature for use	T_{max} (°C)	2,000–2,100	1,350–2,100	1,100–1,600	1,000–1,100

3.7.6.5 Other Uses

- In burners, ovens, hot gas pipes, heat exchangers.
- For the nuclear industry: SiC/SiC coatings for reactors (three-dimensional reinforcement with crystalline SiC fibers, stable at high temperatures).
- For steam plants pumps (water at 160°C, 20 bars): axial and radial bearings. The pumped liquid is used as a lubricant.
- For machining: cutting tools.

3.8 BIOCOMPOSITE MATERIALS

3.8.1 NATURAL PLANT FIBERS

3.8.1.1 Natural Fibers

These are derived from plants and from animals and have long been woven, knitted, or braided to make textiles. They were used also in the past for the reinforcement of matrices (cob for building, cotton/phenolic, hemp/phenolic for technical parts).

Today, because of the significance of the environmental impacts, the development of composite reinforced with natural fibers is rapidly emerging.

The vegetable fibers take the form of bundles of tens of elementary fibers (20–50) bonded with tacky substances. The degumming of these bundles is necessary to release basic fibers. These fibers are composed largely of cellulose fibrils. The fibrils follow helical curves around the axis of the fiber, with a helix angle of a few degrees called the microfibrillar angle. The cellulose has an almost crystalline structure. Its longitudinal modulus of elasticity is 135,000 MPa, compared with that of the “R” glass (86,000 MPa). It thus appears possible to obtain mechanical performances comparable to these of glass.

3.8.1.2 Pros

- They are biodegradable
- They are neutral with respect to emissions of carbon dioxide
- They have a low energy cost (however, fiber processing requires a lot of water, and it is a polluting industry)
- They are light, and many of them have interesting values of specific modules combined with excellent damping and shock-resistant properties
- Some, such as flax and hemp, are native plants. This ensures the supply and offers a significant and valuable perspective for agricultural industry

3.8.1.3 Cons

The use of natural fibers requires prerequisite solutions for the following problems:

- While conventional fibers have well-controlled reproducible characteristics, the quality of natural fibers depends on the environment in which they are produced: the season, where they were planted and harvested, characteristics of the soil on which they have grown, or location from which they originate in the plant (peripheral part or internal part of the stem, leaf, etc.). All these cause the disadvantage of a dispersion of characteristics: varying diameter along fibers, various lengths and degrees of polymerization, and shape defects caused or amplified by the handling and implementation.
- Natural fibers are hydrophilic. The possibility of moisture absorption for composites reinforced by these fibers is thus large (up to 8% or 10%), accompanied by a degradation of the fiber leading to a reduction in performances of the material over time.
- Natural fibers are not resistant to high temperatures. They lose their stiffness to 160°C and degrade at a temperature of approximately 200°C. Applications with thermoplastic matrices thus exclude the use of high-performance types such as PEEK resins (see Section 1.6).
- The tensile strength is not very high. They can be used for rigid parts rather than resistant.
- The risk of microbial contamination must be taken into account.

3.8.1.4 Examples

• Flax fibers

They are taken from the plant on the outskirts of the stem. After selection, cleaning, and separation, the fiber looks generally like a six-sided polygonal cylinder with faces remarkably smooth. It is composed of a hemicellulose matrix, of lignin, with a reinforcement of cellulose fibrils in crystalline form ($V_f \approx 70\%$) that are oriented at a microfibrillar angle about 10° with the axis of the fiber.

• Hemp fibers

The growing (cultivation) of the hemp requires neither pesticides nor herbicides. The average fiber yield is about 250 kg/ha. The fiber, composed of a bundle of a few tens of elementary fibers, is located on the outer periphery of the stem to ensure structural stiffness of the latter.

Table 3.12 shows the characteristics of some natural fibers used as reinforcements. The significant variations for a same type of fibers should be noted, due to the reported parameters earlier in combination with the specific treatment received.

Note: Failure values on industrial rovings are *much lower* than in Table 3.8. For example, a failure value to the tune of 60 MPa for the flax (up to 85 MPa on rovings) and 35 MPa for hemp.

3.8.2 NATURAL VEGETABLE FIBER–REINFORCED COMPOSITES

3.8.2.1 Mechanical Properties

The mechanical properties of this type of composite depend on the volume fraction of fibers, orientation of these fibers, and quality of bonding between fiber and matrix. It so happens that the cellulose is scarcely compatible with the polymer matrices. For **technical fibers**, therefore, a prior surface treatment is a clear need in view of improving the fiber–matrix linkage:

- For flax fibers: combination with polyester and epoxy resins
- For hemp fibers: combination with polyurethane and polyvinyl chloride (PVC) resins

The flax and hemp can be used as **technical fibers** in the form of unidirectional, woven reinforcement, mat (nonwoven), and short fibers (compound).

TABLE 3.12 Characteristics of Some Natural Fibers Used as Reinforcements							
Nature of the Fiber	Flax	Hemp	Sisal	Jute	Cotton	Silk Thread	Spider Thread
Diameter	4–77; Average: 19	10–51	50–400	5–200	12–25		
Fiber length	Average: 33	5–55	0.8–8; Average: 3	2–5	2–40		
Fiber volume fraction of cellulose	64–71	73–78	67–78	61–71	90		
Microfibrillar angle	10	6	20	8			
Density	1,400–1,540	1,070–1,480	1,330–1,450	1,370–1,460	1,500–1,600		
Longitudinal modulus of elasticity	12,000–85,000	30,000–70,000	9,000–38,000	10,000–30,000	5,500–13,000	5,000–16,000	7,000
Tensile strength	600–2,000	380–900	350–700	383–800	287–597	200–650	600
Elongation at break	1–4	1.6–2.7	2–14	1.5–2	3–10	15–18	30
Moisture regain	7	8	11	12	8–25		

• **Example: Characteristics of a Pultruded Unidirectional Flax/Polyester**

	Fiber Volume Fraction, V_f (%)	Density, ρ (kg/m ³)	Tensile Longitudinal Elastic Modulus, E (MPa)	Coefficient of Thermal Conductivity, λ (W/m °C)
Flax/unsaturated polyester resin	60	1,400	35,000	0.3

3.8.2.2 Biodegradable Matrices

After manufacturing, it becomes impossible for a composite to dissociate reinforcement and matrix. So for a complete recycling, the use of natural fibers as part of a composite respectful of the environment must be associated with a biodegradable matrix, that is to say a biopolymer.

Some examples of biopolymers (biodegradable resins) today are as follows:

- Biopolyethylene high density (HDPE)
- Biodegradable polyester: polycaprolactone (PCL)
- Biodegradable polyester: polylactic acid (PLA)
- Thermoplastic starch derived: **Mater-bi®**

Example: Biodegradable Composite *Hemp/Resin*

Table 3.13 shows the mechanical characteristics of the resins given earlier, pure and reinforced by short hemp fibers.

3.8.3 MANUFACTURING PROCESSES¹⁹

3.8.3.1 With Thermosetting Resins

- Contact molding (polyester)
- SMC (flax/polyester)
- Compression molding (cotton/polyester)
- Filament winding (jute/polyester)
- Pultrusion (jute/vinylester)
- RTM (hemp/phenolic resin)

TABLE 3.13

Mechanical Characteristics of Biodegradable Composite *Hemp/Resin*

Biodegradable Composite	Tensile Longitudinal Elastic Modulus		Tensile Strength	
	$V_f = 0\%$ (Pure Resin) E (MPa)	$V_f = 30\%$ Multiplication Factor	$V_f = 0\%$ (Pure Resin) $\sigma_{rupture}$ (MPa)	$V_f = 30\%$ Multiplication Factor
Volume Fraction of <i>Hemp</i> (Short Fibers)				
Resin				
HDPE	750	×2.8	22	×1.13
Biodegradable polyester: PCL	375	×5.7	17	×1.43
Biodegradable polyester: PLA	3,250	×2.3	70	×1.06
Thermoplastic starch derived: Mater-bi®	225	×7.7	12	×1.83

3.8.3.2 With Thermoplastic Resins

- Injection molding (hemp/acrylonitrile-butadiene-styrene “ABS” resin)
- Pultrusion (flax/PP resin), TRE (flax/PE resin)
- Extrusion (hemp/PVC resin)
- **Examples**
 - *Nonwoven mats* (50% of hemp fiber+50% of polymer fiber): They are made up by the needling of nonwoven laps and are then thermoformed
 - *Compounds* reinforced with hemp fiber (30% of hemp fibers+70% of polymer): They are used in injection molding

There are numerous applications in the areas of building, infrastructure, furniture, navigation, sports and recreation, and especially in the automotive industry (see Chapter 8).

3.9 NANOCOMPOSITE MATERIALS

These terms refer to composite materials with polymer matrices for the most; they are mechanically more resistant than the matrix but offer other significant benefits in terms of resistance to fire, electrical, optical, and surface properties.

3.9.1 NANOREINFORCEMENT

A material is called nanocomposite when at least one of the dimensions of the reinforcement is less than 100 nm: it is then called nanoreinforcement.

3.9.1.1 Nanoreinforcement Shapes

Figure 3.26 illustrates the typical geometrical shapes of nanoreinforcements.

Using the term **nanocomposite material** to describe any addition of adjuvants in a polymer should be avoided, although some may be of nanosize. In fact, in a nanocomposite, the association **matrix + nanoreinforcement** is specific: the interest is to make the best of atoms of the nanoparticles.

For example, consider a compact spherical cluster of atoms, of radius r , as described in Figure 3.27. The surface/volume ratio of this cluster is

$$\frac{4\pi r^2}{\left(\frac{4}{3}\right)\pi r^3} = 3 / r$$

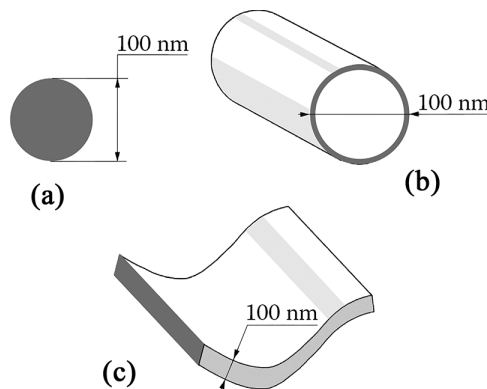


FIGURE 3.26 Geometrical shapes of nanoreinforcements: (a) grain (nanoparticle), (b) tube (nanowire or nanofiber), and (c) lamellae or layer (nanoplatelet).

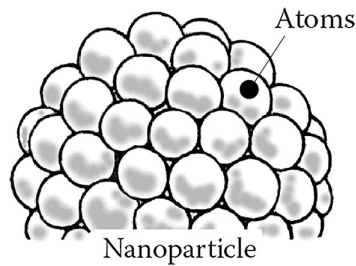


FIGURE 3.27 Spherical cluster of atoms.

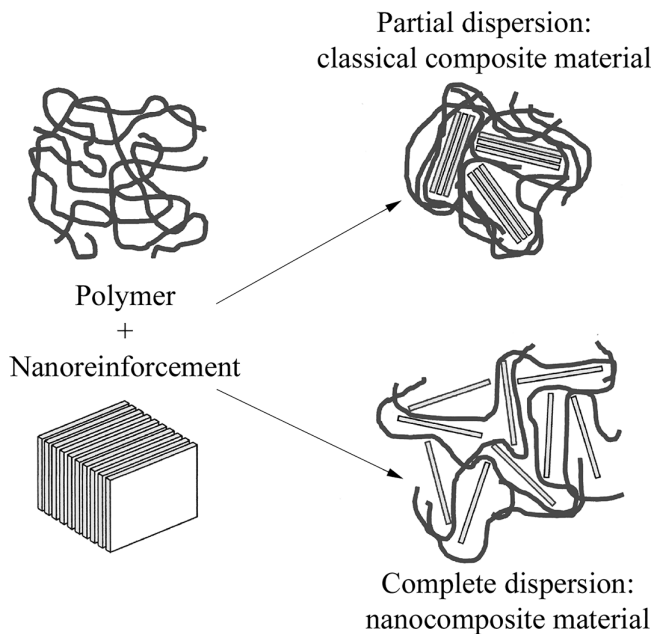


FIGURE 3.28 Dispersion of nanoreinforcement.

We see therefore that this ratio increases when the cluster size decreases, which means that an increasing number of atoms of the cluster are exposed to the external environment. Thus, when the size of the cluster is of the order of the nanometer, the number of cluster atoms exposed exceeds 90%.

It then comes to take full advantage of the **connection** of this available atom **surface** with a matrix, polymer, for example. We can see in Figure 3.28 that the quality of this bonding is characterized by a **degree** of dispersion of the nanoreinforcements. When this dispersion becomes complete, the interactions at the atomic level become more complex than for the interfaces **matrix-reinforcement** of conventional composites. Such a mechanism can significantly improve some of the properties of the created products.

Although we are most interested in structural applications of nanocomposite materials, we will also consider the other types of applications, important and diverse.

3.9.1.2 Properties of Nanoreinforcements

- **Grains or nanoparticles**

They are often of spherical shape (solid or hollow spheres) of a few nanometers to 100 nm in diameter.

The use of such particles is not recent. As old nanoparticles can be considered silica, carbon black, and nanocalcium carbonate, which is classical mineral filler in many applications, where it is often associated with PVC matrix. This allows to increase the modulus of elasticity, the flexural strength, and to strengthen the dimensional stability. The chemical compounds available today leading to nanoparticles are numerous (about 150) and are involved in a broad variety of applications. As seen before concerning the advantages of exposition of the nanoparticle atoms to the external environment, it is of interest to be able to define an **outer mean surface area of nanoparticles** expressed in m^2/g . To evaluate such a surface, one of the techniques consists of measuring a specific surface area referred as **B.E.T.**²⁰ Some of these measurement values are given in Table 3.14.

- **Lamellae or nanosheet or nanoplatelet**

- *Silicates*: They include nanosheets of clay, nanosheets of mica (aluminum silicate, potassium silicate) having the form of lamellae of a few nanometers in thickness, with a ratio in both others directions greater than 25. For example, the most used is the **montmorillonite**, a lamellar aluminosilicate characterized by nanometer-sized thickness.
- *Graphene*: Consisting of carbon atoms, it is the unique case of 2D crystal. Its atoms are arranged in hexagons like a honeycomb and form a planar molecule of the thickness of a single carbon atom, that is, 0.1 nm. As an example, when sheets are stacked one on top of the other, we obtain the graphite of a pencil lead. Figure 3.29 shows a graphene sheet. The available processing methods provide stacks of sheets, for example,

TABLE 3.14
Some Values of B.E.T.-Specific Surface Area

Nanoparticle	B.E.T.-Specific Surface Area (m^2/g)	Average Grain Size (nm)
Carbon black	24	
Carbon particles	60–100	45
Titanium silicate	95	20
Titanium dioxide	50–250	6–30
Alumina silicate	215	
Alumina	20–70	7–13
Tin–silver alloy	5	<150
Calcium carbonate	>25	80–100

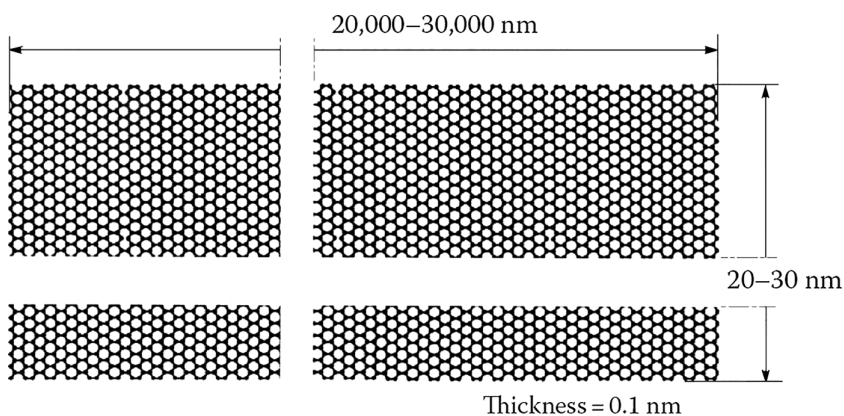


FIGURE 3.29 Graphene sheet.

TABLE 3.15
Some Mechanical Properties of Nanosheets

	B.E.T.-Specific Surface Area (m ² /g)	Longitudinal Modulus of Elasticity (in the Plane of Sheet), <i>E</i> (MPa)	Shear Modulus (in the Plane of Sheet), <i>G</i> (MPa)	Poisson Ratio, <i>ν</i>	Tensile Strength, σ_{rupture} (MPa)	Elongation at Break, <i>A</i> (%)
Aluminosilicate (montmorillonite)	800					
Graphene sheet	2,600	1,000,000	40,000	0.16	130,000	20
Stack of graphene sheets (<5)	640	500,000			100,000	

from two to several tens of sheets. It is worth noting that the absence of defects on the sheet of the crystal makes the latter the most resistant of all materials, as can be seen in Table 3.15.

- **Nanotubes, nanowires, nanofibers**

- *Nanotubes*: They include carbon, alumina, clay, and tungsten disulfide. The presence of carbon nanotubes improves
 - The electrical and thermal conductivity
 - The mechanical properties
 - The thermal withstand and the fire resistance

Figure 3.30 shows the structure of a single-wall carbon nanotube.

- *Nanowires*: Carbide silicon, silicon nitride, and carbon
- *Nanofibers*: Polyester, silicon with diameter <100 nm and slenderness (length-to-diameter ratio) $\ell / \phi > 100$, and fibrous clays

A few geometrical characteristics of nanofibers can be found in the following:

	Diameter (nm)	Length (μm)	B.E.T.-Specific Surface Area (m ² /g)
Aluminum nanofiber	10	160	
Single-wall carbon nanotube	1–2	1–1,000	1,000
Multiwall carbon nanotube	8–50	1–1,000	
High-strength carbon fiber (HR) (see Section 1.6)	7,000		

Table 3.16 compares the mechanical and thermal properties of carbon nanotubes to other types of reinforcements already cited in Section 1.6.

3.9.2 NANOCOMPOSITE MATERIAL

Nanocomposite materials with polymeric matrices (thermoplastics, thermosets, and elastomers) are reinforced by small amounts of nanoparticles (less than 5% by mass) having a high shape

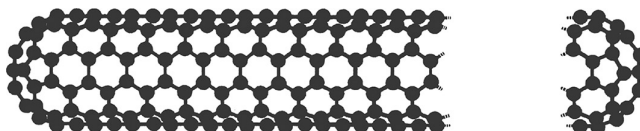


FIGURE 3.30 Carbon nanotube.

TABLE 3.16
Comparative Mechanical and Thermal Properties of Carbon Nanotubes

	Density, ρ (kg/m ³)	Longitudinal Modulus of Elasticity, E (MPa)	Poisson Ratio, ν	Tensile Strength, σ_{rupture} (MPa)	Elongation at Break, A (%)	Coefficient of Thermal Conductivity 20°C, λ (W/m °C)
Single-wall carbon nanotube	1,300–2,000	1,000,000	0.25	100,000	10	2,000
Multiwall carbon nanotube		700,000		100,000		2,000
High-strength carbon fiber (HR)	1,750	230,000	0.3	3,200	1.3	200
High-modulus carbon fiber (HM)	1,800	390,000	0.35	2,500	0.6	200
Glass (R)	2,500	86,000	0.2	3,200	4	1
Glass (E)	2,600	74,000	0.25	2,500	3.5	1
Kevlar® 49	1,450	130,000	0.4	2,900	2.3	
Steels	7,800	205,000	0.3	400–1,600	1.8–10	
Copper	8,800	125,000	0.3	200–500		380

factor $(\ell / h) > 300$. The optimum interaction between polymer matrix and nanoparticles may result in an increase of mechanical properties similar to what one would observe with a mass content M_f ten times higher with conventional fillers such as talc or mica, as shown in Table 3.17.

TABLE 3.17
Comparative Mechanical Properties of Nanocomposites

	Volume Fraction of Nanoreinforcement, V_f (%)	Mass Fraction of Nanoreinforcement, M_f (%)	Increase in Longitudinal Modulus of Elasticity, E (%)	Increase in Tensile Strength, $\sigma_{\text{rupt.}}$ (%)	Increase in Elongation at Break (A (%)) (%)
Nanosheets aluminosilicate/ polyamide matrix	2–5		70 (at 23°C); 220 (at 120°C)	40 (at 23°C); 20 (at 120°C)	
Nanosheets aluminosilicate/ polypropylene matrix		2.5 6	60 80		
Nanosheets aluminosilicate/poly (methyl) methacrylate matrix		2.5 5	40 38	0 0	
Nanosheets aluminosilicate/ polyethylene matrix		3	14	0	35
Carbon nanotubes/ epoxy matrix		4 0.1	100 3	50 14	
Nanosheets graphene/ epoxy matrix		0.1	30	40	

Today, the polymer matrix nanocomposites are the most common because their manufacturing processes are under better control. A few examples of applications in use or in development are shown hereafter.

3.9.3 MECHANICAL APPLICATIONS

3.9.3.1 Improvement in Mechanical Properties

These include stiffness, mechanical strength, abrasion resistance, and impact strength.

- Since a long time ago, the gum of the tires is strengthened by the addition of black carbon and for more than 15 years by the addition of nanoparticles of silica SiO_2 , about 2 kg per tire: what is known as **green tire**.
- Aircraft parts (secondary structure).

Example: The fighter aircraft **F-35 Lightning II/Lockheed Martin** (US) uses wing tips of epoxy resin reinforced by carbon nanotubes (price divided by 10 compared to that of the original carbon fiber reinforcement).

- Electric conductors are made of extra-reinforced materials for nondestructive coils, allowing the production of high-pulsed magnetic fields close to 100 Tesla and of long duration. The Lorentz forces on electric conductors generate mechanical stresses, able to lead to yielding or even to rupture of the coils. Nanocomposite conductors made of niobium nanofilaments with copper matrix have a high mechanical resistance, high electrical conductivity, and a very good deformability: $\sigma_{\text{rupture}} = 1,900 \text{ MPa}$ at 77°K for an electrical conductor of 5 mm^2 section that contains 30% of niobium distributed in the form of 52×10^6 of 140 nm diameter fibers. This strength value reveals a significant difference compared to the results of the law of mixtures (see Section 3.3.2), which is due to the nanosize of fibers.
- Aeronautical-panels-reinforced carbon: In addition to the enhancement of mechanical properties such as the improvement of impact resistance, the dispersion of carbon nanotubes in a polymer matrix allows that a low current applied heats the nanotubes. This is allowing the use of a thermographic camera to detect a defect.
- The introduction of carbon nanotubes in an adhesive provides monitoring of conduction in the nanocomposite material. To do this, the principle of **percolation** is involved. The material is defined statistically as a system consisting of a network of a large number of objects that can be linked together. The conductance is either possible or impossible depending on the number of objects and connections: There is a precise transition threshold (or percolation threshold) between those two regimes.
- To detect excessive deformation of wind turbine blades, sensors located in sensitive regions use the same resin as that of the blade, with addition of carbon nanotubes. The continuity of the deformable network of nanotubes provides a conductance sensitive to deformation, analog of a **piezoresistive** property.
- Improvement of the mechanical resistance of bonded joints is achieved by dispersing nanoparticles of alumina in epoxy resins.
- Improvement of the mechanical resistance of ceramics is obtained by dispersion of nanoreinforcements: they become stronger and more ductile than traditional ceramics.

3.9.3.2 Further Examples of Nonmechanical Applications

- As noted earlier, one may **improve the electrical conductivity** of a matrix. Insertion of carbon nanotubes can render it conductive. Another example of its application is as follows:
 - Electrostatic paint: dissipation of static electricity of some equipment
- **Improvement of coating properties** using dispersion of carbon nanotubes:
 - Coatings absorbing radar waves (stealth technology)

- **Improvement of chemical properties:** Dye affinity
- **Improvement of thermal properties** such as thermal conductivity, heat resistance, or fire resistance (fireproof quality): in case of fire, the introduction of nanosheets of clay in a polymer matrix decreases the rate of heat release and reduces the speed of propagation of the fire
- **Improved barrier properties:** Ability to retain some molecules (liquids or gases) by adding small amounts of clay in the starting material:
 - Reduction in the permeability of film coating for food packaging
 - Coating of tennis balls
- **Improvement of optical properties** such as light absorption capacity, fluorescent emission, and transparency: nanoparticle introduction provides nanocomposite polymer/mineral fillers, which are transparent to visible light. This eliminates the light scattering and can also bring new properties to the thus achieved transparent material:
 - The inclusion of clay in thermoplastic films increases their transparency
 - Luminescent nanoparticles are used in the production of certain types of screen
 - Metallic pigments added in paints or in pottery (is quite well known from ancient times)
- **Improvement of the UV resistance:** nanoparticles of titanium and zinc oxides are used as anti-UV additives because they have a large absorption range of the UV spectrum without affecting the transparency from the polymer matrix
- Titanium dioxide is also used for the manufacture of **self-cleaning surfaces**

3.9.4 MANUFACTURING OF NANOCOMPOSITE MATERIALS

While manufacturing a nanocomposite material, it is essential to ensure a homogeneous distribution of the nanoparticles in the material, that is, to avoid particles to congregate in clusters, which would result in loss of all the expected properties. Manufacturing techniques vary depending on the nature of the matrix (polymer, ceramic, metal) and on that of nanoreinforcements. The following can thus be found:

- Direct mixture of nanoreinforcements with the starting material that has been melted in advance (ex situ manufacturing)
- The incorporation of nanoparticles in a matrix that has been priorly dissolved in a solvent
- Direct growth of the nanoreinforcements within the matrix by chemical reactions (in situ manufacturing)

For polymeric matrices, the manufacturing processes require action at the level of the polymer/nanoparticle interfaces to ensure the dispersion of nanoparticles: grafting of compounds onto the surface of the nanoparticles; introduction of ions, so-called organophilic; and introduction of graft polymers. Nanocomposites with polymer matrices are marketed as semi-finished products called **nanocomposite compounds**. They can be formed as classical composite compounds (see Chapter 2). The parts are obtained by injection, extrusion, and blow molding.

Note: Toxicity of nanocomposite materials

The nanometric size of reinforcements provides them the ability to

- Reach the deep ramifications of the respiratory tract (see Figure 3.31)
- Cross biological barriers, such as cell membranes
- Increase the reactivity of some usually inert materials, which can thus become chemically active

Numerous studies are underway in order to assess relevant physicochemical factors (chemical, size, surface, shape, potential contaminants, etc.) and control the risks.

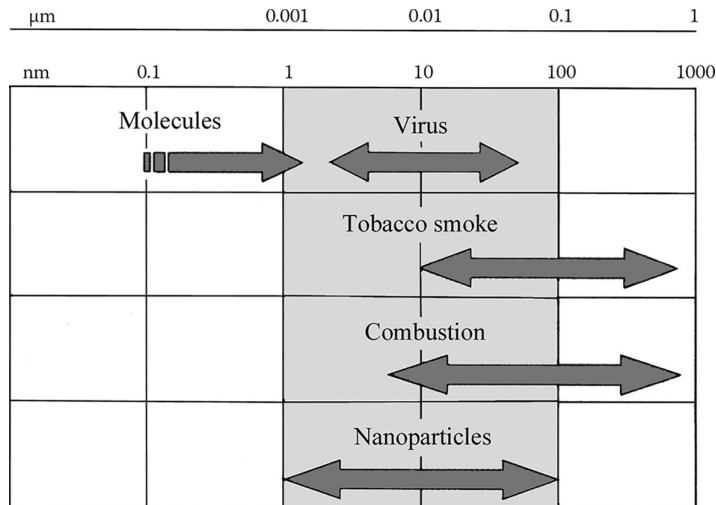


FIGURE 3.31 Sizes of particles.

3.10 TESTS

The relations cited on the previous sections in order to evaluate elastic moduli and Poisson coefficients of composites allow obtaining only an order of magnitude for these mechanical properties. Some of these relations are not quite reliable, particularly for the shear modulus. Also, these properties are very sensitive to the fabrication conditions. It is therefore essential for the design office to have access to the results provided by the suppliers concerning the reinforcements and the matrices or even better to the results obtained after carrying out laboratory tests on coupon specimens. They provide the moduli, Poisson ratios, and strength values. The field of composite testing is vast and obeys many standards: tensile test, bending test, shear test, shock test... Only three examples are cited below for illustrative purposes.

Examples:

- **Tensile test**

The tensile test (ASTM D3039, NF T51-034) on the specimen in Figure 3.32, instrumented with electrical strain gauges, allows the measurement of the strength and the elongation at break.

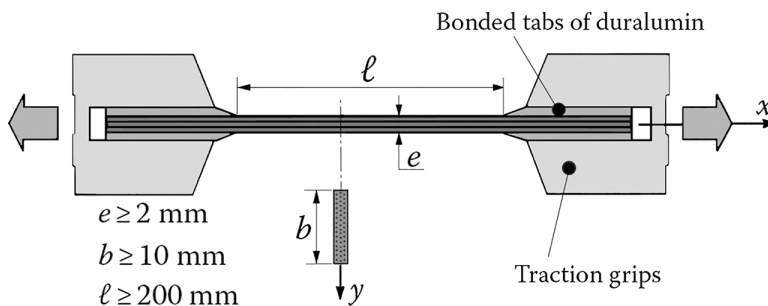


FIGURE 3.32 Tensile test.

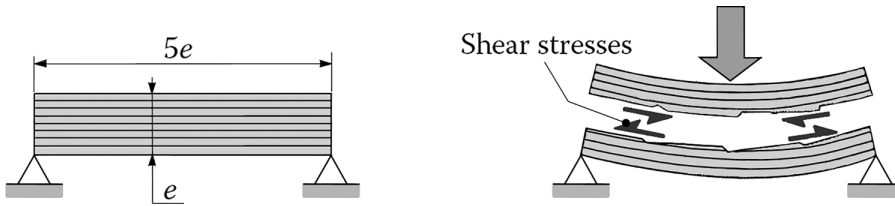


FIGURE 3.33 Short beam shear test.

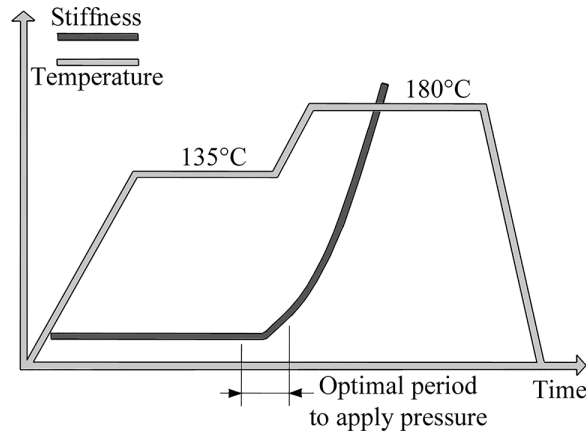


FIGURE 3.34 Stiffness evolution during curing.

- **Delamination test**

The test (NF T57-104) is performed with a specimen having a low slenderness, that is, a short beam, working in bending (see Figure 3.33). The breakage is caused by delamination under the effect of bending stresses and particularly of interlaminar shear stresses. One can thus obtain the interlaminar shear strength²¹.

- **Control of fiber volume fraction**

Further testing is very useful for the manufacture of high performance composites. This is the case in particular for the control of fiber volume content in the matrix. Indeed, during the phase of polymerization under pressure of a fiber/resin composite (see Chapter 2), the resin flows in an absorbent fabric in varying amounts depending on the adopted working pressure cycle compared to the temperature cycle over time. The fiber volume fraction V_f varies accordingly, as well as the dimensional characteristics of the part (thickness). To avoid these leaks of resin, one is brought to assess by means of testing the optimum point in time for pressurization of the installation. This is done by measuring the evolution over time of the bending stiffness of a sample (see Figure 3.34).

NOTES

- 1 In these equations, ϵ_x , ϵ_y , and γ_{xy} are also the small strains (two normal strains and a distortion) that are obtained in a classical manner from the displacements u_x and u_y as $\epsilon_x = (\partial u_x / \partial x)$; $\epsilon_y = (\partial u_y / \partial y)$; $\gamma_{xy} = (\partial u_x / \partial y + \partial u_y / \partial x)$.
- 2 To obtain more development about this point, refer to Section 9.2 and Application 19.2 “Poisson Coefficient of a Unidirectional Layer”.
- 3 Refer to Section 13.2.

- 4 This conditioning is available **as is** on the market. It is called **prepreg**. It is also the case of the **SMC**. In addition to this type of conditioning, nonpreformed mixtures of short fibers and resin can also be found. They are called **premix** or **BMC**. See Section 2.3.
- 5 In fact, the reinforcement/matrix mixture also includes a small volume of voids not occupied by the matrix, characterizing a certain **porosity** of the composite. It would thus be more logical to write $V_m + V_f + V_p = 1$, in which V_p denotes the **porosity volume fraction**, with $V_p \ll 1$ (see Application 19.11 “Determination of Fiber Volume Fraction by Pyrolysis”).
- 6 This is due to the stretching of the carbon and Kevlar fibers during fabrication. This orients the chains of molecules.
- 7 Chapter 10 details the calculation leading to these estimations of the moduli E_ℓ , E_t , $G_{\ell t}$, $\nu_{\ell t}$.
- 8 The calculation of these moduli is shown in detail in Chapter 11.
- 9 Detailed calculation is shown in Section 14.3.
- 10 The values assigned in Table 3.4 can vary significantly depending on the manufacturing process.
- 11 For the calculation of these characteristics, see Section 12.1.2 and also Application 20.12 “Sailboat Hull in Glass/Polyester”.
- 12 Compare, for example, the tensile and compressive strengths in Table 3.6. Compare these values also on Tables 5.1, 5.6, and 5.11 of Section 5.4 by selecting proportions of 50% at 0° and 50% at 90°.
- 13 For more details, see Bibliography: Riley V.R./1990.
- 14 **AkzoNobel/DELFT University** (NL), **Fokker Aerostructures** (NL), **Structural Laminates Company**® (US), **Alcoa** (US).
- 15 Noninclusion of pandemic in this diagram.
- 16 Product of **Safran Group** (FR).
- 17 See Section 2.2.4.
- 18 This notion is shown in detail in Section 13.2.
- 19 For the meaning of acronyms, see Section 2.4.1 and Figure 2.23.
- 20 B.E.T. is the acronym of Brunauer-Emmett-Teller surface characterization (1938).
- 21 This is by using a simplified formula whose precision is insufficient in view of the complexity of the actual state of stresses due to the presence of concentrated forces that are closely spaced. For interlaminar shear stresses, see Chapter 18.

4 Sandwich Structures

The **sandwich** structures occupy an important place in the manufacture of composite parts. They appear in almost all application areas. Historically, these were the first composite structures both lightened and efficient¹. In most cases, they must be designed for a specific purpose. However, some types of sandwich materials are commercially available in the form of semifinished products. In this chapter, emphasis is given on the identification of key properties and the precautions for use of sandwich materials.

4.1 WHAT IS A SANDWICH STRUCTURE?

A sandwich structure results from the assembly by bonding – or welding – of two thin facings or skins on a lighter core that maintains a predetermined spacing between the two skins (see Figure 4.1).

4.1.1 THEIR PROPERTIES ARE SURPRISING

Particularly, noticeable are the following:

- **A very light weight.** As a comparison, the mass per unit area of the dome of Saint Peter's Basilica in Rome (45-m diameter) is 2,600 kg/m², whereas the mass per surface area of a similar dome made of sandwich steel/polyurethane foam (Hanover) is only 33 kg/m².
- **A very high flexural rigidity** due to the distance between the surface skins, which increases the flexural moment of inertia.
- **Excellent thermal insulation properties.**



However, be careful:

- properties (no acoustic insulation).
- Some categories of cores have low fire resistance.
- The risk of **buckling by core crushing** is to be verified by appropriate sizing methods.

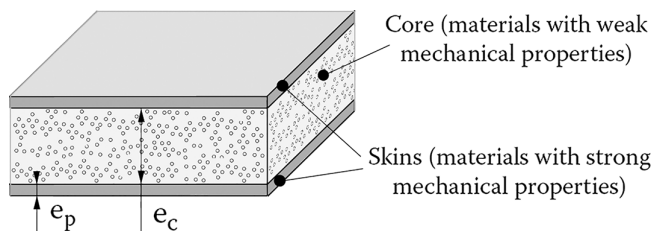


FIGURE 4.1 Sandwich structure: $10 \leq e_c/e_p \leq 100$.

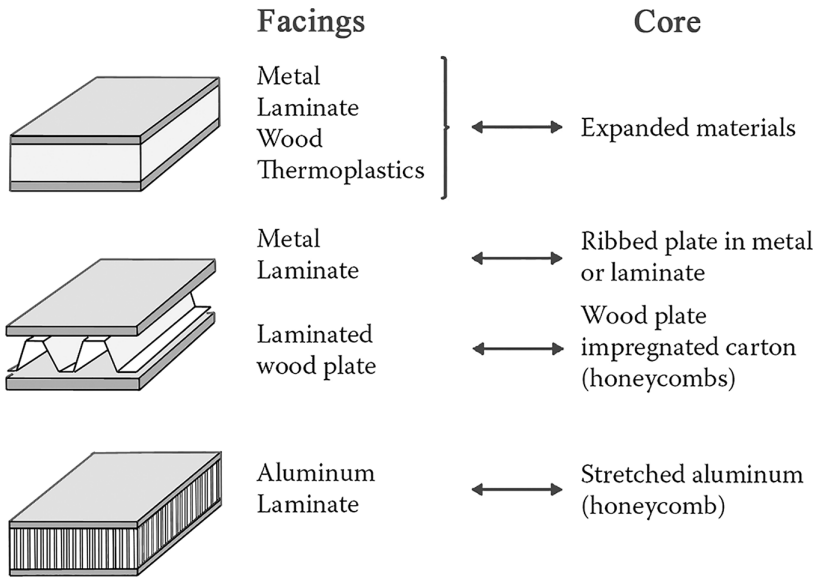


FIGURE 4.2 Constituents of sandwich materials.

4.1.2 CONSTITUENT MATERIALS

The skin materials can be from very diverse nature, while the core materials must be selected as light as possible. Figure 4.2 mentions some pairs of compatible materials to build a sandwich structure.



Be careful: Polyester resins attack polystyrene foams.

Assembly of the skins and the core is achieved by bonding with adhesives or directly with the resin impregnating the fibers of the skins. In some exceptional cases, the skins are welded on the core. The bonding quality is of course fundamental to obtain the best performance and durability of the sandwich part. In general,

$$0.025 \text{ mm} \leq \text{adhesive thickness} \leq 0.2 \text{ mm}$$

4.2 SIMPLIFIED FLEXURE

4.2.1 STRESS

In Figure 4.3, we highlight in a simplified manner the main stresses that arise when a sandwich beam is subject to bending². The beam is clamped at its left end and subjected to a transverse load T at its right end. We isolate an elementary slice dx of the sandwich beam and we magnify the deformation. Thus, we can observe on any cross section a **shear stress resultant T** and a **moment resultant M** according to the classical notations of **strength of materials**.

The shear force T is the result of a shear stress distribution τ . The bending moment M is the result of a normal stress distribution σ .

In order to evaluate σ and τ , the following simplifications can be suggested:

- The normal stress σ is assumed to occur only in the skins and is uniform across the skin thickness due to the thinness of the latter.

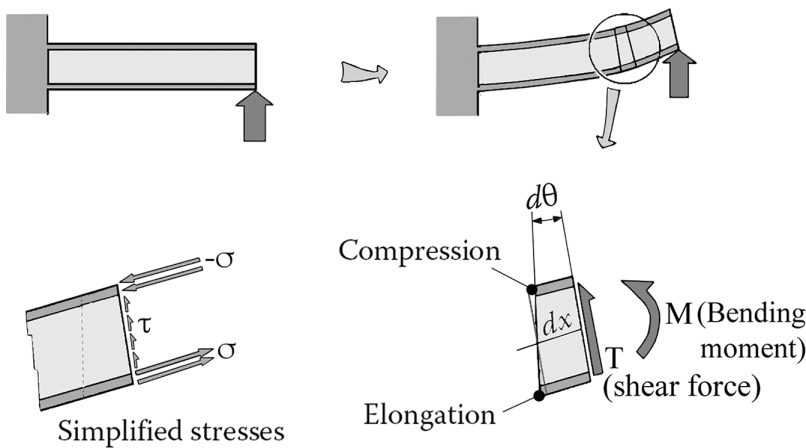


FIGURE 4.3 Flexure representation.

- The shear stress τ is assumed to occur in the core only and is uniform across the core thickness³.

We obtain, therefrom, immediately the approximative expressions shown in Figure 4.4 for σ and τ regarding a thin-skinned sandwich beam of unit width.

4.2.2 DISPLACEMENTS

4.2.2.1 Contributions of Bending Moment M and Shear Force T

Figure 4.5 illustrates a sandwich beam subjected to bending. Here, the deflection Δ is the consequence of

- The deformation due to the normal stress σ
- The deformation created by the shear stress τ

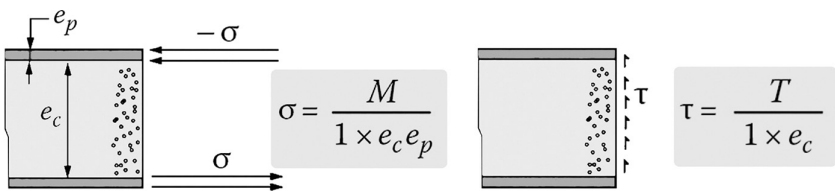


FIGURE 4.4 Stress in sandwich structure.

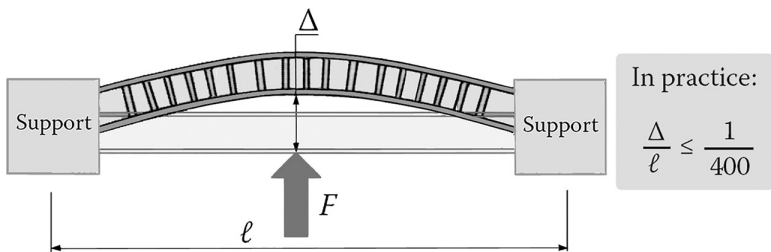


FIGURE 4.5 Sandwich beam under flexure.

To evaluate the deflection Δ we can, among other methods⁴, use the Castigliano theorem:

$$\begin{array}{c}
 \boxed{
 \begin{array}{l}
 W_{\text{elastic energy}} = \frac{1}{2} \int \frac{M^2}{\langle EI \rangle} dx + \frac{1}{2} \int \frac{k}{\langle GS \rangle} T^2 dx \\
 \begin{array}{cc}
 \text{contribution} & \text{contribution} \\
 \text{of bending} & \text{of shear}
 \end{array} \\
 \downarrow \\
 \Delta_{\text{deflection}} = \frac{\partial W(\text{energy})}{\partial F(\text{load})}
 \end{array}
 }
 \end{array}$$

Where the following notations⁵ are used for a beam of unit width

M is the bending moment

T is the shear force

E_p is the modulus of elasticity of the skins material

G_c is the shear modulus of the core material

$$\langle EI \rangle \approx E_p e_p \times 1 \times \frac{(e_c + e_p)^2}{2}; \quad \frac{k}{\langle GS \rangle} = \frac{1}{G_c (e_c + 2e_p) \times 1}$$

4.2.2.2 Example: A Cantilever Sandwich Structure

The cantilever sandwich structure in Figure 4.6 is treated as a sandwich beam hereafter.

Elastic energy is as follows:

$$\begin{aligned}
 W &= \frac{1}{2} \int_0^\ell \frac{F^2 (\ell - x)^2}{\langle EI \rangle} dx + \frac{1}{2} \int_0^\ell \frac{k}{\langle GS \rangle} F^2 dx \\
 W &= \frac{F^2}{2} \left(\frac{\ell^3}{3 \langle EI \rangle} + \frac{k}{\langle GS \rangle} \ell \right)
 \end{aligned}$$

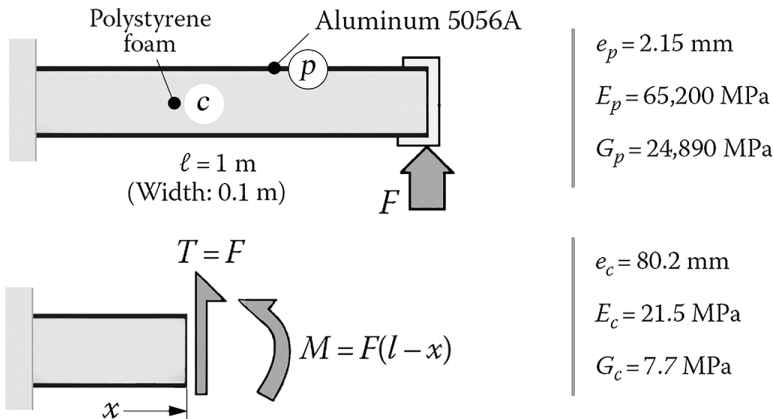


FIGURE 4.6 Cantilever beam.

where

$$\langle EI \rangle = 475 \times 10^2 \left(\text{N} \times \text{m}^2 \right); \quad \frac{\langle GS \rangle}{k} = 650 \times 10^2 \text{ (N)}$$

The end displacement Δ can be written as

$$\Delta = \frac{\partial W}{\partial F}$$

Then, for an applied load of 1 N,

$$\Delta = \underbrace{0.7 \times 10^{-2}}_{\text{flexure}} \text{ mm/N} + \underbrace{1.54 \times 10^{-2}}_{\text{shear}} \text{ mm/N}$$

Note: The share of displacement Δ due to shear appears much higher than that due to bending, whereas in the case of classical homogeneous beams, the shear displacement is very small and usually ignored. Thus, this is a specific property of sandwich structures. This notable difference in behavior has a considerable influence over the estimate of the bending deflections as well as on the stability as mentioned later.

4.3 SOME SPECIAL FEATURES OF SANDWICH STRUCTURES

4.3.1 COMPARISON OF MASS FOR THE SAME FLEXURAL RIGIDITY $\langle EI \rangle$

Figure 4.7 compares the mass of different sandwich structures for the same value of the flexural stiffness $\langle EI \rangle$. According to the note in Section 4.2.2.2, remember that this term only partly reflects the deformability under bending.

4.3.2 DETERIORATION BY BUCKLING OF SANDWICH STRUCTURES

The compression resistance of all or part of a sandwich structure is limited by the so-called critical values of the applied load, above which the deformations become large and uncontrollable. This phenomenon is called **buckling** of the structure (see Figure 4.8). Depending on the type of loading, one can distinguish different types of buckling, which can be global or local.

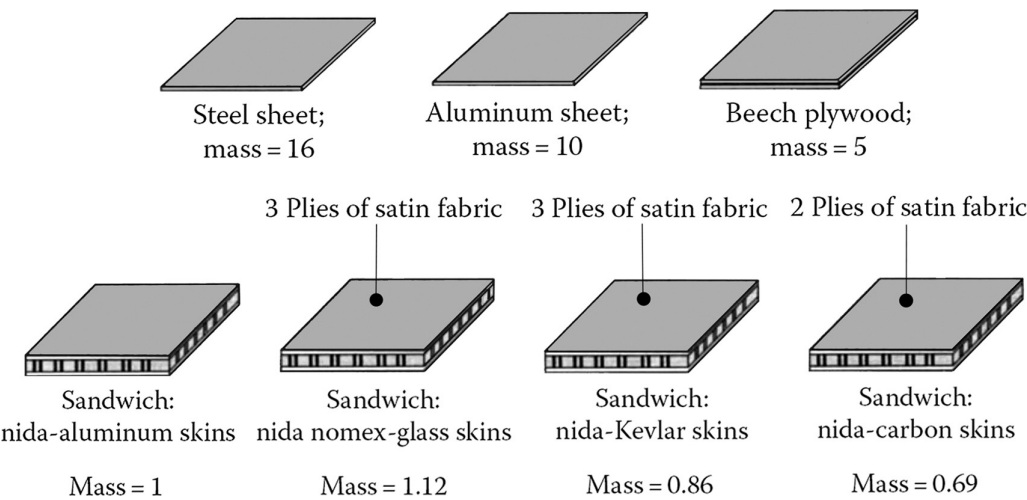


FIGURE 4.7

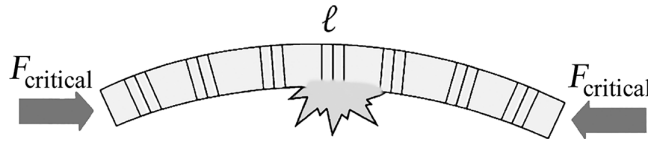


FIGURE 4.8 Buckling of sandwich structure.

4.3.2.1 Global Buckling

Following the geometry of the deformed shape, the critical buckling load F_{critical} is given⁶ by

$$F_{\text{critical}} = K \frac{\pi^2 \langle EI \rangle}{\ell^2 + \pi^2 \frac{\langle EI \rangle}{\langle GS \rangle} kK}$$



4.3.2.2 Local Buckling of the Skins

The skins are subject to buckling due to the low stiffness of the core. Depending on the type of loading, one can find the following modes of deformation:

- As shown in Figure 4.9, the critical compression stress in the skins is given in the following equation, where ν_c is the Poisson coefficient of the core (c identifies the core and p identifies the skins):

$$\sigma_{cr} = a \times (E_p \times E_c^2)^{1/3} \quad \text{with} \quad a = 3 \left\{ 12(3 - \nu_c)^2 (1 + \nu_c)^2 \right\}^{-1/3}$$

- As shown in Figure 4.10, the critical load F_{critical} shown causes local damage by local buckling of a skin.

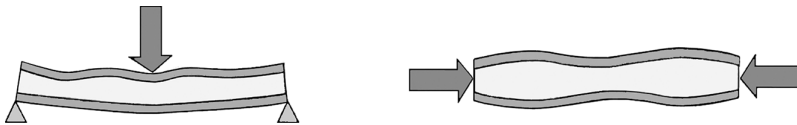


FIGURE 4.9 Local buckling of skins.

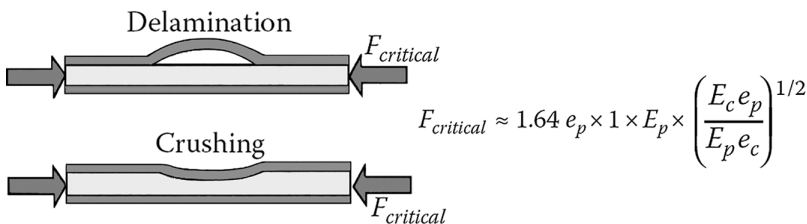
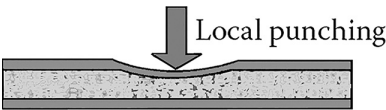


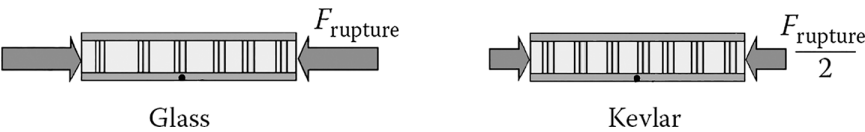
FIGURE 4.10 Damage by local buckling.

4.3.3 OTHER TYPES OF DAMAGE

- **Local punching:** This is the punching of the core material at the location of the load application (see the following figure).



- **Compression failure:** It should be pointed out in this case that the weak compression strength of Kevlar fibers⁷ leads to a compression breaking strength about two times less than for sandwich panels with analogous skins made from glass fibers (see the following figure).



4.4 MANUFACTURING AND DESIGN PROBLEMS

4.4.1 EXAMPLE OF CORE MATERIAL: HONEYCOMB

These widely available core materials are made up of hexagonal cells regularly spaced like that of a honeycomb of hive (by chance, some went as far as to adopt the same color!); hence, the name **honeycomb**. Such geometry is the result of a relatively simple manufacturing principle: thin sheets or foils are partially glued and stacked. Then, they undergo an expansion as shown in Figure 4.11. The honeycomb material can be metal (light alloy, steel) or nonmetal (carton impregnated with phenolic resin, polyamide sheets, or impregnated glass fabrics):

- Nonmetallic honeycombs are corrosion proof and are good thermal insulators.
- Metallic honeycombs are less expensive and more resistant but heavier than nonmetallic honeycombs.

Table 4.1 shows the mechanical and geometrical characteristics of a few current honeycombs, using the notations of Figure 4.11.

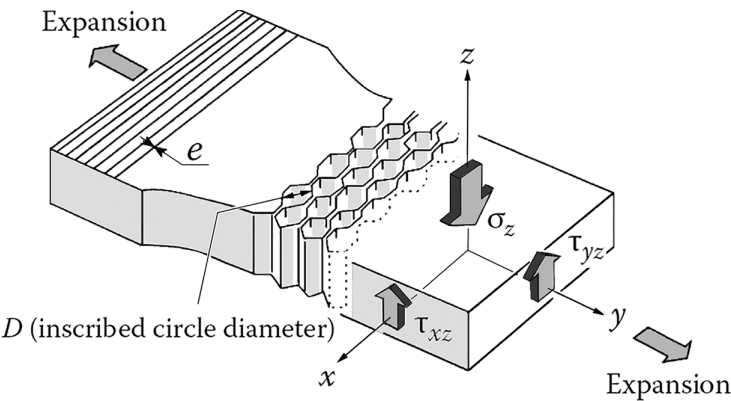


FIGURE 4.11 Honeycomb.

TABLE 4.1
Properties of Some Honeycombs

	Bonded Sheets of Polyamide: Nomex ^{®a}	Light Alloy AA5154A (5154A)	Light Alloy A92024 (2024)
Inscribed circle diameter, D (mm)	5	4	6
Thickness, e (mm)	0.08	0.05	0.04
Specific mass (kg/m ³)	64	80	46
Shear strength, $\tau_{xz\text{rupture}}$ (MPa)	2.5	3.2	1.5
Shear modulus, G_{yz} (MPa) $\approx 1.5 \times G_{\text{mat}} \times (e/D)$	70	520	280
Shear strength, $\tau_{yz\text{rupture}}$ (MPa)	1.1	2	0.9
Shear modulus, G_{yz} (MPa)	35	250	140
Compression strength, $\sigma_{z\text{rupture}}$ (MPa)	3.8	4.4	2

^a Nomex[®] is a product of Du Pont de Nemours (US).

4.4.2 SHAPING PROCESSES

4.4.2.1 Machining

The **machining** of honeycomb-shaped panels is done with a diamond disk (peripheral speed in the order of 30 m/s). The honeycomb is held on the machine table by an aluminum sheet to which it is bonded. The aluminum sheet is kept on the table by a vacuum (see Figure 4.12).

4.4.2.2 Deformation

To achieve the **deformation** of the honeycomb, it is important to keep it firmly in place, because the natural deformation behavior is complex. For example, a honeycomb panel under cylindrical bending shows two reverse curvatures as illustrated in Figure 4.13⁸.

4.4.2.3 Some Other Considerations

- The shaping process is facilitated by the **overexpansion** ability of the honeycomb, which changes the shape of the hexagonal cells as shown in Figure 4.14.
- For the limitations of the curved shape, see Figure 4.15, where R is the radius of the curve and e is the thickness of the sheet that constitutes the honeycomb.
- The schematic for the processing of a structural part of sandwich honeycomb is as in Figure 4.16.
- For moderate loadings (e.g., interior walls or bulkheads), it is possible to bend a sandwich panel following the schematic in Figure 4.17.

4.4.3 INSERTS AND ATTACHMENT FITTINGS

Their role is to transfer loads locally introduced to the overall structure. Depending on their level, it is convenient to distribute them over one or several inserts, as indicated in Figure 4.18⁹.

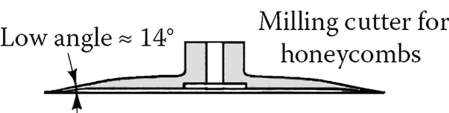


FIGURE 4.12 Machining of honeycomb.

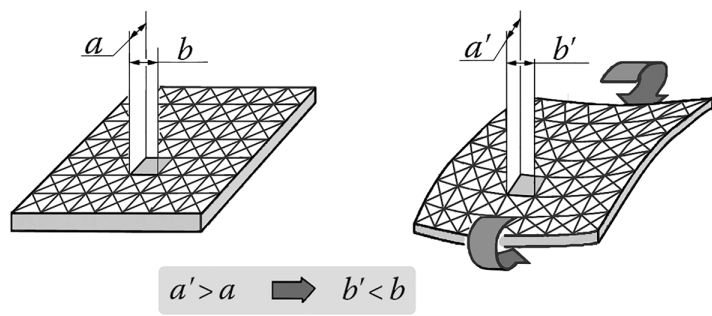


FIGURE 4.13 Deformation of honeycomb.

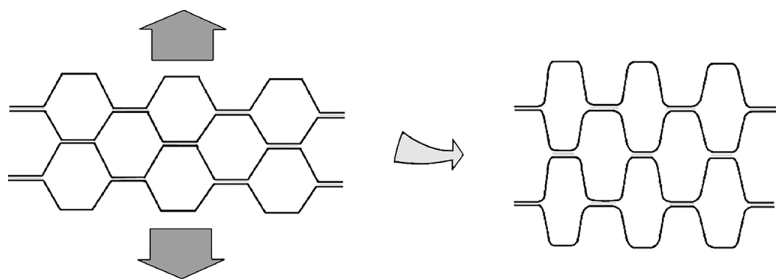


FIGURE 4.14 Overexpansion of honeycomb.

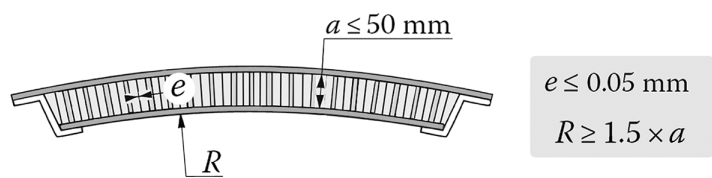


FIGURE 4.15 Curvature of honeycomb.

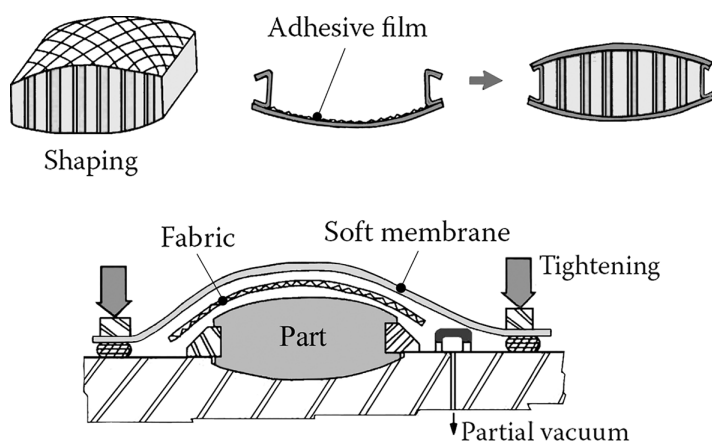


FIGURE 4.16 Processing of a sandwich structural part.

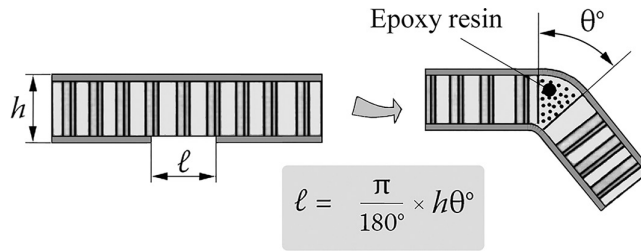


FIGURE 4.17 Bending a sandwich panel.

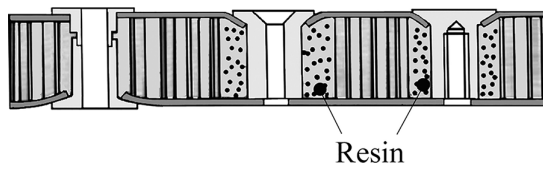


FIGURE 4.18 Inserts and attachment fittings.

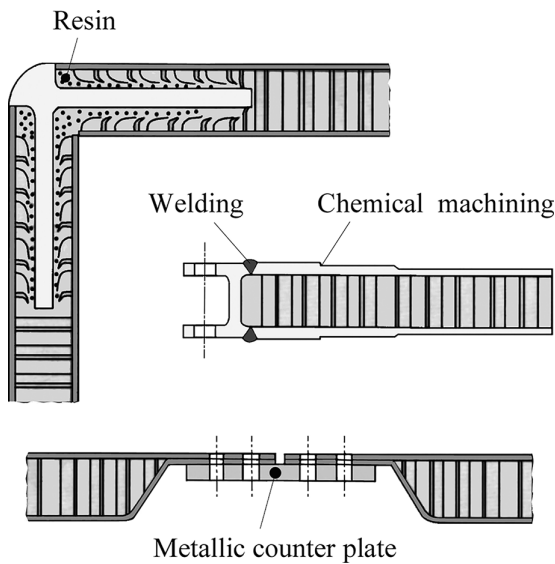


FIGURE 4.19 Some links for sandwich structures.

The filling resin of epoxy type, shown in Figure 4.18, can be made lighter by incorporation of phenolic microspheres with resulting density for the lightened resin of 700–900 kg/m³ and crush strength ≈35 MPa (see Figure 4.19).

4.4.4 REPAIR OF LAMINATED FACINGS

For sandwich materials of the type **honeycombs/laminates**, the repair of local damages is relatively easy. It involves the **patch-type** repair of the laminate. Depending on the care taken, and the speed in the execution, the configuration of the repaired area appears as in Figure 4.20.

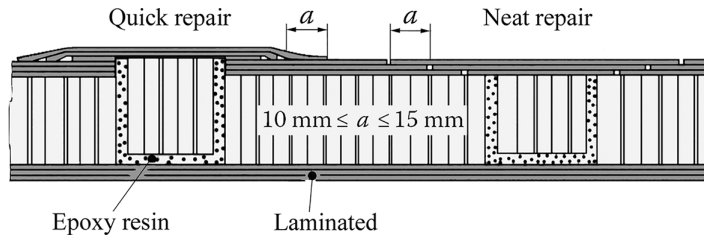


FIGURE 4.20 Repair of a sandwich panel.

4.5 NONDESTRUCTIVE INSPECTION

4.5.1 MAIN NONDESTRUCTIVE INSPECTION METHODS

Apart from using the classical methods for controlling the surface defects (e.g., dye penetrant test), which allow the identification of external delaminations of laminated facings, the following techniques allow the detection and identification of internal defects as a result of fabrication process or due to damage in service. These defects take commonly the following form:

- Imperfect bonding
- Delaminations
- Inclusions (foreign objects or voids)

The main Nondestructive Inspection methods are illustrated in Figure 4.21.

4.5.2 ACOUSTIC EMISSION TESTING

When a composite structure (e.g., a reservoir under pressure) is subjected to loading, various microcracks occur within the piece. Microcracking in the resin, fiber fracture, and disbond between fiber and matrix can occur even within the admissible loading range. These ruptures create acoustic waves that propagate to the surface of the piece. They can be detected and analyzed using **acoustic emission** (AE) sensors (see Figure 4.22).

The number of peaks as well as the duration and the amplitude of the signal can be used to indicate the integrity of the piece. In addition, the accumulated number of peaks may be used to predict the fracture of the piece (see the change in slope of the curve in Figure 4.23).

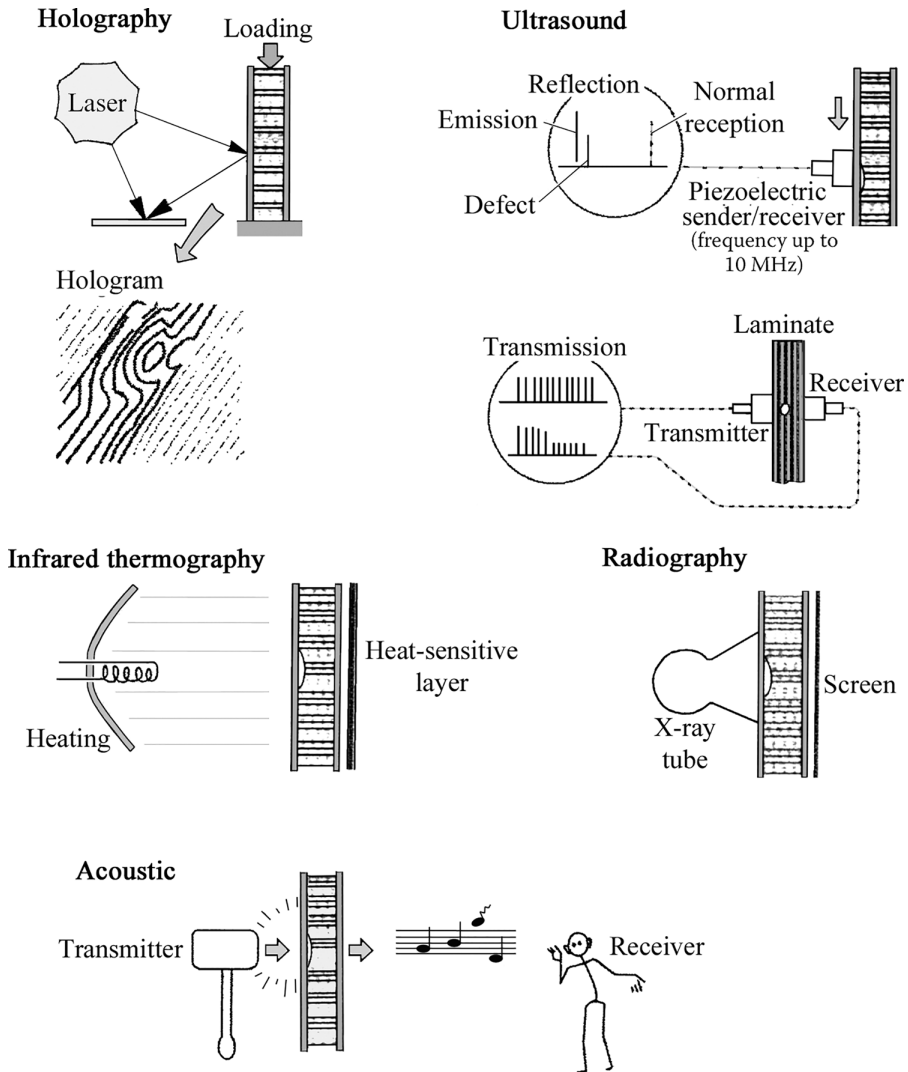


FIGURE 4.21 Main nondestructive testing methods.

(Continued)

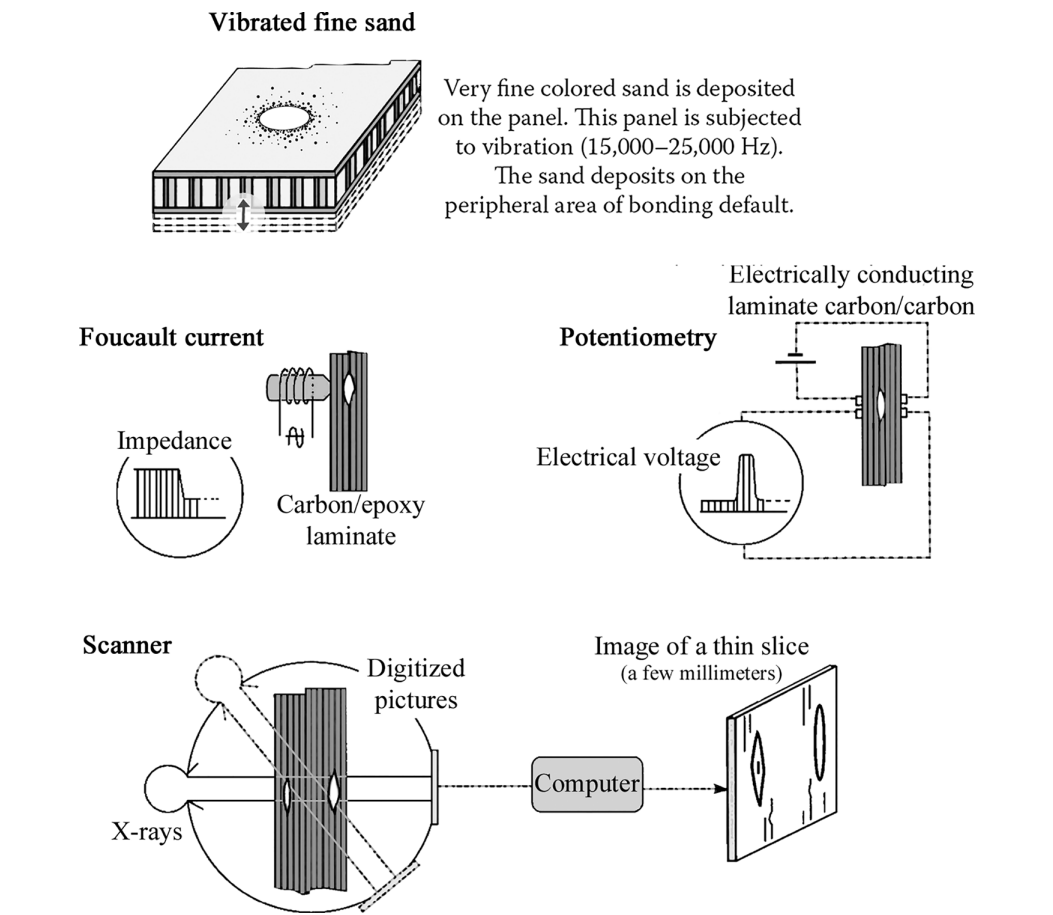


FIGURE 4.21 (CONTINUED) Main nondestructive testing methods.

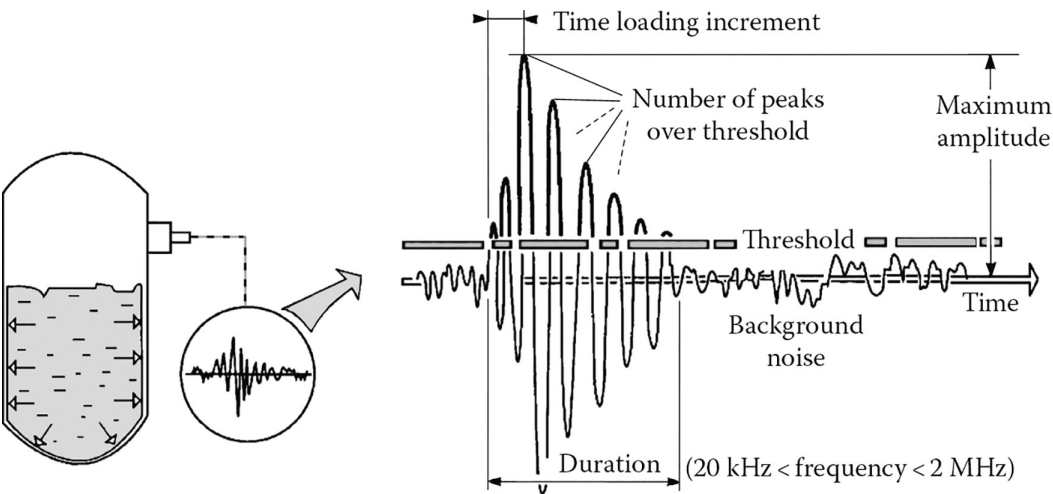


FIGURE 4.22 Acoustic emission (AE) testing.

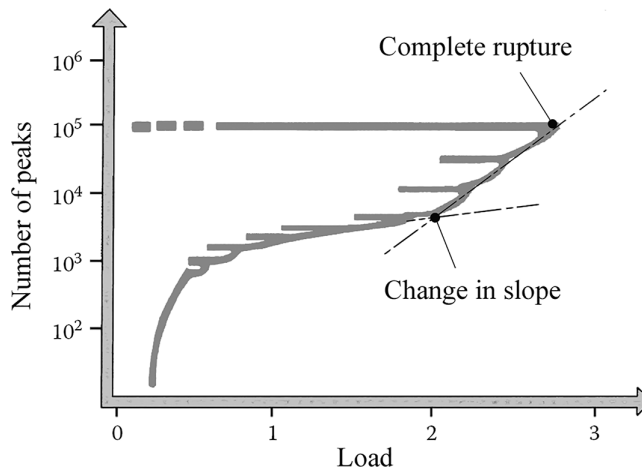


FIGURE 4.23 Plotting of AE events.

NOTES

- 1 See Section 7.1.
- 2 For a more detailed study concerning the bending of this type of structure, see Chapter 16 and Section 18.7.2. See also Applications 20.1, 21.5, and 21.11.
- 3 See Section 18.7.2 and Applications 20.1, and 21.5, for more accurate estimates of the stress distribution.
- 4 See Equation 16.16, which leads to consider this type of beam as a classical homogeneous beam. This enables to use the conventional notions of the strength of materials.
- 5 See Application 20.1 or Chapter 16.
- 6 See Application 21.4.
- 7 See Table 3.4.
- 8 This phenomenon is due to the Poisson effect, particularly noticeable here (see Section 12.1.4).
- 9 See Sections 6.2.4 and 6.3.

5 Conception

Design and Drawing

A different approach: As every mechanical component, a composite part has to fulfill the product specification. Beyond that, the composite design approach has to extend over a wider range than for a component made of **predetermined** classic material. In fact, the following applies:

- For isotropic materials, the conventional approach of the designer consists of the selection of an existing material and then of the sizing of the part thus constituted.
- For a composite part, the designer **builds** the material according to the needs defined by the functional requirements. The designer defines the following:
 - Reinforcement
 - Matrix
 - Forming process

Then follow, being the object of this chapter:

- The definition of the architecture of the part, that is, the arrangement of plies
- The pre-sizing and drawings

5.1 DRAWING A COMPOSITE PART

5.1.1 SPECIFIC PROPERTIES

The following properties must always remain present in the mind of the designer:

- Fiber orientation enables the optimization of the mechanical behavior along a specific direction
- The material is elastic up to rupture. It cannot relax following a local yielding as it would be the case with a classical metallic material
- Fatigue resistance is excellent

Note: A very good fatigue resistance.

Specific fatigue strength is defined as the ratio (σ/ρ), σ being the loading stress and ρ the density. For composite materials, this specific strength is three times higher than that of aluminum alloy and two times higher than that of high-strength steels and titanium alloys. This results from the fact that fatigue strength is equal to 90% of the static tensile strength for a composite instead of 35% for aluminum alloys or 50% for steels and titanium alloys (see Figure 5.1)¹.

- Coefficients of thermal expansion are not the same as that for metals (attention should be paid when joining metal to composite)
- Complex forms can be achieved by molding
- It is possible to reduce the number of parts and limit the machining
- The classical techniques must be adapted for the assemblies and fittings containing composite parts and must take into account their induced problems: local weakening, bearing, fatigue, and thermal stresses

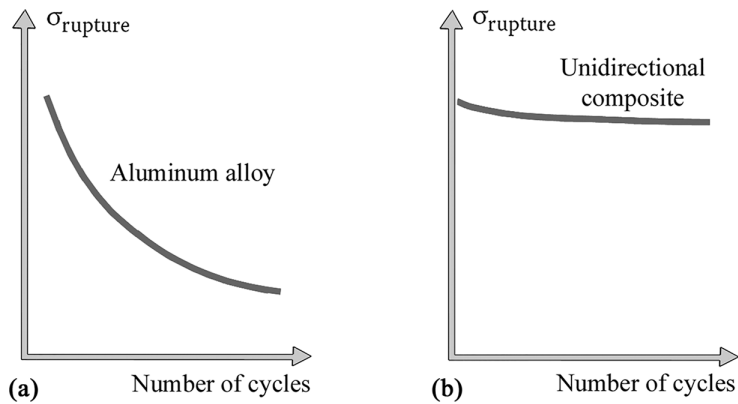


FIGURE 5.1 Comparison of fatigue behavior between (a) aluminum and (b) composite.

5.1.2 GUIDE VALUES OF PRE-SIZING

5.1.2.1 Material Characteristics

Material characteristics, which are compared in Figure 5.2, allow appreciating the potential benefit of a composite at the preliminary project stage.

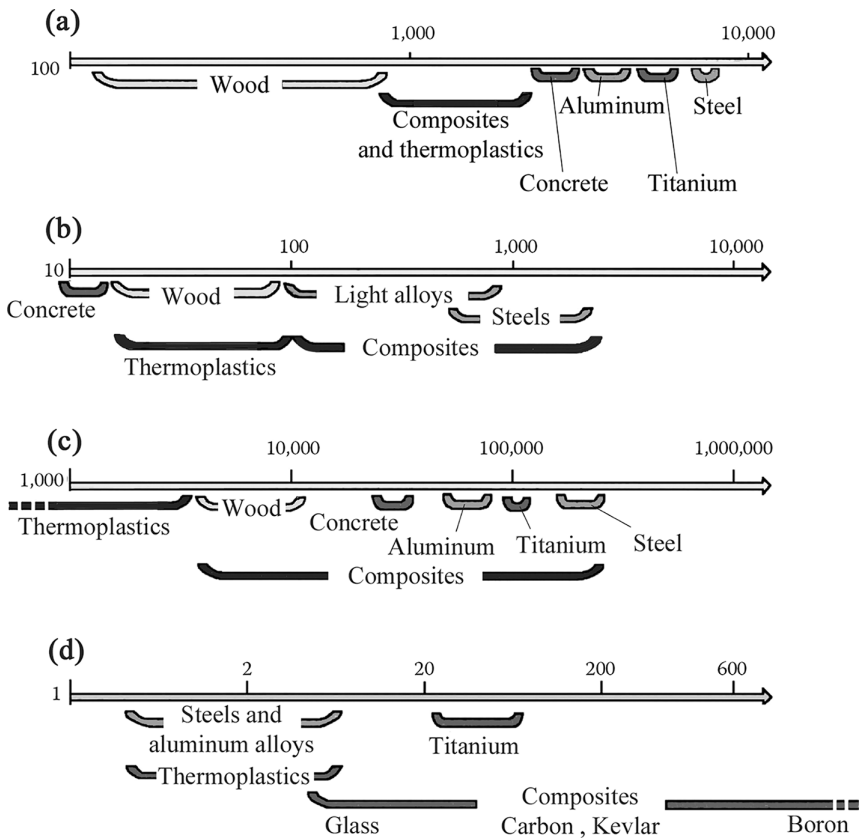


FIGURE 5.2 Comparison of characteristics of different materials: (a) density (kg/m^3), (b) tensile fracture strength (MPa), (c) modulus of elasticity (MPa), and (d) price per unit mass.

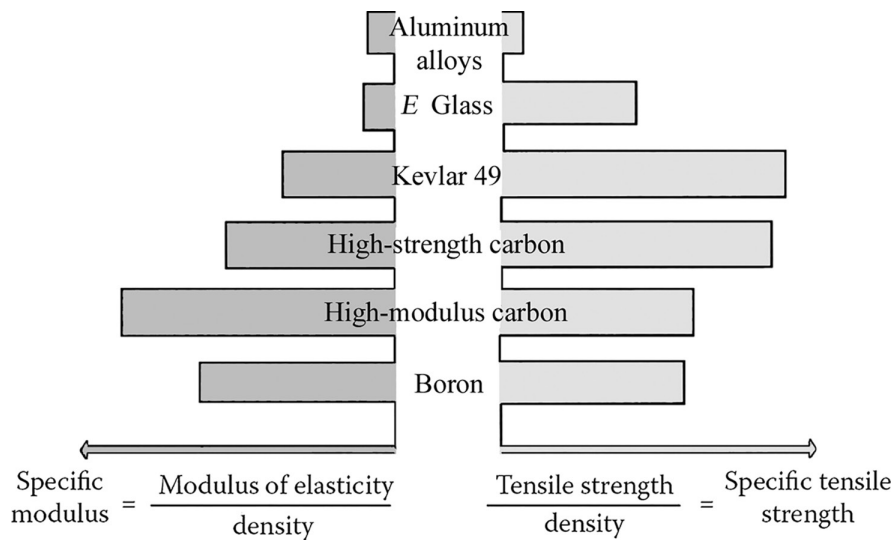


FIGURE 5.3 Specific characteristics of different fibers.

The graph in Figure 5.3 allows comparing the main specific properties of the fibers that constitute the plies, namely, the specific modulus and the specific strength whose definitions are shown. The reference to density makes it possible to bear in mind the performance–lightness correlation.

5.1.2.2 Design Factors

The design factors are defined to take care of uncertainties on

- The magnitude of mechanical characteristics of reinforcement and matrix
- The stress concentrations
- The imperfection of the hypotheses for calculation
- The fabrication process and the associated quality control level
- The aging of materials

The orders of magnitude of the design factors commonly used are as follows:

High-Volume Composites		
Static loading	Short duration	2
	Long duration	4
Intermittent loading over long term		4
Cyclic loading		5
Impact loading		10
High-Performance Composites		1.3–1.8

5.2 LAMINATE

The laminates result in the superimposition of several layers, or plies, or sheets, made of unidirectional layers or fabrics or mats, with for each ply its own orientation. This is the result of the **drap-
ing** or **lay-up** operation.

5.2.1 UNIDIRECTIONAL LAYERS AND FABRICS

5.2.1.1 Unidirectional Layer

Unidirectional layer in its original packing is shown in Figure 5.4.

The advantages of unidirectional layers are the following:

- After curing, they provide a high stiffness along the fiber direction.
- They allow the lay-up of long lengths: continuity of loads transmission is thus ensured.
- There is less offcuts.

The disadvantages of unidirectional layers are as follows:

- The lay-up sequence may be long, depending on its complexity.
- The lay-up cannot follow shapes with tight curves (risk of wrinkles)².

Example: Carbon/epoxy unidirectionals with a width of 300–1,000 mm, pre-impregnated with resin; usable over several months when stored at cold temperature (-18°C)

5.2.1.2 Fabrics

Fabrics are in the form of rolls, dry or pre-impregnated with resin (Figure 5.5).

The advantages of fabrics are

- Reduced lay-up time
- Possibility of manufacturing complex shapes using the deformability of the fabric
- Possibility to combine different types of fibers in the same fabric

The disadvantages of fabrics are

- Lower modulus and strength than for unidirectionals
- Larger amount of waste material after cutting
- Need of connections when manufacturing large parts

5.2.2 CORRECT PLY ORIENTATION

One of the fundamental advantages of laminates is their ability to adapt and control the orientation of fibers, so that the material can best resist to the loadings. It is therefore important to know how the plies contribute to the laminate resistance, taking into account their relative orientation with respect to the loading direction.

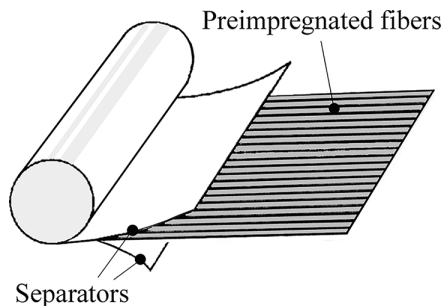


FIGURE 5.4 Unidirectional layer.

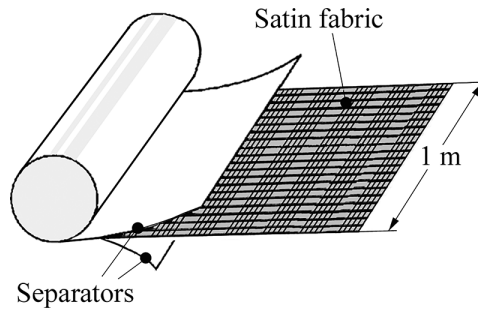
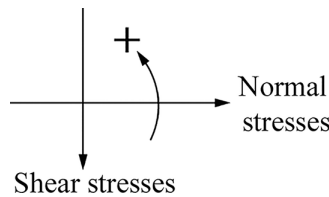
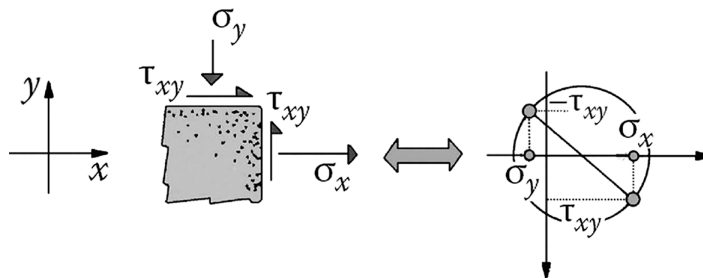


FIGURE 5.5 Fabric layer.

Note: A reminder about Mohr's circle
With the conventions as follows,



We obtain, for example, for the stress state illustrated below, the corresponding Mohr's circle:



Figures 5.6–5.9 show the favorable situations and those that should be avoided. In Figure 5.7, Mohr's circle for stresses shows that the 45° fibers support the compression $\sigma_1 = -\tau$ (τ being the shear stress arithmetic value), while the resin supports the tension $\sigma_2 = \tau$, with low fracture limit. The fibers in Figure 5.8 support the tension $\sigma_1 = \tau$, whereas the resin supports the compression $\sigma_2 = -\tau$. In Figure 5.9, the fiber orientations are 45° and -45° . Taking into account the previous remarks, the 45° fibers can support the tension $\sigma_1 = \tau$, whereas the -45° fibers can support the compression $\sigma_2 = -\tau$. As a result, the resin is less loaded than previously.

5.2.3 THE QUADRANGLE SYMMETRIC (QUAD) LAMINATE

5.2.3.1 Standard Orientations

In accordance with working modes of plies described in the previous paragraph, the most frequently used orientations are as in Figure 5.10. The so-called **0° direction** corresponds to either the direction of main loading, or a preferential direction of the concerned part, or one axis of the chosen coordinates system.

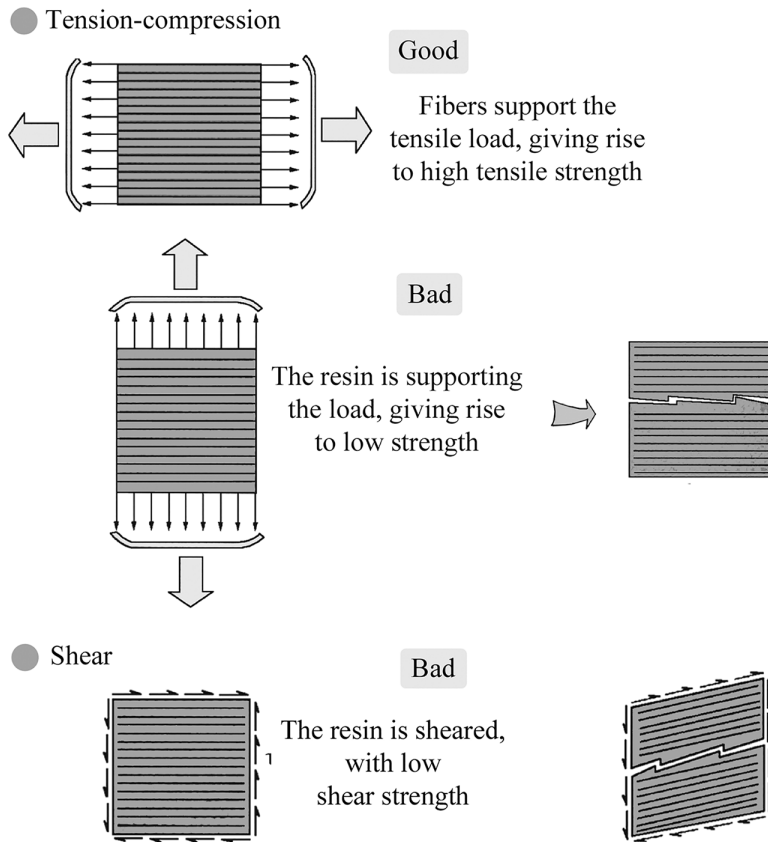


FIGURE 5.6 Effect of ply orientation.

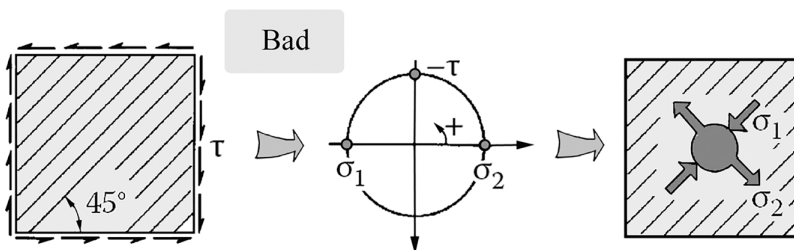


FIGURE 5.7 Bad design.

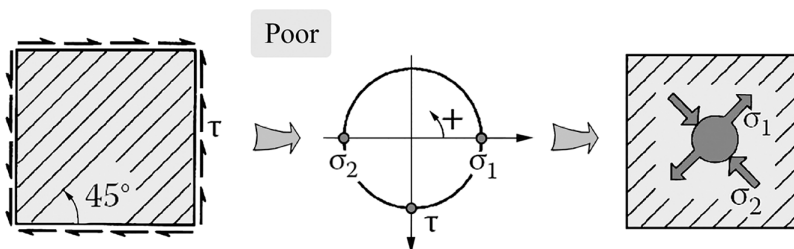


FIGURE 5.8 Poor design.

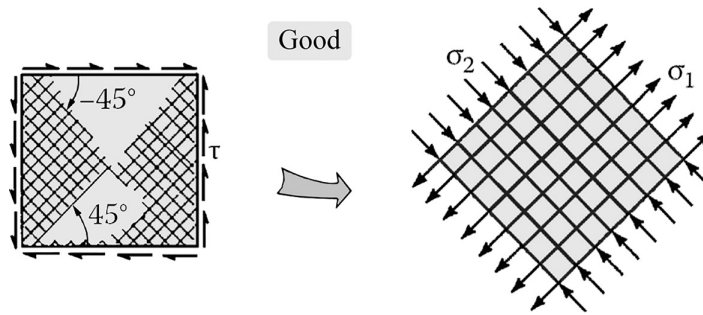


FIGURE 5.9 Good design.

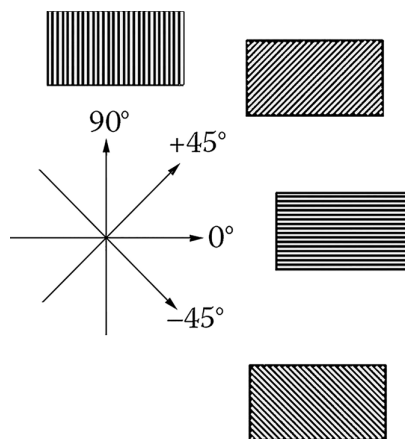


FIGURE 5.10 Standard orientations of a Quadrangle symmetric laminate.

Note: The cases of more general orientations of the $[\pm\Phi / \pm\Psi]$ type are the subject of a specific study (see Chapter 15).

5.2.3.2 Laminate Middle Plane

This is the term used to define the plane that separates the laminate thickness into two half thicknesses. In Figure 5.11, the middle plane, or **Mid-plane**, is the (x, y) plane. In this plane, the z -coordinate value is $z = 0$.

5.2.3.3 Description of the Stacking Order: Drawing Code

The description of the stacking of plies is done by beginning with the lowest ply on the side $z < 0$ and then moving toward the uppermost ply of the side $z > 0$. In so doing, each ply is noted by its orientation:

- The successive plies are separated by a slash “/”
- The grouping of too many plies of the same orientation must be avoided³. However, when this occurs, an index number is used to indicate the number of these identical plies

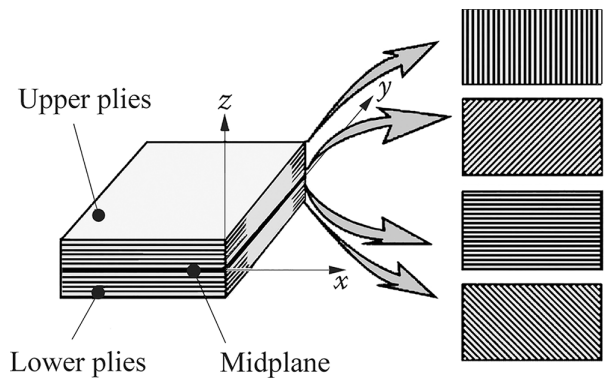


FIGURE 5.11 Quadrangle symmetric laminate and its middle plane (x, y).

5.2.3.4 Mid-plane Symmetry

A laminate has the **Mid-plane symmetry property**, or the **mirror symmetry property**, or is **symmetric**, when the stacking of plies on both sides starting from the middle plane is the same.

- **Example:**

Ply number	Orientation	Conventional notation	Symbol
10	90°	$(90/0_2/-45/45)_s$	
9	0°		
8	0°		
7	-45°		
6	+45°		
5	+45°		
4	-45°		
3	0°		
2	0°		
1	90°		

- **Example:**

Ply number	Orientation	Conventional notation	Symbol
10	90°	$(90/0_2/-45/45)_s$	
9	0°		
8	0°		
7	-45°		
6	+45°		
5	+45°		
4	-45°		
3	0°		
2	0°		
1	90°		

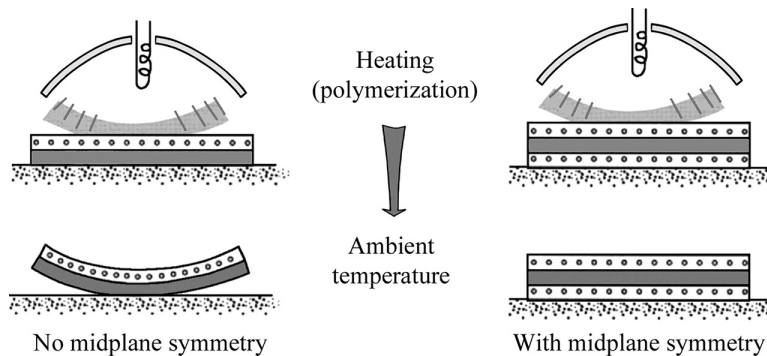


FIGURE 5.12 Effect of laminate lay-up on deformation.

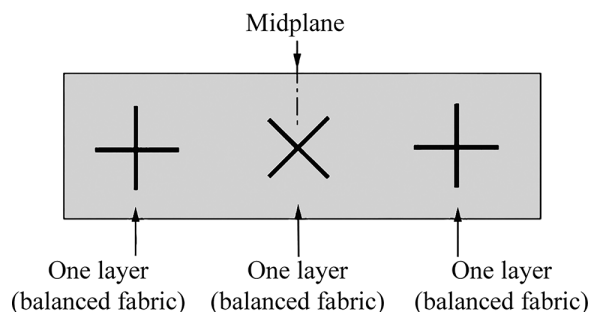
Note: Why the need for Mid-plane symmetry

During the manufacturing of a laminate, the successive impregnated plies are stacked at ambient temperature. Then they are placed within an autoclave for curing. At the high curing temperature, the thermal expansion of the whole laminate takes place without bending or warping. However, during cooling, while the resin is polymerized, the plies have a trend to contract differently depending on the fiber direction or the direction perpendicular to it (transverse direction). The occurrence of thermally related residual stresses follows from this. When Mid-plane symmetry is carried out, it leads to the Mid-plane symmetry of these stresses and thus prevents the overall structure to be deformed as, for example, the twisting or warping shown in Figure 5.12.

5.2.3.5 Specific Case of Balanced Fabrics

Some laminates are made partially or totally of layers of balanced fabric. The designer then needs to describe the drawing of the composition of the laminate.

• **Example:**



The laminate shown above is made up of three layers of balanced fabric. A woven fabric layer is equivalent to two unidirectional layers crossed at 90° , and due to the weaving, we can consider that the layer also has Mid-plane symmetry. Thus, this laminate is considered to have Mid-plane symmetry.

Note: If this hypothesis is well established for a plain weave or a taffeta (see Section 3.4.1), and even for a twill fabric, it becomes less and less accurate when the weave harness number is increasing (for the plain weave, two-harness; for twill fabric, three-harness; for satin, four-harness, five-harness, etc.). If we suppose that this number is indefinitely growing, the woven fabric becomes then the superimposition of two unidirectional layers crossed at 90° . It does not have any more the Mid-plane symmetry⁴.

As indicated in Section 3.4.2, we can consider the resulting laminate in two different ways⁵:

- Each layer of the fabric is replaced by two identical plies crossed at 90° , each with thickness equal to half the thickness e of the fabric layer and each with known elastic properties. This representation is convenient for the determination of the elastic properties of the laminate. The equivalencies are shown in Figure 5.13.
- Each layer of the fabric is replaced by one anisotropic ply with thickness e for which one knows the elastic properties and failure strengths. This representation is useful for the determination of the failure stress of the laminate. Such an equivalency is shown in Figure 5.14.

5.2.3.6 Technical Minimum

- Typically, a minimum amount of plies from 5% to 10% must be used for each direction, namely, 0° , 90° , $+45^\circ$, and -45° .
- The minimum thickness of a laminate should be of the order of one millimeter⁶, for example, eight unidirectional layers or three to four layers of balanced fabric of carbon/epoxy.

5.2.4 ARRANGEMENT OF PLYS

5.2.4.1 Proportion and Number of Plies

The proportion and number of plies along each of the directions (0° , 90° , $+45^\circ$, -45°) must take into account the mechanical loading on the laminate in the area. A common case consists in the loading of the laminate in its own plane. This is called an **In-plane loading**⁷. In such case, the mechanical loading can take the form of overall plane stress components σ_x , σ_y , and τ_{xy} in Figure 5.15a or In-plane stress resultants N_x , N_y , and T_{xy} in Figure 5.15b. Each stress resultant is the product of the overall stress value by the thickness h of the laminate.

Generally, the designer has to decide the arrangement of plies following three objectives:

- Support the loading without deterioration of the laminate (even incomplete)
- Limit the deformation of the loaded part
- Minimize the material weight involved

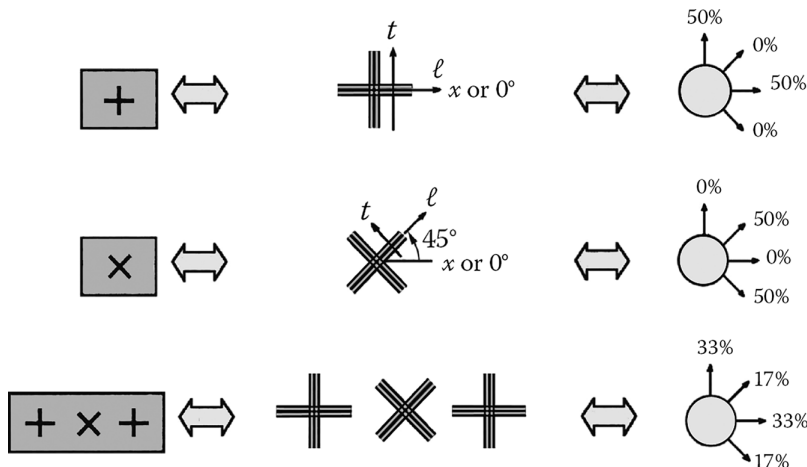


FIGURE 5.13 Laminate with balanced fabrics; representation 1.

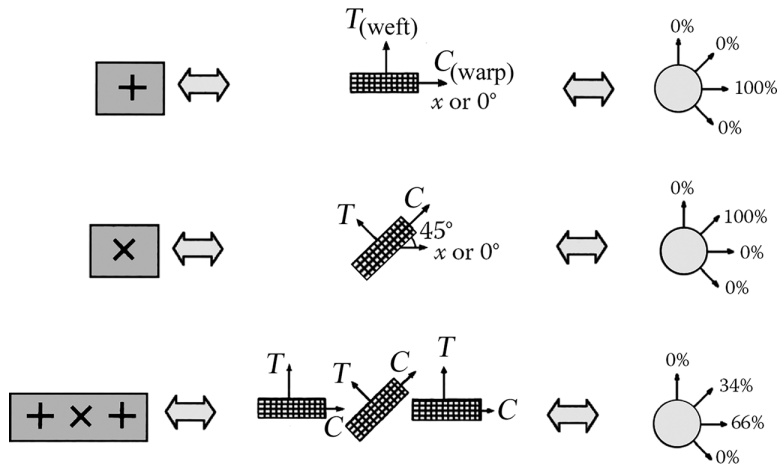


FIGURE 5.14 Laminate with balanced fabrics; representation 2.

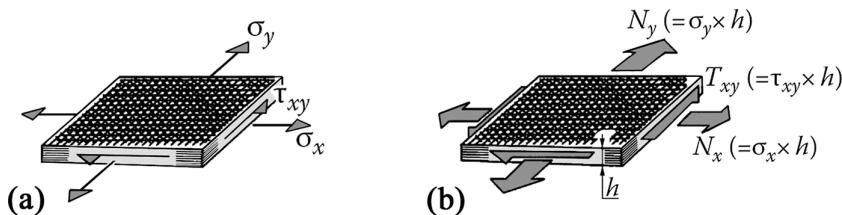


FIGURE 5.15 Stresses and stress resultants: (a) overall stress components and (b) In-plane stress resultants.

All these criteria do not work in a same direction. For example, searching for minimum thickness may not be compatible with high rigidity. Searching for high rigidity may not be compatible with minimum weight. We will see in Section 5.4 guide values for proportions that help to define a laminate with minimum thickness allowing withstanding without damage the specified mechanical loading.

Once a laminate is defined (number of layers and orientations), the designer must respect to the extent possible the following arrangements:

- When the predominant In-plane resultant is oriented along the 0° direction: 90° plies draped on the laminate external surface, then 45° and -45° plies, then 0° plies
- No more than four consecutive plies along the same direction

It should be done without forgetting the technological minimum indicated in Section 5.2.3.6.

5.2.4.2 Example of Pictorial Representation

In Figure 5.16, the symbols indicating the composition of the laminate are shown on top view. The plies drop-offs must be designed in order to obtain a gradual change in thickness (no more than two plies for each 6 mm length increment).

5.2.4.3 Case of Sandwich Structure

The description of the sandwich material is done as in Figure 5.17.

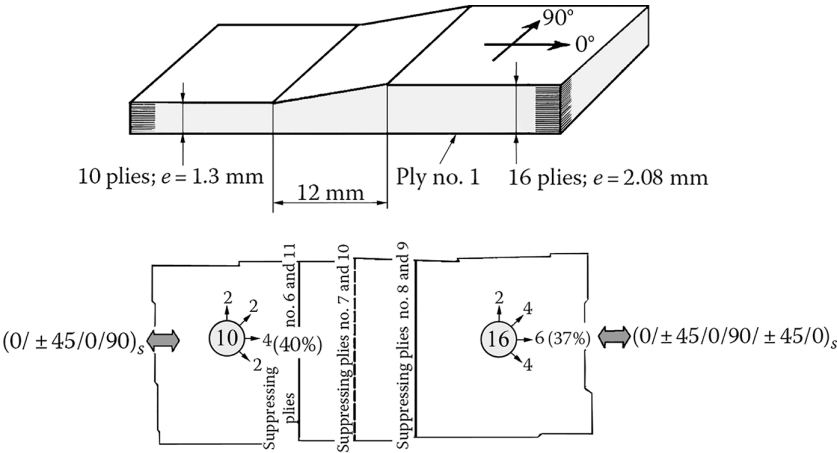


FIGURE 5.16 Pictorial representation.

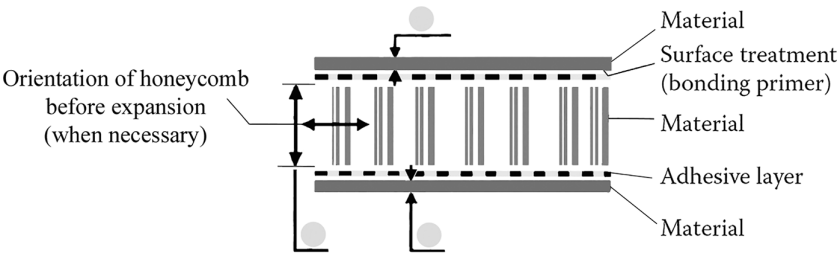


FIGURE 5.17 Description of a sandwich material.

5.3 FAILURE OF LAMINATES

5.3.1 DAMAGES

It should be pointed out that further details about the different phenomena characterizing damage of composite parts are provided in Chapter 14, Section 14.1.

5.3.1.1 Types of Failure

Figure 5.18 shows schematically different types of failure leading to damage of a laminate⁸.

When the loads exceed critical levels, the main modes of damage for the laminate are illustrated in Figure 5.19 (see also Figure 14.5).

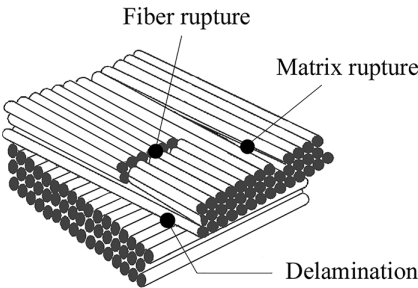


FIGURE 5.18 Different types of failure.

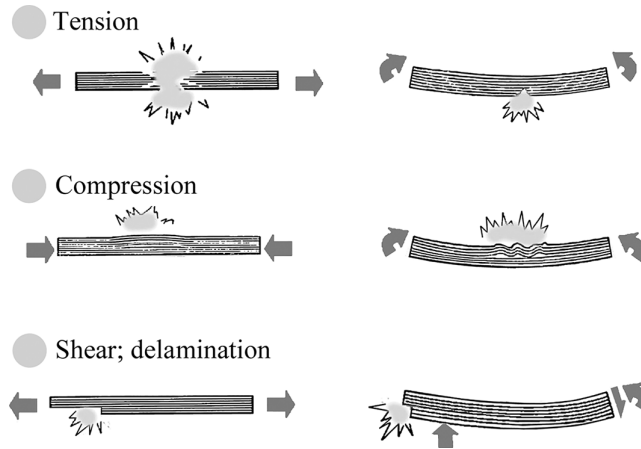


FIGURE 5.19 Modes of damage.

5.3.1.2 Note: Classical Maximum Stress Criterion Shows Its Limits

Figure 5.20 shows a unidirectional laminate loaded successively in two different manners. In the two cases, the maximum normal stress has the same value denoted as σ . In the loading case (a), the unidirectional specimen will rupture when

$$\sigma > \sigma_{\text{rupture along } \ell}$$

This is a maximum stress criterion.

In loading case (b), the maximum normal stress occurs in a direction that is different from that of the fibers (one can obtain this by tracing Mohr's circle as discussed previously). Then the failure strength will decrease as we have seen in Section 3.3.2. It is weaker than that of case (a). The unidirectional laminate therefore fails when

$$\sigma < \sigma_{\text{rupture along } \ell}$$

This phenomenon is more evident if the unidirectional laminate is loaded in a direction transverse to the fibers t . In this case, the laminate failure strength is that of the matrix, which is much less than that of the fibers.

Thus, taking into consideration the evolution of the failure strength with the loading direction, the designer cannot use a simple maximum stress criterion as for the classical metallic materials.

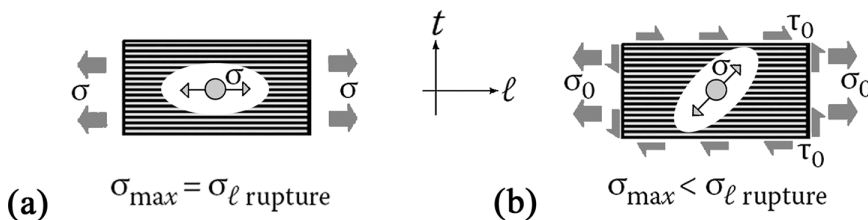


FIGURE 5.20 The strong influence of orientation.

5.3.2 FREQUENTLY USED CRITERION: TSAI-HILL FAILURE CRITERION⁹

5.3.2.1 Tsai-Hill Number

This criterion shall apply successively to **each ply** of the laminate, i.e., for each one of the four orientations (0° , 90° , $+45^\circ$, -45°) that have been considered (Quadrangle symmetric laminates). As already discussed in Chapter 3, the axes of a unidirectional ply are denoted as ℓ for the direction along the fibers and t for the transverse direction. The stress components are denoted as σ_ℓ in the fiber direction, σ_t in the direction transverse to the fibers, and $\tau_{\ell t}$ for the shear stress in plane (ℓ, t) (see Figure 5.21).

The **Tsai-Hill number** is the number α such that

$$\alpha^2 = \frac{\sigma_\ell^2}{\sigma_{\ell \text{ rupture}}^2} + \frac{\sigma_t^2}{\sigma_{t \text{ rupture}}^2} - \frac{\sigma_\ell \sigma_t}{\sigma_{\ell \text{ rupture}}^2} + \frac{\tau_{\ell t}^2}{\tau_{\ell t \text{ rupture}}^2}$$

- If $\alpha < 1$, no ply failure occurs.
- If $\alpha \geq 1$, failure occurs in the ply under consideration. Generally, this deterioration is due to the resin failure¹⁰.

The mechanical properties (modulus of elasticity and failure strength) of a broken ply become almost negligible, except for those along the fiber direction¹¹.

5.3.2.2 Notes

- **Caution:** The failure strength σ_{rupture} (called also **allowable value**) does not have the same value in tension and in compression (see, e.g., Section 3.3.3). It is therefore necessary to put at each denominator (except for shear) of the previous Tsai-Hill expression the allowable value corresponding to the type of loading (traction or compression) that appears in the numerator.
- Using this criterion, when the failure of one of the plies of the laminate occurs (more precisely the failure of the plies along one of the four orientations), this **does not necessarily lead to the failure** of the whole laminate. In most cases, the degraded laminate continues to withstand the applied stress resultants. In increasing these stress resultants, the recalculation criterion can show in which ply orientations can a new rupture occur. This may lead – or not – to complete rupture of the laminate. If complete rupture does not occur, the allowable stress resultants¹² can still be increased. In this way, a design factor can be applied on the initial critical loading, reflecting the gap between the first-ply rupture and the ultimate rupture.
- As a consequence of the previous remark, it appears possible to allow a laminate to remain in service even if it is partially degraded. It is up to the designer to decide whether the partially degraded laminate is appropriate – or not – for the considered application.
- A parallel somewhat crude can be made with the working areas of classical metallic alloys as represented in Figure 5.22.

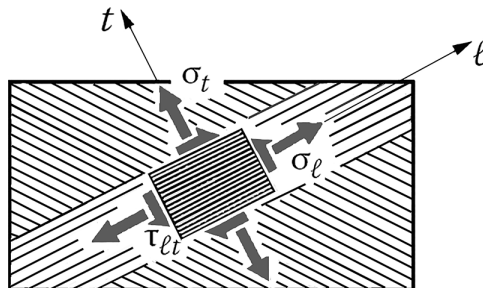


FIGURE 5.21 Ply stresses.

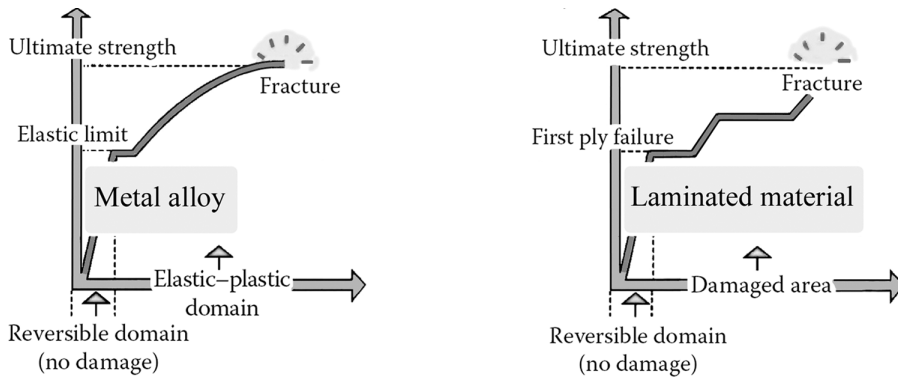


FIGURE 5.22 Stress-strain curves. Comparison of behavior until failure.

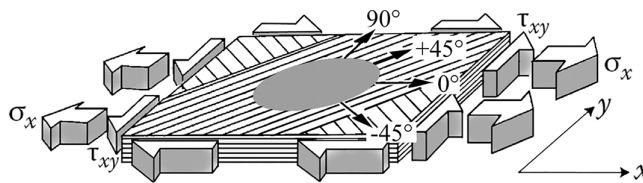


FIGURE 5.23 Overall stresses on the laminate.

5.3.2.3 How to Determine the Stress Components σ_t , σ_r , and τ_{tr} in Each Ply

Consider, for example, the laminate shown in Figure 5.23 consisting of identical plies and on which we know, beside the mechanical properties of the basic ply:

- The proportions (percentages) of plies in each of the directions 0° , 90° , $+45^\circ$, and -45°
- The values of the overall stresses applied, here, for example, σ_x and τ_{xy}

We can consider this loading case as consisting of the superposition of two simple loading cases:

First σ_x only, and then τ_{xy} only. For each of these elementary load cases, we look for the stress values of σ_t , σ_r , and τ_{tr} in each ply. Manual calculation is usually far too long¹³. It should be replaced by computerized calculation.

The resulting tables that provide these stress values can be found in Appendix A for carbon/epoxy plies with 60% fiber volume fraction.

Then, always **for each ply**, the stress values σ_t due to each of the simple loadings σ_x and τ_{xy} are added together. We obtain in the same way the stress value σ_r , then, respectively, the stress value τ_{tr} . We are then able to calculate the Tsai-Hill number to verify the integrity of each of the plies. Application 19.6 shows an example with the aim of determining the thickness of a laminate subject to such a type of combined loading.

5.4 PRE-SIZING OF THE QUADRANGLE SYMMETRIC LAMINATE

5.4.1 MODULUS OF ELASTICITY; DEFORMATION OF THE LAMINATE

5.4.1.1 Varying Proportions of Plies

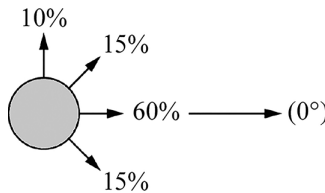
For varying proportions of plies in the directions 0° , 90° , $+45^\circ$, and -45° , the charts that follow allow the determination of the deformation of a Quadrangle symmetric laminated plate subject to the applied overall stress components. For this, we have used a stress-strain relation similar to that described in Section 3.1 for an anisotropic plate, which is repeated below:

$$\begin{Bmatrix} \epsilon_x \\ \epsilon_y \\ \gamma_{xy} \end{Bmatrix} = \begin{bmatrix} \frac{1}{E_x} & -\frac{v_{yx}}{E_y} & 0 \\ -\frac{v_{xy}}{E_x} & \frac{1}{E_y} & 0 \\ 0 & 0 & \frac{1}{G_{xy}} \end{bmatrix} \begin{Bmatrix} \sigma_x \\ \sigma_y \\ \tau_{xy} \end{Bmatrix}$$

E_x , E_y , G_{xy} , v_{xy} , and v_{yx} are the moduli of elasticity and Poisson ratios of the laminate,¹⁴ ϵ_x and ϵ_y are normal strains, and γ_{xy} is the angular distortion in plane (x, y).

5.4.1.2 Example of Using Tables

What are the elastic moduli and thermal expansion coefficients of a glass/epoxy laminate ($V_f = 60\%$) with the following ply configuration?



Answer: Chart 5.14 indicates the following values for this laminate:

$$E_x = 33,100 \text{ MPa}$$

$$E_y = 17,190 \text{ MPa} \quad (\text{This value is obtained by permuting the proportions of } 0^\circ \text{ and } 90^\circ)$$

$$v_{xy} = 0.34$$

$$v_{yx} = 0.17$$

Chart 5.15 shows $G_{xy} = 6,980 \text{ MPa}$.

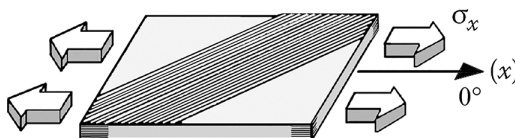
When the overall stress values are known, we then obtain the strains ϵ_x , ϵ_y , and γ_{xy} using the matrix relation mentioned above.

Regarding coefficients of thermal expansion, Chart 5.14 shows $\alpha_x = 0.64 \times 10^{-5}$ and $\alpha_y = 1.21 \times 10^{-5}$ by permuting the proportions of 0° and 90° .

5.4.2 CASE OF SIMPLE LOADING

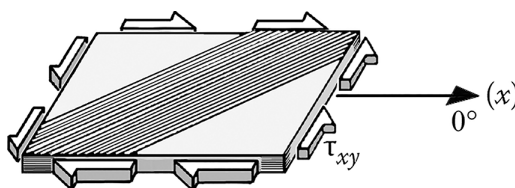
The laminate is subjected to only **one** single overall stress: σ_x or σ_y or τ_{xy} . For a particular set of proportions in the four directions, we would like to know the order of magnitude of the stress that can cause a first-ply failure in this laminate.

- **Example:**



For which value of σ_x (known as $\sigma_{x \max}$) will this laminate start to deteriorate?

- **Example:**



For which value of τ_{xy} (known as $\tau_{xy \max}$) will this laminate start to damage?

Charts 5.1–5.15 indicate these maximum stress values as well as the elastic characteristics and the coefficients of thermal expansion for quadrangle symmetric laminates with the following characteristics:

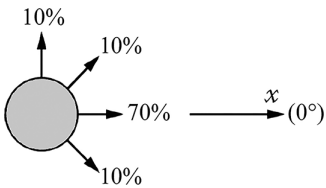
- Materials: **Carbon**, **Kevlar®**, and **glass/epoxy** with $V_f = 60\%$ fiber volume fraction.
- All the plies are of same nature (same unidirectional, same thickness).
- The laminate is balanced (same number of 45° and -45° plies). The Mid-plane symmetry is performed.
- The percentages of plies along the four directions (0° , 90° , $+45^\circ$, -45°) are adjustable in steps of 10%.

Note: The following tables are established from the properties of unidirectionals shown in Table 3.4 (see Chapter 3). Not all reinforcements marketed can be detailed in this book; thus, concerning the carbon/resin plies, one can find about 15 marketed plies (thermosetting or thermoplastic resin) with volume contents of fibers varying from 60% to 70%. To use these other marketed reinforcements, a free dedicated utility can be easily downloaded. This is the LAM SEARCH tool. It was created within the association THINK COMPOSITES whose objective is to promote composite materials in industry and education. The LAM SEARCH tool is fully open and available free to interested parties, manufacturers, and academics. For references about this tool, see Section 15.8.4.

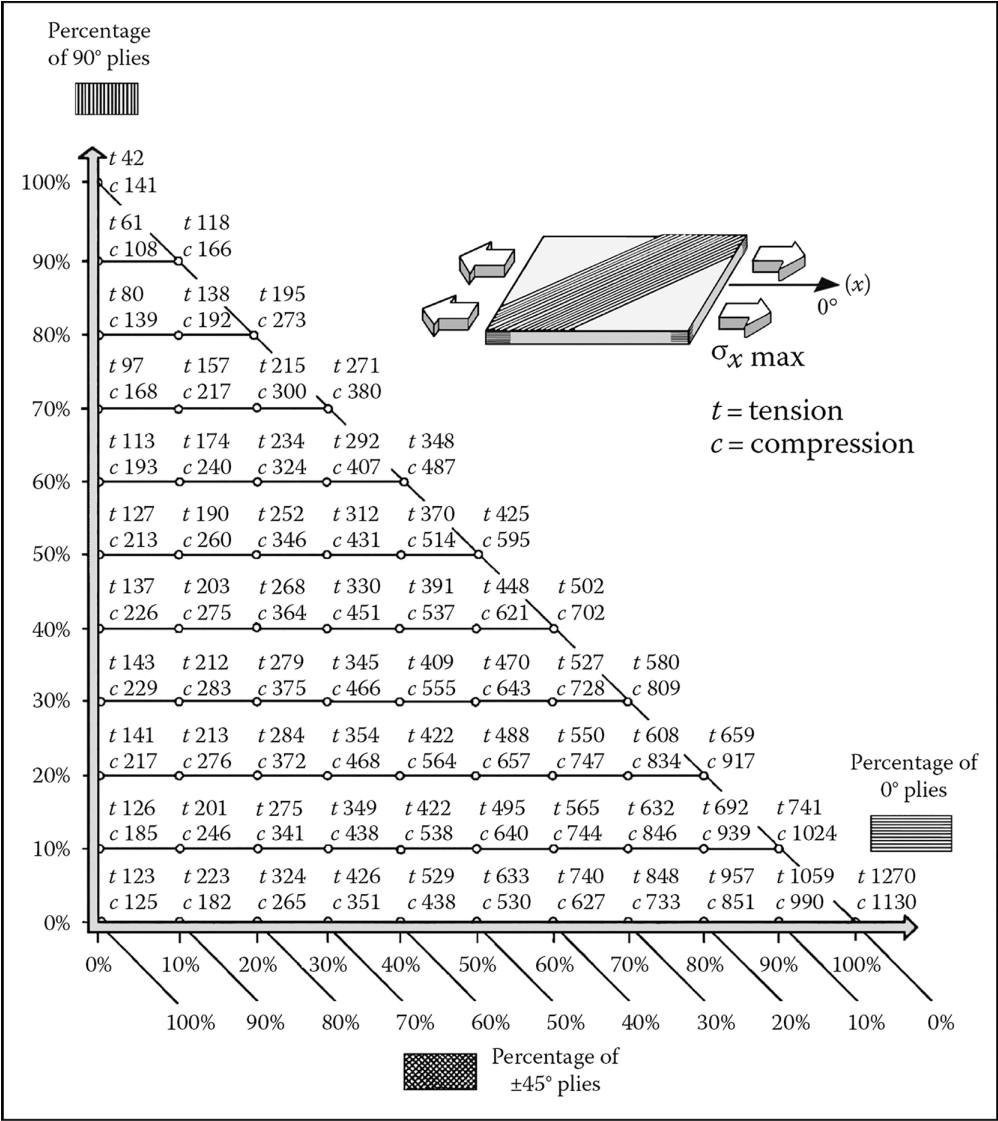
Calculation of maximum overall stress values $\sigma_{x \max}$, $\sigma_{y \max}$, and $\tau_{xy \max}$ is done based on the Tsai-Hill failure criterion¹⁵.

- **Example:**

Which maximum tensile stress along the 0° direction can be applied to a Kevlar/epoxy laminate containing 60% fiber volume with the orientation distribution as shown in the figure below?



Answer: Chart 5.6 indicates the maximum stress in the 0° direction (or x). For the percentages given, we read $\sigma_{x\max}^{\text{tension}} = 308 \text{ MPa}$.

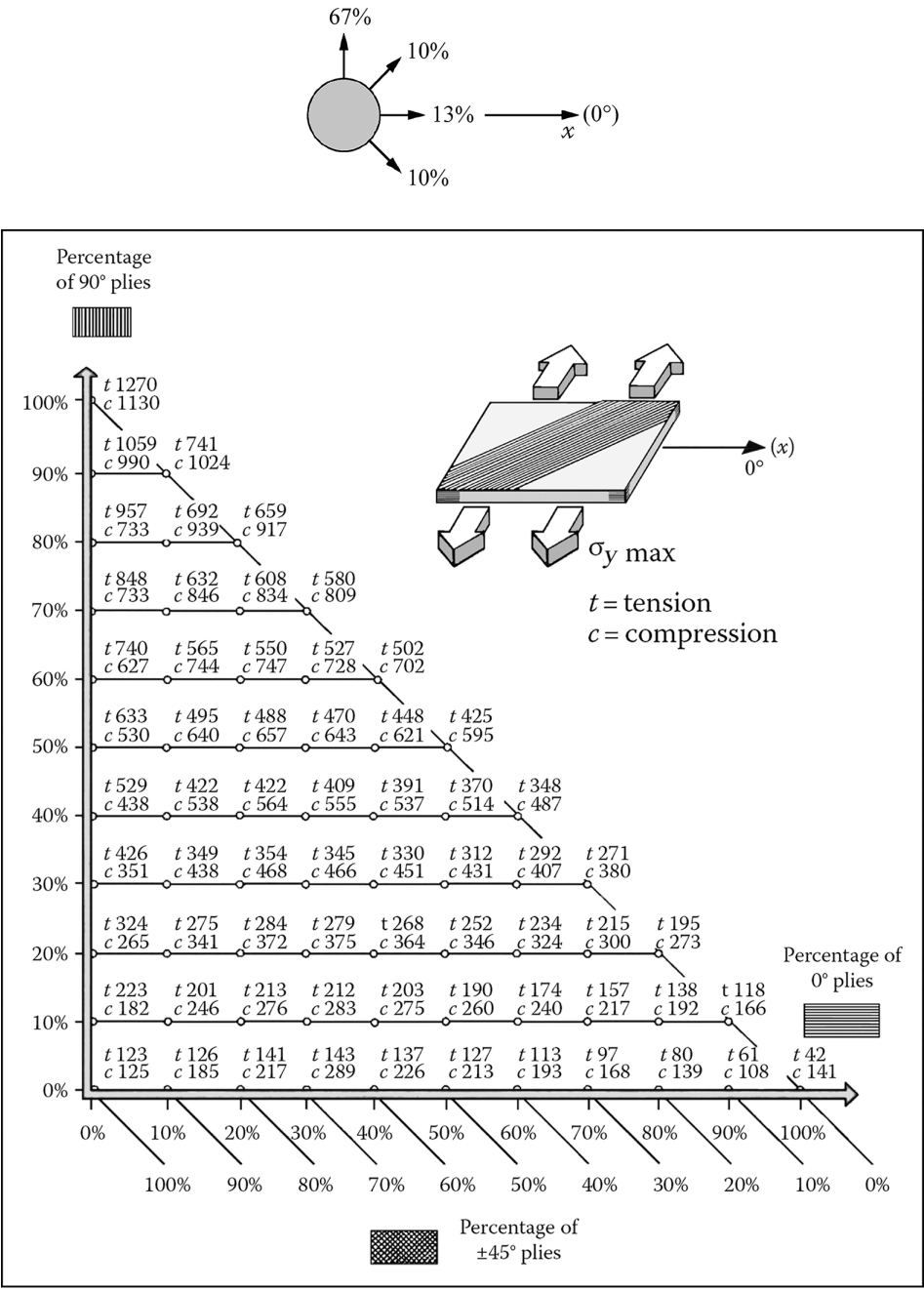


Note: Maximum stress $\sigma_{x\max}$ (MPa) as a function of the ply percentages in the directions 0°, 90°, +45°, and -45°. (For more information on modulus and strength of a basic ply, see Section 3.3.3.)

CHART 5.1 Carbon/epoxy laminate: $V_f = 60\%$, ply thickness = 0.13 mm.

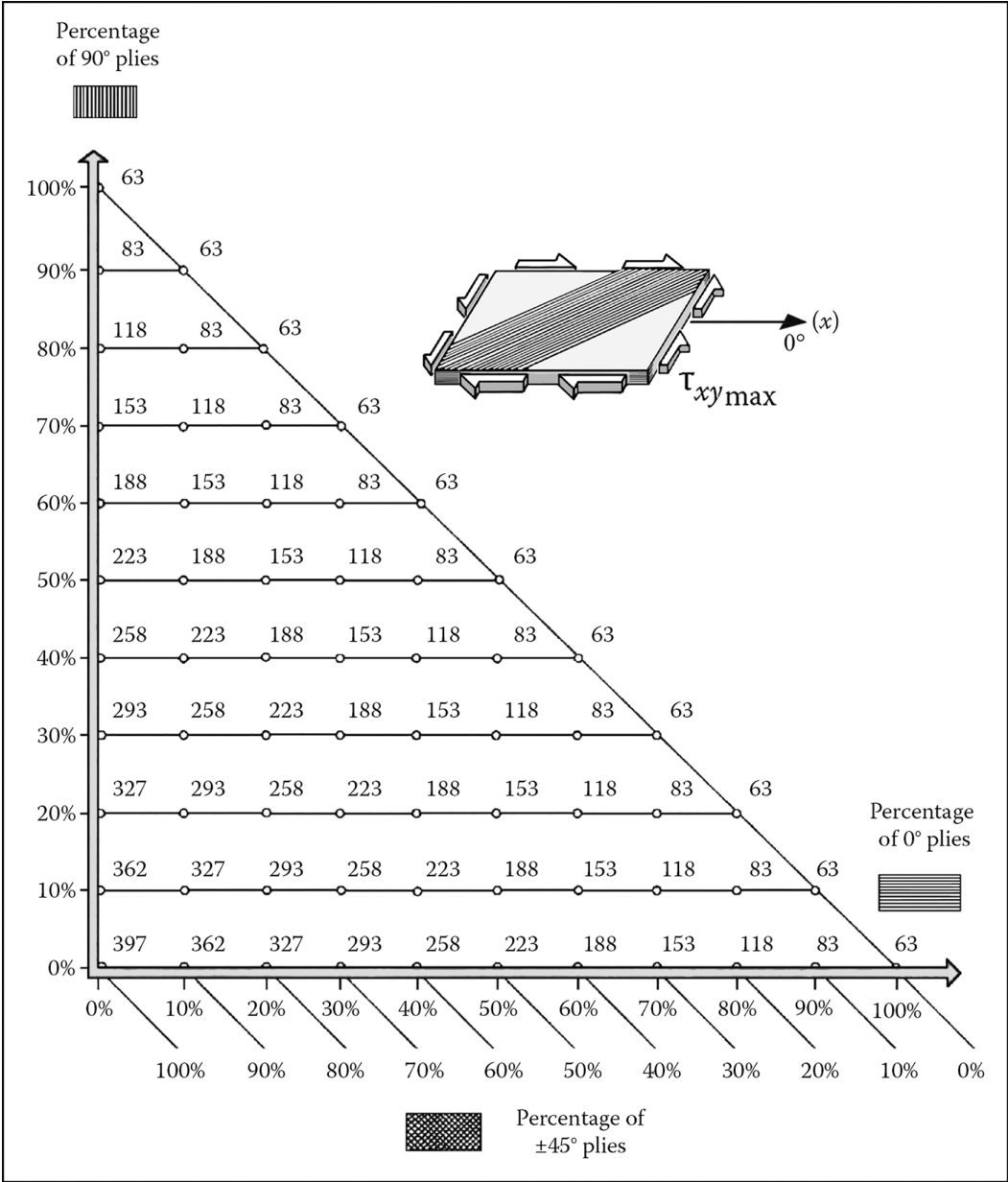
• **Example:**

Which maximum overall compression stress along the 90° direction (or y) can be applied to a carbon/epoxy laminate containing 60% fiber volume fraction with the orientation distribution as shown in the following figure?



Note: Maximum stress $\sigma_{y \max}$ (MPa) as a function of the ply percentages in the directions 0°, 90°, +45°, and -45°. (For more information on modulus and strength of a basic ply, see Section 3.3.3.)

CHART 5.2 Carbon/epoxy laminate: $V_f = 60\%$, ply thickness = 0.13 mm.

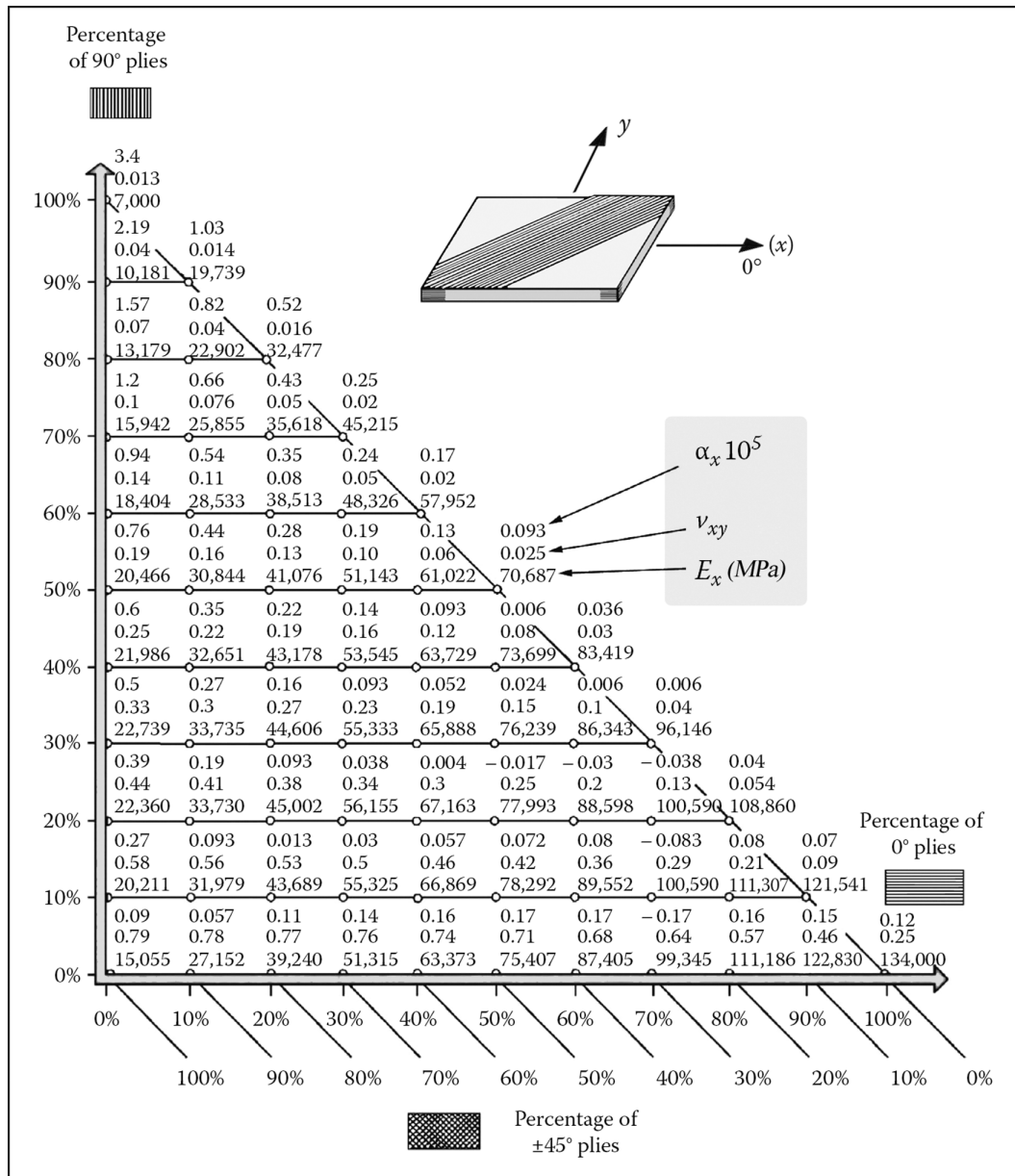


Note: Maximum stress $\tau_{xy \max}$ (MPa) as a function of the ply percentages in the directions 0°, 90°, +45°, and -45°. (For more information on modulus and strength of a basic ply, see Section 3.3.3.)

CHART 5.3 Carbon/epoxy laminate: $V_f=60\%$, ply thickness = 0.13 mm.

Answer: Chart 5.2 shows the maximum stress in the 90° direction. Starting from the immediately adjacent composition (10°|60°|15°|15°), we have

$$\sigma_{y \max} = \sigma(13^\circ|67^\circ|10^\circ|10^\circ) = \sigma(10^\circ|60^\circ|15^\circ|15^\circ) + \Delta\sigma = 744 + \Delta\sigma$$

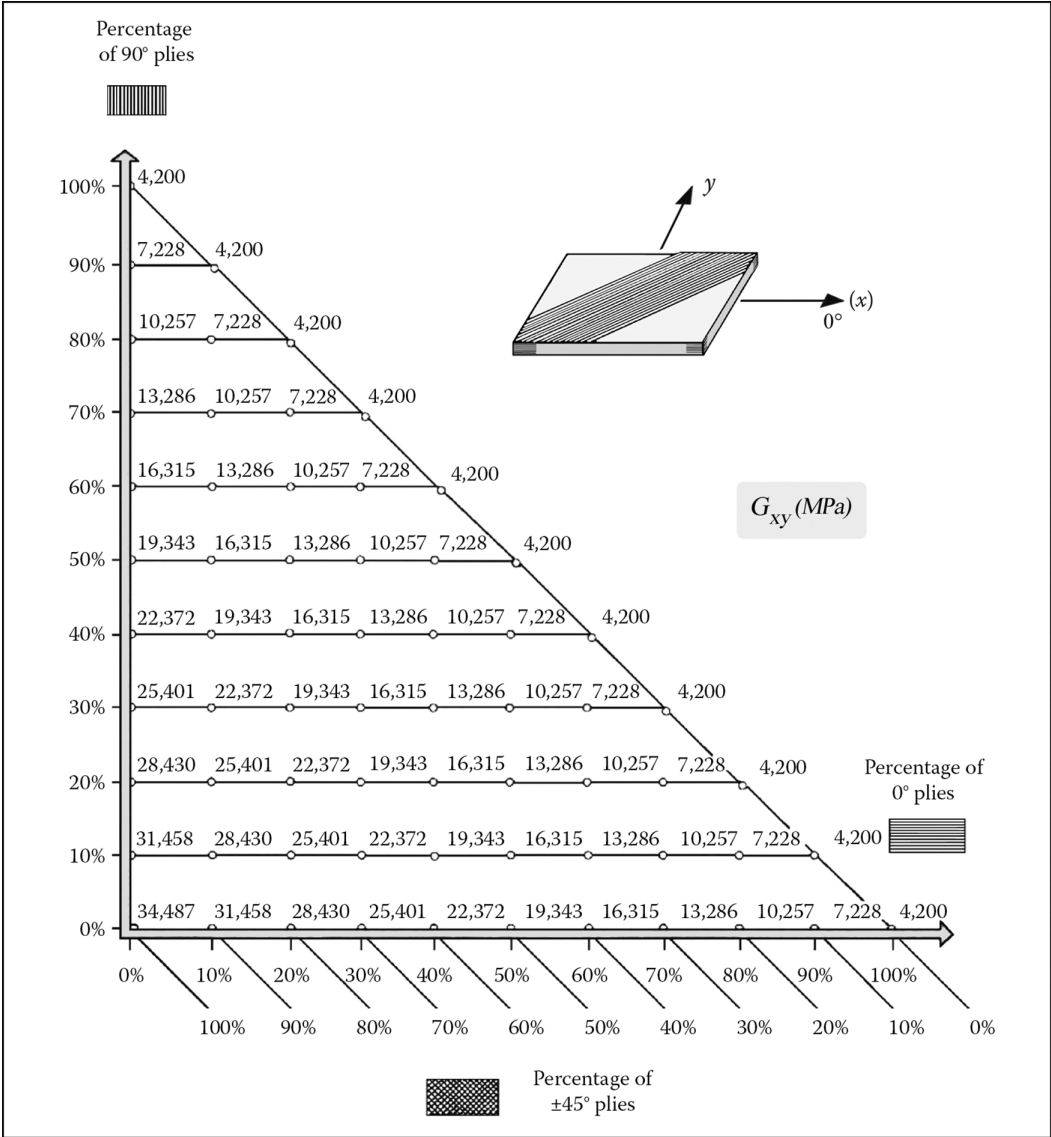


Note: Modulus E_x (MPa), Poisson ratio ν_{xy} , and coefficient of thermal expansion α_x as a function of the ply percentages in the directions 0°, 90°, +45°, and -45°. (For more information on modulus and strength of a basic ply, see Section 3.3.3.)

CHART 5.4 Carbon/epoxy laminate: $V_f = 60\%$, ply thickness = 0.13 mm.

Denoting as p^{0° and p^{90° the proportions of plies along the 0° and 90° directions, respectively, we have

$$\Delta\sigma = \frac{\partial\sigma}{\partial p^{0^\circ}} \times \Delta p^{0^\circ} + \frac{\partial\sigma}{\partial p^{90^\circ}} \times \Delta p^{90^\circ}$$



Note: Shear modulus G_{xy} (MPa) as a function of the ply percentages in the directions 0°, 90°, +45°, and -45°. (For more information on modulus and strength of a basic ply, see Section 3.3.3.)

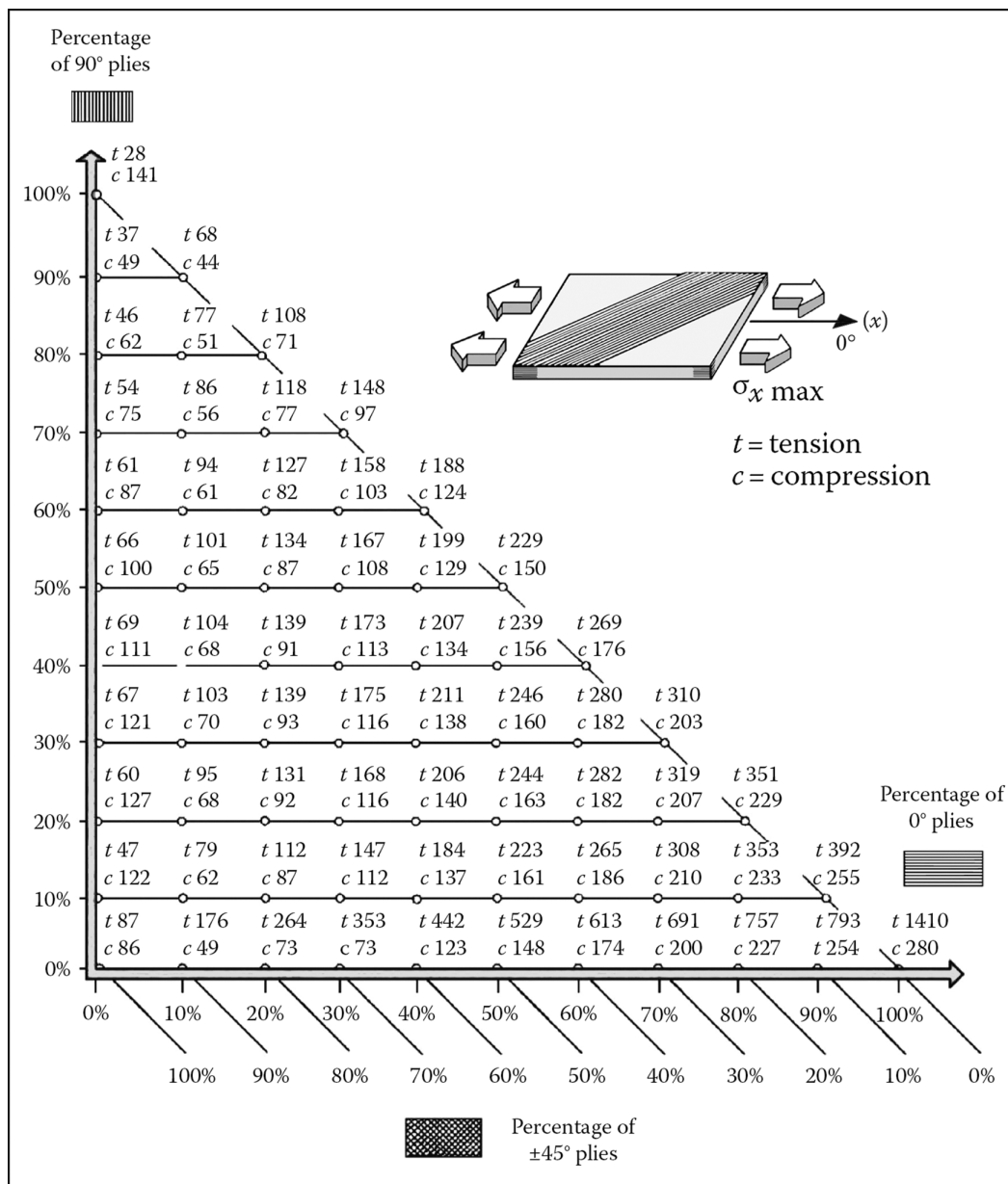
CHART 5.5 Carbon/epoxy laminate: $V_f=60\%$, ply thickness = 0.13 mm.

And we obtain by linear interpolation

$$\Delta\sigma = (747 - 744) \times \frac{3}{10} + (846 - 744) \times \frac{7}{10} = 72 \text{ MPa}$$

Therefore,

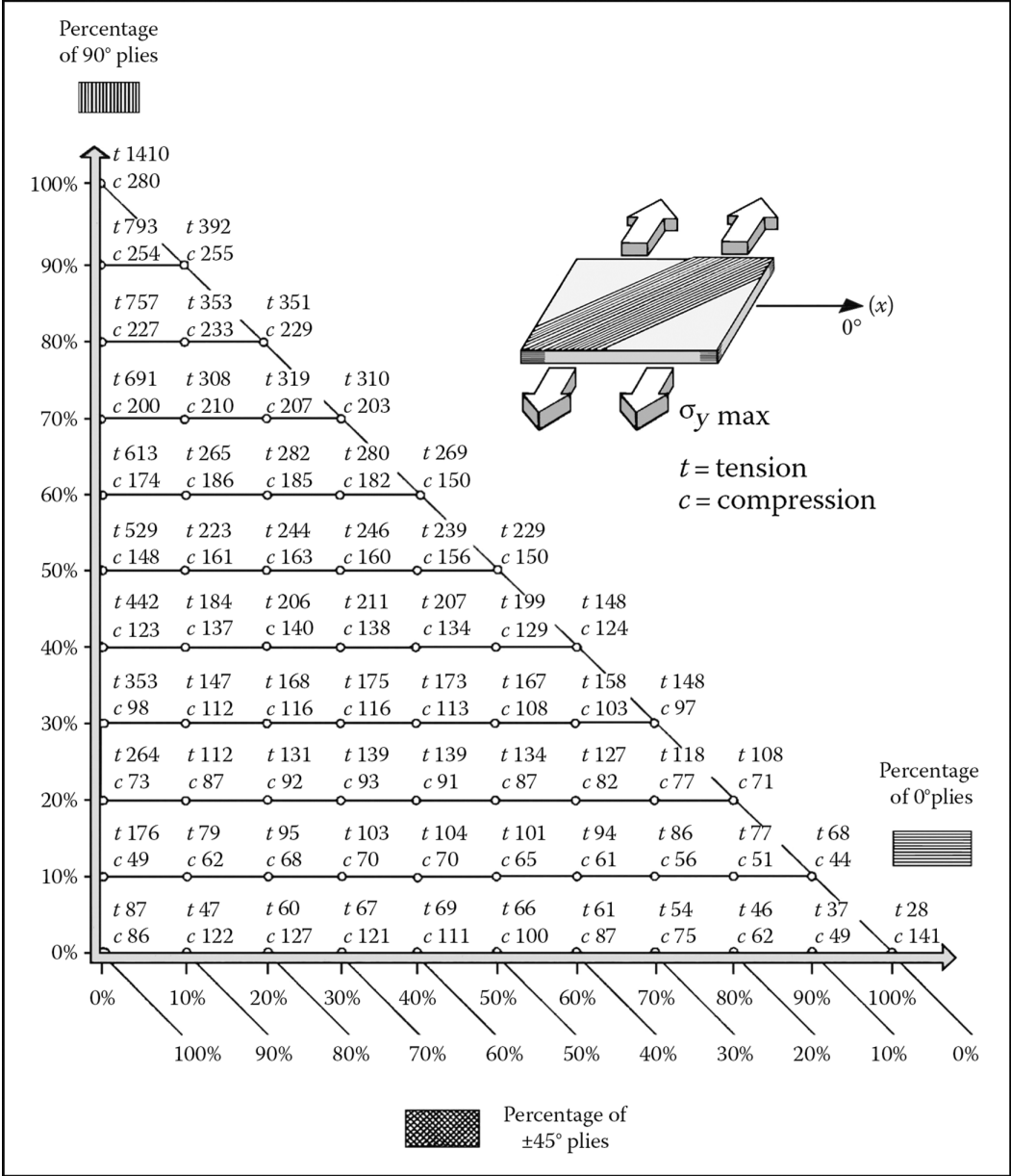
$$\sigma_{y \text{ max}} = 744 + 72 = 816 \text{ MPa}$$



Note: Maximum stress $\sigma_{x \max}$ (MPa) as a function of the ply percentages in the directions 0°, 90°, +45°, and -45°. (For more information on modulus and strength of a basic ply, see Section 3.3.3.)

CHART 5.6 Kevlar/epoxy laminate: $V_f = 60\%$, ply thickness = 0.13 mm.

Note: The charts that provide the maximum overall stresses are not usable for the laminates made of balanced fabrics. In fact, the compression strength value of a layer of balanced fabric is significantly lower than what is obtained when one superimposes two unidirectional plies crossed at 0° and 90° in equal quantities in these two directions¹⁶.



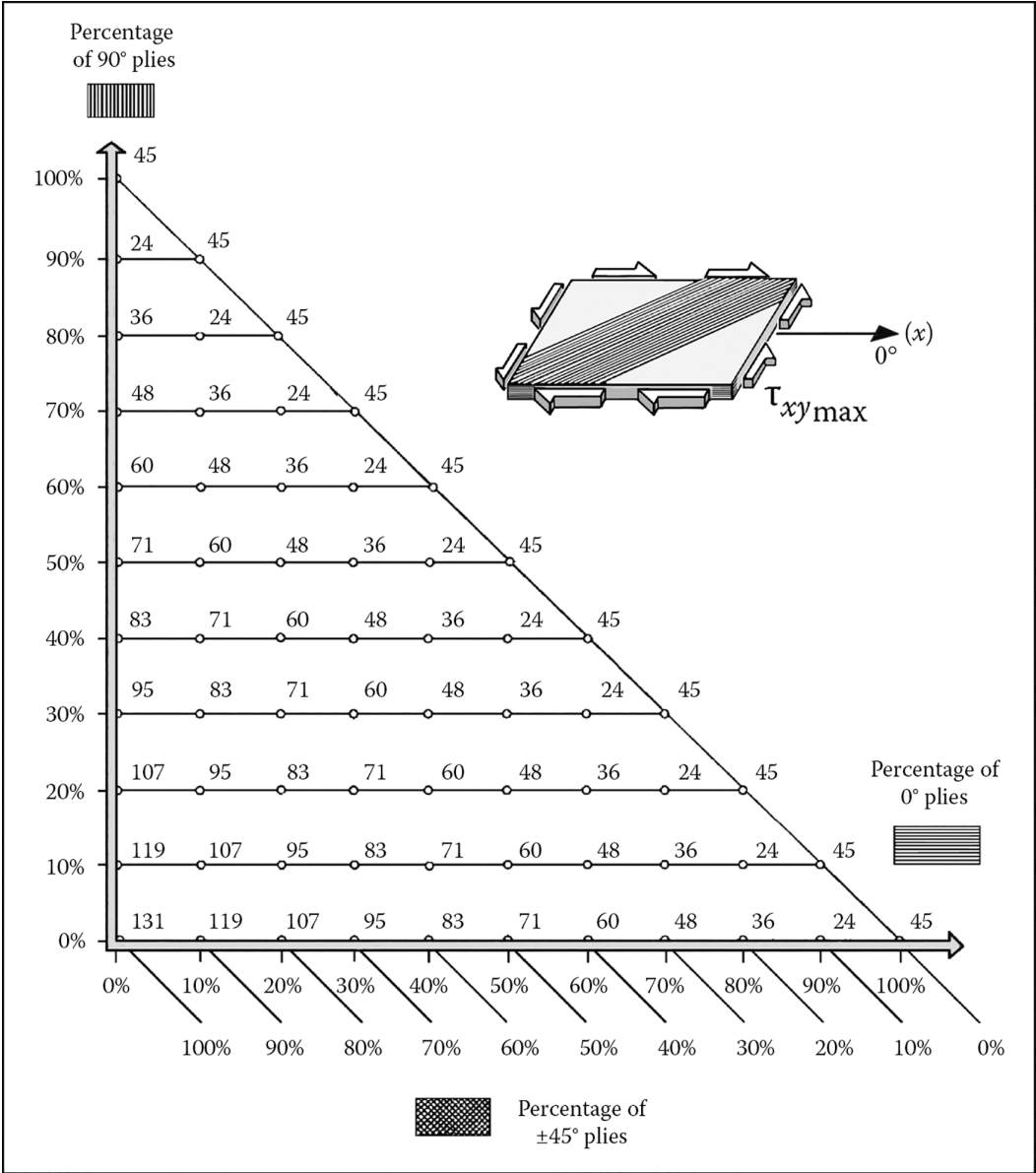
Note: Maximum stress $\sigma_{y \max}$ (MPa) as a function of the ply percentages in the directions 0°, 90°, +45°, and -45°. (For more information on modulus and strength of a basic ply, see Section 3.3.3.)

CHART 5.7 Kevlar/epoxy laminate: $V_f = 60\%$, ply thickness = 0.13 mm.

5.4.3 COMPLEX LOADING CASE: APPROXIMATIVE PROPORTIONS ACCORDING TO ORIENTATIONS

5.4.3.1 When the Normal and Shear Loads Are Applied Simultaneously

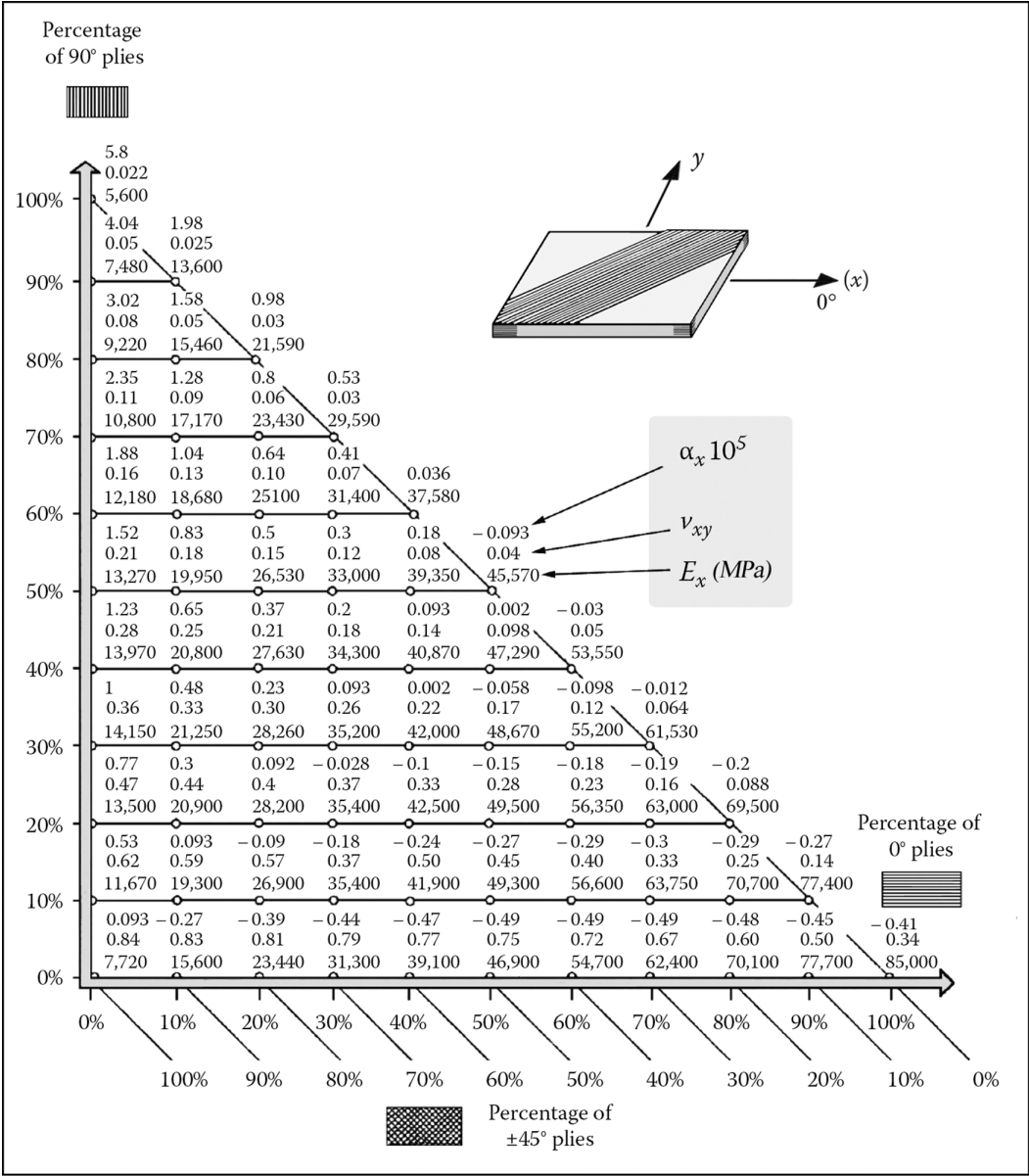
When the normal and tangential (shear) loads are applied simultaneously onto the Quad laminate, the previous tables are not valid because they were established for the cases of simple stress states. However, one can still use them to make a first estimate of ply proportions following the four orientations¹⁷.



Note: Maximum stress $\tau_{xy \max}$ (MPa) as a function of the ply percentages in the directions 0°, 90°, +45°, and -45°. (For more information on modulus and strength of a basic ply, see Section 3.3.3.)

CHART 5.8 Kevlar/epoxy laminate: $V_f = 60\%$, ply thickness = 0.13 mm.

The principle is as follows: consider the case of complex loading and replacing the stress components with the In-plane resultants N_x , N_y , and T_{xy} , which were defined in Section 5.2.4. Generally, these stress resultants constitute the initial numerical data that results from some previous studies. The design department thus knows them. In view of this, each one of the three stress resultants should be associated with an appropriate orientation of the plies following the advice in Section 5.2.2. Using this hypothesis, the normal stress resultant N_x is assumed to be supported by the 0° plies (or along x) and thus requires a global thickness e_x for these plies such that



Note: Longitudinal modulus E_x (MPa), Poisson ratio ν_{xy} , and coefficient of thermal expansion α_x as a function of the ply percentages in the directions 0°, 90°, +45°, and -45°. (For more information on modulus and strength of a basic ply, see Section 3.3.3.)

CHART 5.9 Kevlar/epoxy laminate: $V_f = 60\%$, ply thickness = 0.13 mm.

$$e_x = \frac{N_x}{\sigma_{\ell \text{ rupture}}}$$

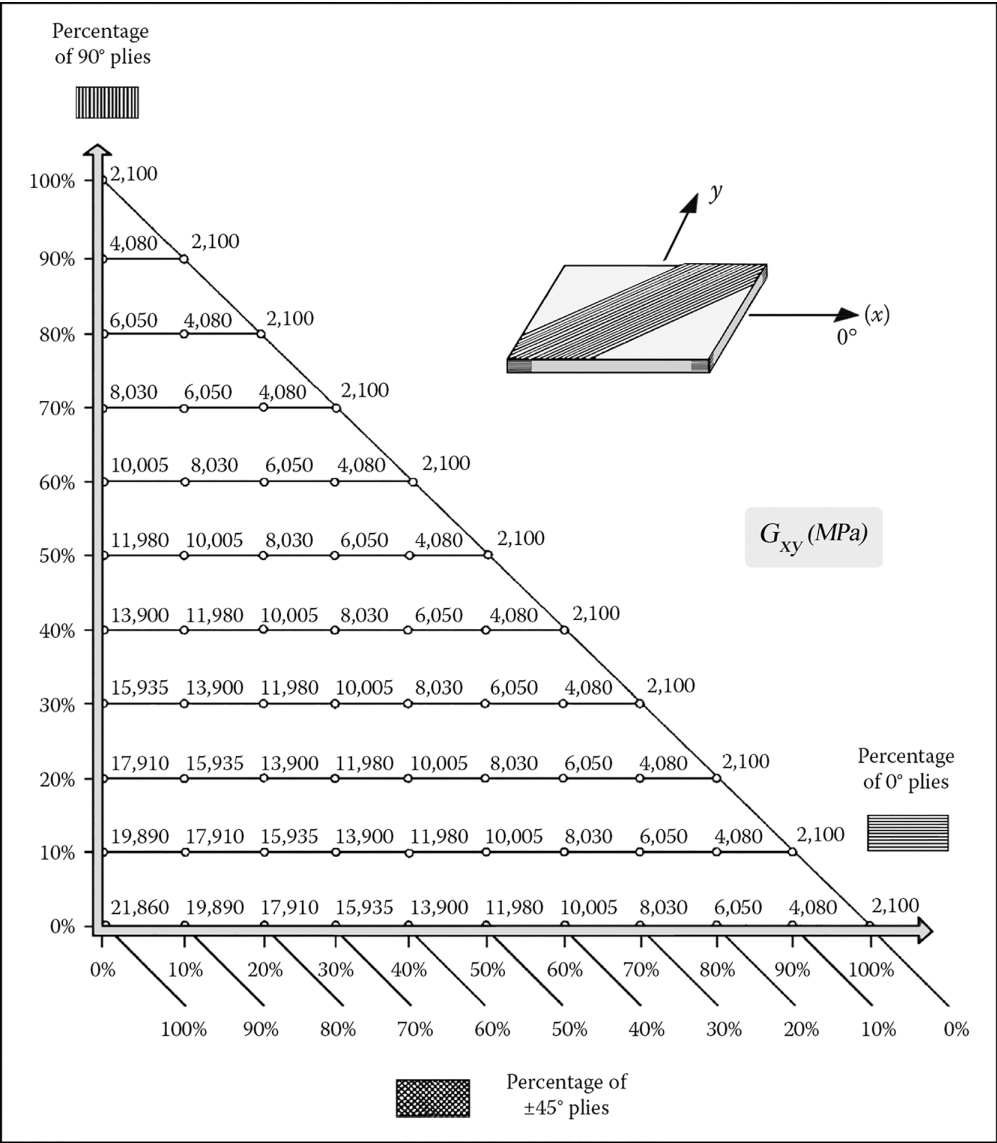
where $\sigma_{\ell \text{ rupture}}$ is the ultimate stress for a unidirectional ply, in the fiber direction (or along x). In the same manner, N_y is supposed to be supported by the 90° plies (or along y) and requires a global thickness for these plies of

$$e_y = \frac{N_y}{\sigma_{\ell \text{ rupture}}}$$

Finally, the shear resultant T_{xy} is assumed to be supported by the $\pm 45^\circ$ plies and requires a global thickness for these plies of

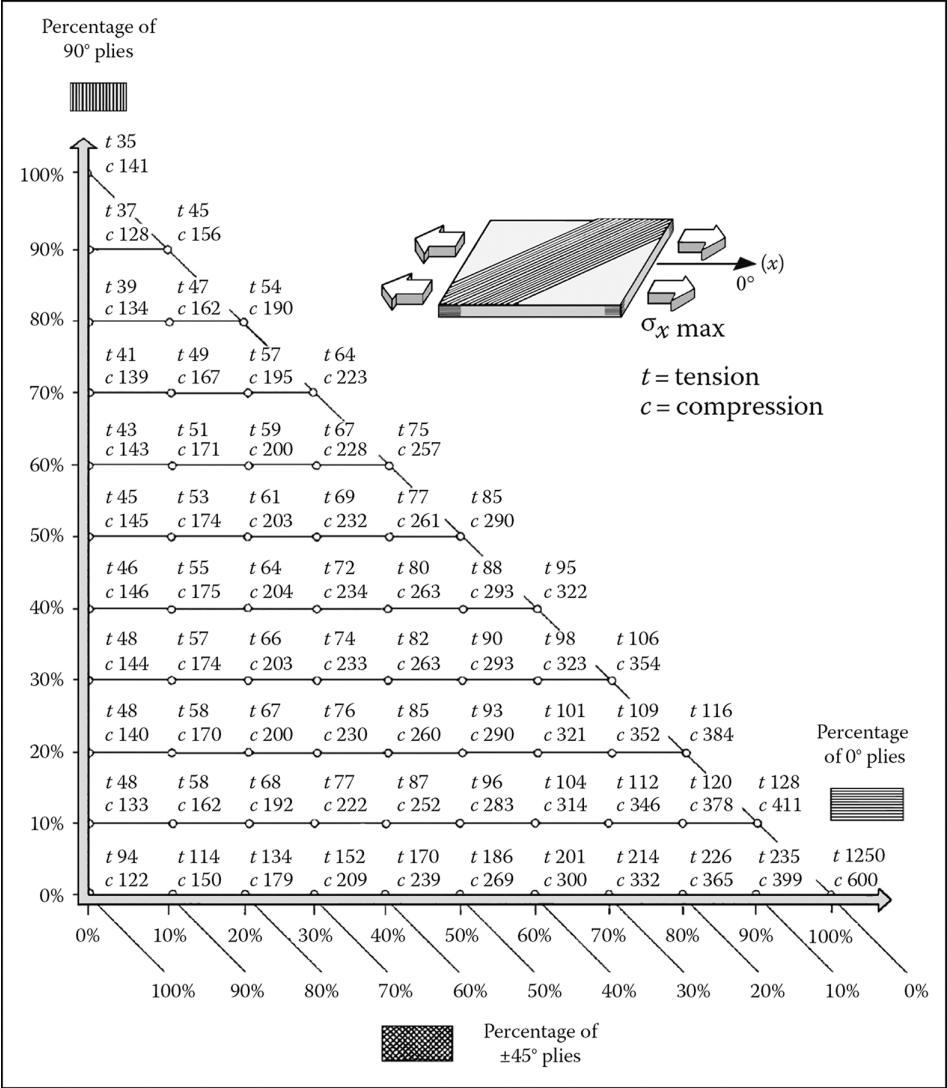
$$e_{xy} = \frac{T_{xy}}{\tau_{\text{rupture}}}$$

where τ_{rupture} is the maximum shear stress that a $\pm 45^\circ$ laminate can support.



Note: Shear modulus G_{xy} (MPa) as a function of the ply percentages in the directions 0° , 90° , $+45^\circ$, and -45° . (For more information on modulus and strength of a basic ply, see Section 3.3.3.)

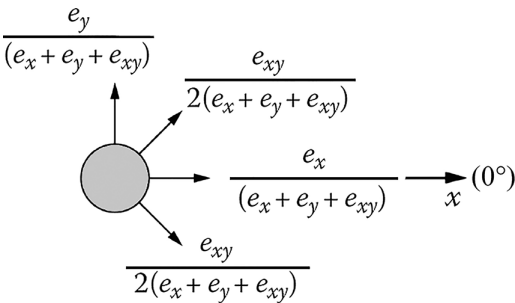
CHART 5.10 Kevlar/epoxy laminate: $V_f = 60\%$, ply thickness =

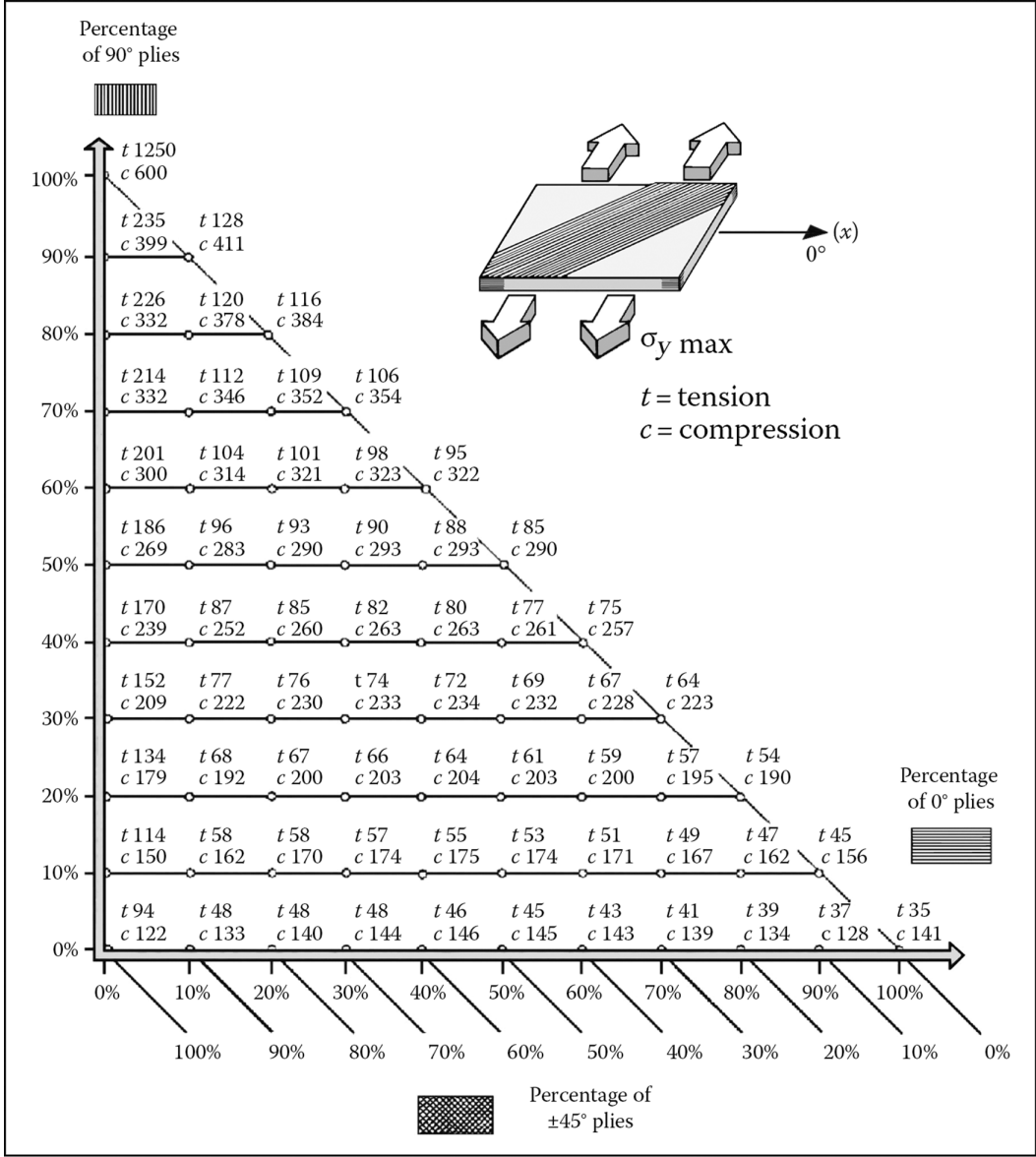


Note: Maximum stress $\sigma_{x \max}$ (MPa) as a function of the ply percentages in the directions 0°, 90°, +45°, and -45°. (For more information on modulus and strength of a basic ply, see Section 3.3.3.)

CHART 5.11 Glass/epoxy laminate: $V_f = 60\%$, ply thickness = 0.13 mm.

Therefore, we can retain for the complete laminate the proportions indicated below.





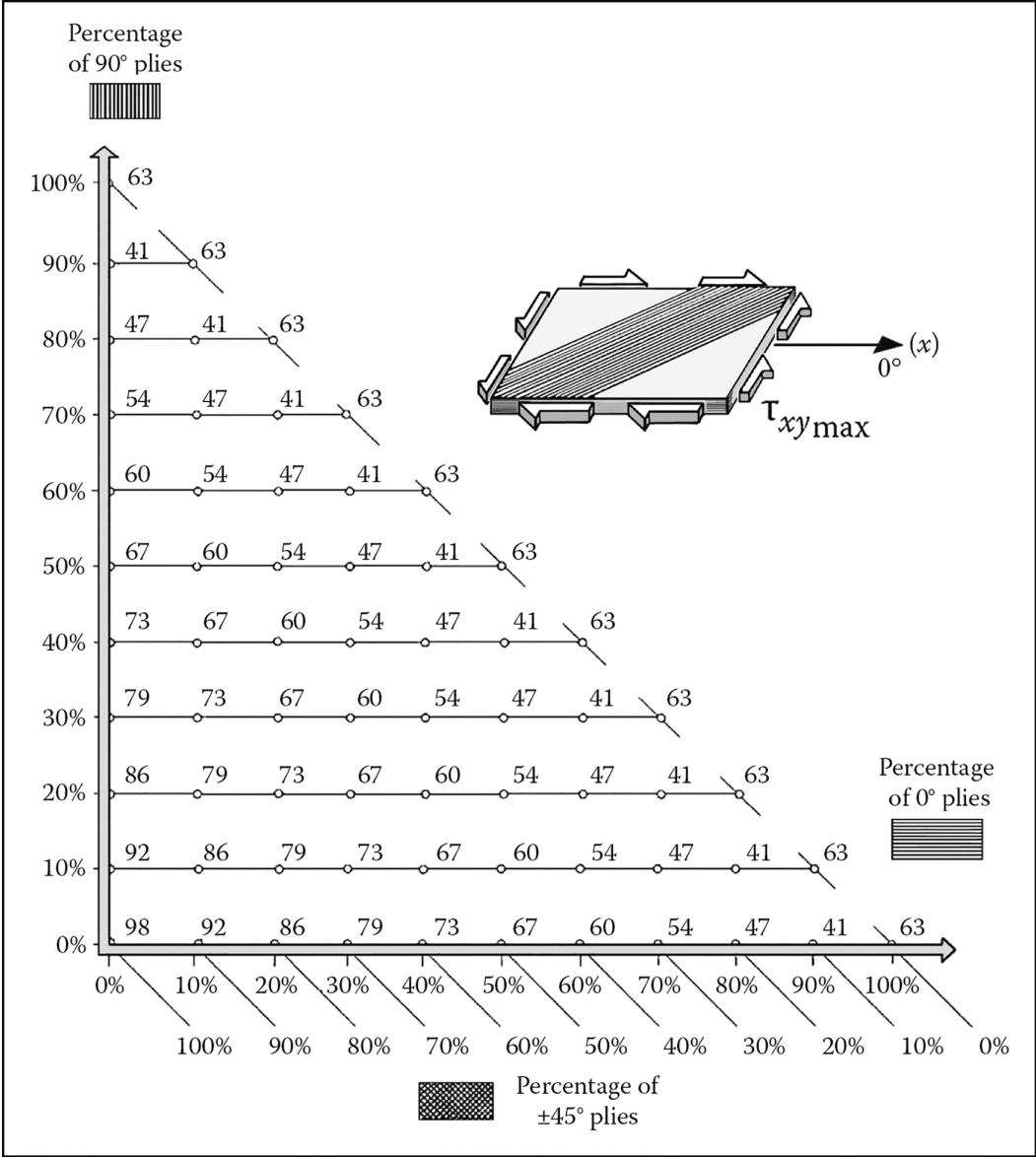
Note: Maximum stress $\sigma_{y \max}$ (MPa) as a function of the ply percentages in the directions 0°, 90°, +45°, and 45°. (For more information on modulus and strength of a basic ply, see Section 3.3.3.)

CHART 5.12 Glass/epoxy laminate: $V_f = 60\%$, ply thickness = 0.13 mm.

5.4.3.2 Example

We would like to determine the composition of a laminate made up of unidirectional plies of carbon/epoxy ($V_f = 60\%$) to support the In-plane stress resultants:

$$N_x = -800 \text{ N/mm}; \quad N_y = -900 \text{ N/mm}; \quad T_{xy} = -340 \text{ N/mm}$$



Note: Maximum stress $\tau_{xy \max}$ (MPa) as a function of the ply percentages in the directions 0°, 90°, +45°, and -45°. (For more information on modulus and strength of a basic ply, see Section 3.3.3.)

CHART 5.13 Glass/epoxy laminate: $V_f = 60\%$, ply thickness = 0.13 mm.

The compression strength $\sigma_{\ell_{\text{rupture}}}$ is 1,130 MPa (see Section 3.3.3 or Chart 5.1 for 100% of 0° plies). Then

$$e_x = \frac{800}{1,130} = 0.71 \text{ mm}; \quad e_y = \frac{900}{1,130} = 0.8 \text{ mm}$$

The optimum shear strength τ_{rupture} is given in Chart 5.3 for 100% of ±45° plies; then

$$\tau_{\text{rupture}} = 397 \text{ MPa}$$

From which

$$e_{xy} = \frac{340}{397} = 0.86 \text{ mm}$$

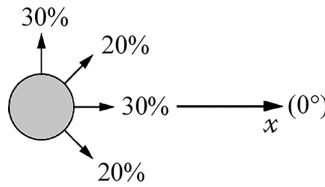
We obtain for the proportions

$$\text{at } 0^\circ \Rightarrow \frac{e_x}{e_x + e_y + e_{xy}} = 0.3$$

$$\text{at } 90^\circ \Rightarrow \frac{e_y}{e_x + e_y + e_{xy}} = 0.34$$

$$\text{at } \pm 45^\circ \Rightarrow \frac{e_{xy}}{e_x + e_y + e_{xy}} = 0.36$$

And we can then retain for the composition of the laminate the following approximate values:



5.4.3.3 Note

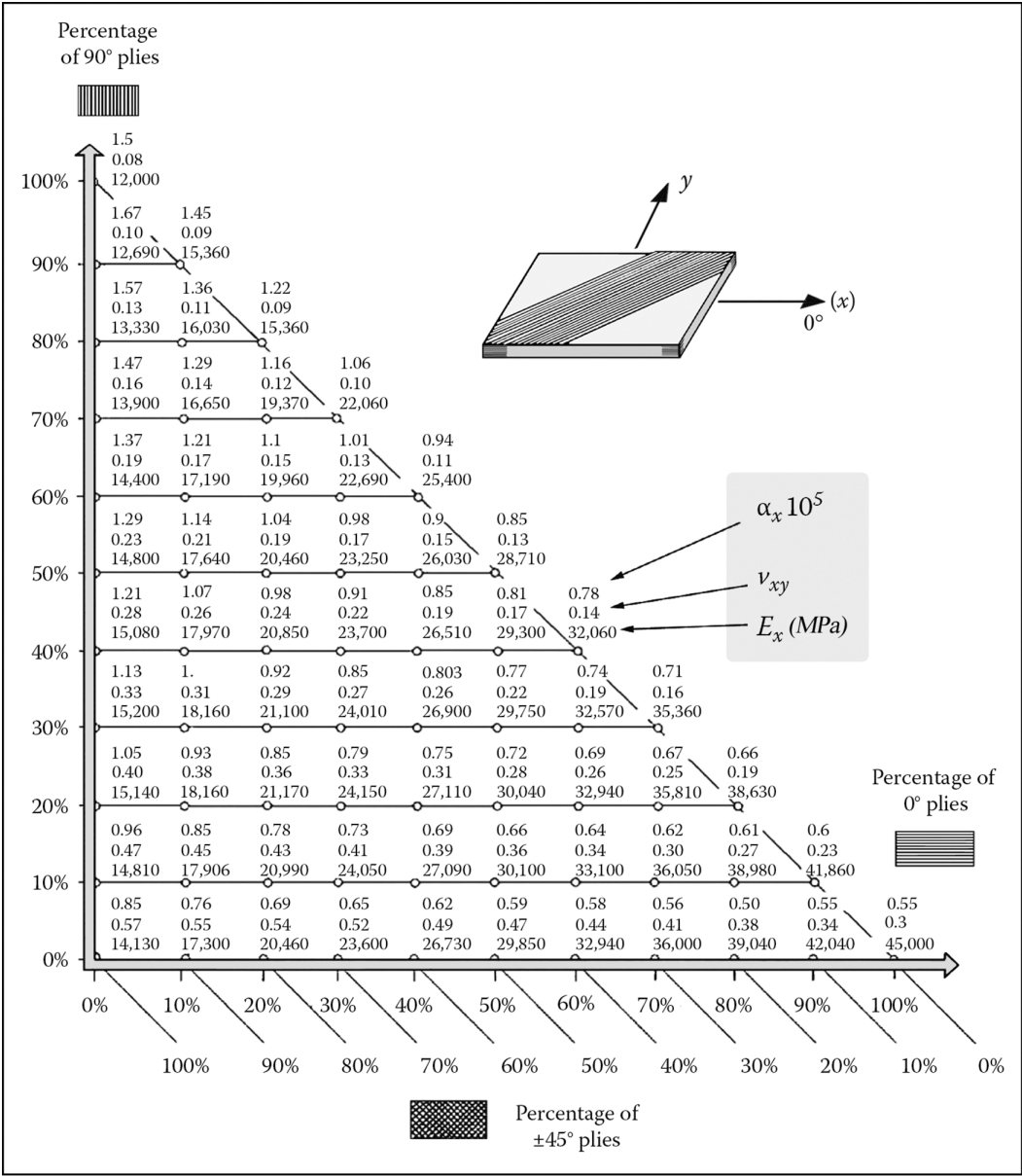
Thicknesses e_x , e_y , and e_{xy} as evaluated above only serve to determine the proportions. After that, they **should not be kept**. This because in fact each orientation really supports a part of each stress resultant. For example, the 0° plies cover the major part of stress resultant N_x , but they **also** support a part of stress resultant N_y **and** a part of stress resultant T_{xy} , thus resulting to a more unfavorable situation for each orientation as compared with what has been assumed previously. The minimum required for the laminate thickness will in fact be larger than the previous result ($e_x + e_y + e_{xy}$), which therefore appears to be **dangerously optimistic**. The practical determination of the minimum thickness of the laminate comes from the Tsai-Hill failure criterion, as indicated at the end of Section 5.3.2 and explained in details in Application 19.6. In this way, with the same stress resultants and proportions as in the previous example, one finds a minimum thickness of 2.64 mm (see Application 19.6, in Chapter 19), whereas the previous sum ($e_x + e_y + e_{xy}$) gave a thickness of 2.37 mm, 10% lower than the required minimum thickness (2.64 mm).

5.4.4 COMPLEX LOADING CASE: OPTIMUM COMPOSITION OF A LAMINATE

5.4.4.1 Optimum Laminate

Estimation of the proportions in the previous paragraph does not generally lead to **an optimum laminate**, that is, a laminate with the smallest thickness among all laminates of different compositions that can support a given set of In-plane stress resultants N_x , N_y , and T_{xy} .

Charts 5.16–5.19, calculated on the base of Tsai-Hill criterion,¹⁸ give the optimum compositions of laminates made of carbon/epoxy unidirectional that can support various sets of In-plane resultants N_x , N_y , and T_{xy} . The indicated compositions (percentages) correspond to laminates that are



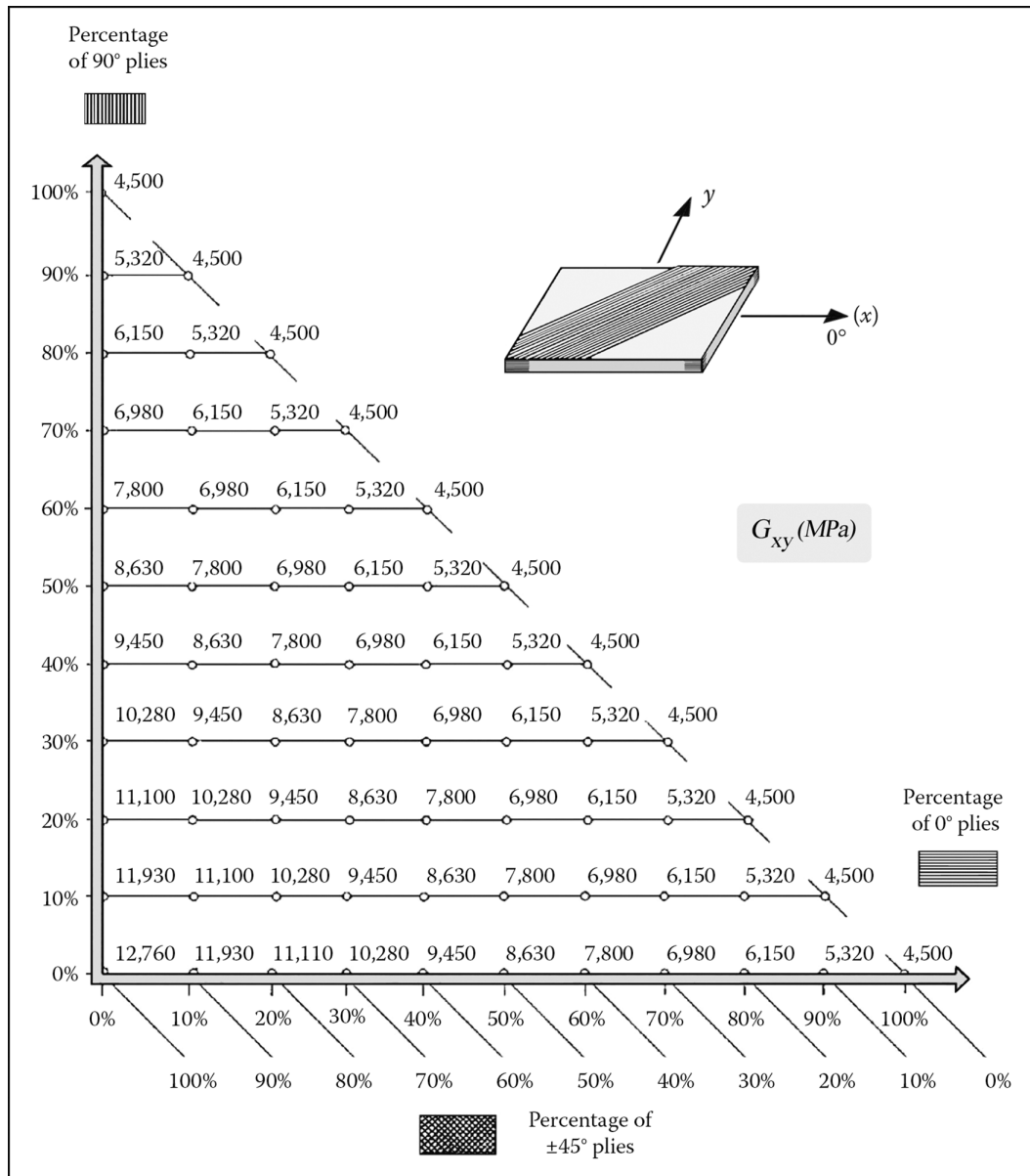
Note: Longitudinal modulus E_x (MPa), Poisson ratio ν_{xy} , and coefficient of thermal expansion α_x as a function of the ply percentages in the directions 0°, 90°, +45°, and -45°. (For more information on modulus and strength of a basic ply, see Section 3.3.3.)

CHART 5.14 Glass/epoxy laminate: $V_f = 60\%$, ply thickness = 0.13 mm

able to support the specified flux resultants while in the same time keeping a minimum thickness. This thickness value can be read in millimeters within the circles. It relates to an *arithmetic* sum of the In-plane resultants equal to 100 N/mm.

Also shown in the charts are the following:

- The direction along which the first damage will occur (first-ply failure).
- The multiplication factor for the In-plane resultants in order to go from first-ply failure to ultimate fracture of the laminate.



Note: Shear modulus G_{xy} (MPa) as a function of percentages of plies in directions 0° , 90° , $+45^\circ$, and -45° . (For more information on modulus and strength of a basic ply, see Section 3.3.3.)

CHART 5.15 Glass/epoxy laminate: $V_f = 60\%$, ply thickness = 0.13 mm.

- The two compositions (a) and (b) that are closest to the optimum composition, obtained by varying from the indicated composition along the direction of the arrows. First, in order to define composition (a), the increasing or decreasing arrows (*solid line*) denote the increase or decrease of 5% as compared to proportions marked. Next, to define composition (b), the increasing or decreasing *dotted* arrows denote the increase or decrease of 5% as compared to proportions marked.

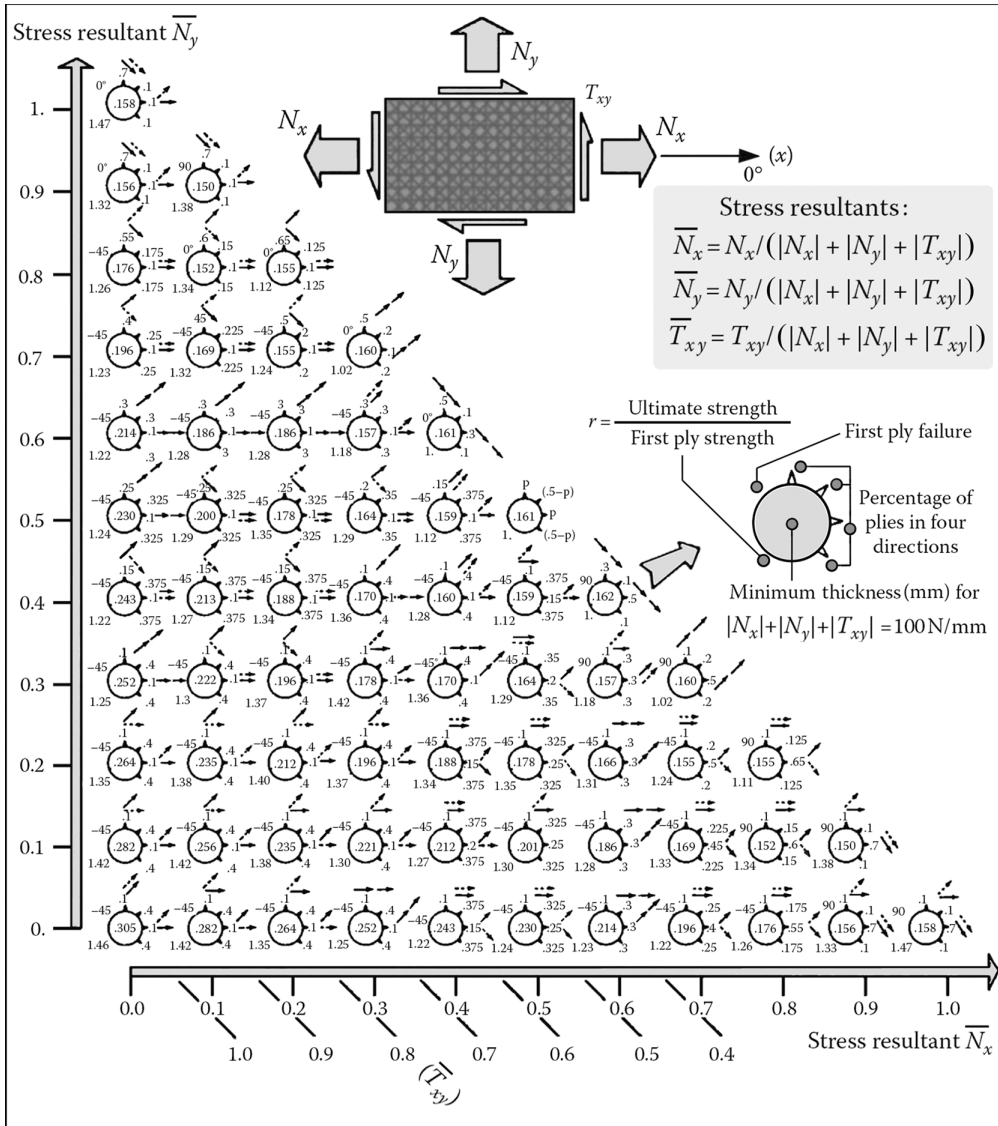


CHART 5.16 Optimum composition of a carbon/epoxy laminate.

5.4.4.2 Example

Given the stress resultants:

$$N_x = 720 \text{ N/mm}; \quad N_y = 0; \quad T_{xy} = 80 \text{ N/mm}$$

We first deduce the values of the reduced flux resultants:

$$\bar{N}_x = \frac{720}{720 + 80} = 0.9; \quad \bar{N}_y = 0; \quad \bar{T}_{xy} = \frac{80}{720 + 80} = 0.1$$

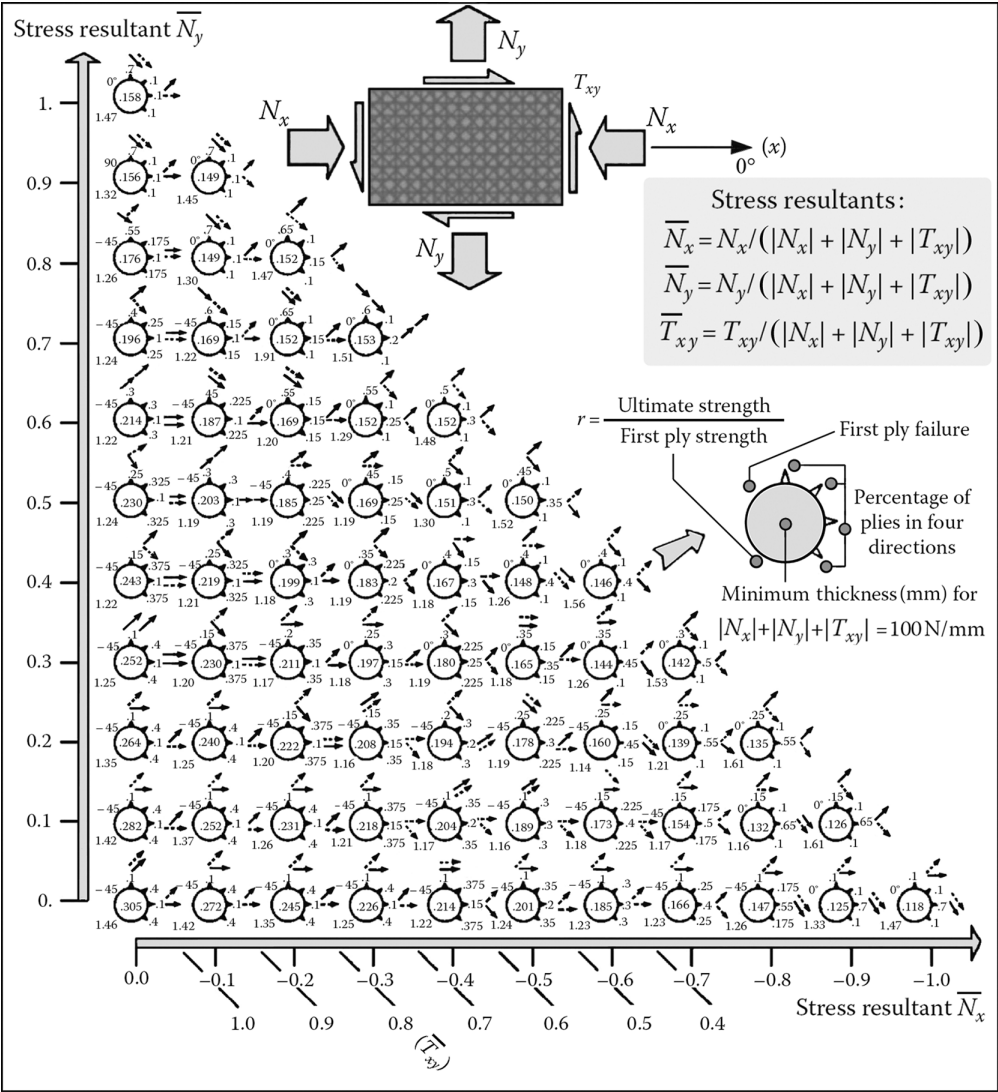
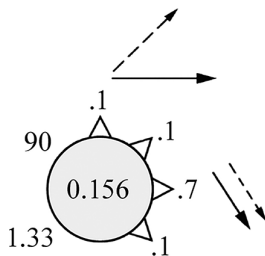
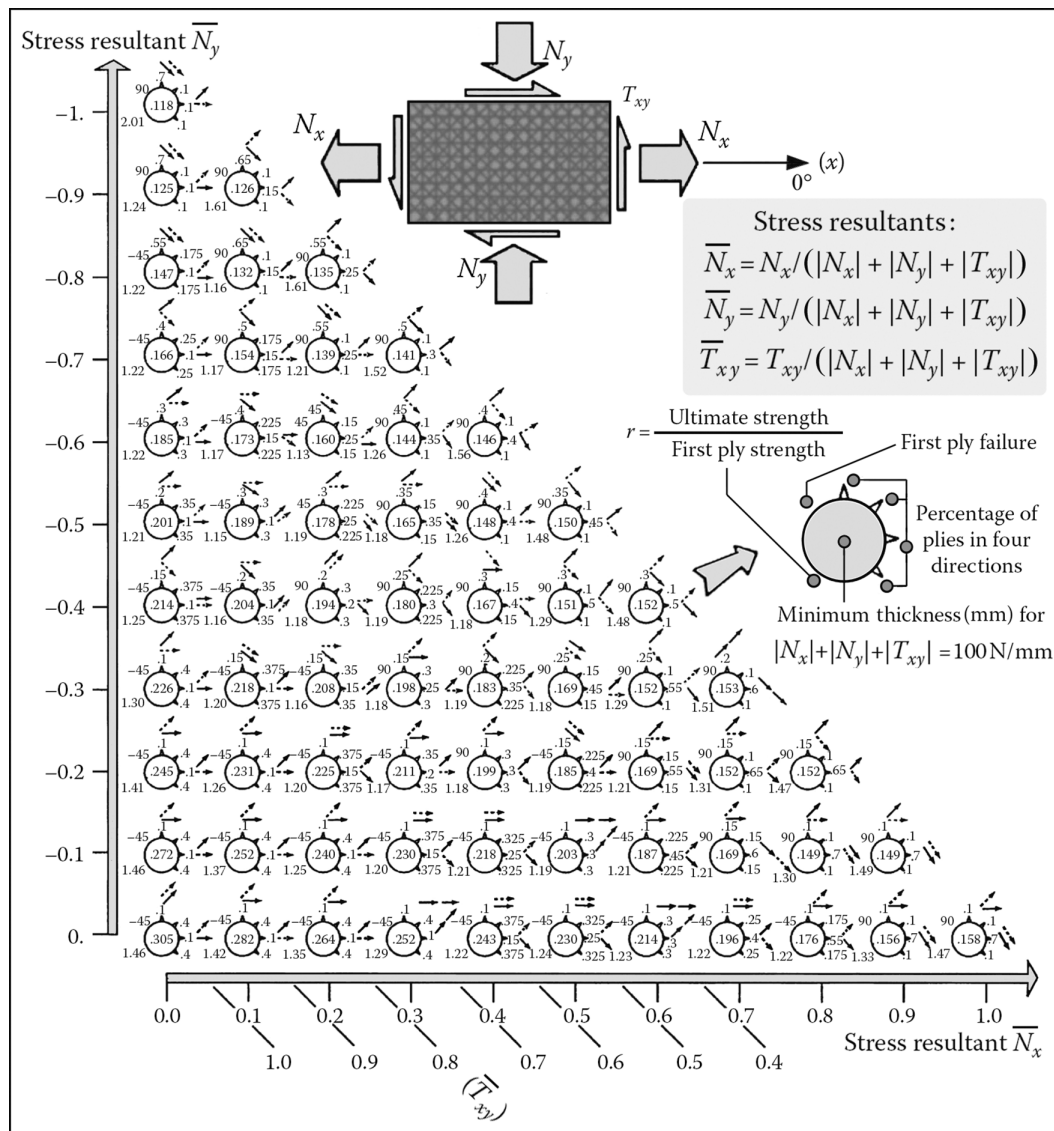


CHART 5.17 Optimum composition of a carbon/epoxy laminate.

We then use Chart 5.16 (all stress resultants are positive), where we note, corresponding to these values of reduced stress resultants, the following pictogram:





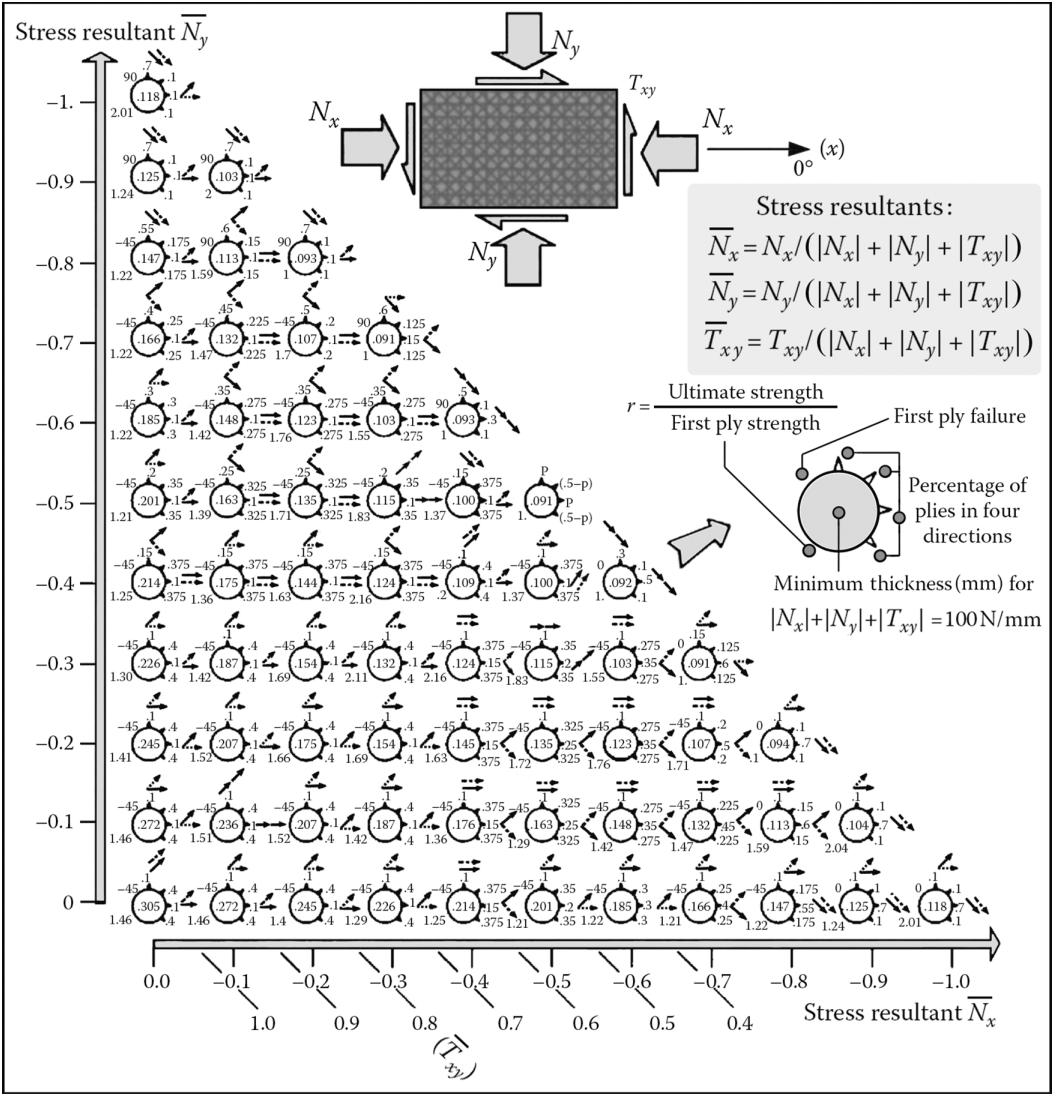
Note: $V_f = 0.6$, 10% minimum in each direction 0° , 90° , $+45^\circ$, and -45° . (For ply characteristics, see Appendix A or Section 3.3.3.)

CHART 5.18 Optimum composition of a carbon/epoxy laminate.

This can be interpreted in the following way:

- **Optimal composition of the laminate:**
 - 70% of 0° plies (along x -direction)
 - 10% of 90° plies
 - 10% of plies at 45° , 10% of plies at -45°

The **critical thickness of the laminate** is 0.156 mm when the arithmetic sum of the three stress resultants is equal to 100 N/mm. For this thickness, the first-ply failure occurs in the 90° plies. However, one can continue to load this laminate until reaching 1.33 times the critical load. At this point, there is complete rupture of the laminate.



Note: $V_f = 0.6$, 10% minimum in each direction 0° , 90° , $+45^\circ$, and -45° . (For ply characteristics, see Appendix A or Section 3.3.3.)

CHART 5.19 Optimum composition of a carbon/epoxy laminate.

Returning to our example, the arithmetic sum of the stress resultants is equal to:

$$720 + 80 = 800 \text{ N/mm} = 8 \times 100 \text{ N/mm}$$

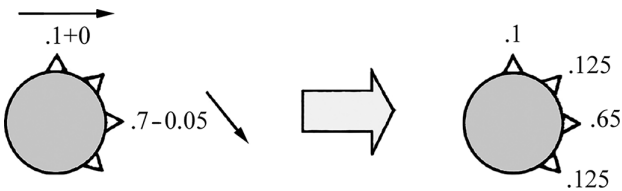
Then, the thickness of the laminate has to be more than

$$8 \times 0.156 = 1.25 \text{ mm}$$

And the complete failure of the laminate will occur if the loading is multiplied by a factor of 1.33, that is, for

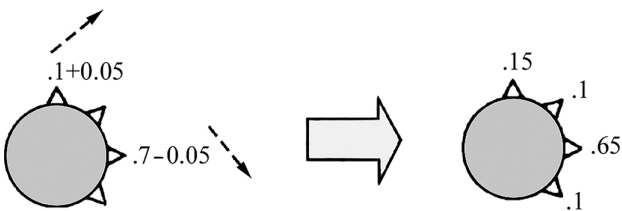
$$N_x = 1.33 \times 720 = 957 \text{ N/mm}; \quad N_y = 0; \quad T_{xy} = 1.33 \times 80 = 106 \text{ N/mm}$$

- **Neighboring compositions:** The second smallest thickness in the vicinity is obtained by modifying the indicated composition in the direction specified by the arrows in solid line, as



We then obtain (not shown on the chart) a thickness of 0.160 mm (increase of 2.5% relative to the previous value) and a multiplication factor to reach the ultimate loading equal to 1.35.

Continuing in the direction of increasing thickness, the third smallest thickness in the immediate vicinity is obtained by modifying the indicated composition in the direction specified by the dotted arrows, as



We then obtain a thickness (not shown on the chart) of 0.165 mm (increase of 6%) and a multiplication factor of 1.3 for the ultimate load.

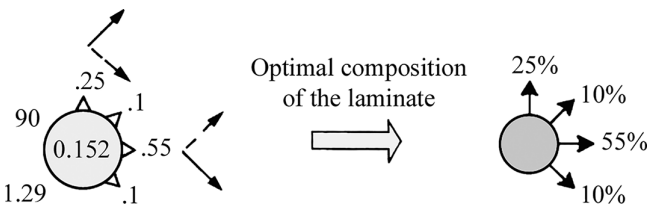
5.4.4.3 Example

Given the stress resultants

$$N_x = 600 \text{ N/mm}; \quad N_y = -300 \text{ N/mm}; \quad T_{xy} = 100 \text{ N/mm}$$

the corresponding reduced stress resultants are

$$\bar{N}_x = 0.6; \quad \bar{N}_y = -0.3; \quad \bar{T}_{xy} = 0.1 \text{ N/mm}$$



We obtain from Chart 5.18

where the critical thickness is $10 \times 0.152 = 1.52$ mm (since the arithmetic sum of the stress resultants is 1,000 N/mm or 10×100 N/mm).

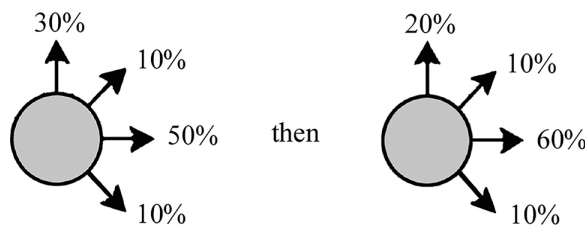
- These are the 90° plies that fail first
- Complete rupture of the laminate occurs when

$$N_x = 1.29 \times 600 = 774 \text{ N/mm}$$

$$N_y = 1.29 \times -300 = -387 \text{ N/mm}$$

$$N_{xy} = 1.29 \times 100 = 129 \text{ N/mm}$$

- The closest critical thicknesses (in increasing order) are obtained with the following suc-

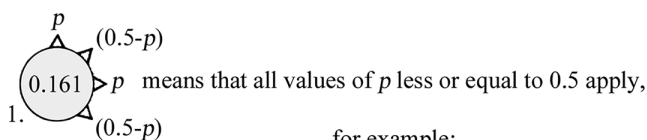
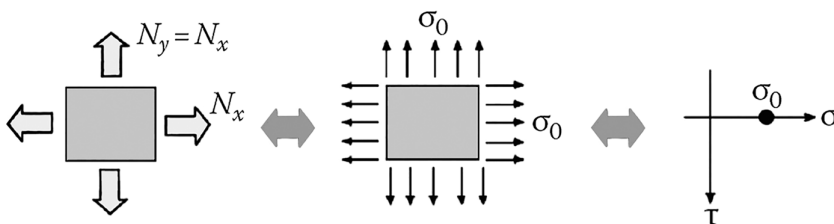


cessive compositions:

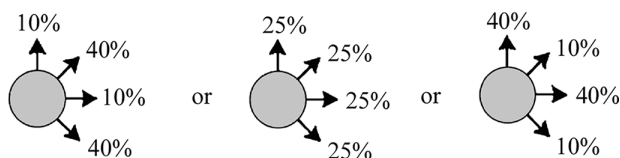
5.4.4.4 Notes

- A few loading cases can lead to several distinct optimum compositions, but with identical thicknesses. For example, the reduced stress resultants

$$\bar{N}_x = \bar{N}_y = 0.5; \quad \bar{T}_{xy} = 0$$



for example:

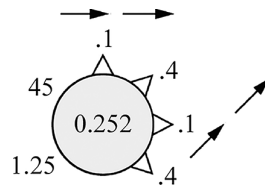


This represents a case of isotropic loading, Mohr's circle being reduced to one point as illustrated below.

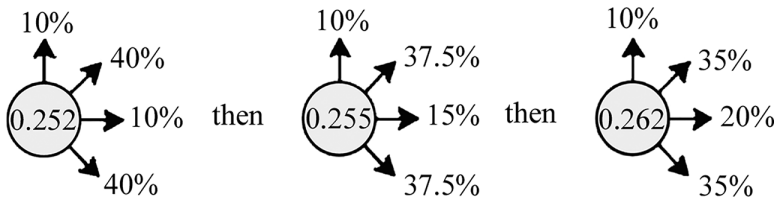
Chart 5.16 indicates

We obtain in this case a unique critical thickness of 0.161 mm (corresponding to a sum $N_x + N_y = 100$ N/mm) **whatever** the proportion p^{19} . The isotropic composition [25% / 25% / 25% / 25%] in the directions 0° , 90° , $+45^\circ$, and -45° might appear intuitive. In fact, it can be replaced by various periodic compositions²⁰.

- In some loading cases, one finds from the table only arrows in a solid line. For example, for the following reduced stress resultants



$$\bar{N}_x = 0.3; \quad \bar{N}_y = 0; \quad \bar{T}_{xy} = 0.7$$



We find from Chart 5.16 the following figure:

The three neighboring optimum compositions in increasing order are

(Thicknesses of 0.255 and 0.262 mm are not indicated on the chart.) The third composition, characterized by an increase in thickness of (0.262–0.252 mm), or 6%, leads to an increase in modulus of elasticity in the x (0°) direction by 36% (see Section 5.4.2, Chart 5.4).

We should finally note that in the majority of cases, the optimum compositions indicated in Charts 5.16–5.19 are not easy to postulate basing on intuition²¹.

5.4.5 NOTES FOR PRACTICAL USE CONCERNING LAMINATES

5.4.5.1 Specific Aspects for the Design of Laminates

- Fabrics can be shaped on double-curved surfaces²² by pushing back in the warp and weft directions (possibility of shrinkage up to 30%).
- The radii of the mold must not be too small. This applies in particular to the inner radius R_i as shown in Figure 5.24a. The graph in Figure 5.24b provides an overview of minimum values required for the inner and outer radii.
- The **thickness** of a polymerized ply is only of 0.8–0.85 times that of the ply before polymerization. Thus, when dimensioning the final thicknesses, one has to take into account a margin of uncertainty of the order of 15%.
- When the surface of the part is too large to be covered by an only sheet of unidirectional taken from the roll, precautions should be taken when cutting out the different elements drawn from the roll. One can see in Figure 5.25 a few lay-up examples.

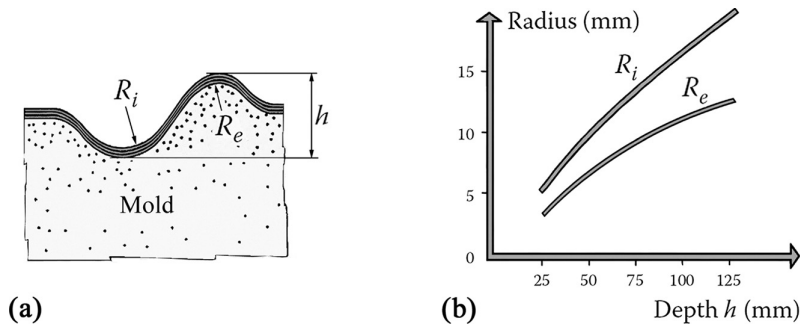


FIGURE 5.24 Minimum required for inner and outer radii of mold.

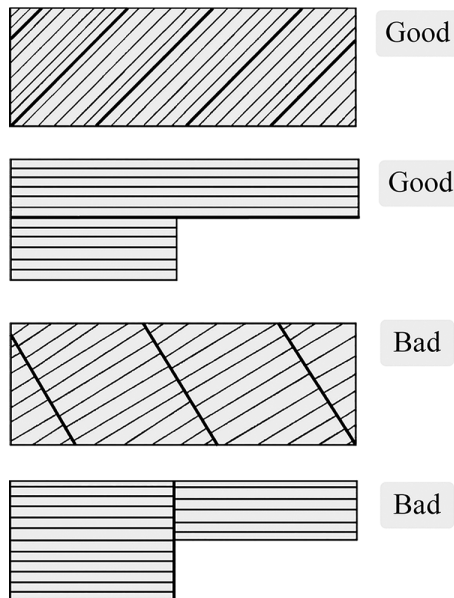


FIGURE 5.25 Disposition of cut elements from unidirectional roll.

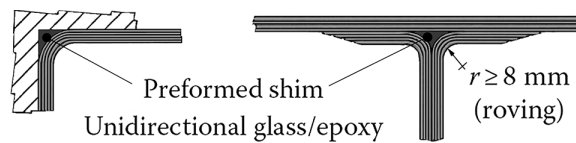


FIGURE 5.26 Laying in a corner.

- The unidirectional sheets cannot have sharp bends in the fiber direction. The schematic in Figure 5.26 shows the design features to achieve sudden curvature changes along the lay-up direction.

5.4.5.2 Delaminations

When some plies making up the laminate separate from each other, it is said that there is **delamination**. Many causes account for this type of damage:

- (a) **An impact** that does not leave apparent traces on the surface but may lead to internal delaminations

Carbon/epoxy laminates are susceptible of such localized delamination, resulting, for example, from the fall of a dense object (tool) on the surface coating. Subsequently, the compressive strength of the part is affected by the damage. Indeed, not only damages to some plies but also delamination of interfaces between plies occur, as shown in the following example. Then, in addition, the risk of a local buckling due to compression occurs, which can spread. This phenomenon has to be carefully monitored in aircraft construction and leads to sizing criteria based not on a maximum compression stress but on a maximum compression strain²³. In practice, the latter is evaluated in microstrain ($\mu\epsilon$), that is, $\epsilon \times 10^6$, where ϵ is the small classic strain already seen. For such applications involving carbon/epoxy parts, the maximum allowable compression strain is linked to a codified intensity for a tool impact and is somewhat above 3,000 $\mu\epsilon$ in terms of absolute value.

Accordingly, one can clearly see here that with unidirectional sheets, the most loaded plies should not be draped on the upper or lower laminate surface²⁴.

Example: Impact of a projectile on a layered plate $[0_n^\circ / 90_n^\circ / 0_n^\circ]$

- Order of magnitude of impact:

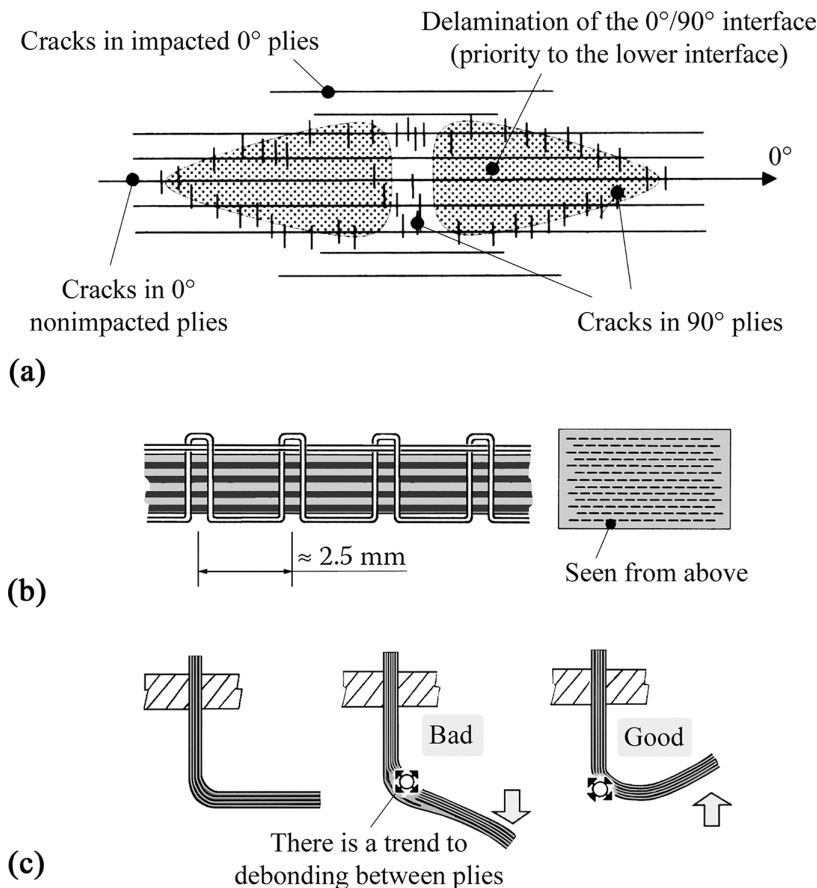


FIGURE 5.27 (a) Impact on a $[0_n^\circ / 90_n^\circ / 0_n^\circ]$ laminate. (b) Sewing stitch on a laminate. (c) Laminated bracket loaded.

- Mass: several kilograms; speed: several m/s

The damage in the impacted area is shown in Figure 5.27a.

- An improvement: the stitch of the laminate. In view of reducing the impact damage, the delamination can be prevented by carrying out sewing stitches (Figure 5.27b) on

- Prepregs
- Dry preforms before injection molding²⁵

(b) **A mode of loading** that leads to the disbond of the plies (tensile load on the interface) as shown in Figure 5.27c

(c) **Shear stresses** on the interfaces between the different plies, which occur very close to the edges of the laminates and that may be illustrated as follows, taking a three-ply laminate as an example:

1. Consider the three plies in Figure 5.28a, uncoupled. Under the effect of loading (the figure at the right-hand side), they deform independently, and therefore, they do not coincide anymore when they are superimposed.
2. Now the plies have built a balanced laminate. Under the same type of loading, they deform together, without showing any difference, as shown in Figure 5.28b.

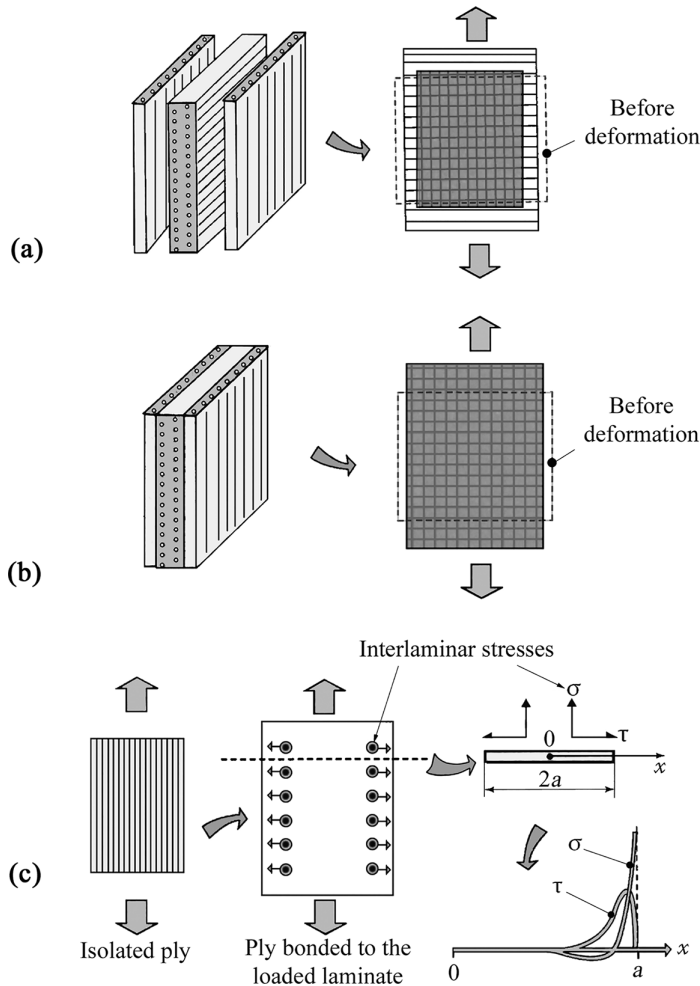


FIGURE 5.28 (a) Three plies considered separately. (b) Three plies bound together. (c) Stresses at free edge.

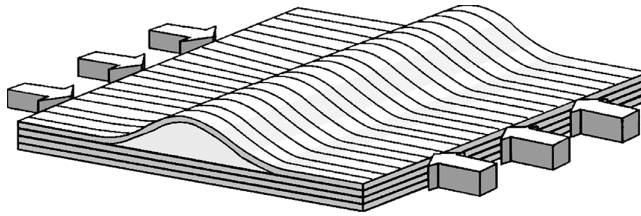


FIGURE 5.29 Delamination due to buckling at interface.

3. That means that interlaminar stress components occur on the bonded faces. It can be shown that these stress components are located very near the edges of the laminate, as illustrated in Figure 5.28c.
- (d) **A complex state of stress** at the interface, caused for example by a local buckling (see Figure 5.29)

Practical as well as theoretical studies of these interlaminar stress components are very difficult, and the phenomenon is still imperfectly controlled.

5.4.5.3 Why Is Fatigue Resistance So Good?

- **Paradox:** Glass is a very brittle material (no plastic deformation). Similarly, a resin is also often an almost brittle material that does not yield (e.g., epoxy). Nonetheless, the reinforcement/matrix association formed by these two materials opposes to the propagation of cracks and makes the resultant composite remarkably fatigue-resistant compared to a metallic alloy.
- **Explanation:** When the crack initiates, for example in the unidirectional layer shown schematically in Figure 5.30 in the form of alternating of fibers and resin, the initial stress concentration at crack tip causes a degradation of the resin as pictured. Accordingly, there is a disbond of fibers from the matrix. Therefore, fibers benefit from a stress relaxation. Thus, there is no stress concentration comparable to what happens in a homogeneous material.

5.4.5.4 Laminated Tubes

Laminated tubes can be obtained by winding of threads, unidirectional tapes, or fabrics. As the first approximation²⁶, the strain and stress values in flexure and in torsion can be estimated from the relations in Figure 5.31 in which the following applies:

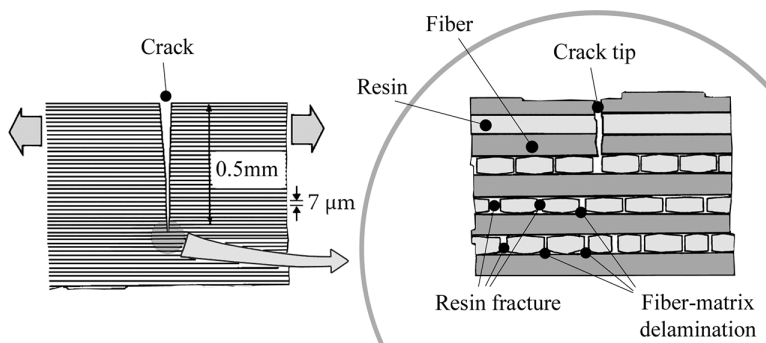
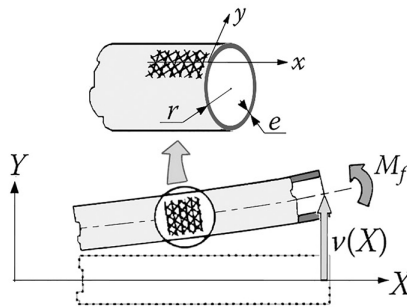


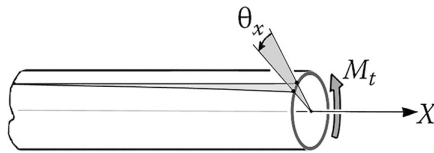
FIGURE 5.30 Crack effects in unidirectional.



Flexure:

$$E_x I \frac{d^2 v}{dX^2} = M_f$$

$$\sigma_x = -\frac{M_f}{I} \times Y$$



Torsion:

$$G_{xy} I_0 \frac{d\theta_x}{dX} = M_t$$

$$\tau_{xy} = \frac{M_t}{I_0} \times r$$

FIGURE 5.31 Composite tube relations.

- E_x and G_{xy} are the moduli of elasticity in the tangent plane (x, y).
- I and I_0 are, respectively, the quadratic moment of inertia and polar moment of inertia of the cross section of the tube (ring section), with $I_0 = 2 \times I$.
- Y is the coordinate of a point in the cross section (in the undeformed position) in the (X, Y, Z) coordinates.
- r is the average radius of the tube.

NOTES

- 1 See Section 5.4.4.
- 2 See Section 2.3.
- 3 This is to limit the interlaminar shear stress (see Section 5.4.5 and Chapter 18). This precaution applies also to the fabrics (e.g., no more than four consecutive fabric layers of carbon/epoxy along the same direction).
- 4 This property can be observed for example on a unique ply of five-harness satin of carbon/epoxy: after curing in an autoclave, it deforms (double curvature shape) after demolding. See Application 20.17 "Thermoelastic Behavior of a Balanced Fabric Ply".
- 5 See also Applications 20.9 and 20.10.
- 6 Apart from space applications, where thicknesses are very small. Then the skins of sandwich plates are laminates that do not necessarily have individually a Mid-plane symmetry. In such cases, these are the sandwich plates themselves which exhibit overall symmetry with respect to their Mid-plane.
- 7 The laminate can also work in bending. This is studied in Chapters 12, 15, and 18.
- 8 See also Chapter 14.
- 9 For more details concerning failure criteria, see Chapter 14.
- 10 See Section 14.1.
- 11 See Section 14.5.
- 12 See Application 20.7 "First Ply Failure of a Laminate; Ultimate Strength".
- 13 The procedure for this calculation is described in Section 12.1.3.

- 14 Recall (Sections 3.1 and 3.2) that $\frac{v_{xy}}{E_x} = \frac{v_{yx}}{E_y}$.
- 15 For calculation steps, see Application 20.2 “Procedure for a Laminate Calculation Program”.
- 16 Also see Note in Section 3.4.2.
- 17 Caution: What follows applies to the determination of *proportions*, but not of *thicknesses*.
- 18 See Section 5.3.2.
- 19 See Application 20.8 “Optimum Laminate for Isotropic Plane Stress”.
- 20 See Section 5.4.2, Chart 5.4.
- 21 See Application 19.6.
- 22 See Figures 3.10 and 14.3. This is much more difficult for the plain weave fabric than for the satins, due to the mode of weaving (see Section 3.4.1).
- 23 The Strain Failure Criterion is detailed in Section 14.4.
- 24 As already noted in Section 5.2.4.1.
- 25 See Sections 2.1.4 and 2.3.1.
- 26 For a complete study of flexure and torsion of composite beams with any cross-sectional shapes, see Chapters 16 and 17. Relations in Figure 5.31 are used in Applications 19.4, 19.13, 19.15, and 21.1.

6 Conception

Fastening and Joining

We saw in Chapter 5 how to design the regular, or typical, or smooth area of a laminate so to sustain overall loads. Even more critical for the designer of a composite part is the careful design of the attachments and joints of the parts between them. Here, we look at the assembly solutions involving riveting, bolting, and bonding for

- A composite part and another composite part between them
- A composite part and a metallic part between them

6.1 RIVETING AND BOLTING

6.1.1 LOCAL LOSS OF STRENGTH

6.1.1.1 Knockdown Factor

In any mechanical component, the presence of holes generates **stress concentration factors**. Especially in composite parts, holes (molded-in holes or drilled holes) induce local reduction of the failure strength in comparison to the same location but without holes. The knockdown factor is in the range of

- **40%–60% in tension**
- **15%–50% in compression**, depending on whether the hole is filled by a fastening pin, or is free

Example: Figure 6.1 illustrates the degradation process before failure of a glass/epoxy laminate containing a free hole, under uniaxial stress.

6.1.1.2 Causes of Hole Degradation

- **Stress concentration factors:** The balance of stress shown in Figure 6.2 demonstrates the increase in stress concentration in the case of a laminate. Considering a slight torquing force provided by the rivet, usually neglected for composite laminate cases, the stresses shown in these figures are such that

$$\sigma' > \sigma$$

In an area where

$$\sigma_{\text{local rupture}} < \sigma_{\text{laminate rupture}}$$

With an order of magnitude for the maximum stress σ'_M in the laminate,

$$\sigma'_M = \sigma' \times \left\{ 1 + \sqrt{2 \left(\sqrt{\frac{E_x}{E_y} - \nu_{xy}} \right) + \frac{E_x}{G_{xy}}} \right\}$$

where

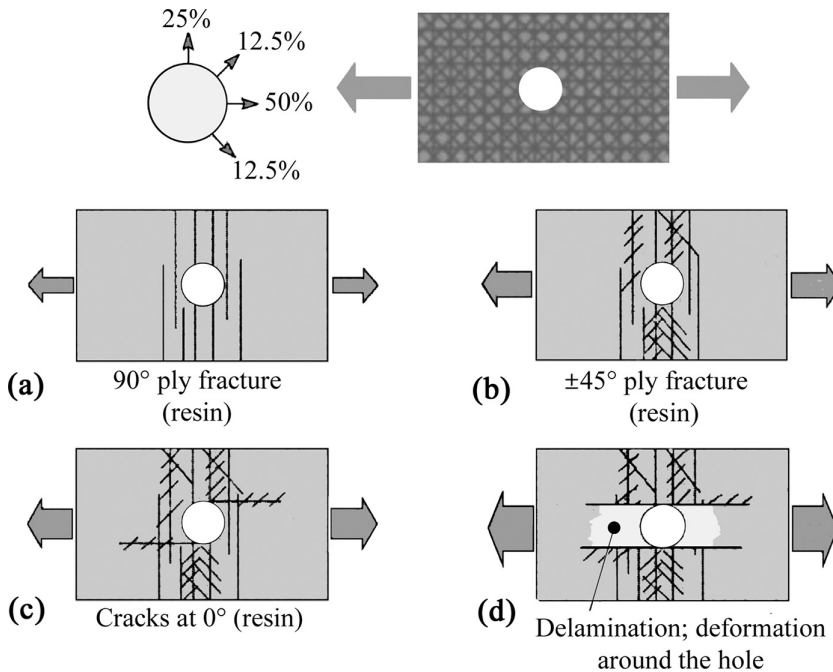


FIGURE 6.1 Progression of damage from (a) to (d) in a laminate with an open hole when load increases.

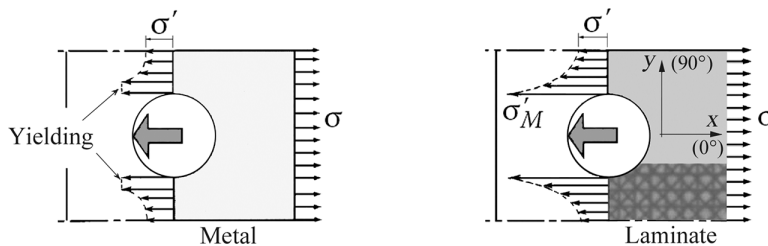


FIGURE 6.2 Stress concentrations.

E_x and E_y are the elastic moduli in the 0° and 90° directions, respectively
 G_{xy} is the shear modulus
 ν_{xy} is the Poisson ratio

In addition to this local stress increase, one should point out local phenomena called edge effects, giving rise to stress gradients near the walls of the hole, In-plane and out of plane of the laminate (see Section 14.1.3 and Figure 14.3).

- **Rupture or misalignment of fibers:** Rupture of fibers occurs during the cutting process of the hole. Another cause of hole degradation is the misalignment of fibers if the hole is made before polymerization: Figure 6.3 illustrates the correlation between the weakened zones consecutive to rupture of fibers and the **overstressed** zones.
- **Bearing stress:** This term designates the contact pressure between the rivet shank or the bolt shaft and the wall of the hole. When this pressure is excessive, it leads to spalling and **delamination** of the laminate¹.

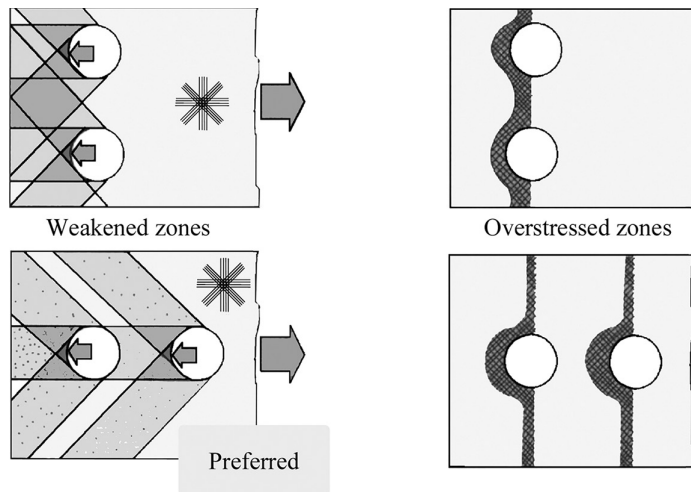


FIGURE 6.3 Weakened zones due to the presence of holes.

6.1.2 MAIN FAILURE MODES IN BOLTED JOINTS OF COMPOSITE MATERIALS

These are demonstrated in Figure 6.4.

6.1.3 SIZING OF THE JOINT

6.1.3.1 Recommended Values

- **Pitch, edge distance, and thickness** (see Figure 6.5).
- **Orientation of plies:** Recommendation for percentages of plies near the holes (see Figure 6.6).
- **Condition for no bearing damage:** In Figure 6.7, F and T designate the normal load and the shear load, respectively, acting on the connected parts, on a width of one pitch value.

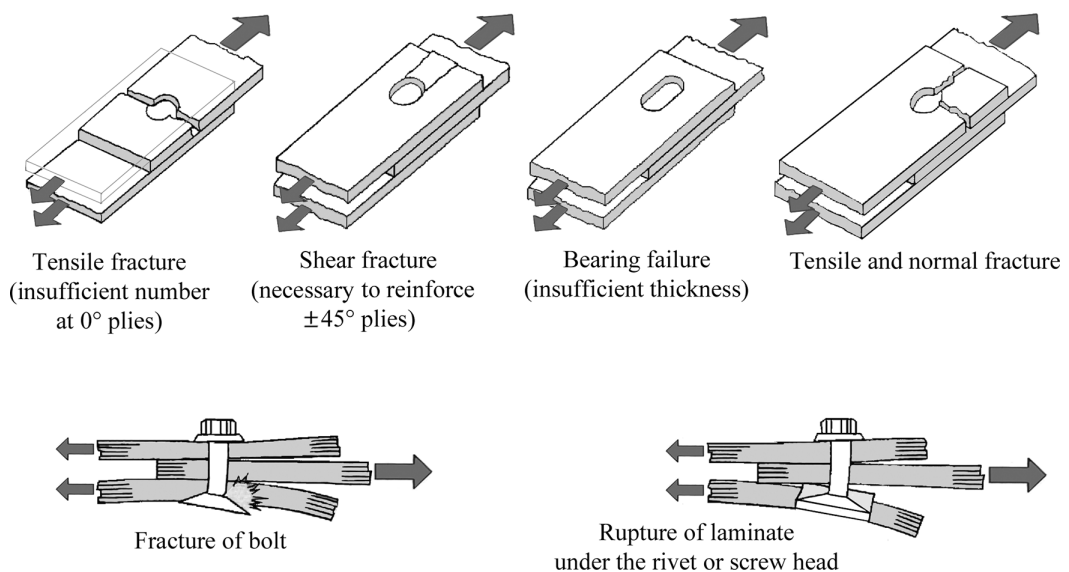


FIGURE 6.4 Main failure modes in bolted joints.

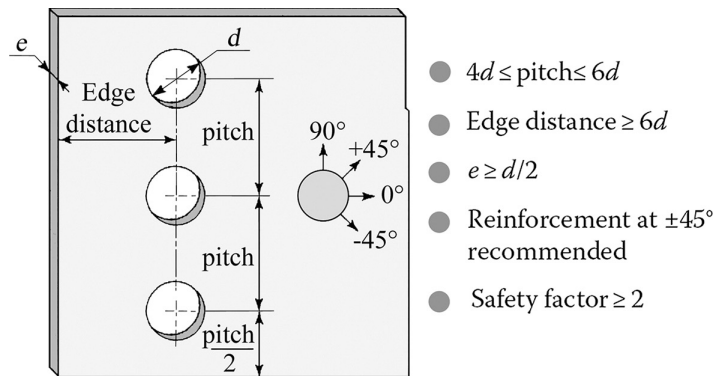


FIGURE 6.5 Recommended pitch, edge distance, and thickness.

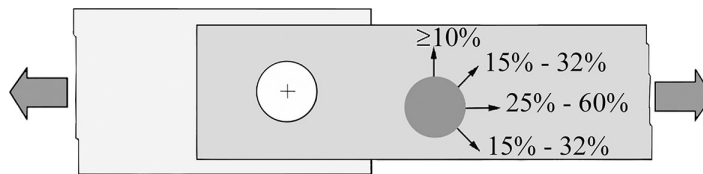


FIGURE 6.6 Recommended proportions.

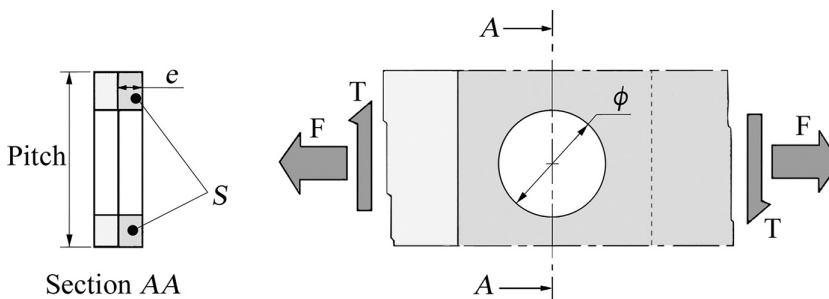


FIGURE 6.7 Normal and shear loads on assembly.

The equivalent bearing pressure, which leads to the crushing of the wall of the hole of diameter ϕ , is $F / (\phi \times e)$. It must remain smaller than a given ultimate bearing strength as

$$\frac{F}{\phi \times e} \leq \sigma_{\text{bearing strength}} \quad \text{carbon : } \sigma_{\text{bearing strength}} = 500 \text{ MPa}$$

$$\text{glass : } \sigma_{\text{bearing strength}} = 300 \text{ MPa}$$

6.1.3.2 Evaluation of Magnified Stress Values

The principle of calculation consists in increasing the stress values that are given by elementary considerations, by means of empirical coefficients of magnification²:

- Due to the presence of the hole
- Due to the pressure of contact or bearing on the wall of the hole (rivet, bolt)

With the notations of Figure 6.7, we have

$$\sigma_{\text{increased}} = \frac{1}{\alpha} \left(\frac{F}{S} + 0.2 \frac{F}{\phi \times e} \right)$$

tension, $\alpha = 0.6$

compression, $\alpha = 0.8$

$$\tau_{\text{increased}} = \frac{1}{0.7} \times \frac{T}{S}$$

Then checking should be carried out in order to ensure that these stress levels are compatible with the allowable values, that is, that they do not lead to the failure of the ply, by using the method of verification of nonfailure described in Section 5.3.2.

6.1.4 RIVETING

The special features and recommendations for riveting the composite parts can be presented as follows:

- **Do not hit the rivets**, due to the poor impact resistance of the laminates.
- Beware of possible **rupture of laminate under the rivet head** (pull-through failure) due to small laminate thickness.
- The **galvanic compatibility** of the rivet with the laminates to be assembled shall be ensured. For example, as a rule, never use aluminum rivets through a carbon laminate.
- **Riveting used along with bonding** of the surfaces to be assembled provides a gain in the mechanical resistance on the order of 20%–30%. On the other hand, the disassembly of the joint becomes impossible, and the weight is increased.

Some characteristics of rivets for composites are shown in Figure 6.8.

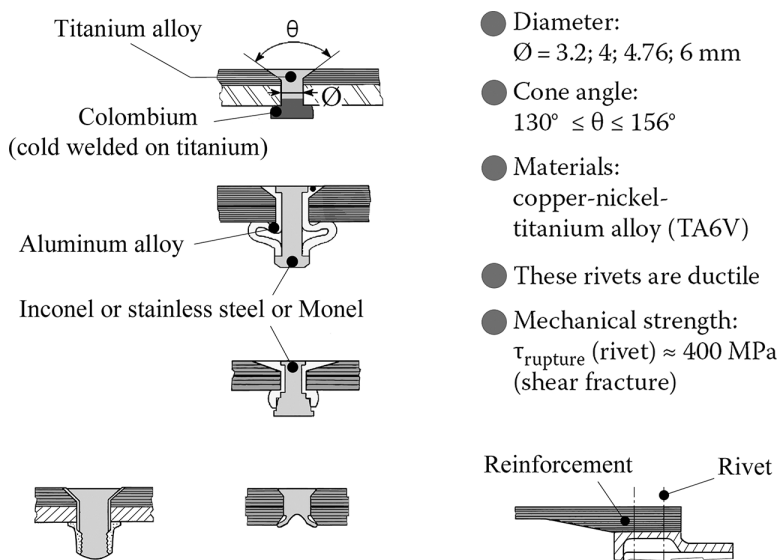


FIGURE 6.8 Different types of riveting.

6.1.5 BOLTING

6.1.5.1 Example of Bolted Joint

Let us look at a practical example that requires a bolted joint (simple case)³. Consider a sandwich panel fixed on a base support and subjected to simple loading represented by a shear load and a bending moment (see Figure 6.9).

A bolt fastening is envisaged. As shown in the schematics of Figure 6.10, even if the bolt is not tightened, it is in principle able to act to equilibrate the bending moment. However, the action of the shear load will work to separate the sandwich skins.

It is the torquing of the bolt that will allow contact pressure distribution between the base support and the skins. The sum of forces accruing from this contact pressure acting on the sandwich panel will balance out the overall shear resultant, while removing any risk of separation of skins (see Figure 6.11).

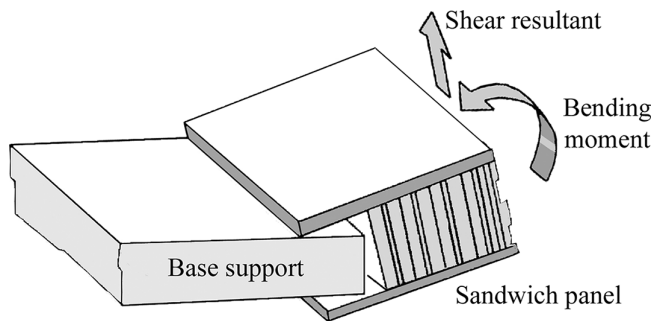


FIGURE 6.9 Fastening a panel using bolted joint.

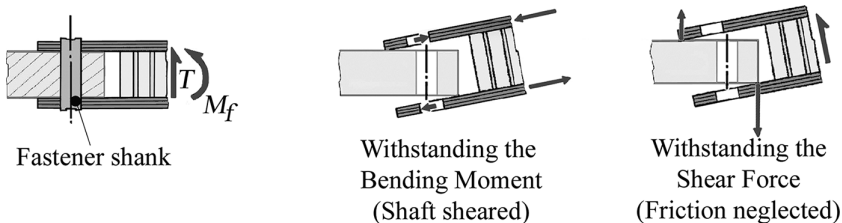


FIGURE 6.10 Local behavior without bolt torquing.

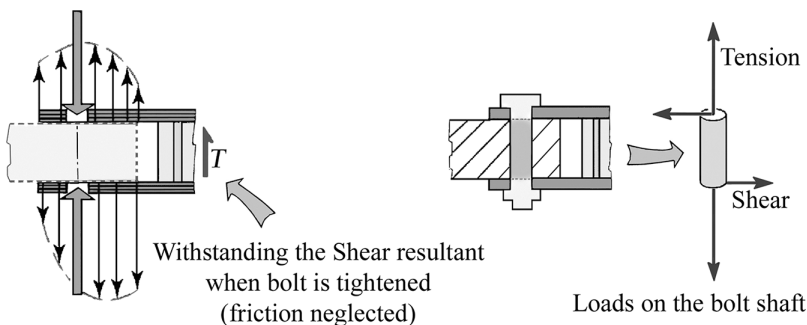


FIGURE 6.11 Advantage of tightening torque.

6.1.5.2 Tightening of the Bolt

The **tightening of the bolt** is therefore mandatory.

- However, the laminated skins are fragile and **cannot admit** high contact pressures under the bolt head and under the nut: there is a need for local metallic devices, allowing a distributed pressure on a larger surface as shown in Figure 6.12.
- The bolting plus bonding of the surfaces provides a gain in mechanical resistance of 20%–30%. On the other hand, the joint cannot be disassembled and is increased in weight.

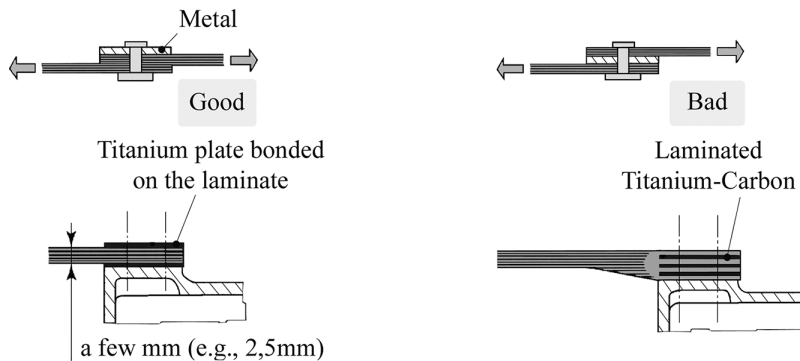


FIGURE 6.12 Some configurations for bolted joints.

6.2 BONDING

Let us mention briefly that this common joining technique is based upon the adhesion by molecular attraction between two parts (the substrates to be bonded) and an adhesive that must be able to transfer loads. We can list the following as **main advantages** of this fastening technique:

- Distribution of stresses throughout a large surface
- Possibility to optimize the geometry and dimensions of bonding area
- Lightweight of the mechanical connection
- Insulation and sealing properties of adhesive

6.2.1 ADHESIVES USED

The adhesives used include

- Epoxies
- Polyesters
- Polyurethanes
- Methacrylates

In all cases, the curing process is shown schematically in Figure 6.13.

The current adhesives are resistant simultaneously to

- High temperatures (>180°C)
- Moisture
- Many chemical agents

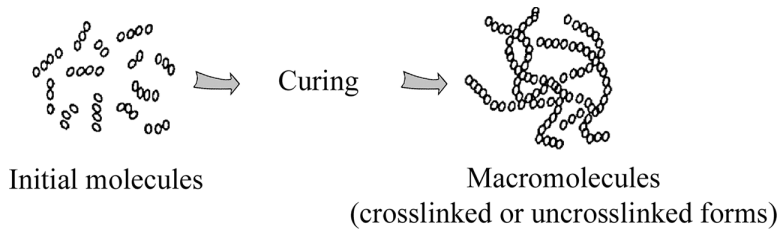


FIGURE 6.13 Curing process of adhesive.

The parts that have to be connected must be surface treated. This involves three steps:

- Degreasing
- Surface pickling
- Protection of the pickled surface

The case of metal/laminate bonding: Due to differences in physical properties of the constituents, the adhesive should compensate the differences between

- Thermal expansions
- Deformation under stress

The schematic in Figure 6.14 indicates in a strongly exaggerated manner the deformed configuration of an adhesively bonded double-lap joint. This demonstrates the role of adhesive in the gradual transmission of the load from the center part to the external components⁴.

Failure of an adhesively bonded joint can occur from different manners, as indicated in Figure 6.15.

6.2.2 GEOMETRY OF THE BONDED JOINTS

As far as possible, adhesively bonded joint geometries should allow to meet the following specifications:

- The adhesive layer must be loaded in shear in its own plane
- A state of tensile stress in the adhesive layer should be avoided



FIGURE 6.14 Deformation of a double-lap bonded joint.

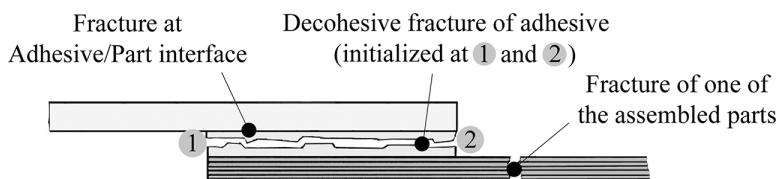


FIGURE 6.15 Failure modes in a bonded joint.

Consequently, transmission of load will be made in more or less favorable conditions depending on the joint geometry, as shown in Figure 6.16. A double-lap bonded joint comprising panels with tapered thicknesses is shown in Figure 6.17.

Transmission of torque is shown in Figure 6.18.

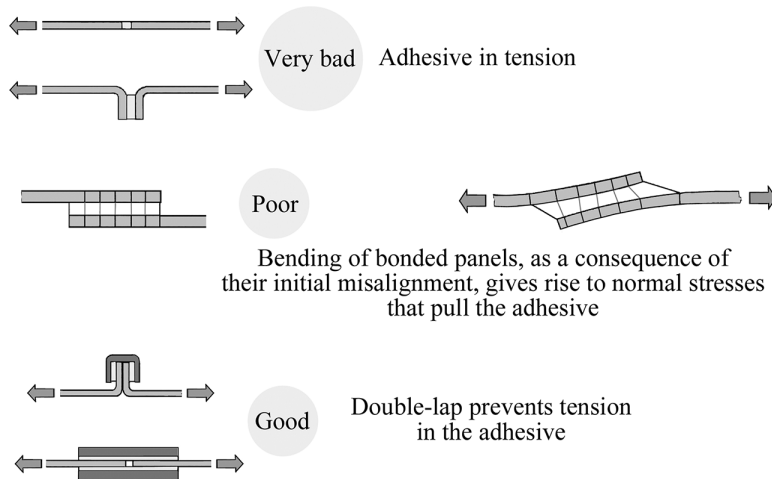


FIGURE 6.16 Some designs for bonded joints.

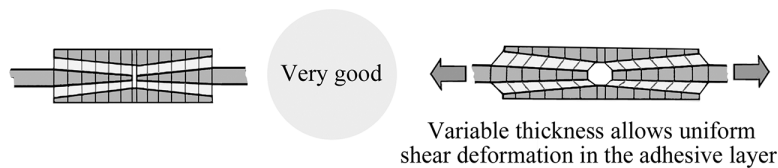


FIGURE 6.17 Double-lap tapered joint.

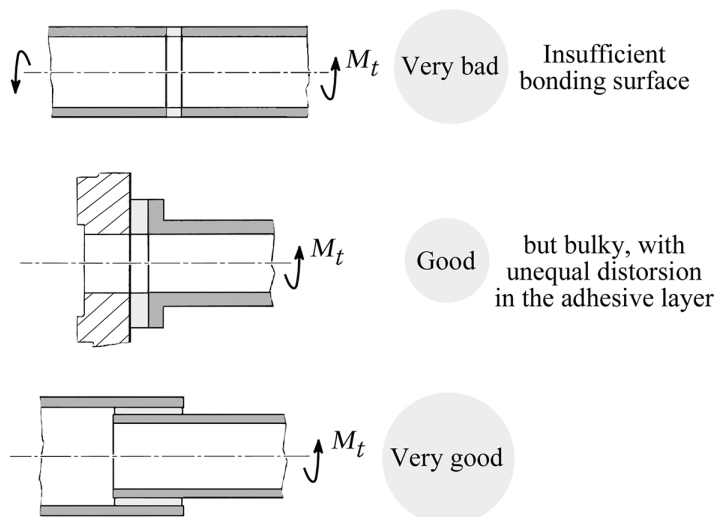


FIGURE 6.18 Design for torque transmission (see Section 20.1).

6.2.3 SIZING OF THE BONDING SURFACE AREA

6.2.3.1 Strength of Adhesive

The strength of adhesive is characterized by its allowable shear strength τ_{rupture} . This strength varies with the curing process of bonding (cold bonding or hot bonding). For epoxy adhesive, the following values can be cited:

- **For cold bonding**, (Araldite®) adhesive thickness = 0.2 mm:

$$\tau_{\text{rupture}} = 10 \text{ MPa at } 20^\circ\text{C}$$

$$\tau_{\text{rupture}} = 3 \text{ MPa at } 80^\circ\text{C}$$

- **For hot bonding**, polymerization temperature is between 120°C and 180°C :

$$\tau_{\text{rupture}} = 15 - 30 \text{ Mpa from } 20^\circ\text{C to } 100^\circ\text{C}$$

The diagram in Figure 6.19 shows, for example, a typical polymerization cycle for an epoxy adhesive.

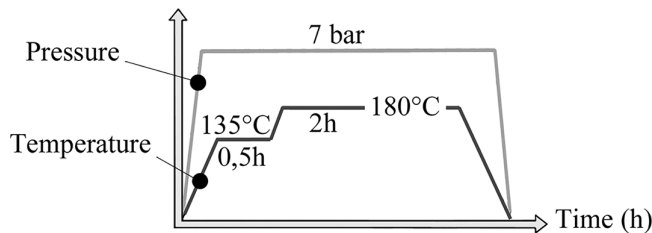


FIGURE 6.19 Curing cycle of epoxy adhesive.

6.2.3.2 Design

- Denoting by e_c the **thickness of the adhesive layer**, the typical values are

$$0.1 \text{ mm} \leq e_c \leq 0.3 \text{ mm}$$

When the adhesive joint is especially thick, the adhesive should be filled with glass powder or with cut fibers.

- **Scarf joint**: This design of joint (see Figure 6.20) allows obtaining a sufficient bonding surface, with limited tensile stress
- **Parallel joint**: As illustrated in Section 6.2.2, there is bending of bonded parts. The geometrical configurations are varied (see Figure 6.21)

6.2.3.3 Stress in Bonded Areas

By focusing on a bonded area, the loading on bonded joint appears as shown in the right-hand side of Figure 6.22 (the bonded joint width is assumed to be unitary).

The state of stress in the adhesive (Figure 6.22) consists mainly in

- A shear stress τ
- A normal stress, so-called **peel stress** σ

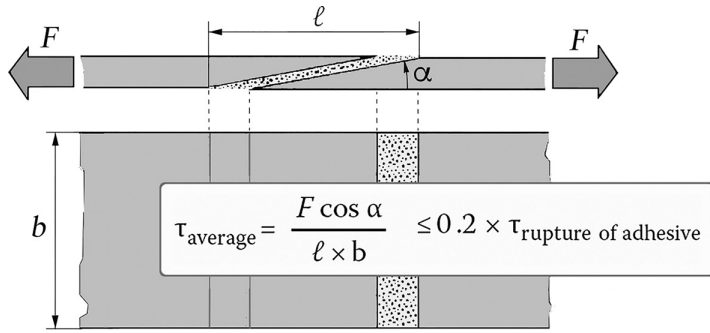


FIGURE 6.20 Scarf joint.

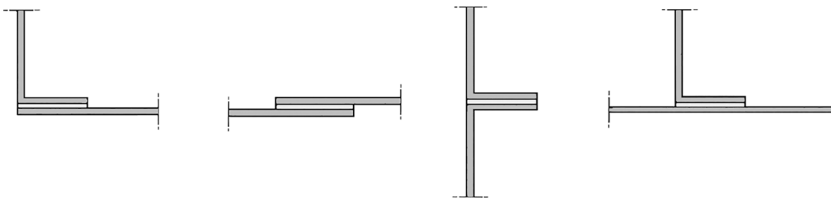


FIGURE 6.21 Configurations of parallel joint.

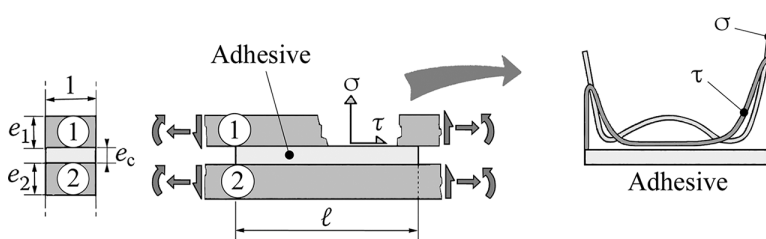


FIGURE 6.22 Stresses in adhesive.

These stress distributions show maximum values σ_M and τ_M very close to the edges along the longitudinal direction ℓ of the adhesive. These maxima can be approached by superimposition of the partial maxima created by each of the resultants N , T , and M_f , respectively, by means of the procedure described hereafter:

a. By writing,

$$\alpha_1 = \frac{G_c}{E_1 e_1 e_c}; \quad \alpha_2 = \frac{G_c}{E_2 e_2 e_c}; \quad \beta_1 = \frac{12 E_c}{E_1 e_1^3 e_c}; \quad \beta_2 = \frac{12 E_c}{E_2 e_2^3 e_c}$$

Expressions in which

E_c is the elastic modulus of the adhesive

G_c is the shear modulus of adhesive

E_1 and E_2 are the elastic moduli of the bonded parts 1 and 2 in the horizontal direction ℓ of the adhesive

e_1 , e_2 , and e_c are thicknesses as shown in Figure 6.22

b. Then we obtain

- Maximum shear stress values as illustrated in Figure 6.23
- Maximum peel stress values as shown in Figure 6.24.

Notes:

- The stress resultants N , T , and M_f are evaluated per unitary width of the bonded joint.
- When several resultant forces and moments exist together, the total maximum shear stress is obtained by superimposition of the maxima of shear stress values and the maximum peel stress by superimposition of the maxima of peel stress values.
- When the lower part is also subject to resultant force and moment, the previous estimate can be used, through permuting indices 1 and 2 and through changing the sign of the second member.
- The range of validity for these approximate formulas⁵ is as follows:

$$0.6 \leq \frac{\alpha_1}{\alpha_2} \quad \text{and} \quad \frac{\beta_1}{\beta_2} \leq 2$$

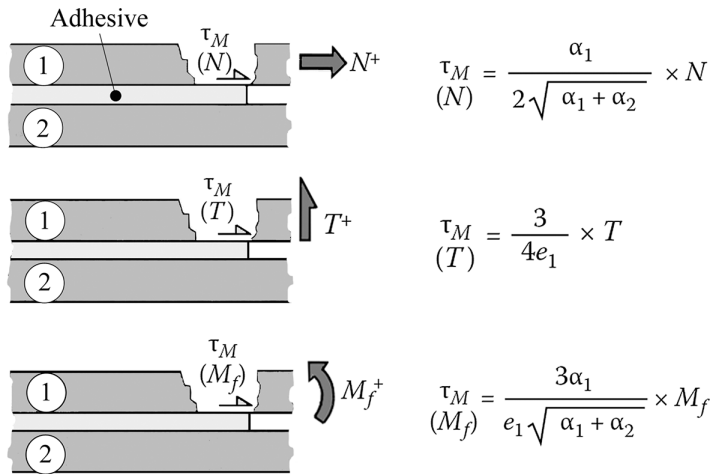


FIGURE 6.23 Maximum shear stress.

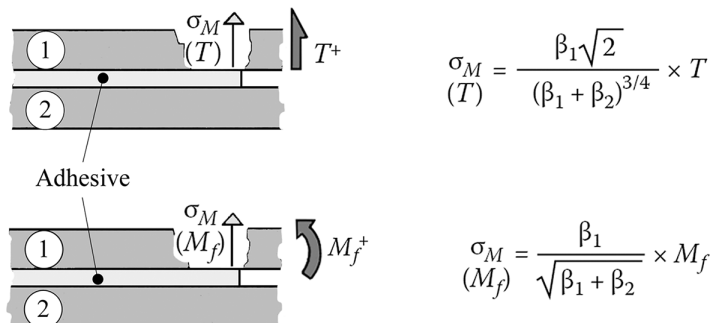


FIGURE 6.24 Maximum peel stress.

$$(\alpha_1 + \alpha_2) \times \ell^2 \geq 9$$

$$(\beta_1 + \beta_2) \times \ell^4 \geq 4 \times 6^4$$

6.2.3.4 Example of Single-Lap Adhesive Joint

For the single-lap adhesive joint below, and with the notations used previously,



$$N = F; \quad M_f = F \times \left(\frac{e_1 + e_2}{2} + e_c \right)$$

$$\tau_M = \tau_{M(N)} + \tau_{M(M_f)}; \quad \sigma_M = \sigma_{M(M_f)}$$

This is relevant only if $\alpha_1, \alpha_2, \beta_1$, and β_2 remain in the range of validity indicated above.

6.2.4 CASE OF BONDED JOINT WITH CYLINDRICAL GEOMETRY

6.2.4.1 Bonded Circular Flange

The maximum shear stress value and the condition of nondamage are given in Figure 6.25.

6.2.4.2 Tubes Fitted and Bonded into One Another

The maximum shear stress value and the condition of nondamage are given in Figure 6.26. For different thicknesses and different materials to be assembled, see Application 21.1 “Cylindrical Bonding”.

6.2.5 EXAMPLES OF BONDING

6.2.5.1 Laminates

- **In a laminate, orientation of plies** that are in contact with the adhesive joint influences strongly the failure by fiber–resin decohesion. This can be easily understood through Figure 6.27.

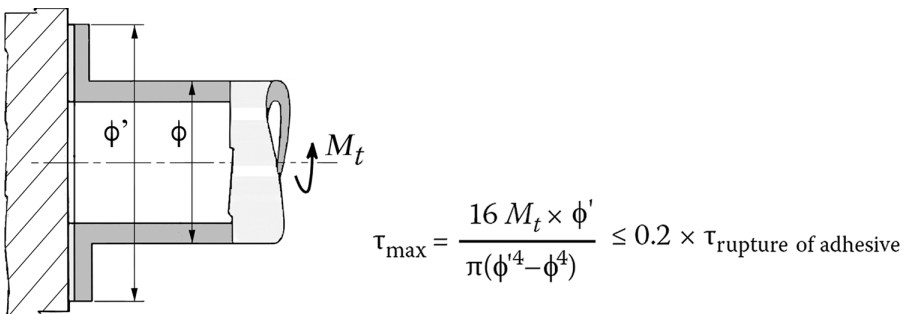


FIGURE 6.25 Bonded circular flange.

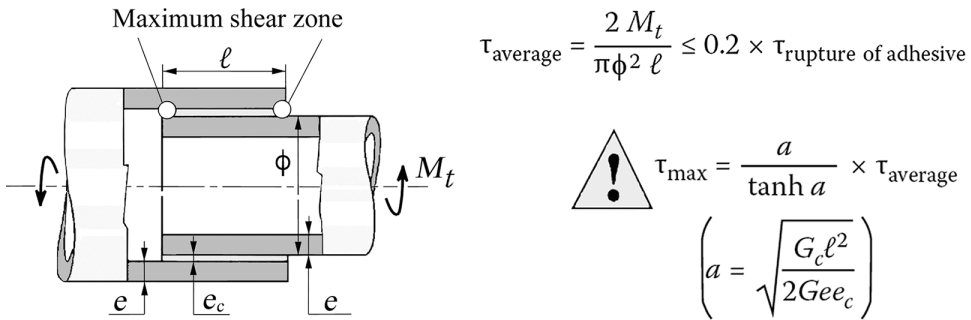


FIGURE 6.26 Tube fitted and bonded into one another.

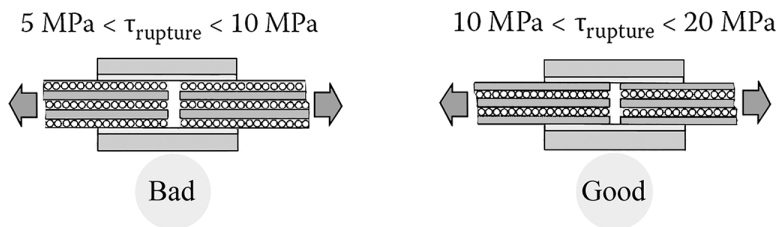


FIGURE 6.27 Importance of ply orientation in bonded laminates.

- Figure 6.28 shows how to achieve stepped thickness on the titanium side with intentionally nonsymmetrical design of the steps, with the aim of limiting the stress concentration in internal angles⁶.
- Sandwiches (see Figure 6.29): The bonding at the borders of sandwich panels must be done in a simple manner (especially for the preparation of the core) and with the best possible contact for the bonded parts, similar to the cases shown in Figure 6.30.

6.3 INSERTS

In composite parts, it is sometimes necessary to use local reinforcement parts, or inserts, which may be used to fasten the concerned composite part to the surrounding structure or to attach equipment. The inserts carry the fastening devices and spread the loads introduced by the fasteners into the composite part.

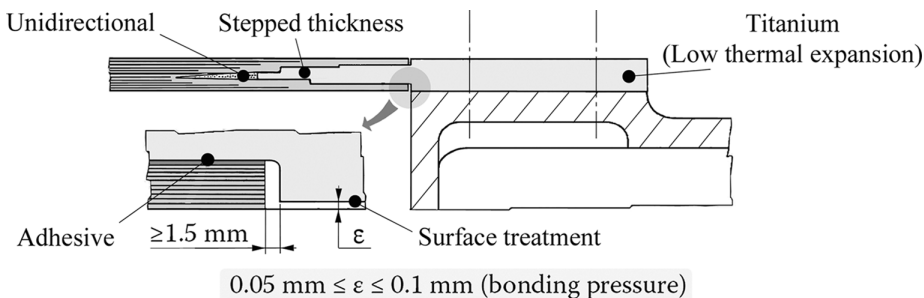


FIGURE 6.28 An example of laminate bonding.

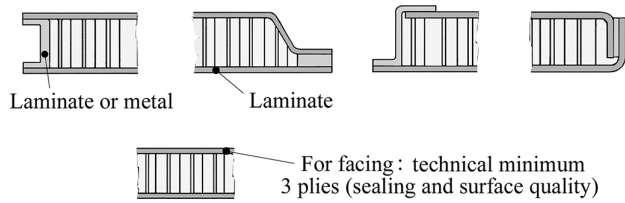


FIGURE 6.29 Bonding of sandwich panels.

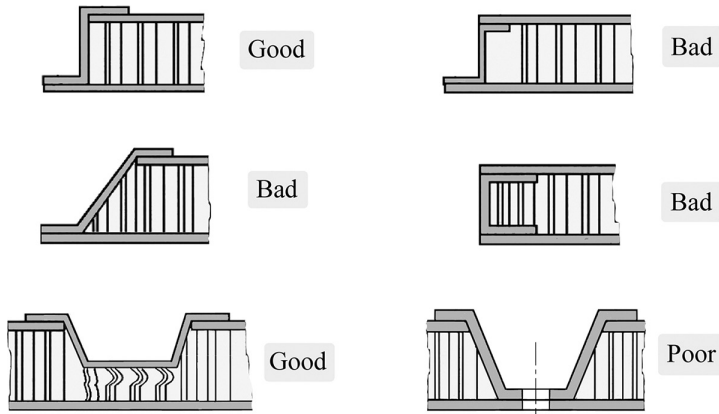


FIGURE 6.30 Borders of sandwich panels.

6.3.1 CASE OF SANDWICH PARTS

Metallic inserts into sandwich parts are frequently designed according to the schematics in Figure 6.31.

6.3.2 CASE OF PARTS UNDER UNIAXIAL LOADS

- **Tensile load:** See Figure 6.32. See also Figure 7.49 “Composite propeller blade”, Figure 8.24 “Riser tube”, and Application 19.3 “Helicopter blade”.
- **Compression load:** See Figure 6.33.
- **Tension–compression load:** See Figure 6.34.

Arrangements that allow the increase of the bonded surfaces are shown in Figure 6.35.

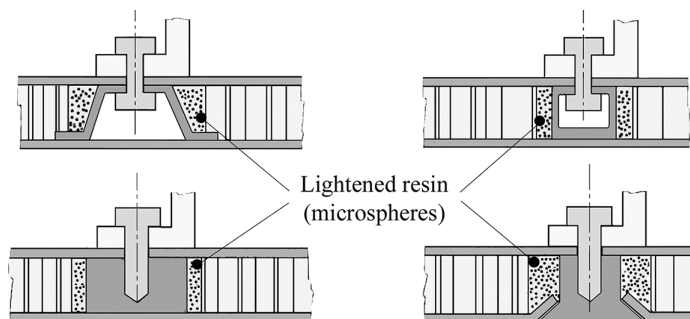


FIGURE 6.31 Inserts in sandwich construction.

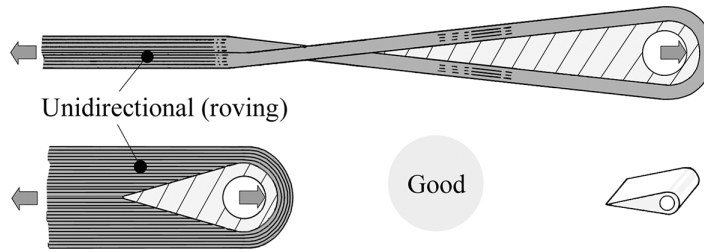


FIGURE 6.32 Composite parts under tensile load.



FIGURE 6.33 Composite part under compression.

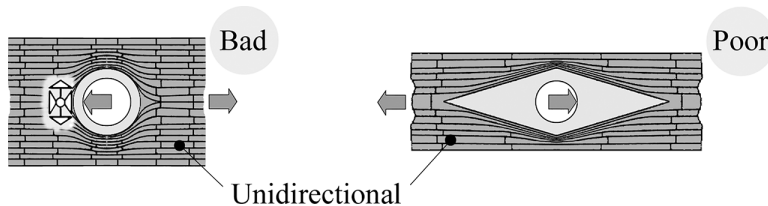


FIGURE 6.34 Tension-compression load.

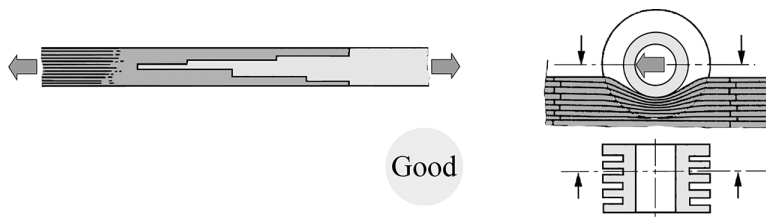


FIGURE 6.35 Devices to increase the bonded area.

NOTES

- 1 Nevertheless, an open hole reduces the mechanical capability of a laminate in a greater proportion than does a filled hole. The reason is that the presence of a fastening pin helps to maintain the shape of the hole and thus limits the deformation under load.
- 2 When the aging of the part must be taken into account, an additional 10% factor must be applied on top of the others. Another approach consists of applying rather a knockdown factor on the allowable stress values or on strains.
- 3 A more complete case of panel fastening is examined in Application 19.6 “Wing Tip made of Carbon/Epoxy”.
- 4 See Application 21.2 “Double Lap Bonded Joint”.
- 5 For more details, see Bibliography: Bigwood D.A. and Grocombe A.D.
- 6 See also Application 19.6 “Wing Tip Made of Carbon/Epoxy”.

7 Composite Materials and Aerospace Construction

A brief history shows that lightness and mechanical robustness requirements have early led aircraft manufacturers to move toward composite solutions:

- In 1938, the fighter aircraft **Morane 406** (FR) had sandwich panels made of plywood core and light alloy skins.
- In 1943, the fighter aircraft **Spitfire Supermarine** (GB) was fitted with composite wing spars and some composite fuselage parts made of hemp fiber and phenolic resin.
- Glass/resin has been used since 1950. Combined with honeycombs, this composite enabled the manufacture of fairings with complex shapes.
- Boron/epoxy was introduced around 1960, with moderate development since that time.
- Carbon/epoxy structural parts were fitted on aircraft from the 1970s.
- Kevlar®/epoxy has been used since 1972.

The experience shows that the use of composites allows weight reduction from 10% to 30% compared to a metallic design with equal performance, together with a cost reduction of 10%–20%.

7.1 AIRCRAFT

7.1.1 COMPOSITE COMPONENTS IN AIRCRAFT

Aircraft construction today uses a wide variety of composite components. They are listed hereafter, depending on the more or less important role they play in the aircraft integrity:

- **Primary structure components** (integrity is vital for the aircraft)
 - Wing panel, wing tip, and wing box
 - Vertical stabilizer (fin box), horizontal stabilizer (empennage box)
 - Center wing box
 - Keel beam
 - Fuselage sections
 - Pressure bulkhead
- **Flight controls**
 - Ailerons
 - Rudder, elevators
 - Wing flaps
 - Spoilers
 - Winglets
- **Fairings**
 - Belly fairing
 - Flap track fairings
 - Leading edge flap (slat)
 - Trailing edge flap
 - Wing fairings **Karmans** and pylon fairings

- Engine nacelle and thrust reversers
- Doors, cargo doors
- Landing gear doors
- Radomes
- Tail cones
- **Interior design**
 - Floors
 - Cabin lining panels
 - Doors

7.1.2 ALLOCATION OF COMPOSITES DEPENDING ON THEIR NATURE

Qualities and defects of composites and corresponding applications can be listed as follows.

7.1.2.1 Glass/Epoxy, Kevlar/Epoxy

- **Pros**
 - High static failure strength¹
 - High elastic allowable deformation
 - Very good fatigue strength
- **Cons**
 - Maximum operating temperature around 80°C
 - Nonconducting material
 - Higher areal weight compared to carbon/epoxy

These were used in fairings, cargo doors, landing gear doors, Karmans, radomes, and leading edge flaps. In most areas, glass and Kevlar have now been replaced by carbon on recent aircraft development.

7.1.2.2 Carbon/Epoxy

- **Pros**
 - High static failure strength²
 - Very good fatigue strength
 - Very good heat and electricity conductor
 - High operating temperature (limited by the resin around 120°C)
 - No dilatation
 - Lower areal weight than glass/epoxy
- **Cons**
 - More delicate fabrication (prone to manufacturing defects)
 - Resistance after impact: two or three times less than glass/epoxy
 - Material prone to lightning strike

This is used in wing box, wing tip, vertical and horizontal stabilizers, fuselage, center wing box, ailerons, spoilers, flaps, traps, struts, floors, and pressure bulkhead.

7.1.2.3 Boron/Epoxy

- **Pros**
 - High static failure strength
 - High stiffness
 - Very good compatibility with epoxy resins
 - Good fatigue resistance

- **Cons**
 - Higher areal weight than the previous composites³
 - Delicate implementing and handling
 - High cost

This was used for vertical and horizontal stabilizer boxes.

7.1.2.4 Honeycombs

- **Pros**
 - Low specific mass
 - High specific modulus and specific strength
 - Very good fatigue resistance
- **Cons**
 - Prone to corrosion
 - Difficult to detect defects

Honeycombs are used to create the core of structural sandwich parts.

7.1.3 FEW COMMENTS

The construction using only glass fiber is increasingly neglected in comparison with a combination of Kevlar and carbon fiber for weight-saving reasons:

- If maximum strength is needed, it is then recommended to use Kevlar.
- If maximum rigidity is wished, it is then recommended to use carbon.
- Kevlar fibers possess excellent vibration damping properties.
- Because of bird impacts, hail impact, or impact from other particles (sand, dirt), the designer usually avoids the use of composites without metallic protection on the leading edges⁴.

Carbon/epoxy composite is a good electrical conductor but prone to lightning strike, with the following consequences:

- Damages at the point of impact: delamination, burning of resin
- Risk of flash event in fasteners inside fuel tanks (bolt heads or nuts)
- Need of mass bonding network for the electrical circuits situated under the composite element

In order to prevent this,

- Placement of a thin metallic mesh or glass fabric in conjunction with a very thin sheet of extended copper foil (20 μm)
- Spray of a protective aluminum coating (aluminum flame spray)

Temperature is an important parameter limiting the possible use of epoxy resins. Some carbon parts are made from bismaleimide resins, in particular for space industry. Bismaleimides are thermoset resins that soften⁵ at temperatures higher than 350°C instead of 210°C for epoxies. Another means consists in using a high-performance thermoplastic resin such as **PEEK**⁶ that softens at 380°C. Laminates made of carbon/PEEK are more expensive than products made of carbon/epoxy. However, they present good performance at higher operating temperatures (continuously at 130°C and periodically at 160°C) with the following additional advantages:

- Superior impact resistance
- Negligible moisture absorption
- Very low smoke generation in the case of fire

7.1.4 SPECIFIC ASPECTS OF STRUCTURAL STRENGTH

- It is necessary to apply to aeronautical composite parts and subassemblies the principle of **fail-safe** design, which consists in predicting the first failure mode (e.g., delamination) and designing in such a manner that this does not lead to the complete collapse of the component during the period between inspections.
- Composite parts are more easily repairable than metallic ones. Repair methods are analogous for laminates made of unidirectionals or fabrics⁷.
- As a result of the drastic reduction of the number of rivets compared to a conventional metallic design, smoother surfaces are obtained, leading to improved aerodynamic performance.
- The environmental aggressions and fatigue cycles do not lead to significant deterioration of the composite parts. Shown in Figure 7.1 are two typical fatigue cycles for an aircraft structure.
- The crash-safety airworthiness requirement is more difficult to fulfill with structures 100% made of composite materials. Indeed, the energy cannot be absorbed by plastic deformation on the composite parts, because of the lack of plasticity of the latter. When well engineered, some metallic internal structures remain in place in order to continue providing plastic deformations required for crash-safety purpose.
- In cabin interiors, phenolic resins are mostly used for their good fire resistance, with low smoke emission. For the same reason, Kevlar fiber was replaced by a combination of glass/carbon (lighter than glass alone and less expensive than carbon alone).
- It is possible to take advantage of the laminate anisotropy for the control of dynamic and aeroelastic behavior of the wing structures.

7.1.5 LARGE TRANSPORT AIRCRAFT

7.1.5.1 Example

The following examples give an idea of increasing trend in the use of composites in the main types of large commercial aircraft.

- **Examples:** **Aérospatiale** (FR), **Airbus** (EU), and **Boeing** (US) (Figure 7.2).

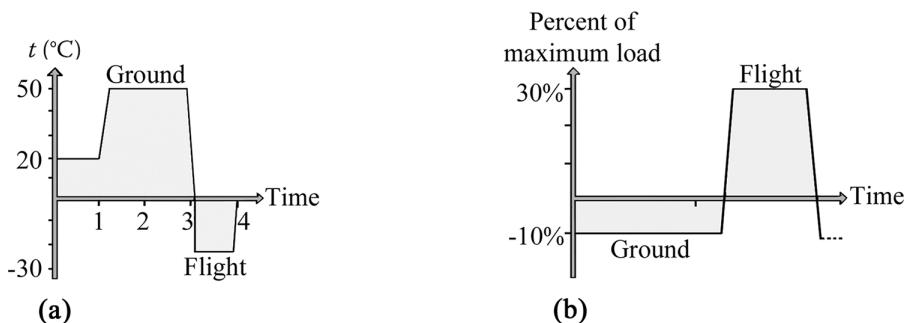


FIGURE 7.1 Typical fatigue cycles on an aircraft structure: (a) cyclic temperature and (b) cyclic loading.

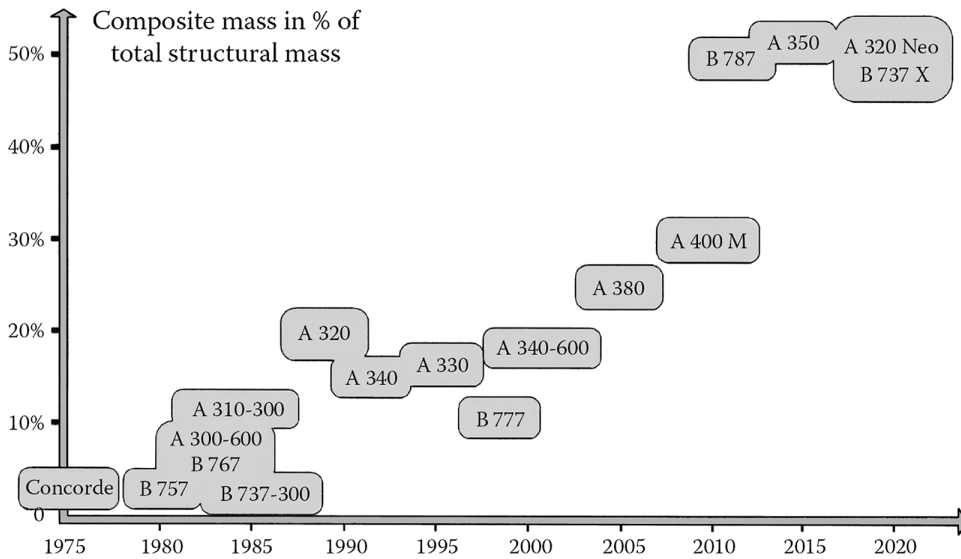


FIGURE 7.2 Evolution of mass of composites in civil transport aircraft.

7.1.5.2 How to Determine the Benefits

- **The principle:** The benefits can be explained by cascading consequences as illustrated in Figure 7.3.
- **Practicality:** In fact, the introduction of composites in aircraft is limited to certain structure areas. It is done case by case and in a progressive manner during the life of the aircraft (improvement operation). This is accomplished after taking into consideration a number of factors.
- **Notion of exchange rate:** It is the cost of every kilogram that can be trimmed from the classical metallic design by substituting a mostly composite design. It can vary depending on the considered part. This cost is balanced out by the **payload** gain as described here.
- **Notion of payload gain:** It is the gain in terms of number of passengers, of increasing freight, or of fuel cost. For example, for a large commercial aircraft, the following applies:

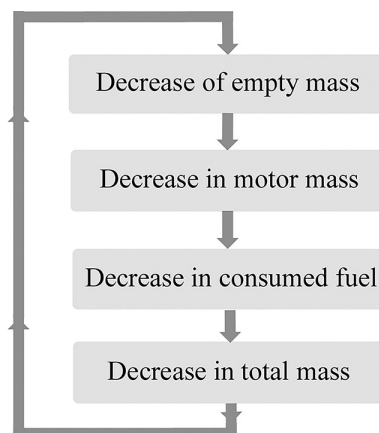


FIGURE 7.3 Cascading effect in mass reduction.

- A 150-ton aircraft, with 250 passengers, comprises a 60-ton structure. A progressive introduction of 1,600 kg of high-performance composite materials leads to a gain of 16 additional passengers along with their luggage.
- A mass reduction of 1 kg leads to decrease fuel consumption around 0.12 m^3 per year.

Note: Why the mass saving (average about 20%) is not more spectacular?

Consider the example of a rudder. The mass balance of a composite rudder can be presented as follows:

- Carbon/epoxy skins: 30% of total mass
- Honeycombs, adhesives: 35% of total mass
- Attachment fittings: 25% of total mass
- Reinforcement of carbon/epoxy: increasing of thickness localized at the fastening systems, oversizing of carbon/epoxy
- Consideration of the aging and of thermal fatigue of carbon/epoxy: oversizing of facings (the stresses are magnified about 10% for a subsonic aircraft and about 13% for a super-sonic aircraft)

Accordingly, the saving in terms of total weight compared to a conventional light alloy solution is only about 15%.

7.1.5.3 Example: Civil Transport Aircraft A380–800, Airbus (EU) (Figure 7.4)

This has the following characteristics:

- Maximum takeoff weight (MTOW): 560 tons
- Maximum weight empty: 240 tons
- Percentage of composites: 25% of the structural mass (mass of carbon/epoxy, 40 tons)
- Some other specifications: length, 72.7 m; wingspan, 79.6 m; height, 24 m; payload, 55 tons (555 passengers) transported over a distance of 14,800 km

Among the main innovations in the use of composites are:

- The center wing box: this structural assembly is 7 m long, 7.9 m wide, 3 m high, and 11 tons heavy. It connects the wings to the fuselage. It is the main mechanical load-carrying area of the aircraft. The box consists of 50% by weight of carbon/epoxy (intermediate modulus

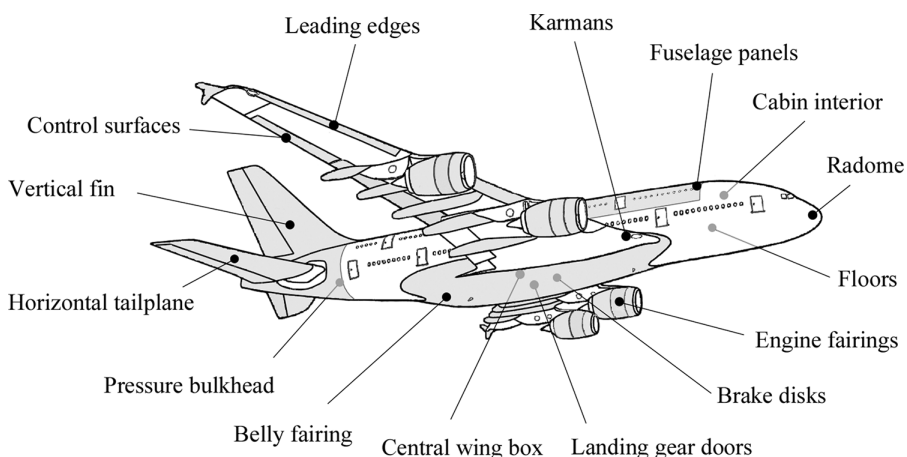


FIGURE 7.4 Composites in an Airbus A-380.

fiber) and of 50% of light alloy. The thickness of carbon skins reaches 44 mm in some locations. Mass gain is 1.5 tons compared to a metal solution.

- The upper fuselage with the use of MMC (metal matrix composite) panels (see Section 7.1.9.3 and Figures 7.32 and 7.33).

7.1.5.4 Example: Civil Transport Aircraft B 787–800, Boeing (US) (Figure 7.5)

The percentage of composites is 50% of the mass of the structure compared to 14% for titanium, 7% for steel, and 20% for aluminum (various others 9%). This aircraft is featured by a very important **technological leap**, with the merging of research and development and of industrial stage. The percentage of composites does more than double compared to previously existing aircraft of the same importance. In addition to the composite parts already produced in other large civil aircraft, we should note the introduction of:

- The wing boxes (carbon/epoxy)
- The fuselage (fiber placement using placement heads on rotating mandrel, with local reinforcements around openings such as windows, doors, and fastenings)
- Some other characteristics that follow: length, 56 m; wingspan, 51 m; and 217 passengers over a range of 15,700 km

7.1.5.5 Example: Civil Transport Aircraft A350–900, Airbus (EU) (Figure 7.6)

- Some characteristics include the following:
 - Length, 67 m; wingspan, 64.75 m; height, 17.1 m; fuselage diameter, 5.96 m; and MTOW, 268 tons
 - 315 passengers; cruising speed, Mach 0.85; range, 15,000 km; and ceiling, 13,000 m

The composites reach 53% of the mass of the primary structure compared to 14% for titanium, 6% for steel, and 19% for aluminum or aluminum–lithium alloys (various others 8%).

- **Center fuselage**
 - **Center wing box** (see Figure 7.7): width 6 m×length 5.5 m×height 1.9 m; weight 5 tons. It is made of parts assembled with up to 50% by weight of carbon/epoxy and with thicknesses up to about 20 mm.

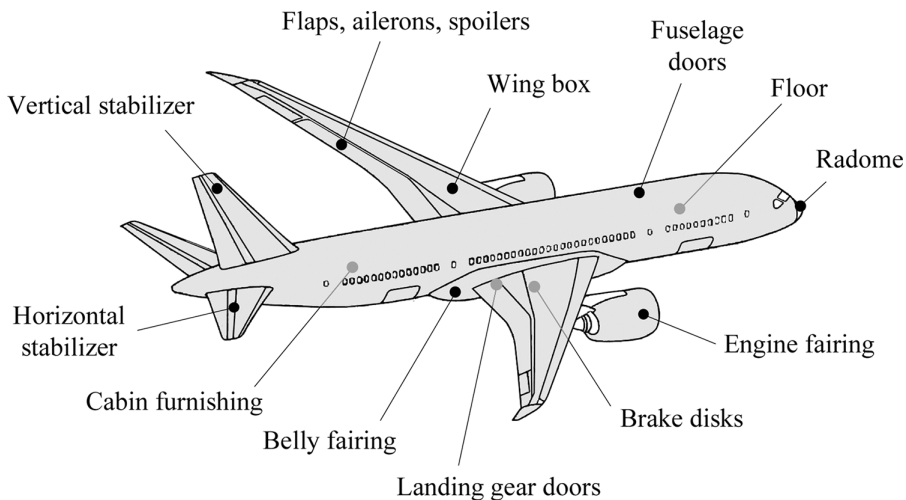


FIGURE 7.5 Composites in a Boeing B-787.

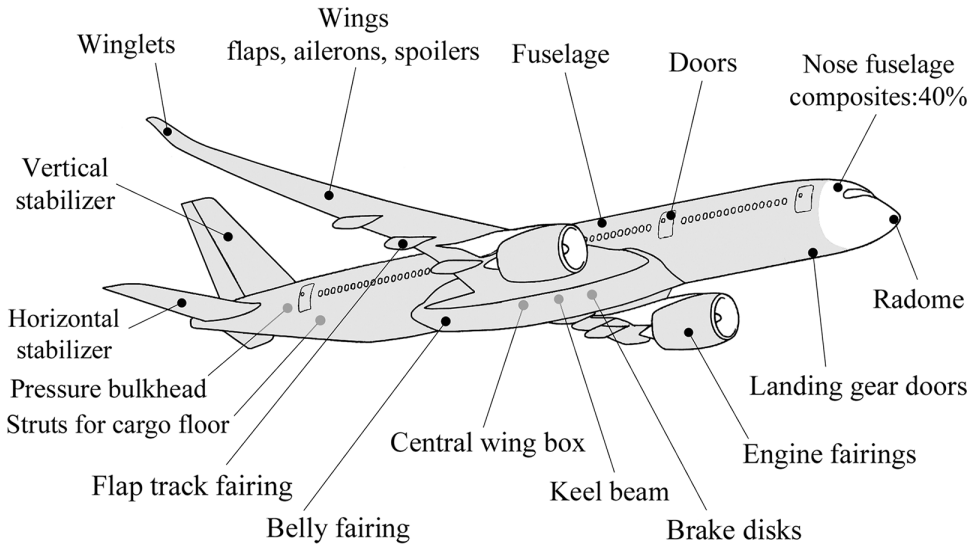


FIGURE 7.6 Composites in an Airbus A-350.

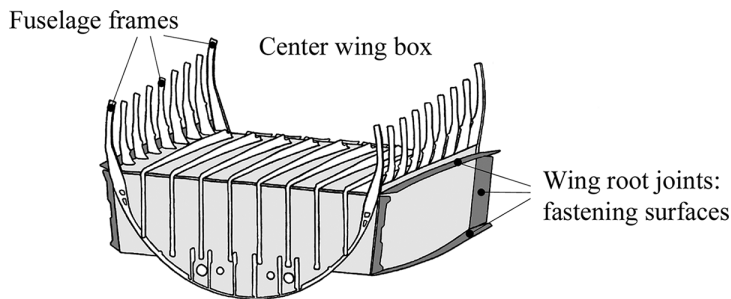


FIGURE 7.7 Center wing box of Airbus A-350.

- **Closing ventral beam** called **keel beam** by aircraft manufacturers. This 16.5×4.3 m subassembly with a mass of 1,200 kg consists of 70% by weight of carbon/epoxy. It closes the fuselage in the hollowed out area of the main landing gear bay, thus ensuring the structural continuity of the fuselage. This significant substructure drives 700 tons of compression load.

On the two aforementioned components is fixed the central cylindrical part of the fuselage or **central fuselage**. It is made of carbon/epoxy, 32 m length. The wing box is bolted on the center wing box at the wing root joint.

- **Typical fuselage**

The front fuselage and the rear fuselage are obtained each from a framework formed by the fuselage frames and by transverse junctional beams (which stabilize the shape of the fuselage and support the floor). This framework is covered by four panels in the form of stiffened cylindrical carbon/epoxy shells. The surface area of these panels may exceed 90 m^2 . Their thickness varies (from less than 2 mm to more than 5 mm) in order to provide proper resistance to local loads in their relevant areas. Such a mechanical optimization leads to a reduced mass. In addition, in view of polymerization, this solution requires a smaller autoclave than for monolithic fuselage section. Furthermore, in case of fabrication

defect or damage, the loss is limited to a single panel. These stiffened panels are fixed on carbon/epoxy common frames of varying thicknesses, by means of carbon/PEEK connecting parts or **attachment fittings**. Heavily loaded frames are made of titanium. The transverse junction beams are metallic (aluminum–lithium).

- **Wings** (see Figure 7.6)

The composite design allows removal of the wing center spar. This gets a wing box made up of lower and upper skins and of front and rear spars. This box is entirely in carbon/epoxy, stiff, and without differential thermal expansion. The lower stiffened skin, slightly larger than the upper one, is 32 m long and 6 m wide at the wing root, constituting the largest one-piece part of carbon/epoxy of civil aviation. The rear spar, 30 m long in three sections assembled, has a mass of 750 kg and a thickness at the wing root ranging from 25 to 30 mm. The front spar is 32 m long, with a mass of 900 kg.

7.1.6 REGIONAL AIRCRAFT AND BUSINESS JETS

7.1.6.1 Example: Regional Aircraft ATR 72–600, ATR (EU-IT)

See Figure 7.8.

Equipped with powerful engines, this aircraft operates on shorter runways and maximizes the payload. It is worth noting that the turboprop engines emit less CO₂ than turbojets for equal capacity.

MTOW, 22.5 tons

Cruising speed, 565 km/h

Autonomy, 1,600 km with 74 passengers (payload: 7,500 kg)

Two propellers (diameter 3.93 m) with six composite blades, **Hamilton Sundstrand** (US)–**Ratier Figeac** (FR) (see Section 7.3.)

Introduction of fuselage composite panels in carbon/epoxy.

Aircraft Interior: Wall panels for windows and ceiling, luggage bins, cabin bulkheads, toilets, galleys, and trolleys made of glass–carbon/phenolic resin/Nomex® honeycomb. The decoration is done by a polyvinyl fluoride film (PVF) **Tedlar®**.

7.1.6.2 Example: Business Aircraft Falcon 10X, Dassault Aviation (FR)

See Figure 7.9.

MTOW: 43 tons

Maximum cruising speed of Mach 0.925.

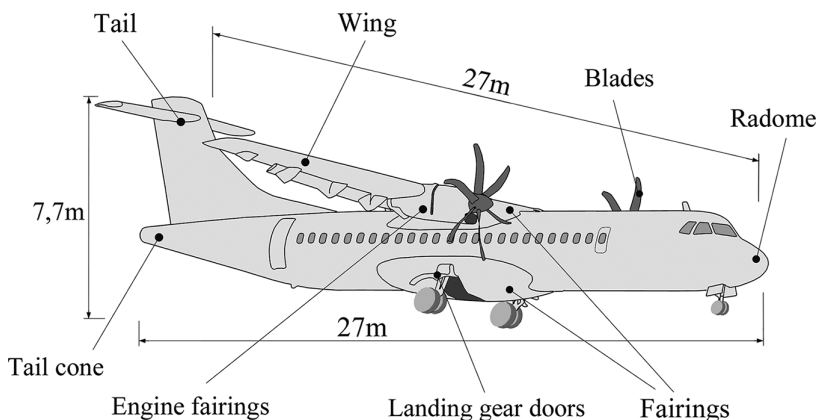


FIGURE 7.8 Composites in regional aircraft ATR 72.

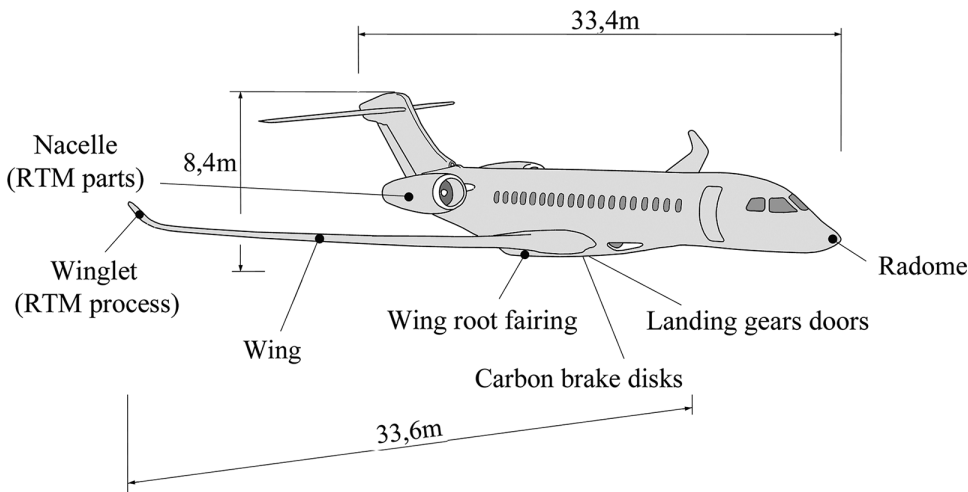


FIGURE 7.9 Business aircraft Falcon 10X.

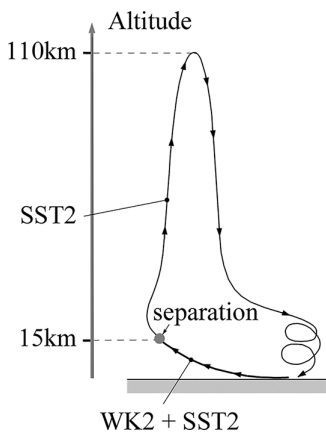


FIGURE 7.10 Operating principle of suborbital space plane.

13,900-km Range
Cabin: 2.03 (height)×2.77×16.4 m

Note: The use of carbon fiber in aircraft cabins and cockpits is growing rapidly. And besides the weight reduction, customers are now using its esthetic features to create a high-end look.

7.1.6.3 Example: Cargo Aircraft WK2 and Suborbital Space Plane
SST2, Scaled Composites (US)-Virgin Group (GB)

The cargo aircraft or “Mothership” VMS Eve **White Knight 2 (WK2)** carries the space plane VSS Unity **SpaceShip2 (SST2)** (see Figure 7.10) up to an altitude of 15 km. The space plane is then dropped and, powered by a rocket engine, leads six passengers and two pilots up to an altitude of 110km. Then, it descends in free fall and lands in gliding.

These two aircraft are entirely in carbon/epoxy (except for engines and landing gear) to reduce as much as possible the structure weight (see Figure 7.11).

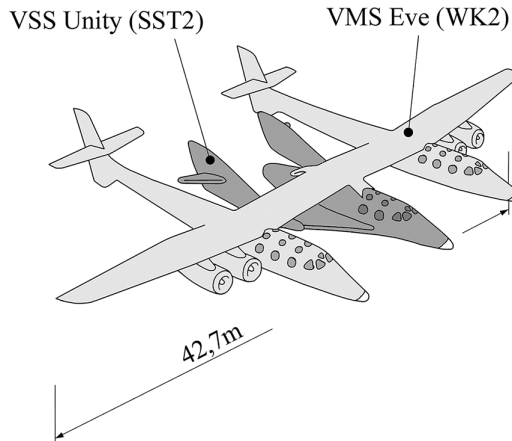


FIGURE 7.11 Cargo aircraft WK2 and suborbital space plane SST2.

- **Some features of WK2 carrier aircraft** include the following:

Wingspan, 42.7 m, making it the largest all-carbon aircraft currently. The wing in carbon/epoxy is of this length.

Length, 24 m; external payload, 16 tons; and maximum flight altitude, 21 km.

With low specific fuel consumption and because of its particular architecture, it is in fact a multipurpose aircraft that is not only intended to take away the space plane but can also be used to

- Take on passengers with the aim of floating in weightlessness (zero-g)
- Allow experiments in microgravity
- Perform missions requiring higher elevation
- Carry other types of payloads, which can be put into orbit if needed (the payload carrying the satellite must communicate to the latter a horizontal speed of 27,720 km/h; it corresponds to a 200 kg maxi satellite, put into low orbit of 160–2,000 km)
- Fight forest fires by carrying a large water tank in carbon/epoxy (this aircraft supports a large payload and a high load factor)

7.1.7 LIGHT AIRCRAFT

7.1.7.1 Trends

Light aircraft comprise **private aircraft**, **gliders**, and **drones**. These new generations of planes are characterized by

- Extensive use of composite materials
- Renovation of aerodynamic solutions

Gains of payload, of range, and of cruising speed allowed by the use of composites are amplified even more on these types of aircraft. The following presents some **all-composite** solutions.

7.1.7.2 Aircraft with Tractor Propeller

- **Example:** Drone **Patroller**, **Safran-Sagem** (FR)–**Stemme AG** (DE) (Figure 7.12)

In this type of plane (equipped as powered glider), the aircraft itself constitutes about 20% of the price of the unmanned system. The equipment then forms a major part of the

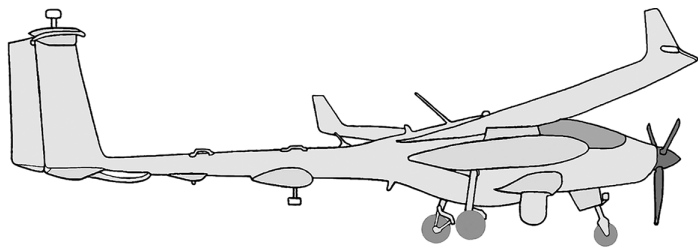


FIGURE 7.12 Drone with tractor propeller.

cost. Optionally with a pilot, the drone can also receive two seats. The engine is located behind the cockpit. A long shaft in carbon/epoxy passes between the pilots to operate the tractor propeller. The latter can retract into the front cone.

The airframe is composed of ready-built modules in carbon/epoxy assembled on a tubular central frame of steel, which also takes up the forces of the landing gear and receives the engine mounting cradle.

- Some characteristics include the following:
Wingspan, 18 m; weight of plane, 750 kg; and payload, 250 kg
Cruising speed, 300 km/h; altitude, 7.6 km; mission duration up to 30 h; and high load factor up to 6 g.
- **Example:** Training aircrafts for flight schools.
The current training planes are said to be fourth generation, which corresponds to the evolution illustrated in Figure 7.13.
- Aircraft with electrical engine, as shown in Figure 7.14
- Aircraft with heat engine, as shown in Figure 7.15

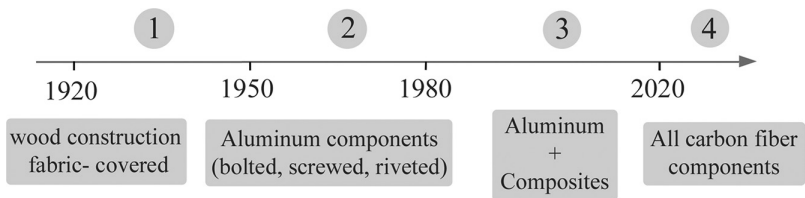


FIGURE 7.13 Four generations of light aviation.

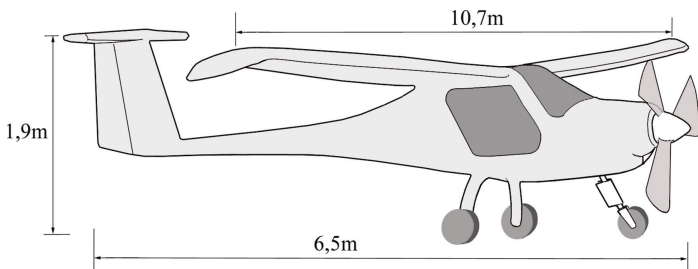


FIGURE 7.14 Training aircraft Velis Pipistrel, Pipistrel Aircraft (SI).

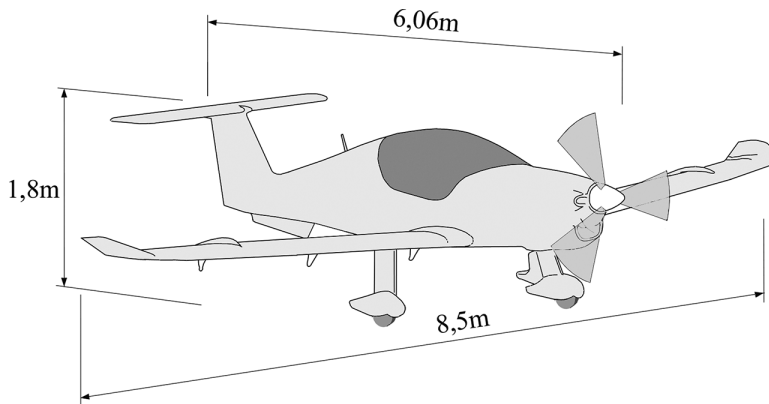


FIGURE 7.15 Training aircraft Elixir, Elixir Aircraft (FR).

Notes:

- The structure of the Elixir aircraft is over 95% carbon, composed only of 8 large components (wing, fuselage, rudder, elevator, and two ailerons and flaps). They are obtained by “One-Shot” technology for the fuselage as well as for the wing, by **C3 Technologies** (FR) specializing in the manufacture of competition boats (see Figure 7.16). This reverses the history sense as one can notice here that it is the naval construction that impels for carbon/epoxy the monolithic manufacture in the aeronautical field: no spar, no ribs, no bonding, no bolts, and no rivets (see Figure 2.7).
- Table 7.1 summarizes the performance of two equivalent training aircraft, typical representatives of the fourth generation.

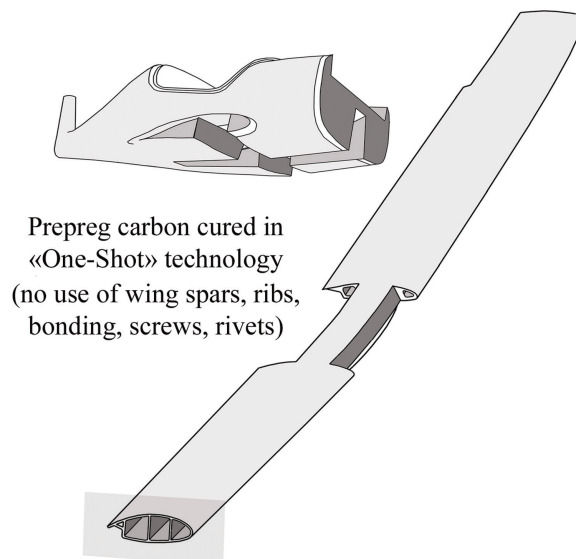


FIGURE 7.16 Training aircraft Elixir, “one-shot” technology.

TABLE 7.1
Two Single-Engine Two-Seat Training Aircraft

Two-Seat Single-Engine Aircraft Fourth Generation (All Carbon)	2020	Electric Engine	Piston-Engine
Engine weight	kg	30	60 (Rotax 912)
Engine power	kW	60	74
Energy stored	kWh	25	855 (Petrol 94 ℓ)
Recharge time	minute	70	2.4 (Fuel pump 40 ℓ/min)
MTOW	kg	600	544
Autonomy max	hour	1,5	6
Cruising speed	km/h	167	240
Operational autonomy at cruising speed	km	250	1,440

7.1.7.3 Aircraft with Pusher Propeller (Backward Propeller)

The pros and cons of principle are illustrated in Figure 7.17.

The change in center of gravity balance due to engine installation position requires a long propeller shaft in carbon/epoxy or (and) a wing with a rear offset.

- **Example: Civil drone Altair, NASA–G. A. Aeronautical Systems (US)**
It is a pusher-propeller aircraft operated by remote control and developed to perform experimental missions of long duration and high altitude (see Figure 7.18). It is entirely in carbon/epoxy and Nomex.
- Some characteristics include the following:
Wingspan, 26 m; length, 10.4 m; total weight, 3.2 tons; and cruising speed, 390 km/h.
Payload, 320 kg at altitude of 15.8 km for mission duration up to 32 h. This payload may be extended to 1,360 kg for shorter missions with low-level flying.

7.1.8 FIGHTER AIRCRAFT

The introduction in the 1970s of composite secondary structures made of sandwich structures of carbon/epoxy, boron/epoxy, and glass/epoxy should be noted. Then, it will be the turn of primary structures in the 1980s. In addition to the previously mentioned specific contributions, the composite

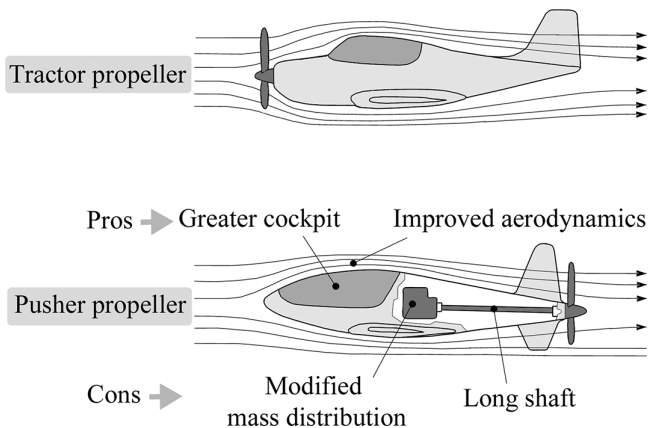


FIGURE 7.17 Tractor and pusher propeller.

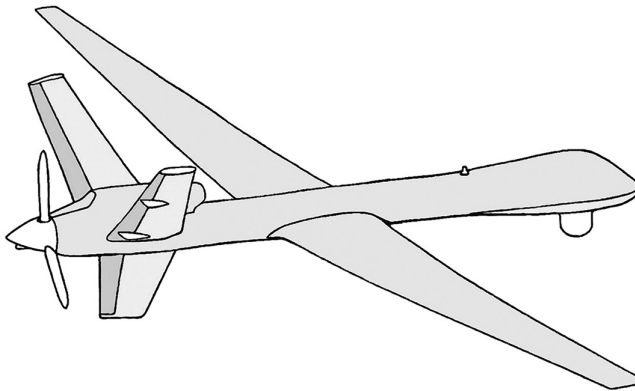


FIGURE 7.18 Pusher propeller: Civil drone Altair.

parts of these aircraft must confer structural stiffness to wings that enable them to maintain the control effectiveness in a wider flight envelope than the other planes.

- **Example:** Fighter aircraft **Rafale, Dassault Aviation** (FR) (see Figure 7.19)

On this plane, great use is made of high-performance composite materials (carbon/epoxy, carbon/PEEK, and Kevlar/epoxy): 29% of the airframe weight and three-quarters of the outer surface or **wet surface** of the aircraft. Thanks to the cascade effect (see Section 7.1.5), the mass saving is 300 kg, which leads to an empty weight of the equipped aircraft of slightly less than 10 tons. In case of a metal construction, this weight would have been from 11 to 12 tons.

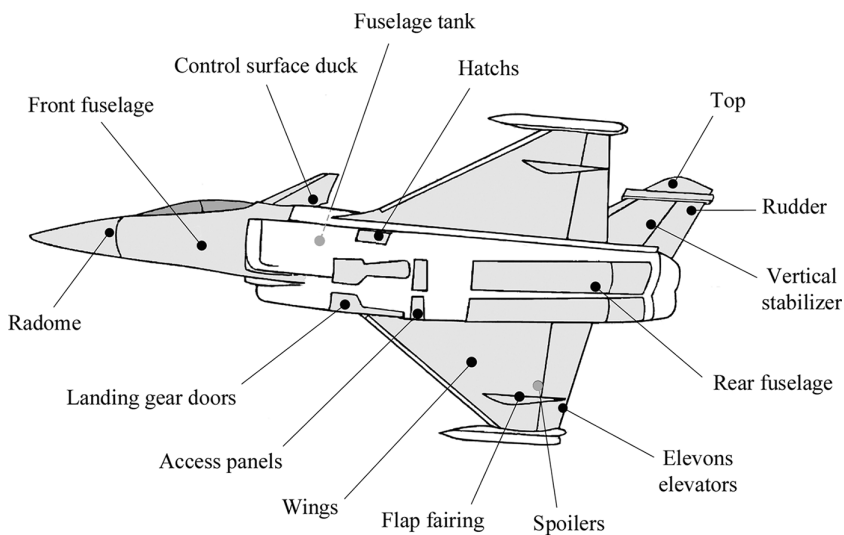


FIGURE 7.19 Rafale fighter aircraft.

- Some characteristics include the following:
 Length, 15.3 m; wingspan, 10.9 m; height, 5.34 m; empty mass of the equipped aircraft, 9.67 tons; and weapon load, 6–8 tons
 Maximum speed, Mach 2; low altitude range, 1,090 km; high altitude range, 1,850 km; rate of climb, 300 m/s; load factor, $-3.6g$ to $+9g$
 Figure 7.19 shows the main components using composites.

7.1.9 ARCHITECTURE AND MANUFACTURE OF COMPOSITE AIRCRAFT PARTS

7.1.9.1 Sandwich Design

a. Sandwich with monolithic honeycomb

According to the nature of the component, two methods of fabrication can be distinguished:

- Multiphase manufacturing:** The skins of the sandwich structure are polymerized separately and then placed on the honeycomb core previously shaped, with interposition of an adhesive film. After that, the assembly is polymerized following the process shown in Section 4.4.2, with the possibility of using an autoclave⁸.
- Monophase manufacturing:** After the honeycomb core is machined, the wet skins are placed directly on this core. The assembly is polymerized using the same method as for the multiphase method.
- Example: Flap box** (Figure 7.20)

The honeycomb core ensures dimensional stability of the component. However, the mass of the part is growing significantly with the thickness of the core.

- Example: Horizontal tail of a fighting aircraft** (Figure 7.21)

Notes

- Drilling of the boron/epoxy laminate is avoided as much as possible. The operation is very expensive and needs ultrasonic machining, together with diamond tool.
- A problem is on the corrosion of metallic honeycombs. This corrosion is due to combined action of water that gradually condenses in the honeycomb and of the mechanical and thermal stresses (fatigue) that occur in the sandwich structure.

Remedies

Coat the metal foils constituting the honeycomb with a resin film.

Introduce an organic inhibitor that recognizes the potential points of attack and fixes itself there to prevent the reaction with water.

b. Sandwich skin panels

When the part becomes too thick (range of 150 mm), the skins are stiffened separately by using a honeycomb core, according to the geometrical arrangements shown in Figure 7.22.

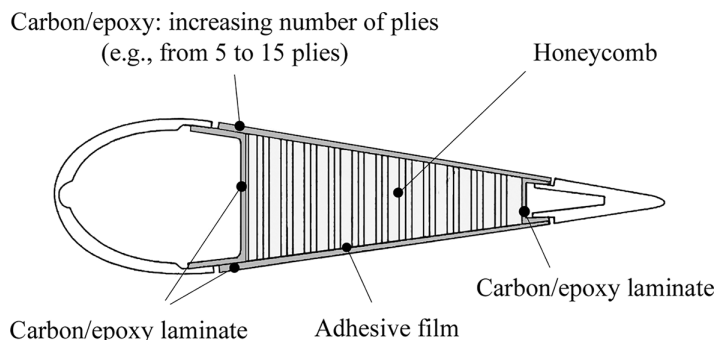


FIGURE 7.20 Flap box.

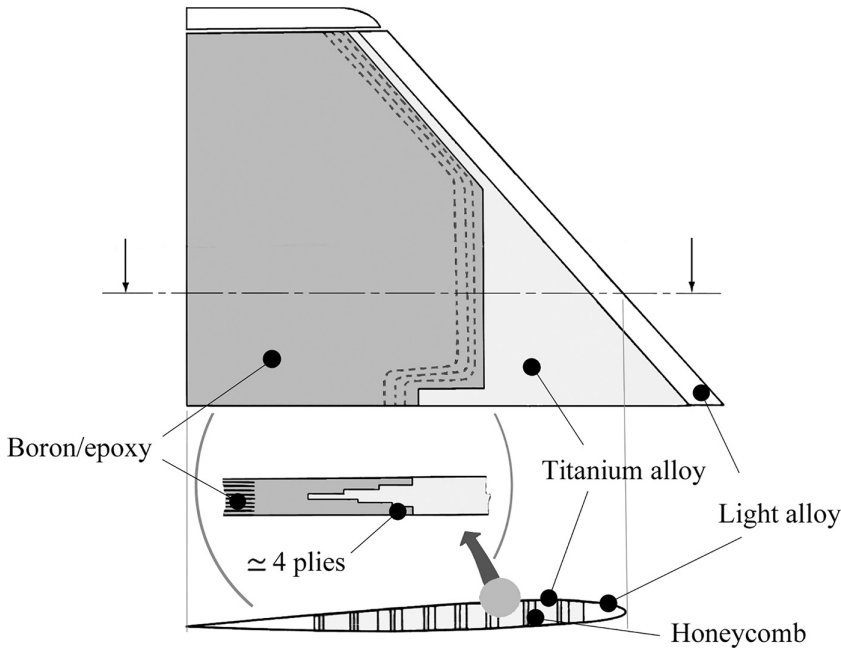


FIGURE 7.21 Horizontal tail.

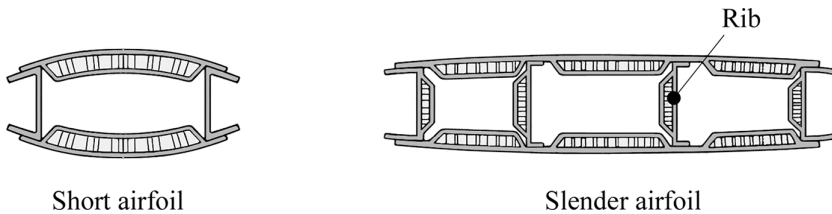


FIGURE 7.22 Sandwich skin panels.

When the part is too long, the requirement of dimensional stability can require the interposition of intermediate longitudinal ribs.

Each component (skins, ribs) is first assembled and polymerized following the monolithic technique described above.

- **Example: Wing flap** (Figure 7.23)

c. Sandwich for the reinforcement of spars and ribs

Introducing honeycombs, as represented in Figure 7.24, can increase the torsional and flexural stiffness.

7.1.9.2 Rib-Stiffened Panels

Rib-stiffened panels are common components in metal construction: the stiffeners are either assembled onto the panel or integrated to the panel. In that case, they are designed as part on the panel itself and machined together with the panel. So, a parallel may be found when obtaining stiffened composite panels.

a. Added stiffeners

The rib shapes used in conventional construction can also be found for composite stiffeners, as shown in Figure 7.25.

- **Example: Wing box** (Figure 7.26)

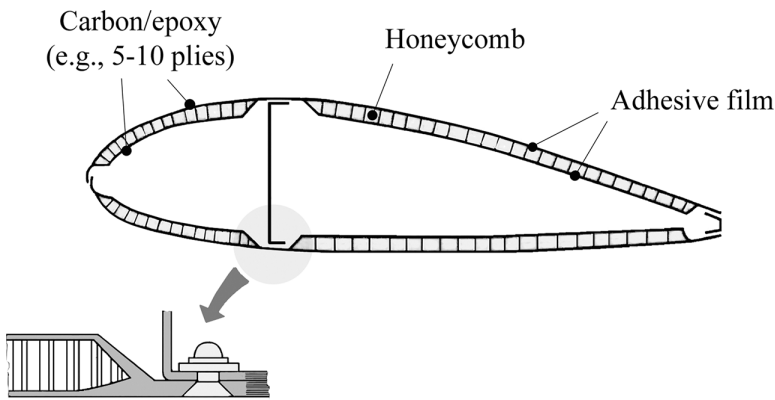


FIGURE 7.23 Wing flap.

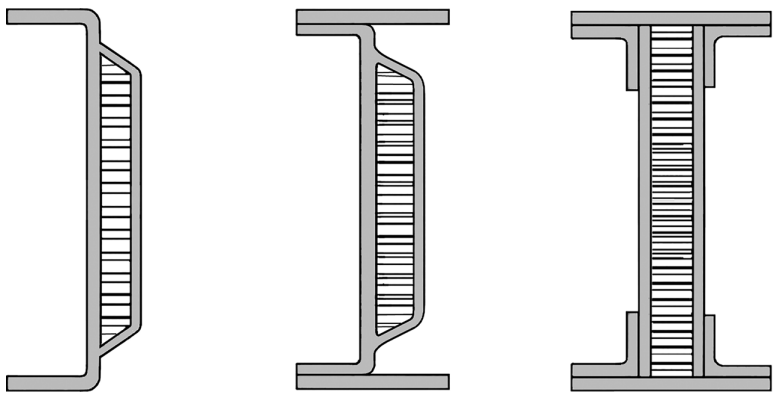


FIGURE 7.24 Reinforcement of spars and ribs.



FIGURE 7.25 Stiffeners shapes.

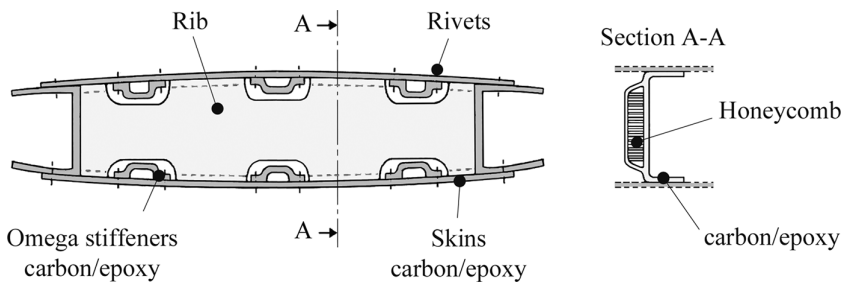


FIGURE 7.26 Wing box with added stiffeners.

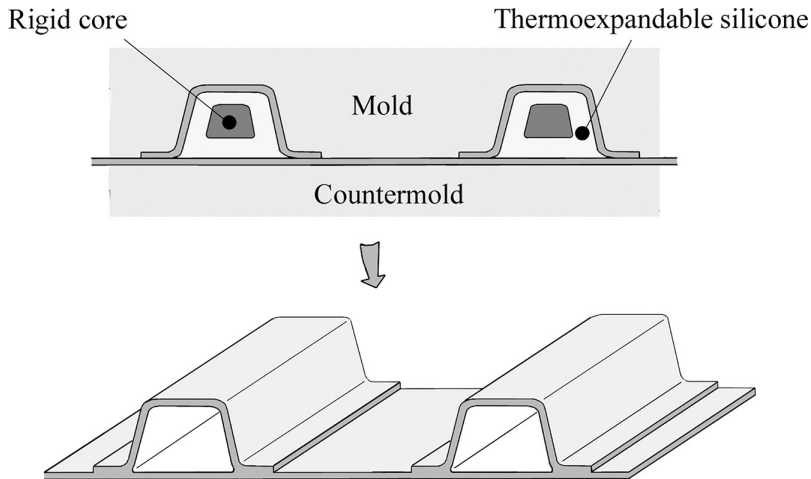


FIGURE 7.27 Monolithic stiffeners.

b. Monolithic stiffeners

These are cured at the same time with the skins. The latter can support higher loads than the previous case, but with higher cost. The mode of fabrication is shown schematically in Figure 7.27 for the so-called **omega** stiffeners. The manufacture requires using removable cores such as

- Silicon core, whose part is thermoexpandable
- Hollow silicon core stiffened by means of compressed air
- Fusible cores at a temperature to the tune of 170°C , that is, a little superior to the polymerization temperature of the part
- **Example: Ribbed plate** (Figure 7.28)
- **Example: Vertical tail skin** (see Figure 7.29)

The carbon/epoxy stiffeners are obtained by combining the autoclave pressure and the thermal dilatation of detachable light alloy modules⁹. The steps of the process are shown schematically in Figure 7.29.

• Example: Outer wing

This is a portion of wing primary structure of aircraft **ATR 72** (see Section 7.1.6). It consists of 2 carbon/epoxy panels with monolithic stiffeners, 2 carbon/epoxy spars, and 18 folded sheet ribs of light alloy as shown schematically in Figure 7.30.

The wing box's weight is 260kg (reduction of 65kg compared to an all-metal solution).

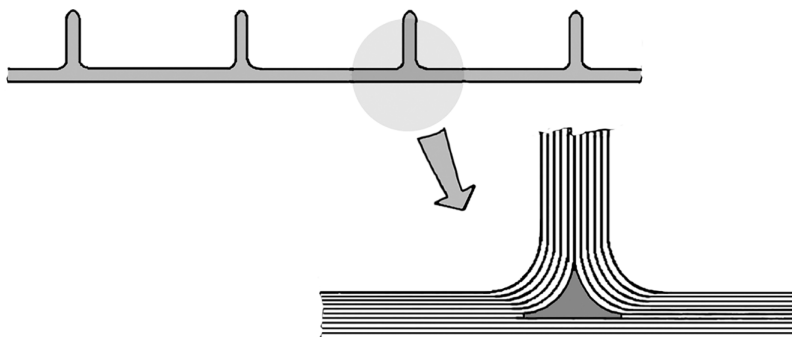


FIGURE 7.28 Ribbed plate.

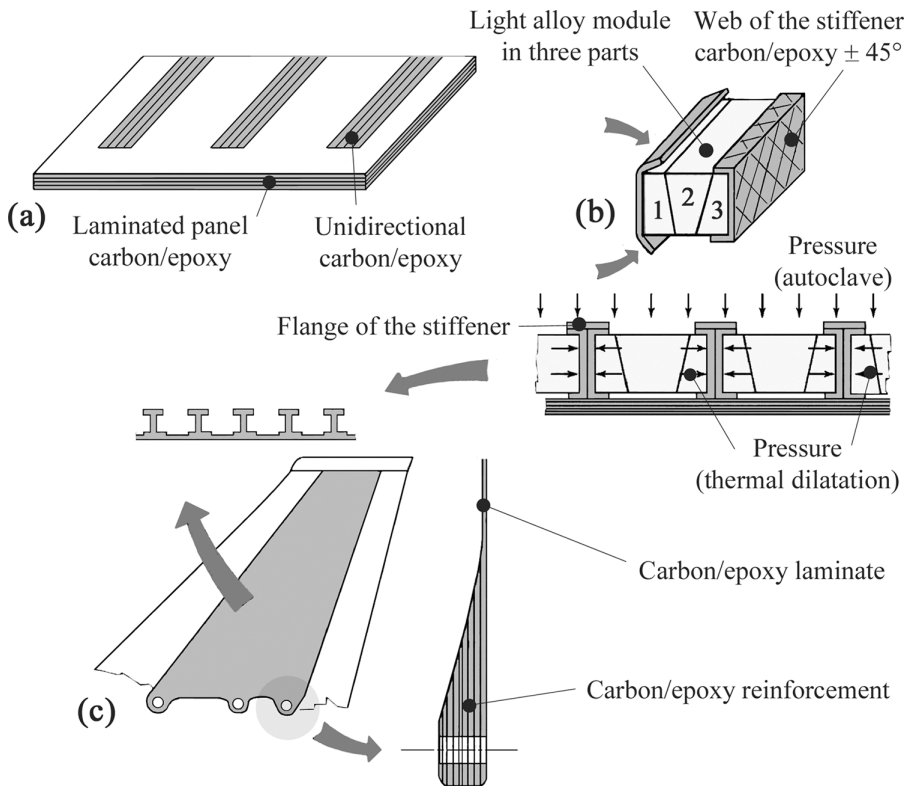


FIGURE 7.29 Vertical tail skin: (a) and (b) steps of draping, (c) finished part.

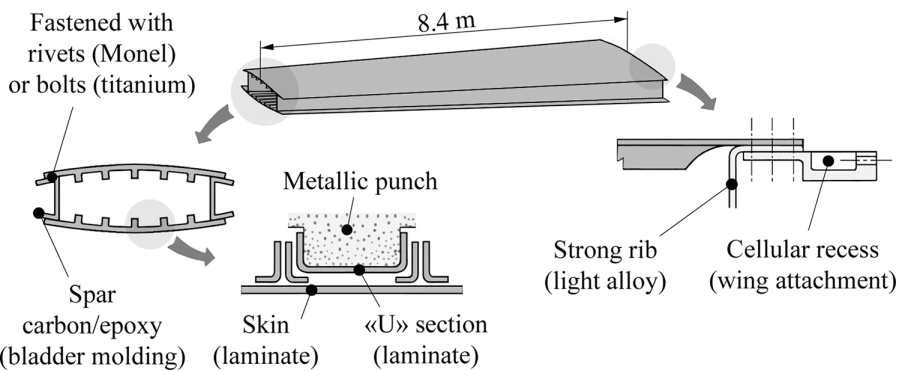


FIGURE 7.30 Outer wing.

Notes: Lightning protection of such a structure requires specific precautions such as:

- Incorporation of a conducting fabric made of bronze wires to the overall aerodynamic surface
- Installation of lightning conductors along the spars
- Protection of fasteners
 - **Example: Airbrake flap** (Figure 7.31)

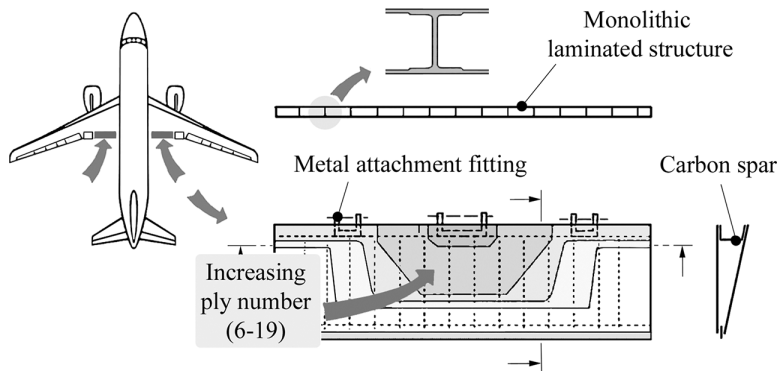


FIGURE 7.31 Airbrake flap.

7.1.9.3 MMC Panels

Figure 7.32 shows the upper fuselage area of an A 380 aircraft made up of GLARE panels (see Section 3.6.2.1). The total area is approximately 470 m^2 for 27 panels. These skin panels are shaped and joined from aluminum sheets of limited width (generally, 1.5 m) and pre-impregnated plies ensuring continuity at the joints (see Figure 7.33).

7.1.10 BRAKING SYSTEMS

Unlike the brakes of motor vehicles, the aircraft brakes are characterized by operating phases that are isolated in time and repeated in almost identical conditions from one landing to the next. These are **heat absorption** brakes, and they are operated for only a few seconds (about 20 s). Afterward, the cooling will perform gradually and monotonically. The heat coming from the transformation of kinetic energy is stored in the components participating in the friction phenomenon, which serve as **heat sinks**. These components must have the following characteristics:

- Being able to create a high braking moment that remains stable as the temperature increases
- Being able to support a very important **thermal shock**, on the order of 10^6 J/kg mass of the component
- Being refractory while retaining a good dimensional stability

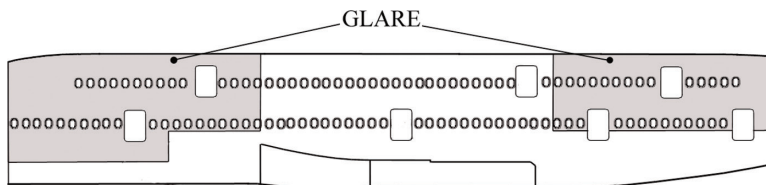


FIGURE 7.32 GLARE panels.

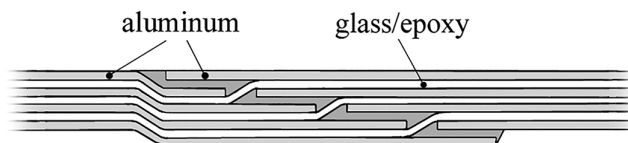


FIGURE 7.33 GLARE panels joining.

- Being able to keep mechanical properties at high temperature
- Having a mass as low as possible

The corresponding brakes are of **disk** type. The candidate materials able to constitute these friction disks are compared in Figure 7.34.

Thus, the interest to use 3D carbon–carbon composite disks as seen in Figure 7.35 is obvious. They have, in the light of the required qualifications, the following characteristics:

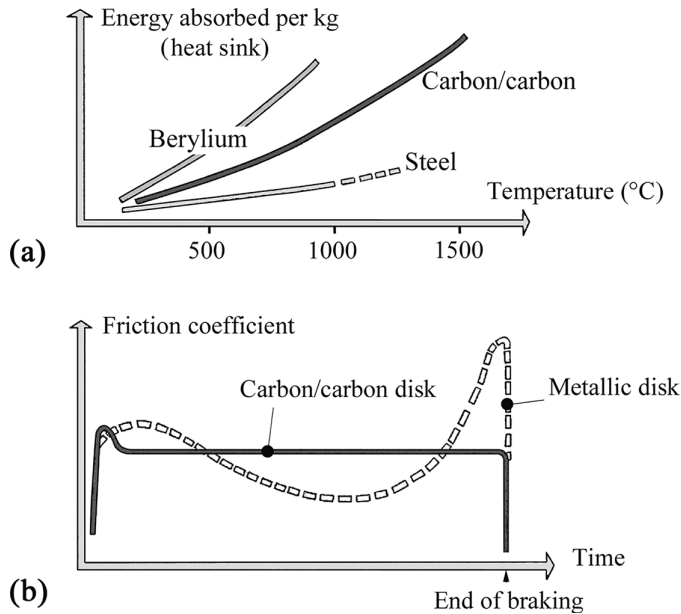


FIGURE 7.34 Materials to constitute friction disks: (a) energy absorbed and (b) friction coefficient.

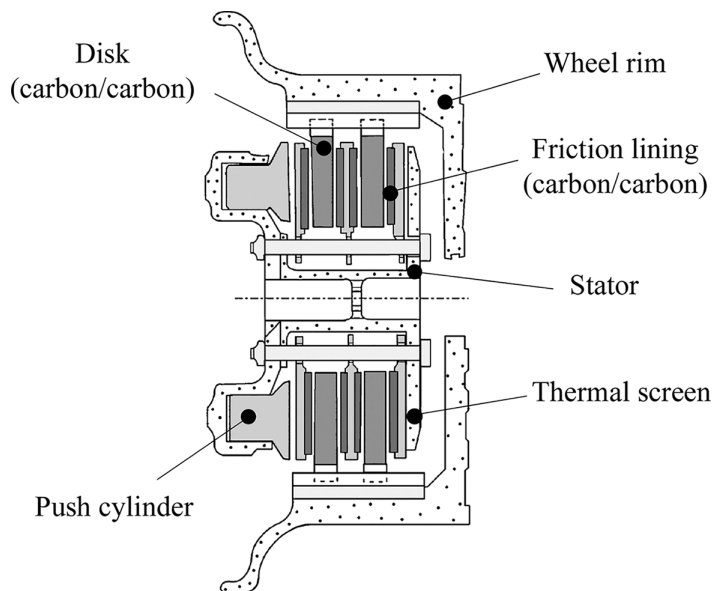


FIGURE 7.35 Carbon/carbon brake disks.

- Their dynamic friction coefficient is stable with respect to temperature, varying from 0.25 to 0.3.
- They resist thermal shock and are refractory until 1,600°C.
- They retain their mechanical properties at high temperature¹⁰.
- They are lightweight (specific mass of 1,900 kg/m³).

Example: Case of aborted takeoff on Airbus A340 (front landing):

Absorbed energy: 100 MJ; temperature: 2,000°C.

7.2 HELICOPTERS

7.2.1 COMPOSITE AREAS

This type of aircraft has undergone rapid change since the mid-1960s, thanks notably to composite materials integration in the airframe and the rotors. After the main rotor (blades and hub), composites were occupying more than 50% of the structure at the end of the 1980s. This latter became an all-composite structure, mainly in carbon/epoxy, during the 1990s (see Figure 7.36).

Compared to the previous metal construction, the weight savings are of

- 15% for secondary structures
- Up to 50% for the working parts such as blades, power transmission, and command parts

7.2.2 SOME EXAMPLES

7.2.2.1 Helicopter H160 Airbus-Helicopter (EU) 2020

This aircraft (see Figure 7.37) is the successor of the **Dolphin**. It should be noted the five-blade rotor with boomerang-shaped blades (**blue edge**) to reduce noise emission and increase the lift. The **Fenestron**® that forms the antitorque tail rotor improves ground security and flight safety. In addition, it reduces noise (3–4 dB) and the aircraft drag. Its rotor is tilted about 12°, which allows it to contribute to lift and improve handling when slowing down.

Cruise speed: 285 km/h

Maximum speed: 315 km/h

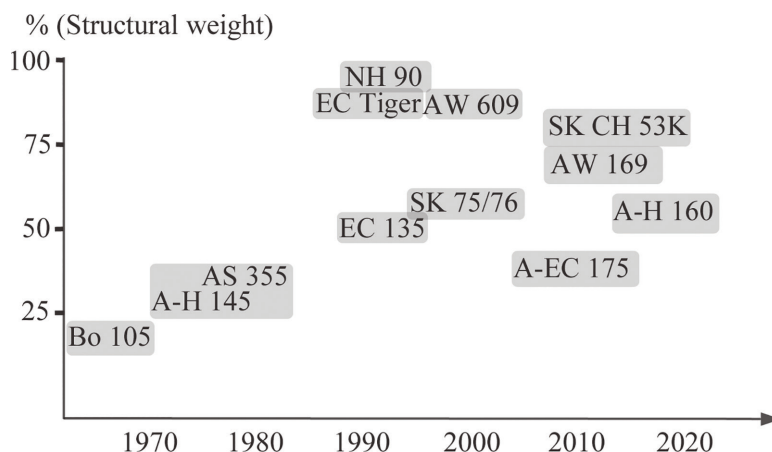


FIGURE 7.36 Percentage of structural composites: MBB (DE); Eurocopter (FR–DE); Eurocopter (EU); Sikorsky Aircraft (US); Agusta-Westland (IT).

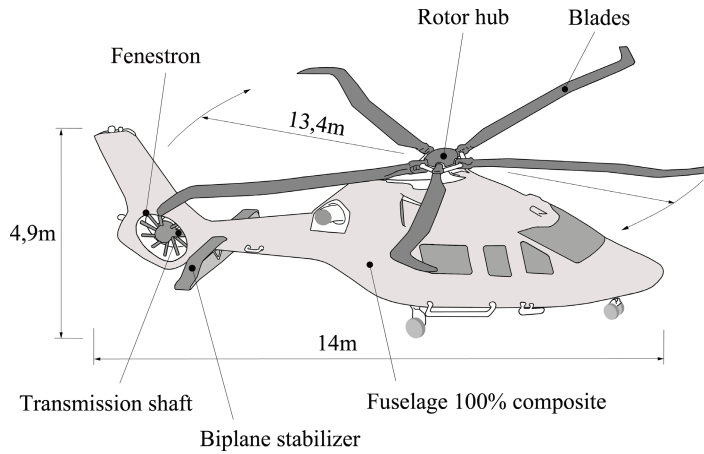


FIGURE 7.37 Composite components in the helicopter H160.

Max takeoff weight: 5,670–6,050 kg

Maximum ceiling: 6,096 m

Flying range: 834 km

7.2.2.2 Racer Airbus-Helicopter (EU)

The « Rapid And Cost-Efficient Rotorcraft » (Racer) Airbus (EU) 2022 (see Figure 7.38)

MTOW: 8 tons

Cruise speed: 400 km/h

Autonomy: 740 km

Composite transmission shafts: length 3 m, 3,000 t/min

Hybrid metallic-composite airframe. Some parts of primary structure are produced using additive manufacturing (see Section 2.2.3).

Double wing provides lift while minimizing perturbation of main rotor airflow.

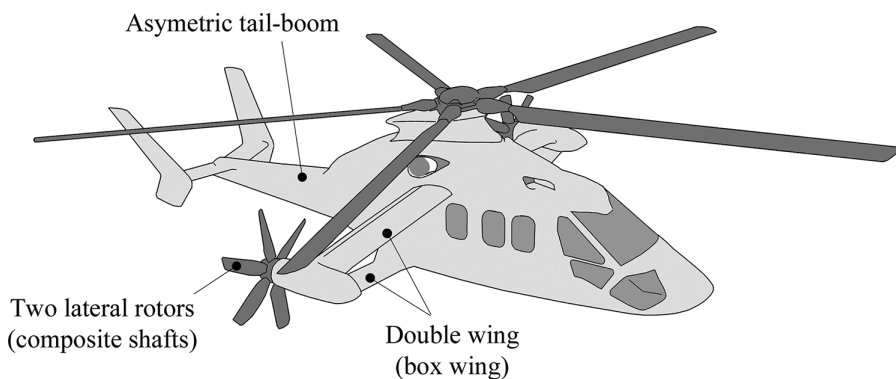


FIGURE 7.38 Racer.

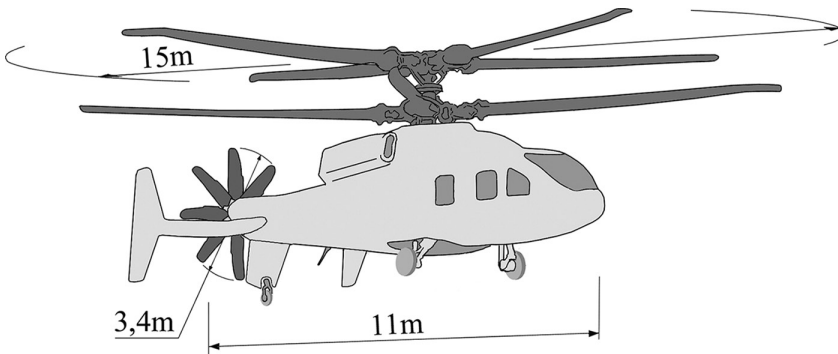
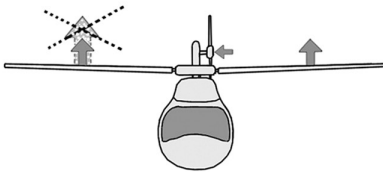


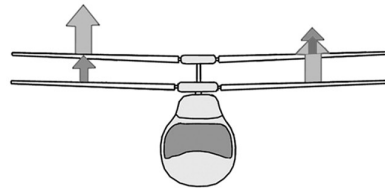
FIGURE 7.39 SB1 Defiant.

The lifts of advancing and retreating rotor blades must be balanced



Classical rotor + tail rotor

The lift of advancing rotor blade can be greater



Coaxial twin rigid rotor system

FIGURE 7.40 Advantage of twin rigid rotors.

7.2.2.3 SB-1 Defiant Sikorsky-Boeing (US)

Coaxial twin rigid rotor system (see Figure 7.39). Each rotor rotating in the opposite direction to reduce the net torque of the other rotor. This design also improves lift (see Figure 7.40) and lowers maintenance costs.

Folding blades reduce machine footprint for parking and transport.

Composite fuselage and all blades.

MTOW: 14 tons

Cruising speed: 450 km/h

Range: 425 km

7.2.2.4 V 280 Valor Bell-Lockheed Martin (US)

Military aircraft with two tilt-rotors (see Figure 7.41)

MTOW: 26 tons

Cruising speed: 520 km/h

980 km ≤ autonomy ≤ 3,900 km

Thermoplastic composites: V-tail and ruddervators

Access panels obtained from waste molding

Blades all carbon (**Eagle Technologies** (US))

The upper and lower carbon/resin wing skins are fixed to the wing box.

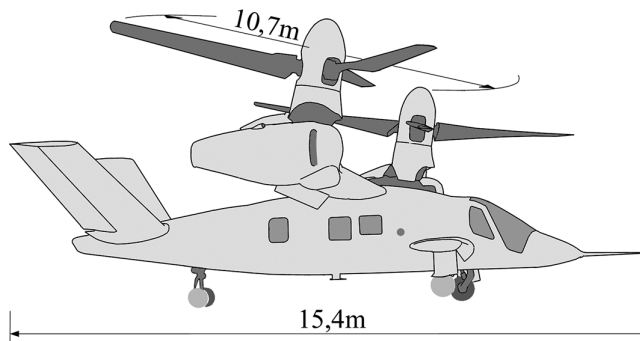


FIGURE 7.41 V280 Valor.

7.2.3 BLADES

7.2.3.1 Design of a Main Rotor Blade

The blades are the key elements of these aircrafts. They consist principally of the following:

- Outer skins forming the **box** that ensures the aerodynamic shape of the blade and the torsion stiffness (the blade does not twist under aerodynamic forces).
- A spar that resists the centrifugal tension on the blade as well as the flexure caused by the lift and drag loads¹¹. It is made of glass/epoxy (“R” glass, more resistant and less susceptible to aging by humidity).
- A rear edge that stiffens the blade in flexure in the drag direction.
- A filler material (foam or honeycomb) that prevents the deformation of the outer skins, thus ensuring the shape stability of the profile.

Figure 7.42 shows the different parts of the blade.

7.2.3.2 Advantages

The list of advantages obtained with this type of design is impressive.

The blade is molded (molding by assembly of two half shells under pressure). This solution allows designing an **optimized profile**, characterized by

- Variable chord and variable thickness
- Nonsymmetric and nonlinear twist of the blade profile
- Flapping and torsion stiffnesses, which can be controlled thanks to judicious usage of composite materials

7.2.3.3 Consequences

The consequences are as follows:

- The takeoff weight is significantly improved.
- The cruising speed is increased for the same power.
- The cost of fabrication is reduced by 50% in comparison with conventional metallic solution.
- The cost of operation is reduced.
- The life duration of the blade is quite unlimited. None of the loads inside the flight envelope of the aircraft can lead to fatigue fracture. The blade is nearly indestructible, even on appropriate testing machines.

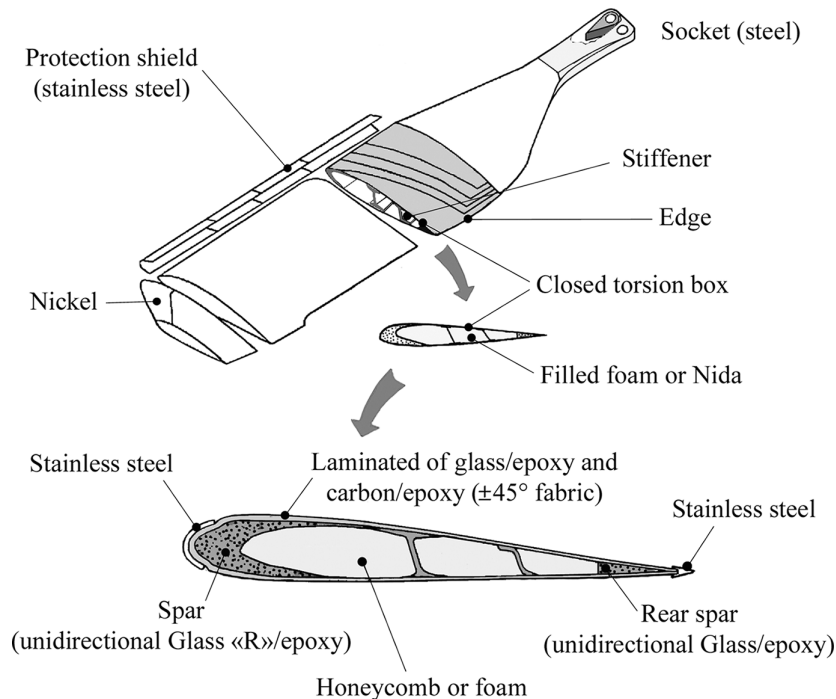


FIGURE 7.42 Helicopter blade.

- For greater safety, the blade has a **fail-safe** design¹². An impact (projectile, collision) causes a local deterioration that does not lead to the fall of the aircraft.
- The repair of the blade is straightforward¹³.
- The blade is insensitive to corrosion.

Note: The blade, as designed, can become ultralight. However, the weight cannot go down below a minimum value that ensures the inertia needed for the good lift of the rotor.

7.2.4 ROTOR HUB

This mechanical device is designed to enable the following:

- Rotation of the blades
- Flapping and dragging, that is, the small amplitude angular displacements of the blades during rotation
- Pitch control, that is, the control of aerodynamic profile incidence of the blades

To ensure these functions, the earlier metallic rotors were very complex. They consisted in many parts – with an extensive use of spherical bearings – and numerous points of lubrication. Thereby, the maintenance was very costly.

The modern rotors – in particular those developed from the 1970s by **Aerospatiale** (FR) and then by **Eurocopter** (FR–DE) – were designed by replacing these classical articulations by other suitable devices, allowing the creation of degrees of freedom by using elastic deformation of

- Composite elastic joints made of metal/elastomer
- Elastic laminated parts

7.2.4.1 Example: Rotor Hub Starflex, Eurocopter (FR-DE)

This hub has the form of a four-pointed flexible star (see Figure 7.43) obtained by draping a large amount of balanced glass/epoxy fabric sheets and molding under heat and pressure.

The different degrees of freedom necessary for the operation are made possible by dedicated features as shown in Figure 7.44:

- The elastic arm ensures the angular deflection called **lift flapping**.
- The elastic articulation joint with spherical deflection acts like a **ball and socket** allowing for the rotation identified as **pitch control** on the figure. This translates into a variation in the profile incidence.
- The elastomer bearing allows for blade angular deflection out of the plane of the figure, which is called **drag deflection**.

The following are the consequences:

- A spectacular decrease in the number of components: from 377 pieces for a classical metallic solution with 30 bearings down to 70 pieces for a composite solution without any bearings
- Accordingly, a weight saving of 40 kg

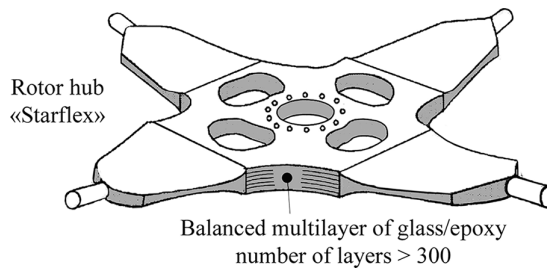


FIGURE 7.43 Starflex rotor hub.

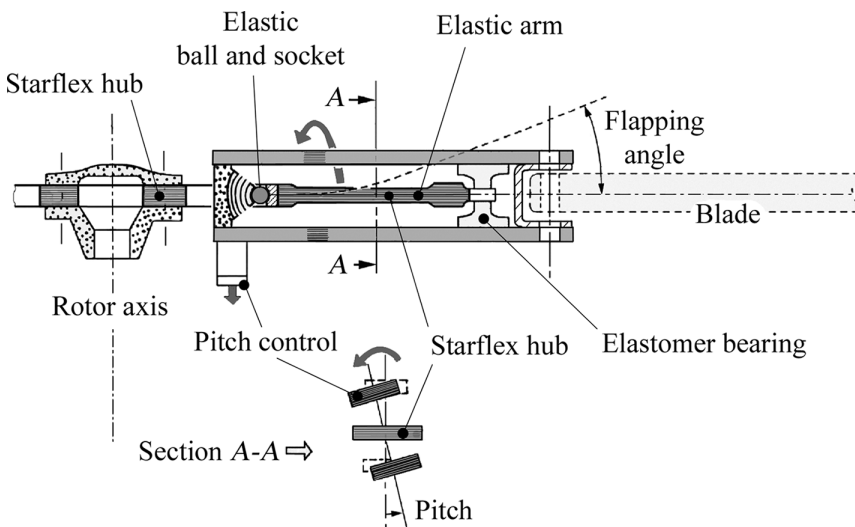


FIGURE 7.44 Details of the Starflex hub.

- A reduced cost of fabrication
- A maintenance that is reduced in considerable proportion, lowering significantly the hourly cost of the flight
- An improved safety (greater reliability of the mechanical assembly)

7.2.4.2 Example: Rotor Hub Spheriflex, Eurocopter (FR-DE), Airbus (EU)

It is characterized by an elastic ball and socket, which includes elastomeric layers between two rigid elements. The latter ensures spherical deflection and, thus, allows various angular displacements required: pitching, flapping, and dragging. The blade root is modified accordingly (see Figure 7.45). The number of components becomes extremely reduced, with a minimal design space (less than the volume of the previous solutions).

7.2.5 OTHER WORKING COMPOSITE PARTS

They are mostly made of carbon/epoxy. The parts already in service include the following:

- Swashplate for the control of the pitch
- Pitch change links
- Pitch levers (see Figure 7.46) where the composite design leads to a weight reduction of 45% as compared with the metallic solution
- Tail rotor blades
- Empennage
- Fenestron
- Transmission shaft to drive the tail rotor
- Tail boom (pylon)
- Winch lifting boom¹⁴

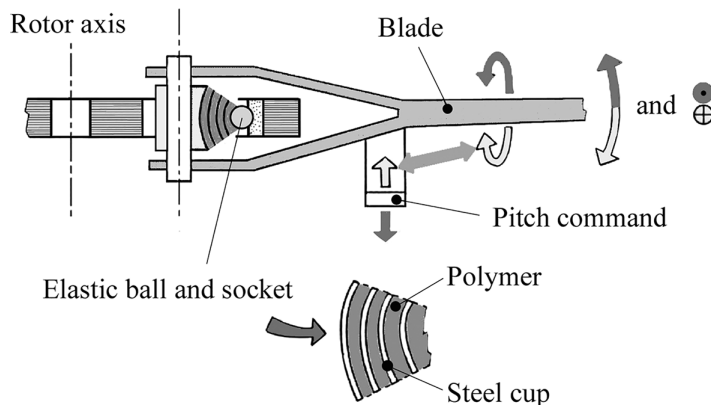


FIGURE 7.45 Spheriflex rotor hub.

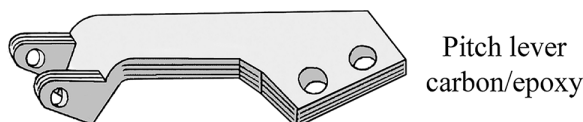


FIGURE 7.46 Pitch lever.

- **Example: Aircraft Dauphin Eurocopter (FR–DE)**

Light Alloy Empennage	Carbon/Epoxy Empennage
231 parts	88 parts
5,900 rivets	0 rivets
Mass = 1	Mass = 0.78
Overall cost = 1	Overall cost = 0.66
Light Alloy Rotor Hub	Carbon/Epoxy Rotor Hub
293 parts	92 parts
Overall cost = 1	Overall cost = 0.35

Notes

- Using composite materials reduces the **radar signature** of the helicopter.
- Damage caused by piercing projectiles to the blades, hub, and command links evolves more slowly in composite parts, allowing the aircraft to be able to return to home base (except for ammunitions with diameters higher than 20 mm).
- Crashworthiness¹⁵ requirements are more difficult to fulfill for a composite structure than for a conventional structure.

7.3 AIRPLANE PROPELLERS

7.3.1 PROPELLERS FOR CONVENTIONAL AERODYNAMICS

The design of composite propellers for conventional aerodynamics is similar to helicopter blade design. These blades consist essentially of a composite torsion box associated with a metallic or composite spar.

7.3.1.1 Example: Propeller Blade, Hamilton Sundstrand (US)-Ratier Figeac (FR)

- a. Propeller of the aircraft **ATR 42**¹⁶:
The design of the blade is shown in Figure 7.47.
 - b. Propeller of the airplane **Transall** (FR–DE):
When the rotor diameter becomes important, the introduction of a spar in unidirectional glass and a torsion box in carbon leads to a significant weight saving as indicated in Figure 7.48.
- Some characteristics include the following:
 - Diameter of the four-blade rotor, 5.5 m
 - Mass of a composite blade, 51 kg

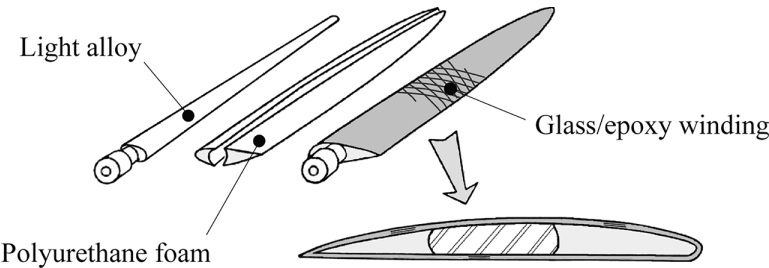


FIGURE 7.47 Composite-metal propeller blade.

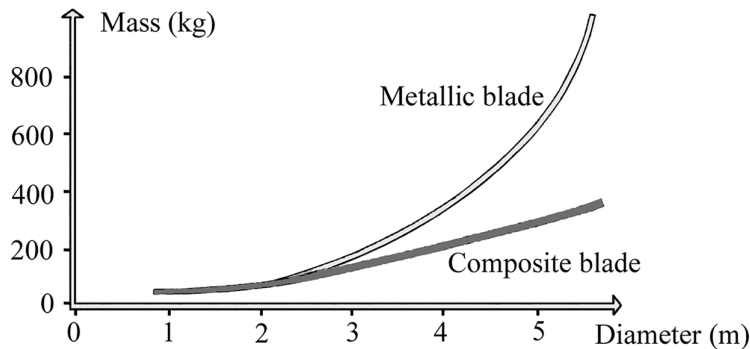


FIGURE 7.48 Weight saving in using composites blades.

- Weight saving as compared to a metal blade, 53 kg (mass of a metal blade, 104 kg)
- Total weight saving, 2×4 blades, or 430 kg

Note: The centrifugal inertia force at the blade root decreases from 105,000 to 30,000 daN. This load is taken by a special position of the spar glass fibers, which are bonded to a steel part shaped like a tulip, together with a circumferential binding by means of filament winding of rovings. This allows for the **fail-safe** design. If there is disbonding from the tulip, the blade is retained on its base by the circumferential winding.

The propeller blade is described in Figure 7.49.

c. Propeller of the airplane **A400M Airbus** (EU):

Each of the four propellers (two on each wing) is composed of eight blades of 5.33 m-diameter and unitary weight of 47 kg (see Figure 7.50). If the form differs from the precedent blade, the composite structure and manufacturing technique are similar.

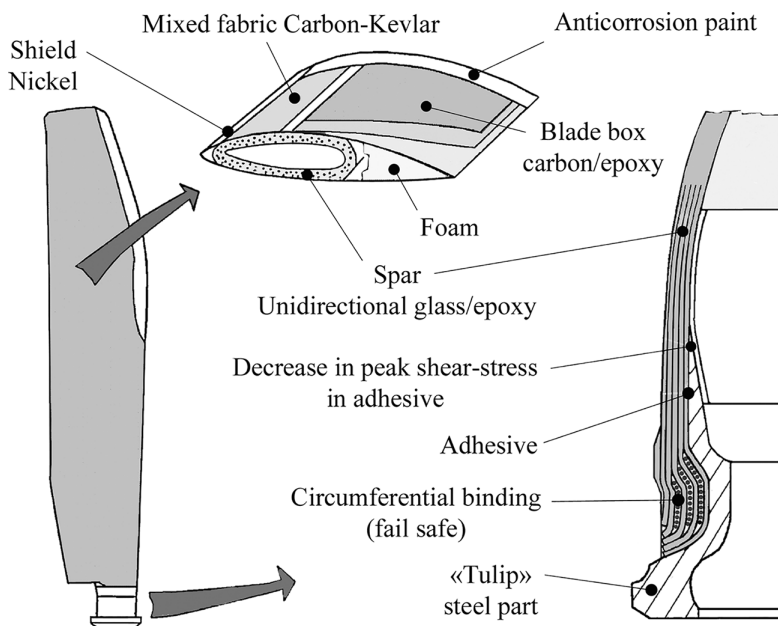


FIGURE 7.49 Composite propeller blade.

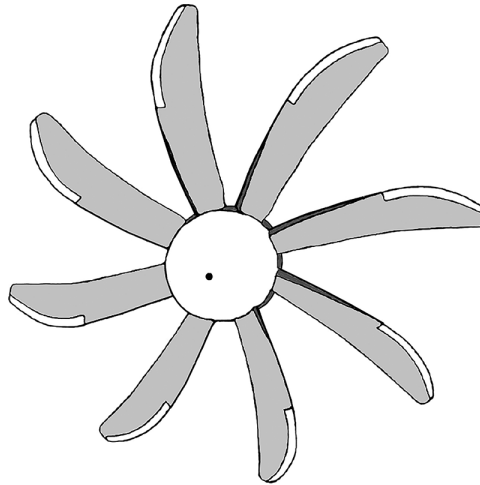


FIGURE 7.50 Composite propeller.

The two propellers located on a same wing rotate in opposite directions, so that the blades go down between the two engines at the middle wing level. This design arrangement creates aerodynamic benefits that bring a weight saving for the wing and the rudder. However, it requires two symmetrical forms of blades and a reversal of the direction of rotation of one motor out of two (interposition of a reverse gear).

7.3.2 HIGH-SPEED PROPELLERS

The high-speed propellers intend to drive commercial aircraft at a speed close to jet engine-propelled aircraft (Mach 0.8–0.85 or more than 850 km/h). The interest of these propellers lies in a higher propulsion efficiency compared to jet engine's one, as shown in the graph of Figure 7.51.

The feasibility of the concept of a nonducted propeller for a turbofan has been already demonstrated in flight in the 1980s. The fan became an open rotor, with two high-speed propellers spinning in opposite directions. Such a configuration reduces the weight and drag of the nacelle. Thus, the diameter may increase. This means that the dilution ratio is also increased (high bypass) and,

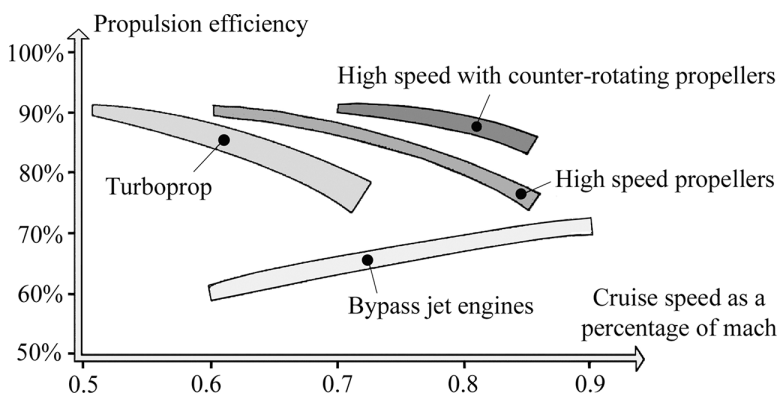


FIGURE 7.51 Propulsion efficiency of propellers.

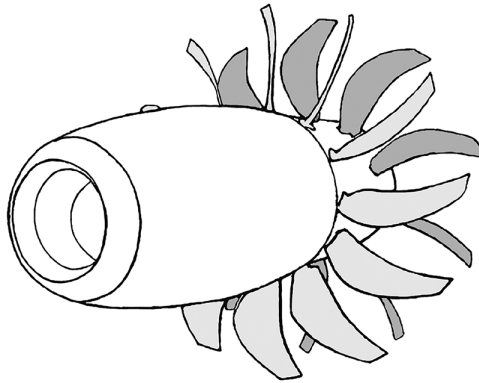


FIGURE 7.52 Open rotor.

thus, the engine performance. For a good aerodynamic and acoustic behavior, the propellers are characterized by a low thickness, a large airfoil chord, and a strong curvature of the blades made of 3D woven carbon/resin (CFRP). The complexity of the geometry combined with important speeds of rotation (more than 4,000 rpm) requires such a composite design. With a very high dilution ratio of 30:1¹⁷ and for a same speed, the fuel saving is of the order of 20% compared to an aircraft equipped with an engine of the current generation. Nevertheless, the challenge is to make these open rotors acoustically more competitive.

- **Example: Open rotor, CFM International, General Electric (US)-SNECMA (FR)** this open rotor consists of two counterrotating propellers (see Figure 7.52). The manufacturing process for the blades is the same as described earlier, with an RTM-injected torsion box.

Note: Current developments are also moving toward large open rotors in which the second crown of blades does not rotate. These variable pitch blades straighten the flow downstream of the fan. Example: **Open Fan RISE, CFM International, and General Electric (US)-Safran Aircraft Engines (FR)**. With such an open rotor, it should be noticed that for a cruise speed of Mach 0.78 is expected a propulsion efficiency identical to that of a turboprop (see Figure 7.51).

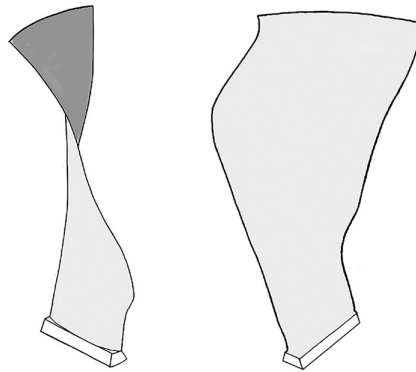
7.4 AIRCRAFT REACTION ENGINE

7.4.1 TECHNOLOGICAL DEVELOPMENTS AND PROGRESS

Since the beginning of the 1960s, the fuel consumption per passenger of civil transport aircraft has decreased by 70% (currently 3–5 ℓ per passenger per 100 km traveled). Progress in motorization has contributed largely to this reduction. The need to reduce the mass of the jet engines leads the designers to introduce low-density materials as much as possible.

7.4.1.1 Example: Jet Engine Leap®, CFM International, General Electric (US) – Safran Aircraft Engines (FR)

This new generation of jet engine presents an important weight reduction and an increased lifetime compared to prior generation. Beside the composite cowl of the engine, the following composite assemblies are noted:

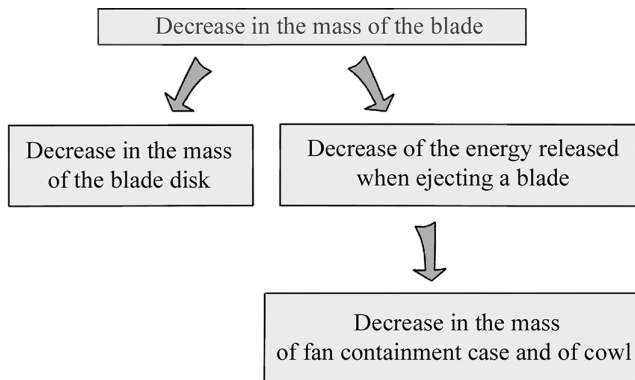


Average diameter of the fan: 1.83m

FIGURE 7.53 Composite blade for engine fan.

- **Fan:** The blades and their containment case are made of composite materials, leading to a weight saving higher than 200kg. The blade number is reduced by half (18 instead of 36), whereas the geometric complexity of the latter increases (see Figure 7.53). Significantly lighter with a mass divided by five, and more sustainable, these blades are obtained on the same design principle described above for the propellers, with a carbon/epoxy box made from 3D woven preforms injected by the RTM process (see Section 2.3.1).

Note: Here again, the consequences of composite design for the fan are to be noted:



- **Low-pressure turbine:** With temperatures about 1,000°C, it is equipped with refractory ceramic matrix composite (CMC) blades, leading to a weight saving of 125 kg.
- **High-pressure turbine:** The high-pressure turbine shrouds are made of composite with ceramic matrix.

Knowing that the temperature range in the combustion chambers of these machines is 1,600°C, we find the following:

- **High-performance alloys** for the rotating metal parts interacting with hot gases.
 - Nickel-based superalloys that are not only essential components of the aircraft turbo-shaft engines but also more widely used in the production of energy. They are polycrystalline for the disks and monocrystalline for the blades before the combustion chamber (high-pressure compressor) or after the combustion chamber.

- New low-density alloys and intermetallic compounds. They are very resistant, combining the high-temperature resistance of ceramics with the malleability of metals. This is the aluminide case (titanium aluminides). They are used for carter components.
- **CMCs** for parts in contact with hot gases downstream of the engine itself.
- **MMC**, usually titanium-based, with silicon carbide fibers (SiC) for next-generation disks.

7.4.2 USE OF CERAMIC MATRIX COMPOSITES (CMCs)

7.4.2.1 Interest of CMCs for Aerospace Engines

CMCs were discussed in Chapter 3 (see Section 3.6). Remember that thermostructural CMCs are intended to be used at high temperature (1,000°C–1,200°C). They were originally developed for the space industry. When extending their use for aeronautical applications, the major problem was that of the duration of use. Indeed, while a rocket engine works for 1–10 min, the jet engine of a military aircraft performs thousands of hours, and in the civil field, durations of tens of thousands of hours must be ensured.

When comparing the performance of CMCs with Ni super alloys (Inconel remains rigid up to 700°C), one can note:

- Weight saving: $\rho_{\text{CMC}} \approx \frac{1}{3} \times \rho_{\text{super-alloy}}$
- Increase in operating temperature: $T_{\text{max}}^{\text{CMC}} - T_{\text{max}}^{\text{super-alloy}} > 280^\circ\text{C}$

Consequences:

- Less cooling air: better fan efficiency
- Engine runs hotter: more complete combustion: reduction in consumption and reduction in pollution.

7.4.2.2 Applications

- C/SiC (carbon fibers/matrix silicon carbide): components of afterburner flaps on the engine of the fighter aircraft **Rafale M88 Snecma** (FR)
- SiC/SiC (silicon carbide fibers)/matrix of silicon carbide): flameholder rings and internal flaps of the jet engine **M88 Snecma** (FR)
- Silicon carbide fibers (SiC/matrix, glass-ceramic of lithium aluminosilicate): spacecraft engine parts by **ONERA**, **Safran-Snecma**, **Dassault Aviation** (FR), **Airbus Group**, and **SEP** (EU)
- Silicon carbide fibers (SiC)/matrix of silicon nitride–silicon carbide (Si_3N_4 –SiC): molds for casting aluminum alloys (US)
- Ox/Ox (alumina fibers/alumina matrix): turbomachinery combustion chambers (**ONERA**, **Safran-Snecma** (FR), **Volvo** (SE), **Rolls-Royce** (GB))
- Silicon carbide fibers (SiC)/matrix of disilicide of molybdenum–silicon nitride (MoSi_2 – Si_3N_4): parts for engines (**NASA** (US))
- Ox/Ox (alumina or aluminosilicate (mullite) fibers/matrix): glass-ceramic aluminosilicate, combustion chambers, nozzles, and missile noses (US)

7.4.2.3 Example: Nozzle: COI Ceramics (US)/Rolls-Royce (GB)

In Figure 7.54, the mixer, an important component located on the back of a jet engine ensuring dilution of hot gas turbine output into cold flow of the fan, is made of composite with ceramic matrix Ox/Ox leading to a weight saving of 40%. In addition to advantages mentioned above (see Section 7.4.2.1), one can add:

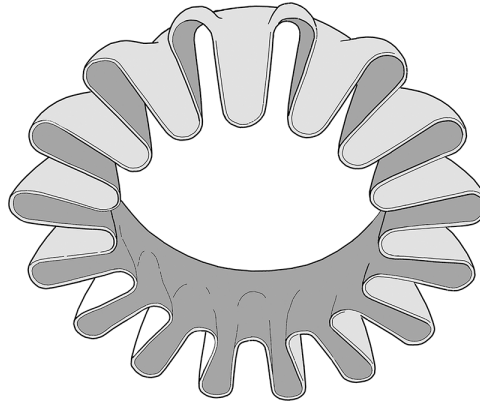


FIGURE 7.54 CMC (Ox/Ox) engine mixer

- Manufacturability: ability to fabricate such advanced component that can't be made with existing metallic materials
- Sufficient strength and modulus at high temperature to maintain lobe shapes, providing improved performance

7.5 SPACE APPLICATIONS

It is undoubtedly in the field of launchers, shuttles, and satellites that the weight saving is the most crucial problem. Thus, **exchange rate** (see Section 7.1.5) can reach tens of thousands of dollars per kilogram for the launcher and satellite components.

7.5.1 SATELLITES

The structure of satellites consists mostly of tubes and plates assembled. The structure should mainly do the following:

- Resist against average and fluctuating accelerations of the launch, counted as number of times the acceleration of gravity ($g = 9.81 \text{ m/s}^2$), up to $5 \times g$ continuously and $5 \times g$ maximum amplitude for sinusoidal state, for frequencies up to 40 Hz. In order to avoid resonance, the structure has to be very rigid. The **rigidity** constitutes the sizing criterion.
- Be quite insensitive to temperature variations (-180°C , $+160^\circ\text{C}$) because of the precision optical instruments such as telescope and high-resolution camera. Here is the main rationale for the use of carbon fibers for tubular structures: they are characterized by a very low thermal expansion coefficient¹⁸ of about 1×10^{-7} per degree.

The primary structure of satellites can also include sandwich panels, with the following design specificities:

- Light alloy honeycomb cores (Nomex is not used¹⁹ due to off-gas emission in vacuum). No risk of corrosion exists between carbon skins and aluminum core, as there is neither oxygen nor humidity in the environment of parts in flight.

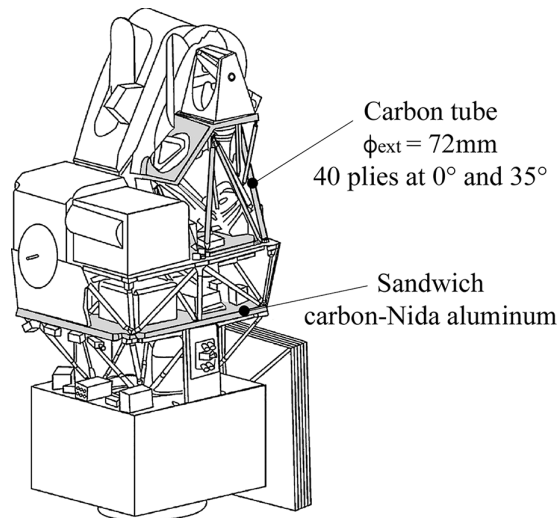


FIGURE 7.55 Camera high-resolution visible (HRV) spot.

- Laminate carbon skins, without midplane symmetry for maximum lightness. The skin thickness is of the order of 0.1 mm. Very twisted during demolding²⁰, the skins are shaped against the aluminum core and then bonded. Hence, the overall midplane symmetry is obtained for the sandwich panel.
- Example: High-resolution visible (**HRV**) camera, **Spot Image** (FR)

It is the upper part of the satellite shown in Figure 7.55.

7.5.2 PROPELLANT TANKS AND PRESSURE VESSELS

These tanks contain the combustible, fuel, or solid propellant providing the propulsion. They are made by winding impregnated carbon fibers strips up on a shaped mandrel. The mandrel must be resistant to thermal shrinkage after polymerization and designed to be removable (see Figure 7.56)²¹.

The **efficiency** of such filament-wound vessels is defined as

$$\text{Efficiency ratio (meters)} = \frac{p_{\text{bursting pressure}}}{(\rho \times g)_{\text{composite specific weight}}}$$

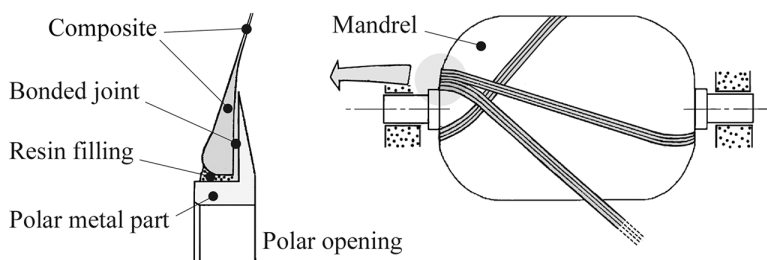


FIGURE 7.56 Filament-wound pressure vessel.

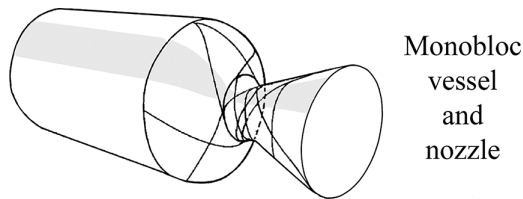


FIGURE 7.57 Monobloc tank and nozzle.

which is dimensionally homogeneous to a length, for example,

- Efficiency of glass/epoxy, 25 km
- Efficiency of Kevlar/epoxy, 35 km

These values justify the predominance of Kevlar/epoxy as the most frequently used material.

For some special cases of applications, the principle of the winding allows to get both tank and nozzle in the same part (see Figure 7.57).

7.5.3 NOZZLES

The propulsion nozzles for solid rocket propellant are characterized today by operating temperatures reaching 3,000°C for several tens of seconds, with pressures ranging from a few bars to several tens of bars²². The inner wall material disappears gradually due to decomposition, melting, vaporization, and sublimation. It is the nozzle **ablation** process. The suitable materials for playing such a role must, therefore, have

- A strong resistance to ablation at a high operating temperature
- A low specific mass
- A good resistance to mechanical and thermal shock

Figure 7.58 reflects the evolution of the nozzle structure until the advent of 3D carbon/carbon composite materials whose mechanical properties are given in Section 3.6.

- **Example:** Carbon/carbon **SepCarb**^{® 23}, **SEP** (FR) (Figure 7.59)

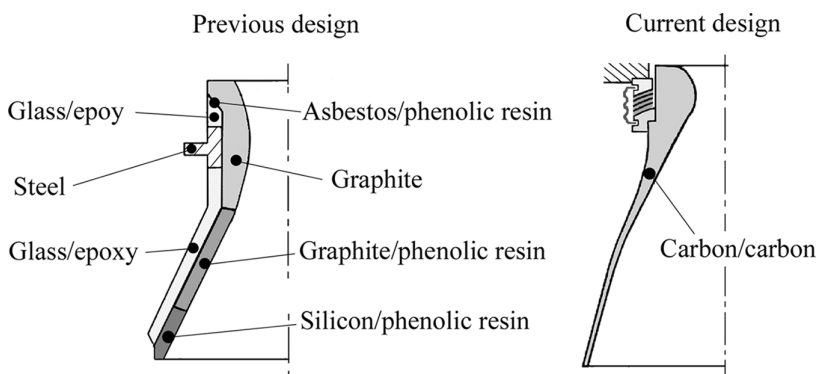


FIGURE 7.58 Development of nozzles.

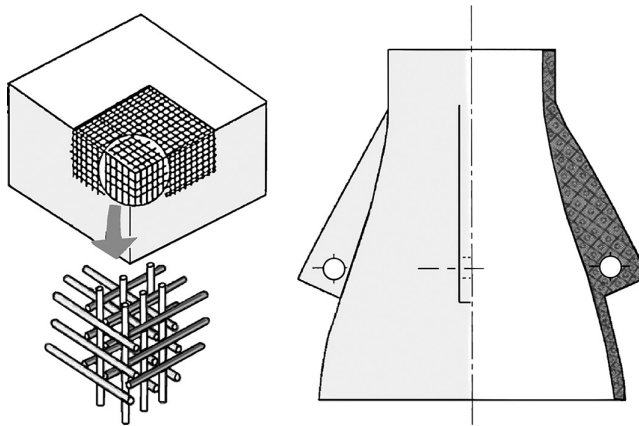


FIGURE 7.59 SepCarb material for propulsion nozzle.

The amount of heat before ablation can reach 84×10^6 J/kg of material. For example, the apogee motor of the launcher **Ariane**, whose nozzle cone is made of carbon/carbon, has the following characteristics:

- Weight saving of 50% in comparison with previous nozzle design
- Gain on the takeoff thrust of 10% thanks to a higher allowed slenderness

Example: Nozzle cone with rosette stratification

Figure 7.60 shows the difference in constitution between this type of nozzle and a classic nozzle with concentric layers and gives a few orders of magnitude.

Compared to the concentric stratification, this design

- Allows more convenient machining (more precise work of the lathe tool)
- Is more resistant to delamination

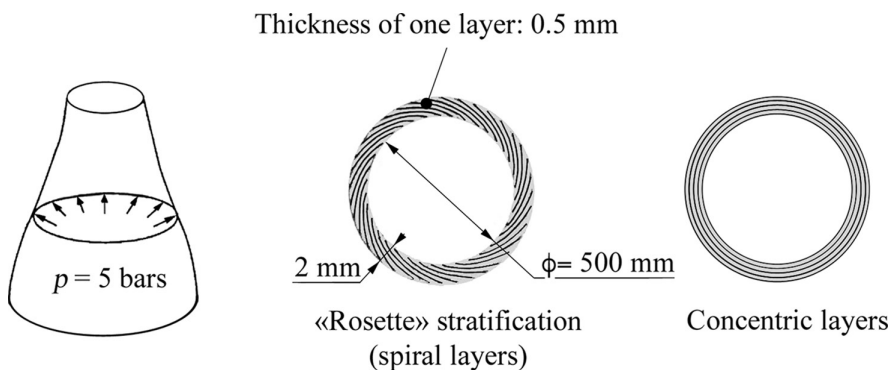


FIGURE 7.60 Nozzle in rosette form.

7.5.4 OTHER COMPOSITE COMPONENTS FOR SPACE APPLICATION

7.5.4.1 For Engines

For refractory composite parts, see Section 7.4.

7.5.4.2 For Thermal Protection

Two modes for the reentry into Earth's atmosphere of an aerospace object can be distinguished:

- **Rapid reentry with strong incidence:** This is the case of ballistic missiles and manned space capsules. The heat flux is very high (on the order of $10,000 \text{ kW/m}^2$) with a relatively short reentry duration. Depending on the intended application, the following materials are found:
 - Heat sinks²⁴ in carbon/carbon or in beryllium (case of ballistic ogive)
 - Ablative materials (see the case of the nozzles above) for the manned space capsules
- **Slow reentry with weak incidence:** This is the case of hypersonic planes or **space shuttles**. The duration of the reentry is on the order of 2,000 s. The heat fluxes are weaker but can attain hundreds of kilowatts per square meter of the plane at the beginning of the entrance (80-km altitude), for example,
 - 500 kW/m^2 at the leading edge
 - $100\text{--}200 \text{ kW/m}^2$ on the shuttle underbelly

The reentry temperature reaches $1,700^\circ\text{C}$, or even $2,000^\circ\text{C}$ at the shuttle nose. The thermal protections are of several types, depending on areas of the shuttle and the possible reuse of the heat shield:

- Heat sinks²⁵ associated with insulation.
- Radiant heat shield (the wall of the vehicle reflects the heat flux it receives).
- Ablative thermal protective coating. The ablative material undergoes an endothermic degradation by fusion, vaporization, and sublimation. The chemical decomposition absorbs the heat, and the vaporized gases cool the remaining protective layer, thereby decreasing the convective heat flux.

The areal masses of these devices are related to the upper temperature limit of underneath structure (see Figure 7.61).

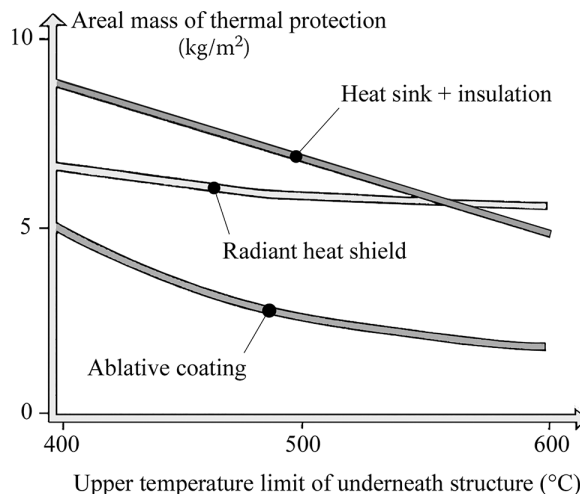


FIGURE 7.61 Areal mass of thermal protection.

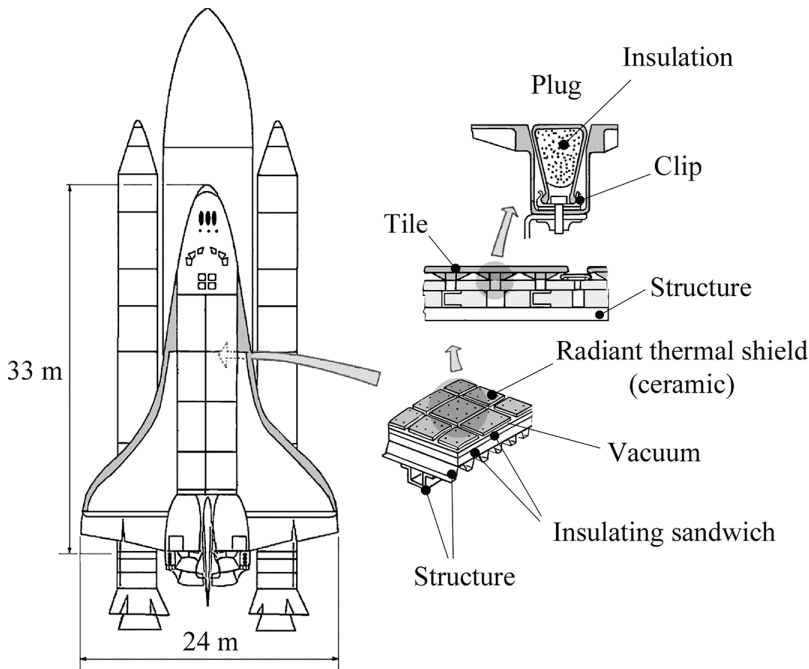


FIGURE 7.62 NASA space shuttle.

- **Example: Space shuttle, NASA (US)**

Its use, which ended in 2011, has allowed many achievements and provided a vast technological experience. It had an empty weight of 70 tons.

Depending on the zones, composite coatings of carbon/carbon or silicon/silicon were used together with underneath boron/aluminum²⁶ structural components (spacers, cross-pieces). The operating temperature was of 300°C continuous and up to 600°C peak.

The shuttle underbelly was protected by composite tiles of silica/silica ceramic²⁷, which constituted a radiant heat shield. They were separated from the underneath structure in light alloy or in laminated boron/aluminum by a sandwich of felt and nonflammable nylon/silicon/Nomex honeycomb. There were about 30,000 tiles. Their assembly is shown in Figure 7.62.

7.5.4.3 For Energy Storage

On board satellites and space stations, the systems using the composite flywheels for the supply of electric power and for the control of attitude provide a mass reduction of 25% as compared with conventional storage methods using batteries and gyroscopic means (specific power of the order of 5 kW/kg of the device). In addition, composite flywheel devices can deliver high levels of specific power output, on the order of 100 kW/kg of the device.

The peripheral speeds can attain 1,400 m/s (carbon filament-wound flywheels) with rotation speeds from 40,000 to 60,000 rpm.

- **Example: An energy storage module (US) (Figure 7.63)**

- Total mass, 200 kg (occupied volume, 0.15 m³)
- Specific energy, 230 kJ/kg (total energy, 46,000 kJ)
- Peripheral speed, 1,100 m/s
- Figure 7.64 shows different designs for carbon/epoxy flywheels²⁸.

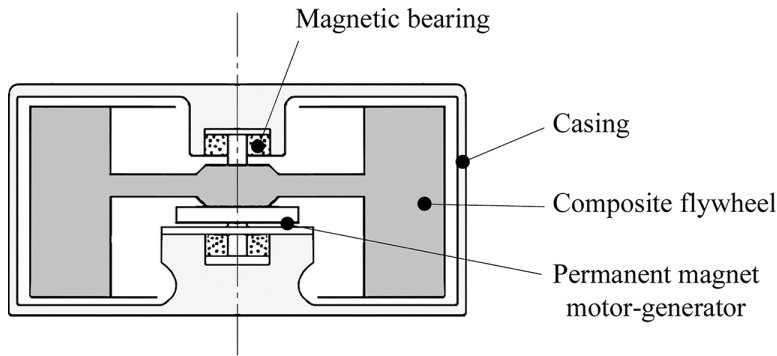


FIGURE 7.63 Flywheel energy storage.

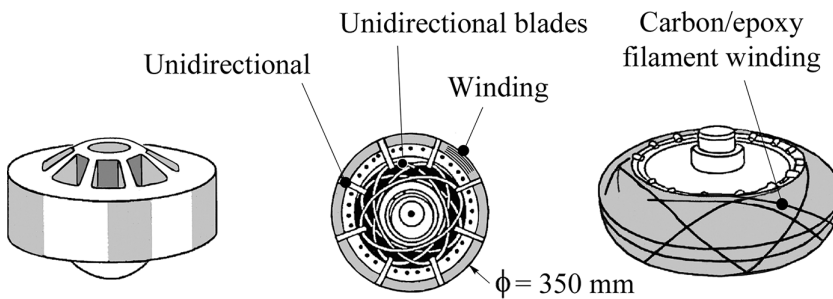


FIGURE 7.64 Some flywheel designs.

NOTES

- 1 See Section 3.3.3.
- 2 See Section 3.3.3.
- 3 See Section 3.3.3.
- 4 Impacts can create internal delaminations that are invisible from outside. This can also happen on the wing panels (e.g., drop of tools on a panel during fabrication or during maintenance work; see Section 5.4.5).
- 5 The mechanical properties of thermoset resins collapse when temperature reaches the **glass transition temperature**.
- 6 See Section 1.6.
- 7 See Section 4.4.4.
- 8 See also Section 2.1.3.
- 9 See Section 1.6 to compare the values of thermal expansion coefficients for light alloy and carbon.
- 10 See orders of magnitude of mechanical properties in Section 3.6.
- 11 See Application 19.3 “Helicopter blade”.
- 12 See Section 7.1.4.
- 13 See Section 4.4.4.
- 14 See Section 1.5.
- 15 See Section 7.1.4.
- 16 See Section 7.1.6.
- 17 Dilution ratio of 11:1 for current jet engines.
- 18 See Section 1.6.
- 19 See Section 1.6.
- 20 See Section 5.2.3.
- 21 See Section 2.1.7 and Applications 19.9 and 19.10.

- 22 1 bar = 0.1 MPa.
- 23 See Section 3.6.
- 24 See Section 7.1.10.
- 25 See Section 7.1.10.
- 26 See Section 3.7.
- 27 See Sections 2.2.4 and 3.6.
- 28 See Application 19.5 “Flywheel in Carbon/Epoxy”.



Taylor & Francis

Taylor & Francis Group

<http://taylorandfrancis.com>

8 Composite Materials for Various Applications

We mentioned in Section 1.3 the diversity of industrial products and of consumer goods that incorporate composite materials. In this chapter, we focus on the industrial areas (excluding aerospace), where these materials have been introduced and are used significantly to increase structural performance.

8.1 COMPARATIVE IMPORTANCE OF COMPOSITES IN APPLICATIONS

The graphs that follow allow comparing the importance of composite applications. In particular, they take into account the volume marketed for the main industrial applications concerned in Figure 8.1 as well as the geographical areas in Figure 8.2.

8.1.1 RELATIVE IMPORTANCE IN TERMS OF MARKET VALUE

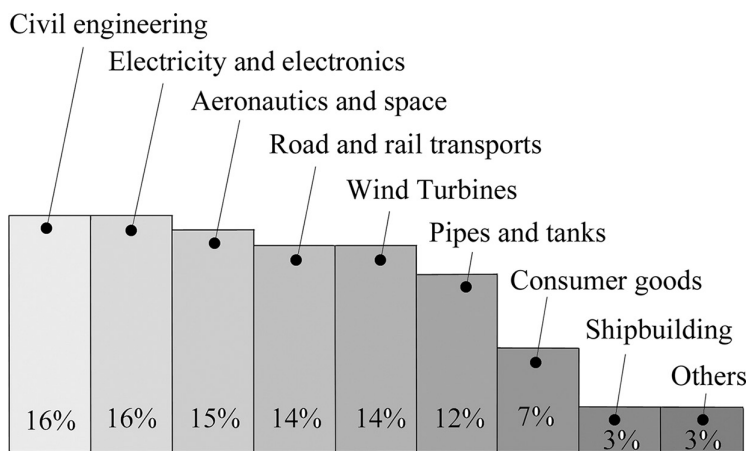


FIGURE 8.1 Percentage distribution of the total value according to application areas.

8.1.2 MASS OF COMPOSITES IMPLEMENTED ACCORDING TO THE GEOGRAPHICAL AREA

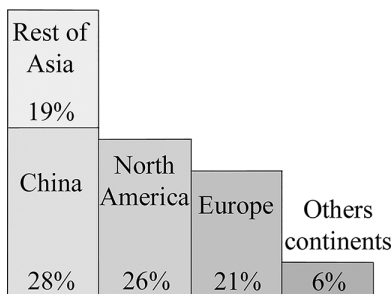


FIGURE 8.2 Composites implemented worldwide.

8.2 COMPOSITE MATERIALS AND AUTOMOTIVE INDUSTRY

8.2.1 INTRODUCTION

Within each manufacturer product range, the mass of vehicles with combustion engines has been steadily growing over time. The average car weight (Europe) has increased from 846 kg in 1953 to 1,250 kg in 2020, with a maximum of 1,283 kg in 2012. See the relative importance of masses in a car in Figure 8.3.

8.2.1.1 Examples

- Fiat 500 Model, **Fiat** (IT), which weighed 490 kg in its 1965 version and 960 kg in 2018.
- Golf Model, **Volkswagen** (DE) through seven generations the vehicle mass has increased from 800 kg in 1979 to 1,400–1,500 kg in 2017.

The main cause is the pressure from users to gain:

- Increased comfort by
 - Increased dimensions of the car (height, footprint) for more room and loading capacity
 - Improvement in equipment level (car radio, air conditioning, and navigation system)
 - Improvement in noise and vibration damping
- Increased safety (by following the evolution of norms)
 - Airbags
 - Nondeformable cabin
 - Electronic equipment
 - Strengthened structural elements

Therefore, to maintain performance, the engine power must grow as well as the mass of the conventional mechanical components, brakes, gearbox, etc., plus the vehicle structure.

8.2.1.2 Relative Weight Importance of Materials

Composite materials have been introduced gradually in cars since the 1950s. They followed the polymeric materials, some of which are used as matrices. They appeared on decorative parts, in structure or mechanical parts, outside and inside the vehicle.

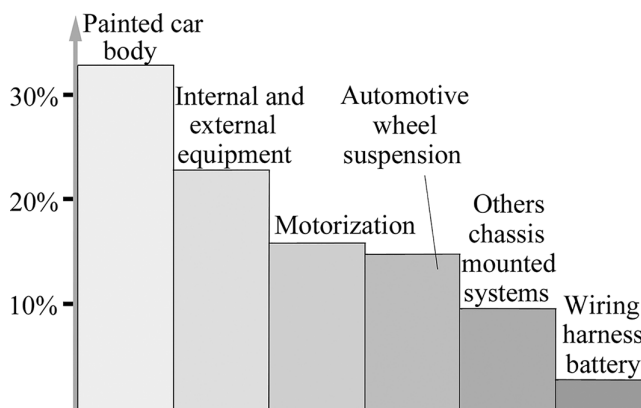


FIGURE 8.3 Mass distributions in a car.

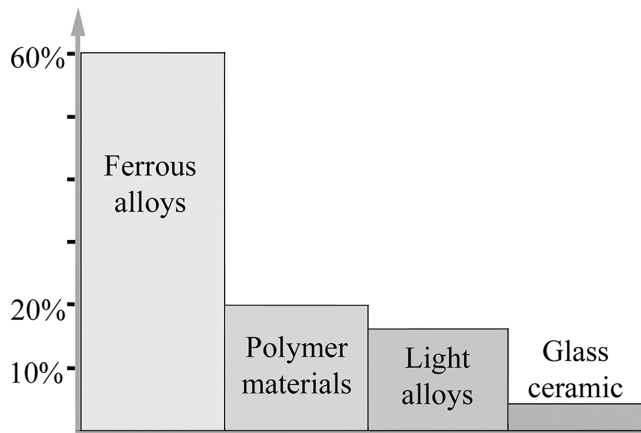


FIGURE 8.4 Allocation in mass of materials in a car.

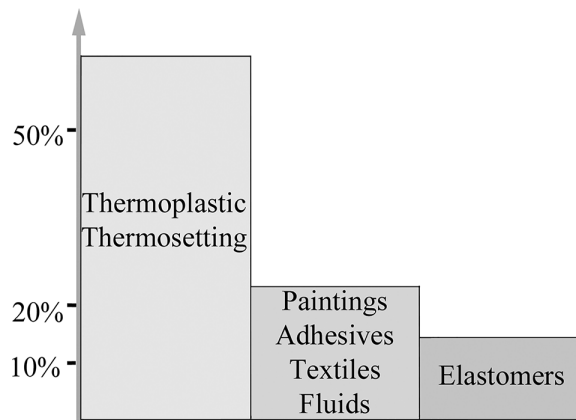


FIGURE 8.5 Mass distribution of polymer materials.

In Figure 8.4, the graph allows determining the relative weight importance of the main materials used in the manufacture of an automobile today. It should be noted that it limits the importance of mass proportion of polymer-based materials. However, although this mass may seem low, it should remain present in mind that the polymer density is about four times lower than that of steel and ferrous materials. This explains that the proportions by volume of materials with thermoplastic or thermosetting matrices as perceived when examining a vehicle could appear far more important.

Automotive polymer materials are shown in Figure 8.5. Here, thermoplastic or thermosetting materials include the reinforcement/matrix composite material.

Thus, for a vehicle of 1,250 kg mass, the mass of thermoplastics and thermosetting represents 160 kg.

8.2.1.3 Need for Making Cars Lighters

- Regulatory evolution

Within the context of the reduction of greenhouse gases emissions, European regulations limited in early 2021 to 95 g/km the average CO₂ emissions of the cars produced.

Compared to this limit, the regulations evolve as indicated below:

2025: -15%

2030: -37.5%

A reduction of 1 g/km requires a reduction of 25 kg of the car. The need to reduce masses, therefore, becomes essential, and it must not impact costs excessively.

Consequences: areas of R&D for weight reduction

It can be seen that the mass saving has become more than ever a key concern (it is estimated that a 100-kg weight saving can reduce by 30 kg the mechanical component mass).

- Improved design and manufacture of light alloy parts
- Improvement of manufacturing processes for composite parts suitable for large series
- Lightening of parts operating at high temperature
- Development of low-cost carbon composite parts
- Eco-design and recycling

8.2.2 COMPOSITE PARTS

8.2.2.1 Brief Reminder

We can see in Figure 8.6 a summary of the evolution of the proportion of plastics in a car. The introduction of reinforcements is slightly posterior.

A few dates for the emergence of mass-produced composite parts with **reinforcement + matrix**:

- The precursors, as shown in Figure 8.7
- 1968: wheel rims in glass/epoxy in car **S.M. Citroën** (FR)
- 1970: shock absorber shield made of glass/polyester in car **R5 Renault** (FR)

8.2.2.2 Current Functional Design

The current functional design of automotive parts and subassemblies leads to retain materials that enable to satisfy technicoeconomic specifications:

- Function
- Production rates
- Durability

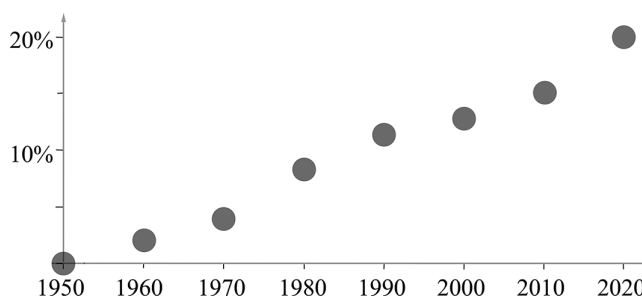


FIGURE 8.6 Evolution of the weight share of plastics in a car.

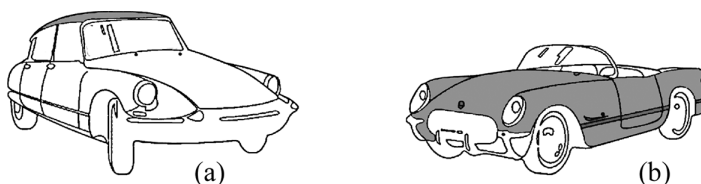


FIGURE 8.7 Composite parts in precursors. (a) 1955, Citroën DS 19 (FR), roof in glass/polyester, 70,000

- Cost
- Suitable to recycling

With this in mind, the following can be listed:

- **Benefits** of polymer solutions
 - Weight saving: up to 60% compared to a metal solution (100 kg of polymer instead of 250 kg of metal).
 - Cost reduction by reducing the number of different parts needed and by integration of several functions.
 - **Example:** Crimped stud by comparison to the welded stud. The cost is reduced up to 80%.
 - Easier to obtain complex shapes and surfaces.
- **Drawbacks** of polymer solutions
 - Mechanical strength generally lower.
 - Difficulties in dealing with the mass production speeds (1,000 vehicles per day).
 - For external body parts, painting is performed at high temperature, as well as surface pretreatment (cataphoresis, 185°C).
 - Potential obligation to protect employees against chemical risks or odorous substance emissions.

The composite parts consist in general the following:

- **For reinforcements:** glass, carbon, and natural fibers (flax, hemp, sisal, etc.) in various forms (continuous fibers, long fibers, short fibers, nonwoven fabric preformed or not)
- **For matrices**
 - Thermoplastic resins: thermoplastic polyester, thermoplastic polyurethane, polyamide, ABS, polyethylene, polypropylene, PVC, and biodegradable (see Section 3.8)
 - Thermosetting resins: epoxy, phenoplast, polyesters, polyurethane, phenolic, and biodegradable (see Sections 1.4 and 3.8)

The graph in Figure 8.8 shows the mass distribution of composites in a passenger car.

Figure 8.9 shows the diversity of car components made of polymer materials, reinforced or not.

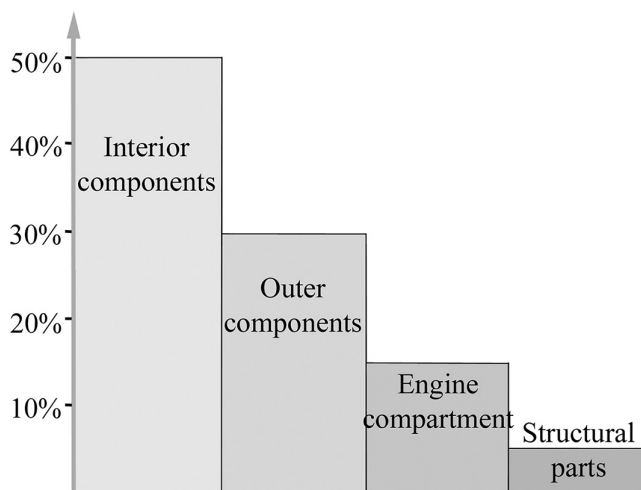


FIGURE 8.8 Distribution of mass of composites in a car.

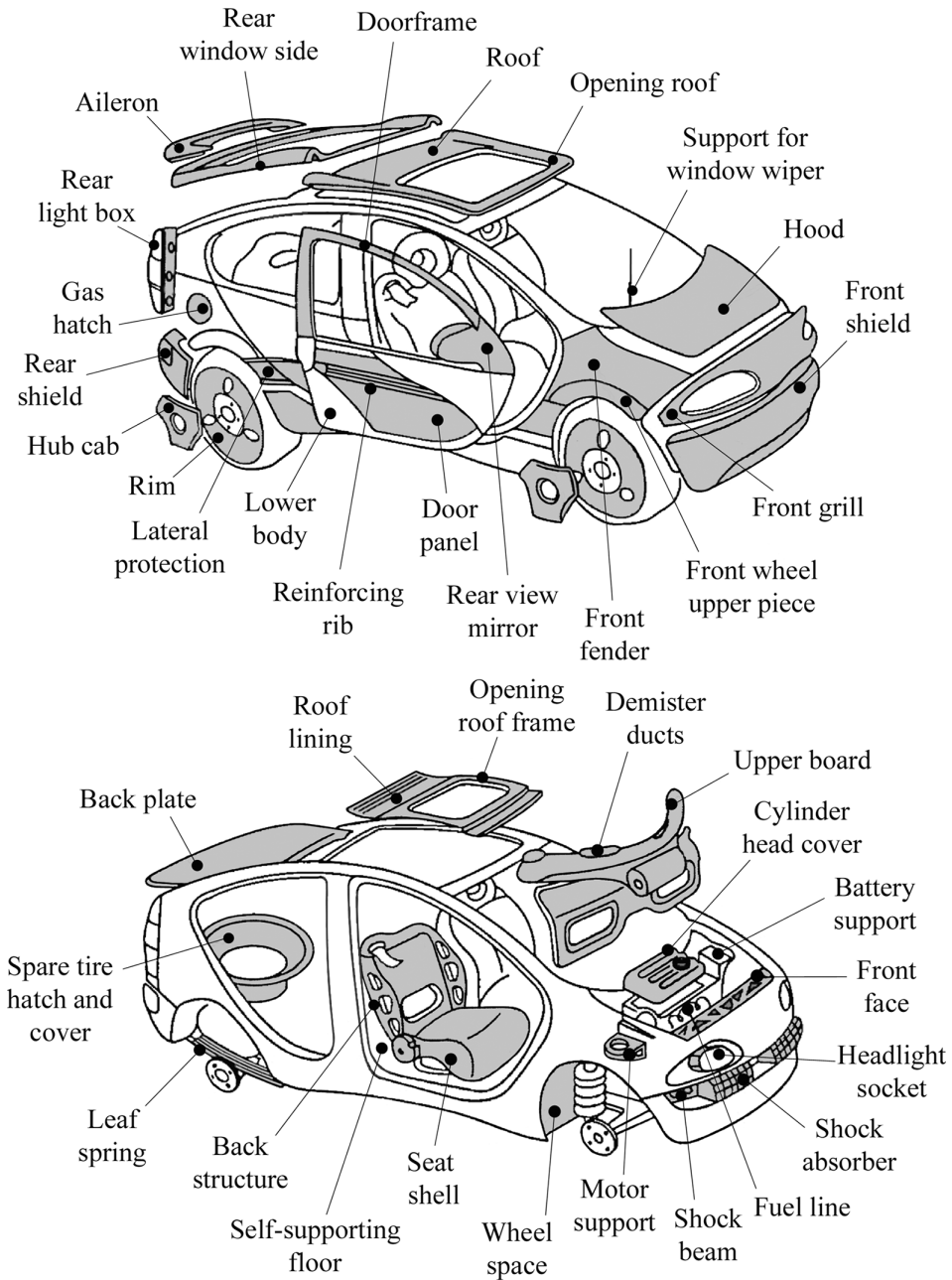


FIGURE 8.9 Composite parts in an automobile.

8.2.2.3 Notable Composite Components

- **Glass/polymer**
 - Short fiber
 - Airbag housing
 - Door module
 - Air inlet manifolds, support for pedals
 - Car body parts
 - Dashboard structure
 - Seat structure
 - Door handle
 - Long fiber
 - Faceplate technical module made of composite metal: a composite part supporting dozens of components and equipment. It is obtained by compression SMC glass (30%–40%)/polypropylene (see Section 2.3.1).
 - Wind deflector
 - Energy-absorbing bumper
 - Wheel arch
 - Cowl grille
 - Panel under tank
 - Battery cover
- **Carbon/polymer**

Apart from the case of competition cars and experimental vehicles (see further example), the introduction of such composite elements is done in progressive stages for reasons of high cost and low production rates, but this introduction is real.

 - **Example:** bumper of the vehicle **M6 BMW** (DE): mass saving of 47% compared to steel solution
- **Kevlar®/polymer**
 - **Example:** tire **SP 8000 Dunlop tires** (GB)

As part of an evolution toward a tire said to be **green**, narrower with a larger diameter, and a higher air pressure, Kevlar replaces several components made of steel or nylon. The sidewall thickness is reduced by 10%. The mass gain is 30%.

8.2.2.4 Notes

- **In the engine compartment**, polymers and glass/polymer can replace certain metal parts:
 - Mechanical parts: housings, gears, bearing cages, lateral wedges of gearboxes, oil pump, and cylinder head cover made of glass/nylon
 - Components resulting from integration of functions, reducing the number of parts: air intake compact module, including air filter, ducts and admission distributor, intake throttle valve, air mass sensor, and injection ramp
 - Supply water pipe, shutter system, small supports, and engine dress-up
- **Suspension**
 - **Spring:** one of the main features of unidirectionals, specifically the unidirectional glass/resin, lies in their ability to accumulate elastic energy. For example, in Figure 3.7, the force-deformation curves of metal and unidirectional materials can be compared. Thus, a glass/resin spring is theoretically capable of storing five to seven times more elastic energy than a steel spring with the same mass. This explains the interest to realize composite springs, particularly in the form of suspension elements.

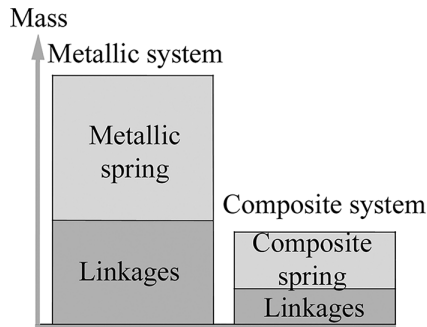


FIGURE 8.10 Comparison between metallic and composite springs.

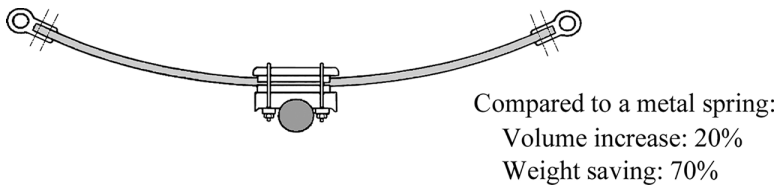


FIGURE 8.11 Single-leaf composite spring.

- *Other advantages of composite springs*
 - Glass/resin composite springs are almost unbreakable because of their large elastic behavior range. A local damage causes a minor behavior change.
 - It is possible to integrate several functions for a particular system, leading, inter alia, to a decrease in the number of parts and to optimal space occupancy and better road handling.
 - Important weight saving (see Figure 8.10).

Drawbacks of composite springs

It is the main difficulty to adapt the product to the requirements of the production: It is not sufficient to only demonstrate the technical feasibility; it is necessary to optimize the triplet **product–process–production** rate (up to several thousand components per day for the mass production).

The positioning on the market concerns leaf springs and torsion bars. The developments involve elastic parts with complex shape.

- **Example: single-leaf spring** (Figure 8.11). A multileaf metal spring is replaced by a single-leaf composite spring made of glass/epoxy ($V_f = 50\%$).

8.2.2.5 Use of Natural Fibers

In the United States, the **Ford Motor Company** had built as early as 1938 an experimental car with a body of 14 composite panels from hemp/phenolic, 3-mm thick. In addition to a reduced mass ($\approx 30\%$), this car showed a remarkable crashworthiness for that time. Nonetheless, the project was abandoned (*O tempora, o mores!*). Starting 2015, all new cars sold in Europe must be 95% recyclable¹. The recyclability requirements constrain, in vehicle construction, the long-term development of conventional composites.

So today, a motor vehicle contains several kilograms of unseen composite parts made from natural fibers (hemp, flax, sisal, jute, kenaf, and abaca) (20%–30%) lighter than glass/polymer composite. This reduces the vehicle weight and the CO₂ emissions and improves crashworthiness.

These natural fibers are associated:

- **With thermoplastic matrices**

- From nonwoven felts (500–2,000 g/m²) obtained by mixing natural and thermoplastic fibers (usually polypropylene). The mixture is carded and then needled. These felts are heated to 200°C and then disposed in a cold mold. Thus, rigid, lightweight, and relatively resistant parts for the automotive and heavy goods vehicles are obtained.
- From compound.

- **With thermosetting matrices**

The reinforcement (e.g., a hemp mat) is used to create composite components for the vehicle body by the SRIM process (molding with reactive resin injection; see Section 2.3).

Note: It is also noteworthy that a composite made of hemp and natural resin is starting to be used in the following parts:

- Rear window frames
- Under-the-hood parts
- Dashboards
- Door trim panels
- Side trim panels
- Armrests
- Inside roof panels
- Plates and lateral rear trunk protection
- Rear cover of spare wheel
- Seat backs
- Rear shelves
- Truck's floors

Other relevant small and medium injected parts

- Propeller fan for cooling
- Inserts
- Air intake systems
- Container valves
- Brake blocks strengthened by addition of fibers
- Parts of clutch
- Parts for rearview mirror
- Airbag casings (if an accident occurs, the rupture of the hemp/resin composite does not make dangerous shards)

8.2.3 RESEARCH AND DEVELOPMENT

The introduction of composites will continue to grow in order to reduce the vehicle mass with the underlying goal of an average weight of 850 kg. Accordingly, in addition to the increased integration of functions like in the cases of bumper, bumper beam, front-end technical module with reduced cost and its accessories (fan unit, radiators, and headlights), and cones of energy absorption connected to the chassis side members, their extension now concerns the following parts.

8.2.3.1 Structure

- Chassis
- Floor
- Bumper

Examples	Mass	Weight Saving Compared to the Metal Solution			Cost
		Metal and Composite	Glass	Carbon	
Prototype of chassis for a four-seat vehicle in sandwich material with composite skins and polypropylene honeycomb core	160 kg			47%	
Rear hatch compression-molded SMC			15%	25%	
Prepreg carbon/thermoplastic for semistructural parts of rear floors		15%			1
			38%		1.2
				47%	2.2

8.2.3.2 Mechanical Parts

- **Suspension wishbones:** parts injected RTM with accelerated cycle (<10 min) characterized by fibers of varying lengths ($V_f \approx 50\%$) and aluminum inserts
- **Brakes:** carbon/carbon (C/C) or C/Sic (see Section 3.7) for sports cars: long life (up to 300,000 km) because of low abrasion, constant friction coefficient even in humid or corrosive environment. The mass is 60% of that of a cast iron disk.
- Composite transmission shaft for 4WD vehicle
- Rack-and-pinion steering gear housing made of glass/polyamide or carbon/epoxy
- **Engine compartment:** bearing cage, seals, bushing, shaft sleeve and ring, and gears in carbon/PEEK (melting temperature higher than 340°C)

Note: Attention is drawn to composite parts in light alloy matrix with the following reinforcements ($V_f = 15\% - 20\%$):

- Short fibers (alumina) of length less than 150 μm , improving the temperature withstand: local stiffening of conrods and pistons and valve spacing on valve block
- Particles (alumina, silicon carbide) improving the temperature-withstanding property and resistance to wear: cylinder head, brake disk, transmission shaft

8.2.4 MOTOR RACING

The following example gives an overview of the use of high-performance composites in a competition car.

- **Example: Formula 1** competition car **R31 Renault** (FR) (Figure 8.12)
 - Overall mass comprising the driver, the cameras, and the ballast: 620 kg.
 - Artificial weight obtained through the airfoils: 1,250 daN at 260 km/h.
 - Composite construction of carbon/epoxy mounted on a tube chassis that must not exceed a mass of 35 kg.

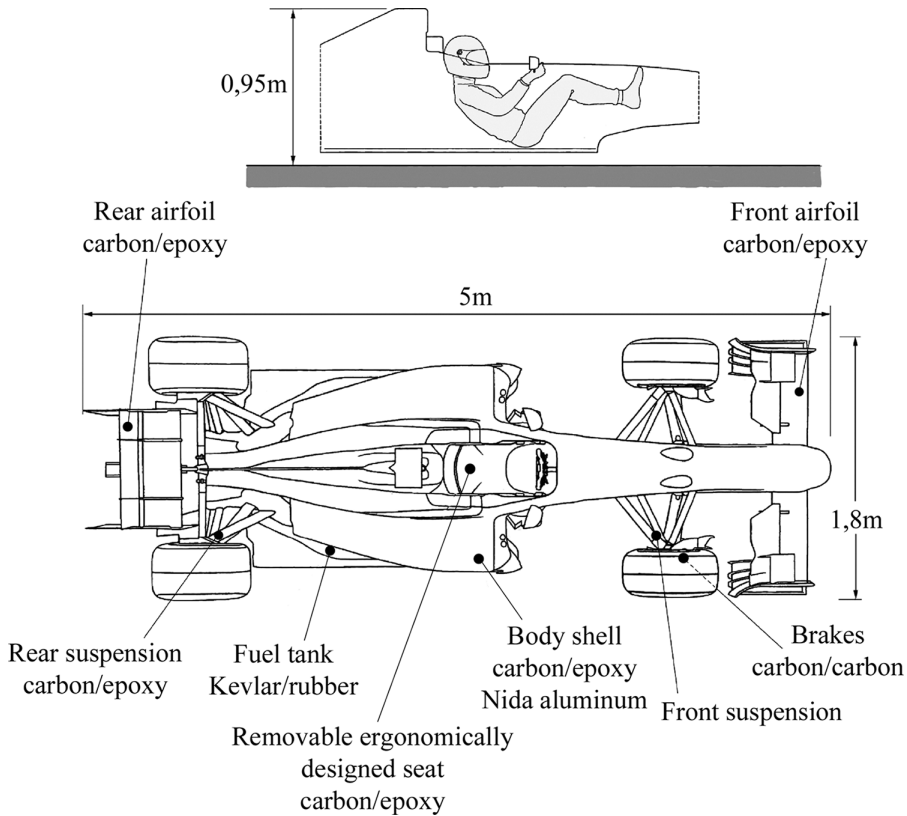


FIGURE 8.12 Formula 1 competition car R31 Renault (FR).

- Carbon/carbon brakes: a heavy braking from 340km/h to 100km/h in 2.8s corresponds to a load factor of $(-2.5) \times g$. The disk temperature can reach up to 1,200°C. For every fraction of a second of delayed braking, this load factor increases, with a competitive strategic advantage for the race: a **Grand Prix** race matches more than 600 braking actions, 200 of which can be considered to be heavy.
- CMC coatings for exhaust pipes and clutch disks of formula 1 (see Section 3.7).

8.3 WIND TURBINES

The electrical energy production from wind turbines is growing very rapidly, and such growth should undoubtedly continue in the medium term as shown in Figure 8.13 for the global wind power cumulative capacity.

8.3.1 COMPONENTS

The structural components of an industrial wind turbine typically consist of three blades, a rotor hub, a nacelle containing the equipment, and a vertical tower. These devices produce currently power ratings ranging from 850 kW to 3 MW, corresponding to a maximum height of rotor axes greater than 120 m with rotor diameters that can exceed 100 m. The current trend is as follows:

- Diameters from 130m to 150m
- Height from 150m to 180m and power ratings up to 4 MW.

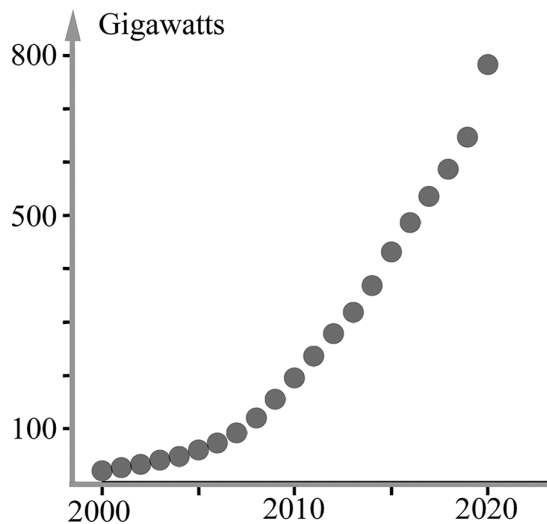


FIGURE 8.13 Evolution of Installed Rated Wind Power (world total cumulative capacity).

Note: The actual average power of a wind turbine is between a quarter and a fifth of its power rating²: thus, a wind turbine with a power rating of 2 MW should deliver an actual average power of 400–500 kW because its operation is discontinuous.

- **The tower:** it is made of metal with tapered shape (base diameter 7 m for a 110 m height tower). It positions the rotor at heights where the wind is stronger and allows a maximum blade length.
- **The rotor:** it consists of three composite blades with lengths between 25 and 60m and more, bolted on a rotor hub enabling the blade adjustments. These blades rotate at a rate of 10–20 rpm. This rotation speed remains low even in strong wind, and, thus, the centrifugal field does not stiffen the blade as for a helicopter blade (see Application 19.3). Consequently, the blades are bending under the wind action. In addition, because the mast is tapered, the blade that moves downward gets close to the tower wall, and the contact of this blade under bending with the tower must be prevented. Thus, the rotor needs to have its axis tilted slightly upward (a few degrees), helping to move the blade away from the lower tower section.
- **The nacelle:** this swivel component is located at the top of the tower. It automatically adjusts itself to keep the rotor facing the dominating wind in order to allow maximum efficiency. It houses the main mechanical and electrical components of the wind turbine: high-speed and low-speed shaft, speed multiplier (when the drive is not direct), brake, and electric generator. The coupling between the multiplier gear and the generator includes a flexible intermediate glass/epoxy ring. The nacelle also contains the device for the pitch control and the system that positions the rotor facing the wind. The nacelle fairing is usually glass/polyester made with acoustic-absorbing coating.
- **The blades:** the smaller blades can be manufactured with cheap materials such as glass/polyester, laminated wood, or aluminum. The longest blades currently weigh 18 tons and more each. They are made of glass/epoxy and (or) carbon/epoxy. With carbon, the weight saving is considerable: 32m blade weighs 6 tons in glass/polyester and 3 tons in carbon/epoxy. The blade design is based on aeronautic applications: a spar resists in bending, and a closed box (blade skin) is torsion resistant. The blade generally consists of three parts, spar, upper skin, and lower skin (see Figure 8.14).

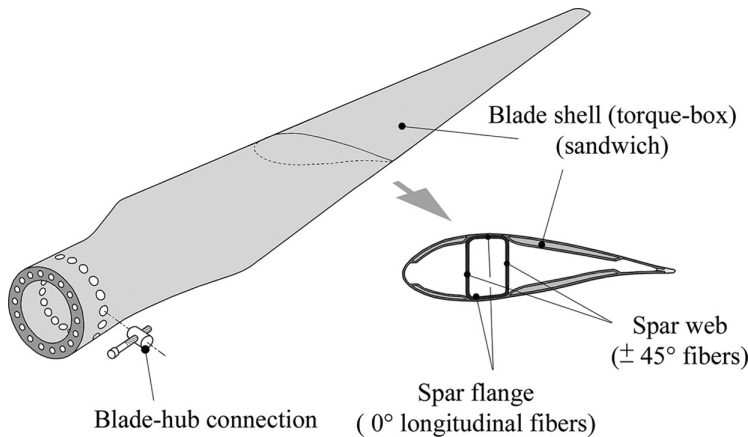


FIGURE 8.14 Wind turbine blade.

8.3.2 MANUFACTURING PROCESSES

The most widely used manufacturing processes for the manufacture of wind turbine composite blades are the filament winding, prepreg molding, resin infusion molding, and RTM:

- **Filament winding** lends itself well to the torsion box constitution but does not allow placing the fibers along longitudinal axis. Moreover, only convex shapes are feasible, eliminating profiles with accentuated concave curvature of the lower surface.
- **Prepreg molding** is used for the following:
 - For the upper and the lower surfaces of large blades: partially, a sandwich structure with core in closed cell foam of styrene acrylonitrile. The use of special prepreg plies on the skin surface avoids using the gel coat.
 - For the spars made of glass-carbon/epoxy: I-shaped (web + flange) or in the form of a closed rectangular box.
- **Resin infusion molding** is a process well suited to obtain an upper and a lower shell due to their geometric shape that excludes any area that is locally complex (see Section 2.1.4).
- **RTM** in a closed mold with internal compaction to obtain a complete blade.

For the blade attachment on the rotor hub, spar fibers are rolled up around steel sockets and adhesively bound. A compound of glass/resin and resin/foam fills in the gaps between the fibers coming from the spar³. For the connection between the blade (steel sockets) and the hub (bolted crown), see Figure 8.14.

- **Example: Wind turbine SWT-2.3–113 Siemens (DE)**
 - Power rating: 2.3 MW
 - Electric generator in direct drive (halving of the number of parts of the rotating assembly, elimination of specific operating problems of a speed multiplier)
 - Three glass/epoxy blades with a seamless one-piece design
 - Length: 55 m
 - Root chord: 4.2 m
 - Tip chord: 0.63 m
 - Area swept by the rotor: 1 ha
 - Rotation speed between 6 and 13 rpm
 - Masses
 - Rotor: 66.7 tons
 - Nacelle: 73 tons
 - Tower (minimum height 100 m): >200 tons

8.4 COMPOSITES AND SHIPBUILDING

We know about the great consumption of composite glass/polyester and polymer foams in the manufacture of pleasure boats of all types as well as of medium-sized vessels. This fabrication method started as early as the 1950s and is now classical. Also classical are the associated problems, comprising the phenomenon of osmosis damage on hulls and problems of dismantling due to the accumulated amounts of ships⁴. In relation to the last point, ongoing R&D efforts to introduce natural fibers should be mentioned, for example, (FR):

- Small sailboat (6.5 m) with 50% of the structure in linen/epoxy (hull, deck, helm, and foot bar)
- Sea kayak made of fully biodegradable composites (reinforcement and matrix)

8.4.1 COMPETITION

It continues to be characterized by the use of composites with carbon reinforcement.

8.4.1.1 Example: Ocean-Going Maxi-Trimaran

This example concerns the Ocean-Going Maxi-Trimaran Banque Populaire XI designed by **CDK Technologies/VPLP Design** (FR) (see Figure 8.15). The structure, appendages, and spars (masts) of this large trimaran are made of carbon/epoxy.

Weight (fully fitted): 16 tons; Draft < 5 m

Max speed: 50 knots or 92 km/h

Average speed: 35 knots or 65 km/h

Note: no motorboat can follow such a sailboat during a round-the-world trip.

- **Advantages of the trimaran formula**

For a platform of this size, the triple hull configuration is lighter than double hulls. It offers, in addition, other benefits:

- A precisely localized control zone: the crew is almost never exposed in the safety nets known to be dangerous.
- The opportunity to optimize the weight balancing, the cockpit area, the maneuvering zones, and the integration of adjustment devices.
- Four submerged appendages make the boat fly up to 1.5m above the water: the central hull rudder, the leeward foil, the leeward float rudder, and the central hull rudder. On the leeward float, the curved foil (see Figure 8.15) goes down in water to relieve this float (thanks to its curvature) for the purpose to limit the drag, thus acting on the speed and on the vessel's trim.

- **Structure**

The structure of the X-shaped platform is made of sandwich carbon honeycomb Nomex®, or sandwich carbon-PVC foam, according to the areas. For each of the parts of the boat, a model is prepared, then two female molds, and finally the piece (two half shells). Curing at 120°C under vacuum is performed in an oven up to 45 m in length × 10 m wide × 8 m high. The shells are then assembled. The skins are preimpregnated fabrics in carbon/epoxy, compacted, and cured under vacuum.

Sandwich areas with foam core:

- Under the fairings of the linking arms
- On the shell plating of each float, between the two linking arms (parts in one piece of 18-m long and 1 m wide, requiring only one vacuum placing instead of several in the case of the honeycomb); finishing with epoxy undercoating and paint.

The spars and particularly the main mast are obtained from carbon/epoxy prepregs molded and cured in a tubular autoclave with prior incorporation of the rails.

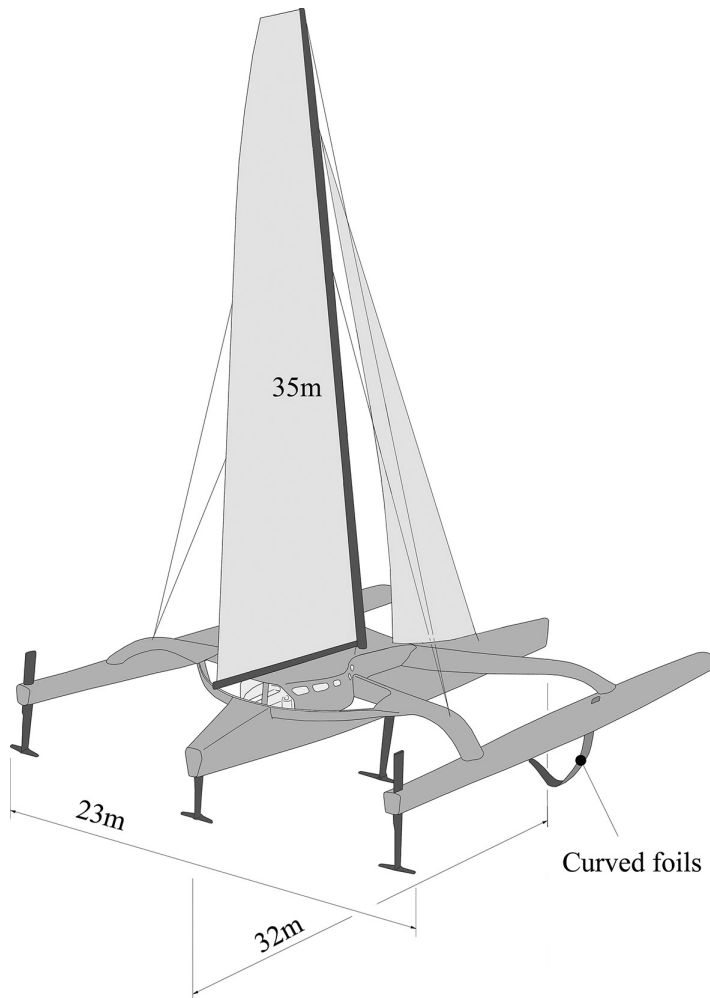


FIGURE 8.15 Maxi-trimaran Banque Populaire XI.

- **Sails**

Sails **North Sails** (US). Five sails: mainsail, large gennaker, small gennaker, genoas, and jib. Sail surface upwind: 610 m^2 . Sail area downwind: 890 m^2 .

They are made of ultrathin unidirectional filament tapes, thin layers of unidirectional prepregs ($\approx 25\text{ }\mu\text{m}$ thickness) of polyethylene, carbon, or aramid, preimpregnated with a thermosetting adhesive, arranged in a multidirectional orientation (automated tape placement) and molded on a mold made of a one-piece membrane (3DL technology for “three-dimensional laminated”). The resulting sails allow flexion without loss of strength.

8.4.1.2 Example: Monohull IMOCA 60

(IMOCA for “International Monohull Open Class Association”)

Hull: 18.3 m (60 feet); width: 5.85 m; weight: 9 tons; speed: up to 70 km/h (38 knots); and 55 km/h (30 knots) continuously.

Entirely made in monolithic and sandwich carbon

As shown in Figure 8.16, the current versions (2022) make it possible to lift 100% of the boat’s weight (9 tons), which can, therefore, “fly” above the water surface from 22 to 28 km/h (12–15 knots). Gain of up to 18 km/h (10 knots).

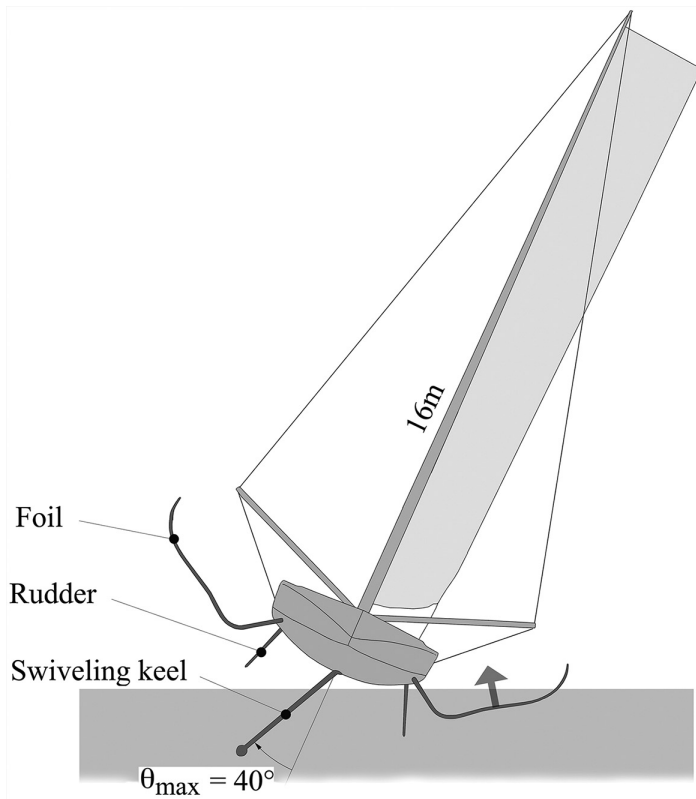


FIGURE 8.16 Monohull IMOCA 60.

- **Foils:** Long and thin carbon fiber blades: 5–6 m. They are made up of three parts:
 - The shaft: the longest part, most often straight,
 - The supporting plane: the curved part,
 - The tip: the straight and more or less vertical part, which serves as an anti-drift plane.
 Foil thrust: 3 tons. The deflection under load can reach 1 m
 The foils are effective at certain speeds from reaching to downwind.
 The leeward foil and the keel tilted to the wind allow the boat to “lift off”, that is to say to lift the hull at downwind speeds in order to reduce the drag and the wet surface and, therefore, increase the speed.
- **Keel:** Bulb weight: 3 tons. The keel is pendular, actuated by a hydraulic cylinder. Lateral angle $-40^\circ \leq \theta \leq +40^\circ$.
 The inclined keel blade generates lift. The keel also makes it possible to straighten up after a capsize.
 It is associated with ballasts.
- **Ballasts:** 10 in total. Side: 1,000 kg, rear: 350 kg in order to maintain the balance of the boat when it passes through the waves (average list: 15°).
- **Mast and outriggers:** carbon tubes. The wing mast supported by giant outriggers pivots on its axis to promote laminar airflow.
- **Rudder blades:** one on starboard and one on port. Straight or curved, they slow down the lateral drift of the boat upwind. They are pivoting or sliding in the “drift well”.
- **Sails:** Sloop rig type.

Sail upwind: 350 m^2

Asymmetric spinnaker: 400 m^2

Righting moment: $25.5 \text{ tons} \times \text{m}$ for 25° of list.

Note: very hard physically for the skippers: loud noises and violent shocks due to the waves and the brutal “take-off-ditching” transitions.

8.4.1.3 Example: Single Scull

See Figure 8.17.

8.4.1.4 Example: Surfboard

See Figure 8.18.

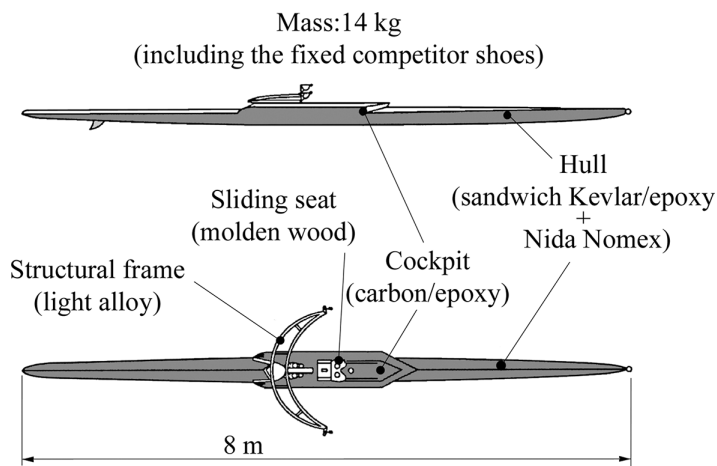


FIGURE 8.17 Single scull.

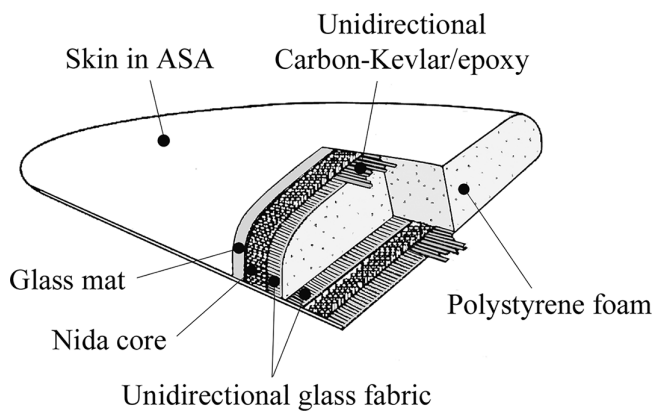


FIGURE 8.18 Surfboard.

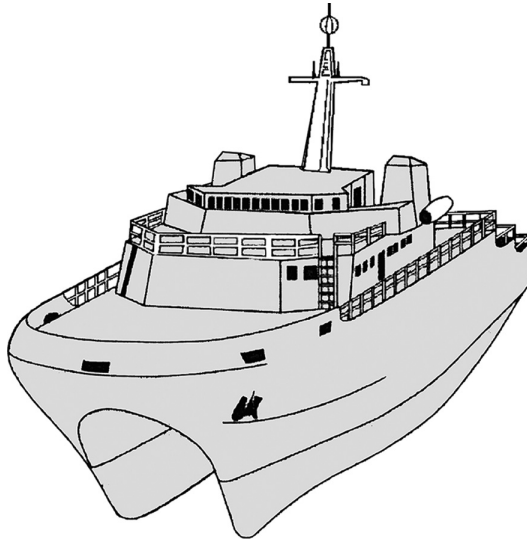


FIGURE 8.19 Oceanic minesweeper.

8.4.2 VESSELS

In the defense area, some glass/resin composite boats are built with lengths exceeding 50 m, as well as some superstructures of larger vessels. One example is an element of frigate of mass 80 tons on length 125 m, which lightens the ship with respect to the metallic solution.

- **Example: Oceanic Minesweeper (FR)** (see Figure 8.19)
Catamaran hull: length 52 m; width 15 m; molded in eight parts, implementing 300 tons of composite glass/polyester of monolithic structure or sandwich structure with balsa core for walls and bridges.

8.5 SPORTS AND LEISURE

8.5.1 SKIS

8.5.1.1 Equipment of a Skier

The significant use of polymers reinforced or not must be noted in the equipment of a skier today:

- **Clothing:** polyesters and polyamides.
- Helmets, sunglasses: polyurethane, polymethylmethacrylate, polycarbonate, and poly-ABS.
- **Shoes:** polyurethane, polyamide, and polypropylene.
- **Ski:** Different types of skis are adjusted to numerous practices (Alpine skiing, Nordic skiing, etc.), as well as to levels of skiers. The current ski shows another typical example of the advances enabled by the development of the means of simulation for the definition of a complex product and of its associated manufacturing tools. It should be noted, in particular, the treatment of the change in the shapes of downhill skis (the parabolic ski), which reduced the skier turning radius by half.

8.5.1.2 Main Components of a Ski

The requirements for a ski are as follows:

- Need to be lightweight
- Admit large elastic displacements in bending without breaking, for example, for a ski in three-point bending, of thickness 15–20 mm in central part and 7–8 mm at the ends: deflection of 100 mm under an ultimate central force of 500 daN
- Be torsionally rigid
- Ensure vibration dampening
- **Structure**

This part determines the elastic behavior and resistance of the ski. It is assembled around a central core. The transverse sections are shown in Figure 8.20.

- **Core:** It occupies the heart of the ski structure. When participating in the flexural stiffness (this is the case for 50% of the skis), it is a glue-laminated structure with several tens of vertical slats of lightweight wood: ash, poplar, and okoume. The composition can vary from the center to the ends. In addition, wood has damping properties and is insensitive to temperature changes. Also, the polyurethane foam (molded cores) is used, which is resistant to moisture, or the Nomex honeycomb.
- **Facings:** they are of
 - Metal: Zircal A97075 (7075), titanium
 - Composite:
 - Carbon/epoxy: oriented $\pm 45^\circ$ for the torsion box
 - Unidirectional in the upper part, as a result of a good compressive strength.
 - Kevlar/epoxy: in the lower part (good tensile strength, elongation at break important, damping) (Figure 8.21)

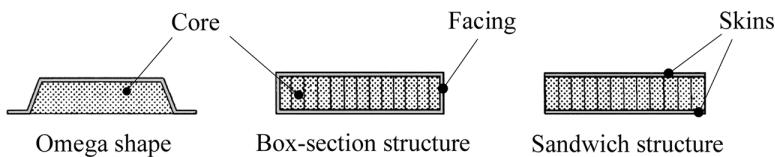


FIGURE 8.20 Transverse section of a ski.

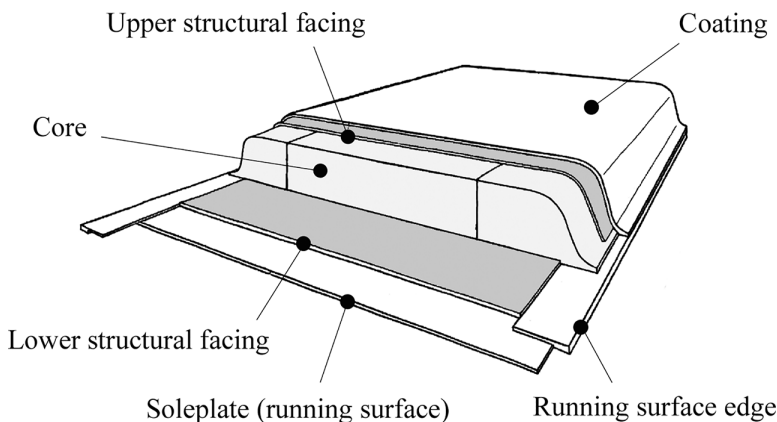


FIGURE 8.21 Ski structure.

- **Edges**

Placed laterally, they protect the core.

- **Running surface edges**

Dimensions: approximately 7×2 mm, punched out and reshaped sheet metal (curved to the shape of the ski), made from quenched and tempered spring steel of high strength and high wear resistance (e.g., steel X39 CrMo17-1).

- **Soleplate**

A (good) skier moves at speeds of 20–40 m/s. The sole has to function as follows:

- Create the thin film of air-water mixture formed in contact with the melt snow and evacuate it. To do this, it has special grooves that structure its surface.
- Resist abrasion.

It is usually made of polyethylene (hydrophobic), possibly filled with carbon particles.

Note: Dampening is increased through composite viscoelastic metal/polymer plates placed at the upper external part and inside of the ski under the core.

8.5.2 BICYCLES

As for a skier, the equipment of the cyclist is largely based on polymers.

8.5.2.1 Machine

Since the first **Tour de France** in 1903, the winner's speed has increased in a century from 20 to 42 km/h. At the same time, the mass of the machine decreased from 20 to 7.7 kg.

Today, this mass is limited to a statutory minimum of 6.8 kg actually reached in the races through the use of carbon/epoxy. The minimum masses reached for frames (less than 0.85 kg) and wheels (0.55 kg) associated with Kevlar saddles enable to make lighter machines. In 2011, the collaboration of 21 companies allowed to get an experimental machine of 2.85 kg whose nearly all of the parts were in carbon/epoxy.

Note: The contribution of natural fibers should be also pointed out, with an association flax carbon for the bicycle frame resulting in increased vibration damping.

8.5.2.2 Other Specific Equipment

- **Cycle helmet**

It is very light (average weight of 250 g), with an outer shell in polyethylene, polycarbonate, or carbon/epoxy (which, more resistant, allows greater ventilation) and an inner shell polystyrene.

- **Cycling shorts**

- Polyethylene, polypropylene, and polyurethane (Lycra®) for the stretch textiles allowing muscle compression and vibration reduction.
- Polytetrafluoroethylene for breathable fabrics: the Gore-Tex® fabric has more than 10 million pores per mm². These pores are 20,000 times smaller than a drop of water, making the fabric waterproof, but they are much larger than clusters of molecules resulting from perspiration, which can pass through.
- In fabrics with thermoregulation: with microcapsules of paraffin wax (melting temperature of between 22°C and 37°C) incorporated in the polymer fibers. The excessive body heat is absorbed by fusion of the paraffin. When the temperature decreases, the paraffin solidifies, giving off heat.

8.5.3 TENNIS RACKETS

The racket frames are frequently in carbon/epoxy. The interposition of linen fibers sandwiched between two layers of carbon, that is, 75% carbon+25% linen/epoxy, confers improved damping properties to these frames.

8.6 DIVERSE APPLICATIONS

8.6.1 PRESSURE GAS BOTTLE

These composite cylinders in wrapped fiber are made of glass/epoxy or Kevlar/epoxy (see Figure 8.22) reinforcing a thin load-sharing liner of light alloy that provides sealing:

- The service pressure can reach 350 bars (rupture at more than 1,000 bar).
- The **gas volume/bottle weight** ratio is multiplied by 4 compared with the steel solution.
- **Applications**
 - Breathing apparatus (scuba) much more lighter
 - Gaseous fuel tank
 - Gas supply for rockets and missiles

8.6.2 BOGIE FRAME

The mass of bogies represents near 40% of the total wagon mass. Inside the bogie, the classic steel frame has a mass of 1–2 tons. Thus, lightening the bogie weight is essential for lightweight vehicle design.

One can see in Figure 8.23 the schematic of the **efWING** bogie, **Kawasaki KHI** (JP), with spring function integration inside the frame structure. It is lighter (40% weight gain) with fewer parts compared to metal solution and highly fatigue resistant, as already reported⁵.

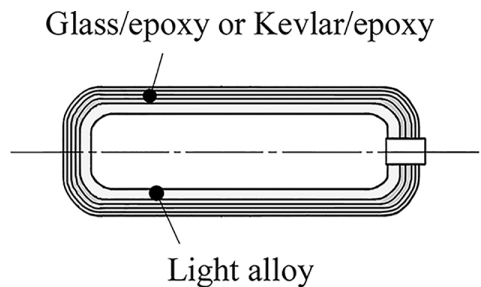


FIGURE 8.22 Pressure gas bottle.

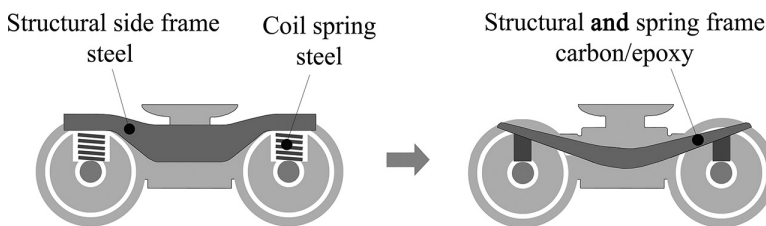


FIGURE 8.23 Bogie with composite frame.

8.6.3 TUBES FOR OFFSHORE INSTALLATIONS

In deep water, the weight of the tubing – the risers – grows proportionally to the depth and can reach high values (e.g., one-third of the traction strength for a depth of 1,000 m). Therefore, it is of interest to use **carbon–glass/resin** tubes, which are three to four times lighter than steel tubes:

- **Example:** tubing for **tension leg platform**. The platform is pulled by cables toward the bottom of the sea (see Figure 8.24). Many connecting tubings from the seafloor to the platform undergo static and dynamic stresses (undercurrents) of
 - Traction
 - Bending
 - Extension and circumferential compression due to external and internal pressures

The safety factor compared to the complete failure is 2–3.

The resin is microcracked, requiring internal and external elastomeric sealing sheaths.

8.6.4 BIOMECHANICAL APPLICATIONS

The carbon/carbon composite (see Section 2.2) has the rare property of not causing fibrous growths when exposed to the bloodstream, what is called a **thromboresistant property**. In addition, the following qualities also promote its implantation in the human body:

- Resistance and chemical inertia
- Mechanical strength and fatigue resistance
- Adjustable flexibility characteristics on the basis of the composite nature of the material
- Low density
- Transparency to rays
- Possible sterilization at high temperatures

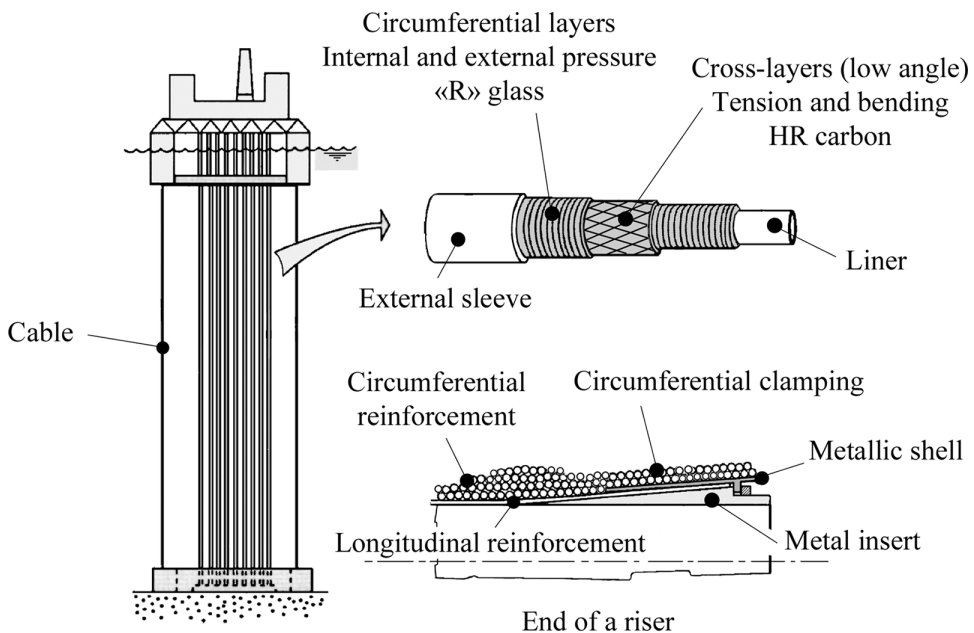


FIGURE 8.24 Riser tube.

The main applications include as follows:

- Artificial hip and knee joints
- Osteosynthesis plating system
- Dental implants
- Implanted devices

8.6.5 CABLE CAR

A composite substitution solution to traditional constructive solutions of metallic cable car allows, at equal weight, a significant increase in payload:

- **Example:** cable car of **Argentières, Ingenix Company (FR)**
- The purpose was to increase capacity while maintaining the existing facilities, that is, the cables, towers, and motorization:
 - Previous **metallic cable car**: 50-passenger cabin
 - New **composite cable car, carbon–Kevlar/epoxy** (see Figure 8.25):
 - Payload: 60 passengers plus the fully equipped cabin with a total mass that remains unchanged.
 - The weight of the hanger and cab assembly has been greatly reduced from 2 tons to 1.2 tons, increasing the capacity from 50 to 60 people. A ballast system could be installed under the cabin in windy conditions, and in such a case the capacity was limited to 50 people as on the old cabin.
 - Comparative costs:
 - In the case of a renewal of the entire facility: 1

Actual renewal of two cable cars: 0.1 (cost divided by 10)

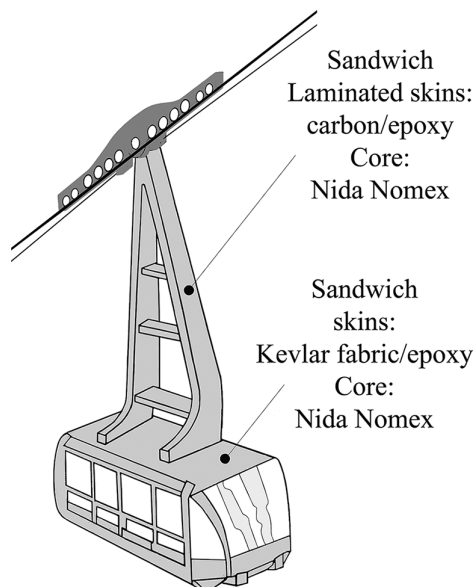


FIGURE 8.25 Cable car.

NOTES

- 1 European Directive 2000/53/EC.
- 2 Based on the energy actually returned over a year.
- 3 Analogy with helicopter blade; see Application 19.3.
- 4 See Section 2.5.
- 5 See Section 5.4.5.3.

Part II

Mechanical Behavior of Laminated Materials

In Section I, we pointed out the anisotropic properties of a composite material from a qualitative point of view¹, and we showed the features of the elastic coefficients for an anisotropic laminate.

We have also mentioned the relations that allow predicting the mechanical behavior of a fiber/matrix combination starting from the properties of the individual constituents². In Chapter 5³, we have also given elements necessary for the sizing of laminates made of carbon/epoxy, Kevlar®/epoxy, and glass/epoxy, in terms of strength and deformation.

Section II is dedicated to the justification of these properties and of mentioned results. It requires a detailed study of the behavior of anisotropic composite layer and of the stacking that makes up the laminate. It is useful to note that the essential bases of mechanics of continuous media, namely, the states of stress and strain at a point, which is explained in detail in many textbooks on elasticity or strength of materials, are supposed to be already known.

NOTES

1 See Section 3.1.

2 See Section 3.3.1.

3 See Sections 5.2 and 5.3.



Taylor & Francis

Taylor & Francis Group

<http://taylorandfrancis.com>

9 Anisotropic Elastic Medium

9.1 SOME REMINDERS

9.1.1 CONTINUUM MECHANICS

We take for granted the following concepts and notations of classical mechanics of continuous media:

- **State of stress at a point:** This is defined by a second-order **tensor** with the symbol Σ . The 3×3 matrix associated with this tensor is symmetric and has, therefore, six distinct terms, which are denoted as σ_{ij} :

$$\sigma_{11}; \sigma_{22}; \sigma_{33}; \sigma_{23}; \sigma_{13}; \sigma_{12}$$

- **State of strain at a point:** This is defined as a second-order tensor with the symbol \mathcal{E} . The 3×3 matrix for this tensor is symmetric due to the form of the small deformations. It consists of six distinct terms denoted as ϵ_{ij} :

$$\epsilon_{11}; \epsilon_{22}; \epsilon_{33}; \epsilon_{23}; \epsilon_{13}; \epsilon_{12}$$

- **Linear elastic material:** The strains are linear and homogeneous functions of the stresses. The corresponding relations are

$$\epsilon_{ij} = \varphi_{ijkl} \times \sigma_{kl}^1$$

- **Homogeneous material:** In this case, the matrix terms φ_{ijkl} characterizing the elastic behavior of the medium are not point functions. They are the same at any point in the considered medium.

9.1.2 NUMBER OF DISTINCT φ_{ijkl} TERMS

The above stress–strain relation can be written in matrix form as

$$\begin{Bmatrix} \epsilon_{11} \\ \epsilon_{22} \\ \epsilon_{33} \\ \epsilon_{23} \\ \epsilon_{13} \\ \epsilon_{12} \\ \epsilon_{32} \\ \epsilon_{31} \\ \epsilon_{21} \end{Bmatrix} = \begin{bmatrix} & & & & & & & & \\ & & & & & & & & \\ & & & & & & & & \\ & & & & & & & & \\ & & & & & & & & \\ & & & & & & & & \\ & & & & & & & & \\ & & & & & & & & \\ & & & & & & & & \end{bmatrix} \begin{Bmatrix} \sigma_{11} \\ \sigma_{22} \\ \sigma_{33} \\ \sigma_{23} \\ \sigma_{13} \\ \sigma_{12} \\ \sigma_{32} \\ \sigma_{31} \\ \sigma_{21} \end{Bmatrix}$$

6×6 6×3
 φ_{ijkl}
 3×6 3×3

- Due to the symmetry of the stresses ($\sigma_{kl} = \sigma_{lk}$), the corresponding coefficients are the same, that is, $\varphi_{ijkl} = \varphi_{ijlk}$.
- Due to the symmetry of the strains ($\varepsilon_{ij} = \varepsilon_{ji}$), the corresponding coefficients are the same, that is, $\varphi_{ijkl} = \varphi_{jikl}$.
- In other words, the knowledge of only the coefficients of the 6×6 matrix above is required.
- In addition, the application of the theorem of virtual work for particular states of stress shows that coefficients φ_{ijkl} are symmetric, meaning

$$\varphi_{ijkl} = \varphi_{klij}^2$$

Therefore, the 6×6 matrix mentioned previously is symmetric. The number of distinct coefficients is

$$\frac{6 \times (6+1)}{2} = 21 \text{ coefficients}$$

- In summary,

Stress reciprocity : $\varphi_{ijk\ell} = \varphi_{ij\ell k}$

Strain definition : $\varphi_{ijk\ell} = \varphi_{jik\ell}$

Symmetry : $\varphi_{ijk\ell} = \varphi_{klij}$

(9.1)

There remain 21 distinct coefficients $\varphi_{ijk\ell}$

The previous stress–strain relation can then be written as

$$\left\{ \begin{array}{c} \varepsilon_{11} \\ \varepsilon_{22} \\ \varepsilon_{33} \\ \varepsilon_{23} \\ \varepsilon_{13} \\ \varepsilon_{12} \end{array} \right\} = \left[\begin{array}{cccccc} \varphi_{1111} & \varphi_{1122} & \varphi_{1133} & 2\varphi_{1123} & 2\varphi_{1113} & 2\varphi_{1112} \\ \varphi_{2211} & \varphi_{2222} & \varphi_{2233} & 2\varphi_{2223} & 2\varphi_{2213} & 2\varphi_{2212} \\ \varphi_{3311} & \varphi_{3322} & \varphi_{3333} & 2\varphi_{3323} & 2\varphi_{3313} & 2\varphi_{3312} \\ \varphi_{2311} & \varphi_{2322} & \varphi_{2333} & 2\varphi_{2323} & 2\varphi_{2313} & 2\varphi_{2312} \\ \varphi_{1311} & \varphi_{1322} & \varphi_{1333} & 2\varphi_{1323} & 2\varphi_{1313} & 2\varphi_{1312} \\ \varphi_{1211} & \varphi_{1222} & \varphi_{1233} & 2\varphi_{1223} & 2\varphi_{1213} & 2\varphi_{1212} \end{array} \right] \left\{ \begin{array}{c} \sigma_{11} \\ \sigma_{22} \\ \sigma_{33} \\ \sigma_{23} \\ \sigma_{13} \\ \sigma_{12} \end{array} \right\} \quad (9.2)$$

This matrix **no longer has the general symmetry** as in the general form (9×9) presented previously (note the coefficients 2 in this matrix). We can get around this inconvenience by doubling the terms ε_{23} , ε_{13} , ε_{12} , that is to say by highlighting the *angular distortion* components:

$$\gamma_{23} = 2\varepsilon_{23}; \quad \gamma_{13} = 2\varepsilon_{13}; \quad \gamma_{12} = 2\varepsilon_{12}$$

From which the stress–strain behavior can then be written in a symmetric form as

$$\left\{ \begin{array}{c} \varepsilon_{11} \\ \varepsilon_{22} \\ \varepsilon_{33} \\ 2\varepsilon_{23} \\ 2\varepsilon_{13} \\ 2\varepsilon_{12} \end{array} \right\} \begin{array}{c} \\ \\ \gamma_{23} \\ \gamma_{13} \\ \gamma_{12} \end{array} = \left[\begin{array}{cccccc} \varphi_{1111} & \varphi_{1122} & \varphi_{1133} & 2\varphi_{1123} & 2\varphi_{1113} & 2\varphi_{1112} \\ \varphi_{2211} & \varphi_{2222} & \varphi_{2233} & 2\varphi_{2223} & 2\varphi_{2213} & 2\varphi_{2212} \\ \varphi_{3311} & \varphi_{3322} & \varphi_{3333} & 2\varphi_{3323} & 2\varphi_{3313} & 2\varphi_{3312} \\ 2\varphi_{2311} & 2\varphi_{2322} & 2\varphi_{2333} & 4\varphi_{2323} & 4\varphi_{2313} & 4\varphi_{2312} \\ 2\varphi_{1311} & 2\varphi_{1322} & 2\varphi_{1333} & 4\varphi_{1323} & 4\varphi_{1313} & 4\varphi_{1312} \\ 2\varphi_{1211} & 2\varphi_{1222} & 2\varphi_{1233} & 4\varphi_{1223} & 4\varphi_{1213} & 4\varphi_{1212} \end{array} \right] \left\{ \begin{array}{c} \sigma_{11} \\ \sigma_{22} \\ \sigma_{33} \\ \sigma_{23} \\ \sigma_{13} \\ \sigma_{12} \end{array} \right\} \quad (9.3)$$

9.2 ORTHOTROPIC MATERIAL

- **Definition:** We define an orthotropic elastic material as a homogeneous linear elastic material having at every point *two* planes of symmetry in terms of mechanical properties, these two planes being perpendicular to each other.

Then we can show that³ the number of independent elastic constants is **nine**. The constitutive relation is expressed in the so-called **orthotropic** axis (axis of the trihedron built on the two orthogonal planes and their intersection line). This relation can be written in the following form, also known as **engineering notation**, because it shows the elastic moduli and Poisson ratios:

$$\left\{ \begin{matrix} \epsilon_{11} \\ \epsilon_{22} \\ \epsilon_{33} \\ \gamma_{23} \\ \gamma_{13} \\ \gamma_{12} \end{matrix} \right\} = \begin{bmatrix} \frac{1}{E_1} & -\frac{\nu_{21}}{E_2} & -\frac{\nu_{31}}{E_3} & 0 & 0 & 0 \\ -\frac{\nu_{12}}{E_1} & \frac{1}{E_2} & -\frac{\nu_{32}}{E_3} & 0 & 0 & 0 \\ -\frac{\nu_{13}}{E_1} & -\frac{\nu_{23}}{E_2} & \frac{1}{E_3} & 0 & 0 & 0 \\ 0 & 0 & 0 & \frac{1}{G_{23}} & 0 & 0 \\ 0 & 0 & 0 & 0 & \frac{1}{G_{13}} & 0 \\ 0 & 0 & 0 & 0 & 0 & \frac{1}{G_{12}} \end{bmatrix} \left\{ \begin{matrix} \sigma_{11} \\ \sigma_{22} \\ \sigma_{33} \\ \sigma_{23} \\ \sigma_{13} \\ \sigma_{12} \end{matrix} \right\} \quad (9.4)$$

where

E_1, E_2, E_3 are the longitudinal elastic moduli

G_{23}, G_{13}, G_{12} are the shear moduli

$\nu_{12}, \nu_{13}, \nu_{23}, \nu_{21}, \nu_{31}, \nu_{32}$ are the Poisson ratios

In addition, the symmetry of the stress–strain matrix above leads to the following relationships:

$$\frac{\nu_{21}}{E_2} = \frac{\nu_{12}}{E_1}, \quad \frac{\nu_{31}}{E_3} = \frac{\nu_{13}}{E_1}, \quad \frac{\nu_{32}}{E_3} = \frac{\nu_{23}}{E_2} \quad (9.5)$$

9.3 TRANSVERSELY ISOTROPIC MATERIAL

- **Definition:** A transversely isotropic material is a homogeneous linear elastic material such that any plane passing through a privileged axis is a plane of mechanical symmetry.

It is then shown that⁴ the constitutive relation holds five independent elastic constants. For the fiber/matrix composite shown in Figure 9.1, the preferred axis is ℓ . The fibers are arranged regularly in the ℓ direction. All directions perpendicular to the fibers characterize the transverse direction t .

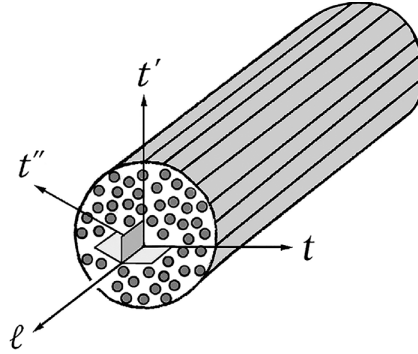


FIGURE 9.1 Example of a transversely isotropic material: unidirectional composite.

The engineering stress–strain relation has the form

$$\left\{ \begin{array}{c} \varepsilon_{\ell\ell} \\ \varepsilon_{tt} \\ \varepsilon_{t't'} \\ \gamma_{tt'} \\ \gamma_{t\ell} \\ \gamma_{t\ell} \end{array} \right\} = \left\{ \begin{array}{cccccc} \frac{1}{E_\ell} & -\frac{\nu_{t\ell}}{E_t} & -\frac{\nu_{t\ell}}{E_t} & 0 & 0 & 0 \\ -\frac{\nu_{t\ell}}{E_\ell} & \frac{1}{E_t} & -\frac{\nu_t}{E_t} & 0 & 0 & 0 \\ -\frac{\nu_{t\ell}}{E_\ell} & -\frac{\nu_t}{E_t} & \frac{1}{E_t} & 0 & 0 & 0 \\ 0 & 0 & 0 & \frac{2(1+\nu_t)}{E_t} & 0 & 0 \\ 0 & 0 & 0 & 0 & \frac{1}{G_{t\ell}} & 0 \\ 0 & 0 & 0 & 0 & 0 & \frac{1}{G_{t\ell}} \end{array} \right\} \left\{ \begin{array}{c} \sigma_{\ell\ell} \\ \sigma_{tt} \\ \sigma_{t't'} \\ \tau_{tt'} \\ \tau_{t\ell} \\ \tau_{t\ell} \end{array} \right\} \quad (9.6)$$

- **Comments**

- The independent elastic constants are
 - Young modulus along the ℓ direction: E_ℓ
 - Young modulus along any transverse direction t : E_t
 - Shear modulus in any plane such (ℓ, t) : $G_{t\ell}$
 - Poisson coefficients: $\nu_{t\ell}$ and ν_t
- The symmetry of coefficients in the constitutive relationship leads to

$$\frac{\nu_{t\ell}}{E_\ell} = \frac{\nu_t}{E_t}$$

- Note that the shear modulus in the plane (t, t') can be written as

$$\frac{E_t}{2(1+\nu_t)}$$

This is a classical expression that adequately reflects a transverse isotropic nature.

NOTES

1 For example,

$$\epsilon_{11} = \varphi_{1111}\sigma_{11} + \varphi_{1112}\sigma_{12} + \varphi_{1113}\sigma_{13} + \varphi_{1121}\sigma_{21} + \varphi_{1122}\sigma_{22} + \varphi_{1123}\sigma_{23} + \varphi_{1131}\sigma_{31} + \varphi_{1132}\sigma_{32} + \varphi_{1133}\sigma_{33}.$$

2 Consider two simple stress states:

- State no. 1: One single stress, $(\sigma_{k\ell})_1$, which causes the strain

$$(\epsilon_{ij})_1 = \varphi_{ijk\ell} (\sigma_{k\ell})_1$$

- **State no. 2:** One single stress, $(\sigma_{pq})_2$, which causes the strain

$$(\epsilon_{mn})_2 = \varphi_{mnpq} (\sigma_{pq})_2$$

The work of the stress in state no.1 on the strain in state no.2 is equal to the work of the stress in state no.2 on the strain in state no.1, as

$$(\sigma_{k\ell})_1 \times (\epsilon_{k\ell})_2 = (\sigma_{pq})_2 \times (\epsilon_{pq})_1$$

which means $(\sigma_{k\ell})_1 \times \varphi_{k\ell pq} \times (\sigma_{pq})_2 = (\sigma_{pq})_2 \times \varphi_{pqk\ell} \times (\sigma_{k\ell})_1$ from which $\varphi_{k\ell pq} = \varphi_{pqk\ell}$

3 Proof is detailed in Section 13.1.

4 Proof is detailed in Section 13.2.



Taylor & Francis

Taylor & Francis Group

<http://taylorandfrancis.com>

10 Elastic Constants of Unidirectional Composites

In this chapter, we examine a combination of two distinct materials (matrix and parallel fibers), with simple geometry and loading conditions. This in order to estimate the elastic and hygrothermal properties of the equivalent material, i.e. of the unidirectional composite layer.

10.1 LONGITUDINAL MODULUS E_ℓ

The two materials are shown schematically in Figure 10.1 where

- m stands for matrix
- f stands for fiber

Hypothesis: The two materials are in principle bonded together. More precisely, we make the following assumptions:

- Both matrix m and fiber f have the same longitudinal strain value noted ϵ_ℓ .
- There is a freedom along z on the interface between the two materials, allowing distinct values of normal strain in each of the two materials:

$$\epsilon_{z_m} \neq \epsilon_{z_f}$$

The state of stress resulting from an applied force F can, therefore, be written as

$$\Sigma_m \Rightarrow \begin{bmatrix} \sigma_\ell & 0 & 0 \\ 0 & 0 & 0 \\ 0 & 0 & 0 \end{bmatrix}_m ; \quad \Sigma_f \Rightarrow \begin{bmatrix} \sigma_\ell & 0 & 0 \\ 0 & 0 & 0 \\ 0 & 0 & 0 \end{bmatrix}_f$$

And the corresponding state of strain as

$$\mathcal{E}_m \Rightarrow \begin{bmatrix} \epsilon_\ell & 0 & 0 \\ 0 & \epsilon_t & 0 \\ 0 & 0 & \epsilon_z \end{bmatrix}_m ; \quad \mathcal{E}_f \Rightarrow \begin{bmatrix} \epsilon_\ell & 0 & 0 \\ 0 & \epsilon_t & 0 \\ 0 & 0 & \epsilon_z \end{bmatrix}_f$$

Each material being assumed linearly elastic and isotropic, its behavior law (so-called Hooke's law), is written in the form

$$\mathcal{E} = \frac{(1+\nu)}{E} \Sigma - \frac{\nu}{E} \times \text{trace}(\Sigma) \mathbf{I} \quad (10.1)$$

In which, \mathcal{E} represents the strain tensor, Σ the stress tensor, and \mathbf{I} the unitary tensor. E and ν are the elastic constants of the considered material.

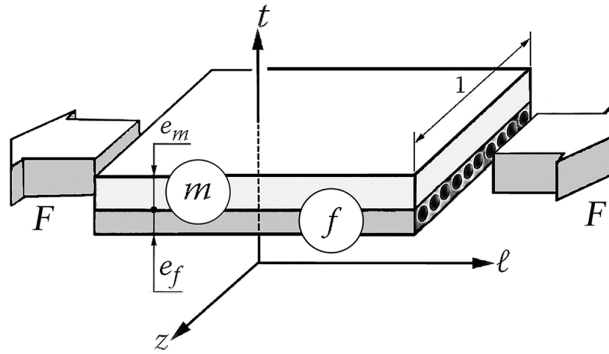


FIGURE 10.1 Longitudinal modulus E_ℓ .

For the composite $(m+f)$, Equation 9.5 is used with restriction to the plane (ℓ, t) . It reduces to

$$\begin{Bmatrix} \epsilon_\ell \\ \epsilon_t \\ \gamma_{\ell t} \end{Bmatrix} = \begin{bmatrix} \frac{1}{E_\ell} & -\frac{\nu_{\ell t}}{E_t} & 0 \\ -\frac{\nu_{t\ell}}{E_\ell} & \frac{1}{E_t} & 0 \\ 0 & 0 & \frac{1}{G_{\ell t}} \end{bmatrix} \begin{Bmatrix} \sigma_\ell \\ \sigma_t \\ \tau_{\ell t} \end{Bmatrix}$$

The stress $\sigma_{\ell(m+f)}$ can be written as (see Figure 10.1)

$$\sigma_{\ell(m+f)} = \frac{F}{S} = \frac{F}{(e_m + e_f) \times 1} = \sigma_{\ell_m} \times \frac{e_m}{e_m + e_f} + \sigma_{\ell_f} \times \frac{e_f}{e_m + e_f}$$

which can be rewritten in terms of volume fraction of the fiber and the matrix as¹

$$\sigma_{\ell(m+f)} = \sigma_{\ell_m} V_m + \sigma_{\ell_f} V_f$$

Taking into account the corresponding behavior law, we can express stress in terms of strain for each material:

$$E_\ell \epsilon_\ell = E_m \epsilon_\ell V_m + E_f \epsilon_\ell V_f$$

Then,

$$E_\ell = E_m V_m + E_f V_f \quad (10.2)$$

Note: Among the real phenomena that are not taken into account in the estimation of E_ℓ , the absence of perfect straightness of fiber in the matrix should be noted. Thus, the module E_ℓ depends on the sign of the solicitation (traction or compression). The material is strictly **bimodulus**.

- **Example:** Unidirectional layers with 60% fiber volume fraction ($V_f = 0.60$) with epoxy matrix:

	Kevlar®	HR Carbon	HM Carbon
E_ℓ tension (MPa)	85,000	134,000	180,000
E_ℓ compression (MPa)	80,300	134,000	160,000

10.2 POISSON COEFFICIENT

Considering again the loading defined in the previous paragraph, the transverse strain for the matrix m and fiber f can be written as

$$\epsilon_t = -\frac{\nu}{E} \sigma_\ell = -\nu \epsilon_\ell$$

And for the composite $(m+f)$ as

$$\epsilon_{t(m+f)} = -\frac{\nu_{t\ell}}{E_\ell} \times \sigma_{\ell(m+f)} = -\nu_{t\ell} \epsilon_\ell$$

On the other hand, the transverse length variations are written as

$$\begin{aligned} \epsilon_{t(m+f)} &= \frac{\Delta(e_m + e_f)}{e_m + e_f} = \frac{\Delta e_m}{e_m} V_m + \frac{\Delta e_f}{e_f} V_f \\ \epsilon_{t(m+f)} &= \epsilon_{tm} V_m + \epsilon_{tf} V_f \end{aligned}$$

Thus, taking into account a common value of ϵ_ℓ in the fiber and the matrix,

$$\begin{aligned} -\nu_{t\ell} \epsilon_\ell &= -\nu_m \epsilon_\ell V_m - \nu_f \epsilon_\ell V_f \\ \nu_{t\ell} &= \nu_m V_m + \nu_f V_f \end{aligned} \quad (10.3)$$

10.3 TRANSVERSE MODULUS E_t

To evaluate the modulus along the transverse direction, that is, E_t , the two materials are symbolized in the same way as previously. The loading is shown in Figure 10.2. In addition, we use the following simplifications:

- **Assumption:** At the interface between the two materials, we assume the following:
 - Freedom of movement in the ℓ direction allowing distinct values for strain in the two materials:

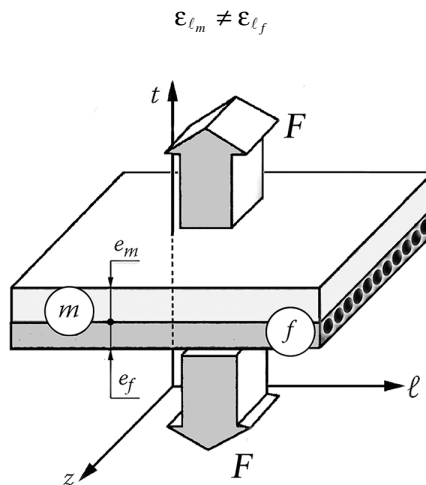


FIGURE 10.2 Transverse modulus E_t .

- Freedom of movement in the z direction allowing distinct values for strain in the two materials:

$$\epsilon_{z_m} \neq \epsilon_{z_f}$$

Then, the state of stress created by a load F (see Figure 10.2) can be reduced for each material to the following:

$$\Sigma \Rightarrow \begin{bmatrix} 0 & 0 & 0 \\ 0 & \sigma_t & 0 \\ 0 & 0 & 0 \end{bmatrix}$$

The strain components can be written as

$$\mathcal{E} \Rightarrow \begin{bmatrix} \epsilon_\ell & 0 & 0 \\ 0 & \epsilon_t & 0 \\ 0 & 0 & \epsilon_z \end{bmatrix}_{m \text{ or } f}$$

Then for the composite ($m+f$), we have

$$\epsilon_t = \frac{1}{E_t} \sigma_t$$

On the other hand, using direct calculation leads to (see Figure 10.2)

$$\epsilon_t = \frac{\Delta(e_m + e_f)}{e_m + e_f} = \epsilon_{t_m} V_m + \epsilon_{t_f} V_f$$

From where

$$\begin{aligned} \frac{1}{E_t} \sigma_t &= \frac{1}{E_m} \sigma_t V_m + \frac{1}{E_f} \sigma_t V_f \\ \frac{1}{E_t} &= \frac{V_m}{E_m} + \frac{V_f}{E_f} \quad \text{or} \quad E_t = E_m \left[\frac{1}{(1 - V_f) + \frac{E_m}{E_f} V_f} \right] \end{aligned} \quad (10.4)$$

- **Note:** Due to the above simplifications enabling a relative sliding along the ℓ and z directions at the interface, the transverse modulus E_t above is approached by default, the actual assembly being more rigid due to a strict interface bonding.
- Some more complex formulae giving E_t can be found in the technical literature. However, none can guarantee good results.
 - Taking into consideration the applied load (see Figure 10.2), the modulus E_f that appears in Equation 10.4 is the fiber modulus in a direction that is **perpendicular** to the fiber axis. This modulus can be very different from the modulus along the axis of the fiber, due to the anisotropy of the latter².

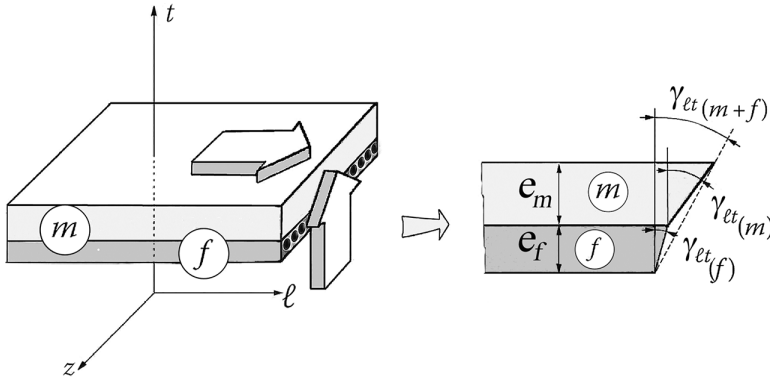


FIGURE 10.3 Shear modulus G_{lt} .

10.4 SHEAR MODULUS G_{lt}

Load application that can be used to evaluate the shear modulus G_{lt} is shown schematically in Figure 10.3, both with the angular deformations that are produced.

The state of stress, identical for both the matrix and the fiber materials, can be written as

$$\Sigma \Rightarrow \begin{bmatrix} 0 & \tau_{lt} & 0 \\ \tau_{lt} & 0 & 0 \\ 0 & 0 & 0 \end{bmatrix}$$

The corresponding strains can be written as

$$\mathcal{E}_m \text{ or } f \Rightarrow \begin{bmatrix} 0 & \epsilon_{lt} & 0 \\ \epsilon_{lt} & 0 & 0 \\ 0 & 0 & 0 \end{bmatrix}$$

Using the constitutive equation, one has

$$\epsilon_{lt} = \frac{(1+\nu)}{E} \tau_{lt} = \frac{\tau_{lt}}{2G}$$

Then with $\gamma_{lt} = 2\epsilon_{lt}$

$$\gamma_{lt} = \frac{\tau_{lt}}{G}$$

Also, from Figure 10.3, we have

$$\gamma_{lt(m+f)} (e_m + e_f) = \gamma_{lt_m} e_m + \gamma_{lt_f} e_f$$

which can be rewritten as

$$\gamma_{lt(m+f)} = \gamma_{lt_m} V_m + \gamma_{lt_f} V_f$$

$$\frac{\tau_{lt}}{G_{lt}} = \frac{\tau_{lt}}{G_m} V_m + \frac{\tau_{lt}}{G_f} V_f$$

$$\frac{1}{G_{lt}} = \frac{V_m}{G_m} + \frac{V_f}{G_f}$$

$$G_{lt} = G_m \left[\frac{1}{(1 - V_f) + \frac{G_m}{G_f} V_f} \right] \quad (10.5)^3$$

10.5 THERMOELASTIC PROPERTIES

10.5.1 ISOTROPIC MATERIAL: RECALL

When the influence of temperature variation is taken into consideration, the so-called **Hooke's** law

$$\boldsymbol{\varepsilon} = \frac{(1 + \nu)}{E} \boldsymbol{\Sigma} - \frac{\nu}{E} \times \text{trace}(\boldsymbol{\Sigma}) \mathbf{I}$$

is replaced by the **Hooke and Duhamel** law:

$$\boldsymbol{\varepsilon} = \frac{(1 + \nu)}{E} \boldsymbol{\Sigma} - \frac{\nu}{E} \times \text{trace}(\boldsymbol{\Sigma}) \mathbf{I} + (\alpha \times \Delta T) \mathbf{I} \quad (10.6)$$

where

$\boldsymbol{\varepsilon}$ is the strain tensor

$\boldsymbol{\Sigma}$ is the stress tensor

\mathbf{I} is the unitary tensor

E, ν are the elastic constants for the considered material

α is the coefficient of thermal expansion⁴

ΔT is the variation in temperature with respect to a reference temperature at which stress and strains are zero in the absence of any mechanical loading

10.5.2 CASE OF UNIDIRECTIONAL COMPOSITE

The coefficient of thermal expansion (CTE) of the matrix is usually much higher (more than ten times) than the one of the fiber⁵. In Figure 10.4, we can imagine that even in the absence of mechanical loading, a change in temperature ΔT will produce a longitudinal strain in the composite. The

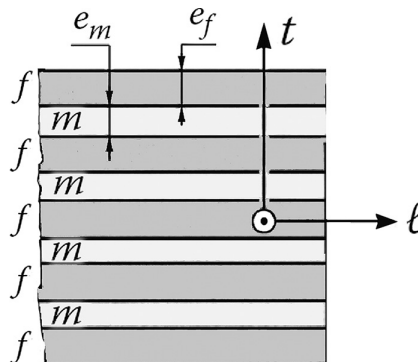


FIGURE 10.4 Unidirectional composite.

value of this longitudinal strain is intermediate between the strain of the fiber alone and that of the matrix alone. Therefore, in the composite **fiber/matrix**, internal stress arises along the direction ℓ , and it is externally balanced (along the direction t , fiber and matrix can expand differently). We then have

- For stress,

$$\Sigma_m \Rightarrow \begin{bmatrix} \sigma_\ell & 0 & 0 \\ 0 & 0 & 0 \\ 0 & 0 & 0 \end{bmatrix}_m ; \quad \Sigma_f \Rightarrow \begin{bmatrix} \sigma_\ell & 0 & 0 \\ 0 & 0 & 0 \\ 0 & 0 & 0 \end{bmatrix}_f$$

- For strain,

$$\mathcal{E}_m \Rightarrow \begin{bmatrix} \varepsilon_\ell & 0 & 0 \\ 0 & \varepsilon_t & 0 \\ 0 & 0 & \varepsilon_z \end{bmatrix}_m ; \quad \mathcal{E}_f \Rightarrow \begin{bmatrix} \varepsilon_\ell & 0 & 0 \\ 0 & \varepsilon_t & 0 \\ 0 & 0 & \varepsilon_z \end{bmatrix}_f$$

10.5.2.1 Coefficient of Thermal Expansion along the Direction ℓ

For the fiber and the matrix, respectively, we can write

$$\varepsilon_{\ell_m} = \frac{\sigma_{\ell_m}}{E_m} + \alpha_m \Delta T = \varepsilon_{\ell_f} = \frac{\sigma_{\ell_f}}{E_f} + \alpha_f \Delta T$$

The external equilibrium can be written as (see Figure 10.4)

$$\sigma_{\ell_m} \times e_m + \sigma_{\ell_f} \times e_f = 0$$

The matrix and the fiber being subject to same deformation,

$$\begin{aligned} \frac{\sigma_{\ell_m}}{E_m} + \alpha_m \Delta T &= -\sigma_{\ell_m} \times \frac{e_m}{e_f} \times \frac{1}{E_f} + \alpha_f \Delta T \\ \sigma_{\ell_m} &= \frac{(\alpha_f - \alpha_m) \Delta T}{\frac{1}{E_m} + \frac{e_m}{e_f} \times \frac{1}{E_f}} = \frac{(\alpha_f - \alpha_m) \Delta T}{\frac{1}{E_m} + \frac{V_m}{V_f} \times \frac{1}{E_f}} \end{aligned}$$

V_m and V_f represent the volume fractions. The longitudinal strain can then be written as

$$\varepsilon_{\ell_m} = \varepsilon_{\ell_f} = \frac{(\alpha_f E_f V_f + \alpha_m E_m V_m)}{E_f V_f + E_m V_m} \times \Delta T$$

Such strain corresponds also to the longitudinal strain that is created by the only effect of temperature:

$$\varepsilon_{\ell(m+f)} = \alpha_\ell \Delta T$$

where α_ℓ is the longitudinal CTE of the unidirectional. When identifying the two equalities above

$$\alpha_\ell = \frac{\alpha_f E_f V_f + \alpha_m E_m V_m}{E_f V_f + E_m V_m} \quad (10.7)$$

10.5.2.2 Coefficient of Thermal Expansion along the Transverse Direction t

The global thermal strain is readily written as (see Figure 10.4)

$$\varepsilon_{t(m+f)} = \frac{\Delta(e_m + e_f)}{e_m + e_f} = \varepsilon_{tm} \frac{e_m}{e_m + e_f} + \varepsilon_{tf} \frac{e_f}{e_m + e_f}$$

Then,

$$\varepsilon_{t(m+f)} = \varepsilon_{tm} \times V_m + \varepsilon_{tf} \times V_f$$

Using the Hooke and Duhamel law (Equation 10.6),⁶

$$\varepsilon_{t(m+f)} = \left(-\frac{\nu_m}{E_m} \sigma_{\ell m} + \alpha_m \Delta T \right) V_m + \left(-\frac{\nu_f}{E_f} \sigma_{\ell f} + \alpha_f \Delta T \right) V_f$$

With the stress values calculated above, we get

$$\varepsilon_{t(m+f)} = \left\{ \left(\alpha_m V_m + \alpha_f V_f \right) + \frac{(\nu_f E_m - \nu_m E_f)}{E_m V_m + E_f V_f} V_m V_f (\alpha_f - \alpha_m) \right\} \Delta T$$

The quantity between brackets represents the CTE of the unidirectional along the transverse direction t , namely, α_t , which can be written as

$$\alpha_t = \alpha_m V_m + \alpha_f V_f + \frac{(\nu_f E_m - \nu_m E_f)}{\frac{E_m}{V_f} + \frac{E_f}{V_m}} \times (\alpha_f - \alpha_m) \quad (10.8)$$

Notes:

- In practice, there is important difference of orders of magnitude between the coefficients of thermal expansion of fiber and matrix: $\alpha_m \gg \alpha_f$. For example, for carbon/epoxy (see Tables 1.3 and 1.4), we can simplify Equations 10.7 and 10.8 which reduce to:

$$\alpha_f \ll \alpha_m; \quad E_m \ll E_f \quad \Rightarrow \quad \alpha_\ell \approx \frac{\alpha_m E_m V_m}{E_m V_m + E_f V_f}; \quad \alpha_t \approx \alpha_m V_m (1 + \nu_m) \quad (10.9)$$

- After curing a thermosetting matrix, cooling to room temperature causes an overall ply-contraction involving the coefficients of thermal expansion defined above. In the absence of any external stress, this phenomenon generates internal stresses of so-called thermal origin.

10.5.3 THERMOMECHANICAL BEHAVIOR OF A UNIDIRECTIONAL LAYER

Accordingly, under the combined effects of stress and temperature, the global thermomechanical strain components of a unidirectional layer can be obtained using the following relation:

$$\begin{Bmatrix} \varepsilon_\ell \\ \varepsilon_t \\ \gamma_{t\ell} \end{Bmatrix} = \begin{bmatrix} \frac{1}{E_\ell} & -\frac{\nu_{t\ell}}{E_t} & 0 \\ -\frac{\nu_{\ell t}}{E_\ell} & \frac{1}{E_t} & 0 \\ 0 & 0 & \frac{1}{G_{t\ell}} \end{bmatrix} \begin{Bmatrix} \sigma_\ell \\ \sigma_t \\ \tau_{t\ell} \end{Bmatrix} + \Delta T \begin{Bmatrix} \alpha_\ell \\ \alpha_t \\ 0 \end{Bmatrix} \quad (10.10)$$

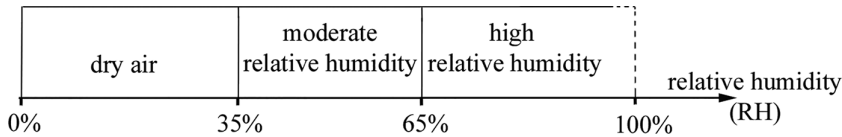
In which the values of the coefficients E_ℓ , E_t , $\nu_{t\ell}$, $G_{t\ell}$, α_ℓ , and α_t are given in Equations 10.2–10.9, respectively.

10.6 HYGROSCOPIC EFFECTS

10.6.1 MOISTURE INFLUENCE

10.6.1.1 Relative Humidity

Remember that ambient air always includes a particular moisture level. Relative humidity (RH) is the ratio of the partial pressure of the water vapor contained in the air to the saturated vapor pressure (or vapor pressure) under the same temperature and pressure conditions. The RH is expressed in %.



Polymer matrix composites exposed to ambient humidity absorb moisture, which mainly diffuses into the matrix. It is considered that the fibers are little affected by the phenomenon.

There is then an increase in volume and an increase in the mass of the resin. The phenomenon is reversible: when the laminate loses moisture, it contracts.

Notes:

- Expansion due to humidity should be compared to the phenomenon of expansion due to an increase in temperature. Thus, for thermosetting matrices, after curing in an oven with zero RH, there is shrinkage due to the decrease in temperature, and residual stresses occur (see Section 5.2.3.4 and Application 20.4). The ambient RH will then contribute over time to an expansion of the resin, which partially compensates residual curing stresses.
- In addition, in the usual areas of temperature and humidity, the phenomena of thermal or hygrometric expansion are quasi-linear and can be approached in a quasi-parallel manner. In fact, the increase in volume induced by moisture absorption varies proportionally to this absorption until a mass gain of around 2%.
- Some composite applications, particularly in aeronautics and marine industries, are subject to significant variations in temperature, pressure, and humidity.
 - Thus, cyclic variations, for example, in airplanes, lead to alterations in mechanical performance. For example, related to the change in humidity of the fiber-matrix interface.
 - In marine applications, variations in pressure and humidity induce stresses due to the expansion of the matrix. These are residual stresses similar to thermal stresses.

10.6.1.2 Moisture Concentration

This is the value that figures moisture amount absorbed per unit mass of the material, noted

$$\Delta M_c(\%) = \frac{\text{mass of moist material} - \text{mass of dry material}}{\text{mass of dry material}} \times 100$$

Thus, for a relative mass increase of $0.006 \rightarrow \Delta M_c = 0.6\%$

Example of extreme value:

	Temperature	Relative Humidity	ΔM_c
Epoxy	85°C	85%	1.5%

10.6.2 COEFFICIENT OF MOISTURE EXPANSION

Alongside with the coefficient of thermal expansion of a material, noted α and previously used, we define the coefficient of moisture expansion noted β defined as the quotient:

$$\beta_{([\%_{\text{H}_2\text{O}}]^{-1})} = \frac{\left(\frac{\Delta L}{L}\right)}{\Delta M_c}$$

where $\Delta L/L$ is the longitudinal strain measured by a dilatometer when varying by ΔM_c the moisture concentration.

We will bring this relation closer to the classic one of thermal expansion for the same material:

$$\alpha_{(^{\circ}\text{C}^{-1})} = \frac{\left(\frac{\Delta L}{L}\right)}{\Delta T}$$

Note: For unidirectional plies, as with coefficients α , one observes a large difference between orders of magnitude of β_f and β_m .

$$\beta_f \ll \beta_m$$

For example, for carbon fibers and epoxy matrix (see Tables 1.3 and 1.4)

	$\alpha_{(^{\circ}\text{C}^{-1})}$	$\beta_{([\%_{\text{H}_2\text{O}}]^{-1})}$
Carbon HR	$0.2E-6$	$< 1E-6$
Epoxy	$0.11E-3$	$3.2E-3$

10.6.3 HYGROTHERMAL BEHAVIOR OF A UNIDIRECTIONAL LAYER

10.6.3.1 Coefficients of Moisture Expansion along ℓ and t Directions

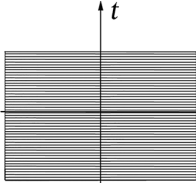
Taking into account the previous remarks, hygroelastic properties for a unidirectional ply can be studied by following the same steps as those we saw in Section 10.5 for the thermoelastic properties. By resuming calculations similar to those adopted in paragraph 10.5.2 for the thermal expansion coefficients, we obtain β_ℓ and β_t formally identical to 10.7 and 10.8 where α_m and α_f are, respectively, replaced by β_m and β_f .

Taking into account that $\beta_f \ll \beta_m$ one can retain in practice expressions similar to Equation 10.9, that is to say here:

$$\beta_f \ll \beta_m; \quad E_m \ll E_f \quad \Rightarrow \quad \beta_\ell \approx \frac{\beta_m E_m V_m}{E_m V_m + E_f V_f}; \quad \beta_t \approx \beta_m V_m (1 + \nu_m) \quad (10.11)$$

10.6.3.2 Constitutive Equation

Under the combined effects of stress, temperature, and moisture, the induced strains are as follows:

$$\begin{Bmatrix} \varepsilon_\ell \\ \varepsilon_t \\ \gamma_{\ell t} \end{Bmatrix} = \begin{bmatrix} \frac{1}{E_\ell} & -\frac{\nu_{\ell t}}{E_t} & 0 \\ -\frac{\nu_{t\ell}}{E_\ell} & \frac{1}{E_t} & 0 \\ 0 & 0 & \frac{1}{G_{\ell t}} \end{bmatrix} \begin{Bmatrix} \sigma_\ell \\ \sigma_t \\ \tau_{\ell t} \end{Bmatrix} + \Delta T \begin{Bmatrix} \alpha_\ell \\ \alpha_t \\ 0 \end{Bmatrix} + \Delta M_c \begin{Bmatrix} \beta_\ell \\ \beta_t \\ 0 \end{Bmatrix} \quad (10.12)$$


E_ℓ longitudinal modulus (see Equation 10.2)

E_t transverse modulus (see Equation 10.4)

$\nu_{\ell t}$ Poisson coefficient (see Equation 10.3)

$G_{\ell t}$ shear modulus (see Equation 10.5)

ΔT algebraic increase in temperature

ΔM_c algebraic increase in moisture concentration

α_ℓ coefficient of thermal expansion along the direction ℓ (see Equation 10.7 or 10.9)

α_t coefficient of thermal expansion along the transverse direction t (see Equation 10.8 or 10.9)

β_ℓ coefficient of moisture expansion along the direction ℓ (see Equation 10.11)

β_t coefficient of moisture expansion along the transverse direction t (see Equation 10.11)

NOTES

- 1 See Section 3.2.2.
- 2 This point is referred to in Section 3.3.1.
- 3 A few values of the shear modulus G_f are shown in Section 3.3.1.
- 4 See Section 1.6, Main Physical Properties.
- 5 *Ibid.*
- 6 For the Poisson coefficients of common fibers, see Section 3.3.1.



Taylor & Francis

Taylor & Francis Group

<http://taylorandfrancis.com>

11 Elastic Constants of a Ply in Any Direction

Studying the behavior of a laminate made up of many plies with different orientations requires knowledge of the behavior of each of these plies, along directions that are different from the principal material directions of the ply. We propose to determine the elastic constants corresponding to such a ply behavior using relatively simple calculations.

11.1 FLEXIBILITY COEFFICIENTS

The ply was already defined in Chapter 3¹. Let ℓ , t , and z be the orthotropic axes of a ply as shown in Figure 11.1².

For a thin laminate made up by a stacking of several plies, we assume that the stress value σ_{zz} is zero. It is then possible, for an orthotropic material, to write the stress–strain relation in plane (ℓ, t) starting from Equation 9.5 in the form

$$\begin{Bmatrix} \varepsilon_{\ell} \\ \varepsilon_t \\ \gamma_{\ell t} \end{Bmatrix} = \begin{bmatrix} \frac{1}{E_{\ell}} & -\frac{\nu_{t\ell}}{E_t} & 0 \\ -\frac{\nu_{\ell t}}{E_{\ell}} & \frac{1}{E_t} & 0 \\ 0 & 0 & \frac{1}{G_{\ell t}} \end{bmatrix} \begin{Bmatrix} \sigma_{\ell} \\ \sigma_t \\ \tau_{\ell t} \end{Bmatrix} \quad (11.1)$$

Problem: How this relationship transforms when it is expressed in axes (x, y) distinct from (ℓ, t) and forming any angle θ with the (ℓ, t) coordinates as in Figure 11.1?³

First, let us recall the following:

- **Recall 1:** The stress $\vec{\sigma}$ acting on a facet with normal vector \vec{n} is given by

$$\begin{array}{ccccc} & \uparrow & \{\sigma\} = [\sigma_{ij}]\{n\} & \nwarrow & \\ \text{Column matrix} & & \text{Stress matrix} & & \text{Column matrix} \\ \text{of components of stress } \vec{\sigma} & & & & \text{of directional cosines of } \vec{n} \end{array} \quad (11.2)$$

- **Recall 2:** The coordinates of a same vector \vec{V} in two distinct coordinate systems (x, y) and (ℓ, t) , such that $(\vec{x}, \vec{\ell}) = \theta$, are

$$\vec{V} = V_{\ell}\vec{\ell} + V_t\vec{t} = V_x\vec{x} + V_y\vec{y}$$

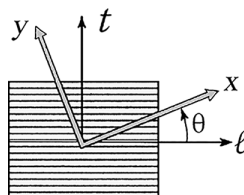


FIGURE 11.1 Orthotropic axes and arbitrary direction in the plane of a ply.

with the relation

$$\begin{Bmatrix} V_x \\ V_y \end{Bmatrix} = \begin{Bmatrix} c & s \\ -s & c \end{Bmatrix} \begin{Bmatrix} V_\ell \\ V_t \end{Bmatrix} \begin{pmatrix} c = \cos \theta \\ s = \sin \theta \end{pmatrix} \quad (11.3)$$

In axes (ℓ, t) , let us express, through the relationship in Equation 11.2, the stress acting on a facet of normal \vec{x} :

$$\{\sigma_{/x}\}_{\ell,t} = [\sigma_{ij}]_{\ell,t} \{x\}_{\ell,t} = [\sigma_{ij}]_{\ell,t} \begin{Bmatrix} c \\ s \end{Bmatrix}$$

where

$\{\sigma_{/x}\}$ is the stress vector
 $[\sigma_{ij}]$ is the stress matrix

And in axes (x, y) , following Equation 11.3,

$$\{\sigma_{/x}\}_{x,y} = \begin{Bmatrix} c & s \\ -s & c \end{Bmatrix} [\sigma_{ij}]_{\ell,t} \begin{Bmatrix} c \\ s \end{Bmatrix}$$

In a similar manner, the stress acting on a facet with the normal \vec{y} is written in the (x, y) axes as

$$\{\sigma_{/y}\}_{x,y} = \begin{Bmatrix} c & s \\ -s & c \end{Bmatrix} [\sigma_{ij}]_{\ell,t} \begin{Bmatrix} -s \\ c \end{Bmatrix}$$

Therefore, the stress matrix in (x, y) axes is

$$[\sigma_{ij}]_{x,y} = [\sigma_{/x}, \sigma_{/y}] = \begin{Bmatrix} c & s \\ -s & c \end{Bmatrix} [\sigma_{ij}]_{\ell,t} \begin{Bmatrix} c & -s \\ s & c \end{Bmatrix}$$

By setting

$$[P] = \begin{Bmatrix} c & s \\ -s & c \end{Bmatrix}$$

and observing that matrix $[P]$ is orthogonal, that is, ${}^t[P] = [P]^{-1}$, where ${}^t[P]$ is the transpose of matrix $[P]$, we have⁴

$$[\sigma_{ij}]_{\ell,t} = {}^t[P][\sigma_{ij}]_{x,y}[P]$$

in developing that expression,

$$\begin{bmatrix} \sigma_\ell & \tau_{\ell t} \\ \tau_{\ell t} & \sigma_t \end{bmatrix} = \begin{bmatrix} c & -s \\ s & c \end{bmatrix} \begin{bmatrix} \sigma_x & \tau_{xy} \\ \tau_{xy} & \sigma_y \end{bmatrix} \begin{bmatrix} c & s \\ -s & c \end{bmatrix}$$

which can be rearranged to give

$$\left\{ \begin{array}{c} \sigma_\ell \\ \sigma_t \\ \tau_{\ell t} \end{array} \right\} = \underbrace{\left[\begin{array}{ccc} c^2 & s^2 & -2cs \\ s^2 & c^2 & 2cs \\ sc & -sc & (c^2 - s^2) \end{array} \right]}_{[T]} \left\{ \begin{array}{c} \sigma_x \\ \sigma_y \\ \tau_{xy} \end{array} \right\} \quad (11.4)$$

Then

$$[\sigma]_{\ell,t} = [T][\sigma]_{x,y}$$

with

$$[T] = \left[\begin{array}{ccc} c^2 & s^2 & -2cs \\ s^2 & c^2 & 2cs \\ sc & -sc & (c^2 - s^2) \end{array} \right]$$

- **Note:** this $[T]$ transfer matrix is readily established when starting from the relationship that allows expressing the tensor components in a given base as functions of components of the same tensor in another base. For our case, this relation is (see Section 13.1)

$$\sigma_{IJ} = \cos_I^m \cos_J^n \sigma_{mn} \text{ with } \cos_I^m = \cos(\vec{m}, \vec{I})$$

With the consideration of strains allowing a similar calculation procedure, we can write parallel to this

$$\left\{ \begin{array}{c} \epsilon_x \\ \epsilon_y \\ \epsilon_{xy} \end{array} \right\} = \left[\begin{array}{ccc} c^2 & s^2 & 2cs \\ s^2 & c^2 & -2cs \\ -cs & cs & (c^2 - s^2) \end{array} \right] \left\{ \begin{array}{c} \epsilon_\ell \\ \epsilon_t \\ \epsilon_{\ell t} \end{array} \right\}$$

or with $\gamma_{ij} = 2\epsilon_{ij}$

$$\left\{ \begin{array}{c} \epsilon_x \\ \epsilon_y \\ \gamma_{xy} \end{array} \right\} = \left[\begin{array}{ccc} c^2 & s^2 & cs \\ s^2 & c^2 & -cs \\ -2cs & 2cs & (c^2 - s^2) \end{array} \right] \left\{ \begin{array}{c} \epsilon_\ell \\ \epsilon_t \\ \gamma_{\ell t} \end{array} \right\}$$

Then

$$\left\{ \begin{array}{c} \epsilon \\ \gamma \end{array} \right\}_{x,y} = {}^t[T] \left\{ \begin{array}{c} \epsilon \\ \gamma \end{array} \right\}_{\ell,t}$$

In this way, we can express Equation 11.1 in axes (x, y) , since we have written

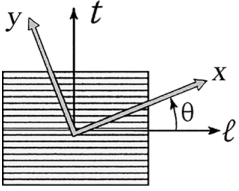
$$\begin{Bmatrix} \varepsilon \\ \gamma \end{Bmatrix}_{x,y} = {}^t [T] \begin{Bmatrix} \varepsilon \\ \gamma \end{Bmatrix}_{\ell,t} ; \quad \begin{Bmatrix} \varepsilon \\ \gamma \end{Bmatrix}_{\ell,t} = \begin{bmatrix} \frac{1}{E_\ell} & -\frac{\nu_{t\ell}}{E_t} & 0 \\ -\frac{\nu_{\ell t}}{E_\ell} & \frac{1}{E_t} & 0 \\ 0 & 0 & \frac{1}{G_{t\ell}} \end{bmatrix} \{\sigma\}_{\ell,t} ; \quad \{\sigma\}_{\ell,t} = [T] \{\sigma\}_{x,y}$$

From which by substituting

$$\begin{Bmatrix} \varepsilon_x \\ \varepsilon_y \\ \gamma_{xy} \end{Bmatrix} = {}^t [T] \begin{bmatrix} \frac{1}{E_\ell} & -\frac{\nu_{t\ell}}{E_t} & 0 \\ -\frac{\nu_{\ell t}}{E_\ell} & \frac{1}{E_t} & 0 \\ 0 & 0 & \frac{1}{G_{t\ell}} \end{bmatrix} [T] \begin{Bmatrix} \sigma_x \\ \sigma_y \\ \tau_{xy} \end{Bmatrix}$$

new matrix of elastic coefficients in x, y axes

After calculation, the following behavior relationship appears, written in technical form in coordinates (x, y) that make an angle θ with axes (ℓ, t) . It reveals the elastic moduli and Poisson's ratios relating to these directions. The nonconventional coupling coefficients denoted by η and μ^5 show, for example, that a normal stress induces a distortion⁶.

 <p style="margin-left: 100px;"> $c = \cos \theta$ $s = \sin \theta$ </p>	$\begin{Bmatrix} \varepsilon_x \\ \varepsilon_y \\ \gamma_{xy} \end{Bmatrix} = \begin{bmatrix} \frac{1}{E_x} & -\frac{\nu_{yx}}{E_y} & \frac{\eta_{xy}}{G_{xy}} \\ -\frac{\nu_{xy}}{E_x} & \frac{1}{E_y} & \frac{\mu_{xy}}{G_{xy}} \\ \frac{\eta_{yx}}{E_x} & \frac{\mu_{yx}}{E_y} & \frac{1}{G_{xy}} \end{bmatrix} \begin{Bmatrix} \sigma_x \\ \sigma_y \\ \tau_{xy} \end{Bmatrix}$
$E_x(\theta) = \frac{1}{\frac{c^4}{E_\ell} + \frac{s^4}{E_t} + c^2 s^2 \left(\frac{1}{G_{t\ell}} - 2 \frac{\nu_{t\ell}}{E_t} \right)}$	$E_y(\theta) = \frac{1}{\frac{s^4}{E_\ell} + \frac{c^4}{E_t} + c^2 s^2 \left(\frac{1}{G_{t\ell}} - 2 \frac{\nu_{t\ell}}{E_t} \right)}$
	$G_{xy}(\theta) = \frac{1}{4c^2 s^2 \left(\frac{1}{E_\ell} + \frac{1}{E_t} + 2 \frac{\nu_{t\ell}}{E_t} \right) + \frac{(c^2 - s^2)^2}{G_{t\ell}}}$
$\frac{\nu_{yx}}{E_y}(\theta) = \frac{\nu_{t\ell}}{E_t} (c^4 + s^4) - c^2 s^2 \left(\frac{1}{E_\ell} + \frac{1}{E_t} - \frac{1}{G_{t\ell}} \right)$	$\frac{\eta_{xy}}{G_{xy}}(\theta) = -2cs \left\{ \frac{c^2}{E_\ell} - \frac{s^2}{E_t} + (c^2 - s^2) \left(\frac{\nu_{t\ell}}{E_t} - \frac{1}{2G_{t\ell}} \right) \right\}$
	$\frac{\mu_{xy}}{G_{xy}}(\theta) = -2cs \left\{ \frac{s^2}{E_\ell} - \frac{c^2}{E_t} - (c^2 - s^2) \left(\frac{\nu_{t\ell}}{E_t} - \frac{1}{2G_{t\ell}} \right) \right\}$

11.2 STIFFNESS COEFFICIENTS

When we invert Equation 11.1 written in coordinate axes (ℓ, t) of a ply, we obtain

$$\begin{Bmatrix} \sigma_\ell \\ \sigma_t \\ \tau_{\ell t} \end{Bmatrix} = \begin{bmatrix} \frac{E_\ell}{(1-\nu_{\ell t}\nu_{t\ell})} & \frac{\nu_{t\ell}E_\ell}{(1-\nu_{\ell t}\nu_{t\ell})} & 0 \\ \frac{\nu_{\ell t}E_t}{(1-\nu_{\ell t}\nu_{t\ell})} & \frac{E_t}{(1-\nu_{\ell t}\nu_{t\ell})} & 0 \\ 0 & 0 & G_{\ell t} \end{bmatrix} \begin{Bmatrix} \varepsilon_\ell \\ \varepsilon_t \\ \gamma_{\ell t} \end{Bmatrix}$$

where appear elastic **stiffness** coefficients as opposed to those of Equation 11.1 referred to as **flexibility** coefficients. To ease writing, it will be preferably noted:

$$\begin{Bmatrix} \sigma_\ell \\ \sigma_t \\ \tau_{\ell t} \end{Bmatrix} = \begin{bmatrix} \bar{E}_\ell & \nu_{t\ell}\bar{E}_\ell & 0 \\ \nu_{\ell t}\bar{E}_t & \bar{E}_t & 0 \\ 0 & 0 & G_{\ell t} \end{bmatrix} \begin{Bmatrix} \varepsilon_\ell \\ \varepsilon_t \\ \gamma_{\ell t} \end{Bmatrix}; \quad \bar{E}_\ell = \frac{E_\ell}{(1-\nu_{\ell t}\nu_{t\ell})}; \quad \bar{E}_t = \frac{E_t}{(1-\nu_{\ell t}\nu_{t\ell})} \quad (11.6)$$

An identical procedure to that followed above to obtain strain–stress behavior leads to the stress–strain relation:

$$\begin{Bmatrix} \sigma_x \\ \sigma_y \\ \tau_{xy} \end{Bmatrix} = \underbrace{\begin{bmatrix} c^2 & s^2 & 2cs \\ s^2 & c^2 & -2cs \\ -cs & cs & (c^2 - s^2) \end{bmatrix}}_{[T_1]} \begin{Bmatrix} \sigma_\ell \\ \sigma_t \\ \tau_{\ell t} \end{Bmatrix}$$

$$\begin{Bmatrix} \varepsilon_\ell \\ \varepsilon_t \\ \gamma_{\ell t} \end{Bmatrix} = \underbrace{\begin{bmatrix} c^2 & s^2 & -cs \\ s^2 & c^2 & cs \\ 2cs & -2cs & (c^2 - s^2) \end{bmatrix}}_{{}^t[T_1]} \begin{Bmatrix} \varepsilon_x \\ \varepsilon_y \\ \gamma_{xy} \end{Bmatrix} \quad (11.7)$$

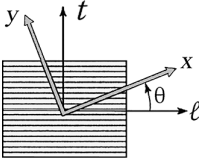
Recall that axes (x, y) are derived from axes (ℓ, t) by rotation θ about the third axis z . Substituting Equations 11.7 into 11.6, we obtain

$$\begin{Bmatrix} \sigma_x \\ \sigma_y \\ \tau_{xy} \end{Bmatrix} = [T_1] \begin{bmatrix} \bar{E}_\ell & \nu_{t\ell}\bar{E}_\ell & 0 \\ \nu_{\ell t}\bar{E}_t & \bar{E}_t & 0 \\ 0 & 0 & G_{\ell t} \end{bmatrix} {}^t[T_1] \begin{Bmatrix} \varepsilon_x \\ \varepsilon_y \\ \gamma_{xy} \end{Bmatrix}$$

which can be rewritten as

$$\begin{Bmatrix} \sigma_x \\ \sigma_y \\ \tau_{xy} \end{Bmatrix} = \begin{bmatrix} \bar{E}_{11} & \bar{E}_{12} & \bar{E}_{13} \\ \bar{E}_{21} & \bar{E}_{22} & \bar{E}_{23} \\ \bar{E}_{31} & \bar{E}_{32} & \bar{E}_{33} \end{bmatrix} \begin{Bmatrix} \varepsilon_x \\ \varepsilon_y \\ \gamma_{xy} \end{Bmatrix}$$

Once the calculation is performed, the following expressions of stiffness coefficients \bar{E}_{ij} are obtained, in which $c = \cos \theta$ and $s = \sin \theta$:

 <p style="margin-left: 100px;"> $c = \cos \theta$ $s = \sin \theta$ </p>	$\begin{Bmatrix} \sigma_x \\ \sigma_y \\ \tau_{xy} \end{Bmatrix} = \begin{bmatrix} \bar{E}_{11} & \bar{E}_{12} & \bar{E}_{13} \\ \bar{E}_{21} & \bar{E}_{22} & \bar{E}_{23} \\ \bar{E}_{31} & \bar{E}_{32} & \bar{E}_{33} \end{bmatrix} \begin{Bmatrix} \varepsilon_x \\ \varepsilon_y \\ \gamma_{xy} \end{Bmatrix}$
	$\bar{E}_{11}(\theta) = c^4 \bar{E}_\ell + s^4 \bar{E}_t + 2c^2 s^2 (v_{t\ell} \bar{E}_\ell + 2G_{t\ell})$
	$\bar{E}_{22}(\theta) = s^4 \bar{E}_\ell + c^4 \bar{E}_t + 2c^2 s^2 (v_{t\ell} \bar{E}_\ell + 2G_{t\ell})$
	$\bar{E}_{33}(\theta) = c^2 s^2 (\bar{E}_\ell + \bar{E}_t - 2v_{t\ell} \bar{E}_\ell) + (c^2 - s^2)^2 G_{t\ell}$
	$\bar{E}_{12}(\theta) = c^2 s^2 (\bar{E}_\ell + \bar{E}_t - 4G_{t\ell}) + (c^4 + s^4) v_{t\ell} \bar{E}_\ell$
	$\bar{E}_{13}(\theta) = -cs \left\{ c^2 \bar{E}_\ell - s^2 \bar{E}_t - (c^2 - s^2) (v_{t\ell} \bar{E}_\ell + 2G_{t\ell}) \right\}$
	$\bar{E}_{23}(\theta) = -cs \left\{ s^2 \bar{E}_\ell - c^2 \bar{E}_t + (c^2 - s^2) (v_{t\ell} \bar{E}_\ell + 2G_{t\ell}) \right\}$
	<p>In which</p> $\bar{E}_\ell = \frac{E_\ell}{(1 - v_{t\ell} v_{t\ell})}; \quad \bar{E}_t = \frac{E_t}{(1 - v_{t\ell} v_{t\ell})}$

(11.8)

The variation of these stiffness coefficients \bar{E}_{ij} as functions of angle θ is pictured in Figure 11.2 for a ply characterized by very different values of moduli E_ℓ and E_t , corresponding, for example, to the case of unidirectional fiber/resin layers⁷.

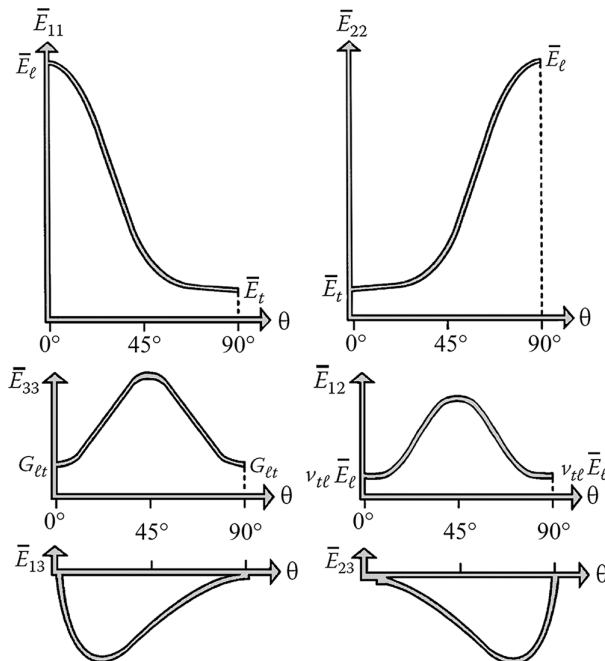


FIGURE 11.2 V

11.3 CASE OF THERMOMECHANICAL LOADING

11.3.1 COMPLIANCE COEFFICIENTS

When considering the temperature variations⁸, the behavior relation in Equation 11.1 should be replaced with the amended form in Equation 10.10, namely,

$$\begin{Bmatrix} \varepsilon_\ell \\ \varepsilon_t \\ \gamma_{\ell t} \end{Bmatrix} = \begin{bmatrix} \frac{1}{E_\ell} & -\frac{\nu_{t\ell}}{E_t} & 0 \\ -\frac{\nu_{\ell t}}{E_\ell} & \frac{1}{E_t} & 0 \\ 0 & 0 & \frac{1}{G_{\ell t}} \end{bmatrix} \begin{Bmatrix} \sigma_\ell \\ \sigma_t \\ \tau_{\ell t} \end{Bmatrix} + \Delta T \begin{Bmatrix} \alpha_\ell \\ \alpha_t \\ 0 \end{Bmatrix}$$

In which α_ℓ and α_t are the thermal expansion coefficients of the unidirectional layer along the longitudinal direction ℓ and transverse direction t , respectively. Following the same procedure as in Section 11.1 with the same notations, we can write

$$\begin{Bmatrix} \varepsilon \\ \gamma \end{Bmatrix}_{x,y} = {}^t[T] \begin{Bmatrix} \varepsilon \\ \gamma \end{Bmatrix}_{\ell,t} ; \{\sigma\}_{\ell,t} = [T] \{\sigma\}_{x,y}$$

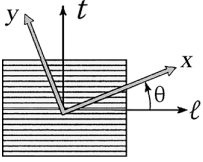
From where, by substituting,

$$\begin{Bmatrix} \varepsilon_x \\ \varepsilon_y \\ \gamma_{xy} \end{Bmatrix} = {}^t[T] \begin{bmatrix} \frac{1}{E_\ell} & -\frac{\nu_{t\ell}}{E_t} & 0 \\ -\frac{\nu_{\ell t}}{E_\ell} & \frac{1}{E_t} & 0 \\ 0 & 0 & \frac{1}{G_{\ell t}} \end{bmatrix} [T] \begin{Bmatrix} \sigma_x \\ \sigma_y \\ \tau_{xy} \end{Bmatrix} + \frac{\Delta T}{\text{temp.}} {}^t[T] \begin{Bmatrix} \alpha_\ell \\ \alpha_t \\ 0 \end{Bmatrix}$$

In this relationship, we find again the flexibility matrix on the right side, the terms of which are described in details in Equation 11.5. The second term on the right side is written as

$$\Delta T \begin{bmatrix} c^2 & s^2 & cs \\ s^2 & c^2 & -cs \\ -2cs & 2cs & (c^2 - s^2) \end{bmatrix} \begin{Bmatrix} \alpha_\ell \\ \alpha_t \\ 0 \end{Bmatrix} = \Delta T \begin{Bmatrix} c^2\alpha_\ell + s^2\alpha_t \\ s^2\alpha_\ell + c^2\alpha_t \\ 2cs(\alpha_t - \alpha_\ell) \end{Bmatrix}$$

Therefore, the thermomechanical behavior relationship for a unidirectional layer, written in axes (x, y) other than the specific coordinates (ℓ, t) of unidirectional, can be summarized as follows:



$c = \cos \theta$
 $s = \sin \theta$

$$\begin{Bmatrix} \epsilon_x \\ \epsilon_y \\ \gamma_{xy} \end{Bmatrix} = \begin{bmatrix} \frac{1}{E_x} & -\frac{\nu_{yx}}{E_y} & \frac{\eta_{xy}}{G_{xy}} \\ -\frac{\nu_{xy}}{E_x} & \frac{1}{E_y} & \frac{\mu_{xy}}{G_{xy}} \\ \frac{\eta_x}{E_x} & \frac{\mu_y}{E_y} & \frac{1}{G_{xy}} \end{bmatrix} \begin{Bmatrix} \sigma_x \\ \sigma_y \\ \tau_{xy} \end{Bmatrix} + \Delta T \begin{Bmatrix} \alpha_x \\ \alpha_y \\ \alpha_{xy} \end{Bmatrix}$$

$E_x, E_y, G_{xy}, \nu_{xy}, \nu_{yx}, \eta_{yx}, \mu_{xy}$ are given by Equation 11.5

$$\alpha_x = c^2 \alpha_\ell + s^2 \alpha_t$$

$$\alpha_y = s^2 \alpha_\ell + c^2 \alpha_t$$

$$\alpha_{xy} = 2cs(\alpha_t - \alpha_\ell)$$

$$c = \cos \theta; \quad s = \sin \theta$$

(11.9)

11.3.2 STIFFNESS COEFFICIENTS

By inversion of Equation 10.10, we get

$$\begin{Bmatrix} \sigma_\ell \\ \sigma_t \\ \tau_{\ell t} \end{Bmatrix} = \begin{bmatrix} \frac{E_\ell}{(1-\nu_{\ell t}\nu_{t\ell})} & \frac{\nu_{t\ell}E_\ell}{(1-\nu_{\ell t}\nu_{t\ell})} & 0 \\ \frac{\nu_{\ell t}E_t}{(1-\nu_{\ell t}\nu_{t\ell})} & \frac{E_t}{(1-\nu_{\ell t}\nu_{t\ell})} & 0 \\ 0 & 0 & G_{\ell t} \end{bmatrix} \begin{Bmatrix} \epsilon_\ell \\ \epsilon_t \\ \gamma_{\ell t} \end{Bmatrix} - \Delta T \begin{Bmatrix} \frac{E_\ell}{(1-\nu_{\ell t}\nu_{t\ell})}\alpha_\ell + \frac{\nu_{t\ell}E_\ell}{(1-\nu_{\ell t}\nu_{t\ell})}\alpha_t \\ \frac{\nu_{\ell t}E_t}{(1-\nu_{\ell t}\nu_{t\ell})}\alpha_\ell + \frac{E_t}{(1-\nu_{\ell t}\nu_{t\ell})}\alpha_t \\ 0 \end{Bmatrix}$$

Following the procedure of Section 11.2, with the same notations, we can write

$$\{\sigma\}_{x,y} = [T_1]\{\sigma\}_{\ell,t}; \quad \begin{Bmatrix} \epsilon \\ \gamma \end{Bmatrix}_{\ell,t} = {}^t[T_1] \begin{Bmatrix} \epsilon \\ \gamma \end{Bmatrix}_{x,y}$$

From where, by replacing,

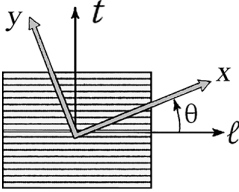
$$\begin{Bmatrix} \sigma_x \\ \sigma_y \\ \tau_{xy} \end{Bmatrix} = [T_1] \begin{bmatrix} \bar{E}_\ell & \nu_{t\ell}\bar{E}_\ell & 0 \\ \nu_{\ell t}\bar{E}_t & \bar{E}_t & 0 \\ 0 & 0 & G_{\ell t} \end{bmatrix} {}^t[T_1] \begin{Bmatrix} \epsilon_x \\ \epsilon_y \\ \gamma_{xy} \end{Bmatrix} - \Delta T [T_1] \begin{Bmatrix} \bar{E}_\ell\alpha_\ell + \nu_{t\ell}\bar{E}_\ell\alpha_t \\ \nu_{\ell t}\bar{E}_t\alpha_\ell + \bar{E}_t\alpha_t \\ 0 \end{Bmatrix}$$

In the first term on the right side, we find again the matrix detailed in Equation 11.8. The second term can be developed as follows:

$$-\Delta T \begin{bmatrix} c^2 & s^2 & 2cs \\ s^2 & c^2 & -2cs \\ -cs & cs & (c^2 - s^2) \end{bmatrix} \begin{Bmatrix} \bar{E}_\ell\alpha_\ell + \nu_{t\ell}\bar{E}_\ell\alpha_t \\ \nu_{\ell t}\bar{E}_t\alpha_\ell + \bar{E}_t\alpha_t \\ 0 \end{Bmatrix} = \dots$$

$$\dots - \Delta T \begin{Bmatrix} c^2 \bar{E}_\ell (\alpha_\ell + \nu_{t\ell} \alpha_t) + s^2 \bar{E}_t (\nu_{t\ell} \alpha_\ell + \alpha_t) \\ s^2 \bar{E}_\ell (\alpha_\ell + \nu_{t\ell} \alpha_t) + c^2 \bar{E}_t (\nu_{t\ell} \alpha_\ell + \alpha_t) \\ cs [\bar{E}_t (\nu_{t\ell} \alpha_\ell + \alpha_t) - \bar{E}_\ell (\alpha_\ell + \nu_{t\ell} \alpha_t)] \end{Bmatrix}$$

Therefore, the thermomechanical behavior relationship written in axes (x, y) other than the specific unidirectional coordinates (ℓ, t) can be summarized as follows:

 <div style="margin-top: 10px;"> $c = \cos \theta$ $s = \sin \theta$ </div>	$\begin{Bmatrix} \sigma_x \\ \sigma_y \\ \tau_{xy} \end{Bmatrix} = \begin{bmatrix} \bar{E}_{11} & \bar{E}_{12} & \bar{E}_{13} \\ \bar{E}_{21} & \bar{E}_{22} & \bar{E}_{23} \\ \bar{E}_{31} & \bar{E}_{32} & \bar{E}_{33} \end{bmatrix} \begin{Bmatrix} \epsilon_x \\ \epsilon_y \\ \gamma_{xy} \end{Bmatrix} - \Delta T \begin{Bmatrix} \bar{\alpha E}_1 \\ \bar{\alpha E}_2 \\ \bar{\alpha E}_3 \end{Bmatrix}$ <p>$\bar{E}_{11} \bar{E}_{22} \bar{E}_{33} \bar{E}_{12} \bar{E}_{13} \bar{E}_{23}$ are given by Equation 11.8</p> $\bar{\alpha E}_1 = c^2 \bar{E}_\ell (\alpha_\ell + \nu_{t\ell} \alpha_t) + s^2 \bar{E}_t (\nu_{t\ell} \alpha_\ell + \alpha_t)$ $\bar{\alpha E}_2 = s^2 \bar{E}_\ell (\alpha_\ell + \nu_{t\ell} \alpha_t) + c^2 \bar{E}_t (\nu_{t\ell} \alpha_\ell + \alpha_t)$ $\bar{\alpha E}_3 = cs [\bar{E}_t (\nu_{t\ell} \alpha_\ell + \alpha_t) - \bar{E}_\ell (\alpha_\ell + \nu_{t\ell} \alpha_t)]$ $\bar{E}_\ell = \frac{E_\ell}{(1 - \nu_{t\ell} \nu_{t\ell})}; \quad \bar{E}_t = \frac{E_t}{(1 - \nu_{t\ell} \nu_{t\ell})}$
---	---

(11.10)

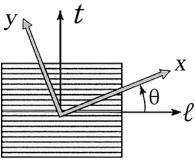
11.4 CASE OF HYGROTHERMAL LOADING

11.4.1 PRELIMINARY REMARK

We noted in Chapter 10 formal similarities between thermal expansion and hygrometric expansion. We notice it, for example, on Equation 10.12. It is, thus, possible to resume the previous calculations from Section 11.3 with Equation 10.12. By following the same steps, one obtains the results below.

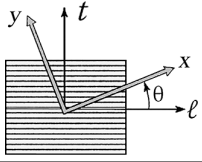
11.4.2 COMPLIANCE COEFFICIENTS

Expressed in axes (x, y) of the unidirectional ply, we obtain:

$\begin{Bmatrix} \epsilon_x \\ \epsilon_y \\ \gamma_{xy} \end{Bmatrix} = \begin{bmatrix} \frac{1}{E_x} & -\frac{\nu_{yx}}{E_y} & \frac{\eta_{xy}}{G_{xy}} \\ -\frac{\nu_{xy}}{E_x} & \frac{1}{E_y} & \frac{\mu_{xy}}{G_{xy}} \\ \frac{\eta_x}{E_x} & \frac{\mu_y}{E_y} & \frac{1}{G_{xy}} \end{bmatrix} \begin{Bmatrix} \sigma_x \\ \sigma_y \\ \tau_{xy} \end{Bmatrix} + \Delta T \begin{Bmatrix} \alpha_x \\ \alpha_y \\ \alpha_{xy} \end{Bmatrix} + \Delta M_c \begin{Bmatrix} \beta_x \\ \beta_y \\ \beta_{xy} \end{Bmatrix}$	
$E_x, E_y, G_{xy}, \nu_{xy}, \nu_{yx}, \eta_{xy}, \mu_{xy}$ are given by Equation 11.5 ΔT algebraic increase in temperature ΔM_c algebraic increase in moisture concentration (see Section 10.6.2)	
$\alpha_x = c^2 \alpha_\ell + s^2 \alpha_t$	$\beta_x = c^2 \beta_\ell + s^2 \beta_t$
$\alpha_y = s^2 \alpha_\ell + c^2 \alpha_t$	$\beta_y = s^2 \beta_\ell + c^2 \beta_t$
$\alpha_{xy} = 2cs(\alpha_t - \alpha_\ell)$	$\beta_{xy} = 2cs(\beta_t - \beta_\ell)$
$c = \cos \theta; \quad s = \sin \theta$	

11.4.3 STIFFNESS COEFFICIENTS

Following the procedure of Section 11.3.2 leads to:

$\begin{Bmatrix} \sigma_x \\ \sigma_y \\ \tau_{xy} \end{Bmatrix} = \begin{bmatrix} \bar{E}_{11} & \bar{E}_{12} & \bar{E}_{13} \\ \bar{E}_{21} & \bar{E}_{22} & \bar{E}_{23} \\ \bar{E}_{31} & \bar{E}_{32} & \bar{E}_{33} \end{bmatrix} \begin{Bmatrix} \epsilon_x \\ \epsilon_y \\ \gamma_{xy} \end{Bmatrix} - \Delta T \begin{Bmatrix} \bar{\alpha E}_1 \\ \bar{\alpha E}_2 \\ \bar{\alpha E}_3 \end{Bmatrix} - \Delta M_c \begin{Bmatrix} \bar{\beta E}_1 \\ \bar{\beta E}_2 \\ \bar{\beta E}_3 \end{Bmatrix}$	
$\bar{E}_{11}, \bar{E}_{22}, \bar{E}_{33}, \bar{E}_{12}, \bar{E}_{13}, \bar{E}_{23}$ are given by Equation 11.8 ΔT algebraic increase in temperature ΔM_c algebraic increase in moisture concentration (see Section 10.6.2)	
$\bar{\alpha E}_1 = c^2 \bar{E}_t (\alpha_\ell + \nu_{t\ell} \alpha_t) + s^2 \bar{E}_t (\nu_{t\ell} \alpha_\ell + \alpha_t)$	$\bar{\beta E}_1 = c^2 \bar{E}_t (\beta_\ell + \nu_{t\ell} \beta_t) + s^2 \bar{E}_t (\nu_{t\ell} \beta_\ell + \beta_t)$
$\bar{\alpha E}_2 = s^2 \bar{E}_t (\alpha_\ell + \nu_{t\ell} \alpha_t) + c^2 \bar{E}_t (\nu_{t\ell} \alpha_\ell + \alpha_t)$	$\bar{\beta E}_2 = s^2 \bar{E}_t (\beta_\ell + \nu_{t\ell} \beta_t) + c^2 \bar{E}_t (\nu_{t\ell} \beta_\ell + \beta_t)$
$\bar{\alpha E}_3 = cs [\bar{E}_t (\nu_{t\ell} \alpha_\ell + \alpha_t) - \bar{E}_t (\alpha_\ell + \nu_{t\ell} \alpha_t)]$	$\bar{\beta E}_3 = cs [\bar{E}_t (\nu_{t\ell} \beta_\ell + \beta_t) - \bar{E}_t (\beta_\ell + \nu_{t\ell} \beta_t)]$
$c = \cos \theta; \quad s = \sin \theta$	
$\bar{E}_\ell = \frac{E_\ell}{(1 - \nu_{t\ell} \nu_{t\ell})}; \quad \bar{E}_t = \frac{E_t}{(1 - \nu_{t\ell} \nu_{t\ell})}$	

(11.12)

NOTES

- 1 See Section 3.2.
- 2 The orthotropic axes (1, 2, 3) in Equation 9.3 are now called (ℓ, t, z), respectively.
- 3 What follows is treated more globally and completely in Section 13.2.2.
- 4 We have $[\sigma]_{x,y} = [P][\sigma]_{\ell,t}$; $[\sigma]_{\ell,t} = [P][\sigma]_{x,y}$; $[P][\sigma]_{\ell,t} = [\sigma]_{x,y}$; $[\sigma]_{\ell,t} = [P][\sigma]_{x,y}$.
- 5 Recall that the matrix of elastic coefficients is symmetric, that is, in particular, $(\eta_{xy}/G_{xy}) = (\eta_x/E_x)$ and $(\mu_{xy}/G_{xy}) = (\mu_y/E_y)$.
- 6 See a descriptive example in Section 3.1.
- 7 See characteristics of the fiber/resin unidirectionals in Section 3.3.3.
- 8 See Section 10.5.

12 Mechanical Behavior of Thin Laminated Plates

The laminate has already been defined¹ in Chapter 5. In the same chapter, practical calculation methods for the laminate have also been described. We propose here to justify these methods. The aim is to study the behavior of the laminate when subjected to combined loads. This study is essential in order to achieve correct sizing. The case of quadrangular symmetric laminates is examined (Quad laminates). Depending on the application case, it is necessary to verify either that the deformation of the laminate does not exceed the admissible value, or that the state of stress remains within an acceptable envelope².

12.1 LAMINATE WITH MID-PLANE SYMMETRY

12.1.1 IN-PLANE BEHAVIOR

We consider in the following a plane laminate with **Mid-plane symmetry** property³, (x, y) being the plane of symmetry. The total thickness of the laminate is denoted as h . It consists of n plies. Ply number k has a thickness denoted as e_k (see Figure 12.1).

12.1.1.1 Loadings

The laminate is loaded in its plane. The stress resultants are denoted as N_x , N_y , and $T_{xy} = T_{yx}$. These are the In-plane stress resultants. They are defined as follows:

- N_x , normal stress resultant in the x -direction per unit width along the y -direction:

$$N_x = \int_{-h/2}^{h/2} (\sigma_x \times 1) \times dz = \sum_{k=1st\ ply}^{nth\ ply} (\sigma_x)_k \times e_k \quad (12.1)$$

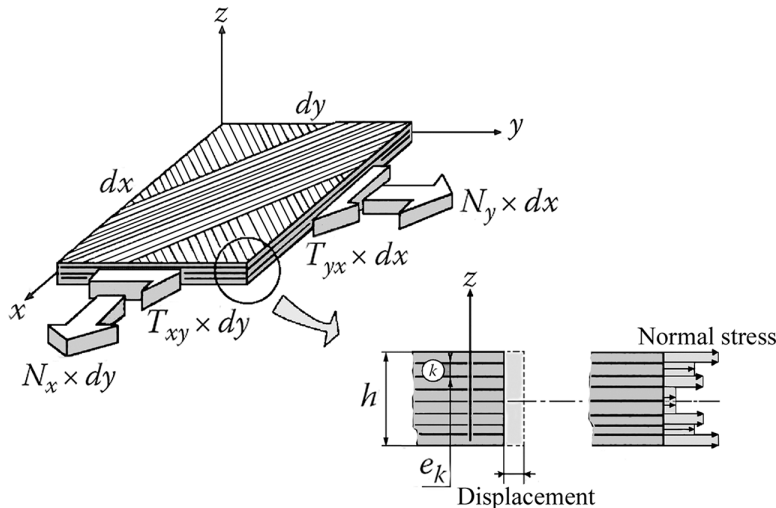


FIGURE 12.1 In-plane loading.

- N_y , normal stress resultant along the y -direction per unitary width along the x -direction:

$$N_y = \int_{-h/2}^{h/2} (\sigma_y \times 1) \times dz = \sum_{k=1}^{nth \text{ ply}} (\sigma_y)_k \times e_k \quad (12.2)$$

- $T_{xy} = T_{yx}$, shear resultant per unit width along the y -direction (or, respectively, along the x -direction):

$$T_{xy} = \int_{-h/2}^{h/2} (\tau_{xy} \times 1) \times dz = \sum_{k=1}^{nth \text{ ply}} (\tau_{xy})_k \times e_k \quad (12.3)$$

12.1.1.2 Displacement Field

The elastic displacement at each point of the laminate is assumed to be two dimensional, in the (x, y) Mid-plane of the laminate. Its components are noted: $u_0(x, y)$, $v_0(x, y)$. The corresponding plane strains and angular variation can be written as

$$\epsilon_{0x} = \frac{\partial u_0}{\partial x}; \quad \epsilon_{0y} = \frac{\partial v_0}{\partial y}; \quad \gamma_{0xy} = \frac{\partial u_0}{\partial y} + \frac{\partial v_0}{\partial x}$$

We have detailed in the previous chapter (Equation 11.8) how, in a given coordinate system, the stresses in a ply could be expressed as functions of the strains. Thus, the normal stress resultant N_x as defined in Equation 12.1 can be written as follows:

$$N_x = \sum_{k=1}^{nth \text{ ply}} \left\{ \bar{E}_{11}^k \epsilon_{0x} + \bar{E}_{12}^k \epsilon_{0y} + \bar{E}_{13}^k \gamma_{0xy} \right\} \times e_k$$

Then

$$N_x = A_{11} \epsilon_{0x} + A_{12} \epsilon_{0y} + A_{13} \gamma_{0xy}$$

with

$$A_{11} = \sum_{k=1}^{nth \text{ ply}} \bar{E}_{11}^k e_k; \quad A_{12} = \sum_{k=1}^{nth \text{ ply}} \bar{E}_{12}^k e_k; \quad A_{13} = \sum_{k=1}^{nth \text{ ply}} \bar{E}_{13}^k e_k$$

In the same manner, we obtain from Equation 12.2

$$N_y = A_{21} \epsilon_{0x} + A_{22} \epsilon_{0y} + A_{23} \gamma_{0xy}$$

with

$$A_{2j} = \sum_{k=1}^{nth \text{ ply}} \bar{E}_{2j}^k e_k$$

And for the shear resultant T_{xy} , we can write, starting from Equation 12.3,

$$T_{xy} = A_{31} \epsilon_{0x} + A_{32} \epsilon_{0y} + A_{33} \gamma_{0xy}$$

with

$$A_{3j} = \sum_{k=\text{1st ply}}^{\text{nth ply}} \bar{E}_{3j}^k e_k$$

Therefore, it is possible to express the stress resultants in the following matrix form⁴:

$$\begin{Bmatrix} N_x \\ N_y \\ T_{xy} \end{Bmatrix} = \begin{bmatrix} A_{11} & A_{12} & A_{13} \\ A_{21} & A_{22} & A_{23} \\ A_{31} & A_{32} & A_{33} \end{bmatrix} \begin{Bmatrix} \epsilon_{0x} \\ \epsilon_{0y} \\ \gamma_{0xy} \end{Bmatrix}$$

with

$$A_{ij} = \sum_{k=\text{1st ply}}^{\text{nth ply}} \bar{E}_{ij}^k e_k = A_{ji} \quad (12.4)$$

Comments

- It can be noted from the above that coefficients A_{ij} are independent of the stacking order of the plies.
- As seen in Equation 12.4, the normal stress resultants N_x or N_y give rise to angular distortions. This coupling will disappear if the laminate is **balanced**, that is, in addition to the Mid-plane symmetry, it presents as many plies at an angle of $+\theta$ with the x -direction as plies at an angle of $-\theta$, these plies being identical⁵. Indeed, \bar{E}_{13} and \bar{E}_{23} are antisymmetric with respect to θ (see Equation 11.8) and, therefore, cancel each other out for the pairs of plies at $\pm\theta$ when the terms A_{13} and A_{23} are calculated. The result is then

$$A_{13} = A_{23} = 0$$

And the resultant stress–strain relationship for the laminate is reduced to

$$\begin{Bmatrix} N_x \\ N_y \\ T_{xy} \end{Bmatrix} = \begin{bmatrix} A_{11} & A_{12} & 0 \\ A_{21} & A_{22} & 0 \\ 0 & 0 & A_{33} \end{bmatrix} \begin{Bmatrix} \epsilon_{0x} \\ \epsilon_{0y} \\ \gamma_{0xy} \end{Bmatrix} \quad (12.5)$$

- The overall average stresses (which are fictitious) may be a substitute for the stress resultants N_x , N_y , and T_{xy} . They take the following form:

$$\sigma_{0x} = \frac{N_x}{h}; \quad \sigma_{0y} = \frac{N_y}{h}; \quad \tau_{0xy} = \frac{T_{xy}}{h} \quad (12.6)$$

Then the In-plane stress–strain relationship for the homogenized laminate can be derived from Equation 12.4 in the form

$$\begin{Bmatrix} \sigma_{0x} \\ \sigma_{0y} \\ \tau_{0xy} \end{Bmatrix} = \frac{1}{h} \begin{bmatrix} A_{11} & A_{12} & A_{13} \\ A_{21} & A_{22} & A_{23} \\ A_{31} & A_{32} & A_{33} \end{bmatrix} \begin{Bmatrix} \epsilon_{0x} \\ \epsilon_{0y} \\ \gamma_{0xy} \end{Bmatrix} \quad (12.7)$$

- According to Equation 12.4, the terms of the matrix $(1/h)[A]$ above can be written as

$$\frac{1}{h} \times A_{ij} = \sum_{k=1}^{nth \text{ ply}} \bar{E}_{ij}^k \times \frac{e_k}{h}$$

It can be noted that the ratios (e_k/h) can be rearranged to obtain each percentage of plies having the same orientation. In so far as these percentages were previously fixed (and so are numerically known), it becomes possible to calculate the terms $(1/h)A_{ij}$ **without knowledge of the thickness h** . For example, if the selected orientations are 0° , 90° , $+45^\circ$, and -45° , and by denoting $p^k(\%)$ the percentages of plies along these different orientations, we have

$$\frac{1}{h} \times A_{ij} = \bar{E}_{ij}^{0^\circ} \times p^{0^\circ} + \bar{E}_{ij}^{90^\circ} \times p^{90^\circ} + \bar{E}_{ij}^{+45^\circ} \times p^{+45^\circ} + \bar{E}_{ij}^{-45^\circ} \times p^{-45^\circ} \quad (12.8)$$

12.1.2 APPARENT ELASTIC MODULI OF THE LAMINATE

Inversion of Equation 12.7 allows obtaining the **apparent elastic moduli** and the associated coupling coefficients that characterize the membrane behavior in plane (x, y) . These coefficients appear through the identification that follows:

$$\begin{Bmatrix} \epsilon_{0x} \\ \epsilon_{0y} \\ \gamma_{0xy} \end{Bmatrix} = h[A]^{-1} \begin{Bmatrix} \sigma_{0x} \\ \sigma_{0y} \\ \tau_{0xy} \end{Bmatrix} = \begin{Bmatrix} \frac{1}{\bar{E}_x} & -\frac{\bar{\nu}_{yx}}{\bar{E}_y} & \frac{\bar{\eta}_{xy}}{\bar{G}_{xy}} \\ -\frac{\bar{\nu}_{xy}}{\bar{E}_x} & \frac{1}{\bar{E}_y} & \frac{\bar{\mu}_{xy}}{\bar{G}_{xy}} \\ \frac{\bar{\eta}_x}{\bar{E}_x} & \frac{\bar{\mu}_y}{\bar{E}_y} & \frac{1}{\bar{G}_{xy}} \end{Bmatrix} \begin{Bmatrix} \sigma_{0x} \\ \sigma_{0y} \\ \tau_{0xy} \end{Bmatrix} \quad (12.9)$$

12.1.3 CONSEQUENCE: PRACTICAL DETERMINATION OF A LAMINATE SUBJECT TO IN-PLANE LOADING

12.1.3.1 Givens of the Problem

- The stress resultants are given and denoted as N_x , N_y , and T_{xy} .
- Using these values, we can estimate the ply proportions in the four orientations⁶. We will assume in the following that all plies are identical, that is, made of same material with same thickness (see Figure 12.2).

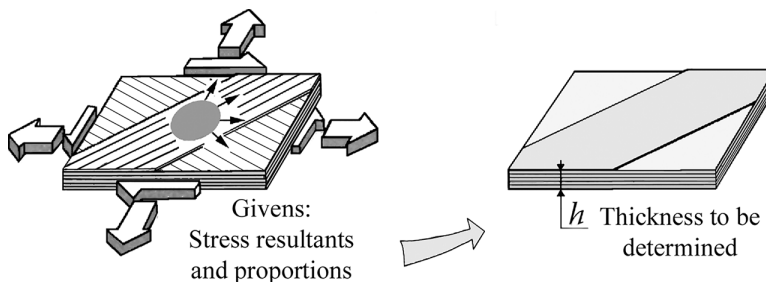


FIGURE 12.2 Practical determination of a laminate subject to In-plane loading.

The problem then is to determine

- The apparent elastic moduli of the laminate and the coupling coefficients, in order to estimate strain under loading
- The minimum laminate thickness noted h in order to prevent failure of any constitutive ply

12.1.3.2 Principle of Calculation

1. **Apparent moduli of the laminate:** The matrix $(1/h)[A]$ evaluated using Equation 12.8 can be inverted, and we obtain Equation 12.9 recalled here:

$$\begin{Bmatrix} \varepsilon_{0x} \\ \varepsilon_{0y} \\ \gamma_{0xy} \end{Bmatrix} = \begin{bmatrix} \frac{1}{\bar{E}_x} & -\frac{\bar{\nu}_{yx}}{\bar{E}_y} & \frac{\bar{\eta}_{xy}}{\bar{G}_{xy}} \\ -\frac{\bar{\nu}_{xy}}{\bar{E}_x} & \frac{1}{\bar{E}_y} & \frac{\bar{\mu}_{xy}}{\bar{G}_{xy}} \\ \frac{\bar{\eta}_x}{\bar{E}_x} & \frac{\bar{\mu}_y}{\bar{E}_y} & \frac{1}{\bar{G}_{xy}} \end{bmatrix} \begin{Bmatrix} \sigma_{0x} \\ \sigma_{0y} \\ \tau_{0xy} \end{Bmatrix}$$

And we have already determined the apparent moduli and the coupling coefficients of the laminate.

2. **Nonfailure of the laminate:** Let σ_ℓ , σ_t , and $\tau_{\ell t}$ be the stress state in orthotropic axes (ℓ, t) of one of the ply orientations making up the laminate, when subject to the loadings N_x , N_y , and T_{xy} . Let h be the thickness of the laminate (still unknown until now) such that this ply orientation is just reaching its failure strength within the meaning of the Tsai-Hill failure criterion.

Saturation of the Tsai-Hill criterion for the concerned orientation is written as⁷

$$\frac{\sigma_\ell^2}{\sigma_{\ell \text{ rupt.}}^2} + \frac{\sigma_t^2}{\sigma_{t \text{ rupt.}}^2} - \frac{\sigma_\ell \sigma_t}{\sigma_{\ell \text{ rupt.}}^2} + \frac{\tau_{\ell t}^2}{\tau_{\ell t \text{ rupt.}}^2} = 1$$

Multiplying the two sides of this equation with the square of thickness h ,

$$\frac{(\sigma_\ell \times h)^2}{\sigma_{\ell \text{ rupt.}}^2} + \frac{(\sigma_t \times h)^2}{\sigma_{t \text{ rupt.}}^2} - \frac{(\sigma_\ell \times h)(\sigma_t \times h)}{\sigma_{\ell \text{ rupt.}}^2} + \frac{(\tau_{\ell t} \times h)^2}{\tau_{\ell t \text{ rupt.}}^2} = h^2 \quad (12.10)$$

On the other hand, we obtain the values $(\sigma_\ell \times h)$, $(\sigma_t \times h)$, and $(\tau_{\ell t} \times h)$ by multiplying with h the average stress values σ_{0x} , σ_{0y} , and τ_{0xy} that apply on the laminate, to become $(\sigma_{0x} \times h)$, $(\sigma_{0y} \times h)$, and $(\tau_{0xy} \times h)$, which are precisely the known stress resultants:

$$N_x = (\sigma_{0x} \times h); \quad N_y = (\sigma_{0y} \times h); \quad T_{xy} = (\tau_{0xy} \times h)$$

So, for a given ply, calculation of the Tsai-Hill criterion can be done by substitution of the known stress resultants N_x , N_y , and T_{xy} to the unknown average stress values. This leads to the calculation of the thickness h necessary to ensure the nonrupture of the ply orientation under analysis.

In this way, each ply orientation k leads to a laminate thickness value denoted as h_k . The final thickness value to be retained will be the highest one.

12.1.3.3 Calculation Procedure

1. **Complete calculation:** The ply proportions are given, and the matrix $(1/h)[A]$ in Equation 12.7 is known. Then, after inverting, we obtain the elastic moduli of the laminate (Equation 12.9)⁸. Multiplying Equation 12.9 with the laminate thickness h (unknown),

$$\begin{Bmatrix} h\epsilon_{0x} \\ h\epsilon_{0y} \\ h\gamma_{0xy} \end{Bmatrix} = \begin{bmatrix} \frac{1}{\bar{E}_x} & -\frac{\bar{\nu}_{yx}}{\bar{E}_y} & \frac{\bar{\eta}_{xy}}{\bar{G}_{xy}} \\ -\frac{\bar{\nu}_{xy}}{\bar{E}_x} & \frac{1}{\bar{E}_y} & \frac{\bar{\mu}_{xy}}{\bar{G}_{xy}} \\ \frac{\bar{\eta}_x}{\bar{E}_x} & \frac{\bar{\mu}_y}{\bar{E}_y} & \frac{1}{\bar{G}_{xy}} \end{bmatrix} \begin{Bmatrix} N_x \\ N_y \\ T_{xy} \end{Bmatrix}$$

Then the stress values in the group of plies corresponding to the orientation k are obtained, adjusted by the thickness h (see Equation 11.8):

$$\begin{Bmatrix} h\sigma_x \\ h\sigma_y \\ h\tau_{xy} \end{Bmatrix}_{\text{ply } n^{\circ}k} = \begin{bmatrix} \bar{E}_{11} & \bar{E}_{12} & \bar{E}_{13} \\ \bar{E}_{21} & \bar{E}_{22} & \bar{E}_{23} \\ \bar{E}_{31} & \bar{E}_{32} & \bar{E}_{33} \end{bmatrix}_{\text{ply } n^{\circ}k} \begin{Bmatrix} h\epsilon_{0x} \\ h\epsilon_{0y} \\ h\gamma_{0xy} \end{Bmatrix}_{\text{laminate}}$$

And in the ply coordinates for the considered orientation (see Equation 11.4):

$$\begin{Bmatrix} h\sigma_\ell \\ h\sigma_t \\ h\tau_{\ell t} \end{Bmatrix}_{\text{ply } n^{\circ}k} = \begin{bmatrix} c^2 & s^2 & -2cs \\ s^2 & c^2 & 2cs \\ sc & -sc & (c^2 - s^2) \end{bmatrix}_{\text{ply } n^{\circ}k} \begin{Bmatrix} h\sigma_x \\ h\sigma_y \\ h\tau_{xy} \end{Bmatrix}_{\text{ply } n^{\circ}k} \quad c = \cos \theta; \quad s = \sin \theta$$

Saturation of the Tsai-Hill criterion leads then to Equation 12.10 where the above known stress resultant values $h\sigma_\ell$, $h\sigma_t$, and $h\tau_{\ell t}$ appear in the numerator as

$$\frac{(h\sigma_\ell)^2}{\sigma_{\ell \text{rupt}}^2} + \frac{(h\sigma_t)^2}{\sigma_{t \text{rupt}}^2} - \frac{(h\sigma_\ell)(h\sigma_t)}{\sigma_{\ell \text{rupt}}^2} + \frac{(h\tau_{\ell t})^2}{\tau_{\ell t \text{rupt}}^2} = h^2 \times 1$$

By writing this expression for each orientation k , we must retain for final thickness value the maximum of the values found for h_k .

2. **Simplified calculation:** Equation 12.10 can be written more quickly if, for each ply orientation, the stress state due to an average unit stress acting on the laminate is already known: the average unit stress will be first $\sigma'_{0x} = 1$, for example, 1 MPa; then $\sigma''_{0y} = 1$ MPa and then again $\tau'''_{0xy} = 1$ MPa.

- Assume first the following state of stress:

$$\begin{cases} \sigma'_{0x} = 1_{(\text{MPa})} \\ \sigma'_{0y} = 0 \\ \tau'_{0xy} = 0 \end{cases}$$

Inverting Equation 12.9 leads to strain values:

$$\begin{Bmatrix} \varepsilon'_{0x} \\ \varepsilon'_{0y} \\ \gamma'_{0xy} \end{Bmatrix} = \begin{bmatrix} \frac{1}{\bar{E}_x} & -\frac{\bar{\nu}_{yx}}{\bar{E}_y} & \frac{\bar{\eta}_{xy}}{\bar{G}_{xy}} \\ -\frac{\bar{\nu}_{xy}}{\bar{E}_x} & \frac{1}{\bar{E}_y} & \frac{\bar{\mu}_{xy}}{\bar{G}_{xy}} \\ \frac{\bar{\eta}_x}{\bar{E}_x} & \frac{\bar{\mu}_y}{\bar{E}_y} & \frac{1}{\bar{G}_{xy}} \end{bmatrix} \begin{Bmatrix} 1_{(\text{MPa})} \\ 0 \\ 0 \end{Bmatrix}$$

which can be considered as **unitary strain values** for the laminate. They are used to calculate the stress values in each ply orientation through Equation 11.8 and then Equation 11.4, that is successively (see Equation 11.8):

$$\begin{Bmatrix} \sigma'_x \\ \sigma'_y \\ \tau'_{xy} \end{Bmatrix}_{\text{ply } n^{\circ}k} = \begin{bmatrix} \bar{E}_{11} & \bar{E}_{12} & \bar{E}_{13} \\ \bar{E}_{21} & \bar{E}_{22} & \bar{E}_{23} \\ \bar{E}_{31} & \bar{E}_{32} & \bar{E}_{33} \end{bmatrix}_{\text{ply } n^{\circ}k} \begin{Bmatrix} \varepsilon'_{0x} \\ \varepsilon'_{0y} \\ \gamma'_{0xy} \end{Bmatrix}_{\text{laminate}}$$

and in the coordinates of the ply orientation in consideration (see Equation 11.4):

$$\begin{Bmatrix} \sigma'_\ell \\ \sigma'_t \\ \tau'_{\ell t} \end{Bmatrix}_{\text{ply } n^{\circ}k} = \begin{bmatrix} c^2 & s^2 & -2cs \\ s^2 & c^2 & 2cs \\ sc & -sc & (c^2 - s^2) \end{bmatrix}_{\text{ply } n^{\circ}k} \begin{Bmatrix} \sigma'_x \\ \sigma'_y \\ \tau'_{xy} \end{Bmatrix}_{\text{ply } n^{\circ}k} \quad \begin{matrix} c = \cos \theta \\ s = \sin \theta \end{matrix}$$

- *Consider then the second state of stress:*

$$\begin{matrix} \sigma_{0x}'' = 0 \\ \sigma_{0y}'' = 1_{(\text{MPa})} \\ \tau_{0xy}'' = 0 \end{matrix}$$

Following the same procedure, σ''_ℓ , σ''_t , and $\tau''_{\ell t}$ are calculated in orthotropic axes of each ply orientation for an average unit stress value on the laminate that is reduced to $\sigma''_{0y} = 1 \text{ MPa}$.

- *Finally, let us consider the third state of stress:*

$$\begin{matrix} \sigma_{0x}''' = 0 \\ \sigma_{0y}''' = 0 \\ \tau_{0xy}''' = 1_{(\text{MPa})} \end{matrix}$$

Following the same procedure, σ'''_ℓ , σ'''_t , and $\tau'''_{\ell t}$ are calculated in orthotropic axis of each ply orientation for an average unit stress value applied on the laminate, which is reduced to $\tau'''_{0xy} = 1 \text{ MPa}$.

Note: In Appendix A at the end of the book are given the values $(\sigma'_\ell, \sigma'_t, \tau'_{\ell t})$, $(\sigma''_\ell, \sigma''_t, \tau''_{\ell t})$, and $(\sigma'''_\ell, \sigma'''_t, \tau'''_{\ell t})$ corresponding to the particular case of a balanced Quad carbon/epoxy laminate with various percentages of plies oriented at 0° , 90° , $+45^\circ$, and -45° . These values are available in Figures A.1–A.12.

It is then easy to determine by simple rule of proportion (or multiplication)¹⁰ the values $(\sigma_\ell \times h)$, $(\sigma_t \times h)$, and $(\tau_{\ell t} \times h)$ in each ply orientation, corresponding to loadings that are no longer unitary but equal successively to

$$N_x = (\sigma_{0x} \times h)$$

Then

$$N_y = (\sigma_{0y} \times h)$$

Then again

$$T_{xy} = (\tau_{0xy} \times h)$$

Subsequently, the **principle of superimposition** allows the determination of $(\sigma_\ell \times h)_{\text{total}}$, $(\sigma_t \times h)_{\text{total}}$, and $(\tau_{\ell t} \times h)_{\text{total}}$ in the ply orientation under consideration when N_x , N_y , and T_{xy} are applied **simultaneously** on the whole laminate. Hence, it is possible to write the modified Tsai-Hill expression for this ply orientation using Equation 12.10, which will provide the thickness needed for the laminate to avoid failure of the plies *having the orientation in consideration*.

If h_k is the value of the laminate thickness obtained from the ply orientation k , after reviewing all the orientations ($k=1 \dots n$), we will retain only the highest value

$$h_{\text{laminate}} = \sup\{h_k\}$$

Note: The calculation principle is retained even if the plies have different thicknesses with any orientations. Then, it becomes necessary to computerize the procedure or to use existing software. A complete composition of the laminate can then be proposed, and it can be verified that the solution is satisfactory with regard to the criteria mentioned above (deformation, failure). The user-friendly aspect of the software, allowing for rapid consideration of input data, makes the process easier.¹¹

12.1.4 FLEXURE BEHAVIOR

In the previous paragraph, discussion was limited to loads of N_x , N_y , and T_{xy} applied in the Mid-plane of the laminate. We will now examine the loading cases that cause out-of-plane bending of the laminate. As before, the laminate considered is supposed to have **Mid-plane symmetry**.

12.1.4.1 Displacement Field

- **Assumption:** Assume that a line perpendicular to the Mid-plane of laminate before deformation (see Figure 12.3) remains perpendicular to the mean surface that results, after bending, from the deformation of the previous Mid-plane¹².
- **Consequence:** If we denote as before by $u_0(x, y)$ and $v_0(x, y)$ the components of the displacement in the Mid-plane and by $w_0(x, y)$ the displacement out of the plane (see Figure 12.3), the displacement of any point in the laminate, with coordinate z in the undeformed configuration, can be written as

$$\begin{cases} u = u_0 - z \frac{\partial w_0}{\partial x} \\ v = v_0 - z \frac{\partial w_0}{\partial y} \\ w = w_0 \end{cases} \quad (12.11)$$

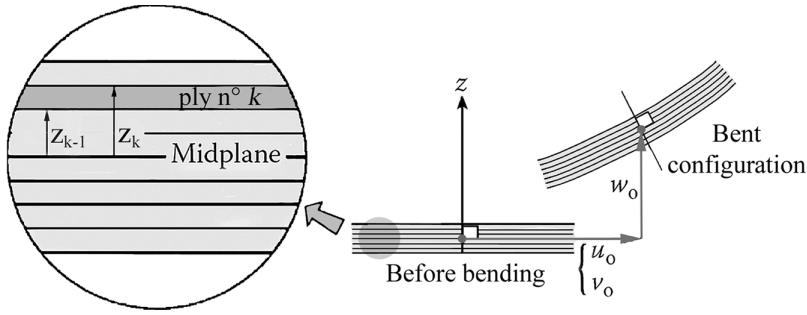


FIGURE 12.3 Bending of the laminate.

From which we deduce the nonzero strain values:

$$\begin{cases} \epsilon_x = \epsilon_{0x} - z \frac{\partial^2 w_0}{\partial x^2} \\ \epsilon_y = \epsilon_{0y} - z \frac{\partial^2 w_0}{\partial y^2} \\ \gamma_{xy} = \gamma_{0xy} - z \times 2 \frac{\partial^2 w_0}{\partial x \partial y} \end{cases} \quad (12.12)$$

12.1.4.2 Loadings

In addition to the In-plane stress resultants N_x , N_y , and T_{xy} of the previous paragraphs, we can add the **bending** and **twisting moments** per unitary width about the x - and y -directions (see Figure 12.4).

As with the In-plane resultants, the bending and twisting moments also serve to synthesize the cohesive forces that appear on cuts normal to x - and y -axes, following a classic method common to all structures (beams, plates, etc.). They should be interpreted as unitary moments of cohesive forces¹³. They are written as

- M_y , bending moment about the y -axis due to the stress σ_x , per unitary width along the y -direction:

$$M_y = \int_{-h/2}^{h/2} \sigma_x \times z \, dz \quad (12.13)$$

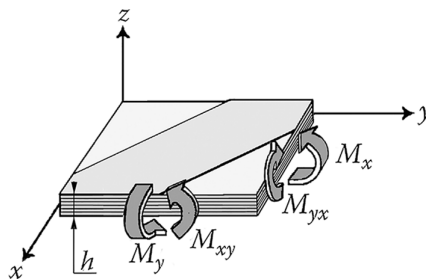


FIGURE 12.4 Bending and twisting moments.

- M_x , bending moment about the x -axis, due to the stress σ_y , per unitary width along the x -direction:

$$M_x = - \int_{-h/2}^{h/2} \sigma_y \times z \, dz \quad (12.14)$$

- M_{xy} (or $-M_{yx}$), twisting moment about the x -axis (respectively, y -axis), due to the shear stress τ_{xy} , per unitary width along the y -direction (respectively, x -direction):

$$M_{xy} = - \int_{-h/2}^{h/2} \tau_{xy} \times z \, dz \quad (12.15)$$

Taking Equation 11.8 into consideration, which allows expressing, in any coordinate system, the stress state in a ply as function of strains, the bending moment M_y (Equation 12.13) can be written as

$$M_y = \sum_{k=1st \, ply}^{nth \, ply} \left\{ \int_{z_{k-1}}^{z_k} \left(\bar{E}_{11}^k \epsilon_x + \bar{E}_{12}^k \epsilon_y + \bar{E}_{13}^k \gamma_{xy} \right) \times z \, dz \right\}$$

Which becomes, when using Equation 12.12,

$$M_y = \sum_{k=1st \, ply}^{nth \, ply} \left\{ \int_{z_{k-1}}^{z_k} \left\{ \bar{E}_{11}^k \left(z \times \epsilon_{0x} - z^2 \times \frac{\partial^2 w_0}{\partial x^2} \right) + \bar{E}_{12}^k \left(z \times \epsilon_{0y} - z^2 \times \frac{\partial^2 w_0}{\partial y^2} \right) \dots \right. \right. \\ \left. \left. \dots + \bar{E}_{13}^k \left(z \times \gamma_{0xy} - z^2 \times 2 \frac{\partial^2 w_0}{\partial x \partial y} \right) \right\} dz \right\}$$

Due to Mid-plane symmetry, every integral of the form $\int_{z_{k-1}}^{z_k} \bar{E}_{1j}^k \times z \, dz$ in the above expression can be

associated with an integral of the form $\int_{-z_k}^{-z_{k-1}} \bar{E}_{1j}^k \times z \, dz$ from opposite sign. The sum of integrals of this type is zero and only remains

$$M_y = \sum_{k=1st \, ply}^{nth \, ply} \left\{ - \bar{E}_{11}^k \frac{(z_k^3 - z_{k-1}^3)}{3} \times \frac{\partial^2 w_0}{\partial x^2} + \bar{E}_{12}^k \frac{(z_k^3 - z_{k-1}^3)}{3} \times \frac{\partial^2 w_0}{\partial y^2} \dots \right. \\ \left. \dots + \bar{E}_{13}^k \frac{(z_k^3 - z_{k-1}^3)}{3} \times 2 \frac{\partial^2 w_0}{\partial x \partial y} \right\}$$

or

$$M_y = -C_{11} \frac{\partial^2 w_0}{\partial x^2} - C_{12} \frac{\partial^2 w_0}{\partial y^2} - C_{13} \times 2 \frac{\partial^2 w_0}{\partial x \partial y}$$

with

$$C_{1j} = \sum_{k=1st \text{ ply}}^{nth \text{ ply}} \bar{E}_{1j}^k \frac{(z_k^3 - z_{k-1}^3)}{3}$$

By proceeding in a similar way with M_x and M_{xy} (Equations 12.14 and 12.15), we obtain the following matrix form:

$$\begin{Bmatrix} M_y \\ -M_x \\ -M_{xy} \end{Bmatrix} = \begin{bmatrix} C_{11} & C_{12} & C_{13} \\ C_{21} & C_{22} & C_{23} \\ C_{31} & C_{32} & C_{33} \end{bmatrix} \begin{Bmatrix} -\frac{\partial^2 w_0}{\partial x^2} \\ -\frac{\partial^2 w_0}{\partial y^2} \\ -2\frac{\partial^2 w_0}{\partial x \partial y} \end{Bmatrix} \quad (12.16)$$

with :

$$C_{ij} = \sum_{k=1st \text{ ply}}^{nth \text{ ply}} \bar{E}_{ij}^k \frac{(z_k^3 - z_{k-1}^3)}{3} = C_{ji}$$

12.1.4.3 Notes

- It can be observed in Equation 12.16 that coefficients C_{ij} **depend** on the stacking sequence of the plies.
- Does such a laminated plate bend under In-plane loading? To determine this, let us consider the flexure displacement field in order to express, for example, the stress resultant N_x (Equation 12.11). This yields

$$N_x = \sum_{k=1st \text{ ply}}^{nth \text{ ply}} \left\{ \int_{z_{k-1}}^{z_k} \left[\bar{E}_{11}^k \left(\epsilon_{0x} - z \frac{\partial^2 w_0}{\partial x^2} \right) + \bar{E}_{12}^k \left(\epsilon_{0y} - z \frac{\partial^2 w_0}{\partial y^2} \right) \right] \dots \right. \\ \left. \dots + \bar{E}_{13}^k \left(\gamma_{0xy} - z \times 2 \frac{\partial^2 w_0}{\partial x \partial y} \right) \right\} dz$$

Making use of the remark mentioned above, the Mid-plane symmetry causes the elimination of integrals of the type

$$\int_{z_{k-1}}^{z_k} \bar{E}_{1j}^k z \, dz$$

As a consequence, we find again Equation 12.4 as

$$N_1 = A_{11}\epsilon_{0x} + A_{12}\epsilon_{0y} + A_{13}\gamma_{0xy}$$

For laminates with Mid-plane symmetry, the In-plane behavior is decoupled from the flexural behavior.

- Even for the balanced laminate case (same number of plies making angle θ with the x -axis, as plies making angle $-\theta$ in addition of Mid-plane symmetry), terms C_{13} and C_{23} in Equation 12.16 are not zero. This modifies the deformed shape compared with the isotropic case as outlined in Figure 12.5.
- Terms C_{13} and C_{23} disappear only in the following cases:
 - a. The plies are oriented uniquely along the 0° and 90° directions. Then the product $\cos\theta \times \sin\theta$ is zero and¹⁴

$$\bar{E}_{13}^k = \bar{E}_{23}^k = 0 \quad \forall k$$

- b. The laminate $[0^\circ/90^\circ/+45^\circ/-45^\circ]$ is made of:
 - Balanced fabric layers (in each fabric layer, warp and weft fibers are first approximation¹⁵ overall at the same z -elevation)
 - Almost isotropic mats layers
 - A combination of the two types of layers above
- The stress state in each ply derives from Equation 11.8. For example, for ply number k ,

$$\sigma_x = \bar{E}_{11}^k \epsilon_x + \bar{E}_{12}^k \epsilon_y + \bar{E}_{13}^k \gamma_{xy}$$

And considering Equation 12.12 for the strains,

$$\begin{aligned} \sigma_x = & \left[\bar{E}_{11}^k \epsilon_{0x} + \bar{E}_{12}^k \epsilon_{0y} + \bar{E}_{13}^k \gamma_{0xy} \right] - z \left[\bar{E}_{11}^k \frac{\partial^2 w_0}{\partial x^2} \dots \right. \\ & \left. \dots + \bar{E}_{12}^k \frac{\partial^2 w_0}{\partial y^2} + \bar{E}_{13}^k \times 2 \frac{\partial^2 w_0}{\partial x \partial y} \right] \end{aligned}$$

Which can be summarized by

$$\sigma_x = \sigma_{0x} \text{ (In-plane)} + \sigma_{xf} \text{ (flexure)}$$

The stress appears, therefore, along the thickness of the laminate as the superposition of a piecewise constant distribution and a piecewise linear distribution, as seen in Figure 12.6. One can also observe analogous forms for σ_y and for τ_{xy} .

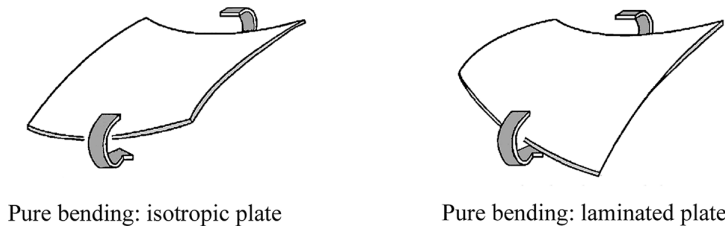


FIGURE 12.5 Isotropic and laminate plates in bending.

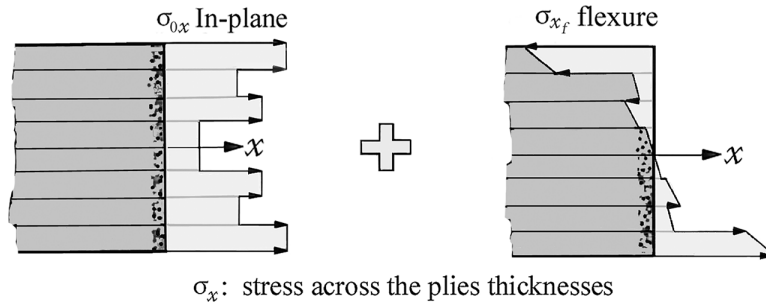


FIGURE 12.6 Total normal stress σ_x in a laminate.

12.1.5 CONSEQUENCE: PRACTICAL DETERMINATION OF A QUAD-LAMINATE SUBJECT TO FLEXURE

Givens

- The bending and twisting moments M_y , M_x , and M_{xy} are known¹⁶.
- Using these resultants leads to estimate proportions of plies for a quadrangle symmetric laminate¹⁷, and to **predict** the stacking sequence.

Principle of Calculation

- **Nonfailure of the laminate:** Following a similar approach as in Section 12.1.3, it is possible to calculate for each of the plies the stress values σ_ℓ , σ_t , and $\tau_{\ell t}$ in (ℓ, t) axes. This allows checking the ply strength using the Tsai-Hill criterion. This requires user-friendly software as already mentioned allowing optimization of the plies proportion in each direction within the laminate¹⁸.
- **Bending deformation:** Determination of the deformed configuration under bending is as complex as for an isotropic plate: apart from a few cases of academic interest, it is necessary to use a computer program based on the finite element methods¹⁹.

12.1.6 SIMPLIFIED CALCULATION FOR BENDING

It appears possible, for a first estimate, to perform simplified calculations by considering that the moment M_y is related uniquely to the curvature $(\partial^2 w_0 / \partial x^2)$, and the moment M_x to the curvature $(\partial^2 w_0 / \partial y^2)$. Then the following elements can be determined.

12.1.6.1 Apparent Failure Strength in Bending

A test conducted on a coupon provides the moment value at failure, denoted by $M_{\text{rupt.}}$ on Figure 12.7 (moment per unitary width of the sample).

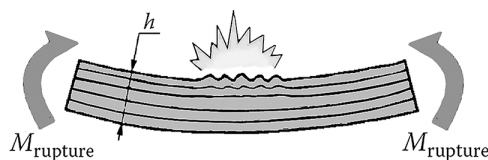


FIGURE 12.7 Bending failure.

Analogy with a beam in bending leads to

$$\|\sigma_{\text{rupt.}}\| = \frac{M_{\text{rupt.}} \times h/2}{h^3/12} \quad \text{then : } \|\sigma_{\text{rupt.}}\| = M_{\text{rupt.}} \times \frac{6}{h^2}$$

12.1.6.2 Apparent Flexure Moduli

These are obtained starting from a comparison between the behavior relationships for **composite** and for **homogeneous** samples. From Figure 12.8a, the relation between the bending moment and the curvature for a homogeneous beam with unitary width is obtained by integration of the local behavior relationship²⁰:

$$\epsilon_x = \frac{\sigma_x}{E} \rightarrow \frac{h^3 \times 1}{12} \times \frac{d^2 w_0}{dx^2} = -\frac{M_f}{E}$$

Equation 12.16 is recalled below:

$$\begin{Bmatrix} M_y \\ -M_x \\ -M_{xy} \end{Bmatrix} = [C] \begin{Bmatrix} -\partial^2 w_0 / \partial x^2 \\ -\partial^2 w_0 / \partial y^2 \\ -2 \times \partial^2 w_0 / \partial x \partial y \end{Bmatrix}$$

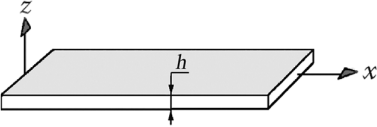
We note that it can be inverted, and by writing,

$$[C]^{-1} = \begin{bmatrix} 1/\overline{EI}_{11} & 1/\overline{EI}_{12} & 1/\overline{EI}_{13} \\ 1/\overline{EI}_{21} & 1/\overline{EI}_{22} & 1/\overline{EI}_{23} \\ 1/\overline{EI}_{31} & 1/\overline{EI}_{32} & 1/\overline{EI}_{33} \end{bmatrix}$$

We obtain

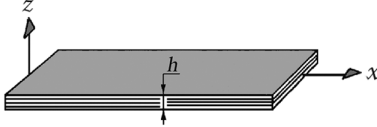
$$\frac{\partial^2 w_0}{\partial x^2} = \frac{-1}{\overline{EI}_{11}} \times M_y + \frac{1}{\overline{EI}_{12}} \times M_x + \frac{1}{\overline{EI}_{13}} \times M_{xy}$$

By comparing the Equation noted in Figure 12.8a with only the first part (moment M_y) on the right-hand side of Equation in Figure 12.8b,



(a)

$$\frac{d^2 w_0}{dx^2} = -\frac{M_f}{E \times \left(\frac{h^3 \times 1}{12}\right)}$$



(b)

$$\frac{\partial^2 w_0}{\partial x^2} = \frac{-1}{\overline{EI}_{11}} M_y \dots + \left(\frac{1}{\overline{EI}_{12}} M_x + \frac{1}{\overline{EI}_{13}} M_{xy} \right)$$

FIGURE 12.8 (a) Homogeneous and (b) laminated beam.

$$\overline{EI}_{11} \Leftrightarrow E \times \frac{h^3 \times 1}{12}$$

we obtain an approximate form for a modulus E that can be interpreted as a **flexure modulus** along the x -direction of the homogenized material:

$$E_{\text{flexure along } x} = \frac{12}{h^3} \times \overline{EI}_{11}$$

Note: When the plies of the laminate have only orientations 0° and 90° , or when the laminate $[0^\circ/90^\circ/+45^\circ/-45^\circ]$ is made only of balanced fabrics and of mats, excluding the unidirectional layers, we then have in matrix $[C]$

$$C_{13} = C_{23} = 0$$

Then

$$\frac{1}{\overline{EI}_{11}} = \frac{C_{22}}{C_{11}C_{22} - C_{12}^2}$$

$$\overline{EI}_{11} = C_{11} - \frac{C_{12}^2}{C_{22}}$$

12.1.7 THERMOMECHANICAL LOADING CASE

12.1.7.1 In-plane Behavior

When temperature variation has to be taken into account, the latter being assumed **identical** in all plies of the laminate, the stresses are given by the modified Equations 11.10. Following the procedure of Section 12.1.1, with the same assumptions and notations, the stress resultant N_x (Equation 12.1) becomes

$$N_x = \sum_{k=1st \text{ ply}}^{nth \text{ ply}} \left\{ \overline{E}_{11}^k \epsilon_{0x} + \overline{E}_{12}^k \epsilon_{0y} + \overline{E}_{13}^k \gamma_{0xy} \right\} \times e_k - \Delta T \sum_{k=1st \text{ ply}}^{nth \text{ ply}} \overline{\alpha E}_1^k \times e_k$$

Then

$$N_x = A_{11} \epsilon_{0x} + A_{12} \epsilon_{0y} + A_{13} \gamma_{0xy} - \Delta T \times \langle \alpha E h \rangle_x$$

with

$$A_{1j} = \sum_{k=1st \text{ ply}}^{nth \text{ ply}} \overline{E}_{1j}^k e_k; \quad \langle \alpha E h \rangle_x = \sum_{k=1st \text{ ply}}^{nth \text{ ply}} \overline{\alpha E}_1^k \times e_k$$

Following the same procedure for N_y and T_{xy} , the In-plane resultants are expressed as

$$\begin{Bmatrix} N_x \\ N_y \\ T_{xy} \end{Bmatrix} = \begin{bmatrix} A_{11} & A_{12} & A_{13} \\ A_{21} & A_{22} & A_{23} \\ A_{31} & A_{32} & A_{33} \end{bmatrix} \begin{Bmatrix} \epsilon_{0x} \\ \epsilon_{0y} \\ \gamma_{0xy} \end{Bmatrix} - \Delta T \begin{Bmatrix} \langle \alpha E h \rangle_x \\ \langle \alpha E h \rangle_y \\ \langle \alpha E h \rangle_{xy} \end{Bmatrix}$$

with :

$$A_{ij} = \sum_{k=1 \text{st ply}}^{n \text{th ply}} \bar{E}_{ij}^k \times e_k = A_{ji} \quad \text{cf. [11.8]} \quad (12.17)$$

$$\left. \begin{aligned} \langle \alpha E h \rangle_x &= \sum_{k=1 \text{st ply}}^{n \text{th ply}} \bar{\alpha E}_1^k \times e_k \\ \langle \alpha E h \rangle_y &= \sum_{k=1 \text{st ply}}^{n \text{th ply}} \bar{\alpha E}_2^k \times e_k \\ \langle \alpha E h \rangle_{xy} &= \sum_{k=1 \text{st ply}}^{n \text{th ply}} \bar{\alpha E}_3^k \times e_k \end{aligned} \right\} \quad \text{cf. [11.10]}$$

Inversion of the above relation allows highlighting, in addition to the apparent moduli of the laminate (see Section 12.1.2), the In-plane thermal strain:

$$\begin{Bmatrix} \epsilon_{0x} \\ \epsilon_{0y} \\ \gamma_{0xy} \end{Bmatrix} = h[A]^{-1} \begin{Bmatrix} \sigma_{0x} \\ \sigma_{0y} \\ \tau_{0xy} \end{Bmatrix} + \Delta T[A]^{-1} \begin{Bmatrix} \langle \alpha E h \rangle_x \\ \langle \alpha E h \rangle_y \\ \langle \alpha E h \rangle_{xy} \end{Bmatrix}$$

or with Equation 12.9

$$\begin{Bmatrix} \epsilon_{0x} \\ \epsilon_{0y} \\ \gamma_{0xy} \end{Bmatrix} = \begin{bmatrix} \frac{1}{\bar{E}_x} & -\frac{\bar{\nu}_{yx}}{\bar{E}_y} & \frac{\bar{\eta}_{xy}}{\bar{G}_{xy}} \\ -\frac{\bar{\nu}_{xy}}{\bar{E}_x} & \frac{1}{\bar{E}_y} & \frac{\bar{\mu}_{xy}}{\bar{G}_{xy}} \\ \frac{\bar{\eta}_x}{\bar{E}_x} & \frac{\bar{\mu}_y}{\bar{E}_y} & \frac{1}{\bar{G}_{xy}} \end{bmatrix} \begin{Bmatrix} \sigma_{0x} \\ \sigma_{0y} \\ \tau_{0xy} \end{Bmatrix} + \Delta T[A]^{-1} \begin{Bmatrix} \langle \alpha E h \rangle_x \\ \langle \alpha E h \rangle_y \\ \langle \alpha E h \rangle_{xy} \end{Bmatrix}$$

which can be rewritten as

$$\begin{Bmatrix} \epsilon_{0x} \\ \epsilon_{0y} \\ \gamma_{0xy} \end{Bmatrix} = h[A]^{-1} \begin{Bmatrix} \sigma_{0x} \\ \sigma_{0y} \\ \tau_{0xy} \end{Bmatrix} + \Delta T \times h[A]^{-1} \begin{Bmatrix} \frac{1}{h} \langle \alpha E h \rangle_x \\ \frac{1}{h} \langle \alpha E h \rangle_y \\ \frac{1}{h} \langle \alpha E h \rangle_{xy} \end{Bmatrix}$$

Notes

- Evaluation of terms $(1/h)\langle\alpha Eh\rangle_x$, $(1/h)\langle\alpha Eh\rangle_y$, and $(1/h)\langle\alpha Eh\rangle_{xy}$ only requires the knowledge of ply **proportions** along the different orientations and not the knowledge of thicknesses²¹.
- The matrix $h[A]^{-1}$ already mentioned in Section 12.1.2 contains the global moduli of the laminate. Then we can write (see Equation 12.9)

$$\begin{Bmatrix} \epsilon_{0x} \\ \epsilon_{0y} \\ \gamma_{0xy} \end{Bmatrix} = \begin{bmatrix} \frac{1}{\bar{E}_x} & -\frac{\bar{\nu}_{yx}}{\bar{E}_y} & \frac{\bar{\eta}_{xy}}{\bar{G}_{xy}} \\ -\frac{\bar{\nu}_{xy}}{\bar{E}_x} & \frac{1}{\bar{E}_y} & \frac{\bar{\mu}_{xy}}{\bar{G}_{xy}} \\ \frac{\bar{\eta}_x}{\bar{E}_x} & \frac{\bar{\mu}_y}{\bar{E}_y} & \frac{1}{\bar{G}_{xy}} \end{bmatrix} \begin{Bmatrix} \sigma_{0x} \\ \sigma_{0y} \\ \tau_{0xy} \end{Bmatrix} + \Delta T \begin{bmatrix} \frac{1}{\bar{E}_x} & -\frac{\bar{\nu}_{yx}}{\bar{E}_y} & \frac{\bar{\eta}_{xy}}{\bar{G}_{xy}} \\ -\frac{\bar{\nu}_{xy}}{\bar{E}_x} & \frac{1}{\bar{E}_y} & \frac{\bar{\mu}_{xy}}{\bar{G}_{xy}} \\ \frac{\bar{\eta}_x}{\bar{E}_x} & \frac{\bar{\mu}_y}{\bar{E}_y} & \frac{1}{\bar{G}_{xy}} \end{bmatrix} \begin{Bmatrix} \frac{1}{h}\langle\alpha Eh\rangle_x \\ \frac{1}{h}\langle\alpha Eh\rangle_y \\ \frac{1}{h}\langle\alpha Eh\rangle_{xy} \end{Bmatrix}$$

The last part of the right-hand side of equation above allows to note the global thermal expansion coefficients of the laminate, which are denoted as α_{0x} , α_{0y} , and α_{0xy} , with the correspondence

$$\begin{Bmatrix} \alpha_{0x} \\ \alpha_{0y} \\ \alpha_{0xy} \end{Bmatrix} = \begin{bmatrix} \frac{1}{\bar{E}_x} & -\frac{\bar{\nu}_{yx}}{\bar{E}_y} & \frac{\bar{\eta}_{xy}}{\bar{G}_{xy}} \\ -\frac{\bar{\nu}_{xy}}{\bar{E}_x} & \frac{1}{\bar{E}_y} & \frac{\bar{\mu}_{xy}}{\bar{G}_{xy}} \\ \frac{\bar{\eta}_x}{\bar{E}_x} & \frac{\bar{\mu}_y}{\bar{E}_y} & \frac{1}{\bar{G}_{xy}} \end{bmatrix} \begin{Bmatrix} \frac{1}{h}\langle\alpha Eh\rangle_x \\ \frac{1}{h}\langle\alpha Eh\rangle_y \\ \frac{1}{h}\langle\alpha Eh\rangle_{xy} \end{Bmatrix} \quad (12.18)$$

In summary, the thermomechanical In-plane behavior of a laminate with Mid-plane symmetry can be written as

$$\begin{Bmatrix} \epsilon_{0x} \\ \epsilon_{0y} \\ \gamma_{0xy} \end{Bmatrix} = \begin{bmatrix} \frac{1}{\bar{E}_x} & -\frac{\bar{\nu}_{yx}}{\bar{E}_y} & \frac{\bar{\eta}_{xy}}{\bar{G}_{xy}} \\ -\frac{\bar{\nu}_{xy}}{\bar{E}_x} & \frac{1}{\bar{E}_y} & \frac{\bar{\mu}_{xy}}{\bar{G}_{xy}} \\ \frac{\bar{\eta}_x}{\bar{E}_x} & \frac{\bar{\mu}_y}{\bar{E}_y} & \frac{1}{\bar{G}_{xy}} \end{bmatrix} \begin{Bmatrix} \sigma_{0x} \\ \sigma_{0y} \\ \tau_{0xy} \end{Bmatrix} + \Delta T \begin{Bmatrix} \alpha_{0x} \\ \alpha_{0y} \\ \alpha_{0xy} \end{Bmatrix} \quad (12.19)$$

In which, Equations 12.17 and 12.18 give α_{0x} , α_{0y} , and α_{0xy} ²².

12.1.7.2 Behavior under Bending

Following the procedure in Section 12.1.4 with the same notations, the bending moment M_y (Equation 12.13) becomes, using the modified Equations 11.10,

$$M_y = \sum_{k=1st\ ply}^{nth\ ply} \left\{ \int_{z_{k-1}}^{z_k} (\bar{E}_{11}^k \epsilon_x + \bar{E}_{12}^k \epsilon_y + \bar{E}_{13}^k \gamma_{xy}) \times z \, dz \right\} \dots$$

$$\dots - \Delta T \sum_{k=1st\ ply}^{nth\ ply} \left(\int_{z_{k-1}}^{z_k} \alpha \bar{E}_1^k \times z \, dz \right)$$

The plate being assumed having Mid-plane symmetry, any integral of the form $\int_{z_{k-1}}^{z_k} \overline{\alpha E_1^k} z \, dz$ at the right-hand side of equation is associated with another integral such as $\int_{-z_k}^{-z_{k-1}} \overline{\alpha E_1^k} z \, dz$ that is equal and opposite in sign. After calculation, only the following expression with notations of Section 12.1.4 remains:

$$M_y = -C_{11} \frac{\partial^2 w_0}{\partial x^2} - C_{12} \frac{\partial^2 w_0}{\partial y^2} - C_{13} \times 2 \frac{\partial^2 w_0}{\partial x \partial y}$$

Due to the Mid-plane symmetry, the behavior under bending (Equation 12.16) is unchanged when the laminate is subjected to thermomechanical loading.

Note: Bear in mind that the temperature field is assumed uniform through thickness of the laminate.

12.1.8 HYGROTHERMAL LOADING CASE

When taking into account variations in the moisture content of the laminate, hygrometric behavior of plies has to be included in the preceding calculations by introducing the coefficients of moisture expansion and the increase in moisture concentration ΔM_c (see Section 10.6).

Equations 11.12 give the stresses. Following the procedure of Section 12.1.7, with the same assumptions and notations we obtain:

a. In place of 12.17:

$$\begin{Bmatrix} N_x \\ N_y \\ T_{xy} \end{Bmatrix} = \begin{bmatrix} A_{11} & A_{12} & A_{13} \\ A_{21} & A_{22} & A_{23} \\ A_{31} & A_{32} & A_{33} \end{bmatrix} \begin{Bmatrix} \epsilon_{0x} \\ \epsilon_{0y} \\ \gamma_{0xy} \end{Bmatrix} - \Delta T \begin{Bmatrix} \langle \alpha E h \rangle_x \\ \langle \alpha E h \rangle_y \\ \langle \alpha E h \rangle_{xy} \end{Bmatrix} - \Delta M_c \begin{Bmatrix} \langle \beta E h \rangle_x \\ \langle \beta E h \rangle_y \\ \langle \beta E h \rangle_{xy} \end{Bmatrix}$$

$$A_{ij} = \sum_{k=1st \text{ ply}}^{nth \text{ ply}} \overline{E}_{ij}^k \times e_k = A_{ji} \quad cf. [11.8]$$

$$\left. \begin{aligned} \langle \alpha E h \rangle_x &= \sum_{k=1st \text{ ply}}^{nth \text{ ply}} \overline{\alpha E}_1^k \times e_k \\ \langle \alpha E h \rangle_y &= \sum_{k=1st \text{ ply}}^{nth \text{ ply}} \overline{\alpha E}_2^k \times e_k \\ \langle \alpha E h \rangle_{xy} &= \sum_{k=1st \text{ ply}}^{nth \text{ ply}} \overline{\alpha E}_3^k \times e_k \end{aligned} \right\} cf. [11.10]$$

$$\left. \begin{aligned} \langle \beta E h \rangle_x &= \sum_{k=1st \text{ ply}}^{nth \text{ ply}} \overline{\beta E}_1^k \times e_k \\ \langle \beta E h \rangle_y &= \sum_{k=1st \text{ ply}}^{nth \text{ ply}} \overline{\beta E}_2^k \times e_k \\ \langle \beta E h \rangle_{xy} &= \sum_{k=1st \text{ ply}}^{nth \text{ ply}} \overline{\beta E}_3^k \times e_k \end{aligned} \right\} cf. [11.12]$$

b. In place of 12.18:

$$\left\{ \begin{array}{c} \alpha_{0x} \\ \alpha_{0y} \\ \alpha_{0xy} \end{array} \right\} = \left[\begin{array}{ccc} \frac{1}{\bar{E}_x} & -\frac{\bar{\nu}_{yx}}{\bar{E}_y} & \frac{\bar{\eta}_{xy}}{\bar{G}_{xy}} \\ -\frac{\bar{\nu}_{xy}}{\bar{E}_x} & \frac{1}{\bar{E}_y} & \frac{\bar{\mu}_{xy}}{\bar{G}_{xy}} \\ \frac{\bar{\eta}_x}{\bar{E}_x} & \frac{\bar{\mu}_y}{\bar{E}_y} & \frac{1}{\bar{G}_{xy}} \end{array} \right] \left\{ \begin{array}{c} \frac{1}{h} \langle \alpha E h \rangle_x \\ \frac{1}{h} \langle \alpha E h \rangle_y \\ \frac{1}{h} \langle \alpha E h \rangle_{xy} \end{array} \right\}$$

$$\left\{ \begin{array}{c} \beta_{0x} \\ \beta_{0y} \\ \beta_{0xy} \end{array} \right\} = \left[\begin{array}{ccc} \frac{1}{\bar{E}_x} & -\frac{\bar{\nu}_{yx}}{\bar{E}_y} & \frac{\bar{\eta}_{xy}}{\bar{G}_{xy}} \\ -\frac{\bar{\nu}_{xy}}{\bar{E}_x} & \frac{1}{\bar{E}_y} & \frac{\bar{\mu}_{xy}}{\bar{G}_{xy}} \\ \frac{\bar{\eta}_x}{\bar{E}_x} & \frac{\bar{\mu}_y}{\bar{E}_y} & \frac{1}{\bar{G}_{xy}} \end{array} \right] \left\{ \begin{array}{c} \frac{1}{h} \langle \beta E h \rangle_x \\ \frac{1}{h} \langle \beta E h \rangle_y \\ \frac{1}{h} \langle \beta E h \rangle_{xy} \end{array} \right\}$$

c. In place of 12.19:

$$\left\{ \begin{array}{c} \epsilon_{0x} \\ \epsilon_{0y} \\ \gamma_{0xy} \end{array} \right\} = \left[\begin{array}{ccc} \frac{1}{\bar{E}_x} & -\frac{\bar{\nu}_{yx}}{\bar{E}_y} & \frac{\bar{\eta}_{xy}}{\bar{G}_{xy}} \\ -\frac{\bar{\nu}_{xy}}{\bar{E}_x} & \frac{1}{\bar{E}_y} & \frac{\bar{\mu}_{xy}}{\bar{G}_{xy}} \\ \frac{\bar{\eta}_x}{\bar{E}_x} & \frac{\bar{\mu}_y}{\bar{E}_y} & \frac{1}{\bar{G}_{xy}} \end{array} \right] \left\{ \begin{array}{c} \sigma_{0x} \\ \sigma_{0y} \\ \tau_{0xy} \end{array} \right\} + \Delta T \left\{ \begin{array}{c} \alpha_{0x} \\ \alpha_{0y} \\ \alpha_{0xy} \end{array} \right\} + \Delta M_c \left\{ \begin{array}{c} \beta_{0x} \\ \beta_{0y} \\ \beta_{0xy} \end{array} \right\}$$

12.2 LAMINATE WITHOUT MID-PLANE SYMMETRY

12.2.1 COUPLED IN-PLANE-FLEXURE BEHAVIOR

If we consider the calculations of Section 12.1.4 without Mid-plane symmetry, we note again the presence of integrals as

$$\int_{z_{k-1}}^{z_k} \bar{E}_{ij}^k z \times dz = \bar{E}_{ij}^k \left(\frac{z_k^2 - z_{k-1}^2}{2} \right)$$

This characterizes each ply k . This time, after summing over all plies of the laminate, these integrals bring to nonzero terms with the form

$$B_{ij} = \sum_{k=\text{1st ply}}^{\text{nth ply}} \bar{E}_{ij}^k \left(\frac{z_k^2 - z_{k-1}^2}{2} \right) = B_{ji}$$

Thus, the development of the bending moment M_y will be (see Section 12.1.4)

$$M_y = -C_{11} \frac{\partial^2 w_0}{\partial x^2} - C_{12} \frac{\partial^2 w_0}{\partial y^2} - C_{13} \times 2 \frac{\partial^2 w_0}{\partial x \partial y} + B_{11} \epsilon_{0x} + B_{12} \epsilon_{0y} + B_{13} \gamma_{0xy}$$

It should be noted in this relationship the coupling between bending and In-plane behavior.

In a similar manner, the normal stress resultant N_x that was developed in Section 12.1.4 is rewritten as

$$N_x = A_{11} \epsilon_{0x} + A_{12} \epsilon_{0y} + A_{13} \gamma_{0xy} - B_{11} \frac{\partial^2 w_0}{\partial x^2} - B_{12} \frac{\partial^2 w_0}{\partial y^2} - B_{13} \times 2 \frac{\partial^2 w_0}{\partial x \partial y}$$

where the previous coupling occurs again.

By using the same approach for M_x , M_{xy} , N_y , and T_{xy} , the relationships obtained can be grouped, bringing to the global behavior relationship hereafter:

$\begin{Bmatrix} N_x \\ N_y \\ T_{xy} \\ M_y \\ -M_x \\ -M_{xy} \end{Bmatrix} = \begin{bmatrix} [A]_{(3 \times 3)} & [B]_{(3 \times 3)} \\ [B]_{(3 \times 3)} & [C]_{(3 \times 3)} \end{bmatrix} \begin{Bmatrix} \epsilon_{0x} \\ \epsilon_{0y} \\ \gamma_{0xy} \\ -\partial^2 w_0 / \partial x^2 \\ -\partial^2 w_0 / \partial y^2 \\ -2\partial^2 w_0 / \partial x \partial y \end{Bmatrix}$		
$A_{ij} = \sum_{k=1st \text{ ply}}^{nth \text{ ply}} \bar{E}_{ij}^k e_k$	$C_{ij} = \sum_{k=1st \text{ ply}}^{nth \text{ ply}} \bar{E}_{ij}^k \left(\frac{z_k^3 - z_{k-1}^3}{3} \right)$	$B_{ij} = \sum_{k=1st \text{ ply}}^{nth \text{ ply}} \bar{E}_{ij}^k \left(\frac{z_k^2 - z_{k-1}^2}{2} \right)$

(12.20)

12.2.2 CASE OF THERMOMECHANICAL LOADING

Considering the development for the bending moment M_y as shown in Section 12.1.7.2, the following integral forms are found for each ply k :

$$\int_{z_{k-1}}^{z_k} \bar{\alpha E}_1^k \times z \, dz = \bar{\alpha E}_1^k \left(\frac{z_k^2 - z_{k-1}^2}{2} \right)$$

After summing over all plies of the laminate, it appears a nonzero term as

$$\langle \alpha E h^2 \rangle_x = \sum_{k=1st \text{ ply}}^{nth \text{ ply}} \bar{\alpha E}_1^k \left(\frac{z_k^2 - z_{k-1}^2}{2} \right)$$

A similar development for the other stress resultants and moments leads to the following relationship, characterizing the thermomechanical behavior:

$$\begin{Bmatrix} N_x \\ N_y \\ T_{xy} \\ M_y \\ -M_x \\ -M_{xy} \end{Bmatrix} = \begin{bmatrix} [A]_{(3 \times 3)} & [B]_{(3 \times 3)} \\ [B]_{(3 \times 3)} & [C]_{(3 \times 3)} \end{bmatrix} \begin{Bmatrix} \epsilon_{0,x} \\ \epsilon_{0,y} \\ \gamma_{0,xy} \\ -\partial^2 w_0 / \partial x^2 \\ -\partial^2 w_0 / \partial y^2 \\ -2\partial^2 w_0 / \partial x \partial y \end{Bmatrix} - \Delta T \begin{Bmatrix} \langle \alpha E h \rangle_x \\ \langle \alpha E h \rangle_y \\ \langle \alpha E h \rangle_{xy} \\ \langle \alpha E h^2 \rangle_x \\ \langle \alpha E h^2 \rangle_y \\ \langle \alpha E h^2 \rangle_{xy} \end{Bmatrix}$$

$$A_{ij} = \sum_{k=1 \text{st ply}}^{n \text{th ply}} \bar{E}_{ij}^k e_k$$

$$C_{ij} = \sum_{k=1 \text{st ply}}^{n \text{th ply}} \bar{E}_{ij}^k \left(\frac{z_k^3 - z_{k-1}^3}{3} \right)$$

$$B_{ij} = \sum_{k=1 \text{st ply}}^{n \text{th ply}} \bar{E}_{ij}^k \left(\frac{z_k^2 - z_{k-1}^2}{2} \right)$$

$$\langle \alpha E h \rangle_x = \sum_{k=1 \text{st to } n \text{th ply}} \bar{\alpha E}_1^k e_k$$

$$\langle \alpha E h \rangle_y = \sum_{k=1 \text{st to } n \text{th ply}} \bar{\alpha E}_2^k e_k$$

$$\langle \alpha E h \rangle_{xy} = \sum_{k=1 \text{st to } n \text{th ply}} \bar{\alpha E}_3^k e_k$$

$$\langle \alpha E h^2 \rangle_x = \sum_{k=1 \text{st to } n \text{th ply}} \bar{\alpha E}_1^k \left(\frac{z_k^2 - z_{k-1}^2}{2} \right)$$

$$\langle \alpha E h^2 \rangle_y = \sum_{k=1 \text{st to } n \text{th ply}} \bar{\alpha E}_2^k \left(\frac{z_k^2 - z_{k-1}^2}{2} \right)$$

$$\langle \alpha E h^2 \rangle_{xy} = \sum_{k=1 \text{st to } n \text{th ply}} \bar{\alpha E}_3^k \left(\frac{z_k^2 - z_{k-1}^2}{2} \right)$$

(12.21)

12.2.3 HYGROTHERMAL LOADING CASE

Hygrometric behavior of plies has to be included in the preceding calculations. Recalling below the stresses expressed from Equation 11.12

$$\begin{Bmatrix} \sigma_x \\ \sigma_y \\ \tau_{xy} \end{Bmatrix} = \begin{bmatrix} \bar{E}_{11} & \bar{E}_{12} & \bar{E}_{13} \\ \bar{E}_{21} & \bar{E}_{22} & \bar{E}_{23} \\ \bar{E}_{31} & \bar{E}_{32} & \bar{E}_{33} \end{bmatrix} \begin{Bmatrix} \epsilon_x \\ \epsilon_y \\ \gamma_{xy} \end{Bmatrix} - \Delta T \begin{Bmatrix} \bar{\alpha E}_1 \\ \bar{\alpha E}_2 \\ \bar{\alpha E}_3 \end{Bmatrix} - \Delta M_c \begin{Bmatrix} \bar{\beta E}_1 \\ \bar{\beta E}_2 \\ \bar{\beta E}_3 \end{Bmatrix}$$

By following the procedure of the preceding sections, one obtains the behavior equations taking into account the hygrothermal effects:

$$\begin{Bmatrix} N_x \\ N_y \\ T_{xy} \\ M_y \\ -M_x \\ -M_{xy} \end{Bmatrix} = \begin{bmatrix} [A]_{(3 \times 3)} & [B]_{(3 \times 3)} \\ [B]_{(3 \times 3)} & [C]_{(3 \times 3)} \end{bmatrix} \begin{Bmatrix} \epsilon_{0x} \\ \epsilon_{0y} \\ \gamma_{0xy} \\ -\partial^2 w_0 / \partial x^2 \\ -\partial^2 w_0 / \partial y^2 \\ -2\partial^2 w_0 / \partial x \partial y \end{Bmatrix} - \Delta T \begin{Bmatrix} \langle \alpha E h \rangle_x \\ \langle \alpha E h \rangle_y \\ \langle \alpha E h \rangle_{xy} \\ \langle \alpha E h^2 \rangle_x \\ \langle \alpha E h^2 \rangle_y \\ \langle \alpha E h^2 \rangle_{xy} \end{Bmatrix} - \Delta M_c \begin{Bmatrix} \langle \beta E h \rangle_x \\ \langle \beta E h \rangle_y \\ \langle \beta E h \rangle_{xy} \\ \langle \beta E h^2 \rangle_x \\ \langle \beta E h^2 \rangle_y \\ \langle \beta E h^2 \rangle_{xy} \end{Bmatrix}$$

$$A_{ij} = \sum_{k=1st \text{ to } nth \text{ ply}} \bar{E}_{ij}^k e_k \quad C_{ij} = \sum_{k=1st \text{ to } nth \text{ ply}} \bar{E}_{ij}^k \left(\frac{z_k^3 - z_{k-1}^3}{3} \right) \quad B_{ij} = \sum_{k=1st \text{ to } nth \text{ ply}} \bar{E}_{ij}^k \left(\frac{z_k^2 - z_{k-1}^2}{2} \right)$$

$$\langle \alpha E h \rangle_x = \sum_{k=1st \text{ to } nth \text{ ply}} \bar{\alpha E}_1^k e_k \quad \langle \beta E h \rangle_x = \sum_{k=1st \text{ to } nth \text{ ply}} \bar{\beta E}_1^k e_k$$

$$\langle \alpha E h \rangle_y = \sum_{k=1st \text{ to } nth \text{ ply}} \bar{\alpha E}_2^k e_k \quad \langle \beta E h \rangle_y = \sum_{k=1st \text{ to } nth \text{ ply}} \bar{\beta E}_2^k e_k$$

$$\langle \alpha E h \rangle_{xy} = \sum_{k=1st \text{ to } nth \text{ ply}} \bar{\alpha E}_3^k e_k \quad \langle \beta E h \rangle_{xy} = \sum_{k=1st \text{ to } nth \text{ ply}} \bar{\beta E}_3^k e_k$$

$$\langle \alpha E h^2 \rangle_x = \sum_{k=1st \text{ to } nth \text{ ply}} \bar{\alpha E}_1^k \left(\frac{z_k^2 - z_{k-1}^2}{2} \right) \quad \langle \beta E h^2 \rangle_x = \sum_{k=1st \text{ to } nth \text{ ply}} \bar{\beta E}_1^k \left(\frac{z_k^2 - z_{k-1}^2}{2} \right)$$

$$\langle \alpha E h^2 \rangle_y = \sum_{k=1st \text{ to } nth \text{ ply}} \bar{\alpha E}_2^k \left(\frac{z_k^2 - z_{k-1}^2}{2} \right) \quad \langle \beta E h^2 \rangle_y = \sum_{k=1st \text{ to } nth \text{ ply}} \bar{\beta E}_2^k \left(\frac{z_k^2 - z_{k-1}^2}{2} \right)$$

$$\langle \alpha E h^2 \rangle_{xy} = \sum_{k=1st \text{ to } nth \text{ ply}} \bar{\alpha E}_3^k \left(\frac{z_k^2 - z_{k-1}^2}{2} \right) \quad \langle \beta E h^2 \rangle_{xy} = \sum_{k=1st \text{ to } nth \text{ ply}} \bar{\beta E}_3^k \left(\frac{z_k^2 - z_{k-1}^2}{2} \right)$$

\bar{E}_{ij}^k are defined in Equation 11.8; $\bar{\alpha E}_i^k$ and $\bar{\beta E}_i^k$ are defined in Equation 11.12

(12.22)

NOTES

- 1 See Section 5.2.
- 2 For stability criteria of the loaded laminate (buckling criteria), not discussed in this chapter, see Appendix B.
- 3 Or **mirror symmetry** property; see Section 5.2.3.
- 4 The entire expressions of \bar{E}_{ij}^k are given in Equation 11.8.
- 5 See Figure 12.1 and Figure in Equation 11.8.
- 6 See Section 5.4.3.
- 7 For the Tsai-Hill failure criterion, see Section 5.3.2 and the detailed explanation in Section 14.3.

8 We can read directly these moduli in Tables 5.1 through 5.15 of Section 5.4.2 for balanced quadrangle symmetric laminates of carbon, Kevlar®, and glass/epoxy with $V_f = 60\%$ fiber volume fraction. As already mentioned in Section 5.4.2, for other marketed reinforcements not detailed in this book, a dedicated free access calculation tool can be readily download: www.think-composites.com (See Bibliography: S. Tsai et al., Composite Laminate Theory and Practice of Analysis, Design and Automated Lay-up, 2017).

9 This calculation can be easily computerized: see Application 20.2.

10 For example, noting the following correspondence,

$$\sigma'_{0x} = 1 \text{ MPa} \rightarrow \sigma'_\ell, \sigma'_t, \tau'_{\ell t}$$

$$\sigma_{0x} (\text{MPa}) \rightarrow \sigma_\ell, \sigma_t, \tau_{\ell t}$$

$$\text{then } \frac{\sigma_{0x}}{\sigma'_{0x}} = \frac{\sigma_\ell}{\sigma'_\ell} \Rightarrow \sigma_\ell = \sigma'_\ell \times \frac{\sigma_{0x}}{1}, \quad \text{thus } h\sigma_\ell = \frac{\sigma'_\ell}{1} \times N_x$$

11 See footnote in Section 12.1.3.3.

12 Such a simplification will be questioned in Chapter 18.

13 In this way, M_y is written in integral form as

$$M_y = \left[\int_{-h/2}^{h/2} z \bar{z} \wedge \sigma_x \bar{x} dz \right] \cdot \bar{y} = \int_{-h/2}^{h/2} \sigma_x z dz \quad \text{Also, } M_x = \left[\int_{-h/2}^{h/2} z \bar{z} \wedge \sigma_y \bar{y} dz \right] \cdot \bar{x} = - \int_{-h/2}^{h/2} \sigma_y z dz \quad \text{And finally,}$$

$$M_{xy} = \left[\int_{-h/2}^{h/2} z \bar{z} \wedge \tau_{xy} \bar{y} dz \right] \cdot \bar{x} = - \int_{-h/2}^{h/2} \tau_{xy} z dz$$

14 See Equations 11.8.

15 See Section 5.2.3.5.

16 For example, as nodal forces obtained from finite element analysis.

17 See Section 5.2. For a more general framework, see Chapter 15.

18 See footnote in Section 12.1.3.3.

19 These elements are constituted on the basis presented above and can include other effects that were not taken into account previously: in particular, the transverse shear stress in flexure due to the transverse shear stress resultants as seen in Chapter 18.

20 Recall that $\epsilon_x = \partial u / \partial x$ with $u = -z \times (dw_0/dx)$; then $z^2 \times (d^2 w_0/dx^2) = -z \times (\sigma_x/E)$, which can be integrated through the thickness.

21 See Application 20.4.

22 In Charts 5.4, 5.9, and 5.14 of Section 5.4 are given the values of thermal expansion coefficients for balanced quadrangle symmetric laminates made of carbon/epoxy, Kevlar/epoxy, and glass/epoxy with $V_f = 60\%$ fiber volume fraction. For other marketed reinforcements not detailed in this book, see footnote in Section 12.1.3.3.



Taylor & Francis

Taylor & Francis Group

<http://taylorandfrancis.com>

Part III

Justifications, D-D Laminates, Composite beams, and Transverse Shear Behavior of Multilayered Plates

A number of elements of fundamental interest for a better understanding of the calculation principles applied to composite parts have been grouped in this section. Chapters 13 and 14 relate to anisotropic properties and strength properties of orthotropic materials and then of transversely isotropic materials. Chapter 15 is devoted to quasi-orthotropic laminates also called “Double-Double”. It presents the recent work initiated by Pr. SW Tsai in order to define and manufacture more efficient and lighter laminates. Based on an original approach, Chapters 16 and 17 demonstrate that slender composite parts regarded as beams can be **homogenized**, making their study similar to ordinary homogeneous beams in classic literature. Finally, Chapter 18 based on a similar original approach describes the transverse shear behavior of laminated plates subject to transverse or buckling loads.



Taylor & Francis

Taylor & Francis Group

<http://taylorandfrancis.com>

13 Elastic Coefficients

A linear elastic anisotropic medium was defined in Chapter 9. At that stage, we reported, without justification, the elastic behavior relationships characterizing the particular case of orthotropic materials, then isotropic transverse. We propose now to examine more closely the elastic constants that appear in stress–strain relationship for these materials. In the case of transversely isotropic materials, we will study also the manner in which the constants change with the coordinate system.

13.1 ELASTIC COEFFICIENTS FOR AN ORTHOTROPIC MATERIAL

13.1.1 REMINDERS

We consider here again the elastic behavior relationship written in Section 9.1.1 in the form

$$\epsilon_{mn} = \varphi_{mnpq} \times \sigma_{pq}$$

It should be recalled that the φ_{mnpq} tensor components expressed in the coordinate system (1, 2, 3) take the form Φ_{IJKL} in another coordinate system (I, II, III) using the relationship

$$\Phi_{IJKL} = \cos_I^m \cos_J^n \cos_K^p \cos_L^q \times \varphi_{mnpq} \quad (13.1)$$

in which

$$\cos_I^m = \cos(\vec{m}, \vec{I})$$

By definition¹, an orthotropic medium shows, at every point, two symmetries of elastic behavior, each with respect to a plane, the two planes being mutually perpendicular.

13.1.2 ELASTIC BEHAVIOR EQUATION IN ORTHOTROPIC AXES

Under these conditions, we consider two coordinate systems (1, 2, 3) and (I, II, III), which are built on these two planes and their intersection and which can be deduced from each other, thanks to a 180° rotation around axis 3 as shown in Figure 13.1.

We deduce

$$\begin{bmatrix} \cos_I^m \end{bmatrix} = \begin{bmatrix} -1 & 0 & 0 \\ 0 & -1 & 0 \\ 0 & 0 & 1 \end{bmatrix}$$

The application of Equation 13.1 leads to

$$\begin{array}{lll} \Phi_{IIIII} = \varphi_{1111}; & \Phi_{IIIII} = \varphi_{1122}; & \Phi_{IIIII} = \varphi_{1133} \\ \Phi_{IIIII} = \varphi_{2222}; & \Phi_{IIIII} = \varphi_{2233}; & \Phi_{IIIII} = \varphi_{3333} \\ \Phi_{IIIII} = \varphi_{2323}; & \Phi_{IIIII} = \varphi_{1313}; & \Phi_{IIIII} = \varphi_{1212} \end{array}$$

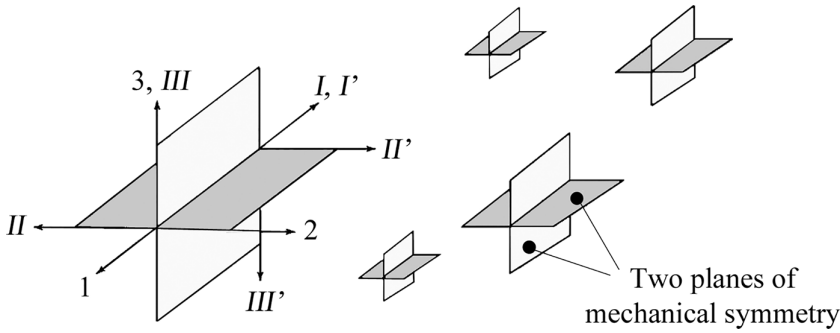


FIGURE 13.1 Orthotropic medium.

and

$$\Phi_{I I I I I I} = -\phi_{1123}$$

However, due to identical elastic properties in coordinates (1, 2, 3) and (I, II, III), we must also have

$$\Phi_{I I I I I I} = \phi_{1123}$$

From this,

$$\Phi_{I I I I I I} = \phi_{1123} = -\phi_{1123} = 0$$

In an analogous manner,

$$\begin{aligned} \Phi_{I I I I I I} &= 0; & \Phi_{I I I I I I} &= 0 \\ \Phi_{I I I I I I} &= 0; & \Phi_{I I I I I I} &= 0; & \Phi_{I I I I I I} &= 0 \\ \Phi_{I I I I I I} &= 0; & \Phi_{I I I I I I} &= 0 \end{aligned}$$

And finally,

$$\begin{aligned} \Phi_{I I I I I I} &= \phi_{1112}; & \Phi_{I I I I I I} &= \phi_{2212}; & \Phi_{I I I I I I} &= \phi_{3312} \\ \Phi_{I I I I I I} &= \phi_{2313} \end{aligned}$$

We have considered so far the symmetry with respect to plane (1, 3). Now coordinates (1, 2, 3) and (I', II', III') (see Figure 13.1) are considered, which are deduced one from the other, thanks to a 180° rotation around axis 2 (symmetry with respect to plane (1, 2)). We have

$$[\cos_I^m] = \begin{bmatrix} -1 & 0 & 0 \\ 0 & 1 & 0 \\ 0 & 0 & -1 \end{bmatrix}$$

The same procedure as above will lead to

$$\begin{aligned} \Phi_{I' I' I' I' I' I'} &= -\phi_{1112} = \phi_{1112} = 0; & \Phi_{I' I' I' I' I' I'} &= -\phi_{2212} = \phi_{2212} = 0 \\ \Phi_{I' I' I' I' I' I'} &= -\phi_{3312} = \phi_{3312} = 0; & \Phi_{I' I' I' I' I' I'} &= -\phi_{2313} = \phi_{2313} = 0 \end{aligned}$$

Considering the symmetry of coefficients ϕ_{mnpq} indicated in Equation 9.1², we have written here the only nonzero terms. From the simplification of Equation 9.2, we obtain the behavior relationship

$$\begin{Bmatrix} \epsilon_{11} \\ \epsilon_{22} \\ \epsilon_{33} \\ \gamma_{23} \\ \gamma_{13} \\ \gamma_{12} \end{Bmatrix} = \begin{bmatrix} \phi_{1111} & \phi_{1122} & \phi_{1133} & 0 & 0 & 0 \\ \phi_{2211} & \phi_{2222} & \phi_{2233} & 0 & 0 & 0 \\ \phi_{3311} & \phi_{3322} & \phi_{3333} & 0 & 0 & 0 \\ 0 & 0 & 0 & 4\phi_{2323} & 0 & 0 \\ 0 & 0 & 0 & 0 & 4\phi_{1313} & 0 \\ 0 & 0 & 0 & 0 & 0 & 4\phi_{1212} \end{bmatrix} \begin{Bmatrix} \sigma_{11} \\ \sigma_{22} \\ \sigma_{33} \\ \tau_{23} \\ \tau_{13} \\ \tau_{12} \end{Bmatrix} \quad (13.2)$$

It remains, therefore, **nine** distinct elastic coefficients, which can be written in the form of Young's moduli and Poisson ratios as

$$\begin{Bmatrix} \epsilon_{11} \\ \epsilon_{22} \\ \epsilon_{33} \\ \gamma_{23} \\ \gamma_{13} \\ \gamma_{12} \end{Bmatrix} = \begin{bmatrix} \frac{1}{E_1} & \frac{-\nu_{21}}{E_2} & \frac{-\nu_{31}}{E_3} & 0 & 0 & 0 \\ \frac{-\nu_{12}}{E_1} & \frac{1}{E_2} & \frac{-\nu_{32}}{E_3} & 0 & 0 & 0 \\ \frac{-\nu_{13}}{E_1} & \frac{-\nu_{23}}{E_2} & \frac{1}{E_3} & 0 & 0 & 0 \\ 0 & 0 & 0 & \frac{1}{G_{23}} & 0 & 0 \\ 0 & 0 & 0 & 0 & \frac{1}{G_{13}} & 0 \\ 0 & 0 & 0 & 0 & 0 & \frac{1}{G_{12}} \end{bmatrix} \begin{Bmatrix} \sigma_{11} \\ \sigma_{22} \\ \sigma_{33} \\ \tau_{23} \\ \tau_{13} \\ \tau_{12} \end{Bmatrix} \quad (13.3)$$

13.2 ELASTIC COEFFICIENTS FOR A TRANSVERSE ISOTROPIC MATERIAL

13.2.1 ELASTIC BEHAVIOR EQUATION

Reminders: By definition³, a transversely isotropic material (Figure 13.2) is such that any plane, including a privileged axis, shall be a mechanical mirror plane. We may already point out that it is a special case of orthotropic material. Therefore, the only nonzero elastic constants are shown in Figure 13.2.⁴

The preferred direction referred to in the definition above being axis 1 in Figure 13.2, let us consider the coordinates (1, 2, 3) and (I, II, III) that can be deduced one from the other, thanks to a rotation of any angle θ . We then have

$$[\cos^m] = \begin{bmatrix} 1 & 0 & 0 \\ 0 & c & -s \\ 0 & s & c \end{bmatrix} \quad \text{with} \quad \begin{aligned} c &= \cos \theta \\ s &= \sin \theta \end{aligned}$$

From the definition of such material, the matrix of elastic coefficients has to remain invariant in this rotation. Equation 13.1 allows writing

- $\Phi_{IIII} = \phi_{1111}$
- $\Phi_{I II II} = \phi_{1122}c^2 + \phi_{1133}s^2 = \phi_{1122}$

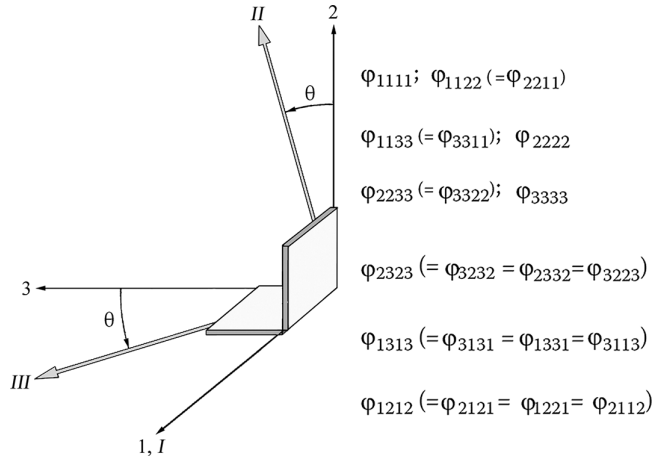


FIGURE 13.2 Transverse isotropic material.

Then,

$$\varphi_{1122}(c^2 - 1) + \varphi_{1133}s^2 = 0$$

$$\varphi_{1122} = \varphi_{1133}$$

$$\Phi_{\text{II III II II}} = \varphi_{2222}c^4 + \varphi_{2233}s^2c^2 + \varphi_{2323}s^2c^2 + \varphi_{2332}s^2c^2 \dots$$

•

$$\dots + \varphi_{3223}s^2c^2 + \varphi_{3232}s^2c^2 + \varphi_{3322}s^2c^2 + \varphi_{3333}s^4$$

and

$$\Phi_{\text{II III II II}} = \varphi_{2222}$$

Then, taking the symmetries into account, we obtain

$$\varphi_{2222}(c^4 - 1) + \varphi_{3333}s^4 + 2s^2c^2(\varphi_{2233} + 2\varphi_{2323}) = 0 \quad (13.4)$$

$$\Phi_{\text{III III III III}} = \varphi_{2222}s^4 + \varphi_{2233}s^2c^2 + \varphi_{2323}s^2c^2 + \varphi_{2332}s^2c^2 \dots$$

$$\dots + \varphi_{3232}s^2c^2 + \varphi_{3223}s^2c^2 + \varphi_{3322}s^2c^2 + \varphi_{3333}s^4$$

and

$$\Phi_{\text{III III III III}} = \varphi_{3333}$$

Then, taking into account the symmetry, we have

$$\phi_{2222}s^4 + \phi_{3333}(c^4 - 1) + 2s^2c^2(\phi_{2233} + 2\phi_{2323}) = 0 \quad (13.5)$$

Subtracting the relationships shown in (13.4) and (13.5),

$$\phi_{2222} = \phi_{3333}$$

Replacing in Equation 13.4,

$$\phi_{2222}(c^4 + s^4 - 1) + 2s^2c^2(\phi_{2233} + 2\phi_{2323}) = 0$$

$$-2s^2c^2\phi_{2222} + 2s^2c^2(\phi_{2233} + 2\phi_{2323}) = 0$$

$$2\phi_{2323} = \phi_{2222} - \phi_{2233}$$

•

$$\Phi_{I\text{III}I\text{III}} = \phi_{1212}s^2 + \phi_{1313}c^2 = \phi_{1313}$$

Then,

$$\phi_{1212}s^2 + \phi_{1313}(c^2 - 1) = 0$$

$$\phi_{1212} = \phi_{1313}$$

Four relations for the nine coefficients have been written. There remain, thus, five distinct elastic coefficients. Equation 13.2 is reduced to

$$\left\{ \begin{array}{c} \epsilon_{11} \\ \epsilon_{22} \\ \epsilon_{33} \\ \gamma_{23} \\ \gamma_{13} \\ \gamma_{12} \end{array} \right\} = \left[\begin{array}{cccccc} \phi_{1111} & \phi_{1122} & \phi_{1122} & 0 & 0 & 0 \\ \phi_{2211} & \phi_{2222} & \phi_{2233} & 0 & 0 & 0 \\ \phi_{2211} & \phi_{3322} & \phi_{2222} & 0 & 0 & 0 \\ 0 & 0 & 0 & 2(\phi_{2222} - \phi_{2233}) & 0 & 0 \\ 0 & 0 & 0 & 0 & 4\phi_{1212} & 0 \\ 0 & 0 & 0 & 0 & 0 & 4\phi_{1212} \end{array} \right] \left\{ \begin{array}{c} \sigma_{11} \\ \sigma_{22} \\ \sigma_{33} \\ \tau_{23} \\ \tau_{13} \\ \tau_{12} \end{array} \right\} \quad (13.6)$$

Or, in the form of Young's moduli and Poisson ratios,

$$\left\{ \begin{array}{c} \epsilon_{11} \\ \epsilon_{22} \\ \epsilon_{33} \\ \gamma_{23} \\ \gamma_{13} \\ \gamma_{12} \end{array} \right\} = \left[\begin{array}{cccccc} \frac{1}{E_1} & \frac{-\nu_{21}}{E_2} & \frac{-\nu_{21}}{E_2} & 0 & 0 & 0 \\ \frac{-\nu_{12}}{E_1} & \frac{1}{E_2} & \frac{-\nu}{E_2} & 0 & 0 & 0 \\ \frac{-\nu_{12}}{E_1} & \frac{-\nu}{E_2} & \frac{1}{E_2} & 0 & 0 & 0 \\ 0 & 0 & 0 & \frac{2(1+\nu)}{E_2} & 0 & 0 \\ 0 & 0 & 0 & 0 & \frac{1}{G_{12}} & 0 \\ 0 & 0 & 0 & 0 & 0 & \frac{1}{G_{12}} \end{array} \right] \left\{ \begin{array}{c} \sigma_{11} \\ \sigma_{22} \\ \sigma_{33} \\ \tau_{23} \\ \tau_{13} \\ \tau_{12} \end{array} \right\} \quad (13.7)$$

13.2.2 ROTATION ABOUT AN ORTHOTROPIC TRANSVERSE AXIS

13.2.2.1 Problem

Rather than the orthotropic axes $(\ell, t, z)^5$, we propose to rewrite the behavior relationship in axes $(x, y, \text{ and } z)$ deduced thanks to a rotation of any angle θ around the z -axis, as shown in Figure 13.3. This is in order to know how the previous elastic coefficients are changing according to angle θ .

Let us recall Equation 13.1 that allows the calculation of components Φ_{IJKL} in coordinate axes $(x, y, \text{ and } z)$ as functions of components φ_{mnpq} in coordinate axes $(\ell, t, \text{ and } z)$:

$$\begin{array}{ccc} \Phi_{IJKL} & = \cos_I^m \cos_J^n \cos_K^p \cos_L^q \times \varphi_{mnpq} \\ \text{(axes } x, y, z) & & \text{(axes } \ell, t, z) \end{array}$$

With (see Figure 13.3)

$$[\cos_I^m] = \begin{bmatrix} \cos(\ell, x) & \cos(\ell, y) & \cos(\ell, z) \\ \cos(t, x) & \cos(t, y) & \cos(t, z) \\ \cos(z, x) & \cos(z, y) & \cos(z, z) \end{bmatrix} = \begin{bmatrix} c & -s & 0 \\ s & c & 0 \\ 0 & 0 & 1 \end{bmatrix}$$

Noting that the only nonzero coefficients φ_{mnpq} appear in Equation 13.6, we obtain

$$\begin{aligned} \bullet \quad \Phi_{IIII} &= c^4 \varphi_{IIII} + c^2 s^2 \varphi_{I122} + c^2 s^2 \varphi_{1212} + c^2 s^2 \varphi_{1221} + c^2 s^2 \varphi_{2112} \cdots \\ &\quad \cdots + c^2 s^2 \varphi_{2121} + c^2 s^2 \varphi_{2211} + s^4 \varphi_{2222} \\ \Phi_{IIII} &= c^4 \varphi_{IIII} + s^4 \varphi_{2222} + 2c^2 s^2 (\varphi_{I122} + 2\varphi_{1212}) \end{aligned}$$

When expressed as a function of **technical** constants, which appear in Equation 13.7, this coefficient becomes

$$\Phi_{IIII} = \frac{c^4}{E_\ell} + \frac{s^4}{E_t} + s^2 c^2 \left(\frac{1}{G_{\ell t}} - 2 \frac{\nu_{t\ell}}{E_t} \right)$$

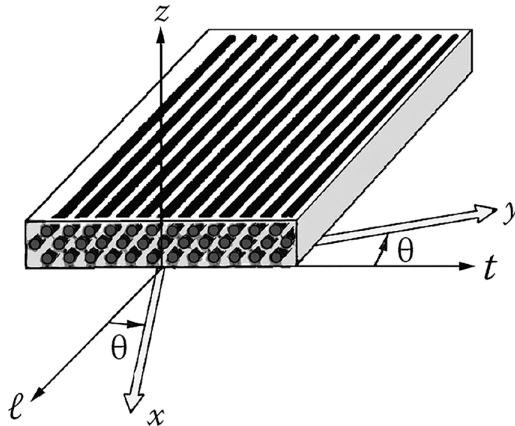


FIGURE 13.3 Rotation about an orthotropic transverse axis.

- $$\begin{aligned}\Phi_{\text{I I I I I I}} &= c^2 s^2 \varphi_{1111} + c^4 \varphi_{1122} - c^2 s^2 \varphi_{1212} - c^2 s^2 \varphi_{1221} - c^2 s^2 \varphi_{2112} \cdots \\ &\quad \cdots - c^2 s^2 \varphi_{2121} + s^4 \varphi_{2211} + s^2 c^2 \varphi_{2222} \\ \Phi_{\text{I I I I I I}} &= (c^4 + s^4) \varphi_{1122} + c^2 s^2 (\varphi_{1111} + \varphi_{2222} - 4c^2 s^2 \varphi_{1212})\end{aligned}$$

Or in the **technical** form,

- $$\begin{aligned}\Phi_{\text{I I I I I I}} &= -\frac{\nu_{t\ell}}{E_t} (c^4 + s^4) + c^2 s^2 \left(\frac{1}{E_\ell} + \frac{1}{E_t} - \frac{1}{G_{t\ell}} \right) \\ \Phi_{\text{I I I I I I}} &= c^2 \varphi_{1133} + s^2 \varphi_{2233} \quad \text{and as } \varphi_{1133} = \varphi_{1122}^6 \\ \Phi_{\text{I I I I I I}} &= c^2 \varphi_{1122} + s^2 \varphi_{2233}\end{aligned}$$

Or in the **technical** form (with Young's modulus and Poisson coefficients),

- $$\Phi_{\text{I I I I I I}} = -\left(c^2 \frac{\nu_{t\ell}}{E_t} + s^2 \frac{\nu}{E_t} \right)$$
- $$\Phi_{\text{I I I I I I}} = 0$$
- $$\Phi_{\text{I I I I I I}} = 0$$
- $$\begin{aligned}\Phi_{\text{I I I I I I}} &= -c^3 s \varphi_{1111} + c^3 s \varphi_{1122} + c^3 s \varphi_{1212} - c s^3 \varphi_{1221} + c^3 s \varphi_{2112} \cdots \\ &\quad \cdots - c s^3 \varphi_{2121} - c s^3 \varphi_{2211} + c s^3 \varphi_{2222} \\ \Phi_{\text{I I I I I I}} &= -s c \left\{ c^2 \varphi_{1111} - s^2 \varphi_{2222} - (c^2 - s^2) (\varphi_{1122} + 2\varphi_{1212}) \right\}\end{aligned}$$

Or in **technical** form,

- $$\begin{aligned}\Phi_{\text{I I I I I I}} &= -c s \left\{ \frac{c^2}{E_\ell} - \frac{s^2}{E_t} + (c^2 - s^2) \left(\frac{\nu_{t\ell}}{E_t} - \frac{1}{2G_{t\ell}} \right) \right\} \\ \Phi_{\text{I I I I I I}} &= s^4 \varphi_{1111} + s^2 c^2 \varphi_{1122} + s^2 c^2 \varphi_{1212} + s^2 c^2 \varphi_{1221} + s^2 c^2 \varphi_{2112} \cdots \\ &\quad \cdots + s^2 c^2 \varphi_{2121} + s^2 c^2 \varphi_{2211} + c^4 \varphi_{2222} \\ \Phi_{\text{I I I I I I}} &= s^4 \varphi_{1111} + c^4 \varphi_{2222} + s^2 c^2 (4\varphi_{1212} + 2\varphi_{1122})\end{aligned}$$

Or in **technical** form,

$$\Phi_{\text{I I I I I I}} = \frac{s^4}{E_\ell} + \frac{c^4}{E_t} + s^2 c^2 \left(\frac{1}{G_{t\ell}} - 2 \frac{\nu_{t\ell}}{E_t} \right)$$

- $\Phi_{\text{II II III III}} = s^2 \varphi_{1133} + c^2 \varphi_{2233}$ and as $\varphi_{1133} = \varphi_{1122}$ ⁷

$$\Phi_{\text{II II III III}} = s^2 \varphi_{1122} + c^2 \varphi_{2233}$$

Or in **technical** form,

$$\Phi_{\text{II II III III}} = - \left(s^2 \frac{v_{t\ell}}{E_t} + c^2 \frac{v}{E_t} \right)$$

- $\Phi_{\text{II II II III}} = 0$

- $\Phi_{\text{II III I III}} = 0$

- $\Phi_{\text{II III II}} = -s^3 c \varphi_{1111} + s^3 c \varphi_{1122} - s c^3 \varphi_{1212} + s^3 c \varphi_{1221} - s c^3 \varphi_{2112} \cdots$
 $\cdots + s^3 c \varphi_{2121} - s c^3 \varphi_{2211} + c^3 s \varphi_{2222}$

$$\Phi_{\text{II III II}} = -s c \left\{ s^2 \varphi_{1111} + c^2 \varphi_{2222} + (c^2 - s^2) (\varphi_{1122} + 2 \varphi_{1212}) \right\}$$

Or in **technical** form,

$$\Phi_{\text{II III II}} = -c s \left\{ \frac{s^2}{E_\ell} - \frac{c^2}{E_t} - (c^2 - s^2) \left(\frac{v_{t\ell}}{E_t} - \frac{1}{2G_{t\ell}} \right) \right\}$$

- $\Phi_{\text{III III III III}} = \varphi_{3333}$

In **technical** form,

$$\Phi_{\text{III III III III}} = \frac{1}{E_t}$$

- $\Phi_{\text{III III II III}} = 0$

- $\Phi_{\text{III III I III}} = 0$

- $\Phi_{\text{III III II}} = -s c \varphi_{3311} + s c \varphi_{3322}$ and as $\varphi_{3311} = \varphi_{1122}$ ⁸

$$\Phi_{\text{III III II}} = -s c \varphi_{1122} + s c \varphi_{2233}$$

In **technical** form,

$$\Phi_{\text{III III II}} = -s c \left(\frac{v - v_{t\ell}}{E_t} \right)$$

- $$\Phi_{\text{II III II III}} = s^2 \varphi_{1313} + c^2 \varphi_{2323}$$

We know⁸ that for a transverse isotropic material, we have

$$\varphi_{1313} = \varphi_{1212} \text{ and } 2\varphi_{2323} = \varphi_{2222} - \varphi_{2233}$$

Then,

$$\Phi_{\text{II III II III}} = s^2 \varphi_{1212} + c^2 \left(\frac{\varphi_{2222} - \varphi_{2233}}{2} \right)$$

In **technical** form,

$$\Phi_{\text{II III II III}} = \frac{s^2}{4G_{tt}} + \frac{c^2(1+\nu)}{2E_t}$$

- $$\Phi_{\text{II III I III}} = -sc\varphi_{1313} + sc\varphi_{2323}$$

or⁹

$$\Phi_{\text{II III I III}} = -sc \left(\varphi_{1212} - \frac{1}{2}(\varphi_{2222} - \varphi_{2233}) \right)$$

Or in **technical** form,

$$\Phi_{\text{II III I III}} = -sc \left(\frac{1}{4G_{tt}} - \frac{(1+\nu)}{2E_t} \right)$$

- $$\Phi_{\text{II III I II}} = 0$$

- $$\Phi_{\text{I III I III}} = c^2 \varphi_{1313} + s^2 \varphi_{2323}$$

or

$$\Phi_{\text{I III I III}} = c^2 \varphi_{1212} + s^2 \frac{(\varphi_{2222} - \varphi_{2233})}{2}$$

Or in **technical** form,

$$\Phi_{\text{I III I III}} = \frac{c^2}{4G_{tt}} + s^2 \frac{(1+\nu)}{2E_t}$$

- $$\Phi_{\text{I III I II}} = 0$$

- $$\begin{aligned} \Phi_{\text{I II I II}} = & s^2 c^2 \varphi_{1111} - s^2 c^2 \varphi_{1122} + c^4 \varphi_{1212} - s^2 c^2 \varphi_{1221} - s^2 c^2 \varphi_{2112} \cdots \\ & \cdots + s^4 \varphi_{2121} - s^2 c^2 \varphi_{2211} + s^2 c^2 \varphi_{2222} \end{aligned}$$

$$\Phi_{IIII} = s^2 c^2 (\phi_{1111} + \phi_{2222} - 2\phi_{1122}) + (c^2 - s^2)^2 \phi_{1212}$$

Or in **technical** form,

$$\Phi_{IIII} = s^2 c^2 \left\{ \frac{1}{E_\ell} + \frac{1}{E_t} + 2 \frac{\nu_{t\ell}}{E_t} \right\} + (c^2 - s^2)^2 \frac{1}{4G_{t\ell}}$$

All the nonzero coefficients Φ_{IJKL} found above allow writing the elastic behavior relationship in the form¹⁰

$$\begin{Bmatrix} \epsilon_{xx} \\ \epsilon_{yy} \\ \epsilon_{zz} \\ \gamma_{yz} \\ \gamma_{xz} \\ \gamma_{xy} \end{Bmatrix} = \begin{bmatrix} \Phi_{IIII} & \Phi_{IIIII} & \Phi_{IIIIII} & 0 & 0 & 2\Phi_{IIII} \\ \Phi_{IIIII} & \Phi_{IIIIII} & \Phi_{IIIIIII} & 0 & 0 & 2\Phi_{IIIII} \\ \Phi_{IIIIII} & \Phi_{IIIIIII} & \Phi_{IIIIIIII} & 0 & 0 & 2\Phi_{IIIIII} \\ 0 & 0 & 0 & 4\Phi_{IIIIIIII} & 4\Phi_{IIIIIII} & 0 \\ 0 & 0 & 0 & 4\Phi_{IIIIIII} & 4\Phi_{IIIIII} & 0 \\ 2\Phi_{IIII} & 2\Phi_{IIIII} & 2\Phi_{IIIIII} & 0 & 0 & 4\Phi_{IIII} \end{bmatrix} \begin{Bmatrix} \sigma_{xx} \\ \sigma_{yy} \\ \sigma_{zz} \\ \tau_{yz} \\ \tau_{xz} \\ \tau_{xy} \end{Bmatrix} \quad (13.8)$$

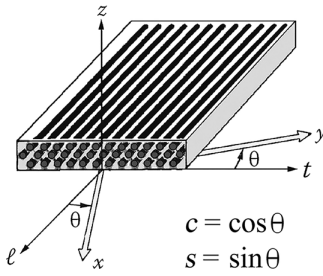
13.2.2.2 Technical Form

By analogy with the **technical** form of Equation 13.7, in orthotropic axes, the constitutive equation in axes (x, y, z) can be written in terms of equivalent moduli and Poisson coefficients as follows:

$$\begin{Bmatrix} \epsilon_{xx} \\ \epsilon_{yy} \\ \epsilon_{zz} \\ \gamma_{yz} \\ \gamma_{xz} \\ \gamma_{xy} \end{Bmatrix} = \begin{bmatrix} \frac{1}{E_x} & \frac{-\nu_{yx}}{E_y} & \frac{-\nu_{zx}}{E_z} & 0 & 0 & \frac{\eta_{xy}}{G_{xy}} \\ \frac{-\nu_{xy}}{E_x} & \frac{1}{E_y} & \frac{-\nu_{zy}}{E_z} & 0 & 0 & \frac{\mu_{xy}}{G_{xy}} \\ \frac{-\nu_{xz}}{E_x} & \frac{-\nu_{yz}}{E_y} & \frac{1}{E_z} & 0 & 0 & \frac{\zeta_{xy}}{G_{xy}} \\ 0 & 0 & 0 & \frac{1}{G_{yz}} & \frac{\xi_{xz}}{G_{xz}} & 0 \\ 0 & 0 & 0 & \frac{\xi_{yz}}{G_{yz}} & \frac{1}{G_{xz}} & 0 \\ \frac{\eta_x}{E_x} & \frac{\mu_y}{E_y} & \frac{\zeta_z}{E_z} & 0 & 0 & \frac{1}{G_{xy}} \end{bmatrix} \begin{Bmatrix} \sigma_{xx} \\ \sigma_{yy} \\ \sigma_{zz} \\ \tau_{yz} \\ \tau_{xz} \\ \tau_{xy} \end{Bmatrix} \quad (13.9)$$

In this equation, the coupling terms characterized by the coefficients η_{xy} , μ_{xy} , ζ_{xy} , and ξ_{xz} should be noted, which are not similar to Poisson coefficients.

The values of elastic constants that appear above can be deduced immediately from the technical forms of coefficients Φ_{IJKL} . These constants are detailed below, and subsequently, the elastic moduli and Poisson coefficients in axes (x, y, z) are obtained:



$$\frac{1}{E_x} = \frac{c^4}{E_\ell} + \frac{s^4}{E_t} + s^2 c^2 \left(\frac{1}{G_{\ell t}} - 2 \frac{\nu_{\ell t}}{E_t} \right) \Rightarrow$$

$$\frac{1}{E_y} = \frac{s^4}{E_\ell} + \frac{c^4}{E_t} + s^2 c^2 \left(\frac{1}{G_{\ell t}} - 2 \frac{\nu_{\ell t}}{E_t} \right) \Rightarrow$$

$$\frac{1}{E_z} = \frac{1}{E_t} \Rightarrow$$

$$-\frac{\nu_{yx}}{E_y} = -\frac{\nu_{t\ell}}{E_t} (c^4 + s^4) + c^2 s^2 \left(\frac{1}{E_\ell} + \frac{1}{E_t} - \frac{1}{G_{\ell t}} \right) \Rightarrow$$

$$-\frac{\nu_{zx}}{E_z} = -\left(c^2 \frac{\nu_{t\ell}}{E_t} + s^2 \frac{\nu}{E_t} \right) \Rightarrow$$

$$-\frac{\nu_{zy}}{E_z} = -\left(s^2 \frac{\nu_{t\ell}}{E_t} + c^2 \frac{\nu}{E_t} \right) \Rightarrow$$

$$\frac{1}{G_{yz}} = c^2 \frac{2(1+\nu)}{E_t} + \frac{s^2}{G_{\ell t}} \Rightarrow$$

$$\frac{1}{G_{xz}} = s^2 \frac{2(1+\nu)}{E_t} + \frac{c^2}{G_{\ell t}} \Rightarrow$$

$$\frac{1}{G_{xy}} = 4c^2 s^2 \left(\frac{1}{E_\ell} + \frac{1}{E_t} + 2 \frac{\nu_{t\ell}}{E_t} \right) + \frac{(c^2 - s^2)^2}{G_{\ell t}} \Rightarrow$$

$$\frac{\eta_{xy}}{G_{xy}} = -2cs \left\{ \frac{c^2}{E_\ell} - \frac{s^2}{E_t} + (c^2 - s^2) \left(\frac{\nu_{t\ell}}{E_t} - \frac{1}{2G_{\ell t}} \right) \right\}$$

$$\frac{\xi_{xy}}{G_{xy}} = -2cs \frac{(\nu - \nu_{t\ell})}{E_t}$$

$$E_x(\theta) = \frac{1}{\frac{c^4}{E_\ell} + \frac{s^4}{E_t} + s^2 c^2 \left(\frac{1}{G_{\ell t}} - \frac{2\nu_{t\ell}}{E_t} \right)}$$

$$E_y(\theta) = \frac{1}{\frac{s^4}{E_\ell} + \frac{c^4}{E_t} + s^2 c^2 \left(\frac{1}{G_{\ell t}} - \frac{2\nu_{t\ell}}{E_t} \right)}$$

$$E_z(\theta) = E_t \quad (\forall \theta)$$

$$\frac{\nu_{yx}}{E_y}(\theta) = \frac{\nu_{t\ell}}{E_t} (c^4 + s^4) - c^2 s^2 \left(\frac{1}{E_\ell} + \frac{1}{E_t} - \frac{1}{G_{\ell t}} \right)$$

$$\nu_{zx}(\theta) = c^2 \nu_{t\ell} + s^2 \nu$$

$$\nu_{zy}(\theta) = s^2 \nu_{t\ell} + c^2 \nu$$

$$G_{yz}(\theta) = \frac{1}{c^2 \frac{2(1+\nu)}{E_t} + \frac{s^2}{G_{\ell t}}}$$

$$G_{xz}(\theta) = \frac{1}{s^2 \frac{2(1+\nu)}{E_t} + \frac{c^2}{G_{\ell t}}}$$

$$G_{xy}(\theta) = \frac{1}{4c^2 s^2 \left(\frac{1}{E_\ell} + \frac{1}{E_t} + 2 \frac{\nu_{t\ell}}{E_t} \right) + \frac{(c^2 - s^2)^2}{G_{\ell t}}}$$

$$\frac{\mu_{xy}}{G_{xy}} = -2cs \left\{ \frac{s^2}{E_\ell} - \frac{c^2}{E_t} - (c^2 - s^2) \left(\frac{\nu_{t\ell}}{E_t} - \frac{1}{2G_{\ell t}} \right) \right\}$$

$$\frac{\xi_{xz}}{G_{xz}} = -cs \left(\frac{1}{G_{\ell t}} - \frac{2(1+\nu)}{E_t} \right)$$

(13.10)

13.3 CASE OF A PLY

In Equation 13.9, we may note that the stress–strain relationship in axes (x, y) appears to be decoupled when $\sigma_{zz} = 0$. We will assume this to be the case for a thin laminate. Each ply will be, therefore, characterized in its plane by what follows, extracted from Equations 13.7¹¹ and 13.9:

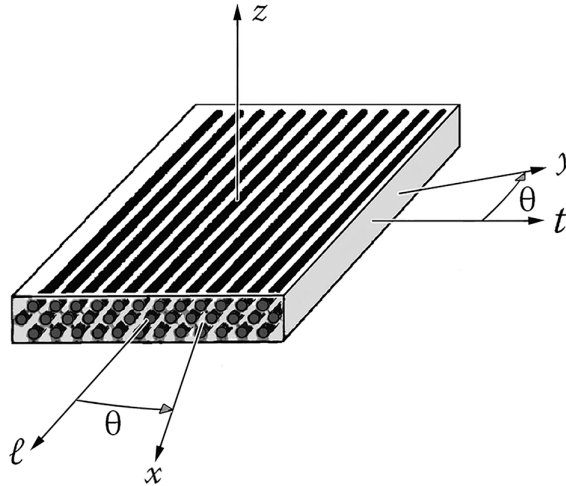


FIGURE 13.4 Axes (x, y) , making an angle θ with the orthotropic axes (ℓ, t) .

- In orthotropic axes (ℓ, t) ,

$$\begin{Bmatrix} \varepsilon_{\ell} \\ \varepsilon_t \\ \gamma_{\ell t} \end{Bmatrix} = \begin{bmatrix} \frac{1}{E_{\ell}} & \frac{-\nu_{t\ell}}{E_t} & 0 \\ \frac{-\nu_{\ell t}}{E_{\ell}} & \frac{1}{E_t} & 0 \\ 0 & 0 & \frac{1}{G_{\ell t}} \end{bmatrix} \begin{Bmatrix} \sigma_{\ell} \\ \sigma_t \\ \tau_{\ell t} \end{Bmatrix} \quad (13.11)$$

- In axes (x, y) , making an angle θ with the orthotropic axes (ℓ, t) (Figure 13.4)

$$\begin{Bmatrix} \varepsilon_{xx} \\ \varepsilon_{yy} \\ \gamma_{xy} \end{Bmatrix} = \begin{bmatrix} \frac{1}{E_x} & \frac{-\nu_{yx}}{E_y} & \frac{\eta_{xy}}{G_{xy}} \\ \frac{-\nu_{xy}}{E_x} & \frac{1}{E_y} & \frac{\mu_{xy}}{G_{xy}} \\ \frac{\eta_x}{E_x} & \frac{\mu_y}{E_y} & \frac{1}{G_{xy}} \end{bmatrix} \begin{Bmatrix} \sigma_{xx} \\ \sigma_{yy} \\ \tau_{xy} \end{Bmatrix} \quad (13.12)$$

The values of elastic constants above are listed in Equation 13.10.

NOTES

- 1 See Section 9.2.
- 2 Recall the symmetry properties: $\varphi_{ijkl} = \varphi_{ijlk}$; $\varphi_{ijkl} = \varphi_{jkl i}$; $\varphi_{ijkl} = \varphi_{klij}$.
- 3 See Section 9.3.
- 4 By involving symmetries in Equation 9.1, which are also mentioned in the footnote in Section 13.1.2.
- 5 From now on, orthotropic axes $(1, 2, 3)$ of Equation 13.7 are denoted as (ℓ, t, z) .
- 6 See Equations 9.2 and 13.6.
- 7 See Equations 9.2 and 13.6.
- 8 See Equations 9.2 and 13.6.
- 9 See Equations 9.2 and 13.6.
- 10 This is deduced from the general Equation 9.2.
- 11 Orthotropic axes $(1, 2, 3)$ of Equation 13.7 are denoted as (ℓ, t, z) for a ply (see Section 3.3.1).

14 Damage in Composite Parts; Failure Criteria

In Section I, Chapters 5 and 6, we have reported some specific degradation processes of laminated composite parts (see Sections 5.3.1, 5.4.5, and 6.1). We return more broadly in this chapter to the damage and failure criteria. First of all, we focus on the overall problem of damage and degradation of composite parts. We then talk about the characteristics and the general shape of a fracture criterion, in particular in the case of an orthotropic material. Then, we concentrate on the general form of the quadratic failure criterion for the particular plane stress case with the Tsai-Wu criterion and the Tsai-Hill criterion. Finally, to allow an application in the next chapter to D-D laminates, we translate the Tsai-Wu stress criterion in the strain space and take into account the mechanical properties of the damaged ply.

14.1 DAMAGE IN COMPOSITE PARTS

14.1.1 INDUSTRIAL EMPHASIS OF THE PROBLEM

14.1.1.1 Causes of Damage

As an example with regard to the field of aviation, we know the crucial importance of sizing for the various structural elements of an aircraft, in order to withstand the relevant loads. During the life of appliance, in addition to this sizing aspect, which takes already account of fatigue, consideration should also be given to the incidence of damage in service. As shown in the graph in Figure 14.1, this occurs for most of the parts during maintenance or during stopovers.

14.1.1.2 Diversity of Composite Parts

The term **composite** covers a wide scope of

- Ranges and geometries of reinforcements
- Matrices

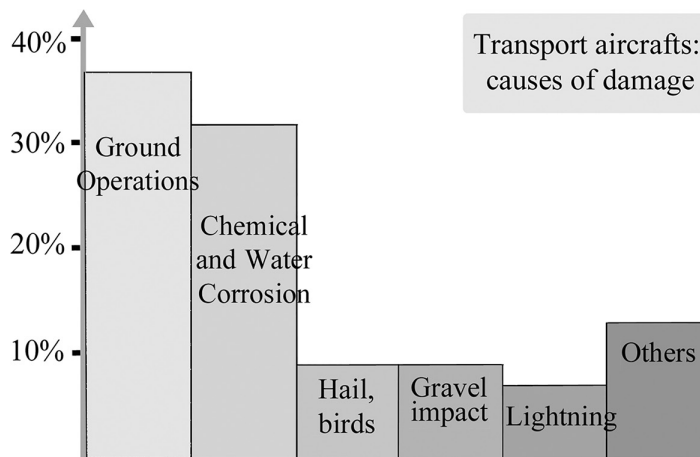


FIGURE 14.1 Damage in transport aircraft.

- Manufacturing processes
- Shapes of parts

In such a context, initialization of damages and monitoring of their growth appear to be a very broad topic of studies. Such studies are aimed at the construction of reliable digital models taking into account the degradation processes in the part area where a defined load that is growing is imposed. These models must rely upstream on experimental damage study and then be validated by the experience. After that, they are incorporated into numerical simulation tools, the goal being to **try virtually** an industrial part (**virtual testing**) in order to limit too expensive physical testing¹. The expected time and money savings are a crucial economic issue today. They involve a considerable scientific work upstream, as well as a coordination of efforts the most extensive possible, often exceeding the national level.

14.1.2 INFLUENCE OF MANUFACTURING PROCESS

Even before considering the specific shape of a part, should be noted the importance of manufacturing process and its impact on mechanical properties.

14.1.2.1 Example: Injected Part with Short Fibers

The diagram in Figure 14.2 shows the cross section through thickness of a mold and a plate injected with short fibers (e.g., a plate of a few millimeters thick, with short fibers of average length about $250\mu\text{m}$, average slenderness of the order of $1/25$). We note that the proximity of the mold wall guides the fibers along the flow direction. These are indeed areas of high values for velocity gradient, that is, the boundary layers of the flow following the injection.

Thus, the microscopic arrangements of reinforcement in this composite part are varying depending on the areas. Therefore, there is a variability of the mechanical properties relating to stiffness, thermoelasticity, and strength (mass fraction of short glass fiber today is reaching $M_f = 50\%$ and volume fraction $V_f > 30\%$).

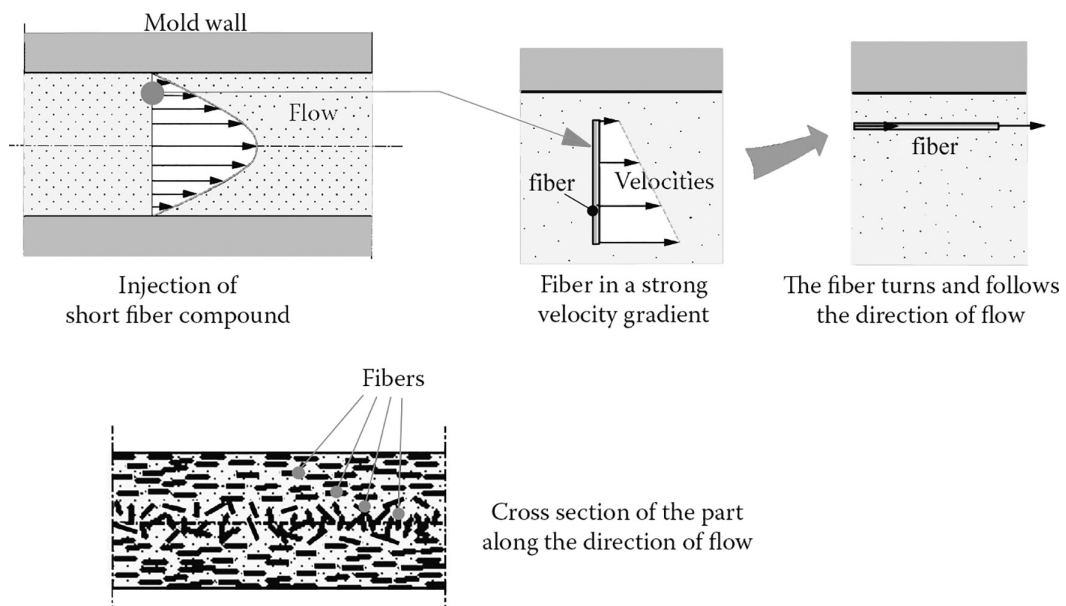


FIGURE 14.2 Injected plate with short fibers.

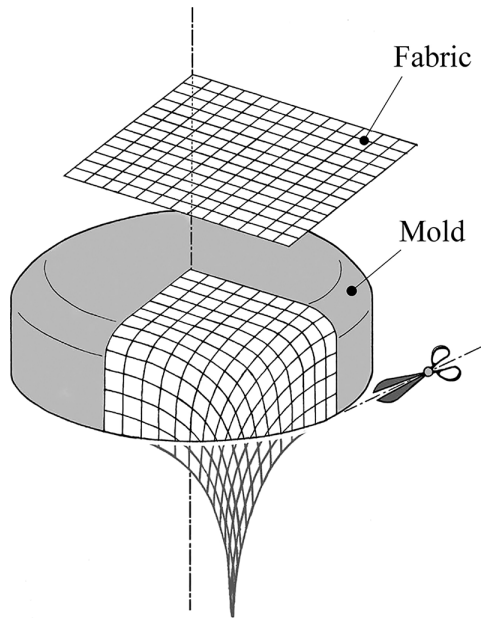


FIGURE 14.3 Draping of a fabric ply over a mold.

14.1.2.2 Example: Parts with Pronounced Curvatures

Figure 14.3 shows the draping of a fabric ply over a mold with a double curvature, which is a frequent geometrical characteristic in applications. The fabric must be equipped with appropriate draping weave, for example, a satin of high modulus (see Section 3.4.1).

Here also, the mechanical properties of the fabric ply will evolve following the level of curvature of the areas concerned. In these areas, the ply remains orthotropic but shows different orthotropic directions with different mechanical and strength characteristics, due to the high level of curvature. And this phenomenon is repeated during stacking of successive plies of fabric, with their specific orientations, to constitute the final layered part.

14.1.3 SMOOTH AREA AND SINGULARITIES IN A SAME PART

Structural composite parts generally show areas so-called **regular** or **smooth**, or **typical**, as well as specific local adaptations allowing their fastening or their reinforcement, called **singularities**. Figure 14.4 illustrates such a composite laminated part under sollicitation of In-plane tension. Within the smooth area, the state of plane stress is uniform. The singularities, characterized by localized geometry changes, are the seat of rapidly varying In-plane stresses (stress gradient), as well as out-of-plane stresses, as shown in Figure 14.4 and also Figure 5.28c for the **free edge** effect².

The accidental defects create localized damage, as already indicated (see Figure 14.1). The most common are impact damages, and their consideration is very important (see the typical example of aerospace industry in Section 5.4.5).

14.1.4 DEGRADATION PROCESS WITHIN THE SMOOTH AREA

Geometric imperfections and microdefects, such as localized absence of sizing agent on fiber surface and porosity in the matrix, are always at the microscopic scale. That will foster initiation of degradation process.

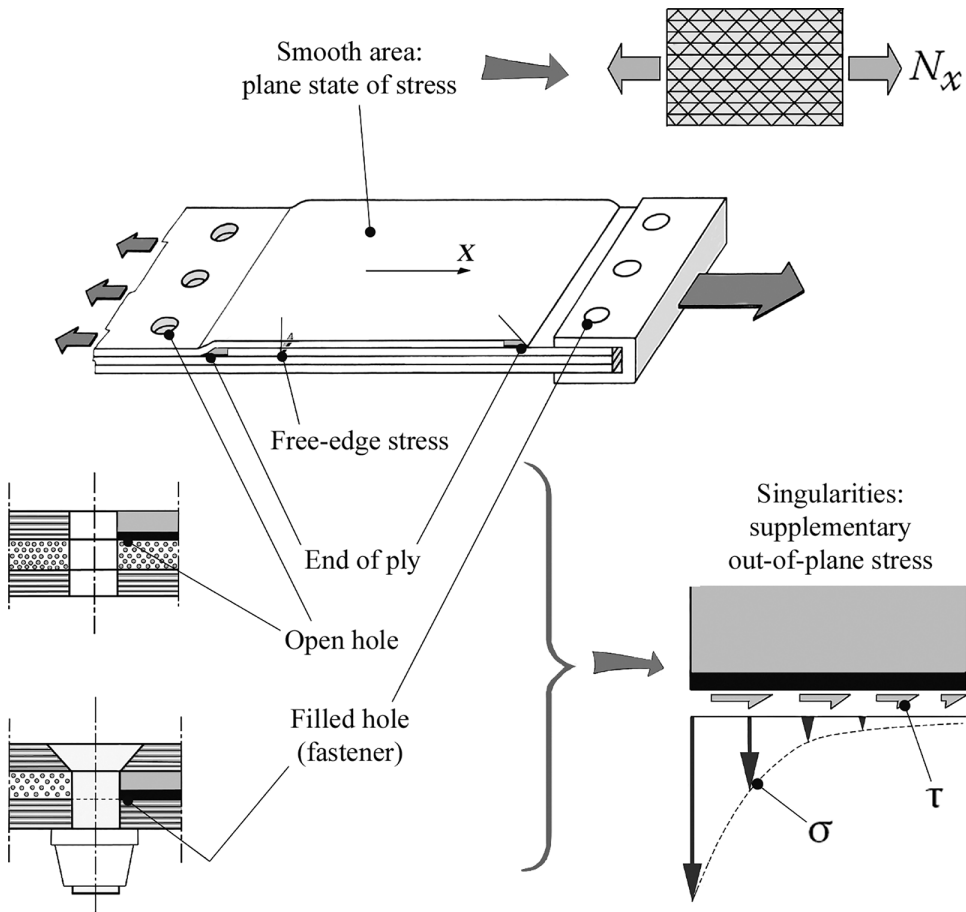


FIGURE 14.4 Typical smooth area and singularities in a part.

14.1.4.1 Example: Composite Short Fiber Plate

In the case of the abovementioned composite plate (see Section 14.1.2.1), Figure 14.5 shows the process at microscopic scale that leads to failure under tension along the direction of injected short fibers.

Notes

- The matrix separates from the fiber by *adhesive rupture* (matrix disbonding, subsequent to a sizing defect) or *cohesive rupture* (rupture of matrix in the vicinity of the fiber wall).
- Here, short fibers are not broken, even at ultimate failure stage.

14.1.4.2 Example: Laminate Consisting of Unidirectional Plies

When the load gradually increases, for example, in the x -direction of Figure 14.6, initiation of degradation usually takes the form of microcracks development in the resin, in areas of stress concentration, due to the presence of microdefects. This is the **microscopic**-level phenomenon. In a second step, there is growth or **coalescence** of these defects that reach the fibers and cause fiber disbonding.

The cracking now propagates across a ply and its mechanical and strength characteristics change. The damage has reached the **mesoscopic** level.

As loading continues to grow, so-called **macroscopic** phenomena appear across the plies themselves: longitudinal cracking of plies (along the fiber direction), delamination between two

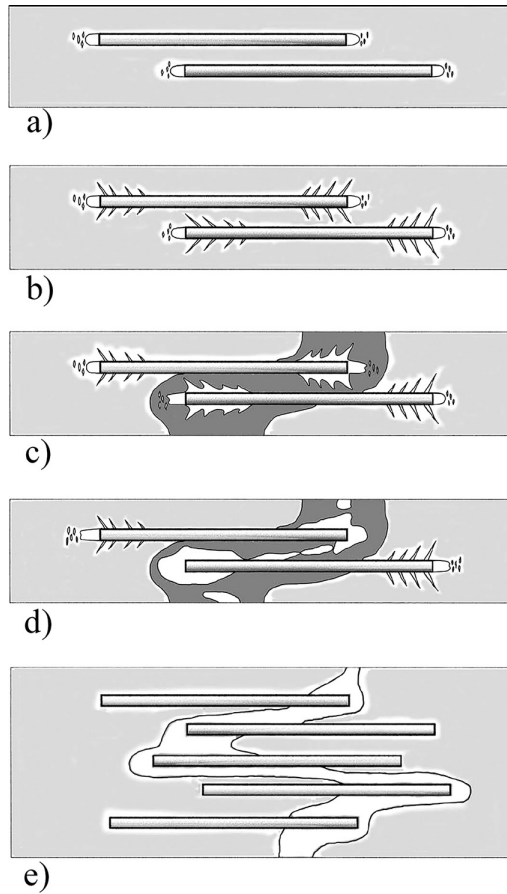


FIGURE 14.5 Degradation of a short fiber composite: (a) Microcracks and voids at the end of fibers (*note*: at the end of short-cut fiber, there is no sizing agent); (b) initiation and propagation of microcracks along the surface of fibers; (c) development of a plasticized zone; (d) small cracks coalesce and grow together in the plasticized zone; and (e) the cracked ductile zone reaches a critical size resulting in the brutal spread of a brittle cracking.

consecutive plies having different orientations, and finally breaking of fibers themselves, which corresponds generally to the ultimate failure of the laminate.

Notes

- Stiffness and strength characteristics of the degraded ply: degradation of the unidirectional ply as described results in an alteration of the elastic properties and mainly of the E_t and G_{tt} modulus, and of Poisson's ratio ν_{tt} ³. We return in Section 14.5 on these degraded moduli (see Equation 14.17).
- The previous illustration is linked to a laminate made of unidirectional plies and should not be extrapolated to woven plies. Interlacing of warp and weft threads (the weaving) is the source of specific stress concentration, and this can significantly change the process of degradation.
- We did not mention the nature of mechanical behavior of components. This behavior varies within the plies: linear elastic along the direction governed by the reinforcement but which may become nonlinear or anelastic in the direction governed by the matrix.
- The damage process in the singularities abovementioned is specific for these singularities.

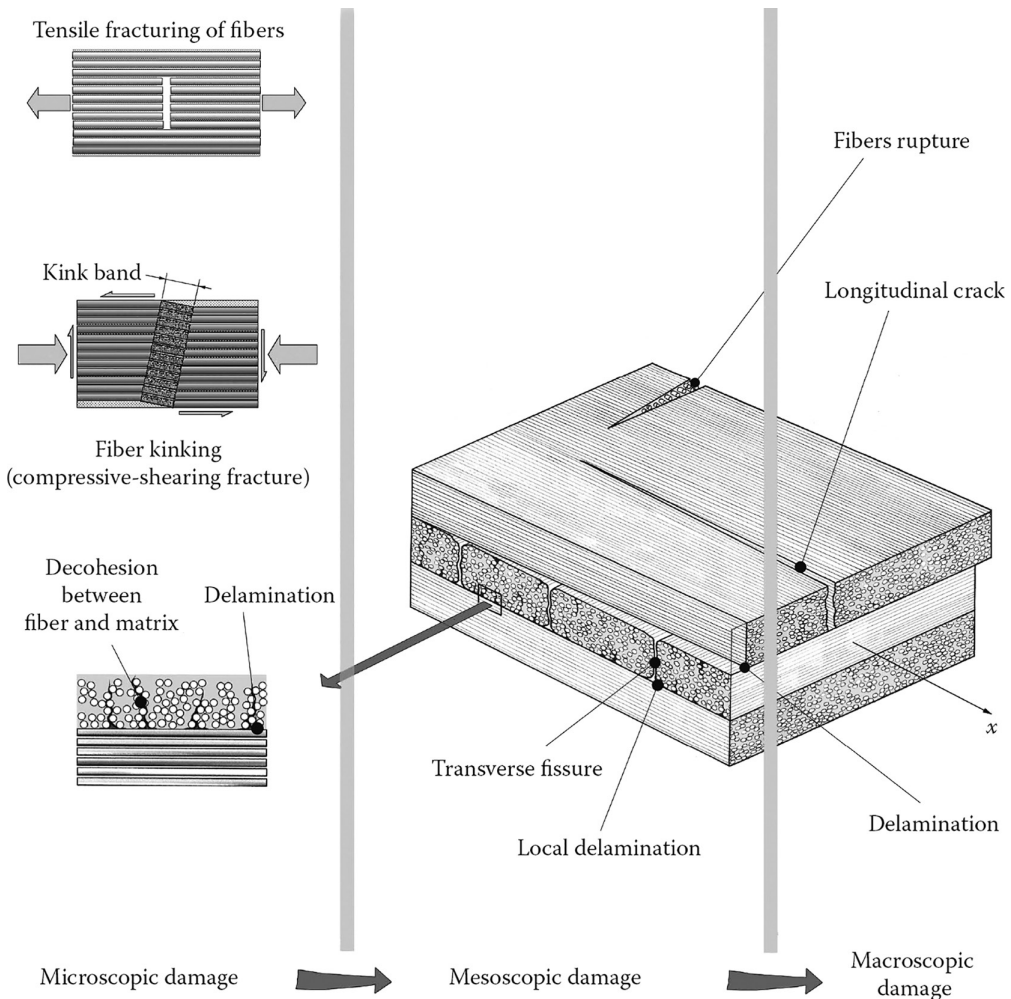


FIGURE 14.6 Different levels of damage in a laminate consisting of unidirectional plies.

- The allowable damage limit does not necessarily correspond to final failure but should be related to the envisaged application.

Example: Composite pipe carried out by filament winding. When the internal pressure is increasing, microcracking of resin causes fluid leakage. The outer layer begins to **weep**, a weeping phenomenon that, while linked to a microscopic damage level, is particularly problematic (see Application 19.8).

Thus, we can note that detailed study of a failure process in a composite part requires knowledge of the following features:

- State of stress in the typical areas or in the singular areas concerned
- Local mechanical properties of each phase
- Nature of the cracks in order to consider their propagation
- Mechanical properties of the interface between reinforcement and matrix

Then, the modeling coupled to a progressive and homogeneous loading of the part should allow following up the damage, up to a limit characterizing the failure of the area under study.

14.2 FORM OF A FAILURE CRITERION

14.2.1 FEATURES OF A FAILURE CRITERION

14.2.1.1 Failure Criterion Is a Design Tool

- A failure criterion must, therefore, provide a convenient means for predicting the loss of integrity that could lead to ultimate strength of the area studied in the part.
- Directly usable by the designer, a failure criterion must provide a result at the macroscopic level, which is the area studied in the composite part (the part itself being representative of the **global** level).
- It should integrate the results of tests from specimens, the structure of which must be consistent with that of areas under study.
- The implementation of a failure criterion should not take into account the details of damage evolution. It is positioned downstream from studies based on fracture mechanics where the microscopic and mesoscopic phenomena above are successively evoked.

Note: In the case of a smooth laminate area, damage starts in a certain ply orientation. The plies referred to this orientation have their mechanical properties (elastic properties and, later, strength) degraded, mainly in the transverse direction to fibers. Thus, the initial laminate definition should be replaced with a new definition, structurally degraded as compared to the initial laminate, and on which the loading continues to grow. The criterion must be able to adapt to this iterative approach to lead to ultimate failure⁴.

14.2.1.2 Many Criteria

Many criteria have been proposed, more or less in line with this philosophy, since the 1960s. The approach followed here is not to establish an exhaustive list (many works from literature are doing this). However, the problem arises of their choice, based on their assessment.

In the early 2000s, the first results of an international campaign (**Worldwide Failure Exercises**) designed to compare the rupture criteria of monolayers or laminates in typical area were published. The comparisons of criteria were made both among themselves and with experimental results, which come almost entirely from biaxial testing with well-defined protocols.

Some twenty criteria were evaluated. No final conclusion could be drawn on the emergence of a dominant criterion that could provide an accurate rupture prediction for all the loading combinations.

So probably, there will never be a single criterion resulting from a theory of rupture of laminates, which would provide a sufficient range of precision to be fully accepted.

Therefore, we will limit ourselves here to present the bases on which a criterion is built, before examining in detail convenient forms among the most commonly used for examination of smooth areas.

14.2.2 GENERAL FORM OF A FAILURE CRITERION

14.2.2.1 Development of a Criterion

The development of a criterion results in a mathematical expression built on the stress tensor Σ prevailing in the study area, which also contains experimental strength values of the concerned material.

The condition of no damage takes the general form of a scalar inequality such as

$$f(\Sigma) \leq 1$$

When equality is achieved, the criterion is said to be **saturated**, leading to a **boundary surface** in the space of stresses, or **failure envelope**, which marks the occurrence of failure.

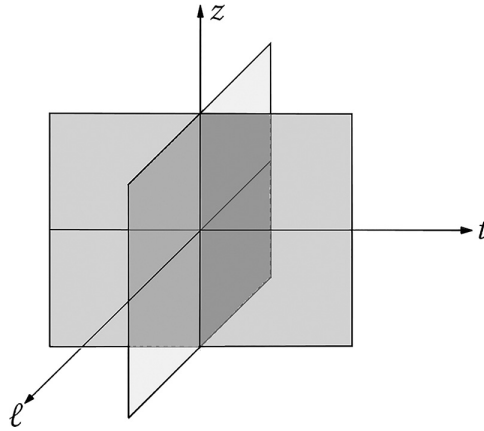


FIGURE 14.7 Orthotropic axes built on planes of mechanical symmetry for damage.

14.2.2.2 Case of an Orthotropic Material

We should define an **orthotropic-for-damage** material on a similar basis than already used for the elastic coefficients in the previous chapter (see Section 13.1), that is, assuming the existence of two mechanical symmetry planes for damage⁵. These two planes are supposed to be orthogonal. The mechanism of damage is characteristic of the symmetry plane considered. Starting from these two planes of symmetry and their intersection (z -axis noted on Figure 14.7), we define three orthogonal axes, which are the axes of orthotropy (z, ℓ, t)⁶. When changing from coordinate system by 180° rotation around ℓ -axis or around t -axis, the scalar form constituting the failure criterion should in principle remain invariant for the given state of stress resulting from the loading.

Notes

- Experimental values of failure strength are algebraically measured in the orthotropy axes, and the criterion is expressed in the corresponding coordinate system.
- The criterion depends on a final state of stress, but not on the **loading path**. Therefore, it masks the microscopic and mesoscopic evolutionary phenomena that lead to the rupture.
- However, any linearly increasing loading path must pierce the failure envelope of the criterion at a single point. This is a sufficient condition to refer $f(\Sigma)$ as a **convex functional** of the stress tensor.

We describe below some forms of criteria built on these principles.

14.2.3 LINEAR FAILURE CRITERION

$$f(\Sigma) = a_{ij}\sigma_{ij} \leq 1$$

14.2.3.1 Example: Plane State of Stress in an Orthotropic Material

In orthotropic axes (ℓ, t), the expression above is reduced to⁷

$$f(\Sigma) = a_{\ell\ell}\sigma_{\ell} + a_{tt}\sigma_t + (a_{\ell t} + a_{t\ell})\tau_{\ell t} \leq 1$$

For simple states of stress, results of test on samples provide failure strength values for traction, compression, and shear, that is, in algebraic form,

$$\sigma_{\ell \text{ rupt.}}^{\text{tens.}} > 0; \quad \sigma_{\ell \text{ rupt.}}^{\text{comp.}} < 0; \quad \sigma_t^{\text{tens.}} > 0; \quad \sigma_t^{\text{comp.}} < 0; \quad \tau_{\ell t \text{ rupt.}} \leq 0$$

Stating that the criterion is saturated for each simple state of stress corresponding to each of the failure strength taken successively, the criterion takes the form

$$\frac{\sigma_{\ell}}{\sigma_{\ell \text{ rupt.}}} + \frac{\sigma_t}{\sigma_t \text{ rupt.}} + \frac{\tau_{\ell t}}{\tau_{\ell t \text{ rupt.}}} \leq 1$$

In the 3D space defined by the coordinate system σ_{ℓ}, σ_t , and $\tau_{\ell t}$, this criterion translates into eight equations of planes corresponding to the different failure strengths seen above.

Thus, the boundary surface or failure envelope in the coordinate system $(\sigma_{\ell}, \sigma_t, \tau_{\ell t})$ corresponds to the volume bounded by these eight planes. It is an octahedron, as shown in Figure 14.7.

It should be noted⁸ that this criterion form provides quite satisfactory results for a unidirectional ply in plane (σ, τ_{ℓ}) for the quadrant I and in plane $(\sigma_{\ell}, \sigma_t)$ for the quadrants II and IV. However, it is too **pessimistic** in the same plane $(\sigma_{\ell}, \sigma_t)$ for the quadrants I and III (biaxial state of stress in tension and especially in compression).

Note: Possibly because of that, or due to a lack of sufficient experimental knowledge until recently, this criterion is apparently never cited in the literature. This is surprising because it has the merit of never being dangerously optimistic and a little regrettable given its simplicity.

14.2.3.2 Example: Maximum Stress Failure Criterion

The previous criterion is most commonly replaced by a simplistic derivative that is to neglect the physical stress coupling that is observed on the previous relationship. We then get the following **maximum stress failure criterion**:

$$\frac{\sigma_{\ell}}{\sigma_{\ell \text{ rupt.}}} \leq 1; \quad \frac{\sigma_t}{\sigma_t \text{ rupt.}} \leq 1; \quad \frac{\tau_{\ell t}}{\tau_{\ell t \text{ rupt.}}} \leq 1$$

where the algebraic failure strength value corresponding to the numerator algebraic stress value is placed at denominator. The failure envelope now is the parallelepiped shown in Figure 14.8.

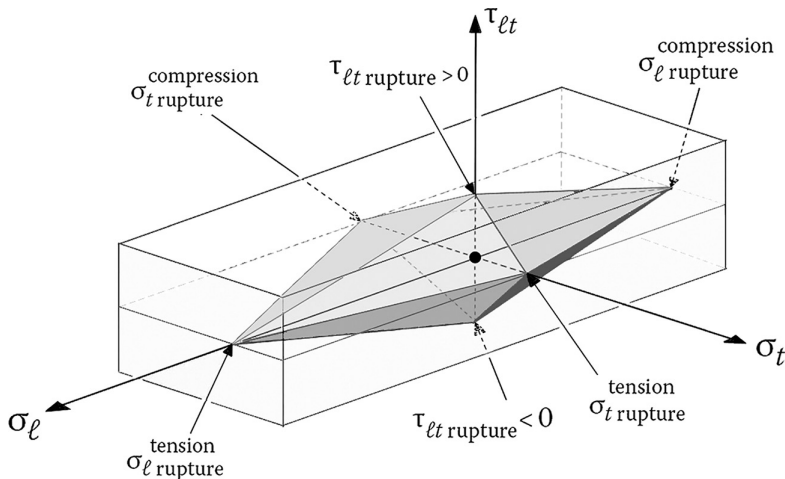


FIGURE 14.8 Failure envelope in the coordinate system $(\sigma_{\ell}, \sigma_t, \tau_{\ell t})$.

This gets an **often optimistic** criterion, that is, where the actual failure occurs before saturation of the criterion. From the reliability perspective, this is no better than the previous criterion. However, this criterion is commonly used as a first approximation by linking it to safety factors.

14.2.3.3 Note: Maximum Eligible Strain Criterion

In such a simple way, a noninteractive failure criterion based on maximum deformation by introducing practical values of maximum allowable strains can be defined. Then a cuboid in the space of strains $(\epsilon_\ell, \epsilon_t, \gamma_{\ell t})$ is obtained for boundary surface. It will be recalled that allowable strains are a major concern of aircraft industry, as we have already reported (see Section 5.4.5). We return in more detail below to the conversion of a stress criterion in terms of strains (see Sections 14.4 and 15.4.1).

14.2.4 QUADRATIC FAILURE CRITERION

14.2.4.1 General Form

$$f(\Sigma) = b_{ijkl}\sigma_{ij}\sigma_{kl} + a_{ij}\sigma_{ij} \leq 1 \quad (14.1)$$

Because of the symmetry property $\sigma_{ij} = \sigma_{ji}$, the developed form of this criterion shows linear terms characterized by 6 separate coefficients, by grouping of terms a_{ij} , and quadratic terms with 21 separate coefficients, by grouping⁹ of terms b_{ijkl} .

14.2.4.2 Orthotropic Material

As reported in Section 14.2.2, when changing axis system by pivoting 180° around the ℓ -axis, or around the t -axis, the quadratic form making up the criterion should remain invariant for a same stress state. Thus, 12 coefficients among the 21 of this quadratic form disappear¹⁰, and it is expressed by means of 9 separate coefficients. Similarly, separate coefficients of linear part are reduced to 3.

14.2.4.3 Specific Case of Plane Stress: The Tsai-Wu Criterion

For an orthotropic material and a plane state of stress in symmetry plane (ℓ, t) , the criterion can be written in the following form¹¹:

$$f(\Sigma) = b_\ell \sigma_\ell^2 + 2 \times b_0 \sigma_\ell \sigma_t + b_t \sigma_t^2 + b_{\ell t} \tau_{\ell t}^2 + a_\ell \sigma_\ell + a_t \sigma_t \leq 1 \quad (14.2)$$

which can also take the form:

$$f(\Sigma) = \begin{Bmatrix} \sigma_\ell \\ \sigma_t \\ \tau_{\ell t} \end{Bmatrix}^t \begin{bmatrix} b_\ell & b_0 & 0 \\ b_0 & b_t & 0 \\ 0 & 0 & b_{\ell t} \end{bmatrix} \begin{Bmatrix} \sigma_\ell \\ \sigma_t \\ \tau_{\ell t} \end{Bmatrix} + \begin{Bmatrix} \sigma_\ell \\ \sigma_t \\ 0 \end{Bmatrix}^t \begin{bmatrix} a_\ell \\ a_t \\ 0 \end{bmatrix} \leq 1 \quad (14.3)$$

When this criterion is saturated, the representative point of stresses $(\sigma_\ell, \sigma_t, \tau_{\ell t})$ moves on the failure envelope. In fact, this surface is an ellipsoid provided that the three matrix eigenvalues in Equation 14.3 are positive, i.e., if:

$$b_\ell > 0; \quad b_t > 0; \quad b_{\ell t} > 0; \quad (b_\ell b_t - b_0^2) > 0 \quad (14.4)$$

In order to evaluate the b_i and a_i coefficients in Equation 14.3, one can perform five strength tests in order to provide the stresses for rupture:

$$\sigma_{\ell \text{rupt.}}^{\text{tens.}} > 0; \quad \sigma_{\ell \text{rupt.}}^{\text{comp.}} < 0; \quad \sigma_{t \text{rupt.}}^{\text{tens.}} > 0; \quad \sigma_{t \text{rupt.}}^{\text{comp.}} < 0; \quad \tau_{\ell t \text{rupt.}} \leq 0$$

By using these experimental stress values that saturate the criterion:

- Uniaxial tension along ℓ :

$$b_\ell \times (\sigma_{\ell \text{rupt.}}^{\text{tens.}})^2 + a_\ell \times \sigma_{\ell \text{rupt.}}^{\text{tens.}} = 1$$

- Uniaxial compression along ℓ :

$$b_\ell \times (\sigma_{\ell \text{rupt.}}^{\text{comp.}})^2 - a_\ell \times \|\sigma_{\ell \text{rupt.}}^{\text{comp.}}\| = 1$$

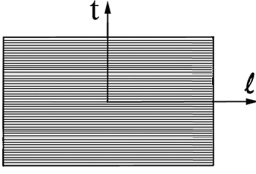
etc. Remembering that due to the predominant influence of fibers:

$$\sigma_{\ell \text{rupt.}}^{\text{tens.}} > \|\sigma_{\ell \text{rupt.}}^{\text{comp.}}\|$$

and due to the matrix prevalence:

$$\sigma_{t \text{rupt.}}^{\text{tens.}} < \|\sigma_{t \text{rupt.}}^{\text{comp.}}\|$$

one obtains for coefficients in Equation 14.3 and for the condition $(b_\ell b_t - b_0^2) > 0$:



$$f(\Sigma) = \begin{Bmatrix} \sigma_\ell \\ \sigma_t \\ \tau_{\ell t} \end{Bmatrix}^t \begin{bmatrix} b_\ell & b_0 & 0 \\ b_0 & b_t & 0 \\ 0 & 0 & b_{\ell t} \end{bmatrix} \begin{Bmatrix} \sigma_\ell \\ \sigma_t \\ \tau_{\ell t} \end{Bmatrix} + \begin{Bmatrix} \sigma_\ell \\ \sigma_t \\ 0 \end{Bmatrix}^t \begin{bmatrix} a_\ell \\ a_t \\ 0 \end{bmatrix} \leq 1$$

$$b_\ell = \frac{1}{\sigma_{\ell \text{rupt.}}^{\text{tens.}} \times \|\sigma_{\ell \text{rupt.}}^{\text{comp.}}\|} > 0$$

$$b_t = \frac{1}{\sigma_{t \text{rupt.}}^{\text{tens.}} \times \|\sigma_{t \text{rupt.}}^{\text{comp.}}\|} > 0$$

$$b_{\ell t} = \frac{1}{\tau_{\ell t \text{rupt.}}^2} > 0$$

$$a_\ell = \frac{1}{\sigma_{\ell \text{rupt.}}^{\text{tens.}}} - \frac{1}{\|\sigma_{\ell \text{rupt.}}^{\text{comp.}}\|} < 0$$

$$a_t = \frac{1}{\sigma_{t \text{rupt.}}^{\text{tens.}}} - \frac{1}{\|\sigma_{t \text{rupt.}}^{\text{comp.}}\|} < 0$$

$$b_0 = \frac{b_0^*}{\sqrt{\sigma_{\ell \text{rupt.}}^{\text{tens.}} \times \|\sigma_{\ell \text{rupt.}}^{\text{comp.}}\| \times \sigma_{t \text{rupt.}}^{\text{tens.}} \times \|\sigma_{t \text{rupt.}}^{\text{comp.}}\|}}; \quad -1 < b_0^* < 1$$

(14.5)

Note: We note that the coupling term b_0 is just framed. Its experimental determination involves biaxial stresses tests difficult to implement and providing scattered values. If limiting ourselves to:

$$-1 < b_0^* \leq 0$$

We, thus, obtain the criterion known as the **Tsai-Wu** criterion. To mark the start of damage on initially intact ply, the following is commonly used:

$$b_0^* = -0.5 \tag{14.6}$$

TABLE 14.1
Unidirectional Carbon/Epoxy Ply (See Table 3.4)

b_ℓ (Pa ⁻²)	b_t (Pa ⁻²)	b_0 (Pa ⁻²)	$b_{\ell t}$ (Pa ⁻²)	a_ℓ (Pa ⁻¹)	a_t (Pa ⁻¹)
7 E^{-19}	1.7 E^{-16}	-0.54 E^{-17}	2.5 E^{-16}	-9.8 E^{-11}	1.7 E^{-8}
$f(\Sigma) = b_\ell \sigma_\ell^2 + 2 \times b_0 \sigma_\ell \sigma_t + b_t \sigma_t^2 + b_{\ell t} \tau_{\ell t}^2 + a_\ell \sigma_\ell + a_t \sigma_t < 1$					

This is the most used value because when the material becomes isotropic (identical rupture strengths in tension and in compression), one brings back to the von Mises criterion for normal stresses as described in Section 14.3.2.1.

Example: Consider the unidirectional carbon/epoxy ply whose characteristics are presented in Table 3.4. Starting from Equation 14.5 and writing the Tsai-Wu criterion with $b_0^* = -0.5$, we obtain the coefficients in Table 14.1.

14.2.4.4 Note: Simplified Form for the Quadratic Criterion

It consists of the homogeneous form

$$f(\Sigma) = b_{ijkl} \sigma_{ij} \sigma_{kl} \leq 1$$

Such writing provides significant advantages:

- a. For a given state of plane stress $(\sigma_\ell, \sigma_t, \tau_{\ell t})$ such as

$$f(\sigma_\ell, \sigma_t, \tau_{\ell t}) = \alpha^2 < 1$$

It is possible to multiply the loading by a specific loading factor k in order to reach saturation, that is,

$$f(k\sigma_\ell, k\sigma_t, k\tau_{\ell t}) = k^2 f(\sigma_\ell, \sigma_t, \tau_{\ell t}) = k^2 \alpha^2 = 1$$

which allows setting the **safety margin**:

$$\frac{k\sigma_\ell - \sigma_\ell}{\sigma_\ell} = k - 1 = \frac{1}{\alpha} - 1$$

It should be noted that this is not as simple when using a nonhomogeneous criterion (e.g., the previous failure criterion), in which

$$f(k\sigma_\ell, k\sigma_t, k\tau_{\ell t}) \neq k^2 f(\sigma_\ell, \sigma_t, \tau_{\ell t})$$

- b. This simplified criterion form appears as an extension toward composite materials of the classical **von Mises** criterion characterizing the yield strength. Then for an orthotropic material, the constants in the general quadratic form can be derived from nine basic tests:

- Six longitudinal tests: three tensile and three compression testing
- Three shear tests

This results in the so-called **Tsai–Hill** criterion, which is studied in Section 14.3.

- c. As noted above, there is no criterion that would totally fit everyone. Nevertheless, the Tsai–Hill criterion is the most used among quadratic criteria, particularly for Quad laminates, and in the aeronautic industry, as shown in Figure 14.9.

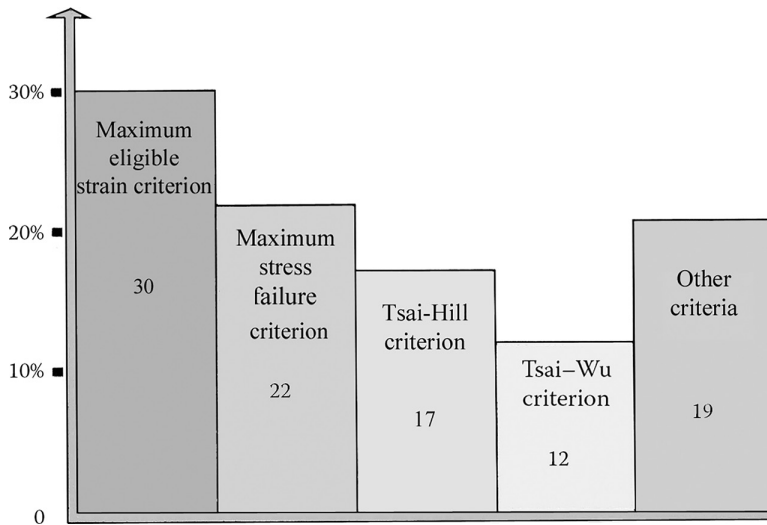


FIGURE 14.9 Use of failure criteria in aerospace industry.

So we will expose the detailed approach leading to the best known form of this stress criterion. Its application to laminates in typical regular areas is already being used in Sections 5.3, 5.4, and 12.1.3. This criterion is also used in several Applications in Section IV of the book¹².

14.3 TSAI-HILL FAILURE CRITERION

14.3.1 ISOTROPIC MATERIAL: THE VON MISES CRITERION

14.3.1.1 Distortion Strain Energy

In Figure 14.10, we denote by (I, II, III) the principal directions of the stress tensor Σ for a given point. The corresponding matrix is

$$\begin{bmatrix} \sigma_I & 0 & 0 \\ 0 & \sigma_{II} & 0 \\ 0 & 0 & \sigma_{III} \end{bmatrix}$$

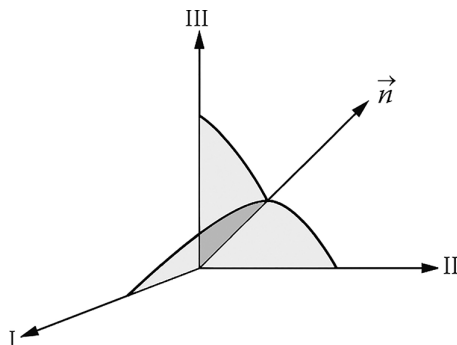


FIGURE 14.10 Principal directions of the stress tensor.

The general formula of the strain energy dW_{total} for an elementary volume dV surrounding the point under consideration can be written as

$$dW_{\text{total}} = \frac{1}{2} \sum_i \sum_j \sigma_{ij} \epsilon_{ij} dV$$

which is reduced here to

$$dW_{\text{total}} = \frac{1}{2} (\sigma_I \epsilon_I + \sigma_{II} \epsilon_{II} + \sigma_{III} \epsilon_{III}) dV$$

$\epsilon_I, \epsilon_{II}, \epsilon_{III}$ are the principal strain values that can be expressed as functions of stress using the constitutive Equation 10.1 as

$$\boldsymbol{\epsilon} = \frac{(1+\nu)}{E} \boldsymbol{\Sigma} - \frac{\nu}{E} \times \text{trace}(\boldsymbol{\Sigma}).$$

This leads to

$$\left(\frac{dW}{dV} \right)_{\text{total}} = \frac{1}{2} \left\{ \frac{(1+\nu)}{E} (\sigma_I^2 + \sigma_{II}^2 + \sigma_{III}^2) - \frac{\nu}{E} (\sigma_I + \sigma_{II} + \sigma_{III})^2 \right\}$$

(Note that (dW/dV) represents the strain energy density.)

The total elastic deformation above is due to the dilatation and distortion of the material. The von Mises criterion postulates that the material resists to an isotropic (or spherical) state of stress but will plastify when the distortion strain energy density reaches a critical value. This latter is written as

$$\left(\frac{dW}{dV} \right)_{\text{distortion}} = \left(\frac{dW}{dV} \right)_{\text{total}} - \left(\frac{dW}{dV} \right)_{\text{spherical stress}}$$

Here, the isotropic portion of the stress state is written as $(\sigma_I + \sigma_{II} + \sigma_{III})/3$. It creates an isotropic dilatation (Equation 10.1):

$$\epsilon = \frac{(1+\nu)}{E} \left(\frac{\sigma_I + \sigma_{II} + \sigma_{III}}{3} \right) - \frac{\nu}{E} (\sigma_I + \sigma_{II} + \sigma_{III})$$

Then

$$\begin{aligned} \left(\frac{dW}{dV} \right)_{\text{spherical stress}} &= \frac{1}{2} \left\{ 3 \times \left(\frac{\sigma_I + \sigma_{II} + \sigma_{III}}{3} \right) \times \epsilon \right\} \\ \left(\frac{dW}{dV} \right)_{\text{spherical stress}} &= \frac{1}{2} \left\{ \frac{(1+\nu)}{E} \frac{(\sigma_I + \sigma_{II} + \sigma_{III})^2}{3} - \frac{\nu}{E} (\sigma_I + \sigma_{II} + \sigma_{III})^2 \right\} \end{aligned}$$

We obtain then by replacing

$$\begin{aligned} \left(\frac{dW}{dV} \right)_{\text{distortion}} &= \frac{1}{2} \left\{ \frac{(1+\nu)}{E} (\sigma_I^2 + \sigma_{II}^2 + \sigma_{III}^2) - \frac{\nu}{E} (\sigma_I + \sigma_{II} + \sigma_{III})^2 \right. \\ &\quad \left. \dots - \frac{(1+\nu)}{E} \frac{(\sigma_I + \sigma_{II} + \sigma_{III})^2}{3} + \frac{\nu}{E} (\sigma_I + \sigma_{II} + \sigma_{III})^2 \right\} \end{aligned}$$

Hence,

$$\left(\frac{dW}{dV}\right)_{\text{distortion}} = \frac{1}{4G} \left\{ (\sigma_I^2 + \sigma_{II}^2 + \sigma_{III}^2) - \frac{(\sigma_I + \sigma_{II} + \sigma_{III})^2}{3} \right\} \quad (14.7)$$

We can rewrite the quantity in brackets as follows:

$$\begin{aligned} & \frac{2}{3} \{ \sigma_I^2 + \sigma_{II}^2 + \sigma_{III}^2 - \sigma_I \sigma_{II} - \sigma_{II} \sigma_{III} - \sigma_{III} \sigma_I \} \\ & \frac{2}{3} \{ (\sigma_I + \sigma_{II} + \sigma_{III})^2 - 3(\sigma_I \sigma_{II} + \sigma_{II} \sigma_{III} + \sigma_{III} \sigma_I) \} \\ \left(\frac{dW}{dV}\right)_{\text{distortion}} &= \frac{1}{6G} \{ (\sigma_I + \sigma_{II} + \sigma_{III})^2 - 3(\sigma_I \sigma_{II} + \sigma_{II} \sigma_{III} + \sigma_{III} \sigma_I) \} \end{aligned} \quad (14.8)$$

14.3.1.2 Notes

Following Figure 14.10, if we denote as \vec{n} the direction making the same angle with each of the principal directions, we observe on the facet with the normal \vec{n} a stress vector $\vec{\sigma}$ such that $\vec{\sigma} = \Sigma(\vec{n})$.

That is,

$$\{\sigma\} = \begin{Bmatrix} \sigma_I / \sqrt{3} \\ \sigma_{II} / \sqrt{3} \\ \sigma_{III} / \sqrt{3} \end{Bmatrix}$$

which can be decomposed as follows:

- A **normal** stress:

$$\sigma_n = \vec{\sigma} \cdot \vec{n}$$

Then,

$$\sigma_n = \frac{\sigma_I + \sigma_{II} + \sigma_{III}}{3}$$

It is the average stress value or isotropic stress from stress tensor¹³.

- A **shear** stress:

$$\tau = \sqrt{\sigma^2 - \sigma_n^2}$$

Then,

$$\tau^2 = \frac{1}{3} \left\{ \sigma_I^2 + \sigma_{II}^2 + \sigma_{III}^2 - \left(\frac{\sigma_I + \sigma_{II} + \sigma_{III}}{3} \right)^2 \right\}$$

which can be compared with Equation 14.7. Thus,

$$\left(\frac{dW}{dV}\right)_{\text{distortion}} = \frac{1}{2G} \left(\frac{3}{2} \tau^2 \right)$$

This shear value τ appears to be characteristic of the distortion energy.

- We should recognize in Equation 14.8 the presence of the first and second scalar invariants of the stress tensor that are independent of the coordinate system. In coordinate axes other than the principal directions, the second invariant can be written as

$$(\sigma_{11}\sigma_{22} - \tau_{12}^2) + (\sigma_{22}\sigma_{33} - \tau_{23}^2) + (\sigma_{33}\sigma_{11} - \tau_{31}^2)$$

Then we have for any coordinate system

$$\left(\frac{dW}{dV}\right)_{\text{distortion}} = \frac{1}{6G} \left\{ (\sigma_{11} + \sigma_{22} + \sigma_{33})^2 - 3 \left[(\sigma_{11}\sigma_{22} - \tau_{12}^2) + (\sigma_{22}\sigma_{33} - \tau_{23}^2) + (\sigma_{33}\sigma_{11} - \tau_{31}^2) \right] \right\}$$

or

$$\left(\frac{dW}{dV}\right)_{\text{distortion}} = \frac{1}{12G} \left\{ (\sigma_{11} - \sigma_{22})^2 + (\sigma_{22} - \sigma_{33})^2 + (\sigma_{33} - \sigma_{11})^2 + 6(\tau_{12}^2 + \tau_{23}^2 + \tau_{31}^2) \right\}$$

The elastic domain, that is, where the distortion energy is below a certain critical value, can then be characterized by the following condition:

$$a \left\{ (\sigma_{11} - \sigma_{22})^2 + (\sigma_{22} - \sigma_{33})^2 + (\sigma_{33} - \sigma_{11})^2 + 6(\tau_{12}^2 + \tau_{23}^2 + \tau_{31}^2) \right\} < 1 \quad (14.9)$$

To determine the constant, a single uniaxial test is sufficient. Indeed, if we denote by σ_e the elastic limit obtained from a tension–compression test, we have

$$a \times 2\sigma_e^2 = 1$$

Then,

$$a = \frac{1}{2\sigma_e^2}$$

14.3.2 ORTHOTROPIC MATERIAL: THE TSAI–HILL CRITERION

14.3.2.1 Notes

For an orthotropic material, a parallel with the von Mises criterion can be seen with the following observations:

- For an orthotropic material, the principal directions for the stresses do not coincide with the orthotropic directions, unlike the isotropic case.
- A uniaxial test is not enough to determine all the terms of the criterion equation, because the mechanical behavior varies with the direction of loading.
- For the application to fiber/resin composites, the limit of elasticity corresponds to the rupture limit.

We should then write in an orthotropic coordinate system noted (ℓ, t, z) an expression similar to Equation 14.9, that is,

$$a(\sigma_\ell - \sigma_t)^2 + b(\sigma_t - \sigma_z)^2 + c(\sigma_z - \sigma_\ell)^2 + d\tau_{\ell z}^2 + e\tau_{tz}^2 + f\tau_{t\ell}^2 \leq 1 \quad (14.10)$$

That must now be regarded as a failure criterion and no longer as a yield criterion.

14.3.2.2 Case of a Transversely Isotropic Material

As a simplification, in the following, we shall limit ourselves to the consideration of a transversely isotropic material¹⁴. It is represented in Figure 14.11 with the plane of isotropy (t, z). Then,

- The failure strength values are very different depending on whether we load the longitudinal direction ℓ or the transverse direction t .
- The failure strength values are different in uniaxial tension and compression.
- The constants a, b, c, d, e, f in Equation 14.10 will be determined from the following test results:
- Test along the longitudinal direction ℓ :

$$a + c = \frac{1}{\sigma_{\ell \text{rupt.}}^2}$$

- Test along the transverse direction t :

$$a + b = \frac{1}{\sigma_{t \text{rupt.}}^2}$$

- Test along the transverse direction z , due to transverse isotropy:

$$b + c = \frac{1}{\sigma_{t \text{rupt.}}^2}$$

Then,

$$a = c = \frac{1}{2\sigma_{\ell \text{rupt.}}^2}$$

$$b = \frac{1}{\sigma_{t \text{rupt.}}^2} - \frac{1}{2\sigma_{\ell \text{rupt.}}^2}$$

- Shear tests:

$$\tau_{\ell t} \rightarrow f = \frac{1}{\tau_{\ell t \text{rupt.}}^2}$$

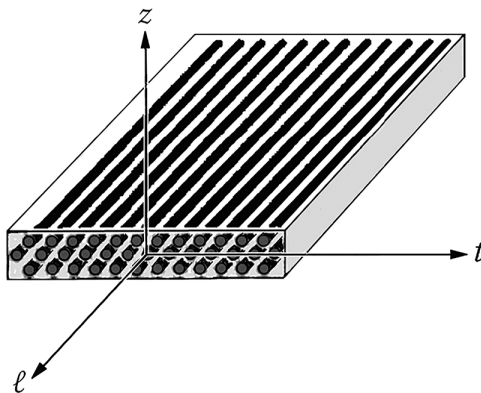


FIGURE 14.11 Transversely isotropic material.

$$\tau_{tz} \rightarrow e = \frac{1}{\tau_{tz,rupt.}^2}$$

$$\tau_{\ell t} \rightarrow d = \frac{1}{\tau_{\ell t,rupt.}^2} \text{ (due to transverse isotropy)}$$

Replacing in Equation 14.10,

$$\frac{1}{2\sigma_{\ell,rupt.}^2} \{(\sigma_{\ell} - \sigma_t)^2 + (\sigma_{\ell} - \sigma_z)^2\} - \left(\frac{1}{2\sigma_{\ell,rupt.}^2} - \frac{1}{\sigma_{t,rupt.}^2} \right) (\sigma_t - \sigma_z)^2 + \frac{1}{\tau_{\ell t,rupt.}^2} (\tau_{\ell t}^2 + \tau_{\ell z}^2) + \frac{\tau_{tz}^2}{\tau_{tz,rupt.}^2} \leq 1$$

And after calculation¹⁵

$$\frac{\sigma_{\ell}^2}{\sigma_{\ell,rupt.}^2} + \frac{\sigma_t^2 + \sigma_z^2}{\sigma_{t,rupt.}^2} - \frac{\sigma_{\ell}}{\sigma_{\ell,rupt.}^2} (\sigma_t + \sigma_z) + \sigma_z \sigma_t \left(\frac{1}{\sigma_{\ell,rupt.}^2} - \frac{2}{\sigma_{t,rupt.}^2} \right) + \frac{\tau_{\ell t}^2 + \tau_{\ell z}^2}{\tau_{\ell t,rupt.}^2} + \frac{\tau_{tz}^2}{\tau_{tz,rupt.}^2} \leq 1 \quad (14.11)$$

Note: For the case of a **3D** orthotropic material, similar reasoning starting from Equation 14.10 leads to a more general writing of the criterion, which takes the form

$$\begin{aligned} & \frac{\sigma_{\ell}^2}{\sigma_{\ell,rupt.}^2} + \frac{\sigma_t^2}{\sigma_{t,rupt.}^2} + \frac{\sigma_z^2}{\sigma_{z,rupt.}^2} - \left(\frac{1}{\sigma_{\ell,rupt.}^2} + \frac{1}{\sigma_{t,rupt.}^2} - \frac{1}{\sigma_{z,rupt.}^2} \right) \sigma_{\ell} \sigma_t \dots \\ & \dots - \left(\frac{1}{\sigma_{\ell,rupt.}^2} + \frac{1}{\sigma_{z,rupt.}^2} - \frac{1}{\sigma_{\ell,rupt.}^2} \right) \sigma_t \sigma_z - \left(\frac{1}{\sigma_{z,rupt.}^2} + \frac{1}{\sigma_{\ell,rupt.}^2} - \frac{1}{\sigma_{t,rupt.}^2} \right) \sigma_z \sigma_{\ell} \dots \\ & \dots + \frac{\tau_{\ell t}^2}{\tau_{\ell t,rupt.}^2} + \frac{\tau_{tz}^2}{\tau_{tz,rupt.}^2} + \frac{\tau_{z\ell}^2}{\tau_{z\ell,rupt.}^2} \leq 1 \end{aligned}$$

14.3.2.3 Case of Unidirectional Ply under In-plane Loading

For a plane state of stress in the plane (ℓ , t) (see Figure 14.9), we have

$$\sigma_z = \tau_{tz} = \tau_{tz} = 0$$

Equation 14.11 simplifies, and we obtain what is called the **Tsai–Hill** criterion for a ply that works within its plane:

$$\frac{\sigma_{\ell}^2}{\sigma_{\ell,rupt.}^2} + \frac{\sigma_t^2}{\sigma_{t,rupt.}^2} - \frac{\sigma_{\ell} \sigma_t}{\sigma_{\ell,rupt.}^2} + \frac{\tau_{\ell t}^2}{\tau_{\ell t,rupt.}^2} < 1 \quad (14.12)$$

Notes

- As already pointed out, the failure strength values of the **fiber/matrix** plies are different in tension and in compression¹⁶. Do not forget to place in denominator of each of the first three terms in Equation 14.12, the algebraic failure strength values corresponding to the nature of solicitations that are represented in numerators (tension or compression).
- Safety factor:** Let $\alpha^2 < 1$ the Tsai–Hill expression found for a state of stress $(\sigma_{\ell}, \sigma_t, \tau_{\ell t})$. As reported at the end of Section 14.2.4, we then can increase the loading via a multiplicative load factor k up to a limit value such as

$$\frac{(k\sigma_\ell)^2}{\sigma_{\ell \text{rupt.}}^2} + \frac{(k\sigma_t)^2}{\sigma_{t \text{rupt.}}^2} - \frac{(k\sigma_\ell)(k\sigma_t)}{\sigma_{\ell \text{rupt.}}^2} + \frac{(k\tau_{\ell t})^2}{\tau_{\ell t \text{rupt.}}^2} = k^2 \alpha^2 = 1$$

We define as safety margin the ratio

$$\frac{(k\sigma_\ell) - \sigma_\ell}{\sigma_\ell} = k - 1$$

which can also be written as

$$\text{Safety margin} = \frac{1}{\alpha} - 1$$

- The Tsai–Hill criterion generally provides quite satisfactory results for unidirectional plies in plane $(\sigma_t, \tau_{\ell t})$, in quadrants I and II. In the plane $(\sigma_\ell, \tau_{\ell t})$, the results are never dangerously optimistic in quadrants I and II. In plane (σ_ℓ, σ_t) , it gives good results for quadrants I and II. It is dangerously optimistic for quadrant III (biaxial state of stress in compression). In quadrant IV, the linear criterion that was already seen in Section 14.2.3 is of similar accuracy¹⁷.

14.3.3 EVOLUTION OF STRENGTH PROPERTIES OF A UNIDIRECTIONAL PLY DEPENDING ON THE DIRECTION OF SOLICITATION

14.3.3.1 Tensile and Compressive Strength

We intend evaluating the maximum stress σ_x that can be exerted on the ply in the x -direction in Figure 14.12.

The stress values $(\sigma_\ell, \sigma_t, \tau_{\ell t})$ in orthotropic axes are given by Equation 11.4 as

$$\begin{Bmatrix} \sigma_\ell \\ \sigma_t \\ \tau_{\ell t} \end{Bmatrix} = \begin{bmatrix} c^2 & s^2 & -2cs \\ s^2 & c^2 & 2cs \\ cs & -cs & (c^2 - s^2) \end{bmatrix} \begin{Bmatrix} \sigma_x \\ 0 \\ 0 \end{Bmatrix}$$

where we recall that $c = \cos \theta$ and $s = \sin \theta$. Thus,

$$\sigma_\ell = c^2 \times \sigma_x; \quad \sigma_t = s^2 \times \sigma_x; \quad \tau_{\ell t} = sc \times \sigma_x$$

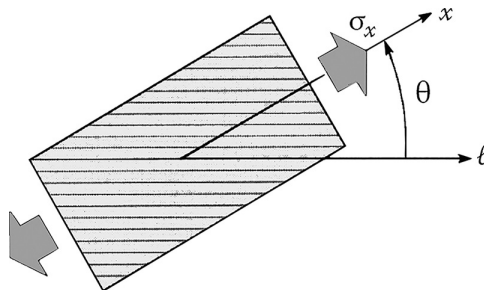


FIGURE 14.12 Loading direction distinct from orthotropic axes.

Substituting into the Tsai–Hill criterion of Equation 14.12, we have

$$\sigma_x^2 \left\{ \frac{c^4}{\sigma_{\ell \text{rupt.}}^2} + \frac{s^4}{\sigma_{t \text{rupt.}}^2} - \frac{c^2 s^2}{\sigma_{\ell \text{rupt.}}^2} + \frac{c^2 s^2}{\tau_{\ell t \text{rupt.}}^2} \right\} \leq 1$$

Then,

$$\sigma_{x \text{rupt.}} = \frac{1}{\sqrt{\frac{c^4}{\sigma_{\ell \text{rupt.}}^2} + \frac{s^4}{\sigma_{t \text{rupt.}}^2} + c^2 s^2 \left(\frac{1}{\tau_{\ell t \text{rupt.}}^2} - \frac{1}{\sigma_{\ell \text{rupt.}}^2} \right)}}$$

Notes

- If σ_x is a tensile stress, then $\sigma_{\ell \text{rupt.}}$ and $\sigma_{t \text{rupt.}}$ are failure strength values in tension. Indeed:
When $\theta=0^\circ$: $\sigma_{x \text{rupt.}} = \sigma_{\ell \text{rupt.}}$.
When $\theta=90^\circ$: $\sigma_{x \text{rupt.}} = \sigma_{t \text{rupt.}}$.
- When θ varies, the progression of $\sigma_{x \text{rupt.}}$ is represented by the curve in Figure 3.8 (see Section 3.3.2).

14.3.3.2 Shear Strength

For pure shear state as represented in Figure 14.13, we will have in an analogous manner:

$$\begin{Bmatrix} \sigma_\ell \\ \sigma_t \\ \tau_{\ell t} \end{Bmatrix} = \begin{bmatrix} c^2 & s^2 & -2cs \\ s^2 & c^2 & 2cs \\ cs & -cs & (c^2 - s^2) \end{bmatrix} \begin{Bmatrix} 0 \\ 0 \\ \tau_{xy} \end{Bmatrix}$$

$$\sigma_\ell = -2cs \times \tau_{xy}; \quad \sigma_t = 2cs \times \tau_{xy}; \quad \tau_{\ell t} = (c^2 - s^2) \times \tau_{xy} \quad (14.13)$$

Using this in the Tsai–Hill criterion in Equation 14.12,

$$\tau_{xy}^2 \left\{ \frac{4c^2 s^2}{\sigma_{\ell \text{rupt.}}^2} + \frac{4c^2 s^2}{\sigma_{t \text{rupt.}}^2} + \frac{4c^2 s^2}{\sigma_{\ell \text{rupt.}}^2} + \frac{(c^2 - s^2)^2}{\tau_{\ell t \text{rupt.}}^2} \right\} \leq 1$$

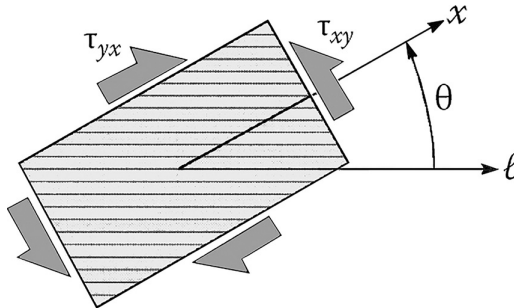


FIGURE 14.13 Pure shear in (x, y) axes.

Then,

$$\tau_{xy\text{rupt.}} = \frac{1}{\sqrt{4c^2s^2\left(\frac{2}{\sigma_{\ell\text{rupt.}}^2} + \frac{1}{\sigma_{t\text{rupt.}}^2}\right) + \frac{(c^2 - s^2)^2}{\tau_{\ell t\text{rupt.}}^2}}}$$

Note: Here, taking into account the arrangement in Figure 14.13 ($\tau_{xy} > 0$) and Equations 14.13, $\sigma_{\ell\text{rupt.}}$ will be the compression failure strength and $\sigma_{t\text{rupt.}}$ the tensile failure strength, and this applies for $0^\circ \leq \theta \leq 90^\circ$.

14.4 STRESS CRITERION TRANSLATED INTO STRAIN SPACE

14.4.1 ADVANTAGE OF THE APPROACH

- A maximum allowable strain-based criterion is often preferred for high performance applications. A typical example being aircraft construction, as already mentioned (see Sections 5.4.5, 14.2.3 and Figure 14.9). Particularly suited to quasi-orthotropic D-D laminates, this approach will be detailed and implemented in Chapter 15.
- Consider a laminate made up of plies of different orientations with respect to reference axes. When this laminate is subjected to In-plane loading or to bending and torsional moments, we saw in Chapter 12 how to calculate stresses in each ply constituting the laminate. Along a transverse cut of the laminate, these stresses vary depending on the orientation of considered plies (see Figure 12.6). On the other hand, strains of every ply coincide with the overall laminate strain¹⁸.
- Finally, one can notice that the quadratic criterion (see Equation 14.3) built on a positive definite symmetric matrix is analogous to an energy quadratic form built on the elastic constitutive law and transforms in the same way.

14.4.2 FORM OF THE CRITERION IN THE PLY AXES (ℓ, t)

Using Equation 11.6 that we recall:

$$\begin{Bmatrix} \sigma_\ell \\ \sigma_t \\ \tau_{\ell t} \end{Bmatrix} = \begin{bmatrix} \bar{E}_\ell & \nu_{\ell t}\bar{E}_\ell & 0 \\ \nu_{t\ell}\bar{E}_t & \bar{E}_t & 0 \\ 0 & 0 & G_{\ell t} \end{bmatrix} \begin{Bmatrix} \varepsilon_\ell \\ \varepsilon_t \\ \gamma_{\ell t} \end{Bmatrix} = [\bar{E}]_{\ell t} \begin{Bmatrix} \varepsilon_\ell \\ \varepsilon_t \\ \gamma_{\ell t} \end{Bmatrix}$$

with

$$\bar{E}_\ell = \frac{E_\ell}{1 - \nu_{\ell t}\nu_{t\ell}} \quad ; \quad \bar{E}_t = \frac{E_t}{1 - \nu_{\ell t}\nu_{t\ell}} \quad (14.14)$$

and rewriting the Tsai-Wu criterion (see Equations 14.5, 14.6) as:

$$f(\Sigma) = \begin{Bmatrix} \varepsilon_\ell \\ \varepsilon_t \\ \gamma_{\ell t} \end{Bmatrix}^t [\bar{E}]_{\ell t} \begin{bmatrix} b_\ell & b_0 & 0 \\ b_0 & b_t & 0 \\ 0 & 0 & b_{\ell t} \end{bmatrix} [\bar{E}]_{\ell t} \begin{Bmatrix} \varepsilon_\ell \\ \varepsilon_t \\ \gamma_{\ell t} \end{Bmatrix} + \begin{Bmatrix} \varepsilon_\ell \\ \varepsilon_t \\ 0 \end{Bmatrix}^t [\bar{E}]_{\ell t} \begin{Bmatrix} a_\ell \\ a_t \\ 0 \end{Bmatrix} < 1$$

leads to:

$$\begin{aligned}
 f(\Sigma) &= \begin{Bmatrix} \varepsilon_\ell \\ \varepsilon_t \\ \gamma_{\ell t} \end{Bmatrix}^T \begin{bmatrix} b'_\ell & b'_0 & 0 \\ b'_0 & b'_t & 0 \\ 0 & 0 & b'_{\ell t} \end{bmatrix} \begin{Bmatrix} \varepsilon_\ell \\ \varepsilon_t \\ \gamma_{\ell t} \end{Bmatrix} + \begin{Bmatrix} \varepsilon_\ell \\ \varepsilon_t \end{Bmatrix}^T \begin{Bmatrix} a'_\ell \\ a'_t \end{Bmatrix} < 1 \\
 b'_\ell &= b_\ell \bar{E}_\ell^2 + b_t (\nu_{\ell t} \bar{E}_\ell)^2 + 2b_0 \nu_{\ell t} \bar{E}_\ell^2 \\
 b'_t &= b_t \bar{E}_t^2 + b_\ell (\nu_{\ell t} \bar{E}_t)^2 + 2b_0 \nu_{\ell t} \bar{E}_t^2 \\
 b'_0 &= b_\ell \nu_{\ell t} \bar{E}_\ell^2 + b_t \nu_{\ell t} \bar{E}_t^2 + b_0 \bar{E}_\ell \bar{E}_t (1 + \nu_{\ell t} \nu_{t\ell}) \\
 b'_{\ell t} &= b_{\ell t} G_{\ell t}^2 \\
 a'_\ell &= a_\ell \bar{E}_\ell + a_t \nu_{\ell t} \bar{E}_t; \quad a'_t = a_t \nu_{\ell t} \bar{E}_\ell + a_\ell \bar{E}_t
 \end{aligned} \tag{14.15}$$

14.4.3 EXAMPLE: UNIDIRECTIONAL CARBON/EPOXY

With elastic characteristics as defined in Table 3.4, we will have the values in (Table 14.2):

Considering these values and writing the Tsai-Wu criterion (see Equation 14.15) expressed in strains with $b'_0 = -0.5$ (see Equation 14.5), one obtains the dimensionless coefficients in Table 14.3.

Later in Section 15.5 of Chapter 15, we return to the advantages of such writing.

TABLE 14.2

Unidirectional Carbon/Epoxy

Table 3.4	$V_f(\%)$	$E_\ell(\text{GPa})$	$E_t(\text{GPa})$	$G_{\ell t}(\text{GPa})$	$\nu_{\ell t}$	Equation 11.6	$\bar{E}_\ell(\text{GPa})$	$\bar{E}_t(\text{GPa})$	$G_{\ell t}(\text{GPa})$	$\nu_{\ell t} \bar{E}_\ell(\text{GPa})$
	60%	134	7	4.2	0.25		134.4	7	4.2	1.75

TABLE 14.3

Tsai-Wu Criterion Converted in Strain

b'_ℓ	b'_t	b'_0	$b'_{\ell t}$	a'_ℓ	a'_t
10,600	8,200	-2,850	4,400	17	118
$f(\Sigma) = b'_\ell \varepsilon_\ell^2 + b'_t \varepsilon_t^2 + 2b'_0 \varepsilon_\ell \varepsilon_t + b'_{\ell t} \gamma_{\ell t}^2 + a'_\ell \varepsilon_\ell + a'_t \varepsilon_t < 1$					

14.5 TAKING INTO ACCOUNT THE PLY FAILURE

14.5.1 MECHANICAL PROPERTIES OF DAMAGED PLY

Saturation of failure criterion indicates that plies in a same orientation deteriorate according to the process described in Section 14.1.4. The laminate is at the first stage of ply failure, or “First Ply Failure”. The first damage is considered to relate to stiffness, not to strength. The damaged plies see some of their elastic properties reduced while initial mechanical strengths remain unchanged, as indicated in Table 14.4.

One has to use semi empirical relations to estimate the degraded properties values. In Equation 14.16, E_m and G_m are the resin moduli and V_f the volume content of fibers¹⁹.

TABLE 14.4**Matrix Degradation: Degraded and Intact Properties**

Degraded properties	E_t	\searrow	E'_t	$G_{\ell t}$	\searrow	$G'_{\ell t}$	$\nu_{\ell t}$	\searrow	$\nu'_{\ell t}$	b_0^*	\searrow	$b_0'^*$	
Intact properties	E_ℓ			$\sigma_{\ell \text{rupt.}}^{\text{tens.}}$			$\sigma_{\ell \text{rupt.}}^{\text{comp.}}$			$\sigma_{t \text{rupt.}}^{\text{tens.}}$		$\sigma_{t \text{rupt.}}^{\text{comp.}}$	$\tau_{\ell t \text{rupt.}}$

$$\begin{aligned}
 E'_t &= \frac{1 + 0.516 \times \left(\frac{1}{V_f} - 1 \right)}{\frac{1}{E_t} + 0.516 \times \left(\frac{1}{V_f} - 1 \right) \left(\frac{1}{E_t} + \frac{5.67}{E_m} \right)} \\
 G'_{lt} &= \frac{1 + 0.316 \times \left(\frac{1}{V_f} - 1 \right)}{\frac{1}{G_{lt}} + 0.316 \times \left(\frac{1}{V_f} - 1 \right) \left(\frac{1}{G_{lt}} + \frac{5.67}{G_m} \right)} \\
 \nu'_{lt} &= 0.15 \times \nu_{lt}; \quad b_0'^* = 0.15 \times b_0^*
 \end{aligned}$$

(14.16)

14.5.2 EXAMPLE

For the unidirectional carbon/epoxy ply, the characteristics of which are given in Section 3.3.3, and with the epoxy resin properties in Table 1.4, we obtain the results in Table 14.5.

14.5.3 CONSEQUENCES FOR STRENGTH-LAMINATE ANALYSIS

When analyzing a loaded laminate with initially intact plies and when some plies are damaged, their mechanical properties have to be modified according to Table 14.4. A new “damaged” laminate is, thus, recomposed. From there:

TABLE 14.5**Intact and Degraded Carbon/Epoxy Unidirectional Ply**

$V_f = 60\%$	Intact	Degraded	Epoxy Resin
E_t (GPa)	134	134	E_m (GPa) = 4.5
E_ℓ (GPa)	7	2.15	
ν_{lt}	0.25	0.04	
G_{lt} (GPa)	4.2	1.17	G_m (GPa) = 1.6
$\sigma_{\ell \text{rupt.}}^{\text{tens.}}$ (MPa)	1,270	1,270	
$\sigma_{\ell \text{rupt.}}^{\text{comp.}}$ (MPa)	1,130	1,130	
$\sigma_{t \text{rupt.}}^{\text{tens.}}$ (MPa)	42	42	
$\sigma_{t \text{rupt.}}^{\text{comp.}}$ (MPa)	141	141	
$\tau_{lt \text{rupt.}}$ (MPa)	63	63	
b_0^*	-0.5	-0.075	

- One can constitute a model with progressive damage. The damaged laminate obtained is analyzed again ply by ply. The process continues until failure occurs for all plies²⁰.
- Alternatively, a possible ply failure can also be taken into account from the start. This method is implemented in Chapter 15 (see Section 15.5).

NOTES

- 1 In this context, dedicated numerical finite element models are helpful in order to simulate the degradation process in the part area where the loads are concentrating.
- 2 See also Figure 6.1 for damage around a drilled hole.
- 3 See Application 20.7.
- 4 See Application 20.7.
- 5 Such an assumption, made without any consideration of the limitations of a strict analogy, should be taken with caution.
- 6 The modeling implicitly assumes that these axes are identical to the orthotropic ones considered up to now.
- 7 It should be noted that after a 180° rotation around the ℓ -axis, on Figure 14.7, we observe a change in the sign of shear $\tau_{\ell t}$ leading to an antisymmetric term in the criterion, which, thus, should disappear. We will retain, however, here the term $\tau_{\ell t}$ in the criterion, in order to take into account reality of physical stress coupling effects.
- 8 Based on the results of the **World Wide Failure Exercises** already mentioned (see Bibliography).
- 9 For example, the coefficient of term in $\sigma_{13}\sigma_{23}$ is written as

$$(b_{1323} + b_{1332} + b_{2313} + b_{2331} + b_{3123} + b_{3132} + b_{3213} + b_{3231})$$

- 10 For example, after a rotation by 180° about the ℓ -axis, the change in sign of stresses $\sigma_{\ell z}$ and $\sigma_{t\ell}$ can be observed, giving rise to antisymmetry of terms in $\sigma_{zz}\sigma_{\ell z}$, $\sigma_{zz}\sigma_{t\ell}$, $\sigma_{tt}\sigma_{\ell z}$, $\sigma_{tt}\sigma_{t\ell}$, etc.
- 11 It remains then four coefficients for the quadratic part and two for the linear part.
- 12 See Applications 19.6, 20.2, 20.4, 20.8, 20.10, 20.12, and 20.16.
- 13 Recall the expression $(\sigma_I + \sigma_{II} + \sigma_{III})$ that constitutes the first scalar invariant of the stress tensor.
- 14 For an orthotropic material, the procedure is identical. See hereafter.
- 15 Beware, this is not valid for a fabric that is not transversely isotropic! See Application 20.10.
- 16 See values in Section 3.3.3.
- 17 See Bibliography: Hinton M.J. et al., World Wide Failure Exercises.
- 18 For example, the midplane strains are the same regardless the considered ply.
- 19 See Bibliography: Tsai S.W. and Melo J.D.D., Composite Materials/Design and Testing, 2015.
- 20 See Application 20.7.

15 Quasi-Orthotropic Homogenized Laminates or D-D Laminates

This chapter presents a recent approach to enable an optimized design of high-performance laminates. Based on the work of Professor Stephen Tsai and his team, the concept allows to build quasi-orthotropic laminates by stacking Sub-Laminate sets so-called D-D Sub-Laminates. In so doing, each set is composed of four plies and characterized by two privileged directions (Φ , Ψ), each doubled according to the pattern $\pm\Phi$ and $\pm\Psi$. This approach includes numerous advantages over Quadrangle Symmetric laminates $[0^\circ; \pm 45^\circ; 90^\circ]$ so-called Quad laminates previously described (see Section 5.2). Furthermore, manufacturing of such D-D laminates is well suited to the automated tape laying (ATL). The digital implementation of the laminate optimization process requires a specific calculation tool. Given at the end of the chapter is useful information about this tool and its free access.

15.1 TSAI MODULUS AND STIFFNESS CHARACTERIZATION OF A LAMINATE

15.1.1 TSAI MODULUS

15.1.1.1 Constitutive Equation of a Ply

Starting from the general relationship $\varepsilon_{ij} = \phi_{ijk} \times \sigma_{kl}$ (see Section 9.1), reduced to plane stresses $\{\sigma_{\ell\ell}; \sigma_{tt}; \tau_{\ell t}\}$ for a transversely isotropic ply (see Equation 9.5¹) leads to

$$\begin{Bmatrix} \varepsilon_{\ell\ell} \\ \varepsilon_{tt} \\ \varepsilon_{\ell t} \end{Bmatrix} = \begin{bmatrix} \frac{1}{E_\ell} & \frac{-\nu_{\ell t}}{E_t} & 0 \\ \frac{-\nu_{\ell t}}{E_\ell} & \frac{1}{E_t} & 0 \\ 0 & 0 & \frac{1}{2G_{\ell t}} \end{bmatrix} \begin{Bmatrix} \sigma_{\ell\ell} \\ \sigma_{tt} \\ \tau_{\ell t} \end{Bmatrix} \quad (15.1)$$

The first of the three behavior tensor invariants is the trace of the matrix above, constituting the so-called “compliance” invariant:

$$I_{\text{compliance}} = \frac{1}{E_\ell} + \frac{1}{E_t} + \frac{1}{2G_{\ell t}}$$

When inverting the previous constitutive equation and with the more convenient notations ℓ and t already seen:

$$\begin{Bmatrix} \sigma_\ell \\ \sigma_t \\ \tau_{\ell t} \end{Bmatrix} = \begin{bmatrix} \bar{E}_\ell & \nu_{\ell t} \bar{E}_\ell & 0 \\ \nu_{\ell t} \bar{E}_t & \bar{E}_t & 0 \\ 0 & 0 & 2G_{\ell t} \end{bmatrix} \begin{Bmatrix} \varepsilon_\ell \\ \varepsilon_t \\ \varepsilon_{\ell t} \end{Bmatrix} \quad (15.2)$$

With

$$\bar{E}_\ell = \frac{E_\ell}{1 - \nu_{\ell t} \nu_{t\ell}}; \quad \bar{E}_t = \frac{E_t}{1 - \nu_{\ell t} \nu_{t\ell}}$$

In the matrix above, the trace is the first “stiffness” invariant so-called the **Tsai modulus**² as

$$I_{\text{Tsai}} = \bar{E}_\ell + \bar{E}_t + 2G_{\ell t} \quad (15.3)$$

15.1.1.2 Unidirectional Ply in a Plane Laminate

Laminate axes are denoted (x, y) in Figure 15.1. As already shown (see Figure 11.1), the x axis of the laminate makes an angle θ with the fiber direction of the ply.

Writing the behavior of a ply in the (x, y) axes by following the procedure of Chapter 11, Section 11.2 leads to an equation similar to relation 11.8 with $\gamma_{xy} = 2\epsilon_{xy}$, that is:

$$\begin{Bmatrix} \sigma_x \\ \sigma_y \\ \tau_{xy} \end{Bmatrix} = \begin{bmatrix} \bar{E}_{11} & \bar{E}_{12} & \bar{E}_{13} \\ \bar{E}_{21} & \bar{E}_{22} & \bar{E}_{23} \\ \bar{E}_{31} & \bar{E}_{32} & 2\bar{E}_{33} \end{bmatrix} \begin{Bmatrix} \epsilon_x \\ \epsilon_y \\ \epsilon_{xy} \end{Bmatrix}$$

With off-axis stiffnesses \bar{E}_{ij} given by Equation 11.8.

The Tsai modulus can therefore be written alternatively:

$$I_{\text{Tsai}} = \bar{E}_\ell + \bar{E}_t + 2G_{\ell t} = \bar{E}_{11} + \bar{E}_{22} + 2\bar{E}_{33} \quad (15.4)$$

It can be noted that the Tsai modulus synthesizes the main stiffness properties of the layer.

15.1.1.3 Trace-Normalized Moduli

Trace-normalized moduli \bar{E}_{ij}^* are thus defined as:

$$\bar{E}_\ell^* = \frac{\bar{E}_\ell}{I_{\text{Tsai}}}; \quad \bar{E}_t^* = \frac{\bar{E}_t}{I_{\text{Tsai}}}; \quad G_{\ell t}^* = \frac{G_{\ell t}}{I_{\text{Tsai}}} \quad \text{and} \quad \bar{E}_{ij}^* = \frac{\bar{E}_{ij}}{I_{\text{Tsai}}} \quad (15.5)$$

- **Example:** For the carbon/epoxy unidirectional of Table 3.4, the trace-normalized values are summarized in Table 15.1.

The stiffness components vary with orientation θ as in Figure 11.2 (see Chapter 11). For example, for the previous carbon/epoxy ply, we obtain with trace-normalized form the values in Figure 15.2 where:

$$\bar{E}_{11}^* + \bar{E}_{22}^* + 2\bar{E}_{33}^* = 1$$

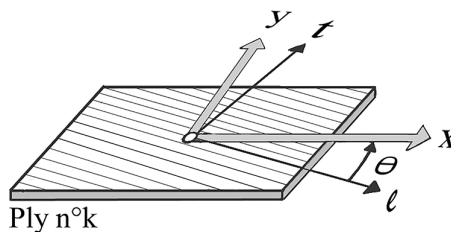


FIGURE 15.1 Ply n°k.

TABLE 15.1
Carbon/Epoxy Unidirectional: Moduli and Trace-Normalized Stiffness Components

Ply Moduli								
V_f	E_ℓ (GPa)	E_t (GPa)	G_{α} (GPa)	ν_{α}				
60%	134	7	4.2	0.25				
\bar{E}_ℓ (GPa)	\bar{E}_t (GPa)	G_{α} (GPa)	$\nu_{\ell t} \bar{E}_\ell$ (GPa)	I_{Tsal} (GPa)	\bar{E}_ℓ^*	\bar{E}_t^*	G_{α}^*	$\nu_{\ell t} \bar{E}_\ell^*$
134.4	7	4.2	1.75	149.8	0.897	0.047	0.028	0.012

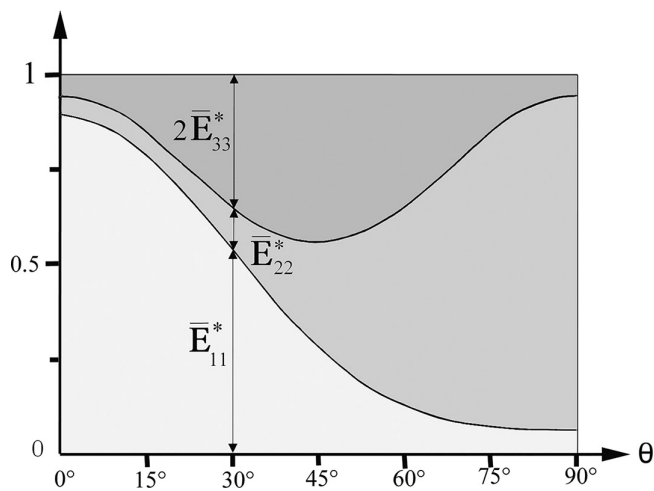


FIGURE 15.2 Trace-normalized stiffness coefficients varying with θ .

15.1.2 MASTER PLY

Concerning carbon/resin (CFRP) unidirectional plies, there is a range of about 15 marketed plies (thermosetting or thermoplastic resin) with fiber volume contents varying from 60% to 70%. Comparing the mechanical characteristics of these 15 products³ revealed a remarkable property: the trace-normalized moduli as defined in the previous paragraph show a low scatter. So much that they can all be assimilated to a single trace-normalized ply so-called the “**master ply**”. The characteristic values for this master ply are in Table 15.2 as well as the standard deviations observed for the 15 marketed plies.

Thus, to characterize the moduli of a unidirectional CFRP layer, it appears essential to know the value of its Tsai modulus (its stiffness trace), as well as the variations of the latter with environmental conditions.

TABLE 15.2
Characteristic Values of Master Ply

	E_ℓ^* (E_ℓ/I_T)	E_t^* (E_t/I_T)	G_{α}^* (G_{α}/I_T)	ν_{α}	\bar{E}_ℓ^* (\bar{E}_ℓ/I_T)	\bar{E}_t^* (\bar{E}_t/I_T)	G_{α}^* (G_{α}/I_T)	$\nu_{\ell t} \bar{E}_\ell^*$ ($\nu_{\ell t} \bar{E}_\ell/I_T$)
Master ply	0.880	0.052	0.031	0.32	0.885	0.052	0.031	0.017
Standard deviations	1.3%	0.05%	0.06%					

The Tsai modulus makes it possible to go back to the stiffness components of the ply from the knowledge of the master ply.

- **Example:** We want to determine the elastic moduli of a certain CFRP unidirectional. To this end, a tensile test is carried out on a coupon specimen in the fiber direction. This test provides the value $E_{\ell_{\text{measured}}}$ (GPa). We then deduce the Tsai modulus from Table 15.2:

$$E_{\ell}^{\text{th}} = 0.880 = \frac{E_{\ell_{\text{measured}}}}{I_{\text{Tsai}}} \Rightarrow I_{\text{Tsai}} = \frac{E_{\ell_{\text{measured}}}}{0.880}$$

Then, from Table 15.2, the other moduli can be deduced as follows

$$E_t = 0.052 \times I_{\text{Tsai}} ; \quad G_{\ell t} = 0.031 \times I_{\text{Tsai}}$$

It is worth to note greater precision than that which one would obtain from tests, particularly for the shear modulus $G_{\ell t}$, the experimental determination of which remaining difficult.

In the following we examine the extension of the use of the Tsai modulus.

15.1.3 TSAI MODULUS OF A LAMINATE

15.1.3.1 Reminder: Behavior Relationship

Let us first limit ourselves to the elastic behavior relationship of a laminated plate given by Equation 12.20 which we recall here (each of the n transversely isotropic plies being *a priori* different, with its own thickness e_k):

$$\begin{aligned} \begin{Bmatrix} N_x \\ N_y \\ T_{xy} \\ M_y \\ -M_x \\ -M_{xy} \end{Bmatrix} &= \begin{bmatrix} [A] & [B] \\ [B] & [C] \end{bmatrix} \begin{Bmatrix} \epsilon_{0x} \\ \epsilon_{0y} \\ \gamma_{0xy} \\ -\partial^2 w_0 / \partial x^2 \\ -\partial^2 w_0 / \partial y^2 \\ -2\partial^2 w_0 / \partial x \partial y \end{Bmatrix} \\ A_{ij} &= \sum_{k=1}^{\text{nth ply}} \bar{E}_{ij}^k e_k & C_{ij} &= \sum_{k=1}^{\text{nth ply}} \bar{E}_{ij}^k \left(\frac{z_k^3 - z_{k-1}^3}{3} \right) & B_{ij} &= \sum_{k=1}^{\text{nth ply}} \bar{E}_{ij}^k \left(\frac{z_k^2 - z_{k-1}^2}{2} \right) \end{aligned}$$

(15.6a)

Remember that:

- In equation above, off-axis stiffnesses \bar{E}_{ij}^k are given by Equation 11.8, z_k and z_{k-1} being the heights of the upper face, respectively lower of the ply n° k .
- N_x , N_y , T_{xy} are the In-plane resultants, and M_y , M_x , M_{xy} are the bending and twisting moments acting on the laminate (Cf. Equations 12.13, 12.14, and 12.15).
- The displacement field in the plate is described in Chapter 12 (see Section 12.1.4) and shown in Figure 12.3. We recall its form:

$$\begin{cases} u = u_0 - z \frac{\partial w_0}{\partial x} \\ v = v_0 - z \frac{\partial w_0}{\partial y} \\ w = w_0 \end{cases}$$

Where $u_0(x, y)$ and $v_0(x, y)$ are the displacement components in the mid-plane, and $w_0(x, y)$ the displacement out of this initial plane. Recall that for a laminate thickness h , we have

$$-\frac{h}{2} \leq z \leq \frac{h}{2}$$

- From this the strain field in the plate (Equation 12.12):

$$\begin{cases} \epsilon_x = \epsilon_{0x} - z \frac{\partial^2 w_0}{\partial x^2} \\ \epsilon_y = \epsilon_{0y} - z \frac{\partial^2 w_0}{\partial y^2} \\ \gamma_{xy} = \gamma_{0xy} - z \times 2 \frac{\partial^2 w_0}{\partial x \partial y} \end{cases} \quad (15.6b)$$

where ϵ_{0x} , ϵ_{0y} , γ_{0xy} are the Mid-plane strains and

$$-\frac{\partial^2 w_0}{\partial x^2}, -\frac{\partial^2 w_0}{\partial y^2}, -\frac{2\partial^2 w_0}{\partial x \partial y}$$

are curvatures of the middle surface.

15.1.3.2 In-plane Stiffness Matrix $[A]$

In the following, we limit ourselves to a laminate obtained by stacking of *identical* unidirectional layers with any orientations.

Writing the diagonal terms of $[A]$, we have successively:

$$A_{11} = \bar{E}_{11}^{k=1} \times e + \bar{E}_{11}^{k=2} \times e + \dots + \bar{E}_{11}^{k=n} \times e = e \times \sum_{k=1}^{k=n} \bar{E}_{11}^k$$

$$A_{22} = e \times \sum_{k=1}^{k=n} \bar{E}_{22}^k; \quad A_{33} = e \times \sum_{k=1}^{k=n} \bar{E}_{33}^k$$

Then considering the sum $A_{11} + A_{22} + 2A_{33}$

$$A_{11} + A_{22} + 2A_{33} = e \times \sum_{k=1}^{k=n} (\bar{E}_{11}^k + \bar{E}_{22}^k + 2\bar{E}_{33}^k)$$

Where we recognize the Tsai modulus (See Equation 15.4), a unique value whatever the ply orientation, namely:

$$\left(\bar{E}_{11}^k + \bar{E}_{22}^k + 2\bar{E}_{33}^k\right) = \left(\bar{E}_\ell + \bar{E}_t + 2G_{\ell t}\right) = I_{\text{Tsaï}} \quad \forall k$$

The laminate thickness being noted $h = n \times e$ we have:

$$A_{11} + A_{22} + 2A_{33} = n \times e \times \left(\bar{E}_\ell + \bar{E}_t + 2G_{\ell t}\right) = h \times I_{\text{Tsaï}}$$

From which we deduce:

$$I_{\text{Tsaï}} = \frac{1}{h} (A_{11} + A_{22} + 2A_{33}) \quad (15.7)$$

15.1.3.3 Flexural Stiffness Matrix [C]

We have successively, writing the diagonal terms of matrix [C] and starting from the underside of the laminate:

$$C_{11} = \bar{E}_{11}^{k=1} \times \frac{(z_1^3 - z_0^3)}{3} + \bar{E}_{11}^{k=2} \times \frac{(z_2^3 - z_1^3)}{3} + \dots + \bar{E}_{11}^{k=n} \times \frac{(z_n^3 - z_{n-1}^3)}{3}$$

$$C_{22} = \bar{E}_{22}^{k=1} \times \frac{(z_1^3 - z_0^3)}{3} + \bar{E}_{22}^{k=2} \times \frac{(z_2^3 - z_1^3)}{3} + \dots + \bar{E}_{22}^{k=n} \times \frac{(z_n^3 - z_{n-1}^3)}{3}$$

$$C_{33} = \bar{E}_{33}^{k=1} \times \frac{(z_1^3 - z_0^3)}{3} + \bar{E}_{33}^{k=2} \times \frac{(z_2^3 - z_1^3)}{3} + \dots + \bar{E}_{33}^{k=n} \times \frac{(z_n^3 - z_{n-1}^3)}{3}$$

Then considering the sum $C_{11} + C_{22} + 2C_{33}$:

$$\begin{aligned} C_{11} + C_{22} + 2C_{33} &= \left(\bar{E}_{11}^{k=1} + \bar{E}_{22}^{k=1} + 2\bar{E}_{33}^{k=1}\right) \times \frac{(z_1^3 - z_0^3)}{3} + \dots \\ &\dots + \left(\bar{E}_{11}^{k=n} + \bar{E}_{22}^{k=n} + 2\bar{E}_{33}^{k=n}\right) \times \frac{(z_n^3 - z_{n-1}^3)}{3} \end{aligned}$$

where appears the Tsai modulus of the ply. From where:

$$\begin{aligned} C_{11} + C_{22} + 2C_{33} &= I_{\text{Tsaï}} \times \left[\frac{(z_1^3 - z_0^3)}{3} + \frac{(z_2^3 - z_1^3)}{3} + \dots + \frac{(z_n^3 - z_{n-1}^3)}{3} \right] \\ C_{11} + C_{22} + 2C_{33} &= I_{\text{Tsaï}} \times \frac{(z_n^3 - z_0^3)}{3} \end{aligned}$$

h being the laminate thickness: $z_n = h/2$, $z_0 = -h/2$. Then:

$$I_{\text{Tsaï}} = \frac{12}{h^3} (C_{11} + C_{22} + 2C_{33}) \quad (15.8)$$

15.1.3.4 Coupling Stiffness Matrix $[B]$

The diagonal terms of matrix $[B]$ are written:

$$B_{11} = \bar{E}_{11}^{k=1} \times \frac{(z_1^2 - z_0^2)}{2} + \bar{E}_{11}^{k=2} \times \frac{(z_2^2 - z_1^2)}{2} + \dots + \bar{E}_{11}^{k=n} \times \frac{(z_n^2 - z_{n-1}^2)}{2}$$

$$B_{22} = \bar{E}_{22}^{k=1} \times \frac{(z_1^2 - z_0^2)}{2} + \bar{E}_{22}^{k=2} \times \frac{(z_2^2 - z_1^2)}{2} + \dots + \bar{E}_{22}^{k=n} \times \frac{(z_n^2 - z_{n-1}^2)}{2}$$

$$B_{33} = \bar{E}_{33}^{k=1} \times \frac{(z_1^2 - z_0^2)}{2} + \bar{E}_{33}^{k=2} \times \frac{(z_2^2 - z_1^2)}{2} + \dots + \bar{E}_{33}^{k=n} \times \frac{(z_n^2 - z_{n-1}^2)}{2}$$

Considering the sum $B_{11} + B_{22} + 2B_{33}$:

$$B_{11} + B_{22} + 2B_{33} = I_{\text{Tsay}} \times \frac{(z_n^2 - z_0^2)}{2} = I_{\text{Tsay}} \times \frac{(h^2 - h^2)}{8} = 0$$

- **Conclusion:** the stiffness properties of a unidirectional ply and of any laminate constructed from this ply are summarized by a unique invariant, the Tsai modulus, independently of any ply stacking sequence.

15.1.3.5 Guide Values for the Stiffness of a Carbon/Resin Laminate

Recall that in Equation 15.6, $[A]$ represents the In-plane stiffness matrix of the laminate. Since the plies are of identical properties, we have:

$$A_{ij} = \sum_{k=1}^{k=n} \bar{E}_{ij}^k \times e_k = e \times \sum_{k=1}^{k=n} \bar{E}_{ij}^k = h \times \frac{(\bar{E}_{ij}^1 + \dots + \bar{E}_{ij}^n)}{n}$$

By introducing the Tsai modulus:

$$A_{ij}^* = \frac{A_{ij}}{I_{\text{Tsay}}} = h \times \frac{(\bar{E}_{ij}^{*1} + \dots + \bar{E}_{ij}^{*n})}{n}$$

For example, for the longitudinal stiffness, we note the trace-normalized value:

$$\frac{1}{h} A_{11}^* = \frac{(\bar{E}_{11}^{*1} + \dots + \bar{E}_{11}^{*n})}{n}$$

Stiffness components \bar{E}_{11}^* are obtained for various orientations θ starting from Equation 11.8 and from the master ply characteristics in Table 15.2.

When considering the four orientations $[0^\circ; \pm 45^\circ; 90^\circ]$ of classical Quadrangle Symmetric laminates or “Quad” laminates, one obtain for the above dimensionless longitudinal stiffness some typical values summarized in Figure 15.3, valid for *all* marketed unidirectional CFRP plies.

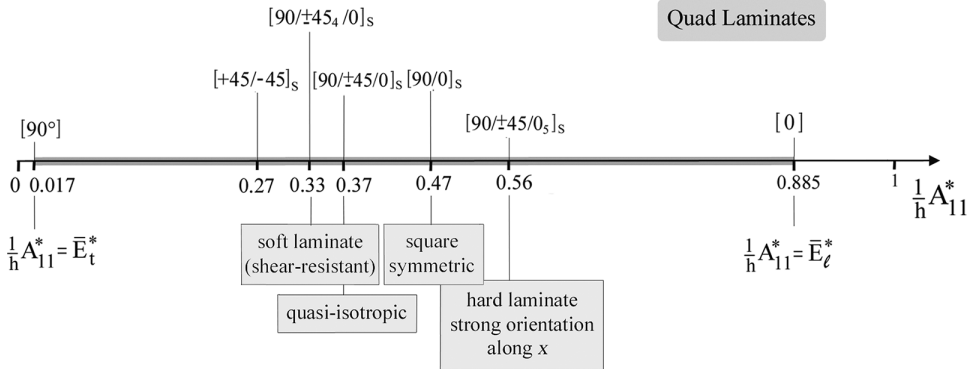


FIGURE 15.3 Dimensionless longitudinal stiffness of carbon/epoxy Quad laminates.

15.2 THE DOUBLE-DOUBLE SUB-LAMINATED SET

15.2.1 NOTES ON CLASSICAL QUADRANGLE SYMMETRIC LAMINATES OR “QUAD LAMINATES”

From Figure 15.3, the four-orientation design $[0^\circ, +45^\circ, -45^\circ, 90^\circ]$ of classic Quad Laminates leads to the following remarks:

- The values of $(1/h)A_{11}^*$ which can be obtained in this way are necessarily discrete. It appears difficult to envisage covering continuously the entire range $[0.017-0.885]$ using a realistic number of plies.
- We have seen⁴ in Chapter 5 that Mid-plane symmetry generally requires a minimum ply percentage of 10% in each of the four orientations. Consequently and apart from a localized minimum of 7 plies, the number of plies is more frequently greater than ten when directional stiffness must be reinforced (tensile-compression, shear, etc.).
- When increasing the loads acting on the laminate, it is necessary to increase the plies number, while respecting the symmetry. Recalling that one must avoid the accumulation of plies with same orientation (see Section 5.2.4.1) in order to limit free edge stresses (see Figure 14.3), and provide for minimal angular deviation as the orientation changes, it becomes very difficult to adopt a systematic approach to define the stacking order of plies. Indeed, the number of possible combinations quickly becomes too high.
- As a result, the final thickness of the Quad laminate has other disadvantages:
 - It can become too bulky, with an unacceptable mass for the envisaged application.
 - It is difficult to vary the thickness along the part because the progressive ply-elimination modifies the initial composition (see Figure 5.16).
 - Patch repair is tricky in order to restore the original composition.
 - A panel with thick edges is subject to edge effects (see Figure 14.3).

In what follows, the purpose is to define laminates offering greater simplicity and flexibility, both at the design stage and at the implementation stage in order to overcome these drawbacks.

15.2.2 DEFINITION OF THE “DOUBLE-DOUBLE” SUB-LAMINATED SET

A so-called “Double-Double” Sub-Laminated set, or more briefly “D-D set” is defined as consisting of four plies arranged in two “doubled” directions (sign + and sign –). With respect to the laminate x -axis in its plane (x, y) , we locate the orientation of these plies respectively by $\pm\Phi$ and $\pm\Psi$, with the conventions already used (see Figure 15.1).

This is shown schematically in Figure 15.4.

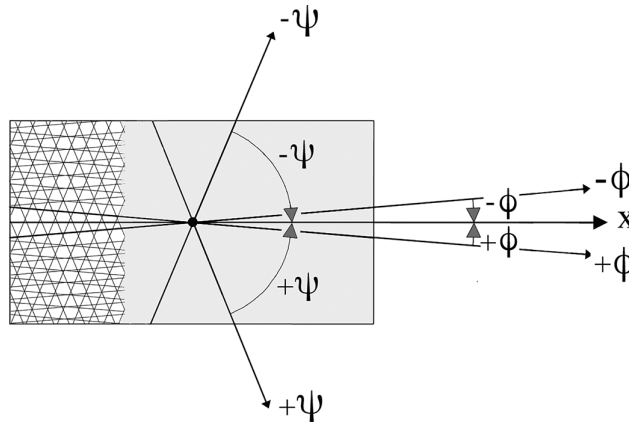


FIGURE 15.4 “Double-Double” sublaminated set.

15.2.3 PROPERTIES OF THE “DOUBLE-DOUBLE” SET

- The “Double-Double” set thus defined is balanced but does not present mirror symmetry.
- The possibility of varying continuously and independently the angles Φ and Ψ leads to a doubly continuous field of Sub-Laminates. This greatly expands the potential of performance. It can be seen, for example, in Figure 15.6 that it is possible to continuously cover the whole range of values of $(1/h)A_{11}^*$ unlike Quad-type laminates.
- **Example:** Figure 15.5 shows “Quad versus D-D” equivalence for the quasi-isotropic⁵ “historical” laminate⁶.
- In all cases, the “D-D” set has only four plies. It is thin. For example with the carbon/resin ply from Table 3.2, a D-D set will have a thickness of $4 \times 0.13 = 0.52$ mm.
- Let us compare the “Quad” and “D-D” designs based on the trace-normalized stiffnesses built on the Tsai modulus, that is to say:

$$\frac{1}{h}A_{11}^*; \quad \frac{1}{h}A_{22}^*; \quad \frac{1}{h}A_{33}^*$$

Table 15.3 shows equivalences between (non-symmetrical) Quad sets and D-D sets.

Figure 15.6 shows some D-D sets on the scale of trace-normalized longitudinal stiffness for *all* CFRP laminates. It is worthy to note the possibility of very significant stiffness values.

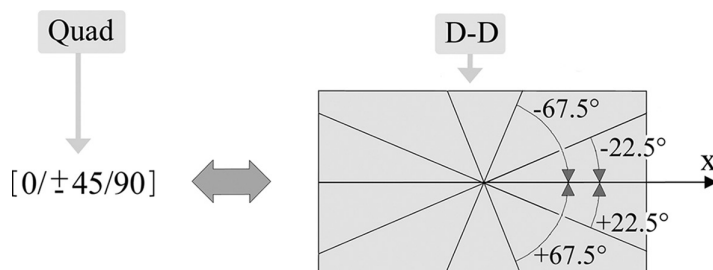


FIGURE 15.5 Quasi-isotropic D-D set.

TABLE 15.3

Some Typical Equivalences between Sub-Laminated Sets (Quad versus D-D)

Equivalence Quad Set \Leftrightarrow D-D set	$\frac{1}{h} A_{11}^*$	$\frac{1}{h} A_{22}^*$	$\frac{2}{h} A_{33}^*$
$[0/\pm 45/90]$ (4 plies) $\Leftrightarrow [\pm 22.5/\pm 67.5]$ (4 plies) <i>quasi-isotropic</i>	0.37	0.37	2×0.128
$[90/\pm 45_4/0]$ (10 plies) $\Leftrightarrow [\pm 29/\pm 60]$ (4 plies) <i>shear resistant (soft laminate)</i>	0.33	0.33	2×0.17
$[90/\pm 45/0_5]$ (8 plies) $\Leftrightarrow [\pm 0/\pm 53]$ (4 plies) <i>strongly oriented along x (hard laminate)</i>	0.56	0.22	2×0.11

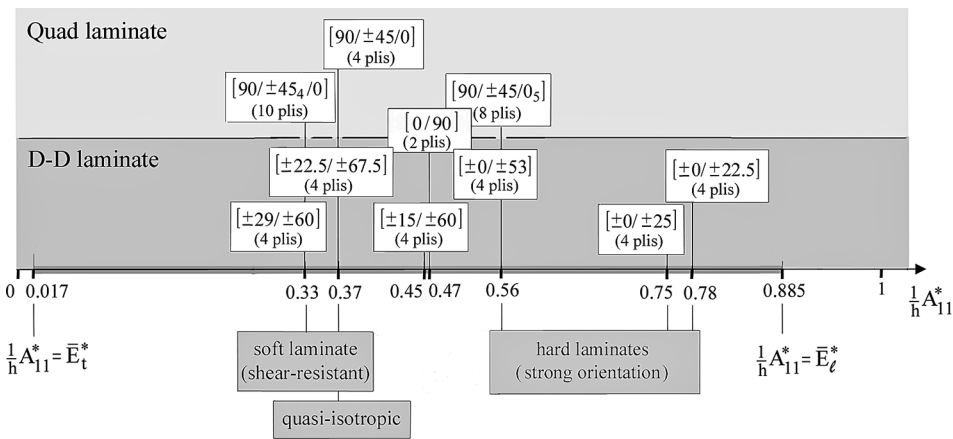


FIGURE 15.6 Trace-normalized longitudinal stiffness $(1/h)A_{11}^*$ of Quad versus D-D Sub-Laminated sets.

15.2.4 ARRANGEMENT OF PLYS

As shown in Figure 15.4, we have for the four plies constituting the D-D set:

$$0 \leq \Phi < \Psi \leq \frac{\pi}{2}$$

A laminate built on the basis of such a D-D set will result in a stack of “ r ” identical D-D sets or “blocks”, r being the number of repeats.

By adopting the convention:

$$1 \leftrightarrow +\Psi; \quad 2 \leftrightarrow +\Phi; \quad 1' \leftrightarrow -\Psi; \quad 2' \leftrightarrow -\Phi$$

Among the possible basic arrangements for the laminate, we can mention for example⁷:

$$\begin{array}{l}
 \mathcal{A} \quad \dots \quad 1 \quad 2 \quad 2' \quad 1' \quad 1 \quad 2 \quad 2' \quad 1' \quad 1 \quad 2 \quad 2' \quad 1' \quad 1 \quad 2 \quad 2' \quad 1' \quad 1 \quad 2 \quad 2' \quad 1' \quad \dots \\
 \quad \quad \Psi \quad \Phi \quad -\Phi \quad -\Psi \quad \Psi \quad \Phi \quad -\Phi \quad -\Psi \quad \Psi \quad \Phi \quad -\Phi \quad -\Psi \quad \Psi \quad \Phi \quad -\Phi \quad -\Psi \quad \Psi \quad \Phi \quad -\Phi \quad -\Psi \quad \dots \\
 \mathcal{B} \quad \dots \quad 1 \quad 1' \quad 2 \quad 2' \quad 1 \quad 1' \quad 2 \quad 2' \quad 1 \quad 1' \quad 2 \quad 2' \quad 1 \quad 1' \quad 2 \quad 2' \quad 1 \quad 1' \quad 2 \quad 2' \quad \dots \\
 \quad \quad \Psi \quad -\Psi \quad \Phi \quad -\Phi \quad \Psi \quad -\Psi \quad \Phi \quad -\Phi \quad \Psi \quad -\Psi \quad \Phi \quad -\Phi \quad \Psi \quad -\Psi \quad \Phi \quad -\Phi \quad \Psi \quad -\Psi \quad \Phi \quad -\Phi \quad \dots
 \end{array}$$

\longleftrightarrow « r » repetitions \longrightarrow

(15.9)

15.3 CONTRIBUTIONS FROM A D-D SUB-LAMINATED SET

15.3.1 ARRANGEMENT \mathcal{A}

15.3.1.1 Notations

Let retain as an example the arrangement \mathcal{A} , that is $[+\Psi / +\Phi / -\Phi / -\Psi]$; ($\Phi < \Psi$). On this basis, we propose to evaluate the contributions of a block or D-D set to the matrices $[A]$, $[C]$, $[B]$ of the behavior relation (Equation 15.6). The D-D set is shown in Figure 15.7. It is located at altitude Z_0 above the middle plane of the entire laminate. The ply-thickness is denoted e . The number of repeats being r , the total thickness of the laminate is noted

$$h = r \times (4e)$$

15.3.1.2 In-plane Stiffness Matrix $[A]$

Recalling (Equation 15.6) that:

$$A_{ij} = \sum_{k=\text{1st ply}}^{k=\text{nth ply}} \bar{E}_{ij}^k \times e_k$$

Noting ΔA_{ij} the D-D set contribution to the term A_{ij} , we have:

$$\Delta A_{ij} = \bar{E}_{ij}^{+\Psi} \times e + \bar{E}_{ij}^{+\Phi} \times e + \bar{E}_{ij}^{-\Phi} \times e + \bar{E}_{ij}^{-\Psi} \times e$$

The coefficients \bar{E}_{ij}^0 are detailed in Equation 11.8.

- $ij = 11; 22; 12; 33$

Then $\bar{E}_{ij}^{+\Psi} = \bar{E}_{ij}^{-\Psi}$; $\bar{E}_{ij}^{+\Phi} = \bar{E}_{ij}^{-\Phi}$ and:

$$\Delta A_{ij} = \bar{E}_{ij}^{+\Psi} \times 2e + \bar{E}_{ij}^{+\Phi} \times 2e = \left(\frac{\bar{E}_{ij}^{+\Psi} + \bar{E}_{ij}^{+\Phi}}{2} \right) \times 4e$$

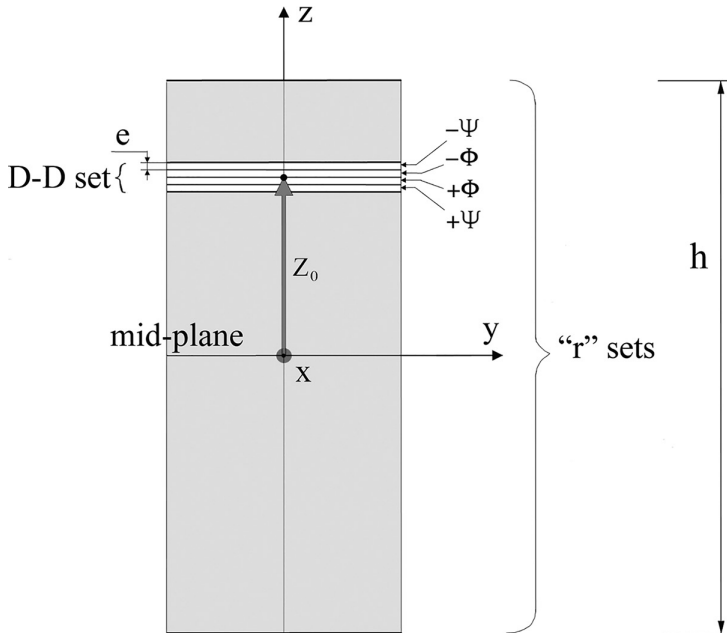


FIGURE 15.7 Stacking of Sub-Laminated D-D sets.

where $4e$ is the D-D set thickness

- $ij = 13; 23$

Then $\bar{E}_{ij}^{-\Psi} = -\bar{E}_{ij}^{+\Psi}$; $\bar{E}_{ij}^{-\Phi} = -\bar{E}_{ij}^{+\Phi}$ and $\Delta A_{ij} = 0$

When considering the stacking of “ r ” repeats of D-D sets, we obtain as terms of $[A]$ matrix for the full laminate with thickness $h = (4e) \times r$:

$$\begin{aligned} ij = 11; 22; 12; 33 & : A_{ij} = \frac{1}{2}(\bar{E}_{ij}^{+\Psi} + \bar{E}_{ij}^{+\Phi}) \times h \\ ij = 13; 23 & : A_{ij} = 0 \end{aligned} \quad (15.10)$$

15.3.1.3 Flexural Stiffness Matrix $[C]$

Recalling (Equation 15.6) that:

$$C_{ij} = \sum_{k=1st \text{ ply}}^{k=nth \text{ ply}} \bar{E}_{ij}^k \times \frac{(z_k^3 - z_{k-1}^3)}{3}$$

Let ΔC_{ij} be the D-D set contribution to the term C_{ij}

- $ij = 11; 22; 12; 33$

We then note for the Sub-Laminate D-D set, in Figure 15.7 a contribution ΔC_{ij} such that:

$$\Delta C_{ij} = \frac{\bar{E}_{ij}^{+\Psi}}{3} [(Z_0 - e)^3 - (Z_0 - 2e)^3 + (Z_0 + 2e)^3 - (Z_0 + e)^3] + \frac{\bar{E}_{ij}^{+\Phi}}{3} [(Z_0 + e)^3 - (Z_0 - e)^3]$$

i.e. after development:

$$\Delta C_{ij} = \frac{1}{2}(\bar{E}_{ij}^{+\Psi} + \bar{E}_{ij}^{+\Phi}) \times 4e \times Z_0^2 + \frac{1}{8}(7\bar{E}_{ij}^{+\Psi} + \bar{E}_{ij}^{+\Phi}) \times \frac{16}{3}e^3$$

When considering a stacking with a number r of D-D sets, we get:

$$C_{ij} = \frac{1}{2}(\bar{E}_{ij}^{+\Psi} + \bar{E}_{ij}^{+\Phi}) \times 4e \times S + \frac{1}{8}(7\bar{E}_{ij}^{+\Psi} + \bar{E}_{ij}^{+\Phi}) \times \frac{16}{3}e^3 \times r$$

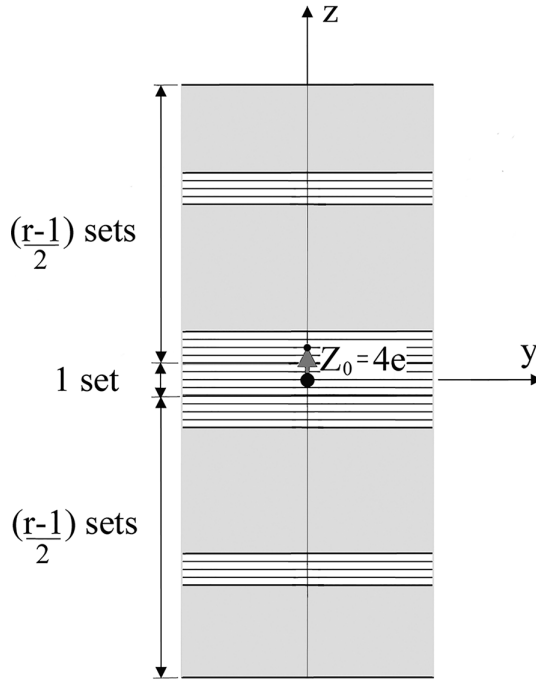
With S such as, $n = 1, \dots, r$, n identifying the successive D-D sets

$$S = Z_{0(n=1)}^2 + Z_{0(n=2)}^2 + \dots + Z_{0(n=r)}^2$$

a. if r is odd, then S takes the form (Figure 15.8)⁸

$$S = 0 + 2 \times [(4e)^2 + (8e)^2 + (12e)^2 + (16e)^2 \dots] \left(\frac{r-1}{2} \right) \text{ terms}$$

$$S = 0 + 2 \times (4e)^2 [1^2 + 2^2 + 3^2 + 4^2 \dots] = \frac{(4e)^2}{12} \times (r^3 - r) \left(\frac{r-1}{2} \right) \text{ terms}$$

FIGURE 15.8 Odd number of repeats “ r ”.

From which

$$C_{ij} = \frac{1}{2}(\bar{E}_{ij}^{+\Psi} + \bar{E}_{ij}^{+\Phi}) \times \frac{(4e)^3}{12} \times (r^3 - r) + \frac{1}{8}(7\bar{E}_{ij}^{+\Psi} + \bar{E}_{ij}^{+\Phi}) \times \frac{16}{3}e^3 \times r$$

$$C_{ij} = \frac{1}{2}(\bar{E}_{ij}^{+\Psi} + \bar{E}_{ij}^{+\Phi}) \times \frac{(4e \times r)^3}{12} + \frac{1}{2}(\bar{E}_{ij}^{+\Psi} - \bar{E}_{ij}^{+\Phi}) \times 4e^3 \times r$$

That is to say:

$$(ij = 11; 22; 12; 33) \quad C_{ij} = \frac{1}{2}(\bar{E}_{ij}^{+\Psi} + \bar{E}_{ij}^{+\Phi}) \times \frac{h^3}{12} + \frac{1}{2}(\bar{E}_{ij}^{+\Psi} - \bar{E}_{ij}^{+\Phi}) \times e^2 h$$

b. if r is even: by modifying accordingly the diagram in Figure 15.8, the D-D set occupying the middle plane disappears. One can check that S is then written⁹:

$$S = 0 + 2 \times (2e)^2 [1^2 + 3^2 + 5^2 + 7^2 \dots] = \frac{(4e)^2}{12} \times (r^3 - r)$$

$$\left(\frac{r}{2}\right) \text{ terms}$$

The expression for C_{ij} is unchanged.

- $ij = 13; 23;$

For the D-D set of Figure 15.7 and taking into account the form of off-axis stiffnesses \bar{E}_{ij}^9 detailed in Equation 11.8: $\bar{E}_{ij}^{-\Psi} = -\bar{E}_{ij}^{+\Psi}$; $\bar{E}_{ij}^{-\Phi} = -\bar{E}_{ij}^{+\Phi}$

Then:

$$\Delta C_{ij} = \frac{\bar{E}_{ij}^{+\Psi}}{3} \left[(Z_0 - e)^3 - (Z_0 - 2e)^3 - ((Z_0 + 2e)^3 - (Z_0 + e)^3) \right] \dots$$

$$+ \frac{\bar{E}_{ij}^{+\Phi}}{3} \left[Z_0^3 - (Z_0 - e)^3 - ((Z_0 + e)^3 - Z_0^3) \right]$$

And after calculation:

$$\Delta C_{ij} = -(\bar{E}_{ij}^{+\Phi} + 3\bar{E}_{ij}^{+\Psi}) \times 2e^2 \times Z_0$$

Hence for the entire laminate and remembering that (x, y) is the middle plane:

$$(ij = 13; 23) \quad C_{ij} = -(\bar{E}_{ij}^{+\Phi} + 3\bar{E}_{ij}^{+\Psi}) \times 2e^2 \times \sum_{n=1}^{n=r} Z_{0(n)} = 0$$

Summarizing the matrix $[C]$:

$$\begin{aligned} ij = 11; 22; 12; 33 \quad : \quad C_{ij} &= \frac{1}{2}(\bar{E}_{ij}^{+\Phi} + \bar{E}_{ij}^{+\Psi}) \times \frac{h^3}{12} - \frac{1}{2}(\bar{E}_{ij}^{+\Phi} - \bar{E}_{ij}^{+\Psi}) \times e^2 h \\ ij = 13; 23 \quad : \quad C_{ij} &= 0 \end{aligned} \quad [C] = \begin{bmatrix} C_{11} & C_{12} & 0 \\ C_{21} & C_{22} & 0 \\ 0 & 0 & C_{33} \end{bmatrix} \quad (15.11)$$

15.3.1.4 Coupling Stiffness Matrix $[B]$

We recall that (see Equation 15.6):

$$B_{ij} = \sum_{k=1st \text{ ply}}^{k=nth \text{ ply}} \bar{E}_{ij}^k \times \frac{(z_k^2 - z_{k-1}^2)}{2}$$

Let ΔB_{ij} be the contribution of a D-D set to the term B_{ij} .

- $ij = 11; 22; 12; 33$

Following the diagram in Figure 15.7, we have

$$\Delta B_{ij} = \frac{\bar{E}_{ij}^{+\Psi}}{2} \left[(Z_0 - e)^2 - (Z_0 - 2e)^2 + (Z_0 + 2e)^2 - (Z_0 + e)^2 \right] + \frac{\bar{E}_{ij}^{+\Phi}}{2} \left[(Z_0 + e)^2 - (Z_0 - e)^2 \right]$$

After calculation:

$$\Delta B_{ij} = \frac{1}{2}(\bar{E}_{ij}^{+\Phi} + \bar{E}_{ij}^{+\Psi}) \times 4e \times Z_0$$

Hence for the full laminate:

$$B_{ij} = \frac{1}{2}(\bar{E}_{ij}^{+\Phi} + \bar{E}_{ij}^{+\Psi}) \times 4e \times \sum_{n=1}^{n=r} Z_{0(n)} = 0$$

- $ij = 13; 23$

Remember that in this case $\bar{E}_{ij}^{-\Psi} = -\bar{E}_{ij}^{+\Psi}$; $\bar{E}_{ij}^{-\Phi} = -\bar{E}_{ij}^{+\Phi}$

According to (Figure 15.7):

$$\Delta B_{ij} = \frac{\bar{E}_{ij}^{+\Psi}}{2} \left[(Z_0 - e)^2 - (Z_0 - 2e)^2 - ((Z_0 + 2e)^2 - (Z_0 + e)^2) \right] \dots$$

$$+ \frac{\bar{E}_{ij}^{+\Phi}}{2} \left[Z_0^2 - (Z_0 - e)^2 - ((Z_0 + e)^2 - Z_0^2) \right]$$

After calculation:

$$\Delta B_{ij} = -\frac{1}{4} \left(\bar{E}_{ij}^{+\Phi} + 3\bar{E}_{ij}^{+\Psi} \right) \times 4e^2$$

And for the full laminate:

$$B_{ij} = -\frac{1}{4} \left(\bar{E}_{ij}^{+\Phi} + 3\bar{E}_{ij}^{+\Psi} \right) \times e \times h$$

Summarizing the matrix $[B]$:

$$\begin{array}{l} ij = 11; 22; 12; 33 \quad : \quad B_{ij} = 0 \\ ij = 13; 23 \quad : \quad B_{ij} = -\frac{1}{4} \left(\bar{E}_{ij}^{+\Phi} + 3\bar{E}_{ij}^{+\Psi} \right) \times e \times h \end{array} \quad B_{ij} = \begin{bmatrix} 0 & 0 & B_{13} \\ 0 & 0 & B_{23} \\ B_{31} & B_{32} & 0 \end{bmatrix} \quad (15.12)$$

15.3.1.5 Thermomechanical Loading

On the basis of the thermomechanical behavior (Equation 12.21), we evaluate the terms related to the temperature effects, noted $\langle \alpha E h \rangle$ and $\langle \alpha E h^2 \rangle$.

- Terms $\langle \alpha E h \rangle$:

$$\langle \alpha E h \rangle_x = \sum_{k=1}^{k=n} \bar{\alpha E}_1^k \times e_k$$

For the D-D set in Figure 15.7:

$$\Delta \langle \alpha E h \rangle_x = \bar{\alpha E}_1^{+\Psi} \times e + \bar{\alpha E}_1^{+\Phi} \times e + \bar{\alpha E}_1^{-\Psi} \times e + \bar{\alpha E}_1^{-\Phi} \times e$$

Since (Equation 11.10): $\bar{\alpha E}_1^{-\Phi} = \bar{\alpha E}_1^{+\Phi}$; $\bar{\alpha E}_1^{-\Psi} = \bar{\alpha E}_1^{+\Psi}$

$$\Delta \langle \alpha E h \rangle_x = \left(\bar{\alpha E}_1^{+\Phi} + \bar{\alpha E}_1^{+\Psi} \right) \times 2e$$

And for the full laminate with thickness $h = (4e) \times r$, r being the D-D set repeats number:

$$\langle \alpha E h \rangle_x = \frac{1}{2} \left(\bar{\alpha E}_1^{+\Phi} + \bar{\alpha E}_1^{+\Psi} \right) \times h$$

$$\langle \alpha E h \rangle_y = \sum_{k=1}^{k=n} \bar{\alpha E}_2^k \times e_k$$

We obtain in a similar way:

$$\langle \alpha E h \rangle_y = \frac{1}{2} \left(\bar{\alpha E}_2^{+\Phi} + \bar{\alpha E}_2^{+\Psi} \right) \times h$$

$$\bullet \quad \langle \alpha E h \rangle_{xy} = \sum_{k=1}^{k=n} \overline{\alpha E}_3^k \times e_k$$

Noting in Equation 11.10 that $\overline{\alpha E}_3^{-\Phi} = -\overline{\alpha E}_3^{+\Phi}$; $\overline{\alpha E}_3^{-\Psi} = -\overline{\alpha E}_3^{+\Psi}$

$$\langle \alpha E h \rangle_{xy} = 0$$

• Terms $\langle \alpha E h^2 \rangle$:

$$\bullet \quad \langle \alpha E h^2 \rangle_x = \sum_{k=1}^{k=n} \overline{\alpha E}_1^k \times (z_k^2 - z_{k-1}^2) / 2$$

The contribution of D-D set (Figure 15.7) becomes:

$$\begin{aligned} \Delta \langle \alpha E h^2 \rangle_x &= \frac{1}{2} \overline{\alpha E}_1^{+\Psi} \left[(Z_0 - e)^2 - (Z_0 - 2e)^2 + (Z_0 + 2e)^2 - (Z_0 + e)^2 \right] \dots \\ &\quad + \frac{1}{2} \overline{\alpha E}_1^{+\Phi} \left[(Z_0 + e)^2 - (Z_0 - e)^2 \right] \end{aligned}$$

And after calculation:

$$\Delta \langle \alpha E h^2 \rangle_x = \frac{1}{2} \left(\overline{\alpha E}_1^{+\Phi} + \overline{\alpha E}_1^{+\Psi} \right) \times 4e \times Z_0$$

For the full laminate, (x, y) being the mid-plane, $\langle \alpha E h^2 \rangle_x = 0$; in a similar way $\langle \alpha E h^2 \rangle_y = 0$.

$$\bullet \quad \langle \alpha E h^2 \rangle_{xy} = \sum_{k=1}^{k=n} \overline{\alpha E}_3^k \times (z_k^2 - z_{k-1}^2) / 2$$

Noting in Equation 11.10 that $\overline{\alpha E}_3^{-\Phi} = -\overline{\alpha E}_3^{+\Phi}$; $\overline{\alpha E}_3^{-\Psi} = -\overline{\alpha E}_3^{+\Psi}$

$$\begin{aligned} \Delta \langle \alpha E h^2 \rangle_{xy} &= \frac{\overline{\alpha E}_3^{+\Psi}}{2} \left[(Z_0 - e)^2 - (Z_0 - 2e)^2 - ((Z_0 + 2e)^2 - (Z_0 + e)^2) \right] \dots \\ &\quad + \frac{\overline{\alpha E}_3^{+\Phi}}{2} \left[Z_0^2 - (Z_0 - e)^2 - ((Z_0 + e)^2 - Z_0^2) \right] \end{aligned}$$

And after calculus:

$$\Delta \langle \alpha E h^2 \rangle_{xy} = -\frac{1}{4} \left(\overline{\alpha E}_3^{+\Phi} + 3\overline{\alpha E}_3^{+\Psi} \right) \times 4e^2$$

For the full laminate with thickness $h = (4e) \times r$ (r being the D-D set repeats number):

$$\langle \alpha E h^2 \rangle_{xy} = -\frac{1}{4} \left(\overline{\alpha E}_3^{+\Phi} + 3\overline{\alpha E}_3^{+\Psi} \right) \times e \times h$$

Summarizing:

$$\begin{aligned} \langle \alpha E h \rangle_x &= \frac{1}{2} \left(\overline{\alpha E}_1^{+\Phi} + \overline{\alpha E}_1^{+\Psi} \right) \times h; \quad \langle \alpha E h \rangle_y = \frac{1}{2} \left(\overline{\alpha E}_2^{+\Phi} + \overline{\alpha E}_2^{+\Psi} \right) \times h; \quad \langle \alpha E h \rangle_{xy} = 0 \\ \langle \alpha E h^2 \rangle_x &= 0; \quad \langle \alpha E h^2 \rangle_y = 0; \quad \langle \alpha E h^2 \rangle_{xy} = -\frac{1}{4} \left(\overline{\alpha E}_3^{+\Phi} + 3\overline{\alpha E}_3^{+\Psi} \right) \times e \times h \end{aligned}$$

(15.13)

15.3.1.6 Hygromechanical Loading

When taking into account the variations in moisture content (assumed to be identical for all plies), terms denoted $\langle \beta Eh \rangle$ and $\langle \beta Eh^2 \rangle$ in Equation 12.22 have to be evaluated. Using Equations 11.11 and 11.12 leads to the following analogous results:

$$\begin{aligned} \langle \beta Eh \rangle_x &= \frac{1}{2} \left(\overline{\beta E_1^{+\Phi}} + \overline{\beta E_1^{+\Psi}} \right) \times h; \quad \langle \beta Eh \rangle_y = \frac{1}{2} \left(\overline{\beta E_2^{+\Phi}} + \overline{\beta E_2^{+\Psi}} \right) \times h; \quad \langle \beta Eh \rangle_{xy} = 0 \\ \langle \beta Eh^2 \rangle_x &= 0; \quad \langle \beta Eh^2 \rangle_y = 0; \quad \langle \beta Eh^2 \rangle_{xy} = -\frac{1}{4} \left(\overline{\beta E_3^{+\Phi}} + 3\overline{\beta E_3^{+\Psi}} \right) \times e \times h \end{aligned} \quad (15.14)$$

15.3.1.7 Resulting Constitutive Relationship

Equations 15.10–15.14 obtained for arrangement A lead to the following constitutive relationship where hygrothermal effects are taken into account.

(15.15)

Arrangement \mathcal{A} : $[+\Psi / +\Phi / -\Phi / -\Psi]$; $(\Phi < \Psi)$.

$$\begin{Bmatrix} N_x \\ N_y \\ T_{xy} \\ M_y \\ -M_x \\ -M_{xy} \end{Bmatrix} = \begin{bmatrix} A_{11} & A_{12} & 0 & 0 & 0 & B_{13} \\ A_{21} & A_{22} & 0 & 0 & 0 & B_{23} \\ 0 & 0 & A_{33} & B_{31} & B_{32} & 0 \\ 0 & 0 & B_{13} & C_{11} & C_{12} & 0 \\ 0 & 0 & B_{23} & C_{21} & C_{22} & 0 \\ B_{31} & B_{32} & 0 & 0 & 0 & C_{33} \end{bmatrix} \begin{Bmatrix} \varepsilon_{0x} \\ \varepsilon_{0y} \\ \gamma_{0,xy} \\ -\partial^2 w_0 / \partial x^2 \\ -\partial^2 w_0 / \partial y^2 \\ -2\partial^2 w_0 / \partial x \partial y \end{Bmatrix} - \Delta T \begin{Bmatrix} \langle \alpha Eh \rangle_x \\ \langle \alpha Eh \rangle_y \\ 0 \\ 0 \\ 0 \\ \langle \alpha Eh^2 \rangle_{xy} \end{Bmatrix} - \Delta M_c \begin{Bmatrix} \langle \beta Eh \rangle_x \\ \langle \beta Eh \rangle_y \\ 0 \\ 0 \\ 0 \\ \langle \beta Eh^2 \rangle_{xy} \end{Bmatrix}$$

 $ij = 11; 22; 12; 33$ $ij = 13; 23$

$$[A] \quad A_{ij} = \frac{1}{2} \left(\overline{E_{ij}^{+\Phi}} + \overline{E_{ij}^{+\Psi}} \right) \times h$$

$$A_{ij} = 0$$

$$[C] \quad C_{ij} = \frac{1}{2} \left(\overline{E_{ij}^{+\Phi}} + \overline{E_{ij}^{+\Psi}} \right) \times \frac{h^3}{12} - \frac{1}{2} \left(\overline{E_{ij}^{+\Phi}} - \overline{E_{ij}^{+\Psi}} \right) \times e^2 h \quad C_{ij} = 0$$

$$[B] \quad B_{ij} = 0$$

$$B_{ij} = -\frac{1}{4} \left(\overline{E_{ij}^{+\Phi}} + 3\overline{E_{ij}^{+\Psi}} \right) \times eh$$

$$\langle \alpha Eh \rangle_x = \frac{1}{2} \left(\overline{\alpha E_1^{+\Phi}} + \overline{\alpha E_1^{+\Psi}} \right) \times h$$

$$\langle \beta Eh \rangle_x = \frac{1}{2} \left(\overline{\beta E_1^{+\Phi}} + \overline{\beta E_1^{+\Psi}} \right) \times h$$

$$\langle \alpha Eh \rangle_y = \frac{1}{2} \left(\overline{\alpha E_2^{+\Phi}} + \overline{\alpha E_2^{+\Psi}} \right) \times h$$

$$\langle \beta Eh \rangle_y = \frac{1}{2} \left(\overline{\beta E_2^{+\Phi}} + \overline{\beta E_2^{+\Psi}} \right) \times h$$

$$\langle \alpha Eh \rangle_{xy} = 0$$

$$\langle \beta Eh \rangle_{xy} = 0$$

$$\langle \alpha Eh^2 \rangle_x = 0$$

$$\langle \beta Eh^2 \rangle_x = 0$$

$$\langle \alpha Eh^2 \rangle_y = 0$$

$$\langle \beta Eh^2 \rangle_y = 0$$

$$\langle \alpha Eh^2 \rangle_{xy} = -\frac{1}{4} \left(\overline{\alpha E_3^{+\Phi}} + 3\overline{\alpha E_3^{+\Psi}} \right) \times eh \quad \langle \beta Eh^2 \rangle_{xy} = -\frac{1}{4} \left(\overline{\beta E_3^{+\Phi}} + 3\overline{\beta E_3^{+\Psi}} \right) \times eh$$

15.3.2 ARRANGEMENT \mathcal{B}

Recall that the previous result (Equation 15.15) was obtained on the basis of the D-D sublamine set defined in Equation 15.9 as the arrangement

$$\mathcal{A} \rightarrow [+ \Psi / + \Phi / - \Phi / - \Psi]; (\Phi < \Psi)$$

When watching at the angular deviations between two consecutive plies when draping either of arrangements \mathcal{A} or \mathcal{B} , we find a greater standard deviation by using arrangement \mathcal{B} . With this second arrangement the calculation of the matrices $[A], [C], [B]$ with an identical approach to that followed for arrangement \mathcal{A} leads to the results summarized in Equation below.

Arrangement \mathcal{B} : $[+ \Psi / - \Psi / + \Phi / - \Phi]; (\Phi < \Psi)$.		
$ij = 11; 22; 12; 33$	$ij = 13; 23$	
$[A] \quad A_{ij} = \frac{1}{2}(\bar{E}_{ij}^{+\Phi} + \bar{E}_{ij}^{+\Psi}) \times h$	$A_{ij} = 0$	
$[C] \quad C_{ij} = \frac{1}{2}(\bar{E}_{ij}^{+\Phi} + \bar{E}_{ij}^{+\Psi}) \times \frac{h^3}{12}$	$C_{ij} = -\frac{1}{2}(\bar{E}_{ij}^{+\Phi} - \bar{E}_{ij}^{+\Psi}) \times e^2 h$	
$[B] \quad B_{ij} = \frac{1}{2}(\bar{E}_{ij}^{+\Phi} - \bar{E}_{ij}^{+\Psi}) \times eh$	$B_{ij} = -\frac{1}{2}(\bar{E}_{ij}^{+\Phi} + \bar{E}_{ij}^{+\Psi}) \times \frac{e}{2} h$	
$\langle \alpha E h \rangle_x = \frac{1}{2}(\overline{\alpha E}_1^{+\Phi} + \overline{\alpha E}_1^{+\Psi}) \times h$	$\langle \beta E h \rangle_x = \frac{1}{2}(\overline{\beta E}_1^{+\Phi} + \overline{\beta E}_1^{+\Psi}) \times h$	(15.16)
$\langle \alpha E h \rangle_y = \frac{1}{2}(\overline{\alpha E}_2^{+\Phi} + \overline{\alpha E}_2^{+\Psi}) \times h$	$\langle \beta E h \rangle_y = \frac{1}{2}(\overline{\beta E}_2^{+\Phi} + \overline{\beta E}_2^{+\Psi}) \times h$	
$\langle \alpha E h \rangle_{xy} = 0$	$\langle \beta E h \rangle_{xy} = 0$	
$\langle \alpha E h^2 \rangle_x = \frac{1}{2}(\overline{\alpha E}_1^{+\Phi} - \overline{\alpha E}_1^{+\Psi}) \times eh$	$\langle \beta E h^2 \rangle_x = \frac{1}{2}(\overline{\beta E}_1^{+\Phi} - \overline{\beta E}_1^{+\Psi}) \times eh$	
$\langle \alpha E h^2 \rangle_y = \frac{1}{2}(\overline{\alpha E}_2^{+\Phi} - \overline{\alpha E}_2^{+\Psi}) \times eh$	$\langle \beta E h^2 \rangle_y = \frac{1}{2}(\overline{\beta E}_2^{+\Phi} - \overline{\beta E}_2^{+\Psi}) \times eh$	
$\langle \alpha E h^2 \rangle_{xy} = -\frac{1}{2}(\overline{\alpha E}_3^{+\Phi} + \overline{\alpha E}_3^{+\Psi}) \times \frac{e}{2} h$	$\langle \beta E h^2 \rangle_{xy} = -\frac{1}{2}(\overline{\beta E}_3^{+\Phi} + \overline{\beta E}_3^{+\Psi}) \times \frac{e}{2} h$	

Arrangement \mathcal{B} (Equation 15.16) presents a greater number of couplings. Arrangement \mathcal{A} makes it possible to approach more quickly the behavior of a homogeneous orthotropic material as presented in the following section. Nevertheless we will see hereafter that when “ r ” increases, the results obtained from the constitutive relations corresponding to arrangements \mathcal{A} and \mathcal{B} merge.

15.4 HOMOGENIZATION OF A DOUBLE-DOUBLE LAMINATE

15.4.1 BEHAVIOR OF A HOMOGENEOUS ORTHOTROPIC PLATE

15.4.1.1 Recall

Consider a plate made of homogeneous orthotropic material, the Mid-plane (x, y) being a plane of mechanical symmetry, and (x, y) being orthotropy-axes. We can deduce from Equation 9.3 the behavior relationship reduced to the (x, y) In-plane behavior as follows:

The strain field in the plate remains unchanged (see Equation 15.6b)

$$\left\{ \begin{array}{c} \sigma_x \\ \sigma_y \\ \tau_{xy} \end{array} \right\} = \left[\begin{array}{ccc} \bar{E}_x & \nu_{yx}\bar{E}_x & 0 \\ \nu_{xy}\bar{E}_y & \bar{E}_y & 0 \\ 0 & 0 & G_{xy} \end{array} \right] \left\{ \begin{array}{c} \epsilon_x \\ \epsilon_y \\ \gamma_{xy} \end{array} \right\}$$

$$\bar{E}_x = \frac{E_x}{1 - \nu_{xy}\nu_{yx}}; \quad \bar{E}_y = \frac{E_y}{1 - \nu_{xy}\nu_{yx}}$$

$$\left\{ \begin{array}{l} \epsilon_x = \epsilon_{0x} - z \frac{\partial^2 w_0}{\partial x^2} \\ \epsilon_y = \epsilon_{0y} - z \frac{\partial^2 w_0}{\partial y^2} \\ \gamma_{xy} = \gamma_{0xy} - z \times 2 \frac{\partial^2 w_0}{\partial x \partial y} \end{array} \right.$$

15.4.1.2 Constitutive Relationship with In-plane Forces and Flexure Moments

We should write the equivalent of Equation 15.15 for this homogeneous orthotropic plate. With the In-plane forces N_x , N_y , T_{xy} we have successively for a plate of thickness h :

$$N_x = \int_{-\frac{h}{2}}^{\frac{h}{2}} \sigma_x dz = \int_{-\frac{h}{2}}^{\frac{h}{2}} (\bar{E}_x \epsilon_x + \nu_{yx} \bar{E}_x \epsilon_y) dz = h \bar{E}_x \epsilon_{0x} + h \nu_{yx} \bar{E}_x \epsilon_{0y}$$

analogously:

$$N_y = \int_{-\frac{h}{2}}^{\frac{h}{2}} \sigma_y dz = h \nu_{xy} \bar{E}_y \epsilon_{0x} + h \bar{E}_y \epsilon_{0y}; \quad T_{xy} = h G_{xy} \gamma_{0xy}$$

And for the bending and twisting moments (cf. Equations 12.13, 12.14, and 12.15)

$$M_y = \int_{-\frac{h}{2}}^{\frac{h}{2}} \sigma_x z dz = \int_{-\frac{h}{2}}^{\frac{h}{2}} \left\{ \bar{E}_x \left(\epsilon_{0x} - z \frac{\partial^2 w_0}{\partial x^2} \right) + \nu_{yx} \bar{E}_x \left(\epsilon_{0y} - z \frac{\partial^2 w_0}{\partial y^2} \right) \right\} z dz$$

$$M_y = \frac{h^3}{12} \bar{E}_x \times -\frac{\partial^2 w_0}{\partial x^2} + \frac{h^3}{12} \nu_{yx} \bar{E}_x \times -\frac{\partial^2 w_0}{\partial y^2}$$

$$M_x = - \int_{-\frac{h}{2}}^{\frac{h}{2}} \sigma_y z dz = \frac{h^3}{12} \nu_{xy} \bar{E}_y \times \frac{\partial^2 w_0}{\partial x^2} + \frac{h^3}{12} \bar{E}_y \times \frac{\partial^2 w_0}{\partial y^2}$$

$$M_{xy} = - \int_{-\frac{h}{2}}^{\frac{h}{2}} \tau_{xy} z dz = \frac{h^3}{12} G_{xy} \times 2 \frac{\partial^2 w_0}{\partial x \partial y}$$

Hence the constitutive relationship for a homogeneous and orthotropic plate:

$$\begin{Bmatrix} N_x \\ N_y \\ T_{xy} \\ \hline M_x \\ M_y \end{Bmatrix} = \begin{bmatrix} h \begin{bmatrix} \bar{E}_x & \nu_{yx} \bar{E}_x & 0 \\ \nu_{xy} \bar{E}_y & \bar{E}_y & 0 \\ 0 & 0 & G_{xy} \end{bmatrix} & [0] \\ [0] & \frac{h^3}{12} \begin{bmatrix} \bar{E}_x & \nu_{yx} \bar{E}_x & 0 \\ \nu_{xy} \bar{E}_y & \bar{E}_y & 0 \\ 0 & 0 & G_{xy} \end{bmatrix} \end{bmatrix} \begin{Bmatrix} \epsilon_{0x} \\ \epsilon_{0y} \\ \gamma_{0xy} \\ \hline -\partial^2 w_0 / \partial x^2 \\ -\partial^2 w_0 / \partial y^2 \\ -2\partial^2 w_0 / \partial x \partial y \end{Bmatrix} \quad (15.17)$$

That we rewrite in the form:

$$\begin{Bmatrix} N_x \\ N_y \\ T_{xy} \\ \hline M_x \\ M_y \end{Bmatrix} = \begin{bmatrix} [A] & [B]=[0] \\ [B]=[0] & [C] = \frac{h^2}{12} [A] \end{bmatrix} \begin{Bmatrix} \epsilon_{0x} \\ \epsilon_{0y} \\ \gamma_{0xy} \\ \hline -\partial^2 w_0 / \partial x^2 \\ -\partial^2 w_0 / \partial y^2 \\ -2\partial^2 w_0 / \partial x \partial y \end{Bmatrix} \quad (15.18)$$

We can observe the absence of coupling between In-plane and bending behaviors, and note the proportionality of In-plane stiffness matrix $[A]$ and flexural stiffness matrix $[C]$, that is:

$$\frac{1}{h} [A] = \frac{12}{h^3} [C] \quad (15.19)$$

15.4.1.3 Stress-Strain Constitutive Relationship

Starting from the previous form 15.18, we wish to show the most significant stresses and strains in the plate of thickness h .

- **For the stresses:** we will have, for example, from the behavior equation and the strain field that are recalled above (see Section 15.4.1.1)

$$\sigma_x = \bar{E}_x \epsilon_{0x} + \nu_{yx} \bar{E}_x \epsilon_{0y} - z \times \left[\bar{E}_x \frac{\partial^2 w_0}{\partial x^2} + \nu_{yx} \bar{E}_x \frac{\partial^2 w_0}{\partial y^2} \right]$$

That is to say also:

$$\sigma_x = \sigma_{0x(\text{In-plane})} + \sigma_{xf(\text{flexure})}$$

- a. In-plane stress: σ_{0x} , σ_{0y} , τ_{0xy}

$$N_x = \int_{-\frac{h}{2}}^{\frac{h}{2}} \sigma_x dz = h \bar{E}_x \epsilon_{0x} + h \nu_{yx} \bar{E}_x \epsilon_{0y} \Rightarrow N_x = \sigma_{0x} \times h$$

Likewise for σ_y and τ_{xy} . So:

$$N_x = \sigma_{0x} \times h; \quad N_y = \sigma_{0y} \times h; \quad T_{xy} = \tau_{0xy} \times h$$

- b. flexural stress: σ_{xf} , σ_{yf} , τ_{xyf}

$$\sigma_{xf} = -z \times \left[\bar{E}_x \frac{\partial^2 w_0}{\partial x^2} + \nu_{yx} \bar{E}_x \frac{\partial^2 w_0}{\partial y^2} \right]$$

When comparing with M_y already written above as

$$M_y = \frac{h^3}{12} \bar{E}_x \times -\frac{\partial^2 w_0}{\partial x^2} + \frac{h^3}{12} \nu_{yx} \bar{E}_x \times -\frac{\partial^2 w_0}{\partial y^2}$$

We can observe¹⁰

$$\sigma_{xf} = z \times \frac{M_y}{h^3/12}$$

Introducing the outer surface stress $(\sigma_{0xf})_{\frac{h}{2}}$ observed when $z = h/2$

$$(\sigma_{0xf})_{\frac{h}{2}} = \frac{h}{2} \times \frac{M_y}{h^3/12}$$

or

$$M_y = (\sigma_{0xf})_{\frac{h}{2}} \times \frac{h^2}{6}$$

And in analogous manner

$$-M_x = (\sigma_{0yf})_{\frac{h}{2}} \times \frac{h^2}{6}; \quad -M_{xy} = (\tau_{0xyf})_{\frac{h}{2}} \times \frac{h^2}{6}$$

- **For the corresponding strains:** recalled above (see Section 15.4.1.1)

$$\epsilon_x = \underbrace{\epsilon_{0x}}_{\text{In-plane strain}} - z \times \underbrace{\frac{\partial^2 w_0}{\partial x^2}}_{\text{flexural strain}} \Rightarrow \epsilon_{xf} = -z \frac{\partial^2 w_0}{\partial x^2}$$

Let for $z = h/2$:

$$(\epsilon_{0xf})_{\frac{h}{2}} = -\frac{h}{2} \times \frac{\partial^2 w_0}{\partial x^2} \Rightarrow -\frac{\partial^2 w_0}{\partial x^2} = \frac{2}{h} \times (\epsilon_{0xf})_{\frac{h}{2}}$$

Analogously:

$$-\frac{\partial^2 w_0}{\partial y^2} = \frac{2}{h} \times (\epsilon_{0,yf})_{\frac{h}{2}}; \quad -2 \frac{\partial^2 w_0}{\partial x \partial y} = \frac{2}{h} \times (\gamma_{0,xyf})_{\frac{h}{2}}$$

Carrying in Equation 15.18

$$\left\{ \begin{array}{c} h\sigma_{0x} \\ h\sigma_{0y} \\ h\tau_{0xy} \\ \frac{h^2}{6}(\sigma_{0,xf})_{\frac{h}{2}} \\ \frac{h^2}{6}(\sigma_{0,yf})_{\frac{h}{2}} \\ \frac{h^2}{6}(\tau_{0,xyf})_{\frac{h}{2}} \end{array} \right\} = \left[\begin{array}{cc} [A] & [B]=[0] \\ [B]=[0] & [C]=\frac{h^2}{12}[A] \end{array} \right] \left\{ \begin{array}{c} \epsilon_{0x} \\ \epsilon_{0y} \\ \gamma_{0xy} \\ \frac{2}{h}(\epsilon_{0,xf})_{\frac{h}{2}} \\ \frac{2}{h}(\epsilon_{0,yf})_{\frac{h}{2}} \\ \frac{2}{h}(\gamma_{0,xyf})_{\frac{h}{2}} \end{array} \right\}$$

or also:

$$\left\{ \begin{array}{c} \sigma_{0x} \\ \sigma_{0y} \\ \tau_{0xy} \\ \hline (\sigma_{0,xf})_{\frac{h}{2}} \\ (\sigma_{0,yf})_{\frac{h}{2}} \\ (\tau_{0,xyf})_{\frac{h}{2}} \end{array} \right\} = \left[\begin{array}{cc} \frac{1}{h}[A] & \frac{2}{h^2}[B]=[0] \\ \frac{6}{h^2}[B]=[0] & \frac{12}{h^3}[C]=\frac{1}{h}[A] \end{array} \right] \left\{ \begin{array}{c} \epsilon_{0x} \\ \epsilon_{0y} \\ \gamma_{0xy} \\ \hline (\epsilon_{0,xf})_{\frac{h}{2}} \\ (\epsilon_{0,yf})_{\frac{h}{2}} \\ (\gamma_{0,xyf})_{\frac{h}{2}} \end{array} \right\} \quad (15.20a)$$

Note: Recall that this relation is also written (see Equation 15.17):

$$\left\{ \begin{array}{c} \sigma_{0x} \\ \sigma_{0y} \\ \tau_{0xy} \\ \hline (\sigma_{0,xf})_{\frac{h}{2}} \\ (\sigma_{0,yf})_{\frac{h}{2}} \\ (\tau_{0,xyf})_{\frac{h}{2}} \end{array} \right\} = \left[\begin{array}{cc} \left[\begin{array}{ccc} \bar{E}_x & \nu_{yx}\bar{E}_x & 0 \\ \nu_{xy}\bar{E}_y & \bar{E}_y & 0 \\ 0 & 0 & G_{xy} \end{array} \right] & \frac{2}{h^2}[B]=[0] \\ \frac{6}{h^2}[B]=[0] & \left[\begin{array}{ccc} \bar{E}_x & \nu_{yx}\bar{E}_x & 0 \\ \nu_{xy}\bar{E}_y & \bar{E}_y & 0 \\ 0 & 0 & G_{xy} \end{array} \right] \end{array} \right] \left\{ \begin{array}{c} \epsilon_{0x} \\ \epsilon_{0y} \\ \gamma_{0xy} \\ \hline (\epsilon_{0,xf})_{\frac{h}{2}} \\ (\epsilon_{0,yf})_{\frac{h}{2}} \\ (\gamma_{0,xyf})_{\frac{h}{2}} \end{array} \right\} \quad (15.20b)$$

15.4.1.4 Comparison with D-D Laminate

We propose to reconsider the constitutive relationship (see Equation 15.15) of a laminate made up of r repeats of D-D sets in order to highlight the differences with the homogeneous orthotropic plate above.

- *Strains*

Across the D-D laminate thickness, strain evolves following Equation 15.6b, like for the homogeneous plate. One can thus take again the preceding expressions where appear the extreme bending strains:

$$-\frac{\partial^2 w_0}{\partial x^2} = \frac{2}{h} \times (\epsilon_{0xf})_{\frac{h}{2}}; \quad -\frac{\partial^2 w_0}{\partial y^2} = \frac{2}{h} \times (\epsilon_{0yf})_{\frac{h}{2}}; \quad -2 \frac{\partial^2 w_0}{\partial x \partial y} = \frac{2}{h} \times (\gamma_{0xyf})_{\frac{h}{2}}$$

- *Stresses*

On the other hand, we note stress discontinuity when going from one ply to the next. For example, we will have for a ply orientation Φ

$$\sigma_x^\Phi = \bar{E}_{11}^{+\Phi} \epsilon_x + \bar{E}_{12}^{+\Phi} \epsilon_y + \bar{E}_{13}^{+\Phi} \gamma_{xy}$$

And considering Equation 15.6b for the strains,

$$\begin{aligned} \sigma_x^\Phi = & \left[\bar{E}_{11}^{+\Phi} \epsilon_{ox} + \bar{E}_{12}^{+\Phi} \epsilon_{oy} + \bar{E}_{13}^{+\Phi} \gamma_{oxy} \right] - z \left[\bar{E}_{11}^{+\Phi} \frac{\partial^2 w_o}{\partial x^2} \dots \right. \\ & \left. \dots + \bar{E}_{12}^{+\Phi} \frac{\partial^2 w_o}{\partial y^2} + \bar{E}_{13}^{+\Phi} \times 2 \frac{\partial^2 w_o}{\partial x \partial y} \right] \end{aligned}$$

which can be summarized by

$$\sigma_x^\Phi = \sigma_{x(\text{In plane})}^\Phi + \sigma_{x(\text{flexure})}^\Phi$$

We can see the corresponding stress-distribution on Figure 15.9b for a laminate made up of 19 repetitions ($r = 19$).

Let us consider In-plane forces and bending moments, and substitute for them the *fictitious* overall stresses defined as

$$N_x = \sigma_{0x} \times h; \quad N_y = \sigma_{0y} \times h; \quad T_{xy} = \tau_{0xy} \times h$$

$$M_y = (\sigma_{0xf})_{\frac{h}{2}} \times \frac{h^2}{6}; \quad -M_x = (\sigma_{0yf})_{\frac{h}{2}} \times \frac{h^2}{6}; \quad -M_{xy} = (\tau_{0xyf})_{\frac{h}{2}} \times \frac{h^2}{6}$$

These stresses look like average stresses for both the In-plane and bending stresses, as observed when comparing (a) and (b) in Figure 15.9. Note that they are expressions of simple and convenient form drawn from the actual stress resultants and from thickness h .

By considering these extrema for flexural strains and the corresponding equivalent average stresses we obtain from Equation 15.15 the following (Equation 15.21) in which the hygrothermal effects have been preserved:

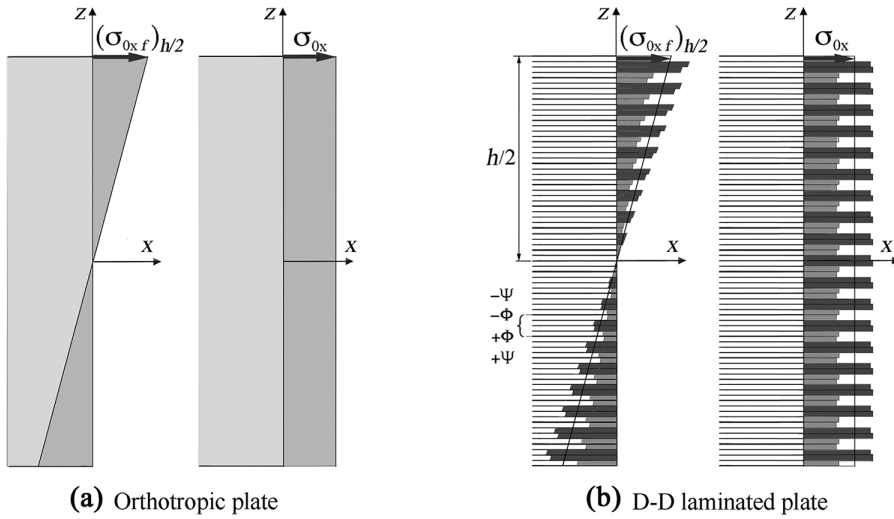


FIGURE 15.9 Flexure and In-plane stress in orthotropic plate (a) and D-D laminate (b).

$$\begin{Bmatrix} \sigma_{0x} \\ \sigma_{0y} \\ \tau_{0xy} \\ (\sigma_{0xf})\frac{h}{2} \\ (\sigma_{0yf})\frac{h}{2} \\ (\tau_{0xyf})\frac{h}{2} \end{Bmatrix} = \begin{bmatrix} \frac{1}{h}[A] & \frac{2}{h^2}[B] \\ \frac{6}{h^2}[B] & \frac{12}{h^3}[C] \end{bmatrix} \begin{Bmatrix} \epsilon_{0x} \\ \epsilon_{0y} \\ \gamma_{0xy} \\ (\epsilon_{0xf})\frac{h}{2} \\ (\epsilon_{0yf})\frac{h}{2} \\ (\gamma_{0xyf})\frac{h}{2} \end{Bmatrix} - \Delta T \begin{Bmatrix} \frac{1}{h}\langle \alpha E h \rangle_x \\ \frac{1}{h}\langle \alpha E h \rangle_y \\ 0 \\ 0 \\ 0 \\ \frac{6}{h^2}\langle \alpha E h^2 \rangle_{xy} \end{Bmatrix} - \Delta M_c \begin{Bmatrix} \frac{1}{h}\langle \beta E h \rangle_x \\ \frac{1}{h}\langle \beta E h \rangle_y \\ 0 \\ 0 \\ 0 \\ \frac{6}{h^2}\langle \beta E h^2 \rangle_{xy} \end{Bmatrix} \quad (15.21)$$

15.4.2 EVOLUTION OF THE LAMINATE BEHAVIOR WITH THE NUMBER OF REPEATS r

15.4.2.1 Evolution of the Constitutive Equation

Let us examine the terms of matrices in Equation 15.21:

From Equation 15.15 and remembering that the laminate thickness is written $h = (4e) \times r$ where r is the number of repeats of D-D sets:

- Terms A_{ij} , ($ij = 11, 22, 12, 33$)

$$\frac{1}{h} A_{ij} = \frac{1}{2} (\bar{E}_{ij}^{+\Phi} + \bar{E}_{ij}^{+\Psi})$$

- Terms C_{ij} , ($ij = 11, 22, 12, 33$)

$$\frac{12}{h^3} C_{ij} = \frac{1}{2} (\bar{E}_{ij}^{+\Phi} + \bar{E}_{ij}^{+\Psi}) \left[1 - \frac{(\bar{E}_{ij}^{+\Phi} - \bar{E}_{ij}^{+\Psi})}{(\bar{E}_{ij}^{+\Phi} + \bar{E}_{ij}^{+\Psi})} \times \frac{3}{4} \times \frac{1}{r^2} \right]$$

- Terms B_{ij} , ($ij = 13, 23$)

$$\frac{2}{h^2} B_{ij} = -\frac{1}{4} (\bar{E}_{ij}^{+\Phi} + 3\bar{E}_{ij}^{+\Psi}) \times \frac{1}{2r}$$

- Terms $\langle \alpha E h \rangle_x$, $\langle \alpha E h \rangle_y$

$$\frac{1}{h} \langle \alpha E h \rangle_x = \frac{1}{2} (\overline{\alpha E_1^{+\Phi}} + \overline{\alpha E_1^{+\Psi}}); \quad \frac{1}{h} \langle \alpha E h \rangle_y = \frac{1}{2} (\overline{\alpha E_2^{+\Phi}} + \overline{\alpha E_2^{+\Psi}})$$

- Term $\langle \alpha E h^2 \rangle_{xy}$

$$\frac{6}{h^2} \langle \alpha E h^2 \rangle_{xy} = -\frac{1}{4} (\overline{\alpha E_3^{+\Phi}} + 3\overline{\alpha E_3^{+\Psi}}) \times \frac{3}{2} \times \frac{1}{r}$$

And formally identical terms for hygrometric effects:

$$\frac{1}{h} \langle \beta E h \rangle_x; \quad \frac{1}{h} \langle \beta E h \rangle_y; \quad \frac{6}{h^2} \langle \beta E h^2 \rangle_{xy}$$

15.4.2.2 Consequence: Homogenized Laminate

We see from these expressions that while the number r of D-D blocks increases, some terms stabilize while others decrease and become negligible. For example for 5 D-D sets, the terms of the matrix $(12/h^3)C_{ij}$ become

$$\frac{12}{h^3} C_{ij} = \frac{1}{2} (\bar{E}_{ij}^{+\Phi} + \bar{E}_{ij}^{+\Psi}) [1 - \varepsilon] \quad \text{with } \varepsilon < 3\%$$

And to the limit

$$\frac{12}{h^3} C_{ij} = \frac{1}{h} A_{ij}$$

In the same way the coupling terms responsible for the warping lose their influence:

$$\frac{2}{h^2} B_{ij}, \quad \frac{6}{h^2} \langle \alpha E h^2 \rangle_{xy}, \quad \frac{6}{h^2} \langle \beta E h^2 \rangle_{xy} \searrow \varepsilon \text{ as } r \nearrow$$

Practically, for $r > 5$ ¹¹ one observes for the laminate a quasi-orthotropic behavior (see Equation 15.20a).

Note that for $r = 5$ the laminate is still relatively thin. For example, for carbon/epoxy (see Table 3.2), we will have:

$$h = 4e \times 5 = 20 \times 0.13 \text{ mm} = 2.6 \text{ mm}$$

A “homogenization threshold” is thus reached for the laminate.

• Notes

- With the equality

$$\frac{12}{h^3} C_{ij} = \frac{1}{h} A_{ij}$$

Only four constants $(1/h)A_{ij}$, $ij = 11, 22, 12, 33$ characterize the homogenized D-D laminate, and we note

$$\frac{1}{h}A_{ij} = \frac{1}{2}(\bar{E}_{ij}^{+\Phi} + \bar{E}_{ij}^{+\Psi})$$

- Particularly, the notion of stacking sequence for the plies, fundamental for Quad laminates, disappears here.
- Also equality $(12/h^3)C_{ij} = (1/h)A_{ij}$ makes it possible to simplify the characterization tests on coupons taken from the laminate. It is thus possible to substitute bending tests for tensile-compression tests (see Section 12.1.6). They are easier to implement and less expensive.
- Moreover, as we have seen (see Section 15.1.2.5), we can substitute values normalized with the Tsai modulus, that is $(1/h)A_{ij}^*$, which further reduces the number of characteristics. Thus we will have as coefficient characterizing the laminate stiffness along the x direction:

$$\frac{1}{h}A_{11}^* = \frac{(\bar{E}_{11}^{+\Phi} + \bar{E}_{11}^{+\Psi})}{2}$$

- **Example:** We know, based on the characteristics of the master ply (See Table 15.2 and Equation 11.8) the trace-normalized values $\bar{E}_{11}^{+\Phi}$ and $\bar{E}_{11}^{+\Psi}$ and therefore the term $(1/h)A_{11}^*$. The result of a *bending* test on a DD-laminate with carbon/resin plies provides the numerical value $(1/h)A_{11}$. Thus we derive the value of the Tsai modulus of the unidirectional used, namely:

$$I_{\text{Tsai}} = \frac{1}{h}A_{11} / \frac{1}{h}A_{11}^*$$

From which we deduce the elastic constants of the ply with Table 15.2.

- Equation 15.21 was written considering the arrangement $\mathcal{A} : [+ \Psi / + \Phi / - \Phi / - \Psi]; (\Phi < \Psi)$ (see Section 15.3.1). As already seen, the arrangement $\mathcal{B} : [+ \Psi / - \Psi / + \Phi / - \Phi]; (\Phi < \Psi)$ involves other forms for coupling terms. However, the latter have the same orders of magnitude and the homogenization process works the same when the number of repetitions r increases.
- Thus, for $r > 5$, it can be considered that a D-D laminate is quasi-orthotropic in its plane, that is to say characterized by the constitutive equation derived from Equation 15.21:

$$\left\{ \begin{array}{c} \sigma_{0x} \\ \sigma_{0y} \\ \tau_{0xy} \\ (\sigma_{0xf})_{\frac{h}{2}} \\ (\sigma_{0yf})_{\frac{h}{2}} \\ (\tau_{0xyf})_{\frac{h}{2}} \end{array} \right\} = \left\{ \begin{array}{cc} \frac{1}{h}[A] & [0] \\ [0] & \frac{12}{h^3}[C] = \frac{1}{h}[A] \end{array} \right\} \left\{ \begin{array}{c} \epsilon_{0x} \\ \epsilon_{0y} \\ \gamma_{0xy} \\ (\epsilon_{0xf})_{\frac{h}{2}} \\ (\epsilon_{0yf})_{\frac{h}{2}} \\ (\gamma_{0xyf})_{\frac{h}{2}} \end{array} \right\} - \Delta T \left\{ \begin{array}{c} \frac{1}{h}\langle \alpha E h \rangle_x \\ \frac{1}{h}\langle \alpha E h \rangle_y \\ 0 \\ 0 \\ 0 \\ 0 \end{array} \right\} - \Delta M \left\{ \begin{array}{c} \frac{1}{h}\langle \beta E h \rangle_x \\ \frac{1}{h}\langle \beta E h \rangle_y \\ 0 \\ 0 \\ 0 \\ 0 \end{array} \right\} \quad (15.22)$$

Or without hygrothermal effects:

$$\left\{ \begin{array}{c} \sigma_{0x} \\ \sigma_{0y} \\ \tau_{0xy} \\ (\sigma_{0xf})_{\frac{h}{2}} \\ (\sigma_{0yf})_{\frac{h}{2}} \\ (\tau_{0xyf})_{\frac{h}{2}} \end{array} \right\} = \left[\begin{array}{ccc} \frac{1}{h} \begin{bmatrix} A_{11} & A_{12} & 0 \\ A_{21} & A_{22} & 0 \\ 0 & 0 & A_{33} \end{bmatrix} & [0] & \\ [0] & \frac{12}{h^3} [C] = \frac{1}{h} \begin{bmatrix} A_{11} & A_{12} & 0 \\ A_{21} & A_{22} & 0 \\ 0 & 0 & A_{33} \end{bmatrix} & \end{array} \right] \left\{ \begin{array}{c} \epsilon_{0x} \\ \epsilon_{0y} \\ \gamma_{0xy} \\ (\epsilon_{0xf})_{\frac{h}{2}} \\ (\epsilon_{0yf})_{\frac{h}{2}} \\ (\gamma_{0xyf})_{\frac{h}{2}} \end{array} \right\}$$

$$\frac{1}{h} A_{ij} = \frac{1}{2} (\bar{E}_{ij}^{+\Phi} + \bar{E}_{ij}^{+\Psi}) \quad (15.23a)$$

That we can compare to Equation 15.20a

By explaining terms $(1/h)A_{ij}$, this equation is therefore written as

$$\left\{ \begin{array}{c} \sigma_{0x} \\ \sigma_{0y} \\ \tau_{0xy} \\ (\sigma_{0xf})_{\frac{h}{2}} \\ (\sigma_{0yf})_{\frac{h}{2}} \\ (\tau_{0xyf})_{\frac{h}{2}} \end{array} \right\} = \left[\begin{array}{ccc} \frac{1}{2} (\bar{E}_{11}^{+\Phi} + \bar{E}_{11}^{+\Psi}) \frac{1}{2} (\bar{E}_{12}^{+\Phi} + \bar{E}_{12}^{+\Psi}) & 0 & \\ \frac{1}{2} (\bar{E}_{12}^{+\Phi} + \bar{E}_{12}^{+\Psi}) \frac{1}{2} (\bar{E}_{22}^{+\Phi} + \bar{E}_{22}^{+\Psi}) & 0 & [0] \\ 0 & 0 & \frac{1}{2} (\bar{E}_{33}^{+\Phi} + \bar{E}_{33}^{+\Psi}) \end{array} \right] \left\{ \begin{array}{c} \epsilon_{0x} \\ \epsilon_{0y} \\ \gamma_{0xy} \\ (\epsilon_{0xf})_{\frac{h}{2}} \\ (\epsilon_{0yf})_{\frac{h}{2}} \\ (\gamma_{0xyf})_{\frac{h}{2}} \end{array} \right\} + \left[\begin{array}{ccc} \frac{1}{2} (\bar{E}_{11}^{+\Phi} + \bar{E}_{11}^{+\Psi}) \frac{1}{2} (\bar{E}_{12}^{+\Phi} + \bar{E}_{12}^{+\Psi}) & 0 & \\ \frac{1}{2} (\bar{E}_{12}^{+\Phi} + \bar{E}_{12}^{+\Psi}) \frac{1}{2} (\bar{E}_{22}^{+\Phi} + \bar{E}_{22}^{+\Psi}) & 0 & \\ 0 & 0 & \frac{1}{2} (\bar{E}_{33}^{+\Phi} + \bar{E}_{33}^{+\Psi}) \end{array} \right] \left\{ \begin{array}{c} \epsilon_{0x} \\ \epsilon_{0y} \\ \gamma_{0xy} \\ (\epsilon_{0xf})_{\frac{h}{2}} \\ (\epsilon_{0yf})_{\frac{h}{2}} \\ (\gamma_{0xyf})_{\frac{h}{2}} \end{array} \right\} \quad (15.23b)$$

That we can compare to Equation 15.20b. A form which better shows the quasi-orthotropic state of the laminate, because the thickness h is no longer involved in the matrix terms.

To sum up, the paralleling of Equation 15.23 above with Equation 15.20 for an orthotropic plate shows what can be called an equivalent orthotropic plate associated with the homogenized D-D laminate, with the main characteristics:

	Homogenized D-D Laminate Equation 15.23a,b	Associated Orthotropic Plate Equation 15.20a,b
$\frac{1}{h} A_{11}$	$\frac{1}{2} (\bar{E}_{11}^{+\Phi} + \bar{E}_{11}^{+\Psi})$	$\bar{E}_x = \frac{1}{2} (\bar{E}_{11}^{+\Phi} + \bar{E}_{11}^{+\Psi})$
$\frac{1}{h} A_{12}$	$\frac{1}{2} (\bar{E}_{12}^{+\Phi} + \bar{E}_{12}^{+\Psi})$	$\nu_{yx} \bar{E}_x = \frac{1}{2} (\bar{E}_{12}^{+\Phi} + \bar{E}_{12}^{+\Psi})$
$\frac{1}{h} A_{22}$	$\frac{1}{2} (\bar{E}_{22}^{+\Phi} + \bar{E}_{22}^{+\Psi})$	$\bar{E}_y = \frac{1}{2} (\bar{E}_{22}^{+\Phi} + \bar{E}_{22}^{+\Psi})$
$\frac{1}{h} A_{33}$	$\frac{1}{2} (\bar{E}_{33}^{+\Phi} + \bar{E}_{33}^{+\Psi})$	$G_{xy} = \frac{1}{2} (\bar{E}_{33}^{+\Phi} + \bar{E}_{33}^{+\Psi})$
$\frac{12}{h^3} C_{ij} = \frac{1}{h} A_{ij}$		

15.4.3 PARTICULAR CASE OF VERY THIN LAMINATES

This is the case when the number r of repeats of D-D Sub-Laminated sets is low ($1 < r < 5$). One must then consider the constitutive law Equation 15.15 with its couplings, that is to say:

$$B_{13} ; B_{23} ; \langle \alpha E h^2 \rangle_{xy} ; \langle \beta E h^2 \rangle_{xy}$$

Consequently, due to the non-zero terms B_{13} and B_{23} , applying, for example, an In-plane stress resultant induces a warping of the laminate, i.e. non-zero value of $(-2\partial^2 w_0 / \partial x \partial y)$.

Moreover, even in the case of zero applied forces, warping can also occur due to temperature (or humidity) variations, especially when cooling the plate after curing (see Application 20.17). Here this warping is also influenced by the non-zero term $\langle \alpha E h^2 \rangle_{xy}$.

In such cases with a low number of repetitions (typical example $r = 1$), one cannot of course claim quasi-homogeneity. On the other hand, from $r_{\text{even}} \geq 2$, it is possible to remove the above couplings if necessary. In this way, it just has to mirror each new D-D set with respect to the previous one, that is to say to change the strict repetition such as:

$$\dots [+ \Psi / + \Phi / - \Phi / - \Psi] + [+ \Psi / + \Phi / - \Phi / - \Psi] + [+ \Psi / + \Phi / - \Phi / - \Psi] + [+ \Psi / + \Phi / \dots$$

In an alternating repetition such as:

$$\dots [+ \Psi / + \Phi / - \Phi / - \Psi] + [- \Psi / - \Phi / + \Phi / + \Psi] + [+ \Psi / + \Phi / - \Phi / - \Psi] + [- \Psi / - \Phi / \dots$$

Thus when considering the coupling terms detailed above, the contributions of two consecutive sets involving odd stiffness coefficients in Φ and Ψ cancel each other out. As an example for $ij = 13; 23$ and for a set $[+ \Psi / + \Phi / - \Phi / - \Psi]$ (see Section 15.3.1.4):

$$\Delta B_{ij[+ \Psi / + \Phi / - \Phi / - \Psi]} = -\frac{1}{4} (\bar{E}_{ij}^{+\Phi} + 3\bar{E}_{ij}^{+\Psi}) \times 4e^2$$

And for the next set $[- \Psi / - \Phi / + \Phi / + \Psi]$

$$\Delta B_{ij[-\Psi/-\Phi/+ \Phi/+ \Psi]} = -\frac{1}{4}(\bar{E}_{ij}^{-\Phi} + 3\bar{E}_{ij}^{-\Psi}) \times 4e^2 = -\Delta B_{ij[+\Psi/+ \Phi/- \Phi/- \Psi]}$$

The same property is valid for $\Delta \langle \alpha E h^2 \rangle_{xy}$ (see Section 15.3.1.5) and for $\Delta \langle \beta E h^2 \rangle_{xy}$ (See Section 15.3.1.6).

In return arise coupling terms C_{13} and C_{23} for r_{even}^{12} . But it should be noted that very thin laminates are not designed to withstand bending moments¹³. They essentially resist to traction In-plane stress resultants.

Anyway, this is a convenient arrangement to “accelerate” the homogenization of thin laminates. A means which combines the advantages, including by limiting in this way the path of movement made by the laying machine during layup.

15.4.4 TRANSVERSE SHEAR BEHAVIOR

Transverse loading of laminates induces transverse shears denoted τ_{xz} and τ_{yz} . Then we are led to take into account additional stress resultants, i.e. the transverse shear resultants:

$$Q_x = \int_{-h/2}^{+h/2} \tau_{xz} dz; \quad Q_y = \int_{-h/2}^{+h/2} \tau_{yz} dz$$

Studying bending with transverse shear is carried out in Chapter 18.

Notes:

- In all cases of laminates it may happens necessary to take into account the transverse shear stiffness. This is typically the case in a buckling stability study.
- In Section 18.8, we study the transverse shear stresses in a laminate with a particular D-D sequence and we compare the transverse shear behavior of this D-D laminated plate with that of its equivalent homogeneous orthotropic plate.

15.4.5 TAPE LAYING OF D-D LAMINATES

15.4.5.1 A Look Back on Sub-Laminate D-D Sets Arrangements

We have used as an example in Section 15.2.4 two types of D-D set arrangements denoted \mathcal{A} and \mathcal{B} . Of course, they are not the only ones. When we come back to the order of ply stacking, we can note other combinations that can be summarized by the two types of successions:

- ...1 1 2 2 1 1 2 2..., for example 1 2 2' 1' that is to say also $[+\Psi / +\Phi / -\Phi / -\Psi]$, which is the arrangement \mathcal{A} . For example, 1 1' 2 2' which is the arrangement \mathcal{B} , but also 1 2' 2 1'.
- There are four distinct D-D laminates with the succession ...11221122...
- ...1 2 1 2 1 2 1..., for example 1 2 1' 2', i.e. $[\Psi / \Phi / -\Psi / -\Phi]$ (let us call this arrangement \mathcal{C}), and also 1' 2 1 2'. It is worthy to note that arrangement \mathcal{C} appears to be the one which leads the most rapidly to homogenization¹⁴. This homogenization begins when $3 \leq r \leq 5$.
- There are two distinct D-D laminates with the succession ...12121212...

It has already been seen (see Equations 15.15 and 15.16) that the laminate stiffness characteristics obtained with \mathcal{A} or \mathcal{B} were similar and merged when the number of repetitions increased. It is the same with the arrangements mentioned above in b). For example, for arrangement \mathcal{C} , the matrices $[A], [C], [B]$ as well as the hygrothermal characteristics are almost identical to those shown in Equation 15.16. In other words, the homogenized constants are the same regardless of the stacking sequence in a set. Only matter the values of the angles Φ and Ψ to define the homogenized laminate.

15.4.5.2 Classical Tape Laying

The layup of D-D laminates can be done with the conventional method so-called Automated Tape Laying (ATL) (see Section 2.2.5) which allows to deposit plies of preimpregnated fibers.

When using this usual method of laying, it is preferable to limit the angular standard deviation when draping the four plies constituting the D-D set. Thus, arrangement **A** combines the advantages of a moderate average angular deviation $\Delta\theta$ when going from one layer to the next and of a low standard deviation σ , for example:

$$\mathcal{A} : \{\Phi = 10^\circ; \Psi = 60^\circ\} \Rightarrow \Delta\theta = \frac{\pi}{4}; \quad \sigma = \frac{\pi}{12} = 15^\circ$$

15.4.5.3 Bidirectional Tape Laying

This variant of the process consists in ATL with bidirectional Non-Crimp Fabric (NCF)¹⁵. The tape is made up of two unidirectional plies superimposed and joined together. A first ply along the direction of the tape (long fibers) and a second ply making an angle $(\Psi - \Phi)$ with the previous one (short fibers). Each ply is thinner than a conventional unidirectional ply, in view of rapid homogenization. With such a tape, the D-D set is draped in two passes¹⁶.

15.5 STRENGTH OF HOMOGENIZED D-D LAMINATES

15.5.1 PLY FAILURE CRITERION IN ANY ORIENTATION

15.5.1.1 Criterion Expressed in Laminate Axes

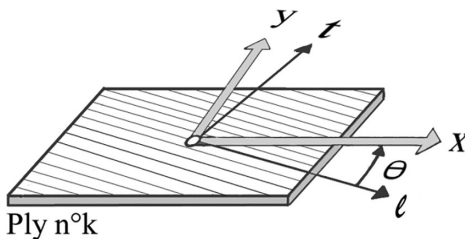
We start from the Tsai-Wu stress criterion translated previously into strain space and in the (ℓ, t) axes of a unidirectional ply (see Equation 14.15) in the form:

$$f(\Sigma) = \begin{Bmatrix} \varepsilon_\ell \\ \varepsilon_t \\ \gamma_{\ell t} \end{Bmatrix}^t \begin{bmatrix} b'_\ell & b'_0 & 0 \\ b'_0 & b'_t & 0 \\ 0 & 0 & b'_{\ell t} \end{bmatrix} \begin{Bmatrix} \varepsilon_\ell \\ \varepsilon_t \\ \gamma_{\ell t} \end{Bmatrix} + \begin{Bmatrix} \varepsilon_\ell \\ \varepsilon_t \\ 0 \end{Bmatrix}^t \begin{bmatrix} a'_\ell \\ a'_t \\ 0 \end{bmatrix} < 1 \quad (15.24)$$

This ply is oriented in the (x, y) axes of the laminate with angle θ (see Figure 15.10). The failure criterion, initially written in stress terms, transforms like the components of the elasticity tensor (invariant criterion). For that purpose, we use Equations written in Section 11.5 and that we recall in Figure 15.10.

Or also:

$$\begin{Bmatrix} \varepsilon_\ell \\ \varepsilon_t \\ \gamma_{\ell t} \end{Bmatrix} = \begin{bmatrix} c^2 & s^2 & -cs \\ s^2 & c^2 & cs \\ 2cs & -2cs & (c^2 - s^2) \end{bmatrix} \begin{Bmatrix} \varepsilon_x \\ \varepsilon_y \\ \gamma_{xy} \end{Bmatrix} = [T_0] \begin{Bmatrix} \varepsilon_x \\ \varepsilon_y \\ \gamma_{xy} \end{Bmatrix}$$



$$\begin{Bmatrix} \varepsilon_x \\ \varepsilon_y \\ \varepsilon_{xy} \end{Bmatrix} = \begin{bmatrix} c^2 & s^2 & 2cs \\ s^2 & c^2 & -2cs \\ -cs & cs & (c^2 - s^2) \end{bmatrix} \begin{Bmatrix} \varepsilon_\ell \\ \varepsilon_t \\ \varepsilon_{\ell t} \end{Bmatrix}$$

$$c = \cos\theta ; \quad s = \sin\theta$$

FIGURE 15.10 Ply n°k with its orientation in the (x, y) laminate axes.

The criterion in the form 15.24 becomes for the ply $n^{\circ}k$:

$$f(\Sigma) = \begin{Bmatrix} \epsilon_x \\ \epsilon_y \\ \gamma_{xy} \end{Bmatrix}^t \begin{bmatrix} b'_\ell & b'_0 & 0 \\ b'_0 & b'_t & 0 \\ 0 & 0 & b'_{t\ell} \end{bmatrix} \begin{Bmatrix} \epsilon_x \\ \epsilon_y \\ \gamma_{xy} \end{Bmatrix} + \begin{Bmatrix} \epsilon_x \\ \epsilon_y \\ 0 \end{Bmatrix}^t \begin{bmatrix} a'_\ell \\ a'_t \\ 0 \end{bmatrix} < 1$$

Terms $b'_\ell, b'_t, b'_0, b'_{t\ell}$ have been written in Equation 14.15. We obtain:

$$\boxed{\begin{aligned} f(\Sigma) &= \begin{Bmatrix} \epsilon_x \\ \epsilon_y \\ \gamma_{xy} \end{Bmatrix}^t \begin{bmatrix} g_{11} & g_{12} & g_{13} \\ & g_{22} & g_{23} \\ \text{sym.} & & g_{33} \end{bmatrix} \begin{Bmatrix} \epsilon_x \\ \epsilon_y \\ \gamma_{xy} \end{Bmatrix} + \begin{Bmatrix} \epsilon_x \\ \epsilon_y \\ 0 \end{Bmatrix}^t \begin{bmatrix} g_x \\ g_y \\ 0 \end{bmatrix} < 1 \\ &\text{Ply } n^{\circ}k \\ g_{11} &= c^4 b'_\ell + s^4 b'_t + 2c^2 s^2 (b'_0 + 2b'_{t\ell}) \\ g_{22} &= s^4 b'_\ell + c^4 b'_t + 2c^2 s^2 (b'_0 + 2b'_{t\ell}) \\ g_{33} &= c^2 s^2 (b'_\ell + b'_t - 2b'_0) + (c^2 - s^2)^2 b'_{t\ell} \\ g_{12} &= c^2 s^2 (b'_\ell + b'_t - 4b'_{t\ell}) + (c^4 + s^4) b'_0 \\ g_{13} &= -cs [c^2 b'_\ell - s^2 b'_t - (c^2 - s^2)(b'_0 + 2b'_{t\ell})] \\ g_{23} &= -cs [s^2 b'_\ell - c^2 b'_t + (c^2 - s^2)(b'_0 + 2b'_{t\ell})] \\ g_x &= c^2 a'_\ell + s^2 a'_t; \quad g_y = s^2 a'_\ell + c^2 a'_t \\ c &= \cos \theta; \quad s = \sin \theta \end{aligned}} \quad (15.25)$$

15.5.1.2 Notes

- The strains $\epsilon_x, \epsilon_y, \gamma_{xy}$ of any constitutive ply *coincide* with the strains of the laminate.
- The failure envelope corresponding to saturation of the criterion, that is to say $f(\Sigma) = 1$ is an ellipsoid. It intersects the plane (ϵ_x, ϵ_y) following an ellipse with equation:

$$g_{11}\epsilon_x^2 + 2g_{12}\epsilon_x \epsilon_y + g_{22}\epsilon_y^2 + g_x\epsilon_x + g_y\epsilon_y = 1 \quad (15.26)$$

This ellipse is not centered due to the presence of first-degree terms for (ϵ_x, ϵ_y) . We note also that its axes are distinct from the axes (ϵ_x, ϵ_y) and that the origin is well inside the ellipse (see Figure 15.11).

15.5.2 EXTENSION TO LAMINATE LEVEL

15.5.2.1 Variation with Angle θ

As already pointed out, laminates built on the basis of D-D Sub-Laminate sets form a doubly continuous field when the angles Φ and Ψ are varied between 0° and 90° . This gives all possible laminates built on unidirectional plies, unlike Quad laminates built on four angles. Thus considering D-D laminates, to every value $\theta = \Phi$ or $\theta = \Psi$ corresponds in these laminates a certain set of unidirectional plies, and to each value of θ corresponds an ellipse with the form of Equation 15.26. The ellipsoid (see Equation 15.25) is conserved while its orientation in space $(\epsilon_x, \epsilon_y, \gamma_{xy})$ changes with θ . Thus its intersection with (ϵ_x, ϵ_y) plane evolves in shape and direction.

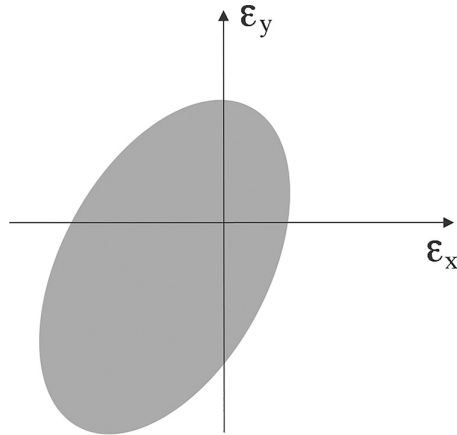


FIGURE 15.11 Intersection of $f(\Sigma) = 1$ with $(\varepsilon_x, \varepsilon_y)$ plane.

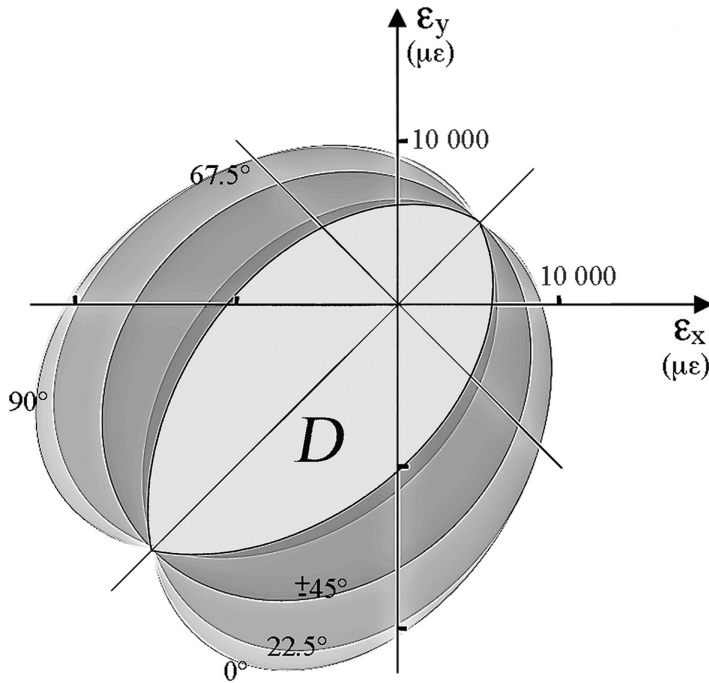


FIGURE 15.12 Domain \mathcal{D} for the First Ply Failure (FPF).

15.5.2.2 Example

Let us consider the laminate made of unidirectional carbon/epoxy plies from Table 14.2. When θ varies, we obtain the network of ellipses shown in Figure 15.12. Note that these ellipses are symmetrical in pairs with respect to the first bisector (see coefficients in Equations 15.25 and 15.26).

We note as domain \mathcal{D} the common intersection to all ellipses when θ varies between 0° and 90° .

Although characterizing every θ , this domain is in fact only delimited by the extreme plies 0° and 90° . The laminate will not undergo any deterioration if the applied average stresses, for example (see Equation 15.23)¹⁷,

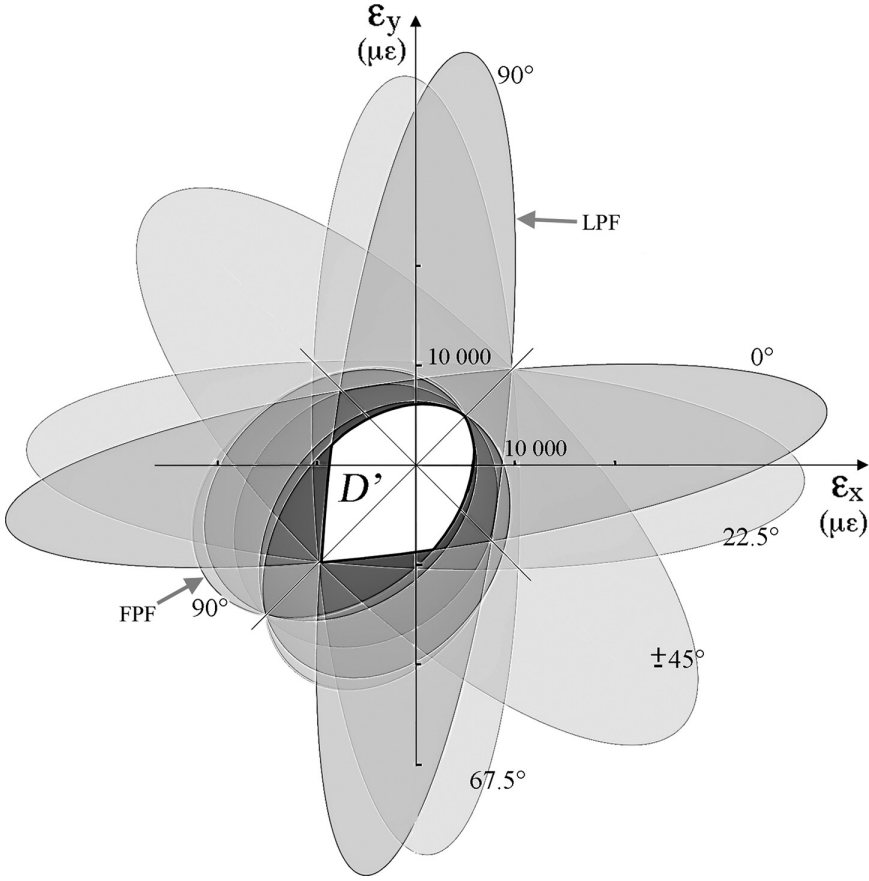


FIGURE 15.13 The First (FPF) and Last (LPF) Ply Failures. Domain \mathcal{D}' .

$$\{\sigma_{0x}; \sigma_{0y}; \tau_{0xy}\} \quad (15.27)$$

lead to laminate strains within domain \mathcal{D} . The domain envelope thus signals the First Ply Failure (FPF).

When increasing the loading, for example proportionally with the loading written in Equation 15.27, some plies deteriorate and neighboring plies are overloaded. So Figure 15.12 is no longer representative because we must take into account the degraded plies.

Degraded ply characteristics were discussed in Section 14.5. Thus for the carbon/epoxy plies here considered, “intact ply” and “degraded ply” characteristics appear in Table 14.5. Rewriting Equation 15.26 for degraded plies leads to a new network of ellipses shown in Figure 15.13. It is shown superimposed on the previous network. Intersection common to the two networks is denoted \mathcal{D}' . It reflects the area in which none loading causes permanent damage.

15.5.3 PRACTICAL FORM OF THE FAILURE CRITERION

15.5.3.1 Preliminary Remarks

- Remember that here the D-D laminate $[\pm\Phi / \pm\Psi]$ consists of plies with orientations: $\Phi \in [0^\circ, 90^\circ]$; $\Psi \in [0^\circ, 90^\circ]$. The envelope limiting the domain \mathcal{D}' in Figure 15.13 concerns all laminates built in this way. And we must consider all the possible orientations from 0° to 90° even if we are dealing with a single Double-Double laminate, i.e. with twice two orientations. We justify this in the following.

- The network with orientations noted in Figure 15.13 relates to the (x, y) axes of a laminate. Let us choose for this laminate another set of axes distinct from the previous ones, let (I, II) , such that (x, y) make the angle δ with (I, II) , i.e. $(\vec{x}, \vec{I}) = \delta$. If we sweep in the same way all the possible ply orientations as before, we will obtain in axes (I, II) a network of identical ellipses. Simply an ellipse which in Figure 15.13 characterizes a (ℓ, t) ply such that $(\vec{x}, \vec{\ell}) = \theta$ (see Figure 15.10) will now represent another ply (ℓ', t') such that $(\vec{x}, \vec{\ell}') = \theta + \delta$. In fact this other ply makes an angle $(\vec{I}, \vec{\ell}') = \theta$ with respect to the new axes (I, II) . We will see in what follows the usefulness of this remark.

15.5.3.2 Principal Strain Components $\epsilon_I, \epsilon_{II}$

The overall stresses in Equation 15.27, i.e. $\{\sigma_{0x}; \sigma_{0y}; \tau_{0xy}\}$ cause plane strains (see Equation 15.23) written as:

$$\{\epsilon_{0x}; \epsilon_{0y}; \gamma_{0xy}\} \quad (15.28)$$

With generally a non-zero shear strain γ_{0xy} . The latter is not taken into account in (ϵ_x, ϵ_y) plane, in Figure 15.13. To make it appear, it would be necessary to show the intersections of the envelope in Equation 15.25 with $(\epsilon_x, \gamma_{xy})$ and $(\epsilon_y, \gamma_{xy})$ planes. One get around this by calculating from Equation 15.28 the principal strain-components noted ϵ_I and ϵ_{II} and their associated directions (I, II) shown in Figure 15.14.

For this, we draw the Mohr circle (see Section 5.2.2) for strains $\{\epsilon_{0x}; \epsilon_{0y}; \epsilon_{0xy} = (\gamma_{0xy}/2)\}$ of the loaded laminate. We can deduce

- The principal strain-components:

$$\begin{matrix} \epsilon_I \\ \epsilon_{II} \end{matrix} = \left(\frac{\epsilon_{0x} + \epsilon_{0y}}{2} \right) \pm \sqrt{\left(\frac{\epsilon_{0x} - \epsilon_{0y}}{2} \right)^2 + \left(\frac{\gamma_{0xy}}{2} \right)^2}$$

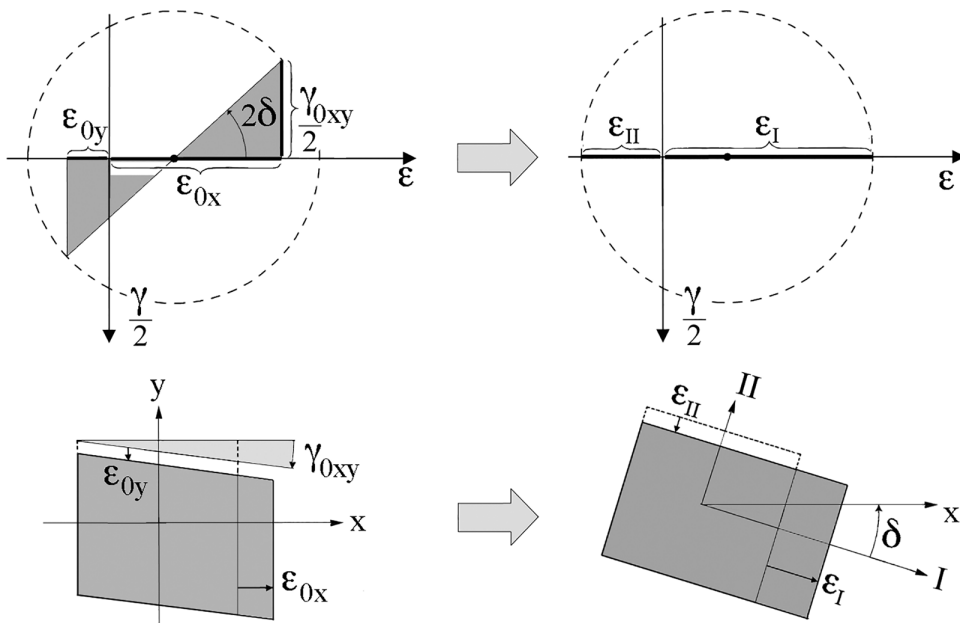


FIGURE 15.14 Principal strain components $(\epsilon_I, \epsilon_{II})$ and associated directions.

- The angle $(\vec{x}, \vec{I}) = \delta$ between axes (x, y) and principal directions (I, II)

$$\tan 2\delta = \frac{\gamma_{0,xy}}{(\epsilon_{0,x} - \epsilon_{0,y})}$$

As already noticed in the previous section, the failure criterion will be shown in (I, II) directions by the same network of ellipses. The envelope \mathcal{D}' in Figure 15.13 is thus usable for all possible cases of plane loadings, each of these cases creating distinct orientations for the principal strain directions. Hence the possibility of replacing (ϵ_x, ϵ_y) axes with ϵ_I and ϵ_{II} , on which are plotted the principal strain values.

Note:

It has already been noted that \mathcal{D}' , constructed from all the ply orientations, is valid for all the D-D laminates produced from the same basic unidirectional ply. \mathcal{D}' therefore appears as a *characteristic of the material* constituted by a given unidirectional layer.

15.5.3.3 Unit Circle

For a more convenient use of the criterion, one substitutes for the outline of domain \mathcal{D}' (see Figure 15.13) a more restrictive contour but with simpler definition. An auxiliary *unit circle* is used for that purpose as shown in Figure 15.15. The so-normalized circle is defined with the correspondences:

$$\text{Along } OA' : \epsilon_I^* = \frac{\epsilon_I}{\epsilon_A}; \quad \text{along } OB' : \epsilon_{II}^* = \frac{\epsilon_{II}}{\epsilon_B}; \quad \text{along } OC' : \epsilon_I^* = \frac{\epsilon_I}{\epsilon_C}; \quad \text{along } OD' : \epsilon_{II}^* = \frac{\epsilon_{II}}{\epsilon_D}$$

The unit circle allows to construct an outline delimiting the domain \mathcal{D}'' limited by two quarter circles and two quarter ellipses. For example with the ply in Table 14.2, definition of domain \mathcal{D}'' is done from the only values:

$$\epsilon_A = \epsilon_B = 6,000 \mu\epsilon; \quad \epsilon_C = \epsilon_D = -8,960 \mu\epsilon$$

It should be noted that the domain \mathcal{D}'' , more conservative, is also more convenient to handle digitally.

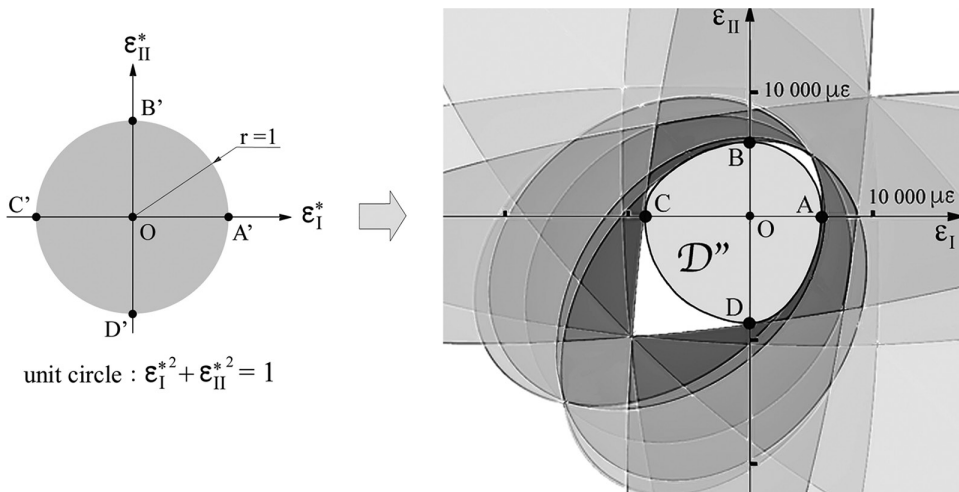


FIGURE 15.15 Limitation of criterion to the “unit circle”.

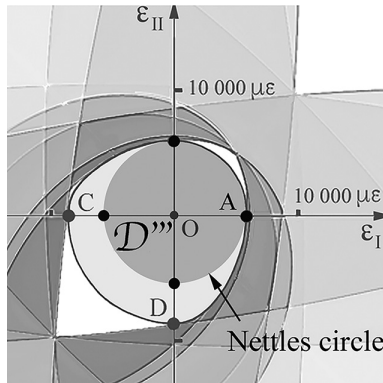


FIGURE 15.16 The Nettles circle.

15.5.3.4 The Nettles Circle

We have already pointed out (see Section 5.4.5.2) that for certain applications and notably in aeronautics, the risk of delamination in compression was significant, particularly at the laminates outer surfaces. For a first faster approach, one can then simplify by substituting for the preceding envelope-outline a circle of radius ϵ_A as in Figure 15.16, also called “Nettles circle”¹⁸. We thus obtain the domain D''' , a more restrictive criterion in compression, which is the intended purpose.

15.6 INCIDENCE FOR THE DESIGN

15.6.1 PRELIMINARY REMARKS

- Remember that the sizing of a loaded structure is subject to a set of specifications, i.e. for the most basic:
- **Strength calculation:** The structure must withstand a set of loads. For example, an aeronautical structure must remain intact under external and internal loads and overloads, in flight or on landing. These loads can act on:
 - regular (or smooth) areas, and can remain constant or vary when moving through these areas.
 - singular areas: open or filled holes, free edges (see Figure 14.3).
- **Stiffness sizing:** One must control the structure stiffness to ensure:
 - Control of overall deformations that must be limited to ensure proper operation (airplane wing, aeroelastic control, etc.).
 - Vibration control (natural frequencies)
 - Control of local or overall stability (buckling)
- Another dimensioning characteristic specific to composite structures: the starting material is not the final material. It must be defined during the sizing process, which involves loops within the digital process. For example, prior modeling by orthotropic finite elements provides nodal forces (stress resultants and moments) making it possible to initiate the process on the basis of specifications to be respected including the above ones.

15.6.2 DEFINING THE LAMINATE ANISOTROPY

We have noted in Equation 15.23 that the stiffness of homogenized D-D laminates was characterized by $(1/h)A_{11}$, $(1/h)A_{22}$, $(1/h)A_{12}$, $(1/h)A_{33}$. We have also described in Section 15.1.2.5 the normalization of these stiffness coefficients by means of the Tsai modulus I_{Tsai} leading to trace-normalized stiffnesses that can be applied to *all* marketed CFRP unidirectionals. One thus obtains for the stiffness characterization (In-plane and bending) the only values:

$$\frac{1}{h}A_{11}^*; \quad \frac{1}{h}A_{22}^*; \quad \frac{1}{h}A_{12}^*; \quad \frac{1}{h}A_{33}^*$$

with

$$\frac{1}{h}A_{11}^* + \frac{1}{h}A_{22}^* + \frac{2}{h}A_{33}^* = 1 \quad (15.29)$$

These normalized values are shown in Figure 15.17 for the homogenized D-D laminates field $\{\pm\Phi / \pm\Psi\}$ and for some values of Ψ .

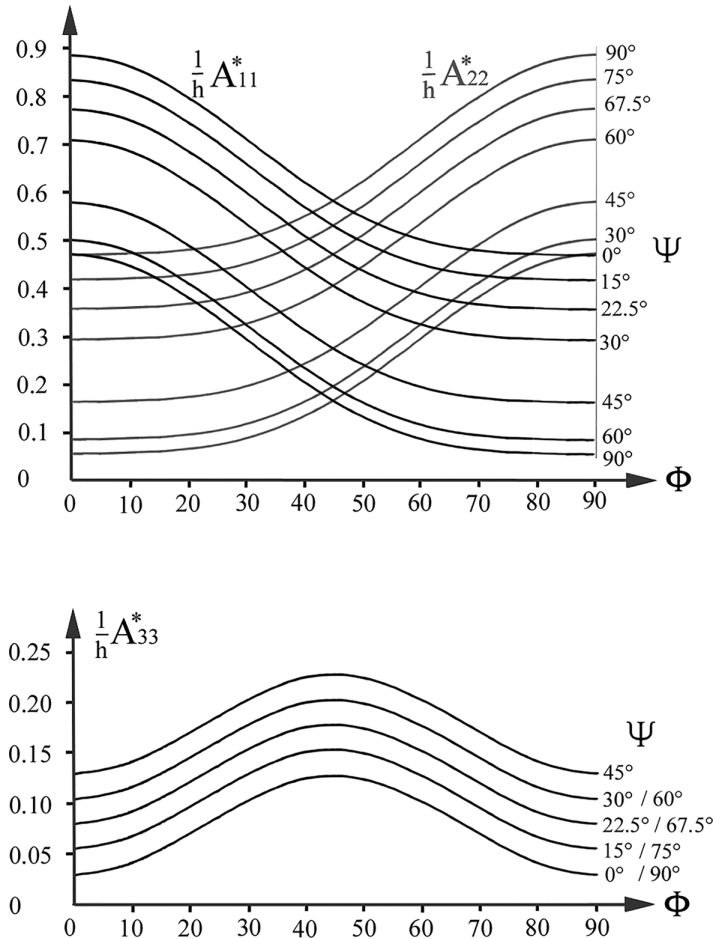


FIGURE 15.17 Normalized characteristics for homogenized CFRP D-D laminates.

These values are linked to the stiffness coefficients of plies (see Equation 11.8).

When one specifies a pair of values, for example $(1/h)A_{11}^*$ and $(1/h)A_{33}^*$ ($(1/h)A_{22}^*$ can be deduced with Equation 15.29), the database characterizing the laminate field allows to obtain the appropriate definition for $\{\pm\Phi / \pm\Psi\}$.

15.6.3 STRENGTH OF THE LAMINATE

15.6.3.1 Preliminary Remark

The strength sizing approach takes into account coefficients that increase loading. These are the *safety factors* specific to each of applications in consideration. This is assumed to be already included upstream to lead to the applied loads considered in what follows.

15.6.3.2 Load Factor

Let us consider the relationship in Equation 15.23a limited to the In-plane behavior, that is to say:

$$\begin{Bmatrix} \sigma_{0x} \\ \sigma_{0y} \\ \tau_{0xy} \end{Bmatrix} = \frac{1}{h} \begin{bmatrix} A_{11} & A_{12} & 0 \\ A_{21} & A_{22} & 0 \\ 0 & 0 & A_{33} \end{bmatrix} \begin{Bmatrix} \epsilon_{0x} \\ \epsilon_{0y} \\ \gamma_{0xy} \end{Bmatrix} \quad (15.30)$$

Remember that this Equation can be written indifferently as (see Equation 15.23b)

$$\begin{Bmatrix} \sigma_{0x} \\ \sigma_{0y} \\ \tau_{0xy} \end{Bmatrix} = \begin{bmatrix} \frac{1}{2}(\bar{E}_{11}^{\Phi} + \bar{E}_{11}^{\Psi}) & \frac{1}{2}(\bar{E}_{12}^{\Phi} + \bar{E}_{12}^{\Psi}) & 0 \\ \frac{1}{2}(\bar{E}_{12}^{\Phi} + \bar{E}_{12}^{\Psi}) & \frac{1}{2}(\bar{E}_{22}^{\Phi} + \bar{E}_{22}^{\Psi}) & 0 \\ 0 & 0 & \frac{1}{2}(\bar{E}_{33}^{\Phi} + \bar{E}_{33}^{\Psi}) \end{bmatrix} \begin{Bmatrix} \epsilon_{0x} \\ \epsilon_{0y} \\ \gamma_{0xy} \end{Bmatrix}$$

- **Simple loading:** let us reduce the loading to the only average stress σ_{0x} , in practice taken equal to the unit, i.e. a unit stress ($\sigma_{0x} = 1 \text{ N/mm}^2$). Then:

$$\begin{Bmatrix} \epsilon_{0x} \\ \epsilon_{0y} \\ \gamma_{0xy} \end{Bmatrix} = h \times [A]^{-1} \begin{Bmatrix} \sigma_{0x(1 \text{ N/mm}^2)} \\ 0 \\ 0 \end{Bmatrix}$$

Thus one deduces the principal strains ϵ_{0I} and ϵ_{0II} ¹⁹ (see Section 15.5.3.2). As shown in Figure 15.18, they are associated with the domain \mathcal{D}'' already defined in Figure 15.15.

Point noted E_0 characterizes the loading $\sigma_{0x(1 \text{ N/mm}^2)}$. Extending \overline{OE}_0 gives point E on the outline of domain \mathcal{D}'' . For that purpose, one must multiply \overline{OE}_0 by a positive factor R so-called “load factor” such as:

$$R = \frac{\overline{OE}}{\overline{OE}_0}$$

In other words, the laminate can withstand without any damage a maximum average stress corresponding to

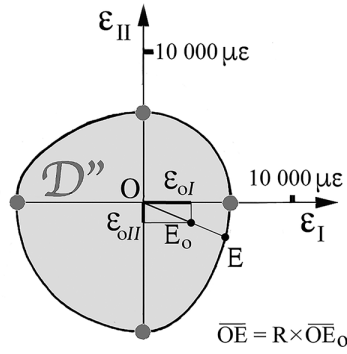


FIGURE 15.18 Load factor “R”.

$$\overline{OE} = R \times \overline{OE_0}, \text{ i.e. equal to } R \times \sigma_{0x} \left(1 \text{ N/mm}^2 \right)$$

15.6.3.3 In-plane Loading

- **Simple loading:**

Given the actual stress-resultant $N_{x(N/mm)}$ that the laminate of thickness h must withstand, the corresponding overall stress (N_x/h) should be such that

$$\frac{N_x}{h} \leq R \times \sigma_{0x} \left(1 \text{ N/mm}^2 \right)$$

i.e.

$$h \geq \frac{N_x \text{ (N/mm)}}{R \times \sigma_{0x} \left(1 \text{ N/mm}^2 \right)} = \frac{N_x}{R} \text{ (mm)} \quad (15.31)$$

- **Example:**

Given the loading $N_x = 3,000 \text{ (N/mm)}$ leads to check the inequality:

$$h_{\text{(mm)}} \geq \frac{3,000}{R}$$

which allows the calculus of h when R is known.

Note: The above implies that N_x and $\sigma_{0x} \left(1 \text{ N/mm}^2 \right)$ are of the same sign chosen here as positive. If $N_x < 0$, then σ_{0x} should be chosen as $\sigma_{0x} = -1 \text{ N/mm}^2 < 0$ which leads in Figure 15.18 to opposite values of the principal strains ϵ_{0I} and ϵ_{0II} and therefore to a load factor $R' \neq R$. Then from Equation 15.31:

$$h \geq \frac{\|N_x\|}{R'} \text{ (mm)}$$

- **Complex loading:**

Consider the combined loading $\{N_x, N_y, T_{xy}\}$

Let us define a unit average stress, for example $\sigma_{0x} = 1 \text{ (N/mm}^2 \text{)}$ if $N_x > 0$.

We will define the other two average stresses σ_{0y} and τ_{0xy} such that $\left\{ \sigma_{0x(1 \text{ N/mm}^2)}, \sigma_{0y}, \tau_{0xy} \right\}$ is taken homothetic with $\{N_x, N_y, T_{xy}\}$.

Then we obtain the laminate strains from Equation 15.30

$$\begin{Bmatrix} \epsilon_{0x} \\ \epsilon_{0y} \\ \gamma_{0xy} \end{Bmatrix} = h \times [A]^{-1} \begin{Bmatrix} \sigma_{0x(1 \text{ N/mm}^2)} \\ \sigma_{0y} \\ \tau_{0xy} \end{Bmatrix}$$

These strains are converted into principal strains ϵ_{0I} and ϵ_{0II} in the domain \mathcal{D}'' in Figure 15.18. They allow definition of a load factor R , i.e. the laminate can withstand the loading $\left\{ R \times \sigma_{0x(1 \text{ N/mm}^2)}; R \times \sigma_{0y}; R \times \tau_{0xy} \right\}$. By returning to the actual loading $\{N_x, N_y, T_{xy}\}$, this leads to:

$$\frac{N_{x(\text{N/mm})}}{h_{(\text{mm})}} \leq R \times \sigma_{0x(1 \text{ N/mm}^2)}; \quad \frac{N_{y(\text{N/mm})}}{h_{(\text{mm})}} \leq R \times \sigma_{0y}; \quad \frac{T_{xy(\text{N/mm})}}{h_{(\text{mm})}} \leq R \times \tau_{0xy}$$

Or, by considering the homothetic values

$$\frac{N_{x(\text{N/mm})}}{\sigma_{0x(1 \text{ N/mm}^2)}} = \frac{N_{y(\text{N/mm})}}{\sigma_{0y}} = \frac{T_{xy(\text{N/mm})}}{\tau_{0xy}} \leq R \times h_{(\text{mm})} \quad (15.32)$$

- **Example:**

Given the stress resultants

$$N_x = 3,000_{(\text{N/mm})}; \quad N_y = -1,500_{(\text{N/mm})}; \quad T_{xy} = -1,500_{(\text{N/mm})}$$

We define the average stresses $\left\{ \sigma_{0x(1 \text{ N/mm}^2)}; \sigma_{0y}; \tau_{0xy} \right\}$ as the homothetic values:

$$\sigma_{0x} = 1_{(\text{N/mm}^2)}; \quad \sigma_{0y} = -0.5_{(\text{N/mm}^2)}; \quad \tau_{0xy} = -0.5_{(\text{N/mm}^2)}$$

After determining the load factor R we have (See Equation 15.32)

$$\frac{3,000_{(\text{N/mm})}}{1_{(\text{N/mm}^2)}} = \frac{-1,500_{(\text{N/mm})}}{-0.5_{(\text{N/mm}^2)}} = \frac{-1,500_{(\text{N/mm})}}{-0.5_{(\text{N/mm}^2)}} \leq R \times h_{(\text{mm})} \Rightarrow 3,000 \leq R \times h_{(\text{mm})}$$

which allows the calculation of h .

15.6.3.4 Flexure Loading

Considering Equation 15.23a limited to the bending behavior, that is to say:

$$\begin{Bmatrix} (\sigma_{0xf})_{\frac{h}{2}} \\ (\sigma_{0yf})_{\frac{h}{2}} \\ (\tau_{0xyf})_{\frac{h}{2}} \end{Bmatrix} = \frac{1}{h} \begin{bmatrix} A_{11} & A_{12} & 0 \\ A_{21} & A_{22} & 0 \\ 0 & 0 & A_{33} \end{bmatrix} \begin{Bmatrix} (\epsilon_{0xf})_{\frac{h}{2}} \\ (\epsilon_{0yf})_{\frac{h}{2}} \\ (\gamma_{0xyf})_{\frac{h}{2}} \end{Bmatrix}$$

Remember that this Equation can be written indifferently (See Equation 15.23b)

$$\left\{ \begin{array}{c} (\sigma_{0,xf})_{\frac{h}{2}} \\ (\sigma_{0,yf})_{\frac{h}{2}} \\ (\tau_{0,xyf})_{\frac{h}{2}} \end{array} \right\} = \left[\begin{array}{ccc} \frac{1}{2}(\bar{E}_{11}^{+\Phi} + \bar{E}_{11}^{+\Psi}) & \frac{1}{2}(\bar{E}_{12}^{+\Phi} + \bar{E}_{12}^{+\Psi}) & 0 \\ \frac{1}{2}(\bar{E}_{12}^{+\Phi} + \bar{E}_{12}^{+\Psi}) & \frac{1}{2}(\bar{E}_{22}^{+\Phi} + \bar{E}_{22}^{+\Psi}) & 0 \\ 0 & 0 & \frac{1}{2}(\bar{E}_{33}^{+\Phi} + \bar{E}_{33}^{+\Psi}) \end{array} \right] \left\{ \begin{array}{c} (\epsilon_{0,xf})_{\frac{h}{2}} \\ (\epsilon_{0,yf})_{\frac{h}{2}} \\ (\gamma_{0,xyf})_{\frac{h}{2}} \end{array} \right\}$$

The average bending stresses considered exert on the upper face ($z = h/2$). As for the previous loadings, these bending stresses are deduced from the nodal forces obtained from finite element analysis, namely $M_{y(N)}$; $M_{x(N)}$; $M_{xy(N)}$ ²⁰. With $M_{y(N)}$ for example, we will have (See Section 15.4.1.3):

a. *Upper face of the laminate:*

$$(\sigma_{0,xf})_{\frac{h}{2}} = \frac{6}{h^2} \times M_y$$

Let us define a unit average bending stress with the same sign as $M_{y(N)}$, for example $(\sigma_{0,xf})_{\frac{h}{2}} = 1_{(N/mm^2)}$ provided that $M_{y(N)} > 0$

The corresponding strains are written as:

$$\left\{ \begin{array}{c} (\epsilon_{0,xf})_{\frac{h}{2}} \\ (\epsilon_{0,yf})_{\frac{h}{2}} \\ (\gamma_{0,xyf})_{\frac{h}{2}} \end{array} \right\} = h \times [A]^{-1} \left\{ \begin{array}{c} \underbrace{(\sigma_{0,xf})_{\frac{h}{2}}}_{(1N/mm^2)} \\ 0 \\ 0 \end{array} \right\}$$

From that we deduce the upper surface strains $(\epsilon_{0,xf})_{\frac{h}{2}}$ and $(\epsilon_{0,yf})_{\frac{h}{2}}$ which allow defining a load factor R_{upper} (See Figure 15.19). The laminate can therefore withstand:

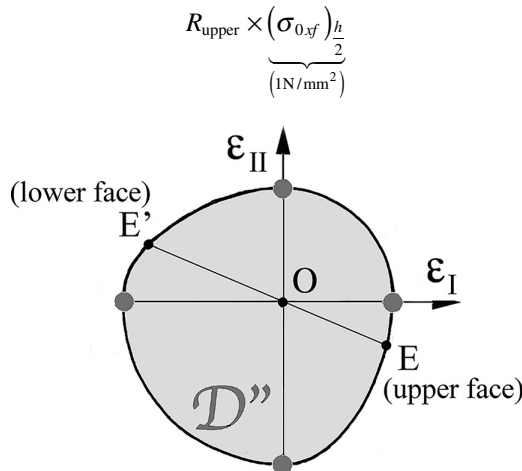


FIGURE 15.19 Upper and lower face to define load factors R_{upper} and R_{lower} .

If now it is subjected to the actual loading $M_{y(N)}$, the laminate thickness being noted h , we must respect:

$$\frac{6}{h^2} \times M_{y(N)} \leq R_{\text{upper}} \times \underbrace{(\sigma_{0,xf})_{\frac{h}{2}}}_{(1\text{N/mm}^2)}$$

b. *Lower face of the laminate:*

The bending stress is then opposite in sign: $(\sigma_{0,xf})_{-\frac{h}{2}} = -(\sigma_{0,xf})_{\frac{h}{2}}$. This case should also be considered. For this stress we will obtain a load factor $R_{\text{lower}} \neq R_{\text{upper}}$ as shown in Figure 15.19 where

$$\frac{R_{\text{lower}}}{R_{\text{upper}}} = \frac{\|OE'\|}{\|OE\|}$$

To summarize, we have: (a) on the upper face of the laminate:

$$\frac{6M_y}{h^2} \leq R_{\text{upper}} \times \underbrace{(\sigma_{0,xf})_{\frac{h}{2}}}_{(1\text{N/mm}^2)}$$

(b) on the lower face:

$$\frac{6M_y}{h^2} \leq R_{\text{lower}} \times \left\| \underbrace{(\sigma_{0,xf})_{-\frac{h}{2}}}_{(-1\text{N/mm}^2)} \right\|$$

We must therefore retain:

$$\frac{6M_y}{h^2} \leq \min(R_{\text{lower}}, R_{\text{upper}}) \times \underbrace{(\sigma_{0,xf})_{\frac{h}{2}}}_{(1\text{N/mm}^2)}$$

$$h^2 \geq \frac{6M_{y(N)}}{\min(R_{\text{lower}}, R_{\text{upper}}) \times \underbrace{(\sigma_{0,xf})_{\frac{h}{2}}}_{(1\text{N/mm}^2)}} \Rightarrow h_{(\text{mm}^2)}^2 \geq \frac{6M_{y(N)}}{\min(R_{\text{lower}}, R_{\text{upper}})}$$

Which allows the calculation of thickness h .

Note: When using the Nettles circle (See Figure 15.16) instead of the domain \mathcal{D}'' , then $R_{\text{lower}} = R_{\text{upper}}$ and the above case simplify.

15.7 PRACTICAL BENEFITS OF HOMOGENIZED D-D LAMINATES

15.7.1 IMPACT ON DESIGN

Taking into account the properties resulting from the D-D laminates homogenization, it is possible to vary the thickness of laminated parts by interrupting the layup of plies (ply drop) on any of outer surfaces without alteration of the laminate stiffness matrix $(1/h)[A]$ (see Equation 15.22).

Consider, for example, the basic arrangement \mathcal{A} (see Section 15.3.1) which we recall:

$\mathcal{A} \dots \begin{matrix} 1 & 2 & 2' & 1' & 1 & 2 & 2' & 1' & 1 & 2 & 2' & 1' & 1 & 2 & 2' & 1' & 1 & 2 & 2' & 1' \dots \\ \Psi & \Phi & -\Phi & -\Psi & \Psi & \Phi & -\Phi & -\Psi & \Psi & \Phi & -\Phi & -\Psi & \Psi & \Phi & -\Phi & -\Psi & \Psi & \Phi & -\Phi & -\Psi \dots \end{matrix}$
 $\leftarrow \hspace{10em} \text{« 5 » repetitions} \hspace{10em} \rightarrow$

Twenty plies resulting from five D-D Sub-Laminated sets are shown here. Either a thickness for a unidirectional CFRP²¹ of 2.6mm considered as a minimum for homogenization. The plies not shown on either side (dotted lines) reinforce the homogenized nature. By increasing the ply-number beyond what is shown, thickness can vary by adding plies on either lower or upper surface, or both, according for example to the schemas in Figure 15.20. Another arrangement is to use the so-called “card-sliding technique” scheme, as shown in Figure 15.21. Figure 15.22 shows an Omega stiffener obtained with this method, with an important weight saving.

- **Note:** In this way internal structure of the D-D laminate remains intact. This advantage does not occur in Quad laminates where mirror symmetry has to be maintained. Thus, when the thickness has to vary, ply drop has to be done within the draping, causing internal defects. In addition, the stiffness characteristics related to the ply-percentages in the four directions are altered (see Figure 5.16).
It will therefore be retained that for D-D laminates one can vary the thickness h in significant proportions when the In-plane and moment resultants vary, while keeping constant the stiffness terms $(1/h)A_{ij}$, with as consequences:
 - Weight saving which can be a decisive advantage when choosing a manufacturing process.
 - Possibility of obtaining tapered edges reducing edge effects (out of plane stresses, see Figure 14.3).
 - Possibility of more efficient repair of a damaged area by means of a D-D patch to rigorously restore the homogenized characteristics.
- It is worthy to note that such advantages – not possible with Quad laminates – are in line with the development and possibilities of unidirectional and NCF tapes and with tape laying machines.

Figure 15.22 shows an Omega stiffener obtained with the card sliding technique²².

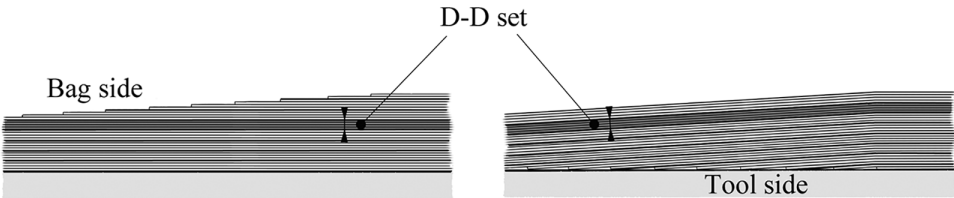


FIGURE 15.20 Varying thickness.

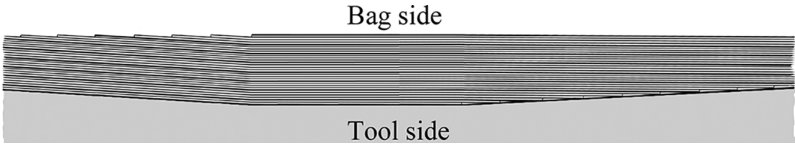


FIGURE 15.21 Card-sliding technique.

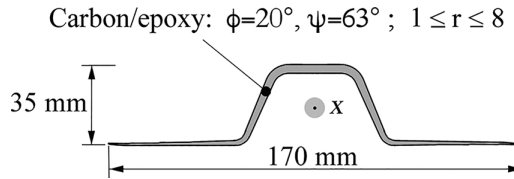


FIGURE 15.22 Example: Omega stiffener, weight saving 41.5%. (Cf. Bibliography: Arteiro A. et al., A case of Tsai Modulus, an Invariant-based Approach to Stiffness /2020.)

15.8 CALCULATION TOOL

15.8.1 PRESENTATION

The calculation tool is based on the principles explained in the previous section. It also incorporates additional functions. In its directly available and usable form, it consists of an Excel® or MATLAB® spreadsheet entitled “LAM SEARCH”, freely accessible and accompanied by a user manual.

15.8.2 CHARACTERISTICS

This tool first incorporates elements presented in this chapter, summarized as follows:

- Elastic properties of plies synthesized thanks to the Tsai modulus.
 - The concept of homogenized laminate resulting from repeatedly stacked D-D sets.
 - Resistance properties transferred to the maximum allowable laminate strains.
- Moreover the tool also integrates additional functions not mentioned in the above, and particularly:
- Taking into account of other constituent plies such as glass / resin or extension to sandwich plates, while we have limited ourselves here to unidirectional CFRP plies.
 - Taking into account of singularities in laminated parts (see Figure 14.3) and particularly open and filled holes that is dimensioning case for many applications such as aeronautics.
 - Sizing of laminated parts stiffened by means of ribs network.
 - Study of partial or overall part buckling.
 - Blending of areas subject to spatially non-uniform loads.
 - Sizing of predefined substructures such as tubes, pressure tanks, and beams.
- **Note:** With regard to this last point, some particular substructures work under well-defined single loading rather than under multiple loadings. The example of pressure vessel envelopes is typical. It is well known that, depending on the case, the envelope requires two or three winding angles²³. These types of laminates appear as simplifications of D-D laminates, and lend themselves better to optimization due to the particular loading.

15.8.3 COMPUTERIZED INTEGRATION

Association of the tool in question with several marketed calculation codes²⁴ is constantly evolving. The goal is always to build an iterative procedure capable of providing optimized stratified zones, for example by following the diagram in Figure 15.23.

15.8.4 REFERENCES

The LAM SEARCH tool was created within the non-profit association THINK COMPOSITES²⁵, the aim of which is to promote composite materials in industry and education. Composed of an international network of high-level scientists working around Professor Stephen Tsai²⁶ this association

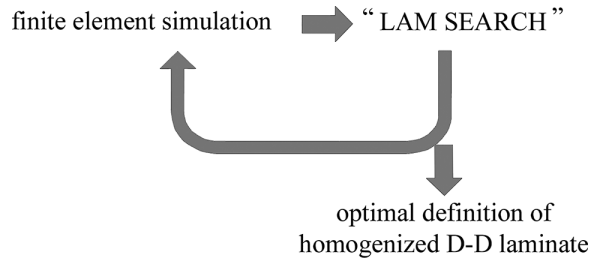


FIGURE 15.23 Searching an optimal composition and thickness.

has been working since the early 1980s for composite materials in various fields ranging from theoretical aspects to manufacturing and characterization. The association also offers services to industry by means of advice, specific design tools, training.

As already mentioned, the LAM SEARCH tool is completely open and available free of charge to interested parties, manufacturers and academics.

For more information and to take advantage of it: www.think-composites.com

NOTES

- 1 Remember that in Equation 9.5: $\gamma_{tr} = 2\epsilon_{tr}$.
- 2 Cf. Bibliography: Arteiro A. et al., A case of Tsai Modulus, an Invariant-based Approach to Stiffness /2020.
- 3 See Bibliography: Tsai S.W. et al., Composite Laminate Theory and Practice of Analysis, Design and Automated Lay-up /2017.
- 4 See Section 5.2.3.
- 5 See Application 19.14.
- 6 « Historical » because chronologically it is the first carbon / epoxy laminate designed during the 1960s (**General Dynamics** (US)) to obtain mechanical characteristics similar to those of an aluminum alloy with a much lower density and therefore known as “black aluminum”.
- 7 Choices for arrangements will be considered later (see Section 15.4.5.1).
- 8 Recall that $[1^2 + 2^2 + 3^2 + 4^2 \dots + N^2] = N(N+1)(2N+1)/6$.
- 9 Recall that $[1^2 + 3^2 + 5^2 \dots]_{N \text{ terms}} = N(2N-1)(2N+1)/3$.
- 10 We can also write: $M_y = \int_{-\frac{h}{2}}^{\frac{h}{2}} \sigma_x z dz = \int_{-\frac{h}{2}}^{\frac{h}{2}} \sigma_{xf} z dz = \int_{-\frac{h}{2}}^{\frac{h}{2}} (\sigma_{0xf})_{\frac{h}{2}} \times \frac{z}{(h/2)} \times z \times dz = (\sigma_{0xf})_{\frac{h}{2}} \times \frac{h^2}{6}$.
- 11 Cf. Bibliography: Tsai S.W. et al., Composite Laminate Theory and Practice of Analysis, Design and Automated Lay-up /2017.
- 12 Such couplings do not appear for r_{odd} . For r_{even} , relative values of these terms decreases rapidly in the same way as seen in Section 15.4.2.2.
- 13 Except in special cases of buckling risk.
- 14 Cf. Bibliography: Tsai S. W., Double–Double: New Family of Composite Lamina /2021.
- 15 Cf. for example **Chomar** (FR, US, CN, TN).
- 16 In addition, the laying involves more complexity in that the short fibers should alternate with the long ones following each direction.
- 17 More generally, one can see from Equation 15.23 how obtaining (after inversion) global strains from the addition of average In-plane and flexural stresses.
- 18 See Bibliography: Nettles A.T., 2021.
- 19 Note that in this pure traction case, principal strains merge with ϵ_{0x} , ϵ_{0y} .
- 20 Remember that M_y is expressed in ($N \times \text{mm} / \text{mm}$) that is to say in (N).
- 21 See Table 3.2.
- 22 Cf. Bibliography: Tsai S.W., *AIAA Journal*, 2021 and Keppel E./2022.

- 23 See Applications 19.9 and 19.10.
- 24 Among which stand out @: ANSYS, CATIA, NASTRAN, ABAQUS, MATLAB.
- 25 Association which has been operating since 1983 by Pr. Stephen W. Tsai and Dr. Thierry Massard.
<https://www.think-composites.com>.
- 26 Cf. Bibliography: Arteiro A. et al., A case of Tsai Modulus, an Invariant-based Approach to Stiffness/
2020.

16 Bending of Composite Beams of Any Section Shape

Due to their slenderness, a number of composite elements (mechanical components or structural parts) can be considered as beams. A few typical examples are shown schematically in Figure 16.1. The behavior under loading of these elements (evaluation of stress and displacements) becomes a very complex problem when the 3D aspect is discussed. We propose in this chapter a monodimensional approach of the phenomenon through an original method. It is based on the definition of resultants for displacements, which will constitute the counterpart of the traditional stress resultants (shear force, normal force, and bending moment). This leads to a **homogenized** formulation for bending and for torsion. This means that equilibrium and behavior relationships are formally identical to those of classical homogeneous beams. Then using similar equations to those of classical beams does the application of these relationships to the calculation of stress values and displacements.

We shall limit the study to composite beams with constant characteristics from one cross section to another (geometry, materials), with any-shaped components that we will call **phases**, which are assumed to be perfectly bonded to each other.

To clarify the procedure, a maximum simplicity in calculation is reached with isotropic phases. The extension to transversely isotropic phases is immediate. When the phases become orthotropic, with orthotropic directions changing from one point to another in the cross section, the study is analogous, with a much more complicated formulation¹.

16.1 BENDING OF BEAMS WITH ISOTROPIC PHASES AND PLANE OF SYMMETRY

In the following, D symbolizes the cross-sectional domain in the (y, z) plane. The **external** boundary is denoted as ∂D . The **internal** boundaries are denoted by ℓ_{ij} for two contiguous phases i and j (see Figure 16.2). The area of phase i is denoted as S_i . E_i and G_i denote its moduli of elasticity.

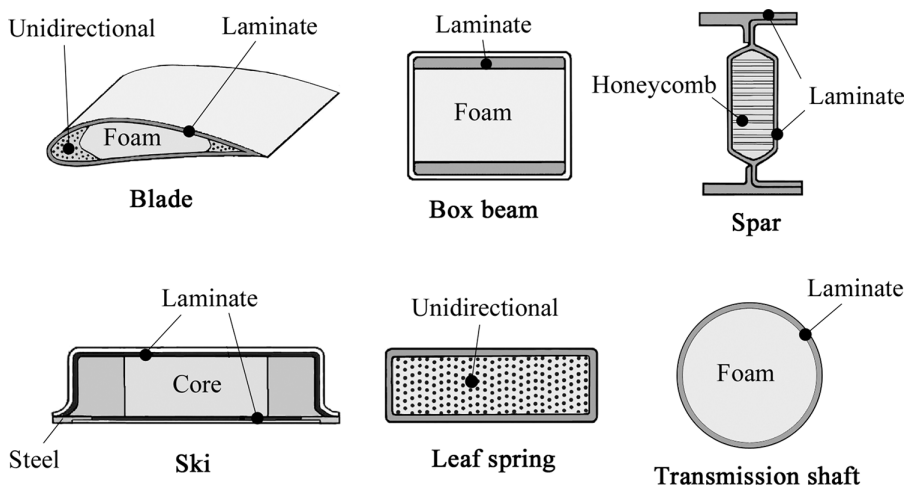


FIGURE 16.1 Composite beams.

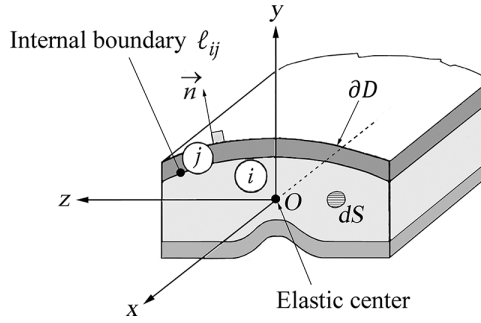


FIGURE 16.2 Composite beam with a plane of symmetry.

The elastic displacement at any point of the beam has the following components: $u_x(x, y, z)$, $u_y(x, y, z)$, and $u_z(x, y, z)$.

The beam is bending in the symmetry plane (x, y) under external loads that are also symmetric with respect to this plane.

16.1.1 DEGREES OF FREEDOM

16.1.1.1 Equivalent Stiffnesses

We will note in condensed form the following integrals, taken on the whole cross section and that we define as the equivalent stiffnesses for bending²:

$$\begin{aligned}
 \langle ES \rangle &= \int_D E_i dS \quad \text{or} = \sum_{\substack{i \\ \text{number of phases}}} E_i S_i \\
 \langle EI_z \rangle &= \int_D E_i y^2 dS \quad \text{or} = \sum_{\substack{i \\ \text{number of phases}}} E_i I_{zi} \\
 \langle GS \rangle &= \int_D G_i dS \quad \text{or} = \sum_{\substack{i \\ \text{number of phases}}} G_i S_i
 \end{aligned} \tag{16.1}$$

16.1.1.2 Longitudinal Displacement

By definition, the longitudinal displacement denoted by $u(x)$ is written as

$$u(x) = \frac{1}{\langle ES \rangle} \times \int_D E_i u_x(x, y, z) dS$$

Such definition of $u(x)$ allows writing

$$u_x(x, y, z) = u(x) + \Delta u_x(x, y, z)$$

where it should be noted that

$$\int_D E_i \Delta u_x dS = 0 \tag{16.2}$$

16.1.1.3 Rotation of the Section

By definition, this is the fictitious rotation or **equivalent rotation** given by the following:

$$\theta_z(x) = \frac{-1}{\langle EI_z \rangle} \int_D E_i u_x(x, y, z) \times y \, dS$$

Or, with the above:

$$\theta_z(x) = \frac{-1}{EI_z} \left\{ u(x) \int_D E_i y \, dS + \int_D E_i \Delta u_x(x, y, z) y \, dS \right\}$$

16.1.1.4 Elastic Center

Origin O of coordinate y is chosen such that the following integral is zero:

$$\int_D E_i y \times dS = 0$$

We refer this point O as the **elastic center**. Then Δu_x takes the form

$$\Delta u_x(x, y, z) = -y\theta_z(x) + \eta_x(x, y, z)$$

with³

$$\int_D E_i \eta_x y \, dS = \int_D E_i \eta_x \, dS = 0$$

The displacement $u_x(x, y, z)$ can then take the form

$$u_x(x, y, z) = u(x) - y\theta_z(x) + \eta_x(x, y, z)$$

16.1.1.5 Transverse Displacement along y -Direction

By definition, this is $v(x)$ given by the following:

$$v(x) = \frac{1}{\langle GS \rangle} \int_D G_i u_y(x, y, z) \, dS$$

From this definition,

$$u_y(x, y, z) = v(x) + \eta_y(x, y, z)$$

where we should note that

$$\int_D G_i \eta_y \, dS = 0$$

16.1.1.6 Transverse Displacement along z -Direction

By definition, this is $w(x)$ given by

$$w(x) = \frac{1}{\langle GS \rangle} \int_D G_i u_z(x, y, z) dS$$

It follows from this definition and from the existence of the symmetry plane (x, y) a zero average transverse displacement as $w(x) = 0$:

$$u_z(x, y, z) = 0 + \eta_z(x, y, z), \quad \text{with} \quad \int_D G_i \eta_z dS = 0$$

In summary, we obtain the elastic displacement field:

$$\begin{cases} u_x = u(x) - y\theta_z(x) + \eta_x(x, y, z) \\ u_y = v(x) + \eta_y(x, y, z) \\ u_z = \eta_z(x, y, z) \end{cases} \quad (16.3)$$

The origin of axes is the elastic center O such that

$$\int_D E_i y \times dS = 0 \quad (16.4)$$

The 3D incremental displacement field $(\eta_x, \eta_y \text{ and } \eta_z)$ is superimposed on the unidimensional approximation $(u(x), v(x), \theta_z(x))$ and verifies the following:

$$\begin{aligned} \int_D E_i \eta_x dS &= \int_D E_i y \times \eta_x dS = 0 \\ \int_D G_i \eta_y dS &= 0 \\ \int_D G_i \eta_z dS &= 0 \end{aligned} \quad (16.5)$$

Notes:

- η_x represents the **longitudinal warping** of a cross section, that is, the displacement of each point in this section, **out of the plane** that would represent this section if it were moving in accordance with the unidimensional displacement field $(u(x), v(x), \theta_z(x))$.
- η_y and η_z are displacements that characterize the change of cross-sectional shape in its initial plane.

16.1.2 PERFECT BONDING BETWEEN THE PHASES

16.1.2.1 Displacements

The bonding of phases is assumed to be perfect. Therefore, the displacements are continuous when crossing through the interface between two phases in contact. Thus, on the interface between two phases i and j , we have

$$u_{x(i)} = u_{x(j)}; \quad u_{y(i)} = u_{y(j)}; \quad u_{z(i)} = u_{z(j)}$$

16.1.2.2 Strains

Strains are identical for phases i and j (see Figure 16.3) in the plane of an elemental interface with normal vector \vec{n} . ϵ being the strain tensor, we will, thus, have in phases i and j

$$\begin{aligned}\vec{x} \cdot \epsilon(\vec{x})_{(i)} &= \vec{x} \cdot \epsilon(\vec{x})_{(j)} \\ \vec{t} \cdot \epsilon(\vec{x})_{(i)} &= \vec{t} \cdot \epsilon(\vec{x})_{(j)} \\ \vec{t} \cdot \epsilon(\vec{t})_{(i)} &= \vec{t} \cdot \epsilon(\vec{t})_{(j)}\end{aligned}$$

which can also be written as

$$\begin{aligned}\epsilon_{xx} &= \epsilon_{xx} \\ \epsilon_{xy} n_z + \epsilon_{xz} n_y &= \epsilon_{xy} n_z + \epsilon_{xz} n_y \\ \epsilon_{yy} n_z^2 - 2\epsilon_{yz} n_y n_z + \epsilon_{zz} n_y^2 &= \epsilon_{yy} n_z^2 - 2\epsilon_{yz} n_y n_z + \epsilon_{zz} n_y^2\end{aligned}$$

16.1.2.3 Stresses

The stress vector $\vec{\sigma} = \Sigma(\vec{n})$, where Σ represents the stress tensor, remains continuous across an interface element with normal \vec{n} as

$$\begin{aligned}\tau_{xy} n_y + \tau_{xz} n_z &= \tau_{xy} n_y + \tau_{xz} n_z \\ \sigma_{yy} n_y + \tau_{yz} n_z &= \sigma_{yy} n_y + \tau_{yz} n_z \\ \tau_{yz} n_y + \sigma_{zz} n_z &= \tau_{yz} n_y + \sigma_{zz} n_z\end{aligned} \tag{16.6}$$

16.1.3 EQUILIBRIUM RELATIONSHIPS

Starting from the local equilibrium, in the absence of body forces, we have

$$\frac{\partial \sigma_{ij}}{\partial x_j} = 0$$

By integrating over the cross section, we have the following successively.

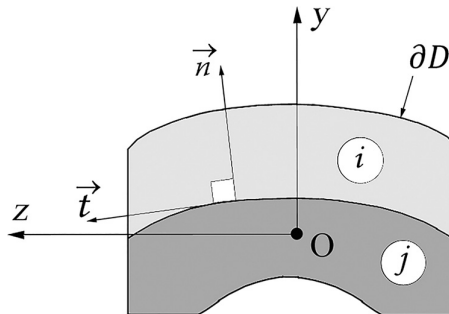


FIGURE 16.3 Interface between two phases.

16.1.3.1 Longitudinal Equilibrium

$$\frac{d}{dx} \int_D \sigma_{xx} dS + \int_D \left(\frac{\partial \tau_{xy}}{\partial y} + \frac{\partial \tau_{xz}}{\partial z} \right) dS = 0$$

Where the **normal stress resultant** N_x appears as

$$N_x = \int_D \sigma_{xx} dS$$

Then, converting the second integral into an integral over the external boundary ∂D of D^4 ,

$$\frac{dN_x}{dx} + \int_{\partial D} (\tau_{xy} n_y + \tau_{xz} n_z) d\Gamma = 0$$

In which n_y and n_z are the cosines of the outward normal \vec{n} and $d\Gamma$ is an element of external boundary ∂D . Assuming the absence of shear stress over the lateral surface of the beam, then $\tau_{xy} n_y + \tau_{xz} n_z = 0$ along the external boundary ∂D . Thus, for longitudinal equilibrium, we have⁵

$$\frac{dN_x}{dx} = 0$$

16.1.3.2 Transverse Equilibrium

$$\frac{d}{dx} \int_D \tau_{xy} dS + \int_D \left(\frac{\partial \sigma_{yy}}{\partial y} + \frac{\partial \tau_{yz}}{\partial z} \right) dS = 0$$

Where we recognize the shear stress resultant

$$T_y = \int_D \tau_{xy} dS.$$

Then transforming the second integral into an integral over the external boundary ∂D of the cross-sectional domain D^6 ,

$$\frac{\partial T_y}{\partial x} + \int_{\partial D} (\sigma_{yy} n_y + \tau_{yz} n_z) d\Gamma = 0$$

Noting that

$$\int_{\partial D} (\sigma_{yy} n_y + \tau_{yz} n_z) d\Gamma = \int_{\partial D} \vec{y} \cdot \Sigma(\vec{n}) d\Gamma = \vec{y} \cdot \int_{\partial D} \vec{\sigma} d\Gamma = p_y \text{ (N/m)}$$

which is the transverse load per unit length acting on the lateral surface of the beam, transverse equilibrium can be written as

$$\frac{dT_y}{dx} + p_y = 0$$

16.1.3.3 Moment Equilibrium

$$\frac{d}{dx} \int_D -y \sigma_{xx} dS + \int_D -y \left(\frac{\partial \tau_{xy}}{\partial y} + \frac{\partial \tau_{xz}}{\partial z} \right) dS = 0$$

Where appears the **bending moment**

$$M_z = \int_D -y \sigma_{xx} dS.$$

Then transforming the second integral⁷,

$$\frac{dM_z}{dx} + \int_{\partial D} -y (\tau_{xy} n_y + \tau_{xz} n_z) d\Gamma + \int_D \tau_{xy} dS = 0$$

It should be noted that

$$\int_{\partial D} -y (\tau_{xy} n_y + \tau_{xz} n_z) d\Gamma = \int_{\partial D} -y \vec{x} \cdot \Sigma(\vec{n}) d\Gamma = \int_{\partial D} -y (\vec{\sigma} \cdot \vec{x}) d\Gamma = \mu_z \text{ (m} \times \text{N/m)}$$

which can be called a moment per unit length exerted on the beam. Then we obtain the following equilibrium relationship:

$$\frac{dM_z}{dx} + T_y + \mu_z = 0$$

A loading giving a moment per unit length in statics being highly exceptional, we will, therefore, assume that $\mu_z = 0$ in what follows.

In summary, we obtain the following equations of equilibrium:

$$\begin{aligned} \frac{dN_x}{dx} &= 0 \\ \frac{dT_y}{dx} + p_y &= 0 \\ \frac{dM_z}{dx} + T_y &= 0 \end{aligned} \tag{16.7}$$

16.1.4 CONSTITUTIVE EQUATIONS

Taking into account the isotropic nature of the different phases, the constitutive equation can be written in tensor form for phase i as

$$\boldsymbol{\varepsilon} = \frac{(1 + \nu_i)}{E_i} \boldsymbol{\Sigma} - \frac{\nu_i}{E_i} \text{tr}(\boldsymbol{\Sigma}) \mathbf{I} \quad (\mathbf{I} = \text{unity tensor})$$

We deduce, by integrating over the domain D occupied by the cross section of the beam,

$$\text{a. } \int_D \varepsilon_{xx} E_i dS = \int_D \sigma_{xx} dS - \int_D \nu_i (\sigma_{yy} + \sigma_{zz}) dS$$

Taking into account the displacements in Equation 16.3, we can write

$$\int_D \epsilon_{xx} E_i dS = \int_D \frac{\partial u_x}{\partial x} E_i dS = -\frac{d\theta_z}{dx} \int_D y E_i dS + \frac{du}{dx} \int_D E_i dS + \frac{\partial}{\partial x} \int_D E_i \eta_x dS$$

which leads, with notation of Equation 16.1, to

$$N_x = \langle ES \rangle \frac{du}{dx} + \int_D v_i (\sigma_{yy} + \sigma_{zz}) dS \quad (16.8)$$

$$\text{b. } \int_D -y \epsilon_{xx} E_i dS = \int_D -y \sigma_{xx} dS + \int_D v_i y (\sigma_{yy} + \sigma_{zz}) dS$$

Taking into account the displacements in Equation 16.3, we can write

$$\int_D -y \epsilon_{xx} E_i dS = \frac{d\theta_z}{dx} \int_D E_i y^2 dS - \frac{du}{dx} \int_D E_i y dS - \frac{\partial}{\partial x} \int_D E_i y \eta_x dS$$

This leads, with notation of Equation 16.1, to

$$M_z = \langle EI_z \rangle \frac{d\theta_z}{dx} - \int_D v_i y (\sigma_{yy} + \sigma_{zz}) dS \quad (16.9)$$

$$\text{c. } \int_D 2\epsilon_{xy} G_i dS = \int_D \tau_{xy} dS$$

Similarly, with the displacements in Equation 16.3,

$$\begin{aligned} \int_D 2\epsilon_{xy} G_i dS &= \int_D \left(\frac{\partial u_x}{\partial y} + \frac{\partial u_y}{\partial x} \right) G_i dS = -\theta_z \int_D G_i dS \dots \\ &\dots + \int_D G_i \frac{\partial \eta_x}{\partial y} dS + \frac{dv}{dx} \int_D G_i dS + \frac{\partial}{\partial x} \int_D \eta_y G_i dS \end{aligned}$$

And with notation in Equation 16.1,

$$T_y = \langle GS \rangle \left(\frac{dv}{dx} - \theta_z \right) + \int_D G_i \frac{\partial \eta_x}{\partial y} dS \quad (16.10)$$

16.1.5 TECHNICAL FORMULATION

16.1.5.1 Assumptions

The classical assumptions made for homogeneous beams are extended here to composite beams:

1. We assume that σ_{yy} and $\sigma_{zz} \ll \sigma_{xx}$ at almost every point of the cross section⁸.
2. When calculating the flexure stress values σ_{xx} , τ_{xy} and τ_{xz} , we neglect the warping variation (η_x, η_y, η_z) between two cross sections that are infinitely close to one another⁹.

15.1.5.2 Expression of Normal Stress

Considering the constitutive equation

$$\epsilon_{xx} = \frac{\sigma_{xx}}{E_i} - \frac{\nu_i}{E_i} (\sigma_{yy} + \sigma_{zz})$$

and taking into account the previous simplifications, we can extract the following simplified form:

$$\frac{\sigma_{xx}}{E_i} \approx \frac{\partial u_x}{\partial x} = -y \frac{d\theta_z}{dx} + \frac{du}{dx} + \cancel{\frac{\partial \eta_x}{\partial x}}$$

Then, with $M_z \approx \langle EI_z \rangle \times (d\theta_z/dx)$ (see Equation 16.9) and $N_x \approx \langle ES \rangle \times (du/dx)$ (see Equation 16.8),

$$\sigma_{xx} = -E_i \underbrace{\frac{M_z}{\langle EI_z \rangle}}_{\text{bending}} y + E_i \underbrace{\frac{N_x}{\langle ES \rangle}}_{\text{extension}} \quad (16.11)$$

Note: The strain continuity¹⁰ $(\epsilon_{xx})_i = (\epsilon_{xx})_j$ at the interface between phases i and j leads to

$$\frac{(\sigma_{xx})_i}{E_i} = \frac{(\sigma_{xx})_j}{E_j}$$

which shows the **discontinuity of normal stress** due to different values of longitudinal moduli, as illustrated in Figure 16.4.

16.1.5.3 Expression of Shear Stress

1. Characterization of warping

Starting from the local equilibrium described by

$$\frac{\partial \sigma_{ij}}{\partial x_j} = 0$$

we study the flexure shear stress in the cross section, noted as

$$\vec{\tau} = \tau_{xy} \vec{y} + \tau_{xz} \vec{z}$$

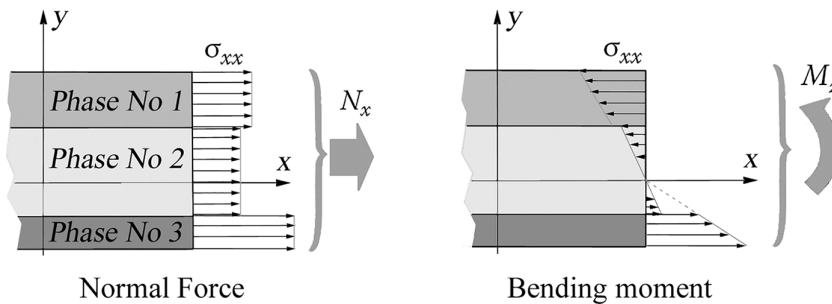


FIGURE 16.4 Normal and bending stresses.

Taking into consideration Equations 16.11 and 16.7 and the aforementioned Assumption 2,

$$\frac{\partial \tau_{xy}}{\partial y} + \frac{\partial \tau_{xz}}{\partial z} = -\frac{\partial \sigma_{xx}}{\partial x} = \frac{E_i}{\langle EI_z \rangle} \frac{dM_z}{dx} y - \frac{E_i}{\langle ES \rangle} \frac{dN_x}{dx} = -\frac{E_i}{\langle EI_z \rangle} T_y \times y$$

with

$$\tau_{xy} = G_i \left(\frac{\partial u_x}{\partial y} + \frac{\partial u_y}{\partial x} \right); \quad \tau_{xz} = G_i \left(\frac{\partial u_x}{\partial z} + \frac{\partial u_z}{\partial x} \right)$$

and inserting the displacement field of Equation 16.3

$$G_i \left(\frac{\partial^2 \eta_x}{\partial y^2} + \frac{\partial^2 \eta_x}{\partial z^2} \right) = -T_y \frac{E_i}{\langle EI_z \rangle} \times y$$

Putting η_x in the form

$$\eta_x = \frac{T_y}{\langle GS \rangle} \times g(y, z) \quad (16.12)$$

leads to

$$\nabla^2 g = -\frac{E_i}{G_i} \frac{\langle GS \rangle}{\langle EI_z \rangle} \times y \quad (16.13)$$

And Equation 16.10 becomes

$$T_y = GS \left(\frac{dv}{dx} - \theta_z \right) + \int_D G_i \frac{T_y}{\langle GS \rangle} \frac{\partial g}{\partial y} ds$$

$$T_y = \left(1 - \frac{1}{\langle GS \rangle} \int_D G_i \frac{\partial g}{\partial y} ds \right) = \langle GS \rangle \left(\frac{dv}{dx} - \theta_z \right)$$

or

$$T_y = \frac{\langle GS \rangle}{k} \left(\frac{dv}{dx} - \theta_z \right) \quad (16.14)$$

In the above relationship appears a coefficient k , which is the analog of the shear coefficient for homogeneous beams and which is worked out in what follows.

2. External boundary condition

Recalling that the lateral surface of the beam is assumed free from shear, this gives, along the external contour ∂D of the cross section,

$$\vec{\tau} \cdot \vec{n} = \tau_{xy} n_y + \tau_{xz} n_z = 0$$

Then, using the displacement field of Equation 16.3 and assumptions above (see Section 16.1.5.1),

$$\left(\frac{dv}{dx} - \theta_z \right) n_y + \overline{\text{grad}} \eta_x \cdot \vec{n} = 0$$

Introducing the function $g(y, z)$ (Equation 16.12) with Equation 16.14,

$$\overrightarrow{\text{grad}} g \cdot \vec{n} = \frac{\partial g}{\partial y} = -kn_y$$

Let us substitute $g(y, z)$ with $g_o(y, z)$ defined as

$$g_o(y, z) = g(y, z) + k \times y \quad (16.15)$$

Then, $g_o(y, z)$ appears as the solution to the problem:

$$\left\{ \begin{array}{l} \nabla^2 g_o = -\frac{E_i}{G_i} \frac{\langle GS \rangle}{\langle EI_z \rangle} \times y \text{ in domain } D \\ \frac{\partial g_o}{\partial n} = 0 \text{ on the boundary } \partial D \end{array} \right.$$

$g_o(y, z)$ will be referred to as the **longitudinal warping function** of the cross section under consideration.

3. Internal boundary conditions

Due to continuity conditions already described in Section 16.1.2, we can note at the boundary ℓ_{ij} between two phases i and j :

$$g_{oi} = g_{oj}$$

and

$$\tau_{xy(i)} n_y + \tau_{xz(i)} n_z = \tau_{xy(j)} n_y + \tau_{xz(j)} n_z$$

By using the displacement field, where is introduced the warping function,

$$G_i \frac{\partial g_{oi}}{\partial n} = G_j \frac{\partial g_{oj}}{\partial n}$$

4. Uniqueness of the solution

Given by Equation 16.5 that translates here into

$$\int_D E_i g_o \, dS = 0$$

5. Form of shear stress

We can easily verify the following expressions for shear stress:

$$\tau_{xy} = G_i \frac{T_y}{\langle GS \rangle} \frac{\partial g_o}{\partial y}$$

$$\tau_{xz} = G_i \frac{T_y}{\langle GS \rangle} \frac{\partial g_o}{\partial z}$$

or equally

$$\bar{\tau} = G_i \frac{T_y}{\langle GS \rangle} \overline{\text{grad}} g_o$$

16.1.5.4 Shear Coefficient for the Section

When the warping function g_o is known, the shear coefficient for the section is obtained starting from Equation 16.5:

$$\int_D E_i \eta_x dS = 0$$

Noting that this relationship can be rewritten as

$$\int_D E_i \frac{T_y}{\langle GS \rangle} (g_o - k \times y) \times y dS = 0$$

We obtain

$$k = \frac{1}{\langle EI_z \rangle} \int_D E_i g_o y dS$$

16.1.5.5 Summary

In summary, in the absence of body forces (e.g., inertia forces), the bending of a composite beam in its plane of symmetry (see Figure 16.5) can be characterized by a homogenized formulation equivalent to that of a classical homogeneous beam in the following manner:

Summary (see Figure 16.5)

- **Elastic center O :** it is such that

$$\int_D E_i y dS = 0$$

- **Equivalent stiffnesses:**

$$\langle ES \rangle = \sum_i E_i S_i \quad ; \quad \langle EI_z \rangle = \sum_i E_i I_{zi} \quad ; \quad \frac{\langle GS \rangle}{k} = \frac{1}{k} \times \sum_i G_i S_i$$

- **Equilibrium relationships:** (stress resultants calculated at elastic center O)

$$\frac{dN_x}{dx} = 0 \quad ; \quad \frac{dT_y}{dx} + p_y = 0 \quad ; \quad \frac{dM_z}{dx} + T_y = 0$$

- **Constitutive equations:**

$$N_x = ES \frac{du}{dx} \quad ; \quad T_y = \frac{GS}{k} \left(\frac{dv}{dx} - \theta_z \right) \quad ; \quad M_z = EI_z \frac{d\theta_z}{dx}$$

(16.16a)

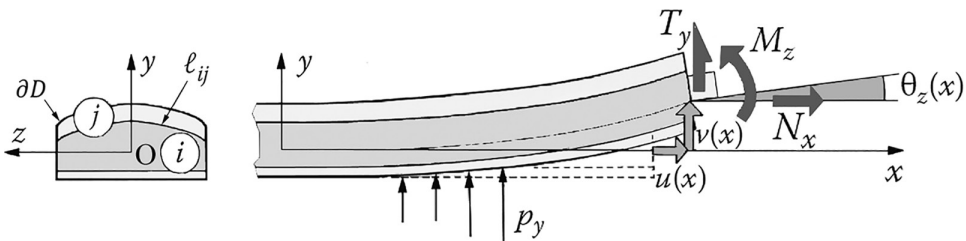


FIGURE 16.5 Notations.

<ul style="list-style-type: none"> • Stress values <p>Normal stress σ_{xx}</p> $\sigma_{xx} = -E_i \frac{M_z}{\langle EI_z \rangle} \times y + E_i \frac{N_x}{\langle ES \rangle}$ <p>Shear stress $\vec{\tau} = \tau_{xy} \vec{y} + \tau_{xz} \vec{z}$</p> $\vec{\tau} = \frac{G_i}{\langle GS \rangle} T_y \times \overline{\text{grad}} g_o \left\{ \begin{array}{l} \tau_{xy} = G_i \frac{T_y}{\langle GS \rangle} \frac{\partial g_o}{\partial y} \\ \tau_{xz} = G_i \frac{T_y}{\langle GS \rangle} \frac{\partial g_o}{\partial z} \end{array} \right.$
<ul style="list-style-type: none"> • Longitudinal warping function $g_o(y, z)$: in domain D of the cross section, it is the solution to the problem $\frac{\partial^2 g_o}{\partial y^2} + \frac{\partial^2 g_o}{\partial z^2} = -\frac{E_i}{G_i} \frac{\langle GS \rangle}{\langle EI_z \rangle} \times y$ <p>with on the external boundary ∂D</p> $\frac{\partial g_o}{\partial n} = 0$ <p>and internal continuities along internal boundaries ℓ_{ij}</p> $g_{oi} = g_{oj} \quad ; \quad G_i \frac{\partial g_{oi}}{\partial n} = G_j \frac{\partial g_{oj}}{\partial n}$ <p>Uniqueness condition</p> $\int_D E_i g_o dS = 0$
<ul style="list-style-type: none"> • Shear coefficient k: it is given by the formula¹¹ $k = \frac{1}{\langle EI_z \rangle} \int_D E_i g_o y dS$

(16.16b)

16.1.6 ENERGY INTERPRETATION

16.1.6.1 Energy Due to Normal Stress σ_{xx}

Denoting dW_σ as the deformation energy of an elementary beam portion with length dx , under normal stress σ_{xx} , we have

$$dW_\sigma = \frac{1}{2} \int_D \sigma_{xx} \epsilon_{xx} dV = \left\{ \frac{1}{2} \int_D \frac{\sigma_{xx}^2}{E_i} dS \right\} dx$$

Taking into account Equation 16.11 for the normal stress,

$$\begin{aligned} \frac{dW_\sigma}{dx} &= \frac{1}{2} \int_D \frac{1}{E_i} \left[-\frac{E_i}{\langle EI_z \rangle} M_z y + \frac{E_i}{\langle ES \rangle} N_x \right]^2 dS \\ &= \frac{1}{2} \int_D E_i \frac{M_z^2}{\langle EI_z \rangle^2} y^2 dS + \frac{1}{2} \int_D E_i \frac{N_x^2}{\langle ES \rangle^2} dS \dots \\ &\quad \dots + \int_D E_i \frac{M_z N_x}{\langle EI_z \rangle \langle ES \rangle} y dS \end{aligned}$$

The above expression simplifies due to the definition of elastic center O in Equation 16.16. Therefore,

$$\frac{dW_\sigma}{dx} = \frac{1}{2} \frac{M_z^2}{\langle EI_z \rangle} + \frac{1}{2} \frac{N_x^2}{\langle ES \rangle}$$

16.1.6.2 Energy Due to Shear Stress $\bar{\tau}$

Due to shear stress $\bar{\tau}$, the deformation energy dW_τ of an elementary beam portion with length dx takes the form

$$dW_\tau = \frac{1}{2} \int_D 2(\tau_{xy} \epsilon_{xy} + \tau_{xz} \epsilon_{xz}) dV = \frac{1}{2} \left\{ \int_D \frac{1}{G_i} (\tau_{xy}^2 + \tau_{xz}^2) dS \right\} dx$$

Taking into account the form of shear stress in Equation 16.16,

$$\begin{aligned} \frac{dW_\tau}{dx} &= \frac{1}{2} \int_D G_i \frac{T_y^2}{\langle GS \rangle^2} \left\{ \left(\frac{\partial g_o}{\partial y} \right)^2 + \left(\frac{\partial g_o}{\partial z} \right)^2 \right\} dS \\ \frac{dW_\tau}{dx} &= \frac{1}{2} \frac{T_y^2}{\langle GS \rangle^2} \int_D G_i \left\{ \frac{\partial}{\partial y} \left(g_o \frac{\partial g_o}{\partial y} \right) + \frac{\partial}{\partial z} \left(g_o \frac{\partial g_o}{\partial z} \right) - g_o \nabla^2 g_o \right\} dS \end{aligned}$$

With the Laplacian value of the warping function g_o taken from Equation 16.16¹²,

$$\frac{dW_\tau}{dx} = \frac{1}{2} \frac{T_y^2}{\langle GS \rangle^2} \left\{ \int_D G_i g_o \frac{E_i}{G_i} \frac{\langle GS \rangle}{\langle EI_z \rangle} y dS + \int_{\partial D} G_i g_o \frac{\partial g_o}{\partial n} d\Gamma \right\}$$

In the above, we can recognize the shear coefficient k for the section (see Equation 16.16). Then,

$$\frac{dW_\tau}{dx} = \frac{1}{2} k \frac{T_y^2}{\langle GS \rangle}$$

In summary, the strain energy density can be written as

$$\frac{dW}{dx} = \frac{1}{2} \frac{N_x^2}{\langle ES \rangle} + \frac{1}{2} \frac{M_z^2}{\langle EI_z \rangle} + \frac{1}{2} k \frac{T_y^2}{\langle GS \rangle} \quad (16.17)$$

Notes:

- Note the analogy between this expression and that for the strain energy of a classical homogeneous beam, which should be written here:

$$\frac{dW}{dx} = \frac{1}{2} \frac{N_x^2}{ES} + \frac{1}{2} \frac{M_z^2}{EI_z} + \frac{1}{2} k \frac{T_y^2}{GS}$$

- As a practical consequence of this homogenization, it becomes possible to determine the **equivalent characteristics** that are necessary in the process of data entry into a computer program utilizing finite elements of classical homogeneous beams. The problem then comes to the numerical evaluation of the following values:

- Equivalent moduli: $E_{\text{equiv.}}$, $G_{\text{equiv.}}$, (or $\nu_{\text{equiv.}}$)
- Geometrical characteristics: $S_{\text{equiv.}}$, $I_{z \text{ equiv.}}$, and k

Taking $S_{\text{equiv.}} = S$ (actual area of the cross section), we can easily verify that

$$E_{\text{equiv.}} = \frac{\langle ES \rangle}{S}; \quad G_{\text{equiv.}} = \frac{\langle GS \rangle}{S}$$

$$I_{z_{\text{equiv.}}} = \frac{\langle EI_z \rangle}{E_{\text{equiv.}}}; \quad \nu_{\text{equiv.}} = \frac{1}{2} \frac{\langle ES \rangle}{\langle GS \rangle} - 1$$

However, as for classical beams, knowledge of the shear coefficient k is not direct, as noted in the following (see Section 16.2.2).

16.1.7 EXTENSION TO THE DYNAMIC CASE

16.1.7.1 Inertia Forces

Equilibrium relationships of Section 16.1.3 were written in the absence of body forces. During vibratory motions, these body forces exist as inertia forces. Then we have

$$\frac{\partial \sigma_{ij}}{\partial x_j} - \rho \ddot{u}_i = 0$$

By repeating the main calculation steps as described in Section 16.1.3, we obtain the following for a beam that oscillates freely¹³:

(a)

$$\frac{\partial N_x}{\partial x} = \frac{\partial^2}{\partial t^2} \int_D \rho u_x \, dS$$

which leads, with Equation 16.3, to

$$\frac{\partial N_x}{\partial x} = \langle \rho S \rangle \frac{\partial^2 u}{\partial t^2} - y_G \langle \rho S \rangle \frac{\partial^2 \theta_z}{\partial t^2}$$

where we denote

$$\langle \rho S \rangle = \int_D \rho \, dS \quad \text{and} \quad y_G \times \langle \rho S \rangle = \int_D \rho y \, dS.$$

y_G appears here as the **mass center** ordinate of the section. It should be noted that we have neglected the secondary coupling due to η_x .

(b)

$$\frac{\partial T_y}{\partial x} = \frac{\partial^2}{\partial t^2} \int_D \rho u_y \, dS$$

With Equation 16.3 and neglecting the secondary coupling due to η_x :

$$\frac{\partial T_y}{\partial x} = \langle \rho S \rangle \frac{\partial^2 v}{\partial t^2}$$

(c)

$$\frac{\partial M_z}{\partial x} + T_y = \frac{\partial^2}{\partial t^2} \int_D -y \rho u_x \, dS$$

With Equation 16.3, posing $\langle \rho I_z \rangle = \int_D \rho y^2 dS$ and neglecting the secondary coupling due to η_x :

$$\frac{\partial M_z}{\partial x} + T_y = \langle \rho I_z \rangle \frac{\partial^2 \theta_z}{\partial t^2} - y_G \langle \rho S \rangle \frac{\partial^2 u}{\partial t^2}$$

The above relations are to be linked to constitutive relationships in Equation 16.16. However, we should note that the latter were written in the absence of body forces. Nevertheless, we will consider them as relevant, under the condition that the concerned frequencies are not too high. Generally, this corresponds to the mechanical frequency domain, also denoted as **quasistatic** domain.

16.1.7.2 Summary

In summary, for the dynamic case, we must replace the equilibrium and behavior relationships, which appear in Equation 16.16, with the following:

Equations of motion (<i>stress resultants calculated in elastic center O</i>)
$\frac{\partial N_x}{\partial x} = \langle \rho S \rangle \frac{\partial^2 u}{\partial t^2} - y_G \langle \rho S \rangle \frac{\partial^2 \theta_z}{\partial t^2}$
$\frac{\partial T_y}{\partial x} = \langle \rho S \rangle \frac{\partial^2 v}{\partial t^2}$
$\frac{\partial M_z}{\partial x} + T_y = \langle \rho I_z \rangle \frac{\partial^2 \theta_z}{\partial t^2} - y_G \langle \rho S \rangle \frac{\partial^2 u}{\partial t^2}$
$\langle \rho S \rangle = \sum_i \rho_i S_i; \quad \langle \rho I_z \rangle = \sum_i \rho_i I_{zi}; \quad y_G \langle \rho S \rangle = \int_D \rho y dS$
Constitutive equations
$N_x = \langle ES \rangle \frac{\partial u}{\partial x}; \quad T_y = \frac{\langle GS \rangle}{k} \left(\frac{\partial v}{\partial x} - \theta_z \right); \quad M_z = \langle EI_z \rangle \frac{\partial \theta_z}{\partial x}$

(16.18)

Note: We can observe in the above relations a nonclassical coupling between longitudinal oscillations $u(x,t)$ and flexural oscillations $v(x,t)$ and $\theta_z(x,t)$. This coupling disappears when the elastic center O is coincident with the mass center (or center of gravity)¹⁴.

16.2 CASE OF BEAMS OF ANY CROSS SECTION (ASYMMETRIC)

16.2.1 TECHNICAL FORMULATION

Now, the beam cross section does not present any particular symmetry (see Figure 16.6).

The procedure adopted in Section 16.1 for symmetric beams is still considered for this general case. First, we note the supplementary equivalent stiffness:

$$\langle EI_y \rangle = \int_D E_i z^2 dS = \sum_i \left(E_i \times I_{yi} \right)$$

number of phases

Besides the equivalent rotation $\theta_z(x)$, we also define an equivalent rotation $\theta_y(x)$ defined by the expression:

$$\theta_y(x) = \frac{1}{\langle EI_y \rangle} \int_D E_i u_x(x, y, z) \times z dS$$

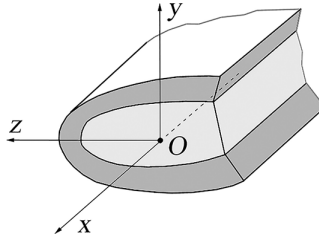


FIGURE 16.6 Composite beam with any cross-sectional shape.

It follows from definitions of θ_y , u , and θ_z (Section 16.1.1) that

$$\theta_y(x) = \frac{1}{\langle EI_y \rangle} \int_D E_i \{u - y\theta_z + \eta_{ox}\} \times z \, dS$$

This expression simplifies if we choose the origin of z -coordinate such that

$$\int_D E_i z \, dS = 0; \quad \int_D E_i (y \times z) dS = 0$$

This, together with the condition already established in the previous paragraph, that is, $\int_D E_i \times y \, dS = 0$,

allows us to define the position of the **elastic center** O of the section, as well as the orientation of axes y and z that will be called **principal axes** of the section. Then, in summary,

The contribution η_{ox} to the longitudinal displacement u_x , which appears above, can then be rewritten as

Elastic center	$\int_D E_i y \, dS = 0$
	$\int_D E_i z \, dS = 0$
Principal axes	$\int_D E_i yz \, dS = 0$

$$\eta_{ox}(x, y, z) = z \times \theta_y + \eta_x(x, y, z)$$

And from the definition of the degree of freedom θ_y , it can be verified that

$$\int_D E_i \eta_x z \, dS = 0$$

The displacement $u_x(x, y, z)$ then takes the form

$$u_x(x, y, z) = u(x) - y\theta_z(x) + z\theta_y(x) + \eta_x(x, y, z)$$

In addition, due to the disappearance of symmetry in the section, the average displacement $w(x)$ (see Section 16.1.1.6) is not zero.

We then obtain the elastic displacement field

$$u_x = u(x) - y\theta_z + z\theta_y + \eta_x$$

$$u_y = v(x) + \eta_y$$

$$u_z = w(x) + \eta_z$$

The incremental displacement field (η_x, η_y, η_z) verifies (see Section 16.1.1.6)

$$\int_D E_i \eta_x \, dS = \int_D E_i \eta_x y \, dS = \int_D E_i \eta_x z \, dS = 0$$

$$\int_D G_i \eta_y \, dS = 0$$

$$\int_D G_i \eta_z \, dS = 0$$

Analysis may be carried out starting from the above and following the same procedure as in Section 16.1, successively for bending in (x, y) plane, with identical results, then in (x, z) plane. We summarize these in the following.

16.2.2 SUMMARY

- **Degrees of freedom:**

along $x : u(x)$

along $y : v(x); \theta_y(x)$

along $z : w(x); \theta_z(x)$

- **Elastic center O :** See Figure 16.6. It is such that

$$\int_D E_i y \, dS = \int_D E_i z \, dS = 0$$

- **Principal axes y and z :** they are such that

$$\int_D E_i y z \, dS = 0$$

- **Equivalent stiffnesses:**

$$\langle ES \rangle = \sum_i E_i S_i$$

$$\langle EI_z \rangle = \sum_i E_i I_{zi} \quad ; \quad \langle EI_y \rangle = \sum_i E_i I_{yi}$$

$$\frac{\langle GS \rangle}{k_y} = \sum_i G_i S_i \times \frac{1}{k_y} \quad ; \quad \frac{\langle GS \rangle}{k_z} = \sum_i G_i S_i \times \frac{1}{k_z}$$

(16.19a)

- **Equilibrium relationships:** (stress resultants calculated at elastic center O)

$$\frac{dN_x}{dx} = 0$$

$$\frac{dT_y}{dx} + p_y = 0; \quad \frac{dT_z}{dx} + p_z = 0$$

$$\frac{dM_z}{dx} + T_y = 0; \quad \frac{dM_y}{dx} - T_z = 0$$

- **Constitutive equations:**

$$N_x = \langle ES \rangle \frac{du}{dx}$$

$$T_y = \frac{\langle GS \rangle}{k_y} \left(\frac{dv}{dx} - \theta_z \right); \quad T_z = \frac{\langle GS \rangle}{k_z} \left(\frac{dw}{dx} + \theta_y \right)$$

$$M_z = \langle EI_z \rangle \frac{d\theta_z}{dx}; \quad M_y = \langle EI_y \rangle \frac{d\theta_y}{dx}$$

(16.19b)

- **Normal stress:**

$$\sigma_{xx} = -E_i \frac{M_z}{\langle EI_z \rangle} y + E_i \frac{M_y}{\langle EI_y \rangle} z + E_i \frac{N_x}{\langle ES \rangle}$$

- **Shear stress:**

$$\tau_{xy} = \frac{G_i}{\langle GS \rangle} \left(T_y \frac{\partial g_o}{\partial y} + T_z \frac{\partial h_o}{\partial y} \right)$$

$$\tau_{xz} = \frac{G_i}{\langle GS \rangle} \left(T_y \frac{\partial g_o}{\partial z} + T_z \frac{\partial h_o}{\partial z} \right)$$

That is,

$$\vec{\tau} = \frac{G_i}{\langle GS \rangle} \left(T_y \overline{\text{grad}} g_o + T_z \overline{\text{grad}} h_o \right)$$

(16.19c)

Longitudinal Warping Functions

function $g_o(y, z)$: it is the solution to the problem

$$\begin{cases} \frac{\partial^2 g_o}{\partial y^2} + \frac{\partial^2 g_o}{\partial z^2} = -\frac{E_i}{G_i} \frac{\langle GS \rangle}{\langle EI_z \rangle} y & \text{in domain } D \text{ of the section,} \\ \frac{\partial g_o}{\partial n} = 0 & \text{on the external boundary } \partial D \end{cases}$$

with internal continuity

$$\left. \begin{aligned} g_{oi} &= g_{oj} \\ G_i \frac{\partial g_{oi}}{\partial n} &= G_j \frac{\partial g_{oj}}{\partial n} \end{aligned} \right\} \text{along internal boundaries } \ell_{ij}$$

and the uniqueness condition $\int_D E_i g_o \, dS = 0$

<p>function $h_o(y, z)$: it is the solution to the problem</p> $\begin{cases} \frac{\partial^2 h_o}{\partial y^2} + \frac{\partial^2 h_o}{\partial z^2} = -\frac{E_i}{G_i} \frac{\langle GS \rangle}{\langle EI_z \rangle} z \text{ in domain } D \text{ of the section,} \\ \frac{\partial h_o}{\partial n} = 0 \text{ on the external boundary } \partial D \end{cases}$ <p>with internal continuity</p> $\left. \begin{aligned} h_{oi} &= h_{oj} \\ G_i \frac{\partial h_{oi}}{\partial n} &= G_j \frac{\partial h_{oj}}{\partial n} \end{aligned} \right\} \text{along internal boundaries } \ell_{ij}$ <p>and the uniqueness condition $\int_D E_i h_o \, dS = 0$</p>
Shear Coefficients
<p>coefficient k_y : it is given by the formula $k_y = \frac{1}{\langle EI_z \rangle} \int_D E_i g_o y \, dS$</p>
<p>coefficient k_z : it is given by the formula $k_z = \frac{1}{\langle EI_y \rangle} \int_D E_i h_o z \, dS$</p>
Strain Energy
$\frac{dW}{dx} = \frac{1}{2} \frac{N_x^2}{\langle ES \rangle} + \frac{1}{2} \frac{M_z^2}{\langle EI_z \rangle} + \frac{1}{2} \frac{M_y^2}{\langle EI_y \rangle} + \frac{1}{2} k_y \frac{T_y^2}{\langle GS \rangle} + \frac{1}{2} k_z \frac{T_z^2}{\langle GS \rangle}$

(16.19d)

16.2.2 NOTES

- In fact in Equation 16.19b, instead of the constitutive relationship,

$$T_y = \frac{\langle GS \rangle}{k_y} \left(\frac{dv}{dx} - \theta_z \right)$$

it comes to a form such as

$$k_y T_y + k_{yz} T_z = \langle GS \rangle \left(\frac{dv}{dx} - \theta_z \right)$$

where appears a coupling shear coefficient k_{yz} . This means that a unique shear resultant T_z leads also to flexure in the y -axis direction, which is perpendicular to it. This secondary effect has been neglected here. Analogous remark holds for the constitutive relationship

$$T_z = \frac{\langle GS \rangle}{k_z} \left(\frac{dw}{dx} + \theta_y \right)$$

It results in the simplification of the relationship

$$k_{zy} T_y + k_z T_z = \langle GS \rangle \left(\frac{dw}{dx} + \theta_y \right)$$

where we are led in a similar way to neglect a coupling coefficient k_{zy} (which furthermore checks the equality $k_{zy} = k_{yz}$).

- As already mentioned in Section 16.1.6 for a symmetric beam, it is possible to evaluate the equivalent characteristics that are necessary in the process of data entry in order to utilize computer programs for finite element calculation of classical beams¹⁵. The characteristics

$$E_{\text{equiv.}}; \quad G_{\text{equiv.}}; \quad I_{z \text{ equiv.}}; \quad \text{and} \quad I_{y \text{ equiv.}}$$

can be obtained right away.

- On the contrary, as for classical beams, calculation of shear coefficients k_y and k_z is not direct. At first, it is necessary to calculate the warping function values g_0 and h_0 , solutions of Poisson problems in the domain occupied by the cross section, as it is noted in Equation 16.19d. The nature of these problems makes it possible for each of functions g_0 and h_0 to write an equivalent functional, allowing, therefore, the function calculation by means of finite element discretization of the cross section¹⁶.

16.2.3 EXAMPLES

Various examples of composite beams are provided in Application Chapters 19 and 21. They are treated in accordance with the results obtained in this chapter, and with simplifications where possible.

One can, thus, consult the following application examples:

- Simply supported sandwich beam: Application 19.1
- Helicopter blade: Application 19.3
- Reversing lever made of carbon/PEEK: Application 19.12
- Glass/resin telegraph pole: Application 19.13
- Manipulator arm for a space shuttle: Application 19.15
- Composite beam with two layers: Application 21.2
- Buckling of a sandwich beam: Application 21.4
- Shear due to bending in a sandwich beam: Application 21.5
- Shear due to bending in a composite box beam: Application 21.6
- Torsion center of a composite U-beam: Application 21.7
- Shear to bending in a composite I-beam: Application 21.8
- Bending vibration of a sandwich beam: Application 21.12
- Two phases circular section beam: Application 21.13

It is useful to note that most of these applications provide results that can be used as tests for numerical modeling.

NOTES

- 1 The only restrictive condition lies in the fact that one orthotropic direction is supposed parallel to the longitudinal axis of the beam. See Bibliography: Tanghe-Carrier F. (1999) and Tanghe-Carrier F., Gay D. (2000).
- 2 I_{z_i} is the quadratic moment of phase i with respect to z -axis.
- 3 The nullity of the second integral is the consequence of Equation 16.2.
- 4 Note that equality $\int_D \left(\frac{\partial \tau_{xy}}{\partial y} + \frac{\partial \tau_{xz}}{\partial z} \right) dS = \int_{\partial D} (\tau_{xy} n_y + \tau_{xz} n_z) d\Gamma$ is made possible due to the continuity of expression $(\tau_{xy} n_y + \tau_{xz} n_z)$ across the interfaces between the different phases (see Equation 16.6).

- 5 In the equation of local equilibrium above, volumic forces have been neglected. They result in the presence of a second member f_x . If these exist, such as inertia forces, centrifugal forces, or vibratory inertial forces, for example, the equilibrium relationship is obtained in the modified form $(dN_x/dx) + p_x = 0$ in which $p_x = \int_D f_x dS$ represents the longitudinal load per unit length.
- 6 Note that equality $\int_D \left(\frac{\partial \sigma_{yy}}{\partial y} + \frac{\partial \tau_{yz}}{\partial z} \right) dS = \int_{\partial D} (\sigma_{yy} n_y + \tau_{yz} n_z) d\Gamma$ is made possible due to the continuity of the expression $(\sigma_{yy} n_y + \tau_{yz} n_z)$ across the internal boundaries between the different phases (see Equation 16.6).
- 7 Same remark as before concerning the continuity of expression $(\tau_{xy} n_y + \tau_{xz} n_z)$ across the internal boundaries (Equation 16.6).
- 8 Such assumption is all the more verified if the Poisson coefficients of the different phases have similar values.
- 9 This assumption is also known in classical literature on homogeneous beams, as the Navier-Bernoulli generalized hypothesis.
- 10 See Section 16.1.2.
- 11 See Applications 21.3, 21.5, 21.6, and 21.8.
- 12 Equality $\int_D G_i \left\{ \frac{\partial}{\partial y} \left(g_o \frac{\partial g_o}{\partial y} \right) + \frac{\partial}{\partial z} \left(g_o \frac{\partial g_o}{\partial z} \right) \right\} dS = \int_{\partial D} G_i g_o \frac{\partial g_o}{\partial n} d\Gamma$ is made possible due to continuity of quantities $G_i \times g_o \times (\partial g_o / \partial n)$ at interfaces ℓ_{ij} (see internal boundary conditions in Section 16.1.5.3).
- 13 We remove all forces and moments per unit length acting on the beam, except inertial forces and moments.
- 14 See Application in Section 21.12 in Chapter 21.
- 15 It should be noted that a computer program based on classical homogeneous beam elements cannot provide correct stress values in a cross section, since these stress values are of particular formulation for composite beams, as can be seen in Equations 16.16b and 16.19c.
- 16 See Bibliography: Nouri and Gay (1994).

17 Torsion of Composite Beams of Any Section Shape

As described in Chapter 16, we consider here composite beams made of isotropic phases. Extrapolation to beams with transversely isotropic phases is straightforward. The study of orthotropic phases with one principal direction parallel to the axis of the beam, the other two principal directions variable in the plane of a cross section, does not present fundamental difficulties¹.

17.1 UNIFORM TORSION

We will keep the conventions and notations of the previous chapter. In Figure 17.1, O is the **elastic center** and (y, z) are the **principal axes**. The beam is slender and uniformly twisted, that is, every cross section is subjected to a pure and constant torsion moment, along the x -axis, denoted as M_x .

When submitted to this moment, each line in the beam, initially parallel to the x longitudinal axis, becomes a **helicoid curve**. Because of the absence of symmetry in the cross section, this property also concerns the line that, initially, was coinciding with the x -axis itself (i.e., the locus of elastic centers). The only line that remains rectilinear is cutting the plane of all cross sections at a point that will be called **torsion center** and denoted as C , with coordinates y_C and z_C in principal axes (see Figure 17.1).

17.1.1 TORSIONAL DEGREE OF FREEDOM

It is defined as the rotation of each cross section about the x -axis and denoted as θ_x ². The torsional moment M_x being constant, θ_x evolves along the x -axis in such a manner that, for any pair of cross sections spaced at dx interval, a same relative rotation $d\theta_x$ can be observed. Thus,

$$\frac{d\theta_x}{dx} = \text{constant}$$

From this, it comes that the rotation of section varies linearly along the x -axis. As a consequence, we assume *a priori* the components of the displacement field u_x , u_y and u_z to be written as

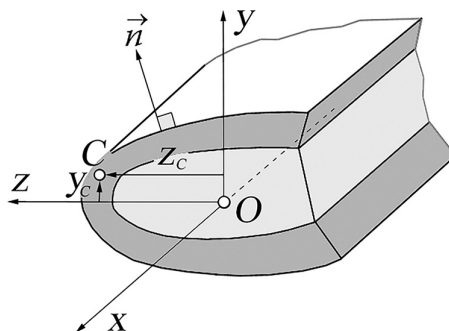


FIGURE 17.1 Elastic center O , torsion center C , and principal axes.

$$\begin{aligned}
u_x &= \frac{d\theta_x}{dx} \times \varphi(y, z) \\
u_y &= -(z - z_c) \theta_x \\
u_z &= (y - y_c) \theta_x
\end{aligned} \tag{17.1}$$

In which the function denoted as $\varphi(y, z)$ is characteristic of the cross-sectional shape and of the materials that constitute the composite beam. This is called the **warping function** for torsion.

17.1.2 CONSTITUTIVE EQUATION

With the displacement field in Equation 17.1, the only nonzero strain values are written as

$$\begin{aligned}
\gamma_{xy} &= \frac{d\theta_x}{dx} \left(\frac{\partial \varphi}{\partial y} - (z - z_c) \right) \\
\gamma_{xz} &= \frac{d\theta_x}{dx} \left(\frac{\partial \varphi}{\partial z} + (y - y_c) \right)
\end{aligned}$$

The only nonzero stress values are then the shear stresses τ_{xy} and τ_{xz} , immediately deduced from the strains above. The torsional moment is readily obtained by integration over the domain D of the cross section as

$$M_x = \int_D (y \tau_{xz} - z \tau_{xy}) dS = \frac{d\theta_x}{dx} \int_D G_i \left\{ y \left(\frac{\partial \varphi}{\partial z} - y_c \right) - z \left(\frac{\partial \varphi}{\partial z} + z_c \right) + y^2 + z^2 \right\} dS$$

Introducing the function $\Phi(y, x)$ such that

$$\Phi(y, x) = \varphi(y, z) + y z_c - z y_c \tag{17.2}$$

Then,

$$M_x = \frac{d\theta_x}{dx} \times \int_D G_i \left(y \frac{\partial \Phi}{\partial z} - z \frac{\partial \Phi}{\partial y} + y^2 + z^2 \right) dS$$

In this expression, it is possible to define the **equivalent stiffness in torsion**:

$$\langle GJ \rangle = \int_D G_i \left(y \frac{\partial \Phi}{\partial z} - z \frac{\partial \Phi}{\partial y} + y^2 + z^2 \right) dS \tag{17.3}$$

So that the constitutive equation takes the form

$$M_x = \langle GJ \rangle \frac{\partial \theta_x}{\partial x}$$

17.1.3 DETERMINATION OF $\Phi(y, z)$

17.1.3.1 Local Equilibrium

The local equilibrium is written as

$$\frac{\partial \tau_{xy}}{\partial y} + \frac{\partial \tau_{xz}}{\partial z} = 0$$

Then, with the displacement field in Equation 17.1,

$$\nabla^2 \varphi = 0$$

and with the form (17.2) of function Φ ,

$$\nabla^2 \Phi = 0$$

17.1.3.2 External Boundary Condition

The lateral surface of the beam being free of any stress, we can write along the external boundary ∂D :

$$\vec{\tau} \cdot \vec{n} = 0,$$

where \vec{n} is the outward unitary vector, perpendicular to the boundary (see Figure 17.1).

With the displacement field in Equation 17.1,

$$\left\{ \frac{\partial \Phi}{\partial y} - (z - z_c) \right\} n_y + \left\{ \frac{\partial \Phi}{\partial z} + (y - y_c) \right\} n_z = 0$$

Then again,

$$\frac{\partial \Phi}{\partial y} n_y + \frac{\partial \Phi}{\partial z} n_z = z n_y - y n_z$$

17.1.3.3 Internal Boundary Conditions

The continuity conditions (see Section 16.1.2) are verified for u_y and u_z . Across an internal boundary ℓ_{ij} between two phases i and j , the continuity of displacement u_x leads to $\varphi_i = \varphi_j$, or

$$\Phi_i = \Phi_j$$

The continuity relations in Equation 16.6 are reducing to the continuity of $(\tau_{xy} n_y + \tau_{xz} n_z)$ when crossing the lines ℓ_{ij} , or

$$\begin{aligned} G_i \left(\frac{\partial \Phi_i}{\partial y} - z \right) n_y + G_i \left(\frac{\partial \Phi_i}{\partial z} + y \right) n_z &= G_j \left(\frac{\partial \Phi_j}{\partial y} - z \right) n_y + G_j \left(\frac{\partial \Phi_j}{\partial z} + y \right) n_z \\ G_i \left[\left(\frac{\partial \Phi_i}{\partial y} n_y + \frac{\partial \Phi_i}{\partial z} n_z \right) - z n_y + y n_z \right] &= G_j \left[\left(\frac{\partial \Phi_j}{\partial y} n_y + \frac{\partial \Phi_j}{\partial z} n_z \right) - z n_y + y n_z \right] \end{aligned}$$

$$G_i \left[\left(\frac{\partial \Phi_i}{\partial n} \right) - zn_y + yn_z \right] = G_j \left[\left(\frac{\partial \Phi_j}{\partial n} \right) - zn_y + yn_z \right]$$

17.1.3.4 Uniqueness of Function Φ

If one superimposes torsion and bending, by using the flexure degrees of freedom defined in Equation 16.3 in the previous chapter, the displacement u_x becomes

$$u_x = u(x) - y\theta_z + z\theta_y + \frac{d\theta_x}{dx}\varphi + \eta_x$$

The longitudinal displacement $u(x)$ has to meet its definition (Section 16.1.1), meaning

$$\begin{aligned} u(x) &= \frac{1}{\langle ES \rangle} \int_D E_i u_x dS \\ u(x) &= \frac{1}{\langle ES \rangle} \left\{ u \int_D E_i dS - \theta_z \int_D E_i y dS + \theta_y \int_D E_i z dS \dots \right. \\ &\quad \left. \dots + \frac{d\theta_x}{dx} \int_D E_i \varphi dS + \int_D E_i \eta_x dS \right\} \end{aligned}$$

This requires that

$$\int_D E_i \varphi dS = 0$$

Moreover, taking into account the form of Φ in Equation 17.2 and properties of the elastic center,

$$\int_D E_i \Phi dS = 0$$

In summary, the function $\Phi(y, z)$ is solution of the problem

$$\begin{cases} \nabla^2 \Phi = 0 & \text{in domain } D \text{ of the section} \\ \frac{\partial \Phi}{\partial n} = zn_y - yn_z & \text{on the external boundary } \partial D \end{cases}$$

With internal continuities: along any internal boundary ℓ_{ij} between two phases i and j

$$\Phi_i = \Phi_j$$

$$G_i \left(\frac{\partial \Phi_i}{\partial n} - zn_y + yn_z \right) = G_j \left(\frac{\partial \Phi_j}{\partial n} - zn_y + yn_z \right)$$

and the condition for uniqueness

$$\int_D E_i \Phi dS = 0$$

17.1.4 ENERGY INTERPRETATION

The strain energy of an elementary segment of beam with thickness dx is written as

$$dW = \frac{1}{2} \int 2(\tau_{xy}\epsilon_{xy} + \tau_{xz}\epsilon_{xz}) dV = \left\{ \frac{1}{2} \int_D G_i (\gamma_{xy}^2 + \gamma_{xz}^2) dS \right\} dx$$

Then, taking into account the displacement field in Equation 17.1,

$$\frac{dW}{dx} = \frac{1}{2} \left(\frac{d\theta_x}{dx} \right)^2 \int_D G_i \left\{ \left(\frac{\partial \Phi}{\partial y} - z \right)^2 + \left(\frac{\partial \Phi}{\partial z} + y \right)^2 \right\} dS$$

which can be rewritten as³

$$\begin{aligned} \frac{dW}{dx} = & \frac{1}{2} \left(\frac{d\theta_x}{dx} \right)^2 \left\{ \int_D G_i \left\{ y \frac{\partial \Phi}{\partial z} - z \frac{\partial \Phi}{\partial y} + y^2 + z^2 \right\} ds - \int_D G_i \Phi \nabla^2 \Phi dS \dots \right. \\ & \left. \dots + \int_{\partial D} G_i \Phi \left\{ \left(\frac{\partial \Phi}{\partial y} - z \right) n_y + \left(\frac{\partial \Phi}{\partial z} + y \right) n_z \right\} d\Gamma \right\} \end{aligned}$$

where we note the torsional stiffness GJ defined by Equation 17.3. Thus,

$$\frac{dW}{dx} = \frac{1}{2} \langle GJ \rangle \left(\frac{d\theta_x}{dx} \right)^2 = \frac{1}{2} \frac{M_x^2}{\langle GJ \rangle}$$

17.2 LOCATION OF THE TORSION CENTER

17.2.1 COORDINATES IN PRINCIPAL AXES

Consider the cantilever beam that is clamped at its left end as shown schematically in Figure 17.2 and, more particularly, the beam segment limited by the cross sections denoted by D_0 and D_1 . In the section D_1 , O is the elastic center and C is the torsion center of which we wish to determine the position.

With this objective, we will apply on the cross section D_1 the two following successive loadings:

- **Loading 1:** On the cross section D_1 , we apply a force \vec{F} in the plane of the section, passing through the torsion center C (see Figure 17.2a).
- **Loading 2:** On the same cross section D_1 , we apply a torsional moment (about x -axis) denoted as M_x (see Figure 17.2b).

When these two loads are applied successively, the end equilibrium state is independent of the application order. As a consequence for the external forces acting on the isolated segment $(D_0 D_1)$, the work corresponding to loading 1 multiplied by the displacements created by loading 2 is equal to the work corresponding to loading 2 multiplied by the displacements created by loading 1. This can be written in the following form:

$$W_{(\text{loading 1} \times \text{displacement 2})} = W_{(\text{loading 2} \times \text{displacement 1})}$$

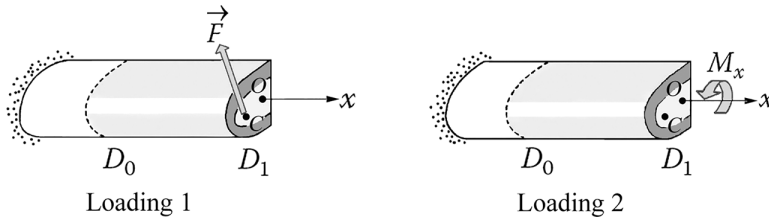


FIGURE 17.2 Cantilever beam under two successive loadings: (a) Loading 1 and (b) Loading 2.

Now, we evaluate these works:

a. W (loading 1 \times displacement 2)

- **On D_0 :** \vec{F} creates the bending moments M_z and M_y and, thus, a normal stress distribution given in principal axes by Equation 16.19 as

$$(\sigma_{xx})_1 = -E_i \frac{M_z}{\langle EI_z \rangle} \times y + E_i \frac{M_y}{\langle EI_y \rangle} \times z$$

Then, taking into account the displacement field in Equation 17.1, the work done on D_0 is

$$\begin{aligned} \int_D (\sigma_{xx})_1 \times (u_x)_2 dS &= \int_D \left\{ -E_i \frac{M_z}{\langle EI_z \rangle} \times y + E_i \frac{M_y}{\langle EI_y \rangle} \times z \right\} \frac{d\theta_x}{dx} \phi dS \\ &= \frac{d\theta_x}{dx} \int_D \left\{ -E_i \frac{M_z}{\langle EI_z \rangle} \times y + E_i \frac{M_y}{\langle EI_y \rangle} \times z \right\} (\Phi - yz_c + zy_c) dS \end{aligned}$$

- **On D_1 :** The torsion center C does not move in the plane of the cross section during torsion. The work done by the force \vec{F} in the displacement field of torsion is nil.

b. W (loading 2 \times displacement 1)

Force \vec{F} as applied to the torsion center C does not lead to the rotation of the cross sections around the longitudinal axis x . From this, the torsional moment M_x does not work together with bending displacement field due to \vec{F} .

Writing the equality of the two works,

$$\frac{d\theta_x}{dx} \int_D \left\{ -E_i \frac{M_z}{\langle EI_z \rangle} \times y + E_i \frac{M_y}{\langle EI_y \rangle} \times z \right\} (\Phi - yz_c + zy_c) dS = 0$$

Then,

$$\begin{aligned} & -\frac{M_z}{\langle EI_z \rangle} \int_D (E_i y \Phi - E_i y^2 z_c + \cancel{E_i y z y_c}) dS \dots \\ & \dots + \frac{M_y}{\langle EI_y \rangle} \int_D (E_i z \Phi + E_i z^2 y_c - \cancel{E_i y z z_c}) dS = 0 \end{aligned}$$

This relationship has to be verified when the force applied on C varies in magnitude and direction in the plane of the cross section. From there, we can deduce that such a relation is valid regardless of the values of M_z and M_y . Both the above integrals are then nil. We extract from this property the coordinates of the torsion center:

$$y_c = -\frac{1}{\langle EI_y \rangle} \int_D E_i z \Phi \, dS$$

$$z_c = \frac{1}{\langle EI_z \rangle} \int_D E_i y \Phi \, dS$$

17.2.2 SUMMARY OF RESULTS

In summary, the uniform torsion of a cylindrical composite beam of any sectional shape, made of perfectly bonded isotropic phases, can be characterized by a homogenized formulation, that is, equivalent to that of a classical homogeneous beam, in the following manner:

Degree of Freedom	θ_x about x -axis
Elastic Center O	It is such that $\int_D E_i y \, dS = \int_D E_i z \, dS = 0$
Principal Axes	They are such that $\int_D E_i y z \, dS = 0$
Equivalent Stiffnesses	$\langle EI_z \rangle = \sum_i E_i I_{z_i}; \quad \langle EI_y \rangle = \sum_i E_i I_{y_i}$ $\langle GJ \rangle = \int_D G_i \left(y \frac{\partial \Phi}{\partial z} - z \frac{\partial \Phi}{\partial y} + y^2 + z^2 \right) dS$
Torsion Center C	Coordinates in principal axes are $y_c = -\frac{1}{\langle EI_y \rangle} \int_D E_i z \Phi \, dS$ $z_c = \frac{1}{\langle EI_z \rangle} \int_D E_i y \Phi \, dS$
Equilibrium Relationship	$\frac{dM_x}{dx} = 0 \quad (M_x = \text{constant})$
Constitutive Equation	$M_x = \langle GJ \rangle \frac{d\theta_x}{dx}$
Shear Stress	$\tau_{xy} = G_i \frac{d\theta_x}{dx} \left(\frac{\partial \Phi}{\partial y} - z \right)$ $\tau_{xz} = G_i \frac{d\theta_x}{dx} \left(\frac{\partial \Phi}{\partial z} + y \right)$

Function $\Phi(y, z)$	<p>It is the solution to the problem</p> $\left\{ \begin{array}{l} \frac{\partial^2 \Phi}{\partial y^2} + \frac{\partial^2 \Phi}{\partial z^2} = 0 \text{ in domain } D \text{ of the section.} \\ \frac{\partial \Phi}{\partial n} = zn_y - yn_z \text{ on the external boundary } \partial D. \end{array} \right.$ <p>with internal continuity</p> $\left. \begin{array}{l} \Phi_i = \Phi_j \\ G_i \left(\frac{\partial \Phi_i}{\partial n} - zn_y + yn_z \right) = G_j \left(\frac{\partial \Phi_j}{\partial n} - zn_y + yn_z \right) \end{array} \right\} \text{along internal boundaries } \ell_{ij}$ <p>and the uniqueness condition : $\int_D E_i \Phi \, dS = 0$</p>
Strain Energy Density	$\frac{dW}{dx} = \frac{1}{2} \frac{M_x^2}{\langle GJ \rangle}$

(17.4b)

Notes

- For simple geometric section cases, direct calculation can be done. See, for example, Section 5.4.5.4 and Applications 19.4, 21.1, and 21.7.
- A finite element computer program for classical homogeneous beams is usable⁴ provided that we could quantify the equivalent torsional stiffness $\langle GJ \rangle$. For complex-shaped cross sections, this requires a numerical computation of the function Φ ⁵. The latter is the solution of a Laplace-type problem, as can be noted in Equation 17.4b. An equivalent functional is possible to define, which leads to the calculation of Φ by the finite element method, by discretizing the cross section⁶.

17.2.3 FLEXION–TORSION COUPLING

When, due to the loads applied on the beam, bending and torsion exist simultaneously, the approach of the previous chapter is always valid. Thus, the definition of degrees of freedom u , v , θ_z , θ_y , seen in Sections 16.1.1 and 16.2, leads to the following displacement field:

$$\left\{ \begin{array}{l} u_x = u - y\theta_z + z\theta_y + \varphi \frac{d\theta_x}{dx} + \eta_x \\ u_y = v - z\theta_x + \eta_y \\ u_z = w + y\theta_x + \eta_z \end{array} \right.$$

Torsion being uniform, equilibrium relationships in Equation 16.19 are getting more restrictive. They reduce to

$$\left\{ \begin{array}{l} \frac{dN_x}{dx} = 0; \quad \frac{dT_y}{dx} = 0; \quad \frac{dT_z}{dx} = 0 \\ \frac{dM_x}{dx} = 0; \quad \frac{dM_z}{dx} + T_y = 0; \quad \frac{dM_y}{dx} - T_z = 0 \end{array} \right. \quad (17.5)$$

Taking into account six degrees of freedom also leads to six constitutive relationships. They are summarized below. It is recalled that coefficients involved in these relations are detailed in Equations 16.16 and 17.4.

$$\left\{ \begin{array}{l} N_x = \langle ES \rangle \frac{du}{dx} \\ T_y = \frac{\langle GS \rangle}{k_y} \left(\frac{dv}{dx} - \theta_z - z_c \frac{d\theta_x}{dx} \right) (*) \\ T_z = \frac{\langle GS \rangle}{k_z} \left(\frac{dw}{dx} + \theta_y + y_c \frac{d\theta_x}{dx} \right) (*) \\ M_x = \langle GJ \rangle \frac{d\theta_x}{dx} - z_c T_y + y_c T_z \\ M_y = \langle EI_y \rangle \frac{d\theta_y}{dx} \\ M_z = \langle EI_z \rangle \frac{d\theta_z}{dx} \end{array} \right. \quad (17.6)$$

Note: While doing calculations, in each of the two relations marked with (*), a supplementary coupling term appears, connected to the existence of a third shear coefficient denoted as k_{yz} . The complete form is then

$$\begin{aligned} k_y T_y + k_{yz} T_z &= \langle GS \rangle \left(\frac{dv}{dx} - \theta_z - z_c \frac{d\theta_x}{dx} \right) \\ k_{yz} T_y + k_z T_z &= \langle GS \rangle \left(\frac{dw}{dx} + \theta_y + y_c \frac{d\theta_x}{dx} \right) \end{aligned}$$

This secondary coupling has been neglected in Equation 17.6.

NOTES

- 1 See Bibliography: Tanghe-Carrier F. and Tanghe-Carrier F., Gay D.
- 2 Here, it is not necessary to define θ_x by means of an integral of displacements, as in Chapter 16 relating to flexure. Indeed, we will see in the following that the displacement field associated with this pure rotation of section leads to the exact solution of the problem in the elastic domain (at least for the torsion case with uniform warping that is being looked at here).
- 3 In effect, we have, for example, $\left(\frac{\partial \Phi}{\partial y} \right)^2 - z \frac{\partial \Phi}{\partial y} = \frac{\partial \Phi}{\partial y} \left(\frac{\partial \Phi}{\partial y} - z \right) = \frac{\partial}{\partial y} \left\{ \Phi \left(\frac{\partial \Phi}{\partial y} - z \right) \right\} - \Phi \frac{\partial^2 \Phi}{\partial y^2}$
- 4 Except if the considered application requires the calculation of shear stress in the cross section (see Bibliography: Nouri T., Gay D., 1994.
- 5 We have to solve analogous problem for homogeneous beams, when we desire to calculate the torsional Saint-Venant Stiffness $J = \int_D \left(y \frac{\partial \Phi}{\partial z} - z \frac{\partial \Phi}{\partial y} + y^2 + z^2 \right) dS$.
- 6 See Bibliography: Nouri T., Gay D., 1994.



Taylor & Francis

Taylor & Francis Group

<http://taylorandfrancis.com>

18 Transverse Shear Behavior of Multilayered Plates

The mechanical behavior of a laminated plate as studied in Chapters 12 and 15 has required the definition of In-plane resultants N_x , N_y , and T_{xy} and of bending and twisting moments M_x , M_y , and M_{xy} . These resultants are constructed using the stress values σ_x , σ_y , τ_{xy} . The other stress components, that is, σ_z , τ_{xz} , τ_{yz} , have not been taken into account so far.

We shall be considering in this chapter how these stresses can exist, particularly the transverse shear stresses τ_{xz} and τ_{yz} , and how they can impact the mechanical behavior of the laminate. We will also examine plate configurations for which the influence of these stresses is significant. Among others, this is the case of plates with high relative thicknesses and of sandwiches plates. However, even for thin laminated plates the transverse shear stiffness can be of importance in dealing with buckling stability problems. Also we will examine the case of a quasi-orthotropic stratification built on Double-Double sequence as examined in Chapter 15, thus in order to compare the transverse shear behavior of a D-D laminate with its associated homogeneous orthotropic plate.

The original method proposed here is based on the prior definition of equivalent displacement parameters, via a similar approach to the one used in Chapter 16, when examining composite beams in flexure.

18.1 PRELIMINARY REMARKS

18.1.1 TRANSVERSE NORMAL STRESS σ_z

The coordinate system of the plate is as in Chapter 12, which explains the name of transverse normal stress for σ_z . Such stress appears when applying a transverse load, concentrated or distributed, which will cause bending of the plate:

- A very local load concentration in a very small zone cannot be carried out within a plate theory, unsuitable to provide a spatial stress distribution in the neighborhood of the point of load application. This phenomenon is complex even in the case of 3D numerical modeling. Therefore, what will be presented will not be valid in the immediate surroundings of a very local transverse load, such as the load on an insert.
- A distributed load, which generally gives rise to quite small values of σ_z compared to σ_x and σ_y . Accordingly, σ_z will be the most often neglected.

18.1.2 TRANSVERSE SHEAR STRESS τ_{xz} AND τ_{yz}

Due to the assumption of perfect bonding between the plies, the stress vector remains continuous across an interfacial element with normal vector $\vec{n} = \vec{z}$, between two consecutive plies of the laminate. Thus, τ_{xz} and τ_{yz} remain continuous when crossing the interface between plies (see Section 16.1.2.3). In addition, the upper and the lower face of the laminate are assumed to be free of tangential forces. The thickness of the laminate is denoted as h . Then,

$$\tau_{xz} = \tau_{yz} = 0 \quad \text{for } z = \pm \frac{h}{2}$$

Assume the In-plane resultants and the bending and twisting moments to be constant in a given area of the laminate, that is, in that area:

$$N_x, N_y, T_{xy}, M_x, M_y, M_{xy} \quad \text{constant} \quad \forall (x, y)$$

Then, by inversion of Equation 12.20, for example, we can note that the following overall strains

$$\epsilon_{0x}; \quad \epsilon_{0y}; \quad \gamma_{0xy}; \quad \frac{\partial^2 w_0}{\partial x^2}; \quad \frac{\partial^2 w_0}{\partial y^2}; \quad 2 \frac{\partial^2 w_0}{\partial x \partial y}$$

are constant in the area under consideration. From this, the local strains in Equation 12.12 depend only on the z -coordinate in the laminate. This is the same for the stress values σ_x , σ_y , τ_{xy} .

With the earlier consideration, and in the absence of body forces, local equilibrium can be written as

$$\begin{aligned} \frac{\partial \sigma_x}{\partial x} + \frac{\partial \tau_{xy}}{\partial y} + \frac{\partial \tau_{xz}}{\partial z} &= 0 \\ \frac{\partial \tau_{xy}}{\partial x} + \frac{\partial \sigma_y}{\partial y} + \frac{\partial \tau_{yz}}{\partial z} &= 0 \end{aligned} \quad (18.1)$$

The transverse shear stresses then appear to be constant across the thickness of a ply. As they are continuous at the interfaces between the plies and null at the locations $z = \pm(h/2)$, they are nil through all the thickness of the laminate.

Notes:

- From this, these stresses do not play systematically an important role: they do not always exist, because their existence is related to stress resultants and moments that vary in the plate.
- An exception: one also finds transverse shear stresses when studying buckling phenomena. In such cases these stresses are induced when taking into account the associated adjacent equilibrium¹.

When they exist and depending on the composition of the laminate, the transverse shear stresses can influence the deformation in bending and the interlaminar adhesion between layers².

Let's assume the existence of this type of stress, associated with the assumptions of the following paragraph.

18.1.3 ASSUMPTIONS

- The plate has Mid-plane symmetry.
- The plies are orthotropic, the orthotropic directions coinciding with axes (x, y, z) of the laminate³.
- The stress σ_z is negligible.

Instead of this hypothesis, the less restrictive hypothesis of a more general balanced laminate case could also be adopted, for example when one wishes to study laminates without mirror symmetry. In such case, the following calculations are much heavier, without appreciable gain on the enlargement of the field of applications examined in Section 18.6.3.

Notes

- For each ply with orthotropic axes (x, y, z), and taking into account the simplification $\sigma_z \approx 0$, the constitutive Equation 13.3 can be written as

$$\begin{Bmatrix} \varepsilon_x \\ \varepsilon_y \\ \gamma_{xy} \\ \gamma_{xz} \\ \gamma_{yz} \end{Bmatrix} = \begin{bmatrix} \frac{1}{E_x} & -\frac{\nu_{yx}}{E_y} & 0 & 0 & 0 \\ -\frac{\nu_{xy}}{E_x} & \frac{1}{E_y} & 0 & 0 & 0 \\ 0 & 0 & \frac{1}{G_{xy}} & 0 & 0 \\ 0 & 0 & 0 & \frac{1}{G_{xz}} & 0 \\ 0 & 0 & 0 & 0 & \frac{1}{G_{yz}} \end{bmatrix} \begin{Bmatrix} \sigma_x \\ \sigma_y \\ \tau_{xy} \\ \tau_{xz} \\ \tau_{yz} \end{Bmatrix}$$

Or in inverted form,

$$\begin{Bmatrix} \sigma_x \\ \sigma_y \\ \tau_{xy} \\ \tau_{xz} \\ \tau_{yz} \end{Bmatrix} = \begin{bmatrix} \bar{E}_{11} & \bar{E}_{12} & 0 & 0 & 0 \\ \bar{E}_{21} & \bar{E}_{22} & 0 & 0 & 0 \\ 0 & 0 & \bar{E}_{33} = G_{xy} & 0 & 0 \\ 0 & 0 & 0 & \bar{E}_{44} = G_{xz} & 0 \\ 0 & 0 & 0 & 0 & \bar{E}_{55} = G_{yz} \end{bmatrix} \begin{Bmatrix} \varepsilon_x \\ \varepsilon_y \\ \gamma_{xy} \\ \gamma_{xz} \\ \gamma_{yz} \end{Bmatrix}$$

$$\text{where } \bar{E}_{11} = \frac{E_x}{1 - \nu_{xy}\nu_{yx}}; \quad \bar{E}_{12} = \frac{\nu_{yx}E_x}{1 - \nu_{xy}\nu_{yx}}; \quad \bar{E}_{22} = \frac{E_y}{1 - \nu_{xy}\nu_{yx}} \quad (18.2)$$

- The transverse shear stress causes distortions as illustrated in Figure 18.1 for the shear stress τ_{xz} (see also Figures 18.7 and 18.8).
- As a consequence, the displacements due to flexion discussed in Section 12.1.4 can be adapted as shown in Figure 18.2.

Figure 18.2a represents a cross section defined as the intersection of the plate with plane (y, z), before and after bending, and Figure 18.2b shows the section evolution as a rigid displacement (parameters u_0 , w_0 , and θ_y) to which are superimposed increments η_x and η_z in plane (x, z). Due to the existence

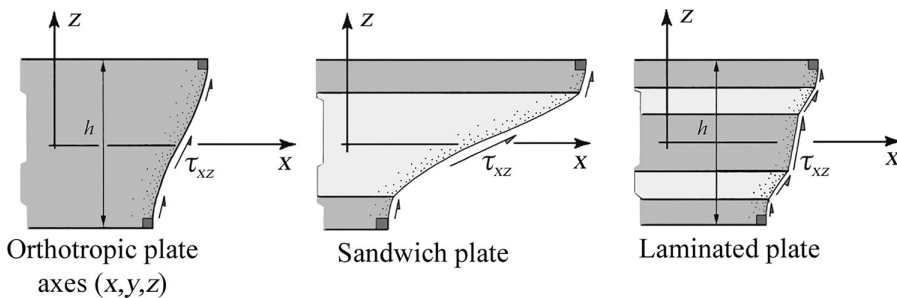


FIGURE 18.1 Distortion of section due to transverse shear τ_{xz} .

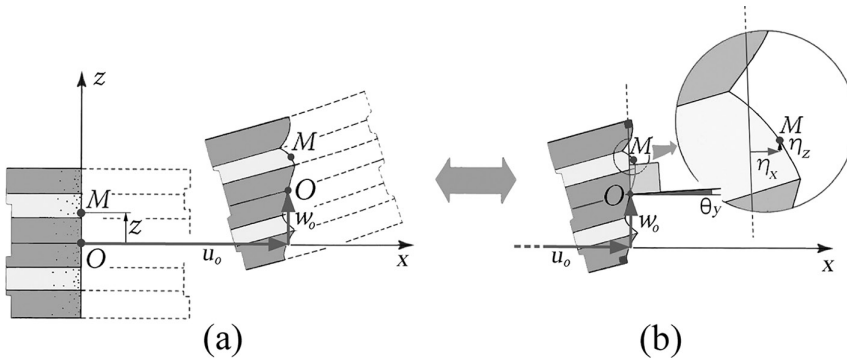


FIGURE 18.2 Flexural displacements: (a) cross section before and after flexure and (b) displacement parameters.

of Mid-plane symmetry, we should note the antisymmetric shape of these increments, with respect to z . They are small but we can neither neglect them *a priori* nor assign them any mathematical form, all the more so we do not have, at this stage, a definition for the equivalent rotation, noted as θ_y , in Figure 18.2b. This justifies the interest in the definition of a displacement field involving permanently these increments. A supplementary interest rests in the ability, during the study, to observe closely the necessary approximations that allow obtaining useful technical formulation⁴.

18.2 DISPLACEMENT FIELD

Components of elastic displacement at each point of the laminate are denoted by $u(x, y, z)$, $v(x, y, z)$, and $w(x, y, z)$. We denote in Figure 18.2b:

- Average translations as u_o and w_o
- Average rotation as θ_y

We will define these average parameters in integral forms as follows:

- **Translation along the x direction:** By definition, this is $u_o(x, y)$ such that

$$u_o = \frac{1}{h} \int_{-h/2}^{h/2} u(x, y, z) dz$$

- **Rotation about the y -axis:** By definition, this is $\theta_y(x, y)$ such that⁵

$$\theta_y = \int_{-h/2}^{h/2} \left(\frac{\bar{E}_{11}}{\bar{E}I_{11}} + \frac{\bar{E}_{12}}{\bar{E}I_{12}} \right) \times u(x, y, z) \times z \times dz$$

In which we have reused the notations of Section 12.1.6 for the terms $1/\bar{E}I_{ij}$ of matrix

$$\left[\frac{1}{\bar{E}I} \right] = [C]^{-1}$$

Where

$$C_{ij} = \int_{-h/2}^{h/2} \bar{E}_{ij} \times z^2 dz \quad \text{or} \quad = \sum_{k=1 \text{st ply}}^{n \text{th ply}} \bar{E}_{ij}^k \left(\frac{z_k^3 - z_{k-1}^3}{3} \right)$$

By superimposing increment η_x , the longitudinal displacement $u(x, y, z)$ then takes the form

$$u(x, y, z) = u_0(x, y) + z \times \theta_y(x, y) + \eta_x(x, y, z)$$

With

$$\int_{-h/2}^{h/2} \left(\frac{\bar{E}_{11}}{EI_{11}} + \frac{\bar{E}_{12}}{EI_{12}} \right) \times \eta_x z \times dz = 0$$

In effect, note that we can obtain, starting from this expression,

$$\int_{-h/2}^{h/2} u dz = h \times u_0 + \theta_y \int_{-h/2}^{h/2} z dz + \int_{-h/2}^{h/2} \eta_x dz$$

Strikethrough integrals disappear due to antisymmetry in z :

$$\begin{aligned} \int_{-h/2}^{h/2} \left(\frac{\bar{E}_{11}}{EI_{11}} + \frac{\bar{E}_{12}}{EI_{12}} \right) \times u z dz &= u_0 \int_{-h/2}^{h/2} \left(\frac{\bar{E}_{11}}{EI_{11}} + \frac{\bar{E}_{12}}{EI_{12}} \right) \times z dz \dots \\ \dots + \theta_y &+ \int_{-h/2}^{h/2} \left(\frac{\bar{E}_{11}}{EI_{11}} + \frac{\bar{E}_{12}}{EI_{12}} \right) \times \eta_x z dz \end{aligned}$$

In the right-hand side of the previous equation, the first integral disappears due to Mid-plane symmetry. In addition, taking into account the definition of θ_y written earlier, the second integral also is zero. Finally, we should notice that the coefficient of θ_y is 1 because

$$\int_{-h/2}^{h/2} \left(\frac{\bar{E}_{11}}{EI_{11}} + \frac{\bar{E}_{12}}{EI_{12}} \right) \times z^2 dz = \frac{C_{11}}{EI_{11}} + \frac{C_{12}}{EI_{12}} = \frac{C_{11}C_{22}}{C_{11}C_{22} - C_{12}^2} - \frac{C_{12}^2}{C_{11}C_{22} - C_{12}^2} = 1$$

- **Translation along the y direction:** This is $v_0(x, y)$ such that

$$v_0 = \frac{1}{h} \int_{-h/2}^{h/2} v(x, y, z) \times dz$$

- **Rotation about the x-axis:** This is θ_x such that

$$\theta_x = - \int_{-h/2}^{h/2} \left(\frac{\bar{E}_{22}}{EI_{22}} + \frac{\bar{E}_{12}}{EI_{12}} \right) \times v(x, y, z) \times z \times dz$$

By superimposing increment η_y , the longitudinal displacement $v(x, y, z)$ then takes the form

$$v(x, y, z) = v_0(x, y) - z \times \theta_x(x, y) + \eta_y(x, y, z)$$

With

$$\int_{-h/2}^{h/2} \left(\frac{\bar{E}_{22}}{EI_{22}} + \frac{\bar{E}_{12}}{EI_{12}} \right) \times \eta_y z \times dz = 0$$

- **Translation along the z direction:** This is $w_0(x, y)$ such that

$$w_0(x, y) = \frac{1}{h} \int_{-h/2}^{h/2} w(x, y, z) \times dz$$

By superimposing increment η_z , the vertical displacement takes the form

$$w(x, y, z) = w_0(x, y) + \eta_z(x, y, z)$$

In summary, we obtain the elastic displacement field:

$$\begin{aligned} u &= u_0 + z\theta_y + \eta_x(x, y, z) \\ v &= v_0 - z\theta_x + \eta_y(x, y, z) \\ w &= w_0 + \eta_z(x, y, z) \end{aligned} \quad (18.3)$$

$$\eta_x, \eta_y, \eta_z \quad \text{antisymmetric in } z. \quad (18.4)$$

$$\int_{-h/2}^{h/2} \left(\frac{\bar{E}_{11}}{EI_{11}} + \frac{\bar{E}_{12}}{EI_{12}} \right) \eta_x z \times dz = \int_{-h/2}^{h/2} \left(\frac{\bar{E}_{22}}{EI_{22}} + \frac{\bar{E}_{12}}{EI_{12}} \right) \eta_y z \times dz = 0 \quad (18.5)$$

18.3 STRAINS

The strain values can be deduced from the previous displacement field as

$$\left\{ \begin{aligned} \epsilon_x &= \epsilon_{0x} + z \frac{\partial \theta_y}{\partial x} + \frac{\partial \eta_x}{\partial x} \\ \epsilon_y &= \epsilon_{0y} - z \frac{\partial \theta_x}{\partial y} + \frac{\partial \eta_y}{\partial y} \\ \gamma_{xy} &= \gamma_{0xy} + z \left(\frac{\partial \theta_y}{\partial y} - \frac{\partial \theta_x}{\partial x} \right) + \frac{\partial \eta_x}{\partial y} + \frac{\partial \eta_y}{\partial x} \\ \gamma_{xz} &= \frac{\partial w_0}{\partial x} + \theta_y + \frac{\partial \eta_x}{\partial z} + \frac{\partial \eta_z}{\partial x} \\ \gamma_{yz} &= \frac{\partial w_0}{\partial y} - \theta_x + \frac{\partial \eta_y}{\partial z} + \frac{\partial \eta_z}{\partial y} \end{aligned} \right. \quad (18.6)$$

18.4 CONSTITUTIVE EQUATIONS

18.4.1 IN-PLANE BEHAVIOR

We proceed in the same way to that already used in Section 12.1.1:

- **Stress resultant** $N_x = \int_{-h/2}^{h/2} \sigma_x dx$

From Equations 18.2 and 18.6,⁶

$$N_x = \int_{-h/2}^{h/2} \bar{E}_{11} \left(\epsilon_{0x} + z \frac{\partial \theta_y}{\partial x} + \frac{\partial \eta_x}{\partial x} \right) dz + \int_{-h/2}^{h/2} \bar{E}_{12} \left(\epsilon_{0y} - z \frac{\partial \theta_x}{\partial y} + \frac{\partial \eta_y}{\partial y} \right) dz$$

$$N_x = A_{11} \epsilon_{0x} + A_{12} \epsilon_{0y} + \frac{\partial}{\partial x} \int_{-h/2}^{h/2} \bar{E}_{11} \eta_x dz + \frac{\partial}{\partial y} \int_{-h/2}^{h/2} \bar{E}_{12} \eta_y dz$$

- **Stress resultant** $N_y = \int_{-h/2}^{h/2} \sigma_y dz$

$$N_y = A_{21} \epsilon_{0x} + A_{22} \epsilon_{0y}$$

- **Stress resultant** $T_{xy} = \int_{-h/2}^{h/2} \tau_{xy} dz$

$$T_{xy} = \int_{-h/2}^{h/2} \bar{E}_{33} \left(\gamma_{0xy} + z \left(\frac{\partial \theta_y}{\partial y} - \frac{\partial \theta_x}{\partial x} \right) + \frac{\partial \eta_x}{\partial y} + \frac{\partial \eta_y}{\partial x} \right) dz$$

$$T_{xy} = A_{33} \times \gamma_{0xy}$$

In summary, relations already established in Chapter 12 are found again (Equation 12.5):

$$\begin{Bmatrix} N_x \\ N_y \\ T_{xy} \end{Bmatrix} = \begin{bmatrix} A_{11} & A_{12} & 0 \\ A_{21} & A_{22} & 0 \\ 0 & 0 & A_{33} \end{bmatrix} \begin{Bmatrix} \epsilon_{0x} \\ \epsilon_{0y} \\ \gamma_{0xy} \end{Bmatrix}$$

Or, in inverse form, by using the notations in Equation 12.9,

$$\begin{Bmatrix} \epsilon_{0x} \\ \epsilon_{0y} \\ \gamma_{0xy} \end{Bmatrix} = h[A]^{-1} \times \frac{1}{h} \begin{Bmatrix} N_x \\ N_y \\ T_{xy} \end{Bmatrix} = \frac{1}{h} \begin{bmatrix} 1/\bar{E}_x & -\bar{\nu}_{yx}/\bar{E}_y & 0 \\ -\bar{\nu}_{xy}/\bar{E}_x & 1/\bar{E}_y & 0 \\ 0 & 0 & 1/\bar{G}_{xy} \end{bmatrix} \begin{Bmatrix} N_x \\ N_y \\ T_{xy} \end{Bmatrix} \quad (18.7)$$

18.4.2 BENDING BEHAVIOR

We start again with the already known moments (see Section 12.2.1).

- **Bending moment** $M_y = \int_{-h/2}^{h/2} \sigma_x z dz$

With Equations 18.2 and 18.5,

$$M_y = \int_{-h/2}^{h/2} \bar{E}_{11} \left(z \epsilon_{0x} + z^2 \frac{\partial \theta_y}{\partial x} + z \frac{\partial \eta_x}{\partial x} \right) dz + \int_{-h/2}^{h/2} \bar{E}_{12} \left(z \epsilon_{0y} - z^2 \frac{\partial \theta_x}{\partial y} + z \frac{\partial \eta_y}{\partial y} \right) dz$$

$$M_y = C_{11} \frac{\partial \theta_y}{\partial x} + C_{12} \times -\frac{\partial \theta_x}{\partial y} + \left(\frac{\partial}{\partial x} \int_{-h/2}^{h/2} \bar{E}_{11} \eta_x z \times dz \right) + \left(\frac{\partial}{\partial y} \int_{-h/2}^{h/2} \bar{E}_{12} \eta_y z \times dz \right)$$

In the last two terms of the right-hand side appear the nonzero integrals of even functions. If we neglect the contribution of the rates of variation along the x -axis and the y -axis that these terms respectively represent, the previous equation is reduced to⁷

$$M_y = C_{11} \frac{\partial \theta_y}{\partial x} + C_{12} \times -\frac{\partial \theta_x}{\partial y}$$

- **Bending moment** $M_x = - \int_{-h/2}^{h/2} \sigma_y z dz$

$$-M_x = \int_{-h/2}^{h/2} \bar{E}_{12} \left(z \epsilon_{0x} + z^2 \frac{\partial \theta_y}{\partial x} + z \frac{\partial \eta_x}{\partial x} \right) dz + \int_{-h/2}^{h/2} \bar{E}_{22} \left(z \epsilon_{0y} - z^2 \frac{\partial \theta_x}{\partial y} + z \frac{\partial \eta_y}{\partial y} \right) dz$$

Which is reduced to

$$-M_x = C_{12} \frac{\partial \theta_y}{\partial x} + C_{22} \times -\frac{\partial \theta_x}{\partial y} + \left(\frac{\partial}{\partial x} \int_{-h/2}^{h/2} \bar{E}_{12} \eta_x z \times dz \right) + \left(\frac{\partial}{\partial y} \int_{-h/2}^{h/2} \bar{E}_{22} \eta_y z \times dz \right)$$

We neglect the contribution of the last two terms of the right-hand side as made earlier for the bending moment M_y :

$$-M_x = C_{12} \frac{\partial \theta_y}{\partial x} + C_{22} \times -\frac{\partial \theta_x}{\partial y}$$

- **Twisting moment** $M_{xy} = - \int_{-h/2}^{h/2} \tau_{xy} z dz$

$$-M_{xy} = \int_{-h/2}^{h/2} \bar{E}_{33} \left(z \gamma_{0xy} + z^2 \left(\frac{\partial \theta_y}{\partial y} - \frac{\partial \theta_x}{\partial x} \right) + z \frac{\partial \eta_x}{\partial y} + z \frac{\partial \eta_y}{\partial x} \right) dz$$

Which is reduced to

$$-M_{xy} = C_{33} \left(\frac{\partial \theta_y}{\partial y} - \frac{\partial \theta_x}{\partial x} \right) + \left(\frac{\partial}{\partial y} \int_{-h/2}^{h/2} \bar{E}_{33} \eta_x z \times dz \right) + \left(\frac{\partial}{\partial x} \int_{-h/2}^{h/2} \bar{E}_{33} \eta_y z \times dz \right)$$

In a similar way, we neglect the contribution of the rates of variation of increments η_x and η_y :

$$-M_{xy} = C_{33} \left(\frac{\partial \theta_y}{\partial y} - \frac{\partial \theta_x}{\partial x} \right)$$

In summary, we find again a similar form as in Equation 12.16 with, in addition, $C_{13} = C_{23} = 0$ due to orientation of plies (see assumptions Section 18.1.3):

$$\begin{Bmatrix} M_y \\ -M_x \\ -M_{xy} \end{Bmatrix} = \begin{bmatrix} C_{11} & C_{12} & 0 \\ C_{21} & C_{22} & 0 \\ 0 & 0 & C_{33} \end{bmatrix} \begin{Bmatrix} \frac{\partial \theta_y}{\partial x} \\ -\frac{\partial \theta_x}{\partial y} \\ \left(\frac{\partial \theta_y}{\partial y} - \frac{\partial \theta_x}{\partial x} \right) \end{Bmatrix} \quad (18.8)$$

Or, in inverse form, by reusing the notations of Section 12.1.6,

$$\begin{Bmatrix} \frac{\partial \theta_y}{\partial x} \\ -\frac{\partial \theta_x}{\partial y} \\ \left(\frac{\partial \theta_y}{\partial y} - \frac{\partial \theta_x}{\partial x} \right) \end{Bmatrix} = \begin{bmatrix} \frac{1}{\bar{E}I_{11}} & \frac{1}{\bar{E}I_{12}} & 0 \\ \frac{1}{\bar{E}I_{21}} & \frac{1}{\bar{E}I_{22}} & 0 \\ 0 & 0 & \frac{1}{C_{33}} \end{bmatrix} \begin{Bmatrix} M_y \\ -M_x \\ -M_{xy} \end{Bmatrix} \quad (18.9)$$

18.4.3 TRANSVERSE SHEAR BEHAVIOR

Starting from transverse shear stress, we define the following supplementary stress resultants denoted as transverse shear resultants:

18.4.3.1 Transverse Shear Resultant $Q_x = \int_{-h/2}^{h/2} \tau_{xz} dz$

Using Equations 18.2 and 18.6,

$$Q_x = \int_{-h/2}^{h/2} G_{xz} \left(\frac{\partial w_0}{\partial x} + \theta_y + \frac{\partial \eta_x}{\partial z} + \frac{\partial \eta_z}{\partial x} \right) dz$$

In setting

$$\langle hG_{xz} \rangle = \int_{-h/2}^{h/2} G_{xz} dz$$

yields

$$Q_x = \langle hG_{xz} \rangle \left(\frac{\partial w_0}{\partial x} + \theta_y \right) + \int_{-h/2}^{h/2} G_{xz} \frac{\partial \eta_x}{\partial z} dz \quad (18.10)$$

Where the integral of an even function can be noted.

18.4.3.2 Transverse Shear Resultant $Q_y = \int_{-h/2}^{h/2} \tau_{yz} dz$

$$Q_y = \int_{-h/2}^{h/2} G_{yz} \left(\frac{\partial w_0}{\partial y} - \theta_x + \frac{\partial \eta_y}{\partial z} + \frac{\partial \eta_z}{\partial y} \right) dz$$

In setting

$$\langle hG_{yz} \rangle = \int_{-h/2}^{h/2} G_{yz} dz$$

Yields

$$Q_y = \langle hG_{yz} \rangle \left(\frac{\partial w_0}{\partial y} - \theta_x \right) + \int_{-h/2}^{h/2} G_{yz} \frac{\partial \eta_y}{\partial z} dz \quad (18.11)$$

18.5 EQUILIBRIUM RELATIONSHIPS

These relationships are characteristic of plates in general, regardless of their compositions, and therefore are classic.

We recall here the equilibrium relationships related to bending.

18.5.1 TRANSVERSE EQUILIBRIUM

- Local equilibrium relationship:

$$\frac{\partial \tau_{zx}}{\partial x} + \frac{\partial \tau_{zy}}{\partial y} + \frac{\partial \sigma_z}{\partial z} + f_z = 0$$

Integrating across the thickness reveals the transverse shear resultants Q_x and Q_y :

$$\frac{\partial Q_x}{\partial x} + \frac{\partial Q_y}{\partial y} + [\sigma_z]_{-h/2}^{h/2} + \int_{-h/2}^{h/2} f_z dz = 0$$

Denoting as p_z the transverse load density that appears in the last terms,

$$\frac{\partial Q_x}{\partial x} + \frac{\partial Q_y}{\partial y} + p_z = 0$$

18.5.2 EQUILIBRIUM IN BENDING

- Local equilibrium relationship:

$$\frac{\partial \sigma_x}{\partial x} + \frac{\partial \tau_{xy}}{\partial y} + \frac{\partial \tau_{xz}}{\partial z} + f_x = 0$$

After multiplication by z , integration over the thickness leads to

$$\begin{aligned} \frac{\partial M_y}{\partial x} - \frac{\partial M_{xy}}{\partial y} + \int_{-h/2}^{h/2} \left[\frac{\partial}{\partial z} (z \tau_{xz}) - \tau_{xz} \right] dz + \int_{-h/2}^{h/2} z \times f_x dz &= 0 \\ \frac{\partial M_y}{\partial x} - \frac{\partial M_{xy}}{\partial y} - Q_x + \left[z \tau_{xz} \right]_{-h/2}^{h/2} + \int_{-h/2}^{h/2} z \times f_x dz &= 0 \end{aligned}$$

The case of a static loading giving a moment density being highly exceptional, we neglect the moment density that appears in the last term:

$$\frac{\partial M_y}{\partial x} - \frac{\partial M_{xy}}{\partial y} - Q_x = 0 \quad (18.12)$$

- Local equilibrium relationship:

$$\frac{\partial \tau_{yx}}{\partial x} + \frac{\partial \sigma_y}{\partial y} + \frac{\partial \tau_{yz}}{\partial z} + f_y = 0$$

A similar calculation leads to

$$\frac{\partial M_{xy}}{\partial x} + \frac{\partial M_x}{\partial y} + Q_y = 0 \quad (18.13)$$

18.6 TECHNICAL FORMULATION FOR BENDING

- We can note in Equations 18.7 and 18.8 that Mid-plane symmetry always decouples the membrane behavior from bending behavior. As a consequence, in what follows, we shall consider only stress due to bending. This will be done by canceling the In-plane stress resultants: $N_x = N_y = T_{xy} = 0$.
- In addition to assumptions in Section 18.1.3, we will neglect, for stress calculation, the variations of increments η_x, η_y , and η_z along x -axis and y -axis⁸.

18.6.1 STRESS DUE TO BENDING

18.6.1.1 Plane Stress Values

We can write successively for a ply number k what follows:

- $\sigma_x = \bar{E}_{11}^k \epsilon_x + \bar{E}_{12}^k \epsilon_y$

Then with Equation 18.6,

$$\sigma_x = \bar{E}_{11}^k \left(\epsilon_{ox} + z \frac{\partial \theta_y}{\partial x} + \frac{\partial \eta_x}{\partial x} \right) + \bar{E}_{12}^k \left(\epsilon_{oy} - z \frac{\partial \theta_x}{\partial y} + \frac{\partial \eta_y}{\partial y} \right)$$

And with Equations 18.7 and 18.9,

$$\begin{aligned} \sigma_x = \bar{E}_{11}^k \left[\frac{N_x}{\cancel{hE_x}} - \frac{v_{yx}}{\cancel{hE_y}} N_y + z \left(\frac{M_y}{EI_{11}} - \frac{M_x}{EI_{12}} \right) \right] \dots \\ \dots + \bar{E}_{12}^k \left[-\frac{v_{xy}}{\cancel{hE_x}} N_x + \frac{N_y}{\cancel{hE_y}} + z \left(\frac{M_y}{EI_{12}} - \frac{M_x}{EI_{22}} \right) \right] \end{aligned} \quad (18.14)$$

$$\sigma_x = z \left(\frac{\bar{E}_{11}^k}{EI_{11}} + \frac{\bar{E}_{12}^k}{EI_{12}} \right) M_y + z \left(\frac{\bar{E}_{11}^k}{EI_{12}} + \frac{\bar{E}_{12}^k}{EI_{22}} \right) \times -M_x$$

- $\sigma_y = \bar{E}_{12}^k \epsilon_x + \bar{E}_{22}^k \epsilon_y$

A similar calculation leads to

$$\sigma_y = z \left(\frac{\bar{E}_{12}^k}{EI_{11}} + \frac{\bar{E}_{22}^k}{EI_{12}} \right) M_y + z \left(\frac{\bar{E}_{12}^k}{EI_{12}} + \frac{\bar{E}_{22}^k}{EI_{22}} \right) \times -M_x \quad (18.15)$$

- $\tau_{xy} = \bar{E}_{33}^k \gamma_{xy} = G_{xy}^k \gamma_{xy}$

Then with Equation 18.6,

$$\tau_{xy} = G_{xy}^k \left(\gamma_{oxy} + z \left(\frac{\partial \theta_y}{\partial y} - \frac{\partial \theta_x}{\partial x} \right) + \frac{\partial \eta_x}{\partial y} + \frac{\partial \eta_y}{\partial x} \right)$$

And with Equations 18.7 and 18.9 and $T_{xy} = 0$,

$$\tau_{xy} = -z \frac{G_{xy}^k}{C_{33}} M_{xy} \quad (18.16)$$

18.6.1.2 Transverse Shear Stress Values

- $\tau_{xz} = \bar{E}_{44}^k \gamma_{xz} = G_{xz}^k \gamma_{xz}$ from Equation 18.2.

And with Equation 18.6 and neglecting the variation $\partial \eta_z / \partial x$,

$$\tau_{xz} = G_{xz}^k \left(\frac{\partial w_0}{\partial x} + \theta_y \right) + G_{xz}^k \frac{\partial \eta_x}{\partial z} \quad (18.17)$$

- $\tau_{yz} = \bar{E}_{55}^k \gamma_{yz} = G_{yz}^k \gamma_{yz}$

which leads in a similar manner to

$$\tau_{yz} = G_{yz}^k \left(\frac{\partial w_0}{\partial y} - \theta_x \right) + G_{yz}^k \frac{\partial \eta_y}{\partial z} \quad (18.18)$$

Thus, the knowledge of transverse shear stress requires the prior calculation of increments η_x , and η_y that characterize warping.

18.6.2 CHARACTERIZATION OF WARPING INCREMENTS IN BENDING η_x AND η_y

- Warping $\eta_x(x, y, z)$

Starting from the first equation of local equilibrium,

$$\frac{\partial \tau_{xz}}{\partial z} = -\frac{\partial \sigma_x}{\partial x} - \frac{\partial \tau_{xy}}{\partial y}$$

Then with Equations 18.14, 18.16, and 18.17,

$$G_{xz}^k \frac{\partial^2 \eta_x}{\partial z^2} = -z \left(\frac{\bar{E}_{11}^k}{EI_{11}} + \frac{\bar{E}_{12}^k}{EI_{12}} \right) \frac{\partial M_y}{\partial x} + z \left(\frac{\bar{E}_{11}^k}{EI_{12}} + \frac{\bar{E}_{12}^k}{EI_{22}} \right) \frac{\partial M_x}{\partial x} + z \frac{G_{xy}^k}{C_{33}} \frac{\partial M_{xy}}{\partial y}$$

Taking into account the equilibrium Equation 18.12, we can rewrite

$$\begin{aligned} G_{xz}^k \frac{\partial^2 \eta_x}{\partial z^2} = & -z \left(\frac{\bar{E}_{11}^k}{EI_{11}} + \frac{\bar{E}_{12}^k}{EI_{12}} \right) Q_x + z \left(\frac{\bar{E}_{11}^k}{EI_{12}} + \frac{\bar{E}_{12}^k}{EI_{22}} \right) \frac{\partial M_x}{\partial x} \dots \\ & \dots + z \left(\frac{G_{xy}^k}{C_{33}} - \frac{\bar{E}_{11}^k}{EI_{11}} - \frac{\bar{E}_{12}^k}{EI_{12}} \right) \frac{\partial M_{xy}}{\partial y} \end{aligned} \quad (18.19)$$

- Warping $\eta_y(x, y, z)$

In the same way, starting from the second equation of local equilibrium,

$$\frac{\partial \tau_{yz}}{\partial z} = -\frac{\partial \sigma_y}{\partial y} - \frac{\partial \tau_{yx}}{\partial x}$$

Then with Equations 18.15, 18.16, and 18.18,

$$\begin{aligned} G_{yz}^k \frac{\partial^2 \eta_y}{\partial z^2} = & -z \left(\frac{\bar{E}_{12}^k}{EI_{11}} + \frac{\bar{E}_{22}^k}{EI_{12}} \right) \frac{\partial M_y}{\partial y} + z \left(\frac{\bar{E}_{12}^k}{EI_{12}} + \frac{\bar{E}_{22}^k}{EI_{22}} \right) \frac{\partial M_x}{\partial y} \dots \\ & \dots + z \frac{G_{xy}^k}{C_{33}} \frac{\partial M_{xy}}{\partial y} \end{aligned}$$

Taking into account the equilibrium Equation 18.13, we can rewrite

$$\begin{aligned}
 G_{yz}^k \frac{\partial^2 \eta_y}{\partial z^2} = & -z \left(\frac{\bar{E}_{22}^k}{EI_{12}} + \frac{\bar{E}_{12}^k}{EI_{11}} \right) \frac{\partial M_y}{\partial y} - z \left(\frac{\bar{E}_{22}^k}{EI_{22}} + \frac{\bar{E}_{12}^k}{EI_{12}} \right) Q_y \cdots \\
 & \cdots + z \left(\frac{G_{xy}^k}{C_{33}} - \frac{\bar{E}_{22}^k}{EI_{22}} - \frac{\bar{E}_{12}^k}{EI_{12}} \right) \frac{\partial M_{xy}}{\partial x}
 \end{aligned} \tag{18.20}$$

18.6.3 PARTICULAR CASES

Equations 18.19 and 18.20 are simplified in the following specific cases:

18.6.3.1 Orthotropic Homogeneous Plate

From Equations 18.2, 18.8, and 18.9,

$$\begin{aligned}
 \bar{E}_{11}^k &= \bar{E}_{11}; \quad \bar{E}_{12}^k = \bar{E}_{12}; \quad \bar{E}_{22}^k = \bar{E}_{22} \\
 \frac{1}{EI_{11}} &= \frac{C_{22}}{C_{11}C_{22} - C_{12}^2} = \frac{\bar{E}_{22}}{\bar{E}_{11}\bar{E}_{22} - \bar{E}_{12}^2} \times \frac{12}{h^3} \\
 \frac{1}{EI_{22}} &= \frac{\bar{E}_{11}}{\bar{E}_{11}\bar{E}_{22} - \bar{E}_{12}^2} \times \frac{12}{h^3} \\
 \frac{1}{EI_{12}} &= -\frac{C_{12}}{C_{11}C_{22} - C_{12}^2} = \frac{-\bar{E}_{12}}{\bar{E}_{11}\bar{E}_{22} - \bar{E}_{12}^2} \times \frac{12}{h^3}; \quad \frac{1}{C_{33}} = \frac{1}{G_{xy}} \times \frac{12}{h^3}
 \end{aligned}$$

Accordingly, Equations 18.19 and 18.20 reduce to

$$\begin{aligned}
 G_{xz} \frac{\partial^2 \eta_x}{\partial z^2} &= -z \times \frac{12}{h^3} \times Q_x \\
 G_{yz} \frac{\partial^2 \eta_y}{\partial z^2} &= -z \times \frac{12}{h^3} \times Q_y
 \end{aligned} \tag{18.21}$$

18.6.3.2 Cylindrical Bending of a Multilayered Plate with Proportionality Properties

We consider the cylindrical bending of a multilayered plate such that for any two plies k and m , we have in plane (x, y) (see Equation 18.2)

$$\frac{\bar{E}_{ij}^k}{\bar{E}_{ij}^m} = \alpha_{km} \quad \forall i, j = 1, 2 \Rightarrow \frac{\bar{E}_{11}^k}{\bar{E}_{11}^m} = \frac{\bar{E}_{12}^k}{\bar{E}_{12}^m} = \frac{\bar{E}_{22}^k}{\bar{E}_{22}^m} = \alpha_{km}$$

Then,

$$C_{ij} = \int_{-h/2}^{h/2} \bar{E}_{ij}^k z^2 dz = \sum_{k=1}^{nth \text{ ply}} \left\{ \bar{E}_{ij}^k \int_{z_{k-1}}^{z_k} z^2 dz \right\}$$

$$C_{ij} = \bar{E}_{ij}^1 \int_{z_0}^{z_1} z^2 dz + \bar{E}_{ij}^2 \int_{z_1}^{z_2} z^2 dz \cdots + \bar{E}_{ij}^n \int_{z_{n-1}}^{z_n} z^2 dz$$

$$C_{ij} = \bar{E}_{ij}^1 \left\{ \int_{z_0}^{z_1} z^2 dz + \alpha_{12} \int_{z_1}^{z_2} z^2 dz \cdots + \alpha_{n-1,n} \int_{z_{n-1}}^{z_n} z^2 dz \right\} = \bar{E}_{ij}^1 \times \frac{\alpha h^3}{12}$$

Where α is a nondimensional coefficient. We therefore have

$$\frac{1}{\bar{E}I_{11}} = \frac{C_{22}}{C_{11}C_{22} - C_{12}^2} = \frac{\bar{E}_{22}^1}{\left(\bar{E}_{11}^1 \bar{E}_{22}^1 - (\bar{E}_{12}^1)^2 \right)} \times \frac{12}{\alpha h^3}$$

$$\frac{1}{\bar{E}I_{22}} = \frac{\bar{E}_{11}^1}{\left(\bar{E}_{11}^1 \bar{E}_{22}^1 - (\bar{E}_{12}^1)^2 \right)} \times \frac{12}{\alpha h^3}$$

$$\frac{1}{\bar{E}I_{12}} = \frac{-\bar{E}_{12}^1}{\left(\bar{E}_{11}^1 \bar{E}_{22}^1 - (\bar{E}_{12}^1)^2 \right)} \times \frac{12}{\alpha h^3}$$

In Equation 18.19, we obtain the following simplification:

$$\frac{\bar{E}_{11}^k}{\bar{E}I_{12}} + \frac{\bar{E}_{12}^k}{\bar{E}I_{22}} = \frac{-\bar{E}_{11}^k \bar{E}_{12}^1 + \bar{E}_{12}^k \bar{E}_{11}^1}{\bar{E}_{11}^1 \bar{E}_{22}^1 - (\bar{E}_{12}^1)^2} \times \frac{12}{\alpha h^3}$$

$$= \frac{\alpha_{k1} (-\bar{E}_{11}^1 \bar{E}_{12}^1 + \bar{E}_{12}^1 \bar{E}_{11}^1)}{\bar{E}_{11}^1 \bar{E}_{22}^1 - (\bar{E}_{12}^1)^2} \times \frac{12}{\alpha h^3} = 0$$

As well as a similar simplification in Equation 18.20:

$$\frac{\bar{E}_{12}^k}{\bar{E}I_{11}} + \frac{\bar{E}_{22}^k}{\bar{E}I_{12}} = 0$$

Then, if we examine the following cylindrical bending cases for this plate:

- Cylindrical bending about y-axis: then in Equation 18.22, $M_{xy} = Q_y = 0$ and Equation 18.20 disappears.
- Cylindrical bending about x-axis: then $M_{xy} = Q_x = 0$ and Equation 18.19 disappears.

Equations 18.19 and 18.20 simplify as follows:

(a) Cylindrical bending about y-axis

$$G_{xz}^k \frac{\partial^2 \eta_x}{\partial z^2} = -z \left(\frac{\bar{E}_{11}^k}{\bar{E}I_{11}} + \frac{\bar{E}_{12}^k}{\bar{E}I_{12}} \right) Q_x$$

or

(b) Cylindrical bending about x-axis

$$G_{yz}^k \frac{\partial^2 \eta_y}{\partial z^2} = -z \left(\frac{\bar{E}_{22}^k}{\bar{E}I_{22}} + \frac{\bar{E}_{12}^k}{\bar{E}I_{12}} \right) Q_y$$

(18.22)

18.6.3.3 Bending of a Multilayered Plate with Proportionality Properties

We focus on the particular case where, for any two of plies k and m , we observe in the plane of the plate the proportionality between elastic coefficients \bar{E}_{ij}^9 :

$$\frac{\bar{E}_{ij}^k}{\bar{E}_{ij}^m} = \alpha_{km} \quad \forall i, j = 1, 2, 3 \Rightarrow \frac{\bar{E}_{11}^k}{\bar{E}_{11}^m} = \frac{\bar{E}_{12}^k}{\bar{E}_{12}^m} = \frac{\bar{E}_{22}^k}{\bar{E}_{22}^m} = \frac{\bar{E}_{33}^k}{\bar{E}_{33}^m} = \alpha_{km}$$

Then Equations 18.19 and 18.20 reduce to:

$$\boxed{\begin{aligned} G_{xz}^k \frac{\partial^2 \eta_x}{\partial z^2} &= -z \left(\frac{\bar{E}_{11}^k}{EI_{11}} + \frac{\bar{E}_{12}^k}{EI_{12}} \right) Q_x \\ \text{and} \\ G_{yz}^k \frac{\partial^2 \eta_y}{\partial z^2} &= -z \left(\frac{\bar{E}_{22}^k}{EI_{22}} + \frac{\bar{E}_{12}^k}{EI_{12}} \right) Q_y \end{aligned}} \quad (18.23)$$

Notes:

- The previous specific cases constitute a significant restriction among the variety of practical laminations. Nevertheless, we will conserve, in the following, the simplified forms of Equations 18.21, 18.22, and 18.23 because they will show the direct connection between the warping functions η_x and η_y and the transverse shear forces Q_x and Q_y , respectively.
- With the aim of a simplified approach of the phenomenon, it can be noted that Equations 18.22 are immediately obtained by considering cylindrical bending of a laminate with the following approximations:
 - A cylindrical bending about y-axis for which we neglect the bending moment M_x in Equation 18.19
 - A cylindrical bending about x-axis for which we neglect the bending moment M_y in Equation 18.20

18.6.3.4 Consequences

Taking into account the preceding remark about the link between warping and shear force, we set η_x and η_y as

$$\begin{cases} \eta_x(x, y, z) = \frac{Q_x}{\langle hG_{xz} \rangle} \times g(z) \\ \eta_y(x, y, z) = \frac{Q_y}{\langle hG_{yz} \rangle} \times p(z) \end{cases} \quad (18.24)$$

Constitutive Equations 18.10 and 18.11 are written as

$$\bullet \quad Q_x = \langle hG_{xz} \rangle \left(\frac{\partial w_0}{\partial x} + \theta_y \right) + \frac{Q_x}{\langle hG_{xz} \rangle} \int_{-h/2}^{h/2} G_{xz} \frac{dg}{dz} \times dz$$

Then by setting

$$k_x = \left(1 - \frac{1}{\langle hG_{xz} \rangle} \int_{-h/2}^{h/2} G_{xz} \frac{dg}{dz} \times dz \right)$$

One obtains

$$Q_x = \frac{\langle hG_{xz} \rangle}{k_x} \left(\frac{\partial w_0}{\partial x} + \theta_y \right) \quad (18.25)$$

$$\bullet \quad Q_y = \langle hG_{yz} \rangle \left(\frac{\partial w_0}{\partial y} - \theta_x \right) + \frac{Q_y}{\langle hG_{yz} \rangle} \int_{-h/2}^{h/2} G_{yz} \frac{dp}{dz} \times dz$$

And then by setting

$$k_y = \left(1 - \frac{1}{\langle hG_{yz} \rangle} \int_{-h/2}^{h/2} G_{yz} \frac{dp}{dz} \times dz \right)$$

One obtains

$$Q_y = \frac{\langle hG_{yz} \rangle}{k_y} \left(\frac{\partial w_0}{\partial y} - \theta_x \right) \quad (18.26)$$

Thus appear two transverse shear coefficients k_x and k_y that require for their calculation the knowledge of functions $g(z)$ and $p(z)$.

18.6.4 WARPING FUNCTIONS

18.6.4.1 Boundary Conditions

We have assumed that upper and lower faces of the plate were free of any shear. Thus, from the transverse shear stress values appearing in Equations 18.17 and 18.18,

$$\bullet \quad \left(\frac{\partial w_0}{\partial x} + \theta_y \right) + \frac{Q_x}{\langle hG_{xz} \rangle} \frac{dg}{dz} = 0 \quad \text{for } z = \pm \frac{h}{2}$$

And with Equation 18.25,

$$k_x + \frac{dg}{dz} = 0 \quad \text{for } z = \pm \frac{h}{2}$$

$$\bullet \quad \left(\frac{\partial w_0}{\partial y} - \theta_x \right) + \frac{Q_y}{\langle hG_{yz} \rangle} \frac{dp}{dz} = 0 \quad \text{for } z = \pm \frac{h}{2}$$

And with Equation 18.26,

$$k_y + \frac{dp}{dz} = 0 \quad \text{for } z = \pm \frac{h}{2}$$

18.6.4.2 Interfacial Continuity

The continuity of transverse shear stress across interfaces between layers is resulting from the assumed perfect bonding between the plies (see Section 16.1.2.3). Thus, at the interface between two consecutive plies (k) and ($k+1$),

$$\tau_{xz}^{(k)} = \tau_{xz}^{(k+1)}; \quad \tau_{yz}^{(k)} = \tau_{yz}^{(k+1)}$$

And with Equations 18.17, 18.18, 18.25, and 18.26,

$$G_{xz}^k \left(k_x + \frac{dg_k}{dz} \right) = G_{xz}^{k+1} \left(k_x + \frac{dg_{k+1}}{dz} \right)$$

$$G_{yz}^k \left(k_y + \frac{dp_k}{dz} \right) = G_{yz}^{k+1} \left(k_y + \frac{dp_{k+1}}{dz} \right)$$

18.6.4.3 Formulation of Warping Functions

By replacing $g(z)$ and $p(z)$ with the following,

$$g_0(z) = g(z) + z \times k_x; \quad p_0(z) = p(z) + z \times k_y$$

$g_0(z)$ and $p_0(z)$ are so-called the **warping functions**. Then, the boundary conditions and interface conditions are simplified, and Equation 18.23 leads to formulate the problems that allow simple calculation of warping functions $g_0(z)$ and $p_0(z)$. We obtain

$$\left\{ \begin{array}{l} \frac{d^2 g_0}{dz^2} = -z \times \frac{\langle hG_{xz} \rangle}{G_{xz}^k} \left(\frac{\bar{E}_{11}^k}{EI_{11}} + \frac{\bar{E}_{12}^k}{EI_{12}} \right) \\ \frac{dg_0}{dz} = 0 \quad \text{for } z = \pm \frac{h}{2} \\ G_{xz}^k \frac{dg_{0k}}{dz} = G_{xz}^{k+1} \frac{dg_{0k+1}}{dz} \quad \text{for } z = z_k \end{array} \right. \quad (18.27)$$

$$\left\{ \begin{array}{l} \frac{d^2 p_0}{dz^2} = -z \times \frac{\langle hG_{yz} \rangle}{G_{yz}^k} \left(\frac{\bar{E}_{22}^k}{EI_{22}} + \frac{\bar{E}_{12}^k}{EI_{12}} \right) \\ \frac{dp_0}{dz} = 0 \quad \text{for } z = \pm \frac{h}{2} \\ G_{yz}^k \frac{dp_{0k}}{dz} = G_{yz}^{k+1} \frac{dp_{0k+1}}{dz} \quad \text{for } z = z_k \end{array} \right. \quad (18.28)$$

Antisymmetric functions $g_0(z)$ and $p_0(z)$ are thus defined in a unique manner.

18.6.5 CONSEQUENCES

18.6.5.1 Expression of Transverse Shear Stress

Equations 18.17 and 18.18 take the following simple forms:

$$\tau_{xz} = Q_x \times \frac{G_{xz}^k}{\langle hG_{xz} \rangle} \frac{dg_0}{dz}; \quad \tau_{yz} = Q_y \times \frac{G_{yz}^k}{\langle hG_{yz} \rangle} \frac{dp_0}{dz} \quad (18.29)$$

18.6.5.2 Transverse Shear Coefficients

These coefficients are obtained from Equation 18.5:

$$\text{a) } \int_{-h/2}^{h/2} \left(\frac{\bar{E}_{11}}{\bar{E}I_{11}} + \frac{\bar{E}_{12}}{\bar{E}I_{12}} \right) \eta_x z \times dz = 0$$

Using Equation 18.24 and the definition of g_o gives

$$\int_{-h/2}^{h/2} \left(\frac{\bar{E}_{11}}{\bar{E}I_{11}} + \frac{\bar{E}_{12}}{\bar{E}I_{12}} \right) \times \frac{Q_x}{\langle hG_{xz} \rangle} (g_0 - k_x z) \times z \times dz = 0$$

Noting that

$$\int_{-h/2}^{h/2} \left(\frac{\bar{E}_{11}}{\bar{E}I_{11}} + \frac{\bar{E}_{12}}{\bar{E}I_{12}} \right) z^2 dz = \frac{C_{11}}{\bar{E}I_{11}} + \frac{C_{12}}{\bar{E}I_{12}} = \frac{C_{11}C_{22} - C_{12}^2}{C_{11}C_{22} - C_{12}^2} = 1$$

We obtain

$$k_x = \int_{-h/2}^{h/2} \left(\frac{\bar{E}_{11}}{\bar{E}I_{11}} + \frac{\bar{E}_{12}}{\bar{E}I_{12}} \right) g_o z \times dz \quad (18.30)$$

$$\text{b) } \int_{-h/2}^{h/2} \left(\frac{\bar{E}_{22}}{\bar{E}I_{22}} + \frac{\bar{E}_{12}}{\bar{E}I_{12}} \right) \eta_y z \times dz = 0$$

$$\int_{-h/2}^{h/2} \left(\frac{\bar{E}_{22}}{\bar{E}I_{22}} + \frac{\bar{E}_{12}}{\bar{E}I_{12}} \right) \times \frac{Q_y}{\langle hG_{yz} \rangle} (p_0 - k_y z) \times z \times dz = 0$$

Leading to

$$k_y = \int_{-h/2}^{h/2} \left(\frac{\bar{E}_{22}}{\bar{E}I_{22}} + \frac{\bar{E}_{12}}{\bar{E}I_{12}} \right) p_0 z \times dz \quad (18.31)$$

In summary, in the absence of body forces, such as inertia forces, the bending behavior, uncoupled from the membrane behavior, of a laminated plate can be simplified in a few particular cases noted below. The characteristic relationships are summarized in the following box.

Bending behavior (no In-plane stress resultants)

- Orthotropic homogeneous plate/orthotropic axes (x, y, z)
- **Or** Laminated plate/Mid-plane symmetry/orthotropic axes of plies (x, y, z) /cylindrical bending about x or y axis/elastic constants \bar{E}_{ij} ($i, j = 1, 2$) being proportional from one ply to another.
- **Or** Laminated plate/Mid-plane symmetry/orthotropic axes of plies (x, y, z) /elastic constants \bar{E}_{ij} ($i, j = 1, 2, 3$) being proportional from one ply to another.
- **Or** Laminated plate/Mid-plane symmetry/orthotropic axes of plies (x, y, z) /simplified cylindrical bending.

• **Constitutive equations**

$$\begin{Bmatrix} M_y \\ -M_x \\ -M_{xy} \\ Q_x \\ Q_y \end{Bmatrix} = \begin{bmatrix} C_{11} & C_{12} & 0 & 0 & 0 \\ C_{21} & C_{22} & 0 & 0 & 0 \\ 0 & 0 & C_{33} & 0 & 0 \\ 0 & 0 & 0 & \frac{\langle hG_{xz} \rangle}{k_x} & 0 \\ 0 & 0 & 0 & 0 & \frac{\langle hG_{yz} \rangle}{k_y} \end{bmatrix} \begin{Bmatrix} \frac{\partial \theta_y}{\partial x} \\ -\frac{\partial \theta_x}{\partial y} \\ \left(\frac{\partial \theta_y}{\partial y} - \frac{\partial \theta_x}{\partial x} \right) \\ \left(\frac{\partial w_0}{\partial x} + \theta_y \right) \\ \left(\frac{\partial w_0}{\partial y} - \theta_x \right) \end{Bmatrix}$$

$$C_{ij} = \int_{-\frac{h}{2}}^{\frac{h}{2}} \bar{E}_{ij} \times z^2 dz \quad \text{or} = \sum_{k=1st \text{ ply}}^{k=nth \text{ ply}} \bar{E}_{ij}^k \times \frac{(z_k^3 - z_{k-1}^3)}{3}; \quad \left[\frac{1}{EI} \right] = [C]^{-1}$$

$$\langle hG_{xz} \rangle = \int_{-h/2}^{h/2} G_{xz} dz \quad \text{or} = \sum_{k=1st \text{ ply}}^{k=nth \text{ ply}} G_{xz}^k \times (z_k - z_{k-1})$$

$$\langle hG_{yz} \rangle = \int_{-h/2}^{h/2} G_{yz} dz \quad \text{or} = \sum_{k=1st \text{ ply}}^{k=nth \text{ ply}} G_{yz}^k \times (z_k - z_{k-1})$$

(18.32a)

k_x and k_y are transverse shear coefficients

• **Stress values**

- Stresses within the ply (ply $n^o k$):

σ_x : see Equation 18.14; σ_y : see Equation 18.15; τ_{xy} : see Equation 18.16.

- Transverse shear stresses:

$$\tau_{xz} = Q_x \frac{G_{xz}^k}{\langle hG_{xz} \rangle} \frac{dg_0}{dz}; \quad \tau_{yz} = Q_y \frac{G_{yz}^k}{\langle hG_{yz} \rangle} \frac{dp_0}{dz}$$

(18.32b)

- **Warping functions**

- $g_0(z)$ is the solution of the problem:

$$\begin{cases} \frac{d^2 g_0}{dz^2} = -z \frac{\langle hG_{xz} \rangle}{G_{xz}^k} \left(\frac{\bar{E}_{11}^k}{EI_{11}} + \frac{\bar{E}_{12}^k}{EI_{12}} \right) \\ \frac{dg_0}{dz} = 0 \quad \text{for } z = \pm \frac{h}{2} \\ G_{xz}^k \frac{dg_{0k}}{dz} = G_{xz}^{k+1} \frac{dg_{0k+1}}{dz} \quad \text{for } z = z_k \end{cases}$$

- $p_0(z)$ is the solution of the problem:

$$\begin{cases} \frac{d^2 p_0}{dz^2} = -z \frac{\langle hG_{yz} \rangle}{G_{yz}^k} \left(\frac{\bar{E}_{22}^k}{EI_{22}} + \frac{\bar{E}_{12}^k}{EI_{12}} \right) \\ \frac{dp_0}{dz} = 0 \quad \text{for } z = \pm \frac{h}{2} \\ G_{yz}^k \frac{dp_{0k}}{dz} = G_{yz}^{k+1} \frac{dp_{0k+1}}{dz} \quad \text{for } z = z_k \end{cases}$$

(18.32c)

- **Transverse shear coefficients k_x and k_y**

They are given by the following formulas:

$$\begin{aligned} k_x &= \int_{-h/2}^{h/2} \left(\frac{\bar{E}_{11}}{EI_{11}} + \frac{\bar{E}_{12}}{EI_{12}} \right) g_0 z \times dz \quad \text{or} = \sum_{k=1st \text{ ply}}^{k=nth \text{ ply}} \left\{ \left(\frac{\bar{E}_{11}^k}{EI_{11}} + \frac{\bar{E}_{12}^k}{EI_{12}} \right) \int_{\text{ply } k} g_{0k} z \times dz \right\} \\ k_y &= \int_{-h/2}^{h/2} \left(\frac{\bar{E}_{22}}{EI_{22}} + \frac{\bar{E}_{12}}{EI_{12}} \right) p_0 z \times dz \quad \text{or} = \sum_{k=1st \text{ ply}}^{k=nth \text{ ply}} \left\{ \left(\frac{\bar{E}_{22}^k}{EI_{22}} + \frac{\bar{E}_{12}^k}{EI_{12}} \right) \int_{\text{ply } k} p_{0k} z \times dz \right\} \end{aligned}$$

(18.32d)

18.6.6 ENERGY INTERPRETATION

We will limit ourselves to the energy density per unitary surface of the plate, due to transverse shear stress as

$$W_\tau = \frac{1}{2} \int_{-h/2}^{h/2} (\tau_{xz} \gamma_{xz} + \tau_{yz} \gamma_{yz}) \times dz = \frac{1}{2} \int_{-h/2}^{h/2} \left(\frac{\tau_{xz}^2}{G_{xz}} + \frac{\tau_{yz}^2}{G_{yz}} \right) \times dz$$

Substituting Equation 18.29, we obtain

$$W_\tau = \frac{1}{2} \int_{-h/2}^{h/2} Q_x^2 \frac{G_{xz}}{\langle hG_{xz} \rangle^2} \left(\frac{dg_0}{dz} \right)^2 \times dz + \frac{1}{2} \int_{-h/2}^{h/2} Q_y^2 \frac{G_{yz}}{\langle hG_{yz} \rangle^2} \left(\frac{dp_0}{dz} \right)^2 \times dz$$

The first integral can be rewritten as

$$\frac{1}{2} \frac{Q_x^2}{\langle hG_{xz} \rangle^2} \int_{-h/2}^{h/2} G_{xz} \left[\frac{d}{dz} \left(g_0 \frac{dg_0}{dz} \right) - g_0 \frac{d^2 g_0}{dz^2} \right] \times dz$$

Or, taking into account Equation 18.27,

$$\frac{1}{2} \frac{Q_x^2}{\langle hG_{xz} \rangle^2} \left\{ G_{xz} \left[g_o \frac{dg_o}{dz} \right]_{-h/2}^{h/2} + \langle hG_{xz} \rangle \int_{-h/2}^{h/2} \left(\frac{\bar{E}_{11}}{\bar{E}I_{11}} + \frac{\bar{E}_{12}}{\bar{E}I_{12}} \right) g_o z \times dz \right\}$$

Only the second term remains where we recognize the transverse shear coefficient k_x of Equation 18.30. The first integral under examination is reduced to

$$\frac{1}{2} k_x \frac{Q_x^2}{\langle hG_{xz} \rangle}$$

Following a similar approach for the second integral and taking into account Equations 18.28 and 18.31 for the transverse shear coefficient k_y , the surface density of energy due to transverse shear takes the form

$$W_\tau = \frac{1}{2} k_x \frac{Q_x^2}{\langle hG_{xz} \rangle} + \frac{1}{2} k_y \frac{Q_y^2}{\langle hG_{yz} \rangle} \quad (18.32e)$$

18.7 EXAMPLES

Examples for plates in bending are shown in details in Section IV of this book, in Chapter 21. We give here a few useful elements to advance treatment of these examples, and we study a particular case of D-D laminate.

18.7.1 ORTHOTROPIC HOMOGENEOUS PLATE

- **Warping functions**

With $\bar{E}_{11}^k = \bar{E}_{11}$; $\bar{E}_{12}^k = \bar{E}_{12}$; $\bar{E}_{22}^k = \bar{E}_{22}$; $G_{xz}^k = G_{xz}$

Equation 18.27 becomes¹⁰

$$\frac{d^2 g_o}{dz^2} = -z \times h \left(\frac{\bar{E}_{11} \bar{E}_{22}}{(\bar{E}_{11} \bar{E}_{22} - \bar{E}_{12}^2)} \frac{12}{h^3} - \frac{\bar{E}_{12}^2}{(\bar{E}_{11} \bar{E}_{22} - \bar{E}_{12}^2)} \frac{12}{h^3} \right) = -z \times \frac{12}{h^2}$$

$$\frac{dg_o}{dz} = 0 \quad \text{for } z = \pm \frac{h}{2}$$

Then

$$\frac{dg_o}{dz} = \frac{3}{2} \left(1 - 4 \frac{z^2}{h^2} \right); \quad g_o = \frac{3}{2} z \left(1 - \frac{4}{3} \frac{z^2}{h^2} \right)$$

- **Transverse shear stress and shear coefficients:** We deduce from Equation 18.32

$$\tau_{xz} = \frac{Q_x}{h} \times \frac{3}{2} \left(1 - 4 \frac{z^2}{h^2} \right) \quad (18.33)$$

$$k_x = \frac{12}{h^3} \int_{-h/2}^{h/2} \frac{3}{2} \left(1 - \frac{4}{3} \frac{z^2}{h^2} \right) \times z^2 dz$$

$$k_x = \frac{6}{5} \quad (18.34)$$

In a similar manner starting from Equation 18.28,

$$p_0(z) = g_0(z)$$

Then,

$$\tau_{yz} = \frac{Q_y}{h} \times \frac{3}{2} \left(1 - 4 \frac{z^2}{h^2} \right) \quad (18.35)$$

$$k_y = \frac{6}{5} \quad (18.36)$$

Note: In Application 21.10, we treat the case of a thick orthotropic homogeneous plate in cylindrical bending about y-axis. The plate supports a uniformly distributed load. We can see there the strong influence of transverse shear on the bending deflection. Two characteristics of the plate are involved that act directly on this deflection:

- The relative thickness h/a , where a is the length of the bent side of the plate
- The ratio E_x/G_{xz} . For the composite case and certain combinations of fiber/matrix, this ratio can become large compared with unity. This is typically the case for unidirectional.

18.7.2 SANDWICH PLATE

18.7.2.1 Case of Two Orthotropic Materials

Material (1) for the skins

Material (2) for the core (see Figure 18.3)

Proportionality of elastic coefficients for both materials is assumed. This leads to (See Section 18.6.3.3)

$$\frac{\bar{E}_{11}^{(2)}}{\bar{E}_{11}^{(1)}} = \frac{\bar{E}_{12}^{(2)}}{\bar{E}_{12}^{(1)}} = \frac{\bar{E}_{22}^{(2)}}{\bar{E}_{22}^{(1)}} = \frac{\bar{E}_{33}^{(2)}}{\bar{E}_{33}^{(1)}} = \alpha_{21}$$

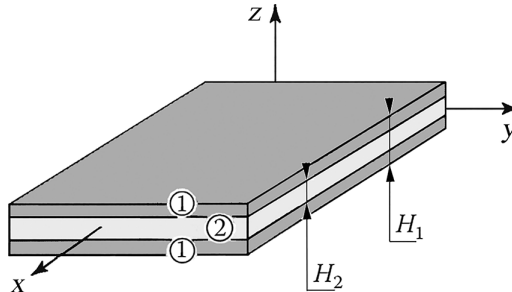


FIGURE 18.3 Sandwich plate.

Note: As an example, this is the case for both isotropic materials (1) and (2) having the same Poisson coefficient.

Then,

$$C_{ij} = \int_{-h/2}^{h/2} \bar{E}_{ij} z^2 dz = \bar{E}_{ij}^{(1)} \int_{-H_1/2}^{-H_2/2} z^2 \times dz + \bar{E}_{ij}^{(2)} \int_{-H_2/2}^{H_2/2} z^2 \times dz + \bar{E}_{ij}^{(1)} \int_{H_2/2}^{H_1/2} z^2 \times dz$$

$$C_{ij} = \bar{E}_{ij}^{(1)} \left(\frac{H_1^3 - H_2^3}{12} \right) + \bar{E}_{ij}^{(2)} \frac{H_2^3}{12}$$

$$C_{ij} = \bar{E}_{ij}^{(1)} \times \frac{\alpha H_1^3}{12} \text{ with } \frac{\alpha H_1^3}{12} = \frac{(H_1^3 - H_2^3)}{12} + \alpha_{21} \frac{H_2^3}{12}$$

From this, we deduce

$$\frac{1}{\bar{E}I_{11}} = \frac{C_{22}}{C_{11}C_{22} - C_{12}^2} = \frac{\bar{E}_{22}^{(1)}}{\bar{E}_{11}^{(1)}\bar{E}_{22}^{(1)} - (\bar{E}_{12}^{(1)})^2} \times \frac{12}{\alpha H_1^3}$$

$$\frac{1}{\bar{E}I_{12}} = \frac{-C_{12}}{C_{11}C_{22} - C_{12}^2} = \frac{-\bar{E}_{12}^{(1)}}{\bar{E}_{11}^{(1)}\bar{E}_{22}^{(1)} - (\bar{E}_{12}^{(1)})^2} \times \frac{12}{\alpha H_1^3}$$

18.7.2.2 Warping Functions

- Based on the foregoing, one can write in Equation 18.32c¹¹

$$\left(\frac{\bar{E}_{11}^k}{\bar{E}I_{11}} + \frac{\bar{E}_{12}^k}{\bar{E}I_{12}} \right) = \frac{E_x^k}{E_x^{(1)}} \times \frac{12}{\alpha H_1^3} = \frac{E_x^k}{E_x^{(1)} \frac{(H_1^3 - H_2^3)}{12} + E_x^{(2)} \frac{H_2^3}{12}}$$

In addition,

$$\langle hG_{xz} \rangle = G_{xz}^{(1)} (H_1 - H_2) + G_{xz}^{(2)} H_2$$

Equation 18.27 then can be written as

$$\left\{ \begin{array}{l} \frac{d^2 g_0}{dz^2} = -z \times \frac{E_x^k}{G_{xz}^k} \times 12 \times \frac{G_{xz}^{(1)} (H_1 - H_2) + G_{xz}^{(2)} H_2}{E_x^{(1)} (H_1^3 - H_2^3) + E_x^{(2)} H_2^3} \\ \frac{dg_0}{dz} = 0 \quad \text{for } z = \pm \frac{H_1}{2} \\ G_{xz}^k \frac{dg_0}{dz} \text{ continuous for } z = \pm \frac{H_2}{2} \end{array} \right.$$

- For the warping function $p_0(z)$, Equation 18.28 takes a similar form. We can indeed write as follows:

$$\left(\frac{\bar{E}_{22}^k}{EI_{22}} + \frac{\bar{E}_{12}^k}{EI_{12}} \right) = \frac{E_y^k}{E_y^{(1)}} \times \frac{12}{\alpha h^3} = \frac{E_y^k}{E_y^{(1)} \frac{(H_1^3 - H_2^3)}{12} + E_y^{(2)} \frac{H_2^3}{12}}$$

The problem (18.28) is then written as

$$\begin{cases} \frac{d^2 p_0}{dz^2} = -z \times \frac{E_y^k}{G_{yz}^k} \times 12 \times \frac{G_{yz}^{(1)}(H_1 - H_2) + G_{yz}^{(2)}H_2}{E_y^{(1)}(H_1^3 - H_2^3) + E_y^{(2)}H_2^3} \\ \frac{dp_0}{dz} = 0 \quad \text{for } z = \pm \frac{H_1}{2} \\ G_{yz}^k \frac{dp_0}{dz} \text{ continuous for } z = \pm \frac{H_2}{2} \end{cases}$$

Note: It should be noted that the two problems presented earlier are identical to the one that allows warping function calculation for a sandwich beam in bending, as can be seen in Section 21.5. We can therefore repeat here for the calculations the same steps that are followed in this application. The results are shown below.

18.7.2.3 Transverse Shear Stress

- **Shear stress τ_{xz}**

$$-\frac{H_2}{2} \leq z \leq \frac{H_2}{2} \rightarrow \tau_{xz} = Q_x \times 6 \times \frac{E_x^{(2)} \left(\frac{H_2^2}{4} - z^2 \right) + E_x^{(1)} \left(\frac{H_1^2}{4} - \frac{H_2^2}{4} \right)}{E_x^{(1)}(H_1^3 - H_2^3) + E_x^{(2)}H_2^3} \quad (18.37)$$

$$\frac{H_2}{2} \leq z \leq \frac{H_1}{2} \rightarrow \tau_{xz} = Q_x \times 6 \times \frac{E_x^{(1)} \left(\frac{H_1^2}{4} - z^2 \right)}{E_x^{(1)}(H_1^3 - H_2^3) + E_x^{(2)}H_2^3}$$

- **Shear stress τ_{yz}**

$$-\frac{H_2}{2} \leq z \leq \frac{H_2}{2} \rightarrow \tau_{yz} = Q_y \times 6 \times \frac{E_y^{(2)} \left(\frac{H_2^2}{4} - z^2 \right) + E_y^{(1)} \left(\frac{H_1^2}{4} - \frac{H_2^2}{4} \right)}{E_y^{(1)}(H_1^3 - H_2^3) + E_y^{(2)}H_2^3} \quad (18.38)$$

$$\frac{H_2}{2} \leq z \leq \frac{H_1}{2} \rightarrow \tau_{yz} = Q_y \times 6 \times \frac{E_y^{(1)} \left(\frac{H_1^2}{4} - z^2 \right)}{E_y^{(1)}(H_1^3 - H_2^3) + E_y^{(2)}H_2^3}$$

18.7.2.4 Transverse Shear Coefficients

$$k_x = \frac{a_x}{8 \left[E_x^{(1)} (H_1^3 - H_2^3) + E_x^{(2)} H_2^3 \right]} \left\{ \frac{E_x^{(2)}}{G_{xz}^{(2)}} H_2^3 \left[E_x^{(1)} H_1^2 + \left(\frac{4}{5} E_x^{(2)} - E_x^{(1)} \right) H_2^2 \right] \dots \right. \\ \left. \dots + \frac{(E_x^{(1)})^2}{G_{xz}^{(1)}} \left(\frac{4}{5} H_1^5 + \frac{H_2^5}{5} - H_1^2 H_2^3 \right) \right\} + \frac{3b_x E_x^{(1)} (H_1^2 - H_2^2)}{E_x^{(1)} (H_1^3 - H_2^3) + E_x^{(2)} H_2^3} \quad (18.39)$$

$$\text{with : } a_x = 12 \times \frac{G_{xz}^{(1)} (H_1 - H_2) + G_{xz}^{(2)} H_2}{E_x^{(1)} (H_1^3 - H_2^3) + E_x^{(2)} H_2^3}$$

$$b_x = \frac{a_x}{16} H_2 \frac{E_x^{(1)}}{G_{xz}^{(1)}} \left\{ \frac{H_2^2}{3} + H_1^2 \left(\frac{G_{xz}^{(1)}}{G_{xz}^{(2)}} - 1 \right) - H_2^2 \frac{G_{xz}^{(1)}}{G_{xz}^{(2)}} \left(1 - \frac{2}{3} \frac{E_x^{(2)}}{E_x^{(1)}} \right) \right\}$$

k_y is given by a formally identical expression in which index x is replaced by y .

In Application 21.10, we treat the case of a rectangular sandwich plate in cylindrical bending, clamped on one side and subjected to uniform force per unit length on another. The plate is free on the two other sides. Influence of transverse shear on the deflection is brought to light. This influence is especially marked because

- The mechanical characteristics (moduli) of the core are weaker than those of the skins
- The relative thickness of the core is important (thin skins)
- The relative thickness of the plate is large (thick plate)

18.8 QUASI-ORTHOTROPIC HOMOGENIZED LAMINATES (D-D LAMINATES)

18.8.1 EXTENSION TO TRANSVERSE SHEAR

18.8.1.1 Reminder

We saw in Chapter 15 that we get quasi-orthotropic laminates by stacking sublaminate sets so-called Double-Double sublaminates. Then each D-D set is composed of four identical unidirectional plies and characterized by two privileged directions (Φ , Ψ), each doubled according to the pattern $\pm\Phi$ and $\pm\Psi$ as recalled in Figure 18.4.

The laminate results from stacking “ r ” repetitions of D-D sublaminates. When the number r is increasing, we have observed that the relations between the overall strains and the average stresses for In-plane and bending behaviors approached those of a fictitious plate of the same thickness, homogeneous and orthotropic. This equivalent plate is defined very simply from the sequence D-D (See Section 15.3) as recalled below.

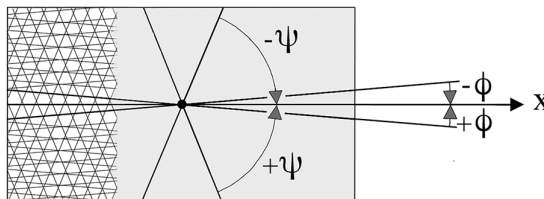


FIGURE 18.4 Four plies D-D set.

18.8.1.2 Equivalent Orthotropic Homogeneous Plate

This *equivalent orthotropic plate* associated to the D-D laminate was defined in Chapter 15. We recall that the behavior described by Equation 15.20 boils down to knowledge of matrices (see Equation 15.19):

$$\frac{12}{h^3}[C] = \frac{1}{h}[A]$$

With

$$\frac{1}{h}A_{ij} = \frac{1}{2}(\bar{E}_{ij}^{+\Phi} + \bar{E}_{ij}^{+\Psi}) \quad (18.40)$$

In what precedes this chapter, we could observe that this constitutive law could be completed by the terms (see Equation 18.32a):

$$\frac{\langle hG_{xz} \rangle}{k_x} \quad \text{and} \quad \frac{\langle hG_{yz} \rangle}{k_y}$$

We will thus have for the D-D laminate as well as for its equivalent orthotropic plate

$$\begin{aligned} \langle hG_{xz} \rangle_{D-D} &= \frac{h}{2}(G_{xz}^{\Phi} + G_{xz}^{\Psi}) = \langle hG_{xz} \rangle_{\text{orthotropic}} \\ \langle hG_{yz} \rangle_{D-D} &= \frac{h}{2}(G_{yz}^{\Phi} + G_{yz}^{\Psi}) = \langle hG_{yz} \rangle_{\text{orthotropic}} \end{aligned} \quad (18.41)$$

Recall that for the orthotropic plate case we have found (see Equations 18.34 and 18.36)

$$k_{x\text{orthotropic}} = k_{y\text{orthotropic}} = \frac{6}{5}$$

However, nothing can be said at this stage about shear coefficients k_{xD-D} and k_{yD-D} of a D-D laminate.

18.8.1.3 Transverse Shear Stiffness

Equations 18.25 and 18.26 relate the transverse shear resultants to the overall shear deformations, that is to say

$$Q_x = \frac{\langle hG_{xz} \rangle}{k_x} \left(\frac{\partial w_0}{\partial x} + \theta_y \right); \quad Q_y = \frac{\langle hG_{yz} \rangle}{k_y} \left(\frac{\partial w_0}{\partial y} - \theta_x \right)$$

One can also consider in an equivalent way the surface density of shear energy (see Equation 18.32), that is to say

$$W_\tau = \frac{1}{2}k_x \frac{Q_x^2}{\langle hG_{xz} \rangle} + \frac{1}{2}k_y \frac{Q_y^2}{\langle hG_{yz} \rangle}$$

In these both expressions appear what we could define as the “*transverse shear stiffnesses*”

$$\frac{\langle hG_{xz} \rangle}{k_x} \quad \text{and} \quad \frac{\langle hG_{yz} \rangle}{k_y}$$

Thus comparison of the transverse shear stiffness for a D-D laminate and its associated orthotropic plate leads to examine the ratios:

a. For bending in the (x, z) plane:

$$q_{(x,z)} = \frac{\left(\frac{\langle hG_{xz} \rangle}{k_x} \right)_{D-D}}{\left(\frac{\langle hG_{xz} \rangle}{k_x} \right)_{\text{orth.}}} = \frac{k_{x\text{orthotropic}}}{k_{xD-D}}$$

$$q_{(x,z)} = \frac{6}{5} \times \frac{1}{k_{xD-D}} \quad (18.42)$$

b. For bending in the (y, z) plane:

$$q_{(y,z)} = \frac{\left(\frac{\langle hG_{yz} \rangle}{k_y} \right)_{D-D}}{\left(\frac{\langle hG_{yz} \rangle}{k_y} \right)_{\text{orth.}}} = \frac{k_{y\text{orthotropic}}}{k_{yD-D}} = \frac{6}{5} \times \frac{1}{k_{yD-D}} \quad (18.43)$$

It can then be noted that the knowledge of transverse shear coefficients obtained from Equations (18.32d) appears necessary and sufficient to compare the transverse shear stiffness of the two plates (laminated and orthotropic).

18.8.1.4 Transverse Shear Stresses

When studying the In-plane and bending behaviors of a laminate (see Chapters 12 and 15), it was observed that the strains in each of the plies coincided with those of the overall laminate, while the stresses showed discontinuities from one ply to the next (see for example Figure 15.9).

It is the *reverse* when we are interested in the mechanism of the transverse shear. Indeed, as we saw above in this chapter, the transverse shear stresses remain continuous by passing from one ply to the next, whereas the distortion undergoes a discontinuity during this passage.

The transverse shear stresses are given by Equations (18.32b) i.e.

$$\tau_{xz} = Q_x \frac{G_{xz}^k}{\langle hG_{xz} \rangle} \frac{dg_0}{dz}; \quad \tau_{yz} = Q_y \frac{G_{yz}^k}{\langle hG_{yz} \rangle} \frac{dp_0}{dz}$$

Where appear the “warping functions” $g_0(z)$ for bending in the plane (x, z) and $p_0(z)$ for bending in the plane (y, z) . These functions are obtained by solving the problems (18.32c). For example for $g_0(z)$

$$\begin{cases} \frac{d^2 g_0}{dz^2} = -z \frac{\langle hG_{xz} \rangle}{G_{xz}^k} \left(\frac{\bar{E}_{11}^k}{EI_{11}} + \frac{\bar{E}_{12}^k}{EI_{12}} \right) \\ \frac{dg_0}{dz} = 0 \quad \text{for } z = \pm \frac{h}{2} \\ G_{xz}^k \frac{dg_{0k}}{dz} = G_{xz}^{k+1} \frac{dg_{0k+1}}{dz} \quad \text{for } z = z_k \end{cases}$$

We study in what follows a particular case of laminate of the Double-Double type.

18.8.2 EXAMPLE OF D-D LAMINATE

18.8.2.1 Definition

Based on arrangement \mathcal{A} , already discussed in Chapter 15 (see Section 15.3.1) that is $[+\Psi/+ \Phi/-\Phi/-\Psi]; (\Phi < \Psi)$, we then examine the sequence

$$[+\Psi/+ \Phi/-\Phi/-\Psi] \Rightarrow [90^\circ/0^\circ/0^\circ/90^\circ]$$

This corresponds to the particular case of passage to the limits $\pm\Phi \Rightarrow 0^\circ$ and $\pm\Psi \Rightarrow 90^\circ$.

We thus obtain a laminate also called “square symmetric”. Such a configuration has the following advantages here:

- We then obtain with unidirectional plies the most important differences between the elastic properties of two consecutive orientations Φ and Ψ . This is where the “delay” in homogenization for transverse shear will be greatest.
- For the same purpose, in order to deliberately delay the homogenization process, we prefer such a sequence to a sequence of type 1 2 1 2 1 2 1 so called arrangement \mathcal{C} (see Section 15.4.5.1).
- Such a configuration with a Mid-plane symmetry makes it possible to exploit Equations 18.32 by limiting ourselves to the study of a simplified cylindrical bending (See Note in Section 18.6.3.3). We can thus decouple the phenomenon of transverse shear from the problems related to bending seen in Chapter 15.

The laminate is shown in Figure 18.5 with 20 layers of thickness “ e ”. The corresponding number of repetitions of D-D sets is $r = 5$. We saw in Chapter 15 (see Section 15.4.2.2) that we then reached an admissible threshold of homogenization for bending.

This number of repetitions is low, corresponding to a thin laminate. However, even for such a case, consideration of transverse shear stiffness can be of importance in dealing with buckling stability problems (adjacent equilibrium associated with transverse shear forces)¹².

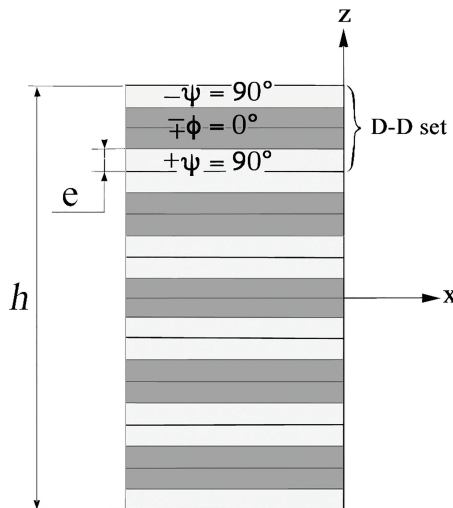


FIGURE 18.5 $[90^\circ/0^\circ/0^\circ/90^\circ]$ Laminate with five repetitions ($h = 5 \times 4e = 20e$).

TABLE 18.1
Unidirectional Carbon/Epoxy Ply

E_t (GPa)	E_l (GPa)	G_{tl} (GPa)	ν_{tl}	ν_{tt}	Equation (11.6)	\bar{E}_t (GPa)	\bar{E}_l (GPa)	$\nu_{tl}\bar{E}_t$ (GPa)	G_{tl} (GPa)	G_{zt} (GPa)
134	7	4.2	0.25	0.013		134.4	7.02	1.7472	4.2	2.7

18.8.2.2 Mechanical Characteristics

In the following we use a unidirectional carbon/epoxy ply. We start with elastic characteristics in Table 3.4. Moreover, taking into account the transverse isotropic nature of the ply (see Equation 13.7) and with Equation 18.2, we have:

$$G_{zt} = \frac{E_t}{2(1 + \nu)}$$

We retain the mean value $\nu = 0.3$ for the Poisson's ratio in the plane (t, z), that is

$$G_{zt} = 2.7 \text{ GPa}$$

The characteristics are summarized in Table 18.1

18.8.2.3 Bending in (x, z) Plane

We must solve Equation (18.32c) as recalled

$$\begin{cases} \frac{d^2 g_0}{dz^2} = -z \frac{\langle h G_{xz} \rangle}{G_{xz}^k} \left(\frac{\bar{E}_{11}^k}{EI_{11}} + \frac{\bar{E}_{12}^k}{EI_{12}} \right) \\ \frac{dg_0}{dz} = 0 \quad \text{for } z = \pm \frac{h}{2} \\ G_{xz}^k \frac{dg_{0k}}{dz} = G_{xz}^{k+1} \frac{dg_{0k+1}}{dz} \quad \text{for } z = z_k \end{cases}$$

a. We have $G_{xz}^\Phi = G_{xz}^{0^\circ} = G_{tl} = 4.2 \text{ GPa}$; $G_{xz}^\Psi = G_{xz}^{90^\circ} = G_{zt} = 2.7 \text{ GPa}$

$$\langle h G_{xz} \rangle = \frac{h}{2} (G_{xz}^\Phi + G_{xz}^\Psi) = h \times 3.45 \text{ GPa}$$

b. Term $\left(\frac{\bar{E}_{11}^k}{EI_{11}} + \frac{\bar{E}_{12}^k}{EI_{12}} \right)$

From Equations 18.2, 18.8, 18.9, and Figure 18.5

$$\bar{E}_{11}^\Phi = \bar{E}_{11}^{0^\circ} = \bar{E}_l = 134.4 \text{ GPa}; \quad \bar{E}_{12}^\Phi = \bar{E}_{12}^{0^\circ} = \nu_{tl} \bar{E}_l = 1.7472 \text{ GPa}; \quad \bar{E}_{22}^\Phi = \bar{E}_{22}^{0^\circ} = \bar{E}_t = 7.02 \text{ GPa}$$

$$\bar{E}_{11}^\Psi = \bar{E}_{11}^{90^\circ} = \bar{E}_t = 7.02 \text{ GPa}; \quad \bar{E}_{12}^\Psi = \bar{E}_{12}^{90^\circ} = \nu_{tl} \bar{E}_l = 1.7472 \text{ GPa}; \quad \bar{E}_{22}^\Psi = \bar{E}_{22}^{90^\circ} = \bar{E}_l =$$

134.4 GPa

$$C_{11} = 2 \times \left\{ \bar{E}_l \times \frac{e^3}{3} + \bar{E}_t \frac{(3e)^3 - e^3}{3} + \dots + \bar{E}_t \frac{(10e)^3 - (9e)^3}{3} \right\} = \frac{h^3}{12} (0.485 \bar{E}_l + 0.515 \bar{E}_t)$$

$$C_{22} = \frac{h^3}{12} (0.485\bar{E}_t + 0.515\bar{E}_\ell); \quad C_{12} = \frac{h^3}{12} \nu_{t\ell} \bar{E}_\ell$$

Then

$$\frac{1}{\bar{E}I_{11}} = \frac{C_{22}}{C_{11}C_{22} - C_{12}^2}; \quad \frac{1}{\bar{E}I_{12}} = -\frac{C_{12}}{C_{11}C_{22} - C_{12}^2}$$

And

$$\left(\frac{\bar{E}_{11}^\Phi}{\bar{E}I_{11}} + \frac{\bar{E}_{12}^\Phi}{\bar{E}I_{12}} \right) = \left(\frac{\bar{E}_\ell}{\bar{E}I_{11}} + \frac{\nu_{t\ell} \bar{E}_\ell}{\bar{E}I_{12}} \right); \quad \left(\frac{\bar{E}_{11}^\Psi}{\bar{E}I_{11}} + \frac{\bar{E}_{12}^\Psi}{\bar{E}I_{12}} \right) = \left(\frac{\bar{E}_t}{\bar{E}I_{11}} + \frac{\nu_{t\ell} \bar{E}_\ell}{\bar{E}I_{12}} \right)$$

• **Note**

As already indicated, the retained number of repetitions ($r = 5$) corresponds to a minimum threshold of homogenization (see Section 15.4.2.2). This can be controlled by comparing the above coefficients with those of the so-called equivalent orthotropic plate (see Equation 18.40). We note for example:

$$C_{11\text{orthotropic}} = \frac{h^3}{12} (0.5\bar{E}_\ell + 0.5\bar{E}_t)$$

To be compared to (see above)

$$C_{11\text{D-D}} = \frac{h^3}{12} (0.485\bar{E}_\ell + 0.515\bar{E}_t)$$

The difference is

$$\frac{C_{11\text{D-D}} - C_{11\text{orthotropic}}}{C_{11\text{orthotropic}}} = -2.7\%$$

And the difference is zero for the coefficient C_{12} .

18.8.2.4 Transverse Shear Stresses

We integrate for each ply the differential equation

$$\frac{d^2 g_0}{dz^2} = -z \times \frac{\langle hG_{xz} \rangle}{G_{xz}^k} \left(\frac{\bar{E}_{11}^k}{\bar{E}I_{11}} + \frac{\bar{E}_{12}^k}{\bar{E}I_{12}} \right)$$

Where G_{xz}^k alternately takes the values $G_{xz}^\Phi = G_{t\ell}$ and $G_{xz}^\Psi = G_{z\ell}$

The connecting condition

$$G_{xz}^k \frac{dg_{0k}}{dz} = G_{xz}^{k+1} \frac{dg_{0k+1}}{dz} \quad \text{for } z = z_k$$

Is written

$$G_{xz}^\Phi \frac{dg_{0\Phi}}{dz} = G_{xz}^\Psi \frac{dg_{0\Psi}}{dz}$$

We thus obtain (dg_o/dz) in each ply, and from Equations 18.32b we deduce the shear stresses

$$\tau_{xz} = Q_x \frac{G_{xz}^k}{\langle hG_{xz} \rangle} \frac{dg_0}{dz} \Rightarrow \frac{\tau_{xz\Phi}}{\left(\frac{Q_x}{h}\right)} = \frac{hG_{xz}^\Phi}{\langle hG_{xz} \rangle} \frac{dg_{0\Phi}}{dz}; \quad \frac{\tau_{xz\Psi}}{\left(\frac{Q_x}{h}\right)} = \frac{hG_{xz}^\Psi}{\langle hG_{xz} \rangle} \frac{dg_{0\Psi}}{dz}$$

At the same time, Equation 18.33 gives the shear stress in the associated homogeneous orthotropic plate with same thickness and for a same transverse shear resultant:

$$\tau_{xz\text{orthotropic}} = \frac{Q_x}{h} \times \frac{3}{2} \left(1 - 4 \frac{z^2}{h^2} \right) \Rightarrow \frac{\tau_{xz\text{orthotropic}}}{\left(\frac{Q_x}{h}\right)} = \frac{3}{2} - 6 \frac{z^2}{h^2}$$

The two distributions are illustrated in Figure 18.6. It is immediately seen that for the D-D laminate, interlaminar shear stress due to the transverse shear resultant is everywhere less than or equal to the *maximum* shear stress in the associated orthotropic plate.

- **Note:** On the warping function $g_0(z)$

To obtain the previous shears, the differential equation

$$\frac{d^2 g_0}{dz^2} = -z \frac{\langle hG_{xz} \rangle}{G_{xz}^k} \left(\frac{\bar{E}_{11}^k}{EI_{11}} + \frac{\bar{E}_{12}^k}{EI_{12}} \right)$$

has been integrated for a first time. A new integration provides the warping function $g_0(z)$ in the form

$$g_0(z) = a_0 e + a_1 z + a_2 \frac{z^3}{h^2}$$

This antisymmetric function is given in Table 18.2 for $z \geq 0$

Knowledge of this function is necessary for the following. Also this function can be used to check the accuracy of the shear determination method. For this purpose, we integrate the shear stresses along the thickness h of the section shown in Figure 18.6. We then obtain (see Equation 18.32b):

$$\sum_{k=1\text{st ply}}^{k=n\text{th ply}} (\Delta Q_x)_{\text{ply } k} = \sum_{k=1\text{st ply}}^{k=n\text{th ply}} \left(\int_{\text{ply } k} \tau_{xz} dz \right) = Q_x \times \sum_{k=1\text{st ply}}^{k=n\text{th ply}} \left(\int_{\text{ply } k} \frac{G_{xz}^k}{\langle hG_{xz} \rangle} \frac{dg_0}{dz} dz \right)$$

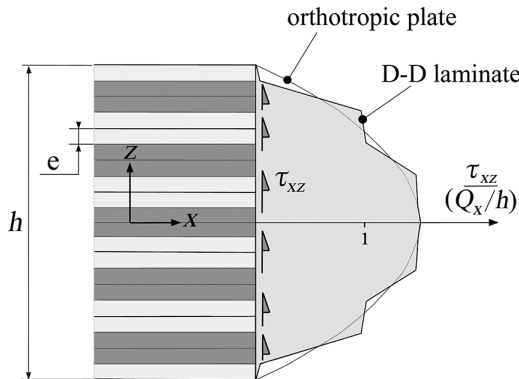


FIGURE 18.6 Shear stress τ_{xz} in D-D laminate and its associated orthotropic plate.

TABLE 18.2
Coefficients of the Warping Function $g_0(z)$

	z	a_0	a_1	a_2
$+\Phi = 0^\circ$	$[0 - e]$	0	1.243565	-3.210313
$\pm\Psi = 90^\circ$	$[e - 3e]$	-0.662739	1.898926	-0.259357
$\pm\Phi = 0^\circ$	$[3e - 5e]$	0.954688	1.426180	-3.210313
$\pm\Psi = 90^\circ$	$[5e - 7e]$	0.509469	1.330789	-0.259357
$\pm\Phi = 0^\circ$	$[7e - 9e]$	-1.462732	1.974024	-3.210313
$+\Psi = 90^\circ$	$[9e - 10e]$	9.174705	0.194518	-0.259357

It comes after calculation

$$\sum_{k=1st \text{ ply}}^{k=nth \text{ ply}} (\Delta Q_x)_{ply \ k} = Q_x \times (1 + 7E^{-6})$$

which gives an idea of the precision of this method.

18.8.2.5 Transverse Shear Coefficient

From Equation 18.32d

$$k_{x_{D-D}} = \sum_{k=1st \text{ ply}}^{k=nth \text{ ply}} \left\{ \left(\frac{\bar{E}_{11}^k}{EI_{11}} + \frac{\bar{E}_{12}^k}{EI_{12}} \right) \int_{ply \ k} g_{0_k} z \, dz \right\}$$

One obtains by means of the warping function $g_0(z)$ defined previously

$$k_{x_{D-D}} = 1,313 \quad (18.44)$$

Then, the transverse shear stiffness of the laminate and that of its associated orthotropic plate can be compared by means of the ratio (see Equation 18.42):

$$q_{(x,z)} = \frac{k_{x_{orthotropic}}}{k_{x_{D-D}}} = \frac{6}{5} \times \frac{1}{1.313} = 0.914 = 1 - 8.6\% \quad (18.45)$$

18.8.2.6 Warping of the Cross Section

The warping, i.e. the displacement of the initially plane section out of its plane as described in Figure 18.2 is given by $\eta_x(z)$ (see Equation 18.24):

$$\eta_x(z) = \frac{Q_x}{\langle hG_{xz} \rangle} \times g(z)$$

With (see Section 18.6.4.3)

$$g(z) = g_0(z) - z \times k_x$$

From where

$$\frac{\eta_x}{(Q_x/h)} = \frac{h}{\langle hG_{xz} \rangle} \times [g_0(z) - z \times k_x] \quad (18.46)$$

• **Note**

For the associated homogeneous orthotropic plate, we have (see Section 18.7.1)

$$\frac{\eta_{x\text{orthotropic}}}{(Q_x/h)} = \frac{h}{\langle hG_{xz} \rangle} \times \left[\frac{3}{2} z \left(1 - \frac{4}{3} \frac{z^2}{h^2} \right) - z \times \frac{6}{5} \right] = \frac{h}{\langle hG_{xz} \rangle} \times \left(0.3z - 2 \frac{z^3}{h^2} \right) \quad (18.47)$$

In Figure 18.7, we compare the warping of the laminated plate D-D with that of its associated homogeneous orthotropic plate with the same thickness h and subjected to the same transverse shear resultant Q_x (N/mm).

18.8.2.7 Bending in (y, z) Plane

By following the same procedure, one obtains for cylindrical bending in the (y, z) plane the results summarized in Figure 18.8

We find for this bending case the shear coefficient value

$$k_{y \text{ D-D}} = 1,238 \quad (18.48)$$

Leading to a shear stiffness ratio of the laminated plate compared to its equivalent orthotropic plate (see Equation 18.43)

$$q_{(y,z)} = \frac{k_{y\text{orthotropic}}}{k_{y \text{ D-D}}} = \frac{6}{5} \times \frac{1}{1,238} = 0.969 = 1 - 3\% \quad (18.49)$$

18.8.2.8 Increase in the Repetitions Number “ r ”

Figure 18.9 summarizes the results obtained for a number of repetitions $r = 9$ for shear stresses, warping and shear stiffness. We can see that the foreseeable evolutions are confirmed when the number of repetitions increases.

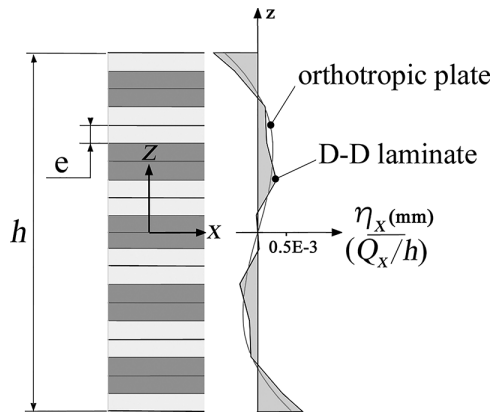


FIGURE 18.7 Warping of cross section (same thickness h and same transverse shear resultant Q_x (N/mm) for each plate).

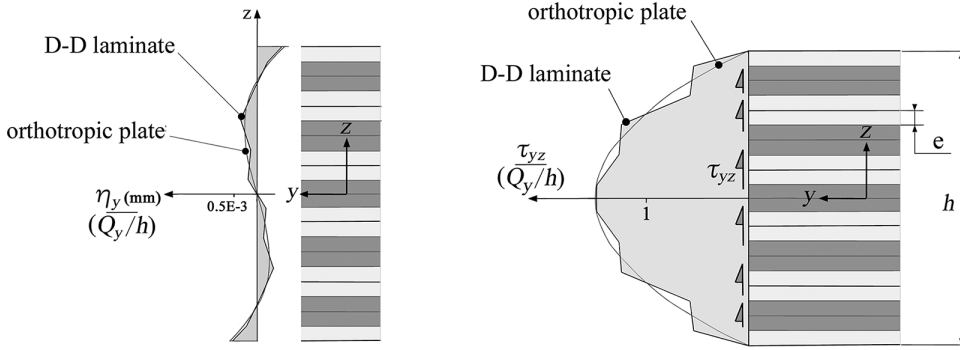


FIGURE 18.8 Shear stress τ_{yz} and warping of cross section for the D-D laminate and associated orthotropic plate.

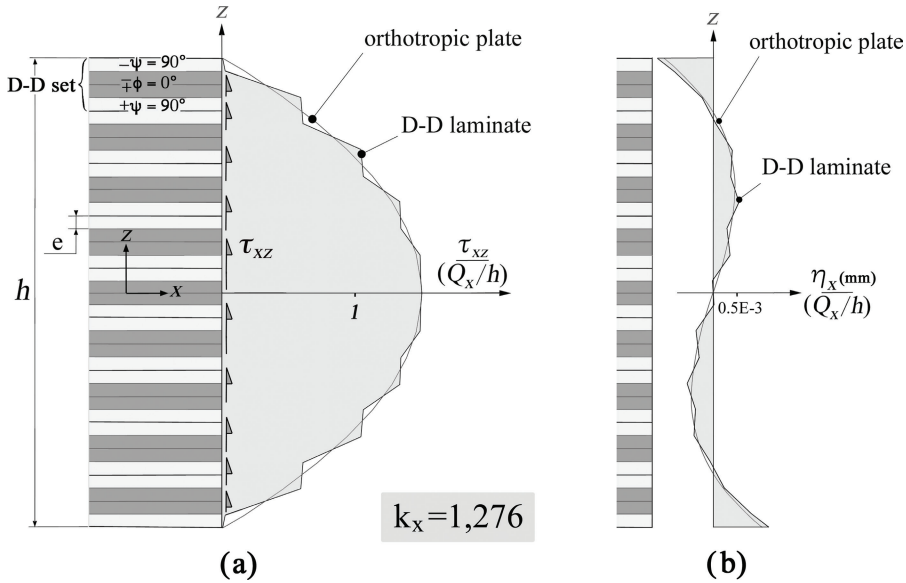


FIGURE 18.9 (a) Shear stress τ_{xz} in a D-D laminate with 9 D-D sets and (b) warping of cross section compared to associated orthotropic plate.

18.8.2.9 Conclusion

The results obtained for the D-D laminated plate are briefly summarized as follows:

- As the number of repetitions increases ($r \geq 5$), the shear distribution becomes similar to that observed in the orthotropic plate with same thickness and for a same transverse shear resultant, given by (see Equation 18.33)

$$\tau_{xz \text{ orthotropic}} = \frac{Q_x}{h} \times \frac{3}{2} \left(1 - 4 \frac{z^2}{h^2} \right); \quad \tau_{yz \text{ orthotropic}} = \frac{Q_y}{h} \times \frac{3}{2} \left(1 - 4 \frac{z^2}{h^2} \right)$$

It is notable that transverse and particularly interlaminar shear stress is everywhere lower than the maximum stress observed in the associated equivalent orthotropic plate.

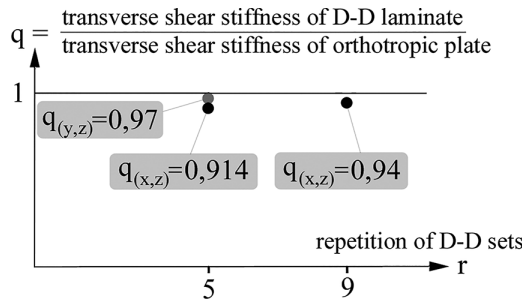


FIGURE 18.10 Comparison of transverse shear stiffness for the D-D laminate and associated orthotropic plate.

- Transverse shear stiffness (see Equations 18.42, 18.43) is similar to that of orthotropic plate one defined from the characteristics G_{xz}^Φ et G_{xz}^Ψ of the D-D laminate as

$$\frac{\langle hG_{xz} \rangle_{\text{orthotropic}}}{1.2}; \quad \frac{\langle hG_{yz} \rangle_{\text{orthotropic}}}{1.2}$$

With

$$\langle hG_{xz} \rangle_{\text{orthotropic}} = \frac{h}{2} (G_{xz}^\Phi + G_{xz}^\Psi); \quad \langle hG_{yz} \rangle_{\text{orthotropic}} = \frac{h}{2} (G_{yz}^\Phi + G_{yz}^\Psi)$$

This is found even for a low number of repetitions “ r ”, the laminated plate appearing slightly more shear-flexible as shown in Figure 18.10.

NOTES

- 1 Application 21.4 shows such a particularity for a sandwich beam.
- 2 Attention, one considers here the transverse shear stresses in smooth zone, not to be confused with the localized interlaminar shear stresses due to singularities (See Section 14.1.3 and Figure 14.3)
- 3 This is, for example, the case of
 - Laminates made of layers of balanced fabric at 0° and 90° or 45° and -45°
 - Unidirectional layers at 0° and 90°
 - Mats
- 4 Approximations that do not always appear clearly in the specialized literature.
- 5 Such a definition for the **average rotation** θ_y will be fundamental in the following to ensure the energy coherence of the transverse shear formulation (see Section 18.6.6).
- 6 Simplifications are due to antisymmetry of integrated functions (midplane symmetry).
- 7 This simplification is also used hereafter (see Section 18.6) and linked to the generalized Navier-Bernoulli principle (see footnote in Section 18.6). The existence of such approximation would not have arisen if the increments η_x , η_y , and η_z in Equation 18.3 had been overlooked *a priori*.
- 8 Such simplification constitutes here the extension to plates of the generalized Navier-Bernoulli principle for beams (see Section 16.1.5).
- 9 See Assumptions Section 18.1.3.
- 10 As g , g_0 is antisymmetric in z (see Equation 18.4).
- 11 See Equation 18.2.
- 12 See an example in Application 21.4.

Part IV

Applications

This section includes 45 examples of applications varied in terms of objectives and levels of difficulty. Moving away from too academic cases with a few exceptions, we have deliberately confined ourselves to practical applications and focused on the numerical aspect of the results. While a few cases are specifically tests for the use of numerical computational tools, almost all of the applications that follow can be used to validate modeling tools such as finite element software.



Taylor & Francis

Taylor & Francis Group

<http://taylorandfrancis.com>

19 Applications Level 1

19.1 SIMPLY SUPPORTED SANDWICH BEAM

Problem Statement

1. In Figure 19.1a, a beam made of aluminum is simply supported at both ends and subjected at midlength to a transverse force of $F = 50$ daN. Calculate the deflection of the beam, denoted as Δ , at the location of force F .
2. By cutting the aluminum beam by its horizontal midplane, we obtain two parts with equal thickness $e_p = 2.5$ mm (Figure 19.1b). Each half is bonded to a parallelepipedic core made of polyurethane foam, constituting the skin of a sandwich beam. In neglecting the mass of the foam and the glue, the latter has quite the same mass as the initial beam. The beam is resting on the same supports and subjected to the same load F . Calculate the deflection at midlength caused by F , denoted as Δ' . Compare with the Δ value found in Question 1. (Take the shear modulus of the foam to be $G_c = 20$ MPa.)

Solution

1. Using the classical formula that gives the deflection at the center of a simply supported beam with such loading,

$$\Delta = \frac{Fl^3}{48EI} \quad \text{with} \quad I = \frac{bh^3}{12}$$

For duralumin (see Section 1.6), $E = 75,000$ MPa. We find

$$\Delta = 16.7 \text{ mm}$$

2. Denoting by W the elastic energy due to flexure, we have, according to Section 4.2.2¹,

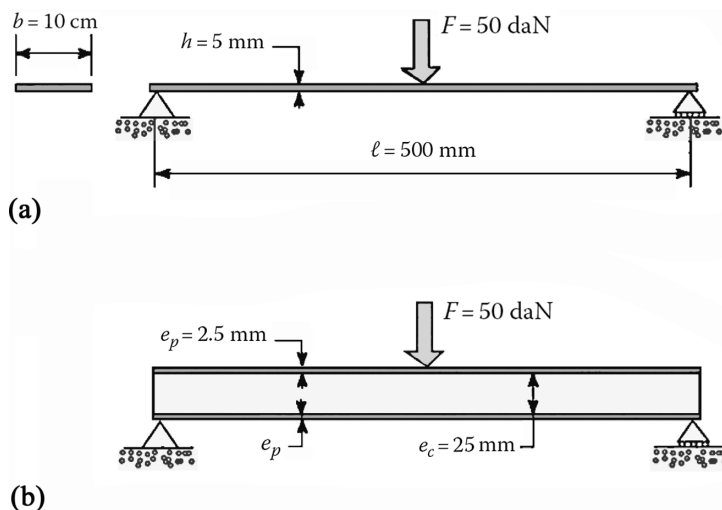


FIGURE 19.1 (a) Aluminum beam and (b) sandwich beam.

$$W = \int_{\text{beam}} \frac{1}{2} \frac{M^2}{\langle EI \rangle} dx + \int_{\text{beam}} \frac{1}{2} \frac{k}{\langle GS \rangle} T^2 dx$$

In the second integral above, we can use the following simple expression calculated hereafter in Application 20.1²:

$$\frac{k}{\langle GS \rangle} \approx \frac{1}{G_c (e_c + 2e_p) \times b}$$

Using the Castigliano theorem gives

$$\Delta' = \frac{\partial W}{\partial F}$$

Then,

$$\Delta' = \int_{\text{beam}} \frac{M}{\langle EI \rangle} \frac{dM}{dF} dx + \int_{\text{beam}} \frac{1}{2} \frac{k}{\langle GS \rangle} T \frac{dT}{dF} dx$$

with

$$0 \leq x \leq \frac{\ell}{2}: M = \frac{F}{2} \times x; T = -\frac{F}{2}$$

$$\frac{\ell}{2} \leq x \leq \ell: M = \frac{F}{2} (\ell - x); T = \frac{F}{2}$$

$$\Delta' = \frac{1}{\langle EI \rangle} \left\{ \int_0^{\ell/2} \frac{Fx}{2} \times \frac{x}{2} dx + \int_{\ell/2}^{\ell} \frac{F}{2} (\ell - x) \frac{(\ell - x)}{2} dx \right\} + \frac{k}{\langle GS \rangle} \left\{ \int_0^{\ell/2} -\frac{F}{2} \times -\frac{dx}{2} + \int_{\ell/2}^{\ell} \frac{F}{2} \times \frac{dx}{2} \right\}$$

$$\Delta' = \frac{F\ell^3}{48\langle EI \rangle} + \frac{F\ell}{4} \frac{k}{\langle GS \rangle}$$

- Approximate calculation

$$\langle EI \rangle \approx E_p \times e_p \times b \times \frac{(e_c + e_p)^2}{2} + E_c \times \frac{e_c^3 b}{12}$$

Then,

$$\langle EI \rangle = 7,090 \text{ MKS} + 7.8 \text{ MKS (negligible)} \text{ with } E_c = 60 \text{ MPa (see Section 1.6)}$$

We obtain for Δ' the following:

$$\Delta' = \underbrace{0.18 \text{ mm}}_{\text{bending moment}} + \underbrace{1.04 \text{ mm}}_{\text{shear resultant}}$$

$$\Delta' = 1.22 \text{ mm}$$

Comparing with the deflection Δ found in Question 1,

$$\frac{\Delta}{\Delta'} = \frac{14}{1}$$

Notes

- The sandwich configuration has allowed to divide the deflection by 14, without significant mass increase: with an adhesive film thickness of 0.2 mm and a specific mass of 40 kg/m³ for the foam, we obtain a total mass of the sandwich:

$$m = 700 \text{ g (duralumin)} + 50 \text{ g (foam)} + 48 \text{ g (adhesive)}$$

This corresponds to a mass increase of 14% with respect to the homogeneous full beam in Question 1.

- The deflection due to shear resultant T is close to six times more important than that due to the bending moment M only. It should be noted that in the case of the classical beam in Question 1, this term is negligible. This is because we have $k=1.2$ for a homogeneous beam of rectangular section. And thus,

$$\frac{k}{GS} = 8.27 \times 10^{-8}$$

- With $G=29,000$ MPa (see Section 1.6), the contribution to deflection Δ of the shear resultant in Question 1 is reduced to

$$\int \frac{k}{GS} T \frac{dT}{dF} dx = 0.002 \text{ mm} \ll \Delta$$

19.2 POISSON COEFFICIENT OF A UNIDIRECTIONAL LAYER

Problem Statement

Consider a unidirectional layer with thickness e as shown schematically in Figure 19.2. E_ℓ (longitudinal direction) and E_t (transverse direction) denote the moduli of elasticity.

Show that two distinct Poisson coefficients $\nu_{\ell t}$ and $\nu_{t\ell}$ are necessary to characterize the elastic behavior of this unidirectional layer in its plane (ℓ , t).

Numerical application: The layer is of glass/epoxy with fiber volume fraction $V_f = 60\%$.

Solution

Two types of loading acting successively will be considered:

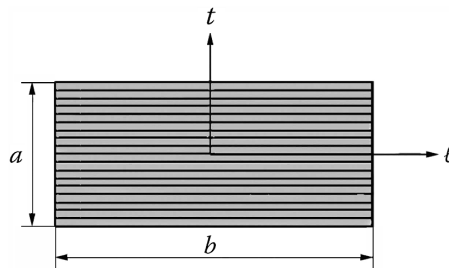


FIGURE 19.2 Unidirectional layer.

1. A uniform stress σ_ℓ along the ℓ direction: The change in length of sides a and b can then be written as

$$\frac{\Delta b_1}{b} = \frac{\sigma_\ell}{E_\ell}; \quad \frac{\Delta a_1}{a} = -\frac{\nu_{\ell t}}{E_\ell} \sigma_\ell$$

2. A uniform stress σ_t along the t direction: For a relatively important elongation of the resin, we should observe a weak shortening of fibers along ℓ . Therefore, we use another notation for the Poisson coefficient. The change in length can be written as

$$\frac{\Delta b_2}{b} = -\frac{\nu_{t\ell}}{E_t} \sigma_t; \quad \frac{\Delta a_2}{a} = \frac{\sigma_t}{E_t}$$

Now let us calculate the elastic energy stored under the cumulated loads above, by considering two successive loading orders:

- i. σ_ℓ is applied first, and then σ_t is applied:

$$W = \frac{1}{2} \sigma_\ell \times a \times e \times \Delta b_1 + \frac{1}{2} \sigma_t \times b \times e \times \Delta a_2 + \sigma_\ell \times a \times e \times \Delta b_2$$

- ii. σ_t is applied first, and then σ_ℓ is applied:

$$W' = \frac{1}{2} \sigma_t \times b \times e \times \Delta a_2 + \frac{1}{2} \sigma_\ell \times a \times e \times \Delta b_1 + \sigma_t \times b \times e \times \Delta a_1$$

The final energies are the same:

$$W = W'$$

Thus,

$$\sigma_\ell \times a \times e \times \Delta b_2 = \sigma_t \times b \times e \times \Delta a_1$$

With the values obtained for Δb_2 and Δa_1 ,

$$\sigma_\ell \times a \times e \times -\frac{\nu_{t\ell}}{E_t} \sigma_t \times b = \sigma_t \times b \times e \times -\frac{\nu_{\ell t}}{E_\ell} \sigma_\ell \times a$$

$$\frac{\nu_{t\ell}}{E_t} = \frac{\nu_{\ell t}}{E_\ell}$$

Numerical application: $\nu_{\ell t} = 0.3$; $E_\ell = 45,000$ MPa; $E_t = 12,000$ MPa (see Section 3.3.3):

$$\nu_{t\ell} = 0.3 \times \frac{12,000}{45,000}$$

$$\nu_{t\ell} = 0.08$$

Note: The same reasoning applies to all balanced laminates, based on axes of mechanical symmetry³. However, depending on the composition of the considered laminate, the Poisson coefficients in the two perpendicular directions may vary in more important ranges:

- In absolute value
- One with respect to the other

It may be noted in Chapter 5, Chart 5.14, the variation range of the global Poisson coefficient ν_{xy} for a Quad glass/epoxy laminate, from which we can deduce the Poisson coefficient ν_{yx} using a formula analogous to the aforementioned one, namely,

$$\frac{\nu_{yx}}{E_y} = \frac{\nu_{xy}}{E_x}$$

19.3 HELICOPTER BLADE

The following study aims to highlight some important features related to the operation of a helicopter blade and particularly the sizing due to centrifugal loading.

Problem Statement

Consider a helicopter blade attached to the rotor hub as shown schematically in Figure 19.3.

The rotor characteristics are as follows:

- Three blades; rotational speed, 500rpm.
- The mass per unit length of a blade at first approximation is assumed to have a constant value of 3.5 kg/m.
- $\ell = 5$ m; $c = 0.3$ m.
- The elementary lift for a blade element dx (see Figure 19.3) is written as

$$dF_2 = \frac{1}{2} \rho (c \times dx) C_z \times V^2$$

In which V is the relative velocity of air with respect to the blade profile. In addition,

- Lift coefficient: $C_z (7^\circ) = 0.35$
- Air density in normal conditions: $\rho = 1.3 \text{ kg/m}^3$

We will not take into account here the drag and its consequences. The helicopter is assumed immobile with respect to the ground (stationary flight in immobile air). If we neglect the blade weight compared with the applied load, and assuming an infinite flexural rigidity, the relative equilibrium configuration in uniform rotation is shown schematically in Figure 19.4:

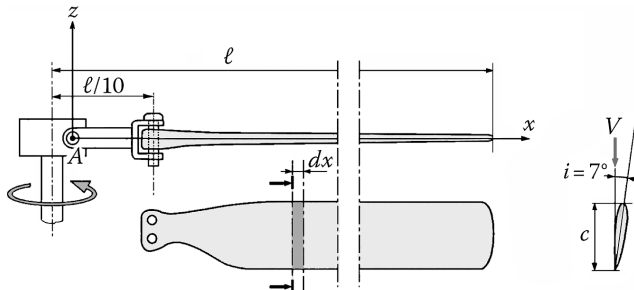


FIGURE 19.3 Helicopter blade.

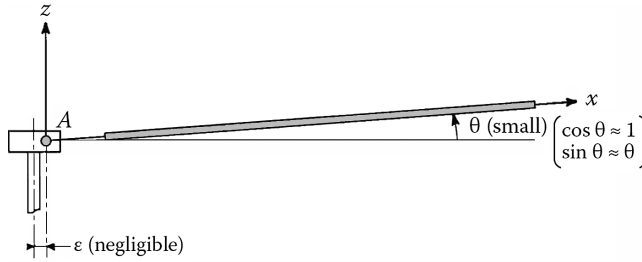


FIGURE 19.4 Relative equilibrium.

1. Justify the presence of the **blade flapping angle** θ and calculate it.
2. Calculate the helicopter weight.
3. Calculate the normal resultant on any cross section of the blade and at the blade root (attachment area).

The spar of the blade⁴ is made of unidirectional glass/epoxy with 60% fiber volume fraction, with “R” glass ($\sigma_{\ell \text{ rupture}} \approx 1,700 \text{ MPa}$). The safety factor is 6. Calculate the following characteristics:

4. Longitudinal modulus of elasticity E_{ℓ} of the unidirectional.
5. Cross-sectional area of the spar for any x value and at the blade root.
6. Total mass of the spar for the whole blade.
7. Elongation of the blade, assuming that only the spar supports the normal loading.
8. Dimensions of the two axes to clamp the blade onto the rotor hub. An alloy steel 30NCD16 has been selected (shear failure strength $\tau_{\text{rupture}} = 500 \text{ MPa}$; bearing strength $\sigma_{\text{bearing}} = 1,600 \text{ MPa}$). Represent the blade attachment on a scheme.

Solution

1. Considering the relative equilibrium of the blade, the latter is subjected to two load distributions:
 - Distributed loads due to driving motion, or centrifugal action. They are radial, meaning that they are in horizontal planes in Figure 19.4, with supports that cut the rotor axis.
 - Distributed loads due to lift, perpendicular to the direction of the blade that is Ax direction in Figure 19.4.

This explains the intermediate equilibrium position characterized by angle θ .

The joint in A does not transmit any couple. Thus, the moment of forces acting on the blade about the y -axis perpendicular to the figure is nil:

$$\int_{\ell/10}^{\ell} dF_z \times x = \int_{\ell/10}^{\ell} dF_c \times x \sin \theta \approx \theta \times \int_{\ell/10}^{\ell} dF_c \times x$$

with

$$dF_z = \frac{1}{2} \times \rho c \, dx C_z \times V^2 = \frac{1}{2} \times \rho c \, dx C_z \times (x \cos \theta \times \omega)^2 \approx \frac{1}{2} \times \rho c \, dx C_z x^2 \omega^2$$

$$dF_c = dm \times \omega^2 x \cos \theta \approx m \times dx \times \omega^2 x \text{ (centrifugal force)}$$

After calculation,

$$\frac{1}{2} \times \rho c C_z \omega^2 \frac{(\ell^4 - \ell^4/10^4)}{4} = \theta m \omega^2 \frac{(\ell^3 - \ell^3/10^3)}{3}$$

$$\theta \approx \frac{3}{8} \frac{\rho c C_z}{m} \times \ell$$

And numerically,

$$\theta = 0.073 \text{ rad} = 4^\circ 11'$$

Notes

- We can verify that $\sin \theta = 0.073 \approx \theta$ and $\cos \theta = 0.997 \approx 1$.
- When the helicopter is no longer immobile but has a horizontal velocity v_0 , the relative velocity of air with respect to the blade varies between $(v_0 + \omega x)$ for the blade that is forward and $(-v_0 + \omega x)$ for a blade that is backward. If the incidence i do not vary, then the lift varies in a cyclical manner, causing a vertical **flapping motion** of the blade. This is why a mechanism for cyclic variation of the incidence is necessary.
- We have not taken account of the drag, in view of simplifying the calculations. The latter can be considered similarly to the case of the lift. It then gives rise to a modified equilibrium position revealing a second small angle, called ϕ , with respect to the radial direction from top view, as represented in Figure 19.5. This is why a supplementary joint, or **drag joint**, is necessary.

2. Weight of the helicopter: The lift and weight balance themselves out. The lift of the blade is

$$F_z = \int_{\ell/10}^{\ell} dF_z \cos \theta \approx \int_{\ell/10}^{\ell} dF_z = \frac{1}{2} \times \rho c C_z \omega^2 \frac{(\ell^3 - \ell^3/10^3)}{3}$$

For the three rotor blades,

$$Mg = 3F_z$$

$$Mg \approx \frac{1}{2} \times \rho c C_z \omega^2 \ell^3$$

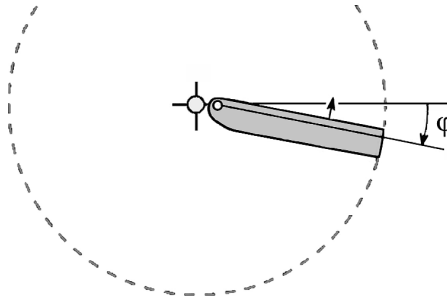


FIGURE 19.5 Drag angle.

Numerically,

$$Mg = 2,340 \text{ daN}$$

3. Normal resultant: It is denoted as $N(x)$ for any cross section with x -abscissa:

$$N(x) = \int_x^\ell dF_c \cos \theta \approx \int_x^\ell dF_c = \int_x^\ell m\omega^2 x \, dx$$

$$N(x) = \frac{m\omega^2}{2} (\ell^2 - x^2)$$

At the blade root ($x = \ell/10$),

$$N(\ell/10) \approx 12,000 \text{ daN}$$

4. Longitudinal modulus of elasticity:

Using the relationship of Section 3.3.1,

$$E_\ell = E_f V_f + E_m V_m$$

with (Section 1.6) $E_f = 86,000 \text{ MPa}$ and $E_m = 4,000 \text{ MPa}$

$$E_\ell = 53,200 \text{ MPa}$$

5. Cross-sectional area of the glass/epoxy spar:

The value of longitudinal tensile failure strength of the unidirectional is given as

$$\sigma_{\ell \text{ rupture}} \approx 1,700 \text{ MPa}$$

With a safety factor of 6, the allowable stress on a section $S(x)$ becomes

$$\sigma = \frac{N(x)}{S(x)} = \frac{1,700}{6} = 283 \text{ MPa}$$

Then,

$$S(x) = \frac{N(x)}{\sigma}$$

$$S(x) = \frac{m\omega^2}{2\sigma} (\ell^2 - x^2)$$

At the blade root,

$$S(\ell/10) = 4.24 \text{ cm}^2$$

6. Mass of the whole spar:

$$m_{\text{spar}} = \int_{\ell/10}^{\ell} \rho_{\text{unidirect.}} S(x) dx$$

$$m_{\text{spar}} = \rho_{\text{unidirect.}} \times \frac{m\omega^2}{\sigma} \times \frac{1.7}{6} \ell^3$$

Specific mass value of unidirectional (see Section 3.2.3):

$$\rho_{\text{unidirect.}} = V_f \rho_f + V_m \rho_m = 1,980 \text{ kg/m}^3$$

Then,

$$m_{\text{spar}} = 2.38 \text{ kg}$$

7. Elongation of the blade spar: The constitutive relationship corresponding to longitudinal behavior is (see Section 3.1)

$$\epsilon_x = \frac{\sigma_x}{E_x} = \frac{N(x)}{E_\ell \times S(x)} = \frac{\sigma}{E_\ell}$$

Elongation of a spar element with length dx : $\epsilon_x(x) \times dx$.

For the whole spar,

$$\Delta\ell = \int_{\ell/10}^{\ell} \epsilon_x dx$$

$$\Delta\ell = 0.9 \frac{\ell \times \sigma}{E_\ell}$$

Then,

$$\Delta\ell = 2.4 \text{ cm}$$

The spar should be reinforced to decrease the elongation rather than to withstand the centrifugal force.

8. Fixing pins: Two 30 NCD16 steel axles with shear failure strength $\tau_{\text{rupture}} = 500 \text{ MPa}$ and bearing strength $\sigma_{\text{bearing}} = 1,600 \text{ MPa}$.

With two sheared sections for *each* pin and a safety factor of 6,

- Diameter:

$$\frac{N\left(\frac{\ell}{10}\right)}{\pi \times \phi^2} \leq \frac{\tau_{\text{rupture}}}{6} \Rightarrow \phi \geq 21.4 \text{ mm}$$

- Length:

$$\frac{N\left(\frac{\ell}{10}\right)}{2h \times \phi} \leq \frac{\sigma_{\text{bearing}}}{6} \Rightarrow h \geq 10.5 \text{ mm}$$

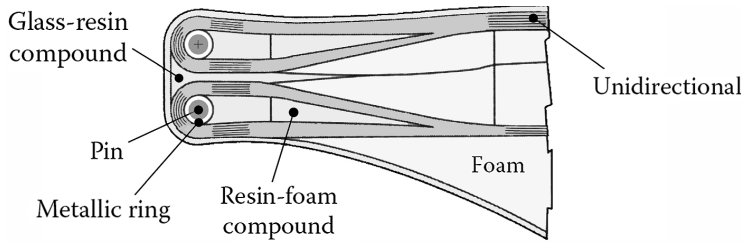


FIGURE 19.6 Blade attachment.

Blade attachment is represented in Figure 19.6.

19.4 DRIVE SHAFT FOR TRUCKS

Problem Statement

The purpose is to replace the classical drive shaft equipped with universal joint and center bearing as shown Figure 19.7a with a single carbon/epoxy shaft and with the measurements noted Figure 19.7b.

The characteristics of the drive shaft are as follows:

- Carbon/epoxy unidirectional: $V_f = 60\%$ fiber volume fraction; thickness of a cured ply, 0.125 mm
- Maximum torsion torque: $M_t = 300 \text{ m} \times \text{daN}$
- Maximum rotation speed: $N = 4,000 \text{ rpm}$

Recall: The first flexural natural frequency of a simply supported beam is given by

$$f_1 = \frac{\pi}{2} \sqrt{\frac{EI}{mL^3}}$$

where m is the mass of the beam and I is the moment of inertia for flexure.

It corresponds to a **critical rotation speed** for the rotating shaft, which should not be reached during actual use:

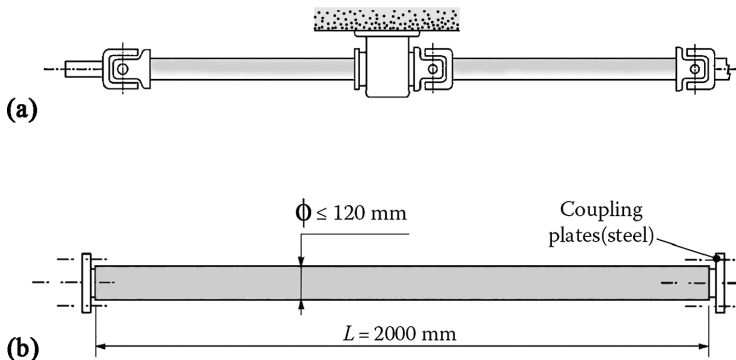


FIGURE 19.7 (a) Classical shaft and (b) carbon/epoxy shaft.

1. Give the characteristics of a suitable composite shaft in carbon/epoxy. Charts in Section 5.4.2 should be used, associated with a safety factor of 6.
2. Bonded fitting of the coupling plates to the shaft will be examined.
3. Carry out an assessment of the weight gain with respect to the **steel shaft** solution (not including the coupling plates).

Solution

1. Characteristics of the shaft:

- **The hollow shaft is assumed to be thin** (small thickness e compared to the average radius r as in Figure 19.8).

The shear stress τ is as follows (see Section 5.4.5.4 and Figure 5.31):

$$\tau = \frac{M_t}{2\pi r^2 e}$$

Taking into account the nature of the loading on the tube (pure shear), the composition of the latter requires

- An important percentage of unidirectional in the directions of $\pm 45^\circ$ (see Section 5.2.2)
- A minimum percentage in the order of 10% in other directions (see Section 5.2.3.6)

This leads, for example, to the distribution in Figure 19.9:

In Section 5.4, Chart 5.3 will be consulted, which gives the maximum shear stress that can be applied to a laminate subject to pure shear, as a function of ply proportions at 0° , 90° , $+45^\circ$, -45° . For these proportions, we can read

$$\tau_{\max} = 327 \text{ MPa}$$

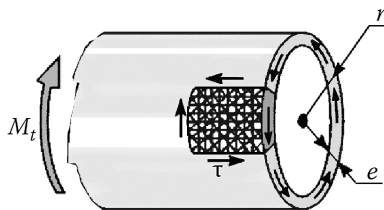


FIGURE 19.8 Thin hollow shaft.

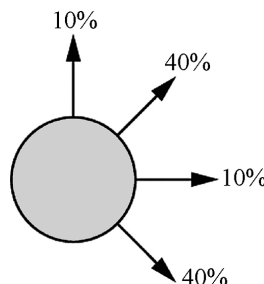


FIGURE 19.9 Proportions.

From which the allowable value, after taking into account a safety factor of 6, is as follows:

$$\tau_{\text{admis.}} = \frac{327}{6} \text{ MPa}$$

We must respect that

$$\frac{M_t}{2\pi r^2 e} \leq \tau_{\text{admis.}}$$

Or numerically,

$$r^2 e \geq 8,760 \text{ mm}^3$$

For the specified radius $r = 60 \text{ mm}$, seen as an average radius, we obtain

$$e \geq 2.43 \text{ mm}$$

And the corresponding number of plies of carbon/epoxy is

$$\frac{2.43}{0.125} \approx 20 \text{ plies}$$

With the corresponding thickness,

$$e = 2.5 \text{ mm}$$

Then, we can verify (see Figure 19.10) that a number of 20 plies can meet

- a. The required proportions
- b. The midplane symmetry, with the sequence

$$\left[90^\circ / 0^\circ / \pm 45^\circ_4 \right]_s$$

- **Critical speed of such a shaft:**

$$f_1 = \frac{\pi}{2} \sqrt{\frac{EI}{mL^3}}$$

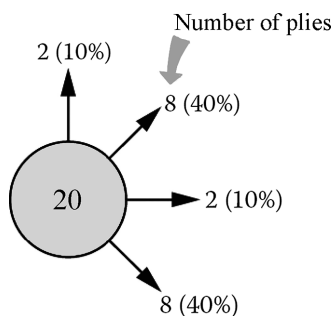


FIGURE 19.10 Composition of the laminate.

- Chart 5.4 in Section 5.4.2 gives the longitudinal modulus E of the laminate in the direction of the shaft:

$$E = 31,979 \text{ MPa}$$

- The specific density of the laminate is (see Section 3.2.3)

$$\rho_{\text{lam}} = V_f \times \rho_f + V_m \times \rho_m$$

with (Section 1.6) $\rho_f = 1,750 \text{ kg/m}^3$ and $\rho_m = 1,200 \text{ kg/m}^3$.

Then, $\rho_{\text{lam}} = 1,530 \text{ kg/m}^3$ (or more directly in Section 3.3.3, Table 3.4).

The moment of inertia of the cross section is $I = \pi r^3 \times e$ from which the first flexure vibration frequency is $f_1 = 76 \text{ Hz}$. It corresponds to a critical speed of 4,562 rpm, higher than the maximum shaft speed⁵.

2. Bonded fitting of coupling plates: We will use the relationship of Section 6.2.3, Figure 6.26, for the sake of simplicity. This implies identical thicknesses for the tube making up the shaft and that of the coupling plate made of steel⁶. The maximum shear stress then has an order of magnitude of

$$\tau_{\text{max}} = \frac{a}{\tanh a} \times \tau_{\text{average}} = \frac{a}{\tanh a} \times \frac{M_t}{2\pi r^2 \ell}$$

where ℓ is the bond length, and

$$a = \ell \sqrt{\frac{G_c}{2Gee_c}}$$

with G_c as the shear modulus of araldite (see Section 1.6): $G_c = 1,700 \text{ MPa}$

$G_{\text{laminate}} = 28,430 \text{ MPa}$ (see Section 5.4.2, Chart 5.5); e_c is the adhesive layer thickness (see Section 6.2.3: $e_c \approx 0.2 \text{ mm}$)

- Thickness within bonding area:
Keeping the thickness found for the tube, as $e = 2.5 \text{ mm}$, we obtain

$$a = \ell \times 244.5$$

The failure criterion can then be written as

$$\tau_{\text{max}} \leq \tau_{\text{rupture}} = 15 \text{ MPa for araldite (see Section 6.2.3)}$$

Then,

$$\frac{a}{\tanh a} \times \frac{M_t}{2\pi r^2 \ell} \leq \tau_{\text{rupture}}$$

or

$$\frac{244.5}{\tanh a} \times \frac{M_t}{2\pi r^2} \leq \tau_{\text{rupture}}$$

Numerically, $\tanh a \geq 2.16 \rightarrow \text{impossible since } \tanh x \in]-1; +1[.$

It is then necessary to augment the thickness of the tube at the bond location. For this purpose, we start from the relation

$$\frac{a}{\tanh a} \times \frac{M_t}{2\pi r^2 \ell} \leq \tau_{\text{rupture}}$$

Placed in the form

$$\frac{\sqrt{\frac{G_c}{2Gee_c}}}{(1-\varepsilon)} \times \frac{M_t}{2\pi r^2} \leq \tau_{\text{rupture}} \quad \text{with } \varepsilon \ll 1$$

Then,

$$\sqrt{\frac{G_c}{2Gee_c}} \leq \tau_{\text{rupture}} \times \frac{2\pi r^2}{M_t} \times (1-\varepsilon)$$

We find numerically the following:

$$e > 11.7 \text{ mm.}$$

We retain

$$e = 12 \text{ mm (then we have } \tanh a = (1-\varepsilon) = 0.987)$$

- Bonded length:

In accordance with Section 6.2.3, the resistance condition is written as

$$\tau_{\text{average}} = \frac{M_t}{2\pi r^2 \ell} \leq 0.2 \times \tau_{\text{rupture}}$$

Then,

$$\ell \geq 44 \text{ mm}$$

The bonded fitting of the coupling plate is shown in Figure 19.11.

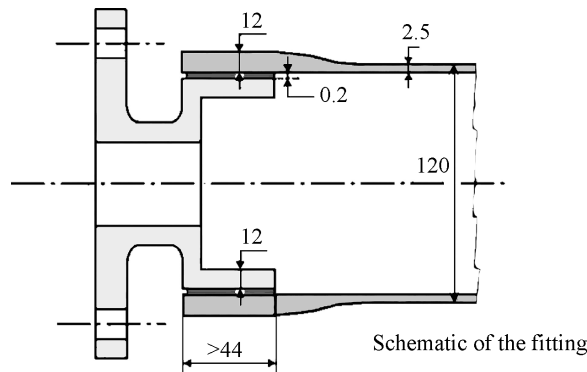


FIGURE 19.11 Assembly of the coupling plate.

3. Mass balance:

- The mass of carbon/epoxy shaft is

$$m_{\text{laminare}} = \rho \times 2\pi r e \times L$$

with numerical values already mentioned,

$$m_{\text{laminare}} = 2.8 \text{ kg.}$$

- If we consider a tubular shaft made of steel ($\tau_{\text{rupture}} = 300 \text{ MPa}$) with a safety factor that is 2 times less, say 3, and a minimum thickness of 2.5 mm, the resistance condition

$$\frac{M_t}{2\pi r^2 e} \leq \frac{300}{3} \text{ MPa}$$

leads to a radius for the tube of

$$r \geq 43 \text{ mm.}$$

From this and with $\rho_{\text{steel}} = 7,800 \text{ kg/m}^3$, we find a mass of

$$m_{\text{steel}} = 10.5 \text{ kg}$$

The saving in mass of the composite solution over the steel solution is 73%. The real saving is higher because it takes into account the disappearance of the intermediate bearing and of a part of the universal joint.

19.5 FLYWHEEL IN CARBON/EPOXY

Problem Statement

We show schematically, in Figure 19.12, a carbon/epoxy flywheel with 60% fiber volume fraction and indicated proportions for fiber orientation.

- Calculate the maximum kinetic energy that can be obtained with a mass of 1 kg of such a flywheel.
- Compare with the maximum kinetic energy that can be obtained with a mass of 1 kg of a steel flywheel ($\sigma_{\text{rupture steel}} = 1,000 \text{ MPa}$).

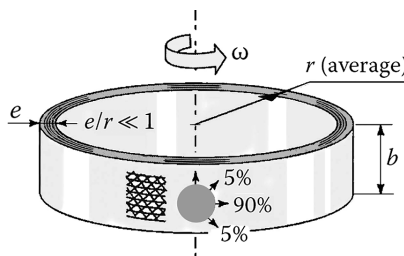


FIGURE 19.12 Carbon/epoxy flywheel.

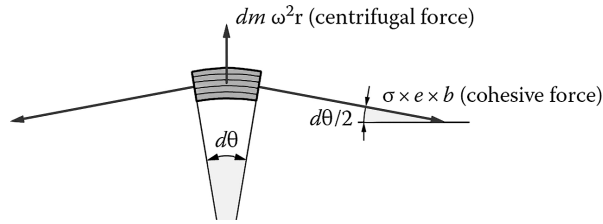


FIGURE 19.13 Equilibrium of a wheel element.

Solution

1. The equilibrium of a wheel element as outlined in Figure 19.13 illustrates clearly the roles of inertia forces and cohesive forces.

We deduce from there the equilibrium equation along the radial direction:

$$dm \times \omega^2 r = 2\sigma \times eb \times \frac{d\theta}{2}$$

Denoting by ρ the specific mass,

$$\rho r \times d\theta \times eb \times \omega^2 r = \sigma \times eb \times d\theta$$

$$\rho(r\omega)^2 = \sigma$$

Denoting by $V = r\omega$ the circumferential speed, the latter reaches its maximum for the rupture strength of carbon/epoxy, as

$$V_{\max} = \sqrt{\frac{\sigma_{\text{rupture}}}{\rho}}$$

- *Numerical application:* With composition of carbon/epoxy laminate indicated above, we read in Section 5.4.2, Chart 5.1, the following:

$$\sigma_{\text{rupture}} = 1,059 \text{ MPa}$$

and with $\rho = 1,530 \text{ kg/m}^3$ (Table 3.4 of Section 3.3.3, or calculation in Section 3.2.3),

$$V_{\max} = 832 \text{ m/s}$$

From this, the maximum kinetic energy obtained with 1 kg of composite⁷ is

$$W_{\text{kinetic}} = \frac{1}{2} \times 1 \text{ kg} \times V_{\max}^2$$

Then,

$$W_{\text{kinetic}} = 346 \text{ kJ}$$

2. The maximum possible circumferential speed with a steel flywheel can be written as

$$V_{\max, \text{steel}} = \sqrt{\frac{\sigma_{\text{rupture steel}}}{\rho_{\text{steel}}}}$$

Therefore, the ratio of kinetic energies **composite/steel** is

$$\frac{W_{\text{kinetic carbon}}}{W_{\text{kinetic steel}}} = \frac{V_{\max \text{ carbon}}^2}{V_{\max \text{ steel}}^2} = \frac{\sigma_{\text{rupture carbon}} \times \rho_{\text{steel}}}{\sigma_{\text{rupture steel}} \times \rho_{\text{carbon}}}$$

with $\rho_{\text{steel}} = 7,800 \text{ kg/m}^3$ and $\sigma_{\text{rupture steel}} = 1,000 \text{ MPa}$, we obtain

$$\frac{W_{\text{kinetic carbon}}}{W_{\text{kinetic steel}}} = 5.4$$

With respect to the same mass, it appears that it is possible to accumulate five times more kinetic energy with a carbon/epoxy flywheel than with a steel flywheel.

19.6 WING TIP MADE OF CARBON/EPOXY

Problem Statement

A wing tip refers to a part of an airplane wing as shown in Figure 19.14.

It is made of a sandwich structure with carbon/epoxy skins (Figure 19.15) fixed to the rest of the wing by titanium borders as shown.

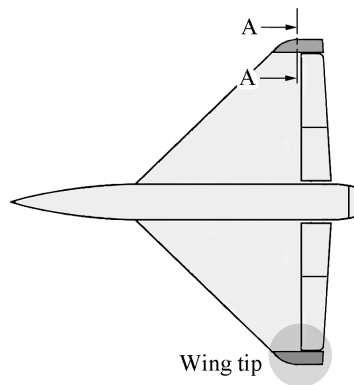


FIGURE 19.14 Location of wing tip.

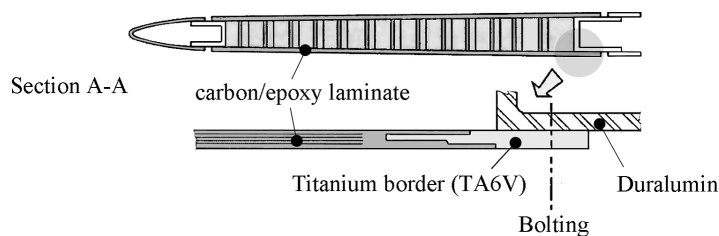


FIGURE 19.15 Section A-A: design of the wing tip.

Under aerodynamic forces (Figure 19.16), the wing tip is subjected to bending moments, twisting moments, and shear resultants (forces per unit length) as shown in Figure 19.17a.

It will be assumed that the sandwich core transmits only shear forces, while skins support the moments. This is represented in Figure 19.17b. In their respective planes, the skins withstand the In-plane resultants N_x , N_y , and T_{xy} . Figure 19.18 shows some values of these stress resultants at a few points of the upper skin.

1. According to Figure 19.17a and b, deduce literal writing of the stress resultants N_x , N_y , and T_{xy} from the knowledge of bending and twisting moments M_x , M_y , and M_{xy} .
2. Using a safety factor of 2, define the carbon/epoxy skin that is suitable in the vicinity of the border made of titanium alloy (proportions, thickness, and number of plies). This will be done using unidirectional plies with $V_f = 60\%$ fiber volume fraction.
3. The skin is bonded on the titanium border (Figure 19.15). Provide the dimensions of the bonded interface by using an average allowable shear stress in the adhesive (epoxy: $\tau_{\text{rupture}} = 30 \text{ MPa}$).
4. The titanium border is bolted to the rest of the wing (Figure 19.2). Determine the dimensional characteristics of the junction, **pitch** of bolting, thickness of the border, and edge distance, with the following data:
 - Bolts, steel, 30 NCD16: $\varnothing = 6.35 \text{ mm}$, tight fitting, with negligible clamping force.
 $\sigma_{\text{rupture}} = 1,100 \text{ MPa}$; $\tau_{\text{rupture}} = 660 \text{ MPa}$; $\sigma_{\text{bearing}} = 1,600 \text{ MPa}$.
 - Titanium alloy R56400 (TA6V):
 $\sigma_{\text{rupture}} = 900 \text{ MPa}$; $\tau_{\text{rupture}} = 450 \text{ MPa}$; $\sigma_{\text{bearing}} = 1,100 \text{ MPa}$.
 - Aluminum alloy A92024 (2024) duralumin:
 $\sigma_{\text{rupture}} = 420 \text{ MPa}$; $\sigma_{\text{bearing}} = 550 \text{ MPa}$

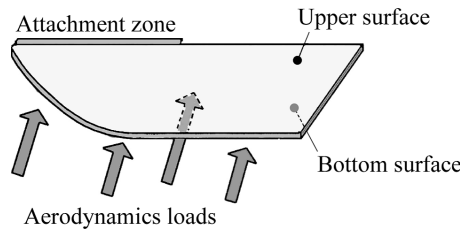


FIGURE 19.16 Aerodynamic loading.

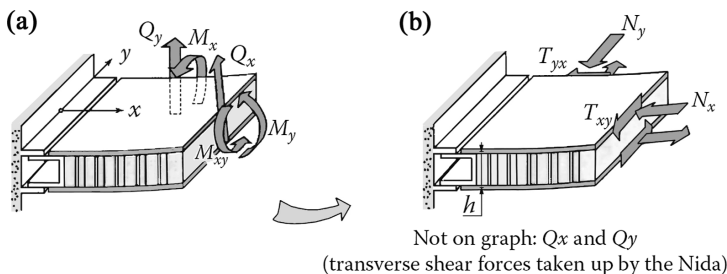


FIGURE 19.17 (a) Bending and twisting moments and (b) equivalent In-plane resultants in the skins.

Solution

1. The bending and twisting moments M_x , M_y , and M_{xy} (and M_{yx} not shown in Figure 19.17a) are taken up by the laminated skins. Thus, in the upper skin (Figure 19.17b), h being the mean distance between the two skins,

$$N_x = \frac{M_y}{h}; \quad N_y = -\frac{M_x}{h}; \quad T_{xy} = -\frac{M_{xy}}{h}$$

Note: The unit of measurement of bending and twisting moments, which are the moments per unit width of skin (1 mm in practice), is 1 daN \times mm / mm. The stress resultants N_x , N_y , and T_{xy} per unit width of skin have for unit of measurement 1 daN/mm.

2. Looking at the most loaded area of the skin in Figure 19.18, we can represent the principal directions and stresses by constructing Mohr's circle shown in Figure 19.19. Then we can note that there should be a nonnegligible proportion of $\pm 45^\circ$ fibers. However, the laminate should also be able to resist compression along the axes x and y . An estimation of proportions can be done following the method presented in Section 5.4.3. We then obtain the composition shown in Figure 19.19⁸:

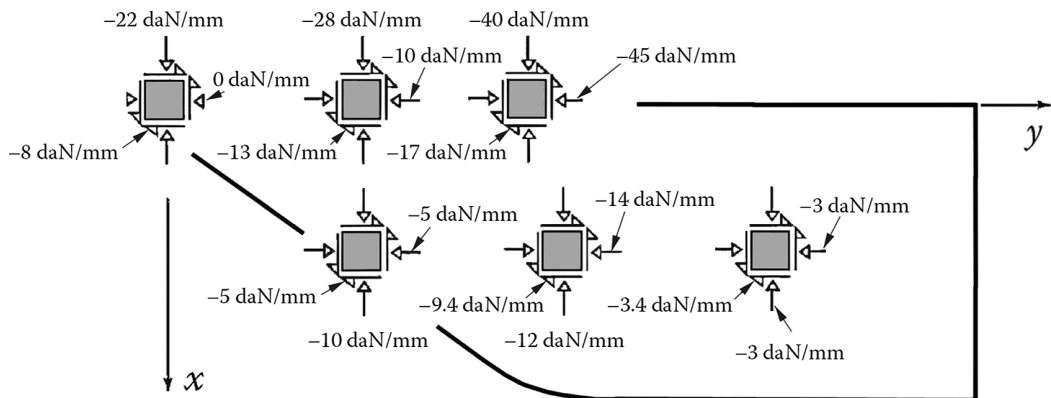


FIGURE 19.18 Some values of stress resultants.

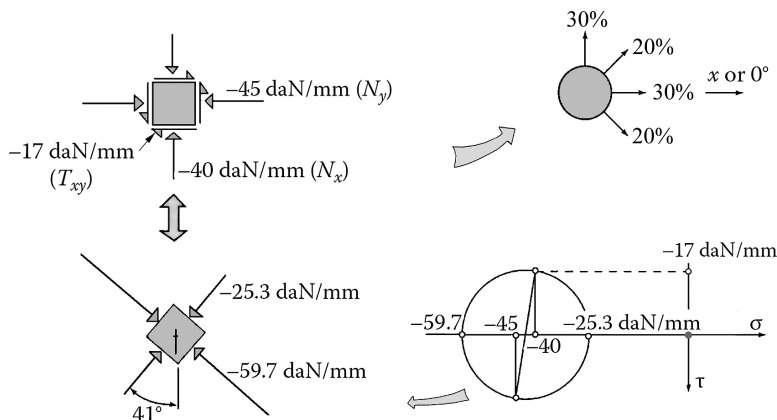


FIGURE 19.19 Most loaded area.

Let σ_ℓ , σ_t , and $\tau_{\ell t}$ be the stress values along the axes (ℓ , t) of one of the plies for the loading given above. The thickness e of the laminate (which is unknown *a priori*) is such that the limit of the Tsai-Hill failure criterion is reached⁹. Then we have

$$\frac{\sigma_\ell^2}{\sigma_{\ell \text{ rupture}}^2} + \frac{\sigma_t^2}{\sigma_{t \text{ rupture}}^2} - \frac{\sigma_\ell \sigma_t}{\sigma_{\ell \text{ rupture}}^2} + \frac{\tau_{\ell t}^2}{\tau_{\ell t \text{ rupture}}^2} = 1$$

If we multiply the two sides by the square of the thickness e ,

$$\frac{(\sigma_\ell \times e)^2}{\sigma_{\ell \text{ rupture}}^2} + \frac{(\sigma_t \times e)^2}{\sigma_{t \text{ rupture}}^2} - \frac{(\sigma_\ell \times e)(\sigma_t \times e)}{\sigma_{\ell \text{ rupture}}^2} + \frac{(\tau_{\ell t} \times e)^2}{\tau_{\ell t \text{ rupture}}^2} = e^2 \quad (19.1)$$

We should obtain the values $(\sigma_\ell \times e)$, $(\sigma_t \times e)$, and $(\tau_{\ell t} \times e)$ by multiplying the global stress values σ_x , σ_y , and τ_{xy} by the thickness e , as $(\sigma_x \times e)$, $(\sigma_y \times e)$, and $(\tau_{xy} \times e)$, which are precisely the stress resultants defined previously:

$$N_x = (\sigma_x \times e); \quad N_y = (\sigma_y \times e); \quad T_{xy} = (\tau_{xy} \times e)$$

Units: The failure strengths are given in MPa (or N/mm²) in Appendix A. As a consequence, we should write from Figure 19.19 the following:

$$N_x = -400 \text{ MPa} \times \text{mm}$$

$$N_y = -450 \text{ MPa} \times \text{mm}$$

$$T_{xy} = -170 \text{ MPa} \times \text{mm}$$

With a safety factor of 2, the following values will be retained:

$$N'_x = -800 \text{ MPa} \times \text{mm}$$

$$N'_y = -900 \text{ MPa} \times \text{mm}$$

$$T'_{xy} = -340 \text{ MPa} \times \text{mm}$$

We use the Figures in Appendix A that show stress values σ_ℓ , σ_t and $\tau_{\ell t}$ in each ply due to a global applied stress with unit value (e.g., 1 MPa):

a. 0° Plies

- Loading $N'_x = -800 \text{ MPa} \times \text{mm}$ alone:

For the proportions defined in the previous question, we can read on Figure A.1 the following:

$$\left. \begin{array}{l} \sigma_\ell = 2.4 \\ \sigma_t = 0.0 \\ \tau_{\ell t} = 0 \end{array} \right\} \rightarrow \left\{ \begin{array}{l} (\sigma_\ell \times e) = 2.4 \times -800 = -1,920 \text{ MPa} \times \text{mm} \\ (\sigma_t \times e) = 0 \\ (\tau_{\ell t} \times e) = 0 \end{array} \right.$$

- Loading $N'_x = -900 \text{ MPa} \times \text{mm}$ alone:

From Figure A.5:

$$\left. \begin{array}{l} \sigma_\ell = -0.54 \\ \sigma_t = 0.12 \\ \tau_{\ell t} = 0 \end{array} \right\} \rightarrow \left\{ \begin{array}{l} (\sigma_\ell \times e) = -0.54 \times -900 = 486 \text{ MPa} \times \text{mm} \\ (\sigma_t \times e) = 0.12 \times -900 = -108 \text{ MPa} \times \text{mm} \\ (\tau_{\ell t} \times e) = 0 \end{array} \right.$$

- Loading $T'_{xy} = -340 \text{ MPa} \times \text{mm}$ alone:

From Figure A.9:

$$\left. \begin{array}{l} \sigma_\ell = 0 \\ \sigma_t = 0 \\ \tau_{\ell t} = 0.26 \end{array} \right\} \rightarrow \left\{ \begin{array}{l} (\sigma_\ell \times e) = 0 \\ (\sigma_t \times e) = 0 \\ (\tau_{\ell t} \times e) = 0.26 \times -340 = -89 \text{ MPa} \times \text{mm} \end{array} \right.$$

Superposing the three loadings leads to a total state of stress in the 0° plies:

$$(\sigma_\ell \times e) = -1,920 + 486 = -1,434 \text{ MPa} \times \text{mm}$$

$$(\sigma_t \times e) = -108 \text{ MPa} \times \text{mm}$$

$$(\tau_{\ell t} \times e) = -89 \text{ MPa} \times \text{mm}$$

Then the Tsai-Hill criterion is written in the modified form of Equation 19.1, the denominator of which being provided with failure strength values indicated in Appendix A:

$$e^2 = \frac{1,434^2}{1,130^2} + \frac{108^2}{141^2} - \frac{1,434 \times 108}{1,130^2} + \frac{89^2}{63^2} = 4.07$$

$$e_{(0^\circ)} = 2.02 \text{ mm}$$

The previous calculation may be summarized as follows:

Ply at 0°	$(\sigma_\ell \times e)$	$(\sigma_t \times e)$	$(\tau_{\ell t} \times e)$	
N'_x	-1920	0	0	
N'_y	486	-108	0	$e = 2.02 \text{ mm}$
T'_{xy}	0	0	-89	
Total (MPa \times mm)	-1,434	-108	-89	

b. 90° Plies

Repeating the same calculation procedure by using Figures A.2, A.6, and A.10 leads to the following analogous table and to a thickness e calculated as previously (remember that this is the minimum thickness of the whole laminate, below which there will be failure of the 90° plies):

Plies at 90°	$(\sigma_l \times e)$	$(\sigma_t \times e)$	$(\tau_{lt} \times e)$	
N'_x	432	-96	0	
N'_y	-2,160	0	0	$e = 2.16 \text{ mm}$
T'_{xy}	0	0	89	
Total (MPa \times mm)	-1,728	-96	89	

c. **+45° Plies**

Figures A.3, A.7, and A.11 allow to obtain the following:

Plies at 45°	$(\sigma_l \times e)$	$(\sigma_t \times e)$	$(\tau_{lt} \times e)$	
N'_x	-752	-48	72	
N'_y	-846	-54	-81	$e = 2.64 \text{ mm}$
T'_{xy}	-1,384	55	0	
Total (MPa \times mm)	-2,982	-47	-9	

d. **-45° Plies**

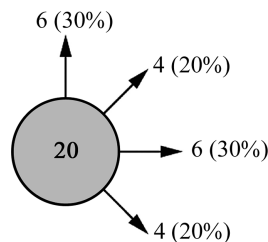
By using Figures A.4, A.8, and A.12, we obtain the following:

Plies at -45°	$(\sigma_l \times e)$	$(\sigma_t \times e)$	$(\tau_{lt} \times e)$	
N'_x	-752	-48	-72	
N'_y	-846	-54	81	$e = 1.13 \text{ mm}$
T'_{xy}	1,384	-55	0	
Total (MPa \times mm)	-214	-157	9	

Therefore, the theoretical thickness that should be kept here is the largest out of the four thicknesses found above, that is to say

$$e = 2.64 \text{ mm (rupture of plies at } +45^\circ).$$

The thickness of each ply is 0.13 mm. It takes $2.64/0.13=20$ plies minimum, from which we deduce the following composition allowing for midplane symmetry:



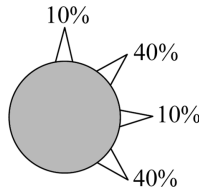
Note: Optimal composition of the laminate: for the complex loading considered here, we may directly obtain the composition leading to the minimum thickness by using the charts of Section 5.4.4. As specified in these charts, the reduced flux resultants should be used. They are deduced from the flux resultants considered above. Namely,

$$\bar{N}_x = -\frac{800}{(\|800\| + \|900\| + \|340\|)} = -39\%$$

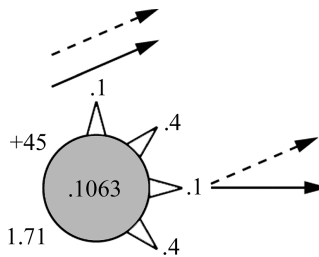
$$\bar{N}_y = -\frac{900}{(\|800\| + \|900\| + \|340\|)} = -44\%$$

$$\bar{T}_{xy} = -17\%$$

Chart 5.19 of Section 5.4.4 allows identifying, as an optimal one, a composition close to the following one

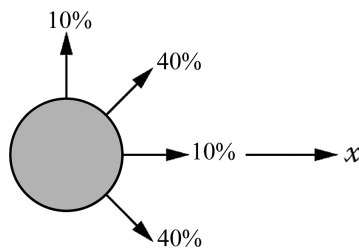


When using the previous exact values of flux resultants, the calculation by computer of the optimal composition leads to the following result, which should be interpreted as described in Section 5.4.4.



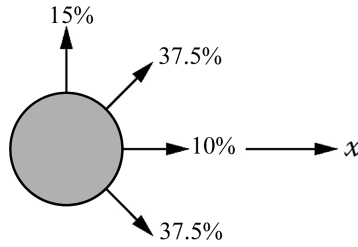
The minimum thickness of the optimum laminate is, thus, obtained:

$$\text{Thickness : } e = 0.1063 \times \frac{(\|800\| + \|900\| + \|340\|)}{100} = 2.17 \text{ mm}$$

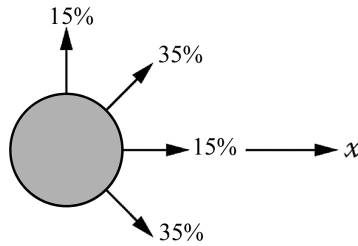


And for the two laminates that are immediately adjacent,

$$\text{Thickness : } e = 0.1068 \times \frac{(\|800\| + \|900\| + \|340\|)}{100} = 2.18 \text{ mm}$$



$$\text{Thickness : } e = 0.1096 \times \frac{(\|800\| + \|900\| + \|340\|)}{100} = 2.24 \text{ mm}$$

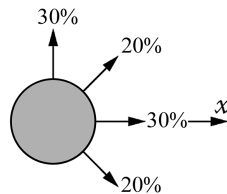


It should be noted the significant difference between the initial composition estimated by the designer and the optimal composition. This difference in composition causes a relative variation in thickness:

$$\frac{2.64 - 2.17}{2.17} = 21\%$$

which indicates impact on thickness and thus on mass. As a result, this translates into a supplementary advantage: the possibility to reinforce the rigidity in given directions without penalizing too heavily the thickness. We can note this if we compare the elastic moduli obtained starting from the approximate proportions estimated previously, following the method of Section 5.4.3, with the optimal composition. We obtain (Section 5.4.2, Charts 5.4 and 5.5) the noticeably different values noted below:

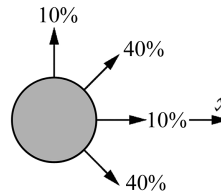
Approximative composition



$$E_x = 55,333 \text{ Mpa}$$

$$G_{xy} = 16,315 \text{ Mpa}$$

Optimum composition



$$E_x = 31,979 \text{ Mpa}$$

$$G_{xy} = 28,430 \text{ Mpa}$$

3. *Bonding of the laminate:* In the immediate vicinity of the titanium border, we represent in Figure 19.20a the principal loading values, as well as their directions, deduced from stress resultant values in Figure 19.18.

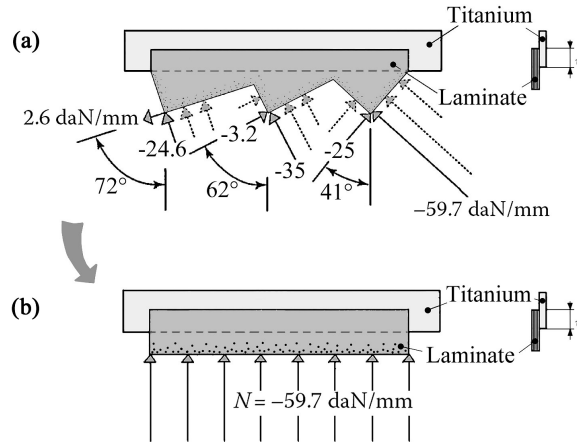


FIGURE 19.20 Vicinity of the titanium border.

For example, we could overestimate these loadings by substituting them with a fictitious distribution based on the largest of them. Taking -59.7 daN/mm as a relevant value, the simplified schematic in Figure 19.20b is then obtained.

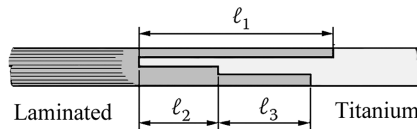
The width ℓ of bonding area needs to be evaluated. Each millimeter in width of the border corresponds to a bonding surface of $\ell \times 1 \text{ mm}$. Taking into account a failure criterion of average shear in the adhesive, we can write (see Section 6.2.3)

$$\frac{N}{\ell \times 1} \leq 0.2 \times \tau_{\text{rupture adhesive}}$$

Then with $\tau_{\text{rupture adhesive}} = 30 \text{ MPa}$,

$$\ell \geq \frac{597}{0.2 \times 30} \approx 100 \text{ mm}$$

From there is the following design proposition, in which $(\ell_1 + \ell_2 + \ell_3) = 100 \text{ mm}$.



4. Bolting on the rest of the wing:

- Pitch of bolting: The clamping force of bolts is assumed to be low. Thus, the bolts are calculated based on shear of the shanks. The load transmitted by a bolt being denoted as ΔF , we have (see the following figure)

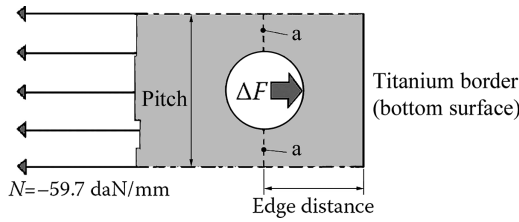
$$\Delta F = N \times \text{pitch} \leq \frac{\pi \times \phi^2}{4} \times \tau_{\text{rupture}}$$

where

ϕ is the diameter

τ_{rupture} is the shear strength of the bolt shank

We find a pitch equal to 35 mm.



This value is a little high. In practice, preference will be given to values such that $\text{pitch} \leq 5\phi$, that is,

$$\text{pitch} = 30 \text{ mm.}$$

- Thickness of the border: The bearing condition is written as

$$\frac{N \times \text{pitch}}{\phi \times e_{\text{titanium}}} \leq \sigma_{\text{bearing}}$$

Then,

$$e_{\text{titanium}} \geq 2.55 \text{ mm}$$

- Verification of titanium sheet resistance in the two zones denoted “a” in the previous figure: The stress resultant in this zone, noted as N' , is such that

$$N \times \text{pitch} = N' \times (\text{pitch} - \phi)$$

Then,

$$N' = N \times \frac{\text{pitch}}{(\text{pitch} - \phi)} = 75.4 \text{ daN/mm}$$

The failure stress being $\sigma_{\text{rupture}} = 900 \text{ MPa}$ and with a minimum thickness of 2.55 mm, we must verify that

$$\frac{N'(\text{daN/mm})}{e(\text{mm})} \leq \sigma_{\text{rupture}} (\text{daN/mm}^2)$$

Indeed, we can see that

$$\frac{75.4}{2.55} \leq 90$$

- Verification of the edge distance (see previous figure): We must respect the following shear condition:

$$\frac{\Delta F}{2 \times \text{edge distance} \times e} \leq \tau_{\text{titanium rupture}}$$

Then,

$$\text{edge distance} \geq 7.8 \text{ mm}$$

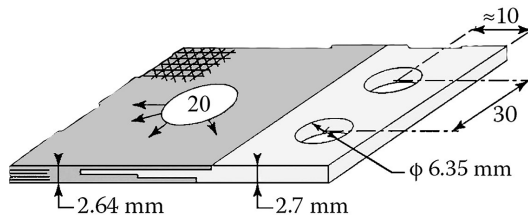


FIGURE 19.21 Fastening.

The corresponding partial dimensioning of the fastening is shown in Figure 19.21.

19.7 CARBON FIBER COATED WITH NICKEL

Problem Statement

With the objective of enhancing the electrical and thermal conductivities of a carbon/epoxy laminated panel, a thin layer of nickel with a thickness e coats the carbon fibers by means of electrolytic plating process (see Figure 19.22).

1. Calculate the longitudinal modulus of elasticity of a coated fiber.
2. Calculate the thermal expansion coefficient in the coated fiber direction.

Solution

1. Hooke's law applied to a fiber with length ℓ subject to a load F (see Figure 19.23) can be written as

$$F = E_f \times s \times \frac{\Delta \ell}{\ell}$$

where E_f is the modulus of the coated fiber that we wish to determine, and

$$s = \pi \left(\frac{d}{2} + e \right)^2$$

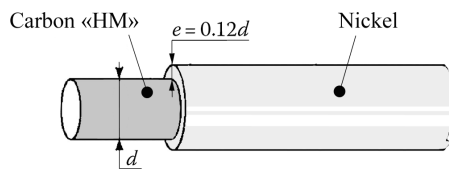


FIGURE 19.22 Carbon fiber coated with nickel.

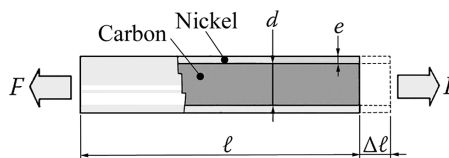


FIGURE 19.23 Loaded fiber.

The load F is divided into F_C on the carbon fiber and F_N on the nickel coating. The same elongation for the two components allows writing the following:

$$F_C = E_C \times \pi \frac{d^2}{4} \times \frac{\Delta \ell}{\ell}; \quad F_N = E_N \times \pi \left[\left(\frac{d}{2} + e \right)^2 - \frac{d^2}{4} \right] \frac{\Delta \ell}{\ell}$$

Then, taking into account that $F = F_C + F_N$,

$$E_f \times \pi \left(\frac{d}{2} + e \right)^2 = E_C \times \pi \frac{d^2}{4} + E_N \times \pi \left[\left(\frac{d}{2} + e \right)^2 - \frac{d^2}{4} \right]$$

$$E_f = E_C \frac{1}{\left(1 + \frac{2e}{d} \right)^2} + E_N \left[1 - \frac{1}{\left(1 + \frac{2e}{d} \right)^2} \right]$$

Numerical application:

$$E_C = 390,000 \text{ MPa}; \quad E_N = 220,000 \text{ MPa}; \quad d = 6.5 \text{ } \mu\text{m (Section 1.6)}$$

$$E_f = 330,500 \text{ MPa}$$

2. Thermal expansion of an unloaded rod with length $\ell = 1 \text{ m}$ due to a temperature variation ΔT can be written as

$$\Delta \ell_1 = \alpha \times \Delta T \times 1$$

where α is the thermal expansion coefficient of the material making up the rod. In addition, when this rod is subjected to a longitudinal stress σ , Hooke's law indicates a second elongation:

$$\Delta \ell_2 = \frac{\sigma}{E} \times 1$$

When the two cases occur simultaneously,

$$\Delta \ell = \Delta \ell_1 + \Delta \ell_2$$

or

$$\Delta \ell = \left(\frac{\sigma}{E} + \alpha \times \Delta T \right) \times 1$$

When the coated fiber is subjected to a temperature variation ΔT , each of its constituents will elongate an identical amount Δ . This coated fiber is not subjected to any external forces. The difference in the coefficients of thermal expansion of carbon and of nickel that would lead to different free thermal expansions leads here to a self-equilibrium of loads within the components of the coated fiber.

Let α_f be the thermal expansion coefficient of the coated fiber. Then,

$$\Delta \ell = \alpha_f \Delta T \times 1$$

On the other hand, for the carbon and for the nickel,

$$\Delta \ell = \frac{\sigma_C}{E_C} + \alpha_C \Delta T = \frac{\sigma_N}{E_N} + \alpha_N \Delta T \quad (19.2)$$

The forces being self-balanced,

$$\pi \left[\left(\frac{d}{2} + e \right)^2 - \frac{d^2}{4} \right] \sigma_N + \pi \frac{d^2}{4} \times \sigma_C = 0 \quad (19.3)$$

Equations 19.2 and 19.3 lead to

$$\sigma_C = \frac{(\alpha_N - \alpha_C) \Delta T}{\frac{1}{E_C} + \frac{1}{E_N} \times \frac{1}{\left[\left(1 + \frac{2e}{d} \right)^2 - 1 \right]}}$$

And taking into account that

$$\alpha_f \Delta T = \Delta \ell = \frac{\sigma_C}{E_C} + \alpha_C \Delta T$$

we obtain

$$\alpha_f = \frac{\alpha_N + \alpha_C \frac{E_C}{E_N} \frac{1}{\left[\left(1 + \frac{2e}{d} \right)^2 - 1 \right]}}{1 + \frac{E_C}{E_N} \frac{1}{\left[\left(1 + \frac{2e}{d} \right)^2 - 1 \right]}}$$

19.8 TUBE MADE OF GLASS/EPOXY UNDER PRESSURE

Problem Statement

Consider a thin tube made by filament winding of glass/epoxy with a winding angle of $\pm 45^\circ$. The fiber volume fraction is $V_f = 0.6$. The tube is fixed at one end to a rigid undeformable mass and mounted to a sliding joint at the other end as outlined in Figure 19.24.

The thickness e is considered to be small as compared with the average radius r ($e/r \ll 1$). The inside of the tube undergoes a pressure $p_o = 1$ MPa (or 10 bar). A safety factor of 8 will be considered in order to include the aging effect:

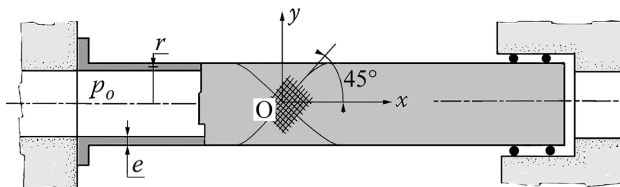


FIGURE 19.24 Tube under pressure.

1. Calculate the stress values σ_x and σ_y , in axes (x, y) of the tangent plane to the tube at point O.
2. What is the maximum stress value allowable for the indicated winding? Deduce the minimum thickness of the tube for an average radius $r=100$ mm.
3. What are the moduli E_x , E_y , and G_{xy} of the laminate and the Poisson coefficients ν_{xy} and ν_{yx} ? Write the stress–strain behavior relationship for the laminate in axes (x, y) .
4. Calculate the strain values ϵ_x and ϵ_y within this composite tube. From there, deduce the strain in the direction that is perpendicular to the fibers of a $+45^\circ$ ply, denoted as ϵ_r . This strain characterizes essentially the strain in the resin.

This strain has to be less than 0.1% to avoid microfractures, which can lead to fluid leakage across the tube thickness, known as **weeping** phenomenon.

Solution

1. The thin tube being free in axial direction, $\sigma_x = 0$.

The equilibrium of a half cylinder is represented in Figure 19.25:

2. Maximum admissible stress: For ply proportions of 50% at $\pm 45^\circ$, we can read on Chart 5.12, Section 5.4.2, the following:

$$\sigma_{y \max (\text{tension})} = 94 \text{ MPa}$$

Then with $\sigma_{y \max} = p_0 \times \frac{r}{e}$, the theoretical minimum thickness is

$$e_{\text{theoretical}} = \frac{p_0 \times r}{\sigma_{y \max}} = \frac{1 \text{ MPa} \times 100 \text{ mm}}{94 \text{ MPa}} = 1.064 \text{ mm}$$

Taking into account the safety factor of 8 for aging effect,

$$e = 8.5 \text{ mm}$$

3. Moduli of the laminate: We can read on Chart 5.14, Section 5.4.2, the following:

$$E_x = 14,130 \text{ MPa} = E_y$$

$$\nu_{xy} = 0.57 = \nu_{yx}$$

and from Chart 5.15,

$$G_{xy} = 12,760 \text{ MPa}.$$

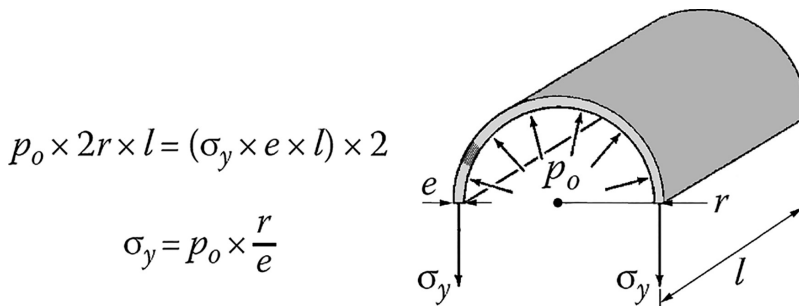


FIGURE 19.25 Equilibrium of a half cylinder.

The stress–strain relationship for an anisotropic material described in Section 3.1 is recalled hereafter:

$$\begin{Bmatrix} \varepsilon_x \\ \varepsilon_y \\ \gamma_{xy} \end{Bmatrix} = \begin{bmatrix} \frac{1}{E_x} & -\frac{\nu_{yx}}{E_y} & 0 \\ -\frac{\nu_{xy}}{E_x} & \frac{1}{E_y} & 0 \\ 0 & 0 & \frac{1}{G_{xy}} \end{bmatrix} \begin{Bmatrix} \sigma_x \\ \sigma_y \\ \tau_{xy} \end{Bmatrix}$$

Here, we have

$$\begin{Bmatrix} \varepsilon_x \\ \varepsilon_y \\ \gamma_{xy} \end{Bmatrix} = \frac{1}{14,130} \begin{bmatrix} 1 & -0.57 & 0 \\ -0.57 & 1 & 0 \\ 0 & 0 & 1.107 \end{bmatrix} \begin{Bmatrix} \sigma_x \\ \sigma_y \\ \tau_{xy} \end{Bmatrix}$$

4. Strain values: For $p_o = 1$ MPa and $e = 8.5$ mm,

$$\sigma_y = \frac{1 \text{ MPa} \times 100}{8.5} = 11.8 \text{ MPa}$$

Then,

$$\begin{Bmatrix} \varepsilon_x \\ \varepsilon_y \\ \gamma_{xy} \end{Bmatrix} = \frac{1}{14,130} \begin{bmatrix} 1 & -0.57 & 0 \\ -0.57 & 1 & 0 \\ 0 & 0 & 1.107 \end{bmatrix} \begin{Bmatrix} 0 \\ 11.8 \\ 0 \end{Bmatrix}$$

From which

$$\varepsilon_x = -4.76 \times 10^{-4}$$

$$\varepsilon_y = 8.35 \times 10^{-4}$$

Mohr's circle for strains in Figure 19.26 allows obtaining the strain ε_t perpendicular to the fibers.

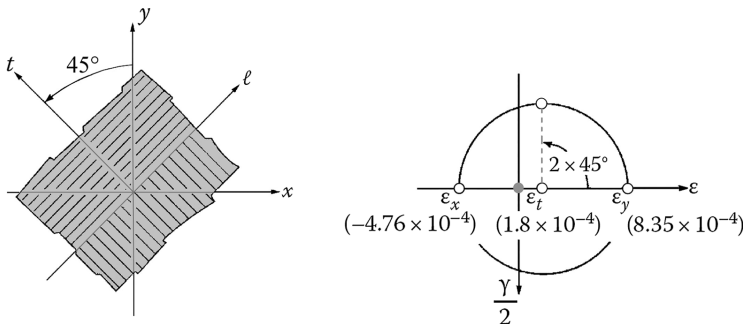


FIGURE 19.26 Strain ε_t .

We obtain

$$\epsilon_t = \frac{\epsilon_x + \epsilon_y}{2} = 1.8 \times 10^{-4}$$

$$\epsilon_t = 0.018\%$$

Thus, we can check that the strain in the matrix is less than 0.1%, which is the maximum allowed value.

19.9 FILAMENT-WOUND PRESSURE VESSEL: WINDING ANGLE

Problem Statement

We will consider a pressure vessel as a thin shell of revolution, obtained by winding of “R” glass/epoxy rovings. The cylindrical portion (see Figure 19.27) has a small thickness e_0 compared to the average radius R . An internal pressure p_0 loads this tank.

1. The resin epoxy is assumed to bear no load. Denoting by e the thickness of the reinforcement alone, calculate in the tangent plane (x, y) (see figure) the stress values σ_{0x} and σ_{0y} in the thin wall, due to pressure p_0 .
2. In the cylindrical part of the pressure vessel, the winding consists of layers at alternating angles $\pm\alpha$ with the cylinder's generatrix (see figure). It is wished to obtain a uniform tension value σ_ℓ in each fiber along its own direction ℓ (such a uniform tension in all fibers confers the characteristic so-called **isotenoid**).
 - a. Evaluate the stresses σ_x and σ_y in the fibers as functions of σ_ℓ .
 - b. Deduce from the above the helical angle α and the tension σ_ℓ in fibers, as functions of pressure p_0 .
 - c. What will be the thickness e_0 for a reservoir of 80 cm in diameter supporting a 200 bar pressure, with 80% fiber volume fraction?

Solution

1. Preliminary remark: The elementary force due to a pressure p_0 acting on a surface dS projects on the x -axis as (see figure below):

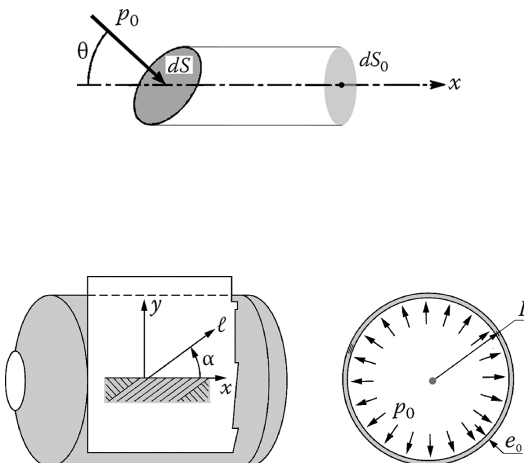


FIGURE 19.27 Pressure vessel.

$$p_o \, dS \cos \theta = p_o \, dS_o$$

where dS_o is the projection of dS along the x -axis in a plane perpendicular to this axis.

- Equilibrium of a vessel bottom along the axial direction: The equilibrium and associated relationship are represented in Figure 19.28
- Equilibrium of a semicylindrical portion along the circumferential direction: The

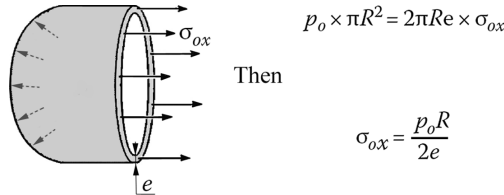


FIGURE 19.28 Equilibrium along axial direction.

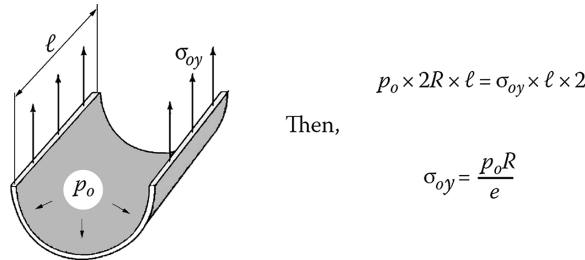
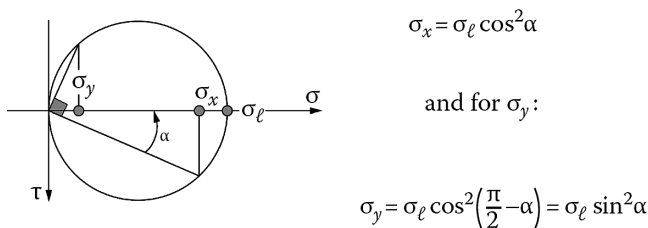


FIGURE 19.29 Equilibrium along circumferential direction.

equilibrium and associated relationship are represented in Figure 19.29

2.

- Stress components σ_x and σ_y in the fibers:* We can represent Mohr's circle of stress starting from the pure normal stress σ_ℓ acting on a facet normal to axis ℓ (see Figure 19.27). From there, we note as follows¹⁰ the construction leading to the stress values σ_x and σ_y



- Helical angle α :* Identification of these stress values with σ_{0x} and σ_{0y} found earlier leads to

$$\sigma_\ell \cos^2 \alpha = \frac{p_o R}{2e}; \quad \sigma_\ell \sin^2 \alpha = \frac{p_o R}{e}$$

From which

$$\tan^2 \alpha = 2$$

Then,

$$\sin \alpha = \sqrt{\frac{2}{3}}; \quad \alpha = 54.7^\circ$$

Tension in fiber is then

$$\sigma_\ell = \frac{3}{2} p_o \frac{R}{e}$$

c. *Thickness e_o* : For “R” glass¹¹, $\sigma_{\ell \text{ rupture}} = 3,200 \text{ MPa}$.

which leads to the reinforcement thickness e :

$$e = \frac{3}{2} \frac{p_o R}{\sigma_{\ell \text{ rupture}}} = 3.75 \text{ mm}$$

V_f being the fiber volume fraction, the thickness of the glass/epoxy composite is

$$e_o = \frac{e}{V_f} = 4.7 \text{ mm}$$

19.10 FILAMENT-WOUND PRESSURE VESSEL: CONSIDERATION OF OPENINGS IN THE BOTTOM HEADS

Problem Statement

A reservoir in the form of a thin shell of revolution is wound with fibers and resin. It is subjected to an internal pressure p_o . The circular heads at the two ends of the reservoir have radius of r_0 . We propose to study the cylindrical part of this reservoir, with an average radius R .

One part of the winding consists of filaments in helical windings making angles of $\pm\alpha_1$ with the generatrices (see Figure 19.30) and using the same proportions. The other part consists of similar filaments wound circumferentially ($\alpha_2 = \pi/2$).

The resin is assumed to carry no load. Tension in filaments of helical layers is denoted as $\sigma_{\ell 1}$ and tension in filaments of circumferential layers as $\sigma_{\ell 2}$.

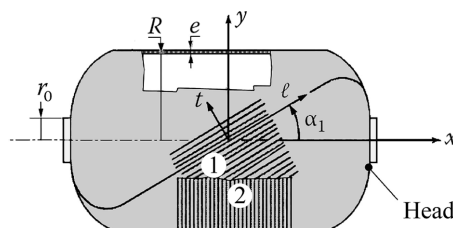


FIGURE 19.30 Filament-wound vessel with openings in the bottom heads.

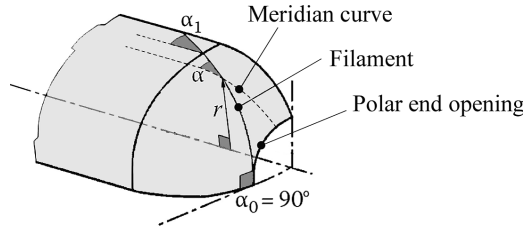


FIGURE 19.31 Geodesic line.

1. What is the value α_1 if the filaments are layered toward the heads along lines of shortest distance?
2. Calculate the thickness e_1 of fibers of the helical layers and thickness e_2 of fibers of the circumferential layer as functions of p_o , R , α_1 , $\sigma_{\ell 1}$, $\sigma_{\ell 2}$.
3. What is the minimum total thickness of fibers e_m that the envelope should have? What are the corresponding ratios e_1/e_m and e_2/e_m ? What is the real corresponding thickness of the envelope with a fiber volume percentage V_f identical for the two types of layers?

Note: It can be shown – and we will agree with this property – that on a surface of revolution, lines of shortest distance, so-called the **geodesic** lines, satisfy the following relation (see Figure 19.31 for the notations):

$$r \times \sin \alpha = \text{constant}$$

Solution

1. Filaments wound helically (angle $\pm\alpha_1$) in the cylindrical part are following geodesic lines toward the heads such that $r \times \sin \alpha = \text{constant}$. The circle making up the head is a geodesic line characterized by $r = r_o$. Then,

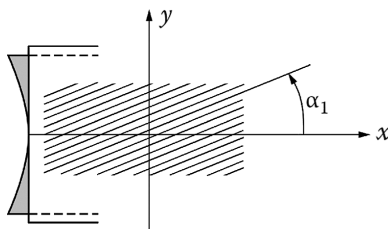
$$\alpha = \alpha_o = \frac{\pi}{2}$$

Thus, for the filaments linking the cylindrical part to the head,

$$r_o \sin \frac{\pi}{2} = R \sin \alpha_1$$

$$\sin \alpha_1 = \frac{r_o}{R}$$

2. Thickness of layers: For an internal pressure p_o , the state of stress in the cylindrical part of the thin envelope is defined in the tangent plane (x, y) shown in the following figure as¹²



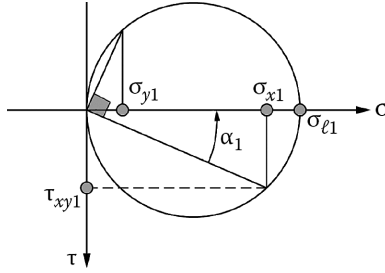
$$\begin{pmatrix} \sigma_{ox} = \frac{p_o R}{2e} \\ \sigma_{oy} = \frac{p_o R}{e} \\ \tau_{oxy} = 0 \end{pmatrix}$$

The resin being assumed to bear no load, e represents the thickness of the reinforcement alone. We can follow by direct calculation¹³. Then, the state of stress in helical layers $\pm\alpha_1$ reduces to $\sigma_{\ell 1} \neq 0$, and $\sigma_{t1} = \tau_{\ell t1} = 0$.

Starting from Mohr's circle illustrated below¹⁴, we obtain for stress in plane (x, y) the following:

$$\sigma_{x1} = \cos^2 \alpha_1 \times \sigma_{\ell 1}; \quad \sigma_{y1} = \sin^2 \alpha_1 \times \sigma_{\ell 1}$$

$$\tau_{xy1} = \cos \alpha_1 \times \sin \alpha_1 \times \sigma_{\ell 1}$$



And for the circumferential layers $\alpha_2 = \pi/2$

$$\sigma_{x2} = 0; \quad \sigma_{y2} = \sigma_{\ell 2}; \quad \tau_{xy2} = 0$$

When calculating the resultant force on unit width section with normal direction x , and then y successively, we obtain the following equivalencies:

- Along x ,

$$\sigma_{x1} \times e_1 \times 1 + \sigma_{x2} \times e_2 \times 1 = \sigma_{ox} \times e \times 1$$

Then,

$$e_1 \times \cos^2 \alpha_1 \times \sigma_{\ell 1} = e \times \sigma_{ox} = e \times p_o \frac{R}{2e}$$

from which

$$e_1 = \frac{p_o}{\sigma_{\ell 1}} \times \frac{R}{2 \cos^2 \alpha_1}$$

- Along y ,

$$\sigma_{y1} \times e_1 \times 1 + \sigma_{y2} \times e_2 \times 1 = \sigma_{oy} \times e \times 1$$

$$e_1 \times \sin^2 \alpha_1 \times \sigma_{\ell 1} + e_2 \times \sigma_{\ell 2} = e \times \sigma_{oy} = e \times \frac{p_o R}{e}$$

$$e_2 = \frac{p_o}{\sigma_{\ell 2}} R \left(1 - \frac{\tan^2 \alpha_1}{2} \right)$$

3. *Minimum envelope thickness:* With the previous results, the reinforcement thickness is written as

$$e = e_1 + e_2 = p_o R \left\{ \frac{1}{2\sigma_{\ell 1} \cos^2 \alpha_1} + \frac{(2 - tg^2 \alpha_1)}{2\sigma_{\ell 2}} \right\}$$

The reinforcements for helical and circumferential layers being of the same type, they can support an identical maximum tension. Therefore, at failure,

$$\sigma_{\ell 1} = \sigma_{\ell 2} = \sigma_{\ell \text{ rupture}}$$

Then,

$$e_{\min} = \frac{p_o R}{2\sigma_{\ell \text{ rupture}}} \left(\frac{1}{\cos^2 \alpha_1} + 2 - tg^2 \alpha_1 \right)$$

$$e_{\min} = \frac{3}{2} \times \frac{p_o R}{\sigma_{\ell \text{ rupture}}}$$

Ratios of thicknesses:

$$\frac{e_1}{e_{\min}} = \frac{1}{3 \cos^2 \alpha_1} ; \quad \frac{e_2}{e_{\min}} = \frac{2 - tg^2 \alpha_1}{3}$$

Actual envelope thickness taking into account the fiber volume percentage V_f :

$$\frac{dv_{\text{reinforcement}}}{dv_{\text{actual}}} = V_f = \frac{2\pi R e_{\min} \times dx}{2\pi R e_{\text{actual}} \times dx}$$

$$e_{\text{actual}} = \frac{3}{2} \times \frac{p_o R}{\sigma_{\ell \text{ rupture}}} \times \frac{1}{V_f}$$

19.11 DETERMINATION OF FIBER VOLUME FRACTION BY PYROLYSIS

Problem Statement

A sample is removed from a carbon/epoxy laminate made up of identical layers of balanced fabric. The measured specific mass of the laminate is ρ . The specific mass of carbon is ρ_f and that of the matrix is ρ_m .

The epoxy matrix is completely burned in an oven. The mass of the residual fiber, denoted as M_f (see Section 3.2.1), is compared with the initial sample mass:

1. Express the following in terms of ρ , ρ_f , ρ_m , M_f :
 - a. The fiber volume fraction V_f
 - b. The matrix volume fraction V_m
 - c. The volume fraction of porosities, or voids V_p

2. Numerical application:

$$\rho = 1,500 \text{ kg/m}^3 ; \quad \rho_f = 1,750 \text{ kg/m}^3 ; \quad \rho_m = 1,200 \text{ kg/m}^3 ; \quad M_f = 0.7$$

Solution

1.

a. By definition (Section 3.2.2), one has

$$V_f = \frac{v_{\text{fibers}}}{v_{\text{total}}} = \frac{m_{\text{fibers}}}{\rho_f} \times \frac{\rho}{m_{\text{total}}} = M_f \times \frac{\rho}{\rho_f}$$

$$V_f = M_f \times \frac{\rho}{\rho_f}$$

b. In an analogous manner,

$$V_m = M_m \times \frac{\rho}{\rho_m}$$

and with $M_f + M_m = 1$,

$$V_m = (1 - M_f) \times \frac{\rho}{\rho_m}$$

c. Noting (Section 3.2.2) that

$$V_f + V_m + V_p = 1$$

we can deduce

$$V_p = 1 - \rho \times \left(\frac{M_f}{\rho_f} + \frac{(1 - M_f)}{\rho_m} \right)$$

Numerical application:

$$V_f = 60\%; \quad V_m = 37.5\%; \quad V_p = 2.5\%$$

Note: In practice, a small amount of carbon fibers is also pyrolyzed: about 0.125% is pyrolyzed per hour.

19.12 REVERSING LEVER MADE OF CARBON/PEEK (UNIDIRECTIONAL AND SHORT FIBERS)

Problem Statement

In Figure 19.32 is shown a lever with three points linked at *A*, *B*, *C*. It is subjected to indicated loads. The external skin is obtained from a plate of thermoformed unidirectional carbon/PEEK¹⁵, 2.8 mm in thickness. The latter is placed in a mold into which short fibers of carbon/PEEK are injected at high temperature.

1. Verify the good resistance of this part by a simplified calculation.
2. Estimate the order of magnitude of elastic displacements at points *A* and *B* relative to *C*, due to the specified loads.
3. Determine the mass balance of the part.

		Density, ρ (kg/m ³)	σ_{rupture} (MPa)	Modulus of Elasticity (MPa)
Carbon/PEEK unidirectional	$V_f = 65\%$	1,600	2,100	$E_f = 125,000$ $G_{ft} = 4,000$
Short fibers of carbon/PEEK	$V_f = 18\%$	1,400	127	$E = 21,000$ $G = 8,000$

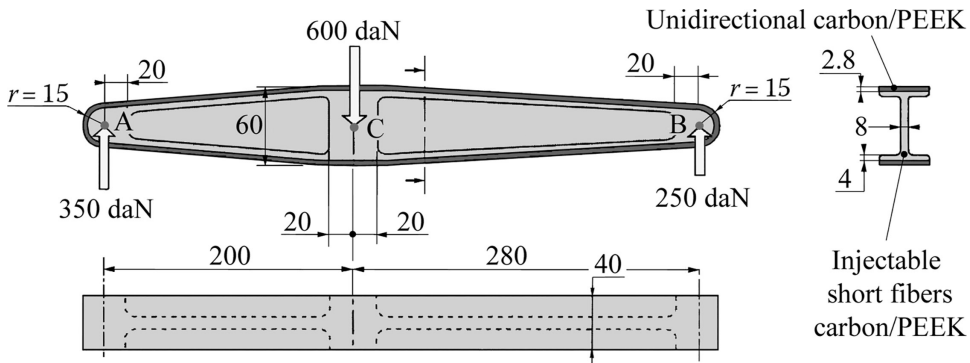
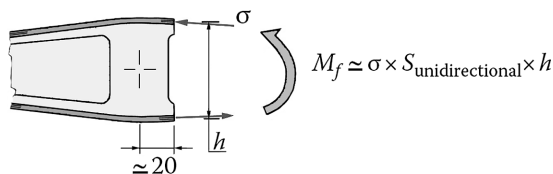


FIGURE 19.32 Carbon/PEEK reversing lever.

Solution

1. Verification of resistance:

- **Unidirectional:** As a simplified calculation, assume that the applied moment is taken up essentially by unidirectional skins¹⁶. When considering the cross section with maximum bending moment (see the following figure), we can express this moment as follows:



With

$$S_{\text{unidirectional}} = 2.8 \times 40 \text{ mm}^2; \quad h = 60 - 2 - 2.8 \approx 55 \text{ mm}$$

$$M_f = 650 \times 10^3 \text{ N} \times \text{mm}.$$

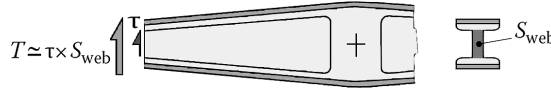
$$\sigma = 106 \text{ MPa}$$

Safety factor:

$$\frac{\sigma_{\text{rupture}}}{\sigma} - 1 = 18.8 \quad (1,880\%)$$

Note: In the injected flange just under the unidirectional skin, the order of magnitude of normal stress is six times smaller (the elasticity modulus E_ℓ of unidirectional is six times higher than that of injected short fibers).

- **Injected core:** We assume that the web, as in the following figure, takes up shear stress due to the shear force essentially:

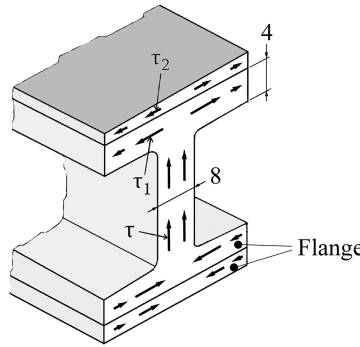


With

$$S_{\text{web}} = (33 - 5.6 - 8) \times 8 \text{ (mm}^2\text{)}; T = 3,500 \text{ N}$$

$$\tau \approx 23 \text{ MPa}$$

Note: In fact, the shear stress is distributed in each flange zone (injected zone and unidirectional zone in the following figure). The bonding being assumed perfect, distortion is the same in injected and unidirectional zones:



$$\gamma = \frac{\tau_2}{G_{\ell t}} = \frac{\tau_1}{G}$$

And accounting for equilibrium of junction of the web with the flange¹⁷

$$\tau \times 8 \approx (\tau_1 \times 4 + \tau_2 \times 2.8) \times 2$$

Then, with $\tau = 23 \text{ MPa}$

$$\tau_1 = 17 \text{ MPa}; \quad \tau_2 = 8.5 \text{ MPa}$$

2. **Displacements under load:** When keeping the central area around C fixed in translation and in rotation, the deformation energy of each arm (right or left) is written as

$$W = \frac{1}{2} \int_{\text{arm}} \sigma \times \varepsilon dV + \frac{1}{2} \int_{\text{arm}} \tau \times \gamma dV$$

with previous approximations,

$$W = \frac{1}{2} \int_{\text{flange}} \frac{\sigma^2}{E_{\ell \text{ unidir.}}} dS \times dx + \frac{1}{2} \int_{\text{web}} \frac{\tau^2}{G} dS \times dx$$

$$W = \frac{1}{2} \int \frac{M_f^2}{E_{\text{unid.}} (S_{\text{unid.}} \times h)^2} \times 2S_{\text{unid.}} dx + \frac{1}{2} \int \frac{T^2}{G \times S_{\text{web}}^2} \times S_{\text{web}} \times dx$$

In view of an estimation, with $M_f = F(\ell - x)$; $T = F$; $h = h_{\text{average}}$ and $S_{\text{web}} = S_{\text{average}}$ (web at midlength of the arm),

$$W = \frac{1}{2} \frac{F^2 \ell^3 / 3}{E_{\ell \text{ unidir.}} \left(S_{\text{unid.}} \times \frac{h_{\text{average}}^2}{2} \right)^2} + \frac{1}{2} \frac{F^2 \ell}{G S_{\text{web average}}}$$

Displacement at point loaded by F is obtained from the Castigliano theorem:

$$\Delta = \frac{\partial W}{\partial F} = \left\{ \frac{\ell^3 / 3}{E_{\ell \text{ unidir.}} \times S_{\text{unid.}} \times \frac{h_{\text{average}}^2}{2}} + \frac{\ell}{G \times S_{\text{web average}}} \right\} \times F$$

From which, we can write the following:

- Displacement at point B (right arm):

$$\ell = 280 \text{ mm}; F = 2,500 \text{ N}; h_{\text{average}} = 45 \text{ mm} - 2.8 \text{ mm}$$

$$\Delta_B = 1.8 \text{ mm}$$

- Displacement at point A (left arm):

$$\ell = 200 \text{ mm}; F = 3,500 \text{ N}; h_{\text{average}} = 45 \text{ mm} - 2.8 \text{ mm}; S_{\text{web average}} = 31.4 \times 8 (\text{mm}^2)$$

$$\Delta_A = 1.1 \text{ mm}$$

3. **Mass balance:** Unidirectional, 189 g; short fibers, 525 g; total mass before drilling:

$$m = 714 \text{ g}$$

Notes:

- Taking into account the low stress level in unidirectional, the part may be lightened by decreasing uniformly and progressively its thickness (40mm here). For example, reduction from 40 to 30mm leads to a mass reduction of 18% and increases displacements by 22% at point A and 26% at point B.
- To obtain a comparable mass with light alloy, folded and welded sheet should be used. The price of the piece is higher. The composite piece is obtained here by one single operation of injection after performing unidirectional reinforcements.

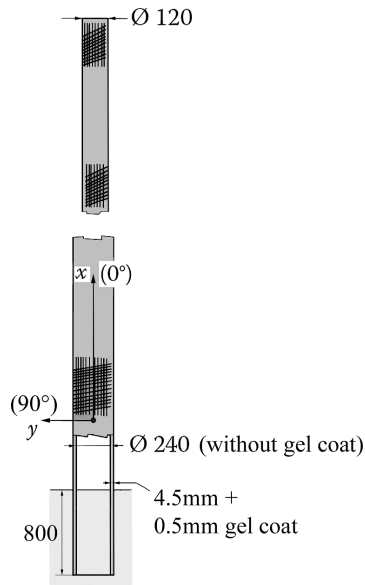


FIGURE 19.33 Glass/resin pole.

19.13 GLASS/RESIN TELEGRAPH POLE

Problem Statement

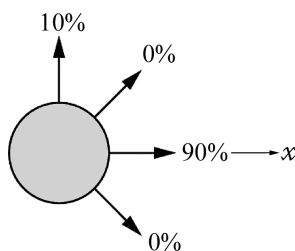
A telegraph pole 8 m long (of which 80 cm is buried in the ground) in glass/epoxy with 60% fiber volume fraction has the characteristics shown in Figure 19.33.

The lower zone of the pole is characterized by

- 27 layers at 0° (x -direction)
- 3 layers oriented in helix with an angle that will be taken practically equal to 90°
 1. Give the elastic constants of the laminate in this zone.
 2. What is, regarding this lower zone, the maximum horizontal load allowable at the top of the pole?
 3. Give an estimate of the horizontal displacement at the top under this load.

Solution

1. The laminate composition in the lower part is as follows:



Charts 5.14 and 5.15 of Section 5.4.2 give for this composition:

$$E_x = 41,860 \text{ MPa}; E_y = 15,360 \text{ MPa}$$

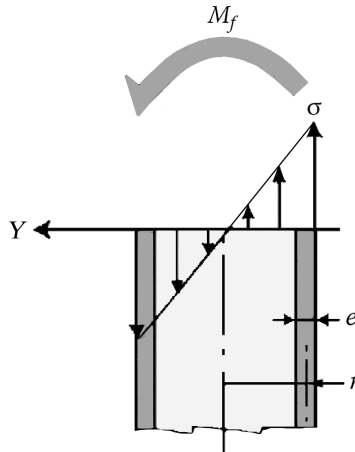
$$\nu_{xy} = 0.23; \nu_{yx} = 0.09$$

$$G_{xy} = 4,500 \text{ MPa}$$

2. In view of evaluating the maximum horizontal load at the top, three risks need to be taken into account:

- Risk of failure due to classical flexure in this lower zone when the bending moment is too high
- Risk of shear failure due to shear force
- Risk of buckling by ovalization and then flattening of the tube

a. **Bending moment:** We derive from the following figure¹⁸



$$\sigma = -\frac{M_f}{I} \times Y \quad \text{with} \quad I = \pi r^3 e$$

The maximum value is obtained when $Y = -r$

$$\sigma_{\max} = \frac{M_f}{\pi r^2 e}$$

Chart 5.11 in Section 5.4.2 shows for the laminate in question a first ply failure when

$$\sigma_{\text{rupture}}^{\text{tensile}} = 128 \text{ MPa}$$

Hence,

$$M_f \leq 26 \times 10^6 \text{ N} \times \text{mm}$$

Corresponding to a horizontal load value at the top,

$$\frac{F_{\max}}{(M_f)} = \frac{26 \times 10^6}{7,200} = 3,600 \text{ N.}$$

- b. **Shear force:** On the average diameter located in the neutral plane of the tubular section, we can write

$$\tau = \alpha \times \frac{T}{S}$$

where

T is the shear force

S is the area of the cross section

α is the amplification factor ($\alpha > 1$)¹⁹

Note that for the laminate considered (Table 5.13, Section 5.4.2), the first ply failure occurs with $\tau_{\text{rupture}} = 63 \text{ MPa}$. Let us imagine that such a value is due to the shear force found before, that is, $T = F_{\max(M_f)} = 3,600 \text{ N}$. Then,

$$\alpha < \frac{63 \times 3,329}{3,600} = 58$$

Such a requirement is certainly satisfied (recall that for a thin circular tube of isotropic material $\alpha = 2$).

- c. **Ovalization of the pole:** From Section B.2,

$$M_{\text{critical}} = \frac{2\sqrt{2}}{9} \pi r e^2 \left[\frac{E_x E_y}{1 - \nu_{xy} \nu_{yx}} \right]^{1/2}$$

That leads here to

$$M_{\text{critical}} = 6 \times 10^7 \text{ N} \times \text{mm}$$

which corresponds to a top horizontal load:

$$F_{\text{critical(Ovalization)}} = 8,360 \text{ N}$$

Therefore, the maximum value that should be retained is

$$F_{\max} = 3,600 \text{ N}$$

3. **Deflection at the top:** If the characteristics of the pole (section, composition) remain constant all along the x -axis, retaining 180 mm for average diameter and considering the previous maximum load, the following deflection would be obtained at the top:

$$\Delta = \frac{F_{\max} \times L^3}{3E_x I_Z} \approx 1 \text{ m}$$

A more accurate value requires discretizing the pole into beam finite elements (four or five) with corresponding sections and moduli (note that due to the decreasing diameter, helical angle increases with x , and the moduli E_x and E_y vary a little).

19.14 UNIDIRECTIONAL LAYER OF HR CARBON

Problem Statement

Consider a unidirectional layer made of HR carbon/epoxy. What is the fiber volume fraction that would confer a modulus of elasticity in the longitudinal direction comparable to duralumin A92024.

Solution

In fiber direction, the modulus of elasticity E_ℓ is given by (see Section 3.3.1)

$$E_\ell = E_f V_f + E_m (1 - V_f)$$

We can read in Tables 1.2, 1.3, and 1.4 in Section 1.6 the following:

$$\text{HR carbon : } E_f = 230,000 \text{ MPa}$$

$$\text{Epoxy resin : } E_m = 4,500 \text{ MPa}$$

$$\text{Duralumin : } E_{A92024} = 75,000 \text{ MPa}$$

The fiber volume fraction V_f has to be such that

$$E_{A92024} = E_f V_f + E_m (1 - V_f)$$

Then,

$$V_f = \frac{E_{A92024} - E_m}{E_f - E_m}$$

$$V_f = 31\%$$

19.15 MANIPULATOR ARM FOR SPACE SHUTTLE

Problem Statement

A manipulator arm is made of two identical carbon/epoxy tubular sections ($V_f = 60\%$; thin cylindrical tubes of revolution). This jointed arm manipulator is shown in Figure 19.34.

Among the different geometric configurations found when the arm is deployed, we consider specifically the ones noted (a), (b), and (c) in Figure 19.35.

F represents the concentrated inertial force.

Note the following:

- E_x is the modulus of elasticity of the tube in the x -direction (Figure 19.34).
- G_{xy} is the shear modulus in tangent plane (x, y) (Figure 19.34).
- I is the quadratic moment of flexure of annular cross section of tube, with respect to its diameter.

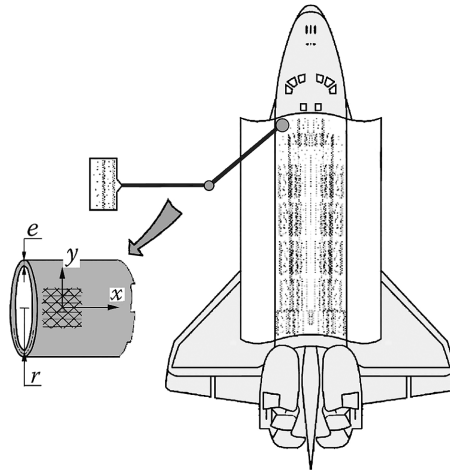


FIGURE 19.34 Jointed arm manipulator.

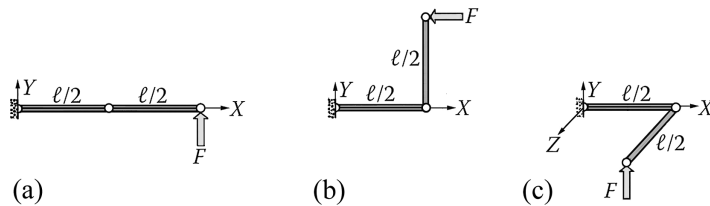


FIGURE 19.35 (a–c) Three geometric configurations.

1. Calculate in terms of F , ℓ , I , E_x , and G_{xy} the deflection components along directions X , Y , Z (Figure 19.35) of the point under the force F for each of configurations (a), (b), and (c). Neglect the strain due to shear and normal forces. Comment on the relative values of these displacements.
2. What should be the ratio between E_x and G_{xy} in order to obtain identical deflections in configurations (a) and (c)?
3. The tube is laminated starting from unidirectional tape. By means of the charts giving moduli E_x and G_{xy} (Section 5.4.2), indicate by simple reading and without interpolation the laminate composition that verifies the ratio found in the previous question within a few percent (choose G_{xy} as large as possible), as well as the elastic characteristics values.
4. Verify that this composition is preferable, in relation to mass balance, to that of another tube with the same diameter, a different thickness, having a modulus of elasticity E'_x as large as possible, and which would show the same deflection as that previously found for configuration (c).
5. Keep the properties determined for the laminate in Question 3. The arm has an average diameter of 0.3 m. Each of the two tubes is 7.5 m long. The minimum stiffness $(F/\Delta)_{\text{minimum}} = 10^4 \text{ N/m}$ is imposed to the arm, where Δ is the deflection under the load F . Calculate the tube thickness and indicate the number of total unidirectional layers and the number of layers in each of the four orientations.
6. With the data given in Figure 19.36, verify that the distributed mass of the arm does not significantly influence the previous results during the stage of operation that adjusts the concentrated mass in position.

Solution

- Starting from the flexure and torsion relationships for composite tubes (see Section 5.4.5.4, Figure 5.31),

$$E_x I \frac{d^2 v}{dX^2} = M_f; \quad G_{xy} I_o \frac{d\theta_x}{dX} = M_t$$

We obtain for displacement components at the end of the arm the following:

- Configuration (a):

$$\Delta_Y = \frac{F\ell^3}{3E_x I}$$

- Configuration (b):

$$\Delta_X = \frac{F \times (\ell/2)}{E_x I} \times \frac{\ell}{2} \times -\frac{\ell}{2} - \frac{F \times \left(\frac{\ell}{2}\right)^3}{3E_x I} = -\frac{F\ell^3}{6E_x I}$$

$$\Delta_Y = \frac{F \times (\ell/2)}{2E_x I} \times \left(\frac{\ell}{2}\right)^2 = \frac{F\ell^3}{16E_x I}$$

- Configuration (c):

$$\Delta_Y = \frac{F \times (\ell/2)^3}{3E_x I} \times 2 + \frac{F \times (\ell/2)}{G_{xy} I_o} \times \frac{\ell}{2} \times \frac{\ell}{2} = \frac{F\ell^3}{8E_x I} \left(\frac{2}{3} + \frac{E_x}{2G_{xy}} \right)$$

Note: For configurations (a) and (b), we can note that the displacement is smaller when the modulus E_x is large. But then (see Section 5.4.2, Charts 5.4 and 5.5), G_{xy} is relatively small, that is, $E_x/G_{xy} \gg 1$, and the displacement of configuration (c) is much larger than the others. This will create problems when operating the arm.

- Deflections will be identical for configurations (a) and (c) if

$$\frac{1}{3} = \frac{1}{8} \left(\frac{2}{3} + \frac{E_x}{2G_{xy}} \right)$$

Then,

$$\frac{E_x}{G_{xy}} = 4$$

- In looking for a modulus G_{xy} as high as possible, we can read on Charts 5.4 and 5.5 (Section 5.4.2) a ratio $E_x/G_{xy} = 3.9 \approx 4$ for the composition indicated below

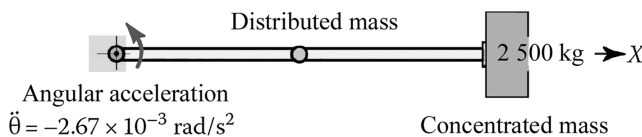
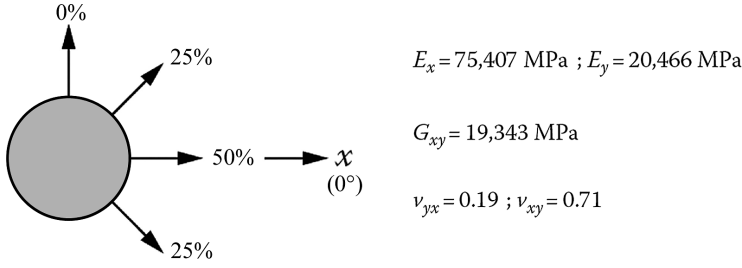


FIGURE 19.36 Inertial loading on the arm.



4. The maximum value of elasticity modulus observed on Chart 5.4 is

$$E'_x = 134,000 \text{ MPa}$$

The corresponding shear modulus is (Chart 5.5)

$$G'_{xy} = 4,200 \text{ MPa}$$

The same deflection as the previous one for the configuration (c) leads to

$$\frac{F\ell^3}{8E'_x I'} \left(\frac{2}{3} + \frac{E'_x}{2G'_{xy}} \right) = \frac{F\ell^3}{3E_x I}$$

Then,

$$\frac{I'}{I} = \frac{\pi r^3 e'}{\pi r^3 e} = \frac{3E_x}{8E'_x} \left(\frac{2}{3} + \frac{E'_x}{2G'_{xy}} \right) = 3.5$$

$$\frac{e'}{e} = 3.5$$

The tube with thickness e' and modulus E'_x would be stiffer for configuration (a) but would have a mass multiplied by 3.5 to keep the stiffness of configuration (c).

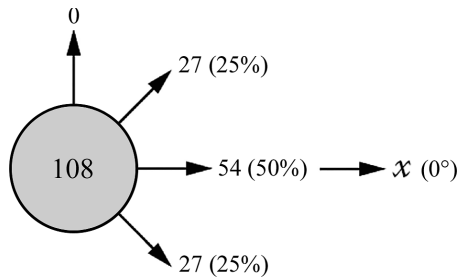
5. Configurations (a) and (c) are the more deformable. We must meet

$$\frac{F}{\Delta_Y} = \frac{3E_x I}{\ell^3} \geq \left(\frac{F}{\Delta} \right)_{\min}$$

$$\text{with } \ell = 15 \text{ m}; I = \pi r^3 e; r = 0.15 \text{ m}$$

$$(F/\Delta)_{\min} = 10^4 \text{ N/m}; E_x = 75,407 \text{ MPa}; e \geq 14 \text{ mm}$$

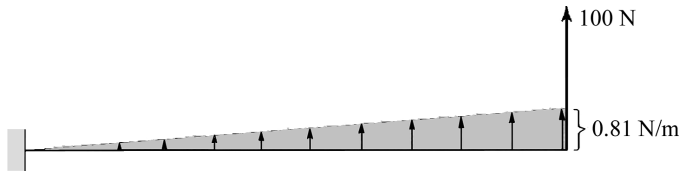
The ply thickness being 0.13 mm, we obtain 108 layers oriented as follows:



6. The specific mass of the laminate is $\rho = 1,530 \text{ kg/m}^3$ (see Section 3.3.3).
The distributed mass of the arm is then

$$\frac{m}{\ell} = \rho \times 2\pi r e = 20.2 \text{ kg/m}$$

With the angular acceleration indicated in Figure 19.36, the following inertial load distribution is obtained:



We deduce from there the deflections at the end of the arm:

- Due to the concentrated mass:

$$\Delta_{\text{concent}} = \frac{100\ell^3}{3E_x I}$$

- Due to distributed load²⁰:

$$\Delta_{\text{distributed}} = \frac{11}{120} \times \frac{0.81 \times \ell^4}{E_x I}$$

From which the total deflection is

$$\Delta_{\text{total}} = \frac{100\ell^3}{3E_x I} (1 + 0.033) \approx \frac{100\ell^3}{3E_x I}$$

The rigidity (F/Δ_{total}) appears well to be related essentially to the concentrated inertial load at the arm extremity.

NOTES

- 1 To establish this relation, see Chapter 16, Equation 16.17.
- 2 See a simplified calculation of coefficient k in Application 20.1 and a more precise calculation in Application 21.5.
- 3 The so-called orthotropic axes: See Chapters 12 and 15.
- 4 See Section 7.2.3.

- 5 The absence of buckling due to torsion of the shaft should also be verified (see Appendix B for this subject).
- 6 If the carbon/epoxy tube and the coupling plate have thicknesses that are different, the more general relation established in Application 21.1 should be used. This also allows different shear moduli for each of the two materials.
- 7 Recall the rotational kinetic energy for a mass m placed at a radius r and rotating at a speed of ω :

$$W_{\text{kinetic}} = \frac{1}{2} I \omega^2 = \frac{1}{2} m r^2 \omega^2 = \frac{1}{2} m V_{\text{circumfer}}^2.$$
- 8 The calculation to estimate these proportions is detailed in Example of Section 5.4.3, where we use the same values as the ones here for In-plane resultants, with a safety factor of 2, as $N_x = -800$ N/mm; $N_y = -900$ N/mm; $T_{xy} = -340$ N/mm
- 9 See Section 5.3.2 and also Chapter 14.
- 10 This result is immediate by using Equation 11.4.
- 11 See Section 1.6.
- 12 See Application 19.9.
- 13 We could also consider a balanced laminate with ply angles $+\alpha_1, -\alpha_1$, and $\pi/2$, the role of the matrix being neglected. The elastic coefficients of a ply (see Equation 11.1) reduce to only one nonzero, namely, E_ℓ . Calculation is carried out as shown in detail in Section 12.1.3. It is longer than by the direct method followed here for the particular case in question.
- 14 See also Equation 11.4 inverted.
- 15 PEEK resin, thermoplastically deformable (see Section 1.6).
- 16 This is because the elasticity modulus E_ℓ of unidirectional is six times higher than that of injected short fibers. For a more accurate calculation of stress values, see Equation 16.16.
- 17 To write this, we have to neglect the area of the corner. Then the shear flow is conservative.
- 18 See Section 5.4.5.4, Figure 5.31, for the distribution of stress in a laminated tube. See also Equation 16.16 in Chapter 16.
- 19 The exact value of α should be obtained from the complete shear stress study for this particular composite beam (see Equation 16.16 and Application 21.13).
- 20 Result obtained from the following differential equation:

$$EI_x \frac{d^2 v}{dX^2} = -\frac{0.81}{6} \times \ell^2 \left[2 - 3(X/\ell) + (X/\ell)^3 \right]$$

20 Applications Level 2

20.1 SANDWICH BEAM: SIMPLIFIED CALCULATION OF THE SHEAR COEFFICIENT

Problem Statement

Represented in Figure 20.1 is the cross section of a sandwich beam. The skin thickness is small compared with that of the core. Under a shear force T , shear stress values in the section are assumed to vary in a piecewise linear fashion¹ along the y -direction. The constitutive materials, denoted as 1 and 2, are assumed to be isotropic, or transversely isotropic in plane (y, z) . Shear moduli are G_1 for material 1 (skin) and G_2 for material 2 (core). The beam is of unitary width.

1. Calculate the shear coefficient k for flexure in (x, y) plane.
2. Give a simplified expression for the case, current in the applications, where $G_1 \gg G_2$ and with thicknesses denoted by e_1 and e_2 such that:

$$e_1 = \frac{(H_1 - H_2)}{2} \ll e_2 = H_2$$

Solution

1. Let W be the strain energy due to shear stress. Consideration of an elementary beam slice allows writing (Equation 16.17)

$$\frac{dW}{dx} = \frac{1}{2} k \frac{T^2}{\langle GS \rangle} = \frac{1}{2} \int_{\text{cross section}} \frac{\tau_{xy}^2}{G_i} dy$$

In the upper skin, we have

$$\tau_{xy} = \frac{(H_1 - 2y)}{(H_1 - H_2)} \times \tau_o$$

On the other hand, in the core, $\tau_{xy} = \tau_o$.

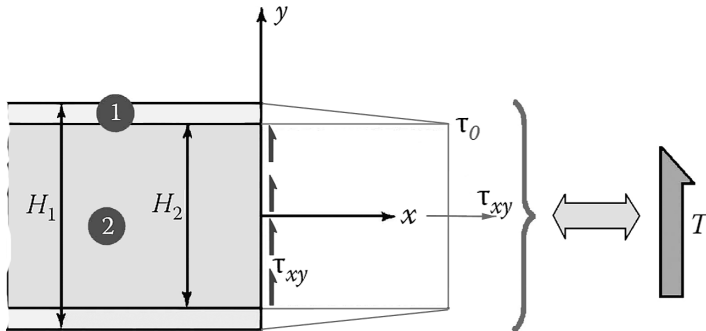


FIGURE 20.1 Sandwich beam.

Then with

$$T = \int_{\text{cross section}} \tau_{xy} (dy \times 1)$$

We deduce the maximum shear stress τ_0

$$\tau_0 = T \times \frac{2}{(H_1 + H_2)}$$

And the strain energy density

$$\frac{dW}{dx} = \frac{1}{2} \int \frac{\tau_{xy}^2}{G_i} dy = \int_0^{H_2/2} \frac{\tau_o^2}{G_2} dy + \int_{H_2/2}^{H_1/2} \frac{\tau_o^2}{G_1} \frac{(H_1 - 2y)^2}{(H_1 - H_2)^2} dy$$

After calculation,

$$\frac{1}{2} \int \frac{\tau_{xy}^2}{G_i} dy = \frac{\tau_o^2}{2} \left(\frac{H_2}{G_2} + \frac{H_1 - H_2}{3G_1} \right) = \frac{2 \times T^2}{(H_1 + H_2)^2} \left(\frac{H_2}{G_2} + \frac{H_1 - H_2}{3G_1} \right)$$

Then

$$\frac{1}{2} k \frac{T^2}{\langle GS \rangle} = \frac{2 \times T^2}{(H_1 + H_2)^2} \left(\frac{H_2}{G_2} + \frac{H_1 - H_2}{3G_1} \right)$$

$$k = \frac{4 \langle GS \rangle}{(H_1 + H_2)^2} \left(\frac{H_2}{G_2} + \frac{H_1 - H_2}{3G_1} \right)$$

With (Equation 16.16)

$$\langle GS \rangle = G_1(H_1 - H_2) + G_2H_2,$$

$$k = \frac{4[G_1(H_1 - H_2) + G_2H_2]}{(H_1 + H_2)^2} \times \left(\frac{H_2}{G_2} + \frac{H_1 - H_2}{3G_1} \right)$$

2. Case $G_1 \gg G_2$: we can rewrite

$$k = \frac{4 \langle GS \rangle}{(e_2 + 2e_1 + e_2)^2} \times \frac{e_2}{G_2} \left[1 + \frac{2}{3} \frac{e_1 G_2}{e_2 G_1} \right]$$

$(\ll 1)$

Then

$$k \approx \frac{\langle GS \rangle}{e_2^2 \left(1 + \frac{e_1}{e_2} \right)^2} \times \frac{e_2}{G_2}$$

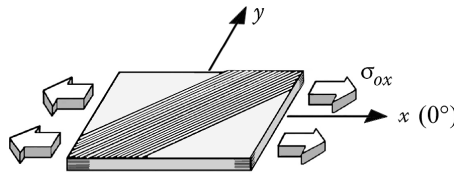
From which the following simplified form, valid when $e_1 \ll e_2$ and $G_2 \ll G_1$

$$\frac{k}{\langle GS \rangle} = \frac{1}{G_2(e_2 + 2e_1)}$$

20.2 PROCEDURE FOR A QUAD-LAMINATE CALCULATION PROGRAM

Problem Statement

Consider a balanced carbon/epoxy laminate with respect to the 0° direction (or x), with midplane symmetry. The plies are oriented 0° , 90° , $+45^\circ$, and -45° with certain proportions (there are as many $+45^\circ$ plies as -45° plies). This Quadrangle Symmetric laminate is subject to uniaxial stress $\sigma_{0x} = 1 \text{ MPa}$ (see the following figure).



Propose a procedure establishing a simple program to allow obtaining

1. Elasticity modulus E_x of the laminate and Poisson coefficient ν_{xy} ²
2. Stress state in orthotropic axes of each ply³
3. The Tsai-Hill⁴ expression for each ply
4. Largest stress value $\sigma_{0x \text{ max}}$ admissible without failure of any ply

The following gives the unidirectional ply characteristics (the laminate is made up of identical plies):

Carbon/epoxy ply with $V_f = 60\%$ fiber volume fraction (See Chapter 3, Table 3.4)

$$E_\ell = 134,000 \text{ MPa}; \quad E_t = 7,000 \text{ MPa}; \quad G_{\ell t} = 4,200 \text{ MPa}; \quad \nu_{\ell t} = 0.25$$

Ultimate strengths

$$\begin{aligned} \sigma_{\ell \text{ rupt.}}^{\text{tens.}} &= 1,270 \text{ MPa}; & \sigma_{\ell \text{ rupt.}}^{\text{comp.}} &= 1,130 \text{ MPa} \\ \sigma_{t \text{ rupt.}}^{\text{tens.}} &= 42 \text{ MPa}; & \sigma_{t \text{ rupt.}}^{\text{comp.}} &= 141 \text{ MPa} \\ \tau_{\ell t \text{ rupt.}} &= 63 \text{ MPa} \end{aligned}$$

Solution

The procedure for calculation is as follows (see also Section 12.1.3):

1. **Modulus E_x and Poisson coefficient ν_{xy}** : The laminate behavior with midplane symmetry can be written in this plane (Equation 12.7):

$$\left\{ \begin{array}{c} \sigma_{ox} \\ \sigma_{oy} \\ \tau_{oxy} \end{array} \right\} = \frac{1}{h} \left[\begin{array}{ccc} A_{11} & A_{12} & A_{13} \\ A_{21} & A_{22} & A_{23} \\ A_{31} & A_{32} & A_{33} \end{array} \right] \left\{ \begin{array}{c} \epsilon_{ox} \\ \epsilon_{oy} \\ \gamma_{oxy} \end{array} \right\} \quad (20.1)$$

With

$$\frac{1}{h} A_{ij} = \sum_{k=1st \text{ ply}}^{nth \text{ ply}} \bar{E}_{ij}^k \frac{e_k}{h}$$

e_k is the thickness of ply k , and h is the total laminate thickness. $[\bar{E}_{ij}^k]_k$ is the stiffness matrix in axes (x, y) for the ply k (see Equation 11.8), as

$$\begin{Bmatrix} \sigma_x \\ \sigma_y \\ \tau_{xy} \end{Bmatrix}_{ply k} = \begin{bmatrix} \bar{E}_{11} & \bar{E}_{12} & \bar{E}_{13} \\ \bar{E}_{21} & \bar{E}_{22} & \bar{E}_{23} \\ \bar{E}_{31} & \bar{E}_{32} & \bar{E}_{33} \end{bmatrix}_{ply k} \begin{Bmatrix} \epsilon_{ox} \\ \epsilon_{oy} \\ \gamma_{oxy} \end{Bmatrix}_{ply k} \quad (20.2)$$

$p^{0^\circ}(\%)$, $p^{90^\circ}(\%)$, $p^{+45^\circ}(\%)$, and $p^{-45^\circ}(\%)$ being the respective ply proportions at 0° , 90° , $+45^\circ$, and -45° , the previous terms $(1/h)A_{ij}$ can be rewritten as

$$\frac{1}{h} A_{ij} = \bar{E}_{ij}^{0^\circ} p^{0^\circ} + \bar{E}_{ij}^{90^\circ} p^{90^\circ} + \bar{E}_{ij}^{+45^\circ} p^{+45^\circ} + \bar{E}_{ij}^{-45^\circ} p^{-45^\circ} \quad (20.3)$$

Note that $(1/h)A_{13}$, $(1/h)A_{23}$, and their symmetrical counterparts are zero because the laminate is balanced (see Equation 11.8).

Equation 20.1 is then inverted as

$$\begin{Bmatrix} \epsilon_{ox} \\ \epsilon_{oy} \\ \gamma_{oxy} \end{Bmatrix} = \begin{bmatrix} \frac{1}{\bar{E}_x} & -\frac{\bar{v}_{yx}}{\bar{E}_y} & 0 \\ -\frac{\bar{v}_{xy}}{\bar{E}_x} & \frac{1}{\bar{E}_y} & 0 \\ 0 & 0 & \frac{1}{\bar{G}_{xy}} \end{bmatrix} \begin{Bmatrix} \sigma_{ox} \\ \sigma_{oy} \\ \tau_{oxy} \end{Bmatrix} \quad (20.4)$$

where \bar{E}_x , \bar{E}_y , \bar{G}_{xy} , \bar{v}_{xy} , \bar{v}_{yx} are the global moduli and Poisson coefficients of the laminate. This laminate is subjected to uniaxial stress $\sigma_{ox} = 1 \text{ MPa}$; then

$$\epsilon_{ox} = \frac{\sigma_{ox}}{\bar{E}_x} = \frac{1 \text{ MPa}}{\bar{E}_x (\text{MPa})}; \epsilon_{oy} = -\frac{\bar{v}_{xy}}{\bar{E}_x} \sigma_{ox} = -\frac{\bar{v}_{xy}}{\bar{E}_x (\text{MPa})} \times 1 \text{ MPa}$$

We obtain as well the modulus and the Poisson coefficient required:

$$\bar{E}_x (\text{MPa}) = \frac{1}{\epsilon_{ox}}$$

$$\bar{v}_{xy} = -\epsilon_{oy} \times \frac{\bar{E}_x (\text{MPa})}{1 \text{ MPa}}$$

- 2. Stress in each ply:** The previous result gives us the global strain of the laminate, strain that each ply should follow as

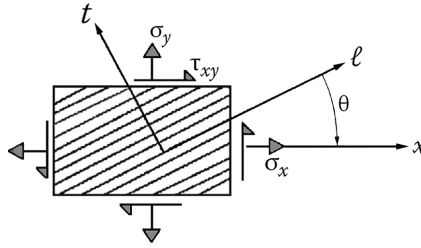
$$\epsilon_{ox} = \frac{1}{\bar{E}_x} \sigma_{ox}; \epsilon_{oy} = -\frac{\bar{v}_{xy}}{\bar{E}_x} \sigma_{ox}; \gamma_{oxy} = 0$$

For a ply k , Equation 20.2 is then written as

$$\begin{Bmatrix} \sigma_x \\ \sigma_y \\ \tau_{xy} \end{Bmatrix}_k = \begin{bmatrix} \bar{E}_{11} & \bar{E}_{12} & \bar{E}_{13} \\ \bar{E}_{21} & \bar{E}_{22} & \bar{E}_{23} \\ \bar{E}_{31} & \bar{E}_{32} & \bar{E}_{33} \end{bmatrix}_k \begin{Bmatrix} \varepsilon_{ox} \\ \varepsilon_{oy} \\ 0 \end{Bmatrix} \quad (20.5)$$

This gives the stress state in ply k and in (x, y) coordinates. In orthotropic axes of that ply (axes (ℓ, t) in the following figure), Equation 11.4 recalled below gives

$$\begin{Bmatrix} \sigma_\ell \\ \sigma_t \\ \tau_{\ell t} \end{Bmatrix}_{ply\ k} = \begin{bmatrix} c^2 & s^2 & -2cs \\ s^2 & c^2 & 2cs \\ sc & -sc & (c^2 - s^2) \end{bmatrix}_{ply\ k} \begin{Bmatrix} \sigma_x \\ \sigma_y \\ \tau_{xy} \end{Bmatrix}_{ply\ k} \quad \begin{matrix} c = \cos \theta \\ s = \sin \theta \end{matrix} \quad (20.6)$$



3. **The Tsai-Hill criterion:** Following Equation 14.12 (see also Section 5.3.2),

$$\alpha^2 = \frac{\sigma_\ell^2}{\sigma_{\ell\text{rupt.}}^2} + \frac{\sigma_t^2}{\sigma_{t\text{rupt.}}^2} - \frac{\sigma_\ell \sigma_t}{\sigma_{\ell\text{rupt.}}^2} + \frac{\tau_{\ell t}^2}{\tau_{\ell t\text{rupt.}}^2}$$

Which provides values $(\alpha^2)_k$ required for each ply k .

4. **The largest stress $\sigma_{ox\text{max}}$ allowable before failure:** The stress values σ_ℓ, σ_t and $\tau_{\ell t}$ are calculated for a global uniaxial stress: $\sigma_{ox} = 1$ MPa. Now let us apply the maximum stress allowable $\sigma_{ox\text{max}}$ (MPa). Then σ_ℓ, σ_t and $\tau_{\ell t}$ in ply k are multiplied by the ratio

$$\frac{\sigma_{ox\text{max}}}{1 \text{ MPa}}$$

And we obtain the critical unitary value of the saturated Tsai-Hill criterion:

$$\frac{\sigma_{ox\text{max}}^2}{(1 \text{ MPa})^2} \times \left\{ \frac{\sigma_\ell^2}{\sigma_{\ell\text{rupt.}}^2} + \frac{\sigma_t^2}{\sigma_{t\text{rupt.}}^2} - \frac{\sigma_\ell \sigma_t}{\sigma_{\ell\text{rupt.}}^2} + \frac{\tau_{\ell t}^2}{\tau_{\ell t\text{rupt.}}^2} \right\} = 1$$

With the values $(\alpha^2)_k$ found in the previous question for the Tsai-Hill expression between brackets, we obtain

$$\sigma_{ox\text{max}}^2 \times \alpha_k^2 = (1 \text{ MPa})^2$$

Then

$$\sigma_{ox\max} = \frac{1\text{MPa}}{\alpha_k}$$

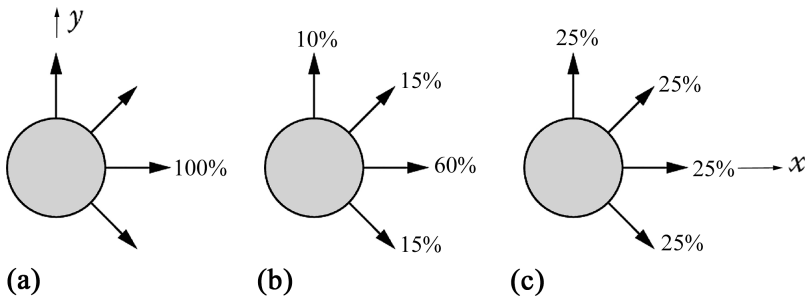
Examination of each ply will lead to a different value for $\sigma_{ox\max}$. We have to keep the minimum value and consider it as the critical stress that should initialize damage (first-ply failure):

$$\sigma_{ox\max} = \min \frac{1}{\alpha_k}$$

20.3 KEVLAR/EPOXY LAMINATES: STIFFNESS IN TERMS OF THE DIRECTION OF LOAD

Problem Statement

We consider balanced Kevlar®/epoxy laminates with $V_f = 60\%$ fiber volume fraction, working in their planes, with the following compositions:



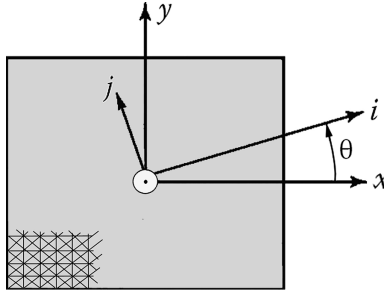
1. Give for these laminates the longitudinal modulus of elasticity denoted as $E(\theta)$ for a direction i in plane (x, y) , making the angle θ with x -direction.
2. For each of these laminates, express the **specific modulus** ($E(\theta)/\rho$), ρ being the mass density. Use for this purpose the charts in Section 5.4.2.
3. Represent in polar coordinates the variations of the specific modulus as a function of θ for each of the laminates.
4. Compare with the specific moduli of conventional materials: steel, aluminum alloy A92024 (2024), and titanium alloy R56400 (TA6V).

Solution

We assume that each of the balanced laminates constitutes a thin plate of orthotropic material, with orthotropic axes (x, y, z) . Thus the constitutive equation, i.e. Equation 12.9, is reduced to

$$\begin{Bmatrix} \epsilon_{ox} \\ \epsilon_{oy} \\ \gamma_{oxy} \end{Bmatrix} = \begin{bmatrix} \frac{1}{E_x} & -\frac{\nu_{yx}}{E_y} & 0 \\ -\frac{\nu_{xy}}{E_x} & \frac{1}{E_y} & 0 \\ 0 & 0 & \frac{1}{G_{xy}} \end{bmatrix} \begin{Bmatrix} \sigma_{ox} \\ \sigma_{oy} \\ \tau_{oxy} \end{Bmatrix}$$

1. E_x , E_y , and G_{xy} are the moduli of the laminate in orthotropic axes (x, y) . In axes (i, j) (see the following figure) making an angle θ with the axes (x, y) , these coefficients transform according to Equation 13.8.



The modulus in the i -direction is⁵

$$E(\theta) = \frac{1}{\frac{\cos^4 \theta}{E_x} + \frac{\sin^4 \theta}{E_y} + \cos^2 \theta \sin^2 \theta \left(\frac{1}{G_{xy}} - \frac{2\nu_{xy}}{E_x} \right)}$$

2. **Specific modulus:** For a Kevlar/epoxy laminate, we find the coefficients E_x , ν_{xy} , and G_{xy} in Charts 5.9 and 5.10 of Section 5.4.2. Chart 5.9 also allows obtaining E_y by permuting the 0° and 90° percentages.

The specific mass ρ is shown in Table 3.4 of Section 3.3.3. It can also be calculated using the relationship in Section 3.2.3. Its value is $\rho = 1,350 \text{ kg/m}^3$. Thus, we obtain the following expressions for the specific modulus:

- *Laminate (a)*

$$E_x = 85,000 \text{ MPa}$$

$$E_y = 5,600 \text{ MPa}$$

$$G_{xy} = 2,100 \text{ MPa}$$

$$\nu_{xy} = 0.34$$

$$\frac{E(\theta)}{\rho} (\text{m/s})^2 = \frac{10^6 / 1,350}{\frac{\cos^4 \theta}{85,000} + \frac{\sin^4 \theta}{5,600} + \cos^2 \theta \sin^2 \theta \left(\frac{1}{2,100} - 2 \times \frac{0.34}{85,000} \right)}$$

- *Laminate (b)*

$$E_x = 56,600 \text{ MPa}$$

$$E_y = 18,680 \text{ MPa}$$

$$G_{xy} = 8,030 \text{ MPa}$$

$$\nu_{xy} = 0.4$$

$$\frac{E(\theta)}{\rho} (\text{m/s})^2 = \frac{10^6 / 1,350}{\frac{\cos^4 \theta}{56,000} + \frac{\sin^4 \theta}{18,680} + \cos^2 \theta \sin^2 \theta \left(\frac{1}{8,030} - 2 \times \frac{0.4}{56,600} \right)}$$

- *Laminate (c)*: The proportions of 25% along the directions 0° and 90° cannot be obtained from Chart 5.9. In this view, we have to evaluate by extrapolation, starting from percentages of 20% and 30%, as⁶

$$E_x = \frac{1}{2}(28,260 + 35,400) = 31,830 \text{ MPa}$$

$$E_y = E_x$$

$$G_{xy} = 11,980 \text{ MPa}$$

$$\nu_{xy} = 0.335$$

$$\frac{E(\theta)}{\rho} (\text{m/s})^2 = \frac{10^6 / 1,350}{\frac{\cos^4 \theta + \sin^4 \theta}{31,830} + \cos^2 \theta \sin^2 \theta \left(\frac{1}{11,980} - 2 \times \frac{0.335}{31,830} \right)}$$

3. Evolution of specific modulus is described in Figure 20.2, where the ability to **control** the anisotropy of the laminate by modifying the ply percentages at 0° , 90° , $+45^\circ$, and -45° can be well observed.
4. For the other materials mentioned, we have immediately (Section 1.6)

$$\left(\frac{E}{\rho} \right)_{\text{steel}} = 26.3 \times 10^6 (\text{m/s})^2; \quad \left(\frac{E}{\rho} \right)_{\text{aluminum A 92,024 (2,024)}} = 26.8 \times 10^6 (\text{m/s})^2;$$

$$\left(\frac{E}{\rho} \right)_{\text{titanium R56400 (TA6V)}} = 23.9 \times 10^6 (\text{m/s})^2$$

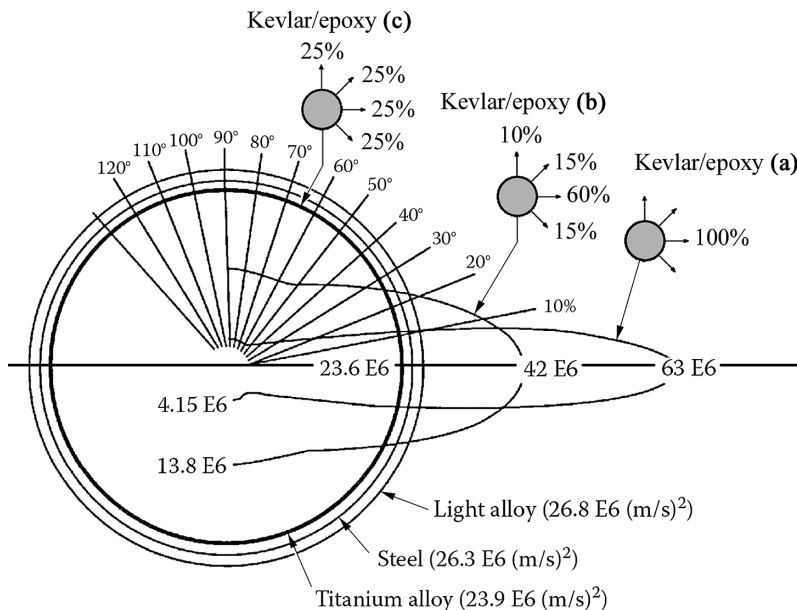


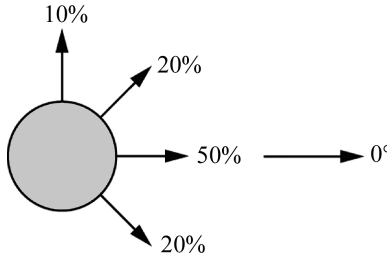
FIGURE 20.2 Specific modulus $(E(\theta)/\rho)(\text{m/s})^2$.

Note: The notion of specific modulus is particularly important in aeronautical construction. When comparing in the above diagram the performances of Kevlar/epoxy laminate with those of steel, aluminum, and titanium, we can see clearly the areas where the use of a laminate is beneficial. As a drawback, we should note the existence of specific angular limits for the loading directions for the Kevlar/epoxy laminate: this is a disadvantage.

20.4 RESIDUAL THERMAL STRESS DUE TO THE LAMINATE CURING PROCESS

Problem Statement

Consider a carbon/epoxy laminated panel with $V_f = 60\%$ fiber volume fraction. It has midplane symmetry, and the composition is shown in the following figure:



This panel is cured in an autoclave at 180°C and demolded at 20°C .

1. Calculate the thermal deformation values observed at the time of demolding.
2. Calculate the thermal residual stress values in the 90° plies.

Solution

1. Thermal deformation

The thermomechanical behavior of the laminate, following Equation 12.19, is

$$\begin{Bmatrix} \epsilon_{ox} \\ \epsilon_{oy} \\ \gamma_{oxy} \end{Bmatrix} = \begin{bmatrix} \frac{1}{\bar{E}_x} & -\frac{\bar{\nu}_{yx}}{\bar{E}_y} & \frac{\bar{\eta}_{xy}}{\bar{G}_{xy}} \\ -\frac{\bar{\nu}_{xy}}{\bar{E}_x} & \frac{1}{\bar{E}_y} & \frac{\bar{\mu}_{xy}}{\bar{G}_{xy}} \\ \frac{\bar{\eta}_x}{\bar{E}_x} & \frac{\bar{\mu}_y}{\bar{E}_y} & \frac{1}{\bar{G}_{xy}} \end{bmatrix} \begin{Bmatrix} \sigma_{ox} \\ \sigma_{oy} \\ \tau_{oxy} \end{Bmatrix} + \Delta T \begin{Bmatrix} \alpha_{ox} \\ \alpha_{oy} \\ \alpha_{oxy} \end{Bmatrix}$$

The panel is not subject to any external mechanical loading. This law then reduces to

$$\begin{Bmatrix} \epsilon_{ox} \\ \epsilon_{oy} \\ \gamma_{oxy} \end{Bmatrix} = \Delta T \begin{Bmatrix} \alpha_{ox} \\ \alpha_{oy} \\ \alpha_{oxy} \end{Bmatrix}$$

The laminate being balanced, Equations 12.18, 12.17, and 11.10 lead to

$$\alpha_{oxy} = 0$$

Then Chart 5.4 of Section 5.4.2 indicates for the laminate with the aforementioned composition:

$$\alpha_{ox} = -0.072 \times 10^{-5}$$

We can also deduce from Chart 5.4, by permutation of the 0° and 90° direction,

$$\alpha_{oy} = 0.44 \times 10^{-5}$$

Therefore, the thermal strain values due to a cooling down of $\Delta T = -160^\circ\text{C}$ are

$$\varepsilon_{ox} = -160 \times (-0.072 \times 10^{-5}); \quad \varepsilon_{oy} = -160 \times (0.44 \times 10^{-5})$$

Or

$$\varepsilon_{ox} = 115 \times 10^{-6}$$

$$\varepsilon_{oy} = -704 \times 10^{-6}$$

$$\gamma_{oxy} = 0$$

2. Residual thermal stress in the 90° plies

Equation 11.10 allows writing

$$\sigma_x = \bar{E}_{11}^{90^\circ} \varepsilon_{ox} + \bar{E}_{12}^{90^\circ} \varepsilon_{oy} - \Delta T \times \overline{\alpha E}_1^{90^\circ}$$

Where

$$\overline{\alpha E}_1^{90^\circ} = \bar{E}_t (\nu_{t\ell} \alpha_\ell + \alpha_t)$$

with (Equation 11.8)

$$\bar{E}_{11}^{90^\circ} = \bar{E}_t \quad \text{and} \quad \bar{E}_{12}^{90^\circ} = \nu_{t\ell} \bar{E}_\ell$$

The elastic moduli and thermal expansion coefficients are given in Table 3.4 of Section 3.3.3⁷. Then

$$\overline{\alpha E}_1^{90^\circ} = 0.237$$

With the known values ε_{ox} and ε_{oy}

$$\sigma_x = 7,021 \times 115 \times 10^{-6} + 1,717 \times (-704 \times 10^{-6}) - (-160) \times 0.237 = 37.5 \text{ MPa}$$

Analogously,

$$\sigma_y = \bar{E}_{21}^{90^\circ} \varepsilon_{ox} + \bar{E}_{22}^{90^\circ} \varepsilon_{oy} - \Delta T \times \overline{\alpha E}_2^{90^\circ}$$

with (see Equation 11.8)

$$\bar{E}_{22}^{90^\circ} = \bar{E}_\ell \quad \text{and} \quad \overline{\alpha E}_2^{90^\circ} = \bar{E}_\ell (\alpha_\ell + \nu_{t\ell} \alpha_t)$$

We obtain

$$\sigma_y = -110.2 \text{ MPa}$$

Finally,

$$\tau_{xy} = 0$$

And with Equation 11.4, we deduce, in axes (ℓ, t) of the 90° plies,

$$\sigma_\ell = -110.2 \text{ MPa}$$

$$\sigma_t = 37.5 \text{ MPa}$$

$$\tau_{\ell t} = 0$$

Note: When writing the Tsai-Hill expression (see Section 5.3.2) for the 90° plies, we obtain, using the failure strengths in Table 3.4 of Section 3.3.3,

$$\left(\frac{-110.2}{1,130} \right)^2 + \left(\frac{37.5}{42} \right)^2 - \left(\frac{(-110.2)(37.5)}{1,130^2} \right) = 0.81$$

The safety factor⁸ equals only

$$\frac{1}{\sqrt{0.81}} - 1 = 11\%$$

This low value is due to high value of σ_t close to the failure strength. From there is the phenomenon of **microfracture** of the resin that happens during cooling. Subsequently, the microcracks favor the absorption of moisture by the resin and secondarily by the fibers, which provokes expansion analogous to that induced by heating, with **hygrometric** expansion coefficients (see Section 12.1.8). The consequence is a reduction of residual stress in the plies, with values weaker than those mentioned earlier.

20.5 THERMOELASTIC BEHAVIOR OF A GLASS/POLYESTER TUBE

Problem Statement

Obtain the thermoelastic behavior of a cylindrical filament-wound tube made of E-glass/polyester, with $\pm 45^\circ$ balanced composition and with fiber volume fraction $V_f = 25\%$.

Solution

In axes (x, y) in Figure 20.3, the stress-strain law takes the form of Equation 12.19:

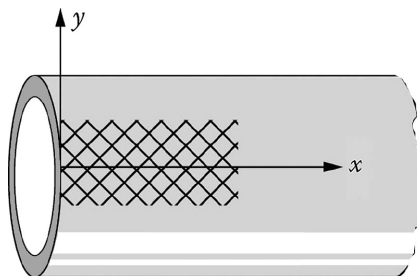


FIGURE 20.3 Filament-wound tube.

$$\left\{ \begin{array}{c} \epsilon_{ox} \\ \epsilon_{oy} \\ \gamma_{oxy} \end{array} \right\} = \left[\begin{array}{ccc} \frac{1}{\bar{E}_x} & -\frac{\bar{\nu}_{yx}}{\bar{E}_y} & \frac{\bar{\eta}_{xy}}{\bar{G}_{xy}} \\ -\frac{\bar{\nu}_{xy}}{\bar{E}_x} & \frac{1}{\bar{E}_y} & \frac{\bar{\mu}_{xy}}{\bar{G}_{xy}} \\ \frac{\bar{\eta}_x}{\bar{E}_x} & \frac{\bar{\mu}_y}{\bar{E}_y} & \frac{1}{\bar{G}_{xy}} \end{array} \right] \left\{ \begin{array}{c} \sigma_{ox} \\ \sigma_{oy} \\ \tau_{oxy} \end{array} \right\} + \Delta T \left\{ \begin{array}{c} \alpha_{ox} \\ \alpha_{oy} \\ \alpha_{oxy} \end{array} \right\}$$

- Calculation of elastic moduli

First, we have to evaluate the matrix $(1/h)[A_{ij}]$ in Equation 12.7. This calculation requires the stiffness coefficients \bar{E}_{ij} for each ply in Equation 11.8.

In this view, we first calculate the elastic moduli of a ply in its axes (ℓ, t). We have, according to Equation 10.2 and those that follow, and numerical values in Tables 1.3 and 1.4 of Section 1.6,

$$E_\ell = 74,000 \times 0.25 + 4,000 \times 0.75 = 21,500 \text{ MPa}$$

$$\nu_{\ell t} = 0.25 \times 0.25 + 0.4 \times 0.75 = 0.36$$

$$E_t = 4,000 \times \frac{1}{0.75 + \frac{4,000}{74,000} \times 0.25} = 5,240 \text{ MPa}$$

$$G_{\ell t} = 1,400 \times \frac{1}{0.75 + \frac{1,400}{30,000} \times 0.25} = 1,840 \text{ MPa}$$

$$\nu_{t\ell} = (5,240 / 21,500) \times 0.36 = 0.088$$

$$\bar{E}_\ell = 22,200 \text{ MPa}; \quad \bar{E}_t = 5,410 \text{ MPa}$$

Then (Equation 11.8)

$$\bar{E}_{11}^{+45^\circ} = \bar{E}_{11}^{-45^\circ} = \bar{E}_{22}^{+45^\circ} = \bar{E}_{22}^{-45^\circ} = 9,720 \text{ MPa}$$

$$\bar{E}_{33}^{+45^\circ} = \bar{E}_{33}^{-45^\circ} = 5,928 \text{ MPa};$$

$$\bar{E}_{12}^{+45^\circ} = \bar{E}_{12}^{-45^\circ} = 6,040 \text{ MPa}$$

$$\bar{E}_{13}^{+45^\circ} = -\bar{E}_{13}^{-45^\circ}; \quad \bar{E}_{23}^{+45^\circ} = -\bar{E}_{23}^{-45^\circ}$$

From which with Equation 12.8

$$\frac{1}{h}[A_{ij}] = \left[\begin{array}{ccc} 9,720 & 6,040 & 0 \\ 6,040 & 9,720 & 0 \\ 0 & 0 & 5,928 \end{array} \right] (\text{MPa})$$

In inverting this matrix (see Equation 12.9),

$$\begin{bmatrix} \frac{1}{\bar{E}_x} & -\frac{\bar{\nu}_{yx}}{\bar{E}_y} & 0 \\ -\frac{\bar{\nu}_{xy}}{\bar{E}_x} & \frac{1}{\bar{E}_y} & 0 \\ 0 & 0 & \frac{1}{\bar{G}_{xy}} \end{bmatrix} = \begin{bmatrix} 1.676 \times 10^{-4} & -1.041 \times 10^{-4} & 0 \\ -1.041 \times 10^{-4} & 1.676 \times 10^{-4} & 0 \\ 0 & 0 & \frac{1}{5,928} \end{bmatrix} (\text{MPa}^{-1})$$

From which by identification

$$\bar{E}_x = \bar{E}_y = 5,966 \text{ MPa}$$

$$\bar{\nu}_{yx} = \bar{\nu}_{xy} = 0.62$$

$$\bar{G}_{xy} = 5,928 \text{ MPa}$$

- Calculation of thermal expansion coefficients

We first calculate from Equation 12.18

$$\frac{1}{h} \langle \alpha E h \rangle_x, \frac{1}{h} \langle \alpha E h \rangle_y, \frac{1}{h} \langle \alpha E h \rangle_{xy}$$

This requires knowledge for each ply of terms $\bar{\alpha E}_1$, $\bar{\alpha E}_2$, and $\bar{\alpha E}_3$ (Equations 12.17 and 11.10 and numerical values in Tables 1.3 and 1.4 of Section 1.6). First, the expansion coefficients α_ℓ and α_t of a ply in its axes (ℓ , t) are obtained from Equations 10.7 and 10.8 and numerical values in Tables 1.3 and 1.4 of Section 1.6:

$$\alpha_\ell = 1.55 \times 10^{-5}; \alpha_t = 7.86 \times 10^{-5}$$

Then

$$\bar{\alpha E}_1^{+45^\circ} = \bar{\alpha E}_1^{-45^\circ} = \bar{\alpha E}_2^{+45^\circ} = \bar{\alpha E}_2^{-45^\circ} = 0.476 \text{ MPa} / ^\circ\text{C}$$

$$\bar{\alpha E}_3^{+45^\circ} = -\bar{\alpha E}_3^{-45^\circ}$$

From which (Equation 12.17)

$$\begin{bmatrix} \frac{1}{h} \langle \alpha E h \rangle_x \\ \frac{1}{h} \langle \alpha E h \rangle_y \\ \frac{1}{h} \langle \alpha E h \rangle_{xy} \end{bmatrix} = \begin{bmatrix} 0.476 \\ 0.476 \\ 0 \end{bmatrix} (\text{MPa} / ^\circ\text{C})$$

Then (Equation 12.18)

$$\begin{bmatrix} \alpha_{\alpha x} \\ \alpha_{\alpha y} \\ \alpha_{\alpha xy} \end{bmatrix} = \begin{bmatrix} 1.676 \times 10^{-4} & -1.041 \times 10^{-4} & 0 \\ -1.041 \times 10^{-4} & 1.676 \times 10^{-4} & 0 \\ 0 & 0 & \frac{1}{5,928} \end{bmatrix} \begin{bmatrix} 0.476 \\ 0.476 \\ 0 \end{bmatrix} = \begin{bmatrix} 3.02 \times 10^{-5} \\ 3.02 \times 10^{-5} \\ 0 \end{bmatrix}$$

In summary, the thermoelastic behavior of the filament-wound tube in glass/polyester can be written as

$$\begin{Bmatrix} \epsilon_{ox} \\ \epsilon_{oy} \\ \gamma_{oxy} \end{Bmatrix} = \underbrace{\begin{bmatrix} \frac{1}{5,966} & -\frac{0.62}{5,966} & 0 \\ -\frac{0.62}{5,966} & \frac{1}{5,966} & 0 \\ 0 & 0 & \frac{1}{5,928} \end{bmatrix}}_{(\text{MPa}^{-1})} \begin{Bmatrix} \sigma_{ox} \\ \sigma_{oy} \\ \tau_{oxy} \end{Bmatrix} + \Delta T \begin{Bmatrix} 3.02 \times 10^{-5} \\ 3.02 \times 10^{-5} \\ 0 \end{Bmatrix} \quad (^\circ\text{C}^{-1})$$

20.6 CREEP OF A POLYMERIC TUBE REINFORCED BY FILAMENT WOUND UNDER THERMAL STRESS

Consider a cylindrical tube of revolution made of polyvinylidene fluoride (PVDF) reinforced externally by filament winding of glass/polyester at $\pm 45^\circ$ from the cylinder generatrices, as in Figure 20.4.

The constituent characteristics are as follows:

- *Polymer tube:*

Thickness $e_1 = 10$ mm; isotropic material; elasticity modulus $E_1 = 260$ MPa; Poisson coefficient $\nu_1 = 0.3$; thermal expansion coefficient $\alpha_1 = 15 \times 10^{-5} (^\circ\text{C}^{-1})$.

- *Glass/polyester reinforcement:*

Thickness $e_2 = 3$ mm; elasticity modulus E_2 ; Poisson coefficient ν_2

Coefficient of thermal expansion $\alpha_2 = 0.7 \times 10^{-5} (^\circ\text{C}^{-1})$. These coefficients are valid in axes (x, y) defining the tangent plane in Figure 20.4. Fiber volume fraction $V_f = 60\%$.

Problem Statement

The thicknesses e_1 and e_2 are small relative to the average radius of the tube, denoted as r .

1. Give the numerical values of E_2 and ν_2 (noting that the elastic moduli of epoxy resins and polyester resins are equivalent).
2. When taking into account a temperature variation ΔT , the mechanical behavior of polymer (1) and reinforcement (2), respectively, can be written in axes (x, y) :

$$\begin{Bmatrix} \epsilon_{1x} \\ \epsilon_{1y} \\ \gamma_{1xy} \end{Bmatrix} = \begin{bmatrix} \frac{1}{E_1} & -\frac{\nu_1}{E_1} & 0 \\ -\frac{\nu_1}{E_1} & \frac{1}{E_1} & 0 \\ 0 & 0 & \frac{1}{G_1} \end{bmatrix} \begin{Bmatrix} \sigma_{1x} \\ \sigma_{1y} \\ \tau_{1xy} \end{Bmatrix} + \alpha_1 \Delta T \begin{Bmatrix} 1 \\ 1 \\ 0 \end{Bmatrix}$$

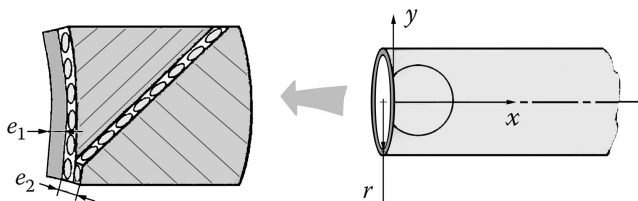


FIGURE 20.4 Polymeric tube reinforced with GFRP.

$$\begin{Bmatrix} \varepsilon_{2x} \\ \varepsilon_{2y} \\ \gamma_{2xy} \end{Bmatrix} = \begin{bmatrix} \frac{1}{E_2} & -\frac{\nu_2}{E_2} & 0 \\ -\frac{\nu_2}{E_2} & \frac{1}{E_2} & 0 \\ 0 & 0 & \frac{1}{G_2} \end{bmatrix} \begin{Bmatrix} \sigma_{2x} \\ \sigma_{2y} \\ \tau_{2xy} \end{Bmatrix} + \alpha_2 \Delta T \begin{Bmatrix} 1 \\ 1 \\ 0 \end{Bmatrix}$$

where we can recognize the strain and stress values in each of the materials. Starting with an assembly (polymer+reinforcement) not stressed nor strained at ambient temperature (20°C), this assembly is heated up to a temperature of 140°C.

- Write the equations describing the external load balance of this assembly.
 - Write the equality of strain. Deduce a system of equations that allows the calculation of stress values $\sigma_{1x}, \sigma_{1y}, \sigma_{2x}, \sigma_{2y}$.
 - Numerical application:* Calculate the stress values in each of the two components (polymer and glass/polyester reinforcement) as well as the strains.
3. Being thereby subject to high temperature, the internal tube in polymer obeys creep law. The stress values calculated previously do not remain constant in time. They evolve and stabilize at a certain final state. When this state is achieved, if the internal polymer tube is separated, by imagination, from its reinforcement and is cooled quickly from 140°C to 20°C, residual strain will be observed, denoted as $\Delta \varepsilon_{1x} = \Delta \varepsilon_{1y} = \Delta \varepsilon$, whereas in the absence of creep, there would be no residual strain in this tube.
- Write the four equations allowing the calculation of stress values in the assembly at 140°C **after** creep in the polymer, denoted as $\sigma'_{1x}, \sigma'_{1y}, \sigma'_{2x}, \sigma'_{2y}$.
 - Numerical application:* It has been found from the experiment that $\Delta \varepsilon = -0.6 \times \alpha_1 \Delta T$. Calculate the stress values after creep.
4. Considering the assembly at 140°C already crept, we cool the whole reinforced tube quickly, from 140°C to 20°C. Calculate the final stress values in the assembly at the end of cooling, denoted as $\sigma''_{1x}, \sigma''_{1y}, \sigma''_{2x}, \sigma''_{2y}$. Comment.

Solution

- For elastic characteristic values of a unidirectional ply in glass/polyester with $V_f = 0.6$, we will take those of a glass/epoxy ply in Table 3.4. For a laminate at $\pm 45^\circ$, Chart 5.14 of Section 5.4.2 shows

$$E_2 = 14,130 \text{ MPa}$$

$$\nu_2 = 0.57$$

- Equilibrium of the assembly:* Section cuts as meridian section and cross section in Figure 20.5 do not show any external resultant force despite of the existence of thermal induced stress.

In addition, because thicknesses are small compared with the radius, each stress value will be taken uniform over the thickness. From there, we have

$$2\pi r (\sigma_{1x} e_1 + \sigma_{2x} e_2) = 0 ; \quad 1 \times 2 (\sigma_{1y} e_1 + \sigma_{2y} e_2) = 0$$

Then

$$\sigma_{1x} e_1 + \sigma_{2x} e_2 = 0$$

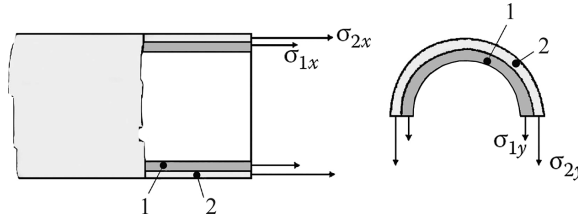


FIGURE 20.5 Equilibrium of the assembly.

$$\sigma_{1y}e_1 + \sigma_{2y}e_2 = 0 \quad (20.8)$$

Due to the symmetry of revolution for the stress distribution, there is no shear stress:

$$\tau_{1xy} = \tau_{2xy} = 0$$

- b. *Equality of strains:* the bonding between components 1 and 2, which is assumed perfect, ensures this equality:

$$\epsilon_{1x} = \epsilon_{2x}; \quad \epsilon_{1y} = \epsilon_{2y}; \quad \gamma_{1xy} = \gamma_{2xy}$$

With the behavior as mentioned in the problem statement, the equalities become

$$\frac{\sigma_{1x}}{E_1} - \frac{\nu_1}{E_1} \sigma_{1y} + \alpha_1 \Delta T = \frac{\sigma_{2x}}{E_2} - \frac{\nu_2}{E_2} \sigma_{2y} + \alpha_2 \Delta T \quad (20.9)$$

$$-\frac{\nu_1}{E_1} \sigma_{1x} + \frac{\sigma_{1y}}{E_1} + \alpha_1 \Delta T = -\frac{\nu_2}{E_2} \sigma_{2x} + \frac{\sigma_{2y}}{E_2} + \alpha_2 \Delta T \quad (20.10)$$

Equations 20.7–20.10 constitute a system of four equations for four unknowns: $\sigma_{1x}, \sigma_{1y}, \sigma_{2x}, \sigma_{2y}$.

- c. *In performing successively* (20.9) – (20.10), (20.9) + (20.10), then substituting σ_{2x}, σ_{2y} obtained from Equations 20.7 and 20.8, we obtain

$$\left\{ \begin{array}{l} \sigma_{1x} - \sigma_{1y} = 0 \\ \sigma_{1x} + \sigma_{1y} = 2\Delta T \times \frac{(\alpha_2 - \alpha_1)}{\left(\frac{1-\nu_1}{E_1}\right) + \frac{e_1}{e_2} \left(\frac{1-\nu_2}{E_2}\right)} \end{array} \right.$$

From which

$$\sigma_{1x} = \sigma_{1y} = \Delta T \times \frac{(\alpha_2 - \alpha_1)}{\left(\frac{1-\nu_1}{E_1}\right) + \frac{e_1}{e_2} \left(\frac{1-\nu_2}{E_2}\right)}$$

We deduce from there, with $\Delta T = 140 - 20 = 120^\circ\text{C}$,

$$\sigma_{1x} = \sigma_{1y} = -6.14 \text{ MPa}$$

$$\sigma_{2x} = \sigma_{2y} = 20.4 \text{ MPa}$$

The internal polymer tube is in biaxial compression. The external tube in glass/polyester is in biaxial tension. The mechanical behavior as given in the problem statement then indicates

$$\epsilon_{1x} = \epsilon_{2x} = \epsilon_{1y} = \epsilon_{2y} = 1.47 \times 10^{-3}$$

3. Creep

a. *The equilibrium relationships* are formally unchanged as

$$\sigma'_{1x}e_1 + \sigma'_{2x}e_2 = 0 \quad (20.11)$$

$$\sigma'_{1y}e_1 + \sigma'_{2y}e_2 = 0 \quad (20.12)$$

The relationships characterizing the perfect bonding are now amended in accordance with Figure 20.6.

With the constitutive equations recalled in the problem statement, these equalities become

$$\frac{\sigma'_{1x}}{E_1} - \frac{\nu_1}{E_1} \sigma'_{1y} + \alpha_1 \Delta T + \Delta \epsilon = \frac{\sigma'_{2x}}{E_2} - \frac{\nu_2}{E_2} \sigma'_{2y} + \alpha_2 \Delta T \quad (20.13)$$

$$-\frac{\nu_1}{E_1} \sigma'_{1x} + \frac{\sigma'_{1y}}{E_1} + \alpha_1 \Delta T + \Delta \epsilon = -\frac{\nu_2}{E_2} \sigma'_{2x} + \frac{\sigma'_{2y}}{E_2} + \alpha_2 \Delta T \quad (20.14)$$

b. *Numerical application:* In performing successively (20.13) – (20.14), (20.13)+(20.14), then substituting σ'_{2x} and σ'_{2y} calculated from Equations 20.11 and 20.12, we obtain

$$\sigma'_{1x} = \sigma'_{1y} = \Delta T \times \frac{(\alpha_2 - 0.4\alpha_1)}{\left(\frac{1-\nu_1}{E_1}\right) + \frac{e_1}{e_2} \left(\frac{1-\nu_2}{E_2}\right)}$$

Then

$$\sigma'_{1x} = \sigma'_{1y} = -2.28 \text{ MPa}$$

$$\sigma'_{2x} = \sigma'_{2y} = 7.6 \text{ MPa}$$

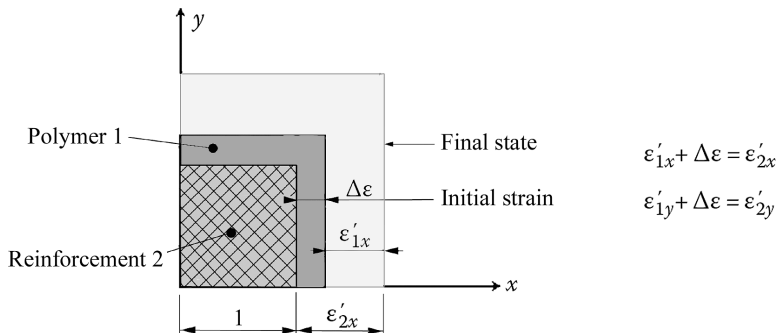


FIGURE 20.6 Creep.

4. *Cooling*: By simply suppressing the increase in temperature ΔT in Equations 20.13 and 20.14, the system of equations becomes

$$\left\{ \begin{array}{l} \sigma''_{1x} e_1 + \sigma''_{2x} e_2 = 0 \\ \sigma''_{1y} e_1 + \sigma''_{2y} e_2 = 0 \\ \frac{\sigma''_{1x}}{E_1} - \frac{\nu_1}{E_1} \sigma''_{1y} + \Delta \varepsilon = \frac{\sigma''_{2x}}{E_2} - \frac{\nu_2}{E_2} \sigma''_{2y} \\ -\frac{\nu_1}{E_1} \sigma''_{1x} + \frac{\sigma''_{1y}}{E_1} + \Delta \varepsilon = -\frac{\nu_2}{E_2} \sigma''_{2x} + \frac{\sigma''_{2y}}{E_2} \end{array} \right.$$

With an analogous resolution method to that used previously, we obtain

$$\sigma''_{1x} = \sigma''_{1y} = \Delta T \times \frac{0.6\alpha_1}{\left(\frac{1-\nu_1}{E_1}\right) + \frac{e_1}{e_2} \left(\frac{1-\nu_2}{E_2}\right)}$$

Then

$$\sigma''_{1x} = \sigma''_{1y} = 3.9 \text{ MPa}$$

$$\sigma''_{2x} = \sigma''_{2y} = -12.9 \text{ MPa}$$

It is worth noting that the polymer tube is loaded now in biaxial tension. Therefore, during an operating cycle, the polymer tube is successively compressed, released by creep, and then extended, as shown in Figure 20.7.

These loading cycles are repeated during the life of the tube, and this increases the risk of fatigue failure. Therefore, an oversizing of the polymer tube is necessary, which leads to low stresses in the polymer, to prevent the risks of:

- Buckling of the compressed tube at the defect locations in adhesive bond between polymer and glass/polyester reinforcement
- Tensile failure during the cooling

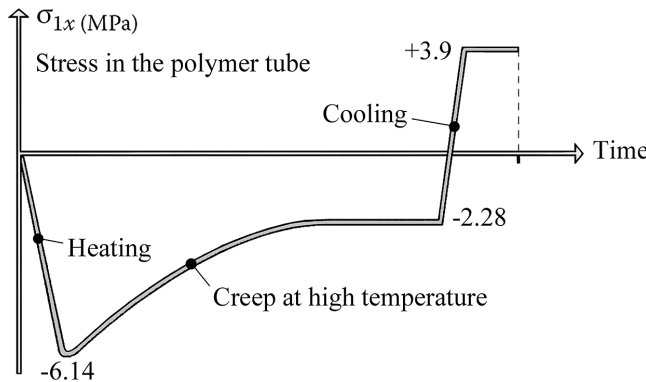


FIGURE 20.7 Operating cycle for the polymer tube.

20.7 FIRST-PLY FAILURE OF A LAMINATE; ULTIMATE STRENGTH

Problem Statement

Consider a carbon/epoxy laminate with 60% fiber volume fraction and the composition as in Figure 20.8.

1.
 - a. Give the elasticity moduli and Poisson coefficients of this laminate.
 - b. What maximum tensile stress denoted as $\sigma_{x\max}$ can be applied without damage?
2. When the value $\sigma_{x\max}$ is exceeded, the 90° plies are damaged by microcracks in epoxy resin, corresponding to the **first-ply** failure. Elastic characteristics of the cracked plies at 90° are therefore decreased with respect to their initial values for intact plies. We shall admit the following damage factors⁹:

$$E'_{\ell\text{fractured}} \simeq E_{\ell\text{intact}}; \quad E'_{t\text{fractured}} \simeq 0.1 \times E_{t\text{intact}}$$

$$G'_{\ell t\text{fractured}} \simeq 0.1 \times G_{\ell t\text{intact}}; \quad \nu'_{\ell t\text{fractured}} \simeq 0.1 \times \nu_{\ell t\text{intact}}$$

- a. Calculate the new terms of matrix $(1/h)[A]$ for the elastic behavior¹⁰. Deduce from there the new elastic moduli of the damaged laminate. Comment.
- b. Calculate the maximum stress σ_{xM} , so-called ultimate strength, leading to complete failure of this laminate, that is, rupture of 0° plies, or **last-ply rupture**.
3. What is the failure strength value, denoted as σ'_{xM} , that would be obtained by eliminating all elastic characteristics of the damaged 90° plies?
How could we obtain rapidly this value σ'_{xM} ?
4. The dimensioning of an aeronautical part is carried out using the previous laminate, with the following considerations:

- a. When the part is subject to a stress along the x -direction, so-called *limit load*, it stays in a reversible elastic domain and is not altered in its structure.
- b. When the part is subject to a stress along the x -direction, so-called *ultimate load*, the result is the total rupture.

Moreover, the regulatory specify

$$\text{Ultimate load} = 1.5 \times \text{limit load}$$

What values of σ_x should be kept here for ultimate load and for limit load, respectively?

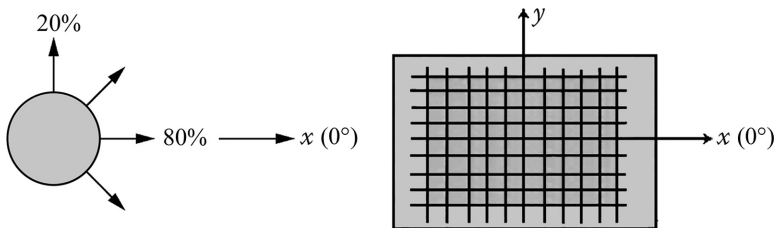


FIGURE 20.8 Composition of the laminate.

Solution

1.

- a. According to Charts 5.4 and 5.5 of Section 5.4.2, we note for the specified composition

$$E_x = 108,860 \text{ MPa}; \quad E_y = 32,447 \text{ MPa}$$

$$\nu_{xy} = 0.054; \quad \nu_{yx} = 0.016 \text{ MPa}$$

$$G_{xy} = 4,200 \text{ MPa}$$

- b. Chart 5.1 of Section 5.4.2 indicates for the first-ply failure:

$$\sigma_x = 659 \text{ MPa}$$

2.

- a. Terms of matrix
- $(1/h)[A]$
- are written as (Equations 12.7 and 12.8)

$$\frac{1}{h} A_{ij} = \bar{E}_{ij}^{0^\circ} \times p^{0^\circ} + \bar{E}_{ij}^{90^\circ} \times p^{90^\circ}$$

Coefficients \bar{E}_{ij} are given by Equation 11.8¹¹:

$$\bar{E}_{11}^{0^\circ} = 134,440 \text{ MPa}; \quad \bar{E}_{22}^{0^\circ} = 7,023 \text{ MPa}; \quad \bar{E}_{12}^{0^\circ} = 1,748 \text{ MPa}$$

$$\bar{E}_{33}^{0^\circ} = 4,200 \text{ MPa}$$

The 90° plies are damaged. Then¹²

$$\bar{E}_{11}^{90^\circ} \Rightarrow \bar{E}'_t = 700 \text{ MPa}; \quad \bar{E}_{22}^{90^\circ} \Rightarrow \bar{E}'_l = 134,000 \text{ MPa}$$

$$\bar{E}_{12}^{90^\circ} \Rightarrow \nu'_{tl} \bar{E}'_l = 17.5 \text{ MPa}; \quad \bar{E}_{33}^{90^\circ} = 420 \text{ MPa}$$

Hence after calculation,

$$\frac{1}{h}[A] = \begin{bmatrix} 107,692 & 1,402 & 0 \\ 1,402 & 32,418 & 0 \\ 0 & 0 & 3,444 \end{bmatrix} (\text{MPa})$$

The new moduli of the damaged laminate are obtained by inverting the matrix. We have (Equation 12.9)

$$h[A]^{-1} = \begin{bmatrix} \frac{1}{E'_x} & -\frac{\nu'_{yx}}{E'_y} & 0 \\ -\frac{\nu'_{xy}}{E'_x} & \frac{1}{E'_y} & 0 \\ 0 & 0 & \frac{1}{G'_{xy}} \end{bmatrix}$$

Which leads to

$$E'_x = 107,630 \text{ MPa}$$

$$E'_y = 32,400 \text{ MPa}$$

$$\nu'_{xy} = 0.043; \quad \nu'_{yx} = 0.013$$

$$G'_{xy} = 3,444 \text{ MPa}$$

Note that only the shear modulus G_{xy} has its value significantly decreased with respect to the intact laminate.

- (b) The 90° plies being damaged, the total failure of the laminate corresponds to rupture of the 0° plies. Let σ_{xM} be the corresponding ultimate failure strength. From the foregoing, the mechanical behavior of the damaged laminate is written as

$$\begin{Bmatrix} \varepsilon_{ox} \\ \varepsilon_{oy} \\ \gamma_{oxy} \end{Bmatrix} = \begin{bmatrix} 9.29 \times 10^{-6} & -4.02 \times 10^{-7} & 0 \\ -4.02 \times 10^{-7} & 3.086 \times 10^{-5} & 0 \\ 0 & 0 & 2.9 \times 10^{-4} \end{bmatrix} \begin{Bmatrix} \sigma_{xM} \\ 0 \\ 0 \end{Bmatrix} = \begin{Bmatrix} 9.29 \times 10^{-6} \times \sigma_{xM} \\ -4.02 \times 10^{-7} \times \sigma_{xM} \\ 0 \end{Bmatrix}$$

From which the stress state in the 0° plies (Equation 11.8)

$$\sigma_x = \bar{E}_{11}^{0^\circ} \varepsilon_{ox} + \bar{E}_{12}^{0^\circ} \varepsilon_{oy} = 1.248 \times \sigma_{xM} = \sigma_\ell$$

$$\sigma_y = \bar{E}_{12}^{0^\circ} \varepsilon_{ox} + \bar{E}_{22}^{0^\circ} \varepsilon_{oy} = 0.0134 \times \sigma_{xM} = \sigma_t$$

$$\tau_{xy} = 0 = \tau_{\ell t}$$

Writing the saturation of the Tsai-Hill criterion for σ_{xM} (see Section 5.3.2) with the failure strength values of Section 3.3.3

$$\left(\frac{1.248 \times \sigma_{xM}}{1,270} \right)^2 + \left(\frac{0.0134 \times \sigma_{xM}}{42} \right)^2 - \frac{1.248 \times 0.0134 \times \sigma_{xM}^2}{1,270^2} = 1$$

We obtain

$$\sigma_{xM} = 973 \text{ MPa}$$

3. If we cancel all elastic characteristics of the damaged plies at 90° , the $\frac{1}{h}[A]$ matrix becomes

$$\frac{1}{h}[A] = 0.8 \begin{bmatrix} \bar{E}_\ell & \nu_{\ell t} \bar{E}_\ell & 0 \\ \nu_{\ell t} \bar{E}_\ell & \bar{E}_t & 0 \\ 0 & 0 & G_{\ell t} \end{bmatrix} \quad \text{then} \quad h[A]^{-1} = \frac{1}{0.8} \begin{bmatrix} \frac{1}{E_\ell} & -\frac{\nu_{\ell t}}{E_t} & 0 \\ -\frac{\nu_{\ell t}}{E_\ell} & \frac{1}{E_t} & 0 \\ 0 & 0 & \frac{1}{G_{\ell t}} \end{bmatrix}$$

Under an ultimate loading σ'_{xM} we note the strain values:

$$\varepsilon_{ox} = \frac{1}{0.8} \frac{\sigma'_{xM}}{E_\ell}; \quad \varepsilon_{oy} = \frac{1}{0.8} \times -\frac{\nu_{\ell t}}{E_t} \sigma'_{xM}; \quad \gamma_{oxy} = 0$$

Then in the 0° plies,

$$\begin{aligned}\sigma_x = \sigma_\ell &= \bar{E}_{11}^{0^\circ} \varepsilon_{ox} + \bar{E}_{12}^{0^\circ} \varepsilon_{oy} = \frac{\sigma'_{x_M}}{0.8} \\ \sigma_y = \sigma_t &= \bar{E}_{12}^{0^\circ} \varepsilon_{ox} + \bar{E}_{22}^{0^\circ} \varepsilon_{oy} = 0\end{aligned}$$

And the saturated Tsai-Hill criterion takes the form

$$\left(\frac{\sigma'_{x_M}}{0.8 \times 1,270} \right)^2 = 1$$

Thus,

$$\sigma'_{x_M} = 1,016 \text{ MPa}$$

We should immediately obtain this value by noting that a stress resultant such as N_x can be written as

$$N_x = \sigma_x \times h = \sigma_x^{0^\circ} \times 0.8h + \cancel{\sigma_x^{90^\circ}} \times 0.2h$$

Then

$$\sigma'_{x_M} = \sigma_{x_M}^{0^\circ} \times 0.8 = 1,270 \times 0.8 = 1,016 \text{ MPa}$$

Note that the failure strength σ_{x_M} corresponding to the last-ply failure calculated in the previous problem is less than σ'_{x_M} . It would have been unwise to reason as if the 0° plies were alone to resist while occupying 80% of the thickness of the laminate.

4. Considering that the limit load corresponds to first-ply rupture, we have $\sigma_{x_{\text{limit}}} = 659 \text{ MPa}$. Hence, the ultimate load will be

$$\sigma_{x_{\text{ultimate}}} = 1.5 \times 659 = 988 \text{ MPa}$$

This is an excessive value because the last-ply failure occurs with $\sigma_{x_M} = 973 \text{ MPa}$. In such a view, we should keep

- For ultimate load, $\sigma_{x_{\text{ultimate}}} = \sigma_{x_M} = 973 \text{ MPa}$
- For limit load,

$$\sigma_{x_{\text{limit}}} = \frac{\sigma_{x_M}}{1.5} = 649 \text{ MPa}$$

Which is less than the value corresponding to first-ply failure.

20.8 OPTIMUM LAMINATE FOR ISOTROPIC PLANE STRESS

Problem Statement

Consider a laminate subjected to the plane stress $\sigma_x = \sigma_y = \sigma_0$; $\tau_{xy} = 0$, characterizing an isotropic state of plane stress.

This laminate presents the composition as in Figure 20.9:

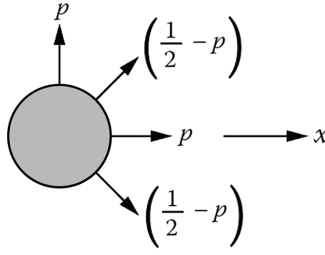


FIGURE 20.9 Composition of the laminate.

1. By a literal calculation, show that the strain of the laminate is invariant for any value of $p \leq 0.5$. Verify this property by means of Chart 5.4 in Section 5.4.2 for $p=0\%$, 30% , 50% .
2. Show that the Tsai-Hill criterion has the same value regardless of the ply, no matter what the proportion p . Comment.
3. Verify the previous property for a carbon/epoxy laminate by means of the figures in Appendix A for $p=0\%$, 30% , 50% .

Solution

1. Determination of apparent moduli of the carbon/epoxy laminate: We begin by calculating the terms of matrix $(1/h)[A]$ (Equations 12.7 and 12.8):

$$\frac{1}{h} A_{11} = \bar{E}_{11}^{0^\circ} \times p + \bar{E}_{11}^{90^\circ} \times p + \bar{E}_{11}^{+45^\circ} \times \left(\frac{1}{2} - p\right) + \bar{E}_{11}^{-45^\circ} \times \left(\frac{1}{2} - p\right)$$

From Equation 11.8,

$$\bar{E}_{11}^{0^\circ} = \bar{E}_\ell; \quad \bar{E}_{11}^{90^\circ} = \bar{E}_t; \quad \bar{E}_{11}^{+45^\circ} = \bar{E}_{11}^{-45^\circ} = \frac{(\bar{E}_\ell + \bar{E}_t)}{4} + \frac{1}{2}(\nu_{t\ell}\bar{E}_\ell + 2G_{t\ell})$$

$$\frac{1}{h} A_{11} = p(\bar{E}_\ell + \bar{E}_t) + 2\left(\frac{1}{2} - p\right)\left[\frac{(\bar{E}_\ell + \bar{E}_t)}{4} + \frac{1}{2}(\nu_{t\ell}\bar{E}_\ell + 2G_{t\ell})\right]$$

$$\frac{1}{h} A_{11} = p\left[\frac{(\bar{E}_\ell + \bar{E}_t)}{2} - \nu_{t\ell}\bar{E}_\ell - 2G_{t\ell}\right] + \frac{1}{2}\left[\frac{(\bar{E}_\ell + \bar{E}_t)}{2} + \nu_{t\ell}\bar{E}_\ell + 2G_{t\ell}\right]$$

$$\frac{1}{h} A_{22} = \frac{1}{h} A_{11}$$

$$\frac{1}{h} A_{12} = 2p \times \nu_{t\ell}\bar{E}_\ell + 2\left(\frac{1}{2} - p\right)\left[\frac{1}{4}(\bar{E}_\ell + \bar{E}_t - 4G_{t\ell}) + \frac{1}{2}\nu_{t\ell}\bar{E}_\ell\right]$$

$$\frac{1}{h} A_{12} = -p\left[\frac{\bar{E}_\ell + \bar{E}_t}{2} - \nu_{t\ell}\bar{E}_\ell - 2G_{t\ell}\right] + \frac{1}{2}\left[\frac{\bar{E}_\ell + \bar{E}_t}{2} + \nu_{t\ell}\bar{E}_\ell - 2G_{t\ell}\right]$$

$$\frac{1}{h} A_{13} = \frac{1}{h} A_{23} = 0$$

The constitutive law in Equation 12.7 here takes the form

$$\begin{Bmatrix} \sigma_o \\ \sigma_o \\ 0 \end{Bmatrix} = \frac{1}{h} \begin{bmatrix} A_{11} & A_{12} & 0 \\ A_{21} & A_{22} & 0 \\ 0 & 0 & A_{33} \end{bmatrix} \begin{Bmatrix} \varepsilon_{ox} \\ \varepsilon_{oy} \\ \gamma_{oxy} \end{Bmatrix}$$

After inversion,

$$\begin{Bmatrix} \varepsilon_{ox} \\ \varepsilon_{oy} \\ \gamma_{oxy} \end{Bmatrix} = \begin{bmatrix} 1/\bar{E}_x & -\bar{\nu}_{yx}/\bar{E}_y & 0 \\ -\bar{\nu}_{xy}/\bar{E}_x & 1/\bar{E}_y & 0 \\ 0 & 0 & 1/\bar{G}_{xy} \end{bmatrix} \begin{Bmatrix} \sigma_o \\ \sigma_o \\ 0 \end{Bmatrix}$$

With

$$\frac{1}{\bar{E}_x} = \frac{\frac{1}{h} A_{22}}{\frac{1}{h^2} (A_{11} A_{22} - A_{12}^2)} = \frac{1}{\bar{E}_y}; \quad \frac{\bar{\nu}_{yx}}{\bar{E}_y} = \frac{\frac{1}{h} A_{12}}{\frac{1}{h^2} (A_{11} A_{22} - A_{12}^2)}$$

And

$$\frac{1}{h^2} (A_{11} A_{22} - A_{12}^2) = 2 \left[p \left(\frac{\bar{E}_\ell + \bar{E}_t}{2} - \nu_{t\ell} \bar{E}_\ell - 2G_{t\ell} \right) + G_{t\ell} \right] \left[\frac{\bar{E}_\ell + \bar{E}_t}{2} + \nu_{t\ell} \bar{E}_\ell \right]$$

Then we obtain the strain values:

$$\varepsilon_{ox} = \sigma_o \left(\frac{1}{\bar{E}_x} - \frac{\bar{\nu}_{yx}}{\bar{E}_y} \right) = \frac{\sigma_o}{\left(\frac{\bar{E}_\ell + \bar{E}_t}{2} + \nu_{t\ell} \bar{E}_\ell \right)} = \varepsilon_{oy}; \quad \gamma_{oxy} = 0$$

In summary¹³,

$$\varepsilon_{ox} = \varepsilon_{oy} = \varepsilon_o = \frac{\sigma_o}{\left(\frac{\bar{E}_\ell + \bar{E}_t}{2} + \nu_{t\ell} \bar{E}_\ell \right)}; \quad \gamma_{oxy} = 0$$

The strain ε_o is independent of the proportion p and of the shear modulus $G_{t\ell}$. Each elastic characteristic that is mentioned has the same weight: $\bar{E}_\ell, \bar{E}_t, \nu_{t\ell} \bar{E}_\ell = \nu_{t\ell} \bar{E}_t$.

- Verification (Chart 5.4 of Section 5.4.2)

$$p = 0\% : \bar{E}_x = \bar{E}_y = 15,055 \text{ MPa}; \quad \bar{\nu}_{xy} = 0.79 = \bar{\nu}_{yx}$$

$$\varepsilon_{ox} = \varepsilon_{oy} = \varepsilon_o = 1.39 \times 10^{-5} \times \sigma_0 \text{ (MPa)}$$

$$p = 30\% : \bar{E}_x = \bar{E}_y = 55,333 \text{ MPa}; \quad \bar{\nu}_{xy} = 0.23 = \bar{\nu}_{yx}$$

$$\varepsilon_{ox} = \varepsilon_{oy} = \varepsilon_o = 1.39 \times 10^{-5} \times \sigma_0 \text{ (MPa)}$$

$$p = 50\% : \bar{E}_x = \bar{E}_y = 70,687 \text{ MPa}; \quad \bar{\nu}_{xy} = 0.025 = \bar{\nu}_{yx}$$

$$\varepsilon_{ox} = \varepsilon_{oy} = \varepsilon_o = 1.38 \times 10^{-5} \times \sigma_0 \text{ (MPa)}$$

2. Tsai-Hill criterion

- 0° plies: following Equation 11.8,

$$\begin{aligned}\sigma_x^{0^\circ} &= \bar{E}_\ell \varepsilon_{ox} + \nu_{t\ell} \bar{E}_\ell \varepsilon_{oy} = \varepsilon_o \bar{E}_\ell (1 + \nu_{t\ell}) \\ \sigma_y^{0^\circ} &= \nu_{t\ell} \bar{E}_\ell \varepsilon_{ox} + \bar{E}_t \varepsilon_{oy} = \varepsilon_o \bar{E}_t (1 + \nu_{t\ell}) \\ \tau_{xy}^{0^\circ} &= 0\end{aligned}$$

And following Equation 11.4,

$$\begin{aligned}\sigma_\ell^{0^\circ} &= \sigma_x^{0^\circ} = \varepsilon_o \bar{E}_\ell (1 + \nu_{t\ell}) \\ \sigma_t^{0^\circ} &= \sigma_y^{0^\circ} = \varepsilon_o \bar{E}_t (1 + \nu_{t\ell}) \\ \tau_{t\ell}^{0^\circ} &= 0\end{aligned}$$

- 90° plies: following Equations 11.8 and 11.4,

$$\begin{aligned}\sigma_\ell^{90^\circ} &= \sigma_y^{90^\circ} = \varepsilon_o \bar{E}_\ell (1 + \nu_{t\ell}) \\ \sigma_t^{90^\circ} &= \sigma_x^{90^\circ} = \varepsilon_o \bar{E}_t (1 + \nu_{t\ell}) \\ \tau_{t\ell}^{90^\circ} &= 0\end{aligned}$$

- $+45^\circ$ plies: following Equations 11.8 and 11.4¹⁴,

$$\begin{aligned}\sigma_\ell^{45^\circ} &= \frac{1}{2} (\sigma_x^{45^\circ} + \sigma_y^{45^\circ}) + \tau_{xy}^{45^\circ} = \varepsilon_o \bar{E}_\ell (1 + \nu_{t\ell}) \\ \sigma_t^{45^\circ} &= \frac{1}{2} (\sigma_x^{45^\circ} + \sigma_y^{45^\circ}) - \tau_{xy}^{45^\circ} = \varepsilon_o \bar{E}_t (1 + \nu_{t\ell}) \\ \tau_{t\ell}^{45^\circ} &= 0\end{aligned}$$

- -45° plies: in an analogous manner,

$$\begin{aligned}\sigma_\ell^{-45^\circ} &= \varepsilon_o \bar{E}_\ell (1 + \nu_{t\ell}) \\ \sigma_t^{-45^\circ} &= \varepsilon_o \bar{E}_t (1 + \nu_{t\ell}) \\ \tau_{t\ell}^{-45^\circ} &= 0\end{aligned}$$

Therefore, the Tsai-Hill criterion (see Section 5.3.2 or Equation 14.6) has the same value in each of the plies, no matter what the proportion p and the shear modulus $G_{t\ell}$.

Notes

- When the Tsai-Hill criterion is saturated, failure occurs simultaneously in all plies.
- We automatically obtain such a laminate with balanced fabric layers at 0° and 45° . It is then convenient to calculate the thickness by considering the proper failure strength of the fabric layer¹⁵.

3. Verification
(see figures in Appendix A.)

$p=0\%$							
Figures A.3 and A.7				Figures A.4 and A.8			
Plies at $+45^\circ$	σ_ℓ	σ_t	$\tau_{\ell t}$	Plies at -45°	σ_ℓ	σ_t	$\tau_{\ell t}$
$\sigma_x=1$ MPa	0.94	0.06	-0.5	$\sigma_x=1$ MPa	0.94	0.06	0.5
$\sigma_y=1$ MPa	0.94	0.06	0.5	$\sigma_y=1$ MPa	0.94	0.06	-0.5
<i>Total</i> (MPa)	1.88	0.12	0.0	<i>Total</i> (MPa)	1.88	0.12	0
Tsai-Hill criterion: 1.02×10^{-5}				Tsai-Hill criterion: 1.02×10^{-5}			
$p=30\%$							
Figures A.1 and A.5				Figures A.2 and A.6			
Plies at 0°	σ_ℓ	σ_t	$\tau_{\ell t}$	Plies at 90°	σ_ℓ	σ_t	$\tau_{\ell t}$
$\sigma_x=1$ MPa	2.4	0.0	0.0	$\sigma_x=1$ MPa	-0.54	0.12	0.0
$\sigma_y=1$ MPa	-0.54	0.12	0.0	$\sigma_y=1$ MPa	2.4	0.0	0.0
<i>Total</i> (MPa)	1.86	0.12	0.0	<i>Total</i> (MPa)	1.86	0.12	0.0
Tsai-Hill criterion: 1.017×10^{-5}				Tsai-Hill criterion: 1.017×10^{-5}			
$p=50\%$							
Figures A.3 and A.7				Figures A.4 and A.8			
Plies at $+45^\circ$	σ_ℓ	σ_t	$\tau_{\ell t}$	Plies at -45°	σ_ℓ	σ_t	$\tau_{\ell t}$
$\sigma_x=1$ MPa	0.94	0.06	-0.09	$\sigma_x=1$ MPa	0.94	0.06	0.09
$\sigma_y=1$ MPa	0.94	0.06	0.09	$\sigma_y=1$ MPa	0.94	0.06	-0.09
<i>Total</i> (MPa)	1.88	0.12	0.0	<i>Total</i> (MPa)	1.88	0.12	0
Tsai-Hill criterion: 1.02×10^{-5}				Tsai-Hill criterion: 1.02×10^{-5}			
$p=50\%$							
Figures A.1 and A.5				Figures A.2 and A.6			
Plies at 0°	σ_ℓ	σ_t	$\tau_{\ell t}$	Plies at 90°	σ_ℓ	σ_t	$\tau_{\ell t}$
$\sigma_x=1$ MPa	1.9	0.02	0.0	$\sigma_x=1$ MPa	-0.02	0.1	0.0
$\sigma_y=1$ MPa	-0.02	0.1	0.0	$\sigma_y=1$ MPa	1.9	0.02	0.0
<i>Total</i> (MPa)	1.88	0.12	0.0	<i>Total</i> (MPa)	1.88	0.12	0.0
Tsai-Hill criterion: 1.02×10^{-5}				Tsai-Hill criterion: 1.02×10^{-5}			

20.9 LAMINATE MADE OF IDENTICAL LAYERS OF BALANCED FABRIC

Problem Statement

A carbon/epoxy laminate consists of a stacking of identical balanced fabric layers with the composition illustrated in Figure 20.10. The fiber volume fraction is $V_f=60\%$.

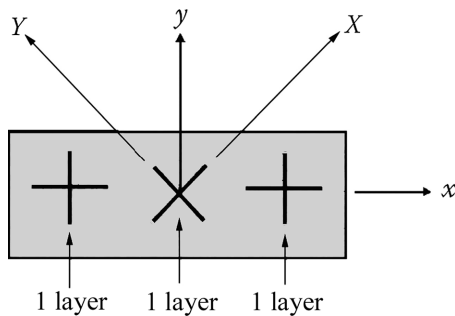


FIGURE 20.10 Laminate made of balanced fabric.

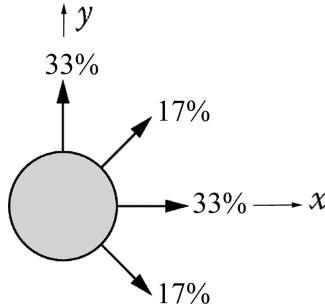
Give the elastic behavior equation of this laminate in axes (x, y) and then in axes (X, Y) .

Solution

- *Axes (x, y) :* The fabric being balanced, each layer can be replaced by two identical unidirectional plies crossed at 90° , with the thickness (see Section 3.4.2)

$$e_{\text{warp}} = e_{\text{weft}} = e / 2$$

The laminate is balanced with composition as in the following figure:



- *Elastic moduli:* From Chart 5.4 of Section 5.4.2,

$$E_x = 55,333 + \Delta E_x \text{ (MPa)}$$

ΔE_x can be evaluated by linear interpolation starting from

$$dE_x = \frac{\partial E}{\partial p^{0^\circ}} \times dp^{0^\circ} + \frac{\partial E}{\partial p^{90^\circ}} \times dp^{90^\circ}$$

As

$$\Delta E_x = (65,888 - 55,333) \times \frac{3}{10} + (53,545 - 55,333) \times \frac{3}{10} = 2,630 \text{ MPa}$$

Then

$$E_x = 57,960 \text{ MPa} = E_y$$

- *Poisson coefficient:* $\nu_{xy} = 0.23 + \Delta \nu_{xy}$.
From an analogous calculation,

$$\nu_{xy} = 0.20 = \nu_{yx}$$

- *Shear modulus:* From Chart 5.5 of Section 5.4.2,

$$G_{xy} = 16,315 + \Delta G_{xy} \text{ (MPa)}$$

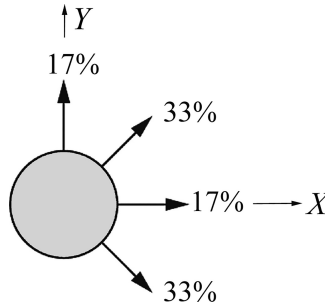
After analogous calculus,

$$G_{xy} = 14,500 \text{ MPa}$$

From which the behavior equation in axes (x, y) (see Equation 12.9) is as follows:

$$\begin{Bmatrix} \epsilon_{ox} \\ \epsilon_{oy} \\ \gamma_{oxy} \end{Bmatrix} = \begin{bmatrix} \frac{1}{57,960} & -\frac{0.2}{57,960} & 0 \\ -\frac{0.2}{57,960} & \frac{1}{57,960} & 0 \\ 0 & 0 & \frac{1}{14,500} \end{bmatrix} \begin{Bmatrix} \sigma_{ox} \\ \sigma_{oy} \\ \tau_{oxy} \end{Bmatrix} \text{ (MPa)}$$

- *Axes (X, Y)*: The laminate is balanced, with the following composition:



In using the same charts as before, we obtain

$$E_X = E_Y = 31,979 + \Delta E_X = 41,400 \text{ MPa}$$

$$\nu_{XY} = \nu_{YX} = 0.56 + \Delta \nu_{XY} = 0.43$$

$$G_{XY} = 28,430 + \Delta G_{XY} = 24,190 \text{ MPa}$$

From which the behavior equation in axes (X, Y) (see Equation 12.9)

$$\begin{Bmatrix} \epsilon_{oX} \\ \epsilon_{oY} \\ \gamma_{oXY} \end{Bmatrix} = \begin{bmatrix} \frac{1}{41,400} & -\frac{0.43}{41,400} & 0 \\ -\frac{0.43}{41,400} & \frac{1}{41,400} & 0 \\ 0 & 0 & \frac{1}{24,190} \end{bmatrix} \begin{Bmatrix} \sigma_{oX} \\ \sigma_{oY} \\ \tau_{oXY} \end{Bmatrix} \text{ (MPa)}$$

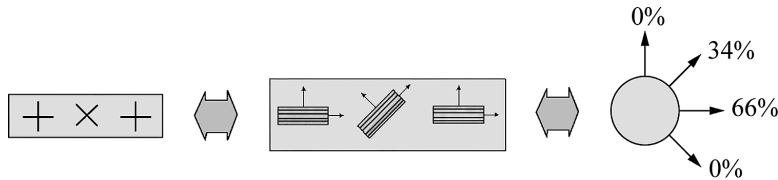
Notes

- We should note that a laminate constituted by layers of balanced fabric with four orientations $(0^\circ, 90^\circ, +45^\circ, -45^\circ)$ admits two systems of orthotropic axes:

$$(x, y) \text{ and } (X, Y).$$

- The elastic properties are reliably estimated when one uses Charts 5.4 and 5.5 in Section 5.4.2. **The same cannot be said** for the maximum admissible stresses indicated in Charts

5.1, 5.2, and 5.3 that are valid only for laminates made of unidirectional layers. In effect, the rupture strength for a layer of balanced fabric is clearly higher in tension than the first-ply failure value for the first ply of an equivalent laminate made up of layers at 0° (50%) and 90° (50%). For a calculation of first-ply failure, or for the failure criterion of the laminate proposed in this application, it would be appropriate to consider a fabric layer as an anisotropic ply with thickness e (see Section 3.4.2) with the rupture stress values $\sigma_{\ell_{\text{rupt}}}, \sigma_{t_{\text{rupt}}}, \tau_{\ell t_{\text{rupt}}}$ of the balanced fabric itself (see examples in Section 3.4.3)¹⁶. The equivalence is then¹⁷



20.10 CARBON/EPOXY WING SPAR

Problem Statement

We consider an airplane control surface, with the internal structure (excluding skins) shown schematically in Figure 20.11. It consists of a spar and several ribs. The spar is a laminate of carbon/epoxy fabric with fiber volume fraction $V_f = 45\%$. The composition varies along the longitudinal coordinate axis x , in the flange (Zone 1), and in the web (Zone 2). A preliminary calculation of the flight surface under loading reveals maximum stress resultants located in the spar areas indicated in the figure.

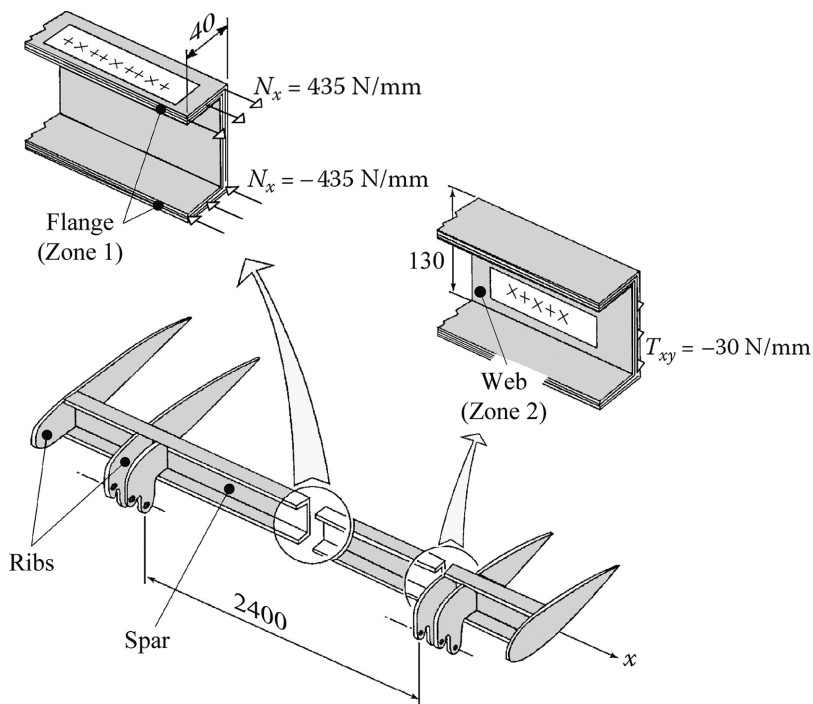


FIGURE 20.11 Wing spar.

For each of these two zones is proposed a laminate composition as indicated in the figure. For each of these laminates,

1. Evaluate the elastic properties
2. Verify the laminate
 - a. At failure
 - b. At buckling

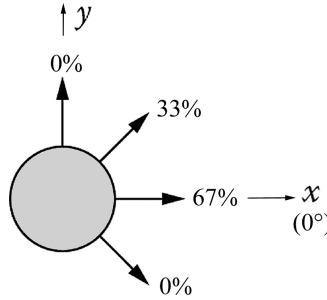
Thickness of a fabric layer is 0.24 mm. Properties of carbon/epoxy fabric are shown in Section 3.4.3.

Solution

1. Elastic properties

a. **Zone 1:** Composition of the laminate¹⁸

Calculation of elastic moduli: From Equations 12.7–12.9 and 11.8,



$$\bar{E}_{11}^{0^\circ} = \bar{E}_\ell; \quad \bar{E}_{12}^{0^\circ} = \nu_{t\ell} \bar{E}_\ell; \quad \bar{E}_{33}^{0^\circ} = G_{t\ell}$$

$$\bar{E}_{11}^{45^\circ} = \frac{\bar{E}_\ell + \bar{E}_t}{4} + \frac{1}{2}(\nu_{t\ell} \bar{E}_\ell + 2G_{t\ell}); \quad \bar{E}_{12}^{45^\circ} = \frac{\bar{E}_\ell + \bar{E}_t}{4} - G_{t\ell} + \frac{1}{2} \nu_{t\ell} \bar{E}_\ell$$

$$\bar{E}_{33}^{45^\circ} = \frac{\bar{E}_\ell + \bar{E}_t}{4} - \frac{1}{2} \nu_{t\ell} \bar{E}_\ell$$

With (See Section 3.4.3)

$$\bar{E}_\ell = \bar{E}_t = \frac{E_x}{(1 - \nu_{xy} \times \nu_{yx})}; \quad E_x = 54,000 \text{ MPa}; \quad \nu_{xy} = \nu_{yx} = 0.045$$

$$G_{t\ell} = G_{xy} = 4,000 \text{ MPa}$$

Then

$$\bar{E}_{11}^{0^\circ} = 54,100 \text{ MPa}; \quad \bar{E}_{12}^{0^\circ} = 2,435 \text{ MPa}; \quad \bar{E}_{33}^{0^\circ} = 4,000 \text{ MPa}$$

$$\bar{E}_{11}^{45^\circ} = 32,270 \text{ MPa}; \quad \bar{E}_{12}^{45^\circ} = 24,270 \text{ MPa}; \quad \bar{E}_{33}^{45^\circ} = 25,840 \text{ MPa}$$

We deduce

$$\frac{1}{h} A_{11} = \bar{E}_{11}^{0^\circ} \times 0.67 + \bar{E}_{11}^{45^\circ} \times 0.33 = 46,900 \text{ MPa} = \frac{1}{h} A_{22}$$

$$\frac{1}{h} A_{12} = \bar{E}_{12}^{0^\circ} \times 0.67 + \bar{E}_{12}^{45^\circ} \times 0.33 = 9,640 \text{ MPa}$$

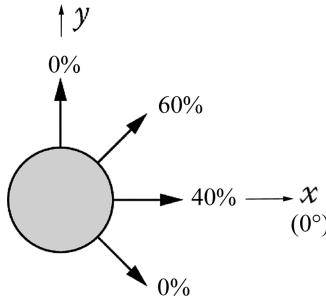
$$\frac{1}{h} A_{33} = \bar{E}_{33}^{0^\circ} \times 0.67 + \bar{E}_{33}^{45^\circ} \times 0.33 = 11,210 \text{ MPa}$$

After calculation of $h [A]^{-1}$, we obtain the behavior equation in zone 1:

$$\left\{ \begin{array}{c} \varepsilon_{ox} \\ \varepsilon_{oy} \\ \gamma_{oxy} \end{array} \right\} = \left[\begin{array}{ccc} \frac{1}{44,920} & -\frac{0.2}{44,920} & 0 \\ -\frac{0.2}{44,920} & \frac{1}{44,920} & 0 \\ 0 & 0 & \frac{1}{11,210} \end{array} \right] \left\{ \begin{array}{c} \sigma_{ox} \\ \sigma_{oy} \\ \tau_{oxy} \end{array} \right\} \quad (20.15)$$

b. **Zone 2:** Composition of the laminate

Following the same method as earlier,



$$\frac{1}{h} A_{11} = \frac{1}{h} A_{22} = \bar{E}_{11}^{0^\circ} \times 0.4 + \bar{E}_{11}^{45^\circ} \times 0.6 = 41,010 \text{ MPa}$$

$$\frac{1}{h} A_{12} = 15,540 \text{ MPa}$$

$$\frac{1}{h} A_{33} = 17,100 \text{ MPa}$$

Then, after inversion,

$$\left\{ \begin{array}{c} \varepsilon_{ox} \\ \varepsilon_{oy} \\ \gamma_{oxy} \end{array} \right\} = \left[\begin{array}{ccc} \frac{1}{35,120} & -\frac{0.38}{35,120} & 0 \\ -\frac{0.38}{35,120} & \frac{1}{35,120} & 0 \\ 0 & 0 & \frac{1}{17,100} \end{array} \right] \left\{ \begin{array}{c} \sigma_{ox} \\ \sigma_{oy} \\ \tau_{oxy} \end{array} \right\} \quad (20.16)$$

2.

a. Verification of nonrupture

- **Zone 1:** Compression in the lower flange: $N_x = -435 \text{ N/mm}$. With nine fabric layers of thickness 0.24 mm, this corresponds to an overall stress

$$\sigma_{ox} = -202 \text{ MPa}$$

From which the strain values with Equation 20.15

$$\varepsilon_{ox} = -4.497 \times 10^{-3}; \quad \varepsilon_{oy} = 9 \times 10^{-4}; \quad \gamma_{oxy} = 0$$

Layers at $0^\circ/90^\circ$ (Equation 11.8):

$$\sigma_x^{0^\circ} = \bar{E}_{11}^{0^\circ} \times \epsilon_{ox} + \bar{E}_{12}^{0^\circ} \times \epsilon_{oy} = -241 \text{ MPa} = \sigma_t^{0^\circ}$$

$$\sigma_y^{0^\circ} = \bar{E}_{21}^{0^\circ} \times \epsilon_{ox} + \bar{E}_{22}^{0^\circ} \times \epsilon_{oy} = 38 \text{ MPa} = \sigma_t^{0^\circ}$$

$$\tau_{xy}^{0^\circ} = 0 = \tau_{lt}$$

When writing the Tsai-Hill expression (see Section 5.3.2 and Chapter 14)¹⁹

$$\frac{-241^2}{360^2} + \frac{38^2}{420^2} - \frac{-241 \times 38}{360^2} = (0.72)^2 < 1$$

A safety factor appears as (see Section 14.2.3)

$$\frac{1}{0.72} - 1 = 38\%$$

Layers at $45^\circ/-45^\circ$: An analogous calculation leads to the much weaker value for the Tsai-Hill expression of $(0.49)^2$. The layers $0^\circ/90^\circ$ fail first.

- **Zone 2:** With a shear resultant $T_{xy} = -30 \text{ N/mm}$ and five fabric layers with 0.24 mm thickness, this corresponds to an overall stress

$$\tau_{oxy} = -25 \text{ MPa}.$$

We obtain then the strain values by means of Equation 20.16:

$$\epsilon_{ox} = 0 ; \epsilon_{oy} = 0 ; \gamma_{oxy} = -1.46 \times 10^{-3}$$

Layers at $45^\circ/-45^\circ$ (Equation 11.8)

$$\sigma_x^{45^\circ} = \sigma_y^{45^\circ} = 0 ; \tau_{xy}^{45^\circ} = -38 \text{ MPa}$$

Equation 11.4

$$\sigma_t^{45^\circ} = -\tau_{xy}^{45^\circ} = 38 \text{ MPa} = -\sigma_t^{45^\circ} ; \tau_{lt}^{45^\circ} = 0$$

Tsai-Hill expression

$$\frac{38^2}{420^2} + \frac{(-38)^2}{360^2} - \frac{-38 \times 38}{420^2} = (0.17)^2$$

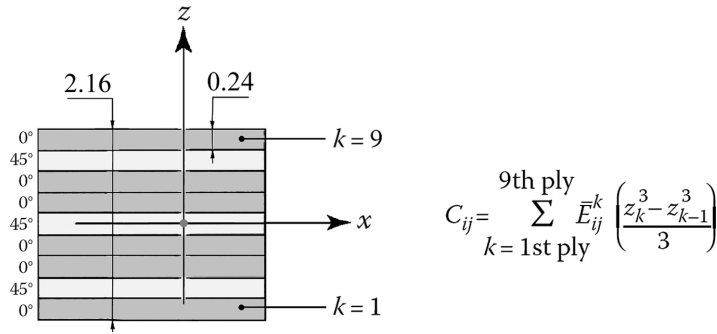
Corresponding to a safety factor of

$$\frac{1}{0.17} - 1 = 500\%$$

Layers at $0^\circ/90^\circ$: A smaller value of $(0.1)^2$ is found for the Tsai-Hill expression. The $45^\circ/-45^\circ$ layers fail first.

- Verification for buckling:* This is done starting from the figures of Appendix B. In this view, we first evaluate the constants C_{11} , C_{22} , C_{12} , C_{33} that appear in the constitutive law for bending (see Equation 12.16):

- Zone 1



Ply no. k	1	2	3	4	5	6	7	8	9
$\frac{(z_k^3 - z_{k-1}^3)}{3}$	0.2223	0.1256	0.0564	0.0150	1.152×10^{-3}	0.0150	0.0564	0.1256	0.2223

From which

$$C_{11} = C_{22} = 39,930 \quad \text{N} \times \text{mm}$$

$$C_{12} = C_{21} = 7,555 \quad \text{N} \times \text{mm}$$

$$C_{33} = 8,870 \quad \text{N} \times \text{mm}$$

Then

$$[C] = \begin{bmatrix} 39,930 & 7,555 & 0 \\ 7,555 & 39,930 & 0 \\ 0 & 0 & 8,870 \end{bmatrix} (\text{N} \times \text{mm})$$

Consider the unfavorable case of a plate simply supported along two of its sides, clamped along the third side, and free on the fourth one (See Figure 20.11). When using Figure B.4 in Appendix B with the values

$$C = \frac{C_{12} + 2C_{33}}{\sqrt{C_{11} \times C_{22}}} = \frac{25,295}{39,930} = 0.63; \quad \frac{a}{b} \left(\frac{C_{22}}{C_{11}} \right)^{1/4} \gg 1$$

We obtain

$$k \approx 1.15$$

From which the critical normal load resultant in compression is

$$N_{x\text{critical}} = 1.15 \times \pi^2 \times \frac{39,930}{40^2}$$

$$N_{x\text{critical}} = 283 \text{ N/mm} < 435 \text{ N/mm applied}$$

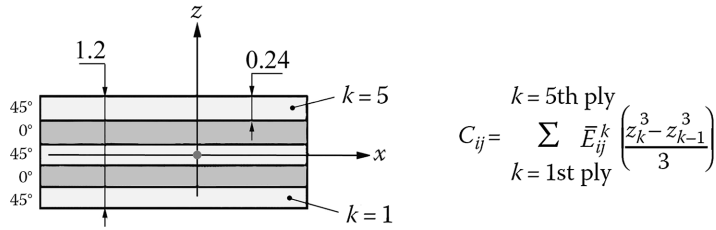
There is a risk of buckling, and we should reinforce the wing in the central part of the spar where the compressive normal resultant is maximum by means of exterior layers at $0^\circ/90^\circ$ in such a way to augment C_{11} and C_{22} . For example, with a supplementary external layer on either side,

$$C'_{11} = 77,475 \text{ N/mm}; C'_{12} = 9,245 \text{ N/mm}; C'_{33} = 11,646 \text{ N/mm}$$

From which $C=0.42$, $k \approx 1$, and

$$N'_{x \text{ critical}} = 477 \text{ N/mm} > 435 \text{ N/mm applied}$$

- Zone 2



We obtain after calculation

$$[C] = \begin{bmatrix} 5,300 & 2,840 & 0 \\ 2,840 & 5,300 & 0 \\ 0 & 0 & 3,065 \end{bmatrix} (\text{N} \times \text{mm})$$

In the unfavorable case of a plate simply supported on four sides (See Figure 20.11), Figure B.6 in Appendix B should be used with the values

$$C = 1.7; \frac{a}{b} \left(\frac{C_{22}}{C_{11}} \right)^{1/4} \gg 1$$

We obtain

$$k \approx 7$$

From which the critical shear stress resultant is

$$T_{xy \text{ critical}} = 7 \times \pi^2 \times \frac{5,300}{130^2}$$

$$T_{xy \text{ critical}} = 21 \text{ N/mm} < 30 \text{ N/mm applied}$$

There is therefore a risk of buckling and the web should be reinforced in this zone of the spar where the shear resultant is at maximum value. A supplementary external layer at $0^\circ/90^\circ$ on either side of this web gives

$$C'_{11} = 18,890 \text{ N/mm}; C'_{12} = 3,450 \text{ N/mm}; C'_{33} = 4,070 \text{ N/mm}$$

From which $C=0.6$, $k \approx 4.3$, and

$$T_{xy \text{ critical}} = 47 \text{ N/mm} > 30 \text{ N/mm applied.}$$

20.11 ELASTIC CONSTANTS OF A CARBON/EPOXY UNIDIRECTIONAL LAYER, BASED ON TENSILE TEST

Problem Statement

Consider a unidirectional carbon/epoxy plate, from which two samples are cut as shown in Figure 20.12. These coupons are tested in a testing machine. Strain values are measured using strain gages arranged as shown. The strain values obtained under different loads are linearized. Values corresponding to a uniform tensile stress σ_x equal to 20 MPa are presented. Calculate the elastic constants of the unidirectional layer subject to In-plane loading.

Solution

We can use the relationships in 11.5:

- *Sample No. 1:* Axes x and y coincide with axes ℓ and t ($\theta=0$), from which

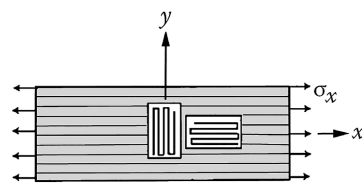
$$\begin{aligned}\epsilon_{1x} &= \frac{\sigma_x}{E_x} = \frac{\sigma_x}{E_\ell} \rightarrow E_\ell = \frac{20}{143 \times 10^{-6}} = 139,860 \text{ MPa} \\ \epsilon_{1y} &= -\frac{\nu_{xy}}{E_x} \times \sigma_x = -\frac{\nu_{\ell t}}{E_\ell} \times \sigma_x \rightarrow \nu_{\ell t} = 0.25\end{aligned}$$

- *Sample No. 2:* Axes x and y make an angle of $\theta=20^\circ$ with axes ℓ and t , from which²⁰

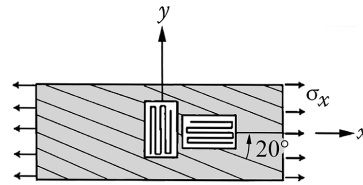
$$\begin{aligned}\epsilon_{2x} &= \frac{\sigma_x}{E_x} = \left\{ \frac{c^4}{E_\ell} + \frac{s^4}{E_t} + c^2 s^2 \left(\frac{1}{G_{\ell t}} - 2 \frac{\nu_{\ell t}}{E_\ell} \right) \right\} \times \sigma_x \\ \epsilon_{2y} &= -\frac{\nu_{xy}}{E_x} \times \sigma_x = -\left\{ \frac{\nu_{\ell t}}{E_\ell} (c^4 + s^4) - c^2 s^2 \left(\frac{1}{E_\ell} + \frac{1}{E_t} - \frac{1}{G_{\ell t}} \right) \right\} \times \sigma_x\end{aligned}$$

Leading to

$$\begin{cases} \frac{1}{G_{\ell t}} + \frac{0.1325}{E_t} = 2.69 \times 10^{-4} \\ \frac{1}{G_{\ell t}} - \frac{1}{E_t} = 1.144 \times 10^{-4} \end{cases}$$



$$\epsilon_{1x} = 143 \times 10^{-6}; \epsilon_{1y} = -36 \times 10^{-6}$$



$$\epsilon_{2x} = 660 \times 10^{-6}; \epsilon_{2y} = -250 \times 10^{-6}$$

FIGURE 20.12 Carbon/epoxy samples.

From which $E_t = 7,320 \text{ MPa}$; $G_{tt} = 3,980 \text{ MPa}$.

In summary,

$$E_\ell = 139,860 \text{ MPa}$$

$$E_t = 7,320 \text{ MPa}$$

$$\nu_{tt} = 0.25 ; \nu_{t\ell} = 0.013$$

$$G_{tt} = 3,980 \text{ MPa}$$

20.12 SAILBOAT HULL IN GLASS/POLYESTER

Problem Statement

Consider a laminated shell plating of a sailboat, in glass/polyester. It is made up of a stack of layers of balanced fabric and glass mat. The reinforcements, in “E” glass, are in the following form:

- *Balanced fabric*: $V_f = 20\%$. Mass of glass per square meter: $m_{0f} = 500 \text{ g/m}^2$
 - *Mat*: $V_{fM} = 15\%$. Mass of glass per square meter: $m_{0fM} = 300 \text{ g/m}^2$
1. Calculate the thickness of
 - a. A glass/polyester fabric layer
 - b. A glass/polyester mat layer
 2. Given the composition of the laminated shell plating as follows:

$$\left[M / F / M / \bar{F} \right]_s \quad \text{with} \quad (M \leftrightarrow \text{mat}; F \leftrightarrow \text{fabric})$$

What is the total thickness, denoted as h , of the shell plating?

3. *Elastic characteristics of a fabric layer*: A layer of balanced fabric is considered to be equivalent to two series of unidirectional plies crossed at 90° , each of these series measuring half of the total fabric layer thickness (see Figure 20.13).

The elastic constants of these unidirectional plies are

$$E_\ell = 18,000 \text{ MPa}; \quad E_t = 4,900 \text{ MPa}; \quad G_{tt} = 1,850 \text{ MPa}; \quad \nu_{tt} = 0.3$$

Calculate the elastic characteristics (moduli, Poisson coefficients) of a fabric layer, in warp (C) and weft (T) axes.

4. The mat layers are considered isotropic in their planes, with

$$E_{\text{mat}} = 8,350 \text{ MPa}; \quad \nu_{\text{mat}} = 0.3$$

Figure 20.14 represents a planar portion of the shell plating. All the fabric plies are oriented at $0^\circ/90^\circ$. Calculate the global elastic constants (moduli, Poisson coefficients) of the shell plating when working in its plane.

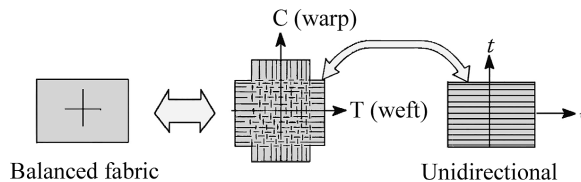


FIGURE 20.13 Equivalence of a balanced fabric layer.

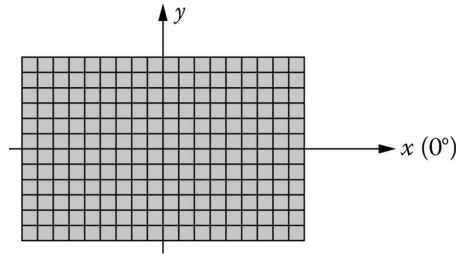


FIGURE 20.14 Planar portion of the shell plating.

Note: Tests on coupons made out of this material indicate a modulus of elasticity along the x -direction to be equal to 9,200 MPa. What can be said about this?

5. *Rupture:* The failure strengths, considered to be equal in tension and in compression, are as follows:
 - Fabric layer along C or T : $\sigma_{\text{rupt-fabric}} = 139 \text{ MPa}$.
 - Mat layer: $\sigma_{\text{rupt-mat}} = 113 \text{ MPa}$.
 - a. Calculate the maximum stress σ_{0x} leading to first-ply failure of the shell plating. What are the damaged layers?
 - b. Apply the maximum stress σ_{0x} . In the previous damaged layers, the glass fibers are supposed entirely broken. What happens to the laminate?

Solution

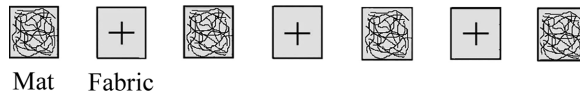
1. The thickness of a layer denoted as h is such that (see Section 3.2.4)

$$h = \frac{m_{of}}{V_f \times \rho_f}$$

The specific mass of “E” glass is (see Section 1.6) $\rho_f = 2,600 \text{ kg/m}^3$, from which

$$h_{\text{fabric}} = 0.96 \text{ mm}; \quad h_{\text{mat}} = 0.77 \text{ mm}.$$

2. The shell plating is constituted of the following stacking sequence:



The total thickness is

$$h = 0.77 \times 4 + 0.96 \times 3 = 5.96 \text{ mm}$$

3. *Elastic characteristics of a fabric layer:* The moduli and Poisson coefficients can be evaluated starting from the simplified relations of Section 3.4.2. We obtain, with $k=0.5$ (balanced fabric),

$$E_C = E_T = 11,450 \text{ MPa}$$

$$G_{CT} = 1,850 \text{ MPa}; \quad \nu_{CT} = \nu_{TC} = 0.128$$

A more precise calculation of these characteristics requires establishing the matrix $h[A]^{-1}$ in Equation 12.9 of Section 12.1.2. We calculate at first $(1/h)[A]$ in Equation 12.8:

$$\frac{1}{h} A_{ij} = \bar{E}_{ij}^{0^\circ} \times 0.5 + \bar{E}_{ij}^{90^\circ} \times 0.5$$

Equation 11.8 gives terms \bar{E}_{ij} . For example, we will have

$$\frac{1}{h} A_{11} = \bar{E}_\ell \times 0.5 + \bar{E}_t \times 0.5 = \frac{1}{2} \frac{(E_\ell + E_t)}{(1 - \nu_{t\ell}\nu_{t\ell})}$$

With

$$\nu_{t\ell} = \nu_{\ell t} \frac{E_t}{E_\ell}$$

We obtain

$$\frac{1}{h} [A] = \begin{bmatrix} 11,737 & 1,507 & 0 \\ 1,507 & 11,737 & 0 \\ 0 & 0 & 1,850 \end{bmatrix} \text{ (MPa)}$$

$$h[A]^{-1} = \begin{bmatrix} \frac{1}{11,540} & -\frac{0.128}{11,540} & 0 \\ -\frac{0.128}{11,540} & \frac{1}{11,540} & 0 \\ 0 & 0 & \frac{1}{1,850} \end{bmatrix}$$

From which

$$E_C = E_T = 11,540 \text{ MPa}$$

$$G_{CT} = 1,850 \text{ MPa}$$

$$\nu_{CT} = \nu_{TC} = 0.128$$

We should note the slight difference between these values and the approximate values estimated using the method described.

4. *Elastic characteristics of the shell plating:* These are deduced from the matrix $h[A]^{-1}$ (Equation 12.9) calculated for all the laminate.

We calculate at first $(1/h)[A]$ in Equation 12.8:

$$\frac{1}{h} A_{ij} = \bar{E}_{ij}^{\text{fabric}} \times p^{\text{fabric}} + \bar{E}_{ij}^{\text{mat}} \times p^{\text{mat}}$$

With

$$p^{\text{fabric}} = \frac{3 \times 0.96}{5.96} = 0.483; \quad p^{\text{mat}} = 0.517$$

$$\bar{E}_{11}^{\text{fabric}} = \bar{E}_{22}^{\text{fabric}} = \bar{E}_C = \frac{E_C}{1 - \nu_{CT}^2}$$

$$\begin{aligned}\bar{E}_{12\text{fabric}} &= \nu_{CT}\bar{E}_C; \quad \bar{E}_{33\text{fabric}} = G_{CT} \\ \bar{E}_{11\text{mat}} &= \bar{E}_{22\text{mat}} = \frac{E_{\text{mat}}}{1-\nu_{\text{mat}}^2}; \quad \bar{E}_{12\text{mat}} = \frac{\nu_{\text{mat}}E_{\text{mat}}}{1-\nu_{\text{mat}}^2} \\ \bar{E}_{33\text{mat}} &= G_{\text{mat}} = \frac{E_{\text{mat}}}{2(1+\nu_{\text{mat}})}\end{aligned}$$

We obtain

$$\begin{aligned}\frac{1}{h}[A] &= \begin{bmatrix} 10,410 & 2,149 & 0 \\ 2,149 & 10,410 & 0 \\ 0 & 0 & 2,554 \end{bmatrix} \text{ (MPa)} \\ h[A]^{-1} &= \begin{bmatrix} \frac{1}{9,966} & -\frac{0.206}{9,966} & 0 \\ -\frac{0.206}{9,966} & \frac{1}{9,966} & 0 \\ 0 & 0 & \frac{1}{2,554} \end{bmatrix}\end{aligned}$$

Then

$$\begin{aligned}E_x &= E_y = 9,966 \text{ MPa} \\ G_{xy} &= 2,554 \text{ MPa} \\ \nu_{xy} &= \nu_{yx} = 0.206\end{aligned}$$

Note: The measured modulus 9,200 MPa is a bit smaller than the one calculated. Indeed, due to curvature of fibers from weaving, a fabric layer is less stiff than the stacking of uni-directionals that are crossed at 90°. However, the approximation obtained by calculation is suitable (difference < 10%).

5. Failure of the shell plating:

- The shell plating is subject to an overall stress σ_{0x} . The resulting strain values are given by Equation 12.9:

$$\begin{Bmatrix} \epsilon_{ox} \\ \epsilon_{oy} \\ \gamma_{oxy} \end{Bmatrix} = h[A]^{-1} \begin{Bmatrix} \sigma_{ox} \\ 0 \\ 0 \end{Bmatrix} = \begin{Bmatrix} \sigma_{ox}/9,966 \\ -0.206 \times \sigma_{ox}/9,966 \\ 0 \end{Bmatrix}$$

These strains give rise to the following stress components:

- In fabric layers (see results from Question 3),

$$\begin{Bmatrix} \sigma_C \\ \sigma_T \\ \tau_{CT} \end{Bmatrix} = \begin{bmatrix} 11,737 & 1,507 & 0 \\ 1,507 & 11,737 & 0 \\ 0 & 0 & 1,850 \end{bmatrix} \begin{Bmatrix} \sigma_{ox}/9,966 \\ -0.206 \times \sigma_{ox}/9,966 \\ 0 \end{Bmatrix} = \begin{Bmatrix} 1.15 \times \sigma_{ox} \\ -0.09 \times \sigma_{ox} \\ 0 \end{Bmatrix}$$

The Tsai-Hill criterion in these layers is saturated for σ_{0x} such that

$$\left(\frac{1.15 \times \sigma_{ox}}{139}\right)^2 + \left(\frac{-0.09 \times \sigma_{ox}}{139}\right)^2 - \frac{-0.09 \times 1.15 \times \sigma_{ox}^2}{139^2} = 1$$

From which

$$\sigma_{ox} = 116 \text{ MPa}$$

- In mat layers, with values of Question 4 for the coefficients $\bar{E}_{ij\text{mat}}$,

$$\begin{Bmatrix} \sigma_x \\ \sigma_y \\ \tau_{xy} \end{Bmatrix} = [\bar{E}_{\text{mat}}] \begin{Bmatrix} \sigma_{ox} / 9,966 \\ -0.206 \times \sigma_{ox} / 9,966 \\ 0 \end{Bmatrix} = \begin{Bmatrix} 0.86 \times \sigma_{ox} \\ 0.087 \times \sigma_{ox} \\ 0 \end{Bmatrix}$$

The Tsai-Hill criterion in mat layers is saturated for σ_{0x} such that²¹

$$\left(\frac{0.86 \times \sigma_{ox}}{113}\right)^2 + \left(\frac{0.087 \times \sigma_{ox}}{113}\right)^2 - \frac{0.86 \times 0.087 \times \sigma_{ox}^2}{113^2} = 1$$

Then

$$\sigma_{ox} = 138 \text{ MPa}$$

The fabric layers are the first to be damaged, for a stress value

$$\sigma_{ox\text{max}} = 116 \text{ MPa}$$

- b. This stress being applied, failure of fabric layers translates into glass-fiber rupture. Considering the normal load resultant corresponding to this stress:

$$N_x = \sigma_{ox\text{max}} \times h = 116 \times 5.96 = 691 \text{ N/mm}$$

This stress resultant is then completely taken up by the layers of mat. Therefore, the stress in these layers is

$$\sigma_{ox\text{mat}} = \frac{N_x}{4 \times h_{\text{mat}}} = \frac{691}{4 \times 0.77} = 224 \text{ MPa}$$

It exceeds the failure strength of the mat (113 MPa), and the latter fails.

The shell plating is therefore completely broken under the stress:

$$\sigma_{ox\text{max}} = 116 \text{ MPa}$$

20.13 BALANCED FABRIC PLY: DETERMINATION OF THE IN-PLANE SHEAR MODULUS

Problem Statement

Consider a coupon cut from a laminated panel made of identical balanced fabric layers, all of them oriented along axes *C* (warp direction) and *T* (weft direction) in Figure 20.15.

The sample is in a state of simple tension in its plane along the *x*-axis shown in the figure:

$$\sigma_{ox} \neq 0; \quad \sigma_{oy} = \tau_{oxy} = 0$$

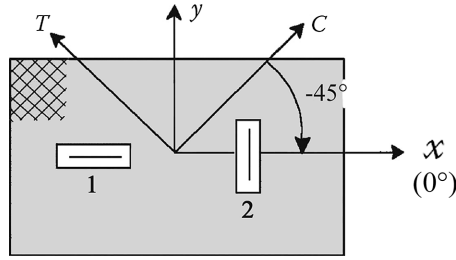


FIGURE 20.15 Strain gages.

Two strain gages, denoted as 1 and 2, are bonded onto the sample (see figure). We can read a strain value ϵ_{0x} from gage 1 and ϵ_{0y} from gage 2.

1. Noting that $\gamma_{0xy} = 0$, give the distortion γ_{CT} in axes (C, T) as a function of ϵ_{0x} and ϵ_{0y} .
2. Express the stress τ_{CT} in axes (C, T) as a function of σ_{0x} .
3. Deduce, from the previous answer, the shear modulus G_{CT} as a function of $\epsilon_{0x}, \epsilon_{0y}, \sigma_{0x}$.

Solution

1. Equation 11.7 allows writing

$$\begin{Bmatrix} \epsilon_C \\ \epsilon_T \\ \gamma_{CT} \end{Bmatrix} = \begin{bmatrix} c^2 & s^2 & -cs \\ s^2 & c^2 & cs \\ 2cs & -2cs & (c^2 - s^2) \end{bmatrix} \begin{Bmatrix} \epsilon_{0x} \\ \epsilon_{0y} \\ \gamma_{0xy} \end{Bmatrix}$$

The laminate under analysis is balanced, with midplane symmetry, loaded in its proper axes (x, y) . Then from Equation 12.9, $\gamma_{0xy} = 0$, from which

$$\gamma_{CT} = 2cs \times \epsilon_{0x} - 2cs \times \epsilon_{0y} \quad \text{with} \quad c = \frac{1}{\sqrt{2}}; s = -\frac{1}{\sqrt{2}}$$

$$\gamma_{CT} = -\epsilon_{0x} + \epsilon_{0y}$$

2. According to Equation 11.4,

$$\begin{Bmatrix} \sigma_C \\ \sigma_T \\ \tau_{CT} \end{Bmatrix} = \begin{bmatrix} c^2 & s^2 & -2cs \\ s^2 & c^2 & 2cs \\ sc & -sc & (c^2 - s^2) \end{bmatrix} \begin{Bmatrix} \sigma_{0x} \\ 0 \\ 0 \end{Bmatrix}$$

Then

$$\tau_{CT} = sc \times \sigma_{0x} = -\frac{\sigma_{0x}}{2}$$

3. The behavior relationship of the fabric in its proper axes can be written, starting from Equation 11.5,

$$\begin{Bmatrix} \varepsilon_C \\ \varepsilon_T \\ \gamma_{CT} \end{Bmatrix} = \begin{bmatrix} \frac{1}{E_C} & -\frac{\nu_{CT}}{E_C} & 0 \\ -\frac{\nu_{CT}}{E_C} & \frac{1}{E_C} & 0 \\ 0 & 0 & \frac{1}{G_{CT}} \end{bmatrix} \begin{Bmatrix} \sigma_C \\ \sigma_T \\ \tau_{CT} \end{Bmatrix}$$

$$\gamma_{CT} = \frac{\tau_{CT}}{G_{CT}}$$

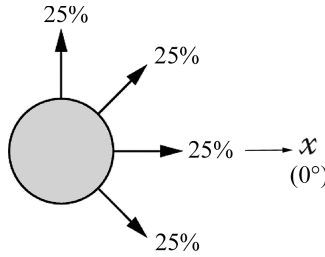
From which

$$G_{CT} = \frac{\sigma_{ox}}{2(\varepsilon_{ox} - \varepsilon_{oy})}$$

20.14 QUASI-ISOTROPIC LAMINATE

Problem Statement

Consider a laminate made up of a number of identical unidirectional plies, with midplane symmetry and the following composition.



Elastic ply characteristics in axes (ℓ, t) are denoted:

$$E_\ell, E_t, G_{\ell t}, \nu_{\ell t}, \nu_{t\ell}$$

We propose to look at the behavior of this laminate under In-plane loading, following Equation 12.9:

$$\begin{Bmatrix} \varepsilon_{ox} \\ \varepsilon_{oy} \\ \gamma_{oxy} \end{Bmatrix} = h[A]^{-1} \begin{Bmatrix} \sigma_{ox} \\ \sigma_{oy} \\ \tau_{oxy} \end{Bmatrix}$$

1. Calculate the matrix coefficients of $(1/h)[A]$.
2. By inversion, deduce the elastic moduli of this laminate.
3. Give a comment. Deduce the laminate behavior under In-plane loading in axes (X, Y) , derived from axes (x, y) by a rotation θ .

Solution

1. Coefficients $(1/h)A_{ij}$ are given by Equation 12.8:

$$\frac{1}{h}A_{ij} = \frac{1}{4}[\bar{E}_{ij}^{0^\circ} + \bar{E}_{ij}^{90^\circ} + \bar{E}_{ij}^{+45^\circ} + \bar{E}_{ij}^{-45^\circ}]$$

The stiffness coefficients \bar{E}_{ij}^0 are obtained from Equation 11.8. In using this relation for $\theta=0^\circ, 90^\circ, +45^\circ, -45^\circ$, we obtain

$$\frac{1}{h} A_{11} = \frac{1}{h} A_{22} = \frac{1}{4} \left[\frac{3}{2} (\bar{E}_\ell + \bar{E}_t) + \nu_{t\ell} \bar{E}_\ell + 2G_{t\ell} \right]$$

$$\frac{1}{h} A_{12} = \frac{1}{4} \left[\frac{1}{2} (\bar{E}_\ell + \bar{E}_t) + 3\nu_{t\ell} \bar{E}_\ell - 2G_{t\ell} \right]$$

$$\frac{1}{h} A_{33} = \frac{1}{4} \left[\frac{1}{2} (\bar{E}_\ell + \bar{E}_t) - \nu_{t\ell} \bar{E}_\ell + 2G_{t\ell} \right]$$

$$\frac{1}{h} A_{13} = \frac{1}{h} A_{23} = 0$$

Bearing in mind that

$$\bar{E}_\ell = \frac{E_\ell}{1 - \nu_{t\ell}\nu_{\ell t}}; \quad \bar{E}_t = \frac{E_t}{1 - \nu_{t\ell}\nu_{\ell t}}$$

The matrix $(1/h)[A]$ reduces to $\frac{1}{h} \begin{bmatrix} A_{11} & A_{12} & 0 \\ A_{21} & A_{11} & 0 \\ 0 & 0 & A_{33} \end{bmatrix}$

2. From the above, the elasticity moduli of the laminate in x - and y -directions and the associated Poisson coefficient are as follows:

$$\frac{1}{E} = \frac{\frac{1}{h} A_{11}}{\frac{1}{h^2} (A_{11}^2 - A_{12}^2)}; \quad -\frac{\nu}{E} = -\frac{\frac{1}{h} A_{12}}{\frac{1}{h^2} (A_{11}^2 - A_{12}^2)}$$

We obtain after calculation

$$E = \frac{\left[2(\bar{E}_\ell + \bar{E}_t) + 4\nu_{t\ell} \bar{E}_\ell \right] \left[\bar{E}_\ell + \bar{E}_t - 2\nu_{t\ell} \bar{E}_\ell + 4G_{t\ell} \right]}{4 \left[\frac{3}{2} (\bar{E}_\ell + \bar{E}_t) + \nu_{t\ell} \bar{E}_\ell + 2G_{t\ell} \right]}$$

$$\nu = \frac{\frac{1}{2} (\bar{E}_\ell + \bar{E}_t) + 3\nu_{t\ell} \bar{E}_\ell - 2G_{t\ell}}{\frac{3}{2} (\bar{E}_\ell + \bar{E}_t) + \nu_{t\ell} \bar{E}_\ell + 2G_{t\ell}}$$

The shear modulus is

$$G = \frac{1}{4} \left[\frac{1}{2} (\bar{E}_\ell + \bar{E}_t) - \nu_{t\ell} \bar{E}_\ell + 2G_{t\ell} \right]$$

3. It can be noted from the above that

$$G = \frac{E}{2(1+\nu)}$$

This leads to an isotropic elastic behavior of this laminate in its plane. As a result, in any coordinate systems (X, Y) derived from (x, y) by rotation of any angle, the constitutive behavior of the laminate is unchanged and is written as

$$\begin{Bmatrix} \epsilon_X \\ \epsilon_Y \\ \gamma_{XY} \end{Bmatrix} = \begin{bmatrix} \frac{1}{E} & -\frac{\nu}{E} & 0 \\ -\frac{\nu}{E} & \frac{1}{E} & 0 \\ 0 & 0 & \frac{1}{G} \end{bmatrix} \begin{Bmatrix} \sigma_X \\ \sigma_Y \\ \tau_{XY} \end{Bmatrix}$$

Note: We show²² that this result generalizes to other groups of ply orientations such as

$$\left[0, \frac{\pi}{3}, \frac{2\pi}{3}\right]; \left[0, \frac{\pi}{5}, \frac{2\pi}{5}, \frac{3\pi}{5}, \frac{4\pi}{5}\right]; \dots$$

More generally, if we consider a laminate made up of n orientations, n being a whole number ($n > 2$), these orientations having the values of

$$\frac{\pi}{n} \times (q-1)$$

With $q=1 \dots n$ and with the same proportion of plies along each orientation denoted as $p = (1/n)$, then this laminate is elastically isotropic. Moreover, for all these laminates, E and ν are *invariable*, keeping the values found above.

20.15 PURE TORSION OF ORTHOTROPIC PLATE

Problem Statement

Consider a square plate ($a \times a$) made of unidirectional glass/epoxy ($V_f = 60\%$), of thickness h , welded at the center point of its lower face on a support. It is subjected to a uniform and constant torsional moment density m_o ($\text{N} \times \text{mm}/\text{mm}$) along its perimeter²³. The proper directions (ℓ, t) of the unidirectional make an angle θ with the (x, y) axes of the plate (see Figure 20.16).

1. Assuming that all load resultants in the plate are zero, except the torsional moment, determine the bending displacement at every midplane point.
2. Determine the state of stress in axes (x, y) then in axes (ℓ, t) of the unidirectional.
3. Numerical application: $\theta = -45^\circ$; $a = 1 \text{ m}$; $h = 5 \text{ mm}$; $m_o = -10 \text{ N} \times \text{mm}/\text{mm}$.

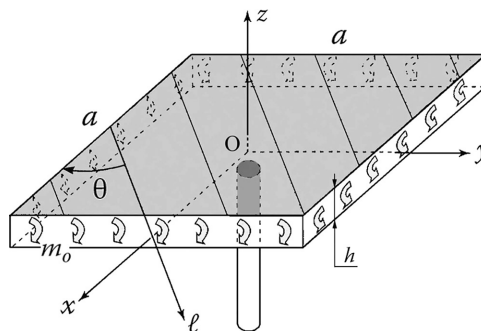


FIGURE 20.16 Glass/epoxy plate.

Solution

1. In the constitutive Equation 12.16, we have

$$C_{ij} = \bar{E}_{ij} \int_{-h/2}^{h/2} z^2 dz = \bar{E}_{ij} \frac{h^3}{12}$$

Then

$$[C] = \frac{h^3}{12} [\bar{E}]$$

Where $[\bar{E}]$ is the matrix shown in Equation 11.8.

By inverting Equation 12.16 and noting that

$$[C]^{-1} = \frac{12}{h^3} [\bar{E}]^{-1} = \frac{12}{h^3} \left[\frac{1}{E} \right]$$

Where $\left[\frac{1}{E} \right]$ is the matrix shown in Equation 11.5, we have

$$\left\{ \begin{array}{c} -\frac{\partial^2 w_o}{\partial x^2} \\ -\frac{\partial^2 w_o}{\partial y^2} \\ -2 \times \frac{\partial^2 w_o}{\partial x \partial y} \end{array} \right\} = \frac{12}{h^3} \left[\frac{1}{E} \right] \left\{ \begin{array}{c} M_y \\ -M_x \\ -M_{xy} \end{array} \right\} \quad (20.17)$$

Assuming the load resultants are all zero except M_{xy}^{24} , we have

$$N_x = N_y = T_{xy} = M_x = M_y = 0 ; M_{xy} = m_o$$

There remains (see Equation 11.5)

$$\frac{\partial^2 w_o}{\partial x^2} = \frac{12}{h^3} \times \frac{\eta_{xy}}{G_{xy}} m_o ; \quad \frac{\partial^2 w_o}{\partial y^2} = \frac{12}{h^3} \times \frac{\mu_{xy}}{G_{xy}} m_o ; \quad 2 \frac{\partial^2 w_o}{\partial x \partial y} = \frac{12}{h^3} \times \frac{1}{G_{xy}} m_o$$

Therefore, one can write $w_o(x, y)$ in the form

$$w_o = \frac{12}{h^3} \frac{m_o}{G_{xy}} (Ax^2 + By^2 + Cxy + Dx + Ey + F)$$

At the center point of the plate, and due to the geometrical and loading symmetry

$$w_o = 0 ; \quad \frac{\partial w_o}{\partial x} = \frac{\partial w_o}{\partial y} = 0$$

From which $D=E=F=0$. And by identification with the second derivatives,

$$2A = \eta_{xy} ; \quad 2B = \mu_{xy} ; \quad 2C = 1$$

The out-of-plane displacement takes the form

$$w_o = \frac{6m_o}{h^3 G_{xy}} (\eta_{xy} x^2 + \mu_{xy} y^2 + xy) \quad (20.18)$$

2. *State of stress*: With Equation 12.12 and taking (20.17) into account, the strain components in axes (x, y) are

$$\begin{Bmatrix} \varepsilon_x \\ \varepsilon_y \\ \gamma_{xy} \end{Bmatrix} = z \times \begin{Bmatrix} -\frac{\partial^2 w_o}{\partial x^2} \\ -\frac{\partial^2 w_o}{\partial y^2} \\ -2\frac{\partial^2 w_o}{\partial x \partial y} \end{Bmatrix} = z \times \frac{12}{h^3} \left[\frac{1}{E} \right] \begin{Bmatrix} 0 \\ 0 \\ -m_o \end{Bmatrix}$$

From which we deduce the stress values in axes (x, y) using Equation 11.8:

$$\begin{Bmatrix} \sigma_x \\ \sigma_y \\ \tau_{xy} \end{Bmatrix} = [\bar{E}] \begin{Bmatrix} \varepsilon_x \\ \varepsilon_y \\ \gamma_{xy} \end{Bmatrix} = z \times \frac{12}{h^3} [\bar{E}] \left[\frac{1}{E} \right] \begin{Bmatrix} 0 \\ 0 \\ -m_o \end{Bmatrix} = z \times \frac{12}{h^3} \begin{Bmatrix} 0 \\ 0 \\ -m_o \end{Bmatrix}$$

Then

$$\sigma_x = 0; \quad \sigma_y = 0; \quad \tau_{xy} = -z \times \frac{12}{h^3} m_o$$

- Stress values in the unidirectional axes: these are obtained by using Equation 11.4:

$$\sigma_\ell = -2cs \tau_{xy} = z \times cs \times \frac{24}{h^3} m_o$$

$$\sigma_t = 2cs \tau_{xy} = -z \times cs \times \frac{24}{h^3} m_o$$

$$\tau_{\ell t} = (c^2 - s^2) \tau_{xy} = -z (c^2 - s^2) \times \frac{12}{h^3} m_o$$

3. Numerical application

Section 3.3.3 gives for glass/epoxy:

$$\begin{aligned} E_\ell &= 45,000 \text{ MPa}; & E_t &= 12,000 \text{ MPa} \\ G_{\ell t} &= 4,500 \text{ MPa}; & \nu_{\ell t} &= 0.3 \quad (\nu_{t\ell} = 0.08) \end{aligned}$$

Then with Equation 11.5 and $\theta = -45^\circ$,

$$\frac{\eta_{xy}}{G_{xy}} = \frac{\mu_{xy}}{G_{xy}} = -\frac{0.1375}{4,500}$$

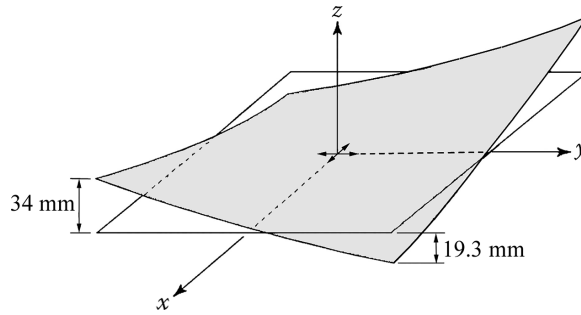


FIGURE 20.17 Deformed configuration of the plate.

w_o takes the form

$$w_{o(mm)} = -\frac{1}{9,375} \left[xy - 0.1375(x^2 + y^2) \right]$$

The deformed configuration is shown in Figure 20.17.

The stress values (in MPa) are written as

$$\sigma_x = \sigma_y = 0; \tau_{xy} = 0.96 \times z \text{ (mm)}$$

$$\sigma_t = -\sigma_l = 0.96 \times z \text{ (mm)}; \tau_{lt} = 0$$

20.16 PLATE MADE BY RESIN TRANSFER MOLDING

Problem Statement

First part

A roll of mat of carbon fibers has the following characteristics:

- Areal mass density: $m_{of} = 30 \text{ g/m}^2$
- Specific mass: $\rho_f = 1,750 \text{ kg/m}^3$

Twenty-one layers of this mat are laid up over a plate in a rectangular mold. The mold is then closed and sealed, as shown in Figure 20.18.

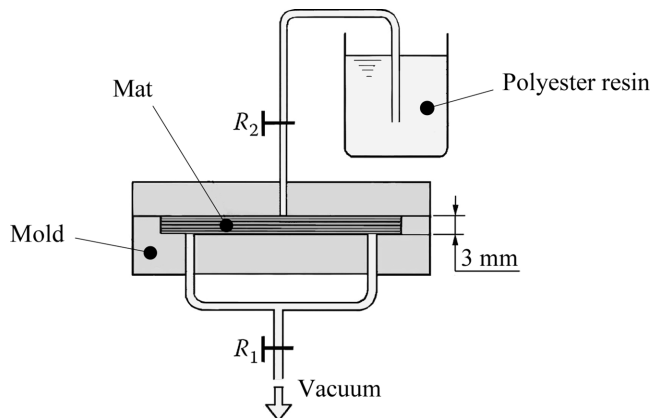


FIGURE 20.18 Plate made by resin transfer molding (RTM).

R_1 and R_2 represent two valves:

- R_2 is closed and R_1 is open. The mold is vacuumed.
- R_2 is open and R_1 is open. The polyester resin is filled into the cavity of the mold. Then the resin begins to flow out through valve R_1 .
- R_1 and R_2 are closed.

The mold is then heated, and the resin polymerizes. After demolding, a plate of mat/polyester is obtained.

- Calculate the fiber volume fraction V_f (%).
- Calculate the modulus of elasticity along longitudinal and transverse directions, denoted, respectively, as E_ℓ and E_t , of a carbon/polyester unidirectional that would have the same amount of fiber volume fraction. The following characteristics are given:

$$E_{f\ell} = 230,000 \text{ MPa}; \quad E_{ft} = 15,000 \text{ MPa} \quad (\text{see Table 3.3 in Section 3.3.1})$$

$$E_{\text{resin}} = 4,000 \text{ MPa} \quad (\text{Section 1.6})$$

- Starting from equation in Section 3.5.1 giving the elasticity modulus of mat (which is assumed to be isotropic in the plane of the plate), deduce the value of E_{mat} . Assume that $\nu_{\text{mat}} = 0.3$.

Second part

On each face of the previous plate are polymerized two plies of preimpregnated carbon/epoxy unidirectionals with $V_f = 60\%$ (see characteristics given in Section 3.3.3). Each ply has a thickness of 0.13 mm. The four plies (two above, two below) are oriented in the same direction denoted as x (or 0°). The midplane of the resulting laminated plate coincides with axes (x, y) .

- Write numerically for the unidirectional and for the mat the constitutive relations in axes (x, y) in the form

$$\begin{Bmatrix} \sigma_x \\ \sigma_y \\ \tau_{xy} \end{Bmatrix} = [\bar{E}] \begin{Bmatrix} \varepsilon_x \\ \varepsilon_y \\ \gamma_{xy} \end{Bmatrix}$$

- Calculate in axes (x, y) the coefficients of the In-plane constitutive equation of the laminated plate (matrix $[A]$ in Section 12.1.1). Deduce from there the apparent elastic moduli and Poisson coefficients of the plate.
- Calculate in axes (x, y) the stiffness coefficients for the bending behavior of the laminated plate (matrix $[C]$ in Section 12.1.4). Deduce from there the apparent bending moduli along x - and y -directions.
- This laminated plate is submitted to a tensile In-plane resultant along the x -direction denoted as N_x (N/mm). The tensile failure strength of mat is 100 MPa. Calculate the stress resultant value N_x that leads to first-ply failure of the laminate. In which component, unidirectional or mat, will this failure occur? This component is supposed to be completely broken (i.e., its mechanical characteristics are reduced to zero). What is then the state of stress in the other component? Comment.

Solution**First part**

1. Carbon fiber volume fraction

$$V_f = \frac{\text{Vol. fibers}}{\text{Total volume}}$$

If s is the rectangular surface forming the base of the mold, the volume of a layer of mat is

$$s \times \frac{m_{of}}{\rho_f}$$

From which, for 21 layers,

$$V_f = \frac{21 \times s \times m_{of} / \rho_f}{s \times 3 \times 10^{-3}} = 12\%$$

2. Elasticity moduli (see Section 3.3.1):

We have

$$E_\ell = E_f V_f + E_m V_m = 31,120 \text{ MPa}$$

$$E_t = E_m \left[\frac{1}{V_m + \frac{E_m}{E_{f_t}} V_f} \right] = 4,386 \text{ MPa}$$

3. Elastic modulus of mat: We have (see Section 3.5.1)

$$E_{\text{mat}} = \frac{3}{8} E_\ell + \frac{5}{8} E_t = 14,410 \text{ MPa}$$

Second part

1. Constitutive equation

- Unidirectional

$$\begin{Bmatrix} \varepsilon_x \\ \varepsilon_y \\ \gamma_{xy} \end{Bmatrix} = \begin{bmatrix} \frac{1}{134,000} & -\frac{0.25}{134,000} & 0 \\ -\frac{0.25}{134,000} & \frac{1}{7,000} & 0 \\ 0 & 0 & \frac{1}{4,200} \end{bmatrix} \begin{Bmatrix} \sigma_x \\ \sigma_y \\ \tau_{xy} \end{Bmatrix}$$

After inversion

$$\begin{Bmatrix} \sigma_x \\ \sigma_y \\ \tau_{xy} \end{Bmatrix} = \begin{bmatrix} 134,400 & 1,756 & 0 \\ 1,756 & 7,023 & 0 \\ 0 & 0 & 4,200 \end{bmatrix} \begin{Bmatrix} \varepsilon_x \\ \varepsilon_y \\ \gamma_{xy} \end{Bmatrix}$$

- Mat

$$\left\{ \begin{array}{c} \epsilon_x \\ \epsilon_y \\ \gamma_{xy} \end{array} \right\} = \left[\begin{array}{ccc} \frac{1}{14,410} & -\frac{0.3}{14,410} & 0 \\ -\frac{0.3}{14,410} & \frac{1}{14,410} & 0 \\ 0 & 0 & \frac{2(1+0.3)}{14,410} \end{array} \right] \left\{ \begin{array}{c} \sigma_x \\ \sigma_y \\ \tau_{xy} \end{array} \right\}$$

After inversion

$$\left\{ \begin{array}{c} \sigma_x \\ \sigma_y \\ \tau_{xy} \end{array} \right\} = \left[\begin{array}{ccc} 15,835 & 4,750 & 0 \\ 4,750 & 15,835 & 0 \\ 0 & 0 & 5,542 \end{array} \right] \left\{ \begin{array}{c} \epsilon_x \\ \epsilon_y \\ \gamma_{xy} \end{array} \right\}$$

2. In-plane behavior of the laminated plate

$$A_{ij} = \sum_{k=1}^{k=n} \bar{E}_{ij}^{(k)} \times e^{(k)}$$

$$A_{11} = 134,440 \times 4 \times 0.13 + 15,835 \times 3 = 117,408 (\text{MPa} \times \text{mm})$$

$$A_{22} = 7,023 \times 4 \times 0.13 + 15,835 \times 3 = 51,151 (\text{MPa} \times \text{mm})$$

$$A_{12} = 1,756 \times 4 \times 0.13 + 4,750 \times 3 = 15,163 (\text{MPa} \times \text{mm})$$

$$A_{13} = A_{23} = 0$$

$$A_{33} = 4,200 \times 4 \times 0.13 + 5,542 \times 3 = 18,810 (\text{MPa} \times \text{mm})$$

From this and with a total plate thickness

$$h = 3 + 4 \times 0.13 = 3.52 \text{ mm}$$

We have

$$[A] = \left[\begin{array}{ccc} 117,408 & 15,163 & 0 \\ 15,163 & 51,151 & 0 \\ 0 & 0 & 18,810 \end{array} \right]$$

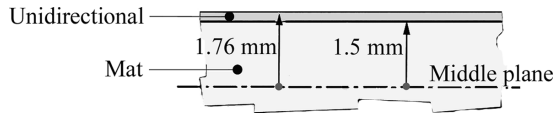
$$h[A]^{-1} = \left[\begin{array}{ccc} \frac{1}{32,078} & -\frac{0.13}{13,975} & 0 \\ -\frac{0.3}{32,078} & \frac{1}{13,975} & 0 \\ 0 & 0 & \frac{1}{5,344} \end{array} \right]$$

From where the apparent elastic moduli of this plate

$$\begin{aligned}\bar{E}_x &= 32,078 \text{ MPa}; \nu_{xy} = 0.3; \bar{G}_{xy} = 5,344 \text{ MPa} \\ \bar{E}_y &= 13,975 \text{ MPa}; \nu_{yx} = 0.13\end{aligned}$$

3. Bending behavior of the laminated plate: From Equation 12.16,

$$C_{ij} = \sum_{k=1}^{k=n} \bar{E}_{ij}^{(k)} \left(\frac{z_k^3 - z_{k-1}^3}{3} \right)$$



$$C_{11} = 134,400 \times \frac{(1.76^3 - 1.5^3)}{3} \times 2 + 15,835 \times \frac{1.5^3}{3} \times 2 = 221,763 \text{ MPa} \times \text{mm}^3$$

$$C_{22} = 7,023 \times \frac{(1.76^3 - 1.5^3)}{3} \times 2 + 15,835 \times \frac{1.5^3}{3} \times 2 = 45,352 \text{ MPa} \times \text{mm}^3$$

$$C_{12} = 1,756 \times \frac{(1.76^3 - 1.5^3)}{3} \times 2 + 4,750 \times \frac{1.5^3}{3} \times 2 = 13,119 \text{ MPa} \times \text{mm}^3$$

$$C_{13} = C_{23} = 0$$

$$C_{33} = 4,200 \times \frac{(1.76^3 - 1.5^3)}{3} \times 2 + 5,542 \times \frac{1.5^3}{3} \times 2 = 18,284 \text{ MPa} \times \text{mm}^3$$

From which (see Section 12.1.6)

$$[C]^{-1} = \begin{bmatrix} \frac{1}{217,968} & -\frac{1}{753,509} & 0 \\ -\frac{1}{753,509} & \frac{1}{44,509} & 0 \\ 0 & 0 & \frac{1}{18,284} \end{bmatrix} = \begin{bmatrix} \frac{1}{\bar{EI}_{11}} & \frac{1}{\bar{EI}_{12}} & 0 \\ \frac{1}{\bar{EI}_{21}} & \frac{1}{\bar{EI}_{22}} & 0 \\ 0 & 0 & \frac{1}{\bar{EI}_{33}} \end{bmatrix}$$

Apparent bending modulus in the x -direction E_{flexure}
(along x)

$$\frac{1}{\bar{EI}_{11}} = \frac{1}{E_{\text{flexure}} \times \frac{h^3}{12}} \Rightarrow E_{\text{flexure}} = 59,972 \text{ MPa} \quad (\text{along } x)$$

Apparent bending modulus in the y-direction E_{flexure}
(along y)

$$\frac{1}{EI_{22}} = \frac{1}{E_{\text{flexure}} \times \frac{h^3}{12}} \Rightarrow E_{\text{flexure}} = 12,264 \text{ MPa} \quad (\text{along y})$$

4. *Rupture*: For a stress resultant N_x , the plate deforms in its plane according to

$$\begin{Bmatrix} \epsilon_x \\ \epsilon_y \\ \gamma_{xy} \end{Bmatrix} = [A]^{-1} \begin{Bmatrix} N_x \\ 0 \\ 0 \end{Bmatrix}$$

Then with the values found for $[A]^{-1}$,

$$\epsilon_x = 8.856 \times 10^{-6} \times N_x; \quad \epsilon_y = -2.66 \times 10^{-6} \times N_x; \quad \gamma_{xy} = 0$$

We obtain for stress values the following:

- In the unidirectional,

$$\sigma_\ell = \sigma_x = 134,440 \times \epsilon_x + 1,756 \times \epsilon_y = 1.183 \times N_x$$

$$\sigma_t = \sigma_y = 1,750 \times \epsilon_x + 7,023 \times \epsilon_y = -0.003 \times N_x$$

$$\tau_{\ell t} = \tau_{xy} = 0.$$

- In the mat,

$$\sigma_x = 15,835 \times \epsilon_x + 4,750 \times \epsilon_y = 0.128 \times N_x$$

$$\sigma_y = 4,750 \times \epsilon_x + 15,835 \times \epsilon_y = 5.5 \times 10^{-5} \times N_x$$

$$\tau_{xy} = 0$$

From which the Tsai-Hill failure criteria values are as follows (see Section 14.2.3):

- In the unidirectional layer,

$$\frac{(1.183 \times N_x)^2}{1,270^2} + \frac{(-0.003 \times N_x)^2}{141^2} - \frac{1.183 \times -0.003 \times N_x^2}{1,270^2} < 1$$

Failure will not occur if $N_x < 1,072 \text{ N/mm}$.

- In the mat layer,

$$\frac{(0.128 \times N_x)^2}{100^2} + \frac{(5.5 \times 10^{-5} \times N_x)^2}{100^2} - \frac{0.128 \times 5.5 \times 10^{-5} \times N_x^2}{100^2} < 1$$

Failure will not occur if $N_x < 781 \text{ N/mm}$.

Therefore, failure will first occur in the mat layer as first-ply failure. The mat is supposed to be completely broken. The load resultant $N_x = 781 \text{ N/mm}$ leads to a state of uniaxial stress in the laminate such that

$$\sigma_\ell = \sigma_x = \frac{N_x}{4 \times 0.13} = \frac{781}{0.52} = 1502 \text{ MPa} > \sigma_{\ell \text{ rupture}}$$

The fibers in the unidirectional are broken.

- **Conclusion:** The first-ply failure leads to ultimate failure of the laminate.

20.17 THERMOELASTIC BEHAVIOR OF A BALANCED FABRIC PLY

Problem Statement

Consider a layer of balanced fabric made of carbon/epoxy ($V_f = 60\%$). The configuration of an elementary cell ($a \times a$) is shown in Figure 20.19. We consider the layer of fabric as equivalent to two layers, each with a thickness e .

First part: Upper layer

We study the upper layer as shown schematically in Figure 20.20.

Assume that the upper layer behavior is similar to the one of two equivalent unidirectional layers ($a \times a$) crossed at 0° and 90° . These layers have equivalent thicknesses denoted, respectively, as

$$e_{\text{equiv.}}^{0^\circ} \text{ and } e_{\text{equiv.}}^{90^\circ}.$$

1.1 Show that

$$e_{\text{equiv.}}^{0^\circ} = \frac{3}{4}e; \quad e_{\text{equiv.}}^{90^\circ} = \frac{1}{4}e$$

- 1.2 Deduce from the above the stiffness matrix $(1/h)[A]$ of this upper layer considered as made up of the two previous unidirectionals, with elastic constants indicated in Section 3.3.3.
- 1.3 Deduce from the above the moduli of elasticity and Poisson coefficients of this upper layer, denoted as $E_x, E_y, G_{xy}, \nu_{xy}$ ²⁵.
- 1.4 The thermal expansion coefficients of this unidirectional are denoted α_ℓ and α_t with values in Section 3.3.3. What are the values of the thermal expansion coefficients $\alpha_{ox}, \alpha_{oy}, \alpha_{oxy}$ of this upper layer? (The terms denoted as $\langle \alpha E h \rangle_i$ of Section 12.1.7 should first be precalculated.)

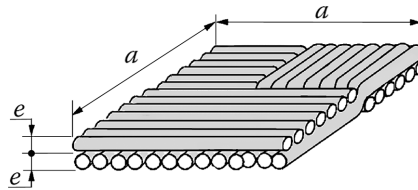


FIGURE 20.19 Elementary cell of balanced fabric.

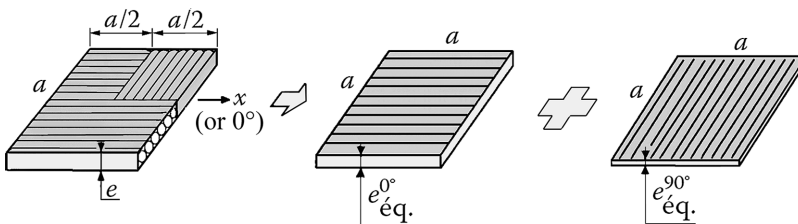


FIGURE 20.20 Modelization of the equivalent upper layer.

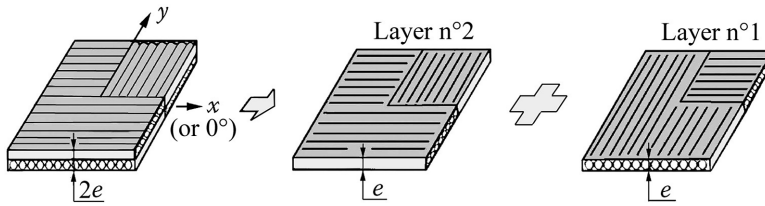


FIGURE 20.21 Modelization of the elementary cell of fabric.

Second part: Complete fabric layer

Now we consider the complete fabric ply (thickness $2e$ in Figure 20.19) as the result of a simple superposition of two layers similar to the one previously studied above, these two layers being crossed at 0° for upper layer (no. 2) and at 90° for lower layer (no. 1), as shown in Figure 20.21.

We retain in the following $e = 0.14 \text{ mm}$.

- 2.1 Write numerically with the previous results the In-plane behavior relationship for layer no. 2, then for layer no. 1 in Figure 20.21 in the form $\{\sigma\} = [\bar{E}] \{\epsilon\}$.
- 2.2 Calculate the coefficients $\alpha \bar{E}_i$ (see Section 11.3.2) of layer no. 2, then of layer no. 1.
- 2.3 Calculate the matrix $[A]$ characterizing the In-plane behavior of the double layer in Figure 20.21 (layer no. 1 + layer no. 2).

Third part (*Independent of the two previous parts until Question 9*)

We consider a laminate consisting of two orthotropic plies noted as 2 and 1, each with a thickness e , crossed at 0° (or x) and at 90° , respectively. We give here the respective thermomechanical behavior of these layers in x - and y -axes (see Equation 11.10):

- Ply no. 1 (lower ply)

$$\begin{Bmatrix} \sigma_x \\ \sigma_y \\ \tau_{xy} \end{Bmatrix}_1 = \begin{bmatrix} a & c & 0 \\ c & b & 0 \\ 0 & 0 & d \end{bmatrix} \begin{Bmatrix} \epsilon_x \\ \epsilon_y \\ \gamma_{xy} \end{Bmatrix} - \Delta T \begin{Bmatrix} f \\ g \\ 0 \end{Bmatrix}$$

- Ply no. 2 (upper ply)

$$\begin{Bmatrix} \sigma_x \\ \sigma_y \\ \tau_{xy} \end{Bmatrix}_2 = \begin{bmatrix} b & c & 0 \\ c & a & 0 \\ 0 & 0 & d \end{bmatrix} \begin{Bmatrix} \epsilon_x \\ \epsilon_y \\ \gamma_{xy} \end{Bmatrix} - \Delta T \begin{Bmatrix} g \\ f \\ 0 \end{Bmatrix}$$

Recalling that the thermomechanical behavior of a laminate is (see Equation 12.21)

$$\begin{Bmatrix} N_x \\ N_y \\ T_{xy} \\ M_x \\ M_y \\ -M_{xy} \end{Bmatrix} = \begin{bmatrix} A & B \\ B & C \end{bmatrix} \begin{Bmatrix} \epsilon_{ox} \\ \epsilon_{oy} \\ \gamma_{oxy} \\ -\frac{\partial^2 w_o}{\partial x^2} \\ -\frac{\partial^2 w_o}{\partial y^2} \\ -2\frac{\partial^2 w_o}{\partial x \partial y} \end{Bmatrix} - \Delta T \begin{Bmatrix} \langle \alpha E h \rangle_x \\ \langle \alpha E h \rangle_y \\ \langle \alpha E h \rangle_{xy} \\ \langle \alpha E h^2 \rangle_x \\ \langle \alpha E h^2 \rangle_y \\ \langle \alpha E h^2 \rangle_{xy} \end{Bmatrix}$$

- 3.1 Write the literal expression of matrix $[A]$.
- 3.2 Write the literal expression of matrix $[C]$.
- 3.3 Write the literal expression of matrix $[B]$.
- 3.4 Calculate the terms $\langle \alpha E h \rangle_x, \langle \alpha E h \rangle_y, \langle \alpha E h \rangle_{xy}, \langle \alpha E h^2 \rangle_x, \langle \alpha E h^2 \rangle_y, \langle \alpha E h^2 \rangle_{xy}$ (see Section 12.2.2).
- 3.5 Write the thermomechanical behavior equation.
- 3.6 This plate is not subject to an external loading. It is subject to a temperature variation ΔT . Deduce from item 3.5 the corresponding system of equations.
- 3.7 Give the strain values $\gamma_{0,xy}$ and $\partial^2 w_o / \partial x \partial y$.
- 3.8 Write the remaining equations that allow the calculation of other strain components.
- 3.9 Taking into account the results obtained in the second part, write numerically this system of equations with $\Delta T = -160^\circ\text{C}$. Give the corresponding strain values. Comment.

Solution

- 1.1 Volume of fibers at 0°

$$v^{0^\circ} = \frac{3a^2}{4} \times e = a^2 \times e_{\text{equiv.}}^{0^\circ}.$$

Volume of fibers at 90°

$$v^{90^\circ} = \frac{a^2}{4} \times e = a^2 \times e_{\text{equiv.}}^{90^\circ}.$$

From which

$$e_{\text{equiv.}}^{0^\circ} = \frac{3e}{4}; \quad e_{\text{equiv.}}^{90^\circ} = \frac{e}{4}$$

- 1.2 Stiffness matrix $(1/h)[A]$

According to Equation 11.8 and values in Section 3.3.3,

$$\bar{E}_{11}^{0^\circ} = \bar{E}_\ell = 134,439 \text{ MPa}; \quad \bar{E}_{12}^{0^\circ} = \nu_{\ell t} \bar{E}_\ell = 1,756 \text{ MPa}$$

$$\bar{E}_{22}^{0^\circ} = \bar{E}_t = 7,023 \text{ MPa}; \quad \bar{E}_{33}^{0^\circ} = G_{\ell t} = 4,200 \text{ MPa}$$

$$\bar{E}_{11}^{90^\circ} = 7,023 \text{ MPa}; \quad \bar{E}_{12}^{90^\circ} = 1,756 \text{ MPa}$$

$$\bar{E}_{22}^{90^\circ} = 134,439 \text{ MPa}; \quad \bar{E}_{33}^{90^\circ} = 4,200 \text{ MPa}$$

$$A_{11} = \bar{E}_{11}^{0^\circ} \times \frac{3e}{4} + \bar{E}_{11}^{90^\circ} \times \frac{e}{4} = 102,585 \times e \text{ (MPa} \times \text{mm)}$$

$$A_{22} = \bar{E}_{22}^{0^\circ} \times \frac{3e}{4} + \bar{E}_{22}^{90^\circ} \times \frac{e}{4} = 38,877 \times e \text{ (MPa} \times \text{mm)}$$

$$A_{12} = 1,756 \times e \text{ (MPa} \times \text{mm)}; \quad A_{33} = 4,200 \times e \text{ (MPa} \times \text{mm)}$$

The stiffness matrix of the upper layer is

$$\frac{1}{h}[A] = \begin{bmatrix} 102,585 & 1,756 & 0 \\ 1,756 & 38,877 & 0 \\ 0 & 0 & 4,200 \end{bmatrix} \text{ (MPa)}$$

1.3 We have, according to Equation 12.9,

$$h[A]^{-1} = \begin{bmatrix} \frac{1}{E_x} & -\frac{\nu_{yx}}{E_y} & 0 \\ -\frac{\nu_{xy}}{E_x} & \frac{1}{E_y} & 0 \\ 0 & 0 & \frac{1}{G_{xy}} \end{bmatrix}$$

From which

$$E_x = 102,506 \text{ MPa}$$

$$E_y = 38,847 \text{ MPa}$$

$$\nu_{yx} = 0.017; \nu_{xy} = 0.045$$

$$G_{xy} = 4,200 \text{ MPa}$$

We therefore observe that

$$\frac{1}{h}[A] \approx \begin{bmatrix} E_x & \nu_{yx}E_x & 0 \\ \nu_{xy}E_y & E_y & 0 \\ 0 & 0 & G_{xy} \end{bmatrix}$$

1.4 We have (Equation 12.18)

$$\begin{Bmatrix} \alpha_{ox} \\ \alpha_{oy} \\ \alpha_{oxy} \end{Bmatrix} = h[A]^{-1} \begin{Bmatrix} \frac{1}{h}\langle \alpha Eh \rangle_x \\ \frac{1}{h}\langle \alpha Eh \rangle_y \\ \frac{1}{h}\langle \alpha Eh \rangle_{xy} \end{Bmatrix}$$

With (Equations 12.17 and 11.10)

$$\langle \alpha Eh \rangle_x = \overline{\alpha E_1}^{0^\circ} \times \frac{3}{4}e + \overline{\alpha E_1}^{90^\circ} \times \frac{e}{4} = \overline{E_t}(\alpha_\ell + \nu_{t\ell}\alpha_t) \times \frac{3}{4}e + \overline{E_t}(\nu_{t\ell}\alpha_\ell + \alpha_t) \times \frac{e}{4}$$

And with (Section 3.3.3) $\alpha_\ell = -0.12 \times 10^{-5}$; $\alpha_t = 3.4 \times 10^{-5}$.

$$\begin{aligned} \frac{1}{h}\langle \alpha Eh \rangle_x &= -1,726 \times 10^{-5} \\ \frac{1}{h}\langle \alpha Eh \rangle_y &= 15,203 \times 10^{-5}; \quad \frac{1}{h}\langle \alpha Eh \rangle_{xy} = 0 \end{aligned}$$

From which we can deduce

$$\alpha_{ox} = -2.3 \times 10^{-7}; \alpha_{oy} = 39 \times 10^{-7}; \alpha_{oxy} = 0$$

2.1 Behavior equation: $\{\sigma\} = [\bar{E}]\{\varepsilon\}$
According to Equation 11.8,

- *Layer no. 2*

$$\bar{E}_{11}^{(2)} = \bar{E}_x = \frac{E_x}{1 - \nu_{yx} \nu_{xy}} = 102,584 \text{ MPa}$$

Etc. We find

$$[\bar{E}]^{(2)} = \begin{bmatrix} 102,584 & 1,744 & 0 \\ 1,744 & 38,877 & 0 \\ 0 & 0 & 4,200 \end{bmatrix}$$

- *Layer no. 1*

$$[\bar{E}]^{(1)} = \begin{bmatrix} 38,877 & 1,744 & 0 \\ 1,744 & 102,584 & 0 \\ 0 & 0 & 4,200 \end{bmatrix}$$

2.2 Coefficients $\bar{\alpha}E_i$:

- *Layer no. 2*

$$\bar{\alpha}E_1^{(2)} = \bar{E}_x (\alpha_{ox} + \nu_{yx} \alpha_{oy}) = -0.0168$$

$$\bar{\alpha}E_2^{(2)} = 0.1512; \bar{\alpha}E_3^{(2)} = 0$$

- *Layer no. 1 (rotation of 90°)*

$$\bar{\alpha}E_1^{(1)} = 0.1512; \bar{\alpha}E_2^{(1)} = -0.0168; \bar{\alpha}E_3^{(1)} = 0$$

2.3 In-plane behavior of the double layer

$$A_{11} = \bar{E}_{11}^{(1)} \times e + \bar{E}_{11}^{(2)} \times e = (102,584 + 38,877) \times 0.14$$

Etc. Then

$$[A] = \begin{bmatrix} 19,804 & 488 & 0 \\ 488 & 19,804 & 0 \\ 0 & 0 & 1,176 \end{bmatrix} (\text{MPa} \times \text{mm})$$

3.1 Matrix [A]

$$[A] = \begin{bmatrix} (a+b)e & 2ce & 0 \\ 2ce & (a+b)e & 0 \\ 0 & 0 & 2de \end{bmatrix}$$

3.2 Matrix [C]

$$C_{11} = a \left(\frac{0 - (-e)^3}{3} \right) + b \left(\frac{e^3 - 0}{3} \right) = (a+b) \frac{e^3}{3}$$

Etc. Then

$$[C] = \begin{bmatrix} (a+b)\frac{e^3}{3} & 2c\frac{e^3}{3} & 0 \\ 2c\frac{e^3}{3} & (a+b)\frac{e^3}{3} & 0 \\ 0 & 0 & 2d\frac{e^3}{3} \end{bmatrix}$$

3.3 Matrix [B]

$$B_{11} = a \left(\frac{0 - (-e)^2}{2} \right) + b \left(\frac{e^2 - 0}{2} \right) = (b - a) \frac{e^2}{2}$$

Etc. Then

$$[B] = \begin{bmatrix} (b-a)\frac{e^2}{2} & 0 & 0 \\ 0 & (a-b)\frac{e^2}{2} & 0 \\ 0 & 0 & 0 \end{bmatrix}$$

3.4 Terms $\langle \alpha E h_i \rangle$ and $\langle \alpha E h_i^2 \rangle$

$$\langle \alpha E h \rangle_x = f e + g e = (f + g) e$$

$$\langle \alpha E h \rangle_y = (f + g) e ; \langle \alpha E h \rangle_{xy} = 0$$

$$\langle \alpha E h^2 \rangle_x = (g - f) \frac{e^2}{2}$$

$$\langle \alpha E h^2 \rangle_y = (f - g) \frac{e^2}{2} ; \langle \alpha E h^2 \rangle_{xy} = 0$$

3.5 Thermomechanical behavior

$$\begin{Bmatrix} N_x \\ N_y \\ T_{xy} \\ M_y \\ -M_x \\ -M_{xy} \end{Bmatrix} = \begin{bmatrix} (a+b)e & 2ce & 0 & (b-a)\frac{e^2}{2} & 0 & 0 \\ 2ce & (a+b)e & 0 & 0 & (a-b)\frac{e^2}{2} & 0 \\ 0 & 0 & 2de & 0 & 0 & 0 \\ (b-a)\frac{e^2}{2} & 0 & 0 & (a+b)\frac{e^3}{3} & 2c\frac{e^3}{3} & 0 \\ 0 & (a-b)\frac{e^2}{2} & 0 & 2c\frac{e^3}{3} & (a+b)\frac{e^3}{3} & 0 \\ 0 & 0 & 0 & 0 & 0 & 2d\frac{e^3}{3} \end{bmatrix} \begin{Bmatrix} \epsilon_{ox} \\ \epsilon_{oy} \\ \gamma_{oxy} \\ -\frac{\partial^2 w_o}{\partial x^2} \\ -\frac{\partial^2 w_o}{\partial y^2} \\ -2\frac{\partial^2 w_o}{\partial x \partial y} \end{Bmatrix} - \Delta T \begin{Bmatrix} (f+g)e \\ (f+g)e \\ 0 \\ (g-f)\frac{e^2}{2} \\ (f-g)\frac{e^2}{2} \\ 0 \end{Bmatrix}$$

3.6 Temperature variation ΔT

In the absence of any external loading,

$$N_x = N_y = T_{xy} = M_x = M_y = M_{xy} = 0$$

From which we have

$$\begin{bmatrix} (a+b)e & 2ce & 0 & (b-a)\frac{e^2}{2} & 0 & 0 \\ 2ce & (a+b)e & 0 & 0 & (a-b)\frac{e^2}{2} & 0 \\ 0 & 0 & 2de & 0 & 0 & 0 \\ (b-a)\frac{e^2}{2} & 0 & 0 & (a+b)\frac{e^3}{3} & 2c\frac{e^3}{3} & 0 \\ 0 & (a-b)\frac{e^2}{2} & 0 & 2c\frac{e^3}{3} & (a+b)\frac{e^3}{3} & 0 \\ 0 & 0 & 0 & 0 & 0 & 2d\frac{e^3}{3} \end{bmatrix} \begin{bmatrix} \epsilon_{ox} \\ \epsilon_{oy} \\ \gamma_{oxy} \\ -\frac{\partial^2 w_o}{\partial x^2} \\ -\frac{\partial^2 w_o}{\partial y^2} \\ -2\frac{\partial^2 w_o}{\partial x \partial y} \end{bmatrix} = \Delta T \begin{bmatrix} (f+g)e \\ (f+g)e \\ 0 \\ (g-f)\frac{e^2}{2} \\ (f-g)\frac{e^2}{2} \\ 0 \end{bmatrix}$$

3.7 It should be noted that

$$\gamma_{oxy} = 0 ; \quad \frac{\partial^2 w_o}{\partial x \partial y} = 0$$

3.8 There remains

$$\begin{bmatrix} (a+b)e & 2ce & (b-a)\frac{e^2}{2} & 0 \\ 2ce & (a+b)e & 0 & (a-b)\frac{e^2}{2} \\ (b-a)\frac{e^2}{2} & 0 & (a+b)\frac{e^3}{3} & 2c\frac{e^3}{3} \\ 0 & (a-b)\frac{e^2}{2} & 2c\frac{e^3}{3} & (a+b)\frac{e^3}{3} \end{bmatrix} \begin{bmatrix} \epsilon_{ox} \\ \epsilon_{oy} \\ -\frac{\partial^2 w_o}{\partial x^2} \\ -\frac{\partial^2 w_o}{\partial y^2} \end{bmatrix} = \Delta T \begin{bmatrix} (f+g)e \\ (f+g)e \\ (g-f)\frac{e^2}{2} \\ (f-g)\frac{e^2}{2} \end{bmatrix}$$

Note: According to the model under analysis, it could reasonably be expected that

$$\epsilon_{ox} = \epsilon_{oy} ; \quad \frac{\partial^2 w_o}{\partial x^2} = -\frac{\partial^2 w_o}{\partial y^2}$$

It is noteworthy that this hypothesis brings two identical systems of equations, each of them written as

$$\begin{bmatrix} (a+b+2c)e & (b-a)\frac{e^2}{2} \\ (b-a)\frac{e^2}{2} & (a+b-2c)\frac{e^3}{3} \end{bmatrix} \begin{bmatrix} \epsilon_{ox} \\ -\frac{\partial^2 w_o}{\partial x^2} \end{bmatrix} = \Delta T \begin{bmatrix} (f+g)e \\ (g-f)e^2 \end{bmatrix}$$

3.9 With the results of the second part, and $\Delta T = -160^\circ\text{C}$, corresponding to the cooling in the autoclave after polymerization of the resin, we have (units: N and mm)

$$(a+b)e = 19,804; \quad 2ce = 488; \quad (a+b)\frac{e^3}{3} = 129; \quad 2c\frac{e^3}{3} = 3.2$$

$$(b-a)\frac{e^2}{2} = 624; \quad (f+g)e = 0.0188; \quad (g-f)\frac{e^2}{2} = -0.00164$$

From which we obtain the strain components and curvatures

$$\epsilon_{ox} = \epsilon_{oy} = -1.7 \times 10^{-4}$$

$$\frac{\partial^2 w_o}{\partial x^2} = -\frac{\partial^2 w_o}{\partial y^2} = -8.6 \times 10^{-4} (\text{mm}^{-1})$$

Therefore, we can conclude that during the cooling, the layer of balanced fabric *not only undergoes a contraction* but also, due to its weave, takes the form of a double curvature surface along the warp and weft directions, that is to say, a **saddle-shaped** surface.

NOTES

- 1 This representation of shear stress is approximate. Application 21.5 sets out in detail the study that provides a more precise distribution of these stress values. In fact, the approximate representation for shear stress proposed here will be as precise as the skins of the sandwich structure will have a small thickness as compared to that of the core.
- 2 See Equation 12.8.
- 3 These are the stresses $\sigma_\ell, \sigma_t, \tau_{\ell t}$ (see, e.g., Equation 11.1).
- 4 See Section 14.3.2.3.
- 5 Recall the relation $v_{xy}/E_x = v_{yx}/E_y$ (Section 9.3 and Application 19.2).
- 6 See also Application 20.14.
- 7 Recall also the property $v_{t\ell}/E_t = v_{\ell t}/E_\ell$ (see Sections 3.1, 3.2, and Application 19.2).
- 8 See Section 14.2.3.
- 9 This as a first approximation. For more precise values see Equation 14.16.
- 10 See Equation 12.7.
- 11 See Section 3.3.3 for the characteristics of unidirectional ply of carbon/epoxy.
- 12 $v'_{t\ell} = v'_{\ell t} \times E'_t/E'_\ell$ (See Application 19.2).
- 13 Recall (see Equation 11.8) that $\bar{E}_\ell = E_\ell/(1 - v_{\ell t}v_{t\ell})$; $\bar{E}_t = E_t/(1 - v_{\ell t}v_{t\ell})$.
- 14 Or still from Equation 11.7, $\epsilon_\ell^{45^\circ} = \frac{1}{2}(\epsilon_{ox} + \epsilon_{oy}) = \epsilon_o$; $\epsilon_t^{45^\circ} = \frac{1}{2}(\epsilon_{ox} - \epsilon_{oy}) = \epsilon_o$; $\gamma_{\ell t}^{45^\circ} = 0$.
Then, following Equation 11.6, $\sigma_\ell^{45^\circ} = \epsilon_o \bar{E}_\ell (1 + v_{\ell t})$; $\sigma_t^{45^\circ} = \epsilon_o \bar{E}_t (1 + v_{\ell t})$; $\tau_{\ell t}^{45^\circ} = 0$.
- 15 See Applications 20.9 and 20.10.
- 16 See also Application 20.10.
- 17 See Section 5.2.3.
- 18 See Section 5.2.3 and Note at the end of previous Application 20.9.
- 19 Recall (see Footnote in Section 14.3.2.2) that a balanced fabric is not transversely isotropic. In such case, the Tsai-Hill criterion (Equation 14.6) should be written as

$$\frac{\sigma_\ell^2}{\sigma_{\ell \text{rupt.}}^2} + \frac{\sigma_t^2}{\sigma_{t \text{rupt.}}^2} - \sigma_\ell \sigma_t \left(\frac{2}{\sigma_{\ell \text{rupt.}}^2} - \frac{1}{\sigma_{t \text{rupt.}}^2} \right) + \frac{\tau_{\ell t}^2}{\tau_{\ell t \text{rupt.}}^2} < 1$$

Without any clear value for $\sigma_{z \text{rupt.}}$ and taking into account the slight difference of the modified term compared to the form used and its weak influence, we shall content ourselves with Equation 14.6.

- 20 Recall that $\nu_{t\ell}/E_t = \nu_{\ell t}/E_\ell$. See Application 19.2.
- 21 A mat layer is not transversely isotropic in axes (y, z) or (x, z) . The Tsai-Hill expression is then modified as already evoked in footnote in Application 20.12. However, we use the form shown here as a first approximation.
- 22 For more details, see Bibliography: Gay and Joubert (1994).
- 23 The practical importance of such a loading is very limited. It is better to consider this example as a mean to validate a computer program using finite elements. It is one of the **patch tests** issued from Matheron G. (1995) (see the Bibliography).
- 24 Note that with this hypothesis, equations of equilibrium, constitutive equation, and boundary conditions are verified.
- 25 Note here that

$$\frac{1}{h}[A] \approx \begin{bmatrix} E_x & \nu_{yx}E_x & 0 \\ \nu_{xy}E_y & E_y & 0 \\ 0 & 0 & G_{xy} \end{bmatrix}$$



Taylor & Francis

Taylor & Francis Group

<http://taylorandfrancis.com>

21 Applications Level 3

21.1 CYLINDRICAL BONDING

Problem Statement

We propose to study, in a simplified approach, an adhesive bond of two cylindrical concentric tubes as in Figure 21.1. The shear moduli of the materials are denoted along with the figure:

Under a torsion torque M_t about the x -axis, the deformed configuration of the generatrices of each of the tubes, viewed from above, is shown in Figure 21.2, with the shear stress components τ_{10} and τ_{20} that are assumed to be uniform across the thickness of each tube. Also shown is the adhesive element.

1. Find the shear stress distribution in the adhesive layer, denoted as τ_c in the previous figure.
2. *Numerical application:*

$G_1 = 28,430 \text{ MPa}$	$G_2 = 79,000 \text{ MPa}$	$G_c = 1,700 \text{ MPa}$
$e_1 = e_2 = 12 \text{ mm}$	$e_c = 0.2 \text{ mm}$	$M_t = 300 \text{ m} \times \text{daN}$
$r_1 = 63.5 \text{ mm}$	$r_2 = 51.5 \text{ mm}$	$\ell = 44 \text{ mm}$

3. Calculate the maximum shear stress in the particular case where materials 1 and 2 are identical with the same thickness e , considered to be small compared with the average radii of tubes.

Solution

1. Shear stress in the adhesive layer. In Figure 21.2 that represents the bonding element, we can read the following equilibrium:

- Equilibrium of material element 1:

$$d\tau_1 e_1 dz + \tau_c dx \quad dz = 0 \rightarrow \frac{d\tau_1}{dx} e_1 + \tau_c = 0 \quad (21.1)$$

- Equilibrium of material element 2:

$$d\tau_2 e_2 dz - \tau_c dx \quad dz = 0 \rightarrow \frac{d\tau_2}{dx} e_2 - \tau_c = 0 \quad (21.2)$$

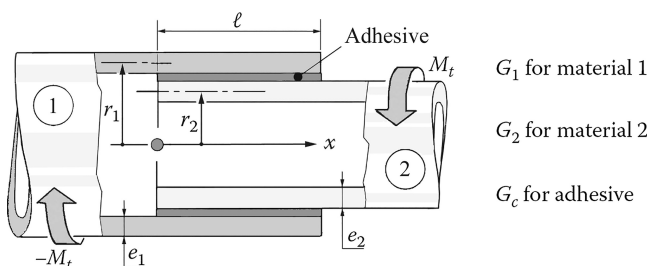


FIGURE 21.1 Two bonded concentric tubes.

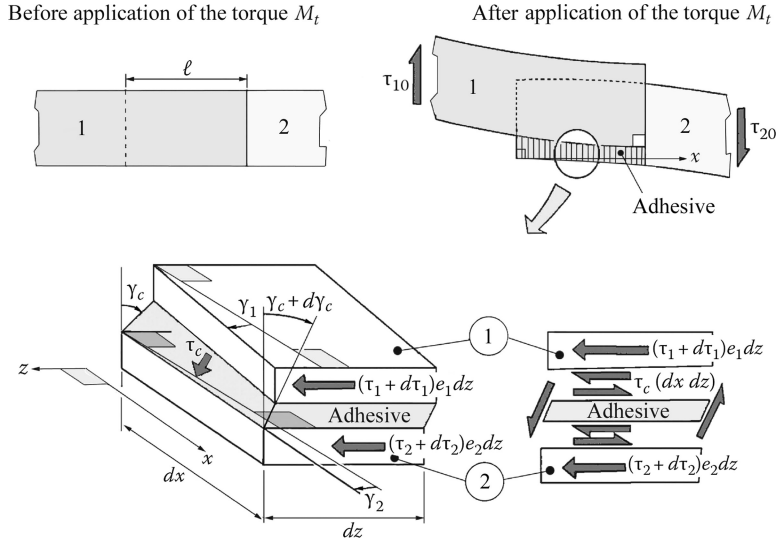


FIGURE 21.2 Deformed configuration.

The shear stress components are proportional to angular distortions, denoted here as γ_1 for material 1, γ_2 for material 2, and γ_c for the adhesive, from which

$$\gamma_1 = \frac{\tau_1}{G_1}; \quad \gamma_2 = \frac{\tau_2}{G_2}; \quad \gamma_c = \frac{\tau_c}{G_c}$$

In addition, we should note the following geometric relation, by equating the tangent and angle (see Figure 21.2):

$$(\gamma_c + d\gamma_c) - \gamma_c \approx \frac{-\gamma_1 dx + \gamma_2 dx}{e_c}$$

Or

$$\frac{d\gamma_c}{dx} = \frac{\gamma_2 - \gamma_1}{e_c}$$

In substituting the stress components,

$$\frac{d\tau_c}{dx} \frac{e_c}{G_c} = \frac{\tau_2}{G_2} - \frac{\tau_1}{G_1} \quad (21.3)$$

We then obtain three relations (21.1) through (21.3), with the three unknowns τ_1 , τ_2 , and τ_c .

Eliminating τ_1 and τ_2 yields

$$\frac{d^2\tau_c}{dx^2} \frac{e_c}{G_c} = \frac{\tau_c}{e_2 G_2} + \frac{\tau_c}{e_1 G_1}$$

Then,

$$\frac{d^2\tau_c}{dx^2} - \lambda^2\tau_c = 0 \quad \text{with} \quad \lambda^2 = \frac{G_c}{e_c} \left(\frac{1}{e_2 G_2} + \frac{1}{e_1 G_1} \right)$$

The general solution for this differential equation is

$$\tau_c = A \cosh \lambda x + B \sinh \lambda x.$$

• *Boundary conditions:*

- For $x = 0$, it is the free edge of material 2, where $\gamma_2 = 0$ and $\gamma_1 = \tau_{10}/G_1$ from which

$$\left. \frac{d\gamma_c}{dx} \right|_{x=0} = \frac{\gamma_2 - \gamma_1}{e_c} = -\frac{\tau_{10}}{e_c G_1}$$

Then,

$$\left. \frac{d\tau_c}{dx} \right|_{x=0} = -\frac{\tau_{10} G_c}{e_c G_1} \quad (21.4)$$

- For $x = \ell$, it is the free edge of material 1, where $\gamma_1 = 0$ and $\gamma_2 = \tau_{20}/G_2$ from which

$$\left. \frac{d\gamma_c}{dx} \right|_{x=\ell} = \frac{\gamma_2 - \gamma_1}{e_c} = \frac{\tau_{20}}{e_c G_2}$$

Then,

$$\left. \frac{d\tau_c}{dx} \right|_{x=\ell} = \frac{\tau_{20} G_c}{e_c G_2} \quad (21.5)$$

Boundary conditions (21.4) and (21.5) allow the calculation of constants A and B of the general solution. We obtain

$$\tau_c = \frac{G_c}{e_c \lambda} \left\{ \left(\frac{\tau_{10}}{G_1} \frac{1}{\tanh \lambda \ell} + \frac{\tau_{20}}{G_2} \frac{1}{\sinh \lambda \ell} \right) \cosh \lambda x - \frac{\tau_{10}}{G_1} \sinh \lambda x \right\}$$

2. *Numerical application:*

$$\tau_{10} = \frac{M_t}{2\pi r_1^2 e_1} = 9.86 \text{ MPa}$$

$$\tau_{20} = \frac{M_t}{2\pi r_2^2 e_2} = 15 \text{ MPa}$$

We obtain in Figure 21.3 the distribution of shear stress τ_c , where stress concentrations at the extremities of assembly can be clearly observed.

This explains that we should not design such a bonding assembly using an average shear stress, which does not exist in reality.

Note: Here, the proposed numerical values correspond to those of application in Application 19.4 relative to the design of a transmission shaft in carbon/epoxy. We can note that the failure strength of araldite, taken to be 15 MPa, is not effectively reached at the location of stress concentration.

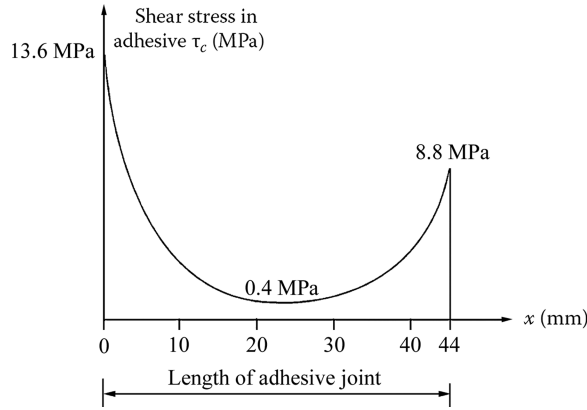


FIGURE 21.3 Shear stress distribution.

3. Particular case

$$G_1 = G_2 = G ; e_1 = e_2 = e \ll r_1 \text{ and } r_2$$

$$r_1 = r_2 + e + e_c \rightarrow \frac{r_1}{r_2} = 1 + \varepsilon \approx 1$$

That is to say for the calculations, $r_1 \approx r_2$.

Comparison of the following terms

$$\tau_{10} = \frac{M_t}{2\pi r_1^2 e} \text{ and } \tau_{20} = \frac{M_t}{2\pi r_2^2 e}$$

Allows us to write approximately

$$\tau_{10} \approx \tau_{20} = \tau_0$$

From which

$$\tau_c = \frac{G_c}{\lambda e_c G} \tau_0 \left\{ \left(\frac{1}{\tanh \lambda \ell} + \frac{1}{\sinh \lambda \ell} \right) \cosh \lambda x - \sinh \lambda x \right\}$$

We can note the presence of identical peaks of stress at $x = 0$ and $x = \ell$ as

$$\tau_{c \max} = \frac{G_c}{\lambda e_c G} \tau_0 \frac{(\cosh \lambda \ell + 1)}{\sinh \lambda \ell} = \frac{G_c}{\lambda e_c G} \tau_0 \frac{1}{\tanh \frac{\lambda \ell}{2}}$$

Taking into account that $\lambda^2 = 2G_c/(e_c G e)$,

$$\tau_{c \max} = \tau_0 \frac{\lambda^2 e}{2\lambda} \frac{1}{\tanh \frac{\lambda \ell}{2}} = \tau_0 e \times \frac{\lambda}{2} \frac{1}{\tanh \frac{\lambda \ell}{2}}$$

Introducing an average stress in the adhesive (fictitious notion as mentioned above) gives

$$\tau_{\text{average}} = \frac{M_t}{2\pi r^2 \ell} = \frac{M_t}{2\pi r^2 e} \frac{e}{\ell} = \tau_o \frac{e}{\ell}$$

From which

$$\tau_{c \text{ max}} = \tau_{\text{average}} \times \frac{\lambda \ell / 2}{\tanh \lambda \ell / 2}$$

In setting $(\lambda \ell) / 2 = a$, we find again the relationship of Section 6.2.4:

$$\tau_{\text{max}} = \frac{a}{\tanh a} \times \tau_{\text{average}}; \quad \text{with } a = \sqrt{\frac{G_c \ell^2}{2G e e_c}}$$

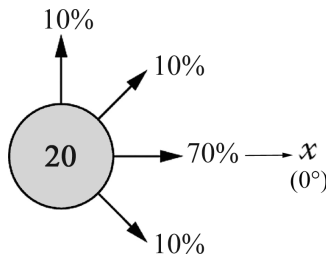
21.2 DOUBLE-LAP BONDED JOINT

Problem Statement

Shown in Figure 21.4 is an assembly consisting of two identical plates of material 1 bonded to a central plate of material 2. This double-lap joint is symmetrical to the midplane, marked by the x -axis in the figure. We propose a simplified study of the shear stress in the adhesive. To this end, it will be assumed that the stress components are just functions of x .

The configuration of a bonding element of length dx is shown in Figure 21.5. The moduli of materials are E_1 for material 1, E_2 for material 2, and G_c for the adhesive.

1. Determine the shear stress distribution in the adhesive $\tau_c(x)$.
2. *Numerical application:* The two external plates are in titanium alloy R56400 (TA6V), with thickness 1.5 mm. The intermediate plate is a Quadrangle symmetric carbon/epoxy laminate, with $V_f = 60\%$ fiber volume fraction and the following composition:



The ply thickness is 0.125 mm. The failure strength of the adhesive (araldite) is 15 MPa. Its thickness is 0.2 mm. What bond length ℓ will allow the bonding assembly to transmit a stress resultant of 20 daN per millimeter width?

3. Calculate the maximum shear stress in the particular case where materials 1 and 2 are identical and $e_1 = e_2 = e$.

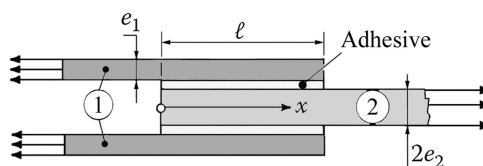


FIGURE 21.4 Symmetrical double-lap joint.

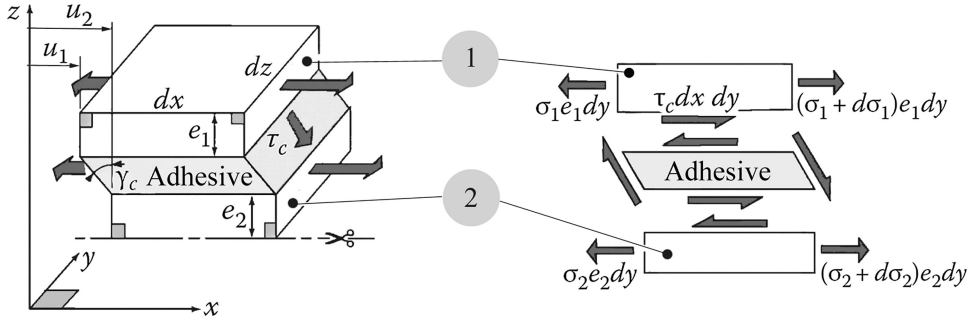


FIGURE 21.5 Deformed configuration.

Solution

1. Shear stress in the adhesive

In the previous figure showing an element of the bond, we can read the following equilibria:

- Element of material 1:

$$d\sigma_1 e_1 dy + \tau_c dx dy = 0 \rightarrow \frac{d\sigma_1}{dx} e_1 + \tau_c = 0 \quad (21.6)$$

- Element of material 2:

$$d\sigma_2 e_2 dy - \tau_c dx dy = 0 \rightarrow \frac{d\sigma_2}{dx} e_2 - \tau_c = 0 \quad (21.7)$$

In addition, we should note the following geometric relation in equating the tangent and angle:

$$\gamma_c \approx \frac{u_2 - u_1}{e_c}$$

Then with the constitutive equations,

$$\gamma_c = \frac{\tau_c}{G_c}; \quad \frac{du_1}{dx} = \frac{1}{E_1} \sigma_1; \quad \frac{du_2}{dx} = \frac{1}{E_2} \sigma_2$$

$$\frac{\tau_c}{G_c} \approx \frac{u_2 - u_1}{e_c}$$

$$\frac{e_c}{G_c} \frac{d\tau_c}{dx} = \frac{\sigma_2}{E_2} - \frac{\sigma_1}{E_1} \quad (21.8)$$

We obtain Equations 21.6 through 21.8 with the three unknowns σ_1 , σ_2 , and τ_c .

We can write

$$\frac{1}{E_1} \frac{d\sigma_1}{dx} = -\frac{\tau_c}{e_1 E_1}; \quad \frac{1}{E_2} \frac{d\sigma_2}{dx} = \frac{\tau_c}{e_2 E_2}$$

$$\frac{1}{E_1} \frac{d\sigma_1}{dx} - \frac{1}{E_2} \frac{d\sigma_2}{dx} = -\tau_c \left(\frac{1}{e_1 E_1} + \frac{1}{e_2 E_2} \right)$$

Taking into account Equation 21.8,

$$\frac{d^2}{dx^2} \left(\frac{\sigma_1}{E_1} - \frac{\sigma_2}{E_2} \right) = \frac{G_c}{e_c} \left(\frac{1}{e_1 E_1} + \frac{1}{e_2 E_2} \right) \left(\frac{\sigma_1}{E_1} - \frac{\sigma_2}{E_2} \right)$$

$$\frac{d^2}{dx^2} \left(\frac{\sigma_1}{E_1} - \frac{\sigma_2}{E_2} \right) - \lambda^2 \left(\frac{\sigma_1}{E_1} - \frac{\sigma_2}{E_2} \right) = 0 \quad \text{with } \lambda^2 = \frac{G_c}{e_c} \left(\frac{1}{e_1 E_1} + \frac{1}{e_2 E_2} \right)$$

The solution of this differential equation is

$$\frac{\sigma_1}{E_1} - \frac{\sigma_2}{E_2} = A \cosh \lambda x + B \sinh \lambda x$$

- *Boundary conditions:*

$$\text{For } x = 0 : \sigma_1 = \sigma_{10} \text{ and } \sigma_2 = 0, \text{ then } \left(\frac{\sigma_1}{E_1} - \frac{\sigma_2}{E_2} \right) \Big|_{x=0} = \frac{\sigma_{10}}{E_1}$$

$$\text{For } x = \ell : \sigma_1 = 0 \text{ and } \sigma_2 = \sigma_{20}, \text{ then } \left(\frac{\sigma_1}{E_1} - \frac{\sigma_2}{E_2} \right) \Big|_{x=\ell} = -\frac{\sigma_{20}}{E_2}$$

From which the constant values

$$A = \frac{\sigma_{10}}{E_1}; \quad B = - \left(\frac{\sigma_{20}}{E_2 \sinh \lambda \ell} + \frac{\sigma_{10}}{E_1 \tanh \lambda \ell} \right)$$

In addition (Equations 21.6 and 21.7),

$$\frac{d\sigma_1}{dx} e_1 + \frac{d\sigma_2}{dx} e_2 = 0$$

Then,

$$\frac{d\sigma_1}{dx} \left[\frac{1}{E_1} + \frac{e_1}{e_2 E_2} \right] = A \lambda \sinh \lambda x + B \lambda \cosh \lambda x$$

That is, according to Equation 21.6,

$$-\tau_c \left[\frac{1}{e_1 E_1} + \frac{1}{e_2 E_2} \right] = A \lambda \sinh \lambda x + B \lambda \cosh \lambda x$$

$$\tau_c = \frac{G_c}{e_c \lambda} \left\{ \left(\frac{\sigma_{10}}{E_1} \frac{1}{\tanh \lambda \ell} + \frac{\sigma_{20}}{E_2} \frac{1}{\sinh \lambda \ell} \right) \cosh \lambda x - \frac{\sigma_{10}}{E_1} \sinh \lambda x \right\} \quad (21.9)$$

- **Comments:**

- Only an approximation of the shear stress τ_c is obtained that way. We could have also deduced directly a differential equation in τ_c from relations (21.6) through (21.8). However, its integration would have revealed zero values of τ_c at the limits $x = 0$ and $x = \ell$ (free surface of the adhesive), making it impossible to obtain a

nonzero solution. In the reverse way, the expression found here for τ_c does not become zero for $x = 0$ and $x = \ell$. This contradicts with reality.

We should conclude from the above that the unidimensional approximation for stress components σ_1 , σ_2 , and τ_c is illegitimate in strict logic. However, the expression found here for τ_c gives an acceptable order of magnitude, except at the immediate vicinity of the free edge. Numerical modeling of the phenomenon by finite element method shows in effect that the shear stress τ_c increases very rapidly from the free edge, up to a peak value very close to the value found here. Apart from this particularity, there is a reasonably good correlation with the values given in relation (21.9).

- Normal peel stress also appears in the adhesive as a peak zone, confined near the free edge. This constitutes another design factor, which is not taken into account in this study.

2. Numerical application:

Longitudinal modulus of titanium (see Section 1.6): $E_1 = 105,000$ MPa.

Shear modulus of the adhesive (araldite): $G_c = 1,700$ MPa.

Longitudinal modulus of the laminate: With the previous ply proportions at 0° , 90° , and $\pm 45^\circ$, we find (Chart 5.4 in Section 5.4.2) $E_2 = 100,590$ MPa.

Thickness of the laminate:

$$2e_2 = 20 \text{ plies} \times 0.125 \text{ mm} = 2.5 \text{ mm} \Rightarrow e_2 = 1.25 \text{ mm}$$

A stress resultant of 20 daN/mm corresponds to the following stress values:

- In the titanium,

$$\sigma_{10} = \frac{200}{2 \times 1.5} = 66.66 \text{ MPa}$$

- In the laminate,

$$\sigma_{20} = \frac{200}{2.5} = 80 \text{ MPa}$$

Numerical calculation of Equation (21.9) allows verifying easily that the failure criterion in adhesive is reached for a length $\ell = 40$ mm, as shown in Figure 21.6.

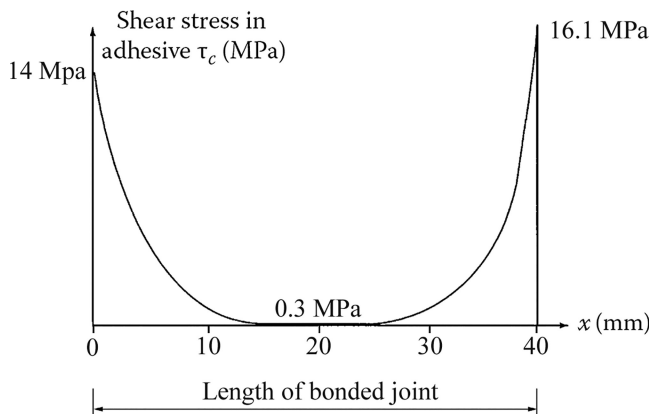


FIGURE 21.6 Shear stress distribution.

3. Particular case

The materials are identical: $e_1 = e_2 = e$. Then $\sigma_{10} = \sigma_{20} = \sigma_0$ and

$$\tau_c = \frac{G_c}{\lambda e_c E} \sigma_0 \left\{ \left(\frac{1}{\tanh \lambda \ell} + \frac{1}{\sinh \lambda \ell} \right) \cosh \lambda x - \sinh \lambda x \right\}$$

We can note identical peak values of stress for $x = 0$ or $x = \ell$:

$$\tau_{c \max} = \frac{G_c}{\lambda e_c E} \sigma_0 \frac{(\cosh \lambda \ell + 1)}{\sinh \lambda \ell} = \frac{G_c}{\lambda e_c E} \sigma_0 \frac{1}{\tanh \frac{\lambda \ell}{2}}$$

Taking into account that $\lambda^2 = 2G_c/(e_c e E)$,

$$\tau_{c \max} = \sigma_0 \frac{e \lambda^2}{2 \lambda} \frac{1}{\tanh \lambda \ell / 2}$$

Introducing an average shear stress value in the adhesive, which is a fictitious stress as can be seen in the previous figure,

$$\tau_{\text{average}} = \sigma_0 \frac{e}{\ell}$$

Then,

$$\tau_{c \max} = \frac{\lambda \ell / 2}{\tanh \lambda \ell / 2} \times \tau_{\text{average}}$$

In posing

$$\lambda \ell / 2 = a$$

$$\tau_{c \max} = \frac{a}{\tanh a} \times \tau_{\text{average}} \quad \text{with } a = \sqrt{\frac{G_c \ell^2}{2 E e e_c}}$$

21.3 COMPOSITE BEAM WITH TWO LAYERS

Problem Statement

A composite beam is made up of two layers of distinct materials, denoted as 1 and 2, bonded together. The beam cross section is shown in Figure 21.7. The thickness of the adhesive is neglected. The materials are elastic and isotropic. The longitudinal and shear moduli of the two materials are denoted E_1 , G_1 and E_2 , G_2 .

Elements that allow the bending behavior study of this beam in its symmetry plane (x , y) are summarized in Equation 16.16.

1. Determine the location of the elastic center denoted as O .
2. Write the equivalent stiffnesses: extensional stiffness, bending stiffness, and shear stiffness (do not provide details about the shear coefficient k).
3. The shear force along y -direction is denoted as T . Calculate the shear stress distribution τ_{xy} . Deduce the shear stress in the adhesive, at the interface between the two materials.

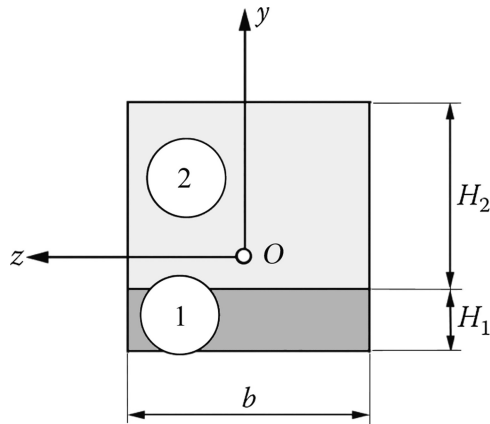


FIGURE 21.7 Beam cross section.

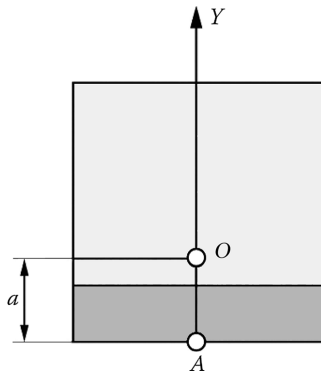
Solution

1. Elastic center

From Equation 16.16, O is the point taken as origin on the y -axis such that

$$\int_{\text{section}} E_i y \, dS = 0$$

Let A be an arbitrary origin that allows defining an ordinate denoted Y . The point O is such that



$$\int_{\text{section}} E_i (Y - a) \, dS = 0$$

Then,

$$a = \frac{\int_{\text{section}} E_i Y \, dS}{\int_{\text{section}} E_i \, dS}$$

$$\int_{\text{section}} E_i Y \, dS = \int_0^{H_1} E_1 Y b \times dY + \int_{H_1}^{(H_1+H_2)} E_2 Y b \times dY$$

We find after calculation

$$a = \frac{1}{2} \left\{ \frac{(E_1 - E_2) H_1^2 + E_2 (H_1 + H_2)^2}{E_1 H_1 + E_2 H_2} \right\}$$

2. Equivalent stiffnesses

- Extensional stiffness:

$$\langle ES \rangle = \sum_i E_i S_i = b(E_1 H_1 + E_2 H_2)$$

- Shear stiffness:

$$\frac{\langle GS \rangle}{k} = \sum_i \frac{G_i S_i}{k} = \frac{b}{k} (G_1 H_1 + G_2 H_2)$$

- Bending stiffness:

$$\langle EI \rangle = \sum_i E_i I_i$$

$$\langle EI \rangle = bE_1 \int_{-a}^{H_1-a} y^2 \, ds + bE_2 \int_{H_1-a}^{H_1+H_2-a} y^2 \, ds$$

$$\langle EI \rangle = \frac{b}{3} \left\{ E_1 \left[(H_1 - a)^3 + a^3 \right] + E_2 \left[(H_1 + H_2 - a)^3 - (H_1 - a)^3 \right] \right\}$$

3. Subject to a shear force T along the y -direction, the shear stress is assumed to be limited to the component τ_{xy} given in material i by the relationship (see Equation 16.16)

$$\tau_{xy} = G_i \frac{T}{\langle GS \rangle} \frac{dg_{oi}}{dy}$$

In which the warping function $g_o(y)$ is the solution of the problem

$$\begin{cases} \frac{d^2 g_o}{dy^2} = -\frac{E_i}{G_i} \frac{\langle GS \rangle}{\langle EI \rangle} \times y & \text{all over in the cross section} \\ \frac{dg_o}{dy} = 0 & \text{for } y = -a \text{ and } y = H_1 + H_2 - a \text{ (free edges)} \end{cases}$$

The uniqueness of function $g_o(y)$ is assured by the condition

$$\int_{\text{section}} E_i g_o \, dS = 0$$

We find in material 1

$$\frac{dg_{o1}}{dy} = \frac{1}{2} \frac{E_1}{G_1} \frac{\langle GS \rangle}{\langle EI \rangle} (a^2 - y^2)$$

and in material 2

$$\frac{dg_{o2}}{dy} = \frac{1}{2} \frac{E_2}{G_2} \frac{\langle GS \rangle}{\langle EI \rangle} [(H_1 + H_2 - a)^2 - y^2]$$

Therefore, the shear follows a parabolic distribution along the beam height

$$-a \leq y \leq (H_1 - a) \rightarrow \tau_{xy} = \frac{T}{2} \frac{E_1}{\langle EI \rangle} (a^2 - y^2)$$

$$(H_1 - a) \leq y \leq (H_1 + H_2 - a) \rightarrow \tau_{xy} = \frac{T}{2} \frac{E_2}{\langle EI \rangle} [(H_1 + H_2 - a)^2 - y^2]$$

The shear variations are shown in Figure 21.8. At junction between the two materials ($y = H_1 - a$), we find the shear in the adhesive:

$$\tau_{xy\text{adhesive}} = \frac{T}{2} \frac{E_1}{\langle EI \rangle} H_1 (2a - H_1)$$

Note: The shear coefficient k is obtained by integration of function $g_0(y)$ by using the following expression (see Equation 16.16):

$$k = \frac{1}{\langle EI \rangle} \int_{\text{section}} E_i g_0 y \, dS$$

This calculation is long but without any particular difficulty. The numerical values of k are shown in Figure 21.9 for different ratios E_1/E_2 and H_2/H_1 , in the particular case where Poisson coefficients are identical for the two materials.

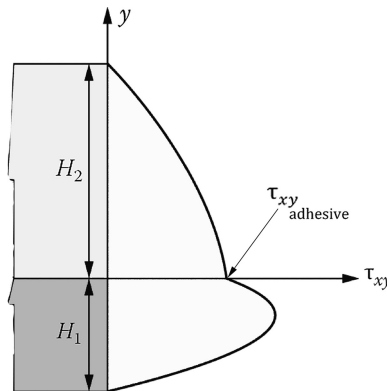


FIGURE 21.8 Shear stress distribution.

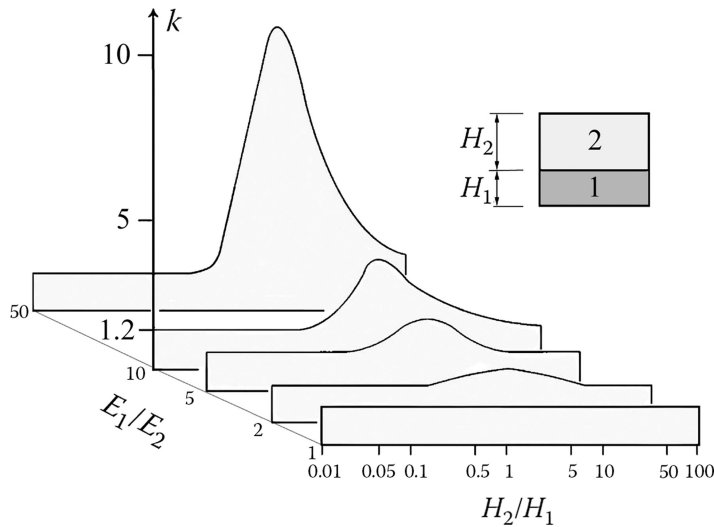


FIGURE 21.9 Variations of “ k ” coefficient.

21.4 BUCKLING OF A SANDWICH BEAM

Problem Statement

A sandwich beam is compressed at its two ends by two opposite forces F . Each end is clamped so that rotation is prevented.

1. For what value of F , denoted as F_{critical} , can we obtain a deformed configuration of the beam other than the rectilinear configuration in compression? For example, a configuration as shown in Figure 21.10 (adjacent equilibrium).
2. What is the error on this value if shear deformation of the beam is neglected? Give a numerical application by using for the beam the characteristics of Application 19.1.

Solution

1. Recall the behavior equations for the beam in Equation 16.16:

$$T_y = \frac{\langle GS \rangle}{k} \left(\frac{dv}{dx} - \theta_z \right); \quad M_z = \langle EI_z \rangle \frac{d\theta_z}{dx}$$

Referring to the following figure, we can write the corresponding relationships, in which C represents the clamping moment on the right-hand side:

$$T_y \approx F \frac{dv}{dx}; \quad M_z = C - Fv$$

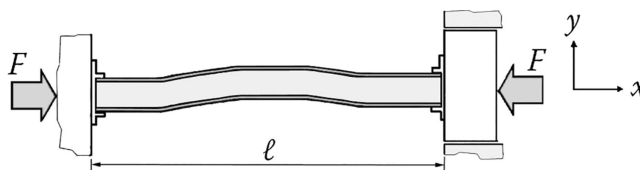
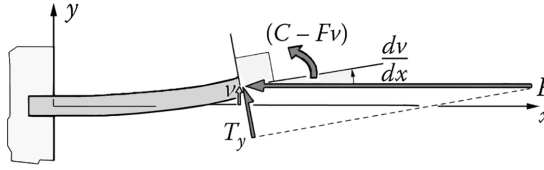


FIGURE 21.10 Sandwich beam under compression.



From which, by substituting in behavior equations,

$$F \frac{dv}{dx} = \frac{\langle GS \rangle}{k} \left(\frac{dv}{dx} - \theta_z \right); \quad C - Fv = \langle EI_z \rangle \frac{d\theta_z}{dx}$$

Elimination of θ_z between these two relationships leads to the following equation:

$$\frac{d^2 v}{dx^2} + \lambda^2 v = \lambda^2 \frac{C}{F} \quad \text{with} \quad \lambda^2 = \frac{F}{\langle EI_z \rangle} \times \frac{1}{\left(1 - \frac{kF}{\langle GS \rangle} \right)} \quad (21.10)$$

Provided that $F < \langle GS \rangle / k$, the general solution is

$$v(x) = A \cos \lambda x + B \sin \lambda x + \frac{C}{F}$$

• *Boundary conditions:*

- For $x = 0$, $v(0) = 0$ and $\theta_z(0) = 0$.

Due to

$$\theta_z = \left(1 - F \times \frac{k}{\langle GS \rangle} \right) \frac{dv}{dx}$$

This last condition leads to

$$\left. \frac{dv}{dx} \right|_{x=0} = 0$$

We then find that

$$B = 0; \quad A = -\frac{C}{F}$$

From which

$$v(x) = \frac{C}{F} (1 - \cos \lambda x)$$

- For $x = \ell$, $v(\ell) = 0$ and $\theta_z(\ell) = 0$

$$\cos \lambda \ell = 1$$

From which

$$\lambda \ell = 2n\pi$$

We obtain

$$v(x) = \frac{C}{F} \left(1 - \cos 2n\pi \frac{x}{\ell} \right) \quad (21.11)$$

With Equation (21.10) and $\lambda^2 = 4n^2\pi^2/\ell^2$, the critical value F_{critical} is as follows:

$$F_{\text{critical}} = \frac{4n^2\pi^2 \langle EI_z \rangle}{\ell^2 \left(1 + \frac{4n^2\pi^2 \langle EI_z \rangle k}{\ell^2 \langle GS \rangle} \right)}$$

The smallest value of F is obtained for $n=1$ as

$$F_{\text{critical}} = \frac{4\pi^2 \langle EI_z \rangle}{\ell^2 \left(1 + \frac{4\pi^2 \langle EI_z \rangle k}{\ell^2 \langle GS \rangle} \right)}$$

• **Comments:**

- We can verify that this value of F_{critical} is less than $\langle GS \rangle/k$. The general solution $v(x)$ in Equation 21.11 is, therefore, appropriate.
- It is worthy to note that $v(x)$ as written in Equation 21.11 is defined only by a multiplication factor, because the clamping moment C is *indeterminate*. We can find this property by writing explicitly as a function of $v(x)$ the relation

$$C = M_x(\ell) = \langle EI_z \rangle \frac{d\theta_z}{dx} \Big|_{x=\ell}$$

2. If shear effect is neglected, it means undeformability under shear and leads to zero value for the corresponding strain energy in Equation 16.16. In other words, $k = 0$.

The critical force then becomes

$$F'_{\text{critical}} = \frac{4\pi^2 \langle EI_z \rangle}{\ell^2}$$

And the relative error to its previous value is

$$\text{Error} = \frac{F'_{\text{critical}}}{F_{\text{critical}}} - 1$$

$$\text{Error} = \frac{4\pi^2 \langle EI_z \rangle k}{\ell^2 \langle GS \rangle}$$

As a numerical example, let us calculate this error for the beam characteristics in Application 19.1 or also in Section 4.2.2. Recall that the beam was made of polyurethane foam with aluminum skins, 1 m long. The following had then been found:

$$\langle EI_z \rangle = 475 \times 10^2; \quad \frac{\langle GS \rangle}{k} = 650 \times 10^2$$

With such values, we note a spectacular error on the critical buckling force evaluation:

$$\text{Error} = 28.84 = (2.884 \times 10^3) \%$$

21.5 SHEAR DUE TO BENDING IN A SANDWICH BEAM

Problem Statement

We consider a sandwich beam cross section as shown in Figure 21.11. The components, assumed

other with an adhesive with negligible thickness. The beam has a unit width. The moduli of elasticity are denoted as shown.

Using the formulation in Equation 16.16 for bending of composite beams,

1. Give a study of the warping function g_0 for bending in the middle plane (x, y) of this beam with such a cross section
2. Deduce from there the shear stress distribution
3. Calculate the shear coefficient for bending in plane (x, y) , as well as the deformed configuration of a cross section under shear
 - *Numerical application:* Calculate k for a beam with the following:
 Core of polystyrene foam with thickness 80.2 mm; $E_2 = 21.5$ MPa; $G_2 = 7.7$ MPa.
 Aluminum skins with thickness 2.15 mm; $E_1 = 65,200$ MPa; $G_1 = 24,890$ MPa.

Solution

1. Longitudinal warping function $g_0(y, z)$

This is the solution of the problem described in Equation 16.16. Assuming here that g_0 does not vary with z leads to

$$\begin{cases} \frac{d^2 g_0}{dy^2} = -\frac{E_i}{G_i} \frac{\langle GS \rangle}{\langle EI_z \rangle} \times y \text{ in the domain of the section} \\ \frac{dg_0}{dy} = 0 \text{ for } y = \pm H_1/2 \end{cases}$$

With g_0 and $G_i (dg_0/dy)$ remaining continuous when crossing from material 1 to material 2.

Taking into account the antisymmetry of function g_0 with respect to y , we find

$$\begin{aligned} \frac{H_2}{2} \leq y \leq \frac{H_1}{2} &\rightarrow g_{o1} = -\frac{E_1}{G_1} \frac{a}{6} y^3 + A_1 y + B_1 \\ -\frac{H_2}{2} \leq y \leq \frac{H_2}{2} &\rightarrow g_{o2} = -\frac{E_2}{G_2} \frac{a}{6} y^3 + A_2 y \\ -\frac{H_1}{2} \leq y \leq -\frac{H_2}{2} &\rightarrow g_{o3} = -\frac{E_1}{G_1} \frac{a}{6} y^3 + A_1 y - B_1 \end{aligned}$$

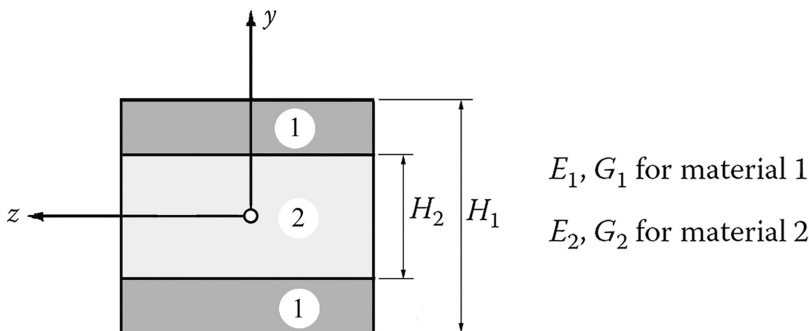


FIGURE 21.11 Sandwich beam cross section.

with

$$a = \frac{\langle GS \rangle}{\langle EI_z \rangle} = 12 \frac{G_2 H_2 + G_1 (H_1 - H_2)}{E_2 H_2^3 + E_1 (H_1^3 - H_2^3)}$$

$$A_1 = \frac{E_1}{G_1} \frac{a}{2} \frac{H_1^2}{4}$$

$$B_1 = a \frac{H_2}{16} \left\{ \left(\frac{1}{G_2} - \frac{1}{G_1} \right) E_1 H_1^2 - \left(\frac{E_1 - E_2}{G_2} \right) H_2^2 - \left(\frac{E_2}{G_2} - \frac{E_1}{G_1} \right) \frac{H_2^2}{3} \right\}$$

$$A_2 = A_1 + \frac{2B_1}{H_2} + \frac{a}{3} \times \frac{H_2^2}{8} \left(\frac{E_2}{G_2} - \frac{E_1}{G_1} \right)$$

2. Shear stress due to bending

It is given by the relationship in Equation 16.16:

$$\bar{\tau} = G_i \frac{T_y}{\langle GS \rangle} \overline{\text{grad } g_o}$$

In the present case,

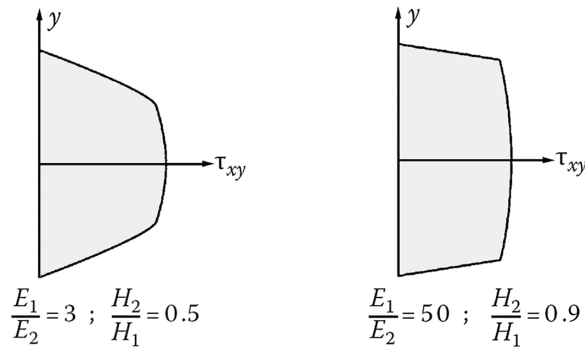
$$\tau_{xy} = G_i \frac{T_y}{\langle GS \rangle} \frac{\partial g_o}{\partial y}; \quad \tau_{xz} = G_i \frac{T_y}{\langle GS \rangle} \frac{\partial g_o}{\partial z} = 0$$

we obtain

$$0 \leq y \leq \frac{H_2}{2} \rightarrow \tau_{xy} = \frac{1}{2} \frac{T_y}{\langle EI_z \rangle} \left\{ E_2 \left(\frac{H_2^2}{4} - y^2 \right) + E_1 \left(\frac{H_1^2}{4} - \frac{H_2^2}{4} \right) \right\}$$

$$\frac{H_2}{2} \leq y \leq \frac{H_1}{2} \rightarrow \tau_{xy} = \frac{1}{2} \frac{T_y}{\langle EI_z \rangle} E_1 \left(\frac{H_1^2}{4} - y^2 \right)$$

The corresponding distribution is illustrated below for two distinct designs of components 1 and 2¹.



3. Shear coefficient

The calculation of k is carried out without difficulty starting from expression in Equation 16.16:

$$k = \frac{1}{\langle EI_z \rangle} \int_D E_i g_{oy} ds$$

We obtain

$$k = \frac{a}{8[E_2 H_2^3 + E_1 (H_1^3 - H_2^3)]} \left\{ \frac{E_2}{G_2} H_2^3 \left[E_1 H_1^2 + \left(\frac{4}{5} E_2 - E_1 \right) H_2^2 \right] \dots \right. \\ \left. \dots + \frac{E_1^2}{G_1} \left(\frac{4}{5} H_1^5 + \frac{H_2^5}{5} - H_1^2 H_2^3 \right) \right\} + \frac{3bE_1 (H_1^2 - H_2^2)}{E_2 H_2^3 + E_1 (H_1^3 - H_2^3)}$$

with

$$a = 12 \frac{G_2 H_2 + G_1 (H_1 - H_2)}{E_2 H_2^3 + E_1 (H_1^3 - H_2^3)} \\ b = \frac{a}{16} H_2 \frac{E_1}{G_1} \left\{ \frac{H_2^2}{3} + H_1^2 \left(\frac{G_1}{G_2} - 1 \right) - H_2^2 \frac{G_1}{G_2} \left(1 - \frac{2}{3} \frac{E_2}{E_1} \right) \right\}$$

Evolution of the shear coefficient k is represented in Figure 21.12 for different ratios (E_1/E_2) and with the same Poisson coefficient (0.3), when varying relative thicknesses of the skins.

• **Comments:**

- In Figure 21.12, the limiting cases $E_2 = E_1$; $H_2 = H_1$; $H_2 = 0$ correspond to a homogeneous beam with rectangular cross section for which we find again the classical value $k = 6/5$ (or 1.2).
- The expression written above for the k coefficient is long. If the skins are thin relative to the total thickness of the beam, we can content ourselves with a simplified expression for easier manipulation, as done in Application 20.1.

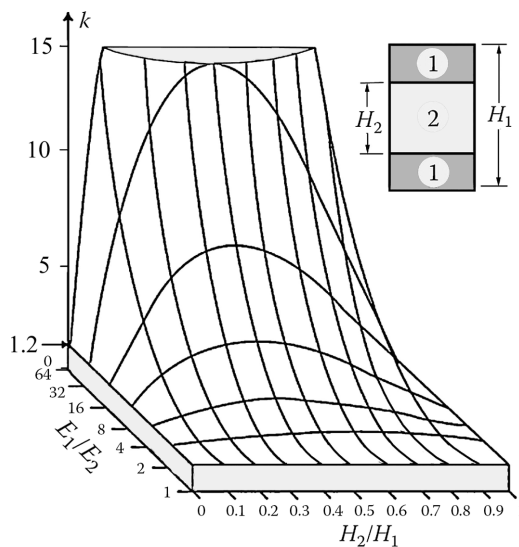
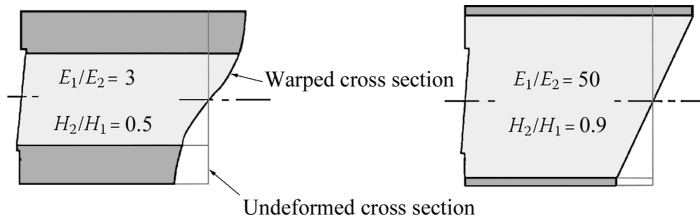


FIGURE 21.12 Variations of “k” coefficient.

- Deformed configuration of a cross section: The displacement of each point of the cross section out of its initial plane is obtained starting from the function g_o through the relationship (see Equations 16.12 and 16.15)

$$\eta_x = \frac{T_y}{\langle GS \rangle} (g_o - k \times y)$$

This displacement is described graphically in the following figure for two distinct sets of properties of components 1 and 2.



- *Numerical application:* We find $k = 165.7$. Note that for this type of beam, the shear coefficient can have very high values, far greater than those of homogeneous beams, which are at most about a few units.

21.6 SHEAR DUE TO BENDING IN A COMPOSITE BOX BEAM

Problem Statement

In Figure 21.13 is shown the cross section of a box beam made of two distinct materials denoted as 1 for vertical parts and 2 for horizontal parts. Each of them is transversely isotropic in plane (y, z) of the cross section. This beam is bending in its midplane (x, z) .

Assuming that e_1 and e_2 have little values compared to h and b ,

1. Calculate the shear stress distribution due to a shear force T_z
2. Calculate the shear coefficient k_z for bending in the plane (x, z)

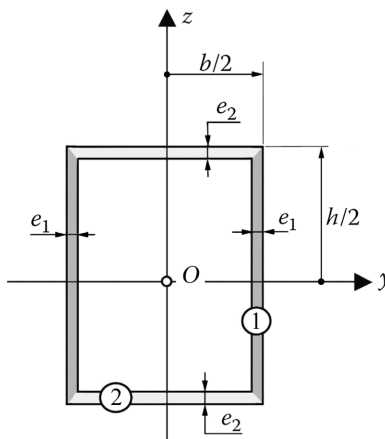


FIGURE 21.13 Composite box beam.

Solution

Note first that the cross section admits y -axis and z -axis as symmetry axes. Accordingly, O is the elastic center in accordance with Equation 16.19.

1. Shear stress due to bending

- **In area 1**, the assumption $e_1 \ll h$ leads to a shear stress denoted as τ_1 directed along z (no component normal to the wall because the latter is free of shear force) and constant across the thickness e_1 . Then with Equation 16.19 and denoting by $h_{01}(z)$ the longitudinal warping function

$$\tau_{xz} = \tau_1 = G_1 \frac{T_y}{\langle GS \rangle} \frac{dh_{01}}{dz}$$

- **In area 2**, the assumption $e_2 \ll b$ leads to a shear stress denoted as τ_2 directed along y (no component normal to the wall because the latter is free) and constant across the thickness e_2 . Then with Equation 16.19 and denoting by $h_{02}(y)$ the longitudinal warping function

$$\tau_{xy} = \tau_2 = G_2 \frac{T_z}{\langle GS \rangle} \frac{dh_{02}}{dy}$$

We have to evaluate (dh_{01}/dz) and (dh_{02}/dy) . From Equation 16.19, the following applies:

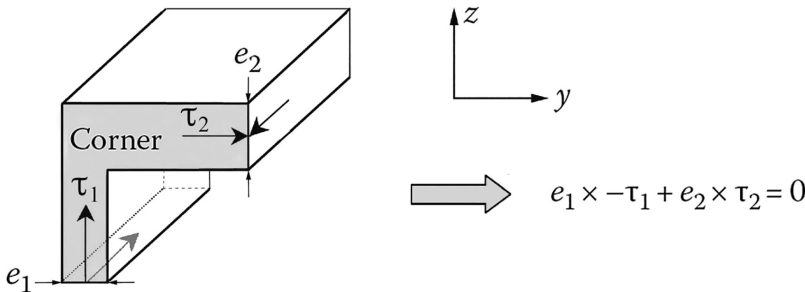
- In area 1, $\frac{d^2 h_{01}}{dz^2} = -\frac{E_1}{G_1} \frac{\langle GS \rangle}{\langle EI_y \rangle} z$ giving $\frac{dh_{01}}{dz} = -\frac{E_1}{G_1} \frac{\langle GS \rangle}{\langle EI_y \rangle} \frac{z^2}{2} + a'_1$
- In area 2, $\frac{d^2 h_{02}}{dy^2} = -\frac{E_2}{G_2} \frac{\langle GS \rangle}{\langle EI_y \rangle} z$ with $z = h/2$ giving $\left. \frac{dh_{02}}{dy} \right|_{z=\frac{h}{2}} = -\frac{E_2}{G_2} \frac{\langle GS \rangle}{\langle EI_y \rangle} \frac{h}{2} y$

(Since z is the axis of symmetry, the integration constant is zero for $y = 0$).

- **Local equilibrium of a corner of the box beam:** for example, in the following figure is shown the corner

$$y = -\frac{b}{2}; \quad z = \frac{h}{2}$$

Consideration of longitudinal equilibrium (along x -direction) in figure below allows writing²



By using expressions of τ_1 and τ_2 above

$$e_1 G_1 \frac{T_z}{\langle GS \rangle} \frac{dh_{01}}{dz} = e_2 G_2 \frac{T_z}{\langle GS \rangle} \frac{dh_{02}}{dy}$$

$$e_1 G_1 \frac{dh_{01}}{dz} = e_2 G_2 \frac{dh_{02}}{dy}$$

$$e_1 G_1 \left(-\frac{E_1}{G_1} \frac{\langle GS \rangle}{\langle EI_y \rangle} \frac{h^2}{8} + a'_1 \right) = e_2 G_2 \left(\frac{E_2}{G_2} \frac{\langle GS \rangle}{\langle EI_y \rangle} \frac{hb}{4} \right)$$

Then,

$$a'_1 = \frac{E_1}{G_1} \frac{\langle GS \rangle}{\langle EI_y \rangle} \frac{h^2}{8} + \frac{e_2 E_2}{e_1 G_1} \frac{\langle GS \rangle}{\langle EI_y \rangle} \frac{hb}{4}$$

From which the shear stress distribution:

- **In vertical walls** (material 1)

$$\tau_1 = G_1 \frac{T_z}{\langle GS \rangle} \frac{dh_{01}}{dz} = \frac{E_1}{\langle EI_y \rangle} T_z \left[-\frac{z^2}{2} + \frac{h^2}{8} + \frac{e_2 E_2}{e_1 E_1} \frac{hb}{4} \right]$$

- **In upper horizontal wall** (material 2; $z = h/2$)

$$\tau_2 = G_2 \frac{T_z}{\langle GS \rangle} \frac{dh_{02}}{dy} \Big|_{z=\frac{h}{2}} = \frac{E_2}{\langle EI_y \rangle} T_z \times -\frac{h}{2} y$$

- **In lower horizontal wall** (material 2; $z = -h/2$)

$$\tau_2 = G_2 \frac{T_z}{\langle GS \rangle} \frac{dh_{02}}{dy} \Big|_{z=-\frac{h}{2}} = \frac{E_2}{\langle EI_y \rangle} T_z \times \frac{h}{2} y$$

2. Shear coefficient k_z

From Section 16.1.6.2, the shear strain energy is

$$\frac{dW_\tau}{dx} = \frac{1}{2} k_z \frac{T_z^2}{\langle GS \rangle} = \frac{1}{2} \left\{ \int_{\text{material 1}} \frac{\tau_1^2}{G_1} e_1 dz + \int_{\text{material 2}} \frac{\tau_2^2}{G_2} e_2 dy \right\}$$

$$\frac{dW_\tau}{dx} = \frac{1}{2} \left\{ 2 \int_{-\frac{h}{2}}^{\frac{h}{2}} \frac{\tau_1^2}{G_1} e_1 dz + 2 \int_{-\frac{b}{2}}^{\frac{b}{2}} \frac{\tau_2^2}{G_2} e_2 dy \right\} = \frac{e_1}{G_1} \int_{-\frac{h}{2}}^{\frac{h}{2}} \tau_1^2 dz + \frac{e_2}{G_2} \int_{-\frac{b}{2}}^{\frac{b}{2}} \tau_2^2 dy$$

With expressions above for τ_1 and τ_2 , we find after calculus

$$\begin{aligned} \frac{dW_\tau}{dx} &= \frac{1}{2} k_z \frac{T_z^2}{\langle GS \rangle} = \frac{e_1}{G_1} \frac{E_1^2}{\langle EI_y \rangle^2} T_z^2 \left[\frac{h^5}{120} + \left(\frac{e_2 E_2}{e_1 E_1} \right)^2 \frac{h^3 b^2}{16} + \frac{e_2 E_2}{e_1 E_1} \frac{h^4 b}{24} \right] \dots \\ &\dots + \frac{e_2}{G_2} \frac{E_2^2}{\langle EI_y \rangle^2} T_z^2 \frac{h^2 b^3}{48} \end{aligned}$$

Then,

$$\frac{k_z}{\langle GS \rangle} = 2 \frac{e_1}{G_1} \frac{E_1^2}{\langle EI_y \rangle^2} \left[\frac{h^5}{120} + \left(\frac{e_2 E_2}{e_1 E_1} \right)^2 \frac{h^3 b^2}{16} + \left(\frac{e_2 E_2}{e_1 E_1} \right) \frac{h^4 b}{24} \right] + \frac{e_2}{G_2} \frac{E_2^2}{\langle EI_y \rangle^2} \frac{h^2 b^3}{24}$$

21.7 TORSION CENTER OF A COMPOSITE U-BEAM

Problem Statement

We consider the cross section of a U-beam as shown in Figure 21.14, made of two distinct materials denoted as 1 (vertical part) and 2 (horizontal parts), each of them being transversely isotropic in plane (Y, Z) of the section. This beam is bending in plane (x, Z) under a shear force T_Z passing through the torsion center C . The latter is located on the Y -axis due to the plane of symmetry (x, Y).

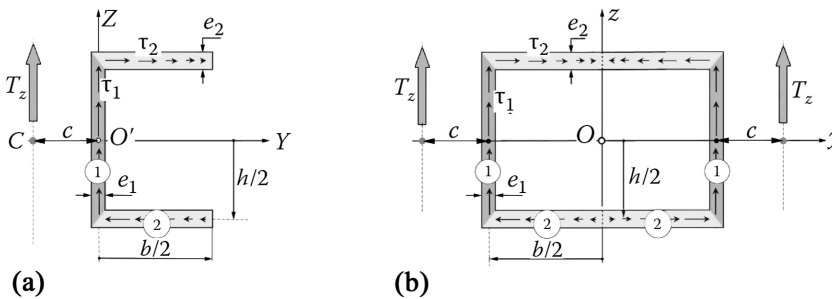
Assuming that e_1 and e_2 have little values compared to $h/2$ and $b/2$,

1. Calculate the shear stress distribution due to the shear force T_Z
2. Calculate the Y -coordinate of the torsion center C , denoted as c

Solution

1. Shear stress due to bending

In Figure 21.14, the Z -axis is not anymore a symmetry axis, and O' is not the elastic center of the section. We could follow the calculation steps described in Equation 16.19 in order to first determine the elastic center O and then calculate shear stress in principal axes y and z . To avoid such calculations, we will note that the U-section shape of the figure above is just the half of the box-beam section examined in the previous Application 21.6. From then, we can observe the equivalence between the loadings of the two cases (a) and (b) summarized in the figure below, when the box beam is subject to a shearing force ($2 \times T_Z$).



Therefore, when the section of the half box beam is considered alone, the shear stress distribution due to T_Z can be deduced from the shear stress distribution in the complete box-beam section written in Application 21.6. We obtain in axes (Y, Z) with $z = Z$ and $y = Y - (b/2)$, the following:

- In vertical wall (material 1),

$$\tau_1 = \frac{E_1}{\langle EI_y \rangle} T_z \left[-\frac{Z^2}{2} + \frac{h^2}{8} + \frac{e_2 E_2}{e_1 E_1} \frac{hb}{4} \right]$$

- In upper horizontal wall (material 2, $Z = h/2$),

$$\tau_2 = \frac{E_2}{\langle EI_y \rangle} T_z \left[\frac{hb}{4} - \frac{h}{2} Y \right]$$

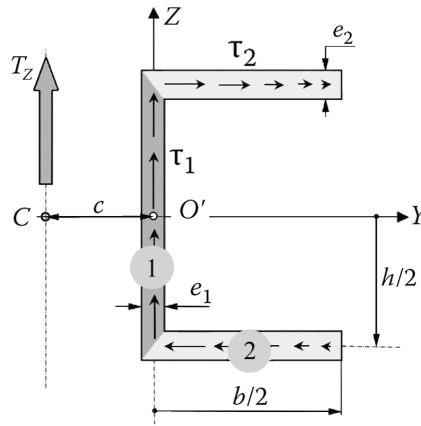


FIGURE 21.14 Composite U-beam.

- **In lower horizontal wall** (material 2, $Z = -h/2$),

$$\tau_2 = \frac{E_2}{\langle EI_y \rangle} T_z \left[\frac{h}{2} Y - \frac{hb}{4} \right]$$

2. Torsion center C

Then the location of the torsion center C can be readily obtained. At this point, we must write that the shear stress distribution (τ_1, τ_2) does not cause any torsional moment. This condition can be written as

$$c \times \int_{-\frac{h}{2}}^{\frac{h}{2}} \tau_1 \times (e_1 dZ) - h \times \int_0^{\frac{b}{2}} \tau_2 \times (e_2 dY) = 0$$

with the forms above for τ_1 and τ_2 , this leads after calculus to

$$c = \frac{b}{4} \frac{1}{\left[1 + \frac{e_1 E_1}{e_2 E_2} \frac{h}{3b} \right]}$$

21.8 SHEAR DUE TO BENDING IN A COMPOSITE I-BEAM

Problem Statement

We consider the cross section of a I-beam as shown in Figure 21.15, made of two distinct materials denoted as 1 (web) and 2 (flanges), each of them being transversely isotropic in the plane (y, z) of the cross section.

This beam is bending in its midplane (x, z) .

Assuming that e_1 and e_2 have little values compared to h and b ,

1. Calculate the shear stress distribution due to a shear force T_z
2. Calculate the shear coefficient k_z for bending in the plane (x, z)

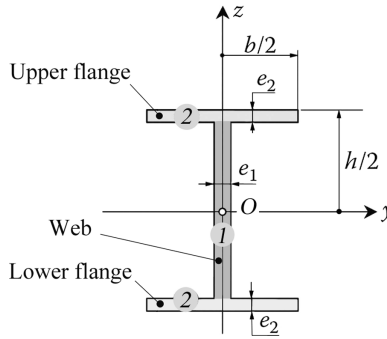


FIGURE 21.15 Composite I-beam.

Solution

Note first that the cross section admits y -axis and z -axis as symmetry axes. Thus, O is the elastic center in accordance with properties in Equation 16.19.

1. Shear stress distribution

- **In area 1**, the assumption $e_1 \ll h$ leads to admit a shear stress τ_1 directed along z (no component normal to the wall because the latter is free) and constant across the thickness e_1 . Then with Equation 16.19 and denoting by $h_{01}(z)$ the longitudinal warping function

$$\tau_{xz} = \tau_1 = G_1 \frac{T_z}{\langle GS \rangle} \frac{dh_{01}}{dz}$$

- **In area 2**, the assumption $e_2 \ll b$ leads to admit a shear stress τ_2 directed along y (no component normal to the wall because the latter is free) and constant across the thickness e_2 . Then with Equation 16.19 and denoting by $h_{02}(y)$ the longitudinal warping function

$$\tau_{xy} = \tau_2 = G_2 \frac{T_z}{\langle GS \rangle} \frac{dh_{02}}{dy}$$

We have to calculate (dh_{01}/dz) and (dh_{02}/dy) . For this, we have from Equation 16.19 the following:

- **In the web** (material 1),

$$\frac{d^2 h_{01}}{dz^2} = -\frac{E_1}{G_1} \frac{\langle GS \rangle}{\langle EI_y \rangle} z$$

From which

$$\frac{dh_{01}}{dz} = -\frac{E_1}{G_1} \frac{\langle GS \rangle}{\langle EI_y \rangle} \frac{z^2}{2} + a'_1$$

- **In the upper flange** (material 2)³

$$0 < y \leq \frac{b}{2} \Rightarrow \frac{d^2 h_{02}}{dy^2} = -\frac{E_2}{G_2} \frac{\langle GS \rangle}{\langle EI_y \rangle} z, \quad \text{and with } z = \frac{h}{2}$$

Then,

$$\left. \frac{dh_{02}}{dy} \right|_{0 < y \leq \frac{b}{2}} = -\frac{E_2}{G_2} \frac{\langle GS \rangle}{\langle EI_y \rangle} \frac{h}{2} y + a'_2.$$

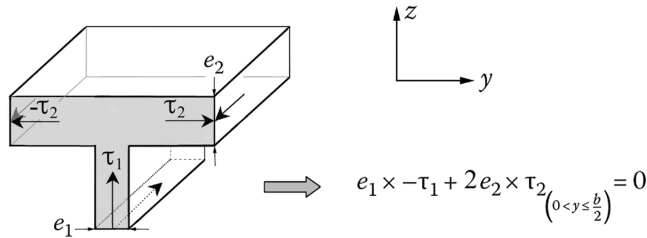
We remark that τ_2 is zero for $y = b/2$ (condition of shear stress reciprocity). Then,

$$\left. \frac{dh_{02}}{dy} \right|_{0 < y \leq \frac{b}{2}} = -\frac{E_2}{G_2} \frac{\langle GS \rangle}{\langle EI_y \rangle} \left[\frac{h}{2} y - \frac{hb}{4} \right]$$

For $-(b/2) \leq y < 0$, an analogous calculus gives

$$\left. \frac{dh_{02}}{dy} \right|_{-\frac{b}{2} \leq y < 0} = -\frac{E_2}{G_2} \frac{\langle GS \rangle}{\langle EI_y \rangle} \left[\frac{h}{2} y + \frac{hb}{4} \right]$$

- **Equilibrium condition at the junction between the web and upper flange:**
Consideration of longitudinal equilibrium along x -direction in figure below for the junction ($y = 0$ and $z = h/2$) allows writing⁴



$$e_1 G_1 \frac{T_z}{\langle GS \rangle} \frac{dh_{01}}{dz} = 2e_2 G_2 \frac{T_z}{\langle GS \rangle} \frac{dh_{02}}{dy} \Big|_{0 < y \leq \frac{b}{2}}$$

$$e_1 G_1 \frac{dh_{01}}{dz} = 2e_2 G_2 \frac{dh_{02}}{dy} \Big|_{0 < y \leq \frac{b}{2}}$$

This continuity condition can be rewritten as

$$e_1 G_1 \left(-\frac{E_1}{G_1} \frac{\langle GS \rangle}{\langle EI_y \rangle} \frac{h^2}{8} + a'_1 \right) = 2e_2 G_2 \left(-\frac{E_2}{G_2} \frac{\langle GS \rangle}{\langle EI_y \rangle} \times -\frac{hb}{4} \right)$$

From which

$$a'_1 = \frac{E_1}{G_1} \frac{\langle GS \rangle}{\langle EI_y \rangle} \frac{h^2}{8} + 2 \frac{e_2 E_2}{e_1 G_1} \frac{\langle GS \rangle}{\langle EI_y \rangle} \frac{hb}{4}$$

Then, the shear stress distribution is obtained as follows:

- **In the web** (material 1),

$$\tau_1 = G_1 \frac{T_z}{\langle GS \rangle} \frac{dh_{01}}{dz} = \frac{E_1}{\langle EI_y \rangle} T_z \left[-\frac{z^2}{2} + \frac{h^2}{8} + \frac{2e_2 E_2}{e_1 E_1} \frac{hb}{4} \right]$$

- **In the upper flange** (material 2),

$$0 < y \leq \frac{b}{2} \Rightarrow \tau_2 = G_2 \frac{T_z}{\langle GS \rangle} \frac{dh_{02}}{dy} \Big|_{0 < y \leq \frac{b}{2}} = \frac{E_2}{\langle EI_y \rangle} T_z \times \left[\frac{hb}{4} - \frac{h}{2} y \right]$$

$$-\frac{b}{2} \leq y < 0 \Rightarrow \tau_2 = G_2 \frac{T_z}{\langle GS \rangle} \frac{dh_{02}}{dy} \Big|_{-\frac{b}{2} \leq y < 0} = -\frac{E_2}{\langle EI_y \rangle} T_z \times \left[\frac{hb}{4} + \frac{h}{2} y \right]$$

Note that the shear stress in the lower flange is readily obtained from an analogous calculation.

2. Shear coefficient k_z

From Section 16.1.6.2,

$$\begin{aligned} \frac{dW_\tau}{dx} &= \frac{1}{2} k_z \frac{T_z^2}{\langle GS \rangle} = \frac{1}{2} \left\{ \int_{\text{material 1}} \frac{\tau_1^2}{G_1} e_1 dz + \int_{\text{material 2}} \frac{\tau_2^2}{G_2} e_2 dy \right\} \\ \frac{dW_\tau}{dx} &= \frac{1}{2} \left\{ \int_{-\frac{h}{2}}^{\frac{h}{2}} \frac{\tau_1^2}{G_1} e_1 dz + 2 \int_{-\frac{b}{2}}^{\frac{b}{2}} \frac{\tau_2^2}{G_2} e_2 dy \right\} = \frac{1}{2} \frac{e_1}{G_1} \int_{-\frac{h}{2}}^{\frac{h}{2}} \tau_1^2 dz + \frac{e_2}{G_2} \int_{-\frac{b}{2}}^{\frac{b}{2}} \tau_2^2 dy \end{aligned}$$

With τ_1 and τ_2 above, we obtain after calculus the following shear energy density:

$$\begin{aligned} \frac{dW_\tau}{dx} &= \frac{1}{2} k_z \frac{T_z^2}{GS} = \dots \\ \dots \frac{1}{2} \left\{ \frac{e_1}{G_1} \frac{E_1^2}{\langle EI_y \rangle^2} T_z^2 \left[\frac{h^5}{120} + \left(\frac{2e_2 E_2}{e_1 E_1} \right)^2 \frac{h^3 b^2}{16} + \frac{2e_2 E_2}{e_1 E_1} \frac{h^4 b}{24} \right] + \frac{e_2}{G_2} \frac{E_2^2}{\langle EI_y \rangle^2} T_z^2 \frac{h^2 b^3}{24} \right\} \end{aligned}$$

From where by identification

$$\frac{k_z}{\langle GS \rangle} = \frac{e_1}{G_1} \frac{E_1^2}{\langle EI_y \rangle^2} \left[\frac{h^5}{120} + \left(\frac{2e_2 E_2}{e_1 E_1} \right)^2 \frac{h^3 b^2}{16} + \left(\frac{2e_2 E_2}{e_1 E_1} \right) \frac{h^4 b}{24} \right] + \frac{e_2}{G_2} \frac{E_2^2}{\langle EI_y \rangle^2} \frac{h^2 b^3}{24}$$

Note: We should point out the close analogy of results for the two section shapes: **I-beam** discussed here and **box beam** of Application 21.6. The results turn identical if we give the value $2e_1$ in place of e_1 for the web thickness of I-beam above. In such case, the areas occupied by material n°1 are strictly identical in both section shapes.

21.9 POLYMERIC COLUMN REINFORCED BY FILAMENT-WOUND FIBERGLASS

Problem Statement

We consider a cylindrical column of revolution designed for the chemical industry (temperature can be high, and it may contain corrosive fluid under pressure) made of PVDF (polyvinylidene fluoride). It is reinforced on the outside by a filament-wound layer of “E” glass/polyester. The characteristics of the two layers are as follows:

- Internal layer in PVDF: Thickness e_1 , isotropic material, modulus of elasticity E_1 , Poisson coefficient ν_1 .
- External layer in glass/polyester: To simplify the calculation, we will neglect the presence of the resin. As a consequence, E_t , ν_{tt} , and G_{tt} (see Chapter 10) are neglected. The total thickness of the glass/polyester layer e_2 consists of a partial thickness denoted as h^{90° of windings along the 90° direction relative to the direction of the generator of the cylinder, and a partial thickness denoted as $h^{\pm 45^\circ}$ of balanced windings along the $+45^\circ$ and -45° direction (as many fibers along the $+45^\circ$ as along the -45° direction). We, thus, have $e_2 = h^{90^\circ} + h^{\pm 45^\circ}$ (see Figure 21.16).

The longitudinal elasticity modulus of the glass/polyester layer is denoted as E_ℓ . Thicknesses e_1 (internal) and e_2 (external) will be considered small, relative to the average radius of the column.

1. The tangent plane to the midsurface of the glass/polyester laminate is denoted as (x, y) in Figure 21.16. Calculate for the reinforcement glass/polyester, in terms of E_ℓ , h^{90° , $h^{\pm 45^\circ}$:
 - The equivalent moduli \bar{E}_x and \bar{E}_y
 - The equivalent coefficients $\bar{\nu}_{yx}$ and $\bar{\nu}_{xy}$
2. A pressure p_o is exerted inside the column, at room temperature (creep of the materials not considered). The resulting stress components are denoted in axes (x, y) :
 - σ_{1x} and σ_{1y} in the internal layer of PVDF
 - σ_{2x} and σ_{2y} in the external layer of glass/polyester
 - a. The assembly of both materials being assumed perfectly bonded, write the equilibrium and behavior equations for this assembly. Deduce from there the system that allows the calculation of σ_{1x} and σ_{2x} .
 - b. *Numerical application:*
 - Internal pressure $p_o = 3 \text{ MPa}$ (30 bar); $r = 100 \text{ mm}$.
 - PVDF, $E_1 = 260 \text{ MPa}$; $\nu_1 = 0.3$; $e_1 = 10 \text{ mm}$.
 - Glass/polyester, $E_\ell = 74,000 \text{ MPa}$; $e_2 = 0.75 \text{ mm}$; $h^{90^\circ} = (h^{\pm 45^\circ}/3)$.
 - Calculate $\sigma_{1x}, \sigma_{1y}, \sigma_{2x}, \sigma_{2y}$.
 - c. Deduce from the previous results the stress values σ_ℓ^{90} in the glass fibers at 90° and $\sigma_\ell^{\pm 45}$ in the fibers at $\pm 45^\circ$. Give comment.

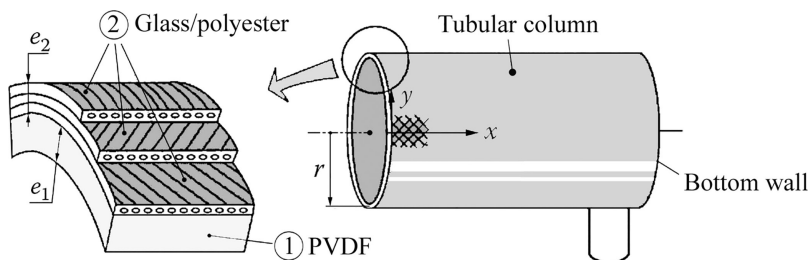


FIGURE 21.16 Reinforced polymeric column.

3. We would like to modify the ratio $(h^{90^\circ}/h^{\pm 45^\circ})$ in order to obtain identical stress in fibers at 90° and at $\pm 45^\circ$, corresponding to an **isotensoid** glass layer.
- What relations have to verify $(h^{90^\circ}/h^{\pm 45^\circ}), \sigma_{2x}, \sigma_{2y}$?
 - Starting from results of Question 2(b), indicate an iterative method that allows the calculation of the suitable ratio $(h^{90^\circ}/h^{\pm 45^\circ})$. Then, give the precise definition of the glass/polyester winding and its true thickness with a fiber volume fraction $V_f = 25\%$.

Solution

1. Equivalent moduli

The constitutive relationship of the laminate in axes (x, y) is written as (see Equation 12.4)

$$\begin{Bmatrix} N_x \\ N_y \\ T_{xy} \end{Bmatrix} = [A] \begin{Bmatrix} \epsilon_{ox} \\ \epsilon_{oy} \\ \gamma_{oxy} \end{Bmatrix} \quad \text{with } A_{ij} = \sum_{k=1st \text{ ply}}^{n^{st} \text{ ply}} \bar{E}_{ij}^k e_k$$

Coefficients \bar{E}_{ij}^k are given by Equation 11.8, in neglecting E_t, ν_{tl} , and G_{tl} :

- Plies at 90° :

$$\bar{E}_{11}^{90} = \bar{E}_{12}^{90} = \bar{E}_{33}^{90} = \bar{E}_{23}^{90} = \bar{E}_{13}^{90} = 0$$

$$\bar{E}_{22}^{90} = E_\ell$$

- Plies at $+45^\circ$:

$$\bar{E}_{11}^{+45} = \bar{E}_{22}^{+45} = \bar{E}_{33}^{+45} = \bar{E}_{12}^{+45} \dots$$

$$\dots = -\bar{E}_{13}^{+45} = -\bar{E}_{23}^{+45} = E_\ell/4$$

- Plies at -45° :

$$\bar{E}_{11}^{-45} = \bar{E}_{22}^{-45} = \bar{E}_{33}^{-45} = \bar{E}_{12}^{-45} \dots$$

$$\dots = \bar{E}_{13}^{-45} = \bar{E}_{23}^{-45} = E_\ell/4$$

From which we deduce the coefficients A_{ij} . For example, we have

$$A_{11} = \bar{E}_{11}^{90} h^{90} + \bar{E}_{11}^{+45} h^{+45} + \bar{E}_{11}^{-45} h^{-45} = \frac{E_\ell}{4} h^{\pm 45}$$

$$A_{12} = \bar{E}_{12}^{90} h^{90} + \bar{E}_{12}^{+45} h^{+45} + \bar{E}_{12}^{-45} h^{-45} = \frac{E_\ell}{4} h^{\pm 45}$$

and so forth. We obtain

$$\begin{Bmatrix} N_x \\ N_y \\ T_{xy} \end{Bmatrix} = \frac{E_\ell}{4} h^{\pm 45} \begin{Bmatrix} 1 & 1 & 0 \\ 1 & \left(1 + 4 \frac{h^{90}}{h^{\pm 45}}\right) & 0 \\ 0 & 0 & 1 \end{Bmatrix} \begin{Bmatrix} \epsilon_{ox} \\ \epsilon_{oy} \\ \gamma_{oxy} \end{Bmatrix}$$

In inverting and introducing average stress components (fictitious) in the external glass layer (with index 2), $\sigma_{2x} = (N_x/e_2)$; $\sigma_{2y} = (N_y/e_2)$; $\tau_{2xy} = (T_{xy}/e_2)$ (see Equation 12.6):

$$\begin{Bmatrix} \epsilon_{ox} \\ \epsilon_{oy} \\ \gamma_{oxy} \end{Bmatrix} = \frac{e_2}{E_\ell h^{90}} \begin{bmatrix} \left(1 + 4 \frac{h^{90}}{h^{\pm 45}}\right) & -1 & 0 \\ -1 & 1 & 0 \\ 0 & 0 & 1 \end{bmatrix} \begin{Bmatrix} \sigma_{2x} \\ \sigma_{2y} \\ \tau_{2xy} \end{Bmatrix}$$

The above relation can be also interpreted as follows (see Equation 12.9):

$$\begin{Bmatrix} \epsilon_{ox} \\ \epsilon_{oy} \\ \gamma_{oxy} \end{Bmatrix} = \begin{bmatrix} \frac{1}{\bar{E}_x} & -\frac{\bar{\nu}_{yx}}{\bar{E}_y} & 0 \\ -\frac{\bar{\nu}_{xy}}{\bar{E}_x} & \frac{1}{\bar{E}_y} & 0 \\ 0 & 0 & \frac{1}{\bar{G}_{xy}} \end{bmatrix} \begin{Bmatrix} \sigma_{2x} \\ \sigma_{2y} \\ \tau_{2xy} \end{Bmatrix}$$

where appear the equivalent moduli of the laminate. From this, by identification,

$$\bar{E}_x = \frac{E_\ell}{e_2 \left(\frac{1}{h^{90}} + \frac{4}{h^{\pm 45}} \right)}; \quad \bar{E}_y = E_\ell \times \frac{h^{90}}{e_2}; \quad \bar{\nu}_{xy} = \frac{1}{\left(1 + 4 \frac{h^{90}}{h^{\pm 45}} \right)}; \quad \bar{\nu}_{yx} = 1 \quad (21.12)$$

• **Comment:**

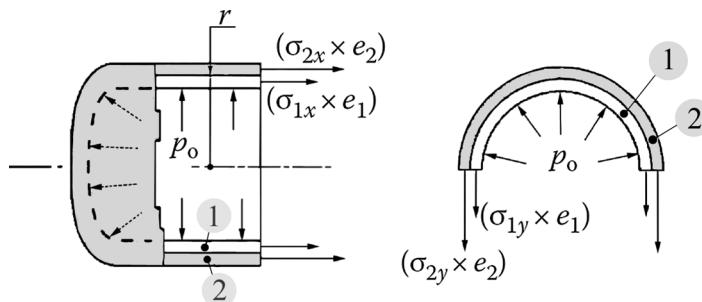
The obtained results are formally simple because of the following reasons:

- The polyester resin is not taken into account. The fibers work only in their directions.
- Decoupling between the external layer (glass/resin) and the internal layer (PVDF) was deliberately preferred to the consideration of a **global** laminate consisting of plies of glass/resin at 90° , $+45^\circ$, and -45° plus one **ply** of PVDF, isotropic, with thickness e_1 .

2.

a. *Equilibrium relationships:*

The isolated portions of the column as shown below allow us to write



$$2\pi r(e_1\sigma_{1x} + e_2\sigma_{2x}) = \pi r^2 p_o$$

$$1 \times 2(e_1\sigma_{1y} + e_2\sigma_{2y}) = 1 \times 2r \times p_o$$

From which the equilibrium relationships

$$e_1\sigma_{1x} + e_2\sigma_{2x} = p_o \frac{r}{2} \quad (21.13)$$

$$e_1\sigma_{1y} + e_2\sigma_{2y} = p_o r \quad (21.14)$$

– *Behavior relationships:*

Elastic behavior of the internal PVDF layer is described by the classical isotropic equation:

$$\begin{Bmatrix} \epsilon_{1x} \\ \epsilon_{1y} \\ \gamma_{1xy} \end{Bmatrix} = \begin{bmatrix} \frac{1}{E_1} & -\frac{\nu_1}{E_1} & 0 \\ -\frac{\nu_1}{E_1} & \frac{1}{E_1} & 0 \\ 0 & 0 & \frac{1}{G_1} \end{bmatrix} \begin{Bmatrix} \sigma_{1x} \\ \sigma_{1y} \\ \tau_{1xy} \end{Bmatrix}$$

The behavior of the external composite filament winding is described in the previous question:

$$\begin{Bmatrix} \epsilon_{ox} \\ \epsilon_{oy} \\ \gamma_{oxy} \end{Bmatrix} = \begin{bmatrix} \frac{1}{\bar{E}_x} & -\frac{\bar{\nu}_{yx}}{\bar{E}_y} & 0 \\ -\frac{\bar{\nu}_{xy}}{\bar{E}_x} & \frac{1}{\bar{E}_y} & 0 \\ 0 & 0 & \frac{1}{\bar{G}_{xy}} \end{bmatrix} \begin{Bmatrix} \sigma_{2x} \\ \sigma_{2y} \\ \tau_{2xy} \end{Bmatrix}$$

Equality of strain under the stress state

$$\epsilon_{1x} = \epsilon_{ox}; \quad \epsilon_{1y} = \epsilon_{oy}$$

leads to

$$\frac{1}{E_1}\sigma_{1x} - \frac{\nu_1}{E_1}\sigma_{1y} = \frac{1}{\bar{E}_x}\sigma_{2x} - \frac{\bar{\nu}_{yx}}{\bar{E}_y}\sigma_{2y} \quad (21.15)$$

$$-\frac{\nu_1}{E_1}\sigma_{1x} + \frac{1}{E_1}\sigma_{1y} = -\frac{\bar{\nu}_{xy}}{\bar{E}_x}\sigma_{2x} + \frac{1}{\bar{E}_y}\sigma_{2y} \quad (21.16)$$

Equations 21.13 through 21.16 constitute a system of four relationships for the four unknowns $\sigma_{1x}, \sigma_{1y}, \sigma_{2x}$, and σ_{2y} . By performing subtraction, (21.15)–(21.16), we obtain

$$\sigma_{1x} \left(\frac{1+v_1}{E_1} \right) - \sigma_{1y} \left(\frac{1+v_1}{E_1} \right) = \sigma_{2x} \left(\frac{1+\bar{v}_{xy}}{\bar{E}_x} \right) - \sigma_{2y} \left(\frac{1+\bar{v}_{yx}}{\bar{E}_y} \right)$$

By performing addition, (21.15) + (21.16), we obtain

$$\sigma_{1x} \left(\frac{1-v_1}{E_1} \right) - \sigma_{1y} \left(\frac{1-v_1}{E_1} \right) = \sigma_{2x} \left(\frac{1-\bar{v}_{xy}}{\bar{E}_x} \right) - \sigma_{2y} \left(\frac{1-\bar{v}_{yx}}{\bar{E}_y} \right)$$

By using Equations 21.13 and 21.14, we obtain a system allowing calculation of σ_{1x} and σ_{1y}

$$\begin{aligned} \sigma_{1x} \left[\left(\frac{1+v_1}{E_1} \right) + \frac{e_1}{e_2} \left(\frac{1+\bar{v}_{xy}}{\bar{E}_x} \right) \right] - \sigma_{1y} \left[\left(\frac{1+v_1}{E_1} \right) + \frac{e_1}{e_2} \left(\frac{1+\bar{v}_{yx}}{\bar{E}_y} \right) \right] &\dots \\ = \frac{p_0 r}{e_2} \left[\left(\frac{1+\bar{v}_{xy}}{2\bar{E}_x} \right) - \left(\frac{1+\bar{v}_{yx}}{\bar{E}_y} \right) \right] \\ \sigma_{1x} \left[\left(\frac{1-v_1}{E_1} \right) + \frac{e_1}{e_2} \left(\frac{1-\bar{v}_{xy}}{\bar{E}_x} \right) \right] + \sigma_{1y} \left[\left(\frac{1-v_1}{E_1} \right) + \frac{e_1}{e_2} \left(\frac{1-\bar{v}_{yx}}{\bar{E}_y} \right) \right] &\dots \\ = \frac{p_0 r}{e_2} \left[\left(\frac{1-\bar{v}_{xy}}{2\bar{E}_x} \right) + \left(\frac{1-\bar{v}_{yx}}{\bar{E}_y} \right) \right] \end{aligned} \quad (21.17)$$

b. *Numerical application:*

Since $h^{90^\circ} = (h^{\pm 45^\circ}/3)$,

$$e_2 = h^{90^\circ} + h^{\pm 45^\circ} = 0.75 \text{ mm}; \quad h^{\pm 45^\circ} = 0.56 \text{ mm}; \quad h^{90^\circ} = 0.19 \text{ mm}$$

Following Equation 21.12,

$$\bar{E}_x = 7,953 \text{ MPa}; \quad \bar{E}_y = 18,747 \text{ MPa}; \quad \bar{v}_{xy} = 0.42$$

The system in Equation 21.17 provides

$$\sigma_{1x} = 1.71 \text{ MPa}; \quad \sigma_{1y} = 3.07 \text{ MPa}$$

Equations 21.15 and 21.16 allow the calculation of σ_{2x} and σ_{2y} :

$$\sigma_{2x} = 188 \text{ MPa}; \quad \sigma_{2y} = 386 \text{ MPa}$$

c. *Stresses in the fibers*

Following Equation 11.8, we have for any ply “k” in the external layer:

$$\begin{Bmatrix} \sigma_x \\ \sigma_y \\ \tau_{xy} \end{Bmatrix}^k = E_\ell \begin{bmatrix} c^4 & c^2 s^2 & -c^3 s \\ c^2 s^2 & s^4 & -cs^3 \\ -c^3 s & -cs^3 & c^2 s^2 \end{bmatrix}^k \begin{Bmatrix} \epsilon_{ox} \\ \epsilon_{oy} \\ \gamma_{oxy} \end{Bmatrix} \quad (21.18)$$

The strain components ϵ_{ox} and ϵ_{oy} are obtained by means of the previous results (see Question 2(a)). For example,

$$\epsilon_{ox} = \epsilon_{1x} = \frac{\sigma_{1x}}{E_1} - \frac{\nu_1}{E_1} \sigma_{1y} = 3.03 \times 10^{-3}$$

$$\epsilon_{oy} = \epsilon_{1y} = -\frac{\nu_1}{E_1} \sigma_{1x} + \frac{\sigma_{1y}}{E_1} = 9.85 \times 10^{-3}$$

If we invert Equation 11.4, taking into account the fact that the only nonzero stress in axes (ℓ, t) of the filament winding is σ_ℓ ,

$$\begin{Bmatrix} \sigma_x \\ \sigma_y \\ \tau_{xy} \end{Bmatrix}^k = \begin{bmatrix} c^2 & s^2 & 2cs \\ s^2 & c^2 & -2cs \\ -sc & sc & (c^2 - s^2) \end{bmatrix}^k \begin{Bmatrix} \sigma_\ell \\ 0 \\ 0 \end{Bmatrix} \quad (21.19)$$

We, thus, have what follows:

- For fibers at 90° ,
 - Following Equation 21.18, $\sigma_x^{90^\circ} = 0$; $\sigma_y^{90^\circ} = E_\ell \epsilon_{oy}$
 - Following Equation 21.19, $\sigma_x^{90^\circ} = 0$; $\sigma_y^{90^\circ} = \sigma_\ell^{90^\circ}$ from which

$$\sigma_\ell^{90^\circ} = E_\ell \times \epsilon_{oy}$$

$$\sigma_\ell^{90^\circ} = 729 \text{ MPa}$$

- For fibers at $+45^\circ$,
 - Following Equation 21.18, $\sigma_x^{+45^\circ} = \sigma_y^{+45^\circ} = \frac{E_\ell}{4} (\epsilon_{ox} + \epsilon_{oy})$
 - Following Equation 21.19, $\sigma_x^{+45^\circ} = \sigma_y^{+45^\circ} = \frac{1}{2} \sigma_\ell^{+45^\circ}$

From which

$$\sigma_\ell^{+45^\circ} = \frac{E_\ell}{2} (\epsilon_{ox} + \epsilon_{oy})$$

$$\sigma_\ell^{+45^\circ} = 477 \text{ MPa}$$

The stress value is identical in the -45° fibers. Note the disparity of stress in the 90° fibers and the $\pm 45^\circ$ fibers. As such, the outer glass layer is not well designed because we want to ensure that all the fibers operate in an identical fashion in order to obtain uniform extension of fiberglass.

3.

- a. Our goal is that $\sigma_\ell^{90^\circ} = \sigma_\ell^{+45^\circ}$.

Referring to the results of the previous question, this equality leads to

$$E_\ell \times \epsilon_{oy} = \frac{E_\ell}{2} (\epsilon_{ox} + \epsilon_{oy})$$

Or

$$\epsilon_{oy} = \epsilon_{ox}$$

The behavior equation of the filament winding (Question 1 and Equation 21.12) indicates then

$$\frac{\sigma_{2x}}{\bar{E}_x} - \frac{\bar{\nu}_{yx}}{\bar{E}_y} \sigma_{2y} = -\frac{\bar{\nu}_{xy}}{\bar{E}_x} \sigma_{2x} + \frac{\sigma_{2y}}{\bar{E}_y}$$

After calculation,

$$\frac{h^{90^\circ}}{h^{\pm 45^\circ}} = \frac{\sigma_{2y} - \sigma_{2x}}{\sigma_{2x}} \quad (21.20)$$

b. With the result of numerical application 2(b), Equation 21.20 indicates

$$\frac{\sigma_{2y} - \sigma_{2x}}{\sigma_{2x}} = 0.53$$

Adopting this new value for the ratio $(h^{90^\circ}/h^{\pm 45^\circ})$ leads to the new result:

$$(h^{90^\circ}/h^{\pm 45^\circ}) = 0.53$$

$$\bar{E}_x = 8,216 \text{ MPa}; \quad \bar{E}_y = 25,653 \text{ MPa}; \quad \bar{\nu}_{xy} = 0.32; \quad \bar{\nu}_{yx} = 1$$

$$\sigma_{1x} = 2.42 \text{ MPa}; \quad \sigma_{1y} = 2.72 \text{ MPa}$$

$$\sigma_{2x} = 167 \text{ MPa}; \quad \sigma_{2y} = 364 \text{ MPa}$$

Equation 21.20 then indicates

$$\frac{\sigma_{2y} - \sigma_{2x}}{\sigma_{2x}} = 0.587$$

The value that we adopt for new ratio

$$(h^{90^\circ}/h^{\pm 45^\circ}) = 0.587$$

$$\bar{E}_x = 8,166 \text{ MPa}; \quad \bar{E}_y = 27,627 \text{ MPa}; \quad \bar{\nu}_{xy} = 0.29; \quad \bar{\nu}_{yx} = 1$$

$$\sigma_{1x} = 2.63 \text{ MPa}; \quad \sigma_{1y} = 2.69 \text{ MPa}$$

$$\sigma_{2x} = 165 \text{ MPa}; \quad \sigma_{2y} = 364 \text{ MPa}$$

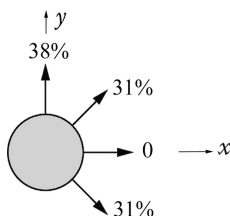
Equation 21.20 then indicates

$$\frac{\sigma_{2y} - \sigma_{2x}}{\sigma_{2x}} = 0.6$$

which corresponds to a 2% relative variation with respect to the ratio value $(h^{90^\circ}/h^{\pm 45^\circ})$ taken to carry out the last calculations above. The iterative procedure seems to quickly converge. Therefore, an external isotenoid layer and an internal layer of PVDF in biaxial tension would be obtained for a ratio

$$\frac{h^{90^\circ}}{h^{\pm 45^\circ}} \approx 0.6$$

The composition of the glass/polyester reinforcement will be as follows:



Taking account of the resin volume with $V_f = 0.25$, the true thickness of the glass/polyester winding will be

$$e'_2 = \frac{e_2}{0.25}$$

$$e'_2 = 3 \text{ mm}$$

21.10 CYLINDRICAL BENDING OF A THICK ORTHOTROPIC PLATE UNDER UNIFORM LOADING

Problem Statement

Consider a thick rectangular plate ($b \times a$) with $b > a$, made of unidirectional glass/resin (see Figure 21.17). It is simply supported at two opposite sides and loaded by a constant pressure noted q_o .

1. Calculate the bending deflection at the midline of the plate located at $x = a/2$ (maximum deflection).
2. *Numerical application:* For this deflection, indicate the contribution of bending moment and of transverse shear, using the following:

$$E_x = 40,000 \text{ MPa}; \quad G_{xz} = 400 \text{ MPa}; \quad \nu_{xy} = 0.3; \quad \nu_{yx} = 0.075; \quad q_o = -1 \text{ MPa}$$

$$a = 150 \text{ mm}; \quad h = 15 \text{ mm}.$$

Comment on this.

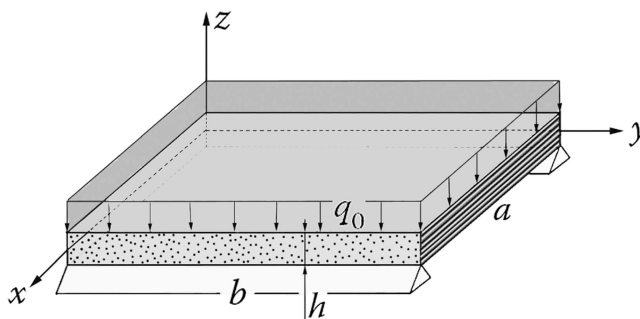


FIGURE 21.17 Thick orthotropic plate.

Solution

1. For the cylindrical bending under analysis, Equation 18.32 allows us to write

$$\frac{dQ_x}{dx} = -q_o; \quad \frac{dM_y}{dx} = Q_x; \quad M_y = C_{11} \frac{d\theta_y}{dx}; \quad Q_x = \frac{hG_{xz}}{k_x} \left(\frac{dw_o}{dx} + \theta_y \right)$$

Elimination of Q_x , M_y , and θ_y leads to

$$\frac{d^4 w_o}{dx^4} = \frac{q_o}{C_{11}}$$

Then,

$$w_o = \frac{q_o}{C_{11}} \left(\frac{x^4}{24} + A \frac{x^3}{6} + B \frac{x^2}{2} + Cx + D \right)$$

The boundary conditions are

$$\left. \begin{array}{l} x=0 \\ x=a \end{array} \right\} \Rightarrow w_o = 0 \quad \text{and} \quad M_y = 0 \Rightarrow \frac{d\theta_y}{dx} = \frac{k_x}{hG_{xz}} q_o - \frac{d^2 w_o}{dx^2} = 0$$

After calculation of constants A , B , C , and D , we obtain the deflection at $x = a/2$:

$$w_o \left(\frac{a}{2} \right) = q_o a^4 \times \frac{12(1 - \nu_{xy}\nu_{yx})}{E_x h^3} \left\{ \frac{5}{384} + k_x \left(\frac{h}{a} \right)^2 \frac{E_x}{G_{xz}} \times \frac{1}{96(1 - \nu_{xy}\nu_{yx})} \right\}$$

The calculation of k_x was done in Section 18.7.1 for this type of plate. It indicates (see Equation 18.34)

$$k_x = \frac{6}{5} = 1.2$$

From which

$$w_o \left(\frac{a}{2} \right) = q_o a^4 \times \frac{12(1 - \nu_{xy}\nu_{yx})}{E_x h^3} \left\{ \frac{5}{384} + \left(\frac{h}{a} \right)^2 \frac{E_x}{G_{xz}} \times \frac{1}{80(1 - \nu_{xy}\nu_{yx})} \right\}$$

The terms between brackets represent, respectively, the contribution of bending moment and that of transverse shear.

2. *Numerical values:*

$$w_o \left(\frac{a}{2} \right) = \underbrace{-0.5727 \text{ mm}}_{\text{moment}} - \underbrace{0.5625 \text{ mm}}_{\text{transverse shear}}$$

$$w_o \left(\frac{a}{2} \right) = -1.1352 \text{ mm}$$

Note: A percentage of 49.5% of this deflection is due to transverse shear. We can see from the above literal expression for $w_0(a/2)$ that the influence of transverse shear on bending deflection increases with the following:

- The relative thickness (h/a) . Here, $(h/a) = 1/10$, corresponding to a thick plate.
- The ratio $(E_x/G_{xz})^5$.

21.11 BENDING OF A SANDWICH PLATE

Problem Statement

A rectangular sandwich plate ($a \times b$) is clamped on one side b and loaded along the opposite side by a constant distributed load f_o (N/mm). The two other sides (length a) are free (see Figure 21.18).

The plate consists of two identical orthotropic skins of material 1 and an orthotropic core made of material 2. The orthotropic axes are parallel to axes (x, y, z) .

1. Assuming cylindrical bending of the plate about the y -axis, calculate the deflection of the loaded side $x = a$.
2. Numerical application: $f_o = -10$ N/mm; $a = b = 1,000$ mm; $H_1 = 2 \times H_2 = 100$ mm.
 - Material 1:

$$E_x^{(1)} = 40,000 \text{ MPa}; \quad G_{xz}^{(1)} = 4,000 \text{ MPa}$$

- Material 2:

$$E_x^{(2)} = 40 \text{ MPa}; \quad G_{xz}^{(2)} = 15 \text{ MPa}$$

For each of the materials, $\nu_{xy} = 0.3$ and $\nu_{yx} = 0.075$,

- a. Calculate the deflection of the side $x = a$, and highlight the contributions of bending moment and of transverse shear
- b. Calculate the transverse shear stress τ_{xz}
 - On the midplane of the plate
 - At the interface between the core and the upper skin
 - At the midthickness of the upper skin

Solution

1. For the cylindrical bending case, consideration of equilibrium (see Section 18.5) and Equation 18.32a allows writing

$$\frac{dQ_x}{dx} = 0; \quad \frac{dM_y}{dx} = Q_x; \quad M_y = C_{11} \frac{d\theta_y}{dx}; \quad Q_x = \frac{\langle hG_{xz} \rangle}{k_x} \left(\frac{dw_0}{dx} + \theta_y \right)$$

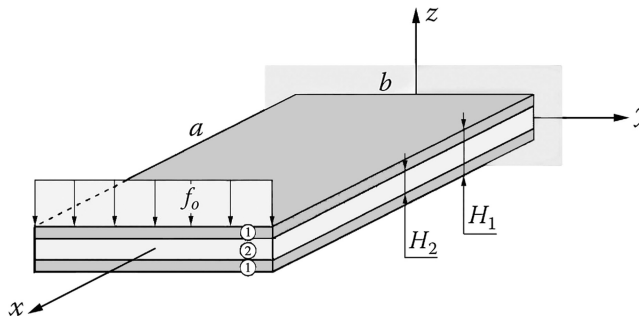


FIGURE 21.18 Sandwich plate.

Here, $Q_x = f_0$, and elimination of M_y and θ_y leads to

$$\frac{d^3 w_o}{dx^3} = -\frac{f_o}{C_{11}}$$

Then,

$$w_o = -\frac{f_o}{C_{11}} \left(\frac{x^3}{6} + A \frac{x^2}{2} + Bx + C \right)$$

The boundary conditions are

$$x = 0 \rightarrow w_o = 0 \text{ and } \theta_y = 0 \Rightarrow k_x \frac{f_o}{\langle hG_{xz} \rangle} - \frac{dw_o}{dx} = 0$$

$$x = a \rightarrow M_y = 0 \Rightarrow \frac{d\theta_y}{dx} = -\frac{d^2 w_o}{dx^2} = 0$$

After the calculation of constants A , B , and C , we obtain the deflection at $x = a$

$$w_o(a) = \frac{f_o a^3}{3C_{11}} + k_x \frac{f_o a}{\langle hG_{xz} \rangle}$$

According to Equations 18.32a and 18.2

$$C_{11} = \bar{E}_{11}^{(1)} \left(\frac{H_1^3 - H_2^3}{12} \right) + \bar{E}_{11}^{(2)} \frac{H_2^3}{12}$$

$$C_{11} = \frac{E_x^{(1)} (H_1^3 - H_2^3) + E_x^{(2)} H_2^3}{12(1 - \nu_{xy} \nu_{yx})}$$

$$\langle hG_{xz} \rangle = G_{xz}^{(1)} (H_1 - H_2) + G_{xz}^{(2)} H_2$$

From which we obtain

$$w_o(a) = \frac{4(1 - \nu_{xy} \nu_{yx}) f_o a^3}{E_x^{(1)} (H_1^3 - H_2^3) + E_x^{(2)} H_2^3} + \frac{k_x f_o a}{G_{xz}^{(1)} (H_1 - H_2) + G_{xz}^{(2)} H_2}$$

The calculation of k_x was carried out in Section 18.7.2 for this type of plate and is given by Equation 18.39.

2. Numerical application:

- a. *Deflection*, from Equation 18.39, $k_x = 110.8$

From which

$$w_o(a) = \underbrace{-1.177 \text{ mm}}_{\text{moment}} - \underbrace{5.519 \text{ mm}}_{\text{transverse shear}}$$

$$w_o(a) = -6.696 \text{ mm}$$

Note: A percentage of 82% of this deflection is due to transverse shear, and this happens despite very thick skins. This important influence is due to

- The very large value (110.8) compared with the unity of the transverse shear coefficient
 - The notable thickness of the plate, $(H_1/a) = 1/10$
- b. *Transverse shear stress* τ_{xz} : from Equation 18.37,
- On the midplane, $z = 0 \rightarrow \tau_{xz} = 0.1286 \text{ MPa}$
 - At the interface between the skin and the core,

$$z = H_2/2 \rightarrow \tau_{xz} = 0.12855 \text{ MPa}$$

- At the midthickness of the upper skin,

$$z = (H_1 + H_2)/4 \rightarrow \tau_{xz} = 0.075 \text{ MPa}$$

Note: We have maintained several decimal places in order to use this example as a test case when evaluating finite element software⁶.

21.12 BENDING VIBRATION OF A SANDWICH BEAM⁷

Problem Statement

Consider a sandwich beam of length ℓ and width d simply supported at its ends (see Figure 21.19). It consists of two identical skins of material 1 (glass/resin) and a core of material 2 (foam). These materials are transversely isotropic in plane (y, z).

The elastic constants are denoted as $E_x^{(1)}$, $G_{xy}^{(1)}$, $E_x^{(2)}$, $G_{xy}^{(2)}$.

Specific masses are ρ_1 and ρ_2 .

1. Write the equation for the natural frequencies of bending vibration in plane of symmetry (x, y) of this beam.
2. *Numerical application:*

$$E_x^{(1)} = 40,000 \text{ MPa}; \quad G_{xy}^{(1)} = 4,000 \text{ MPa}; \quad \rho_1 = 2,000 \text{ kg/m}^3$$

$$E_x^{(2)} = 40 \text{ MPa}; \quad G_{xy}^{(2)} = 15 \text{ MPa}; \quad \rho_2 = 50 \text{ kg/m}^3$$

$$H_1 = 2H_2 = 100 \text{ mm}; \quad \ell = 1,000 \text{ mm}; \quad d = 100 \text{ mm}$$

Calculate the first five flexural natural frequencies.

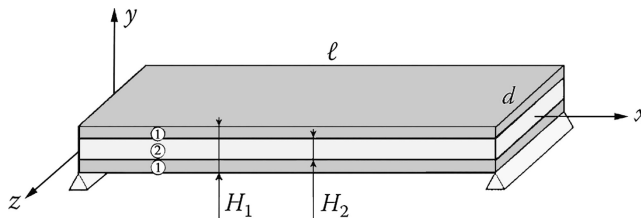


FIGURE 21.19 Simply supported sandwich beam.

Solution

1. Equation for the bending vibrations

We have to formulate the differential equation for the dynamical displacement $v(x, t)$ starting from Equation 16.18. We should note that for the example under analysis, the elastic center and center of gravity of section coincide. Thus, $y_G = 0$, resulting in uncoupling between bending vibrations $v(x, t)$ and longitudinal vibrations $u(x, t)$:

$$\frac{\partial T_y}{\partial x} = \langle \rho S \rangle \frac{\partial^2 v}{\partial t^2}; \quad \frac{\partial M_z}{\partial x} + T_y = \langle \rho I_z \rangle \frac{\partial^2 \theta_z}{\partial t^2}$$

$$T_y = \frac{\langle GS \rangle}{k} \left(\frac{\partial v}{\partial x} - \theta_z \right); \quad M_z = \langle EI_z \rangle \frac{\partial \theta_z}{\partial x}$$

Elimination of T_y , M_z , and θ_z between these four relations leads to the equation for $v(x, t)$:

$$\frac{\partial^4 v}{\partial x^4} - \frac{\langle \rho I_z \rangle}{\langle EI_z \rangle} (1+a) \frac{\partial^4 v}{\partial x^2 \partial t^2} + \frac{\langle \rho S \rangle}{\langle EI_z \rangle} \frac{\partial^2 v}{\partial t^2} + k \frac{\langle \rho I_z \rangle}{\langle GS \rangle} \frac{\langle \rho S \rangle}{\langle EI_z \rangle} \frac{\partial^4 v}{\partial t^4} = 0$$

with

$$a = k \times \frac{\langle \rho S \rangle}{\langle GS \rangle} \frac{\langle EI_z \rangle}{\langle \rho I_z \rangle}$$

Assuming a solution in the form $v(x, t) = v_0(x) \times \cos(\omega t + \phi)$, we can rewrite the differential equation that defines the modal deflection shape $v_0(x)$ in the following nondimensional form:

$$\frac{\partial^4 \bar{v}_o}{\partial \bar{x}^4} + \bar{\omega}^2 (1+a) \frac{\partial^2 \bar{v}_o}{\partial \bar{x}^2} + \bar{\omega}^2 \left(a \bar{\omega}^2 - \frac{1}{\bar{r}^2} \right) \bar{v}_o = 0$$

In which

$$\bar{x} = \frac{x}{\ell}; \quad \bar{v}_o = \frac{v_o}{\ell}; \quad \bar{\omega}^2 = \frac{\langle \rho I_z \rangle}{\langle EI_z \rangle} \omega^2 \ell^2; \quad \bar{r}^2 = \frac{\langle \rho I_z \rangle}{\langle \rho S \rangle} \ell^2$$

After writing the characteristic equation, the reduced modal deflection shape takes the form

$$\bar{v}_o = A \cosh X_1 \bar{x} + B \sinh X_1 \bar{x} + C \cos X_2 \bar{x} + D \sin X_2 \bar{x} \quad (21.21)$$

where

$$\frac{X_2^2}{X_1^2} = \pm \frac{\bar{\omega}^2 (1+a)}{2} + \sqrt{\bar{\omega}^2 \left[\bar{\omega}^2 \left(\frac{1-a}{2} \right)^2 + \frac{1}{\bar{r}^2} \right]} \quad (21.22)$$

The boundary conditions corresponding to simply supported ends are written as

$$x = 0 \text{ or } x = \ell \rightarrow v = 0 \text{ and } M_z = \langle EI_z \rangle \frac{\partial \theta_z}{\partial x} = 0 \quad \forall t$$

which leads in nondimensional form to

$$\bar{x} = 0 \text{ or } \bar{x} = 1 \rightarrow \bar{v}_o = 0 \text{ and } \frac{\partial^2 \bar{v}_o}{\partial \bar{x}^2} + a \bar{\omega}^2 \bar{v}_o = 0$$

With Equation 21.21, these four conditions allow obtaining a linear and homogeneous system with four unknowns A , B , C , and D . By setting the determinant of this system equal to zero, we obtain an equation for circular natural frequencies that reduces to

$$\sin X_2 = 0$$

The solution is

$$X_2 = n\pi, (n = 1, 2, 3 \dots) \quad (21.23)$$

2. Natural frequencies

With the specified numerical values, the shear coefficient k is obtained from the literal expression found in Question 3 of Application 21.5. We find $k = 110.8$.

First, the circular frequencies $\omega_1, \omega_2, \omega_3 \dots$ are extracted from Equation 21.23, in which X_2 takes the form (21.22). The natural frequencies are then obtained:

$$f_i = \frac{\omega_i}{2\pi} (\text{Hz})$$

Numerically⁸,

$$f_1 = 64.476 \text{ Hz}; \quad f_2 = 131.918 \text{ Hz}; \quad f_3 = 198.734 \text{ Hz}$$

$$f_4 = 265.383 \text{ Hz}; \quad f_5 = 331.963 \text{ Hz}$$

21.13 TRANSVERSE SHEAR IN A TWO PHASES CIRCULAR SECTION BEAM

Problem Statement

Consider a circular section beam made up of two concentric phases denoted 1 and 2 as shown in Figure 21.20. The materials constituting each phase are homogeneous and isotropic, with respective moduli of elasticity E_1 , G_1 and E_2 , G_2 . We examine the transverse shear behavior associated to bending of this beam in its symmetry plane (x, y) .

Using the results from Chapter 16 (see Equation 16.16):

1.
 - a. Calculate the warping function g_0 in domain D of the cross section. One can use the polar coordinates r and θ in the plane of the transverse section and put $g_0(r, \theta) = f(r) \times \cos \theta$.
 - b. Give the expression for the shear coefficient k and define the transverse shear stiffness of the beam.

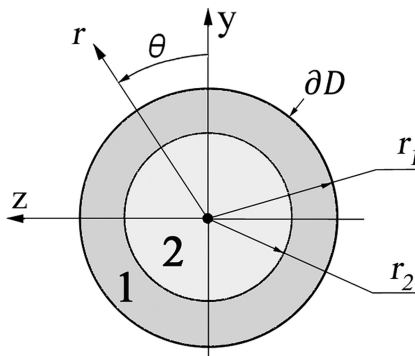


FIGURE 21.20 Two phases circular section beam.

2. Examine the particular case where $r_1 = 1.5 \times r_2$, $E_1 = 10 E_2$, and $\nu_1 = \nu_2 = 0.3$. Calculate the shear coefficient k . Deduce the warping, written as $\eta_x \times (\langle GS \rangle / T_y)$ of the cross section under the effect of transverse shear stress.

Solution

1.

- a. Longitudinal warping function $g_0(r, \theta)$

We have to solve in domain D of the cross section (see Equation 16.16)

$$\frac{\partial^2 g_0}{\partial y^2} + \frac{\partial^2 g_0}{\partial z^2} = \nabla^2 g_0 = -\frac{E_i}{G_i} \frac{\langle GS \rangle}{\langle EI_z \rangle} \times y$$

In polar coordinates

$$\nabla^2 g_0 = \frac{\partial^2 g_0}{\partial r^2} + \frac{1}{r} \frac{\partial g_0}{\partial r} + \frac{1}{r^2} \frac{\partial^2 g_0}{\partial \theta^2}$$

With along external boundary ∂D

$$\frac{\partial g_{01}}{\partial r} = 0$$

And along internal boundary $r = r_2$

$$g_{01} = g_{02}; \quad G_1 \frac{\partial g_{01}}{\partial r} = G_2 \frac{\partial g_{02}}{\partial r}$$

By posing

$$g_0(r, \theta) = f(r) \times \cos \theta$$

We obtain after calculation

$$g_{01} = \frac{a}{8} \left\{ \frac{E_1}{G_1} (3r_1^2 - r^2) + C_1 \left(\frac{1}{r_1^2} + \frac{1}{r^2} \right) \right\} \times r \cos \theta$$

$$g_{02} = \frac{a}{8} \left\{ C_2 - \frac{E_2}{G_2} r^2 \right\} \times r \cos \theta$$

with

$$a = \frac{\langle GS \rangle}{\langle EI_z \rangle} = 4 \times \frac{G_1 r_1^2 + (G_2 - G_1) r_2^2}{E_1 r_1^4 + (E_2 - E_1) r_2^4}$$

$$C_1 = \frac{2r_2^2 \frac{E_2}{G_1} - \frac{E_1}{G_1} \left\{ 3r_1^2 \left(\frac{G_2}{G_1} - 1 \right) - r_2^2 \left(\frac{G_2}{G_1} - 3 \right) \right\}}{\frac{1}{r_1^2} \left(\frac{G_2}{G_1} - 1 \right) + \frac{1}{r_2^2} \left(\frac{G_2}{G_1} + 1 \right)}$$

$$C_2 = C_1 \left(\frac{1}{r_1^2} + \frac{1}{r_2^2} \right) + \frac{E_1}{G_1} (3r_1^2 - r_2^2) + \frac{E_2}{G_2} r_2^2 \quad (21.24)$$

b.

– *Shear coefficient k*

It is given by Equation 16.16b, that is to say

$$k = \frac{1}{\langle EI_z \rangle} \int_D E_i g_0 y \times dS$$

After calculation

$$k = \frac{a}{4} \times \frac{(E_1 A_1 + E_2 A_2)}{(E_1 r_1^4 + (E_2 - E_1) r_2^4)}$$

with

$$A_1 = \frac{E_1}{G_1} \left\{ \frac{3r_1^2}{4} (r_1^4 - r_2^4) - \frac{1}{6} (r_1^6 - r_2^6) \right\} + C_1 \left\{ \frac{r_1^4 - r_2^4}{4r_1^2} + \frac{r_1^2 - r_2^2}{2} \right\}$$

$$A_2 = C_2 \frac{r_2^4}{4} - \frac{E_2}{G_2} \times \frac{r_2^6}{6}$$

– *Transverse shear stiffness of the beam:*

Starting from the constitutive Equation 16.16a:

$$T_y = \frac{\langle GS \rangle}{k} \left(\frac{dv}{dx} - \theta_z \right)$$

One can note the proportionality between the shear stress resultant T_y and the corresponding deformation $((dv/dx) - \theta_z)$. The transverse shear stiffness is, thus, the coefficient of proportionality $(\langle GS \rangle/k)$, that is to say

$$\frac{\langle GS \rangle}{k} = \frac{\pi}{k} \{ G_1 r_1^2 + (G_2 - G_1) r_2^2 \}$$

2. Particular case:

- Shear coefficient k : with $r_1 = 1.5 \times r_2$, $E_1 = 10 \times E_2$, and $\nu_1 = \nu_2 = 0.3$, the formula previously written for k gives

$$k = 1,658 \quad (21.25)$$

- Warping of the cross section: it is written (see Section 16.1.5.3 and Equation 16.15)

$$\eta_x = \frac{T_y}{\langle GS \rangle} \times g(y, z) = \frac{T_y}{\langle GS \rangle} \times [g_0(y, z) - k \times y]$$

i.e.,

$$\eta_x \times \frac{\langle GS \rangle}{T_y} = g_0(y, z) - k \times y$$

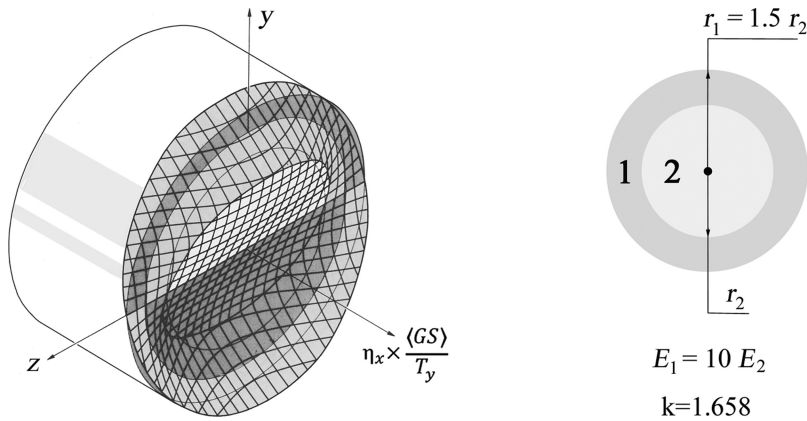
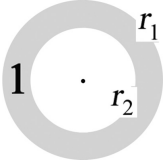


FIGURE 21.21 Warping of the cross section.

With Equations 21.24 and 21.25, one obtains in the plane (y, z) of the cross section:

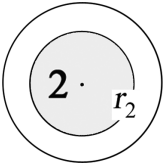
$$\eta_x \times \frac{\langle GS \rangle}{T_y} =$$



1

$r_2 \leq r \leq r_1$

$$\left\{ \frac{E_1}{G_1} \left[3r_1^2 - (y^2 + z^2) \right] + C_1 \left[\frac{1}{r_1^2} + \frac{1}{(y^2 + z^2)} \right] - \frac{8k}{a} \right\} \times \frac{a}{8} \times y$$



2

$0 \leq r \leq r_2$

$$\left\{ C_2 - \frac{8k}{a} - \frac{E_2}{G_2} (y^2 + z^2) \right\} \times \frac{a}{8} \times y$$

a, C_1, C_2 : See Equation 21.24

Figure 21.21 shows the corresponding warped section superimposed on the initial plane cross section.

NOTES

- 1 Evolution of τ_{xy} for the beam with thin skins ($H_2/H_1 = 0.9$) justifies the simplification proposed in Application 20.1.
- 2 To write this, we have to neglect the area of the corner. Then the shear flow is conservative.
- 3 We should note that the assumption of a little value of the flange's thickness is not valid for $y = 0$. From which the occurrence of a strict inequality $y > 0$.
- 4 To write this, we have to neglect the area of the corner. Then the shear flow is conservative.
- 5 This example of thick plate in bending constitutes a test case to evaluate computer programs using finite elements. For complementary information on this topic, see Bibliography: Matheron G.
- 6 This example of thick plate in bending constitutes a test case to evaluate computer programs using finite elements. For complementary information on this topic, see Bibliography: Matheron G.
- 7 This application constitutes another test case for the validation of finite element software. See Bibliography: Matheron G.
- 8 The nonsignificant decimals have intentionally been kept for the purpose of comparison with values obtained from numerical models of finite element software.



Taylor & Francis

Taylor & Francis Group

<http://taylorandfrancis.com>

Appendix A

Stresses in the Plies of a Carbon/ Epoxy Quadrangle Symmetric Laminate Loaded in Its Plane

In this appendix, Figures A.1–A.12 give for each ply of a given Quad laminate, in orthotropic directions ℓ and t of this ply in its plane, the stress components σ_ℓ , σ_t , and $\tau_{\ell t}$.

The laminate is successively subject to three cases of simple loading:

1. $[\pm\Phi / \pm\Psi]$, normal stress along the 0° direction
2. $\sigma_y = 1$ MPa, normal stress along the 90° direction
3. $\tau_{xy} = 1$ MPa, shear stress

A.1 CHARACTERISTICS OF EACH PLY

- $V_f = 60\%$ fiber volume fraction
- Thickness of each ply, 0.13 mm
- Moduli:
 - Modulus along the fiber direction, $E_\ell = 134,000$ MPa
 - Modulus along the transverse direction, $E_t = 7,000$ MPa
 - Shear modulus, $G_{\ell t} = 4,200$ MPa
 - Poisson coefficient, $\nu_{\ell t} = 0.25$
- Failure strength:
 - Tension along the longitudinal direction ℓ , $\sigma_{\ell \text{ rupture}}^{\text{tens.}} = 1,270$ MPa
 - Compression along the longitudinal direction ℓ , $\sigma_{\ell \text{ rupture}}^{\text{comp.}} = 1,130$ MPa
 - Tension along the transverse direction t , $\sigma_{t \text{ rupture}}^{\text{tens.}} = 42$ MPa
 - Compression along the transverse direction t , $\sigma_{t \text{ rupture}}^{\text{comp.}} = 141$ MPa
 - Shear strength, $\tau_{\ell t \text{ rupture}} = 63$ MPa

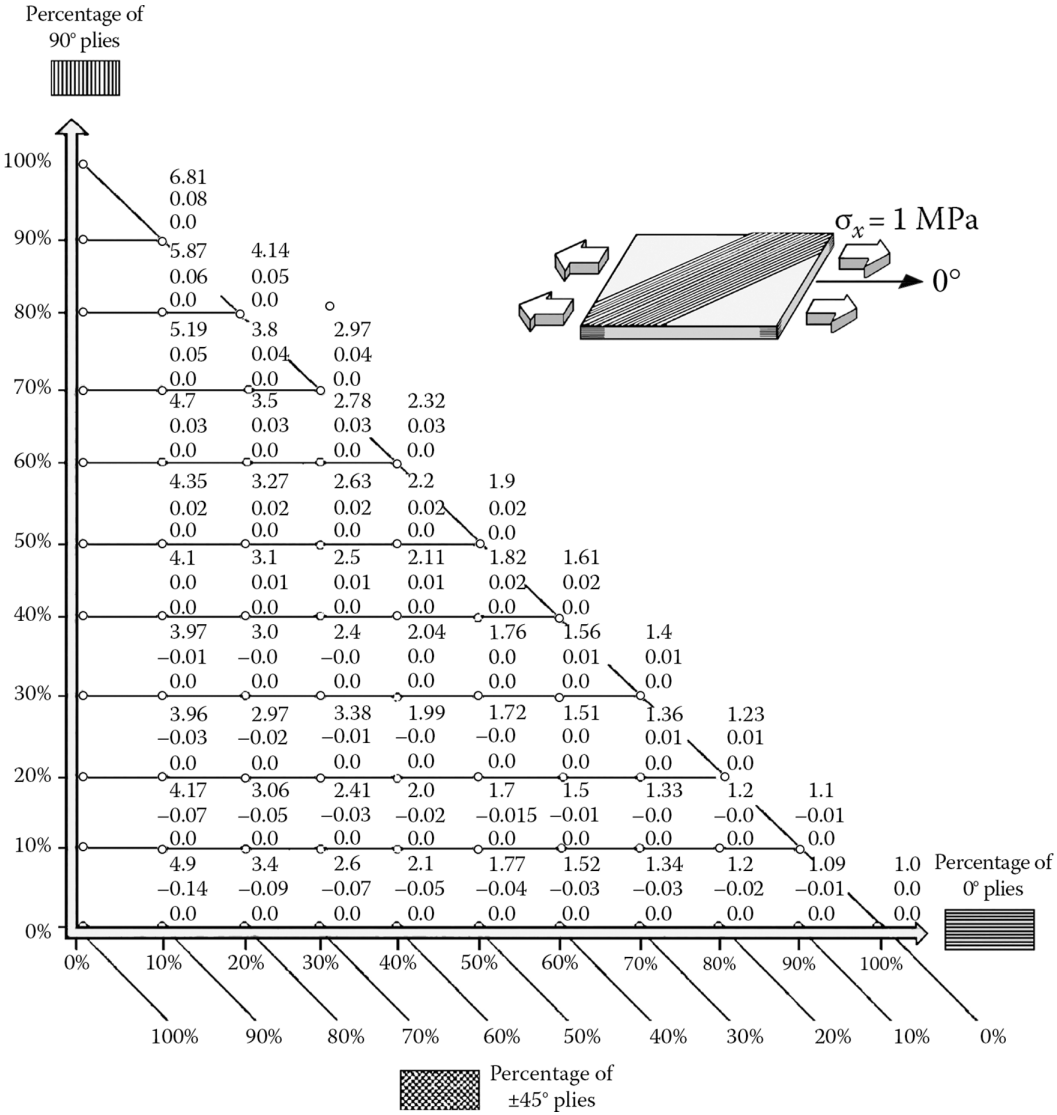


FIGURE A.1 Stresses in 0° plies as functions of the percentage of plies in directions 0°, 90°, +45°, and -45°, for an applied uniaxial stress $\sigma_x = 1 \text{ MPa}$:

$$\begin{cases} \sigma_\ell \\ \sigma_t \\ \tau_{\ell t} \end{cases} \text{ (Mpa)}.$$

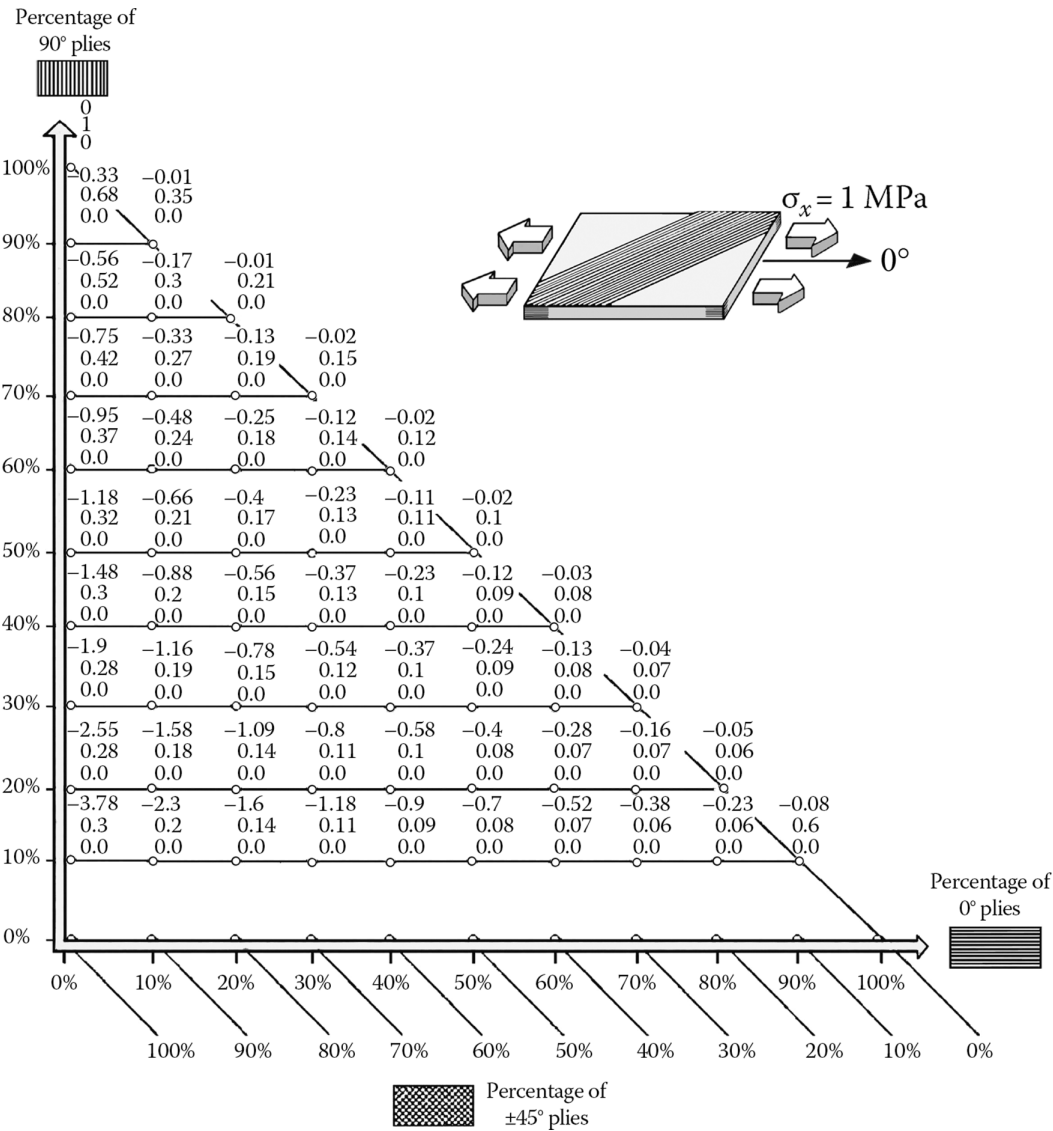


FIGURE A.2 Stresses in 90° plies as functions of the percentage of plies in directions 0°, 90°, +45°, and -45°, for an applied uniaxial stress $\sigma_x = 1 \text{ MPa}$:

$$\begin{cases} \sigma_t \\ \sigma_t \\ \tau_{tt} \end{cases} \text{ (Mpa)}.$$

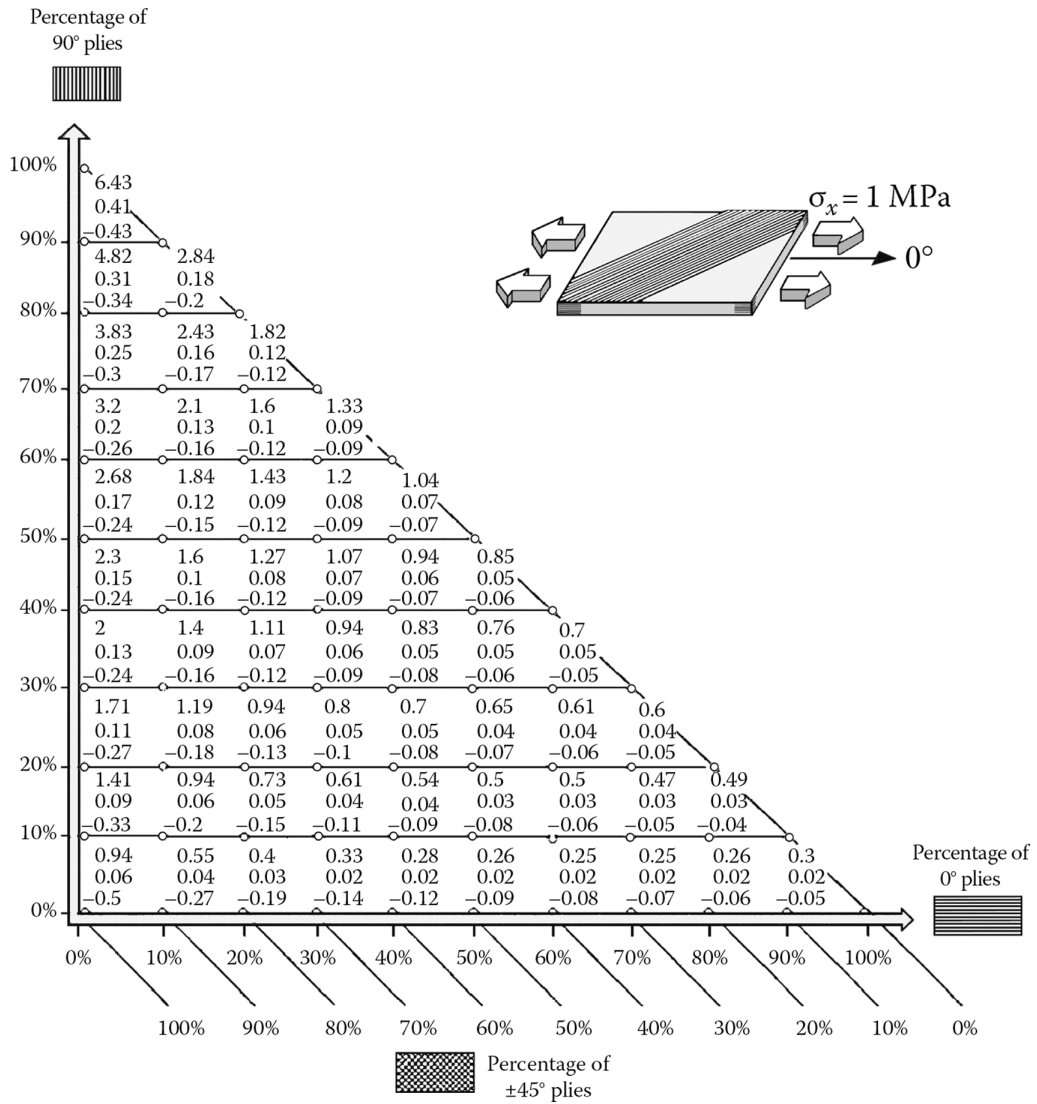


FIGURE A.3 Stresses in +45° plies as functions of the percentage of plies in directions 0°, 90°, +45°, and

−45°, for an applied uniaxial stress $\sigma_x = 1 \text{ MPa}$:

$$\begin{cases} \sigma_\ell \\ \sigma_t \text{ (Mpa)} \\ \tau_{\ell t} \end{cases}$$

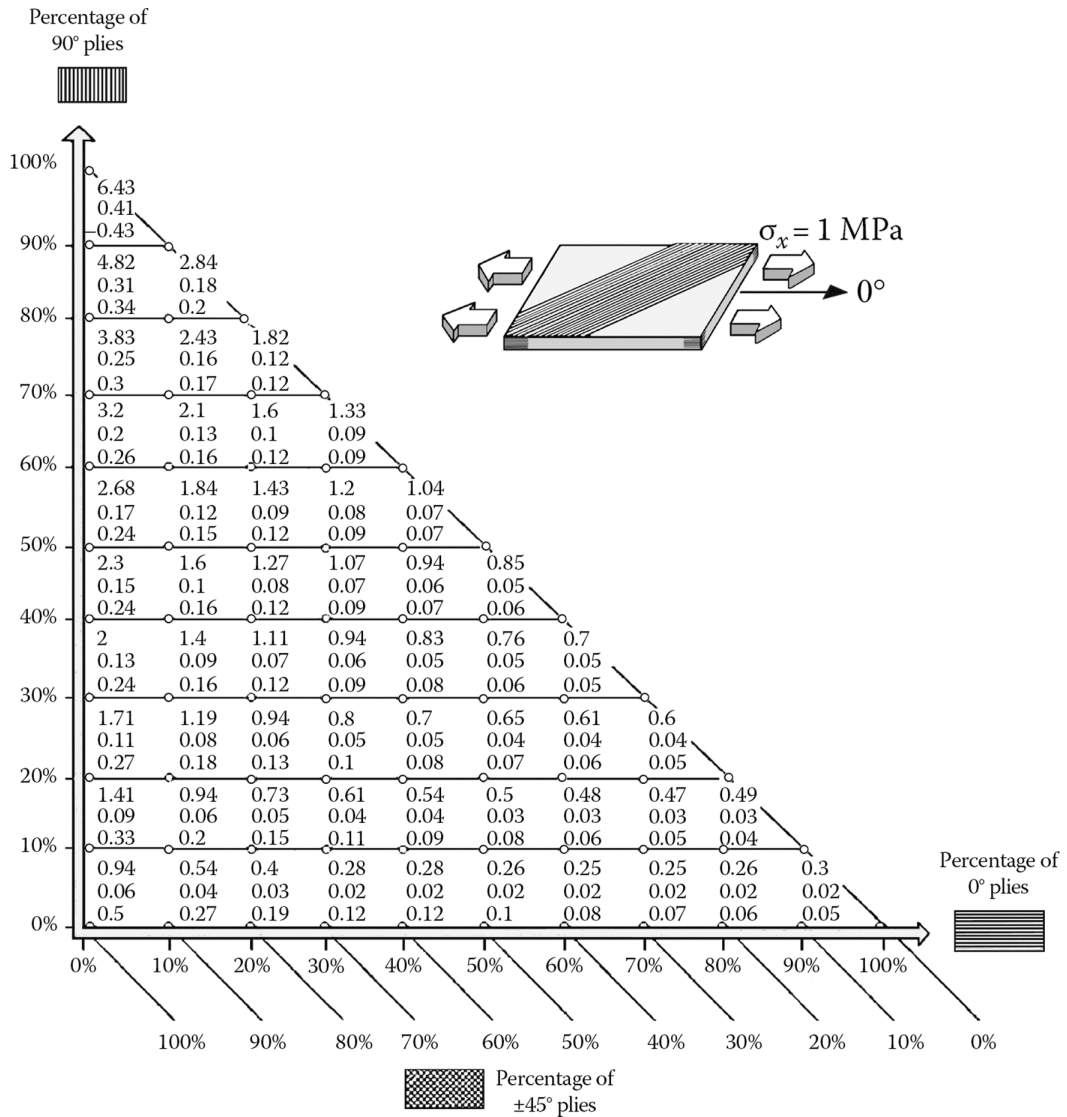


FIGURE A.4 Stresses in -45° plies as functions of the percentage of plies in directions 0° , 90° , $+45^\circ$, and

-45° , for an applied uniaxial stress $\sigma_x = 1 \text{ MPa}$:

$$\begin{cases} \sigma_\ell \\ \sigma_t \text{ (Mpa)} \\ \tau_\alpha \end{cases}$$

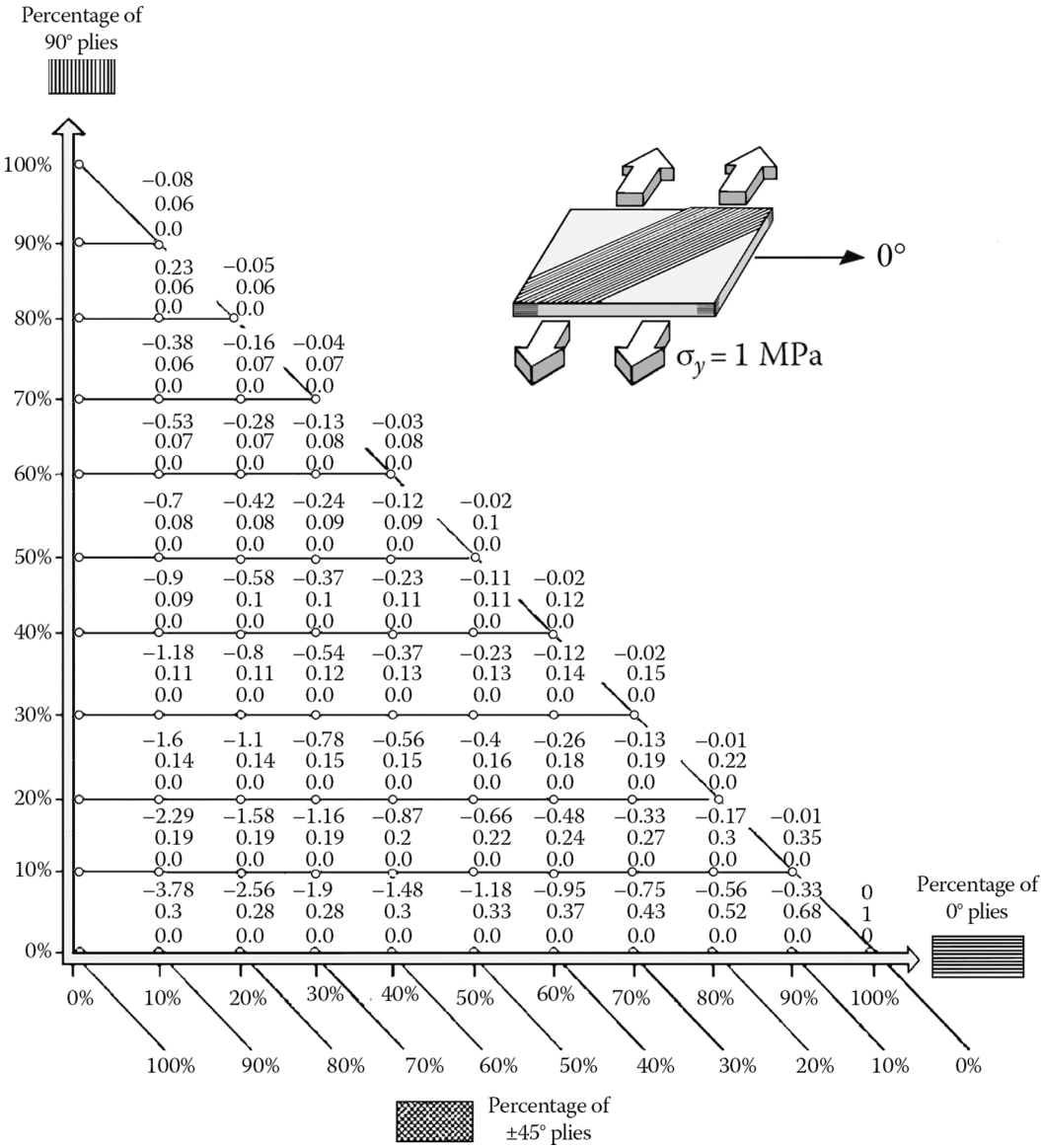


FIGURE A.5 Stresses in 0° plies as functions of the percentage of plies in directions 0°, 90°, +45°, and -45°,

for an applied uniaxial stress $\sigma_y = 1 \text{ MPa}$:

$$\begin{cases} \sigma_\ell \\ \sigma_t \\ \tau_{\ell t} \end{cases} \text{ (Mpa).}$$

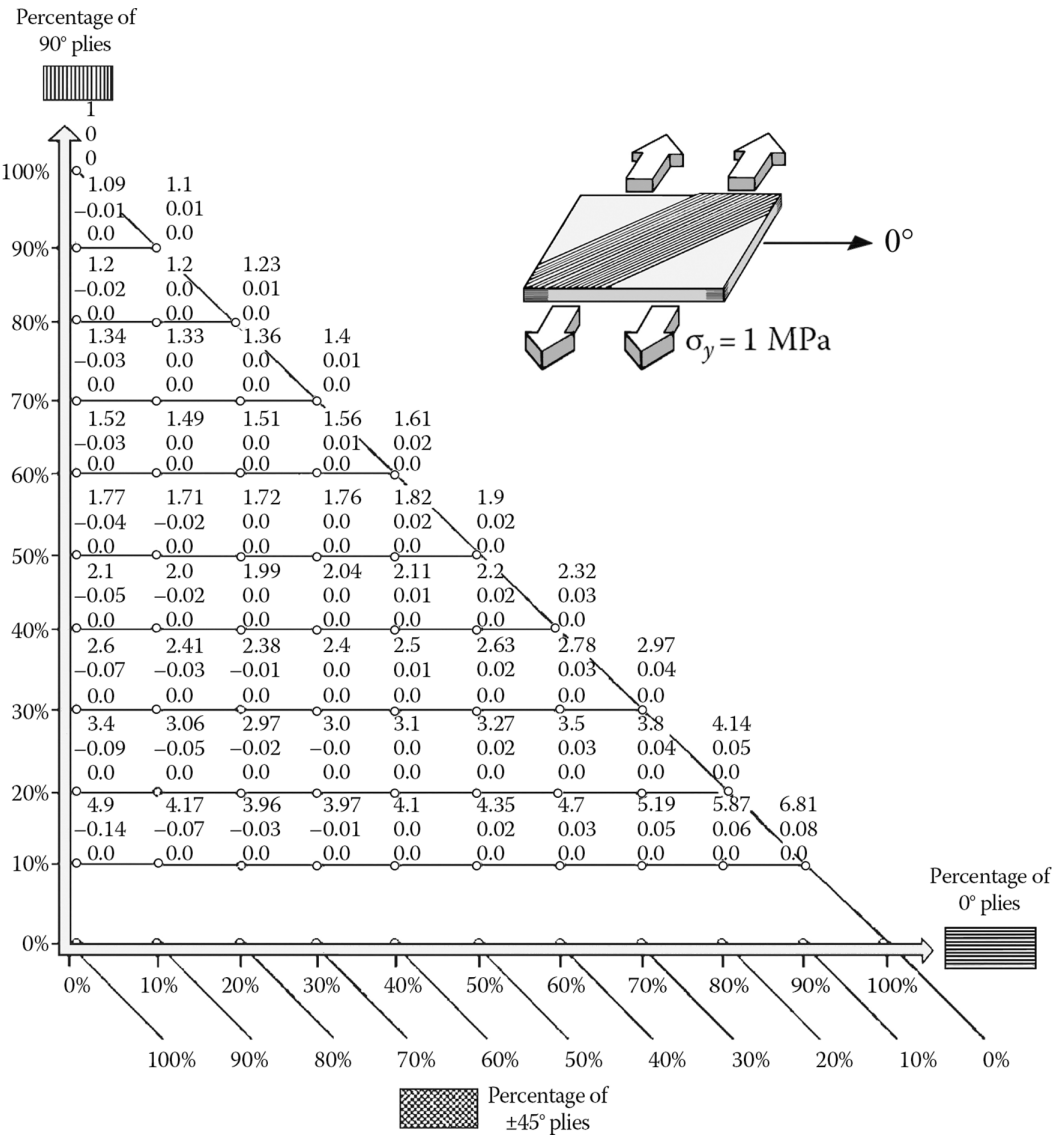


FIGURE A.6 Stresses in 90° plies as functions of the percentage of plies in directions 0°, 90°, +45°, and -45°, for an applied uniaxial stress $\sigma_y = 1 \text{ MPa}$:

$$\begin{cases} \sigma_\ell \\ \sigma_t \text{ (Mpa)} \\ \tau_{\ell t} \end{cases}$$

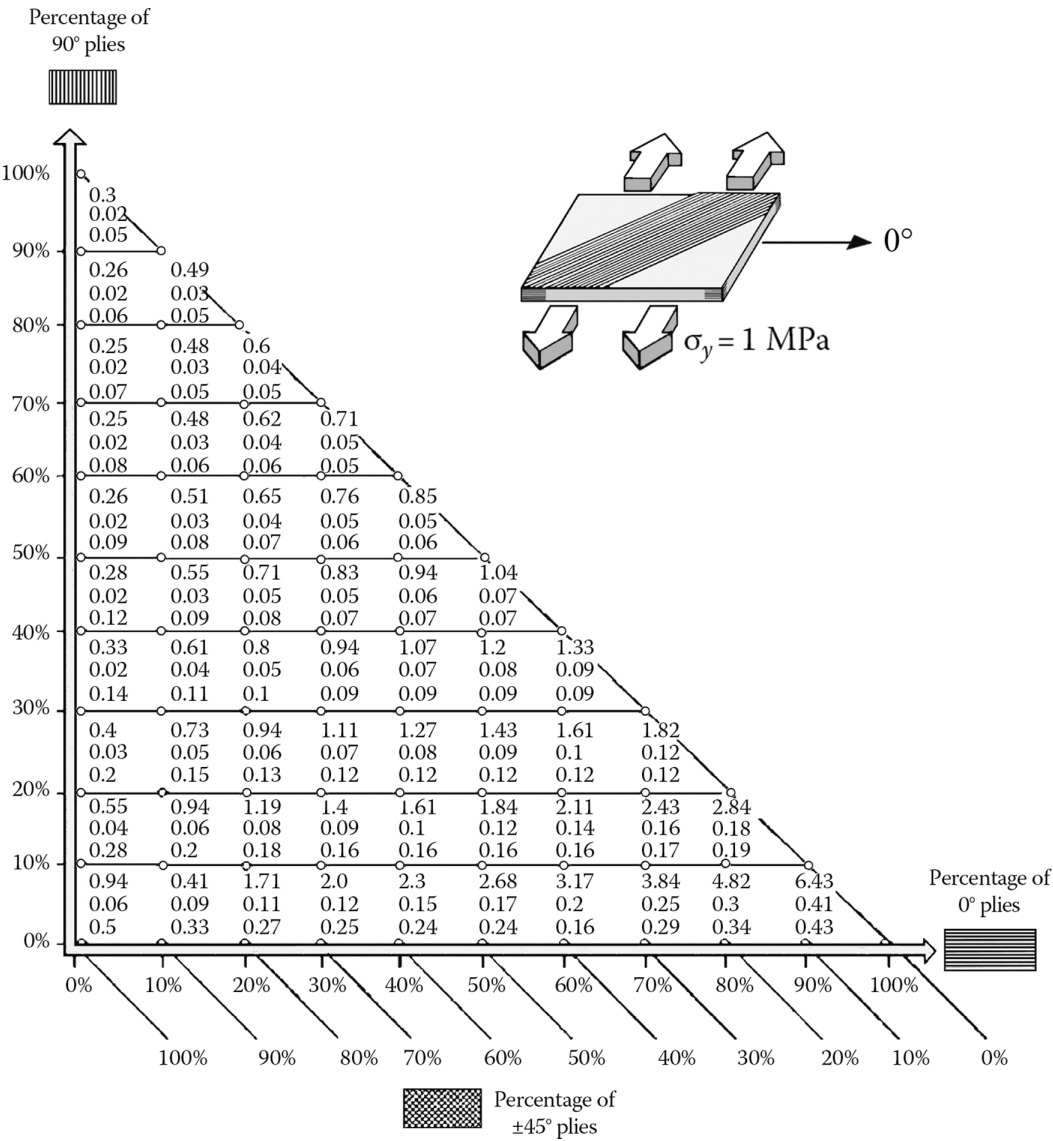


FIGURE A.7 Stresses in +45° plies as functions of the percentage of plies in directions 0°, 90°, +45°, and -45°, for an applied uniaxial stress $\sigma_y = 1 \text{ MPa}$:

$$\begin{cases} \sigma_\ell \\ \sigma_t \\ \tau_{lt} \end{cases} \text{ (Mpa).}$$

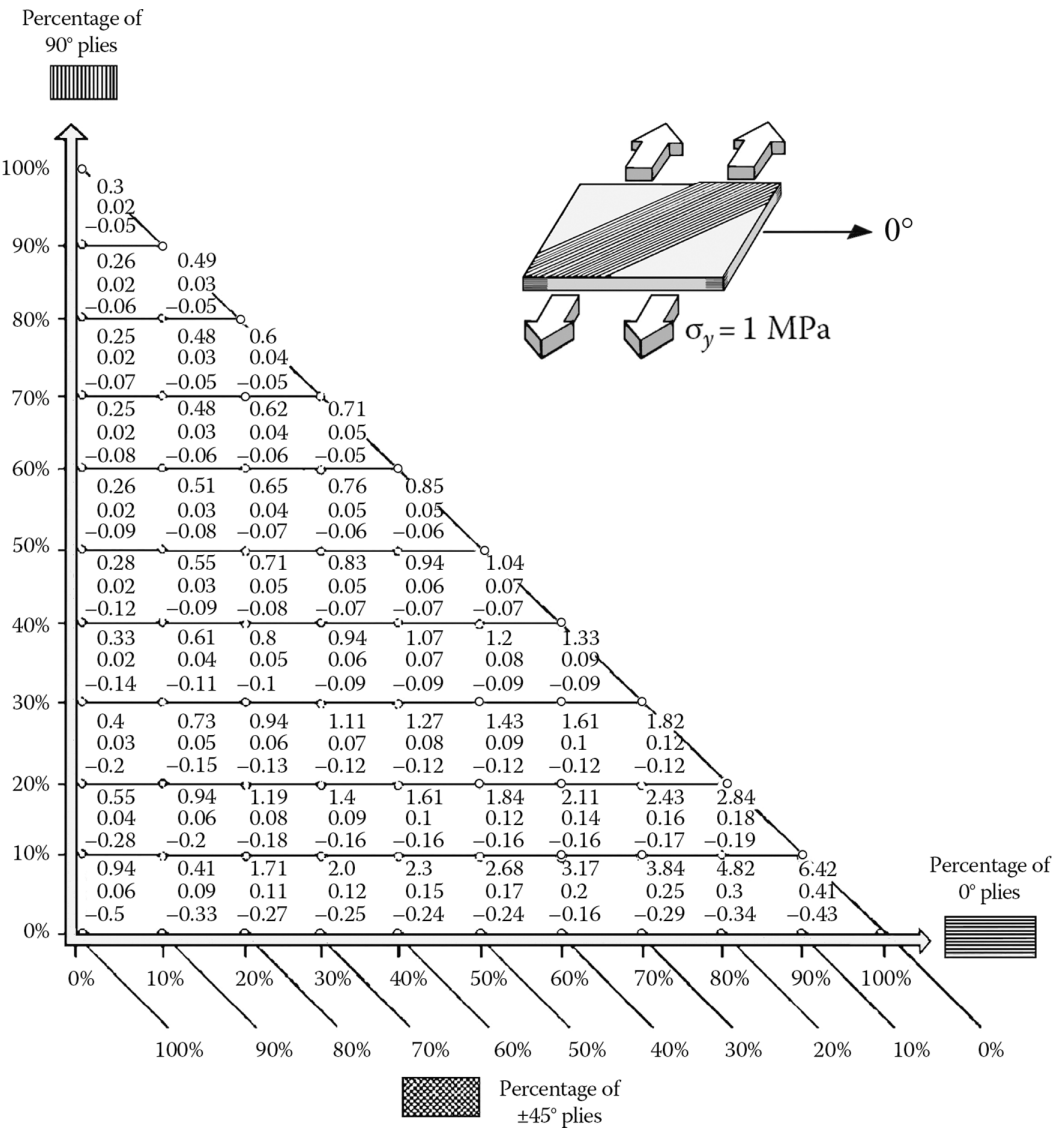


FIGURE A.8 Stresses in -45° plies as functions of the percentage of plies in directions 0° , 90° , $+45^\circ$, and -45° , for an applied uniaxial stress $\sigma_y = 1 \text{ MPa}$:

$$\begin{cases} \sigma_\ell \\ \sigma_t \\ \tau_{lt} \end{cases} \text{ (Mpa).}$$

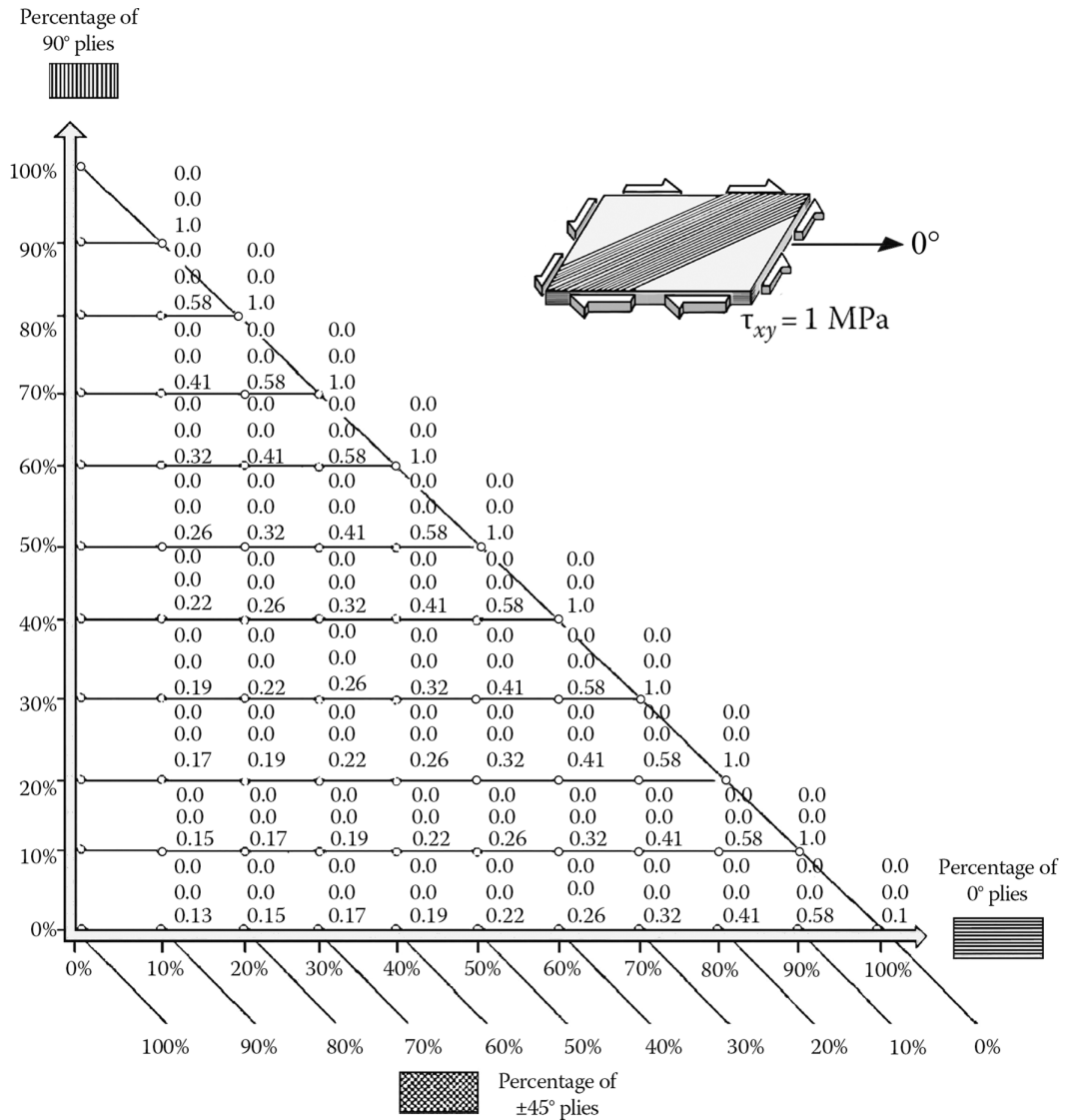


FIGURE A.9 Stresses in 0° plies as functions of the percentage of plies in directions 0°, 90°, +45°, and -45°,

for an applied uniaxial stress $\tau_{xy} = 1 \text{ MPa}$:

$$\begin{cases} \sigma_\ell \\ \sigma_t \text{ (Mpa)} \\ \tau_{\ell t} \end{cases}$$

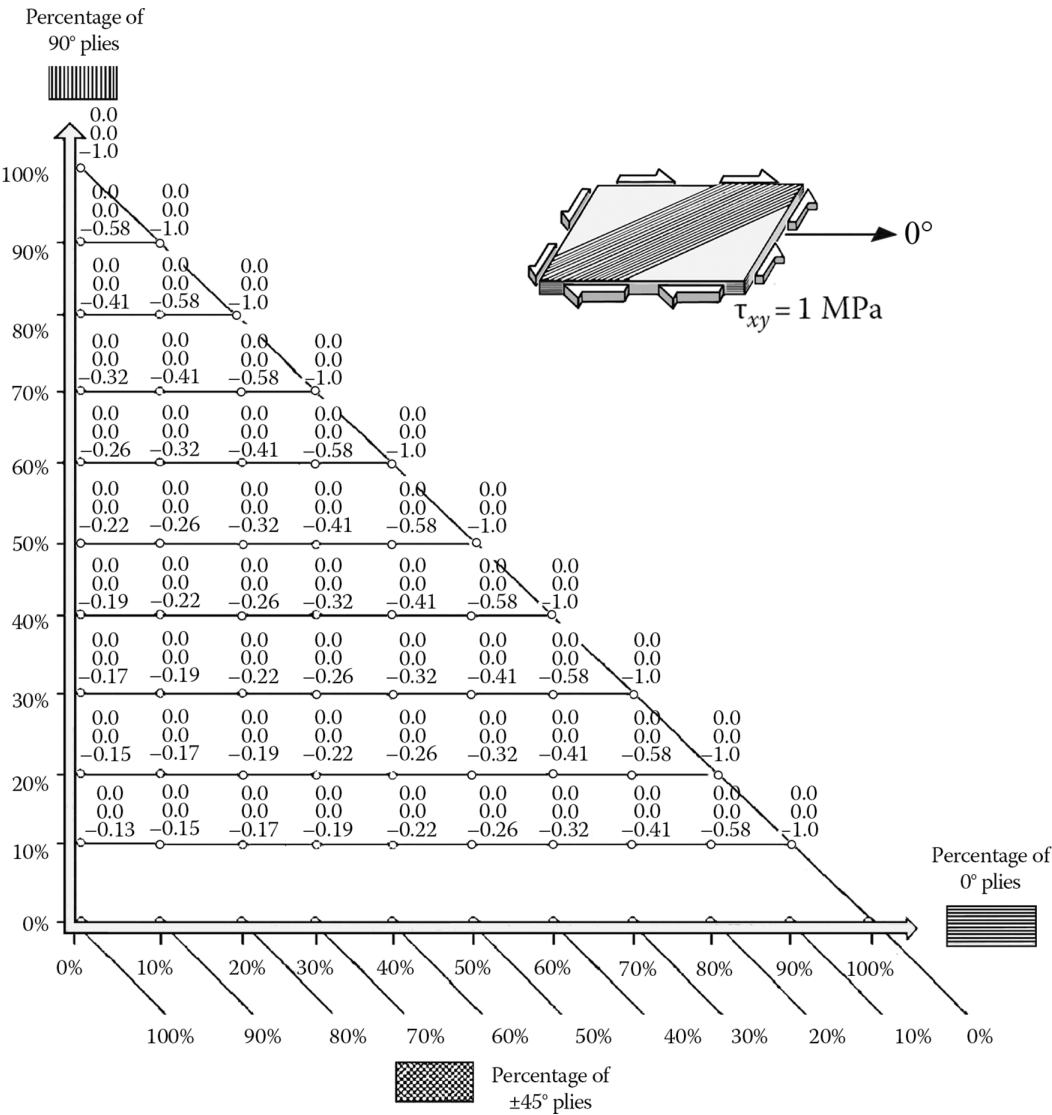


FIGURE A.10 Stresses in 90° plies as functions of the percentage of plies in directions 0°, 90°, +45°, and -45°, for an applied uniaxial stress $\tau_{xy} = 1 \text{ MPa}$:

$$\left\{ \begin{array}{l} \sigma_\ell \\ \sigma_t \text{ (Mpa)} \\ \tau_{lt} \end{array} \right.$$

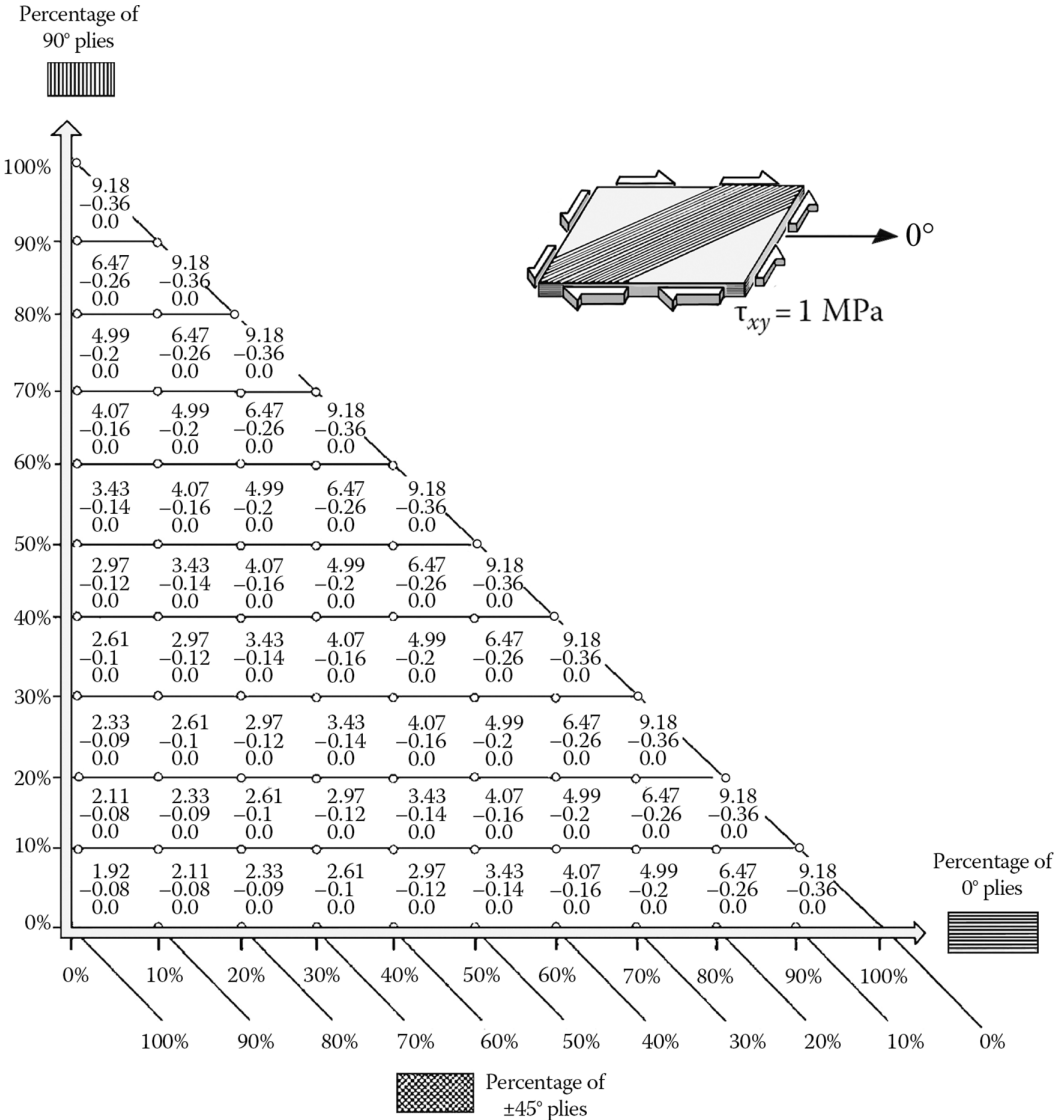


FIGURE A.11 Stresses in +45° plies as functions of the percentage of plies in directions 0°, 90°, +45°, and

−45°, for an applied uniaxial stress $\tau_{xy} = 1 \text{ MPa}$:

$$\left\{ \begin{array}{l} \sigma_{\ell} \\ \sigma_t \\ \tau_{\ell t} \end{array} \right\} \text{ (Mpa)}.$$

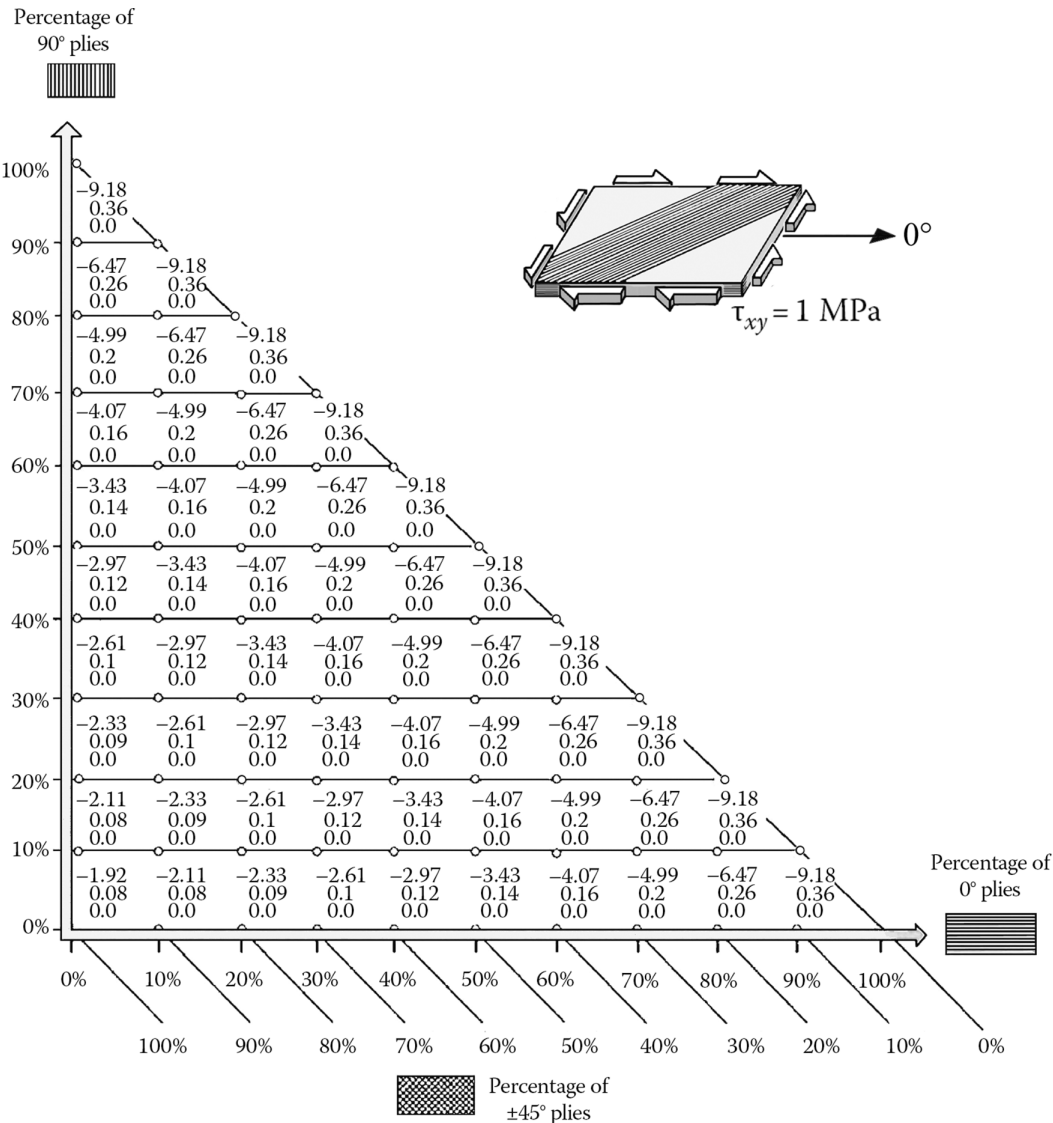


FIGURE A.12 Stresses in -45° plies as functions of the percentage of plies in directions 0° , 90° , $+45^\circ$, and -45° , for an applied uniaxial stress $\tau_{xy} = 1 \text{ MPa}$:

$$\left\{ \begin{array}{l} \sigma_\ell \\ \sigma_t \\ \tau_{\ell t} \end{array} \right\} \text{ (Mpa)}.$$



Taylor & Francis

Taylor & Francis Group

<http://taylorandfrancis.com>

Appendix B

Buckling of Orthotropic Structures

The stability of orthotropic plates and shells is not treated in this book. However, in what follows, we give the way to estimate the magnitude order of loads that can lead to buckling due to compression or shear in orthotropic panels and tubes.

B.1 BUCKLING OF RECTANGULAR PANELS¹

Figures B.1–B.6 allow calculating the critical **In-plane resultants**² in compression and in shear for different support conditions.

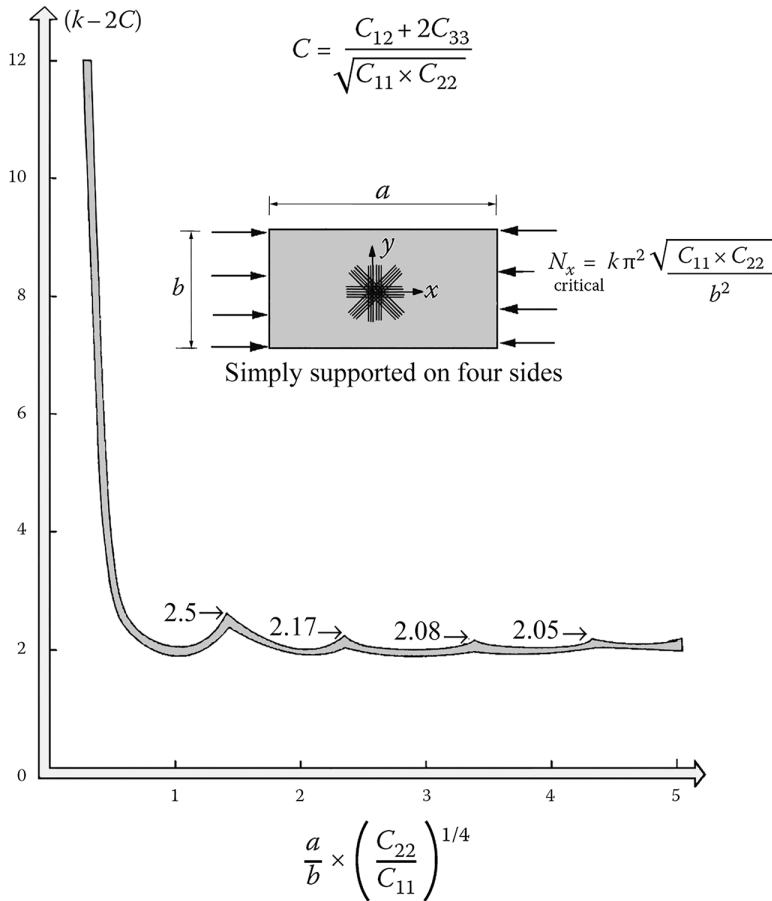


FIGURE B.1 Buckling of a rectangular panel under In-plane loading simply supported on four sides.

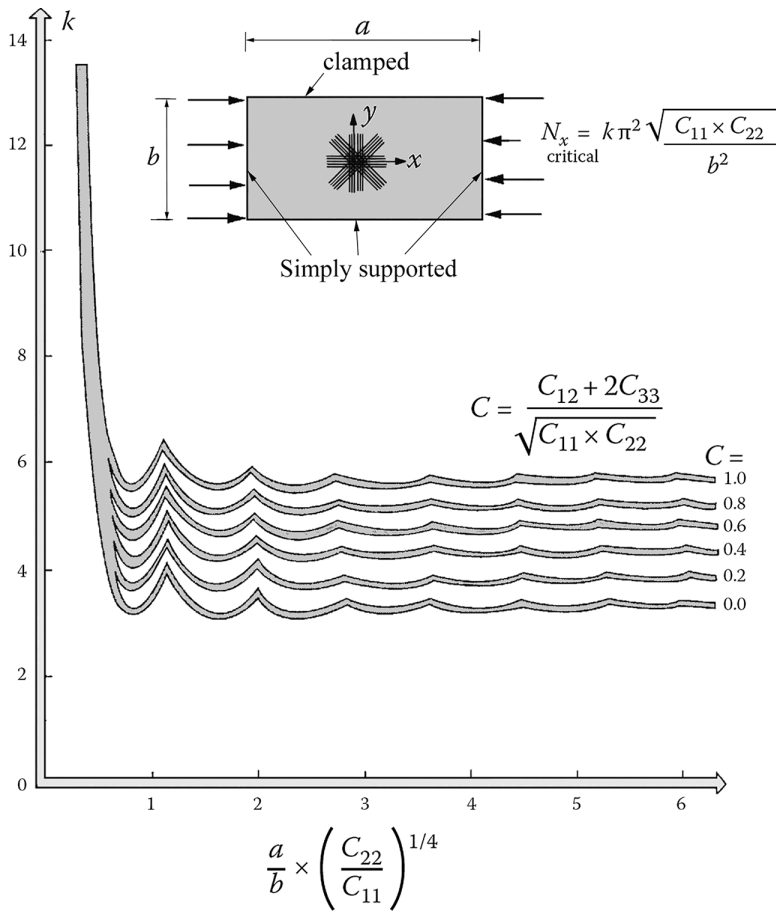


FIGURE B.2 Buckling of a rectangular panel under In-plane loading simply supported on three sides and clamped on the fourth side.

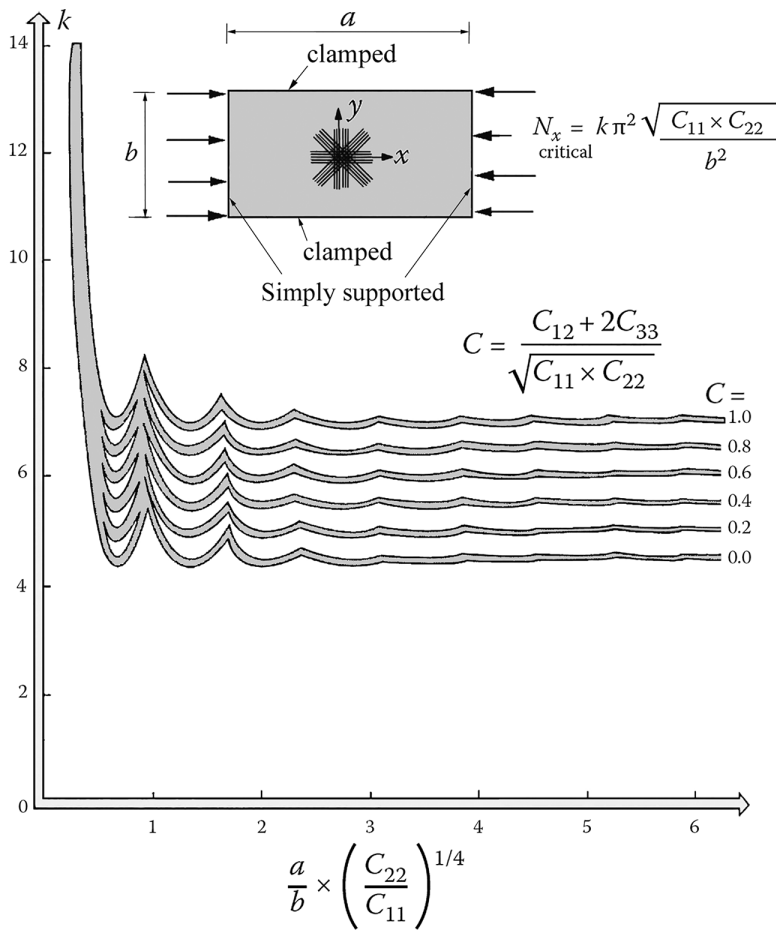


FIGURE B.3 Buckling of a rectangular panel under In-plane loading simply supported on two sides and clamped on the other two sides.

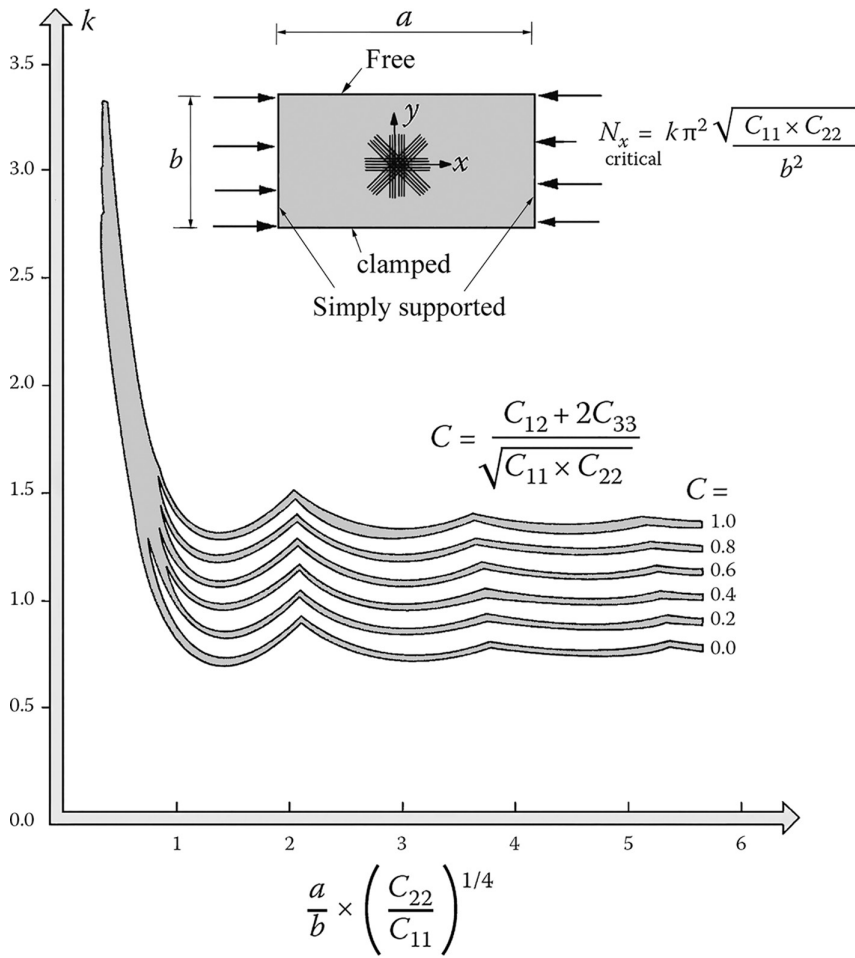


FIGURE B.4 Buckling of a rectangular panel under In-plane loading simply supported on two opposite sides, clamped on the third side, and free on the fourth side.

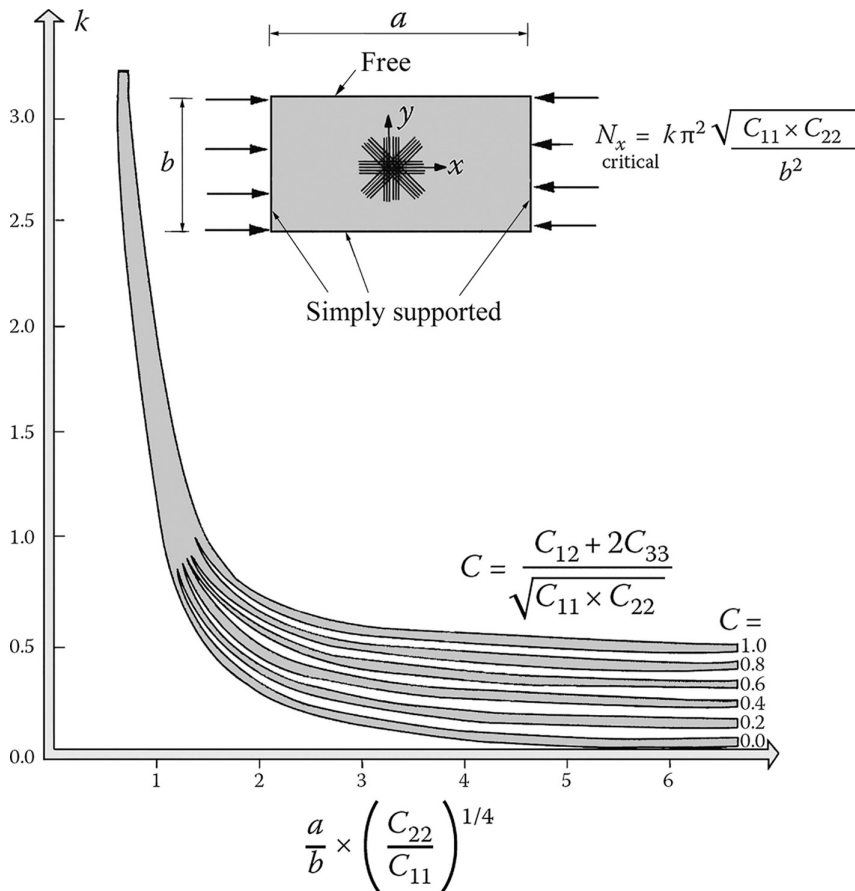


FIGURE B.5 Buckling of a rectangular panel under In-plane loading simply supported on three sides and free on the fourth side.

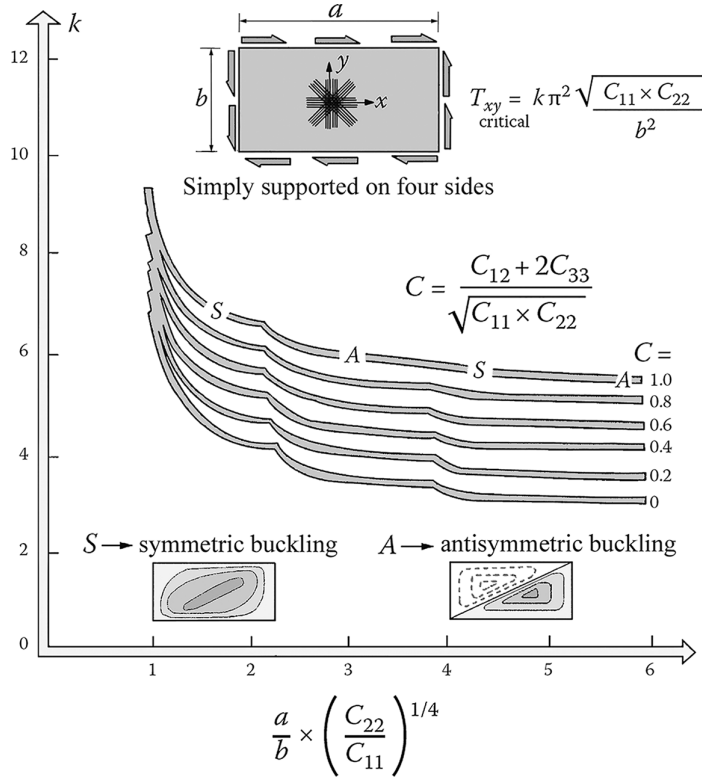


FIGURE B.6 Buckling of a rectangular panel under In-plane shear simply supported on four sides.

B.2 BUCKLING OF ORTHOTROPIC TUBES

- **Buckling in bending, giving rise to ovalization of the thin tube** (Figure B.7)
Bending leads to ovalization of the cross section. Then the moment of inertia for bending that contributes to the bending stiffness decreases, leading to the unstable process. The phenomenon is known as the **Brazier effect**.

$$M_{\text{critical bending}} = \frac{2\sqrt{2}}{9} \pi r_o e^2 \left[\frac{E_x \times E_y}{1 - \nu_{xy} \nu_{yx}} \right]^{1/2}$$

- **Buckling due to external pressure**

The notations in Figure B.7 are kept. L is the length of the tube making the container that is subject to buckling:

$$p_{\text{critical}} = 0.83 \times \frac{E_y}{\left(1 - 0.1 \frac{E_x}{E_y} \right)} \times \left(\frac{E_x}{E_y} \right)^{1/4} \times \frac{r_o}{L} \times \left(\frac{e}{r_o} \right)^{5/2}$$

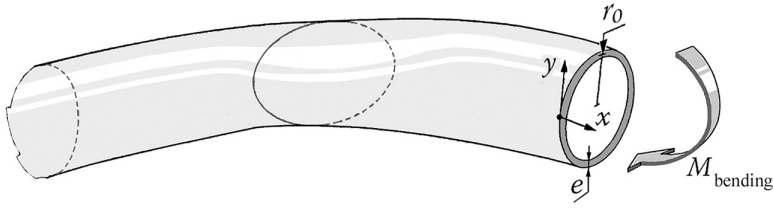


FIGURE B.7 Flexural buckling of a thin-walled orthotropic tube.

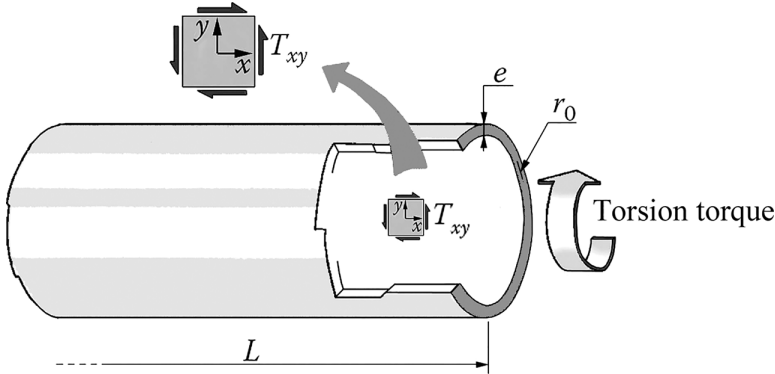


FIGURE B.8 Torsion of a thin-walled orthotropic tube.

- **Buckling due to torsion** (Figure B.8)

The critical shear resultant in torsion is given by

$$T_{xy}^{\text{critical}} = \frac{\pi^2}{12} \left[\frac{e^9}{r_o^3 L^2} \right]^{1/4} \times \left[\frac{E_x^3 E_y^5}{(1 - \nu_{xy} \nu_{yx})^5} \right]^{1/8}$$

- **Buckling due to axial compression**

This aspect is not considered here, because the occurrence of elastic instability is strongly influenced by the geometry defects in the orthotropic cylinder.

NOTES

- 1 See Bibliography “Brunnelle and Oyibo”.
- 2 See Section 5.2.4 or 12.1.1 for the definition of these stress resultants. See in Equation 12.16 the definition of constants C_{11} , C_{22} , C_{12} , and C_{33} that appear in the figures.



Taylor & Francis

Taylor & Francis Group

<http://taylorandfrancis.com>

Bibliography

- Alain G., Nicola P., *Les Composites dans l'Industrie Automobile*, Techniques de l'Ingénieur, Paris, France, April 2011.
- Appert D., Gallet C., *Les Matériaux Polymères et le Secteur du Transport*, Allize-Plasturgie.Org, Plastilien, 72, November 2010.
- Arteiro A., et al., *A case of Tsaï modulus, an invariant-based approach to stiffness*, Composite Structures, 252, November 2020.
- Barbe J., *Structures Coques. Equations Générales et Stabilité*, ENSAE, Toulouse, France, 1983.
- Barrau J.-J., Chambard O., Nuc M., Gay D., *Homogénéisation en Torsion d'une Poutre Composite*, Tendances Actuelles en Calcul des Structures, Bastia, France, 1985.
- Bathias C., Menkes D., *Comptes-Rendus des Cinquièmes Journées Nationales sur les Composites*, Editions Pluralis, Paris, France, 1986.
- Benedict A.V., *An Experimental Investigation of GLARE and Restructured Fiber Metal Laminates*, Embry-Riddle Aeronautical University, Daytona Beach, 2012.
- Berreuer L., Maillard (de) B., Nösperger S., *L'Industrie Française des Matériaux Composites*, DIGITIP/Ministère de l'Economie, des Finances et de l'Industrie, Paris, France, May 2002.
- Bigwood D.A., Grocombe A.D., *Elastic analysis and engineering design formulae for bonded joints*, International Journal of Adhesion and Adhesive, 9(4), 229–242, October 1989.
- Binétruy C., *Structures Sandwiches*, Techniques de l'Ingénieur, Paris, France, October 2008.
- Brunnelle E.J., Oyibo G.A., *Generic buckling curves for specially orthotropic rectangular plates*, AIAA Journal, 21(8), 1150–1154, August 1983.
- CARMA (Regional Activity Center in Advanced Materials), *Glossaire des Matériaux Composites Renforcés par des Fibres d'Origine Renouvelable*, December 2006.
- Ceramic Matrix Composites Market, R-Reports and Data, 2019.
- Chen X., Dupas C., Briand M., Veillet F., Vroman P., Koehl L., *Elaboration d'un Composite Sandwich à Base de Nappes de Chanvre et de Polyuréthane*, ENSAIT, Roubaix, France, 2006.
- Chevalier Y., *Plastiques et Composites*, Techniques de l'Ingénieur, Paris, France, 1989.
- Chrétien G., *Matériaux Composites à Matrice organique*, Technique et Documentation, Lavoisier, Paris, France, 1986.
- Collectif, *Matériaux Composites*, Technea, Marseille, France, 1989.
- Dong L., Blachut J., *Analysis and collapse of thick composite torispheres*, Journal of Process Mechanical Engineering, 212, 103–117, 1998.
- Duquesne J.L., Gonzales M., *Conception et Dimensionnement du Volet Extérieur en Fibres de Carbone du CN235*, ENSICA, Toulouse, France, June 1990.
- Echalier B., Bleut P., Lefebvre F., Tournut C., *Conduites PVDF Renforcées. Contraintes Thermiques et Mécanismes de Rupture*, Composites, 3, 183–188, May/June 1987.
- Editions Pluralis, *Comptes Rendus des Quatrièmes Journées Nationales sur les Composites, 4th JNC-AMAC*, Paris, France, September 1984.
- Faccio R., Fernández-Werner L., Pardo H., Goyenola C., Denis P.A., Mombrú Á.W., *Mechanical and electronic properties of graphene nanostructures*, Physics and Applications of Graphene—Theory, S.A. Mikhailov ed., InTech, Rijeka, Croatia, Chapter 17, pp. 349–366, March 2011.
- Fauner G., Hendlich W., *Manuel des Techniques de Collage*, Editions Soproge S.A., Paris, France, 1984.
- Forcier L.-C., *Conception d'une Pale d'Eolienne de Grande Envergure à l'aide de Techniques d'Optimisation Structurale*, Ecole de Technologie Supérieure, Université du Québec, Montréal, Québec, Canada, September 2010.
- Gallet C., *Les Nanomatériaux: Applications et Perspectives*, Séminaire Nanomatériaux et Nanocomposites: Enjeux et Nouvelles Opportunités pour l'Industrie, Ecole des Mines d'Alès, France, January 2009.
- Gamski C., *Structures Sandwiches*, Techniques de l'Ingénieur, Paris, France, February 1981.
- Gay D., *Transverse Shear Deformation in Bending of Composite Beams of Any Cross Section Shapes*, Mechanics of Structured Media, Part B, pp. 155–171, Elsevier Scientific Publishing Company, Amsterdam, the Netherlands, 1981.
- Gay D., Gambelin J., *Modeling and Dimensioning of Structures*, ISTE Ltd, London; John Wiley & Sons, Inc., Hoboken, NJ, 2008.

- Gay D., Joubert F., *Isotropie de Rigidité et Quasi-isotropie de Resistance des Stratifiés à Orientations Périodiques*, Revue des Composites et des Matériaux Avancés, 4(2), 241–261, 1994.
- Gazeau Y., *Mutation Automobile/Evolutions et Révolutions dans les Matériaux*, Institut Automobile du Mans, Le Mans, France, February 2011.
- Geier M., Duedal D., *Guide Pratique des Matériaux Composites*, Technique et Documentation, Lavoisier, Paris, France, 1985.
- Goncourt (de) L., Sayers K.H., *Les Systèmes Ressort-Composites*, Composites, 3, 145–150, May/June 1988.
- Guibert M.P., *Fabrication des Avions et des Missiles*, Dunod, Paris, France, 1960.
- Guigon M., Kloster A., *Phénomènes Inter faciaux dans les Composites à Matrice Thermoplastique*, Annales des Composites, 1–2, 83–90, 1989.
- Nouailhas H., Saint-Macary L., Fulcrand H., Bergeret A., Caillol S., *Développement de Biocomposites en Résine Epoxy Bio-sourcée/Fibres de Lin par Pultrusion pour la Construction*, Comptes Rendus des JNC 17, Poitiers, France, June 2011.
- Hellard G., *Résistance des Constructions/Matériaux Composites*, ENSICA, Toulouse, France, 1983.
- Hellard G., Hilaire G., Torres M., *Les Applications des Composites dans le Domaine Aéronautique*, Publication “Aérospatiale”, 1985.
- Hellard G., Lafon P., *Les Matériaux Composites*, Conference, Toulouse, France, December 1984.
- Hintona M.J., Kaddourb A.S., Sodenc P.D., *World-wide failure exercise, a comparison of the predictive capabilities of current failure theories for composite laminates, judged against experimental evidence*, Composites Science and Technology, 62, 1725–1797, 2002.
- Jardon A., Costes M., *Composites de Grande Diffusion*, European Conference on Composites Materials, London, July 1987.
- JEC, *Overview of the Worldwide Composites Industry: 2010–2015, 2011 release*, Paris, France, March 2011.
- Johnson W.S., *Impact and residual fatigue behavior of ARALL*, Advances in Composite Materials and Structures, ASME-AMD 82, 9–14, 1989.
- Joubert F., Harry R., *Calcul des Structures en Matériaux Composites*, CODEMAC, Bordeaux, France, 1985.
- Kaufman E.D., *Fibres de Carbone revêtues de Nickel*, Composites, 3, May/June 1988.
- Keppel E., *D-D Laminates and Manufacturing*, Composites Design Workshop XXII, Dpt of Aeronautics and Astronautics, Stanford University, Ca, January 24–27, 2022.
- Kleinholz R., Molinier G., *Fibres de Verre, d'Aramide, de Carbone, des Renforts sur Mesure pour Composites*, Revue Vetrotex, 59, 1986.
- Krawczak P., *Recyclage des Composites*, Techniques de l'Ingénieur, AM5895 v1, jul.2011.
- Lamicq P., *Matériaux et Structures Composites ou l'Adaptation aux Besoins*, 7ème Congrès Français de Mécanique, Bordeaux, France, 1985.
- Lamy B., Pomel C., *Composites Renforcés par des Fibres de Lin*, Ecole Centrale, Nantes, France, 2003.
- Laroche M., *Foreseen Evolutions for Major Aircraft Equipments*, Forum for Aerospace Innovation, Toulouse, France, November 2010.
- Lee C., Wei X., Li Q., Carpick R., Kysar J. W., Hone J., *Elastic and Frictional Properties of Graphene*, Physica Status Solidi B, 246 (11–12), 2562–2567, 2009.
- Lévêque J., *Les Fibres Composites d'Origine Naturelle*, Rencontres Technologiques Matériaux Innovants et Procédés Associés, ISITV, Toulon, France, September 2006.
- Li H., He D., Li T., Genestoux M., Bai J., *Chemical kinetics of catalytic chemical vapor deposition of an acetylene/xylene mixture for improve carbon nanotube production*, Carbon, 48(15), 4330–4342, December 2010.
- Maeder G., *Les Nouveaux Matériaux dans la Mécanique Automobile*, INIST, C&T, 25, 161–166, 1992.
- Maeder G., *De la Difficulté d'introduire des Polymères et Composites dans l'Industrie Automobile*, Colloque National MECAMAT, Aussois, France, January 2008.
- Manera M., Massot J.J., Morel G., Verchery G., *Manuel de Calcul des Composites Verre/Résine*, Editions Pluralis, Paris, France, 1988.
- Manocha L.M., Valand J., Patel N., Varrier A., Manocha S., *Nanocomposites for structural applications*, Indian Journal of Pure and Applied Physics, 44, 135–142, February 2006.
- Manufacturers documentation 1980s and notably VETROTEX News, Dynastar, Aspects of Resins Ciba-Geigy, Dassault-Breguet Information, Aerospace Information.
- Markets and Markets: *Ceramic Matrix Composites Market - Global Forecast to 2029*.
- Marty D., *Conception des Véhicules Spatiaux*, Masson, Paris, France, 1986.
- Massard T., Tsai S.W., Cognet M., Vermes B., *Think Composites*, www.think-composites.com 2021.
- Matheron G., *Progiciels de Calcul de Structures Composites. Exemples de Référence et de Validation (Computer Programs for Composite Structures: Reference Examples for Validation)*, Editions Hermès, Paris, France, 1995.

- Michaud F., *Rhéologie de Panneaux Composites Bois/Thermoplastiques sous Chargement Thermomécanique: Aptitude au Post formage*, Thesis, Université de Laval et Université de Bordeaux 1, France, December 2003.
- Michel R., *Les Composites Aéronautiques 40 ans déjà et ce n'est qu'un début*, Colloque Composite, 48, Toulouse, France, October 2007.
- Naslain R., *Introduction aux Matériaux Composites*, t. 2, *Matrices Métalliques et Céramiques*, Editions du CNRS et de l'Institut des Matériaux Composites, Bordeaux, France, 1985.
- Nettles Alan T. (NASA Marshall Space Flight Center, MSFC, AL); Nelson Jared W. (Keene State College, Keene, NH), *Mechanical Testing of Composites*, Composites Design Workshop XX, Stanford University, January 2021.
- Nouri T., Gay D., *Shear stresses in orthotropic beams*, International Journal of Engineering Science, 32(10), 1647–1667, 1994.
- Odru P., Sparks C., Schmitt J., Fuch J.F., *Conception et Essais de tubes composites Hautes performances*, Matériaux-Mécanique-Electricité, 433, 4–6, February/March 1990.
- Pfletschinger E., *Développement d'une Nouvelle Technologie pour fabriquer des Poteaux*, Composites, 3, 67–72, May/June 1987.
- Pomel C., Baley C., Lamy B., *Influence de Prétraitements et Traitements Chimiques sur l'Adhérence Fibre de Lin/Résine Thermodurcissable Polyester*, XVème Congrès Français de Mécanique, Nancy, France, September 2001.
- Pouteau C., *Quelles Avancées pour les Composites à Fibres Naturelles?* Colloque Chanvre, Conference on Hemp, Poitiers, France, March 2010.
- Publications of the specialized press: Air et Cosmos, Aviation Magazine, Ça m'intéresse, Science et Vie, L'Aéronautique et l'Astronautique. Websites: Vers le Nano Monde, National Research Council of Canada, The Carbon Nanotube Specialist, High Magnetic Field Laboratory, Technology Transfer and Innovative Know-how in Languedoc-Roussillon, etc.
- Rafiee M.A., Rafiee J., Wang Z., Song H., Yu Z.-Z., Koratkar N., *Enhanced mechanical properties of nano-composites at low graphene content*, ACS Nano, 3(12), 3884–3890, 2009.
- Reyne M., *Comment Utiliser au Meilleur Coût les Matériaux Composites*, Editions de l'Usine Nouvelle, Paris, France, 1986.
- Reyne M., *Les Plastiques*, Editions Hermès, Paris, France, 1990a.
- Reyne M., *Technologie des Composites*, Editions Hermès, Paris, France, 1990b.
- Reyne M., *Les Composites*, Presses Universitaires de France, Paris, France, 1995.
- Riley V.R., *Interaction effects in fibre composites*, Polymer Conference Series, University of Utah, June 1990.
- Rouchon J., *Matériaux Composites pour Structures d'Aéronefs*, ENSICA, Toulouse, France, 1980.
- Sanders H., Jena A., *A New Technique Provides Faster Particle Size Analysis at a Lower Cost Compared to Conventional Methods*, Porous Material Inc., Ithaca, NY.
- Sang Y.P., Won J.C., *The Guidelines of Material Design and Process Control on Hybrid Fiber Metal Laminate for Aircraft Structures*, Optimum Composite Structures, IntechOpen. Jan. 2019.
- Sato N., Kurauchi T., Sato S., Kamigaito O., *Microfailure behavior of randomly dispersed short fibre reinforced thermoplastic composites obtained by direct SEM observation*, Journal of Materials Science, 26(14), 3891–3898, 1991.
- Scott B.J., *Mechanical and Electrical Properties of Graphene Sheets*, Thesis, Cornell University, Ithaca, NY, May 2008.
- Sedan D., Pagnoux C., Smith A., Chotard T., *Propriétés Mécaniques de Matériaux Enchevêtrés à Base de Fibre de Chanvre et Matrice Cimentaire*, 18ème Congrès Français de Mécanique, Grenoble, France, 2007.
- Sporn D., Heiko S., Jurgen C., Herborn R., *Polymers for Ceramic Fibers in the System Si-B-N-C—From Laboratory Scale to a Pilot Plant*, Proceedings of the Second WING Conference, Aachen, Germany, 2005.
- Sullins R.T., Smith G.W., Spier E.E., *Manual for Structural Stability Analysis of Sandwich Plates and Shells*, NASA Report CR 1457, Washington, DC, December 1969.
- Sun C.T., Quinn B.J., Tao J., Oplinger D.W., *Comparative Evaluation of Failure Analysis Methods for Composite Laminates*, D0T/FAA/AR-95/109, Office of Aviation Research, Washington, DC, May 1996.
- Tanghe-Carrier F., *Etude des Effets Secondaires en Flexion-Torsion Dynamique à Gauchissement Nonuniforme dans les Poutres Composites à Phases Orthotropes Quelconques*, Thesis, Université Paul Sabatier-Toulouse III, France, December 1999.
- Tanghe-Carrier F., Gay D., *Non-uniform torsion of orthotropic composite beams*, Archive of Applied Mechanics, 99, 70, 635–648, October 2000.

- Temblador Y., *Analyse et Comportement des Reparations dans les Structures Composites Endommagées par un Trou Non Circulaire*, Thèse, Université Paul Sabatier Toulouse III, Toulouse, France, December 1998.
- Thévenin R., *Airbus Composite Maintenance & Repairs Validations*, FAA Workshop for Composite Damage Tolerance and Maintenance, Airbus, Chicago, IL, 2006.
- Thiele G., Poston M., Brown R., *A Case Study in Sizing Nanoparticles*, Micromeritics Analytical Services, MVA Scientific Consultants, Duluth, GA.
- Trovalet M., *Sur un Modèle Micro pour le Calcul des Structures en Composites Stratifiés*, Thesis, ENS Cachan, Cachan, France, March 2010.
- Tsai S.W., *Double-double: New family of composite lamina*, AIAA JOURNAL, vol. 21, n° 11, November 2021.
- Tsai S.W., *Composites 2.0, Think Composites Design Software*, Stanford University/Composite Design Group, 2013.
- Tsai S.W., et al., *Composite Laminate Theory and Practice of Analysis, Design and Automated Lay-up*, Publication of Composite Design Group/Department of Aeronautics & Astronautics/Stanford University, 2017.
- Tsai S.W., Hahn H.T., *Introduction to Composite Materials*, Technomic Publishing & Co, Lancaster, PA, 1980.
- Tsai S.W., Melo J.D., *An invariant-based theory of composites*, Composites Science and Technology, 100, 237–243, 2014.
- Turris F., Loken H.Y., Pinzelli R.F., *Effets des Microfissures de Résine sur les Propriétés des Composites Aéronautiques en Kevlar/époxyde*, Composites, 2, 35–40, March/April 1988.
- Verbruggen M.L., Gunnink J.W., *Metal Laminates –A Family of Advanced Materials*, Plastics/Metals/Ceramics SAMPE European Chapter, pp. 455–465, Bâle, Switzerland, May 1990.
- Volkersen O., *Recherches sur la Théorie des Assemblages Collés*, La Construction Métallique, 4, 3–13, 1965.
- Walder A., *Les Matériaux pour Moteurs d'Avion du Présent et de l'Avenir: les Alliages à Base de Nickel pour Disques, les Composés Intermétalliques, les Composites Céramiques*, Journée SF2M/Section Nord: Les matériaux pour applications à haute température, les matériaux pour moteurs d'avions du présent et de l'avenir, Lille, France, December 1999.
- Weiss J., Bord C., *Les Matériaux Composites*, Publication du Ministère de l'Industrie et de la Recherche, et du CETIM, 1983.

Index

- acoustic emission (AE) testing 83
- aerospace construction 149
 - aircraft (*see* aircraft)
 - space (*see* space applications)
- aircraft
 - aircraft ATR 72-700 157
 - airplane A400M Airbus 179
 - airplane Transall 178
 - architecture and manufacture
 - MMC panels 169
 - rib-stiffened panels 165–167
 - sandwich design 164
 - braking systems
 - carbon/carbon brake disks 169
 - business aircraft Falcon 10X 157
 - cargo aircraft WK2 and suborbital space plane SST2 158
 - components 149, 164
 - fatigue 88, 130
 - fighter aircraft 162
 - large transport aircraft (*see* civil transport aircraft)
 - light aircraft 159
 - regional aircraft 157
 - structural strength aspects 152
- aluminum-reinforced aramid (ARALL) 50
- aluminum-reinforced glass (GLARE) 50, 169
- anisotropic elastic medium
 - continuum mechanics 219
 - distinct ϕ_{ijk} number 219
 - orthotropic material 221
 - transversely isotropic material 221
- aramid *see* Kevlar®
- asymmetric case, of composite beam bending 370
 - elastic center 357
 - normal and shear stress 363
 - principal axes 371
 - shear coefficients 366, 374
 - torsion center 381
- autoclave curing 19
- autoclave molding 29
- automated preform manufacturing 24
- automated tape laying 25
- automated tape laying of D-D laminates 337, 350
- automotive industry 194
- beams 355
 - asymmetric case 370
 - bending stiffness 356
 - dynamic case 369
 - elastic center 357
 - stress distribution 363
 - torsion center 381
- bearing stress 134–135
- bending
 - composite beams 355
 - asymmetric case 370
 - shear
 - in composite box beam 555
 - in composite I-beam 559
 - in sandwich beam 549
- bicycles 212
- biocomposite materials
 - manufacturing process 62
 - natural plant fibers 59
 - natural vegetable fiber-reinforced composites 60
- biodegradable matrices 62
- blades 174
- blade of helicopter 174
 - blade flapping angle 429
 - elongation, of blade spar 433
 - fixing pins 433
 - glass/epoxy spar, cross-sectional area of 432
 - helicopter weight calculation 431
 - rotor hub 175
- BMC *see* bulk molding compound (BMC)
- bogie frame 213
- bolted joints 133, 138
- bonding 139
 - cylindrical geometry 145, 537
 - double-lap 541
 - scarf joint 143
 - single-lap adhesive joint 145
- boron 4–5, 52, 165
- box beam 555
- braking systems
 - carbon/carbon brake disks 169, 203
- Brazier effect 466, 600
- buckling
 - of carbon/epoxy wing spar 503
 - of rectangular panel under in plane loading 595
 - of sandwich beam 549
 - of thin-walled orthotropic tube 600
- bulk molding compound (BMC) 28
- business jets 157
- cable car 7, 215
- calculation tool 103, 352, 477
- cantilever beam 74, 469
- carbon/epoxy flywheel 189, 439
- carbon/epoxy laminate 101, 110, 117, 312, 326, 496, 503, 521
- carbon/epoxy shafts *see* drive shaft, for trucks
- carbon/epoxy wing spar 503
- carbon fibers coated with nickel 451
- carbon nanotube 63
- carbon/PEEK lever 462
- card sliding technique 351
- center wing box 156
- centrifugal molding 21
- Civil Transport Aircraft A350-900 155
- Civil Transport Aircraft A380-800 155
- Civil Transport Aircraft B 787-800 155
- ceramic matrix composites (CMC) 53, 183
- CMC *see* ceramic matrix composites (CMC)
- codes for the representation of names of countries:
 - code ISO 3166-1 /alpha-2. 32

- composite aircraft parts 7, 149
- composite beam with two layers 545
- composite blade 174–178, 429
- composite box beam 555
- composite drive shafts 130, 146, 434, 537
- composite flywheels 439
- composite glass/polyester tube, thermoelastic behavior of 485
- composite material applications
 - aerospace construction 149
 - air transport 152
 - automotive industry (*see* Automotive industry)
 - biomechanical applications 214
 - bogie frame 213
 - buildings and public works 6, 193
 - cable car 7, 215
 - electrical and electronics 6, 68
 - engineering sector 7, 200–204
 - geographical area 193
 - pressure gas bottle 213
 - rail transport 213
 - shipbuilding
 - Monohull IMOCA 60, 207
 - Ocean-Going Maxi-Trimaran 206
 - single scull 209
 - surfboard 209
 - vessels 210
 - space applications 184, 469
 - sports and leisure
 - bicycles 212
 - skis 210
 - tennis rackets 213
 - tubes, offshore installations 214
 - wind turbines 203
- composite propeller blade 174–178, 429
- composite sailboat hull 206, 510
- composite springs 200, 213
- composite U-beam, torsion center of 558
- compression failure 126, 503, 549, 595
- compression molding 18
- contact molding process 17
- continuum mechanics 219
- creep, of PVDF tube 488
- criterion (failure) *see* damage in composite parts
- curing process 17, 71, 95, 230, 264, 323, 527
- cutting tool 80
- cylindrical concentric tubes, adhesive bond of 130, 146, 434, 537
- damage in composite parts
 - failure criterion
 - features of 291
 - maximum eligible strain 294
 - maximum stress 293
 - orthotropic material 292
 - quadratic failure criterion 294
 - state of plane stress 292
 - stress criterion translated into strain space 305
 - industrial emphasis
 - causes of 285
 - diversity of 285
 - manufacturing process
 - injected plate with short fibers 286
 - part with pronounced curvatures 287
 - Tsai-Hill failure criterion
 - isotropic material, von Mises criterion 297
 - orthotropic material 294
 - Tsai-Wu failure criterion 294
 - typical, smooth area
 - damage levels, in laminates 287
 - and singularities 287
- Dauphin Eurocopter 173
- D-D laminate 309, 412
- deflection of sandwich beam 75, 425
- delaminations 71, 78, 83–85, 98–99, 127, 130, 134, 287
- design and drawing
 - composite part
 - design factors 87–89
 - material characteristics 88
 - specific properties 87
 - laminate
 - complex loading 110–117
 - delaminations (*see* delaminations)
 - double-double 309
 - fabrics 90
 - failure (*see* damage in composite parts)
 - fatigue 88, 130
 - midplane symmetry 93
 - modulus of elasticity 101
 - optimum 117
 - ply arrangement 96
 - pre-sizing of quadrangle symmetric laminate 101
 - quadrangle symmetric 91
 - simple loading 102
 - standard orientations 91
 - stress resultants 96, 117, 247, 312
 - tubes 130
 - unidirectional layer 90
- double-double laminate
 - quasi orthotropic laminate 326
 - transverse shear stress 412
- double-double sublaminates set 316
- double-lap bonded joint 541
- double-lap tapered joint 141
- drive shaft, for trucks *see* composite drive shafts
- elastic center
 - asymmetric case, of composite beam bending 370
 - of composite beam with two layers 545
- elastic coefficients
 - carbon/epoxy unidirectional layer 39
 - thermomechanical loading (*see* thermomechanical loading)
 - hygrothermal loading 234
 - longitudinal modulus 38, 225
 - orthotropic material 221
 - of plies 38, 42
 - Poisson coefficient 39, 227
 - shear modulus 39, 229
 - thermoelastic properties 230
 - transverse isotropic material 221
 - transverse modulus 227
 - fabric layer 42
 - glass/epoxy layers 42
 - unidirectional ply 39
- elastic constants of unidirectional composites 225
- epoxy resins 12
- equivalent stiffness in torsion 378
- exchange rate 153

- fabric 95
- failure
 - bending 259
 - bolted joints 135
 - bonded joints 142
 - criterion (*see* damage in composite parts)
 - damage in composite parts (*see* damage in composite parts)
- failure criterion *see* damage in composite parts
- fairings 147
- fastening and joining
 - bolting 133, 138
 - bonding 139
 - causes of hole degradation 133
 - failure modes in bolted joints 135
 - inserts
 - sandwich parts 147
 - uniaxial loads 147
 - riveting 137
- fatigue resistance 88, 130
- fiberglass reinforced polymeric column 563
- fiber placement 25
- fibers
 - mass fraction 36
 - principal materials 4
 - volume fraction 37
- fighter aircraft 68, 162
- filament winding process 22
- filament-wound composites
 - fiberglass reinforced polymeric column 563
 - glass/epoxy tube 453
 - glass/polyester reinforced polymeric tube, creep of 488
 - glass/resin telegraph pole 466
- filament-wound pressure vessels
 - openings in bottom heads 458
 - winding angle 456
- first-ply failure, of carbon/epoxy laminates 306
- flakes 49
- flax fibers 60
- flexibility coefficients 237
- flexure
 - bending of the laminate
 - displacement field 254, 312, 390
 - total normal stress 258, 331, 397
 - twisting moments 256, 394
 - buckling of thin-walled orthotropic tube 600
- flexure loading 570
- flywheel energy storage 189, 439
- forming process *see* manufacturing process
- formula 1 competition car 202
- gel coat 17, 18, 466
- glass
 - fiber 4
 - polyester reinforced polymeric tube, creep of 488
 - polymeric column reinforced by filament wound fiberglass 563
 - sailboat hull in glass/polyester 510
 - telegraph pole 466
 - tube made of glass/epoxy under pressure 453
- grammage 38
- graphene sheet 65
- 5-harness satin 43
 - blades 174, 429
 - elongation, of blade spar 433
 - fixing pins 433
 - flapping angle 430
 - glass/epoxy spar, cross-sectional area of 432
 - helicopter weight calculation 431
 - normal resultant 432
 - rotor characteristics 175
- composite areas
 - Dauphin Eurocopter 178
 - H160 Airbus-Helicopter 171
 - Racer Airbus-Helicopter 172
 - SB-1 Defiant Sikorsky-Boeing 173
 - V 280 Valor Bell-Lockheed Martin 173
- helicopter 171, 429
- percentage of structural composites 171
- pitch lever 177
- rotor hub
 - spheriflex 177
 - starflex 176
- hemp fibers 60
- high-speed propellers 180
- high temperature composites 53, 183, 186, 188
- homogenization of a double-double laminate 326
- honeycomb-shaped panels 79
- Hooke and Duhamel law 230
- hygrothermal loading 234, 264, 323, 325
- impact 127
- injection molding, with prepreg 20
- in-plane behavior, of balanced fabric ply 527
- in-plane loading 247, 326
- inserts
 - sandwich parts 147
 - uniaxial loads 147
- interlaminar shear stress 398
- isotropic plane stress, optimum laminates for 496
- Kevlar® 4, 42, 50, 480
- laminate, double-double, d-d 309, 415
- laminate, quadrangle symmetric 91, 247
- LAM SEARCH 103, 352
- large transport aircraft *see* civil transport aircraft
- light aircraft
 - drone 160
 - training aircrafts 160
- linear elastic material 219, 221
- load factor 493
- manipulator arm for space shuttle 469
- manufacturing process 17
 - acronyms of manufacturing processes 28
- mass fraction, fiber 36
- mats and reinforced matrices 45
- metal matrix composites (MMC) 50, 169
- microspherical fillers 47
- midplane symmetry *see* quad laminates
- moisture 233
- moisture absorption 233
- molding processes *see* manufacturing process
- montmorillonite 65
- motor racing 202
- multidimensional fabric 56

- multilayered plates, transverse shear behavior 387
 - cylindrical bending 405
 - orthotropic homogeneous plate 408
 - technical formulation 405
 - transverse shear coefficients 407
 - transverse shear stress 406
 - warping functions 407
- nanocomposite materials 63
 - manufacturing 69
 - mechanical applications 68
 - mechanical properties 66
- nanoreinforcements
 - geometrical shapes of 63
 - properties of 64
- natural vegetable fiber-reinforced composites 60, 200
- Nettle circle 344
- nickel coated carbon fiber 451
- Nomex® 80
- nondestructive inspection method 83
- nozzles, in space applications 186
- oceanic minesweeper 210
- offshore installations 214
- open rotor 181
- orthotropic material
 - anisotropic elastic medium 219
 - buckling of
 - orthotropic tubes 600
 - rectangular panels 595
 - elastic behavior equation 221
- orthotropic plate
 - homogeneous plate, bending of 326, 570
 - transverse shear stress and shear coefficient 406
 - warping functions 407
- PEEK resin 12, 462
- phenolic resin 12
- physical properties, of composite materials
 - core materials 13
 - reinforcements 11
 - resins 12
 - specific modulus 89, 482
 - specific strength 14, 89
- plain weave fabric 43
- plates
 - bending of
 - sandwich plate 409, 572
 - orthotropic plate 326, 408, 570
 - torsion, of orthotropic plates 518
- ply 38, 42, 50–52, 90–96, 101, 225, 232, 237, 283, 288, 302–309, 469, 498, 514, 527
- poisson coefficient 39, 227
- polyvinylidene fluoride tube, creep of 488
- prepreg molding 20
- pressure gas bottle 213
- pressure vessels
 - filament-wound
 - efficiency ratio 183
 - openings in bottom heads 458
 - winding angle 456
- propellant tanks and pressure vessels 185
- propellers 174–178
 - high-speed propellers 180
- pultrusion 23
- PVDF column, filament-wound fiberglass reinforced 563
- pyrolysis, fiber volume fraction 461
- quad laminate 91, 259
- quadrangle symmetric laminate 91, 259
- quadratic failure criterion 100, 251, 294, 297
 - stress criterion translated into strain space 305
- quasi-isotropic laminate 516
- quasi-orthotropic homogenized laminates 326, 412
 - double-double sub-laminate set 316
- quasi-orthotropic laminate 309, 412
- reaction engine, aircraft 181
- reaction injection molding (RIM / SRIM) 21, 28
- recycling 29
- recycling of polymer matrix composites 31
- regional aircrafts 157
- reinforced-reaction injection molding (R-RIM) 21
- residual thermal stress, in carbon/epoxy laminates 95
- resin transfer molding 19
- Rib-stiffened panels 165
- riveting 137
- rotor hub
 - spheriflex 177
 - starflex 176
- rupture *see* failure
- sailboat hull, glass/polyester 510
- sails 206
- safety factor 89
- sandwich structural part, processing of 81
- sandwich structures
 - beams
 - bending vibration of 369, 574
 - buckling of 78, 549
 - shear coefficient calculation 475, 552
 - shear due to bending 552
 - flexural rigidity 572
 - manufacturing and design problems 79
 - honeycomb 79
 - inserts and attachment fittings 80
 - repair of laminated facings 82
 - shaping process 80
 - plates, bending 409
 - transverse shear coefficients 412
 - transverse shear stress 441
 - simplified flexure 74, 425
- satellite structures *see* space applications
- satin weave fabric 42, 95, 527
- scarf joint 143
- sewing stitch, on laminates 130
- shear modulus *see* elastic coefficients
- shear strength 43, 58, 71, 100, 251, 293–294, 300
- shear stress
 - adhesive 142, 145
 - bending 363, 387, 417
 - composite beam 363
 - cylindrical concentric tubes, adhesive bond of 145, 537
 - deformation energy 368, 407
- shear stiffness 413
- shipbuilding
 - Maxi-trimaran Banque Populaire XI 206
 - Monohull IMOCA 60, 207

- Ocean-Going Maxi-Trimaran 206
- single scull 209
- surfboard 209
- vessels 210
- short fiber composite 286–288
- short beam shear test 71
- short silicon carbide fibers 52
- SiC fibers *see* silicon carbide (SiC) fibers
- skis
 - skier equipment 210
 - structure 211
- SMC 28
- smooth area 287
- space applications 184
- space shuttle
 - manipulator arm for 469
 - thermal protection 188
- spar 166, 168, 175, 503
- sports and leisure
 - bicycles 212
 - skis 210
 - tennis rackets 213
- stacking, of plies 96, 318
- stamp forming 18
- stiffness coefficients 241, 246, 319–320
- stiffness evolution, curing 71
- strain based criterion 128, 294, 305, 338
- strength of homogenized D-D laminates 338
- stress criterion translated into strain space 305
- surfboard 209
- symmetric composite beam bending, dynamic case
 - 369, 574
- symmetric laminates *see* quadrangle symmetric laminates
- tape laying of D-D laminates 337
- tapered lap joints *see* double-lap tapered joint
- tennis rackets 213
- tensile test 70
- thermal expansion coefficients
 - of fiber/epoxy ply 43, 46, 52
 - of nickel coated carbon fiber 451
- thermal stress
 - creep of reinforced polymeric tube 488
 - laminate curing process 483
 - residual thermal stress, in carbon/epoxy laminates 483
- thermoelastic behavior of a glass/polyester tube 485
- thermoelastic behavior, of balanced fabric ply 527
- thermoplastic resins 12
- thermoset resins 12
- think composites 103, 352
- torsion
 - of composite beams of any section shape 377
 - of composite U-beam 558
 - of thin-walled orthotropic tube 131, 537, 601
- training aircraft Elixir 161
- training aircraft Velis Pipistrel 160
- transversely isotropic material 221
- transverse modulus, of unidirectional composites 227
- transverse shear behavior, multilayered plates 387
- transverse shear stress
 - orthotropic homogeneous plate 408
 - quasi-orthotropic D-D plates 412
 - sandwich plate 409
- Tsai-Hill failure criterion 100, 251, 297, 441, 479, 485, 495, 499, 506, 513
- Tsai invariant 309
- Tsai modulus 309
- Tsai-Wu criterion 294
- tubes
 - buckling of orthotropic tubes 596
 - creep of a polymeric tube reinforced by filament
 - wound under thermal stress 488
 - cylindrical bonding 537
 - glass/resin telegraph pole 466
 - laminated tubes 130
 - made of glass/epoxy under pressure 453
 - polymeric column reinforced by filament wound
 - fiberglass 563
 - thermoelastic behavior of a glass/polyester tube 485
- twill weave fabric 42
- U-beam, torsion center of 558
- unidirectional ply *see* ply
- unit circle 343
- vacuum assisted RTM (VARTM) 20
- vessels *see* pressure vessels
- vibrations
 - dynamic case, of symmetric beam bending 369
 - of sandwich beam 574
- volume fraction, fiber 37
- von Mises criterion, isotropic material 297
- warp and weft yarn 42
- warping function, for flexure 365, 367, 373, 403, 407
- warping function, for torsion 378
- waste treatment 29
- wind turbines
 - components 203
 - manufacturing process 205
- wings 161, 164, 166, 168, 441, 503
- world wide failure exercises 291
- woven fabric, forms of 42
- yarns 42



Taylor & Francis Group
an informa business

Taylor & Francis eBooks

www.taylorfrancis.com

A single destination for eBooks from Taylor & Francis with increased functionality and an improved user experience to meet the needs of our customers.

90,000+ eBooks of award-winning academic content in Humanities, Social Science, Science, Technology, Engineering, and Medical written by a global network of editors and authors.

TAYLOR & FRANCIS EBOOKS OFFERS:

A streamlined experience for our library customers

A single point of discovery for all of our eBook content

Improved search and discovery of content at both book and chapter level

REQUEST A FREE TRIAL

support@taylorfrancis.com

 **Routledge**
Taylor & Francis Group

 **CRC Press**
Taylor & Francis Group